Towards a generalized effective nuclear Gogny interaction extended to finite-range spin-orbit and tensor forces

Geoffrey Zietek

université PARIS-SACLAY

Towards a generalized effective nuclear Gogny interaction extended to finite-range spin–orbit and tensor forces

Vers une interaction nucléaire effective de Gogny généralisée étendue à des termes spin–orbite et tenseur de portées finies

Thèse de doctorat de l'université Paris-Saclay

École doctorale n°576 : particules hadrons énergie et noyau : instrumentation, imagerie, cosmos et simulation (PHENIICS)
Spécialité de doctorat : Physique nucléaire
Graduate School : Physique. Référent : Faculté des sciences d'Orsay

Thèse préparée dans l'unité de recherche **Laboratoire Matière en Conditions Extrêmes** (Université Paris-Saclay, CEA), sous la direction de **Marcella GRASSO**, Directrice de recherche et la co-direction de **Nathalie PILLET**, Ingénieur chercheur.

Thèse soutenue à Paris-Saclay, le 15 décembre 2023, par

Geoffrey ZIETEK

Composition du jury

Membres du jury avec voix délibérative

Denis LACROIX Directeur de recherche, IJCLab, Université Paris-Saclay	Président
Karim BENNACEUR Directeur de recherche, IP2I, Université Claude Bernard Lyon 1	Rapporteur & Examinateur
Luís ROBLEDO Professeur des Université, Université autonome de Madrid	Rapporteur & Examinateur
Micaela OERTEL Directrice de recherche, LUTH, Observatoire Paris-Meudon	Examinatrice
Peter RING Professeur des Universités, Université technique de Munich	Examinateur

THESE DE DOCTORAT

NNT : 2023UPASP193

université PARIS-SACLAY

ÉCOLE DOCTORALE
Particules, hadrons, énergie et noyau : instrumentation, imagerie, cosmos et simulation (PHENIICS)

Titre : Vers une interaction nucléaire effective de Gogny généralisée étendue à des forces spin–orbite et tenseur de portées finies

Mots clés : Interaction nucléaire – Force tenseur – Problème à N corps – Structure nucléaire – Fission nucléaire – Énergies d'excitation

Résumé : Peu après son élaboration à la fin des années 1960, l'interaction de Daniel Gogny s'est imposée comme une référence dans le paysage des interactions nucléaires, effectives et phénoménologiques. Sa nature de portée intrinsèquement finie offre en effet la possibilité de traiter sur un même pied d'égalité le champ moyen et les corrélations d'appariement, sans risque de divergences ultraviolettes, même au-delà du champ moyen. Par ailleurs, la force tenseur, composante essentielle des interactions réalistes, a souvent été écartée des formulations effectives. Pourtant, elle s'est très tôt révélée nécessaire à la reproduction des propriétés élémentaires du système nucléaire le plus rudimentaire, le deutéron. Depuis, son action s'est manifestée à bien des égards, de l'arrangement des énergies à une particule, en passant par la description des résonances géantes et des états Gamow–Teller, jusqu'à impacter la magicité de noyaux super lourds.

Dans ce travail de thèse, nous nous proposons d'étendre l'expression analytique de l'interaction de Gogny à des termes spin–orbite et tenseur de portées finies. La forme résultante, voulue de portée intégralement finie, permet de retrouver la plupart des expressions analytiques établies à ce jour. Elle est en ce sens dénommée « interaction de Gogny généralisée ». Le code numérique utilisé pour déduire les paramètres est adapté aux termes nouvellement ajoutés, et une paramétrisation intitulée DG, issue de l'ajustement global de l'ensemble des paramètres, en est extraite. Pour ce faire, les propriétés d'appariement proton–neutron ont notamment été contrôlées pour la première fois dans une interaction de Gogny, via des contraintes sur les éléments de matrice appropriés. La consistance de l'interaction de Gogny généralisée est d'abord évaluée dans la matière nucléaire infinie, en comparaison à diverses paramétrisations antérieures et des calculs réalistes. Les équations d'état des matières symétrique et neutronique, ainsi que des grandeurs physiques tels l'énergie potentielle décomposée en canaux (S, T), les ondes partielles ou des critères de stabilité associés aux paramètres de Landau dans la théorie des liquides de Fermi, sont analysés. Les résultats obtenus dans les noyaux finis, aussi bien au niveau du champ moyen, à partir de l'approximation Hartree–Fock–Bogoliubov, qu'au-delà, par l'intermédiaire de la méthode du mélange des configurations multiparticules–multitrous, sont décisifs. Les caractéristiques substantielles des principales interactions de Gogny sont préservées tandis que de nombreux amendements sont à recenser. Au niveau du champ moyen, le décalage dans les rayons de charge des isotopes du plomb est plus fidèlement décrit, des inversions entre états à une particule sont constatées, la destruction d'une partie de l'énergie d'appariement survient dans des chaînes isotopique et isotonique, la nature des déformations quadrupolaires axiales de certains noyaux mous sont modifiées et les hauteurs des barrières de fission abaissées dans plusieurs pré-actinides et actinides. Au-delà du champ moyen, la reproduction des premières énergies d'excitation de nombreux noyaux légers pairs–pairs, impairs et impairs–impairs est considérablement améliorée. Elle est interprétée la plupart du temps comme la signature d'une compétition subtile entre forces spin–orbite et tenseur dans l'évolution des couches en énergie.

université PARIS-SACLAY

ÉCOLE DOCTORALE
Particules, hadrons, énergie et noyau : instrumentation, imagerie, cosmos et simulation (PHENIICS)

Title: Towards a generalized effective nuclear Gogny interaction extended to finite-range spin–orbit and tensor forces

Keywords: Nuclear interaction – Tensor force – N-body problem – Nuclear structure – Nuclear fission – Excitation energies

Abstract: Soon after its development in the late 1960s, Daniel Gogny's interaction became a reference in the landscape of nuclear, effective and phenomenological interactions. Its intrinsically finite-range nature makes it possible to treat the mean field and pairing correlations on an equal footing, while avoiding ultraviolet divergences, even beyond the mean field. On the other hand, the tensor force, an essential component of realistic interactions, has often been sidelined in effective formulations. Yet, very early on, it proved necessary to reproduce the elementary properties of the most rudimentary nuclear system, the deuteron. Since then, its action has manifested in many ways, from the arrangement of single-particle energies, through the description of giant resonances and Gamow–Teller states, to impacting the magicity of superheavy nuclei.

In this thesis work, we propose to extend the analytical expression of the Gogny interaction to finite-range spin–orbit and tensor terms. The resulting form, which is intended to be entirely of finite range, enables to recover most of the analytical expressions established to date. It is in that sense referred to as the "generalized Gogny interaction". The numerical code used to deduce the parameters is adapted to the newly introduced terms, and a parametrization entitled DG, produced by the global fitting of all the parameters, is extracted. In particular, the proton–neutron pairing properties are controlled for the first time in a Gogny interaction, via constraints on the appropriate matrix elements. The consistency of the generalized Gogny interaction is first evaluated in infinite nuclear matter, in comparison with various previous parametrizations and realistic calculations. The equations of state for symmetric and neutron matters, as well as physical quantities such as the potential energy decomposed into (S, T) channels, partial waves or stability criteria associated with Landau parameters in the theory of Fermi liquids, are analyzed. The results obtained in finite nuclei, both at the mean-field level, from the Hartree–Fock–Bogoliubov approximation, and beyond, via the multiparticle–multihole configuration mixing method, are decisive. Substantial features of the main Gogny interactions are preserved, while numerous amendments are identified. At the mean-field level, the kink in the charge radii of lead isotopes is more accurately described, inversions between single-particle states are observed, the destruction of part of the pairing energy occurs in isotopic and isotonic chains, the nature of the axial quadrupole deformations of certain soft nuclei is modified and the fission barrier heights lowered in several pre-actinides and actinides. Beyond the mean field, the reproduction of first excitation energies of many light even–even, odd and odd–odd nuclei is considerably improved. This effect is most of the time interpreted as the signature of a subtle interplay between spin–orbit and tensor forces in the shell evolution.

Synthèse

L'interaction nucléaire, effective et phénoménologique de Gogny fut élaborée par le physicien français Daniel Gogny vers la fin des années 1960. Sa principale motivation fut de proposer une interaction performante au niveau du champ moyen et au-delà, tenant compte de l'appariement, tout en prévenant l'apparition de divergences ultraviolettes associées aux corrélations retenues, rencontrées avec d'autres interactions effectives telle l'interaction de Skyrme. Pour ce faire, des termes centraux de portées finies furent introduits, en dépit des défis numériques d'ampleur soulevés à l'époque. L'interaction de Gogny dépend d'un ensemble de paramètres qui est déduit de données expérimentales ou de grandeurs physiques évaluées dans la matière nucléaire infinie. Le premier jeu de paramètres – ou paramétrisation – mis au point par Gogny fut dénommé D1. Dès lors, de nouvelles paramétrisations, visant à améliorer la reproduction de certaines quantités physiques et observables, furent façonnées. L'exemple ayant eu la plus importante répercussion dans la littérature spécialisée est certainement la paramétrisation D1S. Proposée par Berger *et al.* en 1991, elle diminue notamment l'appariement ainsi que la hauteur des barrières de fission dans la plupart des actinides, tous deux surévalués par la paramétrisation D1. Une autre manière d'améliorer les prédictions de l'interaction de Gogny est d'étendre son expression analytique, en modifiant certains termes ou en en ajoutant de nouveaux. La forme résultante dépend alors de davantage de paramètres, qui apportent une plus grande latitude à l'interaction et permettent souvent une plus large ou plus précise reproduction de quantités physiques et d'observables ciblées. Il est à noter que cette seconde voie est généralement plus ambitieuse que la première. En effet, elle nécessite le calcul d'éléments de matrice voire de champs propres aux termes nouvellement ajoutés, la recherche de contraintes pertinentes pour déduire un jeu de paramètres, et le choix de la paramétrisation elle-même. L'interaction D2, établie par Chappert en 2006, va en ce sens. Le terme dépendant de la densité, de portée nulle dans l'interaction originelle de Gogny, acquiert une portée finie, de sorte que de nouveaux paramètres sont introduits. L'ajustement de cette interaction a en particulier permis de contrôler la dérive des masses observée avec la paramétrisation D1S.

La force tenseur est connue depuis les années 1940 pour constituer une composante essentielle de l'interaction nucléaire. Elle est à l'origine de certaines propriétés fondamentales comme l'énergie de liaison ou le moment quadrupolaire électrique du système nucléaire le plus rudimentaire, le deutéron. Ces dernières années, son rôle clé a été souligné dans de nombreuses études. La force tenseur intervient notamment dans l'arrangement des états d'énergie à une particule, la description des résonances géantes, des états Gamow–Teller, des propriétés de déformation de noyaux mous, et s'étend jusqu'aux noyaux superlourds loin de la vallée de stabilité. Malgré cela, il faudra attendre les années 1970 pour que celle-ci commence à être prise en compte dans les interactions effectives, de type Skyrme ou M3Y. La raison étant que la force tenseur est liée à des effets fins, et que son traitement est relativement complexe. Elle n'apparaîtra pour la première fois dans l'interaction de

Gogny qu'en 2006, à la suite des travaux d'Otsuka et de collaborateurs, mais l'interaction correspondante ne sera pas sondée en profondeur. Depuis, seules des interactions de Gogny comprenant un terme tenseur ajusté de manière perturbative, c'est-à-dire isolément des autres paramètres, ont vu le jour.

Ce travail de thèse consiste à étendre l'expression analytique de l'interaction de Gogny, à partir de la forme analytique D2, en rendant finie la portée du terme spin–orbite et en incorporant un terme tenseur, directement de portée finie. Cette nouvelle interaction est appelée interaction de Gogny généralisée, et surnommée DG. L'intérêt du terme tenseur a été motivé au paragraphe précédent, tandis que la portée finie du terme spin–orbite assure qu'aucune divergence ultraviolette n'est à craindre dans cette expression voulue intégralement de portée finie. Contrairement aux interactions perturbatives, l'interaction de Gogny généralisée est entièrement réajustée, en ce sens que tous les paramètres sont déterminés ensemble, de façon cohérente.

Dans le Chapitre I, l'interaction de Gogny est située dans le paysage des interactions nucléaires et ses caractéristiques principales comparées à celles de ses homologues. Son évolution historique y est détaillée, avec un inventaire des différentes paramétrisations et extensions analytiques proposées avant l'établissement de l'interaction DG. L'accent est mis sur les expressions analytiques des interactions de type D1 et D2, et leurs spécificités sont discutées. Les procédures d'ajustement des paramètres de D1S et D2 sont exposées, notamment pour préparer le lecteur à la procédure d'ajustement de DG, qui est une généralisation de ces dernières. Le code d'ajustement, rendant possible de telles procédures, y est disséqué ; d'abord dans sa version adaptée à D1S, ensuite dans son extension à D2.

Le formalisme Hartree–Fock restreint (HFR), faisant correspondre les valeurs expérimentales des énergies de liaison et des rayons de charge au cadre théorique choisi, est introduit, et les contraintes et filtres retenus listés. En premier lieu, les contraintes dégagent, au moyen d'un système d'inversion, des jeux de paramètres tandis qu'en second lieu, les filtres ne retiennent que les paramétrisations qui reproduisent avec une certaine précision plusieurs grandeurs physiques dans la matière nucléaire infinie. Ces deux étapes aboutissent, après différents tests dans les noyaux finis, aux paramétrisations D1S et D2.

Le Chapitre II est dédié aux aspects techniques de l'interaction de Gogny généralisée. L'expression analytique de cette nouvelle interaction est fournie et est comparée aux formes précédentes. Il apparaît notamment que l'action du terme spin–orbite est étendue au canal $T = 0$, avec un terme dépendant de l'isospin, et que les expressions de la plupart des interactions de Gogny antérieures peuvent être obtenues en considérant une limite particulière de DG. C'est précisément en cela que cette nouvelle interaction de Gogny a été baptisée « interaction de Gogny généralisée ».

La procédure d'ajustement de DG est ensuite présentée. Le choix des portées des termes spin–orbite et tenseur est guidé par les théories d'échanges de mésons : l'interaction tenseur est principalement véhiculée par le pion tandis que la contribution majeure du terme spin–orbite s'apparente à l'échange d'un méson ω. Le premier agissant à longue distance et le second à courte distance, les portées des termes spin–orbite et tenseur ont été sélectionnées en conséquence. Les contraintes de la procédure d'ajustement de D2 ont été reprises et étendues à DG. En plus, quatre contraintes ont été ajoutées afin de déterminer les nouveaux paramètres spécifiques aux termes spin–orbite et tenseur. Ces contraintes prennent la forme d'éléments de matrice couplés aux nombres quantiques (J, T) dans les couches sd et pf. Il a été demandé à ce que ces éléments de matrice, évalués

via des modèles en couches, soient reproduits avec une erreur de 10% par l'interaction DG. Parmi ces éléments de matrice, certains sont de type appariement et permettent de contrôler pour la première fois dans une interaction de Gogny les propriétés d'appariement proton–neutron dans le canal $T = 0$. Comme pour les contraintes, les filtres utilisés dans le code d'ajustement de D2 ont été repris dans celui de DG, et trois nouveaux filtres ont été considérés. Le premier garantit que l'intensité du terme spin–orbite de portée finie dans le canal $T = 1$ reste proche de celle du terme spin–orbite originel de portée nulle, à la limite d'une portée qui tend vers zéro. Le second a à voir avec un article de Sharma *et al.* publié en 1995. Dans cet article, les auteurs montrent qu'en choisissant convenablement le paramètre dépendant de l'isospin du terme spin–orbite dans une interaction de Skyrme, une meilleure reproduction du décalage isotopique dans les rayons de charge du plomb est obtenue. Puisqu'il est ici question d'une interaction de Gogny, qui plus est pourvue d'un terme spin–orbite de portée finie, seules les paramétrisations pour lesquelles le paramètre dépendant de l'isospin du terme spin–orbite n'était pas trop éloigné de la valeur trouvée dans l'article mentionné ont été conservées. Le troisième s'inspire de l'interaction D1ST2c, dont les paramètres spin–orbite et tenseur ont été ajustés conjointement. Des intervalles de valeurs autorisées pour ces paramètres ont été définis afin de reproduire correctement les écarts en énergie $1f$ des états à une particule neutron dans les noyaux doublement magiques ^{40}Ca, ^{48}Ca et ^{56}Ni. Finalement, plusieurs conditions imposées dans les codes de noyaux finis ont permis de sélectionner l'interaction DG qui est analysée tout au long du document.

Le code d'ajustement fournit directement de nombreux résultats dans la matière nucléaire infinie afin de juger de la fiabilité de l'interaction DG. Il s'avère que les quantités usuelles évaluées à la densité de saturation dans la matière nucléaire symétrique pour l'interaction DG tombent toutes dans les intervalles de valeurs empiriques. L'équation d'état de DG, à savoir l'évolution de l'énergie potentielle en fonction de la densité du milieu, reproduit fidèlement les calculs réalistes, comme l'ensemble des interactions de Gogny étudiées. Pour aller plus loin, l'énergie potentielle a d'abord été décomposée selon son action dans les canaux (S, T). Les interactions D2 et DG, aux courbes très similaires, se présentent comme les meilleurs compromis. Leurs prédictions sont proches des résultats réalistes dans les canaux impairs, tandis qu'elles restent comparables aux autres interactions de Gogny dans les canaux pairs. La décomposition en ondes partielles offre une description encore plus précise de l'énergie potentielle. Il apparaît que certaines ondes partielles, notamment certaines ondes P et D, aux contributions significatives, sont mieux reproduites par DG. Par ailleurs, sont étudiées des différences entre ondes partielles n'impliquant que les termes spin–orbite et tenseur. Le fait qu'elles soient mieux décrites par DG laissent à penser que ces termes ont été correctement ajustés, déjà au niveau de la matière nucléaire. Les masses effectives neutron sont plus importantes que les masses effectives proton avec l'interaction DG, pour toute asymétrie, en accord avec les prédictions réalistes. De même, l'équation d'état dans la matière neutronique obtenue avec DG est semblable à celle de D2, évitant ainsi l'effondrement constaté avec D1S aux grandes densités. Pour terminer, les paramètres de Landau associés au terme tenseur ont été dérivés dans la théorie des liquides de Fermi. Combinés aux paramètres propres aux autres termes de l'interaction de Gogny généralisée, ils sont à l'origine de critères de stabilité et de règles de somme. Les critères de stabilité, issus de la nécessité pour l'état fondamental de quasiparticules de rester stable à toute légère déformation de la surface de Fermi, sont tous satisfaits par l'interaction DG. Ce résultat est notoire dans la mesure où plusieurs de ces critères n'étaient pas respectés par d'autres paramétrisations de type DG, retenues

suite au processus d'ajustement. Quant aux règles de somme, systématiquement violées par les interactions effectives dépendant de la densité, elles le sont davantage avec l'interaction DG qu'avec les interactions D1S et D2. Cependant, elles le sont bien moins que les interactions pourvues d'un terme tenseur perturbatif, que sont D1ST2a et D1ST2c. De plus amples investigations devront être menées pour établir si cette violation se révèle pathologique ou non.

Les résultats dans la matière nucléaire infinie servent de guides, mais ce sont surtout les observations dans les noyaux finis qui permettent de crédibiliser une interaction nucléaire. Pour cette raison, l'interaction DG a été sondée dans une approche de type champ moyen, à l'approximation Hartree–Fock–Bogoliubov (HFB), dans le Chapitre III. Plus précisément, le code HFB utilisé repose sur une base d'oscillateurs harmoniques axiaux à deux centres, dont le formalisme est rappelé en première section. Aussi bien les propriétés de volume, de surface que de déformation de l'interaction DG sont décortiquées.

Les énergies de liaison prédites le long des chaînes isotopiques dans les noyaux légers, de masses intermédiaires et lourds sont satisfaisantes, souvent un peu plus faibles qu'avec l'interaction D2, sauf proche de la magicité. Il en découle que le terme tenseur tend à délier légèrement la plupart des isotopes étudiés. Concernant la dérive des masses, elle est absente des chaînes isotopiques inspectées. Ce résultat était attendu puisque la dérive est contrôlée dès la procédure d'ajustement, en demandant à ce que les différences entre les énergies de liaison expérimentales et évaluées à l'approximation HFB dans les noyaux doublement magiques ^{100}Sn et ^{132}Sn soient identiques. Les rayons de charge de DG sous-évaluent presque toujours les prédictions de D1S, elles-mêmes plus basses que les valeurs expérimentales. À ce stade, il est difficile de conclure, les corrélations au-delà du champ moyen devant être prises en considération pour proposer une comparaison plus juste à l'expérience. L'étude des rayons de charge trouve tout son intérêt pour analyser le décalage isotopique dans les noyaux de plomb et de calcium. Dans les plombs, le décalage isotopique est mieux reproduit avec DG qu'avec les interactions D1S et D2. Cet effet est imputable au gap neutron $(1i_{11/2} - 2g_{9/2})$, plus resserré avec DG et favorisant alors des rayons de charge plus larges pour les isotopes plus lourds que le ^{208}Pb. La diminution de l'intensité du terme spin–orbite de l'interaction DG justifie une telle amélioration. Dans les calciums, en revanche, le comportement singulier des rayons de charge n'est manifestement pas répliqué par l'interaction DG. Enfin, les profils des distributions de densité de charge et de neutrons dans les ^{208}Pb et ^{48}Ca obtenus avec DG et D2 sont assez semblables.

D'une part, l'énergie d'appariement neutron a été calculée le long de la chaîne isotopique des étains. On constate une nette diminution de cette dernière avec DG, comparativement à D1S et D2, entre les isotopes $A = 110$ et $A = 124$. Lorsque les états à une particule neutron sont tracés, on note que les gaps proches du niveau de Fermi sont plus larges avec DG qu'avec D1S et D2. Cette disposition entraîne une probabilité de diffusion vers les états supérieurs moindre et réduit in fine l'énergie d'appariement prédite par DG. Le réarrangement des états à une particule observé avec DG peut s'expliquer par l'action conjointe des forces spin–orbite et tenseur. L'effet est particulièrement marqué, au point d'engendrer deux inversions d'états, l'une pour l'isotope $A = 112$, l'autre pour l'isotope $A = 118$. D'autre part, l'énergie d'appariement proton a été évaluée le long de la chaîne isotonique $N = 50$. À nouveau, un déclin notable de l'énergie d'appariement apparaît avec DG, pour la plupart des isotones. Les termes spin–orbite et tenseur justifient cet effet. En particulier, l'énergie d'appariement est nulle avec DG dans l'isotone ^{90}Zr. L'énergie d'appariement n'étant pas une observable, les propriétés de surface devront être mises à

l'épreuve par l'analyse plus poussée d'observables telles que la différence de masses pairs–impairs le long de chaînes isotopiques et isotoniques. Finalement, la comparaison des écarts énergétiques entre états partenaires de spin et des gaps avec les interactions D1S, D2 et DG révèle que les termes spin–orbite et tenseur seuls ne peuvent rendre compte de l'ensemble des tendances observées. Cela suggère que la renormalisation des termes centraux et dépendant de la densité au passage de D2 à DG joue un rôle prépondérant dans l'agencement des états à une particule.

Les propriétés de déformation ont été scrutées dans de nombreuses chaînes isotopiques. De manière générale, l'énergie de liaison obtenue avec DG dans la majorité des isotopes légers est plus petite que celle des interactions D1S et D2, autour de la sphéricité. Néanmoins, dans les noyaux magiques, d'autres comportements preuvent se présenter. Par exemple, l'interaction DG prédit le ^{36}S plus rigide, avec un puits plus prononcé à déformation quadrupolaire axiale nulle. Dans le ^{44}S, la coexistence de formes est plus marquée avec DG, les puits oblate et prolate étant plus profonds qu'avec les autres interactions. Parfois même, une coexistence de formes fait irruption avec DG, là où le noyau était sphérique avec D1S ; c'est le cas du ^{30}S. Par comparaison avec les résultats d'autres interactions, il apparaît que le terme tenseur est principalement responsable de ces effets. Bien que les données expérimentales ne donnent accès qu'aux valeurs absolues des déformations quadrupolaires axiales, on note que les prédictions de DG sont, pour les isotopes dans lesquels la force tenseur a une action importante, plus en adéquation avec l'expérience.

Les barrières de fission le long des chemins asymétriques sont déterminées pour les pré-actinides que sont les thoriums, et plusieurs actinides standards. Par rapport à l'interaction D1S, les premières barrières de fission sont abaissées de 1 à 1,5 MeV dans les thoriums et d'environ 2 MeV dans les actinides, avec l'interaction DG. Ainsi, elles sont plus proches des valeurs expérimentales pour DG. Les différences restantes peuvent s'expliquer par la nécessité de tenir compte de la triaxialité. Des études réalisées avec D1S montrent en effet que les hauteurs des premières barrières sont réduites de plusieurs MeV dans les calculs triaxiaux, par rapport aux calculs axiaux. Pour ce qui est des secondes barrières de fission, elles sont diminuées d'environ 1 MeV dans la plupart des actinides analysés avec DG. Les valeurs expérimentales sont plus proches mais demeurent éloignées de quelques MeV. Les énergies de référence choisies comme énergies du point zéro plutôt que comme minima HFB devraient davantage réduire la hauteur des secondes barrières de DG, comme ce fut le cas pour D1S. Des décalages en déformation sont également à recenser avec DG. Les déformations quadrupolaires axiales correspondant à l'isomère de fission et au point selle sont généralement plus grandes dans les actinides avec DG qu'avec les autres interactions. Dans ces noyaux, les états isomériques de DG surviennent à des élongations plus prononcées tandis que la séparation des fragments s'enclenche à plus forte contrainte.

Dès sa conception, l'interaction de Gogny a été pensée de manière à fournir des résultats probants au niveau du champ moyen, mais aussi et surtout au-delà, quand davantage de corrélations sont prises en considération. Les résultats HFB étant satisfaisants, l'interaction de Gogny généralisée a été investiguée, dans le Chapitre IV, à l'approximation au-delà du champ moyen que constitue la méthode du mélange de configurations multiparticules–multitrous (MPMH). Les énergies d'excitation des premiers états excités dans les noyaux pairs–pairs, impairs et impairs–impairs de la couche *sd* ont été évaluées. Les valeurs moyennes et écarts-types des différences entre les énergies des premiers états excités prédites théoriquement et expérimentalement sont, pour l'ensemble de ces noyaux,

systématiquement et significativement réduits avec l'interaction DG. Ce succès était à prévoir puisque des filtres visant à améliorer la description des premières énergies d'excitation dans ces noyaux furent placés dans le processus d'ajustement des paramètres. Alors que les contraintes et filtres des codes d'ajustement des interactions de Gogny sont habituellement restreints aux noyaux pairs, l'efficacité de l'interaction DG dans la description des noyaux impairs et impairs–impairs montre l'importance de leur déploiement également pour de tels noyaux.

Une analyse soignée de l'organisation des états à une particule a permis de mettre en évidence que ces améliorations sont *globalement* dues à la diminution de l'intensité du terme spin–orbite et *localement* à la présence du terme tenseur. Dans les noyaux pairs par exemple, la valeur moyenne définie ci-dessus est à peine supérieure à 200 keV avec DG, résultant principalement d'une force spin–orbite d'intensité plus faible que celle des interactions D1S et D2. De façon complémentaire, la meilleure description des isotopes ^{30}Si, ^{30}S et ^{32}S, aux énergies d'excitation fortement surévaluées par D1S et D2, est surtout une conséquence du terme tenseur.

Dans les noyaux impairs et encore plus dans les noyaux impairs–impairs, l'importante densité d'état à basse énergie entraîne des inversions d'états excités dans les spectres prédits par le MPMH. Ainsi, il n'est pas rare que les spins–parités des premiers états excités théoriques et expérimentaux de plusieurs de ces noyaux ne coïncident pas. C'est en l'occurrence ce qui se produit de manière répétée avec l'interaction DG. Le faible écart moyen en énergie entre le premier état excité et le premier état ayant le couple de spin–parité révélé par l'expérience confirme, cependant, que les inversions ont souvent lieu entre des états énergétiquement rapprochés, de l'ordre de quelques centaines de keV. Il est probablement trop tôt pour espérer un tel degré de précision d'une interaction effective comme l'interaction de Gogny. Toutefois, les calculs aboutissant à ces résultats ont été réalisés en ne résolvant que la première des deux équations MPMH. Lorsqu'une résolution complètement auto-consistante de ces dernières sera rendue possible, ces conclusions devront être réévaluées.

Au vu des résultats rapportés dans la matière nucléaire infinie ainsi qu'au niveau du champ moyen et au-delà, l'interaction de Gogny généralisée prend une place de choix dans le panorama des interations de Gogny. Bien entendu, davantage de quantités physiques et d'observables devront être examinées pour accroître son champ d'application ou au contraire pointer des limitations que des interactions ultérieures devront lever. Dans ce dernier cas, une nouvelle paramétrisation de type DG pourra être recherchée, voire même une nouvelle extension analytique proposée. À cette fin, le code d'ajustement a été étendu, de sorte à pouvoir générer des paramétrisations d'une interaction de Gogny comportant jusqu'à deux termes spin–orbite, tenseur et dépendant de la densité. Il appartient aux générations futures de tirer profit (ou non) de ces travaux.

Remerciements

Dans les prochaines lignes, je souhaiterais adresser mes remerciements à l'ensemble des personnes qui ont contribué de près comme de loin à l'élaboration de ce travail de thèse. Sans elles, le présent document n'existerait pas.

En premier lieu, je tiens à remercier chaleureusement tous les membres du Service de Physique Nucléaire du CEA de Bruyères-le-Châtel. À leurs côtés j'ai eu l'opportunité d'évoluer dans un environnement agréable, propice aux discussions stimulantes. Je remercie plus particulièrement Ania Zdeb pour sa douceur et sa sympathie des quelques mois que nous avons partagés ensemble. Je suis très reconnaissant envers Noël Dubray pour son soutien continu dans les derniers mois de thèse. Son aisance avec les outils numériques, toujours surmontée d'une bonne couche d'humour, m'a été d'un grand secours. Je n'oublierai pas non plus la prouesse qu'a constituée la génération des PES en seulement quelques semaines. Mes remerciements vont également à Guillaume Blanchon, pour son authenticité et sa bonhomie d'une part, pour son implication dans le calcul des éléments de matrice sphériques et le développement en ondes partielles d'autre part. Merci à Marc Dupuis pour les échanges utiles et ses recommandations pour la soutenance. C'est avec un large sourire que je mentionne enfin mes collègues doctorants. Merci notamment à Baptiste Fraïsse, Paul Carpentier, Luis Gonzalez-Miret Zaragoza et Alexis Francheteau pour avoir indéniablement participé à rendre mes journées plus animées et moins formelles. Baptiste a été un véritable compagnon de route, je ne compte plus tous les midis qu'il a égayés. Paul a été la voix de la sagesse, toujours ouvert aux débats et aux conservations profondes. Son expertise dans l'implémentation des champs HFB m'a par ailleurs épargné bien des souffrances quand il a fallu s'atteler aux forces spin–orbite et tenseur.

J'aimerais plus particulièrement exprimer dans ce paragraphe ma reconnaissance envers mon encadrante de thèse, Nathalie Pillet. Tant sur les plans humain que professionnel, Nathalie s'est révélée exemplaire. De mes toutes premières questions – certainement peu pertinentes – aux conseils finaux pour la mise en forme de ce document et de la soutenance, Nathalie a toujours répondu présent. J'ai énormément appris à ses côtés, des concepts généraux de la physique nucléaire théorique, en passant par l'historique de l'interaction phénoménologique effective de Gogny, jusqu'aux réjouissances des dérivations analytiques et de l'ajustement d'une interaction de Gogny généralisée. Je la remercie de son accompagnement, de sa patience et de son investissement au quotidien.

Je tiens également à mentionner Stéphane Hilaire et Jean-Paul Ebran, chefs successifs du laboratoire, et Cyril de Saint Jean, chef du service, qui m'ont offert la possibilité de réaliser ma thèse dans les meilleures conditions. J'ai aussi une pensée pour Patricia Brusnel et Fabienne Grenault-Tcholakian, tour à tour secrétaires du service, dont l'aide avec les procédures logistiques et administratives m'a été précieuse.

Je voudrais maintenant avoir quelques mots pour mes collaborateurs et collaboratrices

d'autres laboratoires. Je remercie d'abord Guillaume Hupin (IJCLab, Orsay) pour ses idées dans la dérivation des éléments de matrice sphériques, et ses accueils répétés à Orsay. Rémi Bernard (CEA, Cadarache), tant par son travail préliminaire dans le code d'ajustement que par nos nombreuses discussions, m'a beaucoup accompagné dans ce travail de longue haleine. J'ai également été très bien accueilli durant ma semaine de venue à Cadarache, et je l'en remercie sincèrement. I also wanted to name Marta Anguiano (Universidad de Granada, Spain). I was welcomed with great kindness and consideration in her team. Marta always made her available to discuss, exchange results and help me in general, all with a smile. It goes without saying that if I had chosen to continue in research, I would have definitely asked to do a post-doc with her. I thank her again for everything. Je suis de même redevable à Frédéric Chappert qui est parvenu à se remémorer de lointains souvenirs pour m'aider à mettre au clair certaines curiosités du code d'ajustement. Qu'il en soit ici grandement remercié. Je terminerais en évoquant Marcella Grasso (IJCLab, Orsay), qui a gentiment accepté d'endosser le rôle de directrice de thèse.

I would like to thank all the members of the jury, Denis Lacroix, Karim Bennaceur, Luís Robledo, Micaela Oertel and Peter Ring, for their relevant questions and comments during the defense. It was a real pleasure for me to present my long-term work, and to feel such interest in it.

Dans un dernier temps, il me tenait à cœur de mentionner les proches qui m'ont accompagné et soutenu tout au long de ce cycle universitaire qui prend fin. Je pense d'abord à Pierre-Alexandre. Nos nombreuses discussions n'ont fait qu'accentuer mon goût et ma fascination pour la physique, cependant que les éclats de rire demeurent inoubliables. Yasmin a également été une superbe complice, au sourire et à la bonne humeur permanents. Je les remercie tous deux pour ces belles années de partage et d'entraide. Quant à Jimmy, Mathias et Alexandre, ils ont été des amis dévoués. Je ne les remercierais jamais assez de leur présence dans les périodes de doute, lorsque le lâcher-prise s'imposait. J'ai également une forte pensée pour Emma ; je n'oublierai pas son ouverture d'esprit et la délicatesse dont elle a su faire preuve pour me permettre de mener à bien mes projets.

Enfin, je tiens à exprimer ma gratitude la plus pure et la plus profonde envers celle qui s'est toujours montrée présente, ma mère. Sa bienveillance, sa ténacité et son amour m'ont portés, tant dans mon évolution professionnelle qu'en tant qu'individu. Son soutien, sa sensibilité et son amour se retrouvent assurément dans les fondations des recherches que je présente aujourd'hui. Pour ces raisons, et pour toutes les autres, je lui dédie l'intégralité de ce travail de thèse.

Par-dessus l'horizon aux collines brunies,
Le soleil, cette fleur des splendeurs infinies,
Se penchait sur la terre à l'heure du couchant ;
Une humble marguerite, éclose au bord d'un champ,
Sur un mur gris, croulant parmi l'avoine folle,
Blanche, épanouissait sa candide auréole ;
Et la petite fleur, par-dessus le vieux mur,
Regardait fixement, dans l'éternel azur,
Le grand astre épanchant sa lumière immortelle.
« Et, moi, j'ai des rayons aussi ! » lui disait-elle.

— Victor Hugo, « Unité », *Les Contemplations*

Table of contents

Preamble

We would like to take this opportunity to justify some of the choices we have made in shaping the presentation that follows. Generally speaking, this document is intended, in the manner of the Hartree–Fock–Bogoliubov (HFB) theory, to be self-consistent. By this we mean that it is not overly dependent on external references. There are many reasons for this. The main ones are given below.

Firstly, we hope to be able to guide the neophyte reader who is discovering the Gogny interaction, from a report in the image of what the writer would have liked to find when tackling the subject. Secondly, to gather and disseminate a wealth of information, both published and unpublished, in a single place, and thus provide efficiency. Finally, as we are introducing a so-called "generalized" interaction, it was the right moment to set out the work that made such ambition possible, with a minimum of detail to understand the overall terminology. The first chapter and the lengthy appendices are designed for that matter.

In Chapter I, the symmetries of a realistic two-body interaction are given, as some will be used to deduce symmetries related to HFB fields, at the heart of the derivations carried out to test the generalized Gogny interaction. Similarly, we felt that the reminders about the fitting procedures and the main properties of D1 and D2 analytical expressions, on which our interaction is based, were relevant. Nor was it possible to incorporate a tensor force into the Gogny interaction without mentioning previous attempts.

The appendices supply all the equations for building up the generalized Gogny interaction (Appendix B), as well as analyzing its features in infinite nuclear matter (Appendix A) and at the HFB approximation (Appendix C). Appendix D eventually lists all the formulas and conventions employed, along with some useful considerations. Unless explicitly mentioned, it is not mandatory to consult them to understand the outcomes exposed in the chapters.

Introduction

The nuclear interaction, which depicts the force acting between nucleons (protons and neutrons) within the atomic nucleus, is a key concept as it ensures the cohesion of matter on a microscopic scale. A theoretical formulation, derived from the strong force, one of Nature's four fundamental interactions significantly operating at the smallest distances, should be conceivable. Despite the efforts of physicists since its advent in the 1960s [1, 2], such an undertaking remains perilous, not least because of the non-perturbative aspect of the strong force in the energy range adapted to the nuclear interaction. Usually, the general form of the *realistic* nuclear interaction is constrained from fundamental symmetries, some of which are shared with the strong force [3]. The large number of nucleons making up the nucleus, up to more than three hundred, constitutes another challenge [4]. On the one hand, this implies knowledge of all kinds of interaction, involving two, three or more particles. On the other hand, the description of a system composed of many interacting particles – be it between two, three or more bodies –, referred to as the *many-body problem*, admits no general solution so far.

Several frameworks, based on various levels of approximation, tackle the issue. The ones retained in the following are the so-called *microscopic self-consistent mean-field* approaches [5, 6]. Often founded on a variational principle, they allow a systematic treatment down to the heaviest nuclei, from the main assumption that nucleons are moving independently of each other, in a potential created by all their neighbors, called the *mean field*. Additional long-range correlations are subsequently incorporated step by step through increasingly sophisticated self-consistent mean-field theories. The price to be paid to benefit from these is to abandon the authentic realistic nuclear interaction in favor of a renormalized *effective* interaction, which in essence takes short-range correlations into account [7]. Effective interactions depend on parameters which are drawn from models or directly from experiment, and determined within a fitting procedure. In parallel with relativistic models constructed upon quantum field theories [8, 9], two *non-relativistic* effective interactions were widely developed as early as the end of the 1960s, the Skyrme [10, 11] and Gogny [12, 13] interactions. In their modern expressions, they are comparable in that they account for *two-body* interactions, and *phenomenologically* simulate the correlations generated by higher-body interactions in their density dependence. Conversely, they differ intrinsically in that the Skyrme interaction is of *zero range*, while the Gogny interaction presents *finite-range* central terms. To summarize, the Gogny interaction can then be distinguished by the fact that is it a microscopic but non-relativistic, effective and phenomenological two-body nuclear interaction of finite range.

Although raising analytical and, above all, numerical difficulties for that period, the original Gogny interaction D1 soon became a reference, partly due to its ability to treat the nuclear interaction and the pairing correlations on an equal footing [14]. Moreover, its finite-range nature allowing to avoid the appearance of ultraviolet divergences, and therefore the introduction of cut-offs, as is done with the Skyrme interaction, aroused

interest. Numerous improvements to the original interaction have since been carried out. They take two directions:

(i) The search for a new set of parameters of the original analytical expression;

(ii) The extension of the original analytical expression.

In both cases, extra data associated with the physics to be reproduced must be added in order to adequately deduce the parameters. However, the second option is by far the most ambitious, since it also requires the new analytical terms to be derived and implemented in the fitting and mean-field or beyond mean-field codes. For these reasons, the first option is most of the time preferred. An example of a well-known parametrization (set of parameters) of the original analytical expression still used nowadays is the D1S interaction [15]. It was introduced in 1991 by Berger *et al.* to enhance the description of pairing correlations and lower the fission barrier heights in actinides, which were both too important within mean-field calculations performed with interaction D1 [16]. Obviously, the applications do not stop here, the aim being to probe as many physical phenomena as possible by fitting a limited number of quantities. On the other side, one analytical extension consisting in supplying a finite range to the density-dependent term was elaborated by Chappert in 2006, leading to a parametrization named D2 [17, 18]. Initially built up to correct the binding energies in neutron-rich exotic nuclei underestimated by interaction D1S, it turned out to bring the fission barriers further down, still a bit high with the latter. In spite of these successive refinements, second fission barriers remain high compared to experimental values in some actinides. Besides, when going beyond the mean field, it appears that D1S [19] and D2 [20] interactions fail in reproducing the first excitation energies of a few light nuclei, certain representatives of Si and S isotopic chains being examples.

The tensor force was first introduced in the early 1940s, that is shortly after the birth of nuclear physics. It proved to be of paramount importance to describe both the binding and the electric quadrupole moment of the most rudimentary nuclear system, the deuteron [21, 22]. The tensor force was accordingly systematically incorporated in realistic interactions [23–27].

Nevertheless, the tensor force was dropped for many years in effective interactions, and only quite recently has it enjoyed a revival. It is still rather uncommon, but is drawing more and more attention. The justification lies in the fact that the tensor force is now known to produce effects on a wealth of physical quantities, like binding energies [28, 29], single-particle energies [30–32], giant resonances [33, 34], Gamow–Teller states [35–37] and deformations of low- to heavy-mass nuclei [38–40]. Its action even extends to exotic nuclei far from the stability valley [41] and super-heavy elements [42, 43]. It then becomes delicate to finely describe these quantities without tensor dependence.

The first inclusion of a *zero-range* tensor force in a Skyrme interaction dates back to the 1970s and was done by Stancu *et al.* [44] on top of the parametrization SIII [45]. Afterwards, other attempts were made, either on top on other existing parametrizations [46–50], or by carrying out a global refit of the parameters [51]. *Finite-range* tensor terms are even scarcer. In M3Y interactions [52], two tensor terms with Yukawa form factors are considered, but were only lately applied to mean-field theories, in particular thanks to the work of Nakada [53–56]. In the study of Onishi and Negele [57], a tensor force of Gaussian form factor was added in place of the density-dependent term in a Gogny-type interaction. The first real addition of a tensor force to the original analytical form of the Gogny interaction, though, was performed by Otsuka *et al.* [58], but was not pursued. Other

interactions with tensor terms integrated on top of the D1S parametrization [29, 59, 60] (D1ST2a being an example) or by fitting the tensor and spin–orbit forces together [61] were set up by Anguiano *et al.*

In a recent study [39], a comparison of the fission barriers obtained with D1S and D1ST2a in Th isotopes showed that their heights were modified in a sensitive manner by the tensor force. On the other hand, Otsuka [30] proposed a picture to explain quantitatively how the single-particle energies are shifted by the tensor force. It turns out that in this vision, the tensor force is expected to strongly impact the single-particle spectra of several spin–unsaturated nuclei, like some Si and S isotopes.

The purpose of the present work is to make the connection between the results of the previous paragraph and the limitations exhibited by D1S and D2 interactions. In other words, to expand the analytical expression of the Gogny interaction, starting from D2, to a finite-range tensor term first, in order to amend the reproduction of fission barrier heights at the mean field level, and first excitation energies beyond the mean field. We shall in fact provide a finite range to the spin–orbit force as well, to propose a *fully finite-range* interaction, entirely free from divergences when dealing with Hartree–Fock–Bogoliubov and beyond mean-field calculations. Needless to say, we wish to preserve at the same time the good properties characterizing the former interactions D1S and D2. It should be emphasized that we consider a *long-range* tensor force and a *small-range* spin–orbit force. Actually, it is known that a density-dependent term can mimic the effects of a tensor force [62, 63]. Since the density-dependent term of D2 possesses a relatively small range, we avoid double counting by allocating a long range to the tensor force, in agreement with the one-pion-exchange potential of one-boson-exchange models. As for the spin–orbit force, a small range ensures not to deviate too much from the zero-range term of the original Gogny interaction, while its dominant contribution in one-boson-exchange potentials is also of small range. The new interaction is dubbed as the "generalized Gogny interaction", in the sense that most of the previous Gogny interactions can be recovered from its analytical form. The corresponding parametrization adopted in the following will bear the name "DG". Speaking of the fitting code, we should point out that the parameters related to the newly introduced terms, as well as the old ones, will be determined together, to guarantee *overall consistency* of the interaction. As the different terms influence each other, in particular the spin–orbit and tensor ones, a separate fit of these might indeed display certain limitations. Right from the start, the Gogny interaction was designed to furnish faithful results not at the level of the mean field, but *beyond* it. Consequently, a perfect reproduction of mean-field quantities is not desired; on the contrary, room must be left for beyond mean-field correlations. We shall combine this philosophy with that of constraining matrix elements to control, for the first time, the *proton–neutron* component of the pairing. It should enable to drive the parameters so as to make the predictions better, especially beyond the mean field, where the proton–neutron pairing comes into play in *our* calculations.

The document is divided into four chapters and four appendices. In Chapter I, the place of the Gogny interaction among its counterparts is taken up and discussed in details. Its multiple parametrizations will be presented, with an emphasis on the fitting protocols including tensor forces. Finally, the D1S and D2 fitting procedures will be dissected in order to clarify the parts the parametrization DG depends on. In Chapter II, the generalized Gogny interaction is constructed. Its analytical expression is given and the fitting process explained. Some properties in infinite nuclear matter are also exposed and

compared to other Gogny interactions. Chapters III and IV are dedicated to the results in finite nuclei, at the mean-field level, through the Hartree–Fock–Bogoliubov approach and beyond it, through the mutiparticle–multihole configuration mixing method, respectively. Mean-field outcomes show the bulk and pairing properties of interaction DG, as well as its implications on deformations and fission barrier heights. Beyond mean-field results are focused on the first excitation energies of even–even, odd and odd–odd nuclei, in relation with the shell evolution. All calculations needed to produce the outputs from Chapters I to III can be found in Appendices A, B, C and D.

Chapter I

The Gogny interaction

> « Pour avoir du génie, faut être mort. Pour avoir du talent, faut être vieux, et quand on est jeune, on est des cons. »
>
> — Coluche

In this chapter, we begin by situating the Gogny interaction within the general landscape of nuclear interactions, motivating its analytical expression, its specificities as well as the theoretical framework in which it operates. We focus thereafter on the evolution of its parametrizations and analytical forms over time, introducing the various interactions that will appear throughout the presentation. Specifically, we highlight the foundations of the fitting procedure and certain germane properties of the former interactions that will be taken up and extended to construct the generalized Gogny interaction.

Chapter contents

1. The Gogny interaction in the landscape of nuclear interactions

1.1. The realistic nuclear interaction

The *nuclear force* is the interaction between the nucleons (protons and neutrons) of the atomic nuclei, which ensures their cohesion. Without the nuclear interaction, the nuclei would remain unstable and the Universe as we experience it could just not exist. We empirically know, since the 1930s, that the nuclear force is composed of an attractive part at medium and long ranges, and of a very strong repulsive part at short range, called the *hard-core repulsion*. It is difficult to accurately separate the attractive from the repulsive regions of the nuclear interaction between two nucleons since it depends not only on their relative distance $r \equiv |\vec{r}_1 - \vec{r}_2|$ (where $\vec{r}_1$ and $\vec{r}_2$ are the nucleon locations), but also on their velocities, their spins and, sometimes, on whether they are protons or neutrons (see subsection I.1.2). However, it is agreed that around $r \lesssim 0.7\,\text{fm}$, the hard-core repulsion dominates while beyond, the attractive character of the nuclear force prevails, with an exponential decline that practically vanishes at about $r \sim 3\,\text{fm}$ (see Figure I.1). Protons being electrically charged (unlike neutrons), the nuclear force competes with the Coulomb interaction when both nucleons are protons. At $r \sim 1\,\text{fm}$, the nuclear interaction is about a hundred times stronger than the Coulomb force, that can then be neglected. Nevertheless, because it decreases only as the inverse of the proton distance, it becomes predominant from $r \sim 4\,\text{fm}$, and then cannot be disregarded, as shown in the inset of Figure I.1. As for the weak force, it does not take part in the dynamics of nucleons as it is not intense enough, but it is at the origin of the decay of protons into neutrons, and vice versa.

As early as 1935, Yukawa [64] attempted to describe this singular force by assuming that nucleons were exchanging particles that would mediate the nuclear interaction, in analogy with the electromagnetic force which was, from a quantum mechanical point of view, already understood as originating from exchanges of photons. These force-mediating particles were latter referred to as *mesons* and the pion predicted by Yukawa, was observed for the first time in cosmic rays in 1947. Yukawa was awarded the Nobel Prize of Physics for his discovery in 1949. From there, many theories based on the exchange of various mesons were born and proved to be very fruitful.

In 1964, Gell-Mann [1] and Zweig [2] independently postulated that hadrons, of which nucleons and mesons are the representatives, were not elementary particles, but were composed of more fundamental objects called *quarks*. In 1968, the SLAC's scattering experiments revealed the existence of quarks [65]. Actually the identity of the observed particles was not clearly established at that time, but it was at least indubitable that the proton was formed of smaller constituents. Since mesons were no longer seen as elementary particles, it was necessary to relegate meson theories to the level of models and to try to explain the origin of the nuclear force through the interaction between quarks. The description of the interaction between quarks, mediated by gluons, is rooted in the formalism of quantum chromodynamics (QCD), formulated during the 1970s [66, 67]. This force, called the *strong interaction*, is one of the four fundamental interactions of Nature. The strong force acts attractively or repulsively depending on the color charge associated with the interacting quarks – in the same way that the electromagnetic force depends on the electric charge associated with the interacting bodies –, and has the particularity to be more intense as the distance between quarks increases [68]. More precisely, the strong interaction is marked by two extreme behaviors. At large distances (or, equivalently, at

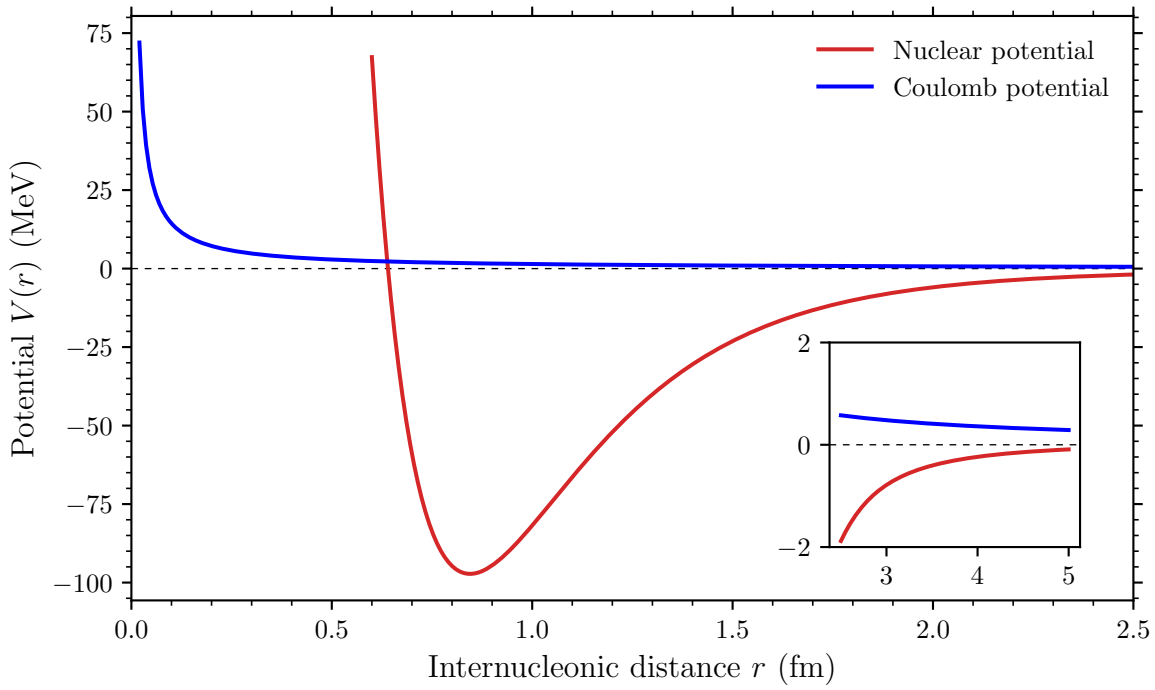

Figure I.1 – Competition between nuclear and Coulomb potentials inside the nucleus. Potentials are represented as functions of the distance between two nucleons (or two protons, in the case of the Coulomb potential). The inset magnifies their behaviors at large distances.

low-energy transfers), the force is so strong that it prevents the existence of free quarks, in a phenomenon called *color confinement* [69]. At small distances (or, equivalently, at high-energy transfers), the force becomes weaker so that quarks behave like nearly unbound particles. As the interaction vanishes at asymptotically high energies, this phenomenon is called *asymptotic freedom* [70]. This last feature of the strong interaction was discovered by Gross and Wilczek [71], and independently by Politzer [72] in 1973. They shared the Nobel Prize of Physics in 2004.

Nucleons are made out of three quarks (two up quarks and one down quark for protons, one up quark and two down quarks for neutrons), which makes them color-neutral particles. Then, to first order, two nucleons are expected not to interact with one another through the strong force. This is indeed what is observed since at large distances ($r > 2.5$ fm), their interaction is almost zero. Nevertheless, this result is not exact (probably due to internal processes in the nucleons) since an interaction remains at smaller distances ($r < 2.5$ fm). For this reason, the nuclear interaction is dubbed the *residual strong force*. Once again, the situation is analogous to electromagnetism as two electrically neutral atoms still feel a residual electromagnetic force through the van der Waals interaction.

In theory, we should then be able to derive an expression for the nuclear interaction from the QCD equations. In practice, two pathological issues arise [73]:

(i) the region in which the strong interaction is particularly intense corresponds to the low-energy regime of nuclear physics;

(ii) nucleons are composite particles constituted of three quarks, so that the interaction between two nucleons actually consists in a six-quark problem.

As it is harsh to solve the QCD equations, physicists often resort to perturbative methods to obtain approximate mathematical solutions. However, to be applied, perturbative methods require the interaction to be weak enough. In the high-energy regime of particle physics, QCD is perturbative as the strong interaction is sufficiently weak, but in the low-energy regime of nuclear physics, QCD turns out to be highly non-perturbative as the strong interaction is a way too intense.

Nowadays, mainly two approaches are developed to deal with these issues. The first one tries to tackle the six-quark problem using computational power. The system is embedded in a four-dimensional discretized lattice on which QCD equations are applied. This is the so-called *lattice quantum chromodynamics* (LQCD) [74]. In 2007, Ishii and collaborators demonstrated, based on LQCD numerical results, that the hard-core repulsion is also a consequence of the strong force [75]. This was a genuine breakthrough as the hard-core repulsion, which is known to be essential to the structure of matter as we know it, escaped a reliable theoretical interpretation so far. It must be emphasized that LQCD necessitates such computational capacities that it cannot be considered a standard technique for nuclear physics.

Standard techniques which seek a relation between low-energy QCD and the nuclear interaction are known as nuclear *effective field theories* (EFTs) [76]. In a broad sense, EFTs are based on a separation between the typical length scale (or energy scale) of the physical phenomena one wants to describe and the typical length scale of the underlying dynamics, which is expressly ignored. The more remarkable this separation, the more effective are the EFT. Specifically, EFTs were extended to low-energy QCD in the 1990s, after the pioneering work of Weinberg [77, 78]. Nuclear EFTs provide a low-energy depiction of QCD in terms of hadrons, instead of quarks and gluons. All nuclear EFTs are constructed in a way that follows a certain scheme. First, typical length scales and relevant degrees of freedom for nuclear physics are identified. Then, appropriate symmetries of low-energy QCD are listed and attention is paid on whether some are broken, to build up the most general Lagrangian consistent with those symmetries and symmetry breakings. Finally, as effective Lagrangians exhibit an infinite number of terms, one has to target the most important contributions to restrict the study to their associated Feynman diagrams. The first and surely the most widespread nuclear EFT is the *chiral EFT* (χEFT) [79]. We use it as an example to briefly describe the mentioned steps. Chiral symmetry imposes, to any massless particle, the existence of a "chiral partner", i.e. another massless particle with opposite parity. Since the nucleons are made of quarks which are nearly massless, an *approximate* chiral symmetry should then manifest. If this symmetry held, we would observe in particular mesons having approximately the same mass, with different parities – since they are themselves composed of the same number of quarks. As it is not the case, we usually state that the (approximate) chiral symmetry is spontaneously broken. According to Goldstone's theorem, this spontaneously symmetry breaking brings out a particle, called the Goldstone boson, which here appears to be the pion. Thus, the pion becomes the main mediator of the nuclear interaction. We can choose its mass to be the typical energy scale $\Lambda_\pi \sim m_\pi \simeq 140\,\mathrm{MeV}$ of the phenomena we wish to describe and the chiral-symmetry breaking energy scale $\Lambda_\chi \sim 1\,\mathrm{GeV}$ as the limit beyond which the phenomena are not reachable by the theory. The last step, allowed by *chiral perturbation theory* (ChPT) [80], is crucial since it permits, by taking back pertubative methods to χEFT, to probe nuclear phenomena in a controlled manner, with the desired degree of accuracy. By accounting for the ever increasing orders of the perturbative expansion, the knowledge of the nuclear interaction is systematically refined, and, besides, in a fundamental way.

Another tactic is simply to drop the quest for a fundamental description of the nuclear interaction from the strong force, attempting to describe it in roundabout ways. We will notably discuss such approaches in the following since this is the path we take in this thesis.

1.2. Expression of the realistic two-body nuclear interaction

Although it is not yet possible to extract a general expression of the nuclear interaction from the more fundamental QCD, we can constrain its analytical expression by imposing some symmetries to be preserved [3, 4, 7]. Some symmetries are quite general whereas others directly stem from QCD, which we shall point out. We highlight that the interaction we want to construct is the *realistic* (or *bare*) nuclear interaction (by opposition to the *effective* nuclear interaction we will defined later on), i.e. the authentic nuclear interaction we introduced in the previous subsection. To describe microscopically such a nuclear interaction, several hypotheses are postulated:

(i) nucleons are the elementary particles of the theory (their quarkish nature is concealed);

(ii) they are considered point-like particles (their spatial extension is neglected);

(iii) they only interact through the nuclear interaction in *vacuum*;

(iv) the interaction propagates instantaneously as nucleons are assumed to obey a *non-relativistic* dynamics.

In the following, we will specifically focus on the form of the two-body interaction v_{12} between nucleons labelled by 1 and 2, called the *(bare) nucleon–nucleon interaction*. Obviously, a similar study for three- or higher-body nuclear interactions is perfectly feasible, though a bit more sophisticated. The nucleon–nucleon interaction may depend on each of the degrees of freedom associated with the two particles, that are their positions $\vec{r}_1$ and $\vec{r}_2$, their momenta $\vec{p}_1$ and $\vec{p}_2$, their spins $\vec{\sigma}_1$ and $\vec{\sigma}_2$ as well as their isospins $\vec{\tau}_1$ and $\vec{\tau}_2$ [1], i.e.

$$v_{12} \equiv v(\vec{r}_1, \vec{p}_1, \vec{\sigma}_1, \vec{\tau}_1; \vec{r}_2, \vec{p}_2, \vec{\sigma}_2, \vec{\tau}_2). \tag{I.1}$$

We start by enumerating all the symmetries we want the two-body realistic nuclear interaction to satisfy:

1. **Symmetry under the exchange of two nucleons**
   This symmetry traduces the fact that the interaction between particle 1 and particle 2 is the same as the interaction between particle 2 and particle 1, i.e. $v_{12} = v_{21}$, or

$$v(\vec{r}_1, \vec{p}_1, \vec{\sigma}_1, \vec{\tau}_1; \vec{r}_2, \vec{p}_2, \vec{\sigma}_2, \vec{\tau}_2) = v(\vec{r}_2, \vec{p}_2, \vec{\sigma}_2, \vec{\tau}_2; \vec{r}_1, \vec{p}_1, \vec{\sigma}_1, \vec{\tau}_1). \tag{I.2}$$

2. **Translational symmetry**
   This symmetry ensures that the interaction between two nucleons does not depend on their absolute position in space, it is the same everywhere in vacuum. If we translate the two particles by an amount $\vec{a}$, positions become $\vec{r}_i' = \vec{r}_i + \vec{a}$ (with $i \in \{1, 2\}$), and the interaction must remain unchanged,

$$v(\vec{r}_1', \vec{p}_1, \vec{\sigma}_1, \vec{\tau}_1; \vec{r}_2', \vec{p}_2, \vec{\sigma}_2, \vec{\tau}_2) = v(\vec{r}_1, \vec{p}_1, \vec{\sigma}_1, \vec{\tau}_1; \vec{r}_2, \vec{p}_2, \vec{\sigma}_2, \vec{\tau}_2), \tag{I.3}$$

1. In fact, those quantities are the Pauli matrices associated with the spin and isospin operators (see relations (D.6) and (D.7)).

for any vector $\vec{a}$. In other words, the interaction does not depend on the center-of-mass position $\vec{R} \equiv (\vec{r}_1 + \vec{r}_2)/2$, but only on the relative position $\vec{r} \equiv \vec{r}_1 - \vec{r}_2$ of the two particles, that is to say

$$v_{12} = v(\vec{r}; \vec{p}_1, \vec{\sigma}_1, \vec{\tau}_1; \vec{p}_2, \vec{\sigma}_2, \vec{\tau}_2). \tag{I.4}$$

3. Symmetry under Galilean transformations

A Galilean transformation consists in providing a constant velocity $\vec{v}_\mathrm{G}$ to the system. Under such transformation, the momenta of the two nucleons become $\vec{p}_i' = \vec{p}_i + m\vec{v}_\mathrm{G}$ (with $i \in \{1, 2\}$), where m is their mass. Imposing the Galilean invariance of the interaction, that is to say

$$v(\vec{r}; \vec{p}_1', \vec{\sigma}_1, \vec{\tau}_1; \vec{p}_2', \vec{\sigma}_2, \vec{\tau}_2) = v(\vec{r}; \vec{p}_1, \vec{\sigma}_1, \vec{\tau}_1; \vec{p}_2, \vec{\sigma}_2, \vec{\tau}_2), \tag{I.5}$$

simply amounts to demanding the principle of inertia to hold for the interaction. Namely, the physics of the interaction is the same regardless of the frame in rectilinear and uniform motion (with respect to a certain fixed frame) from which it is studied. Therefore, the interaction does not depend of the center-of-mass momentum $\vec{P} \equiv \vec{p}_1 + \vec{p}_2$, but only on the relative momentum $\vec{p} \equiv (\vec{p}_1 - \vec{p}_2)/2$ between the two particles, i.e.

$$v_{12} = v(\vec{r}, \vec{p}; \vec{\sigma}_1, \vec{\tau}_1; \vec{\sigma}_2, \vec{\tau}_2). \tag{I.6}$$

4. Full rotational symmetry

This symmetry guarantees that the interaction between the two nucleons does not depend of their absolute orientation in (coordinate plus spin) space. Indeed, if we rotate the two particles by an amount $\mathcal{R}$, the positions and momenta become $\vec{r}' = \mathcal{R}\vec{r}$ and $\vec{p}' = \mathcal{R}\vec{p}$, but the spins are also impacted and turn into $\vec{\sigma}_i' = \mathcal{R}\vec{\sigma}_i$ (with $i \in \{1, 2\}$). This is what we mean by "full" rotation, to be distinguished from separate rotation in coordinate and spin spaces.[2] The interaction must remain unchanged under those transformations, i.e.

$$v(\vec{r}', \vec{p}'; \vec{\sigma}_1', \vec{\tau}_1; \vec{\sigma}_2', \vec{\tau}_2) = v(\vec{r}, \vec{p}; \vec{\sigma}_1, \vec{\tau}_1; \vec{\sigma}_2, \vec{\tau}_2), \tag{I.7}$$

for any matrix $\mathcal{R}$. From a quantum mechanical point of view, this means that the two-body nuclear interaction commutes with the total momentum $\vec{J} \equiv \vec{L} + \vec{S}$, i.e. $[v_{12}, \vec{J}] = 0$. For this to be true, the interaction must be a scalar (in coordinate plus spin space), as rotations do not modify scalar quantities. The full rotational symmetry also implies that the two-body matrix elements of the interaction are diagonal in the quantum numbers J and M_J, and independent of M_J (see subsection B.2.1).

5. Parity (or space reflection) symmetry

As the strong interaction, from which the nuclear interaction should be obtained, is invariant under parity transformations, we expect the nuclear interaction itself to conserve that symmetry. Space reflection, as its name suggests, turns the interaction into its mirror image. In this process, the spatial degrees of freedom are reversed, $\vec{r}' = -\vec{r}$ and $\vec{p}' = -\vec{p}$, while the spins, as pseudovectors, are not modified. Then, the interaction is symmetric under parity transformations if it satisfies

$$v(-\vec{r}, -\vec{p}; \vec{\sigma}_1, \vec{\tau}_1; \vec{\sigma}_2, \vec{\tau}_2) = v(\vec{r}, \vec{p}; \vec{\sigma}_1, \vec{\tau}_1; \vec{\sigma}_2, \vec{\tau}_2). \tag{I.8}$$

2. The distinction is crucial here as the non-central components of the two-body nuclear interaction are invariant under full rotations, as the interaction must be, but not under separate coordinate and spin rotations (see section D.6 for more details).

6. Time-reversal symmetry

Once again, the strong interaction is time-reversal invariant so that we expect the nuclear interaction to respect the time-reversal symmetry itself. Physically, this requirement ensures that the equations of motion do not depend on the direction of the arrow of time. Under a time-reversal transformation, only the momenta and spins are flipped, i.e. $\vec{p}' = -\vec{p}$ and $\vec{\sigma}_i' = -\vec{\sigma}_i$ (with $i \in \{1, 2\}$). Then, time-reversal invariance of the interaction imposes

$$v(\vec{r}, -\vec{p}; -\vec{\sigma}_1, \vec{\tau}_1; -\vec{\sigma}_2, \vec{\tau}_2) = v^*(\vec{r}, \vec{p}; \vec{\sigma}_1, \vec{\tau}_1; \vec{\sigma}_2, \vec{\tau}_2). \tag{I.9}$$

It is important to note that the time-reversal operator involves the complex conjugation, which explains the appearance of the complex conjugate of the interaction in the above relation.

7. Hermiticity

The necessity for the two-body nuclear interaction to be Hermitian is essential since it implies that the associated Hamiltonian is diagonalizable and that its eigenvalues are real. This physical requisite formally reads

$$v_{12}^\dagger = v_{12}. \tag{I.10}$$

8. Charge independence

Charge independence assumes that the interaction between two neutrons has the same strength as the interaction between two protons, as well as the interaction between a neutron and a proton. [3] This is based on the observation that neutrons and protons have practically the same mass. Mathematically speaking, they can be represented as two components of the same state describing an elementary particle (the nucleon) of isospin 1/2, in some abstract space called isospin space. By analogy with the spin formalism, we can picture charge independence as equivalent to a nuclear interaction invariant under any rotation in isospin space. If we rotate the two particles by an amount $\mathcal{R}$ in the isospin space, the isospins become $\vec{\tau}_i' = \vec{\tau}_i$ (with $i \in \{1, 2\}$), and the interaction must remain the same,

$$v(\vec{r}, \vec{p}; \vec{\sigma}_1, \vec{\tau}_1'; \vec{\sigma}_2, \vec{\tau}_2') = v(\vec{r}, \vec{p}; \vec{\sigma}_1, \vec{\tau}_1; \vec{\sigma}_2, \vec{\tau}_2), \tag{I.11}$$

for any matrix $\mathcal{R}$. This means that the two-body nuclear interaction commutes with the total isospin $\vec{T}$, i.e. $[v_{12}, \vec{T}] = 0$. For this to be true, the interaction must be an isoscalar (a scalar in isospin space). The charge independence also implies that the two-body matrix elements of the interaction are diagonal in the quantum numbers T and M_T, and independent of M_T (see subsection B.2.1). Let us emphasize that this symmetry is not exact, the proton and neutron masses not being strictly the same. [4]

When all these eight symmetries are reproduced, we can infer the general expression of the bare two-body nuclear interaction. So as not to slow down the discussion, we have

3. It is important to underline that this statement only makes sense if the two nucleons have the same quantum numbers. Indeed, in the $T = 1$ channel, the proton–neutron interaction in the *symmetric isospin state* $(|\nu\pi\rangle + |\pi\nu\rangle)/\sqrt{2}$ is the same as the neutron–neutron $|\nu\nu\rangle$ and proton–proton $|\pi\pi\rangle$ interactions. In the $T = 0$ channel, however, the *antisymmetric isospin state* $(|\nu\pi\rangle - |\pi\nu\rangle)/\sqrt{2}$ has no neutron–neutron nor proton–proton equivalents and there is no reason for it to be equal to their contributions in the $T = 1$ channel since they do not share the same quantum number T.

4. The neutron is very slightly heavier than the proton, $m_\pi/m_\nu = 0.998\,623\,478\,12(49)$ [81].

deferred the associated demonstration in Appendix D. This interaction reads

$$v_{12} = v^{00} + v^{10}(\vec{\sigma}_1 \cdot \vec{\sigma}_2) + v^{01}(\vec{\tau}_1 \cdot \vec{\tau}_2) + v^{11}(\vec{\sigma}_1 \cdot \vec{\sigma}_2)(\vec{\tau}_1 \cdot \vec{\tau}_2), \tag{I.12}$$

where

$$v^{ST} \equiv \sum_{k=1}^{5} f_k^{ST}(\vec{r}^2, \vec{p}^2, \vec{L}^2) O_k, \quad \text{for } S, T \in \{0, 1\}, \tag{I.13}$$

which is defined in terms of the so-called *form factors* $f_k^{ST}(\vec{r}^2, \vec{p}^2, \vec{L}^2)$ and the operators O_k, taking one of the following form

$$O_k = \begin{cases} \mathbb{1} & \text{if } k = 1, \\ \vec{L} \cdot \vec{S} & \text{if } k = 2, \\ S_{12}(\hat{r}) \equiv (\vec{\sigma}_1 \cdot \hat{r})(\vec{\sigma}_2 \cdot \hat{r}) - \frac{1}{3}\vec{\sigma}_1 \cdot \vec{\sigma}_2 & \text{if } k = 3, \\ S_{12}(\hat{p}) \equiv (\vec{\sigma}_1 \cdot \hat{p})(\vec{\sigma}_2 \cdot \hat{p}) - \frac{1}{3}\vec{\sigma}_1 \cdot \vec{\sigma}_2 & \text{if } k = 4, \\ Q_{12} \equiv \frac{1}{2}\Big[(\vec{\sigma}_1 \cdot \vec{L})(\vec{\sigma}_2 \cdot \vec{L}) + (\vec{\sigma}_2 \cdot \vec{L})(\vec{\sigma}_1 \cdot \vec{L})\Big] & \text{if } k = 5. \end{cases} \tag{I.14}$$

Several remarks should be made concerning these expressions. The set of equations (I.12)–(I.14) defines the most general realistic two-body nuclear interaction we can construct from the eight symmetries. This does not imply that all operators (I.14) or even all components of the interaction (I.13) must be present in some realistic interaction, they are simply allowed by the symmetries. In the expression of the interaction (I.12), we have decided to make the particular spin dependence $(\vec{\sigma}_1 \cdot \vec{\sigma}_2)$ appear. This choice is conventional and any of the other possible spin dependences could have replaced it, but this one is wise since it enables to divide the interaction into four components (I.13), each acting in a different channel (S, T), where S and T are the spin and isospin in the two-nucleon formalism. Then, everything happens as if there were four independent interactions "living" in their own subspace (S, T). This is a consideration that will often be taken up later when analyzing parametrizations of the Gogny interaction. The various possible operators (I.14) are named, in order of appearance, the unity operator, the spin–orbit term, the tensor terms (in coordinate space, with $\hat{r} \equiv \vec{r}/|\vec{r}|$, and in momentum space, with $\hat{p} \equiv \vec{p}/|\vec{p}|$, respectively), and the quadratic spin–orbit term. The factor $-(\vec{\sigma}_1 \cdot \vec{\sigma}_2)/3$ that has been added to the tensor terms ensures that they are isotropic, i.e. that they vanish when integrated over all directions (see subsection D.4.1 for more details). Let us finally note that, with the specific form (I.12) of the interaction, when one of the last four operators of (I.14) intervenes in the subspace $S = 1$, the dependence in Pauli matrices is at least cubic due to the scalar product $(\vec{\sigma}_1 \cdot \vec{\sigma}_2)$. However, this is not a problem since, as explained earlier, we can always convert this dependence into a combination of independent, linear and quadratic terms in Pauli matrices.

1.3. Many-body problem and effective interactions

Until now, we have only considered the interaction between two nucleons in the vacuum which already posed serious problems. Another challenge is that the atomic nuclei we wish to characterize are most of the time made up of more than two nucleons; in general $2 \leq A \lesssim 300$, where A is the number of nucleons. To faithfully describe nuclei, one must in principle know all two-body, three-body and higher-body interactions (since the presence of extra nucleons disturbs the interaction between its neighbors), but also how to describe a system of many interacting particles. In fact, this is the so-called *nuclear*

A-body (or many-body) problem, for which there currently exists no general solution. This problem goes far beyond nuclear physics and is also encountered in condensed matter physics, quantum chemistry as well as atomic and molecular physics, for example. A noticeable particularity of nuclei, though, is that the addition or removal of a single nucleon can drastically change their internal structure and thus their properties, which further complicates their study [4]. To cope with this complexity, a lot of methods have been developed since the 1950s, which can be classified into two categories: *macroscopic* and *microscopic* approaches.

The liquid drop model (LDM) was the first macroscopic model to emerge [82]. It is based on the observation that, under normal conditions, the nucleus has low compressibility and a well-defined surface. In this model, the binding energies are evaluated by means of the semi-empirical mass formula of Bethe and Weizsäcker [83, 84], expressed in terms of global properties (like volume and surface energies) associated with parameters that are phenomenologically determined. It was historically the first model to properly describe the bulk properties of nuclei. As it failed to reproduce the surface properties, it was soon necessary to supplement the model by microscopic shell corrections, in particular through the work of Strutinsky [85, 86]. This *macroscopic-microscopic* approach, taking into account quantum effects, has proved to be very successful, especially after extensive tunings (notably by the work of Myers and Swiatecki [87]), until reaching a high predictive power. It is still used today in an improved version, the finite-range droplet model (FRDM), which provides good predictions of both nuclear masses and deformations [88, 89].

The starting point of a microscopic theory of the nucleus is the nuclear Hamiltonian which governs the behavior of A interacting nucleons,

$$H = \sum_{i=1}^{A} \frac{p_i^2}{2M} + \sum_{i<j} v_{ij} + \sum_{i<j<k} v_{ijk} + \dots, \tag{I.15}$$

where $p_i^2/2M$ denotes the kinetic energy of the i-th nucleon, M its mass, v_{ij} the two-body interaction between nucleons i and j, v_{ijk} the three-body interaction between nucleons i, j and k, and so forth. Note that the inequalities in the summations prevent multiple counting. Thus, the objective is to either solve the time-independent Schrödinger equation

$$H\Psi(\xi_1, \dots, \xi_A) = \mathcal{E}\Psi(\xi_1, \dots, \xi_A), \tag{I.16}$$

or the time-dependent Schrödinger equation for dynamical processes like fission or nuclear collisions,

$$\mathrm{i}\hbar \frac{\partial \Psi}{\partial t}(\xi_1, \dots, \xi_A, t) = H\Psi(\xi_1, \dots, \xi_A, t), \tag{I.17}$$

where Ψ is the A-body wave function and ξ_i the degrees of freedom of the i-th nuclei, with $i \in \{1, \dots, A\}$. Unfortunately, there is no general method to solve this equation exactly, for any value of A. Nevertheless, several microscopic approaches, based on different levels of approximation, satisfactorily tackle the problem. Among those, three main approaches can be distinguished: *ab initio*, *shell model* and *self-consistent mean-field* theories.

Ab initio methods are the most fundamental of the three approaches as they try to solve the many-body problem using the realistic nuclear interaction [90, 91]. Originally, the terminology "*ab initio*" was dedicated to methods capable of solving exactly the Schrödinger equation. Their application was very restrained, only to nuclei with $A \leq 16$. Nowadays, we designate by *ab initio* all the methods that attempt to solve the Schrödinger equation, even in an approximate way, but still from a realistic interaction. According

to this definition, *ab initio* methods are able to describe a wider spectrum of the nuclear chart. It would be difficult to present extensively *ab initio* methods as they are numerous and varied. Let us simply point out that the current trend is to search for a fully consistent approach, deduced from QCD, which would provide exact nuclear structure calculations. To this end, realistic forces deduced from EFT, and more specifically from χEFT, called *chiral interactions*, are commonly used in *ab initio* approaches. Indeed, they allow a direct connection with the QCD Lagrangian and often simplify calculations while χEFT has the ability to generate many-body forces as all forces are treated on the same footing (it suffices to increase the order of the expansion series to get the higher-body contributions to the interaction). At present, *ab initio* methods can handle nuclei up to $A \simeq 100$ (see Figure I.2).

The shell model was independently developed in the end of the 1940s by physicists Goeppert Mayer [92, 93] and Jensen [94] who shared half of the Nobel Prize of Physics in 1963. In the original model, nucleons are described as independent particles immersed in a three-dimensional harmonic oscillator potential with a spin–orbit component [95, 96]. From there, it was possible to show that the energy levels of the nucleons are organized in shells, composed of subshells, whose energy gap is prominent at certain particular values of the number of protons or neutrons. These numbers, later called the *magic numbers* of nucleons provided great success to the shell model as they were experimentally observed from the binding energies of the nuclei close to magicity [97, 98]. The model was efficient to account for the properties of nuclei close to the stability line, but much less so as one moves away from it. Extension to more sophisticated potentials have then been carried out, of which the famous Woods–Saxon potential [99] is an example. One of the obstacles to the shell model calculations is their dimension, which increases extremely rapidly with the size of the system. To circumvent it, the Hilbert space of nucleons is usually divided into an *inert core* of (a magic number of) spectator nucleons that interact little or not, and a *valence space* composed of a few nucleons driving the properties of the nucleus. Additionally, specific diagonalization schemes (like Monte Carlo [100] or Lanczos methods [101]) are requisitioned to cope with large numerical calculations. The shell model allows to deal with nuclei up to $A \simeq 100$.

Finally, the last approach is that of *self-consistent mean-field* (SCMF) theories, also called *energy density functional* (EDF) approaches [5, 6]. We take some time to outline its philosophy, as it will be considerably solicited in the document. Of the three approaches presented, this is truly the only one that can scan almost the entire nuclide chart, as exemplified with the D1M Gogny interaction [102] in Figure I.2. SCMF theories start from the observation that only the one-body problem is exactly solvable. From there, the nuclear Hamiltonian (I.15) is split up into two parts as [7, 103]

$$H = \underbrace{\sum_{i=1}^{A}\left(\frac{p_i^2}{2m} + U_i\right)}_{H_0} + \underbrace{\sum_{i<j} v_{ij} + \sum_{i<j<k} v_{ijk} + \ldots - \sum_{i=1}^{A} U_i}_{U_{\text{res}}}, \tag{I.18}$$

where H_0 is the exactly solvable one-body Hamiltonian and U_{res} the *residual interaction*. In the vision of SCMF theories, particles are moving independently. Their dynamics is dictated by the Hamiltonian H_0 containing a common potential U_i, called the *mean-field*, created by their surrounding neighbors. This description is obviously not so far from that of the shell model. The residual interaction U_{res} then appears as a correction to this independent particle picture by inducing *(long-range) correlations* in their dynamics. In practice, we try to maximize the part of the interaction between nucleons taken

in the mean-field U_i, to minimize the residual interaction U_{res} we neglect. We do so by including the correlations step by step, that is to say by successively incorporating, in the increasingly sophisticated SCMF approaches, different types of correlations that are known to take place in nuclei. In the following, we will introduce the Hartree–Fock (HF) approximation (see subsection A.1.2), which corresponds to the basic SCMF theory, only effective in dealing with doubly magic nuclei. To describe open-shell nuclei, we will use the Hartee–Fock–Bogoliubov (HFB) approximation (see section III.1), which takes into account *pairing correlations*. Note that there exists *beyond mean-field* approaches like random phase approximation (RPA) which integrates correlations associated with *harmonic oscillations* of the mean-field, or generator coordinate method (GCM), dedicated to *large amplitude motions*, for example. As we will illustrate in the thesis for HF and HFB theories, SCMF methods are almost [5] always constructed in the same manner:

(i) the starting wave functions are chosen to be richer and richer as the different types of correlations are taken into account (Slater determinants and BCS wave functions for HF and HFB approaches, respectively);

(ii) unknown quantities of which the wave functions are composed of are obtained using a *variational principle*; it consists in searching for these quantities that minimize the total energy of the nucleus;

(iii) primal equations are eventually obtained and give both the ground state and the excited states of the nucleus.

When one naively employs realistic interactions in HF theory, one ends up with a mean-field having extremely large or even infinite values. Such physically unacceptable result originates in the hard-core repulsion of bare potentials. At normal density, the nucleons remain on average quite far from each other, as a consequence of the Pauli principle. Each nucleon does not often have the opportunity to get close enough to its neighbors to feel the very repulsive core of the nuclear interaction. However, it cannot be excluded that sometimes two nucleons are momentarily at distances involving the hard-core repulsion. In this case, they scatter violently on each other, which induces perturbations referred to as *short-range correlations*. Although quite scarce, these events must be taken into account as their intensity has a strong impact on the behavior of nuclei. Several attempts to take these correlations into account appeared in the 1950s. One of the most widespread is that of Brueckner [104]. Assuming short-range correlations to involve only two nucleons at a time, Brueckner proposed a model consisting in renormalizing the realistic interaction into an *effective* interaction, without a repulsive core, but integrating in essence the effects of short-range correlations. The effective interaction is more elaborated because it depends on the states of the nucleons in the neighborhood, in particular through their energies and the *density of the medium*. Unlike bare interactions acting in vacuum, effective interactions take place in the nuclear medium. Thus, the HF theory becomes applicable provided that an effective interaction is used instead of a realistic one. It is the Brueckner–Hartree–Fock (BHF) theory which justifies the HF approximation in nuclear physics. Since the BHF theory is hard to set up in finite nuclei, especially for heavy and deformed nuclei, its applications were mostly restricted to infinite nuclear matter.

This led physicists to construct *parametrizations* of nuclear effective interactions, i.e. nuclear effective interactions depending on free parameters which are determined:

(i) from theoretical results obtained in Brueckner theory;

5. A notable exception is RPA, which does not use a variational principle to determine the states of the nucleus.

(ii) by adjusting them in order to reproduce key quantities of infinite nuclear matter (saturation point, incompressibility, etc.);

(iii) in a *phenomenological* way, that is to say, by fitting them on experimental data of various types, to be able to describe as many nuclei as possible.

Most of them also retain the explicit density dependence of the medium which is essential in reproducing the standard properties of nuclei, like saturation, but abandon the energy dependence which turns out to be less important. At this point, two schools of thought coexist: those who believe that the effective interaction must retain some signatures of the bare interaction, and those who do not. The former suggest that the interaction is reasonably renormalized by the medium effects, so that the bare interaction can still serve as a guideline. The general expression of the effective interaction is then conducted by the available operators O_k of the bare interactions (see previous subsection), and chosen relatively simple to avoid too expensive calculation times (especially in the 1970s). The latter claim that the various contributions are strongly mixed up when parameters are fitted on experimental data. As a consequence, the choice of these parameters can only be dictated by the desire to reproduce specific observations with the highest accuracy. We also notice that this phenomenological aspect of effective interactions allows, through experimental data, to restore the physical effects (spatial extension, relativistic motion, etc.) which had been put aside for realistic interactions, by the initial assumptions listed in the previous subsection. The two main phenomenological effective interactions that have been widely used and improved since are the so-called Skyrme and Gogny interactions.

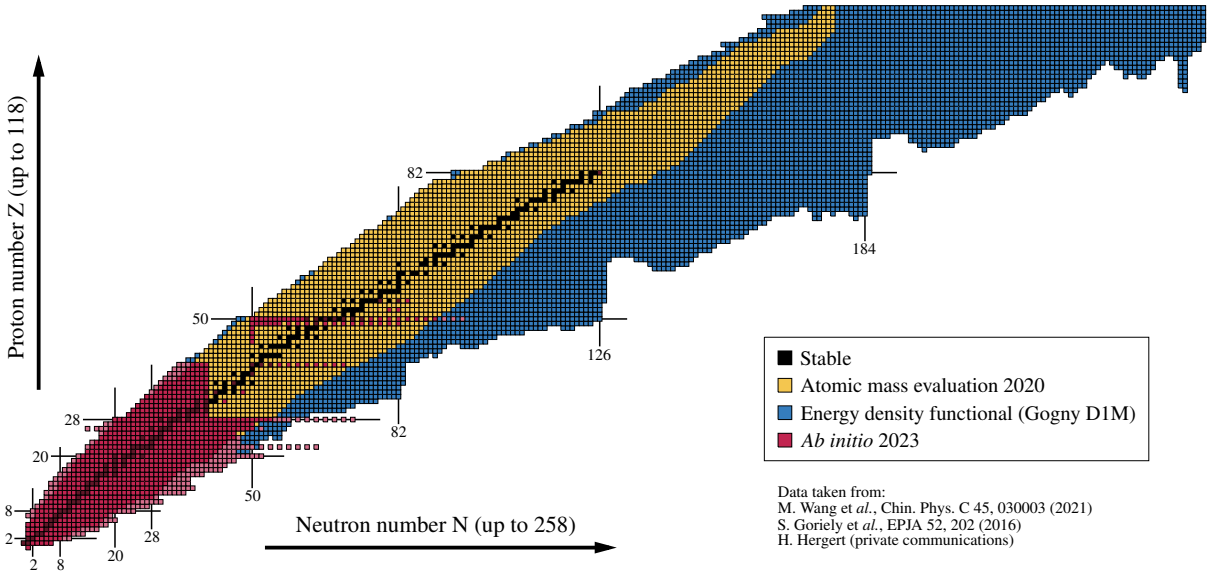

Figure I.2 – The chart of nuclides [105]. Nuclei whose masses are measured experimentally are put into perspective with those recently predicted by *ab initio* approaches and the D1M Gogny interaction.

We now describe the analytical expressions and fitting procedures associated with some important phenomenological effective forces other than the Gogny interaction, which we defer to the next dedicated section. This is important as it reveals a fairly traditional way those interactions are fitted, many aspects of which are common to the Gogny interaction.

The original Skyrme interaction, introduced by Skyrme in 1958 [10, 11] and then popularized by Vautherin and Brink in the 1970s [106, 107], is a fully *zero-range* force, as

evidenced by the (omni)presence of delta functions, of the following form

$$\begin{aligned} v_{12} = {} & t_0(1 + x_0 P_\sigma)\delta(\vec{r}_1 - \vec{r}_2) + \frac{1}{2}t_1\Big[\delta(\vec{r}_1 - \vec{r}_2)k^2 + k'^2\delta(\vec{r}_1 - \vec{r}_2)\Big] \\ & + t_2\vec{k}' \cdot \delta(\vec{r}_1 - \vec{r}_2)\vec{k} \\ & + \frac{1}{6}t_3(1 + P_\sigma)\delta(\vec{r}_1 - \vec{r}_2)\rho\Big(\frac{\vec{r}_1 + \vec{r}_2}{2}\Big) \\ & + \mathrm{i}W_0\Big[\vec{k}' \times \delta(\vec{r}_1 - \vec{r}_2)\vec{k}\Big] \cdot (\vec{\sigma}_1 + \vec{\sigma}_2), \end{aligned} \tag{I.19}$$

where t_0, t_1, t_2, t_3, x_0 and W_0 are the adjustable parameters, $\vec{k}$ and $\vec{k}'$ the momentum operators respectively acting on the right and on the left, defined by $\vec{k} \equiv (\vec{\nabla}_1 - \vec{\nabla}_2)/2\mathrm{i}$ and $\vec{k}' \equiv -(\overleftarrow{\nabla}_1 - \overleftarrow{\nabla}_2)/2\mathrm{i}$, $\vec{\sigma}_1$ and $\vec{\sigma}_2$ the Pauli vectors associated with the first and second particle, defined in (D.1), and P_σ the spin-exchange operator, given by (D.8), allowing to separately constrain the interaction in the spin channels $S = 0$ and $S = 1$. This interaction is, in order, composed of:

(i) a short-range expansion of a Gaussian central term truncated at the second order, leading to a *contact* term;

(ii) a two-body density-dependent term mimicking the three-body interactions evaluated at the center-of-mass position;

(iii) a spin–orbit term.

In the original Skyrme interaction, the parameters were fitted in order to reproduce the binding energy and the density of nuclear matter as well as binding energies and mass differences of light nuclei (in particular ^{4}He, ^{16}O, ^{40}Ca and nuclei of close mass numbers). The goal of such a procedure was to build up a parametrization capable of describing as many nuclei as possible from the limit cases of light and heavy nuclei (whose interiors can be assimilated to nuclear matter). Actually Vautherin and Brink found out too small nuclear radii for heavy nuclei with that fitting procedure, and then decided to improve it. Their parametrization, which serves as the starting point for the Skyrme parametrizations built to date, is adjusted to reproduce:

(i) binding energy and saturation density in nuclear matter;

(ii) binding energy and nuclear radius of ^{16}O, calculated in a harmonic oscillator representation;

(iii) symmetry energy in nuclear matter;

(iv) splitting of $(1p_{3/2} - 1p_{1/2})$ levels in ^{16}O at the HF approximation.

Additionally, in a second step, they performed HF calculations with their parametrization for ^{16}O and ^{208}Pb so as to further refine the nuclear matter and the ^{16}O input values. Finally, the incompressibility of nuclear matter K_∞ was used as a control quantity to ensure the consistency of the parametrizations coming out of the code. It is worthwhile to mention that the spin–orbit parameter W_0 was fixed *independently* of the other parameters, from the fourth point above. This characteristic will be discussed at length in what follows.

The reason why the Skyrme interaction is of zero range, despite the fundamentally finite-range nature of the nuclear interaction, is twofold. First because it greatly simplifies the calculations (both on theoretical and numerical aspects), and second since, in HF calculations for which the Skyrme interaction was primitively designed, only low-momentum matrix elements ($k, k' \leq 2k_\mathrm{F}$, where k_F is the Fermi momentum) are significant. When one

decides to use such an interaction in beyond mean-field approximations, though, ultraviolet divergences appear because the contributions of matrix elements involving momentum transfers above $2k_\mathrm{F}$ become non-negligible.

A finite-range phenomenological effective interaction, less exploited than its Skyrme and Gogny counterparts, is the M3Y interaction. Introduced in the 1970s by Bertsch *et al.* [52] to deal with inelastic scatterings, the M3Y (Michigan three Yukawa) has enjoyed renewed interest in the 2000s, notably via Nakada's work [53] who widely extended its SCMF treatment. Originally, the M3Y interaction read

$$\begin{aligned} v_{12} = &\sum_{i=1}^{3} \Big(t_i^{\mathrm{C}(01)} P_{01} + t_i^{\mathrm{C}(10)} P_{10} + t_i^{\mathrm{C}(00)} P_{00} + t_i^{\mathrm{C}(11)} P_{11} \Big) f_i^{\mathrm{C}}(r_{12}) \\ &+ \sum_{i=1}^{2} \Big(t_i^{\mathrm{SO}(01)} P_{01} + t_i^{\mathrm{SO}(11)} P_{11} \Big) f_i^{\mathrm{SO}}(r_{12}) \vec{L} \cdot (\vec{s}_1 + \vec{s}_2) \\ &+ \sum_{i=1}^{2} \Big(t_i^{\mathrm{T}(01)} P_{01} + t_i^{\mathrm{T}(11)} P_{11} \Big) f_i^{\mathrm{T}}(r_{12}) r_{12}^2 S_{12}, \end{aligned} \tag{I.20}$$

where $P_{01} \equiv (1-P_\sigma)(1+P_\tau)/4$, $P_{10} \equiv (1+P_\sigma)(1-P_\tau)/4$, $P_{00} \equiv (1-P_\sigma)(1-P_\tau)/4$ and $P_{11} \equiv (1+P_\sigma)(1+P_\tau)/4$ respectively project onto the singlet-even ($S=0, T=1$), triplet-even ($S=1, T=0$), singlet-odd ($S=0, T=0$) and triplet-odd ($S=1, T=1$) channels of the interaction. As its name suggests, the M3Y interaction is made up of Yukawa form factors $f_i(r_{12}) \equiv \mathrm{e}^{-\mu_i r_{12}}/\mu_i r_{12}$, with μ_i the range of the interaction and $\vec{r}_{12} \equiv \vec{r}_1 - \vec{r}_2$ the relative position of the nucleon pair. This *fully finite-range* interaction is composed of:

(i) three Yukawa central terms;

(ii) two Yukawa spin–orbit terms;

(iii) two Yukawa tensor terms.

The spin–orbit terms involve the relative orbital angular momentum defined by $\vec{L} \equiv \vec{r}_{12} \times \vec{p}_{12}$, with the relative momentum $\vec{p}_{12} \equiv (\vec{p}_1 - \vec{p}_2)/2$, and the spin operators $\vec{s}_1$ and $\vec{s}_2$. The tensor operator is here defined as $S_{12} \equiv 4[3(\vec{s}_1 \cdot \hat{r}_{12})(\vec{s}_2 \cdot \hat{r}_{12}) - \vec{s}_1 \cdot \vec{s}_2]$, with $\hat{r}_{12} \equiv \vec{r}_{12}/r_{12}$.

In the original M3Y interaction, the three ranges of the central terms were fixed by the values $\mu_1^{\mathrm{C}} = 0.25\,\mathrm{fm}$, $\mu_2^{\mathrm{C}} = 0.4\,\mathrm{fm}$ and $\mu_3^{\mathrm{C}} = 1.414\,\mathrm{fm}$. The medium- and long-range parts of the interaction were interpreted in the light of one-boson-exchange (OBE) models as originating from the interactions between nucleons and mesons ω and π, respectively, while the short range is purely phenomenological. In fact, the set of parameters associated with the third central term is given to exactly replicate the one pion exchange potential. As for the spin–orbit and tensor terms, their respective ranges are $\mu_1^{\mathrm{SO}} = 0.25\,\mathrm{fm}$ and $\mu_2^{\mathrm{SO}} = 0.4\,\mathrm{fm}$, and $\mu_1^{\mathrm{T}} = 0.4\,\mathrm{fm}$ and $\mu_2^{\mathrm{T}} = 0.7\,\mathrm{fm}$, because the spin–orbit force is known to be mainly of short range while the tensor interaction mainly contributes at medium and large distances in OBE models (see subsection II.1.2.1). In the original paper, three procedures for fitting the remaining parameters were proposed, one of which was based on the reproduction of the G-matrix elements of the Reid potential [23] in an harmonic oscillator representation. Still with the aim of describing inelastic scattering, the Reid potential was traded for the Paris potential [24] by Anantaraman *et al.* [108] some years later. It is from their parameters that Nakada applied the M3Y interaction to the HF approach. Nakada started with the original analytical expression given above, along with a zero-range density-dependent term [54]

$$v_{12}^{\mathrm{DD}} = t^{\mathrm{DD}}(1 + x^{\mathrm{DD}} P_\sigma) \delta(\vec{r}_1 - \vec{r}_2) \rho^\alpha(\vec{r}_1), \tag{I.21}$$

similar to that of the Gogny interaction – not evaluated at the center-of-mass position, though –, as it was necessary to get the saturation point of nuclear matter. The parameters were determined so as to reproduce:

(i) binding energies and root mean square radii of some spherical nuclei (^{16}O, ^{40}Ca, ^{48}Ca, ^{90}Zr, ^{132}Sn and ^{208}Pb);

(ii) saturation density and energy in nuclear matter (for the parameters of the density-dependent interaction, $t^{(\mathrm{DD})}$ and $x^{(\mathrm{DD})}$);

(iii) splitting of the neutron ($1p_{3/2}$ – $1p_{1/2}$) levels in ^{16}O, as well as the ordering of single-particle states in ^{208}Pb, at the HF approximation.

Standard quantities evaluated in infinite nuclear matter, similar to those of the Gogny interaction, we shall shortly discuss, were also used as filters. Based on the physical quantities probed with the Gogny interaction, the M3Y interaction was later successfully applied to the HFB theory, first including only the particle-like pairing [55], and then the full pairing [56].

Phenomenological effective interactions, although furnishing convincing outputs, do not take into account the relativistic nature of the nuclear interaction; they are *non-relativistic* interactions. One could then be tempted to take advantage of the relativistic version of Brueckner's theory, the Dirac–Brueckner–Hartree–Fock (DBHF) theory, to build a relativistic effective interaction [109, 110]. Nevertheless, the procedure is even more complex to set up in finite nuclei and involves additional approximations. Instead, the *relativistic mean-field* (RMF) model [8, 9], first introduced in the 1950s by Schiff [111] and by Teller *et al.* [112, 113], and then revived by Walecka and his collaborators [114, 115] in the 1970s, appears a great tool to capture that physics. This model is a relativistic quantum field theory based on the Yukawa vision of an interaction transmitted by exchanges of mesons. In RMF, one considers a Lagrangian bringing into play nucleonic degrees of freedom, through Dirac spinors, interacting by means of mesonic fields. As the coupling constants involved in the Lagrangian are very strong, perturbation methods cannot be applied. However, the mean-field approach appears as a reasonable approximation and is then used in practical calculations. The parameters of the RMF Lagrangian, i.e. the number of mesons, their quantum numbers as well as their masses and coupling constants, are fixed in order to reproduce some chosen quantities in nuclear matter and experimental data in finite nuclei. In this perspective, RMF brings a phenomenological description of the nuclear interaction. As such, it is often considered a relativistic generalization of the self-consistent mean-field approaches employed for the phenomenological interactions cited above, where instantaneous forces are replaced by mesonic degrees of freedom. Note, moreover, that the spin–orbit force naturally comes out of RMF, and the nuclear saturation is easily obtained.

2. Evolution of the Gogny interaction

2.1. The original Gogny interaction D1

Before giving at last the analytical expression of the Gogny interaction, we would like to provide some background to its advent [20, 116, 117]. At the end of the 1960s, Gogny, Pires and de Tourreil [118] proposed a soft-core realistic nucleon–nucleon interaction,

called GPT,[6] aimed at reproducing some physical quantities and observables in both nuclear matter and finite nuclei. The interaction is fully finite range, made out of twelve central, six tensor, two spin–orbit and four quadratic spin–orbit terms, and was fitted so as to faithfully describe:

(i) two-nucleon data (phase shifts up to 300 MeV, deuteron properties, scattering lengths and effective ranges);

(ii) binding energies and charge radii of magic nuclei ^{16}O, ^{40}Ca, ^{90}Zr and ^{208}Pb, with great accuracy at HF approximation;

(iii) reasonable saturation properties in nuclear matter.

Finally, this realistic interaction was shortly after put aside for a phenomenological effective interaction now referred to as the Gogny interaction [12]. Even though the Gogny interaction left out any direct connection with realistic forces, the physics probed by the G-matrix plus higher corrections of GPT was incorporated and simulated by a density dependence, as we will see later on. The initial purpose of the Gogny interaction was to bring out a self-consistent treatment of mean field and pairing correlations at the HFB level. In order to avoid the ultraviolet divergences encountered by the Skyrme interaction then in place, Gogny chose to attribute *finite* ranges to the central terms. In 1964, Gillet and Vinh Mau [119, 120] introduced an interaction composed of one finite-range Gaussian term, with all possible admixtures of spin- and isospin-exchange operators. Compared to a Yukawa, this form factor had the advantage of being easier to handle in theoretical developments and, above all, of being more manageable numerically since no trouble is faced in $r = 0$. In 1967, Brink and Boeker [121] compared different types of interactions, including that one and another composed of two Gaussian central terms proposed by Volkov [122] a year before. The two-Gaussian form turned out to furnish the best set of single-particle energies (SPEs) in ^{16}O and root mean square radii of the tested nuclei. In the same spirit, Gogny introduced two central terms of Gaussian form factors acting in all (S, T) channels. One is repulsive and of short range, the other attractive and of long range, as in the article of Volkov, then catching the essence of the bare nuclear interaction between two nucleons. The finite-range character of the effective Gogny interaction enables short- and long-range correlations to be taken into account on an equal footing. In that sense, it can be said that the original effective Gogny interaction bears a signature of the realistic nuclear interaction. Note that the main effective interactions discussed so far are placed on a timeline in Figure I.6, shown at the end of this chapter.

The original Gogny interaction is formulated in the D1 analytical expression of the form

$$\begin{aligned} v_{12}^{\mathrm{D1}} = &\sum_{i=1}^{2}(W_i + B_i P_\sigma - H_i P_\tau - M_i P_\sigma P_\tau)\,\mathrm{e}^{-(\vec{r}_1-\vec{r}_2)^2/\mu_i^2} \\ &+ t_0(1 + x_0 P_\sigma)\delta(\vec{r}_1 - \vec{r}_2)\rho^\alpha\left(\frac{\vec{r}_1 + \vec{r}_2}{2}\right) \\ &+ \mathrm{i}W_0\left[\vec{k}' \times \delta(\vec{r}_1 - \vec{r}_2)\vec{k}\right]\cdot(\vec{\sigma}_1 + \vec{\sigma}_2). \end{aligned} \tag{I.22}$$

We find, by order of appearance, two Gaussian central terms, a zero-range density-dependent term whose density is evaluated at the center-of-mass position, a zero–range spin–orbit term (the last two being identical to that of the Skyrme interaction). The

6. French speakers must know that this denomination is not coincidence. By saying it aloud, they can appreciate Gogny's subtle sense of humor.

adjustable parameters are $W_i, B_i, H_i, M_i, \mu_i, t_0, x_0, \alpha$ and W_0 (for $i \in \{1,2\}$), while the spin- and isospin-exchange operators P_σ and P_τ, defined in (D.8), allow to modulate the central part of the interaction in all (S,T) channels. When all these parameters are determined, they constitute a parametrization (i.e. a set of parameters) of the D1 analytical expression. It is often said that the Gogny interaction differs from its Skyrme predecessor by the finite-range character of its central terms. This is true, but the density-dependent term was also improved. Where it mimicked the effects of the three-body interaction in the Skyrme interaction, it here mimics the effects of *all* A-body interactions through the phenomenologically determined power α. By phenomenological, we mean that this value affected to α was found out "by hand", that is after several tests to reproduce the saturation point in symmetric nuclear matter.

The Gogny interaction was designed to be treated consistently beyond the mean field. It is essential to bear in mind that in this perspective, a place is deliberately left for beyond mean-field correlations. In other words, the Gogny interaction is not intended to produce mean-field results directly comparable with experiment in general. When going beyond the mean field, ultraviolet divergences pop up in the pairing matrix elements if the interaction is of zero range, as for the Skyrme interaction. This is the main reason, in addition to the intrinsic finite-range nature of the nuclear interaction, that motivated the introduction of finite-range central terms (despite the inherent numerical complications, particularly challenging for that period). However, we have just stated that the density-dependent was of zero range. We then need to justify why this is not a problem. The zero-range density-dependent term (denoted as DD) is even in space, as can be easily inferred from its expression. When evaluated on some two-body antisymmetrized state (a),[7] this implies $P_r = \mathbb{1}$, and it becomes

$$\begin{aligned} v_{\mathrm{DD}}^{\mathrm{D1}} |\vec{r}_1 s_1 t_1 \ \vec{r}_2 s_2 t_2\rangle_{\mathrm{a}}^{(S,T)} &\equiv v_{\mathrm{DD}}^{\mathrm{D1}} (\mathbb{1} - P_r P_\sigma P_\tau) |\vec{r}_1 s_1 t_1 \ \vec{r}_2 s_2 t_2\rangle^{(S,T)} \\ &= v_{\mathrm{DD}}^{\mathrm{D1}} (\mathbb{1} - P_\sigma P_\tau) |\vec{r}_1 s_1 t_1 \ \vec{r}_2 s_2 t_2\rangle^{(S,T)} \\ &= v_{\mathrm{DD}}^{\mathrm{D1}} \Big(1 - (-)^{S+T}\Big) |\vec{r}_1 s_1 t_1 \ \vec{r}_2 s_2 t_2\rangle^{(S,T)}. \end{aligned} \tag{I.23}$$

where $\vec{r}_i$, s_i and t_i respectively denote the space, spin and isospin degrees of freedom of the particle $i \in \{1,2\}$, and where we have benefited from the relations (D.11). We see that the zero-range density-dependent term does not contribute in the $(S=0, T=0)$ and $(S=1, T=1)$ channels of the interaction. Besides, Gogny set $x_0 = 1$ in the D1 analytical expression, so that the zero-range density-dependent term becomes

$$\begin{aligned} v_{\mathrm{DD}}^{\mathrm{D1}} |\vec{r}_1 s_1 t_1 \ \vec{r}_2 s_2 t_2\rangle^{(S,T)} &= t_0 \delta(\vec{r}_1 - \vec{r}_2) \rho^\alpha \left(\frac{\vec{r}_1 + \vec{r}_2}{2}\right) (\mathbb{1} + P_\sigma) |\vec{r}_1 s_1 t_1 \ \vec{r}_2 s_2 t_2\rangle^{(S,T)} \\ &= t_0 \delta(\vec{r}_1 - \vec{r}_2) \rho^\alpha \left(\frac{\vec{r}_1 + \vec{r}_2}{2}\right) \Big(1 - (-)^S\Big) |\vec{r}_1 s_1 t_1 \ \vec{r}_2 s_2 t_2\rangle^{(S,T)}. \end{aligned} \tag{I.24}$$

In these conditions, the zero-range density-dependent term does not contribute in the $(S=0, T=1)$ channel, it only takes part in the $(S=1, T=0)$ channel. Since only the $T=1$ particle-like pairing correlations are taken into account in the original Gogny interaction, no divergences emerge from the zero-range density-dependant term that has not action in this channel. On the other hand, we know the spin–orbit interaction to contribute only to the $S=1$ channel (as we show in subsection II.1.1), while its zero-range character makes it odd in space. These observations can be translated in terms

7. As can be seen in appendices, all quantities of interest involve two-body antisymmetrized matrix elements.

of exchange operators as $P_\sigma = \mathbb{1}$ and $P_r = -\mathbb{1}$, respectively. When evaluated on some two-body antisymmetrized state, the zero-range spin–orbit term (denoted as SO) then becomes

$$\begin{aligned} v_{\mathrm{SO}}^{\mathrm{D1}}|\vec{r}_1 s_1 t_1\ \vec{r}_2 s_2 t_2\rangle_{\mathrm{a}}^{(S,T)} &\equiv v_{\mathrm{SO}}^{\mathrm{D1}}(\mathbb{1} - P_r P_\sigma P_\tau)|\vec{r}_1 s_1 t_1\ \vec{r}_2 s_2 t_2\rangle^{(S,T)} \\ &= v_{\mathrm{SO}}^{\mathrm{D1}}(\mathbb{1} + P_\tau)|\vec{r}_1 s_1 t_1\ \vec{r}_2 s_2 t_2\rangle^{(S,T)} \\ &= v_{\mathrm{SO}}^{\mathrm{D1}}\Big(1 - (-)^T\Big)|\vec{r}_1 s_1 t_1\ \vec{r}_2 s_2 t_2\rangle^{(S,T)}. \end{aligned} \tag{I.25}$$

We see that the zero-range spin–orbit term only contributes to the $(S = 1, T = 1)$ channel, and then *does* take part in the pairing matrix elements taken into account beyond the mean field. However, its contribution is so small that it is either simply discarded or taken into account with a convergence criterion leaving no time for a divergence to show up in oscillator bases.

Note that a contribution of the Coulomb potential, taking into account the electrical nature of protons, is added to the nuclear Gogny interaction, as in the effective interactions discussed in the previous subsection. It is generally written as

$$v_{\mathrm{Coul}} \equiv \frac{1}{4}(1 + 2t_{1z})(1 + 2t_{2z})\frac{e^2}{|\vec{r}_1 - \vec{r}_2|}, \tag{I.26}$$

where $t_{iz} = \pm 1/2$ (for $i \in \{1, 2\}$) denote the projections of the isospin operators along the Oz axis.

We summarize our analysis on the contributions of the different terms of the D1 analytical form to the (S, T) channels in Table I.1.

	Channels			
	$(S = 0, T = 0)$	$(S = 0, T = 1)$	$(S = 1, T = 0)$	$(S = 1, T = 1)$
Terms				
Central	✗	✗	✗	✗
Density-dependent			✗	
Spin–orbit				✗
Coulomb		✗		✗

Table I.1 – Decomposition of the terms involved in the D1 analytical expression according to their actions in the (S, T) channels (when $x_0 = 1$). When a given term acts in a given channel, it is marked by a cross, otherwise its contribution is zero.

The first parametrization associated with the analytical form (I.22) was called the D1 parametrization [14]. As this latter predicted too strong pairing correlations and fission barrier heights [16], it was quickly outperformed in the 1980s by the D1S parametrization [15], fixing these pathologies. The fitting procedure of this still widely-used interaction is the topic of the next subsection.

2.2. The D1S parametrization

In the original fitting procedure of the Gogny interaction, several successive steps allow the extraction of a parametrization [12, 13]. First, some *initial data* are picked up so as to allocate quantitative values to *constraints* involving the parameters to be determined.

Through the *inversion of a system* gathering those constraints, a set of parameters is deduced. Then, this set faces *filters*. If it passes through all the filters, it becomes a potential parametrization associated with the D1 analytical expression (I.22). In the following, we are going to develop the steps that led to the D1S parametrization.

2.2.1. The HFR formalism

We insist on the fact that the fitting procedure is based on the inversion of a system that permits a straight determination of the parameters. For this to be possible, a convenient formalism should be taken [17].

We start from the Hamiltonian of the nucleus, assimilated to a A-body system whose nucleons only interact though two-body forces. In second quantization, it reads

$$H = \sum_{ab} \langle a|t_{\mathrm{K}}|b\rangle c_a^\dagger c_b + \frac{1}{4}\sum_{abcd} \langle ac|v_{12}^{(\mathrm{a})}|bd\rangle c_a^\dagger c_c^\dagger c_d c_b, \tag{I.27}$$

where we recognize the usual creation c_a and annihilation $c_a^\dagger$ operators, the one-body kinetic operator, written in terms of the momentum operator $p \equiv \hbar k$ as

$$t_{\mathrm{K}} \equiv \frac{p^2}{2M}, \tag{I.28}$$

as well as the two-body antisymmetrized Gogny interaction

$$v_{12}^{(\mathrm{a})} \equiv v_{12}(1 - P_r P_\sigma P_\tau). \tag{I.29}$$

To solve the Schrödinger equation associated with the above Hamiltonian, the HF method approximates the wave function of the system by a (normalized) Slater determinant Φ_{HF}. The Slater determinant is fully characterized by an antisymmetrized combination of individual wave functions φ_i^{HF} that must then be determined. In first quantization, it is expressed as

$$\Phi_{\mathrm{HF}}(\xi_1, \ldots, \xi_A) = \frac{1}{\sqrt{A!}} \begin{vmatrix} \varphi_1^{\mathrm{HF}}(\xi_1) & \ldots & \varphi_A^{\mathrm{HF}}(\xi_1) \\ \vdots & \ddots & \vdots \\ \varphi_1^{\mathrm{HF}}(\xi_A) & \ldots & \varphi_A^{\mathrm{HF}}(\xi_A) \end{vmatrix}, \tag{I.30}$$

where ξ_i stands for the degrees of freedom of the i-th individual wave function φ_i^{HF}, with $i \in \{1, \ldots, A\}$. In practice, those are expanded on a basis of functions that are known. The spherical harmonic oscillator (HO) functions were the ones retained in the fitting procedure as they make the calculations with Gaussian form factors quite easy to deal with. Denoting by an integer index a the set of quantum numbers of the spherical HO, the expansion can be written

$$|\varphi_i^{\mathrm{HF}}\rangle = \sum_{a=1}^{\infty} U_{ia}(\hbar\omega)|\phi_a(\hbar\omega)\rangle, \quad \text{for } i \in \{1, \ldots, A\}, \tag{I.31}$$

where $\phi_a(\hbar\omega)$ denotes the HO function of quantum numbers a and frequency $\hbar\omega$. Determining the individual wave functions then comes down to getting the coefficients of the expansion, $U_{ia}(\hbar\omega)$. Obviously, such an infinite series is not numerically tractable and is practically truncated to some finite order n according to

$$|\varphi_i^{\mathrm{HF}}(\hbar\omega)\rangle = \sum_{a=1}^{n} U_{ia}(\hbar\omega)|\phi_a(\hbar\omega)\rangle, \quad \text{for } i \in \{1, \ldots, A\}. \tag{I.32}$$

In this truncation process, some of the information defining the individual wave functions is lost as the basis is no longer complete, and they then become *a priori* frequency-dependent. The choice of this frequency is crucial, since the results of the HF calculation should not depend of its value. As the HF approach is based on the minimization of the HF energy defined by $\mathcal{E}_{\mathrm{HF}} \equiv \langle \Phi_{\mathrm{HF}} | H | \Phi_{\mathrm{HF}} \rangle$, the natural option is to select the frequency for which this energy is minimal. If we now calculate the HF energy, we end up with, using Wick's theorem,

$$\mathcal{E}_{\mathrm{HF}} = \sum_{ab} \langle a | t_{\mathrm{K}} | b \rangle \rho_{ba} + \frac{1}{2} \sum_{abcd} \langle ac | v_{12}^{(\mathrm{a})} | bd \rangle \rho_{ba} \rho_{db}, \tag{I.33}$$

where we have introduced the shorthand notation $|a\rangle \equiv |\phi_a(\hbar\omega)\rangle$ and the one-body density matrix as $\rho_{ba} \equiv \langle \Phi_{\mathrm{HF}} | c_a^\dagger c_b | \Phi_{\mathrm{HF}} \rangle$. Let us now point out that the individual wave functions, characterized by the coefficients $U_{ia}(\hbar\omega)$, are solutions of the HF equations. On the other hand, these equations rely on the Hamiltonian (I.27) which involves the Gogny interaction v_{12}. The coefficients will therefore depend directly on this interaction, what we write as $U_{ia}(\hbar\omega, v_{12})$. Thus, we show that the density matrix can also be expanded with respect to those coefficients as

$$\rho_{ab} = \sum_{i=1}^{A} U_{ia}^*(\hbar\omega, v_{12}) U_{ib}(\hbar\omega, v_{12}). \tag{I.34}$$

Sadly, because of the *iterative* mechanism used to solve the HF equations, there exists no straight relation between the coefficients $U_{ia}(\hbar\omega, v_{12})$ and the interaction v_{12}. This implies that it is not possible to express, at the HF level, the energy directly in terms of the parameters of the interaction as it involves the coefficients $U_{ia}(\hbar\omega, v_{12})$ through the density matrices. This would have been beneficial though, since we could have constrained the parameters from the binding energies of magic nuclei by means of a simple inversion system. As a compromise, the Hartree–Fock restricted (HFR) approximation stipulates that

$$U_{ia} = \delta_{ia}, \tag{I.35}$$

where δ_{ia} stands for the Kronecker delta. The coefficients of the expansion (I.32) no longer depend on either the HO frequency or the interaction, and this expansion simplifies as

$$|\varphi_i^{\mathrm{HF}}(\hbar\omega)\rangle = |\phi_i(\hbar\omega)\rangle, \quad \text{for } i \in \{1, \dots, A\}. \tag{I.36}$$

In other words, the individual HF wave functions are the HO functions, and the density matrix becomes trivial,

$$\rho_{ab} = \delta_{ab}\rho_{aa} = \begin{cases} 1 & \text{if } a \leq A, \\ 0 & \text{otherwise.} \end{cases} \tag{I.37}$$

At the HFR level, the density matrix is diagonal in the HO representation. Its diagonal elements are 1 or 0, depending on whether the corresponding HO eigenstate is occupied or not. With these considerations, the HF energy (I.33) turns into an HFR energy of the form

$$\mathcal{E}_{\mathrm{HFR}} = \sum_{a} \langle a | t_{\mathrm{K}} | a \rangle \rho_{aa} + \frac{1}{2} \sum_{ab} \langle ab | v_{12}^{(\mathrm{a})} | ab \rangle \rho_{aa} \rho_{bb}, \tag{I.38}$$

that can be expressed in terms of the parameters of the Gogny interaction, and eventually be inverted to extract the values of the parameters.

Several remarks should be made. First, the approximation (I.35) may look crude. In fact, *the principle of the fitting procedure is not to perfectly reproduce the input data*

directly, as may be the objective of other methods (that attempt to minimize their predictions with data in the fitting process). Its philosophy consists in rapidly and rather efficiently identifying relevant zones in the space of parameters. It is then the task of the user to discriminate in the output the interactions that are more promising than the others. Second, one must now find a way to consistently choose the values to be allocated to the HFR quantities. We shall evoke this in the next subsection, which will further justify the use of the HFR approximation.

2.2.2. Constraints

Among the fourteen parameters to be determined in the Gogny interaction, we already explained that $x_0 = 1$ was mandatory to avoid pathologies when treating pairing correlations. Moreover, it turned out that taking $\alpha = 1/3$ for the power of the density was also essential in reproducing the saturation point in symmetric nuclear matter. As for the parameters t_3, μ_1 and μ_2, they were left free, and in practice selected in relevant intervals defined by the user. Finally, the strength of the spin–orbit interaction was fixed separately from the other parameters. It was simply chosen in order to reproduce the neutron $(1p_{3/2} - 1p_{1/2})$ splitting in ^{16}O at the HF approximation, as in the original Skyrme interaction. The spin–orbit interaction *does not* take part in the fitting code we here describe. Consequently, the spherical HO states are only specified by their usual quantum numbers n and l, through the occupation of the major shells $N \equiv 2n + l$, in the fitting code. They are not distinguished by the additional quantum numbers j, projections of the total angular momentum, appearing when the spin–orbit force comes into play. Thus, the remaining eight parameters W_i, B_i, H_i and M_i (with $i \in \{1, 2\}$) were gotten from a process we now want to describe, and whose formalism was exposed in the previous subsection.

First system

Two spherical nuclei, ^{16}O and ^{90}Zr, were chosen as representatives of the low- and medium-mass nuclei in the first system. We notice that two constraints for each nucleus can be extracted from our discussion on the HFR approximation. On the one side, the HFR energies of those nuclei are of course constrained. Actually a link between the HF and HFR energies for these nuclei was made, in a similar fashion to the one we detail in the case of the D2 interaction. Basically several reliable D1-type parametrizations were generated, and all of them evaluated the HF and HFR energies of the two nuclei. By plotting the HF energies as a function of the HFR energies, simple relations were successively obtained for each nucleus. On the other side, we have argued that the HO frequency had to be the one rendering the energy minimal. In the fitting code, this requirement takes form through the following constraint on the HFR energy,

$$\frac{\mathrm{d}\mathcal{E}_{\mathrm{HFR}}}{\mathrm{d}(\hbar\omega)}[X] = \frac{\mathrm{d}\mathcal{E}_{\mathrm{HFR}}}{\mathrm{d}b}[X] = 0, \tag{I.39}$$

where X denotes the nucleus and $b \equiv \sqrt{\hbar/M\omega}$ is the spherical oscillator length. It remains to determine how to attribute a value to this quantity. It turns out that, according to the virial theorem, there exists a direct relation between the charge radius of a nucleus at the

HFR approximation and its oscillator length. In our case, these relations read

$$R_{\rm ch}^{\rm HFR}\left[^{16}{\rm O}\right] = \frac{\sqrt{15}}{2} b\left[^{16}{\rm O}\right], \tag{I.40a}$$

$$R_{\rm ch}^{\rm HFR}\left[^{90}{\rm Zr}\right] = \frac{\sqrt{25}}{2} b\left[^{90}{\rm Zr}\right], \tag{I.40b}$$

To find which values to give to the charge radii of the two nuclei, the exact same procedure described for the binding energies was undertaken. As we can see, the few quantities of interest evaluated at the HFR level are straightforwardly connected to those at the HF approximation. This makes the use of the HFR approximation all the more adapted.

The first constraints, on the HFR energies of the two spherical nuclei, split up into kinetic and potential contributions and become

$$\begin{aligned}
\mathcal{E}_{\rm HFR}[X] &\equiv \mathcal{E}_{\rm K}^{\rm HFR}[X] + \mathcal{E}_{\rm P}^{\rm HFR}[X] \\
&= \mathcal{E}_{\rm K}^{\rm HFR}[X] \\
&\quad + \sum_{i=1,2} F_i^{\rm D}[X](4W_i + 2B_i - 2H_i - M_i) \\
&\quad + \sum_{i=1,2} F_i^{\rm E}[X](4M_i + 2H_i - 2B_i - W_i) \\
&\quad + G[X](t_0, x_0).
\end{aligned} \tag{I.41}$$

In this expression, HFR kinetic energies of ^{16}O and ^{90}Zr are explicitly given in (B.172), while $F_i^{\rm D}[X]$ and $F_i^{\rm E}[X]$, direct and exchange contributions of the central terms to the HFR potential energy are calculated in (B.178) and (B.182), respectively. As for the contribution of the zero-range density-dependent term, it is denoted by $G[X](t_0, x_0)$.[8] The same type of relations holds for the constraints on the derivatives of the HFR energies. Explicitly,

$$\begin{aligned}
\mathcal{E}'_{\rm HFR}[X] &\equiv \mathcal{E}'^{\rm HFR}_{\rm K}[X] + \mathcal{E}'^{\rm HFR}_{\rm P}[X] \\
&= \mathcal{E}'^{\rm HFR}_{\rm K}[X] \\
&\quad + \sum_{i=1,2} F_i'^{\rm D}[X](4W_i + 2B_i - 2H_i - M_i) \\
&\quad + \sum_{i=1,2} F_i'^{\rm E}[X](4M_i + 2H_i - 2B_i - W_i) \\
&\quad + G'[X](t_0, x_0),
\end{aligned} \tag{I.42}$$

where the primes stand for the derivative with respect to the oscillator length b. From the expressions of the kinetic energies, we easily find out

$$\mathcal{E}'^{\rm HFR}_{\rm K}\left[^{16}{\rm O}\right]/(A=16) = -\frac{9}{4}\frac{\hbar^2}{Mb^3}, \tag{I.43a}$$

$$\mathcal{E}'^{\rm HFR}_{\rm K}\left[^{90}{\rm Zr}\right]/(A=90) = -\frac{71}{18}\frac{\hbar^2}{Mb^3}. \tag{I.43b}$$

As for the derivations of the potential contributions, a bit more tedious, they were done in the fitting code. These four equations can be formulated in matrix form

$$AX = F, \tag{I.44}$$

8. In the appendices, derivations are done for the finite-range density-dependent term (that will be discussed in the next section). The zero-range density-dependent term can easily be recovered from it at the zero-range limit. As a consequence, all quantities associated with the zero-range density-dependent term can be deduced from the ones associated with its finite-range equivalent.

where A is a 4×4 matrix, and X and F two column vectors reading

$$A \equiv \begin{bmatrix} F_1^{\mathrm{D}}[^{16}\mathrm{O}] & F_2^{\mathrm{D}}[^{16}\mathrm{O}] & F_1^{\mathrm{E}}[^{16}\mathrm{O}] & F_2^{\mathrm{E}}[^{16}\mathrm{O}] \\ F_1'^{\mathrm{D}}[^{16}\mathrm{O}] & F_2'^{\mathrm{D}}[^{16}\mathrm{O}] & F_1'^{\mathrm{E}}[^{16}\mathrm{O}] & F_2'^{\mathrm{E}}[^{16}\mathrm{O}] \\ F_1^{\mathrm{D}}[^{90}\mathrm{Zr}] & F_2^{\mathrm{D}}[^{90}\mathrm{Zr}] & F_1^{\mathrm{E}}[^{90}\mathrm{Zr}] & F_2^{\mathrm{E}}[^{90}\mathrm{Zr}] \\ F_1'^{\mathrm{D}}[^{90}\mathrm{Zr}] & F_2'^{\mathrm{D}}[^{90}\mathrm{Zr}] & F_1'^{\mathrm{E}}[^{90}\mathrm{Zr}] & F_2'^{\mathrm{E}}[^{90}\mathrm{Zr}] \end{bmatrix}, \tag{I.45a}$$

$$X \equiv \begin{bmatrix} 4W_1 + 2B_1 - 2H_1 - M_1 \\ 4W_2 + 2B_2 - 2H_2 - M_2 \\ 4M_1 + 2H_1 - 2B_1 - W_1 \\ 4M_2 + 2H_2 - 2B_2 - W_2 \end{bmatrix}, \tag{I.45b}$$

$$F \equiv \begin{bmatrix} \mathcal{E}^{\mathrm{HFR}}[^{16}\mathrm{O}] - \mathcal{E}_{\mathrm{K}}^{\mathrm{HFR}}[^{16}\mathrm{O}] - G[^{16}\mathrm{O}](t_0, x_0) \\ \mathcal{E}_{\mathrm{K}}'^{\mathrm{HFR}}[^{16}\mathrm{O}] - G'[^{16}\mathrm{O}](t_0, x_0) \\ \mathcal{E}^{\mathrm{HFR}}[^{90}\mathrm{Zr}] - \mathcal{E}_{\mathrm{K}}^{\mathrm{HFR}}[^{90}\mathrm{Zr}] - G[^{90}\mathrm{Zr}](t_0, x_0) \\ \mathcal{E}_{\mathrm{K}}'^{\mathrm{HFR}}[^{90}\mathrm{Zr}] - G'[^{90}\mathrm{Zr}](t_0, x_0) \end{bmatrix}. \tag{I.45c}$$

We can then effortlessly obtain the combinations of parameters belonging to the vector X by simply inverting the matrix A, i.e. $X = A^{-1}F$.

Second system

Three constraints making up two subsystems were elaborated for the second system. As we have said in the previous subsection, only the pairing properties in the $(S = 0, T = 1)$ channel were constrained in the original fitting procedure of the Gogny interaction. To fix the intensity of this pairing, Gogny chose to constrain the values of two two-body matrix elements (TBMEs) in the $(S = 0, T = 1)$ channel. More precisely, TBMEs between $1s$ and $2s$ states of ^{32}S evaluated in a spherical harmonic oscillator basis at the HFR approximation were selected, namely

$$V_{1s} \equiv \langle 1s\,1s|v_{12}^{\mathrm{D1}}|1s\,1s\rangle^{(S=0,T=1)} = \sum_{i=1,2} f_{1s}^i (W_i - B_i - H_i + M_i), \tag{I.46a}$$

$$V_{2s} \equiv \langle 2s\,2s|v_{12}^{\mathrm{D1}}|2s\,2s\rangle^{(S=0,T=1)} = \sum_{i=1,2} f_{2s}^i (W_i - B_i - H_i + M_i). \tag{I.46b}$$

As expected, the contributions only come from central terms, through the quantities f_{1s}^i and f_{2s}^i (with $i \in \{1, 2\}$) given in (B.41). As for the values V_{1s} and V_{2s} attributed to those TBMEs, they were obtained from the requirement that the even–odd mass difference in Sn isotopes reproduces satisfactory pairing effects [13].

Another constraint on the energy difference, at the HFR approximation, between the neutron and proton $2s_{1/2}$ states in ^{48}Ca was also retained. This energy difference, manifestly sensitive to the isospin dependence of the interaction, reads

$$\Delta\varepsilon \equiv \varepsilon_\nu[2s_{1/2}] - \varepsilon_\pi[2s_{1/2}]. \tag{I.47}$$

With the D1 analytical form, we have

$$\Delta\varepsilon = \sum_{i=1,2} f_{\mathrm{D}}^i (2H_i + M_i) + f_{\mathrm{E}}^i (W_i + 2B_i) + g(t_0, x_0), \tag{I.48}$$

where the direct and exchange components of the central terms are denoted by f_{D}^i and f_{E}^i (with $i \in \{1, 2\}$), and are given by (B.200), while $g(t_0, x_0)$ corresponds to the zero-range density-dependent contribution. Actually, there should also be a contribution of the spin–orbit term (see subsection B.6.4), but we have stated that the spin–orbit is neglected in

the fitting procedure. The value assigned to $\Delta\varepsilon$ was found out from a requirement on the symmetry energy a_τ produced by the interaction in nuclear matter. A correction stemming from the Coulomb potential was also added by Gogny to this value.

Note that a more detailed procedure for deducing the values to be assigned to the constraints is proposed in Chappert's thesis, and discussed in subsection I.2.4.2.1. Gathering all the constraints (I.44), (I.46) and (I.48), we end up with seven equations involving eight parameters. In fact, one parameter, B_1, was also set free as the parameters t_3, μ_1 and μ_2 were. By inverting this system, a unique parameter set is obtained.

2.2.3. Filters

Once a set of parameters is generated, it still has to pass through filters nuclear matter to be considered a trustworthy parametrization. There are three steps of filtering, based on:

(i) Standard physical quantities;

(ii) Stability criteria and sum rules in the Landau theory of Fermi liquids;

(iii) The surface energy coefficient.

Basically, for the first point, the parametrization has to reproduce physical quantities at the saturation density of symmetric nuclear matter (total energy, incompressibility, effective mass and symmetry energy) in some intervals defined by empirical values. For the second point, we must recall that criteria ensuring the stability of nuclear matter as well as sum rules derived from the Pauli exclusion principle can be formulated in the Landau theory of Fermi liquids (here in symmetric nuclear matter at saturation point). Those rely on Landau parameters which directly depend on the values of the parameters. In practice, the sum rules are always violated by effective interactions, but by calculating their values, we can discriminate parametrizations whose violations are pathological from those for which they are acceptable. Analytical expressions of standard physical quantities as well as stability criteria and sum rules are reported in Appendix A for clarity. Finally, the last point enables to lower the fission barriers in actinides, by making a link between the surface energy coefficient evaluated in a semi-infinite nuclear matter and the fission barrier heights.

2.2.4. Extraction of the D1S parametrization

We finally sum up and illustrate in Figure I.3 how the D1-type fitting code is working with the example of the fitting process of the D1S parametrization we have just described. As explained earlier, initial data on both bulk and pairing properties were gathered so as to impose constraints on various physical quantities and observables at the HFR approximation. These constraints shape two interdependent systems (as indicated by vertical arrows), from (I.44), and (I.46) and (I.48), respectively, whose inversion leads to a set of fourteen parameters. The potential parametrization is then confronted to filters that it must pass to be considered a promising candidate. If not, the parametrization is thrown away. This operation is automatically repeated with all the possible values authorized for the parameters which are left free (as indicated by arrows on either side of the rectangle at the bottom right of the inversion procedure). At the end, two options are available. Either no parametrization is found, and the initial data needs to be slightly modified, in line with experimental or model uncertainties, so that new constraints emerge and the process can start over. Otherwise, a certain number of parametrizations can be generated,

and it is up to the user to narrow some filters or use his expertise to deduce the most interesting parametrization. This last statement is fundamental since it constitutes the phenomenological aspect of the search for a parametrization of the Gogny interaction.

We can now enumerate the parameters constituting the D1S parametrization of the analytical expression (I.22) in Table I.2. In the order of appearance are the zero-range spin–orbit ($i = 0$), finite-range central ($i \in \{1, 2\}$) and zero-range density-dependent ($i = 3$) terms.

i	μ_i (fm)	α_i	t_0 (MeVfm^4)	x_0	W_i $(-)^a$	B_i $(-)^a$	H_i $(-)^a$	M_i $(-)^a$
0					130.000			
1	0.70				−1720.300	1300.000	−1813.530	1397.600
2	1.20				103.639	−163.483	162.812	−223.934
3		1/3	1390.600	1				

[a] MeVfm^5 ($i = 0$), MeV ($i \in \{1, 2\}$).

Table I.2 – D1S parametrization.

2.3. Other D1-type parametrizations

In this subsection, we evoke the D1-type parametrizations that followed D1S. We detail a bit those of interest for the thesis, and briefly mention the others.

Parametrization D1P

The D1P parametrization, constructed by Farine *et al.* [123] was introduced in 1999 as an improvement to D1S with respect to three major points:

(i) Depth of the optical potential in agreement with experimental data to energies beyond 200 MeV;

(ii) Sum rules associated with Landau parameters less violated and some instabilities cured;

(iii) A realistic behavior of the neutron matter equation of state achieved at high densities.

Although this interaction is not often mentioned in the literature, it has the merit of introducing the need of a better reproduction of the neutron matter equation of state, that will systematically be discussed afterwards.

Parametrization D1N

One important D1-type parametrization established in 2008 as part of Chappert's thesis is the D1N interaction [17, 124]. In the 1990s technological breakthroughs led to the production of radioactive nuclear beams of exotic nuclei, opening the door to new regions of little known or unknown nuclei off the valley of stability [125]. Because no requirements on such nuclei were considered in the D1S fitting code, this parametrization failed in reproducing adequately the binding energies of exotic neutron-rich nuclei. This is peculiarly striking when the energy difference between HFB predictions and experimental values is plotted for many isotopic chains as a function of the neutron number N. In Figure I.4, we indeed observe that the energy difference blows up for D1S, at the tails of isotopic

Figure I.3 – The D1S fitting procedure. The diagram should be read from left to right, in the direction indicated by the horizontal arrows. Boxes dyed in blue correspond to processes proper to the D1S-type fitting procedure (these will be contrasted with other colors in more elaborated fitting procedures to come).

chains, corresponding to exotic nuclei with large numbers of neutrons. This observation was called the *drift* of energy (or masses) along isotopic chains.

To remedy this, a filter on the neutron matter equation of state was added to the D1S fitting procedure. Eight points of the equation of state obtained by realistic calculations of Friedman and Pandharipande [126] in neutron matter had to be reproduced, with chosen accuracies, by the interaction to pass the filter. Since the neutron density remains lower than the saturation density for atomic nuclei ρ_0, five points fixed to densities satisfying $\rho \leq \rho_0$ enabled a faithful description of nuclear structure data. On the other hand, three points at densities such that $\rho > \rho_0$ were demanded, with a view to future astrophysical applications. The resulting parametrization was dubbed D1N and its benefits appears clearly in Figure I.4. This interaction is fundamental since all its successors similarly take up a constraint on the neutron matter equation of state.

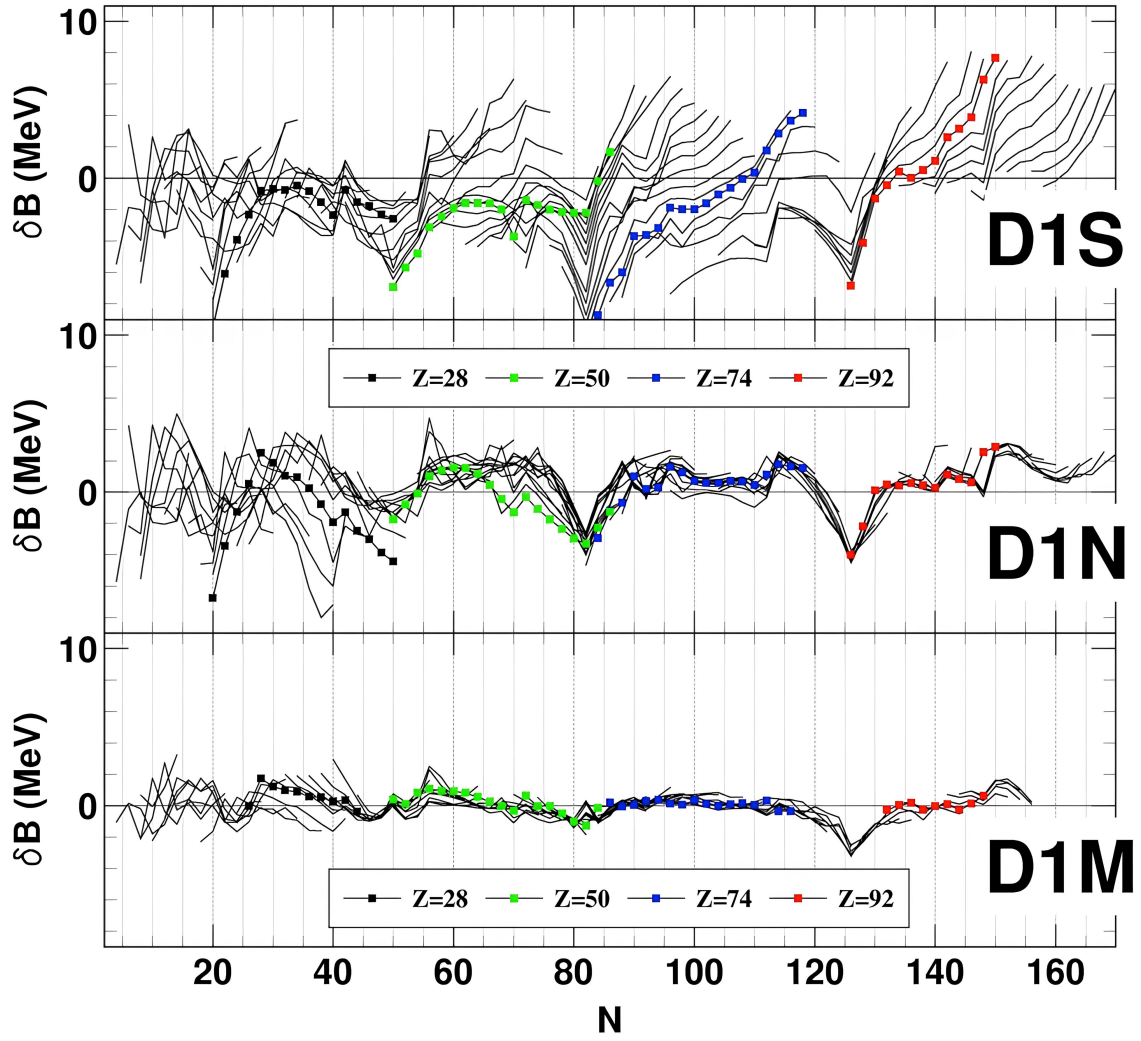

Figure I.4 – Drift of masses along isotopic chains for D1S, D1N and D1M Gogny interactions [127]. The energy difference between 5DCH and experimental masses, defined by $\delta B \equiv B_{\text{5DCH}} - B_{\text{exp}}$, is represented as a function of the neutron number N.

Parametrization D1M

Another remarkable D1-type parametrization built up by Goriely *et al.* in 2009 is the

D1M interaction [102, 127]. The main purpose of this interaction was to improve the overall reproduction of nuclear masses, while further reducing the tiny energy drift of D1N (see Figure I.4). We mention that the fitting code used to create D1M is not an extension of the fitting code we have discussed so far. It is founded on a different procedure. The masses of 2149 nuclei were calculated using a mass formula where the quadrupole collective corrections were taking into account by solving the collective Schrödinger equation with the five-dimensional collection Hamiltonian, and their differences with the experimental data minimized. Some standard physical quantities in infinite nuclear matter alike those of D1S were also included in the fit, as well as requisites to reproduce the neutron matter equation of state. With a better description of binding energies, this interaction seems more suitable than previous D1-type parametrizations for astrophysical purposes.

Parametrization D1M*

In order to enlarge predictions of the Gogny interaction to astrophysical processes, a new parametrization, modelled on D1M, was investigated by Gonzalez-Boquera and collaborators in 2018 [128]. The aim of this interaction was to preserve the finite-nuclei properties of D1M while being competitive with modern Skyrme interactions in catching the physics of neutron stars. Note that astrophysical applications are beyond the scope of this report and will consequently not be inspected.

2.4. The Gogny interaction D2

2.4.1. Analytical expression

In 2007, Chappert broke new ground by extending the expression of the original Gogny interaction, rather than looking for another D1-type parametrization [17]. The density-dependent term acquired a finite range, and the new analytical form, referred to as D2, became

$$\begin{aligned} v_{12}^{\mathrm{D2}} \equiv & \sum_{i=1}^{2}(W_i + B_i P_\sigma - H_i P_\tau - M_i P_\sigma P_\tau) V_i(r_{12}) \\ & + (W_3 + B_3 P_\sigma - H_3 P_\tau - M_3 P_\sigma P_\tau) \frac{V_3(r_{12})}{(\mu_3\sqrt{\pi})^3} \frac{\rho^\alpha(\vec{r}_1) + \rho^\alpha(\vec{r}_2)}{2} \\ & + \mathrm{i} W_0 \Big[\vec{k}' \times \delta(\vec{r}_1 - \vec{r}_2)\vec{k}\Big] \cdot (\vec{\sigma}_1 + \vec{\sigma}_2). \end{aligned} \tag{I.49}$$

The form factor associated with the finite-range density-dependent term is, like the central terms, of Gaussian shape, i.e.

$$V_j(r_{12}) \equiv \mathrm{e}^{-(\vec{r}_1 - \vec{r}_2)^2/\mu_j^2}, \quad \text{with } j \in \{1, 2, 3\}. \tag{I.50}$$

Note that the denominator $(\mu_3\sqrt{\pi})^3$ ensures that one recovers the exact zero-range density-dependent term of the original Gogny interaction by means of the formula

$$\lim_{\mu \to 0} \frac{\mathrm{e}^{-(\vec{r}_1 - \vec{r}_2)^2/\mu^2}}{(\mu\sqrt{\pi})^3} = \delta(\vec{r}_1 - \vec{r}_2). \tag{I.51}$$

According to the Pauli exclusion principle, the exchange operators must satisfy the relation $P_r P_\sigma P_\tau = -\mathbb{1}$. On the other hand, the delta function of the zero-range density-dependent term implies $P_r = \mathbb{1}$, so that $P_\sigma = -P_\tau$. This correspondence make the parameters H_3 and M_3 redundant as they act in the same (S, T) channels as the parameters W_3 and

B_3, respectively. Setting $W_3 = t_0$ and $B_3 = t_0 x_0$, we are eventually able to fall back on the zero-range density-dependent term of the original Gogny interaction (I.22). On the other hand, when the density-dependent term is of finite range, nothing can be inferred regarding P_r contrary to its zero-range counterpart (see discussion in subsection I.2.1). Such density-dependent term then contributes in all (S, T) channels, with no risks of divergences when taking into account pairing correlations (as shown in Table I.3). As for the specific form of the density dependence, it is not founded on theoretical arguments, but on numerical ones. It turns out to be the least numerically time-consuming form among the three proposals made in Chappert's thesis.

	Channels			
Terms	$(S=0,T=0)$	$(S=0,T=1)$	$(S=1,T=0)$	$(S=1,T=1)$
Central	✗	✗	✗	✗
Density-dependent	✗	✗	✗	✗
Spin–orbit				✗
Coulomb		✗		✗

Table I.3 – Decomposition of the terms involved in the D2 analytical expression according to their actions in the (S, T) channels. When a given term acts in a given channel, it is marked by a cross, otherwise its contribution is zero.

Finally, all the other terms of the new analytical expression remain those of the original Gogny interaction. Nonetheless, the fitting code also had to be prolonged to re-determine all the parameters, including the density-dependent ones, in a fully consistent way [17].

2.4.2. Fitting procedure

2.4.2.1. Constraints

With the D2 analytical form, six additional parameters, with respect to the D1 analytical expressions, $W_3, B_3, H_3, M_3, \mu_3$ and α, had to be fitted. This called for new constraints.

For the same reason as before, $\alpha = 1/3$. The range associated with the density-dependent term was set free. Just like the previous ranges, an interval of values was chosen and were only kept those generating relevant parametrizations. All in all four additional constraints were needed to completely specify the D2 interaction. Chappert initially chose to reproduce the binding energy and charge radius of another doubly magic nucleus, the ^{100}Sn, as well as two points driving the slope of the neutron matter equation of state at low densities. The reason is straight, it allowed to constrain the bulk properties of a heavier nucleus while, more importantly, avoiding the collapse of the neutron matter equation of state observed with D1S, and corrected with D1N (see previous subsection). Those constraints can be found in Chappert's thesis. They are not given here as they were ultimately not used to pull out the parametrization D2. Indeed, the inversion system proved unstable for some values of μ_3, which led to this protocol being abandoned. Instead, the four parameters W_3, B_3, H_3 and M_3 were left free to vary in definite intervals, in the manner of μ_3, and the constraints on the neutron matter equation of state was relegated to filters. No additional constraints were actually added in the fitting procedure of D2.

We are thereby simply going to show how the pre-existing constraints are modified by the presence of the finite-range density-dependent term.

According to what we have just said, the first inversion system was only supplemented by the contributions coming from the finite-range density-dependent term. The second inversion system is composed of constraints on pairing TBMEs in the $(S = 0, T = 1)$ channel as well as on the energy difference $\Delta\varepsilon$. This time, the density-dependent term brings a contribution in the $(S = 0, T = 1)$ channel and the relations (I.46) generalize to

$$\begin{aligned} V_{1s} \equiv \langle 1s\,1s|v_{12}^{\mathrm{D2}}|1s\,1s\rangle^{(S=0,T=1)} = &\sum_{i=1,2} f_{1s}^{i}(W_i - B_i - H_i + M_i) \\ &+ g_{1s}(W_3 - B_3 - H_3 + M_3), \end{aligned} \tag{I.52a}$$

$$\begin{aligned} V_{2s} \equiv \langle 2s\,2s|v_{12}^{\mathrm{D2}}|2s\,2s\rangle^{(S=0,T=1)} = &\sum_{i=1,2} f_{2s}^{i}(W_i - B_i - H_i + M_i) \\ &+ g_{2s}(W_3 - B_3 - H_3 + M_3), \end{aligned} \tag{I.52b}$$

where f_{1s}^{i} and f_{2s}^{i} (with $i \in \{1, 2\}$), proper to the central contributions, are given in (B.41), while g_{1s} and g_{2s}, evaluated numerically, account for the density-dependent ones. For the energy difference $\Delta\varepsilon$, the zero-range density-dependent component is replaced by the finite-range one, now made up of direct and exchange parts. Indeed, the constraint (I.48) becomes

$$\begin{aligned} \Delta\varepsilon = &\sum_{i=1,2} f_{\mathrm{D}}^{i}(2H_i + M_i) + f_{\mathrm{E}}^{i}(W_i + 2B_i) \\ &+ g_{\mathrm{D}}(2H_3 + M_3) + g_{\mathrm{E}}(W_3 + 2B_3), \end{aligned} \tag{I.53}$$

where the direct and exchange components of the central terms are denoted by f_{D}^{i} and f_{E}^{i} (with $i \in \{1, 2\}$), and given by (B.200), while g_{D} and g_{E} correspond to the ones associated with the density-dependent ones, computed in (B.203). As in the D1 case, the parameter B_1 was also set free.

Another important element of Chappert's work was to shed more light how the values attributed to the constraints could be defined, as we are going to show.

First system

As we have seen in the previous subsection, the binding energies and charge radii are evaluated at the HFR approximation in the fitting code. It is necessary to find a rigorous way of linking these quantities to the experimental values. Since ^{16}O and ^{90}Zr present no pairing, we can sanely state that their binding energies and charge radii evaluated at the HF approximation are nearly equal to their experimental values. To be precise, Chappert authorized an error of 1% in that reproduction. The next step was to interpret these HF values at the HFR level. To do so, several D2-type parametrizations were generated and for each of them, the binding energies and charge radii of ^{16}O and ^{90}Zr were calculated at both the HF and HFR approximations. For each nucleus, relations between the binding energies (respectively, the charge radii) evaluated at the HF and HFR approximations were established. Taking into account the errors, intervals of allowed values for the binding energies and charge radii evaluated at the HFR level were set up. For the charge radii, a final step was necessary. According to what we have said in subsection I.2.2.2, they can be related to the oscillator lengths at the HFR approximation. Thus, it is by picking up values in the intervals defined for the binding energies and oscillator lengths that Chappert was able to construct the first system.

Second system

The values assigned to the TBMEs V_{1s} and V_{2s} are based on three points. First, V_{1s} was calculated with several D2-type parametrizations, and compared to the pairing energies of ^{16}O predicted by these parametrizations at the HFB level. As the pairing has to be zero in such a closed-shell nucleus, an interval of values for V_{1s} associated with the parametrizations providing no pairing was extracted. Second, knowing that the pairing correlations influence the moment of inertia, moments of inertia of ^{158}Sm were computed with all parametrizations, still at the HFB level, and compared to the values of V_{1s}. The moment of inertia is not an observable, but it is directly related to the energy of the first 2_1^+ excited state, which is. From the corresponding experimental value, the moment of inertia of the nucleus, and subsequently the associated value of V_{1s} was deduced. By allocating an error of 10% on the experimental value, Chappert set up an interval of permissible values for the moment of inertia and therefore restrained the interval of values of V_{1s}. Third, seven values for the difference $V_{2s} - V_{1s}$ were chosen, giving rise to seven combinations of parameters $(W_1 - B_1 - H_1 + M_1)$ and $(W_2 - B_2 - H_2 + M_2)$, by inverting equations (I.52). The spatial form of the interaction in the $(S = 0, T = 1)$ channel,

$$\begin{aligned} v_{12}^{(S=0,T=1)}(r) = (W_1 - B_1 - H_1 + M_1)\mathrm{e}^{-r^2/\mu_1^2} + (W_2 - B_2 - H_2 + M_2)\mathrm{e}^{-r^2/\mu_2^2} \\ + (W_3 - B_3 - H_3 + M_3)\frac{\mathrm{e}^{-r^2/\mu_3^2}}{(\mu_3\sqrt{\pi})^3}\rho^\alpha(\vec{r}), \end{aligned} \tag{I.54}$$

was finally plotted for all parametrizations. By requiring the spatial shape of the above pairing interaction to be close to that of D1S, whose pairing properties were carefully adjusted, it was possible to uniquely determine the values of V_{1s} and V_{2s}.

Finally, the constraint on the energy difference $\Delta\varepsilon$ allows to control the isospin dependence of the interaction. When we look at the semi-empirical mass formula,

$$\mathcal{E} = a_\mathrm{V}A - a_\mathrm{S}A^{2/3} - a_\mathrm{C}\frac{Z^2}{A^{1/3}} + a_\tau\frac{(N-Z)^2}{A} + \delta(N,Z), \tag{I.55}$$

we see that the asymmetry of the nuclear system in terms of protons and neutrons is taken into account through the difference $(N - Z)^2$. For this reason, the coefficient a_τ which regulates the intensity of this contribution to the binding energy is often called the *symmetry energy*. By computing and comparing the symmetry energies a_τ and energy differences $\Delta\varepsilon$ between several D2-type parametrizations, Chappert found a linear relation linking the two quantities. As a consequence, the interval of empirical values for a_τ immediately provided an empirical interval for $\Delta\varepsilon$. To refine the value to be set to $\Delta\varepsilon$, its action on the drift of the binding energies in the tin isotopic chain was studied. Since ^{100}Sn and ^{132}Sn are both doubly magic nuclei, we expect the difference between their binding energies evaluated at the HFB level and experimentally to be the same, i.e.

$$\mathcal{E}_\mathrm{HFB}\left[^{100}\mathrm{Sn}\right] - \mathcal{E}_\mathrm{exp}\left[^{100}\mathrm{Sn}\right] = \mathcal{E}_\mathrm{HFB}\left[^{132}\mathrm{Sn}\right] - \mathcal{E}_\mathrm{exp}\left[^{132}\mathrm{Sn}\right]. \tag{I.56}$$

This requirement obviously depends on the isospin characteristics of the interaction as ^{100}Sn and ^{132}Sn isotopes evince strong differences $(N-Z)$. Indeed, Chappert showed that $\Delta\varepsilon$ had to be chosen with high precision to avoid any drift in the tin isotopic chain, that is for the above relation to hold.

2.4.2.2. Filters

Regarding the filters in infinite nuclear matter, those of the D1S interaction were kept and the zero-range density-dependent contributions replaced by the finite-range ones.

These contributions to the standard physical quantities and to the Landau parameters are reported in Appendix A for clarity.

On top of that, a filter on the neutron matter equation of state, already implemented in the fitting code of D1N and discussed in the previous subsection, was considered. As before, the main purpose of it was to cure the mass drift observed with D1S.

2.4.2.3. Extraction of the parametrization D2

As shown in Figure I.5, the scheme of the D2 fitting procedure is analogous to that of the D1-type version, with an additional filter on the neutron matter equation of state. We dye in green processes proper to the D2 fitting code or at least notably enhanced with respect to that of the D1S parametrization, and in blue the steps already implemented in the D1S fitting code. Obviously, all the constraints and filters had to trade their zero-range density-dependent component for a finite range one. The two interdependent systems were here constructed from (I.44), and (I.52) and (I.53), respectively. We remind that the parameters of this new term, W_3, B_3, H_3, M_3 and μ_3, were all set free (as indicated by arrows on either side of the rectangle at the right of the inversion procedure). Precisions on the way the initial data are obtained were also unveiled. To constrain the values of V_{1s} and V_{2s}, it was asked for:

(i) no pairing in ^{16}O;

(ii) the reproduction of the moment of inertia, deduced from the experimental value of its 2_1^+ first excited state, with an accuracy of 10%;

(iii) a spatial shape of the pairing interaction similar to that of D1S.

As for the value assigned to $\Delta\varepsilon$, the requirements were:

(i) a symmetry energy falling in the empirical values;

(ii) no energy drift in the tin isotopic chain, between isotopes ^{100}Sn and ^{132}Sn.

These modifications we have summed up, connected with the D1-type fitting procedure, make up the D2 fitting code, at the origin of the D2 parametrization (a set of sixteen parameters).

We can now enumerate the parameters constituting the D2 parametrization [9] of the analytical expression (I.49) in Table I.4. In the order of appearance are the zero-range spin–orbit ($i = 0$), finite-range central ($i \in \{1, 2\}$) and finite-range density-dependent ($i = 3$) terms.

i	μ_i (fm)	α_i	W_i (–)[a]	B_i (–)[a]	H_i (–)[a]	M_i (–)[a]
0			130.000			
1	0.80		−1176.440	800.000	−927.366	1115.573
2	1.30		93.741	−161.161	122.414	−223.859
3	0.60	1/3	1800.000	600.000	400.000	−600.000

[a] MeVfm^5 ($i = 0$), MeV ($i \in \{1, 2\}$), MeVfm^4 ($i = 3$).

Table I.4 – D2 parametrization.

9. In Chappert's thesis, two candidates for the D2 interaction, dubbed D2A and D2B, are compared. The final D2 parametrization we discuss here corresponds to D2B.

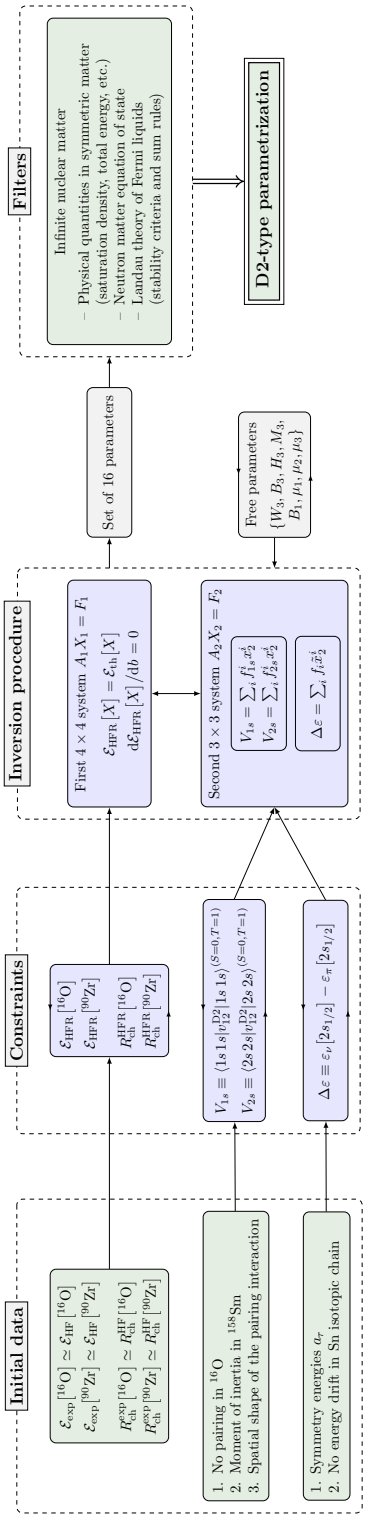

Figure I.5 – The D2 fitting procedure. Boxes colored in blue and green correspond to steps primarily enhances by the D1S and D2 extensions, respectively.

2.5. Other analytical forms

2.5.1. Tensor-dependent interactions

In this subsection, we list the attempts made to incorporate a tensor force in the Gogny interaction. Some of them will indeed be useful in the search and analysis of our own tensor-dependent interaction.

Parametrization GT2

Otsuka *et al.* [58] were the first to introduce in 2006 a tensor term in the Gogny interaction. Basically, they took the D1 analytical expression (I.22) and supplemented it by an isospin-dependent tensor force with a Gaussian shape of the form [10]

$$v_{12}^{\mathrm{T}} = W_{\mathrm{T}}(\vec{\tau}_1 \cdot \vec{\tau}_2)\widetilde{S}_{12}\,\mathrm{e}^{-(\vec{r}_1-\vec{r}_2)^2/\mu_{\mathrm{T}}^2}, \tag{I.57}$$

where their tensor operator is defined as

$$\widetilde{S}_{12} \equiv 3(\vec{\sigma}_1 \cdot \hat{r}_{12})(\vec{\sigma}_2 \cdot \hat{r}_{12}) - \vec{\sigma}_1 \cdot \vec{\sigma}_2. \tag{I.58}$$

All the parameters (including the spin–orbit one) were refitted in a fully consistent way, based on five requirements:

(i) reproduction of the saturation point of D1S in symmetric nuclear matter;

(ii) an incompressibility within empirical values in symmetric nuclear matter;

(iii) binding energies of ^{16}O, ^{40}Ca, ^{48}Ca, ^{56}Ni, ^{132}Sn and ^{132}Sn reproduced with an accuracy of about 1% at the HF level;

(iv) the part of the central terms proportional to $(\vec{\sigma}_1 \cdot \vec{\sigma}_2)(\vec{\tau}_1 \cdot \vec{\tau}_2)$ showing a positive overall strength;

(v) strength W_{T} such that the volume integral of the Gaussian form factor is equal to that of the AV8' potential [129].

Additionally, the range of the tensor force was chosen to be equal to the longest range of the central part of the D1S interaction, namely $\mu_{\mathrm{T}} = 1.2\,\mathrm{fm}$. The corresponding parametrization, named GT2, was only tested regarding its predictions on the single-particle energies at the HF approximation. To our knowledge, there have been no subsequent studies to probe its pairing or beyond mean-field properties.

Parametrizations D1SV8, D1MV8, D1ST and D1MT

Five years later, Co' *et al.* [59] also added an isospin-dependent tensor force on top of the D1 analytical expression of the form

$$v_{12}^{\mathrm{T}} = v_{\mathrm{AV8'}}^{\tau}(r)\left(1 - \mathrm{e}^{-br^2}\right). \tag{I.59}$$

The tensor-isospin dependence is fully contained in the tensor-isospin term of the Argonne V8' potential, denoted as $v_{\mathrm{AV8'}}^{\tau}(r)$ [129]. It is multiplied by a function which incorporates the effects of the short-range correlations [130]. The authors looked at the excitation spectra to target observables particularly sensitive to the tensor force. They found out that the excitation energies of the 0^- levels were good candidates and accordingly fitted

10. Actually the notations used in the article are a bit different, but equivalent to those which are more convenient to be compared with the other tensor-dependent interactions.

the free parameter b, which calibrates the strength of the tensor term, so as to reproduce the first 0^- excited state in ^{16}O. To be precise, they first made HF calculations starting from D1S and D1M parametrizations with no tensor forces to produce the wave functions and SPEs. Then, they switch on the tensor forces in RPA calculations and selected the value of b which reproduced the experimental energy of the 0^- state in ^{16}O. Finally, they evaluated the wave functions and SPEs again with the new interactions and tuned the spin–orbit parameter to find back the neutron $(1p_{3/2} - 1p_{1/2})$ splitting in ^{16}O. New RPA calculations followed and the procedure was repeated until convergence. The outcoming parametrizations were respectively labelled D1SV8 and D1MV8.

We emphasize that this fitting procedure is fundamentally different from that used to elaborate GT2 in the sense that the D1S and D1M parametrizations were kept like they were and the tensor forces (as well as the spin–orbit force) were adjusted aside, on separate observables. We will often say in this situation that the tensor force is adjusted *separately* or *perturbatively*. This is exactly what was already done for the spin–orbit term in the original Skyrme and Gogny interactions. This approach offers the advantage of isolating the effects produced by the term fitted perturbatively (when compared to the primary parametrization), but it is incomplete since each term composing the interaction participates in reproducing the observables. As a consequence, a single-term contribution may be *rearranged* (or *renormalized*) by the contributions of all the other terms.

This fitting process was rapidly taken up step by step by Anguiano *et al.* [29] with the isospin-dependent Argonne V18 potential [27] in place of the V8' version, to build up a tensor force of the form

$$v_{12}^{\mathrm{T}} = v_{\mathrm{AV18}}^{\tau}(r)\left(1 - \mathrm{e}^{-br^2}\right), \tag{I.60}$$

and generated the D1ST and D1MT parametrizations from the tensor-free D1S and D1M interactions.

Parametrizations D1ST2a, D1ST2b and D1ST2c

In 2012, Anguiano *et al.* [60] realized that the expression of the tensor force (I.60) was not general enough to describe both proton–neutron and particle-like tensor effects. They studied the $N = 28$ neutron energy gap, i.e. the energy difference between the neutron $2p_{3/2}$ and $1f_{7/2}$ levels, which is experimentally known to increase when going from ^{40}Ca to ^{48}Ca [131]. This phenomenon is often attributed to the tensor force. Indeed, according to Otsuka's picture (see subsection III.2), the tensor has (almost) no effect on the SPEs of ^{40}Ca as it is both proton and neutron spin-saturated, while it does on those of ^{48}Ca (through a particle-like component) as it is only spin-saturated in protons. Practically, whereas the SLy5 Skyrme interaction predicts an energy decrease in the $N = 28$ gap, the same interaction supplemented by a tensor force managed to reverse this behavior, to recover the trend evidenced by experimental data [48]. With D1S, the neutron $2p_{3/2} - 1f_{7/2}$ gap also moves in the wrong direction but the D1ST interaction worsens the predictions by diminishing even more the energy of the $N = 28$ neutron gap. The pathology can of course be cured by modifying the sign of the strength of the tensor term, but this would alter the nuclear properties which are well described by the D1ST interaction (like the 0^- excitation energy of ^{16}O on which it was adjusted). In order to cope with this issue, the analytical expression of the tensor force was extended in a formulation identical to that

introduced by Onishi and Negele [57]

$$v_{12}^{\mathrm{T}} = (V_{\mathrm{T}1} + V_{\mathrm{T}2}P_\tau)\,\mathrm{e}^{-(\vec{r}_1-\vec{r}_2)^2/\mu_{\mathrm{T}}^2}\widetilde{S}_{12} \tag{I.61}$$
$$= \left[\left(V_{\mathrm{T}1} + \frac{V_{\mathrm{T}2}}{2}\right) + \frac{V_{\mathrm{T}2}}{2}\vec{\tau}_1\cdot\vec{\tau}_2\right]\mathrm{e}^{-(\vec{r}_1-\vec{r}_2)^2/\mu_{\mathrm{T}}^2}\widetilde{S}_{12},$$

with the expression (D.8b) of the isospin-exchange operator P_τ implying the second line where the tensor term splits up into pure and isospin-dependent components. The authors being focused on even–even nuclei, they know that the direct component of the HF tensor field is zero (as we show in the appendices when it comes to the tensor force). The exchange tensor field then involves TBMEs whose isospin part reads [38]

$$\langle t_a t_b|(V_{\mathrm{T}1} + V_{\mathrm{T}2}P_\tau)|t_b t_a\rangle = (V_{\mathrm{T}1} + V_{\mathrm{T}2})\delta_{t_a t_b} + V_{\mathrm{T}2}\delta_{t_a,-t_b}. \tag{I.62}$$

This shows that the strength of the tensor interaction acting between particle-like pairs is given by the sum $V_{\mathrm{T}1}+V_{\mathrm{T}2}$, and by $V_{\mathrm{T}2}$ between protons and neutrons, for even-even nuclei. Thus, the combination $V_{\mathrm{T}1}+V_{\mathrm{T}2}$ was fitted on a particle-like property, the energy difference between the neutron $1f_{5/2}$ and $1f_{7/2}$ states in ^{48}Ca, evaluated at the HF approximation and compared to the experimental value [132]. As for the parameter $V_{\mathrm{T}2}$, directly related to the isospin-dependent component of the tensor force, it was chosen so as to reproduce the 0^- excitation energy of ^{16}O. By the way the adjustment was performed according to the iterative procedure of Co' *et al.* detailed for the previous parametrizations. The parameter of the spin–orbit parameter remains that of the D1S parametrization, and it is the particle-like part of the tensor term, as described above, that is fitted on SPEs, though. This parametrization was dubbed D1ST2a. Another parametrization, where the particle-like part rather had to reproduce the $N = 28$ neutron gap increase was also set up, and referred to as D1ST2b. On the other hand, the tensor range was chosen to be that of the longest central part of D1S, as for GT2, namely $\mu_{\mathrm{T}} = 1.2\,\mathrm{fm}$.

Finally, Anguiano and Grasso [61] built up another parametrization for which the spin–orbit and tensor parameters were *jointly* adjusted so as to reproduce the neutron single-particle energies of three doubly-magic nuclei: ^{40}Ca, ^{48}Ca and ^{56}Ni. This procedure, already employed for other interactions [49, 50], is clever as we know the spin–orbit and tensor interactions to produce fine effects on SPEs, that either tend to add to or cancel each other out, depending on the energy spectra. Technically, the splitting of ^{40}Ca is first reproduced. According to Ostuka's picture (see section III.2), the tensor force has no effects because the spin partners are completely filled, so that the spin–orbit parameter W_0 can be tuned to match alone the experimental value. Then, keeping the new value for the spin–orbit parameter, the splitting of ^{48}Ca is analyzed. This nucleus is spin-saturated in protons, but not in neutrons, so that the tensor shows a particle-like (neutron–neutron) contribution. Since W_0 is fixed, only the particle-like tensor strength $V_{\mathrm{T}1}+V_{\mathrm{T}2}$ is adjusted to recover the experimental value. Finally, the remaining proton–neutron tensor intensity is modulated on the experimental splitting of ^{56}Ni, a spin-unsaturated nucleus, with W_0 and $V_{\mathrm{T}1}+V_{\mathrm{T}2}$ fixed above. It is worth noting that a maximum action of the tensor force is guaranteed in ^{48}Ca (for the particle-like contribution) as $(1f_{7/2})_\nu$ is full and $(1f_{5/2})_\nu$ empty, and in ^{56}Ni (for the proton–neutron contribution) as $(1f_{7/2})_\pi$ is full and $(1f_{5/2})_\pi$ empty (see section III.2). The tensor range is the same as the other D1ST2 versions. This parametrization was labelled D1ST2c.

The D1ST2a parametrization has the advantage of dissociating the tensor effects from those proper to D1S, while the D1ST2c features a fitting protocol that we will (partly) draw on to build up our tensor-dependent interaction. For these reasons, it will be useful to have their parametrizations at hand, which we then record in Table I.5.

Interaction	W_0 (MeVfm^5)	μ_T (fm)	V_{T1} (MeV)	V_{T2} (MeV)
D1ST2a	130	1.2	−135	115
D1ST2c	103	1.2	−135	60

Table I.5 – Spin–orbit and tensor parameters of the perturbative D1ST2a and D1ST2c parametrizations. The central and density-dependent parameters are those of the D1S parametrization, shown in Table I.2.

2.5.2. Three central terms

Lastly, we discuss another very recent analytical extension of the original Gogny interaction, the D3G3 force [133]. In this interaction is added a third Gaussian central term [134], i.e. the form (I.22) remains the same, but the index i now runs from 1 to 3. Two main objectives led to the development of D3G3:

(i) A more faithful reproduction of physical quantities in infinite nuclear matter for astrophysical applications;

(ii) A physical determination of Gaussian ranges.

It is argued that the third central term offers more latitude, that may improve the predictions in nuclear matter, at minimal cost. Indeed, adding an extra central term does not require the analytical derivations and numerical implementation of new terms, as it is the case for D2 and tensor-dependent extensions. The D3G3 interaction was fully refitted from nuclear matter data, some of them being similar to those of D1S (standard quantities as displayed in Table II.4) and neutron matter equation of state), as well as finite-nuclei quantities and observables (binding energies of ^{48}Ca, ^{56}Ni and ^{208}Pb at the HFR level, and pairing TBMEs of $1s$ and $2s$ states in ^{16}O at the HF approximation) [135]. The fitting protocol is, however, different from ours involving the inversion of a system, and relies on an extension of the D1M fitting code. Here the parameters are deduced from a minimization procedure. Selected physical quantities are evaluated at each iteration for a new set of parameters. If a parameter set reproduces these quantities better overall than the previous one (i.e. if its χ^2 is lower), then it is retained, otherwise the previous parameter set instead is. The procedure is repeated a large number of times by exploring the parameter space until some minimum value of χ^2 is reached. As the space of parameters is infinite, the initial values of the parameters entered by the user, from which the space of parameters is traversed, is crucial to determine a reliable parametrization in a reasonable time. Thus, the authors tried to bring more physical insight in the way the central ranges are chosen. In the philosophy of the M3Y interaction, they determined the central ranges as if the force originated from the exchange of mesons between nucleons, as described in OBE models. Contrary to the M3Y interaction, the form factors are Gaussian but not Yukawa. They accordingly adapted the ranges so that the Gaussian form factors reproduced the same physics as the Yukawa ones in infinite nuclear matter. They did so with the short, medium and long ranges respectively accounting for the ρ, σ and π meson exchanges. These ranges served as starting parameters in the fitting procedure which, after minimization of χ^2, resulted in the D3G3 interaction.

The principal parametrizations of the Gogny interaction discussed in this chapter are placed on the timeline of Figure I.6.

Figure I.6 – Timeline of the main effective nuclear interactions (upper part) and parametrizations of the Gogny interaction (lower part).

Chapter II

The generalized Gogny interaction

> « Au centre de cette nébuleuse, quatorze cent mille fois plus considérable que ce globe qu'elle va former un jour, je suis entraîné dans les espaces planétaires ! Mon corps se subtilise, se sublime à son tour et se mélange comme un atome impondérable à ces immenses vapeurs qui tracent dans l'infini leur orbite enflammée ! »
>
> — Jules Verne, *Voyage au centre de la Terre*

In this chapter, we propose an extension of the effective Gogny interaction, hereafter called the "generalized Gogny interaction". Our starting point is an augmented analytical expression introducing new parameters that are determined phenomenologically, with data drawn from models or directly from experiment. The construction of such an interaction is described in great details, both in terms of its theoretical foundations and the numerical challenges raised. The generalized Gogny interaction is finally put to the test in infinite nuclear matter, a simple framework whose key features makes it possible to discriminate between promising sets of parameters.

Chapter contents

1. Construction of the generalized Gogny interaction

1.1. Analytical expression

In order to construct what we are going to call the "generalized Gogny interaction", we take the analytical form of the D2 interaction (I.49), and we extend it by promoting the spin–orbit term to a finite range and by adding a finite-range tensor term. This generalized Gogny interaction has the following "DG" [1] analytical expression,

$$\begin{aligned} v_{12}^{\mathrm{DG}} \equiv & \sum_{i=1}^{2}(W_i + B_i P_\sigma - H_i P_\tau - M_i P_\sigma P_\tau) V_i(r_{12}) \\ & + (W_3 + B_3 P_\sigma - H_3 P_\tau - M_3 P_\sigma P_\tau) \frac{V_3(r_{12})}{(\mu_3\sqrt{\pi})^3} \frac{\rho^\alpha(\vec{r}_1) + \rho^\alpha(\vec{r}_2)}{2} \\ & + B(\mu_5)(W_5 - H_5 P_\tau) V_5(r_{12})\, \vec{L}\cdot\vec{S} \\ & + (W_7 - H_7 P_\tau) V_7(r_{12})\, S_{12}. \end{aligned} \tag{II.1}$$

We identify, in the order of appearance, the central, density-dependent, spin–orbit and tensor terms. The central and density-dependent terms are identical in every respect to those of the D2 interaction. No additional density dependence have been added to the other terms. All the potentials are chosen to be Gaussian form factors reading

$$V_j(r_{12}) \equiv \mathrm{e}^{-(\vec{r}_1-\vec{r}_2)^2/\mu_j^2}, \quad \text{with } j \in \{1,2,3,5,7\}, \tag{II.2}$$

where μ_j is the range of the associated term, with the relative distance between the two nucleons given by $\vec{r}_{12} \equiv \vec{r}_1 - \vec{r}_2$. By essence, the DG Gogny interaction is a *fully finite-range* interaction. As exposed in the previous chapter, this guarantees that no divergences appear when going beyond the mean field.

The *finite-range* spin–orbit force is identified by its spin–orbit operator $\vec{L}\cdot\vec{S}$ composed of a total intrinsic momentum

$$\vec{S} \equiv \frac{\vec{\sigma}_1 + \vec{\sigma}_2}{2}, \tag{II.3}$$

and a total relative orbital momentum

$$\vec{L} \equiv \vec{r}_{12} \times \vec{p}_{12}, \tag{II.4}$$

where the relative momentum of the two-nucleon system is

$$\vec{p}_{12} = \frac{\vec{p}_1 - \vec{p}_2}{2}, \tag{II.5}$$

with

$$\vec{p}_i \equiv -\mathrm{i}\vec{\nabla}_i, \tag{II.6}$$

1. For "D generalized".

the momentum of the particle $i \in \{1,2\}$. Note that the gradient operator $\vec{\nabla}_i$ acts on the spatial degrees of freedom $\vec{r}_i$ of the particle i. The coefficient

$$B(\mu) \equiv -\frac{4}{\mu^2}\frac{1}{(\mu\sqrt{\pi})^3} \tag{II.7}$$

ensures that one recovers the exact zero-range spin–orbit term of the original Gogny interaction at the zero-range limit (i.e. when $\mu_5 \to 0$), as it is shown in appendix D.5.1. The spin–orbit term involves the simple admixture of parameters $(W_5 - H_5 P_\tau)$. The justification is trivial since, according to its definition (II.3), the operator $\vec{S}$ acts symmetrically on the spin degrees of freedom, so that we have, for some two-body state,

$$\vec{S}P_\sigma|\vec{r}_1 s_1 t_1\ \vec{r}_2 s_2 t_2\rangle = \vec{S}|\vec{r}_1 s_2 t_1\ \vec{r}_2 s_1 t_2\rangle = \vec{S}|\vec{r}_1 s_1 t_1\ \vec{r}_2 s_2 t_2\rangle, \tag{II.8}$$

where $\vec{r}_i$, s_i and t_i respectively denote the space, spin and isospin degrees of freedom of the particle i ($i \in \{1,2\}$). The spin exchange operator is then irrelevant when evaluating two-body matrix elements of the spin–orbit force ($P_\sigma = \mathbb{1}$), hence its combination of parameters. Equivalently, the spin–orbit term only contributes to the $S = 1$ channel of the interaction (see relation (D.11a)). Thus, in addition to its finite range, the spin–orbit force of the DG interaction presents an isospin-dependent component.

The *finite-range* tensor force is made up of the tensor operator S_{12}, for which we have conventionally chosen the expression [2]

$$S_{12} \equiv (\vec{\sigma}_1 \cdot \hat{r}_{12})(\vec{\sigma}_2 \cdot \hat{r}_{12}) - \frac{1}{3}\vec{\sigma}_1 \cdot \vec{\sigma}_2, \tag{II.9}$$

where the quantities $\vec{\sigma}_1$ and $\vec{\sigma}_2$ denote the Pauli matrices associated with each of the two particles, and where $\hat{r}_{12}$ corresponds to the unit vector

$$\hat{r}_{12} \equiv \frac{\vec{r}_{12}}{|\vec{r}_{12}|}. \tag{II.10}$$

The tensor force depends on an admixture of parameters of the same type as the spin–orbit term, namely $(W_7 - H_7 P_\tau)$. The reason is similar, and can be demonstrated following (II.8), because the tensor operator acts symmetrically on the spin degrees of freedom as well. The spin exchange operator is also irrelevant for the tensor force ($P_\sigma = \mathbb{1}$), which, in turn, only contributes to the $S = 1$ channel of the interaction. In addition to its finite range, the tensor force of the DG interaction presents an isospin-dependent component. Unlike the spin–orbit term, though, it does not have a global multiplicative factor, since there is no zero-range tensor term in the Gogny interaction to be recovered at the zero-range limit. We summarize the contributions of the different terms of the DG analytical form to the (S,T) channels in Table II.1. The contributions should be compared with those of D1 (Table I.1) and D2 (Table I.3) cases, to see the leeway brought by the DG analytical expression. The terms of DG act in *all* the (S,T) channels in which they are able to act.

One strength of the DG analytical form is that most existing analytical expressions of the Gogny interaction can be obtained from it. To recover D1, if it enough to switch off the tensor interaction ($W_7 = H_7 = 0$) and to take the limits $\mu_3 \to 0$ and $\mu_5 \to 0$, and only $\mu_5 \to 0$ to fall back on D2. For D1ST2-type forms, the same transformations must

2. In fact, we chose this convention as it allows us to avoid carrying around a factor 3 in our calculations, given the equivalent expression for the tensor operator (D.58).

	Channels			
	$(S=0,T=0)$	$(S=0,T=1)$	$(S=1,T=0)$	$(S=1,T=1)$
Terms				
Central	✗	✗	✗	✗
Density-dependent	✗	✗	✗	✗
Spin–orbit			✗	✗
Tensor			✗	✗
Coulomb		✗		✗

Table II.1 – Decomposition of the terms involved in the D2 analytical expression according to their actions in the (S,T) channels. When a given term acts in a given channel, it is marked by a cross, otherwise its contribution is zero.

be performed, and the conventions for the tensor operators, linked by a simple factor 3, adapted (as explained in the next subsection). Finally, even D3G3 is easily reachable with the same limits, and if we set in addition $\alpha = 0$ in the second density-dependent term of the fitting code (see next paragraph), redefining the parameters taking into account the constant $(\mu\sqrt{\pi})^3$. It is in that sense that our Gogny interaction is *generalized*.

All the other quantities appearing in the DG analytical expression were defined in the previous chapter, in section I.2, to which we refer the reader if necessary. The indices allotted to the parameters of the various terms may seem odd. Actually the fitting code was generalized to handle up to two density-dependent, two spin–orbit and two tensor terms. Then, the indices $4, 6$ and 8 are already attached to the second density-dependent, spin–orbit and tensor terms, respectively. In case the reader has to deal with the fitting code at some point, we have chosen to keep these notations. Finally, we will drop the superscript "DG" since the interaction we will be working with by default throughout the thesis will obviously be the generalized Gogny interaction.

1.2. Fitting procedure

In this subsection, we develop the procedure leading to the DG parametrization we have selected. Our aim was to generate an interaction that retained the reliable properties of D1S and D2 while improving those we had targeted. To achieve this, we kept close to the D2 parametrization. It does not mean the parameters of the spin–orbit and tensor forces are determined separately from the other parameters; the interaction is entirely refitted, but looked for in a region of central and density-dependent properties close to those of the D2 interaction.

1.2.1. Ranges

We first want to motivate, from theoretical arguments, our choice for the values of the spin–orbit μ_5 and tensor μ_7 ranges. As we have outlined in the previous chapter, Yukawa introduced a model to explain the long-range behavior of the nuclear interaction in terms of exchanges of a massive particle, the pion [64]. The great success of this approach pushed physicists in the 1960s to extend this idea to other kind of then recently-discovered boson particles. This led to the one-boson-exchange (OBE) models, which proved to be very successful in accounting for the two-nucleon interaction. Within these models, it can

be shown that essentially four bosons, the ω, ρ, σ and π mesons, are needed to describe the short, medium and long parts of the interaction [136]. By means of Lagrangians and rules on Feynman diagrams translating the interaction between nucleons and mesons, it is then possible to obtain the potential created through their interaction [73]. In particular, the potentials involve some of the central, tensor, spin–orbit and quadratic spin–orbit components of the bare interaction we have established in (I.14). The main contribution of the tensor force, already inferred by Yukawa, turns out to be in the so-called one-pion-exchange potential (OPEP),

$$V_\pi(\vec{k}) = -\frac{f_\pi^2}{3m_\pi^2}\frac{k^2}{k^2+m_\pi^2}\left[\widetilde{S}_{12}(\hat{k}) + \vec{\sigma}_1\cdot\vec{\sigma}_2\right]\vec{\tau}_1\cdot\vec{\tau}_2, \tag{II.11}$$

where m_π is the mass of the pion, f_π its coupling constant to a nucleon and $\widetilde{S}_{12}(\hat{k})$ the tensor operator in momentum space. We see there are two components, one proportional to $\vec{\sigma}_1\cdot\vec{\sigma}_2$, which is a central term, another one to the tensor operator, which is the most important contribution of the tensor force to the bare interaction. The same study can be carried out for the spin–orbit force. The main contribution of this latter is contained in the one-omega-exchange potential, whose dominant terms read

$$V_\omega(\vec{k}) \simeq \frac{g_\omega^2}{k^2+m_\omega^2}\left[1 - 3\frac{\vec{L}\cdot\vec{S}}{2M^2}\right], \tag{II.12}$$

where M is the mass of a nucleon, m_ω the mass of the meson omega, g_ω its coupling constant [3] to a nucleon and $\vec{L}\cdot\vec{S}$ the spin–orbit operator. Once again, two components pop up, one proportional to 1, which is a central term, another one to the spin–orbit operator, which is the most important contribution of the spin–orbit force to the bare interaction. An important point lies in that these momentum-space potentials can be Fourier transformed to be expressed in position space as

$$\begin{aligned} V_\pi(\vec{r}) = \frac{f_\pi^2 m_\pi}{12\pi}\Bigg[&\left(1+\frac{3}{m_\pi r}+\frac{3}{(m_\pi r)^2}\right)\frac{\mathrm{e}^{-m_\pi r}}{m_\pi r}\widetilde{S}_{12}(\hat{r}) \\ &+\left(\frac{\mathrm{e}^{-m_\pi r}}{m_\pi r} - \frac{4\pi}{m_\pi^3}\delta(\vec{r})\right)\vec{\sigma}_1\cdot\vec{\sigma}_2\Bigg]\vec{\tau}_1\cdot\vec{\tau}_2, \end{aligned} \tag{II.13a}$$

$$V_\omega(\vec{r}) = \frac{g_\omega^2 m_\omega}{4\pi}\left[\frac{\mathrm{e}^{-m_\omega r}}{m_\omega r} - 3\frac{m_\omega^2}{2M^2}\left(\frac{1}{m_\omega r}+\frac{1}{(m_\omega r)^2}\right)\frac{\mathrm{e}^{-m_\omega r}}{m_\omega r}\vec{L}\cdot\vec{S}\right], \tag{II.13b}$$

where the tensor operator $\widetilde{S}_{12}(\hat{r})$ is now defined in position space, and where Yukawa form factors e^{-mr}/mr appear. The fundamental tour de force made by Yukawa for the OPEP and then extended in OBE potentials, is to identify the range μ of the meson–nucleon potential with the Compton wavelength of the meson according to

$$\mu = \frac{\hbar}{mc}. \tag{II.14}$$

From the experimental masses of pion $m_\pi = 138\,\mathrm{MeV}$ and meson omega $m_\omega = 782\,\mathrm{MeV}$, we can then deduce the ranges of the (main contributions) of the tensor and spin–orbit

3. The vector and tensor couplings appearing in the Lagrangians give rise to different coupling constants, respectively denoted by f and g.

forces in the OBE model. We obtain $\mu_\pi \simeq 1.43\,\text{fm}$ and $\mu_\omega \simeq 0.25\,\text{fm}$. The tensor force plays a major role in the *long-range region* whereas the spin–orbit force principally acts in the *short-range region* of the nucleon–nucleon interaction.

We would like to take into account these considerations when selecting our tensor and spin–orbit ranges. Two remarks are in order. First, we have detailed above how to extract the ranges of the tensor and spin–orbit forces for a *bare* interaction, while the Gogny interaction is *effective*. Actually, we have underlined in the previous chapter that the Gogny interaction is expected to retain signatures of the bare interaction. It is therefore not absurd to say that short- and long-range effects specific to the spin–orbit and tensor terms should also persist in the effective Gogny interaction. Second, the ranges have been derived from Yukawa form factors, while the Gogny interaction involves Gaussian form factors of the type (II.2). The ranges calculated above cannot therefore be taken for granted.

To see things more clearly, let us go back to the GPT interaction we have mentioned in the previous chapter [118]. Even if GPT is a realistic interaction, it is on its fitting procedure that Gogny based the construction of the effective interaction we are dealing with. It can then be insightful to look at the values picked up for the tensor and spin–orbit ranges which are of Gaussian shapes in GPT. For the tensor terms, two ranges of 1.539 fm and 1.687 fm were obtained, compared to 0.6718 fm and 0.9296 fm for the two spin–orbit terms. The values are of the same orders of magnitude than those deduced from the OBE models, although slightly higher, certainly due to the different kinds of form factors. Thus, assuming that the effective interaction keeps a remnant of the bare interaction, we may choose tensor and spin–orbit ranges similar to those of the GPT interaction. Actually, we could go a step further and find out what ranges should be assigned to the Gaussian form factors so that they equal the corresponding Yukawa form factors, for each range μ_π and μ_ω, at some definite distance. This is the way the central ranges of the D3G3 interaction were evaluated in nuclear matter [133] (see subsection I.2.5.2). Nevertheless, we bear in mind that Yukawa's theory and its extensions are *models*, and we do not want to be too restrictive in the way we determine the ranges. We will accordingly limit ourselves to stating that the spin–orbit force must exhibit a short range so that $\mu_5 \in [0.1, 1.0]\,\text{fm}$, and the tensor force a long range such that $\mu_7 \in [1.0, 2.0]\,\text{fm}$.

We finish by noting that a moderate short- to medium-range component of the bare interaction is also often attributed to the tensor force (which is traduced by the exchange of a meson ρ in OBE models). On the other hand, it has been known for years that a density-dependent potential can simulate a tensor force [62, 63]. Since the density-dependent term is more significant within the core of a nucleus than at its surface, there is reason to think that the *short-* to *medium*-range of the tensor force can be absorbed in a density-dependent potential. The D2 interaction from which the DG interaction is built up already has a density-dependent term with a medium range $\mu_3 = 0.6\,\text{fm}$. We consider that at least part of the moderate component of the tensor force is renormalized in this density-dependent term. The remaining part, if it exists, is probably negligible compared with the dominant long-range component that we propose to add in the following.

1.2.2. Constraints

Let us start by looking at how the constraints already present in the fitting procedure of D2, detailed in subsection I.2.4.2.1, are modified by the introduction of one finite-range spin–orbit interaction and one finite-range tensor interaction. The HFR binding energies and charge radii remain the same. Indeed, we show in subsections B.4.2.3 and

B.4.2.4 that these terms do not contribute to the potential energy in our formalism, at the HFR approximation. However, we could establish a direct connection between binding energies (as well as charge radii) at HFR and HF (or HFB) approximations so as to bring out a range of values authorized at the HFR approximation, as Chappert did with D2 (see previous chapter). In practice, this is hard to set up because, contrary to the D2 interaction, the spin–orbit intensity is not fixed (nor can it be, because of the interdependence of the systems, as we shall soon see), and in any case, we have succeeded without invoking such procedure. We then barely allow the binding energies and charge radii to be chosen within the intervals deduced for D2. The constraints on the two-body matrix elements (TBMEs) of the $1s$ and $2s$ states in the $(S = 0, T = 1)$ channel are not changed either. This is a direct consequence of the fact that the spin–orbit and tensor interactions only act on $S = 1$ states. Finally, the tensor component of the energy difference $\Delta\varepsilon$ is zero (see subsection B.6.3) whereas, although neglected in the D1S and D2 fitting procedures, the spin–orbit component is not (see subsection B.6.4). We will not try to evaluate it, but we will gently vary the overall value of $\Delta\varepsilon$ when necessary.

In addition to the ranges, the newly introduced spin–orbit and tensor terms come with four parameters, two for the spin–orbit force, W_5 and H_5, and two for the tensor force, W_7 and H_7, that must be determined. The simplest and most efficient way to do so is to construct a system consisting of four linearly independent equations involving those parameters. On the other hand, we would like this system to constrain the parameters from physical grounds, and more specifically from physical quantities that could improve the predictions of the former Gogny interactions. We know the D1S and D2 parametrizations to be fairly good in describing the particle-like pairing. This is not surprising since particle-like pairing TBMEs were constrained in the D1S and D2 fitting procedure for that purpose (see equations (I.46) and (I.52)). On the other hand, the proton–neutron pairing is not constrained with those interactions, resulting in unsatisfying proton–neutron pairing properties when going beyond the mean field (only particle-like correlations are taken into account in the HFB formalism we consider, see Appendix C). We therefore chose to control this other type of pairing in our interaction to make it more reliable in its applications beyond the mean field. By generalizing the idea consisting in constraining particle-like TBMEs, we built up a system made of TBMEs, some of which are sensitive to the proton–neutron pairing.

The values of the TBMEs chosen as inputs of the fitting code were extracted from the shell-model USD and GPF interactions of Brown *et al.*, related to the *sd* [137, 138] and *pf* [139] shells, respectively. Considered as guidelines, they are coupled to the quantum numbers (J, T), respectively associated with the two-body total angular momentum and isospin operator, in a formalism highlighted in subsection B.2.1. The fitting code being spherically symmetric, the TBMEs of each term of the generalized Gogny interaction, namely the central, density-dependent, spin–orbit and tensor terms, were derived in the spherical harmonic oscillator representation and subsequently coupled to (J, T). This is the subject of section B.2, where we refer the reader for technical details. Those TBMEs are denoted by $\langle V_a^{\mathrm{C}}\rangle^{(J,T)}$, $\langle V_b^{\mathrm{C}}\rangle^{(J,T)}$, $\langle V_a^{\mathrm{DD}}\rangle^{(J,T)}$, $\langle V_b^{\mathrm{DD}}\rangle^{(J,T)}$, $\langle V^{\mathrm{SO}}\rangle^{(J,T)}$ and $\langle V^{\mathrm{T}}\rangle^{(J,T)}$, respectively, from now on. We mention that the central and density-dependent interactions split up into two TBMEs, labelled by the subscripts a and b, associated with two different combinations of parameters (see discussions right after equations (B.28) and (B.43)). Thus, our TBMEs are related to those of Brown *et al.*, called $\langle V^{\mathrm{B}}\rangle^{(J,T)}$, by equations of

the type

$$\begin{aligned} E \equiv \langle V^{\mathrm{B}}\rangle^{(J,T)} - \sum_{i=1,2}\Big[\Big(W_i - B_i + (-)^T H_i - (-)^T M_i\Big)\langle V^{\mathrm{C}}_{a,i}\rangle^{(J,T)} + \Big(B_i - (-)^T M_i\Big)\langle V^{\mathrm{C}}_{b,i}\rangle^{(J,T)}\Big] \\ - \Big[\Big(W_3 - B_3 + (-)^T H_3 - (-)^T M_3\Big)\langle V^{\mathrm{DD}}_{a}\rangle^{(J,T)} + \Big(B_3 + (-)^T M_3\Big)\langle V^{\mathrm{DD}}_{b}\rangle^{(J,T)}\Big] \\ = \Big(W_5 + (-)^T H_5\Big)\langle V^{\mathrm{SO}}\rangle^{(J,T)} + \Big(W_7 + (-)^T H_7\Big)\langle V^{\mathrm{T}}\rangle^{(J,T)}. \end{aligned} \tag{II.15}$$

Since the parameters associated with the central terms are extracted from the previous systems and the ones associated with the density-dependent interaction are left free, all we need is four equations of the form above, two written for the component $T = 0$ and two for the other component $T = 1$, to unequivocally determine the parameters of the tensor and spin–orbit interactions. We can then obtain the parameters from constraints on both $T = 0$ proton–neutron pairing TBMEs and $T = 1$ particle-like TBMEs. The four equations, written E_1, E_2, E_3 and E_4 in the following, that shape the third system of the fitting code of the generalized Gogny interaction, read

$$\begin{cases} E_1 = \Big(W_5 + H_5\Big)\langle V^{\mathrm{SO}}\rangle^{(J_1=1,T=0)}_{sd} + \Big(W_7 + H_7\Big)\langle V^{\mathrm{T}}\rangle^{(J_1=1,T=0)}_{sd}, \\ E_2 = \Big(W_5 - H_5\Big)\langle V^{\mathrm{SO}}\rangle^{(J_2=2,T=1)}_{sd} + \Big(W_7 - H_7\Big)\langle V^{\mathrm{T}}\rangle^{(J_2=2,T=1)}_{sd}, \\ E_3 = \Big(W_5 + H_5\Big)\langle V^{\mathrm{SO}}\rangle^{(J_3=1,T=0)}_{pf} + \Big(W_7 + H_7\Big)\langle V^{\mathrm{T}}\rangle^{(J_3=1,T=0)}_{pf}, \\ E_4 = \Big(W_5 - H_5\Big)\langle V^{\mathrm{SO}}\rangle^{(J_4=2,T=1)}_{pf} + \Big(W_7 - H_7\Big)\langle V^{\mathrm{T}}\rangle^{(J_4=2,T=1)}_{pf}, \end{cases} \tag{II.16}$$

where the quantities E_i, with $i \in \{1, 2, 3, 4\}$, can be deduced from (II.15). Several remarks are in order. First, two kinds of TBMEs were chosen, some coupled to $J = 1$ and others to $J = 2$. When coupled to $T = 0$, $J = 1$ TBMEs indeed describe proton–neutron pairing, while $J = 2$ generally accounts for quadrupole deformation properties. Second, the first two equations were evaluated in the *sd* shell and the last two ones in the *pf* shell, as indicated by the subscripts. The reason is merely that we wanted to catch the physics related to low- and medium-mass nuclei. Third, the nuclei used for *sd*-shell and *pf*-shell calculations are ^{18}O and ^{42}Ca, respectively. As well-known in shell model, the TBMEs can effortlessly be extended to heavier nuclei of mass A that evolve smoothly from a reference nucleus of mass A_{ref}, by means of the formula [137, 139]

$$\langle V^{\mathrm{B}}\rangle^{(J,T)}(A) = \left(\frac{A_{\mathrm{ref}}}{A}\right)^{0.3}\langle V^{\mathrm{B}}\rangle^{(J,T)}(A_{\mathrm{ref}}), \tag{II.17}$$

where $A_{\mathrm{ref}} = 18$ for the *sd* shell and $A_{\mathrm{ref}} = 42$ for the *pf* shell. As for the oscillator lengths, we approximated them thanks to the widely-used Blomqvist–Molinari relation, obtained from a fit on nuclear charge radii [140, 141],

$$b = \sqrt{0.90A^{1/3} + 0.70}. \tag{II.18}$$

From these considerations, the system (II.16) can be inverted to get the tensor and spin–orbit parameters out of it. There are sixty-three *sd*-shell and one hundred and ninety-five *pf*-shell TBMEs among which we can pick up values for the $\langle V^{\mathrm{B}}\rangle^{(J,T)}$ quantities. Moreover, a maximum discrepancy of 10% between those shell-model TBMEs and ours is tolerated as there is no reason for them to be strictly equal to ours, evaluated in a different framework. Then, in practice, a set of four shell-model TBMEs satisfying the

above-mentioned requirements is taken and we keep all the parameters reproducing them in the range $\langle V^{\mathrm{B}}\rangle^{(J,T)} \pm 0.1 \langle V^{\mathrm{B}}\rangle^{(J,T)}$. Considering all the possibilities, – literally – hundreds of thousands of tensor and spin–orbit parameters come out of this process, for a given set of values assigned to the other parameters. With, in addition, all the possible central and density-dependent parameters obtained from the previous constraints, we are left with a staggering number of parametrizations.

1.2.3. Filters

At this stage, we hope the filters are strong enough to discard the bulk of the outcoming parametrizations and retain only a reasonable number of promising ones. As with the constraints, we first used the filters already in place for the D2 interaction (see section I.2.4), except that a contribution of the tensor force to the Landau parameters had to be incorporated (see section II.2.5). Although these filters non-negligibly reduce the number of parametrizations, tens of thousands of them still slip through the net. An additional filtering step of the tensor and spin–orbit parameters had to be implemented. This step is based on the three points discussed below.

We have said at the beginning of this section that we want to generate a fully refitted interaction while trying to stay close to the D2 interaction. The zero-range spin–orbit term of the D2 interaction only acts in the $(S = 1, T = 1)$ channel, with the intensity $W_0 = 130\,\mathrm{MeVfm}^5$. Our finite-range spin–orbit interaction acts in this channel with an intensity $(W_5 - H_5)$ modulated by a Gaussian form factor $\mathrm{e}^{-(\vec{r}_1-\vec{r}_2)^2/\mu_5^2}$. As expected, this finite-range character allows us to gain latitude, since the spin–orbit term now depends on the distance separating the nucleons. We would sadly lose, in this channel, the latitude if we imposed our spin–orbit intensity to be equal to W_0 at all distances. However, if we impose our intensity to be W_0 *at the zero-range limit*, then we retain this latitude while ensuring that we produce, in this channel, a spin–orbit term that coincide with the D2 spin–orbit term at the zero-range limit. At this limit, the intensity of our spin–orbit force is simply given by $(W_5 - H_5)$ (as explained in more details in appendix D.5.1). Since our analytical form is not identical to that of the D2 interaction, and the contribution of the spin–orbit term may be partially modified by the other terms in the fitting process, we only ask to recover approximately the intensity W_0 at the zero-range limit. Quantitatively, we allow a relatively large range such that $(W_5 - H_5) \in [110, 150]\,\mathrm{MeVfm}^5$.

Almost thirty years ago, Sharma *et al.* [142] showed that an extended Skyrme interaction with an isospin-dependent spin–orbit force was able to better reproduce the so-called isotopic shift (or kink) in the charge radii of lead isotopes, than without. In their article, the spin–orbit term takes the following form

$$v_{\mathrm{SO}} \equiv W_0(1 + x_w P_\tau)\Big[\vec{k}' \times \delta(\vec{r}_1 - \vec{r}_2)\vec{k}\Big] \cdot (\vec{\sigma}_1 + \vec{\sigma}_2), \tag{II.19}$$

where $x_w = 0.1032$ is a parameter fixing the intensity of the isospin-dependent spin–orbit force to $W_0 x_w \simeq 28.759\,\mathrm{MeVfm}^5$. The interest of this study is twofold: in addition to giving us an *order of magnitude* for the intensity of the isospin-dependent spin–orbit force, it could enable us to better reproduce the kink. Indeed, among the parametrizations of the Gogny interaction tested to date on this isotopic shift, the best agreement was found for the D2 interaction, but it is still far from experimental data [17, 18]. Nevertheless, this intensity must be considered with caution since the analytical form of the original Skyrme interaction with an isospin-dependent spin–orbit force is quite different from ours. There is in particular no tensor term, and the density-dependent and spin–orbit forces are of zero range. On the contrary, all of our terms are of finite range and have an isospin dependence

that may renormalize the intensity of the isospin-dependent spin–orbit force. This is why we have talked about an "order of magnitude". Moreover, no information is provided on whether the sign of this intensity plays a significant role on the reproduction of the kink. We then decided to add a filter demanding the intensity of our isospin-dependent spin–orbit force to verify $H_5 \in [-50, 50]\,\mathrm{MeVfm}^5$.

More recently, Anguiano and Grasso [61] built up a perturbative D1S-type Gogny interaction supplemented by a finite-range tensor term we have talked about in the previous chapter (see subsection I.2.5.1). For convenience, we here recall the analytical expression chosen for their tensor term,

$$v_{\mathrm{T}} \equiv (V_{\mathrm{T}1} + V_{\mathrm{T}2}P_\tau)\,\mathrm{e}^{-(\vec{r}_1-\vec{r}_2)^2/\mu_{\mathrm{T}}^2}\,\widetilde{S}_{12}, \tag{II.20}$$

where $\widetilde{S}_{12}$ is given in (I.58), and related to our tensor operator by $S_{12} = 3\widetilde{S}_{12}$ (see appendix D.4.1). Their fitting procedure we have detailed in the above-mentioned section, at the origin of the D1ST2c parametrization given in Table I.5, is of great interest to us. Indeed, the combined actions of the spin–orbit and tensor parameters on the SPEs, which are often intertwined, are separated and a convenient way to constrain their parameters is undertaken. Taking into account the factor three linking our conventions for the tensor operator and the signs which are crucial for SPEs to shift in the right direction, their parameters become, in our notations, $(W_7 - H_7) = -225\,\mathrm{MeV}$ and $H_7 = -180\,\mathrm{MeV}$. Once again, we must be careful with these values as our spin–orbit interaction is of finite range, and we aim at carrying out a *complete* refit of all the parameters, unlike this parametrization. Remarkably enough, though, the value of their spin–orbit parameter falls within the range deduced from the two previous paragraphs, for certain values of H_5. We will therefore keep this particular value in a corner of our minds when looking at the spin–orbit intensity of our interaction. Likewise, the rather long range $\mu_{\mathrm{T}} = 1.2\,\mathrm{fm}$ they chose for the tensor interaction is in line with the OBE models (see section II.1.2.1) we rely on. We also recall our desire to stick to the philosophy of the original Gogny interaction, which is to get satisfactory results not only at the mean-field level at which the parameters were obtained here, but also beyond the mean field. Consequently, we will use this study to identify a range of parameters for the tensor term, without being too restrictive. We impose $(W_7 - H_7) \in [-275, -175]\,\mathrm{MeV}$ and $H_7 \in [-230, -130]\,\mathrm{MeV}$.

With these considerations, we are capable of efficiently filtering the parameters associated with the spin–orbit and tensor parameters. Note that filters offer the advantage of being adjustable at will, which is a welcome feature here since we are comparing quite different analytical expressions.

1.2.4. Extraction of the parametrization DG

By adding the above-mentioned constraints and filters to the D2 fitting code, we are in position to extract DG-type parametrizations. The global protocol is summarized and illustrated in Figure II.1. The portions already present in the D1S and D2 fitting procedures are dyed in blue and green, respectively, while the part specific to DG, discussed in the previous subsections of this chapter, is colored in red. Obviously, any new interaction changes most of the steps in the fitting code, so we are here only talking about significant modifications. This fitting protocol must be compared with those of D1S (Figure I.3) and D2 (Figure I.5). In the first place, *initial data* are implemented so as to allocate quantitative values to the *constraints* allowing the *inversion of three systems*. Those three systems are coupled to one another, as indicated by the double vertical arrows. They are constructed from the constraints (I.44), (I.52) and (I.53), and (II.16), respectively.

In addition to the initial data already used in the D2 fitting process, some shell-model TBMEs taken from Brown *et al.* [137, 139] have been added. For conciseness, they are written $V_i \equiv \langle V_i^{\mathrm{B}} \rangle^{(J,T)}$, for $i \in \{1, 2, 3, 4\}$. They permit to fix four TBMEs that, combined to the other constraints, give rise to the inversion procedure, eventually furnishing a parametrization (a set of twenty-two parameters). This method is repeated a huge number of times, and the quantities that can be varied are marked by two arrows on either side of their rectangle. In the second place, the resulting parametrizations face *filters*, established from various criteria in infinite nuclear matter, as for the D1S and D2 interactions, with Landau parameters including tensor forces this time, and from the ranges of authorized values for the spin–orbit and tensor parameters. Each set of parameters, derived from the inversion procedure, that passes through all those filters corresponds to a DG-type parametrization. Let us stress that this method is valid for the DG analytical form exposed in (II.1), containing a single spin–orbit term and a single tensor term. In the fitting code, we have generalized the expressions to simulate up to two spin–orbit and two tensor terms. We can therefore input up to eight shell-model TBMEs, leading to a broader system coupling eight equations. The filters related to the tensor Landau parameters have also been generalized to two ranges. All that remains is to find a way of filtering the new parameters introduced to generate a DG interaction of this kind. Further extending the analytical expression this way might be envisaged in a short future.

We will now try to describe how, in practice, we pulled out the DG parametrization that will be dissected in the rest of the thesis. It is difficult to report, in an organized manner, how we proceeded. First because it involved a never-ending back-and-forth between the fitting code and the finite nuclei codes (HFB3 for mean-field and MPMH for beyond mean-field results, see chapters III and IV). Each time a new looking-good parametrization came out the fitting code, we indeed needed to check whether a bunch of physical quantities and observables was properly reproduced in finite nuclei codes. Reciprocally, the outcomes gave us information on how the values attributed to the parameters influenced those physical quantities and observables, so we modified the parameters accordingly. Then a new parametrization had to be tested in finite nuclei, and so on and so forth. Second because the three systems to be inverted are coupled to one another. This means that each time a constraint or an input is modified, the whole output set of parameters changes.

The main physical quantities and observables we paid deep attention to all along the process are: [4]

(i) binding energies of ^{16}O, ^{90}Zr and ^{208}Pb nuclei;

(ii) pairing energy in doubly magic nuclei;

(iii) SPEs in ^{40}Ca, ^{48}Ca and ^{56}Ni nuclei;

(iv) kink in Pb isotopes;

(v) energy drift in neutron-rich nuclei;

(vi) energies of the first excited states for even–even and odd nuclei in *sd* shell.

All of those were controlled by means of the HFB3 code, except the last point that relied on the MPMH code. Binding energies of ^{16}O and ^{90}Zr are constrained at the

4. In theory, *all* the physical quantities and observables we tried to reproduce had to be controlled. In practice, it is *principally* the listed quantities that have been systematically tested. Either because they vary significantly from one parametrization to the other (the energy drift, for example), or because we wanted to reproduce them at all costs (the pairing energy, for example), all in a way that was relatively easy to test (filtering each parametrization on fission barriers of standard actinides would be insane).

Figure II.1 – The DG fitting process on which the generalized fitting code, referred to as `inter_DG`, is based upon. Boxes colored in blue, green and red correspond to steps primarily enhanced by the D1S, D2 and DG extensions, respectively.

HFR approximation in the fitting code, so we wanted to make sure they were still good at the HFB level. As a representative of heavy nuclei, ^{208}Pb completed the analysis of the binding energies of light and medium-mass nuclei. For an interaction to be reliable enough, the pairing energy had obviously to be zero in doubly-magic nuclei. The third and fourth points are related to the constraints and filters associated with DG, we have mentioned in previous subsections. Indeed, we wanted to improve the SPEs behavior and the experimental agreement of the kink in lead isotopes, with respect to the former Gogny interactions. We also wished to avoid the energy drift of neutron-rich nuclei observed along isotopic chains with D1S. As we have shown in the previous chapter, this drift is corrected by D1N and D2 interactions, by in particular requiring the difference between the HFB and experimental binding energies in ^{100}Sn and ^{132}Sn isotopes to be equal. Lastly, excitation energies allowed us to analyze the actions of spin–orbit and tensor interactions beyond the mean field.

Two-body matrix elements

In concrete terms, we started by attempting to stay close to D2. All the initial data and constraints of the D2 fitting protocol were first kept. Free parameters including the density-dependent ones, and all the ranges were those of D2. We varied the spin–orbit and tensor ranges within the intervals $\mu_5 \in [0.2, 1.0]$ fm and $\mu_7 \in [1.0, 2.0]$ fm – in agreement with our theoretical analysis without being too demanding –, and we looked for a set of TBMEs leading to spin–orbit and tensor parameters that crosses the filters. This first step was already not an easy task, since most sets of TBMEs provided spin–orbit and tensor parameters far removed from the intervals we had defined (as we saw when we lifted the corresponding filters). We tested these parametrizations anyway, but they were far too bad to be retained.

Binding energies

Some of the few dozen parametrizations that passed the filters showed interesting behaviors with regard to the six points mentioned earlier, but all had definite pathologies in terms of binding energies. In the best cases, the difference between HFB and experimental energies was about 11 MeV in ^{100}Sn and about 20 MeV in ^{208}Pb. Even when we changed the parameters or the global intensity of the density-dependent term, and the ranges, moving away from D2, we ended up with the same kind of differences. The reason is a bit subtle. Actually the fitting code takes constraints on binding energies at the HFR approximation, for which there is no spin–orbit contribution, as we have emphasized in the previous chapter. Since the D1S and D2 interactions, that have the same spin–orbit intensity $W_0 = 130\,\text{MeVfm}^5$, produce quite good agreement with experimental binding energies, this means that the constraints on HFR binding energies are relevant for a zero-range spin–orbit force with *this* intensity only. We readily validated this reasoning as, when we imposed by hand the value $130\,\text{MeVfm}^5$ to the spin–orbit intensity (for the channel $(S = 1, T = 1)$) in the parametrizations coming out of the fitting code, we found much more consistent binding energies at the HFB level. Unfortunately, we noticed that such intensity was too strong to reduce the neutron $(1f_{7/2} - 1f_{5/2})$ splitting in ^{40}Ca (in accordance with the value of $103\,\text{MeVfm}^5$ taken by Anguiano and Grasso), as with D1S and D2 interactions. We found a way to conciliate these two observations by slightly modifying the initial data about the ^{16}O and ^{90}Zr HFR binding energies, within the intervals drawn with D2, depending on the range of spin–orbit intensities we decided to probe.

Energy difference $\Delta\varepsilon$

On the other hand, by tuning the HFR binding energies, we altered the HFB binding energies of ^{100}Sn and ^{132}Sn and then broke the same difference to the experimental energies observed with D2. We therefore also had to play with the value of $\Delta\varepsilon$, which is known, together with the filter on the neutron matter equation of state, to shape this energy drift. As exposed for D2, there exists a linear relation between symmetry energies a_τ and energy differences $\Delta\varepsilon$. From a range of empirical values of the symmetry energy, we deduced a range of empirical values for the energy difference from which we picked up values until finding one predicting no energy drift in the Sn isotopic chain at HFB approximation.

Single-particle energies

Finally, we have said in subsection I.2.5.1 that the D1ST2c parametrization was obtained by fitting the neutron $(1f_{7/2} - 1f_{5/2})$ splitting successively in isotopes ^{40}Ca, ^{48}Ca and ^{56}Ni, at the HF level. We took up this procedure, but we simply ensured that the splittings in these nuclei are closer to experimental values with DG than with D1S and D2 interactions. Indeed, as we have mentioned several times, we tried to construct an interaction following the philosophy of the original Gogny interaction, which is to provide reliable results *beyond* the mean field, so that the reproduction of such mean-field results is not expected to be perfect. We have also underlined that the experimental neutron $(1p_{3/2} - 1p_{1/2})$ splitting in ^{16}O was used to fix the intensity of the spin–orbit interaction in the D1 analytical form. We thus made sure not to deteriorate too much the value of this splitting while tuning the intensities of our finite-range spin–orbit and tensor forces on the other three isotopes. The neutron SPEs involved in the splittings discussed above are displayed in Figure II.2, and the corresponding neutron energy splittings $\Delta\varepsilon_\nu$ are listed in Table II.2.

We see that the neutron $(1p_{3/2} - 1p_{1/2})$ splitting in ^{16}O is about 400 keV from the experimental value with DG, which then appears reasonable compared to the 300 keV obtained with D2. Regarding the neutron $(1f_{7/2} - 1f_{5/2})$ splittings in the other isotopes, they are all closer to experimental values, as we wanted.

	Energy difference $\Delta\varepsilon_\nu$			
Interaction	^{16}O (MeV)	^{40}Ca (MeV)	^{48}Ca (MeV)	^{56}Ni (MeV)
DG	5.69	8.05	8.94	7.49
D1S	6.08	9.13	8.37	8.84
D2	6.41	8.81	8.58	8.75
Exp.	6.10	6.80	8.80	7.16

Table II.2 – Energy differences $\Delta\varepsilon_\nu$ between the neutron SPEs $1p_{3/2}$ and $1p_{1/2}$ in ^{16}O, as well as between $1f_{7/2}$ and $1f_{5/2}$ in ^{40}Ca, ^{48}Ca and ^{58}Ni isotopes, calculated at the HF approximation, with DG, D1S and D2 interactions and compared to experimental values [143].

These steps had to be reiterated, again and again, for different constraints (on TBMEs, HFR binding energies or energy differences $\Delta\varepsilon$), different filters (by widening or narrowing the intervals defined in the previous section) and different free parameters (enumerated

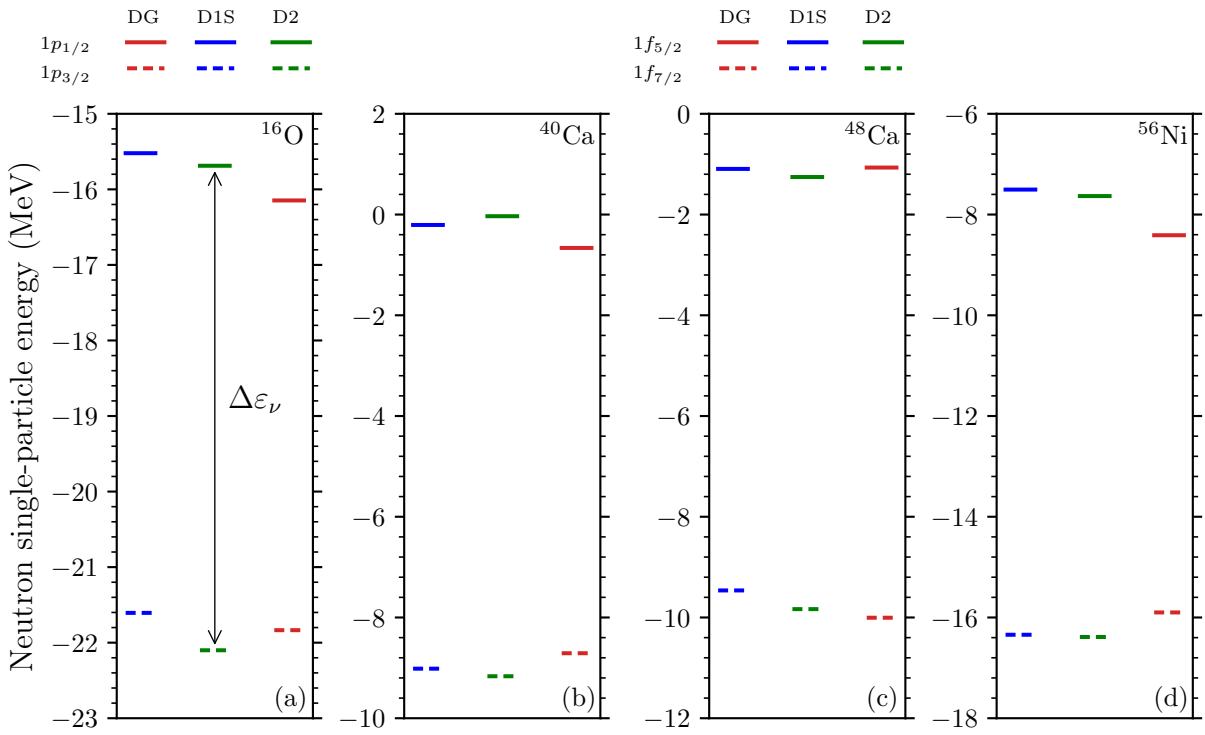

Figure II.2 – Neutron single-particle energies $1p_{3/2}$ and $1p_{1/2}$ in ^{16}O as well as $1f_{7/2}$ and $1f_{5/2}$ in ^{40}Ca, ^{48}Ca and ^{56}Ni isotopes, calculated at the HF approximation, with DG, D1S and D2 interactions.

in the rectangle at the bottom right of the inversion procedure), refining the search as promising parameter areas were identified. This *phenomenological* way of proceeding can be akin to cooking, where a recipe is gradually improved by small pinches of various ingredients, to give it the desired taste. It is no less precise or rigorous, however, and allows us to keep an eye on quantities of interest, knowing the physics we wish our interaction to properly describe. At the end of the day, it is a *compromise* in the reproduction of the physical quantities and observables listed above that led to the DG parametrization we chose.

Before giving the parameters of the DG interaction, we would like to justify that taking the TBMEs of the USD and GXPF1 interactions as guidelines to constrain the TBMEs of Gogny interactions was justified and *a posteriori* relevant. To do so, we compare in Figure II.3 the *sd*-shell TBMEs coupled to (J, T) of DG, D1S and D2 interactions discussed above with those of the USD interaction.

Generally speaking, we see that the TBMEs in both $T = 0$ and $T = 1$ channels of D1S and D2 interactions are comparable to those of the USD interaction. Imposing values obtained from shell-model calculations to constrain the TBMEs of a Gogny interaction to deduce some of its parameters, as we have done with DG, then appears consistent. There are obviously some fluctuations in the overall agreements since the TBMEs of Gogny interactions are not expected, to date, to reach the accuracy of those of the shell model. This is why we have tolerated a maximum discrepancy of 10% in the reproduction of the shell-model TBMEs with interaction DG. On the other hand, it is interesting to notice that the TBMEs of D1S and D2 interactions are closer to the USD predictions in the

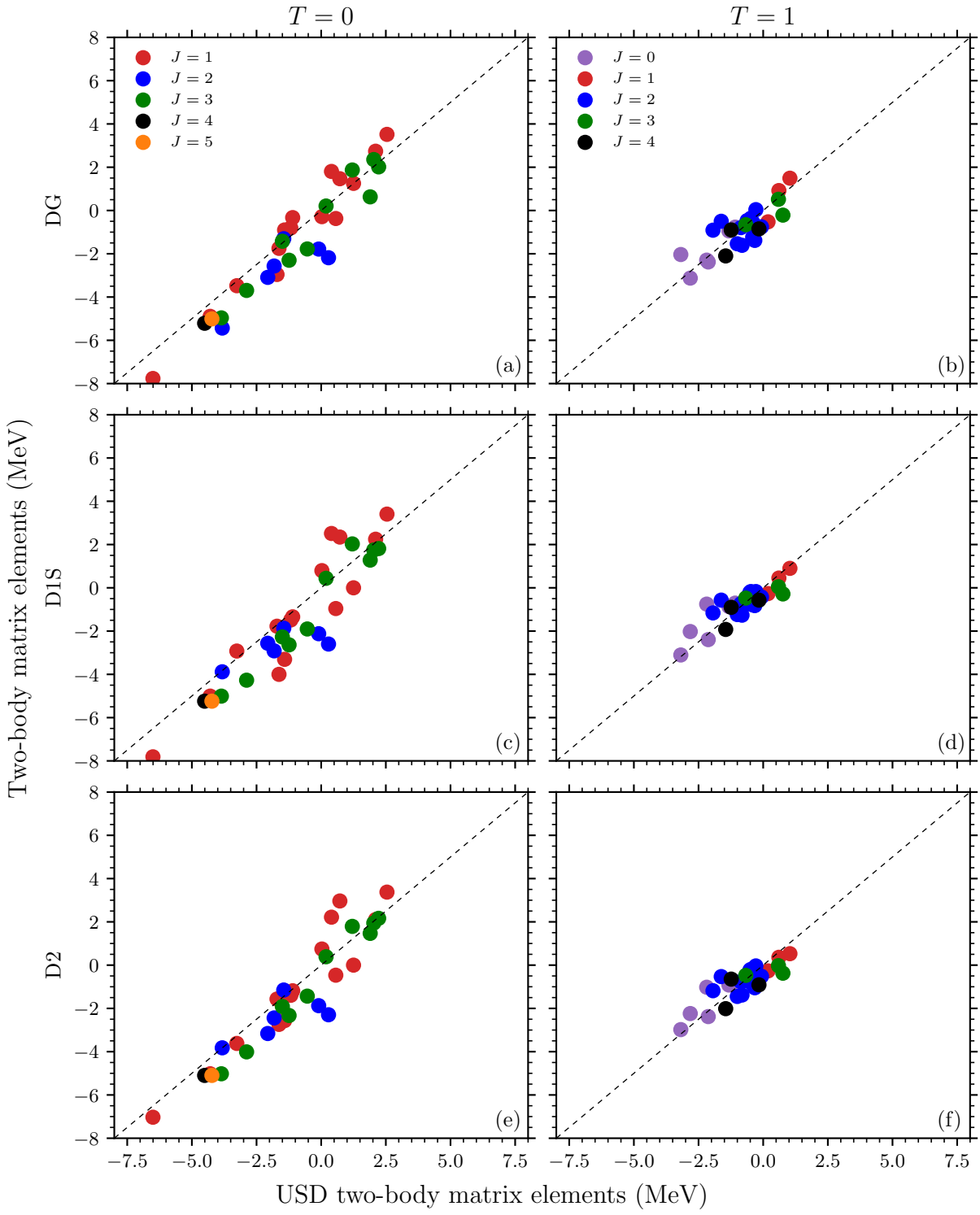

Figure II.3 – Comparison between the *sd*-shell two-body matrix elements, coupled to (J, T), calculated with DG (upper panels), D1S (middle panels) and D2 (lower panels) interactions, and those of the USD interaction. They are displayed for $T = 0$ (left panels) and $T = 1$ (right panels) channels. Diagonal lines show perfect agreement.

$T = 1$ than in the $T = 0$ channel. It is in fact natural since only $T = 1$ TBMEs were constrained in these interactions, as we have explained in the previous chapter. Following this reasoning, the TBMEs of DG, constrained for the first time in the $T = 0$ channel, should be closer to the USD predictions than those of interactions D1S and D2. This is indeed what we observe by looking at panels (a), (c) and (e), since the values are less scattered around the diagonal lines. For simplicity, we have carried out the study with *sd*-shell TBMEs, but similar results are expected in the *pf*-shell when the Gogny interactions are compared to GXPF1.

We can now give the parameters making up the DG parametrization of the analytical expression (II.1) in Table II.3. In the order of appearance are the central ($i \in \{1, 2\}$), density-dependent ($i = 3$), spin–orbit ($i = 5$) and tensor terms ($i = 7$), all of finite range. As expected, the central and density-dependent terms are not too far from those of D2 (see Table I.4), and the spin–orbit and tensor parameters fit the intervals of the previous subsection.

i	μ_i (fm)	α_i	W_i $(-)^a$	B_i $(-)^a$	H_i $(-)^a$	M_i $(-)^a$
1	0.80		−1190.016	800.000	−877.422	1198.923
2	1.24		109.179	−191.226	133.441	−277.509
3	0.60	1/3	1836.200	581.600	377.600	−633.220
5	0.20		145.483		29.634	
7	1.10		−392.544		−196.481	

[a] MeV ($i \in \{1, 2, 5, 7\}$), MeVfm^4 ($i = 3$), MeVfm^5 ($i = 5$).

Table II.3 – DG parametrization.

We insist on the fact that the intensity of our finite-range spin–orbit interaction is entirely driven by the combination of parameters $(W - HP_\tau)$. The overall factor $B(\mu_5)$ only ensures to recover the analytical expression of the original zero-range spin–orbit force at the limit $\mu_5 \to 0$, as detailed in appendix D.5.1. It should not be considered when talking about the intensity, as can be seen from the units, being the same for the parameters of both zero-range and finite-range spin–orbit interactions.

2. Results in infinite nuclear matter

We begin our analysis of the results in infinite nuclear matter (INM). This model can be seen as a theoretical framework giving us a rough idea of the structure and properties of the interior of heavy nuclei. All the calculations used to bring out those outcomes have been carried out in Appendix A, where we show in particular that the spin–orbit and tensor interactions do not contribute (except when their partial waves are considered individually, as studied in section II.2.4). We can then put the central and density-dependent part of the DG interaction to the test, and make sure it does not stray too far from the former convenient parametrizations. Numerous Gogny interactions are displayed. The purpose is not to make a full comparison between them, but to learn how the DG interaction compares with its competitors. On the one side, the D1S and D2 interactions, on which we will mainly focus, were fitted from (successively enhanced versions of) the same code. A comparison between them is a direct testimony of the implications of the

modifications made in the fitting code. On the other side, the D1M and D3G3 interactions, deduced from another process, are often presented as worthy candidates in INM.

2.1. Symmetric infinite nuclear matter

Some results are exposed in symmetric infinite nuclear matter (SNM), which corresponds to a medium composed of as many protons as neutrons, i.e. with an asymmetry parameter equal to zero, $\beta = 0$.

2.1.1. Standard physical quantities

Firstly, numerical values of several common physical quantities evaluated in SNM at the Hartee–Fock approximation for D1S [15], D1M [127], D3G3 [133], D2 [17, 18] and DG interactions are given in Table II.4. Saturation density ρ_0, energy (per nucleon) $\mathcal{E}_0/A \equiv \mathcal{E}^{\mathrm{S}}(\rho_0)/A$ ((A.79) plus (A.80)), incompressibility K_∞ ((A.85) plus (A.89)), effective mass m^*/m (A.107) and symmetry energy $a_\tau \equiv \mathcal{E}_{\mathrm{sym}}(\rho_0)$ ((A.98) plus (A.99)), all evaluated at saturation density, are tabulated. Their formal definitions and physical meanings can be found in Appendix A.

	Physical quantities in SNM				
Interaction	ρ_0 (fm^{-3})	$\mathcal{E}_0/A$ (MeV)	K_∞ (MeV)	m^*/m	a_τ (MeV)
DG	0.163	−16.01	210	0.74	31.1
D1S	0.163	−16.02	210	0.70	31.1
D1M	0.165	−16.03	225	0.75	28.6
D3G3	0.165	−16.05	227	0.68	32.6
D2	0.163	−16.00	209	0.74	31.1

Table II.4 – Various physical quantities evaluated in symmetric nuclear matter (SNM) for different Gogny interactions.

We compare those to some empirical values. The saturation density is obtained from the charge distribution of heavy nuclei taking into account the corrections induced by Coulomb repulsion and surface tension, $\rho_0 = (0.17 \pm 0.02)\,\mathrm{fm}^{-3}$ [144]. Energy per nucleon and symmetry energy appear explicitly in the semi-empirical mass formula. Their values are then deduced from the successive adjustments of this formula on experimental binding energies [145–149], $\mathcal{E}_0/A = (16 \pm 1)\,\mathrm{MeV}$ and $a_\tau = (30 \pm 2)\,\mathrm{MeV}$. Incompressibility was determined using various phenomenological effective interactions to reproduce experimental data of heavy nuclei and the energy of the breathing mode in ^{208}Pb, $K_\infty = (215 \pm 15)\,\mathrm{MeV}$ [150]. Finally, an experimental nucleon-nucleus scattering analyzed in the framework of the optical potential furnished values for the effective mass, $m^*/m = 0.70 \pm 0.05$ [151].

Unsurprisingly, the DG interaction, like its counterparts, sees all its physical quantities fall within the ranges of empirical values. Indeed, as explained in the previous section, these empirical values behave like filters in the fitting code, so that a DG-type interaction with even one of its quantities outside these intervals would be rejected. The DG values are pretty close to those of D2, which corroborates our will not to move too far from D2, underpinned by the similarity of the central and density-dependent part of these

interactions (see Table I.4). Finally, we note that the quantities of these two interactions are not very different from the others, except for the incompressibility, which is lower, and the effective masses of D1S and D3G3, which are the smallest; this is rather encouraging.

2.1.2. Equation of state

In Figure II.4 are drawn the SNM equations of state, that is the energy (per nucleon) $\mathcal{E}_0/A$ as a function of the medium density ρ, for several Gogny interactions, which are compared to realistic calculations.

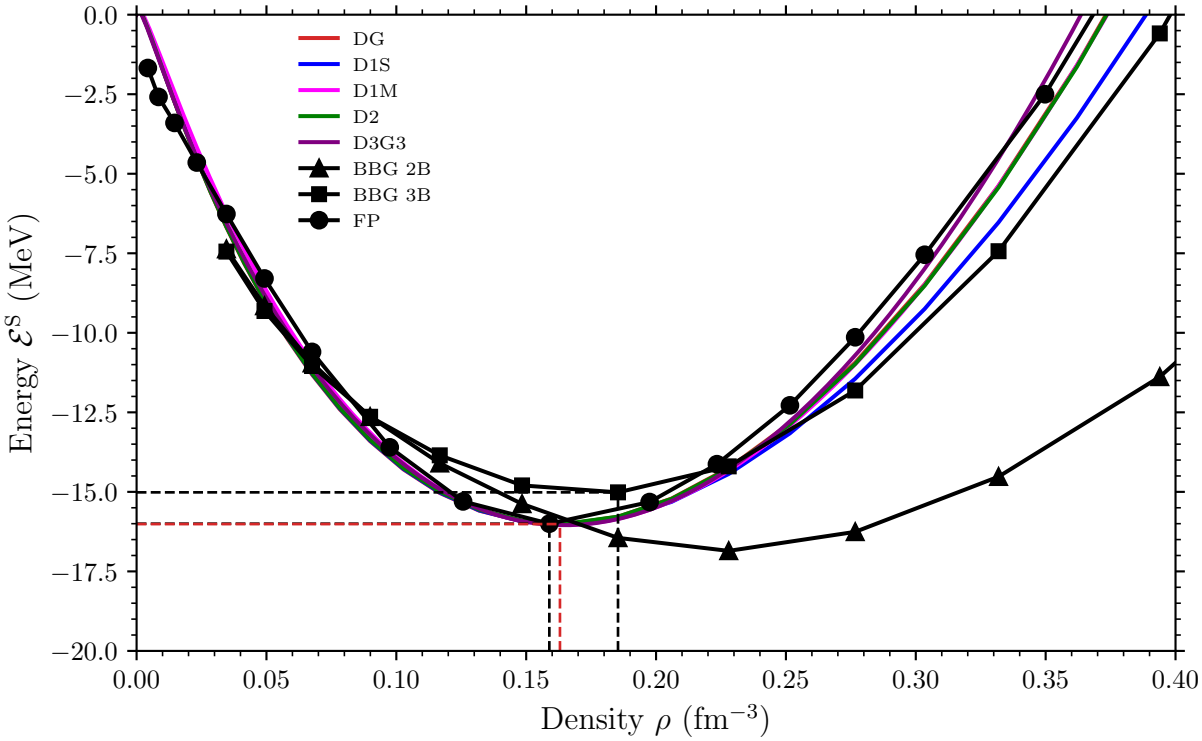

Figure II.4 – Equations of state in symmetric nuclear matter (SNM) for D1S, D1M, D3G3, D2 and DG interactions. Realistic calculations based on Friedman–Pandharipande (FP) and Bethe–Brueckner–Goldstone approaches, with (BBG 3B) and without three-body corrections (BBG 2B), are also represented.

We look at two realistic calculations, based on two different theoretical approaches. The first one utilizes a variational method applied by Friedman and Pandharipande (FP) [126] to the realistic interaction UV14 [152]. The Urbana potential possesses two- and three-body contributions. It reproduces the scattering data in S-, P-, D- and F-waves and fits the ground-state energy, density and compressibility in symmetric nuclear matter.
The second one takes advantage of the Bethe–Brueckner–Goldstone (BBG) method, a generalization of the G-matrix appearing in the Goldstone development, applied by Baldo *et al.* [153] to the realistic interaction AV14 [26]. The Argonne potential presents a good fit to deuteron properties and neutron–proton scattering below 330 MeV. Unfortunately the BBG method does not natively retain the three-body contributions, so that only two-body interactions are taken into account within this approach. Nonetheless, by averaging the position of a third particle by means of Lejeune *et al.* technique [154], a density dependence simulating three-body effects can be adjoined to the BBG method. This is what we dub "BBG 3B" in the following.

Generally speaking, all Gogny interactions, including DG, correctly reproduce the parabolic behavior observed in realistic FP calculations in this low-density regime. It is worth noticing the limitation of realistic two-body calculations, whose parabola is wider, with a minimum located at a lower energy for a higher density. The coordinates of the saturation points $(\rho_0, \mathcal{E}_0/A)$, corresponding to the minima of the curves, are spotted by black dashed lines for three-body realistic calculations, and by a red dashed line for DG. We can check that, as well as falling within the intervals of empirical values (see previous subsection), the DG saturation point is very close to that of the FP calculation $(0.159, -16.00)$. The saturation density of DG is a little bigger than the FP one, but this is not a problem as we know that the saturation density must be close to $0.16\,\mathrm{fm}^{-3}$ for an interaction to provide reliable results in finite nuclei. The saturation density predicted by BBG 3B calculations, $\rho \simeq 0.185\,\mathrm{fm}^{-3}$, then appears to be too high. Since incompressibility is proportional to the second derivative of the energy evaluated at the saturation density (see (A.83)), its magnitude tells us about the curvature of the equation of state around that point. The greater the incompressibility, the steeper the rise of the curve. This is indeed the case, as the D1M and D3G3 curves are rising more sharply than D1S, D2 and DG around the saturation point, in line with the inequalities deduced from Table II.4, $K_\infty^{\mathrm{D1M}} \simeq K_\infty^{\mathrm{D3G3}} > K_\infty^{\mathrm{D1S}} \simeq K_\infty^{\mathrm{D2}} \simeq K_\infty^{\mathrm{DG}}$. Note that this trend is more pronounced at high densities, due to the factor $9\rho^2$ in the definition of K_∞. These curves are therefore closer to the FP results in the range $[\rho_0, 0.30]$ than are D1S, D2 and DG.

2.1.3. Energy in (S,T) channels

In the previous subsection, we have made sure to recover the general shape of the equation of state in SNM, with a consistent saturation point. We would now like to go further and see what our DG nuclear potential looks like in more details. The potential energy can be divided into kinetic and potential parts as

$$\frac{\mathcal{E}^{\mathrm{S}}}{A} = \frac{\mathcal{E}^{\mathrm{S}}_{\mathrm{K}}}{A} + \frac{\mathcal{E}^{\mathrm{S}}_{\mathrm{P}}}{A}, \tag{II.21}$$

with indices K and P standing for "kinetic" and "potential", respectively. The potential contribution (A.80) can itself be expressed as a sum over the coupled spin $S \in \{0,1\}$ and isospin $T \in \{0,1\}$ of the two-nucleon system, i.e.

$$\frac{\mathcal{E}^{\mathrm{S}}_{\mathrm{P}}}{A} = \sum_{ST} \left.\frac{\mathcal{E}^{\mathrm{S}}_{\mathrm{P}}}{A}\right|_{ST}, \tag{II.22}$$

where $\mathcal{E}^{\mathrm{S}}_{\mathrm{P}}/A|_{ST}$ corresponds to the potential energy (per nucleon) in the (S,T) channel. According to this decomposition, the nuclear potential can be viewed as four independent interactions, each acting in its own subspace (S,T). Physically, the $S=0$ component corresponds to the situation where the spins of the two nucleons are opposite, while the *main* contribution of the $S=1$ component corresponds to the situation where they are aligned. On the other hand, the $T=0$ component corresponds to the situation where a neutron interacts with a proton, while the main contributions of the $T=1$ component correspond to the situation where two particles of the same sort interact (two protons or two neutrons). The four possible configurations therefore give rise to four different types of interaction. The technical details associated with this formalism are provided in appendix D.1. The potential energy in the (S,T) channels versus the Fermi momentum

k_F [5] are plotted in Figure II.5, and compared to the former realistic calculations.

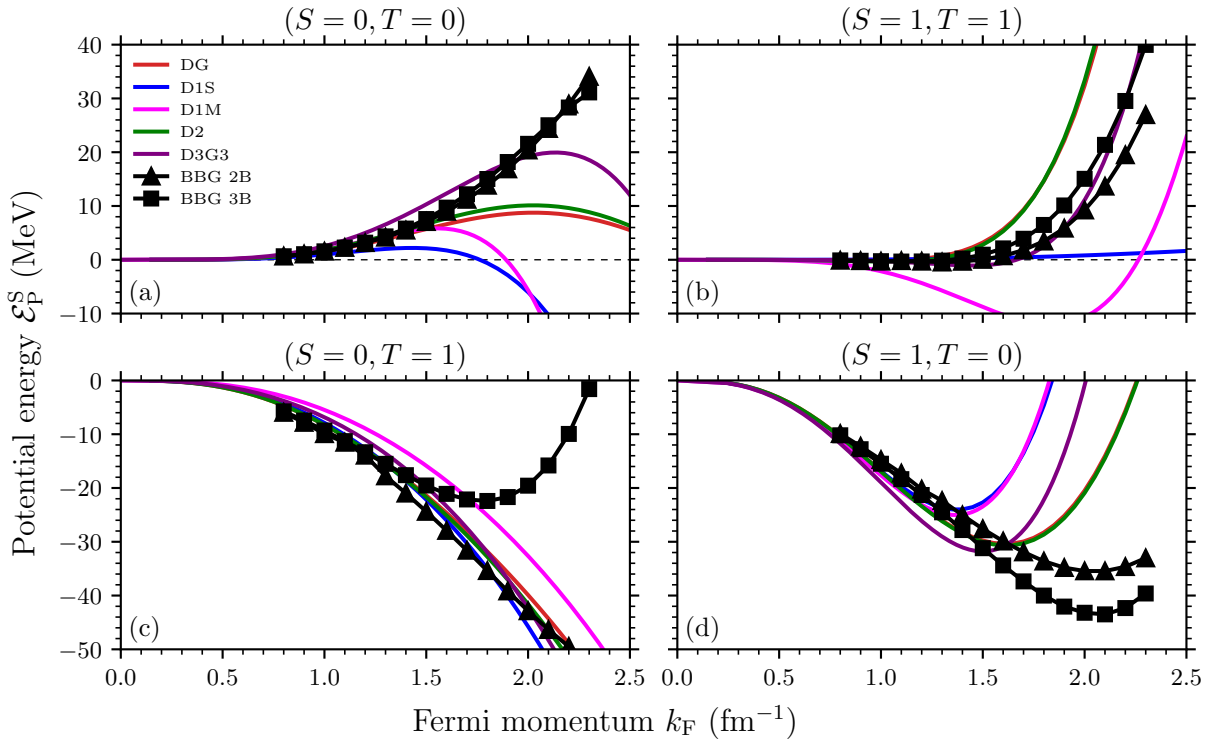

Figure II.5 – Potential energy as a function of the Fermi momentum in symmetric nuclear matter for D1S, D1M, D2, D3G3 and DG interactions. The energy is decomposed in the $(S=0,T=0)$, $(S=1,T=1)$, $(S=0,T=1)$ and $(S=1,T=0)$ channels in panels (a), (b), (c) and (d), respectively. The results are compared to the two-body (BBG 2B) and three-body (BBG 3B) Bethe–Brueckner–Goldstone realistic calculations. The $\mathcal{E}_P^S/A=0$ equation is represented by a dashed line in panels (a) and (b) for clarity.

In the singlet-odd channel $(S=0,T=0)$, realistic calculations are very similar, with or without three-body effects taken into account. They predict positive potential energy and a repulsion between nucleons (k_F is homogeneous to the inverse of a length) that increases with the Fermi momentum. The tested Gogny interactions are also repulsive and fit rather well realistic curves for small values of k_F, before collapsing and then becoming attractive. For D1S, the collapse starts at $k_F \simeq 1.5\,\text{fm}^{-1}$ and makes the energy negative-valued from $k_F \simeq 1.8\,\text{fm}^{-1}$. For D2 and DG, it is carried forward to $k_F \simeq 2.1\,\text{fm}^{-1}$ and $k_F \simeq 2.0\,\text{fm}^{-1}$, with negative-valued energies from $k_F \simeq 2.8\,\text{fm}^{-1}$ and $k_F \simeq 2.7\,\text{fm}^{-1}$, respectively. Equivalently, D1S, D2 and DG become attractive from around $\rho \simeq 1.4\rho_0$, $\rho \simeq 3.8\rho_0$ and $\rho \simeq 3.3\rho_0$, respectively. This is not too pathological for D2 and DG as it is for D1S, since the typical densities found in atomic nuclei reach, at most, a few times the saturation density. Nevertheless, DG declines a little before D2, and we then had to remain vigilant when choosing a DG parametrization to make certain this behavior was not pushed back to even lower densities.

In the triplet-odd channel $(S=1,T=1)$, the two types of realistic calculations are nearly identical until $k_F \simeq 1.5\,\text{fm}^{-1}$; beyond, the inclusion of the three-body effects

5. As some authors do, we could have produced these figures as a function of the density ρ, which is linked to the Fermi momentum k_F by the simple relation (A.27). We preferred to keep the Fermi momentum, as the curves appear to be more explicit that way.

implies a steeper rise. Their contributions are globally repulsive, except around $k_F \simeq 1.3\,\mathrm{fm}^{-1}$, where they exhibit a tenuous attraction that does not exceed 500 keV. The D1S interaction is repulsive at all densities, but fails to reproduce the rise of realistic calculations, contrary to D2 and DG. The ascent is a little too strong with D2 and DG, beginning at $k_F \simeq 1.2\,\mathrm{fm}^{-1}$ compared to $k_F \simeq 1.5\,\mathrm{fm}^{-1}$ for realistic calculations, although very slightly closer to that of the BBG 3B curve in the case of DG. As for the attraction, D2 and DG succeeded in reproducing it even though it takes place a bit earlier for D2 and DG, at $k_F \simeq 1\,\mathrm{fm}^{-1}$, and reaches a maximum value of 350 keV and 200 keV, respectively.

In the singlet-even ($S = 0, T = 1$) channel, two- and three-body realistic calculations blend into each other and are attractive up to $k_F \simeq 1.2\,\mathrm{fm}^{-1}$. Afterwards, while BBG curve continues decreasing, the descent of BBG 3B stops at $k_F \simeq 1.3\,\mathrm{fm}^{-1}$ and evolves into a highly repulsive behavior. This is clearly the channel in which the three-body effects are the most visible. The BBG results are properly reproduced by D1S, without the physics of the three-body interactions. By tuning the intensity of the finite-range density-dependent term in this subspace, Chappert managed to create D2-type interactions following the BBG 3B curve [17]. Regrettably, these interactions manifested non-zero pairing in magic nuclei because of their excessive attractivity at low Fermi momenta. The conclusion was that an interaction should not be too far from D1S in this channel so as not to show pairing in magic nuclei, hence the D2 curve. We followed this recommendation for DG, which in the end deviates very slenderly from D2 and remains close to the two-body realistic predictions.

In the triplet-even ($S = 1, T = 0$) channel, realistic calculations reveal attraction with decreasing energy until $k_F \simeq 2\,\mathrm{fm}^{-1}$, which is a bit more pronounced with the three-body correction. A reduction of the potential energy per particle of about 8 MeV with respect to pure BBG previsions is induced, at the minimum, by this correction. Indeed, it is about -35.5 MeV without, compared to -43.5 MeV with three-body effects taken into consideration. Then the curves go up, as a signature of repulsion. This tendency is observed by D1S, even if the minimum of -24 MeV appears sooner, at $k_F \simeq 1.4\,\mathrm{fm}^{-1}$. Predictions are amended with D2 and DG. Both are attractive and stick to the BBG curve before reaching their minima at the higher Fermi momentum $k_F \simeq 1.7\,\mathrm{fm}^{-1}$, with respective energies -30.5 MeV and -29.5 MeV. These very close points mark the start of the final ascent predicted by realistic calculations.

As we have said in section II.1.2.1, the density-dependent term may include some of the *short-range* effects of the tensor interaction. Albeit the tensor force does not contribute to the energy in nuclear matter, its presence renormalizes the coefficients of the density-dependent term and should, ultimately, affect the behavior of the DG interaction in $S = 1$ channels. However, we have shown that the D2 and DG curves are very similar in these channels. This observation can be attributed to the relatively long range associated with the tensor term and its intensity, which is less than that of the density-dependent interaction. We also point out that the filter on the neutron matter ($\beta = 1$) equation of state (see next subsection) has an influence on the potential energy of symmetric matter ($\beta = 0$), in the $T = 1$ channels. In the ($S = 1, T = 1$) channel, the D2 and DG results, obtained from the same requirements on the neutron matter equation of state, are very close, and improve the D1S results, fitted without such a filter. In the ($S = 0, T = 1$) channel, there are in addition two constraints on the TBMEs of the $1s$ and $2s$ states. Since their intensities remain the same for D1S, D2 and DG, they all produce alike curves.

Finally, D2 and DG interactions appear to us as the best compromises if we take a general outlook of the four (S, T) channels. This is particularly true in the odd channels.

Indeed, D1M and D3G3 collapse before D2 and DG, respectively making the energy negative-valued from $k_F \simeq 1.9\,\mathrm{fm}^{-1}$ and $k_F \simeq 2.6\,\mathrm{fm}^{-1}$ in the $(S = 0, T = 0)$ channel. In the $(S = 1, T = 1)$ channel, they predict maximum attractions of $-12\,\mathrm{MeV}$ and $-1.1\,\mathrm{MeV}$ respectively, which are a bit low compared to the value $-500\,\mathrm{keV}$ of realistic calculations.

Note that our analysis has to be treated with hindsight. Nuclear matter is a model that guides our search for a trustworthy parametrization, but its predictions do not have to be perfectly reproduced. For instance, several D2-type interactions better fitted the realistic curves in the above (S, T) channels than D2, but were found to be unconvincing in finite nuclei [17].

2.2. Neutron matter equation of state

As exposed in subsection I.2.3, a reduction of the energy drift along isotopic chains was achieved by the D1N, D1M, D2 and D3G3 interactions. To do so, requirements on the neutron matter ($\beta = 1$) equation of state was put in the fitting protocols of those interactions. In the specific cases of D1S and D2, eight points of the equation of state obtained by Friedman and Pandharipande (FP) [126] in neutron matter had to be reproduced with chosen accuracies. Contrary to D1M and D3G3, the energy drift was also controlled through a constraint on the energy difference $\Delta\varepsilon$ which can contribute to shrink that drift.

In Figure II.6, the neutron matter equations of state for several Gogny interactions are shown against the (neutron) density, and compared to FP predictions. It can be seen in panel (a) that the realistic calculations describe a strictly increasing and positive energy-valued equation of state at all densities, which ensures the stability of neutron matter. This is not the case of the D1S interaction as it starts decreasing at $\rho \simeq 3.5\rho_0$ until vanishing identically at $\rho = 12\rho_0$. Albeit this is not a good news for astrophysical perspectives, it is not an issue for atomic nuclei. However, even if in the range $\rho \leq \rho_0$ the D1S equation of states overestimates the realistic energies per particle by 3 MeV at worst, this is actually problematic in neutron-rich nuclei for which the difference grows fast. The need to drive the neutron matter equation of state appears to be clear.

In the $\rho \leq \rho_0$ regime, relevant for atomic nuclei, the D2 and DG interactions are no more than 1.5 MeV above the realistic curve. This was expected since the fitting code tolerates a maximum deviation of 10% to the FP values in this regime, and that they reach a maximum energy of 16 MeV at saturation density.

In the $\rho > \rho_0$ regime, potentially interesting for astrophysical purposes, the energy difference to FP predictions enlarges a bit for the D2 and DG interactions, becoming about 2 MeV at $\rho = 1.5\rho_0$, but remaining under control. The D1S interaction, in contrast, goes completely off course and announces its collapse. Beyond $2\rho_0$, the values taken by the energy are of less concern to us, the essential property being that the realistic equation of state is approximately reproduced, and above all that the curves do not break up. This is indeed the case for D2 and DG, with a somewhat better fit for DG at high densities.

2.3. Effective masses

In symmetric nuclear matter, neutron and proton effective masses are the same, with a numerical value that has been given in Table II.4 for different Gogny interactions. This is only because there is an equal number of neutrons and protons in SNM. As long as we move to asymmetric nuclear matter, characterized by a non-zero asymmetry parameter, $\beta \neq 0$, this is no longer true. We propose to study the evolution of the difference between

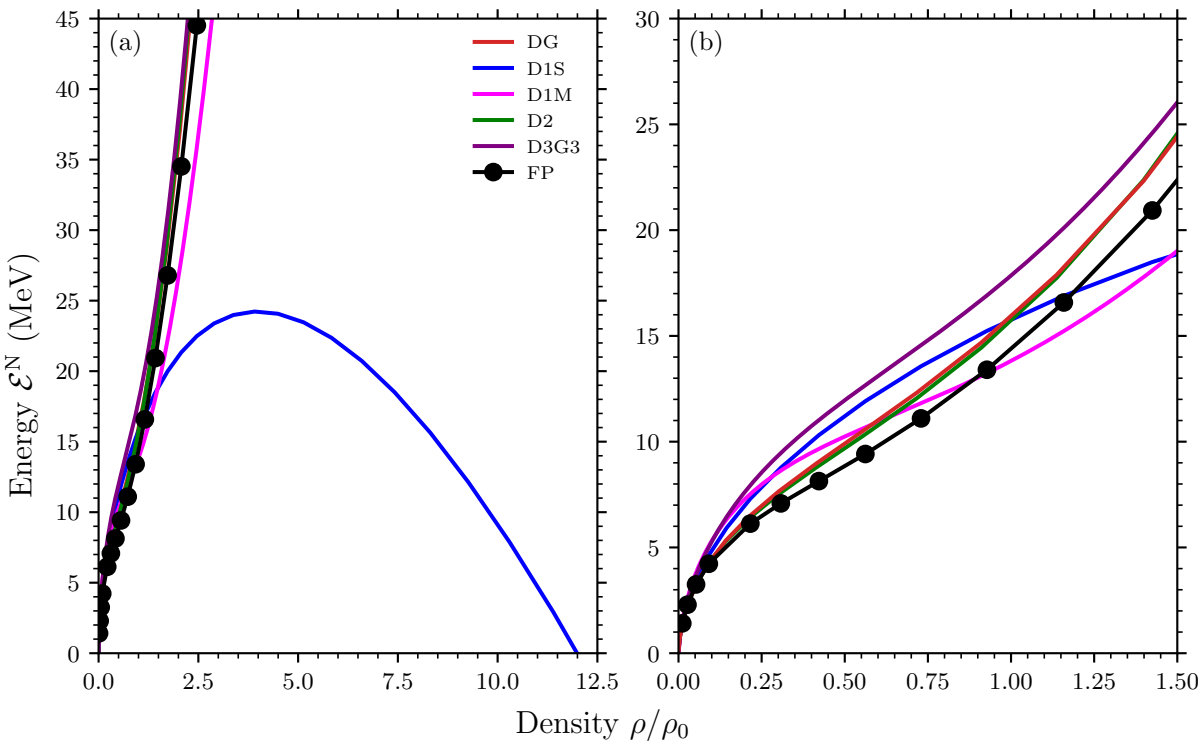

Figure II.6 – Equations of state in neutron matter for D1S, D1M, D3G3, D2 and DG interactions. Realistic calculations based on the work of Friedman and Pandharipande (FP) are also represented. Densities are normalized by the saturation density ρ_0. The results are presented at all densities in the left-hand panel, and at a restricted range of densities in the right-hand panel.

neutron and proton effective masses as a function of the medium asymmetry, for various Gogny interactions, in Figure II.7.

The results are compared to microscopic calculations based on the so-called Brueckner–Hartree–Fock (BHF) approximation of the Bethe–Brueckner–Goldstone (BBG) theory [155]. Within this approach, the effective interaction to be used is evaluated by the self-consistent treatment of the G-matrix. They are denoted BHF-BBG from now on. We first notice that, for zero asymmetry, the effective mass of microscopic calculations $m^*/m = 0.77$ slightly overestimates the empirical values we took on, $m^*/m = 0.70 \pm 0.05$. This is, however, not the case of the other interactions that fit the interval, as already discussed in subsection II.2.1.1. The D1M, D2 and DG interactions in particular are the closest to the microscopic results. As the asymmetry grows, the neutron and proton effective masses of the BHF-BBG scheme split up, with the neutron effective mass always greater than the proton effective mass, reaching a maximum difference of 0.16 for pure neutron matter ($\beta = 1$). It turns out that this behavior is described by both non-relativistic (as considered here) and relativistic (using Dirac–Brueckner–Hartree–Fock approximation) [156] microscopic calculations for neutron-rich nuclear matter. This salient phenomenon must be respected in order to obtain a good reproduction of the neutron single-particle energies, as we will see in section III.4.2. It is predicted by all the Gogny interactions displayed. The maximum difference in neutron and proton effective masses is about 0.32, 0.30 and 0.36, reached at $\beta = 1$, for D1S, D2 and DG, respectively. The D2 interaction is the closest to the microscopic value and DG the furthest away. We expected the filter on

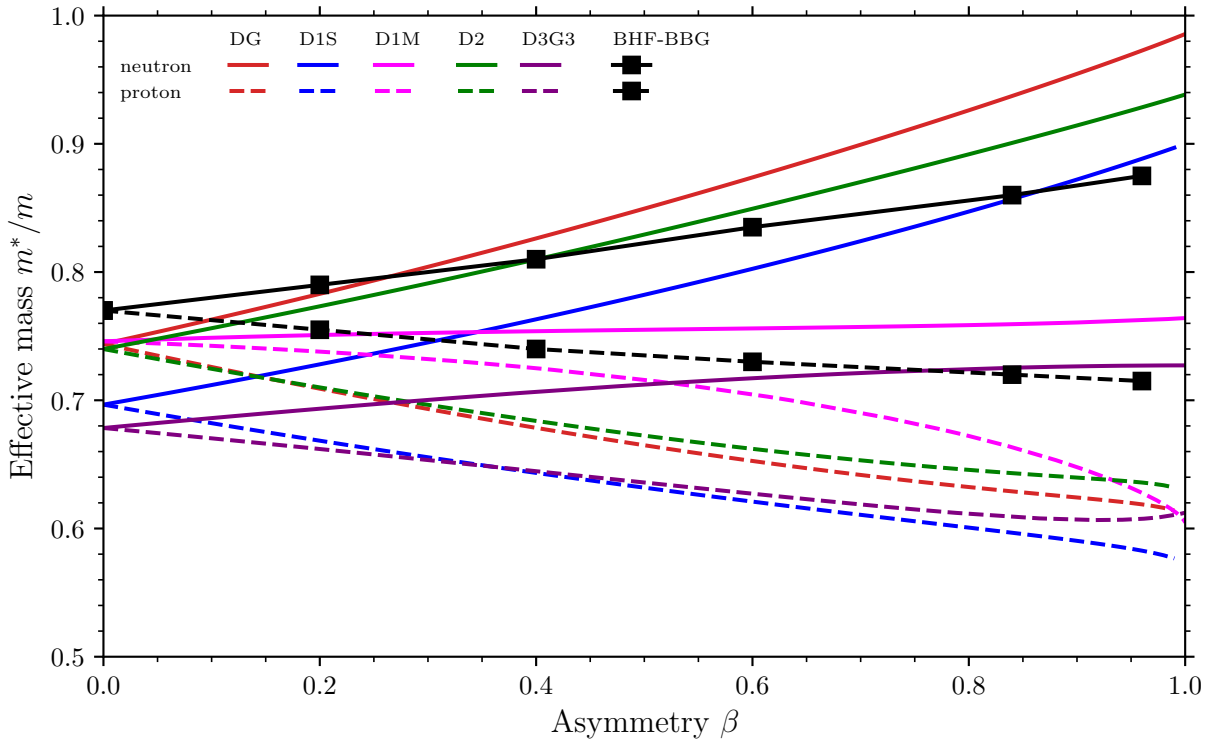

Figure II.7 – Evolution of the proton (full lines) and neutron (dashed lines) effective masses as a function of the asymmetry parameter β for D1S, D2, D1M, D3G3 and DG interactions. Microscopic calculations, founded on the Brueckner–Hartree–Fock approximation of the Bethe–Brueckner–Goldstone (BHF-BBG) theory are also displayed.

the neutron matter equation of state (see previous subsection) to substantially improve the difference in neutron and proton effective masses in neutron matter ($\beta = 1$) for DG, as it did for D2.

2.4. Partial wave decomposition

As we have already explained, neither the spin–orbit nor the tensor terms of the generalized Gogny interaction contribute to infinite nuclear matter. Thus, the quantities we have studied so far do not allow to figure out whether they have been fitted the right way. Actually we can get some clues, as we shall see, by projecting the potential energy per particle in symmetric nuclear matter onto a basis characterized by the orbital $\vec{L}$, intrinsic $\vec{S}$ and total $\vec{J} \equiv \vec{L} + \vec{S}$ angular momenta, according to

$$\frac{\mathcal{E}^{\mathrm{S}}_{\mathrm{P}}}{A} = \sum_{LSJ} \frac{\mathcal{E}^{\mathrm{S}}_{\mathrm{P}}}{A}\left[{}^{2S+1}L_J\right], \tag{II.23}$$

where $\mathcal{E}^{\mathrm{S}}_{\mathrm{P}}/A[{}^{2S+1}L_J]$ denotes the contribution to the potential energy of the state defined by the usual spectroscopic notation ${}^{2S+1}L_J$, where L, S and J refer to the quantum numbers associated with the angular momenta listed above. This expression is called the *partial wave decomposition* of the interaction, where ${}^{2S+1}L_J$ is a partial wave. Finite-range interactions participate to all partial waves, but a careful analysis of BHF calculations [157, 158] performed with the realistic interaction AV18 [27] reveals that the contributions of partial waves decrease as L grows. For $L > 3$, they become negligible, so that

expansion (II.23) can be truncated to order $L = 3$. To justify this statement for the generalized Gogny interaction and the other interactions it is compared to, we focus on the first partial waves P, D and F in Figure II.8.

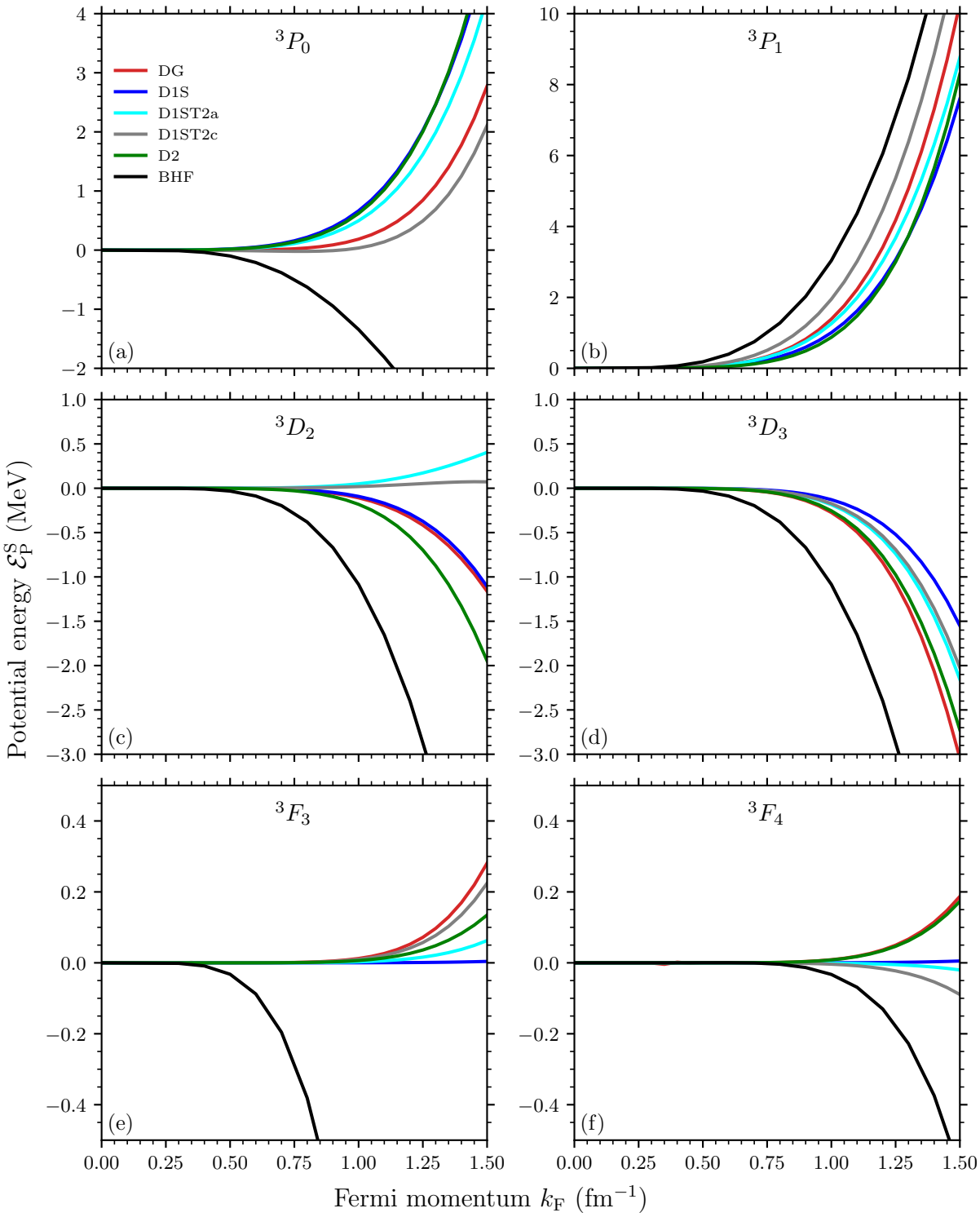

Figure II.8 – Potential energy per particle of the partial waves $^3P_0$,$^3P_1$,$^3D_2$,$^3D_3$,$^3F_3$ and $^3F_4$ versus the Fermi momentum, evaluated in symmetric nuclear matter for DG, D1S, D1ST2a, D1ST2c and D2 interactions. The predictions are compared with realistic calculations using Brueckner–Hartree–Fock approximation [157, 158].

It appears clearly that the contributions of the various Gogny interactions to the potential energy decreases in a significant way as L grows, becoming very small for F waves. Retaining only $L \leq 3$ partial waves in the expansion (II.23) also for Gogny interactions then makes sense. We see that the reproduction of P waves is enhanced by the tensor-dependent interactions DG, D1ST2a and D1ST2c, with respect to D1S and D2, although the monotony of ${}^3P_0$ is not recovered. In D waves, the descent of the BHF curve is less pronounced but observed with Gogny interactions, except for D1ST2-type ones in ${}^3D_2$. In ${}^3D_3$, the predictions of the DG interaction are the most convincing. Finally, the results obtained with DG in F waves tend to worsen the description. However, this is not pathological since the main contribution to the partial wave decomposition is due to the P waves, and to a lesser extent, to the D waves. Indeed, for instance, DG and D2 predictions differ from about 2.5 MeV, 0.8 MeV and 150 keV in ${}^3P_0$,${}^3D_2$ and ${}^3F_3$ waves, respectively, at $k_\mathrm{F} = 1.5\,\mathrm{fm}^{-1}$. Consequently, even if D2 is closer to the BHF calculations in ${}^3D_2$ and ${}^3F_3$, the important improvement is obtained with DG in ${}^3P_0$.

Now, we would like to find a way to use the partial waves studied to discriminate the contributions of the spin–orbit and tensor forces. On the one hand, it has been shown [159] that for given values of L and S, the contributions of central and density-dependent terms to $\mathcal{E}^\mathrm{S}_\mathrm{P}/A[{}^{2S+1}L_J]$ are the same for all values of J, up to a global factor $(2J+1)$. On the other hand, we know the spin–orbit and tensor terms to contribute only to the $S = 1$ channel. As a consequence, the differences

$$\delta_P \equiv \frac{\mathcal{E}^\mathrm{S}_\mathrm{P}}{A}\Big[{}^3P_0\Big] - \frac{1}{3}\frac{\mathcal{E}^\mathrm{S}_\mathrm{P}}{A}\Big[{}^3P_1\Big], \tag{II.24a}$$

$$\delta_D \equiv \frac{1}{5}\frac{\mathcal{E}^\mathrm{S}_\mathrm{P}}{A}\Big[{}^3D_2\Big] - \frac{1}{7}\frac{\mathcal{E}^\mathrm{S}_\mathrm{P}}{A}\Big[{}^3D_3\Big], \tag{II.24b}$$

$$\delta_F \equiv \frac{1}{7}\frac{\mathcal{E}^\mathrm{S}_\mathrm{P}}{A}\Big[{}^3F_3\Big] - \frac{1}{9}\frac{\mathcal{E}^\mathrm{S}_\mathrm{P}}{A}\Big[{}^3F_4\Big], \tag{II.24c}$$

only depend on the spin–orbit and tensor forces. We want to emphasize here that the total contributions of these terms to the partial wave decomposition is zero (when summed up over *all* values of L, S and J in (II.24a)), but that the above differences written for *some* partial waves are not. By comparing the predictions of effective interactions to BHF results with respect to these differences, the spin–orbit and tensor terms are considered separately from the other terms and their relevance can be assessed. This is precisely what was done in [160] with the Skyrme N3LO pseudo-potential and in [161] for D1-type Gogny interactions. We have extended the calculations to carry on this last study for interactions DG, D1ST2a, D1ST2c and D2 [162]. The results are displayed in Figure II.9.

First of all, we notice that the magnitudes of the differences in partial waves evaluated with Gogny interactions decreases sharply as L increases, until becoming very small in F waves, in accordance with what we have said earlier. As expected, the contributions of D1S and D2 interactions are the same since they are tensor-independent and their spin–orbit terms are identical. They additionally provide no contributions in D and F waves as the zero-range spin–orbit force is zero in $L > 1$ states, as one can show [159]. The predictions of δ_P are improved by all tensor-dependent interactions, but deteriorated for the differences δ_D and δ_F, with respect to those of D1S and D2. This is rather encouraging since, among the differences under study, the main contribution to the partial wave decomposition is related to P waves. In particular, a striking change of monotony is observed with DG and D1ST2c curves to get closer to the realistic calculations. It is worth noticing that such behavior is not shared with D1ST2a, whose difference with D1S and D2 is only due to the tensor force, the strength of the spin–orbit term being

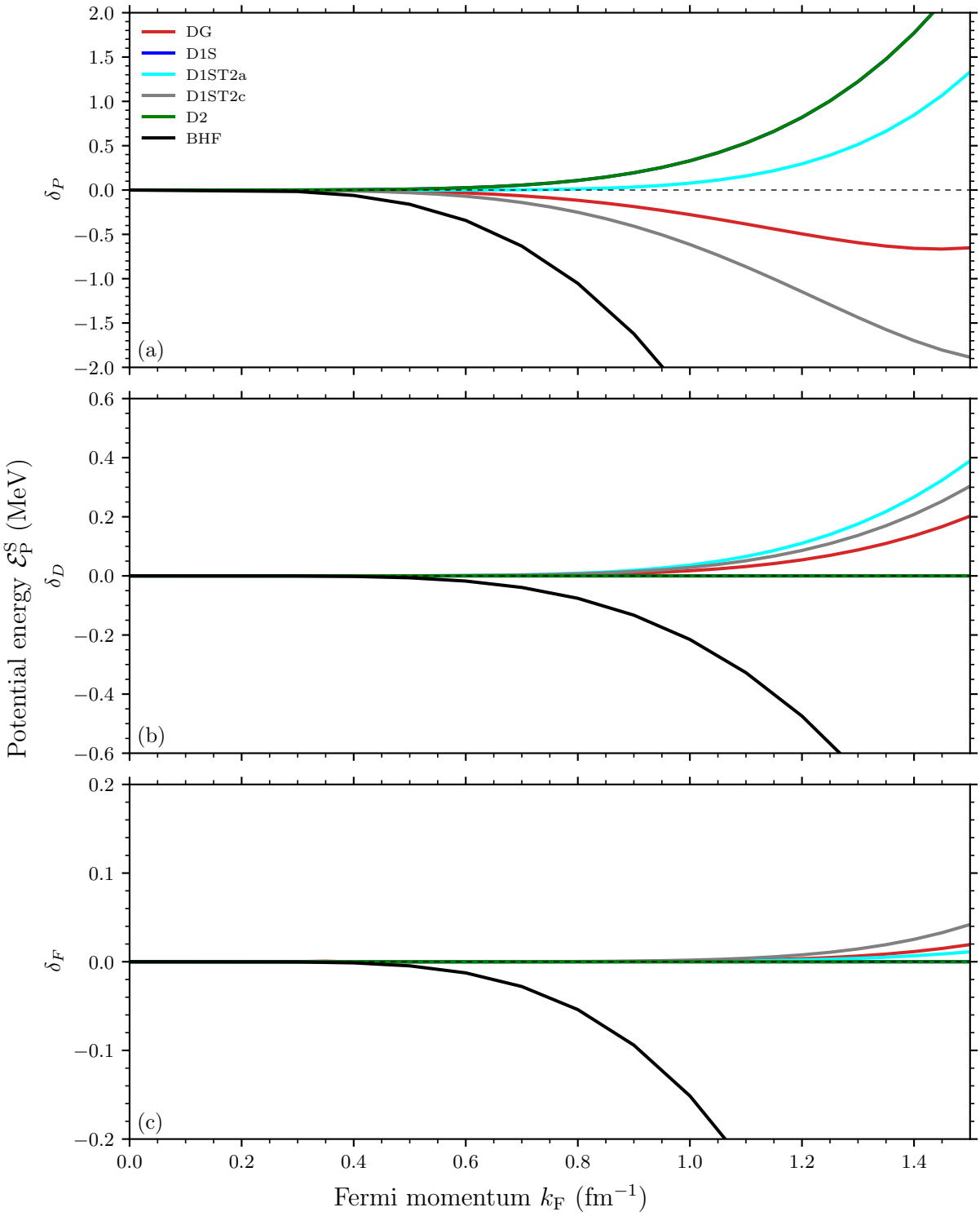

Figure II.9 – Potential energy per particle of the differences in partial waves δ_P, δ_D and δ_D given in (II.24a) versus the Fermi momentum, evaluated in symmetric nuclear matter for DG, D1S, D1ST2a, D1ST2c and D2 interactions. The predictions are compared with realistic calculations using Brueckner–Hartree–Fock approximation [157, 158]. Zero differences are displayed by dashed lines for clarity.

the same ($W_5 = 130\,\text{MeVfm}^5$). Although modifying the outputs in the right direction, the tensor term alone here seems unable to reverse the monotony obtained with D1S

and D2 interactions. For that purpose, the strength of the spin–orbit force must be reduced as well, as for DG ($W_5 - H_5 = 115.849\,\mathrm{MeVfm}^5$) and D1ST2c ($W_5 = 103\,\mathrm{MeVfm}^5$) interactions. The predictions of D1ST2c, whose spin–orbit is the lowest, are by the way the best for P waves. Among the tensor-dependent interactions, DG has the least negative impact on δ_P while it is slightly worse than D1ST2a in the reproduction of δ_F, but the difference is minuscule, reaching at most 10 keV at $k_\mathrm{F} = 1.5\,\mathrm{fm}^{-1}$. On the other side, D1ST2a outcomes in P waves were not satisfactory enough. Gathering our remarks, we can conclude that DG appears as the best comprise, its spin–orbit and tensor part globally enhancing the description in terms of partial waves. In the light of this study, the spin–orbit and tensor forces are correctly fitted at this stage, since they help refine the results locally.

2.5. Landau parameters

We present in this section the Landau parameters as well as the related stability criteria and sum rules obtained for the DG interaction in the framework of the Landau theory of Fermi liquids. We have already discussed the benefits of such quantities in the previous chapter. Let us add that the formalism enables us to test part of the residual interaction, giving an insight into the consistency of our nuclear interaction. Naturally, this study will however need to be extended to more complete RPA calculations for finite nuclei. So as not to slow down the discussion, we have deferred the underlying formalism in appendix A.4. We will content here to recall the key elements, and we urge the reader to, at least, have a look at the dedicated section.

2.5.1. Formalism and physical quantities

We show in appendix A.4, on the one hand, that (the two-body matrix elements of) a particle–hole interaction made up of tensor forces can be parametrized in simple terms. In homogeneous symmetric infinite nuclear matter (SNM), at the long wavelength limit (or Landau limit, corresponding to equal quasiparticle momenta in magnitude, $|\vec{k}_1| \simeq |\vec{k}_2| \simeq k_\mathrm{F}$), the latter reads [163, 164]

$$\begin{aligned} V_\mathrm{ph}^\mathrm{L} = N_0^{-1}\Big[& f^{00}(\theta) + f^{10}(\theta)(\vec{\sigma}_1\cdot\vec{\sigma}_2) + f^{01}(\theta)(\vec{\tau}_1\cdot\vec{\tau}_2) + f^{11}(\theta)(\vec{\sigma}_1\cdot\vec{\sigma}_2)(\vec{\tau}_1\cdot\vec{\tau}_2) \\ & + h^{10}(\theta)\frac{q_\mathrm{F}^2}{k_\mathrm{F}^2}S_{12}(\hat{q}_{12}) + h^{11}(\theta)\frac{q_\mathrm{F}^2}{k_\mathrm{F}^2}S_{12}(\hat{q}_{12})(\vec{\tau}_1\cdot\vec{\tau}_2)\Big], \end{aligned} \tag{II.25}$$

where the density of quasiparticle states at the Fermi surface is given by

$$N_0 \equiv \frac{2m^*\mathcal{V}k_\mathrm{F}}{\pi^2\hbar^2}. \tag{II.26}$$

The parameters f^{ST} and h^{1T}, where S and T respectively refer to the two-nucleon spin and isospin, characterize the quasiparticle interaction and then have to be determined. The parameters f^{ST} are called the central terms since they involve the central part of the nuclear interaction while the parameters h^{1T} are the tensor terms, involving its non-central part, with a tensor operator defined in momentum space as

$$S_{12}(\hat{q}_{12}) \equiv (\vec{\sigma}_1\cdot\hat{q}_{12})(\vec{\sigma}_2\cdot\hat{q}_{12}) - \frac{1}{3}\vec{\sigma}_1\cdot\vec{\sigma}_2, \tag{II.27}$$

where $\hat{q}_{12} \equiv (\vec{q}_1 - \vec{q}_2)/|\vec{q}_1 - \vec{q}_2|$ is the direction pointed by the relative quasiparticle momentum. When evaluated at the Fermi surface, this relative momentum is denoted $q_\mathrm{F} \equiv \vec{k}_\mathrm{F} - \vec{k}'_\mathrm{F}$.

On the other hand, we also show that for a density-dependent interaction like the generalized Gogny interaction (II.1), the TBMEs of its particle–hole interaction can be written [4, 165]

$$\begin{aligned}\langle ph'|V_\mathrm{ph}|hp'\rangle = \langle ph'|v_{12}^{(\mathrm{a})}|hp'\rangle + \sum_i \langle h'i|\frac{\partial v_{12}^{(\mathrm{a})}}{\partial \rho_{hp}}|p'i\rangle + \sum_i \langle pi|\frac{\partial v_{12}^{(\mathrm{a})}}{\partial \rho_{p'h'}}|hi\rangle \\ + \frac{1}{2}\sum_{ij}\langle ij|\frac{\partial^2 v_{12}^{(\mathrm{a})}}{\partial \rho_{hp}\partial \rho_{p'h'}}|ij\rangle,\end{aligned} \tag{II.28}$$

Thus, by calculating the TBMEs using (II.28), and identifying them, at the long wavelength limit, with the expression (II.25), it is possible to obtain the parameters f^{ST} and h^{1T}. More precisely, these are expanded in series of Legendre polynomials according to

$$f^{ST}(\theta) = \sum_l f_l^{ST} P_l(\cos\theta), \tag{II.29a}$$

$$h^{1T}(\theta) = \sum_l h_l^{1T} P_l(\cos\theta), \tag{II.29b}$$

and it is their coefficients f_l^{ST} and h_l^{1T}, the so-called *Landau parameters*, that one needs to evaluate, in principle for all values of $l \in \mathbb{N}$, to fully characterize the particle–hole interaction.

The central, density-dependent and tensor contributions to the TBMEs of (II.28) are derived from subsections A.4.2.1 to A.4.2.4, where we also prove that the spin–orbit TBMEs vanish in this framework. By summing up these components, we can derive the values of the Landau parameters for any l. Table II.5 gives the values of the first six central and non-central Landau parameters, evaluated at saturation density ρ_0, for the DG parametrization. The values of the Landau parameters associated with D1S and 2 interactions are also displayed in Tables II.6, for which non-central components do not exist.

	DG					
l	f_l^{00}	f_l^{10}	f_l^{01}	f_l^{11}	h_l^{10}	h_l^{11}
0	−0.300	0.226	0.869	0.922	0.001	−0.800
1	−0.775	0.027	0.528	0.501	0.001	−0.559
2	−0.845	0.229	0.503	−0.027		−0.148
3	−0.299	0.084	0.159	−0.041		−0.025
4	−0.064	0.018	0.032	−0.011		−0.003
5	−0.010	0.003	0.005	−0.002		
6	−0.001		0.001			

Table II.5 – Numerical values of the first Landau parameters of the interaction DG evaluated at saturation density. Empty boxes correspond to Landau parameters with a magnitude of less than 10^{-3}.

Empirical values for the first Landau parameters can be deduced from experimental data associated with collective states in ^{208}Pb (excitation energies, transition probabilities,

D1S				
l	f_l^{00}	f_l^{10}	f_l^{01}	f_l^{11}
0	−0.376	0.463	0.746	0.633
1	−0.908	−0.182	0.470	0.607
2	−0.555	0.244	0.341	−0.038
3	−0.156	0.090	0.099	−0.035
4	−0.029	0.018	0.019	−0.008
5	−0.004	0.003	0.003	−0.001
6				

D2				
l	f_l^{00}	f_l^{10}	f_l^{01}	f_l^{11}
0	−0.312	0.197	0.850	0.962
1	−0.785	−0.008	0.462	0.498
2	−0.828	0.277	0.532	−0.047
3	−0.310	0.111	0.184	−0.053
4	−0.072	0.026	0.041	−0.015
5	−0.012	0.004	0.007	−0.003
6	−0.002	0.001	0.001	

Tables II.6 – Same as in Table II.5, but for the D1S (left table) and D2 (right table) interactions. [6]

etc.). For a zero-range particle–hole interaction with no tensor forces, Ring *et al.* [166–168] obtained quantities that can be directly related to Landau parameters using Migdal theory [169], if we assume the $l = 0$ component in (II.29) to be the main contribution in the expansions to a large extent. The empirical values read $f_0^{00} \simeq 0.137$, $f_0^{10} \simeq 1.150$, $f_0^{01} \simeq 0.663$ and $f_0^{11} \simeq 1.450$. We see that f_0^{00} and f_0^{11} are closer to the empirical values with DG than with D1S and D2 interactions. As for f_0^{01}, the agreement remains pretty good with all three interactions, but less with f_0^{10}. Obviously, we were not expecting a perfect match with these empirical values as our interaction is of finite range and the tensor force may renormalize the central Landau parameters. On top of that, we see explicitly that the main contribution to the Landau parameter f_l^{00} is not contained in the $l = 0$ component. A comparison with empirical values taking into account one or more of the above hypotheses would certainly be more relevant.

It is not difficult to show that several physical quantities, namely incompressibility, effective mass and symmetry energy, already calculated in SNM in section II.2.1.1, can be related to some central Landau parameters as [169]

$$\frac{m^*}{m} = 1 + \frac{1}{3} f_1^{00}, \tag{II.30}$$

$$K_\infty = \frac{3\hbar^2 k_\mathrm{F}^2}{m^*}\left(1 + f_0^{00}\right), \tag{II.31}$$

$$a_\tau = \frac{\hbar^2 k_\mathrm{F}^2}{6m^*}\left(1 + f_0^{01}\right). \tag{II.32}$$

We emphasize that these three quantities are not impacted by the Landau parameters associated with the tensor force, so they are solely judges of the appropriateness of the central Landau parameters. In Table II.7 are compared the values obtained by means of the Landau parameters to the ones previously deduced from their analytical expressions (see Table II.4).

It appears first that the effective mass is reproduced by both methods to a very good approximation. We were then able to calculate symmetry energy and incompressibility

6. The attentive reader will notice that the values of the D1S and D2 Landau parameters are slightly different from those usually given in the literature [17, 18]. In fact, the version of the fitting code used by Chappert to provide what is found in the literature gives the values tabulated here. In-depth discussions with Chappert did not enable us to determine the source of these (small) disparities. These small differences will have little impact on the stability criteria and sum rules to be discussed.

	Physical quantities in SNM		
Determination method	m^*/m	K_∞ (MeV)	a_τ (MeV)
Analytical expressions	0.741 820	209.961	31.2603
Landau parameters	0.741 820	210.672	31.2603

Table II.7 – Some physical quantities evaluated at the saturation density in SNM for the DG Gogny interaction. The first row shows the numerical values obtained from analytical expressions derived in Appendix A, the second row from Landau parameters using relations (II.30).

from this common numerical value. The same conclusion occurs for the symmetry energy. Nevertheless, incompressibility is about 700 keV higher when evaluated by Landau parameters than by its analytical expression. This discrepancy, although set aside, was already there for the D2 interaction [17, 18].[7] We consider it sufficiently small not to be a cause of concern, and, in any case, it does not play a decisive role in what follows.

2.5.2. Stability criteria

It is explained in appendix A.4.3 that the quasiparticle ground state is stable against small deformations if any variation of the free energy is positive, i.e. if $\delta F > 0$, where the free energy is defined by [170, 171]

$$F \equiv \mathcal{E} - \mu_c A, \tag{II.33}$$

with μ_c the chemical potential and A the number of nucleons. By slightly distorting the ground state and applying this requirement, we can extract stability criteria associated with Landau parameters. In the presence of tensor forces, the stability criteria in the $S = 0$ channel simply read

$$f_l^{0T} + (2l+1) > 0, \quad \text{for } l \in \mathbb{N}. \tag{II.34}$$

In fact this expression remains the same without tensor forces since they do not contribute in this channel. The above quantities evaluated for the first six values of l in the case of the interaction DG are displayed in Table II.8, and in Tables II.9 for the interactions D1S and D2.

The stability criteria in the $S = 1$ channel are effectively complicated when the tensor force is taken into account. The condition becomes that the eigenvalues of the matrix F must all be positive [163]. From the expression of the TBMEs of F, we can easily obtain its eigenvalues. In the $T = 0$ channel, the TBMEs are given by (A.256), and it suffices to replace f_l^{10} by f_l^{11} and h_l^{10} by h_l^{11} to get them in the $T = 1$ channel. We also show that for some value of the total two-nucleon angular momentum J, the associated 3×3 matrix is divided into a diagonal 1×1 sub-block corresponding to $J = l = l'$ (the sub-block $J = 0$ being diagonal as well), and a non-diagonal 2×2 sub-matrix. We then distinguish between two types of eigenvalues. On the one side, we have the TBMEs belonging to the diagonal

7. We envisaged at some point that the discrepancy could be linked to an error in the derivation or implementation of the Landau parameters (in particular in the contribution coming from the rearrangement terms, on which only the parameter f_0^{00} depends). A scrupulous check was carried out and nothing was found. The same applies to the analytical expression of the incompressibility and its implementation.

sub-blocks, directly equal to the eigenvalues denoted $\lambda_0^{(J,T)}$. Their expression for the first six values of $(J, T = 0)$ are given in (A.257). On the other side, we have the non-diagonal sub-matrices that must be diagonalized by means of the procedure described in (A.258), to pull out two eigenvalues denoted $\lambda_\pm^{(J,T)}$. The expressions of the TBMEs composing the sub-matrices for the first four values of $(J, T = 0)$ can be found in (A.261). The stability criteria associated with the Landau parameters in the $S = 1$ channel of the interaction DG are displayed in Table II.10. Note that we cannot compare those values to tensor-free interactions like D1S and D2 since the related stability criteria obey different relations.

DG		
l	$f_l^{00} + (2l+1)$	$f_l^{01} + (2l+1)$
0	0.700	1.869
1	2.225	3.528
2	4.155	5.503
3	6.701	7.159
4	8.936	9.032
5	10.990	11.005
6	12.999	13.001

Table II.8 – Numerical values of the first quantities related to the stability criteria (II.34) of the interaction DG in the $S = 0$ channel. Columns two and three give the results in the $T = 0$ and $T = 1$ channels, respectively.

D1S		
l	$f_l^{00} + (2l+1)$	$f_l^{01} + (2l+1)$
0	0.624	1.633
1	2.092	3.607
2	4.445	4.962
3	6.844	6.965
4	8.971	8.992
5	10.996	10.999
6	13.000	13.000

D2		
l	$f_l^{00} + (2l+1)$	$f_l^{01} + (2l+1)$
0	0.688	1.197
1	2.215	2.992
2	4.172	5.277
3	6.690	7.111
4	8.928	9.026
5	10.988	11.004
6	12.998	13.001

Tables II.9 – Same as in Table II.8, but for the D1S (left table) and D2 (right table) interactions.

In principle, we should check that the stability criteria remain valid for all values of $l \in \mathbb{N}$ and $|l-1| \leq J \leq l+1$. In practice, the Landau parameters converge rapidly (in the sense that their absolute value decreases sharply as l increases), as can either be inferred from their analytical expressions, given from subsections A.4.2.1 to A.4.2.4, or directly from their first numerical values listed in Tables II.5 and II.6. It is worth noticing by the way that the Landau parameters associated with the non-central part of DG follow the same decreasing tendency as those of D1S and D2 interactions. We then reasonably decided to calculate the Landau parameters until their magnitudes fell below 10^{-3}. This took us up to $l = 6$. The stability criteria are based on TBMEs that, for a given value of l, involve Landau parameters of maximum order $l + 1$ (see expression

J	$\lambda_0^{(J,0)}$	$\lambda_+^{(J,0)}$	$\lambda_-^{(J,0)}$	$\lambda_0^{(J,1)}$	$\lambda_+^{(J,1)}$	$\lambda_-^{(J,1)}$
0	1.007			3.106		
1	1.010	2.452	2.091	0.197	4.600	1.641
2	1.046	2.024	2.017	0.791	2.895	1.865
3	1.012	2.092	2.004	0.963	2.139	1.969
4	1.002	2.024	2.001	0.995	2.011	1.993
5	1.000		1.002	0.999		1.000
6			1.000			1.000

Table II.10 – Numerical values of the first eigenvalues of the free energy (II.33) for the interaction DG. The stability criteria in the $S = 1$ channel require these values to be positive. Columns two to four and five to seven give the results in the $T = 0$ and $T = 1$ channels, respectively.

(A.256)). For this reason, we evaluated the stability criteria up to the finite order $l_{\max} = 5$ and $J_{\max} = l_{\max} + 1 = 6$. This choice appears justified since the quantities related to the stability criteria in the $S = 0$ channel seem to converge towards $(2l+1)$, while those in the $S = 1$ channel seem to converge towards 1 for the eigenvalues $\lambda_0^{(J,T)}$ and 2 (up to $J = 4$) for the eigenvalues $\lambda_\pm^{(J,T)}$, [8] according to Tables II.9, II.8 and II.10. This was expected according to the expressions (II.34), (A.257), (A.261) and (A.262). In the $S = 0$ channel, we can see in particular that the DG stability criteria follow the same trend as those of D1S and D2.

Thus, we obtain that the stability criteria are fulfilled in both $S = 0$ and $S = 1$ channels, explicitly up to $l_{\max}$ and $J_{\max}$ – as all quantities in Tables II.8 and II.10 are positive –, and implicitly for all values $l \in \mathbb{N}$ and $|l-1| \leq J \leq l+1$. It should be noted that these criteria are fairly restrictive since most DG-type interactions we studied did not meet all of them.

2.5.3. Sum rules

In appendix A.4.4, we parametrize the forward scattering amplitude of a quasiparticle pair on the Fermi surface as [164, 170]

$$\begin{aligned}\mathcal{S} = N_0^{-1}\Big[&b^{00}(\theta) + b^{10}(\theta)(\vec{\sigma}_1\cdot\vec{\sigma}_2) + b^{01}(\theta)(\vec{\tau}_1\cdot\vec{\tau}_2) + b^{11}(\theta)(\vec{\sigma}_1\cdot\vec{\sigma}_2)(\vec{\tau}_1\cdot\vec{\tau}_2)\\ &+ d^{10}(\theta)\frac{q_{\mathrm{F}}^2}{k_{\mathrm{F}}^2}S_{12}(\hat{q}_{12}) + d^{11}(\theta)\frac{q_{\mathrm{F}}^2}{k_{\mathrm{F}}^2}S_{12}(\hat{q}_{12})(\vec{\tau}_1\cdot\vec{\tau}_2)\Big],\end{aligned} \tag{II.35}$$

where N_0 is given in (II.26). The parameters b^{ST} and h^{1T} fully characterize the forward scattering amplitude. Just like the parameters of the quasiparticle interaction (II.29),

8. As the stability criteria are truncated (at $J_{\max} = 6$), particular attention must be paid at the boundaries. There are only two eigenvalues for $J = 5$, one related to $l = 4$, the other to $l = 5$. For $J = 6$, there is only one eigenvalue related to $l = 5$. The eigenvalue related to $(J = 5, l = 5)$ corresponds to the diagonal matrix element (A.257f). As for the eigenvalues $(J = 5, l = 4)$ and $(J = 6, l = 5)$, they would normally be part of coupled matrix elements like those of (A.261), but written for the corresponding values of J. Here, since the stability criteria are truncated, they simply appears as diagonal matrix elements whose expressions have been calculated in (A.262). For this reason, they converge towards 1 instead of 2, like the other diagonal matrix elements. We have conventionally chosen to denote them $\lambda_-^{(J,T)}$ since they involve the lowest part of their (truncated) sub-matrices, as indicated in Table II.10.

they are expanded in series of Legendre polynomials according to

$$b^{ST}(\theta) = \sum_l b_l^{ST} P_l(\cos\theta), \tag{II.36a}$$

$$d^{1T}(\theta) = \sum_l d_l^{1T} P_l(\cos\theta). \tag{II.36b}$$

On the one hand, when tensor forces are taken into account, one can show the following relations,

$$b_l^{0T} = \frac{f_l^{0T}}{1 + f_l^{0T}/(2l+1)}, \tag{II.37}$$

$$b_l^{1T} = \frac{1}{3}\sum_J \frac{2J+1}{2l+1} \mathcal{S}_{ll}^{JT}, \tag{II.38}$$

where f_l^{0T} are the central Landau parameters in the $S = 0$ channel introduced in the previous subsection, while $\mathcal{S}_{ll}^{JT}$ denotes the forward scattering amplitude coupled to (J, T). Its expression and the related quantities are given in (A.276), (A.277) and (A.278). On the other hand, the Pauli exclusion principle forces the forward scattering amplitude to be antisymmetric under the exchange of the two quasiparticles. This requirement translates into the equation

$$P\mathcal{S} \equiv P_r P_\sigma P_\tau \mathcal{S} = -\mathcal{S}. \tag{II.39}$$

Combining the two last identities, we obtain that the Pauli principle holds if and only if the so-called *sum rules* in the presence of tensor forces (A.280) and (A.281) are verified. In fact, we truncate these two summations at the finite order $l_{\max} = 5$ as we have done for the stability criteria, so that they here become [164]

$$\begin{aligned} S_1 &\equiv \sum_{l=0}^{l_{\max}} \left[\frac{f_l^{00}}{1 + f_l^{00}/(2l+1)} + \frac{f_l^{01}}{1 + f_l^{01}/(2l+1)} + \frac{1}{3}\sum_J \frac{2J+1}{2l+1}\left(\mathcal{S}_{ll}^{J0} + \mathcal{S}_{ll}^{J1}\right)\right] = 0, \\ &\equiv \sum_i T_1^i, \end{aligned} \tag{II.40}$$

$$\begin{aligned} S_2 &\equiv \sum_{l=0}^{l_{\max}} \left[\frac{f_l^{00}}{1 + f_l^{00}/(2l+1)} - \frac{3f_l^{01}}{1 + f_l^{01}/(2l+1)} + \sum_J \frac{2J+1}{2l+1}\left(3\mathcal{S}_{ll}^{J1} - \mathcal{S}_{ll}^{J0}\right)\right] = 0, \\ &\equiv \sum_i T_2^i. \end{aligned} \tag{II.41}$$

We have decomposed the two sum rules into nine components i in order to evaluate their relative contributions T_i. The two first contributions correspond to the sums over l of the terms involving the Landau parameters f_l^{00} and f_l^{01}. The remaining ones correspond to the sums over l of the last term for some given value of J. There are $J_{\max} + 1 = 7$ such quantities. These contributions together with the full sum rules S_1 and S_2 for the interaction DG are listed in Table II.11.

Generally speaking, the sum rules are almost always violated by effective interactions [172]. Calculating their numerical values nonetheless allows us to know to what extent they are. As sum rules are not observables, it is difficult to say whether a definite non-zero value accounts for a significant violation, or not. We then usually compare the predictions of the interactions with each other. We do so in Table II.12, where the interaction DG is in particular compared to D1S and D2, whose sum rules are simplifications of those given above (see relations (A.273) and (A.274)). The value of S_2 is smaller than that of

i	J	T_1^i	T_2^i
1		−2.877	−2.877
2		1.564	−4.691
3	0	0.228	2.027
4	1	−3.482	−34.195
5	2	0.061	−0.739
6	3	0.161	−0.168
7	4	0.041	−0.139
8	5	0.007	−0.038
9	6	0.001	−0.005
		−4.297	−40.826

Table II.11 – Relative contributions of the various terms T_1^i and T_2^i appearing in the sum rules (II.40) and (II.41). The numerical values of the sum rules S_1 and S_2 are displayed in the last row, under the dashed line.

S_1 for DG, as is the case for the D1S and D2 interactions. Even so, their magnitudes are much higher than for D1S and D2. Table II.11 unveils that the dominant contributions to these sums correspond to $i = 4$, that is the third terms of S_1 and S_2 for $J = 1$. We now focus on the contribution $J = 1$ of S_2 as it is the largest. The fitting code reveals that the component $l = 1$ is mainly responsible for it, to be precise, which then corresponds to $3\mathcal{S}_{11}^{J1} - \mathcal{S}_{11}^{J0}$. According to the expression (A.276) of the coupled forward scattering amplitude, we have, in the channel T,

$$\mathcal{S}_{11}^{1T} = 3\frac{\langle 11|F|11\rangle^T - 1}{\langle 11|F|11\rangle^T}, \tag{II.42}$$

where the associated TBMEs are given by (A.257b), i.e.

$$\langle 11|F|11\rangle^T = 1 + \frac{1}{3}f_1^{1T} + \frac{5}{3}h_0^{1T} - \frac{2}{3}h_1^{1T} + \frac{1}{15}h_2^{1T}. \tag{II.43}$$

Plugging the values of the Landau parameters of Table II.5, we get $\langle 11|F|11\rangle^0 \simeq 1.010$, hence $\mathcal{S}_{11}^{10} \simeq 0.030$, and $\langle 11|F|11\rangle^1 \simeq 0.197$, hence $\mathcal{S}_{11}^{11} \simeq -12.228$. It is therefore the high value of $\mathcal{S}_{11}^{11}$, resulting from the low value of $\langle 11|F|11\rangle^1$, that causes the explosion of the magnitude of S_2. Actually, the low value of $\langle 11|F|11\rangle^1$ comes from the prevailing contribution of the tensor Landau parameter h_0^{11}, since $5h_0^{11}/3 \simeq -1.333$. A similar study can be carried out to explain the high value of the component $i = 4$ of S_1. As a consequence, an important part of the violation of the DG sum rules can be attributed to the tensor interaction. To get to the bottom of it, we look at the sum rules for the DG interaction when the tensor interaction is set to zero (see Table II.12). We accordingly find out that the Pauli principle is less violated, the values being of the order of magnitude of those of D2; S_2 is even closer to zero. Although the value of S_2 is still far from that of D1S, that of S_1 is better.

For the sake of completeness, we could compare our values with the sum rules of effective interactions containing a tensor term. Alas we found no such study in the literature.[9] We therefore evaluated the sum rules for other tensor-dependent Gogny

9. There is an article in which sum rules are calculated for a zero-range tensor-dependent Skyrme interaction [173]. However, these are of a different kind.

	Sum rules	
	S_1	S_2
Interaction		
DG	−4.297	−40.826
DG (no tensor)	0.048	−1.718
D1S	−0.175	−0.650
D1ST2a	28.113	254.948
D1ST2c	28.131	254.897
D2	0.007	−2.104

Table II.12 – Numerical values of the sum rules for the D1S, D2, D1ST2a, D1ST2c and DG Gogny interactions. The values obtained by switching off the tensor interaction in DG are also tabulated as "DG (no tensor)".

interactions, the D1ST2a and D1ST2c interactions. These are good candidates since their perturbative natures allow to isolate the tensor effects on the sum rules (the spin–orbit force giving no contribution), while their D1S part is little violated. Table II.12 indicates that the D1ST2a and D1ST2c sum rules have similar values and are by far the most broken of all tested interactions. They are the only ones to be overestimated to that extent. Yet, the D1ST2-type interactions manifest some valuable characteristics, from the point of view of their nuclear structure [60, 174], deformation [38, 40] and fission [39] properties. Comparatively, our tensor-dependent interaction produces reasonable values. In order to settle whether our sum rules are problematic or not, we would definitely need to test it in finite-nuclei RPA calculations, which are beyond the scope of this report. It would also be enlightening to know if there exists other tensor-dependent effective interactions capable of reducing the sum rules to values comparable to those of DG, or even better. On the other hand, it was shown for these latter that the inclusion of the rearrangement terms associated with the density-dependent interaction reduced the violation of the sum rules. It is then legitimate to think that adding a density dependence to the tensor term would produce the same effect.

Chapter III

Mean-field results

> "People say sometimes that Beauty is superficial. That may be so. But at least it is not so superficial as Thought is. To me, Beauty is the wonder of wonders. It is only shallow people who do not judge by appearances. The true mystery of the world is the visible, not the invisible."
>
> — Oscar Wilde, *The Picture of Dorian Grey*

In this chapter, the mean-field properties of the generalized Gogny interaction are analyzed within the Hartree–Fock–Bogoliubov approach. After introducing the related formalism in a two-center axially symmetric representation, as well as the conditions under which the calculations are performed, the bulk and surface characteristics of this interaction are probed. The potential energy surfaces of light- to heavy-mass nuclei are subsequently drawn to underline the specificities of the generalized Gogny interaction regarding deformations and even fission barriers. Particular attention will be paid all along the way to the relative roles of the spin–orbit and tensor forces to these aspects.

Chapter contents

1. General framework

1.1. Hartree–Fock–Bogoliubov formalism in a two-center basis

We first take some time to introduce the formalism of the Hartree–Fock–Bogoliubov (HFB) theory in a *two-center* representation, which is a bit more elaborated compared to the simple one-center version. The main reason, we will return later, is that it provides a more appropriate description of the fission process, during and immediately after the scission. We shall concentrate on the main principles used in Appendix C to derive the HFB fields of the generalized Gogny interaction (II.1). For a more detailed presentation, we refer the reader to the reviews [175, 176]. The formalism is exposed without imposing time-reversal invariance, but the simplifications to be made when it is will be highlighted.

1.1.1. Bogoliubov transformation

The starting point to build up the HFB equations is to define the quasiparticle states of the system, that is to say the elementary excitations of the nucleus in the mean-field approximation with pairing correlations taken into account. Since we want our quasiparticle states to describe both proton and neutron states displaying an axial symmetry, they must be eigenstates of the isospin operator T_z (with eigenvalues $t = \pm 1/2$) and of the angular momentum J_z (with eigenvalues Ω), along the quantization axis Oz. In the following, only the particle-like pairing correlations, i.e. proton–proton and neutron–neutron pairing correlations, are taken into account. Within this formalism, the quasiparticle states are expressed on the axial harmonic oscillator (HO) states by means of the Bogoliubov transformation as

$$\xi^\dagger_{t\Omega n} = \sum_{r_a} \left(U^{t\Omega}_{r_a n} c^\dagger_{t\Omega r_a} + \overline{V}^{t\Omega}_{r_a n} \overline{c}_{t\Omega r_a} \right), \tag{III.1}$$

in such a way that

$$\xi_{t\Omega n} |\widetilde{0}\rangle = 0, \quad \text{for all } t, \Omega, n, \tag{III.2}$$

where we have defined the quasiparticle vacuum by

$$|\widetilde{0}\rangle \equiv \prod_{t\Omega n} \xi_{t\Omega n} |0\rangle, \tag{III.3}$$

with the particle vacuum denoted as $|0\rangle$. In the first expression, r_a denotes the quantum numbers associated with this basis, that turns out to be composed of axially-symmetric harmonic oscillator (HO) wave functions in the `HFB3` code, which we will further specify in subsection III.1.2. As for the additional index n, it distinguishes the quasiparticle states of the same quantum numbers t and Ω. The entities $c_a^\dagger$ and c_a are the creation and annihilation operators of quasiparticles associated with the axial HO states $|a\rangle$, in the second quantization formalism. Quantities topped by a bar indicate that they are reversed in time. We can show that the matrices U and V, acting as coefficients of the Bogoliubov transformation, can be chosen real if we impose the quasiparticle vacuum $|\widetilde{0}\rangle$ to be invariant under the T-simplex transformation (C.20). Note also that, as desired, the Bogoliubov transformation preserves the quantum numbers t and Ω. For this reason, they appear as superscripts in the matrices U and V to indicate that these are diagonal with respect to those quantum numbers. This is a convention we will follow throughout this report.

In the general case where the quasiparticle vacuum $|\widetilde{0}\rangle$ is not time-reversal invariant, we can define two types of density matrices, ρ and $\overline{\rho}$, and a pairing tensor κ, as

$$\rho^{t\Omega} \equiv V^{t\Omega}(V^{t\Omega})^T, \tag{III.4a}$$
$$\overline{\rho}^{t\Omega} \equiv \overline{V}^{t\Omega}(\overline{V}^{t\Omega})^T, \tag{III.4b}$$
$$\kappa^{t\Omega} \equiv V^{t\Omega}(\overline{U}^{t\Omega})^T, \tag{III.4c}$$

or, equivalently, using their components, as

$$\rho_{ab} \equiv \langle\widetilde{0}|c_b^\dagger c_a|\widetilde{0}\rangle, \tag{III.5a}$$
$$\overline{\rho}_{ab} \equiv \langle\widetilde{0}|\overline{c}_b^\dagger \overline{c}_a|\widetilde{0}\rangle, \tag{III.5b}$$
$$\kappa_{ab} \equiv \langle\widetilde{0}|c_a \overline{c}_b|\widetilde{0}\rangle, \tag{III.5c}$$

where the time-reversal operation is defined through its action on the creation operator as $\overline{c}_a \equiv T c_a T^{-1} = \sigma_a c_{-a}$. With this definition, it is not difficult to show that the density matrices are real and symmetric (under the exchange of their indices) while the pairing tensor is only real. When time-reversal invariance is demanded, the two expressions of the density matrices coincide, i.e. $\rho = \overline{\rho}$, and the pairing tensor becomes symmetric (under the exchange of its indices) as well. We have defined the pairing tensor in just this way for this purpose.

1.1.2. Hartree–Fock–Bogoliubov energy

In the second quantization formalism, the effective nuclear Hamiltonian reads

$$H = \sum_{ab} \langle a|t_{\mathrm{K}}|b\rangle c_a^\dagger c_b + \frac{1}{4}\sum_{abcd} \langle ac|v_{12}^{(\mathrm{a})}|bd\rangle c_a^\dagger c_c^\dagger c_d c_b. \tag{III.6}$$

Here, the one-body kinetic energy operator t_{K} takes into account the one-body center-of-mass correction [1] directly in its expression, since

$$t_{\mathrm{K}} = \left(1 - \frac{1}{A}\right)\frac{p^2}{2M}, \tag{III.7}$$

1. In fact, the HFB wave functions break the translational invariance of the Hamiltonian (III.6) since the position of the center-of-mass is defined by the mean-field potential. This induces in particular discrepancies in the evaluation of binding energies and other observables linked to surface properties of nuclei [177]. It this therefore essential to restore this symmetry *a posteriori* through a "center-of-mass correction", composed of one- and two-body contributions in our case, as we neglect higher-body contributions.

where $p \equiv \hbar k$ is the usual momentum operator and A is the number of nucleons in the nucleus under study. The antisymmetrized effective nuclear interaction is given by

$$v_{12}^{(\mathrm{a})} \equiv v_{12}(1 - P_r P_\sigma P_\tau), \tag{III.8}$$

where v_{12} here designates the generalized Gogny interaction (II.1). This interaction directly takes into account the two-body center-of-mass correction, i.e.

$$\langle ac|v_{12}^{(\mathrm{a})}|bd\rangle = \langle ac|V_{12}^{(\mathrm{a})}|bd\rangle + \frac{1}{AM}\Big(\langle a|p|d\rangle\langle c|p|b\rangle - \langle a|p|b\rangle\langle c|p|d\rangle\Big), \tag{III.9}$$

where V_{12} is the interaction without the two-body center-of-mass correction, and A the number of nucleons in the nucleus.

The energy of the nucleus stemming from the Hamiltonian (III.6), $\mathcal{E}_{\mathrm{HFB}} \equiv \langle\tilde{0}|H|\tilde{0}\rangle$, can be deduced using Wick's theorem. We find out

$$\begin{aligned}
\mathcal{E}_{\mathrm{HFB}} = &\sum_{ab>0}\Big[\langle a|t_{\mathrm{K}}|b\rangle\rho_{ba} + \langle\overline{a}|v_{12}^{(\mathrm{a})}|\overline{b}\rangle\overline{\rho}_{ab}\Big] \\
&+ \frac{1}{2}\sum_{abcd>0}\Big[\langle ac|v_{12}^{(\mathrm{a})}|bd\rangle\rho_{ba}\rho_{dc} + \langle\overline{a}c|v_{12}^{(\mathrm{a})}|\overline{b}d\rangle\overline{\rho}_{ab}\rho_{dc} \\
&\qquad + \langle a\overline{c}|v_{12}^{(\mathrm{a})}|b\overline{d}\rangle\rho_{ba}\overline{\rho}_{cd} + \langle\overline{a}\overline{c}|v_{12}^{(\mathrm{a})}|\overline{b}\overline{d}\rangle\overline{\rho}_{ab}\overline{\rho}_{cd}\Big] \\
&+ \frac{1}{4}\sum_{abcd>0}\Big[\langle\overline{a}c|v_{12}^{(\mathrm{a})}|\overline{b}d\rangle\kappa_{ca}\kappa_{db} - \langle\overline{a}c|v_{12}^{(\mathrm{a})}|b\overline{d}\rangle\kappa_{ca}\kappa_{bd} \\
&\qquad - \langle\overline{a}c|v_{12}^{(\mathrm{a})}|\overline{b}d\rangle\kappa_{ac}\kappa_{db} + \langle a\overline{c}|v_{12}^{(\mathrm{a})}|b\overline{d}\rangle\kappa_{ac}\kappa_{bd}\Big],
\end{aligned} \tag{III.10}$$

In order to simplify this expression, we will need to take advantage of some properties of the matrix elements of the kinetic energy operator t_{K} and of the (antisymmetrized) effective nuclear interaction $v_{12}^{(\mathrm{a})}$.[2] These properties will also be useful later, when we will highlight the symmetries of the HFB fields to facilitate their derivation (see subsection C.1.3). Therefore, the next lines are dedicated to demonstrate them.

Since t_{K} is Hermitian and time-reversal invariant,[3] we have

$$\langle\overline{a}|t_{\mathrm{K}}|\overline{b}\rangle = \Big(\langle a|T^\dagger\Big)\, t_{\mathrm{K}}\, \Big(T|b\rangle\Big) = \Big[\langle a|\Big(T^\dagger t_{\mathrm{K}} T|b\rangle\Big)\Big]^* = \Big[\langle a|t_{\mathrm{K}}|b\rangle\Big]^* = \langle b|t_{\mathrm{K}}|a\rangle. \tag{III.12}$$

Note that we have used the identity $TT^\dagger = T^\dagger T = \mathbb{1}$ since the time-reversal operator is antiunitary by definition. The parentheses are also important to precise whether the time-reversal operator, which is antilinear, acts on its left or on its right.[4] Similarly, the

2. Note that the presence of a medium, taken into account through the density dependence of the generalized Gogny interaction, breaks translational and Galilean invariances of the bare nuclear interaction (see subsection I.1.2), evolving in the vacuum.

3. Indeed, the time-reversal operator transforms the momentum vector $\vec{p}$ into its opposite $-\vec{p}$, i.e. $T\vec{p}T^\dagger = -\vec{p}$, so that

$$Tp^2T^\dagger = p^2. \tag{III.11}$$

4. For any states $|\alpha\rangle$ and $|\beta\rangle$, an antilinear operator A satisfies the relation

$$\big(\langle\alpha|A\big)|\beta\rangle = \big[\langle\alpha|\big(A|\beta\rangle\big)\big]^*. \tag{III.13}$$

This notation convention is the one used in [178].

effective nuclear interaction v_{12} is Hermitian and time-reversal invariant (see equations (I.9) and (I.10)), in such a way that

$$\begin{aligned}\langle\overline{ac}|v_{12}|\overline{bd}\rangle &= \Big(\langle ac|T_1^\dagger T_2^\dagger\Big)\, v_{12}\, \Big(T_2T_1|bd\rangle\Big) = \Big[\langle ac|\Big(T_2^\dagger T_1^\dagger v_{12}T_2T_1|bd\rangle\Big)\Big]^* \\ &= \Big[\langle ac|v_{12}|bd\rangle\Big]^* = \langle bd|v_{12}|ac\rangle,\end{aligned} \tag{III.14}$$

where T_1 and T_2 respectively denote the time-reversal operators associated with the first and the second particle. Knowing that v_{12} must remain invariant under the exchange of the two particles $1 \leftrightarrow 2$ (see (I.2)), we also find

$$\langle ac|v_{12}|bd\rangle = \langle ca|v_{21}|db\rangle = \langle ca|v_{12}|db\rangle, \tag{III.15}$$

where the first equality comes from the exchange of the particle coordinates. Note that the last three relations are true in any basis whose states satisfy the identity (C.14), as long as v_{12} is an effective nuclear interaction fulfilling the required symmetries. Now, we are going to prove that, in addition to these properties, the matrix elements of v_{12} are real in the two-center axially-symmetric HO basis, as this is the one we will be working in, in the following. Indeed, one can show that the axial HO states were invariant under the T-simplex symmetry (C.20), hence

$$\begin{aligned}\langle ac|v_{12}|bd\rangle &= \Big(\langle ac|S_{T_1}^\dagger S_{T_2}^\dagger\Big)\, v_{12}\, \Big(S_{T_2}S_{T_1}|bd\rangle\Big) = \Big[\langle ac|\Big(S_{T_2}^\dagger S_{T_1}^\dagger v_{12}S_{T_2}S_{T_1}|bd\rangle\Big)\Big]^* \\ &= \Big[\langle ac|v_{12}|bd\rangle\Big]^*,\end{aligned} \tag{III.16}$$

where S_{T_1} and S_{T_2} respectively denote the T-simplex operators associated with the first and the second particle. Note that the T-simplex operator, being a product of unitary operators, is unitary itself. It is also antilinear since the time-reversal operator is. For the third equality to be true, the nuclear interaction v_{12} has to commute with the T-simplex operator. The nuclear interaction does even more since it commutes with each of the operators composing the T-simplex operator. Indeed, the nuclear interaction remains invariant under a time-reversal transformation, a parity transformation or a full rotation, in both coordinate and spin spaces (see equations (I.7)–(I.9)); it is T-simplex invariant.

Obviously, all these properties still hold for the antisymmetrized nuclear interaction $v_{12}^{(\mathrm{a})}$. Additionally, it verifies

$$\langle ac|v_{12}^{(\mathrm{a})}|bd\rangle \equiv \langle ac|v_{12}|bd\rangle - \langle ac|v_{12}|bd\rangle = -\langle ac|v_{12}^{(\mathrm{a})}|db\rangle, \tag{III.17}$$

as well as

$$\langle ac|v_{12}^{(\mathrm{a})}|bd\rangle = -\langle ca|v_{12}^{(\mathrm{a})}|bd\rangle, \tag{III.18}$$

where we have used property (III.15) with the above equation.

By means of these results, we can show that the HFB energy (III.10) simplifies as

$$\begin{aligned}\mathcal{E}_{\mathrm{HFB}} = &\sum_{ab>0}\langle a|t_{\mathrm{K}}|b\rangle\Big(\rho_{ba}+\overline{\rho}_{ba}\Big) \\ &+\sum_{abcd>0}\Big[\langle ac|v_{12}^{(\mathrm{a})}|bd\rangle\frac{1}{2}\Big(\rho_{ba}\rho_{dc}+\overline{\rho}_{ba}\overline{\rho}_{dc}\Big)+\langle a\overline{c}|v_{12}^{(\mathrm{a})}|b\overline{d}\rangle\rho_{ba}\overline{\rho}_{cd}\Big] \\ &+\sum_{abcd>0}\langle\overline{a}c|v_{12}^{(\mathrm{a})}|\overline{b}d\rangle\kappa_{ca}\kappa_{db}.\end{aligned} \tag{III.19}$$

1.1.3. Hartree–Fock–Bogoliubov fields

Actually, the two-center axial HO basis is not orthogonal and implies the identity $\langle a|b\rangle = S_{ab} \neq \delta_{ab}$, where S_{ab} is the overlap matrix between the states $|a\rangle$ and $|b\rangle$. Yet, to derive and solve the HFB equations, we need an orthogonal basis, called a *bi-orthogonal* basis in such two-center representation. We will not detail the procedure to construct this bi-orthogonal representation but refer the reader to [175, 176] for extensive presentations on how to proceed. In the bi-orthogonal representation, the states are denoted by $|p\rangle, |q\rangle$ and so on, and the HFB energy is still given by (III.19), upon exchanging the states of the two-center HO basis by the ones of the bi-orthogonal basis.
The standard process to obtain the HFB equations consists in minimizing the HFB energy with respect to ρ, $\overline{\rho}$ and κ, given by (III.5), while preserving the average number of protons and neutrons by means of Lagrange multipliers. This amounts to minimizing the functional

$$\mathcal{F}[\rho,\overline{\rho},\kappa] \equiv \mathcal{E}[\rho,\overline{\rho},\kappa] - \sum_t \mu_t \langle\widetilde{0}|N_t|\widetilde{0}\rangle - \Lambda(R^2 - R), \tag{III.20}$$

where N_t is the particle number operator of isospin t, μ_t the chemical potential of an isospin-t particle and R the generalized density matrix expressed in terms of the density matrices and pairing tensor defined in (III.4), as

$$R^{t\Omega} \equiv \begin{pmatrix} \rho^{t\Omega} & -\kappa^{t\Omega} \\ -(\kappa^{t\Omega})^T & \mathbb{1} - \overline{\rho}^{t\Omega} \end{pmatrix}. \tag{III.21}$$

The last constraint, where Λ is some real symmetric matrix composed of Lagrange multipliers, imposes $R^2 = R$, as it is a necessary condition for the Bogoliubov transformation (III.1) to be unitary. The stationary condition $\mathrm{d}\mathcal{F} = 0$ finally leads to the so-called HFB equations

$$[H_{\mathrm{HFB}}, R] = 0. \tag{III.22}$$

The above matrix is defined in the bi-orthogonal basis as

$$\widetilde{H}_{\mathrm{HFB}} \equiv \begin{pmatrix} \widetilde{e} & -\widetilde{\Delta} \\ -\widetilde{\Delta}^T & -\widetilde{\overline{e}} \end{pmatrix}, \tag{III.23}$$

where

$$\widetilde{e}_{pq} \equiv \widetilde{h}_{pq} - \delta_{pq}\mu_{t_p}, \tag{III.24a}$$
$$\widetilde{\overline{e}}_{pq} \equiv \widetilde{\overline{h}}_{pq} - \delta_{pq}\mu_{t_p}, \tag{III.24b}$$

with the mean-field Hamiltonians expressed as

$$\widetilde{h}_{pq} \equiv \frac{1+\delta_{pq}}{2}\frac{\partial \mathcal{E}_{\mathrm{HFB}}}{\partial \widetilde{\rho}_{qp}}, \tag{III.25a}$$
$$\widetilde{\overline{h}}_{pq} \equiv \frac{1+\delta_{pq}}{2}\frac{\partial \mathcal{E}_{\mathrm{HFB}}}{\partial \widetilde{\overline{\rho}}_{qp}}, \tag{III.25b}$$

and the pairing field as

$$\widetilde{\Delta}_{pq} \equiv \frac{1}{2}\frac{\partial \mathcal{E}_{\mathrm{HFB}}}{\partial \widetilde{\kappa}_{pq}}. \tag{III.26}$$

Note that the quantities appearing with a tilde are conventionally expressed in the bi-orthogonal basis. We now have to go back to the two-center HO basis since this is the one we have defined to perform our calculations. Thanks to the relations

$$\rho = M\widetilde{\rho}M^T, \tag{III.27a}$$
$$\overline{\rho} = M\widetilde{\overline{\rho}}M^T, \tag{III.27b}$$
$$\kappa = M\widetilde{\kappa}M^T, \tag{III.27c}$$

where M is the transfer matrix from the bi-orthogonal representation to the two-center HO representation, we can show that we find

$$\widetilde{h} = M^T h M, \tag{III.28a}$$
$$\widetilde{\overline{h}} = M^T \overline{h} M, \tag{III.28b}$$
$$\widetilde{\Delta} = M^T \Delta M, \tag{III.28c}$$

with, explicitly, in the tw-center axial HO basis,

$$h_{ab} \equiv \frac{1+\delta_{ab}}{2}\frac{\partial \mathcal{E}_{\rm HFB}}{\partial \rho_{ba}}, \tag{III.29a}$$
$$\overline{h}_{ab} \equiv \frac{1+\delta_{ab}}{2}\frac{\partial \mathcal{E}_{\rm HFB}}{\partial \overline{\rho}_{ba}}, \tag{III.29b}$$
$$\Delta_{ab} \equiv \frac{1}{2}\frac{\partial \mathcal{E}_{\rm HFB}}{\partial \kappa_{ab}}. \tag{III.29c}$$

Using the expression (III.19) of the HFB energy, we obtain

$$\begin{aligned} h_{ab} = {} & \langle a|t_{\rm K}|b\rangle + \sum_{cd>0}\Big[\langle ac|v_{12}^{(\rm a)}|bd\rangle\rho_{dc} + \langle a\overline{c}|v_{12}^{(\rm a)}|b\overline{d}\rangle\overline{\rho}_{dc}\Big] \\ & + \frac{1+\delta_{ab}}{2}\sum_{a'b'c'd'}\Big[\langle a'c'|\frac{\partial v_{12}^{(\rm a)}}{\partial \rho_{ba}}|b'd'\rangle\frac{1}{2}\Big(\rho_{b'a'}\rho_{d'c'} + \overline{\rho}_{b'a'}\overline{\rho}_{d'c'}\Big) \\ & \qquad + \langle a'\overline{c'}|\frac{\partial v_{12}^{(\rm a)}}{\partial \rho_{ba}}|b'\overline{d'}\rangle\rho_{b'a'}\overline{\rho}_{d'c'}\Big] \\ & + \frac{1+\delta_{ab}}{2}\sum_{a'b'c'd'}\langle\overline{a'}c'|\frac{\partial v_{12}^{(\rm a)}}{\partial \rho_{ba}}|\overline{b'}d'\rangle\kappa_{c'a'}\kappa_{d'b'}, \\ \overline{h}_{ab} = {} & \langle a|t_{\rm K}|b\rangle + \sum_{cd>0}\Big[\langle ac|v_{12}^{(\rm a)}|bd\rangle\overline{\rho}_{dc} + \langle a\overline{c}|v_{12}^{(\rm a)}|b\overline{d}\rangle\rho_{dc}\Big] \\ & + \frac{1+\delta_{ab}}{2}\sum_{a'b'c'd'}\Big[\langle a'c'|\frac{\partial v_{12}^{(\rm a)}}{\partial \overline{\rho}_{ba}}|b'd'\rangle\frac{1}{2}\Big(\rho_{b'a'}\rho_{d'c'} + \overline{\rho}_{b'a'}\overline{\rho}_{d'c'}\Big) \\ & \qquad + \langle a'\overline{c'}|\frac{\partial v_{12}^{(\rm a)}}{\partial \overline{\rho}_{ba}}|b'\overline{d'}\rangle\rho_{b'a'}\overline{\rho}_{d'c'}\Big] \\ & + \frac{1+\delta_{ab}}{2}\sum_{a'b'c'd'}\langle\overline{a'}c'|\frac{\partial v_{12}^{(\rm a)}}{\partial \overline{\rho}_{ba}}|\overline{b'}d'\rangle\kappa_{c'a'}\kappa_{d'b'}, \end{aligned} \tag{III.30, III.31}$$

as well as

$$\Delta_{ab} = \sum_{cd>0}\langle a\overline{b}|v_{12}^{(\rm a)}|c\overline{d}\rangle\kappa_{cd}. \tag{III.32}$$

Alternatively, we can separate the different contributions to the HFB energy (III.19) and express them in terms of HFB fields. To this end, we use the properties of the two-body matrix elements shown in subsection C.1.2. We find

$$\mathcal{E}_{\text{HFB}} = \mathcal{E}_{\text{K}} + \mathcal{E}_{\text{P}} = \mathcal{E}_{\text{K}} + \mathcal{E}_{\text{MF}} + \mathcal{E}_{\text{pair}}. \tag{III.33}$$

On the one hand, the kinetic energy

$$\mathcal{E}_{\text{K}} \equiv \sum_{ab>0} K_{ab}\Big(\rho_{ba} + \overline{\rho}_{ba}\Big), \tag{III.34}$$

is expressed in terms of the kinetic field

$$K_{ab} \equiv \langle a|t_{\text{K}}|b\rangle. \tag{III.35}$$

On the other hand, the potential energy decomposes into a mean-field energy contribution,

$$\mathcal{E}_{\text{MF}} \equiv \frac{1}{2}\sum_{ab>0}\Big[\Gamma_{ab}\rho_{ba} + \overline{\Gamma}_{ab}\overline{\rho}_{ba}\Big], \tag{III.36}$$

expressed in terms of the mean-fields

$$\Gamma_{ab} \equiv \sum_{cd>0}\Big[\langle ac|v_{12}^{(\text{a})}|bd\rangle\rho_{dc} + \langle a\overline{c}|v_{12}^{(\text{a})}|b\overline{d}\rangle\overline{\rho}_{cd}\Big], \tag{III.37}$$

and

$$\overline{\Gamma}_{ab} \equiv \sum_{cd>0}\Big[\langle ac|v_{12}^{(\text{a})}|bd\rangle\overline{\rho}_{dc} + \langle a\overline{c}|v_{12}^{(\text{a})}|b\overline{d}\rangle\rho_{cd}\Big], \tag{III.38}$$

and a pairing energy contribution,

$$\mathcal{E}_{\text{pair}} \equiv \sum_{ab>0}\Delta_{ab}\kappa_{ab}, \tag{III.39}$$

expressed in terms of the pairing field (III.32). Considering this writing of the HFB energy, we can express the mean-field Hamiltonians (III.30) and (III.31) as

$$h_{ab} = K_{ab} + \Gamma_{ab} + \partial\Gamma_{ab} + \partial\Delta_{ab}, \tag{III.40}$$

$$\overline{h}_{ab} = K_{ab} + \overline{\Gamma}_{ab} + \partial\overline{\Gamma}_{ab} + \partial\overline{\Delta}_{ab}, \tag{III.41}$$

where the rearrangement fields, identified by a symbol ∂, are different from zero only if the nuclear interaction under study explicitly depends on the density, as it the case of the generalized Gogny interaction (II.1). Indeed, the rearrangement fields associated with the mean-fields Γ and $\overline{\Gamma}$ read

$$\begin{aligned}\partial\Gamma_{ab} \equiv \frac{1+\delta_{ab}}{2}\sum_{a'b'c'd'}\Bigg[&\langle a'c'|\frac{\partial v_{12}^{(\text{a})}}{\partial\rho_{ba}}|b'd'\rangle\frac{1}{2}\Big(\rho_{b'a'}\rho_{d'c'} + \overline{\rho}_{b'a'}\overline{\rho}_{d'c'}\Big)\\ &+ \langle a'\overline{c'}|\frac{\partial v_{12}^{(\text{a})}}{\partial\rho_{ba}}|b'\overline{d'}\rangle\rho_{b'a'}\overline{\rho}_{d'c'}\Bigg],\end{aligned} \tag{III.42}$$

and

$$\begin{aligned}\partial\overline{\Gamma}_{ab} \equiv \frac{1+\delta_{ab}}{2}\sum_{a'b'c'd'}\Bigg[&\langle a'c'|\frac{\partial v_{12}^{(\text{a})}}{\partial\overline{\rho}_{ba}}|b'd'\rangle\frac{1}{2}\Big(\rho_{b'a'}\rho_{d'c'} + \overline{\rho}_{b'a'}\overline{\rho}_{d'c'}\Big)\\ &+ \langle a'\overline{c'}|\frac{\partial v_{12}^{(\text{a})}}{\partial\overline{\rho}_{ba}}|b'\overline{d'}\rangle\rho_{b'a'}\overline{\rho}_{d'c'}\Bigg],\end{aligned} \tag{III.43}$$

while the rearrangement fields associated with the pairing field read

$$\partial\Delta_{ab} \equiv \frac{1+\delta_{ab}}{2} \sum_{a'b'c'd'} \langle \overline{a'}c'| \frac{\partial v_{12}^{(\mathrm{a})}}{\partial \rho_{ba}} |\overline{b'}d'\rangle \kappa_{c'a'}\kappa_{d'b'}, \tag{III.44}$$

and

$$\partial\overline{\Delta}_{ab} \equiv \frac{1+\delta_{ab}}{2} \sum_{a'b'c'd'} \langle \overline{a'}c'| \frac{\partial v_{12}^{(\mathrm{a})}}{\partial \overline{\rho}_{ba}} |\overline{b'}d'\rangle \kappa_{c'a'}\kappa_{d'b'}. \tag{III.45}$$

To derive these fields, we will thus need an expression for the local nuclear density $\rho(\vec{r})$, defined in (A.25). Inserting two completeness relations based on the two-center axial states of the HO basis (C.1), we find

$$\rho(\vec{r}) = \sum_{st}\sum_{\sigma\tau}\sum_{\substack{m\nu\\ m'\nu'}}\sum_{\Omega,\Omega'>0} \Phi^*_{t\Omega m\nu}(\vec{r},\sigma,\tau)\Phi_{t\Omega' m'\nu'}(\vec{r},\sigma,\tau)\langle t\Omega m\nu|\rho|t\Omega' m'\nu'\rangle\,. \tag{III.46}$$

Using the orthogonality relations associated with the spin and isospin degrees of freedom of the HO states (see (C.6)), the local density reduces to

$$\rho(\vec{r}) = \sum_{st}\sum_{\substack{m\nu\\ m'\nu'}}\sum_{\Omega,\Omega'>0} \phi^*_{m\nu}(\vec{r})\phi_{m'\nu'}(\vec{r})\delta_{ss'}\langle\widetilde{0}|c^\dagger_{t\Omega m\nu}c_{t\Omega' m'\nu'}|\widetilde{0}\rangle\,, \tag{III.47}$$

where we have expressed the density matrix in terms of creation and annihilation operators. The contraction of those imposes $\Omega = \Omega'$. Besides, since $s = s'$, we also have $m = m'$. Note that depending on the sign of Ω, the contraction is equal to the density matrices ρ or $\overline{\rho}$, which are defined in (III.5). Here, $\Omega > 0$, so that

$$\rho(\vec{r}) = \sum_{st}\sum_{m\nu\nu'}\sum_{\Omega>0} \phi^*_{m\nu}(\vec{r})\phi_{m'\nu'}(\vec{r})\delta_{ss'}\Big(\rho^{t\Omega=m+s}_{m'\nu,m\nu} + \overline{\rho}^{t\Omega=m+s}_{m'\nu,m\nu}\Big), \tag{III.48}$$

We can now replace the summations $\sum_m\sum_{\Omega>0}$ by $\sum_{m\geq 0}\sum_{\Omega}\Theta(\Omega)$ to get, benefiting from the Kronecker delta,

$$\rho(\vec{r}) = \sum_{st}\sum_{\substack{m\geq 0\\ \nu\nu'}} \phi^*_{m\nu}(\vec{r})\phi_{m'\nu'}(\vec{r})\Big(\rho^{t\Omega=m+s}_{m'\nu,m\nu} + \overline{\rho}^{t\Omega=m+s}_{m'\nu,m\nu}\Big), \tag{III.49}$$

Finally performing the summation over the spins, the local nuclear density can be written, in a two-center axially symmetric HO basis,

$$\begin{aligned}\rho(\vec{r}) = &\sum_{\substack{m'\geq 0\\ \nu\nu'}} \phi^*_{m\nu}(\vec{r})\phi_{m\nu'}(\vec{r})\\ &\times\sum_t\Big[\rho^{t\Omega=m+1/2}_{m\nu' m\nu} + \overline{\rho}^{t\Omega=m+1/2}_{m\nu' m\nu} + \Theta(m-1/2)\Big(\rho^{t\Omega=m-1/2}_{m\nu' m\nu} + \overline{\rho}^{t\Omega=m-1/2}_{m\nu' m\nu}\Big)\Big],\end{aligned} \tag{III.50}$$

where we have introduced the Heaviside step function $\Theta(\Omega)$ defined in (D.95), where the density matrices $\rho^{t\Omega}_{m\nu' m\nu}$ and $\overline{\rho}^{t\Omega}_{m\nu' m\nu}$ are given by (III.5), and where $\nu = (n_\perp, n_z)$ as well as $\nu' = (n'_\perp, n'_z)$.

Finally, to solve the HFB equations, we first derive all the HFB fields to fully specify h, $\overline{h}$ and Δ, the matrices ρ, $\overline{\rho}$ and κ being assumed known. Then, we transform these quantities into the bi-orthogonal basis, using (III.28). We build the HFB Hamiltonian (III.23) and diagonalize it. This provides the matrices $\widetilde{U}$, $\widetilde{V}$, $\widetilde{\overline{U}}$ and $\widetilde{\overline{V}}$ in the bi-orthogonal

basis. We then move back to the two-center axial HO basis applying the following transformations,

$$U^{t\Omega} = M\widetilde{U}^{t\Omega}, \tag{III.51a}$$
$$\overline{V}^{t\Omega} = M\widetilde{\overline{V}}^{t\Omega}, \tag{III.51b}$$

that furnish the matrices U, V, $\overline{U}$ and $\overline{V}$ in the two-center axial HO basis. These quantities allow us to derive new matrices ρ, $\overline{\rho}$ and κ in this basis using (III.4), which, in turn, provide new values for h, $\overline{h}$ and Δ. We then repeat this same procedure, iteratively, a number of times until we obtain convergence.

1.2. Characteristics and conventions of the HFB3 code

We continue by exposing the characteristics and conventions of the HFB code, called HFB3 [179], we have considered to generate all the results of this chapter. The purpose is not to go into the technical details of the code, but to merely specify its main assumptions and characteristics in order to better understand the outputs.

Currently, HFB3 is a time-reversal invariant HFB code made up of axially-symmetric harmonic oscillator wave functions defined in a two-center basis, allowing parity breaking. As part of this thesis work, we have actually derived the HFB fields associated with all the terms of the generalized Gogny interaction (II.1) *without* imposing time-reversal invariance. It then has been subsequently demanded when implementing the newly finite-range spin–orbit and tensor forces. This restricts the study to even–even nuclei for the moment, but work is in progress to release time-reversal invariance [180]. The choice of harmonic oscillator wave functions is justified on both analytical and numerical aspects. The separable development [175, 181] (see subsection D.3 for more details) enables to simplify the analytical derivations and optimize the numerical calculations of the HFB fields when the quasiparticle states are expanded on a basis of harmonic oscillators, with Gaussian form factors chosen for the potentials. By a two-center axially-symmetric representation, we mean that the two centers display symmetry with respect to rotations around the Oz axis and are separated by a distance d_0 along z. The HFB formalism of this two-center representation has been outlined in the previous subsection. Note that in the HFB3 code, the two centers are equidistant from the origin. Finally, the parity breaking allows to simulate two fragments with different density distributions during the fission process, as illustrated in Figure III.1.

The benefits of having two centers are twofold. First, by choosing a typical distance d_0 of about a few Fermi, a configuration suitable to describe fission is achieved. Indeed, in order to properly describe all possible configurations of the nucleus during the fission process, in particular those corresponding to huge elongations or even two separated fragments, it is natural to decompose the quasiparticle states on two sets of wave functions, the distance between them being modified at will. Second, it enables to reduce the truncation order of the basis (discussed in the next paragraph), i.e. to save computing time while preserving the accuracy of the results. Nevertheless, to account for the structure properties or deformations of low- to medium-mass nuclei, one center is enough. In practice, when the nucleon number is such that $A < 68$, we set $d_0 = 0$ in the HFB3 code, and we fall back on the traditional HFB formalism.

As we have shown in (III.1), the quasiparticle states are expanded on a basis of functions which are here chosen to be axial HO wave functions (C.1). These are characterized by perpendicular $\hbar\omega_\perp$ and longitudinal $\hbar\omega_z$ frequencies and a position $d_0/2$ or $-d_0/2$ in

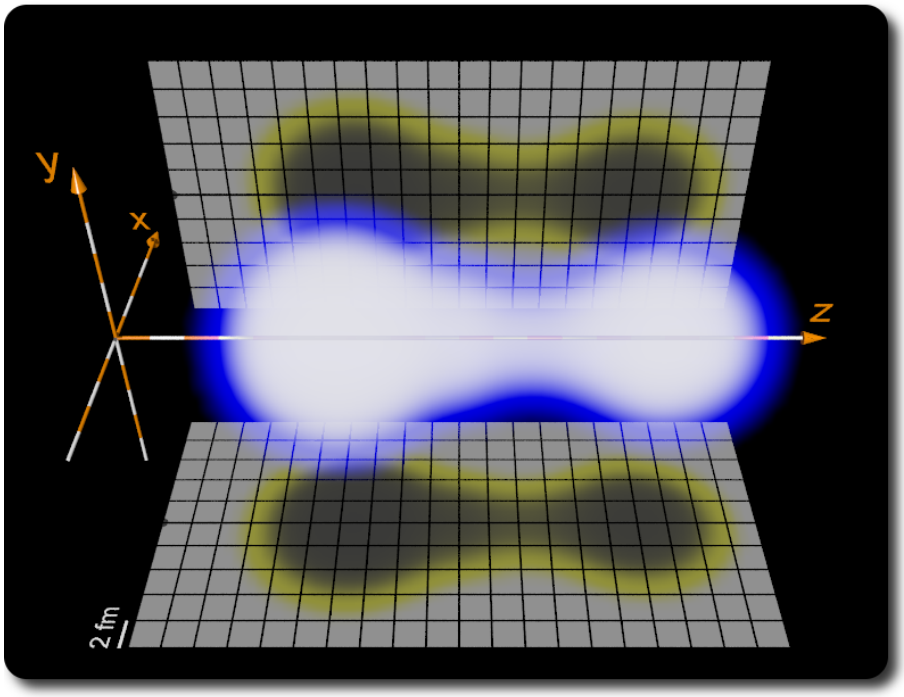

Figure III.1 – Illustration of the two-center axially-symmetric representation, with parity breaking, of `HFB3` [182]. The two centers, separated by a distance d_0, forms a system whose density distribution is not left–right symmetric, because of parity breaking.

the z coordinate. In practice, the infinite series expansion is truncated to a finite order to be numerically tractable. However, in this process, some information about the quasiparticle states is lost as the basis is no longer complete, and they then become dependent on the three parameters $\hbar\omega_\perp, \hbar\omega_z$ and d_0. In practice, since the outputs of HFB calculations must not depend on the parameters of the basis, the truncation order n is chosen sufficiently large such that this dependence fades away (as we show in the next paragraph). On the other hand, since the HFB approach is based on the minimization of the HFB energy, the natural option is to select the parameters $\hbar\omega_\perp, \hbar\omega_z$ and d_0 which minimize the energy. Note that the frequencies of the wave functions in both centers are assumed to be the same. In addition to greatly simplifying the calculation of the HFB fields, on both theoretical and numerical aspects, this hypothesis is justified as supplying different sets of parameters for each center did not significantly modify the results, but complicated the optimization of the parameters [175]. At the level of the off-center axial HO wave functions, three parameters, namely $\hbar\omega_\perp, \hbar\omega_z$ and d_0, are chosen so as to minimize the HFB energy.

Finally, as we have said, the truncation order n also has to be optimized to avoid a strong dependence on the parameters of the basis. It in fact defines the number of quanta of energy in the harmonic oscillators of each center (or the number of major shells), by means of the relation

$$(2n_\perp + |m| + 1)\hbar\Omega_\perp + \left(n_z + \frac{1}{2}\right)\hbar\Omega_z \leq \left(n + \frac{3}{2}\right)\hbar\Omega, \tag{III.52}$$

with $(\hbar\Omega)^3 \equiv (\hbar\Omega_\perp)^2\hbar\Omega_z$. The quantities $\hbar\Omega_\perp$ and $\hbar\Omega_z$ denote the frequencies associated with the size of the two-center representation. They are taken different from the frequencies of the HO wave functions discussed above so as to allow simultaneous optimization of the singular frequencies $\hbar\omega_\perp$ and $\hbar\omega_z$ as well as the two-center basis itself. Indeed, setting

the deformation parameter $Q \equiv \hbar\Omega_\perp/\hbar\Omega_z$, relation (III.52) pushes the quantum numbers to obey the inequalities

$$0 \leq 2n_\perp + |m| \leq n_\perp^{\max} \equiv \Big(n + \frac{3}{2}\Big)Q^{-1/3} - \frac{1}{2Q} - 1, \tag{III.53a}$$

$$0 \leq n_z \leq n_z^{\max} \equiv Q\Big(n_\perp^{\max} - (2n_\perp + |m|)\Big). \tag{III.53b}$$

Then, the truncation of the basis is defined by the parameters n and Q. All in all, the two-center representation is characterized by five parameters: the three parameters $\hbar\omega_\perp, \hbar\omega_z$ and d_0 involved in the off-center axially-symmetric wave functions on the one hand, and the two parameters n and Q which specify the truncation of the basis on the other hand. In the `HFB3` code, it is conventionally the oscillator lengths $b_\perp$ and b_z (which are directly related to the aforementioned frequencies $\hbar\omega$, see equations (C.7)) that are rather chosen so as to minimize the energy. In practice, the truncation order n is fixed for a given nucleus, and the remaining parameters are optimized. We take this occasion to give in Table III.1 the value of the parameter n to treat a nucleus with maximum mass number.

$\leq A$	n
19	7
39	8
59	9
79	10
99	11
119	12
139	13
169	14
189	15
289	16

Table III.1 – Correspondence between the maximum mass number A of a given nucleus and the associated value attributed to the parameter n in order to optimize the basis.

The outputs for the D1S interaction exposed in this chapter are obtained by optimizing the parameters the way we have just described. Doing so with the more sophisticated D2 and DG interactions is feasible but rapidly time-consuming, especially on heavy-mass nuclei. For this reason, their results are most of the time achieved by starting from the optimized parameters found for the D1S solution, and then minimizing the energy without re-optimizing the parameters. This scheme saves a considerable amount of time while almost unaffecting the outcomes.

Another important point lies in that the tensor force added in the generalized Gogny interaction is known to have a strong influence on the deformation properties of some isotopes [38]. Consequently, looking for the minimum energy predicted by DG around the axial deformation for which the HFB energy is minimal with D1S, in a given nucleus, may bring us to a local (and not global) minimum of DG. This is less likely to happen with D2 since no tensor term is considered, but not excluded. We have accordingly decided to calculate the complete potential energy surfaces (PES) with respect to axial quadrupole deformations, for all isotopes of this chapter, with D1S, D2 and DG interactions, to properly extract global energy minima. To achieve this, we have exploited (part of) the power of the CEA/DAM supercomputer.

Finally, we mention that all the results exposed below, with each interaction, are by default performed using the exact Coulomb force, recently implemented in the HFB3 code [183]. Sometimes, we will also consider the outputs using the simpler Slater approximation to underline the role played by the exact Coulomb potential.

2. Tensor effects on single-particle energies

Before introducing the results, we first need to recall the effects of the tensor effects to be expected on single-particle energies (SPEs). The role of the spin–orbit interaction on the SPEs into two subshells is well-known for many years [97, 98]. On the other hand, reductions in the energy gaps of some spin-partner states were already suspected to be due to the tensor force over forty years ago [184–186], but a robust quantitative description of the attached mechanism was only proposed in the 2000s by Otsuka *et al.* [30]. This subsection is meant to introduce the big picture of their interpretation of the tensor effects, referred to as Otsuka's picture in this document [31, 32].

Otsuka *et al.* focus on the *monopole* component of the tensor force, meaning that the many-body effects, related to higher multipole moments, are discarded. In general, the monopole part of a two-body nuclear interaction v_{12} is defined by

$$V^T_{j_1,j_2} \equiv \frac{\sum_J (2J+1) \langle j_1 j_2 | v_{12} | j_1 j_2 \rangle^{JT}}{\sum_J (2J+1)}, \tag{III.54}$$

where $\langle j_1 j_2 | v_{12} | j_1 j_2 \rangle^{JT}$ represents the (diagonal) TBMEs of the interaction, evaluated between states coupled to total angular momentum J and isospin T. We denote by $j_> \equiv l + 1/2$ and $j_< \equiv l - 1/2$ as well as $j'_> \equiv l' + 1/2$ and $j'_< \equiv l' - 1/2$ proton or neutron spin-partner states stemming from the spin–orbit splitting. One can show, provided the radial wave functions in $j_>$ and $j_<$ states are the same (as it is the case of HOs we consider in this chapter), that the monopole components $(V^{\mathrm{T}})^T_{j_1,j_2}$ of the tensor force satisfy the identity

$$(2j_> + 1)(V^{\mathrm{T}})^T_{j_>,j'} + (2j_< + 1)(V^{\mathrm{T}})^T_{j_<,j'} = 0, \tag{III.55}$$

where j' is either $j'_>$ or $j'_<$. From this equality, several properties of the tensor monopole components can be raised:

(i) the interaction acts between protons, between neutrons and also between one proton and one neutron; it is however three times stronger in the $T = 0$ than in the $T = 1$ channel since [5]

$$(V^{\mathrm{T}})^{T=0}_{j,j'} = 3(V^{\mathrm{T}})^{T=1}_{j,j'}, \quad \text{for } j \neq j', \tag{III.56}$$

where j is either $j_>$ or $j_<$;

(ii) the interaction between $j_>$ and j' is opposed to that between $j_<$ and j';

(iii) the interaction never involves s states as they are not separated into two subshells $j_>$ and $j_<$;

(iv) the action of two fully occupied (or empty) $j_>$ and $j_<$ states on j' is zero as the corresponding interactions compensate one another.

5. This relation can be easily obtained by evaluating the isospin TBMEs of the tensor monopole component, thanks to (D.12b).

Note that when all spin-partner states $j_>$ and $j_<$ are filled with nucleons (and the above spin-partner states are empty), we say that the nucleus is *spin-saturated* (and *spin-unsaturated* when it is not the case). We can go a bit further regarding the second point. Relation (III.55) stipulates that the monopole component of the tensor interaction between states $j_>$ and j', weighted by the maximum number of nucleons lying in $j_>$, is counterbalanced by that between states $j_<$ and j', weighted by the maximum number of nucleons lying in $j_<$. Then, as we fill the lower orbital $j_>$, the monopole tensor interaction generated by the nucleons sitting there grows, and is not offset by the upper orbital $j_<$, which is empty. Once the lower orbital is saturated, we start filling the upper orbital $j_<$ and the corresponding monopole tensor interaction progressively compensates that produced by the nucleons lying in the lower orbital $j_>$. When the upper orbital is saturated in turn, the effects compensate exactly and the global monopole component of the tensor force acting on j' is zero. For this reason, Otsuka's picture unveils that (the monopole component of) the tensor force acts maximally on a state j' when one of the spin-partner states is completely filled while the other is empty.

Although $(V^{\mathrm{T}})^T_{j_>,j'}$ and $(V^{\mathrm{T}})^T_{j_<,j'}$ are opposite, we still do not know which one is attractive and which one is repulsive. To settle the question, we can invoke some kind of intuitive toy models or directly compare both possibilities to spectroscopic data. It turns out that $j_>$ and $j'_<$ states attract each other whereas $j_>$ and $j'_>$ (as well as $j_<$ and $j'_<$) repel each other. The attraction *lowers* while the repulsion *raises* the corresponding levels (in energy). [6] An example of a proton–neutron monopole tensor interaction is given schematically in Figure III.2.

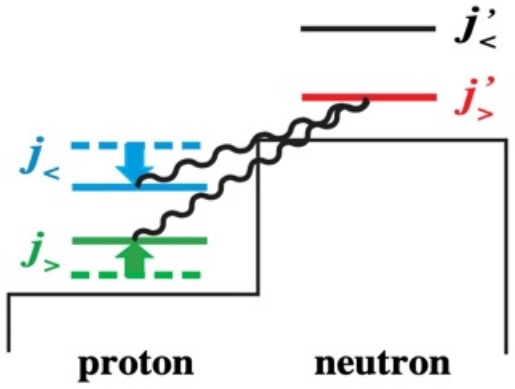

Figure III.2 – Illustration of the tensor monopole force acting between proton and neutron spin-partner single-particle states. If the neutron state $j'_> \equiv l' + 1/2$ is (at least partially) filled, it produces attraction of the higher proton state $j_< \equiv l - 1/2$, lowering its energy, and repulsion of the lower proton state $j_> \equiv l + 1/2$, raising its energy. Similar effects between neutron and between proton states may also occur but are not displayed here for clarity [32].

Since the effects of the tensor force on SPEs will be investigated to a great extent in this chapter and in Chapter IV, in particular in the *sd* shell, we take some time to describe an *sd*-shell nucleus in which the monopole component of the tensor force is expected to be important, namely ^{30}Si ($Z = 14, N = 16$). An illustration of the SPE spectrum of ^{30}Si in the *sd* shell is shown in Figure III.3 to make the analysis clearer.

First, we notice that the proton and neutron spin-partner states below the *sd* shell are completely filled ($1p_{3/2}$ and $1p_{1/2}$ subshells) while those above are empty, so that

6. This terminology, introduced by Otsuka *et al.*, will be used throughout the document.

they do not affect the orbitals we have displayed. We emphasize for what follows that proton and neutron $1d_{5/2}$ states are completely filled with six particles. In the proton sector of the *sd* shell (left side of the diagram), the spin-partner states $j_> = (1d_{3/2})_\pi$ and $j_< = (1d_{5/2})_\pi$ attract each other. This attraction, corresponding to the proton–proton component of the (monopole part of the) tensor force tends to lower $(1d_{5/2})_\pi$ and $(1d_{3/2})_\pi$. Note that according to what we have said, this configuration maximizes the attraction. If $(1d_{5/2})_\pi$ was only partially filled, or if it was entirely but $(1d_{3/2})_\pi$ only partially, the attraction would be less. If $(1d_{3/2})_\pi$ was entirely filled with four protons, no attraction would manifest.

In the neutron sector (right side of the diagram), the conclusions made for protons are exactly the same for neutrons, as the content of the spin-partner states is unchanged. This constitutes the neutron–neutron component of the tensor force. The neutrons filling the state $(2s_{1/2})_\nu$ do not take part in the tensor effects (at least at the first approximation considered in Otsuka's picture).

The subshells $(1d_{3/2})_\pi$ and $(1d_{3/2})_\nu$ being empty, the tensor force between them is zero. However, as $j_< = (1d_{5/2})_\pi$ is completely filled and $j'_> = (1d_{3/2})_\nu$ empty, a strong attraction resulting from the tensor force appears between these states, which tends to lower the $(1d_{3/2})_\nu$ state. Once again, this configuration maximizes the attraction. If $(1d_{5/2})_\pi$ was only partially filled, or if it was entirely but $(1d_{3/2})_\nu$ only partially, the attraction would be less. If $(1d_{3/2})_\nu$ was entirely filled with four protons, no attraction would manifest. Similarly, as $j'_< = (1d_{5/2})_\nu$ is completely filled and $j_> = (1d_{3/2})_\pi$ empty, a strong tensor attraction manifests, contributing in lowering the $j_> = (1d_{3/2})_\pi$ orbital. These effects constitute the proton–neutron component of the (monopole part of the) tensor force, and are expected to be stronger than those associated with the particle-like contributions (see equation (III.56)).

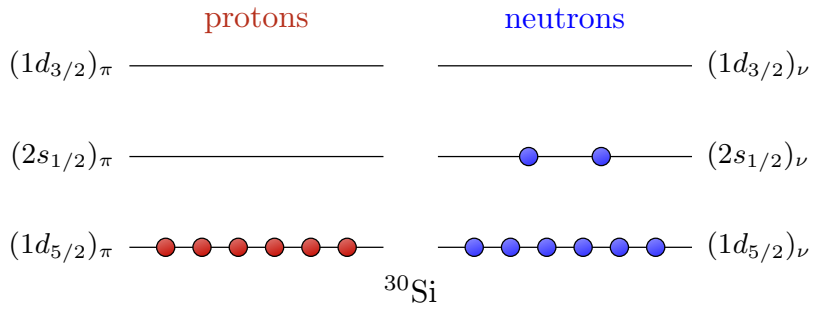

Figure III.3 – Schematic illustration of the single-particle energy spectrum of ^{30}Si in the *sd* shell, separated into proton (left side) and neutron (right side) sectors. Nucleons are placed on the lowest orbitals (HF scheme).

With the example of ^{30}Si, we see how the tensor force can modify the energy gaps between SPEs. It should be kept in mind, though, that we here only take into account monopole effects, which constitutes an approximation. Thus, depending on the nucleus, we do not expect to perfectly reproduce the predictions of this model, but at least to roughly follow its tendency. It should not be forgotten in addition that all the terms of the generalized Gogny interaction have a role to play in shifting the SPEs, and specifically the spin–orbit force.

3. Bulk properties

3.1. Binding energies

We begin our analysis of the generalized Gogny interaction by comparing its bulk properties, and more specifically the binding energies in this subsection, with D1S and D2 predictions as well as with experimental data. To do so, the difference between recent experimental and theoretical HFB binding energies for low- to heavy-mass nuclei along six isotopic chains are displayed in Figure III.4. This difference is defined as

$$\Delta\mathcal{E}_{\rm HFB} \equiv \mathcal{E}_{\rm HFB} - \mathcal{E}_{\rm exp}, \tag{III.57}$$

where $\mathcal{E}_{\rm HFB}$ and $\mathcal{E}_{\rm exp}$ respectively denote the HFB and experimental binding energies.

In O isotopes, DG and D2 outputs are pretty similar, with notable improvements for DG in ^{16}O and ^{24}O which are a bit underestimated by D2. We recall that the binding energy of the doubly magic nucleus ^{16}O was constrained at the HFR approximation in the fitting code. The tuning of that value to generate DG seems to be at the origin of the better reproduction appearing at the HFB level. As for S isotopes, we see that they are all predicted less bound than evidenced experimentally. This is even more pronounced with DG, except for ^{36}S. Actually, this tendency of the tensor force to slightly loosen nuclear systems was observed with the perturbative tensor-dependent Gogny D1ST [29] and D1ST2a [40] interactions. The lower binding energy of ^{36}S, associated with the closure of the $N = 20$ shell, will be further analyzed in subsection III.5.2.

The case of Sn isotopes is of great importance as the energy drift was controlled in the fitting procedure by ensuring that the value of $\Delta\mathcal{E}_{\rm HFB}$ is the same for both doubly magic isotopes ^{100}Sn and ^{132}Sn. This scheme, already undertaken with D2, is clearly visible, unlike D1S. In addition, the energy difference for those nuclei was found to be of about 2 MeV [17].[7] As required, no energy drift takes place in this isotopic chain with DG either. However, the energy differences for ^{100}Sn and ^{132}Sn of about 5.2 MeV look a little too strong. Actually it was harsh to reduce these differences while preserving the other good features of the parametrization at the level of the fitting code. Nevertheless, during the fitting procedure, calculations of the binding energies were done with $n = 15$ harmonic oscillator shells, thus reducing the energy differences further to about 3.5 MeV. Surprisingly, it appears that the arch shape observed with D1S and D2 fades from ^{118}Sn before forming a kind of plateau to the doubly magic nucleus ^{132}Sn. At this stage, we will not give an interpretation, but we will come back to this point in subsection III.4.1.1. In Gd isotopes, no energy drift shows up with D2 based on the binding energies displayed. With D1S, it is known that an energy drift appears. This is indeed what we can discriminate here as an energy of 4.7 MeV already separates the predictions of the two farthest isotopes. For DG, this difference is reduced to 3.5 MeV, and levels off from ^{158}Gd, contrary to D1S that keeps increasing. It seems to indicate that the binding energies are controlled with DG in those isotopes as well, so that no energy drift shows up.

With Pb isotopes, the situation is globally satisfactory with DG as there is no energy drift at this level (only about 1 MeV in the energy differences of ^{194}Pb and ^{214}Pb against

7. In fact, we see that the HFB calculations performed here display almost no difference to experimental data. There are at least two possible reasons for that. First, we have noticed that the higher the truncation order n, the closer we get to the experimental values. We then may have considered a larger value. Second, as we will see, the exact Coulomb potential slenderly increases (the magnitude of) the resulting binding energies, compared to those obtained with the Slater approximation.

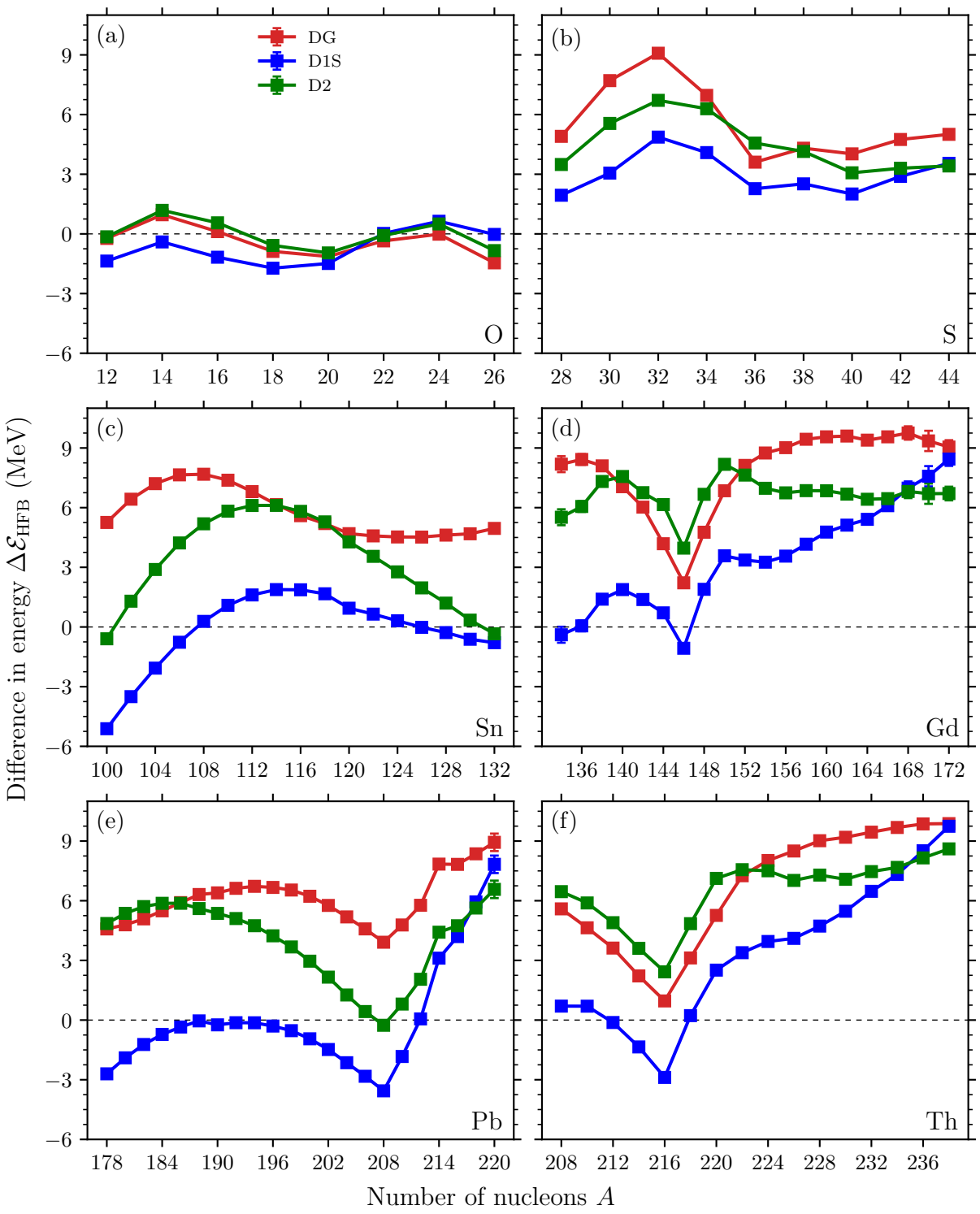

Figure III.4 – Difference between experimental [187] and HFB binding energies, expressed in (III.57), as a function of the number of nucleons A. Results are provided along O, S, Sn, Gd, Pb and Th isotopic chains for DG, D1S and D2 interactions. Horizontal dashed lines display perfect agreement with experiment and vertical bars the experimental errors. Lines are drawn to guide the eye.

3 MeV for D1S). The binding energy of ^{208}Pb, fitted to match the experimental value at the HFB level with D2, reaches an energy difference of 4.1 MeV with DG. As explained

in the fitting procedure, this latter was about 20 MeV in the early attempts. From this point of view, the difference is more reasonable, but still a far from experiment, at the HFB level. Finally, the general tendency observed with Gd isotopes is reproduced with Th isotopes. While a better description of binding energies with DG than with D2 can be seen for the lightest isotopes, a difference of about 3.9 MeV appears when moving towards the neutron-rich isotopes, which remains less important than with D1S, reaching about 5.8 MeV. The conclusion made for Gd isotopes then holds for Th isotopes.

Contrary to D1S, the binding energies predicted at the HFB level by both DG and D2 interactions almost always underestimate the experimental values (except in some O isotopes here). This was desirable since, as a variational method, the HFB approach must provide energies larger than or equal to the actual ground-state energies. Furthermore, we know in particular the dynamic quadrupole correlations taken into account beyond the mean field to bring an increment of energy in soft nuclei that will improve the theoretical predictions. Generally speaking, the pathological energy drifts observed with D1S are softened by DG and D2 interactions. However, it would be necessary to extend the calculations to a large number of isotopic chains, as had been done for D1S, D1N [124], D1M [127] and D2 [17, 18] interactions, to assess the mass drift of DG on a wider scale, including beyond mean-field correlations.

3.2. Charge radii

We continue by looking at the charge radii predicted by the generalized Gogny interaction, in comparison with D1S, D2 and experimental outcomes. We first need to give our definition of the charge radius as different forms exist depending on the corrections which are incorporated. The charge radii of this document are calculated by means of the formula

$$R_{\rm ch}^2 = R_\pi^2 + \frac{3}{2}\Big(P^2 - B^2\Big) + \frac{N}{Z}\,\langle r_\nu^2\rangle, \tag{III.58}$$

where the first term involves the proton radius R_π while the second and third terms are corrections accounting for the spatial extension of the proton and its center-of-mass motion as well as the charge distribution within the neutron, respectively. In the first correction, we have $P \equiv \sqrt{2/3}\sqrt{\langle r_\pi^2\rangle}$, with the root mean square radius of the proton $\sqrt{\langle r_\pi^2\rangle} \simeq 0.8414\,\text{fm}$ [81], as well as $B \equiv \sqrt{\hbar/M\omega A}$, with $\hbar^2/M \simeq 41.47$ and Bethe's formula linking the frequency $\hbar\omega$ to the number of nucleons A, i.e. $\hbar\omega = 1.85 + 35.5A^{-1/3}$. In the second one, the ratio of neutrons over protons is multiplied by the mean square radius of the neutron $\langle r_\nu^2\rangle \simeq -0.110\,\text{fm}^2$ [188]. Actually, this expression of the charge radius can be directly obtained from the common definition

$$R_{\rm ch}^2 \equiv \frac{\displaystyle\int \mathrm{d}^3r\, r^2 \rho_{\rm ch}(r)}{\displaystyle\int \mathrm{d}^3r\, \rho_{\rm ch}(r)} \tag{III.59}$$

and the charge density distribution $\rho_{\rm ch}(r)$ defined in equation (III.64). This ensures cohesion between the various quantities of interest.

Considering the definition (III.58), the difference between recent experimental and theoretical HFB charge radii for low- to heavy-mass nuclei along six isotopic chains are represented in Figure III.5. This difference is defined as

$$\Delta R_{\rm ch}^{\rm HFB} \equiv R_{\rm ch}^{\rm HFB} - R_{\rm ch}^{\rm exp}, \tag{III.60}$$

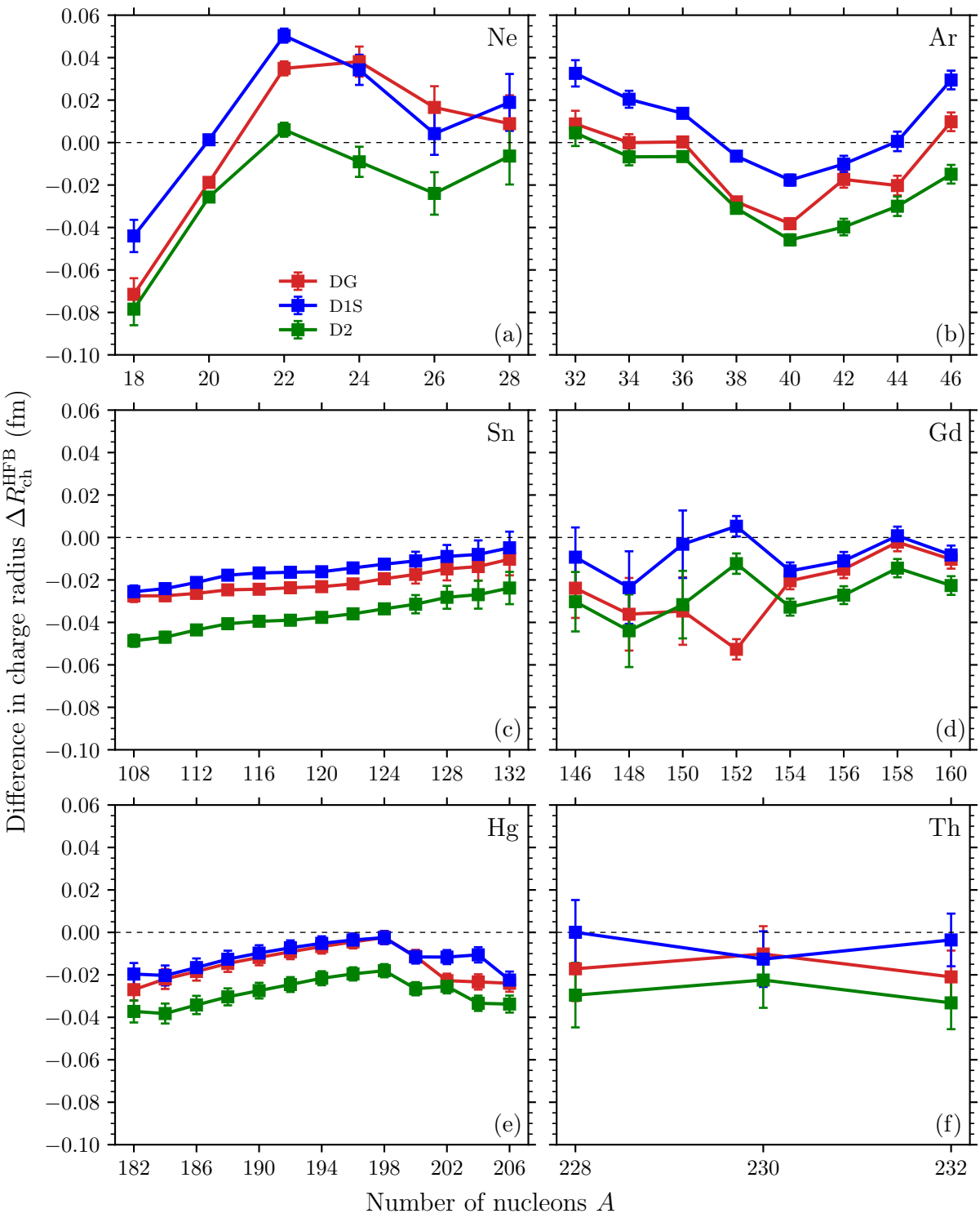

Figure III.5 – Difference between experimental [189] and HFB charge radii, expressed in (III.58), as a function of the number of nucleons A. Results are provided along Ne, Ar, Sn, Gd, Hg and Th isotopic chains for DG, D1S and D2 interactions. Vertical bars indicate the experimental errors.

where $R_{\rm ch}^{\rm HFB}$ and $R_{\rm ch}^{\rm exp}$ respectively denote the HFB and experimental charge radii.

For low-mass nuclei (panels (a) and (b)), the results obtained with the three interactions overall follow the same trend, and are shifted around the horizontal dashed line

such that the charge radii of certain isotopes are better reproduced by one interaction or another; it is not possible to discriminate the most convincing interaction.

This shift also manifests in heavier nuclei but the charge radii are systematically underestimated by all three interactions (putting aside a few exceptions with D1S). Consequently, it appears clearly that the predictions are globally better with D1S, at the HFB level. However, in particular in Sn and Hg isotopes, DG is closer to D1S predictions than D2. Based on these examples, it seems that the DG interaction cures, at least partially and in medium- to heavy-mass nuclei, the lack of precision in the description of charge radii with D2 at the HFB level, as called out in [190].

Once again, it would be useful to generalize the study to more nuclei in order to confirm our results on a larger scale. The underestimation of charge radii by medium- to heavy-mass isotopes supports the fact that they will be raised in soft nuclei when going beyond the mean field, through the incorporation of collective excitations of small or large amplitudes in random phase approximation (RPA) or generator coordinate method (GCM) approaches, for example. This is indeed what was observed for the D1S interaction from the five-dimensional collective quadrupole Hamiltonian (5DCH) method in [191]. The charge radii of D1S were predicted too large within this formalism. It is accordingly satisfactory that the charge radii of DG and D2 are a bit smaller. The same study carried out with these interactions would reveal whether the diminution in charge radii brought by DG is sufficient or if they need to be further diminished, as with interaction D2.

3.3. Isotopic shifts in squared charge radii

The isotopic shift (or kink) in charge radii corresponds to "abnormally" small or high charge radii of one or several isotopes with respect to their neighbors resulting, as its name suggests, in a shift. Usually, to highlight this effect, the following difference between squared charge radii is studied,

$$\Delta R^2_{\rm ch}(A) \equiv R^2_{\rm ch}(A) - R^2_{\rm ch}(A_{\rm ref}), \tag{III.61}$$

where the charge radii $R_{\rm ch}$ are evaluated for a reference nucleus of mass number $A_{\rm ref}$ from which the effect shows up, and for the neighboring isotopes of mass number A.

The best-known and most widely discussed case in the literature is that of the Pb isotopic chain, with which we start our analysis.

3.3.1. Lead isotopic shift

In this Pb isotopic chain, the kink appears at ^{208}Pb, so that the difference in squared charge radii reads

$$\Delta R^2_{\rm ch}(A) \equiv R^2_{\rm ch}(A) - R^2_{\rm ch}(208). \tag{III.62}$$

The charge radii as well as the isotopic shift calculated for the Pb isotopic chain with DG, D1S and D2 interactions and compared to experimental data are shown in Figure III.6.

In panel (a), we see that charge radii predicted by all thee interactions are underestimated with respect to experimental data. This follows the explanation we have given in previous subsection. As detailed in the text, a distinct bent appears with the experimental values at $A = 208$ and extends to heavier isotopes. This phenomenon is visible with D2 and to a lesser extent with D1S, but it is most remarkable with DG. Things are even clearer in panel (b). Indeed, the kink, still lower than experimental predictions, looks better reproduced with DG than with D1S and D2 interactions. In order to be more

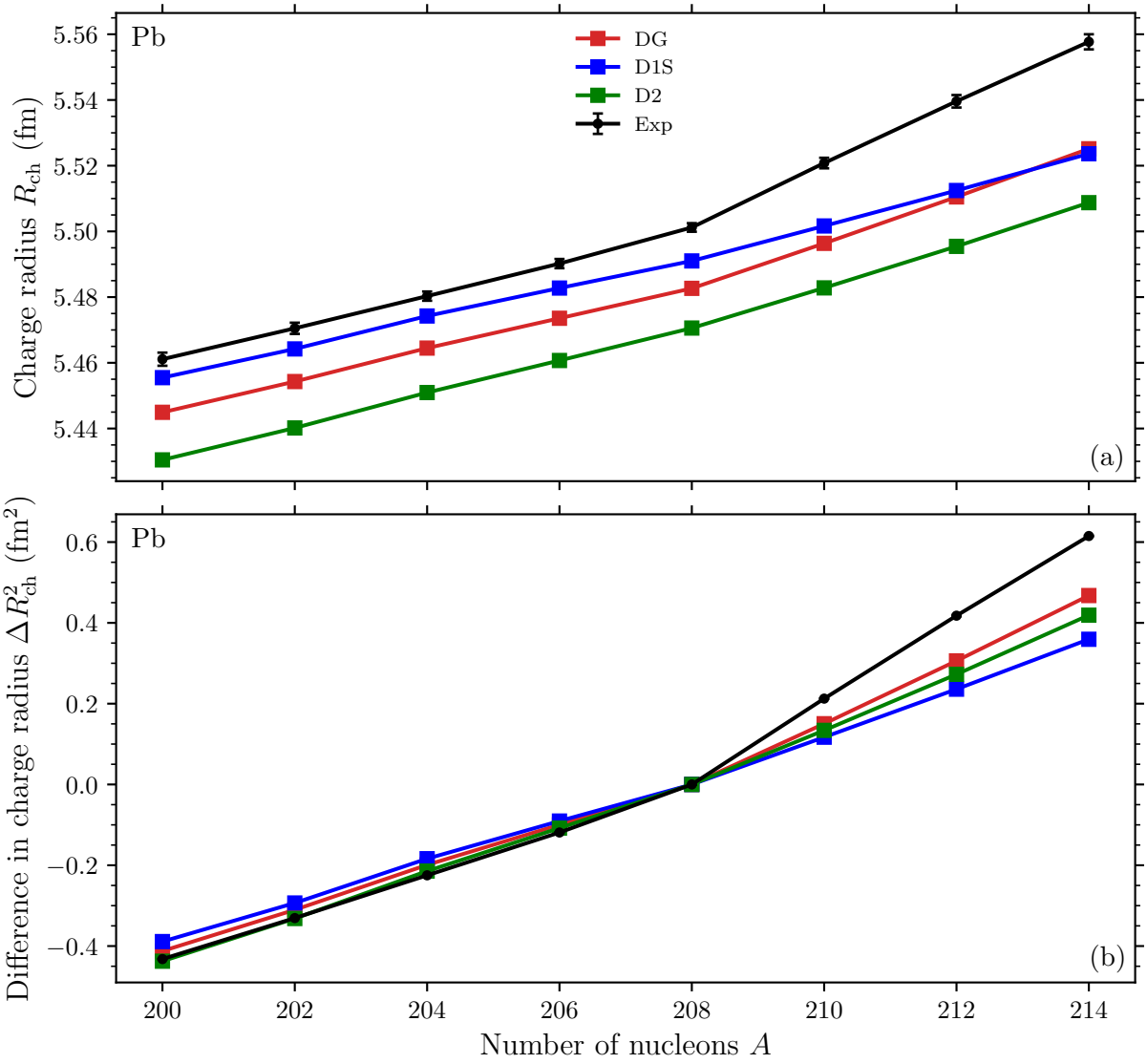

Figure III.6 – The charge radii and differences in squared charge radii, as defined in (III.62) for Pb isotopes, are represented against the neutron number N in panels (a) and (b), respectively, for DG, D2 and D1S interactions. They are compared to experimental data, with vertical bars showing experimental errors [189].

quantitative, we have evaluated the angle formed by the straight lines connecting isotopes ^{200}Pb to ^{208}Pb and ^{208}Pb to ^{214}Pb for various interactions. The results are displayed in Table III.2. The numerical values confirms our observations as the slightly better kink exhibited by D2 is appreciably improved with DG, with respect to D1S.

Now, we would like to understand what peculiarities of DG are responsible for its better reproduction of the isotopic shift. Since the central and density-dependent part of DG remains close to D2, we tend to rather attribute this effect to either the spin–orbit or tensor forces. On the one hand, we have explained in the fitting process that Sharma *et al.* [142] proved that a Skyrme interaction augmented with an isospin-dependent spin–orbit force was able to better reproduce the kink in Pb isotopes. For that reason, a value for our parameter H_5 fixing the intensity of the isospin-dependent spin–orbit term close to theirs was required in the fitting protocol. On the other hand, Colò *et al.* found out no improvement regarding the Pb isotopic shift when they added a tensor force on top of the

Interaction	Angle θ (°)
DG	1.51
DG ($H_5 = 0$)	0.18
DG ($W_7 = H_7 = 0$)	1.65
D1S	0.64
D1ST2a	1.74
D1ST2c	1.11
D2	0.87
Exp	2.76

Table III.2 – Angle formed by the straight lines connecting isotopes ^{200}Pb to ^{208}Pb and ^{208}Pb to ^{214}Pb, used to quantify the kink. The results are provided for Gogny interactions DG, D1S, D1ST2a, D1ST2c, D2 and experimental data, as well as for DG when the spin–orbit parameter H_5 is set to zero or when the tensor is switched off ($W_7 = H_7 = 0$).

Skyrme parametrization SLy5 [48]. Yet, Lesinski *et al.* noticed that this kink was sensitive to tensor terms in Skyrme interactions, even if they could not be held responsible for the entire effect [51]. It seems that under some circumstances, the spin–orbit and tensor forces are both involved in the reproduction of the Pb isotopic shift in Skyrme interactions. To our knowledge, such studies are missing for the Gogny interaction. Then, we propose an attempt to untie the roles of the (finite-range) spin–orbit and tensor forces of the Gogny interaction on this observable.

We have represented in Figure III.7 the isotopic shifts for the perturbative tensor-dependent D1ST2a and D1ST2c interactions, as well as those obtained with the DG parametrization when the isospin-dependent spin–orbit strength is set to zero ($H_5 = 0$) and then when the overall tensor is switched off ($W_7 = H_7 = 0$). This allows to evaluate separately the effects of the spin–orbit and tensor effects with respect to D1S, as well as within the DG interaction.

The results indicate that the spin–orbit and tensor forces of the Gogny interaction are profoundly involved in the reproduction of the kink in Pb isotopes. The numerical values of the isotopic shifts for the above-mentioned interactions are listed in Table III.2. We observe that they are better predicted by D1ST2a and D1ST2c interactions than with D1S. As the former is only supplemented by a tensor force besides the D1S parameters, it reveals that the tensor term unambiguously takes part in the reproduction of the kink. The latter additionally reduces the intensity of the D1S spin–orbit force (from 130 MeVfm^5 to 103 MeVfm^5). Since its kink is notably lowered with respect to D1ST2a, it also reveals that the spin–orbit interaction has a non-negligible influence. Although D1ST2a and D1ST2c do not reach the experimental value, it appears that the isotopic shift is very sensitive to their contributions. We can conclude that, based on these examples, the inclusion of the spin–orbit and tensor forces is necessary to better reproduce the isotopic shift in Pb isotopes when dealing with Gogny interactions. If we now turn into the modified DG parametrizations, we first see than when the small isospin dependence ($H_5 = 29.634$ MeVfm^5) of the spin–orbit interaction is set to zero, the kink nearly disappears. On the contrary, when the tensor force is switched off, the kink is slenderly improved. This implies two interesting features of our interaction. Firstly, the isospin-dependent spin–

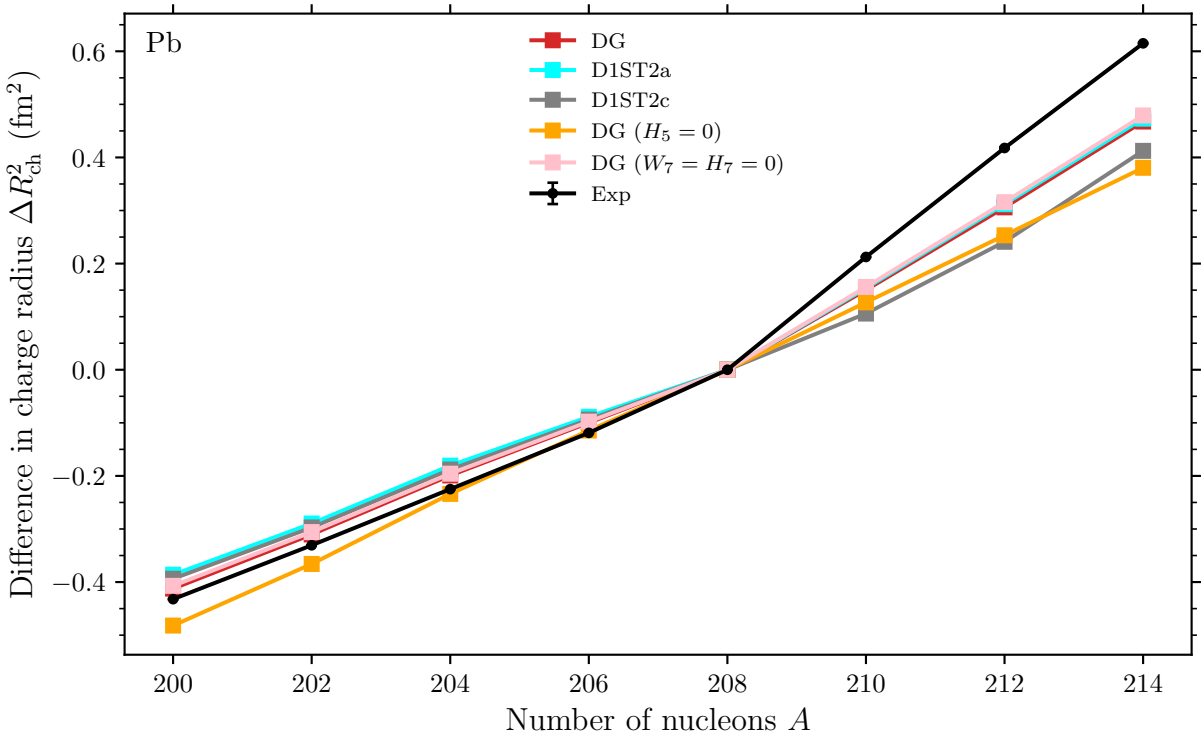

Figure III.7 – Same as in Figure III.6 panel (b), but now for interactions D1ST2a and D1ST2c, as well as interaction DG when the spin–orbit parameter H_5 is set to zero or when the tensor is switched off ($W_7 = H_7 = 0$).

orbit term is mainly responsible for the value of the angle θ, despite its small strength. This was quite expected since it has been fitted for that purpose, but was not guaranteed since the effect showed up for a zero-range spin–orbit term of a Skyrme interaction with a different analytical expression. Secondly, contrary to the D1ST2a and D1ST2c cases, our tensor force destroys part of the good reproduction of the Pb kink. This is astonishing considering that filters deduced from the tensor parameters of the D1ST2c interaction have been set up in the fitting process of DG. Actually we should be careful in our interpretation because the parametrizations D1ST2a and D1ST2c were not completely refitted as DG is, and switching off terms in this latter do not produce fully consistent interactions either since its parameters were determined *all together*. Nonetheless, it would be enlightening to look deeper into the relative contributions of the spin–orbit and tensor forces to the Pb isotopic shift, within the Gogny interaction. If the way in which the tensor terms act on the kink is understood, in the same manner as the isospin component of the spin–orbit force is, an additional filter could be added in the fitting code to select the tensor parameters accordingly.

Finally, we would like to give an explanation from SPE considerations on how the spin–orbit and tensor forces can influence the kink in Pb isotopes. It is often argued that the neutron splitting $(1i_{11/2} - 2g_{9/2})$ in ^{208}Pb is directly related to the kink [51, 192]. Indeed, as these states get closer, the $1i_{11/2}$ level is further filled through pairing correlations from nucleons in the lower $2g_{9/2}$ level, for isotopes with $N > 126$. The partial filling of the $1i_{11/2}$ level increases the neutron radius more than when only the $1i_{13/2}$ is occupied (with no pairing correlations showing up), as for $N \leq 126$ isotopes. Since the charge density distribution follows the evolution of the neutron density distribution in Pb isotopes (and

in particular in ^{208}Pb, as we show in subsection III.3.4.1), the charge radii of $N > 126$ isotopes grow faster than for $N \leq 126$ ones. To expose how this discussion applies to the interactions we have mentioned so far, we represent the neutron $1i_{11/2}$ and $2g_{9/2}$ states in Figure III.8 and enumerate the corresponding neutron energy differences in Table III.3.

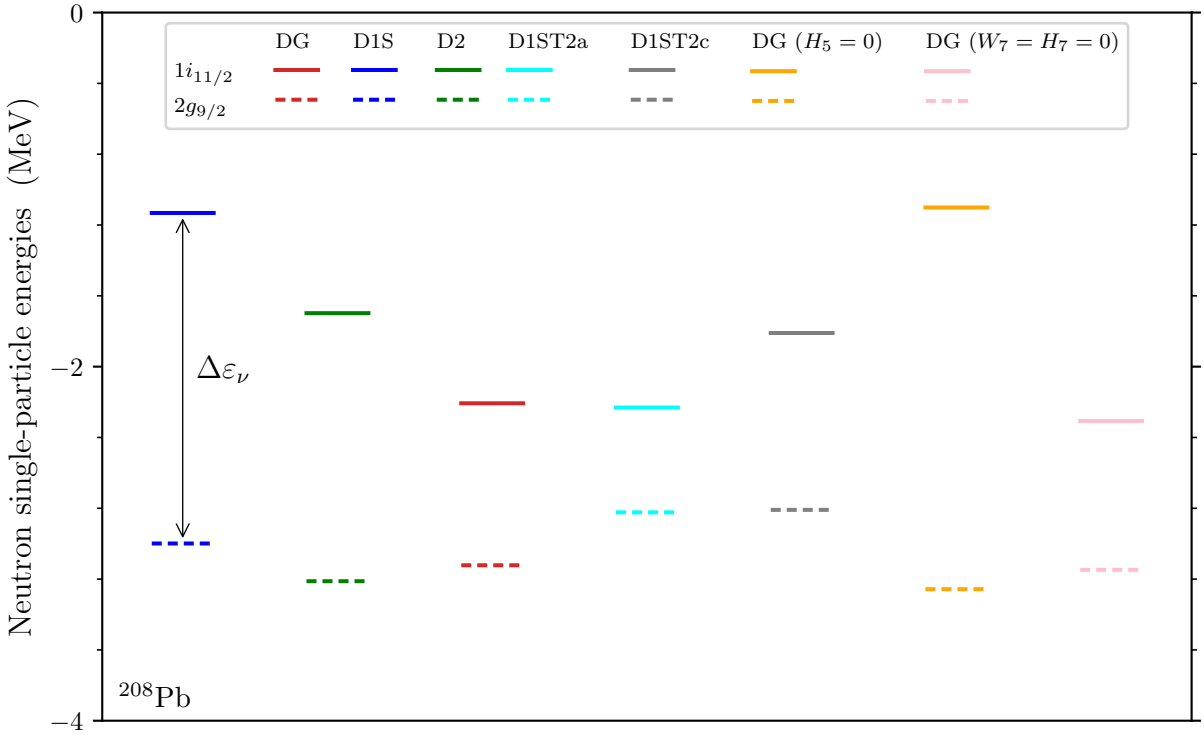

Figure III.8 – Neutron single-particle energies of $1i_{11/2}$ and $2g_{9/2}$ states in ^{208}Pb for DG, D1S, D2, D1ST2a, D1ST2c and DG interactions when $H_5 = 0$ and when $W_7 = H_7 = 0$.

	Energy difference
Interaction	$\Delta\varepsilon_\nu$ (MeV)
DG	0.925
DG ($H_5 = 0$)	2.156
DG ($W_7 = H_7 = 0$)	0.841
D1S	1.867
D1ST2a	0.592
D1ST2c	0.999
D2	1.514

Table III.3 – Energy difference between the neutron $1i_{11/2}$ and $2g_{9/2}$ states in ^{208}Pb for DG, D1S, D1ST2a, D1ST2c, D2 and DG when $H_5 = 0$ and when $W_7 = H_7 = 0$.

Comparison of numerical values in Tables III.2 and III.3 proves that the qualitative description provided above is quantitatively verified by the Gogny interactions we have analyzed. Indeed, the smaller the energy difference between the neutron $1i_{11/2}$ and $2g_{9/2}$ states, the more accurately the experimental Pb isotopic shift is reproduced.

The displacement of the neutron SPEs shown in Figure III.8 can be attributed to the spin–orbit and tensor forces to some extent. We know the spin–orbit term to favor the splitting between spin-partner states proportionally to its intensity. Here, this intensity (in the $T = 1$ channel) was reduced when going from D1S to DG, from 130 MeVfm^5 to $W_5 - H_5 = 115.849$ MeVfm^5, such that it is expected to shrink the neutron $(2g_{9/2} - 2g_{7/2})$ and $(1i_{11/2} - 1i_{13/2})$ splittings, ending up in narrowing the neutron $(1i_{11/9} - 2g_{9/2})$ gap. On the other hand, according to Ostuka's picture (see section III.2), the completely filled $(1i_{13/2})_\nu$ state lowers the $(1i_{11/2})_\nu$ state while the completely filled $(1h_{11/2})_\pi$ state reduces the $(2g_{9/2} - 2g_{7/2})_\nu$ and $(1i_{11/2} - 1i_{13/2})_\nu$ splittings. The global effect of the tensor force is therefore to shrink the neutron gap $(1i_{11/9} - 2g_{9/2})$. Note that such vision does not consider the role of the spin–orbit force in the $T = 0$ channel, whose intensity is given by $W_5 + H_5 = 175.117$ MeVfm^5 with DG. To our knowledge, the action of the proton–neutron component of the spin–orbit interaction on SPEs is not widely discussed in the literature. Yet, this information would be crucial to state whether the spin–orbit force improves the description of the kink because of a lower intensity in the $T = 1$ channel as suggested above, or whether it is related to the isospin-dependent parameter H_5, as highlighted by Sharma *et al.* [142].

Actually, another interpretation can be given to explain this arrangement of neutron SPEs. One can show that the density of states in the vicinity of the Fermi level in finite nuclei is proportional to the effective masses calculated in infinite nuclear matter [17]. The asymmetry of the medium, defined by $\beta \equiv N - Z/N + Z$, reaches $\beta \simeq 0.21$ in ^{208}Pb. From Figure II.7, we can extract the neutron effective masses (m^*_ν/m) at such asymmetry for DG, D1S and D2 interactions. They read $(m^*_\nu/m)^{\rm DG} \simeq 0.78, (m^*_\nu/m)^{\rm D1S} \simeq 0.73$ and $(m^*_\nu/m)^{\rm D2} \simeq 0.77$. Since we have $(m^*_\nu/m)^{\rm DG} > (m^*_\nu/m)^{\rm D2} > (m^*_\nu/m)^{\rm D1S}$, the density of neutron states around the Fermi level in ^{208}Pb should be greater with DG than with D2, and greater with D2 than with D1S. This is indeed what is observed in Figure III.8. Thus, the better reproduction of the kink in Pb isotopes could be associated with a higher neutron effective mass in nuclear matter. It is worth noticing that the neutron effective mass of DG is the closest to that predicted by realistic calculations at $\beta \simeq 0.21$, according to Figure II.7. It is not excluded that these various interpretations are complementary, but further investigations at the fitting stage should be undertaken in the future to settle the question.

As we have pointed out, the isotopic shift is closer to the experimental value with DG than with D1S and D2 interactions. However, this is not satisfactory enough as it reaches only just over half that value with DG. It has already been discussed that adding filters at the fitting stage to constrain the tensor parameters may enhance the outcomes. A recent study conducted by Kanada-En'yo established that allocating a density dependence to the spin–orbit force in the Skyrme interaction remarkably improved the reproduction of the kink in Pb isotopes [192]. This sounds natural since both the spin–orbit and density-dependent terms are known to have a strong action on the arrangement of SPEs, from which the kink can be explained. Following this idea, there is great probability that such analytical extension would also make the predictions of Gogny interactions better. As we have underlined that the position of the neutron SPEs, relevant to justify the kink in Pb isotopes, was the result of a *competition* between spin–orbit and tensor forces, it suggests that supplementing the tensor term with a density dependence as well may further drive the kink in the right direction.

3.3.2. Calcium isotopic shift

In Ca isotopes, a similar phenomenon occurs for ^{42}Ca and ^{44}Ca as well as for ^{48}Ca, whose charge radii are "abnormally" large and small, respectively. As a consequence, the difference in squared charge radii is sometimes defined with respect to $A_{\rm ref} = 40$, and sometimes with respect to $A_{\rm ref} = 46$. We will conventionally choose the first option and study the quantity

$$\Delta R^2_{\rm ch}(A) \equiv R^2_{\rm ch}(A) - R^2_{\rm ch}(40). \tag{III.63}$$

It turns out that Skyrme parametrizations constructed so far fail in reproducing such behavior [5, 51]. In fact, in the region $20 < N < 26$, the disagreement between theoretical and experimental predictions with Skyrme interactions is thought to be due to deformation and pairing effects, while that for ^{48}Ca is not understood yet [192]. For Gogny parametrizations, no extensive studies have been carried out in this direction. Even so, the tensor force is renowned to modify the deformation properties of some nuclei (see section III.5) and, along with the spin–orbit force, to significantly modify the gaps in some nuclei, ending up in altering the pairing properties (see next section). Thus, we wanted to figure out whether the finite-range spin–orbit and tensor forces could improve the description of the kink in Ca isotopes. The charge radii and isotopic shift for Ca isotopes are displayed in Figure III.9 for DG, D1S and D2 interactions, and are compared to experimental data.

In panel (a), we see that the charge radii are globally underestimated by DG and D2 interactions (except for ^{48}Ca which is slightly overestimated by DG). This is in agreement with our general discussion on charge radii (see subsection III.3.2), but not for D1S which substantially overestimates the charge radii of Ca isotopes from ^{46}Ca to ^{50}Ca. The bump appearing for ^{42}Ca and ^{44}Ca is not even sketched by any of the three interactions, and the bent at ^{48}Ca is slightly more pronounced with DG and D2 than with D1S.

These last observations are confirmed by panel (b). Interactions DG, D2 and D1S are all alike and fail in predicting the particular squared charge radii of ^{42}Ca, ^{44}Ca and ^{48}Ca isotopes. The same trend was recently noticed with D1ST2a [195].

We could invoke again that providing density dependences to the spin–orbit and tensor interactions may be a solution. However, the density-dependent spin–orbit term considered by Kanada-En'yo in Skyrme interactions did not solve the problem [192]. As for the effects of a density-dependent tensor term on isotopic shifts, such studies are still missing. Besides, DG does not change the spherical shape of these isotopes, already predicted by D2 and D1S interactions (see subsection III.5.1).

3.4. Nuclear density distributions

We now turn our attention to the nuclear density distributions of two spherical nuclei, namely ^{208}Pb and ^{48}Ca, with DG, D1S and D2 interactions.[8] Contrary to the neutron density distribution, the proton density distribution is not directly accessible to experiment. In fact, different types of corrections need to be taken into account in the proton density distribution, giving rise to the charge density distribution, which can be measured experimentally. For ease of comparison, we detail here the amendments to the proton density distribution we consider. The charge density distribution is defined by

$$\rho_{\rm ch}(r) \equiv \int {\rm d}^3r' \Big[\rho_\pi(r') g_\pi(|\vec{r} - \vec{r}'|) + \rho_\nu(r') g_\nu(|\vec{r} - \vec{r}'|)\Big], \tag{III.64}$$

8. We have checked out that both nuclei were predicted spherical by DG, D1S and D2 interactions.

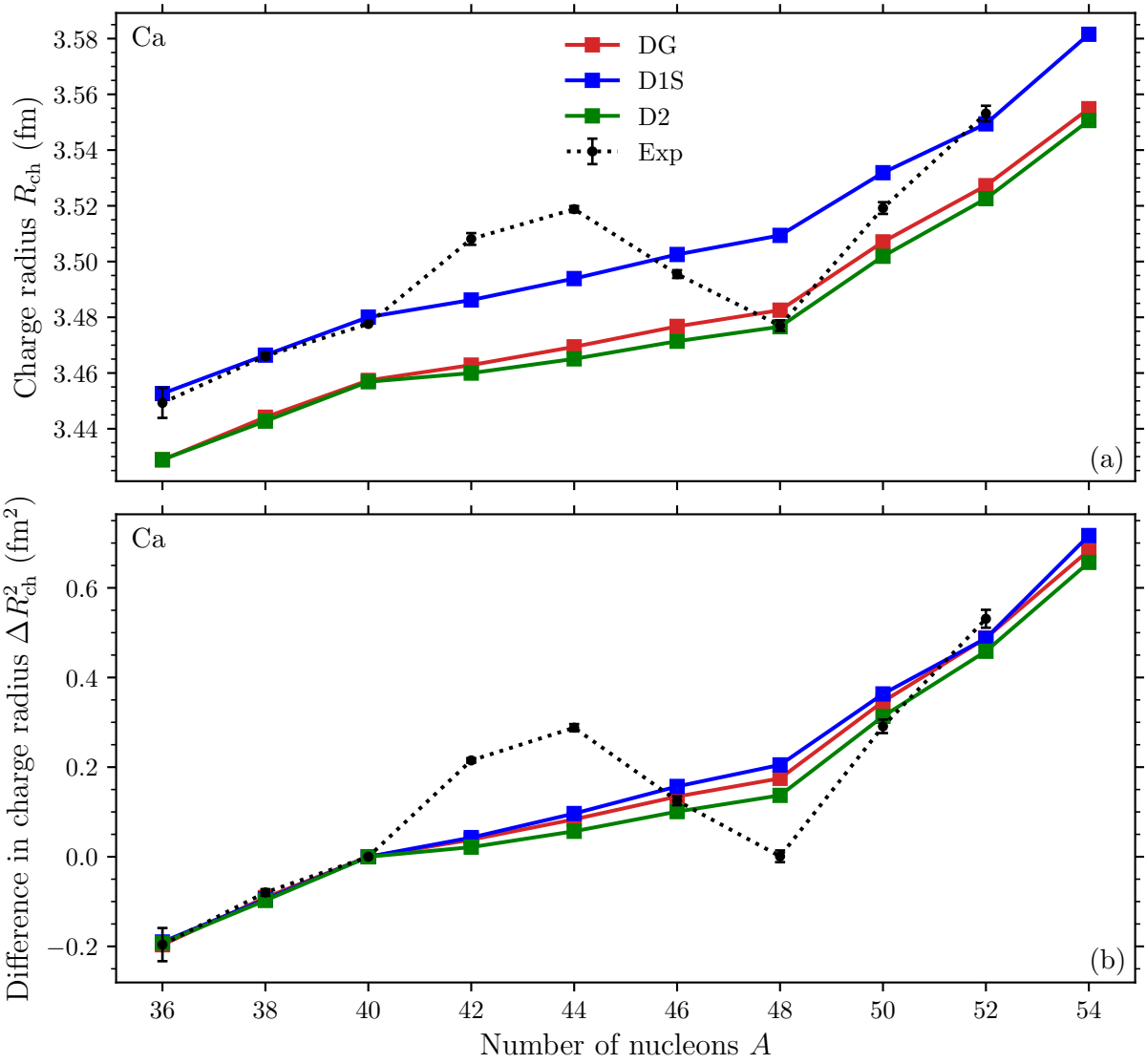

Figure III.9 – The charge radii and differences in squared charge radii, as defined in (III.63) for Ca isotopes, are represented against the neutron number N in panels (a) and (b), respectively, for DG, D2 and D1S interactions. They are compared to experimental data, with vertical bars showing experimental errors [189, 193, 194].

where point-like proton $\rho_\pi(r')$ and neutron $\rho_\nu(r')$ density distributions are folded by proton $g_\pi(|\vec{r}-\vec{r}'|)$ and neutron $g_\nu(|\vec{r}-\vec{r}'|)$ form factors. The proton form factor,

$$g_\pi(|\vec{r}-\vec{r}'|) \equiv \frac{1}{[\pi(P^2-B^2)]^{3/2}} \mathrm{e}^{-(\vec{r}-\vec{r}')^2/(P^2-B^2)}, \tag{III.65}$$

is a distribution which takes into account the spatial extension of the proton as well as its center-of-mass motion, when convoluted with the point-like proton density [196]. As for the neutron form factor,

$$g_\nu(|\vec{r}-\vec{r}'|) \equiv -\frac{2}{3}\frac{\langle r_\nu^2\rangle}{r_1^2(r_1\sqrt{\pi})^3}\left(\frac{r-r'}{r_1}\right)^2\left[1-\frac{2}{5}\left(\frac{r-r'}{r_1}\right)^2\right]\mathrm{e}^{-(\vec{r}-\vec{r}')^2/r_1^2}, \tag{III.66}$$

it is parametrized so as to account for the charge distribution within the neutron, when convoluted with the point-like neutron density [197]. In this distribution, we have $r_1 \equiv$

$\sqrt{2/5} \cdot 0.71\,\text{fm}$. The other quantities appearing in the above definitions have been given in subsection III.3.2.

3.4.1. Density distributions in ^{208}Pb

The neutron and charge density distributions predicted by DG, D1S and D2 interactions for ^{208}Pb are represented in Figure III.10. As the uncertainty in the determination of the neutron density is large, the error is represented by a gray envelope on either side of the experimental measurement.[9] At small distances from the center of the nucleus, $r \leq 0.5\,\text{fm}$, all three interactions are a bit outside the envelope, although DG and D2 are a bit closer. At higher densities, they are almost always contained in the envelope, except around $r \simeq 1.7\,\text{fm}$ and $r \simeq 5.3\,\text{fm}$ where D1S slightly deviates from the experimental area, contrary to D2 and DG interactions. Similarly, at large distances around $r \simeq 7.5\,\text{fm}$, they all thinly underestimate the neutron density distribution. Actually, it is difficult to have a faithful reproduction of the density distributions at small distances at the HFB level since the bump observed is related to the filling the $3s_{1/2}$ orbitals, taken into account through beyond mean-field approaches.

The description of the charge density distribution is pretty well reproduced by all three interactions, with a reasonable discrepancy of about $0.007\,\text{fm}^{-3}$ at zero distance, and gradually fades away until disappearing at about $r \simeq 4\,\text{fm}$. The results provided by the three interactions are once again comparable, and very slightly better at all distances with DG and D2. Note in passing that the three corrections added to the bare proton density distribution are similar for all interactions, with a maximum contribution at zero distance of no more than $0.004\,\text{fm}^{-3}$.

3.4.2. Density distributions in ^{48}Ca

We now carry out the exact same analysis on the nuclear density distributions for ^{48}Ca, whose results are displayed in Figure III.11. Unfortunately, the quantities R_i and $Q_i^\pm$ appearing in the distribution (III.67) are not available for ^{48}Ca, such that we have extracted by hand the envelope from [200], and interpolated the data. At small distances, $r \leq 0.7\,\text{fm}$, all three interactions are outside the envelope, but this time D1S is closer. They then enter the experimental zone, before separating again at about $r \simeq 1.4\,\text{fm}$. Nevertheless DG and D2 quickly return near experimental values, at $r \simeq 2.4\,\text{fm}$, against $r \simeq 3.2\,\text{fm}$ for D1S interaction. Beyond, they all follow the experimental curve and slenderly overestimate the neutron density distribution at large distances, from about $r \simeq 4.2\,\text{fm}$ to $5.2\,\text{fm}$.

As for the charge density distributions of the Gogny interactions, they are all moderately far from experimental predictions, especially in the region $r \leq 2\,\text{fm}$. The phenomenon is more pronounced at zero distance, reaching a difference of $0.017\,\text{fm}^{-3}$ with

9. The upper (+) and lower (−) edges of the envelope are determined using a model-independent sum-of-Gaussians distribution of the form

$$\rho_\nu^\pm(r) = \frac{N}{2\pi^{3/2}\gamma} \sum_{i=1}^{12} \frac{Q_i^\pm}{1 + 2R_i^2/\gamma^2} \left(\mathrm{e}^{-(r-R_i)^2/\gamma^2} + \mathrm{e}^{-(r+R_i)^2/\gamma^2} \right), \tag{III.67}$$

with N the number of neutrons, $\gamma \equiv 1.70/\sqrt{3/2}$ the width of the Gaussians, as well as the position R_i and the fraction of neutrons $Q_i^\pm$ in the i-th Gaussian, which are given for ^{208}Pb in [198].

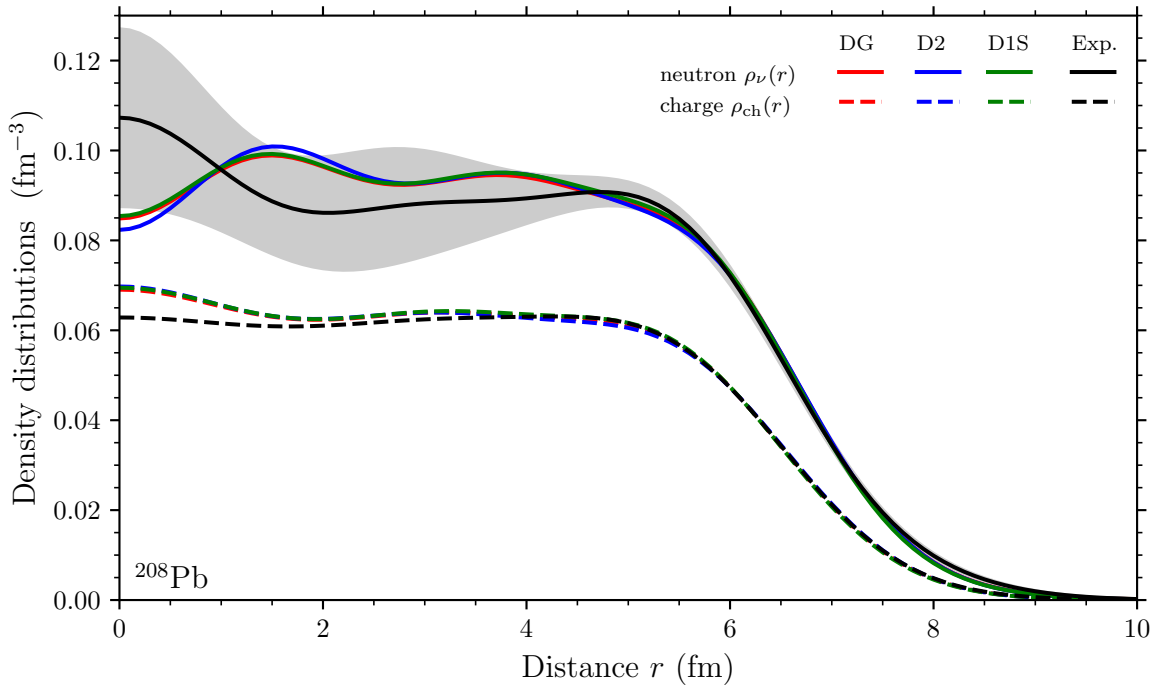

Figure III.10 – Neutron (full lines) and charge (dashed lines) density distributions obtained with DG, D1S and D2 interactions at the HFB approximation, compared to experiment in ^{208}Pb [198, 199]. The gray envelope shows the uncertainty of the experimental neutron density distribution.

D1S and 0.022 fm^{-3} with DG and D2, respectively. At large distances, from $r \simeq 3.4$ fm, all three interactions merge the experimental curve.

Generally speaking, we note that the theoretical predictions are better in ^{208}Pb than in ^{48}Ca. In particular, DG and D2 curves seem to more accurately fit experimental data than D1S. One way of improving our description would be to pull out the density distributions from random phase approximation (RPA) calculations, which would then take into account more correlations in the ground state. The closeness of the DG and D2 results suggests that the spin–orbit and tensor terms have no major influence on the density distributions. If we stick to the HFB outputs, we tend to mainly attribute the good local predictions of DG and D2 interactions to their finite-range density-dependent term. In that logic, it might be worth attaching a density dependence to the spin–orbit and tensor forces.

4. Surface properties

4.1. Pairing energy

4.1.1. Tin isotopic chain

We carry on our analysis of the generalized Gogny interaction by looking at its surface properties, and more particularly its pairing energy in this subsection, which are compared to the D1S and D2 predictions. The pairing energy, drawing its contributions from the central, density-dependent, spin–orbit, tensor and Coulomb pairing fields, for interaction DG, is examined in the Sn isotopic chain. Since these nuclei possess a magic number

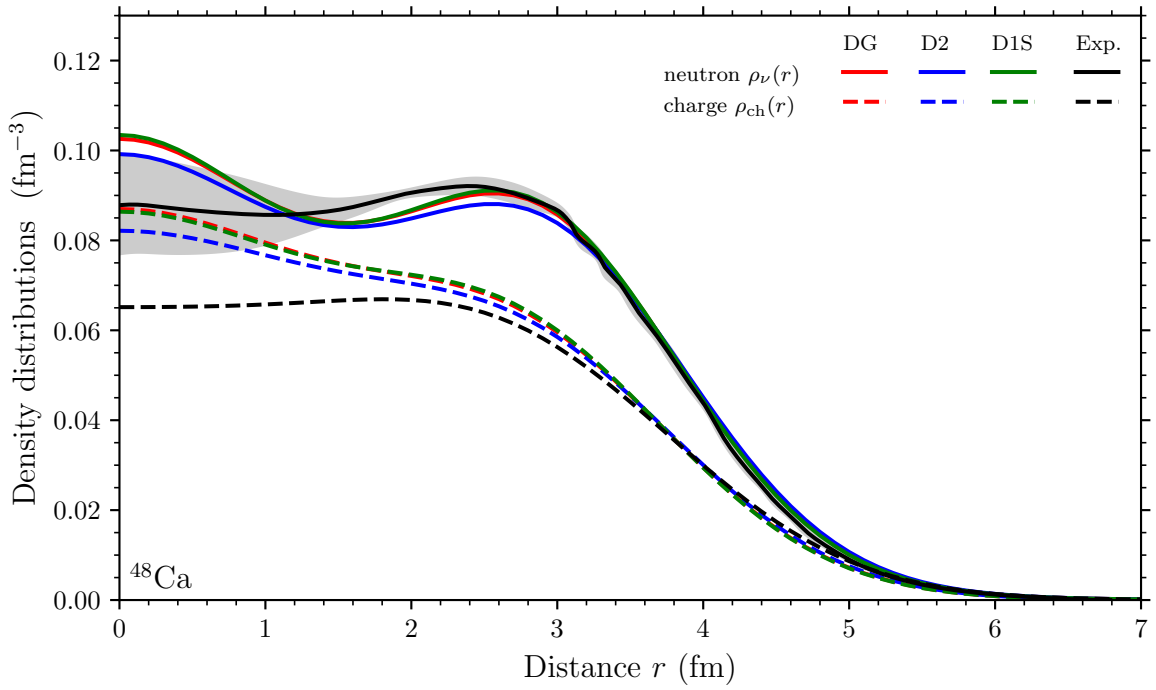

Figure III.11 – Same as in Figure III.10, but now for ^{48}Ca. Experimental data have been extracted from [199, 200].

of protons ($Z = 50$), they allow to isolate the neutron pairing correlations. The pairing energies of DG, D2 and D1S interactions, calculated using the exact exchange Coulomb potential as well as the Slater approximation, are represented in Figure III.12.

We first note we have checked that the proton contribution to the pairing energy is, as expected, zero so that only the neutron pairing energy is responsible for what follows. As required, the pairing energies vanish for all three interactions in the doubly magic isotopes ^{100}Sn and ^{132}Sn. This result was mandatory to guarantee consistency of our parametrization, and was actually systematically verified at the fitting stage. Pairing energies are not significantly changed when the exact Coulomb potential is taken into account. Only for the interaction DG, between $A = 100$ to $A = 116$, the intensity of the pairing energy is increased by at most 300 keV, due to the mean-field rearrangement. This was expected since the Coulomb term contributes to the proton pairing energy exclusively. Once these details have been given, the striking effect is obviously the collapse in pairing energy observed with DG, compared to D1S and D2 interactions. From $A = 110$, the well shape is broken with DG, and the strength of the pairing energy decreases up to $A = 118$ before growing again up to $A = 124$, returning to values comparable to those of D1S and D2 interactions. This phenomenon clarifies the decline of the difference between HFB and experimental binding energies, with respect to D1S and D2 interaction, we have observed sooner along the Sn isotopic chain (see panel (c) of Figure III.4). Indeed, when (the intensity of) the pairing energy starts to fall down with DG, at $A = 110$, the associated binding energy is also reduced. This indicates manifestly the responsibility of the pairing energy in the peculiar diminution of the binding energies, specific to the DG interaction, in the Sn isotopic chain.

To understand what is going on in the region between $60 \leq N \leq 76$, we look at the neutron SPEs of the corresponding isotopes in Figure III.13, with DG, D1S and D2 interactions (employing the exact Coulomb term), extracted from an HF calculation. A

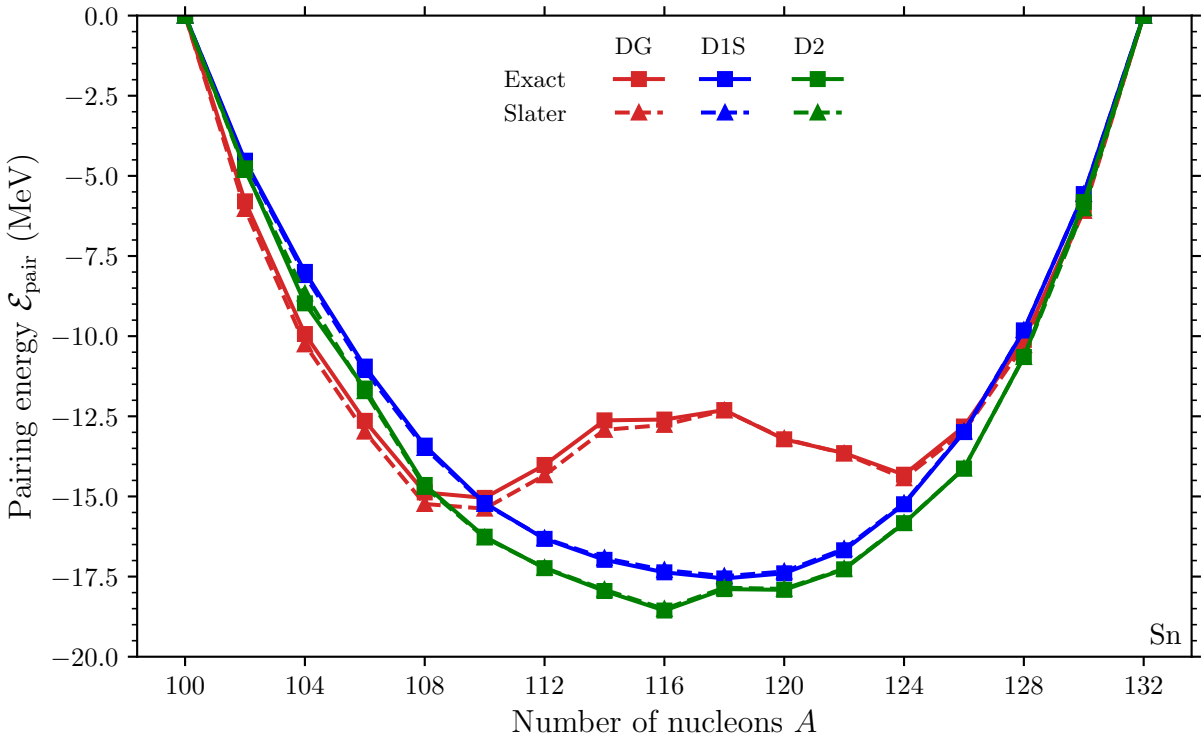

Figure III.12 – Pairing energy as a function of the nucleon number A in the Sn isotopic chain, evaluated for DG, D1S and D2 interactions, with and without the exact Coulomb potential.

quite impressive effect stands out: two inversions of neutron levels, one between $1g_{7/2}$ and $2d_{5/2}$ at $N = 62$ and another between $2d_{3/2}$ and $3s_{1/2}$ states at $N = 68$ appear with DG, compared to D1S and D2 interactions. Even more interestingly, they occur roughly where the monotony of the pairing energy curve changes, as we have described in the previous paragraph. Needless to say, we could be more precise if odd isotopes were also considered, but we can already be quantitative by focusing on the values of the neutron gaps given in Table III.4.

	$(1g_{7/2} - 1g_{9/2})_\nu$			$(2d_{3/2} - 2d_{5/2})_\nu$		
	DG	D1S	D2	DG	D1S	D2
Isotope	(MeV)	(MeV)	(MeV)	(MeV)	(MeV)	(MeV)
^{110}Sn	6.202	8.143	7.953	2.599	2.909	2.754
^{112}Sn	6.153	8.080	7.881	2.544	2.909	2.745
^{114}Sn	6.032	8.014	7.806	2.535	2.911	2.738
^{116}Sn	5.959	7.938	7.713	2.498	2.914	2.729
^{118}Sn	5.913	7.846	7.599	2.438	2.913	2.716
^{120}Sn	5.871	7.735	7.462	2.390	2.907	2.703

Table III.4 – Neutron energy gaps $(1g_{7/2} - 1g_{9/2})_\nu$ and $(2d_{3/2} - 2d_{5/2})_\nu$ of Sn isotopes predicted by DG, D1S and D2 interactions at the HF approximation.

On the one hand, we see that the $(1g_{9/2} - 1g_{7/2})$ neutron gap of DG is considerably reduced compared to that of D1S and D2 interactions in all the Sn isotopes displayed. In

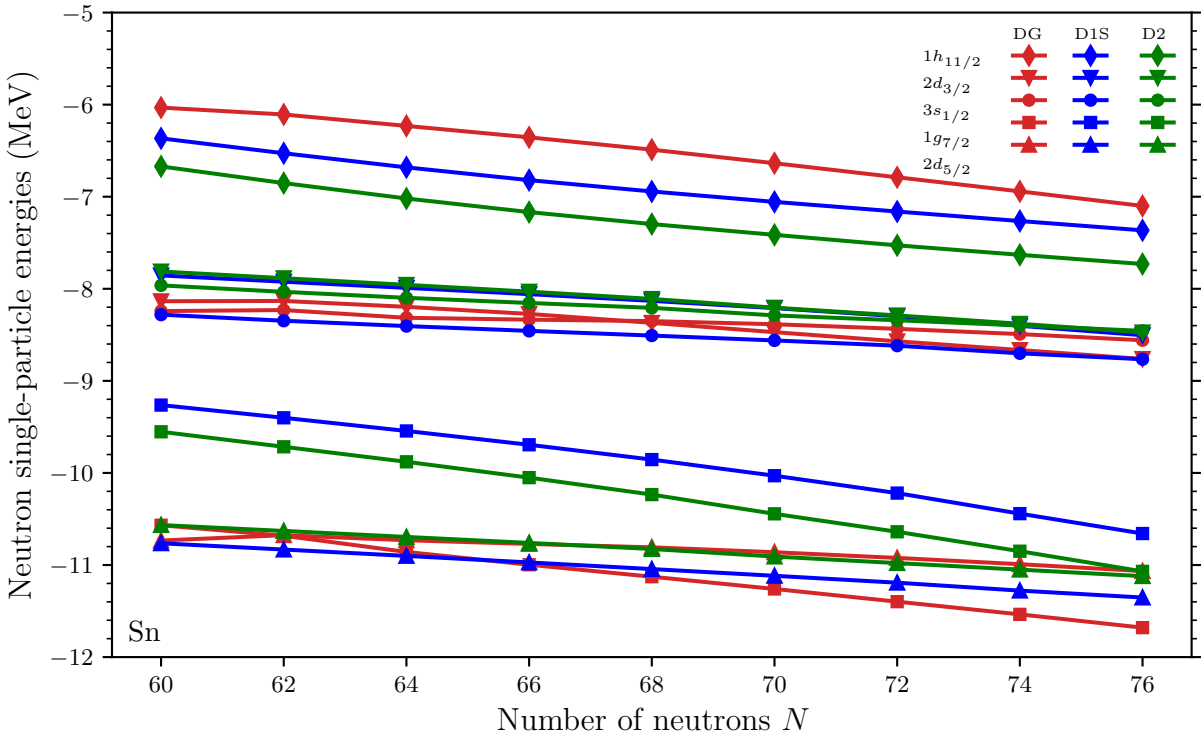

Figure III.13 – Neutron single-particle energies $1h_{11/2}, 2d_{3/2}, 3s_{1/2}, 1g_{7/2}$ and $2d_{5/2}$ as a function of the neutron number N in the Sn isotopic chain, evaluated for DG, D1S and D2 interactions.

^{110}Sn, the difference with D1S (D2) reaches about 1.9 MeV (1.8 MeV) and about 1.9 MeV (1.6 MeV) in ^{120}Sn. Moreover, for all three interactions, the gap is shrunk as the neutron number N grows. On the other hand, the neutron gap $(2d_{3/2} - 2d_{5/2})$ is also predicted smaller by DG than by D1S and D2 interactions, but to a lesser extent since it only differs by 300 keV and 150 keV in ^{110}Sn, and by 500 keV and 300 keV in ^{110}Sn, respectively. We notice in addition that only the gap of DG is significantly reduced when going to heavier isotopes. This corroborates the observations of Figure III.13. Since the gap $(1g_{9/2} - 1g_{7/2})$, rather small with DG (compared to that of D1S and D2), narrows, the $1g_{7/2}$ orbital is lowered while the $2d_{5/2}$ is raised by the same phenomenon in the other gap $(2d_{3/2} - 2d_{5/2})$. The two states end up crossing each other, implying the inversion spotted at $N = 62$. As for the second inversion at $N = 68$, it is also related to the gap $(2d_{3/2} - 2d_{5/2})$ being reduced, as the state $2d_{3/2}$ is lowered when N grows, while $3s_{1/2}$ is not shifted. Note that the second inversion is subtler than the first one as the energy differences between DG, and D1S and D2 gaps are smaller.

These gap reductions also shed light on why the pairing energy of interaction DG is diminished in the region $60 \leq N \leq 76$. From $N = 60$ to $N = 64$, the neutron gap $(3s_{1/2} - 1g_{7/2})$ is enlarged in a significant way with DG because of the decline of the orbital $1g_{7/2}$, thus limiting pairing correlations. This applies from $N = 68$ as well, since the orbital $2d_{3/2}$ continues to move downward right after the inversion with the state $3s_{1/2}$, producing a (small) enlargement of the $(3s_{1/2} - 2d_{3/2})$ gap.

We close this subsection by trying to identify the reasons for the two level inversions we have discriminated. First, we underline that the reductions of the gaps in Table III.4 are not particularly pronounced for specific isotopes, but are quite general, suggesting a

predominance of the spin–orbit force. The intensity of the spin–orbit in the DG interaction has been substantially lowered with respect to D1S and D2 interaction (from 130 MeVfm^5 to 115.849 MeVfm^5). This diminution should be accompanied with a diminution of the spin–orbit splitting, in particular between $2d_{3/2}$ and $2d_{5/2}$, as well as between $1g_{7/2}$ and $1g_{9/2}$ orbitals. This is in line with our observations. It must be emphasized that the splitting of spin-partner states $j_{\gtrless} \equiv l \pm 1/2$ increases with growing values of l, so that the splitting should be more shrunk between $1g_{7/2}$ and $1g_{9/2}$ than between $2d_{3/2}$ and $2d_{5/2}$ states. This is once again what we have noticed above. Obviously the central, density-dependent and tensor forces take part in the overall arrangement exposed so far, but the spin–orbit appears to be mainly responsible for the two inversions of neutron orbitals.

4.1.2. $N = 50$ isotonic chain

The proton twin of the previous analysis is the study of the pairing energy in the $N = 50$ isotonic chain. Indeed, the associated nuclei exhibit a magic number of neutrons and then allow to isolate the proton pairing correlations. The pairing energies of DG, D2 and D1S interactions, computed using the exact exchange Coulomb potential, are shown in Figure III.14. Note that contrary to the Sn isotopes, all isotones of the aforementioned chain are not predicted spherical by the three interactions. We accordingly extracted the pairing energies at the HFB minima.

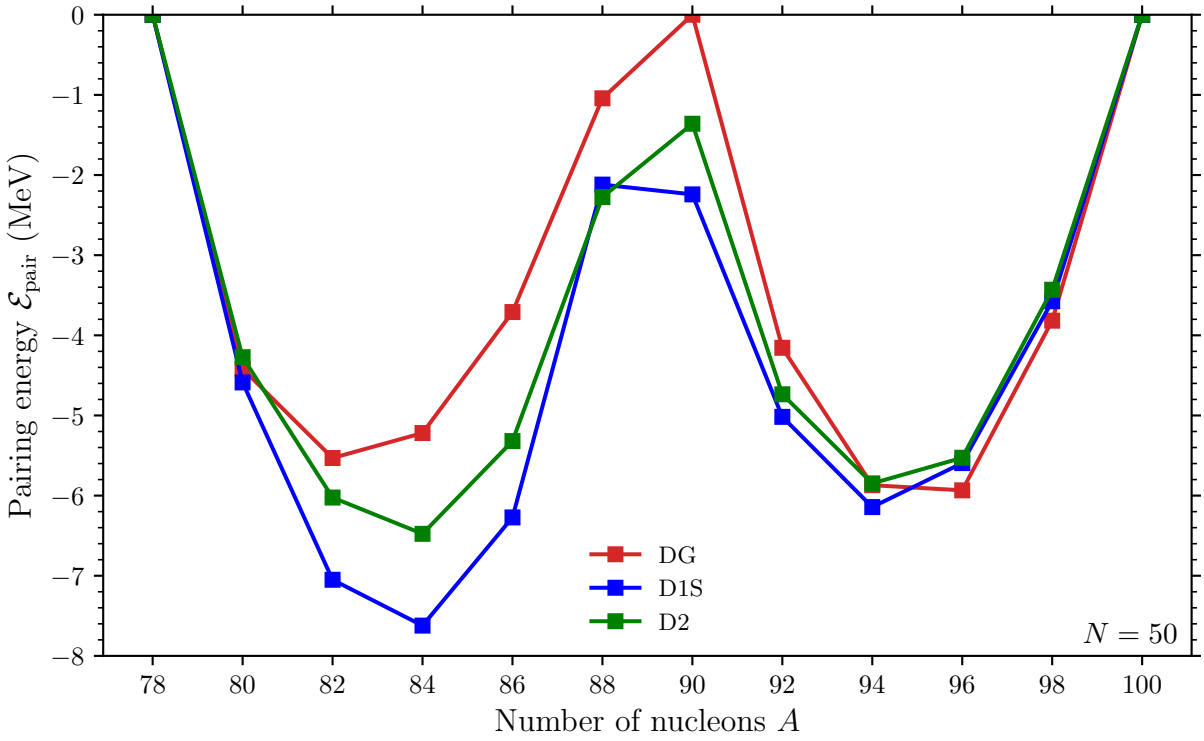

Figure III.14 – Pairing energy as a function of the nucleon number A in the $N = 50$ isotonic chain, evaluated for DG, D1S and D2 interactions, with and without the exact Coulomb potential.

We have first checked that this time the neutron contribution to the pairing energy is zero, so that only the proton pairing energy is involved in the following discussion. As a whole, the same trend is observed with all three interactions, with a DG pairing

energy smaller than those predicted by D1S and D2 interactions from isotones $A = 82$ to $A = 92$, reaching a maximum difference with D2 of about 1.6 MeV for isotone $A = 86$. Pairing energies vanish at magic numbers $Z = 28$ and $Z = 50$, as required, and a distinct diminution of the pairing energy appears at the $Z = 40$ subshell. While the pairing energy at this point is small with D1S and D2 interactions, of about -2.2 MeV and -1.4 MeV respectively, it completely cancels out with DG. We will now interpret this phenomenon in terms of SPE considerations at the HF approximation.

In Figure III.15, the proton SPEs around the Fermi level of $N = 50$ isotones in the region $36 \leq Z \leq 44$ are given for DG, D1S and D2 interactions (employing the exact Coulomb term). Unlike along Sn isotopic chain, no level inversions are observed, but the proton gap $(1g_{9/2} - 2p_{1/2})$, corresponding to the gap of the Fermi level in isotone $Z = 40$, is enlarged in a significant way. To be more quantitative, we furnish the values of some proton energy gaps in Table III.5.

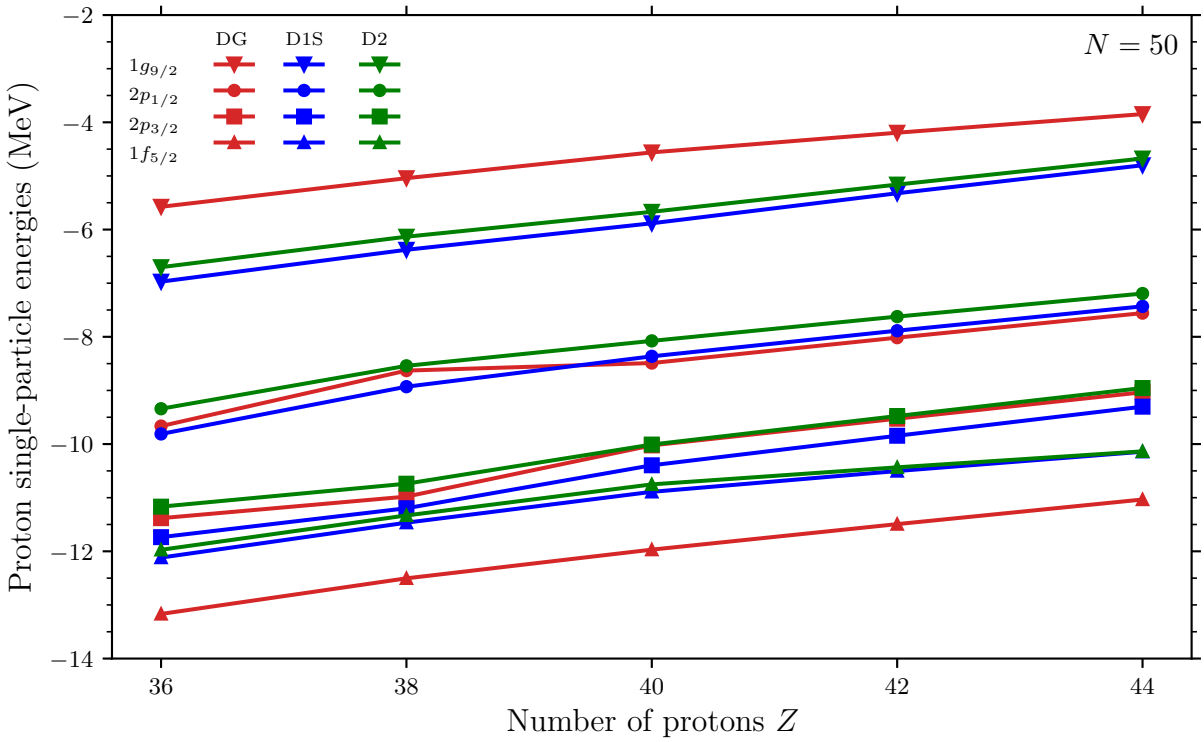

Figure III.15 – Proton single-particle energies $1g_{9/2}, 2p_{1/2}, 2p_{3/2}$ and $1f_{5/2}$ as a function of the number of protons Z in the $N = 50$ isotonic chain, evaluated for DG, D1S and D2 interactions.

In isotone ^{88}Sr, the gap is slightly wider with DG than those of D1S and D2 interactions, resulting in a little smaller proton pairing energy. The level $2p_{1/2}$ is fully filled at $Z = 40$ so that the gap becomes $(1g_{9/2} - 2p_{1/2})$ and is about 2.4 MeV (2.5 MeV) larger with DG than with D1S (D2) interactions; it is almost doubled. This enlargement of the $Z = 40$ gap is at the origin of the zero pairing energy of ^{90}Zr. Finally, in ^{92}Mo, pairing correlations mainly comes from the $1g_{9/2}$ orbital.

The enlargement of the proton gap $(1g_{9/2} - 2p_{1/2})$ observed in ^{90}Zr with DG is also the consequence on a competition between spin–orbit and tensor forces. The reduction of the spin–orbit strength brings spin-partner states $(1g_{7/2})_\pi$ and $(1g_{9/2})_\pi$ as well as $(2p_{1/2})_\pi$ and $(2p_{3/2})_\pi$ closer. On the other side, because the level $(1g_{9/2})_\nu$ is completely filled, a strong

	Proton energy gap		
	DG	D1S	D2
Isotone	(MeV)	(MeV)	(MeV)
^{88}Sr	$(2p_{1/2} - 2p_{3/2})$ 2.350	$(2p_{1/2} - 2p_{3/2})$ 2.267	$(2p_{1/2} - 2p_{3/2})$ 2.198
^{90}Zr	$(1g_{9/2} - 2p_{1/2})$ 3.928	$(1g_{9/2} - 2p_{1/2})$ 2.481	$(1g_{9/2} - 2p_{1/2})$ 2.407
^{92}Mo	$(2d_{5/2} - 1g_{9/2})$ 6.354	$(2d_{5/2} - 1g_{9/2})$ 7.235	$(2d_{5/2} - 1g_{9/2})$ 7.300

Table III.5 – Proton energy gaps of some $N = 50$ isotones predicted by DG, D1S and D2 interactions at the HF approximation.

tensor repulsion with $(1g_{9/2})_\pi$ comes into play and raises the energy of that level. All in all, the spin–orbit and tensor terms contribute to the opening of the proton gap $(1g_{9/2} - 2p_{1/2})$ in ^{90}Zr, killing the small pairing energy displayed by D1S and D2 interactions. Recently, Miyahara and Nakada pointed out, using the M3Y parametrization P6, that the tensor force favored the spherical shape of nucleus ^{90}Zr [201]. This is precisely what we have just shown as the tensor force accentuates the magicity of this nucleus.

4.2. Single-particle energies

We now would like to provide a global picture on the way the splittings and gaps at the Fermi levels transform when going from D1S and D2 to DG interaction, at the HF approximation. For that purpose, we consider several spherical nuclei along the O, Ca, Ni, Zr, Sn and Pb isotopic chains, as carried out for D1ST and D1MT parametrizations in [29]. We will not comment all cases, but simply highlight relevant examples in particular to give evidence of spin–orbit and tensor actions on the shell evolution.

4.2.1. Energy splittings

Proton splittings

We begin with the proton splittings $1p, 1d$ and $1f$, shown for DG, D1S and D2 interactions in Figure III.16.

We first notice that D1S and D2 predictions are rather comparable for all tested nuclei. This informs that the differences in the central and density-dependent parts between D1S and D2 do not have strong implications on the proton splittings (the intensity of their spin–orbit terms being the same). On the opposite, DG sometimes appreciably deviates from them, suggesting, as expected, that the spin–orbit and tensor forces are tied to shell evolution. In O and Ca isotopes for instance, DG systematically reduces the $1p, 1d$ and $1f$ splittings. In O isotopes, no action shows up on the proton $1p$ SPEs as they are spin-saturated in protons. Since the spin–orbit intensity has been lessened (in the $T = 1$ channel) with DG, the $1p$ splitting is lowered via the spin–orbit force only. This explanation holds for the $1p$ and $1d$ splittings of the proton spin-saturated Ca nuclei. When not spin-saturated in neutrons, the tensor force combines with its spin–orbit counterpart to modify $1d$ and $1f$ splittings in O isotopes, as well as $1f$ splittings

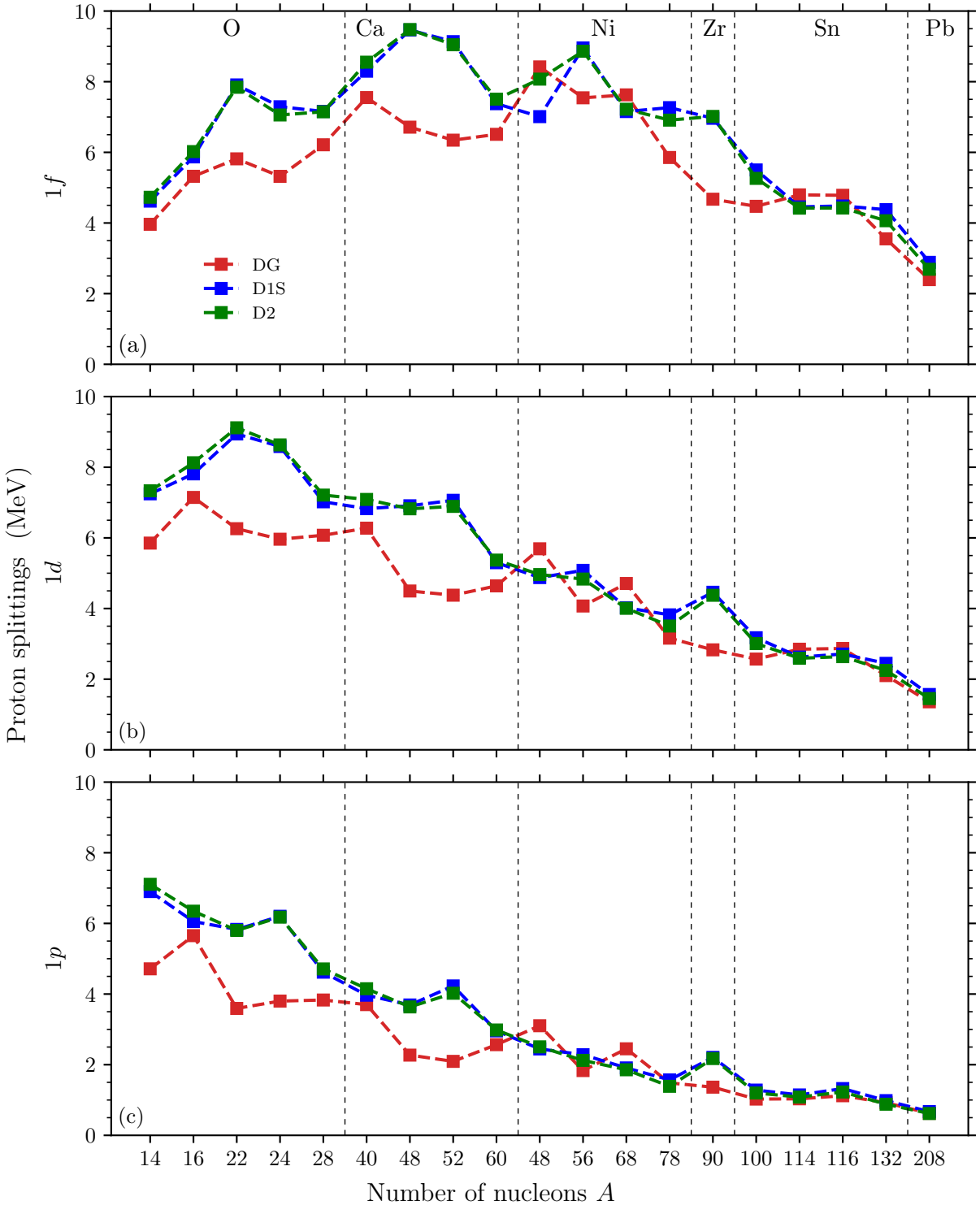

Figure III.16 – Proton splittings displayed for certain nuclei of the O, Ca, Ni, Zr, Sn and Pb isotopic chains, as a function of the neutron number N. The $1f$ ($1f_{7/2}-1f_{5/2}$), $1d$ ($1d_{5/2}-1d_{3/2}$) and $1p$ ($1p_{3/2}-1p_{1/2}$) splittings are represented in panels (a), (b) and (c), respectively.

in Ca isotopes. For example, in ^{22}O, the tensor force *amplifies* the reduction of the $1d$ splitting through its proton–neutron component. The $(1d_{5/2})_\nu$ state, which is completely filled, attracts $(1d_{3/2})_\pi$ and repels $(1d_{5/2})_\pi$ states, which are empty. The addition of the

spin–orbit and tensor contributions explains the particularly broad $1d$ splitting in this nucleus.

In Ni isotopes, an oscillating behavior of the splittings is described by DG, around the D1S and D2 values. This phenomenon is difficult to understand from the point of view of pure spin–orbit and tensor effects, especially for the $1p$ and $1d$ splittings. Indeed, the corresponding states are entirely filled so that the tensor force is zero and only the spin–orbit should contribute to bring those states closer. However, in ^{48}Ni and ^{68}Ni isotopes, the $1p$ and $1d$ splittings are widened by DG, with respect to those of D1S and D2 interactions. The same phenomenon appears in fact for $1f$ splittings. In ^{48}Ni for example, the small proton–proton tensor attraction between orbitals $1f_{7/2}$ and $1f_{5/2}$ is expected to slightly lowers the state $1f_{5/2}$, then contributing to enhance the reduction of the $1f$ splitting, mainly due to the spin–orbit action. This is not what we observe in panel (a). Let us note that these gap expansions have always reasonable amplitudes compared to the splitting reductions in certain O or Ca isotopes. They do not exceed 1 MeV, and could then be related to the central and density-dependent part, that of DG being a bit different from those of D1S and D2 interactions.

From ^{90}Zr, all spin-partner states involved in the $1p, 1d$ and $1f$ splittings are fully occupied, so that only the DG spin–orbit force is supposed to reduce them with respect to D1S and D2 interactions. This is what we see, except in ^{114}Sn and ^{116}Sn, whose small splitting enlargements might also be attributed to the central and density-dependent part. In the other isotopes, it is worth noticing that the splitting reductions are stronger for $1f$ than for $1d$ states, and even more than for $1p$ states, in agreement with the proportionality of the spin–orbit splitting with l.

Neutron splittings

The same study can obviously be performed for neutron splittings. In Figure III.17, the neutron splittings $1p, 1d$ and $1f$ predicted by DG, D1S and D2 interactions are displayed.

Once again, it appears that D1S and D2 predictions are quite similar in the nuclei under study, while DG shows important discrepancies. However, the overall tendency is different from that observed with proton splittings, as the number of protons and neutrons is different (except in ^{40}Ca, ^{56}Ni and ^{100}Sn). With the DG interaction, the results in O and Ca isotopes are closer to those of D1S and D2, Ni and Sn splittings are always reduced while that of ^{90}Zr is broadened. We remind the reader that the DG interaction was fitted to reproduce the neutron $1f$ splittings of isotopes ^{40}Ca, ^{48}Ca and ^{56}Ni better than D1S and D2. In addition, the neutron $1p$ splitting of ^{16}O had to remain appropriate. These constraints unavoidably affect the neutron SPEs of medium-mass nuclei evaluated with the DG interaction.

Once again, the changes observed when going from D1S and D2 to DG cannot be fully explained by the interplay between spin–orbit and tensor forces. Indeed, the neutron splittings should always be reduced with DG for the nuclei selected, but it is not the case. Whereas the evolution of the proton splitting of ^{22}O with DG was correctly understood invoking the relative spin–orbit and tensor contributions, this is no longer true in the neutron sector. The reduction of the neutron splitting $(1d_{5/2} - 1d_{3/2})$ implied by the spin–orbit force should combine with the lowering of the $1d_{3/2}$ level due to its tensor attraction with $1d_{3/2}$, ending up in a narrower neutron $1d$ splitting in this proton spin-saturated nucleus. The opposite effect is actually observed in Figure III.17. This hints again that the central and density-dependent part of DG cannot be discarded from such interpretation. Reciprocally, the evolution of the proton $1f$ splitting of ^{48}Ni, that was not

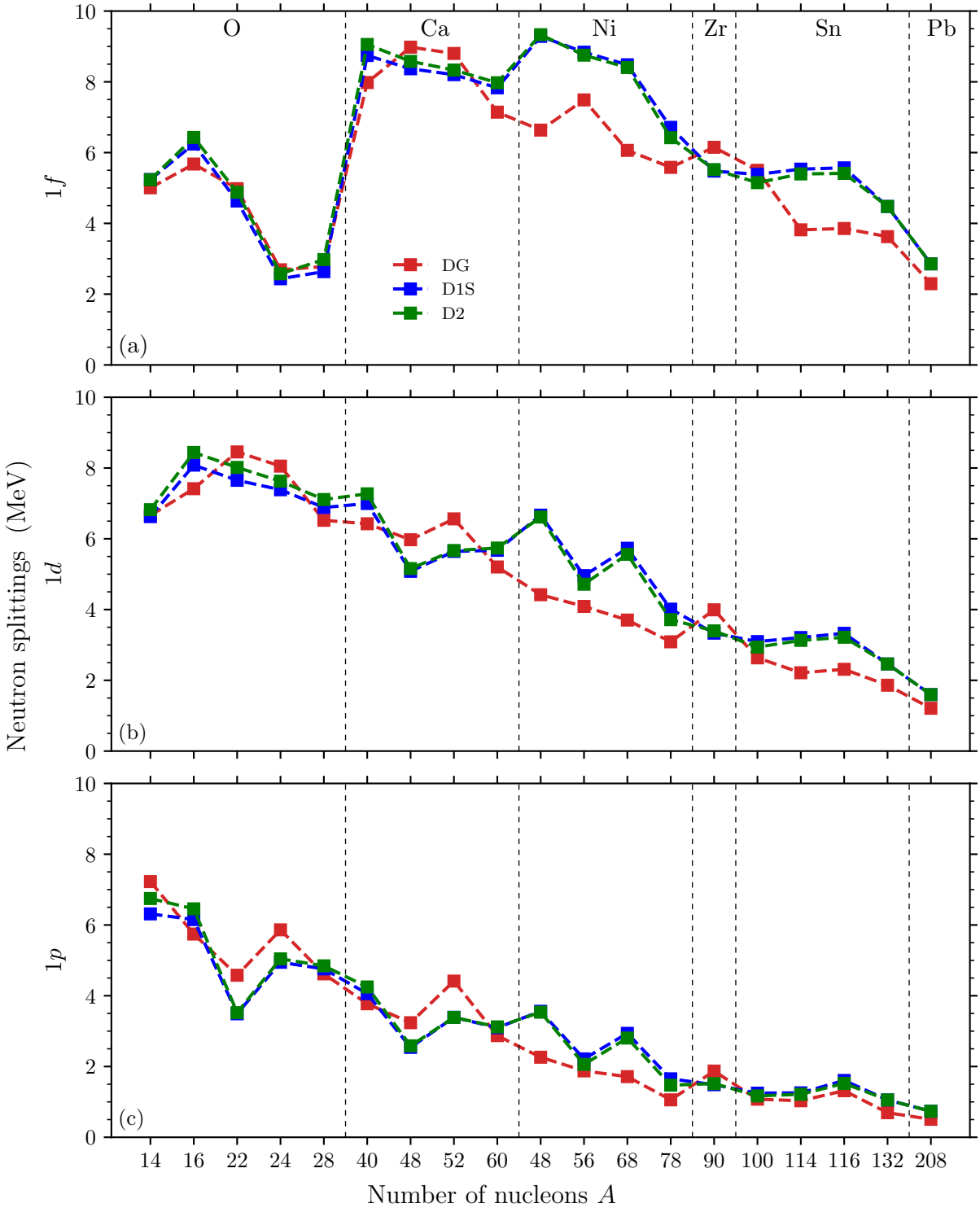

Figure III.17 – Same as in III.16, but now for neutron single-particle energies.

faithfully described by spin–orbit and tensor effects, here is. As usual the $1f$ splitting is shrunk by the spin–orbit force with DG while the state $(1f_{7/2})_\pi$, which is completely filled, lowers $(1f_{5/2})_\nu$ and raises $(1f_{7/2})_\nu$, which are empty. The powerful action of the tensor force combined with that of the spin–orbit term are responsible for the considerable reduction of the neutron $1f$ splitting caused by DG in that isotope.

In heavier isotopes, as in the proton sector, all spin-partner states involved in the

$1p, 1d$ and $1f$ splittings are saturated, so that the tensor force vanishes. We then expect these splittings to be all reduced by the spin–orbit component of DG, with respect to D1S and D2. This is the case, excluding the isotope ^{90}Zr. Central and density-dependent terms may then have a determining role to play in the positioning of the neutron SPEs of this nucleus.

4.2.2. Energy gaps

Finally, the proton and neutron energy gaps of the Fermi levels for the isotopes studied so far are displayed for DG, D1S and D2 interactions, and compared to available experimental data in Figure III.18.

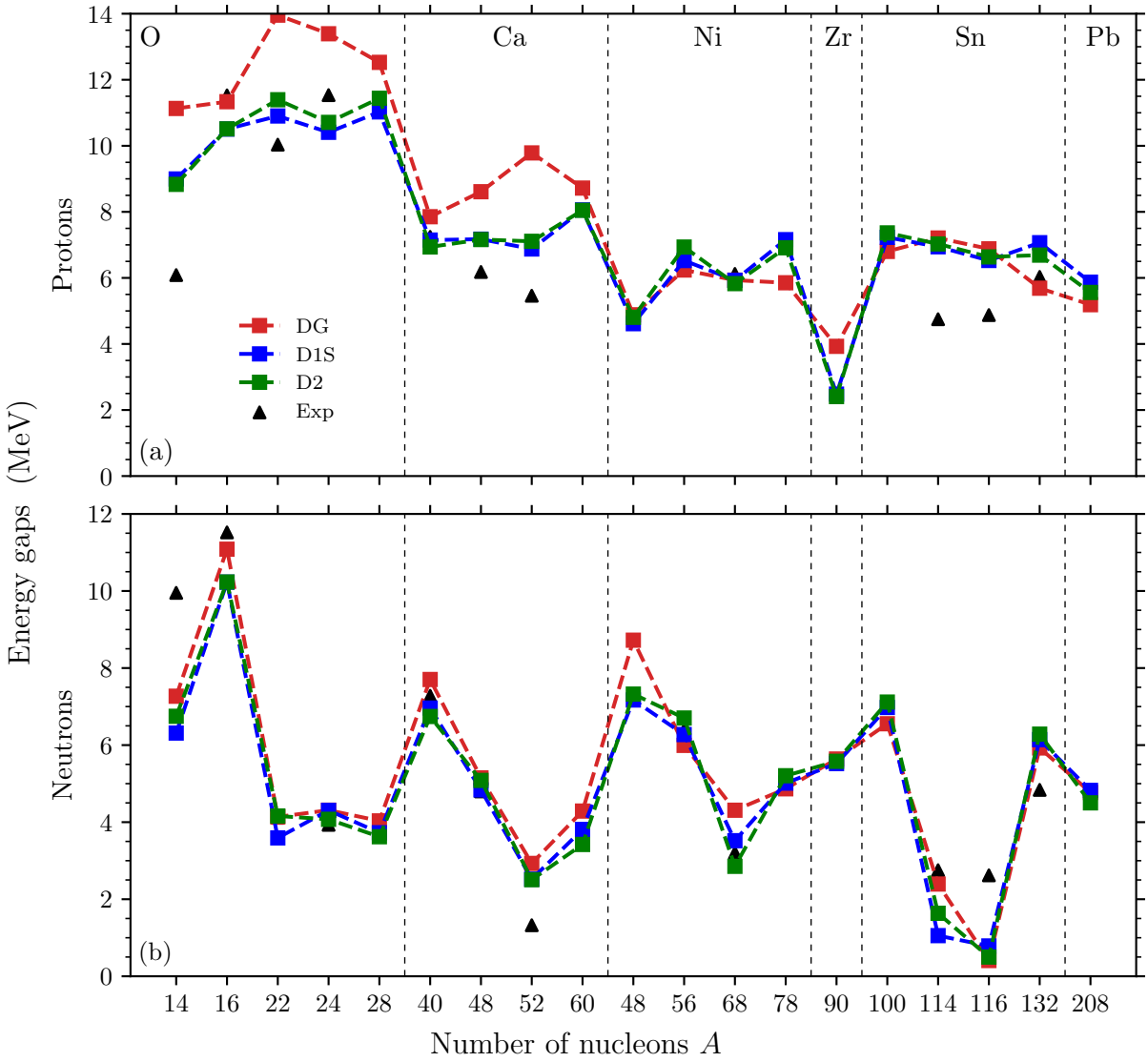

Figure III.18 – Proton (panel (a)) and neutron (panel (b)) energy gaps of the Fermi levels shown for certain nuclei of the O, Ca, Ni, Zr, Sn and Pb isotopic chains, as a function of the nucleon number A. When available, experimental data are represented by black triangles [202, 203]. Note that energy gaps of ^{28}O, ^{48}Ni, ^{60}Ca, ^{78}Ni and ^{100}Sn have not been measured but estimated from the binding energies of the neighboring nuclei.

Contrary to the splittings, we first see here that the proton and neutron gaps are often

enlarged when going from D1S and D2 to DG interactions. The effect is more visible for the proton gaps of O and Ca isotopes. Moreover, the neutron gaps of ^{14}O, ^{16}O, ^{48}Ca, ^{114}Sn and ^{132}Sn better fit experimental values with DG than with the other interactions, while only the proton gaps of ^{16}O and ^{132}Sn do so with DG. This observation confirms that the constraints on the neutron splittings imposed in the fitting process drive the neutron gaps as well.

In ^{132}Sn, the gap $(1g_{7/2} - 1g_{9/2})_\pi$ is reduced with DG because of the spin–orbit force, while the state $(1h_{11/2})_\nu$, which attracts $(1g_{7/2})_\pi$ and repels $(1g_{9/2})_\pi$ by means of the tensor force, favors this reduction. Thus, in this nucleus, the joint actions of the spin–orbit and tensor forces contribute to improve the description of the proton gap.

In the neutron sector, the better agreement with the experimental data for ^{16}O, ^{40}Ca and ^{48}Ca isotopes has believably to do with their respective constraints on the neutron $1p$ and $1f$ splittings. In ^{14}O, the gap $(1p_{3/2} - 1p_{1/2})_\nu$ should be diminished by DG as the spin–orbit force brings the corresponding states closer while the state $(1p_{3/2})_\nu$ attracts $(1p_{1/2})_\nu$ through the tensor term. However, this gap is widened by DG, with respect to those of D1S and D2 interactions according to the figure. This suggests once again that we cannot predict the movements of the SPEs of DG by only calling upon the spin–orbit and tensor forces. For ^{114}Sn, though, we have already pointed out in subsection III.4.1.1 that the spin–orbit force was mainly responsible for an inversion of states, at the origin of the increase of the DG neutron gap $(3s_{1/2} - 2d_{5/2})$. Finally, a combination of spin–orbit and tensor forces seem to account for the reduction of the neutron gap in ^{132}Sn isotope.

It appears from our analysis on the splittings and gaps at the Fermi levels in both proton and neutron sectors, that the spin–orbit and tensor forces definitely have a strong role to play in the arrangement of SPEs with the DG interaction. Nevertheless, its central and density-dependent part is also important and sometimes dominates the spin–orbit and tensor contributions in the shell evolution. Actually the SPEs evaluated at the HF approximation are not quantities directly measurable from experiments, and consequently limits the interpretation. In the next chapter, we will connect such results with the first excitation energies of spin–parity J^π in various nuclei beyond the mean field. This will allow to shed light on the reliability on the DG predictions regarding the evolution of SPEs.

5. Deformations

So far we have studied the characteristics of the interaction DG at the HFB energy minimum only. In this section, we look at how the HFB energy evolves with the deformation, latter called the HFB deformation energy. For that purpose, the axial potential energy surfaces (PES) along Mg, Si, S, Ca and Sn isotopic chains obtained with DG, D1S and D2 interactions are studied with respect to the quadrupole moment Q_{20}. All the other moments appearing in the multipole expansion of the radius are set to zero, in such a way that we are dealing with pure axially symmetric deformations. In fact, for ease of comparisons, we will rather consider the dimensionless quadrupole deformation parameter β_2, related in our conventions with the quadrupole moment by the identity

$$\beta_2 \equiv \frac{4\pi}{3AR^2} Q_{20}, \tag{III.68}$$

where the radius of the nucleus is defined through the empirical formula $R = R_0 A^{1/3}$, with the nucleon number A and $R_0 = 1.2\,\text{fm}$.

5.1. Magnesium potential energy surfaces

We begin with the PES along the Mg isotopic chain, given for the three interactions in Figure III.19.

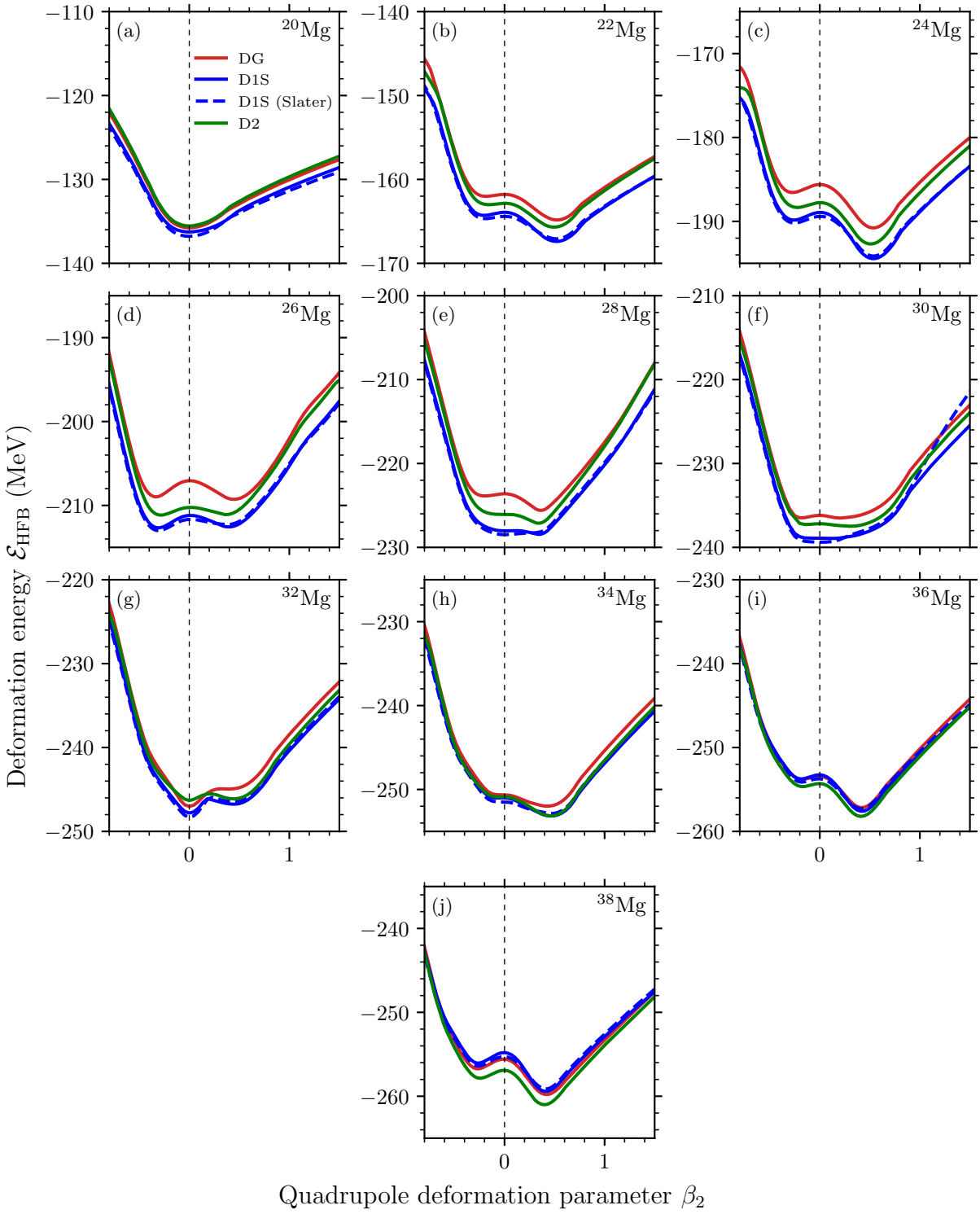

Figure III.19 – Potential energy surfaces of the Mg isotopes as a function of the quadrupole deformation parameter β_2, obtained for DG, D1S (with and without using Slater approximation) and D2 interactions.

First of all, it appears clearly that the results obtained using the exact exchange Coulomb potential (blue full lines) and the Slater approximation (blue dashed lines) with the D1S interaction are not very different. They are shifted by at most of few hundred of keV. Another interesting feature, we have already spotted at HFB minima, is that the interaction DG often provides a bit less binding energy, with respect to D1S and D2 predictions. This is particularly visible from isotopes ^{22}Mg to ^{30}Mg and in ^{34}Mg, and reaches a maximum decrement of 3.2 MeV with respect to D2 in ^{26}Mg at the spherical point ($\beta_2 = 0$). In ^{32}Mg, however, the interaction DG favors sphericity with a more pronounced well than that of D2. By considering quadrupole deformations with axial symmetry assumed using the parametrization P6 of interaction M3Y, Suzuki *et al.* found that the tensor force favored sphericity in magic $N = 20$ nuclei [204]. Observation of this effect with the generalized Gogny interaction seem to indicate that our tensor force acts in the same way as in this M3Y interaction. In ^{22}Mg, we see that two wells, one oblate ($\beta_2 < 0$) and one prolate ($\beta_2 > 0$), start to form and anticipate a competition between the corresponding local minima to become global and fix the shape of the nucleus in the heavier isotopes (expect for ^{30}Mg which displays a rather flat PES around sphericity). Most of the time, all three interactions coincide in predicting oblate or prolate shape for Mg isotopes. Nonetheless, this is not the case of ^{26}Mg, which apparently displays a *shape coexistence*, since two energy wells with relatively equal depths show up. We accordingly study this nucleus in more details in the following.

In Figure III.20, the PES of ^{26}Mg is shown. It appears clearer on this graph that the nucleus is predicted prolate by DG and oblate by D1S and D2 interactions in the ground state (at the HFB level, at least). Quantitatively, the values of the HFB deformation energies $\mathcal{E}_{\text{HFB}}$ at the oblate and prolate local minima β_2 are displayed for DG, D1S and D2 interactions in Table III.6. We see that the oblate and prolate minima of D1S and D2 are separated by 60 keV and 110 keV, respectively. This means that the ground states of ^{26}Mg described by those interactions are not stable as a small amount of energy can tip the system into the other minimum and drastically change its shape. The prolate shape associated with DG is a bit more stable as it is separated by 290 keV from the oblate minimum, but it is still showing a shape coexistence. Note also that these minima are predicted more deformed with DG than with D1S and D2 interactions as the values of $|\beta_2|$ are greater. Interestingly, the tensor force is supposed to have a significant action on the SPEs already at the spherical point in this nucleus. Besides, a study similar to this one carried out with *perturbative* D1ST2a interaction provided comparable results in ^{26}Mg [38]. Because the spin–orbit intensity of D1ST2a is that of D1S, this effect was thought to be due to the tensor force. We here draw the same conclusion, the tensor force is mainly held responsible for these effects.

	Oblate minimum		Prolate minimum	
Interaction	β_2	$\mathcal{E}_{\text{HFB}}$ (MeV)	β_2	$\mathcal{E}_{\text{HFB}}$ (MeV)
DG	−0.331	−208.982	0.433	−209.270
D1S	−0.280	−212.669	0.382	−212.560
D2	−0.306	−211.159	0.357	−211.094

Table III.6 – Deformation energies and quadrupole deformation parameters at the oblate and prolate local minima of ^{26}Mg, predicted by DG, D1S and D2 interactions.

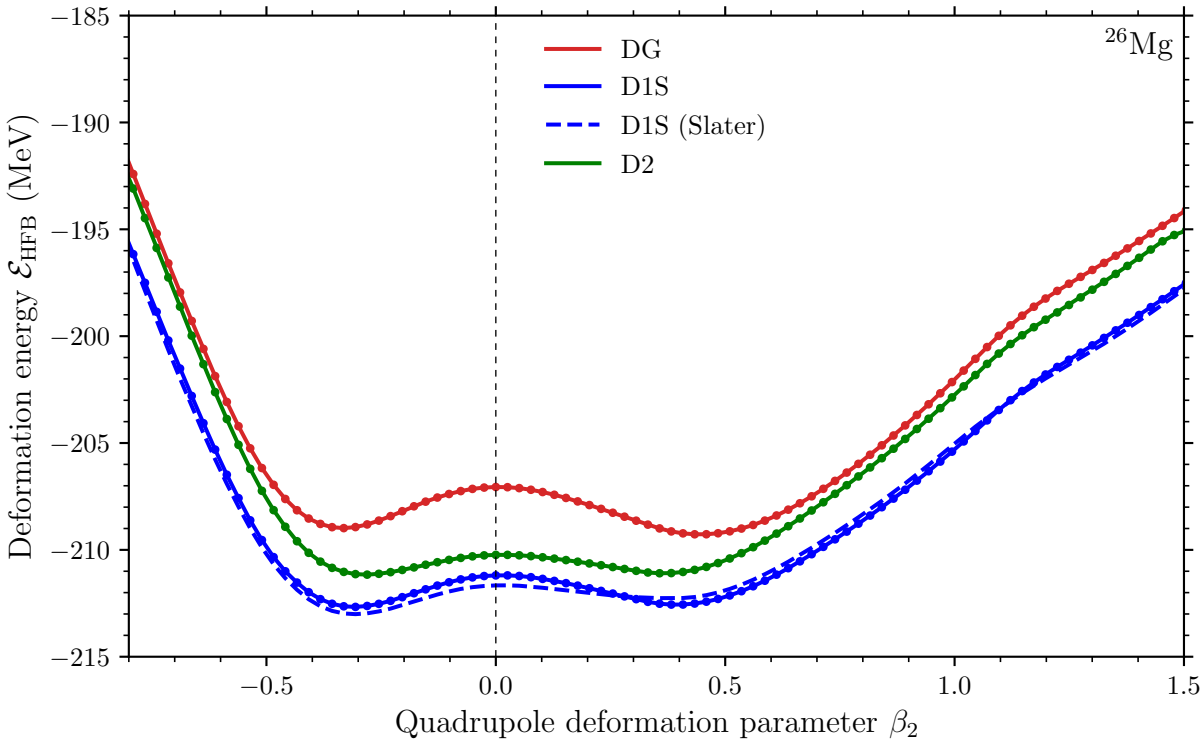

Figure III.20 – Potential energy curve of ^{26}Mg as a function of the quadrupole deformation parameter β_2, obtained for DG, D1S (with and without using Slater approximation) and D2 interactions. The points indicate outputs of HFB calculations.

Finally, we compare the shapes showing up at the HFB minima in Mg isotopes with DG, D1S and D2 interactions with those predicted by the finite-range droplet model (FRDM) and experimental data [202], when available, in Figure III.21.

In panel (a), we check that the nature of the quadrupole deformations (oblate, prolate or spherical shape) among Gogny interactions are, as mentioned above, always the same, except in ^{26}Mg. When we compare these predictions with those of the FRDM, it turns out that they often match. Only in ^{30}Mg, ^{32}Mg and ^{32}Mg they are different from all three interactions. Remarkably, the prolate shape of ^{26}Mg specific to the DG interaction is in line with the FRDM results. On the contrary, the spherical shape of ^{32}Mg accentuated by the interaction DG (in the sense that the nucleus is predicted more rigid) is found prolate by the FRDM. Obviously, this comparison must be considered with caution since the FRDM is, as its name says, a model.

As only the magnitudes of the quadrupole deformations can be related to experimental data, we compare these quantities with the predictions of Gogny interactions in panel (b). Globally, we see that the interaction DG is closer to experiment for ^{22}Mg, ^{26}Mg and ^{28}Mg isotopes. It is worth emphasizing that the prediction is notably amended with DG for ^{26}Mg, corresponding to a nucleus in which the tensor force acts in a predominant manner, changing its shape and increasing the value of β_2, as we have discussed above. We finally notice that the deformations predicted by all three Gogny interactions underestimate the experimental values. Actually, with the HFB approach we have only taken into account static correlations. Going beyond the mean field to incorporate dynamic correlations (vibrations, collective rotations, etc.) should bring up more deformation to the Mg isotopes.

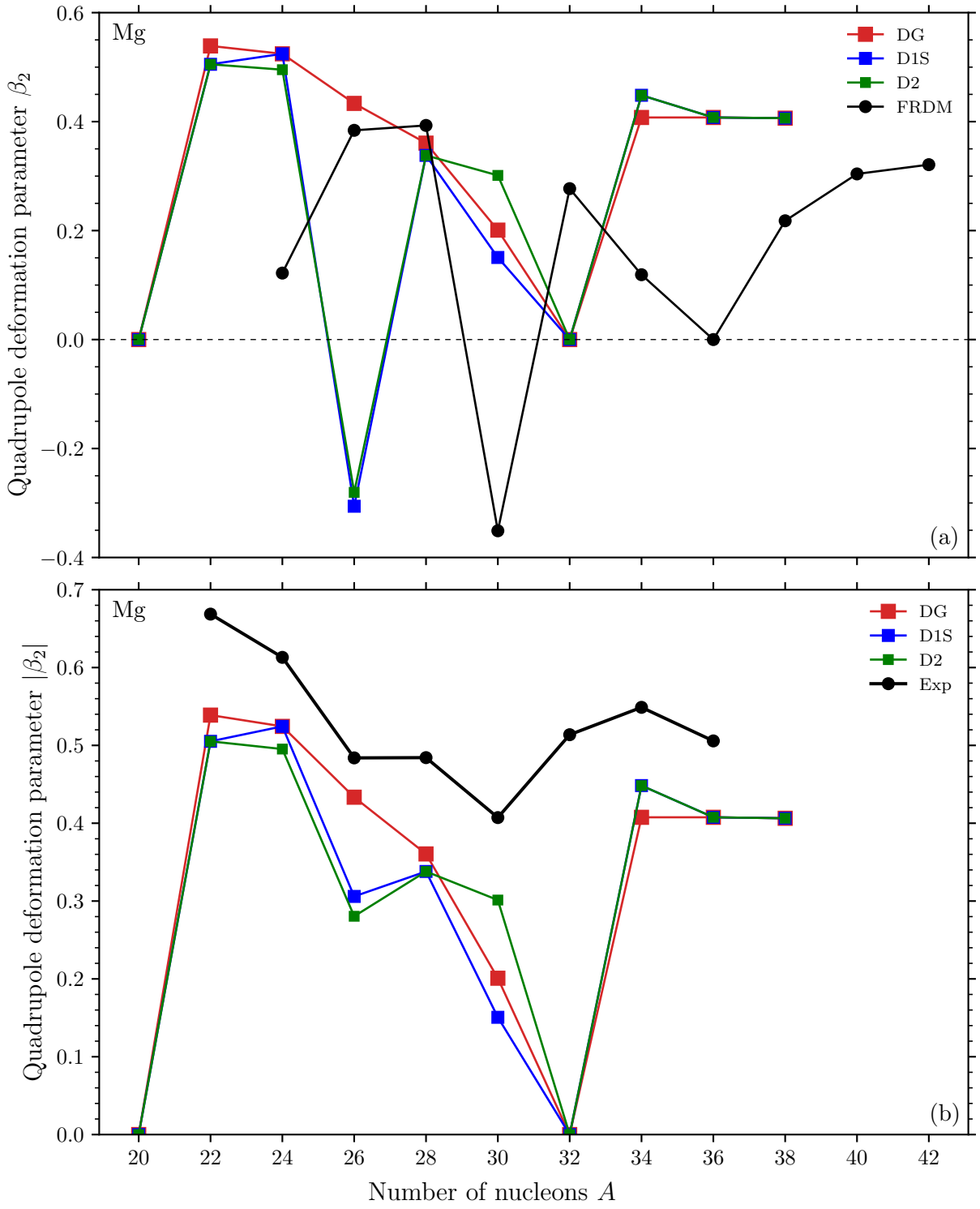

Figure III.21 – The values of the quadrupole deformation parameters β_2 in the ground state for Mg isotopes with DG, D1S and D2 interactions are compared with the predictions of the finite-range droplet model [89] in panel (a). A similar comparison of $|\beta_2|$ with experimental data [202] is carried in panel (b).

5.2. Silicon and Sulfur potential energy surfaces

We continue with the PES along the Si and S isotopic chains, given for the three interactions in Figures III.22 and III.23, respectively. They are studied together as they

present quite alike behaviors on many aspects.

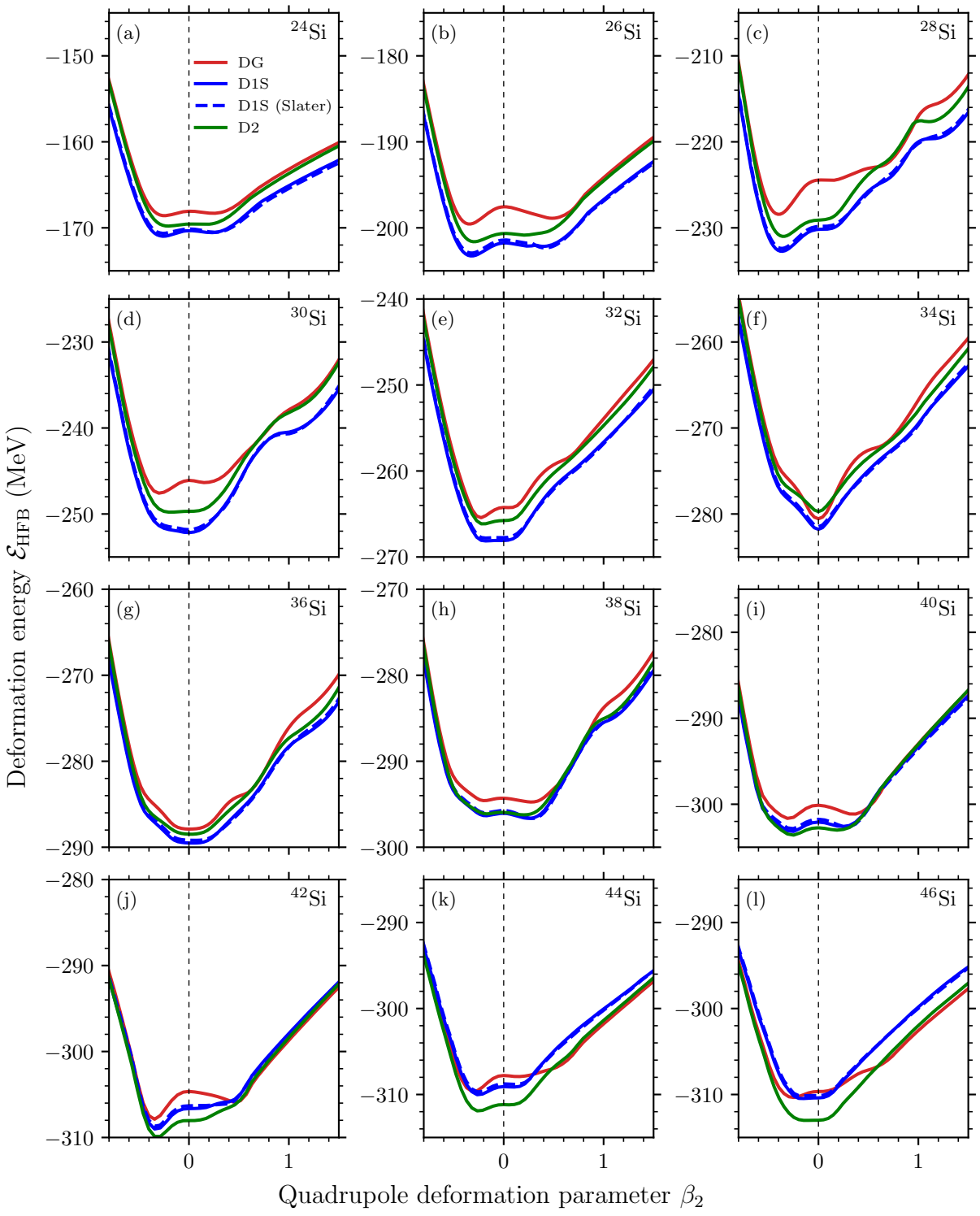

Figure III.22 – Same as in Figure III.19, but now for the Si isotopic chain.

The general remarks made for Mg isotopes remain true. Taking into account the exact Coulomb potential rather that evaluated at the Slater approximation does not change the results in a meaningful way, and the isotopes described by DG are essentially less bound than with D1S and D2 interactions. In ^{34}Si and ^{36}S, though, the spherical shapes are favored with DG, compared to D2, as the wells around $\beta_2 = 0$ are deeper and

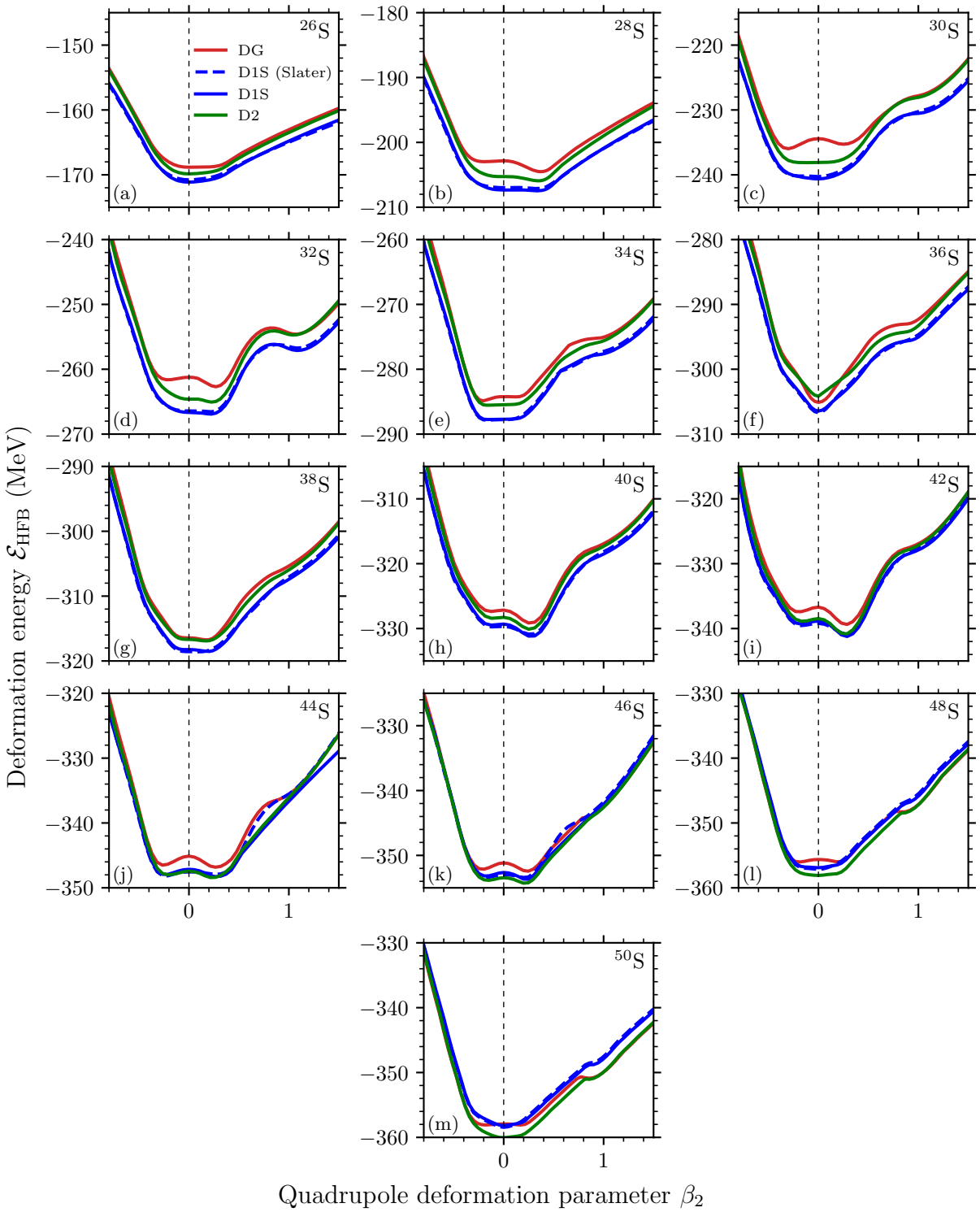

Figure III.23 – Same as in Figure III.19, but now for the S isotopic chain.

less wide in these isotopes. Once again, this corroborates the results obtained by Suzuki *et al.* [204]. On the opposite, the authors show that the tensor favors deformations in magic $N = 28$ nuclei. This is effectively what we get since the energy difference between the prolate minimum and the spherical point reaches 3.2 MeV with DG, against 2.4 MeV and 1.8 MeV, respectively, with D1S and D2 interactions in ^{42}Si. There is also a prolate well taking shape with interaction DG, indicating that deformed configurations are

preferred. The same situation occurs in ^{44}S since the prolate minimum is 1.7 MeV away from the spherical point for interaction DG, versus 1.1 MeV and 1.0 MeV for interactions D1S and D2, respectively. While the nature of the minima is broadly the same for all three interactions (with small energy or deformation shifts), we can see that the interaction DG differs from the other two in isotopes ^{30}Si, ^{30}S, ^{34}S, ^{48}S and ^{50}S. Since the effect is more remarkable in ^{30}S than in ^{34}S, ^{48}S and ^{50}S, we look at ^{30}S in more details from now on (^{30}Si and ^{30}S being mirror nuclei).

In Figure III.24, the PES of ^{30}S is represented. We see on this graph that two distinct wells, one oblate and one prolate, show up with DG, whereas interactions D1S and D2 seem to remain spherical in the ground state. To be more quantitative, the values of the HFB deformation energies $\mathcal{E}_{\text{HFB}}$ at the global minimum and at the spherical point are listed for DG, D1S and D2 interactions in Table III.7. We observe that the nucleus is indeed predicted spherical for D1S, but that it is actually prolate with D2. This was difficult to discriminate as the prolate minimum of D2 is only 30 keV lower than the spherical point. On the contrary, 450 keV separates the oblate from the spherical shape with DG, and even less from the prolate solution, so that ^{30}S is predicted deformed by this interaction. Moreover, the oblate minimum is twice as deformed with DG as with D2 interaction. Qualitative agreement with D1ST2a interaction is found in this nucleus as well [38], so that the tensor force favors deformations here again. Note by the way that the tensor effects in this nucleus, and the neighboring isotopes, already manifesting in the SPEs at the spherical point, will be investigated in the next chapter.

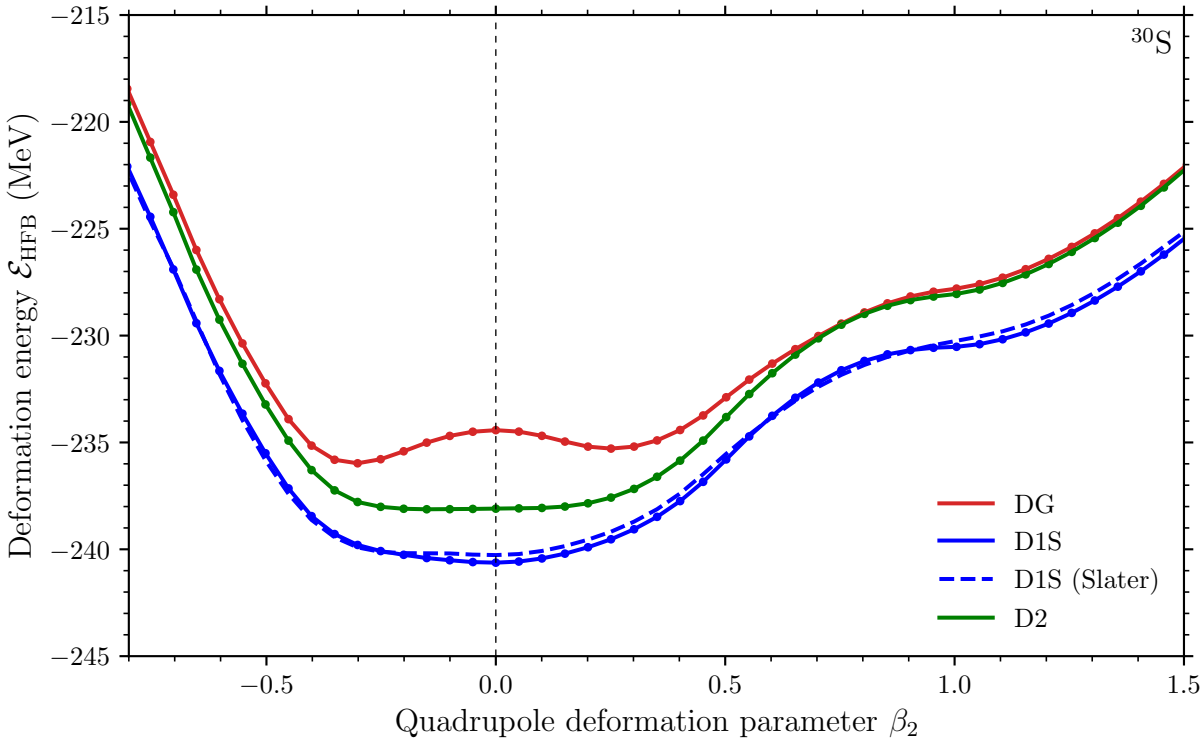

Figure III.24 – Same as in Figure III.20, but now the isotope ^{30}S.

Finally, we compare the shapes appearing at the HFB minima in Si and S isotopes with DG, D1S and D2 interactions with those predicted by the FRDM and experimental data [202], when available, in Figures III.25 and III.26, respectively.

In panels (a), we see that the predictions of Gogny interactions are often in agreement

	Global minimum		Spherical point	
Interaction	β_2	$\mathcal{E}_{\text{HFB}}$ (MeV)	β_2	$\mathcal{E}_{\text{HFB}}$ (MeV)
DG	−0.301	−235.975	0	−234.424
D1S	0	−240.625	0	−240.625
D2	−0.151	−238.127	0	−238.098

Table III.7 – Deformation energies and quadrupole deformation parameters at the global minimum and spherical point of ^{30}S, predicted by DG, D1S and D2 interactions.

with those of the FRDM. In ^{40}Si, ^{26}S, ^{44}S, ^{46}S and ^{50}S, however, the deformation natures are different from those predicted by the three interactions. On the other hand, the oblate shapes of ^{30}Si and ^{30}S, predicted by DG and D2 interactions, are in line with the FRDM results. Likewise, ^{48}S exhibits an oblate shape with DG, in accordance with FRDM predictions, while it remains spherical according to D1S and D2 interactions. Besides, the spherical shapes of ^{34}Si and ^{36}S stressed by the interaction DG are also shared by the FRDM.

In panels (b), it appears that the predictions of interaction DG are closer to the experimental values for ^{28}Si, ^{30}Si, ^{32}Si, ^{30}S, ^{32}S and ^{34}S isotopes (compared to those of D1S only for ^{32}Si). It is worth underlining that the results are in particular improved with DG for the mirror nuclei ^{30}Si and ^{30}S, corresponding to the isotopes in which the tensor force is prominent. Indeed we have shown above that ^{30}S was strongly distorted through its action (the same result holds for ^{30}Si). Finally, we notice that the deformations predicted by all three Gogny interactions underestimate the experimental values, although a bit less than for Mg isotopes. This is due to the limitations of the HFB treatment; extensions beyond the mean field must be undertaken to refine the outcomes.

5.3. Calcium potential energy surfaces

The PES along the Ca isotopic chain are given for the DG, D1S and D2 interactions in Figure III.27.

We see that the ground states of all Ca isotopes are predicted spherical by the three interactions, showing a deep well at $\beta_2 = 0$. Although the solutions are a little less bound away from the spherical point with DG, the spherical wells are systematically predicted narrower with this latter compared to that of D2 from ^{34}Ca to ^{48}Ca, and even compared to D1S from ^{50}Ca. This was to be expected since the remarks we have made for magic $N = 20$ isotones Mg, Si and S, exhibiting similar tensor effects, obviously apply to magic $Z = 20$ isotopes. In the doubly magic $Z = N = 20$ nucleus ^{40}Ca, we consistently find out that the spherical well is more pronounced with DG with respect to D2 interaction than for the neighboring isotopes, reaching a difference of 1.6 MeV. The sphericity is reinforced by the receding prolate minimum with the DG interaction. Actually we have performed the calculations on Ca isotopes to probe the properties of the DG interaction on PES of medium-mass nuclei, but over all to get information for our study on the kink (see subsection III.3.3.2). As it was argued that the deformation properties could influence the isotopic shift, we wanted to analyze the shapes of Ca isotopes. Interaction DG in fact predicts more rigid spherical nuclei, in agreement with the enlargement of both proton and neutron gaps with respect to those of D1S and D2 interactions, as shown in Figure

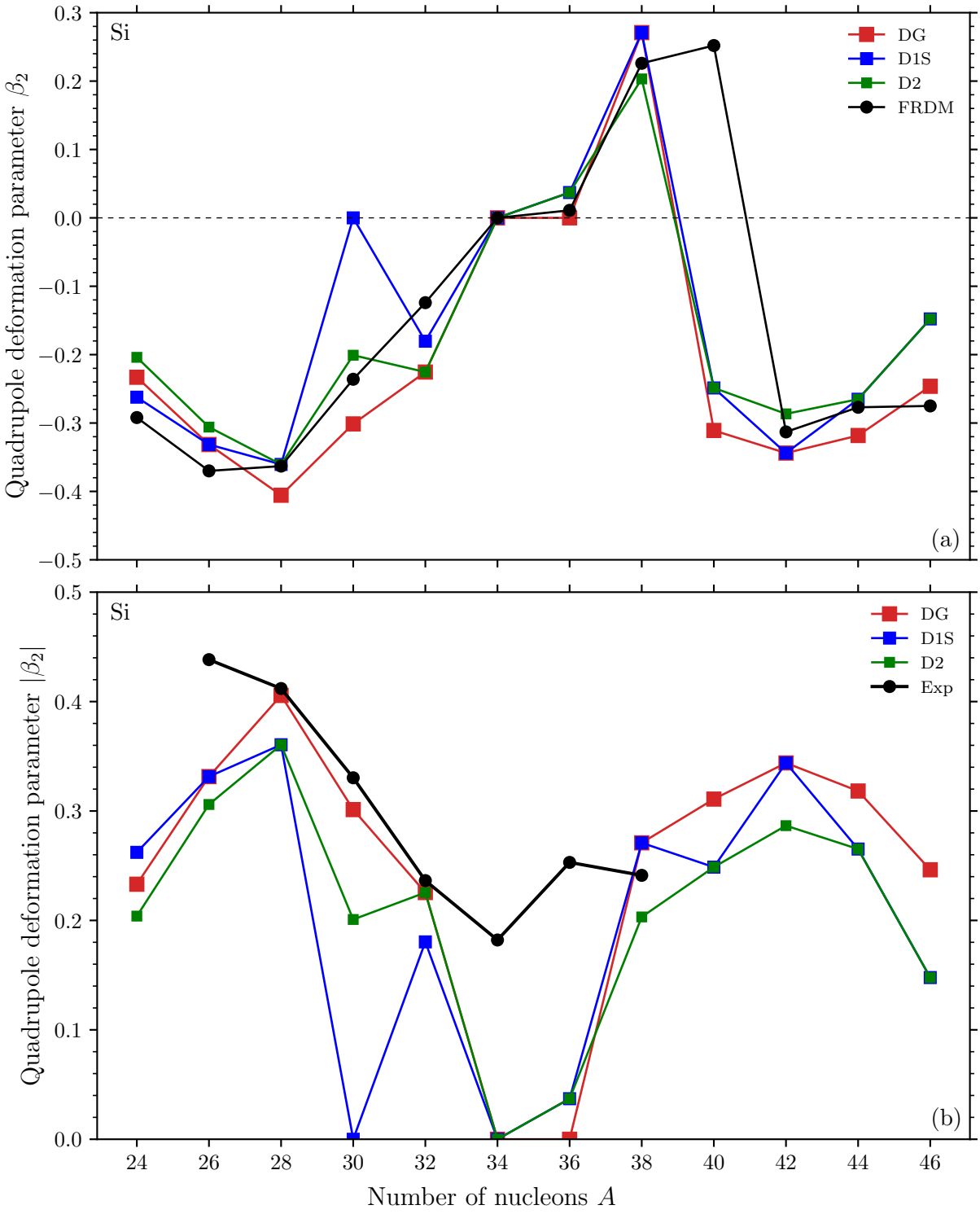

Figure III.25 – Same as in Figure III.21, but now for the Si isotopic chain.

III.18. To go further in the connection of dynamical deformations and pairing correlations to the isotopic shift, beyond mean-field calculations must be carried out.

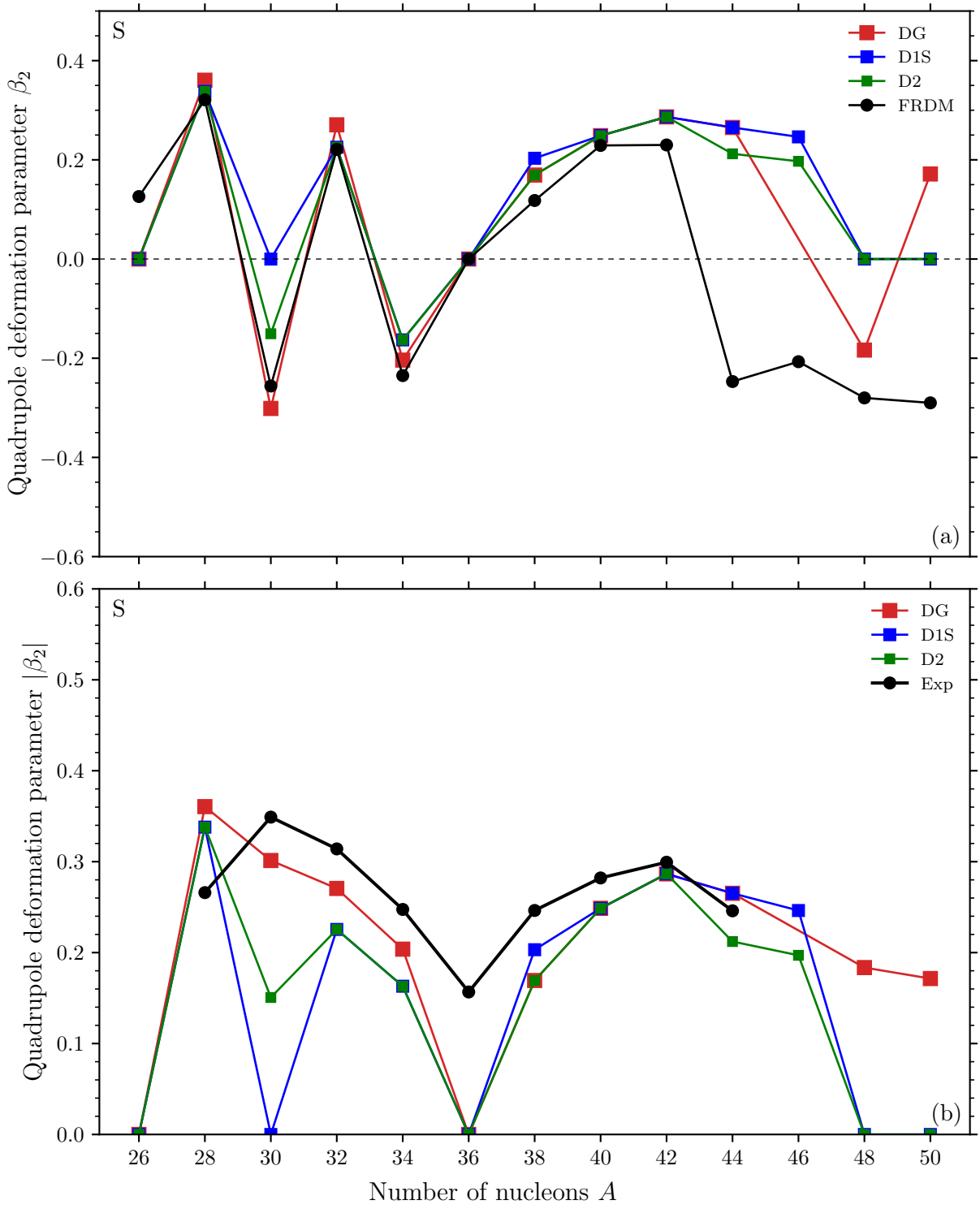

Figure III.26 – Same as in Figure III.21, but now for the S isotopic chain.

5.4. Tin potential energy curves

Finally, the PES along the Sn isotopic chain are represented for the DG, D1S and D2 interactions in Figure III.28.

Here again, the ground states of all Sn isotopes are predicted spherical by the three interactions, with deeper wells at deformation $\beta_2 = 0$ close to the magic nuclei ^{100}Sn and

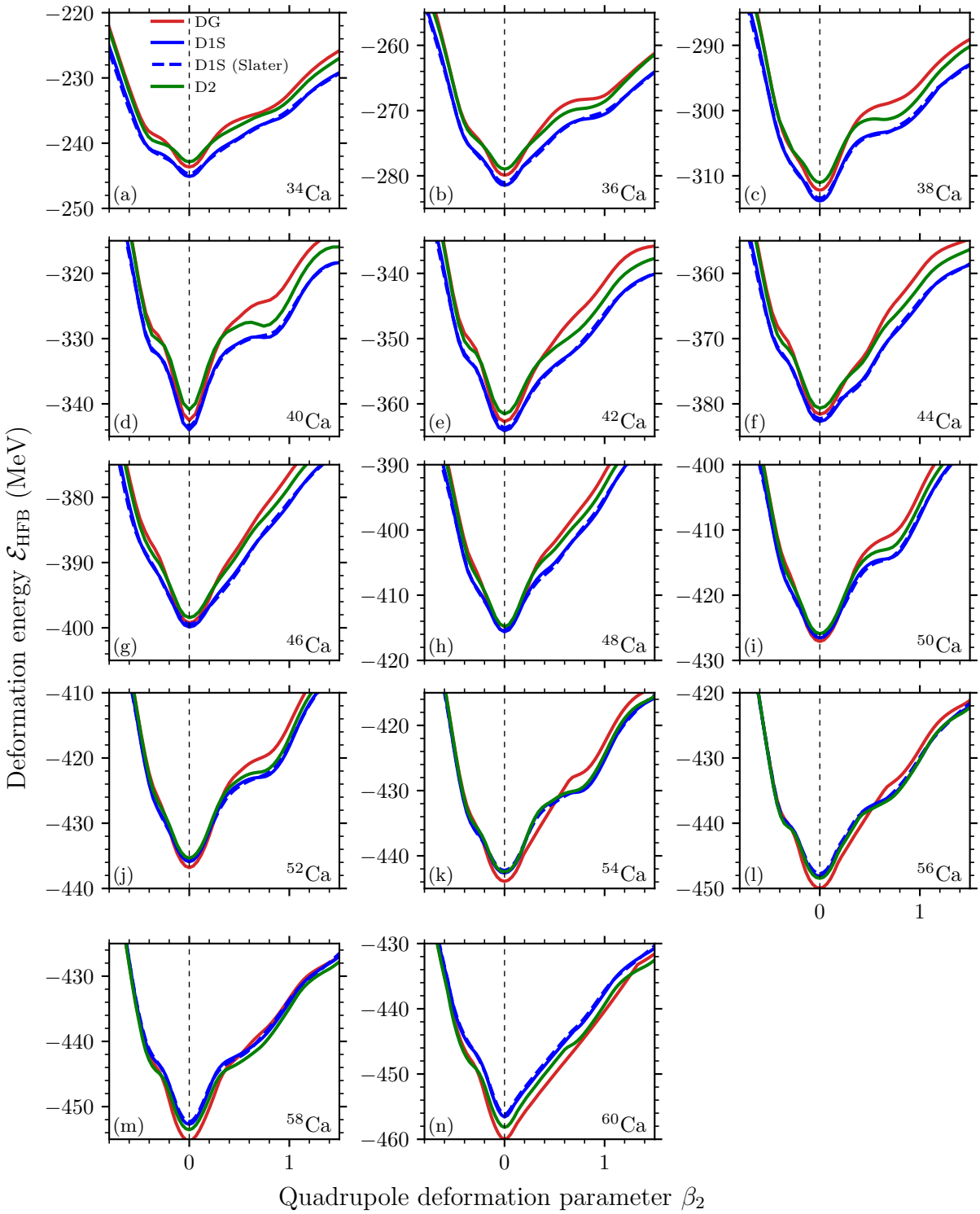

Figure III.27 – Same as in Figure III.19, but now for the Ca isotopic chain.

^{132}Sn, as required. The PES of DG, D1S and D2 interactions follow the same patterns, but are shifted from one another, with D2 overall providing solutions less bound than those of D1S and more bound compared to DG. Specifically at the spherical points, this was already spotted in panel (c) of Figure III.4. In particular, the difference in energy at the spherical point from ^{100}Sn to ^{118}Sn between DG and, D1S and D2, decreases while it then grows up in heavier isotopes. This is in agreement with the results of Figure III.18

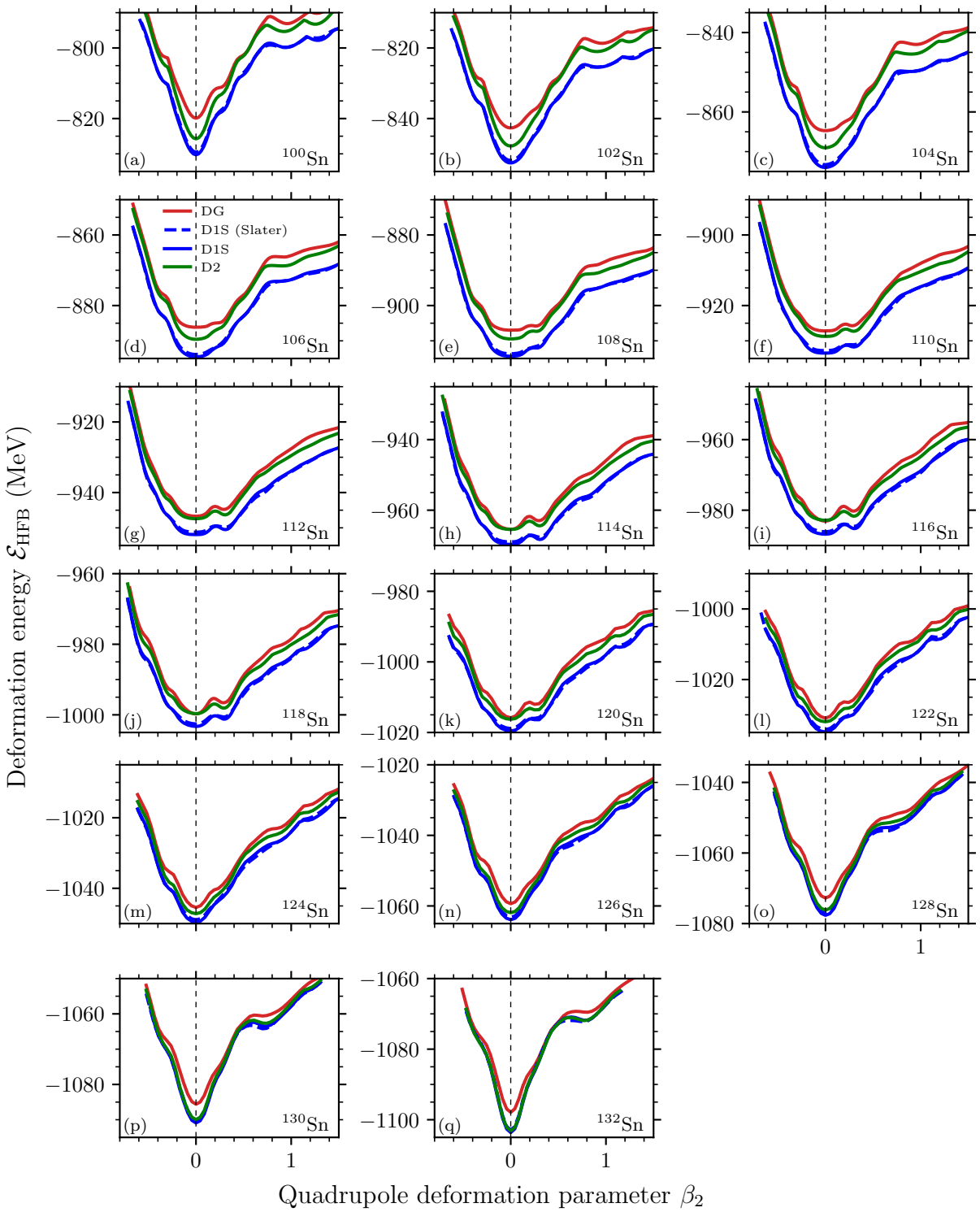

Figure III.28 – Same as in Figure III.19, but now for the Sn isotopic chain.

since the neutron pairing gaps of DG are reduced for isotopes ^{100}Sn and ^{132}Sn, and on the contrary enlarged for isotopes ^{114}Sn and ^{116}Sn, with respect to D1S and D2 interactions at the spherical point. Indeed, we have attributed this effect to the related diminution of neutron pairing energies with DG, observed in Figure III.12.

6. Fission barriers

Finally, we look at the PES of some pre-actinides and actinides to report how their fission barriers are modified by the interaction DG. This kind of nuclei present two barriers. The first one, characterized by a height B_{I}, corresponds to the amount of energy required for the nucleus to move from its ground state (marked by a first well), to a possible metastable state called the *fission isomer* (marked by a second well). There, a second barrier, characterized by a height B_{II}, describes the amount of energy required for the nucleus to undergo fission, i.e. to scission into two lighter fragments.

In the following, the asymmetric (the axial octupole moment Q_{30} is not constrained) fission barriers will be considered to evaluate the fission barrier heights at quadrupole deformations β_2 in Th isotopes and standard actinides. To be able to compare fission barriers more clearly between each of the Gogny interactions, we define the normalized deformation energy by

$$\bar{\mathcal{E}}_{\mathrm{HFB}} \equiv \mathcal{E}_{\mathrm{HFB}} - \mathcal{E}^{\mathrm{GS}}_{\mathrm{HFB}}, \tag{III.69}$$

where $\mathcal{E}^{\mathrm{GS}}_{\mathrm{HFB}}$ is the deformation energy in the ground state for a given nucleus.

6.1. Thorium isotopes

We begin with the PES of four Th isotopes, represented in Figure III.29.

Generally speaking, we see that the PES of all interactions follow the same pattern. Nevertheless, they can be slightly shifted in deformation or in energy in certain regions, from one interaction to another. To quantify these effects, we first compare the first fission barrier heights of DG, D1S (with and without Slater approximation) and D2 interactions in Table III.8.

	First fission barrier height B_{I}			
Interaction	^{226}Th (MeV)	^{228}Th (MeV)	^{232}Th (MeV)	^{234}Th (MeV)
DG	7.3	7.1	8.0	8.4
D1S	8.5	8.7	9.3	9.9
D1S (Slater)	7.6	7.7	8.8	9.4
D2	7.4	7.5	8.2	8.8
Exp		6.2	5.8	6.1

Table III.8 – First fission barrier heights B_{I} of isotopes ^{226}Th, ^{228}Th, ^{232}Th and ^{234}Th obtained with DG, D1S (with and without the exact Coulomb potential) and D2 interactions. They are compared to experimental data when available [205, 206].

It appears that the heights of the first barriers in the Th isotopes under study have comparable sizes with DG and D2 interactions, and are about 1 to 1.5 MeV smaller than those of D1S. It is interesting to see that the exact Coulomb potential tends to increase the heights of these barriers with respect to the same solution using the Slater approximation, for interaction D1S. The effect is moderate on ^{232}Th and ^{234}Th isotopes, not exceeding 500 keV, but more pronounced on ^{226}Th and ^{228}Th isotopes, of about 1 MeV. Since the calculations have been performed with the exact Coulomb force for DG and D2

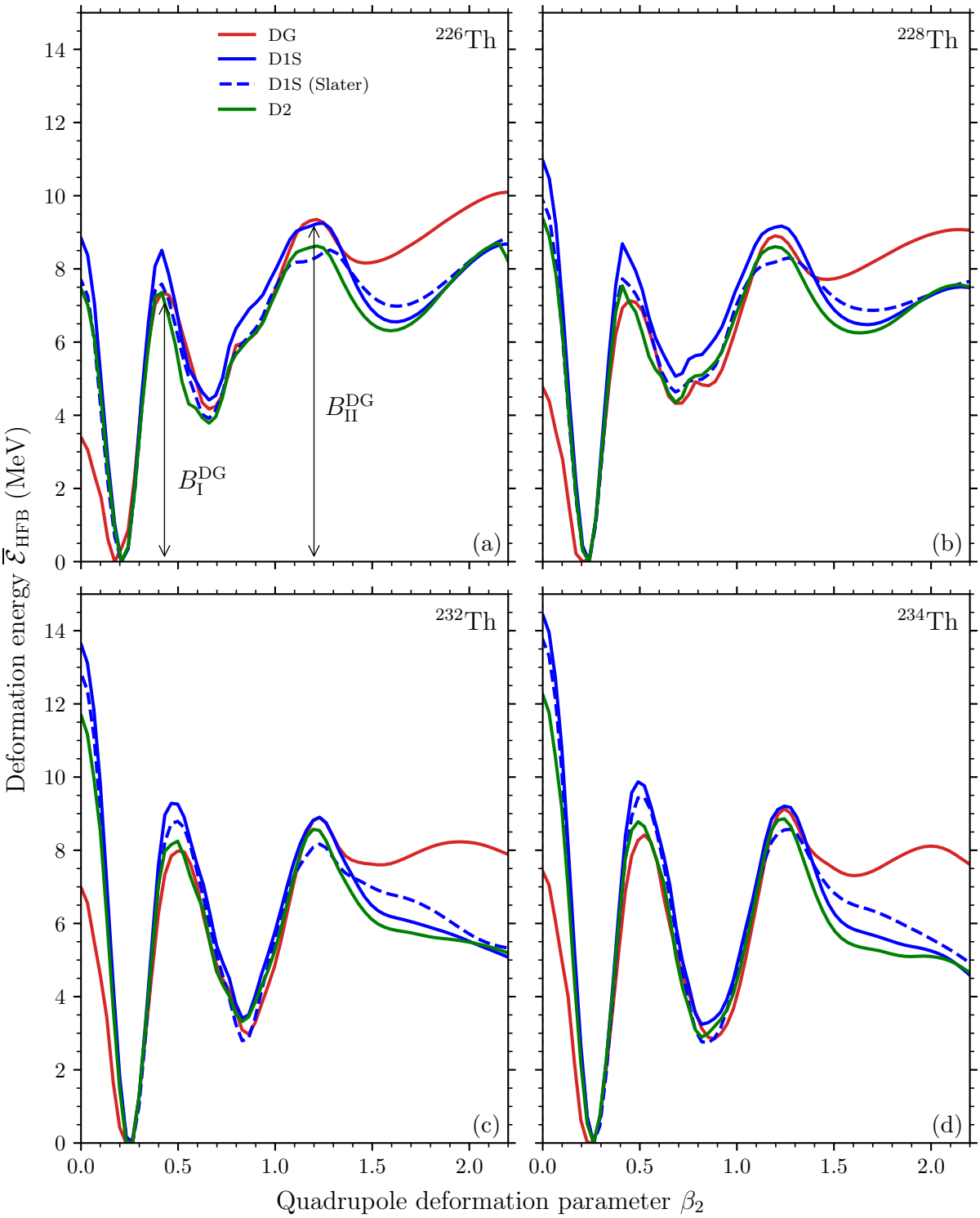

Figure III.29 – Potential energy curves of ^{226}Th, ^{228}Th, ^{232}Th and ^{234}Th as a function of the quadrupole deformation parameter, evaluated at the one-center limit for DG, D1S (with and without the exact Coulomb potential) and D2 interactions. The first $B_{\rm I}^{\rm DG}$ and second $B_{\rm II}^{\rm DG}$ fission barrier heights of DG are represented.

interactions, the comparisons will be priorly made with the exact Coulomb force for interaction D1S. The last row of the above table shows that the heights are systematically overestimated by all Gogny interactions, but are less with DG and D2 interactions, of

about 1 to 2 MeV, compared to experimental values. On the other hand, we know that when triaxial quadrupole deformations are taken into account ($Q_{22} \neq 0$), the heights of the first barriers are diminished by a few MeV. With interaction D1S, it has been shown that triaxiality lowers the first fission barriers by about 1 to 3 MeV, depending on the Th isotope [207]. Triaxial calculations must be performed with D2 and DG interactions to validate such figures, but the predictions are heading in the right direction.

	Second fission barrier height B_{II}			
Interaction	^{226}Th (MeV)	^{228}Th (MeV)	^{232}Th (MeV)	^{234}Th (MeV)
DG	9.4	8.9	8.9	9.1
D1S	9.3	9.2	8.9	9.2
D1S (Slater)	8.5	8.3	8.2	8.6
D2	8.7	8.6	8.6	8.9
Exp		6.5	6.7	6.3

Table III.9 – Same as in Table III.8, but now for the second fission barrier heights B_{II}. When available, experimental data are extracted from [205, 206].

The same analysis is carried out with the second fission barrier heights in Table III.9. Generally speaking, the comments made for the exact Coulomb potential remain true. This time, however, the heights are not significantly reduced by interactions D2 and DG compared to D1S. Those predicted by DG and D1S are comparable, and even higher with DG in the case of ^{226}Th. It then appears that the second fission barriers of DG are about 2 to 3 MeV higher than the experimental values. These observations are not pathological, so far, since the heights are calculated from the HFB ground states, while the zero-point energies should rather be considered to provide relevant comparisons to experiment. Using a D1S interaction, the zero-point energies in these Th isotopes were estimated to be of about 2 to 3 MeV [207]. In the light of such corrections, the fission barriers predicted by D2 and DG seem more reasonable, even though this study must be extended to interactions D2 and DG.

	Deformations							
	^{226}Th		^{228}Th		^{232}Th		^{234}Th	
Interaction	β_2^{isom}	β_2^{II}	β_2^{isom}	β_2^{II}	β_2^{isom}	β_2^{II}	β_2^{isom}	β_2^{II}
DG	0.659	1.214	0.684	1.196	0.863	1.229	0.883	1.244
D1S	0.659	1.248	0.684	1.231	0.830	1.229	0.818	1.244
D1S (Slater)	0.659	1.283	0.684	1.265	0.830	1.229	0.851	1.277
D2	0.659	1.214	0.684	1.196	0.830	1.195	0.818	1.244

Table III.10 – Values of the quadrupole deformation parameters at the second well, β_2^{isom}, and at the second fission barrier, β_2^{II}, for ^{226}Th, ^{228}Th, ^{232}Th and ^{234}Th isotopes, obtained with DG, D1S (with and without Slater approximation) and D2 interactions.

We have discussed the energy shifts of the PES, and we now focus on the deformation ones. In Table III.10 are displayed the values of the quadrupole deformation parameters

where the fission isomer lies, β_2^{isom}, and at the second fission barrier, β_2^{II}, for all three Gogny interactions. We see that the values of β_2^{isom} are slenderly higher with DG in ^{232}Th and ^{234}Th while the values of β_2^{II} are smaller in ^{226}Th and ^{228}Th (compared to those of D1S). This means that with interaction DG, the isomeric states in ^{232}Th and ^{234}Th correspond to more elongated configurations while in ^{226}Th and ^{228}Th, isotopes are found less deformed at the saddle point, when following the asymmetric paths.

We emphasize that the results of this subsection (both shifts in energy and deformation of Th PES with interaction DG) are in qualitative agreement with those obtained by Bernard *et al.* [39] for the interaction D1ST2a. Because this latter was set up by adding a perturbatively fitted tensor force on top of the D1S parametrization, the authors attributed the shifts to the tensor term. Although it is not possible to strictly disentangle the action of the tensor force from that of the other terms in a fully refitted interaction like ours, we then tend to hold the tensor term responsible for these effects as well.

6.2. Standard actinides

We continue our discussion with the same study applied to four actinides, namely ^{236}U, ^{238}U, ^{240}Pu and ^{254}Cf, represented in Figure III.30.

Once again, it is reassuring to see that the PES of all interactions display similar behaviors, with energy and deformation shifts in some regions. The first fission barrier heights of DG, D1S (with and without Slater approximation) and D2 interactions are listed in Table III.11.

	First fission barrier height B_{I}			
Interaction	^{236}U (MeV)	^{238}U (MeV)	^{240}Pu (MeV)	^{252}Cf (MeV)
DG	8.9	9.3	9.9	10.4
D1S	10.8	11.2	11.5	12.4
D1S (Slater)	10.0	10.6	11.0	12.0
D2	9.8	10.2	10.9	11.9
Exp	5.0	6.3	6.1	5.3

Table III.11 – First fission barrier heights B_{I} of nuclei ^{236}U, ^{238}U, ^{240}Pu and ^{252}Cf obtained with DG, D1S (with and without the exact Coulomb potential) and D2 interactions. They are compared to experimental data when available [205, 206].

It turns out that the heights of the first fission barriers in the actinides under study are lowered by about 500 keV to 1 MeV with D2 and about 2 MeV with DG, compared to those of the D1S interaction. As for the exact Coulomb potential, it increases the first fission barriers by 400 to 800 keV, depending on the actinide. The heights are still important with all Gogny interactions with respect to the experimental values, but the successive improvements brought up by D2 and DG interactions are encouraging. Indeed, while the discrepancies with experiment reached 5 to 7 MeV for D1S, they are reduced to 3 to 5 MeV for DG interaction. By the way, the heights of the first barriers of D1S were lowered by 2 to 4 MeV in such actinides when triaxiality was involved in [207]. In the same manner, the zero-point energies are found to be of about 2 to 3 MeV in these latter. Taking into account these considerations should then further lower our first barrier heights, in agreement with experiment.

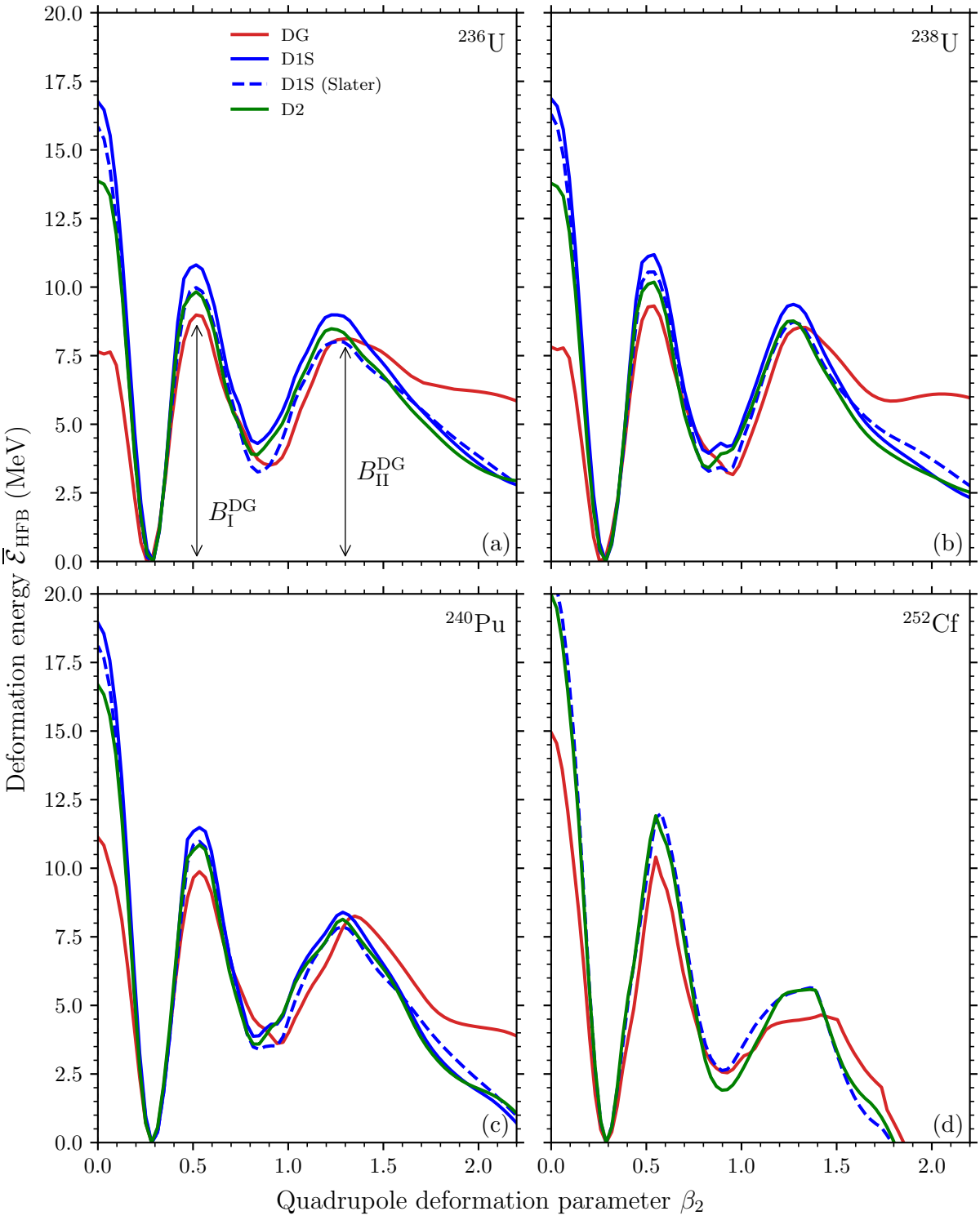

Figure III.30 – Potential energy curves of ^{236}U, ^{238}U, ^{240}Pu and ^{252}Cf as a function of the quadrupole deformation parameter, evaluated at the one-center limit for DG, D1S (with and without the exact Coulomb potential) and D2 interactions. The first $B_{\rm I}^{\rm DG}$ and second $B_{\rm II}^{\rm DG}$ fission barrier heights of DG are represented.

The same analysis is performed with the second fission barrier heights in Table III.12. The heights are reduced by about 500 keV when going from D1S to D2 interactions, in isotopes ^{236}U and ^{238}U, and by about 1 MeV when going from D1S to DG, except in

	Second fission barrier height $B_{\rm II}$			
Interaction	^{236}U (MeV)	^{238}U (MeV)	^{240}Pu (MeV)	^{252}Cf (MeV)
DG	8.1	8.5	8.3	4.7
D1S	9.0	9.4	8.4	5.6
D1S (Slater)	8.0	8.7	7.9	5.6
D2	8.5	8.8	8.1	5.6
Exp	5.7	5.5	5.2	3.5

Table III.12 – Same as in Table III.11, but now for the second fission barrier heights $B_{\rm II}$. When available, experimental data are extracted from [205, 206].

^{240}Pu. The exact Coulomb potential raises the second barriers by 1 MeV in ^{236}U, and by about 500 keV in isotopes ^{238}U and ^{240}Pu. Generally speaking, as for Th isotopes, the predictions are better with DG compared to D1S and D2 interactions, but are still above experimental data. Once again, the discrepancies are rather small, of about 1 to 3 MeV, and the corrections brought by the zero-point energies should improve the agreement with experiment.

	Deformations							
	^{236}U		^{238}U		^{240}Pu		^{252}Cf	
Interaction	$\beta_2^{\rm isom}$	$\beta_2^{\rm II}$	$\beta_2^{\rm isom}$	$\beta_2^{\rm II}$	$\beta_2^{\rm isom}$	$\beta_2^{\rm II}$	$\beta_2^{\rm isom}$	$\beta_2^{\rm II}$
DG	0.903	1.323	0.955	1.337	0.942	1.350	0.926	1.418
D1S	0.839	1.226	0.827	1.273	0.816	1.287	0.926	1.389
D1S (Slater)	0.839	1.259	0.827	1.273	0.847	1.287	0.897	1.360
D2	0.839	1.226	0.827	1.273	0.816	1.287	0.897	1.360

Table III.13 – Values of the quadrupole deformation parameters at the second well, $\beta_2^{\rm isom}$, and at the second fission barrier, $\beta_2^{\rm II}$, for ^{236}U, ^{238}U, ^{240}Pu and ^{252}Cf nuclei, obtained with DG, D1S (with and without Slater approximation) and D2 interactions.

We finally focus on the deformation shifts by looking at the quadrupole deformations at isomer and second fission barrier positions in Table III.13. We see that the values of $\beta_2^{\rm isom}$ and $\beta_2^{\rm II}$ are globally higher in the actinides we have probed with interaction DG. This phenomenon shows that the isomeric states and fission processes show up for more elongated configurations of these nuclei with DG than with D1S and D2 interactions, when following the asymmetric paths.

Such results were qualitatively obtained for the heaviest Th isotopes we studied, and were attributed to the tensor force. We then tend to hold the tensor force responsible for those shifts in actinides as well. Obviously, the analysis should be generalized to more pre-actinides and actinides to validate our observations. Furthermore, triaxial calculations should be carried out for interaction DG as they can also involve shifts in deformation [207].

In fact, to properly model the fission process, both static and dynamic properties of the fissioning system must be known. The HFB treatment we have exposed constitutes the

first step, related to static properties. Then, dynamical calculations based on these results are usually undertaken to describe the time evolution of the nucleus until its scission point. They may incorporate static out-of-equilibrium nuclear configurations, couplings between intrinsic and collective degrees of freedom, and subsequently the dynamics of large-amplitude collective vibrations to refine the dynamical description. An example of such method is the time-dependent generator coordinate method (TDGCM). It is beyond the scope of the present study, but should be handled in the future to directly connect the predictions of interaction DG to well-defined observables like the yield distributions of fission fragments and related quantities.

Chapter IV

Beyond mean-field results

> "Some birds are not meant to be caged, that's all. Their feathers are just too bright, their songs too sweet and wild. So you let them go, or when you open the cage to feed them they somehow fly out past you. And the part of you that knows it was wrong to imprison them in the first place rejoices, but still, the place where you live is that much more drab and empty for their departure."
>
> — Stephen King, *Rita Hayworth and the Shawshank Redemption*

In this chapter, the relevance of the generalized Gogny interaction regarding its spectroscopic properties beyond the mean field is gauged within the multiparticle–multihole configuration mixing method. After succinctly recalling the underlying formalism, the first excitation energies of various Gogny interactions are evaluated, in the *sd* shell, and compared to experimental data. Starting with even–even nuclei, the calculations are subsequently extended for the first time to odd and odd–odd nuclei. In-depth analysis reveals that the predictions of the generalized Gogny interaction stem from a skillful interplay between spin–orbit and tensor forces.

Chapter contents

1. MPMH formalism

In this section, we recall the formalism of the multiparticle–multihole configuration mixing method. It is not our intention to extensively introduce this approach, we shall merely lay the basics and underline the concepts that will be important in the following. For a complete introduction, we refer the reader to [208, 209].

As detailed in the first chapter (see subsection I.1.3), the starting point of self-consistent mean-field (SCMF) approaches is to separate the many-body Schrödinger equation into an exactly solvable one-body Hamiltonian and a residual interaction accounting for long-range correlations. The different types of correlations are incorporated at various levels of approximation through increasingly sophisticated SCMF theories. When taking into account more than simple pairing correlations, treatable at the mean-field level through the HFB approach (see previous chapter), they are referred to as *beyond mean-field theories*. The multiparticle–multihole (MPMH) configuration mixing method is one of those. As a continuation of similar frameworks developed in atomic physics and quantum chemistry (often referred to as multi-configurational self-consistent field methods) [210–212], the MPMH method is a *self-consistent variational* approach. Contrary to these latter, though, the MPMH brings out more complexity since:

(i) two kinds of particles (proton and neutron) come into play;

(ii) the nucleon–nucleon interaction is not known.

The second point results in considering here an effective interaction made up of a density-dependent term which further intricates the problem, as we shall shortly see. Nevertheless, these difficulties also arise in other nuclear SCMF approaches, while the MPMH method allows to:

(i) treat the ground and excited states of even–even, odd–odd and odd nuclei in the same theoretical framework;

(ii) take into account *all* long-range correlations (pairing correlations and correlations associated with collective excitations as well as particle–vibration couplings);

(iii) avoid symmetry breakings.

For example, within the HFB approach, one is often limited to even–even nuclei because the time-reversal symmetry is broken when a nucleus with an odd number of proton or neutron is studied. Even if the time-reversal symmetry is released (which significantly complicates the expressions of the fields, as we have experienced in Appendix C), the particle–vibration coupling is no longer negligible because of the unpaired nucleon. On the other hand, it is well-known that the number of particle is only conserved on average at the HFB level, and that the RPA equations slightly violate the Pauli principle (as a consequence of the quasi-boson approximation). In the MPMH, the proton and neutron numbers are both separately preserved, and the Pauli principle holds.

We begin by giving the Hamiltonian of the nucleus consisting in a A-body system for which we only consider two-body interactions and neglect higher-body contributions. In second quantization, it can be written

$$H^{2\mathrm{B}} = \sum_{ab} \langle a|t_{\mathrm{K}}|b\rangle c_a^\dagger c_b + \frac{1}{4}\sum_{abcd} \langle ac|v_{12}^{(\mathrm{a})}|bd\rangle c_a^\dagger c_c^\dagger c_d c_b, \tag{IV.1}$$

where we recognize the usual creation c_a and annihilation $c_a^\dagger$ operators, the one-body kinetic operator, written in terms of the momentum operator $p \equiv \hbar k$ as

$$t_{\mathrm{K}} \equiv \frac{p^2}{2M}, \tag{IV.2}$$

as well as the two-body antisymmetrized interaction

$$v_{12}^{(\mathrm{a})} \equiv v_{12}(1 - P_r P_\sigma P_\tau), \tag{IV.3}$$

with v_{12} the generalized Gogny force (II.1).

As in any variational approach, the exact wave function of the system $|\Psi\rangle$ is approximated by a trial wave function $|\Phi\rangle$, $|\Psi\rangle \simeq |\Phi\rangle$. In the MPMH approach, the trial wave function is a superposition of Slater determinants $|\phi_\alpha\rangle$, which are themselves expressed as a direct product of proton (π) and neutron (ν) Slater determinants, $|\phi_\alpha\rangle \equiv |\phi_{\alpha_\pi}\rangle \otimes |\phi_{\alpha_\nu}\rangle$, such that

$$|\Phi\rangle \equiv \sum_\alpha A_\alpha |\phi_\alpha\rangle \tag{IV.4a}$$

$$\equiv \sum_{\alpha_\pi \alpha_\nu} A_{\alpha_\pi \alpha_\nu} |\phi_{\alpha_\pi}\rangle \otimes |\phi_{\alpha_\nu}\rangle, \tag{IV.4b}$$

where the *mixing coefficients* A_α represent the weights of the Slater determinants $|\phi_\alpha\rangle$ in the trial wave function. Note that in general we have $A_{\alpha_\pi \alpha_\nu} \neq A_{\alpha_\pi} A_{\alpha_\nu}$ because of the correlations between protons and neutrons. This would only be the case if the residual proton–neutron interaction was neglected. Each Slater determinant, corresponding to a *many-body configuration* of the system, is a multiparticle–multihole (mp–mh) excitation of a reference state $|\phi_0\rangle$, that is to say

$$|\phi_\alpha\rangle \equiv \prod_{i=0}^{M_\alpha} \left(c_{\mathrm{p}_i}^\dagger c_{\mathrm{h}_i}\right) |\phi_0\rangle \tag{IV.5a}$$

$$\equiv \prod_{i_\pi=0}^{M_{\alpha_\pi}} \left(c_{\mathrm{p}_{i_\pi}}^\dagger c_{\mathrm{h}_{i_\pi}}\right) |\phi_{0_\pi}\rangle \otimes \prod_{i_\nu=0}^{M_{\alpha_\nu}} \left(c_{\mathrm{p}_{i_\nu}}^\dagger c_{\mathrm{h}_{i_\nu}}\right) |\phi_{0_\nu}\rangle, \tag{IV.5b}$$

where, in the first equation, we have introduced a pair of creation operators for "particle" (p) and "hole" (h) states. They are divided into proton and neutron operators in the second line, with the reference state being the direct product of proton and neutron reference states, $|\phi_0\rangle \equiv |\phi_{0_\pi}\rangle \otimes |\phi_{0_\nu}\rangle$. The number of particle–hole excitations $c_{\mathrm{p}}^\dagger c_{\mathrm{h}}$ applied to $|\phi_0\rangle$ in order to generate $|\phi_\alpha\rangle$ is called the *excitation order* of the configuration $|\phi_\alpha\rangle$, $M_\alpha \equiv M_{\alpha_\pi} + M_{\alpha_\nu}$. We talk about 0p–0h excitation when no particle–hole excitation is applied, 1p–1h excitation when one particle–hole excitation is applied (which is barely the reference state), 2p–2h excitations when two particle–hole excitations are applied, and so on. This leads to the excited states $|0\mathrm{p}0\mathrm{h}\rangle$, $|1\mathrm{p}1\mathrm{h}\rangle$, $|2\mathrm{p}2\mathrm{h}\rangle$, etc. Obviously, there are many possible configurations for a given excitation order; some of them are illustrated in Figure IV.1. Finally the reference state corresponds to an HF-type ground state obtained by filling the lowest orbitals with the $A = Z + N$ nucleons of the nucleus, i.e.

$$|\phi_0\rangle \equiv \prod_{i=1}^{A} c_i^\dagger |0\rangle \tag{IV.6a}$$

$$\equiv \prod_{i_\pi=1}^{Z} c_{i_\pi}^\dagger |0_\pi\rangle \otimes \prod_{i_\nu=1}^{N} c_{i_\nu}^\dagger |0_\nu\rangle, \tag{IV.6b}$$

where the particle vacuum is expressed as the direct product of proton and neutron vacua, $|0\rangle \equiv |0_\pi\rangle \otimes |0_\nu\rangle$. The reference state is itself made up of an antisymmetrized product of individual orbitals (or single-particle states) $|\varphi_i\rangle \equiv c_i^\dagger|0\rangle$.

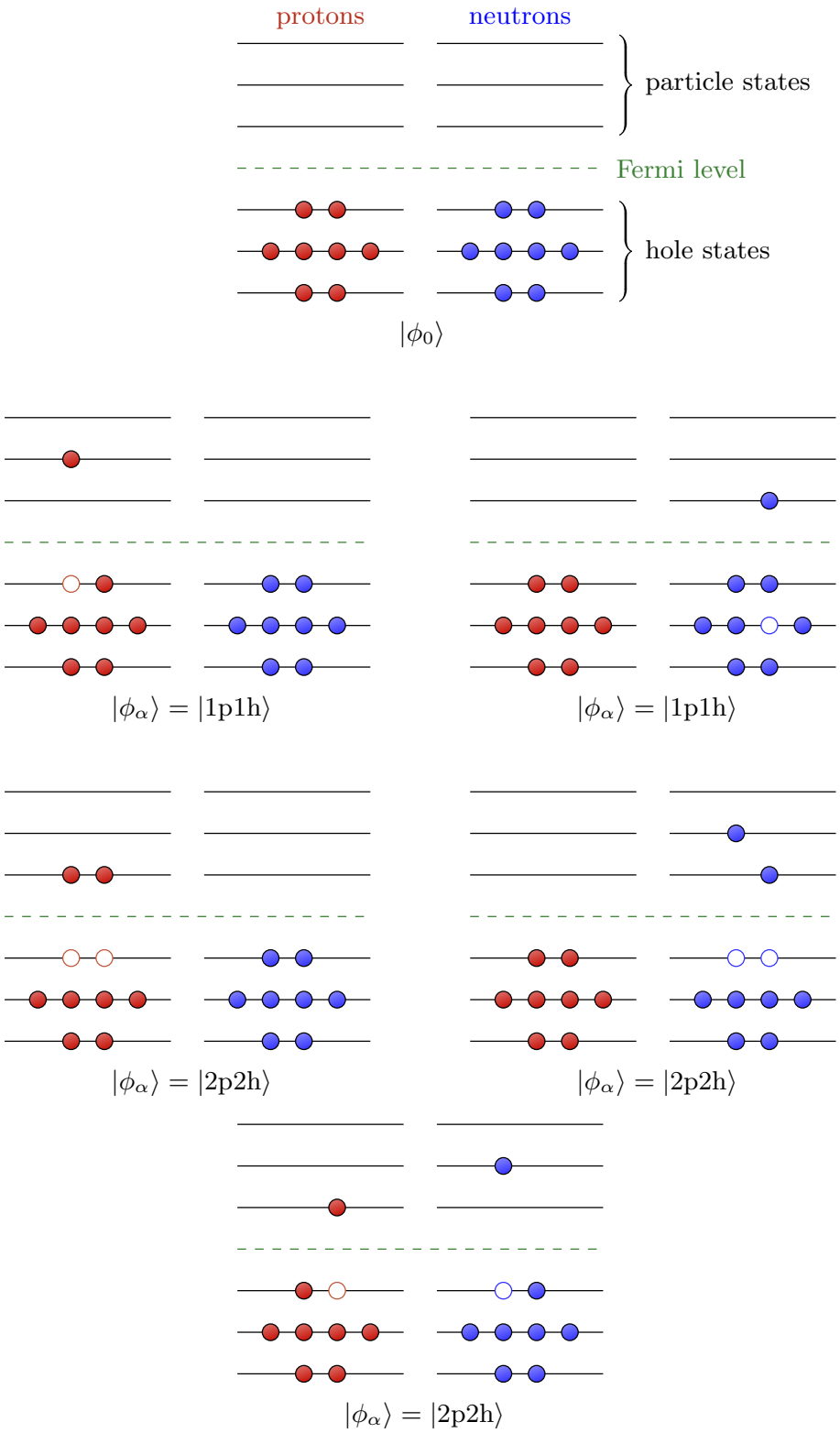

Figure IV.1 – Examples of particle–hole excitations of the reference state $|\phi_0\rangle$ up to $|2\text{p}2\text{h}\rangle$. Protons and neutrons are represented in red and blue, respectively, and the Fermi level, displayed by a green dashed line, separates hole from particle states.

Theoretically, those individual states are expanded on an infinite basis of functions that are known (in the same manner as in the fitting code, see subsection I.2.2.1), which are chosen to be axially-symmetric harmonic oscillator wave functions in the MPMH code. In this case the configurations $|\phi_\alpha\rangle$ span the complete Hilbert space $\mathcal{H}$ and are independent of the individual orbitals. In practice, as it is not possible to numerically deal with an infinite series, this expansion is truncated to some finite order n. The trial wave function $|\Phi\rangle$ can then only be varied in some subspace $\mathcal{S} \subset \mathcal{H}$ and becomes *a priori* dependent on the nature of the single-particle states. If the basis of single-particle states is large enough, the subspace $\mathcal{S}$ covers an important part of $\mathcal{H}$ and the solution remains satisfactory. In practice, the size of the many-body space $\mathcal{S}$ is tremendous as it encompasses all possible excitations of a system composed of A particles with M single-particle states, for both types of nucleons. Thus, the expansion (IV.4a) is further restricted to a subspace $\mathcal{P} \subset \mathcal{S}$ to stay tractable, and becomes

$$|\Phi\rangle = \sum_{\alpha \in \mathcal{P}} A_\alpha |\phi_\alpha\rangle. \tag{IV.7}$$

One drawback of these two successive truncations at both the one- and many-body levels is that the trial wave function may now significantly depend on the nature of the single-particle states $|\varphi_i\rangle$. Consequently, in the MPMH approach, the orbitals are determined so as to *optimize* at best the information contained in $\mathcal{P}$ through a minimization procedure. In other words, the two sets of unknown quantities to be specified are:

(i) The mixing coefficients $\{A_\alpha\}$ characterizing the expansion (IV.7);

(ii) The individual orbitals $\{|\varphi_i\rangle\}$ characterizing the many-body states $|\phi_\alpha\rangle$.

The equation determining the mixing coefficients is obtained by minimizing the energy functional $\mathcal{E} \equiv \langle\Phi|H^{\mathrm{2B}}|\Phi\rangle$ with respect to the mixing coefficients while the individual orbitals are fixed. Conversely, the equation defining the individual orbitals is obtained by minimizing the energy functional with respect to the individual orbitals while the mixing coefficients are fixed. Mathematically speaking these statements amount to imposing

$$\begin{cases} \delta_A \mathcal{E} = 0, \\ \delta_\varphi \mathcal{E} = 0, \end{cases} \tag{IV.8}$$

where δ_A and δ_φ denote the variations with respect to mixing coefficients and individual orbitals, respectively. For a density-dependent force like the generalized Gogny interaction, we can show that these relations lead to the following coupled MPMH equations

$$\begin{cases} \displaystyle\sum_{\beta \in \mathcal{P}} A_\beta \, \langle \phi_\alpha | H[\rho, \sigma] | \phi_\beta \rangle = \lambda A_\alpha, \quad \forall \alpha \in \mathcal{P}, & \text{(IV.9a)} \\ \Big[h[\rho, \sigma], \rho \Big] = G[\sigma]. & \text{(IV.9b)} \end{cases}$$

We will not describe the physics of these equations in detail, but we simply mention a few interesting aspects.

The first equation represents the diagonalization of the modified Hamiltonian in the many-body configuration space, where its associated eigenvalues are denoted λ. It is expressed as

$$H[\rho, \sigma] \equiv H^{\mathrm{2B}}[\rho] + R[\rho, \sigma], \tag{IV.10}$$

with the operator $R[\rho,\sigma]$ defined by

$$\begin{aligned} R[\rho,\sigma] &\equiv \int \mathrm{d}^3r\, \langle\Phi|\frac{\delta v_{12}[\rho]}{\delta\rho(\vec{r})}|\Phi\rangle\rho(\vec{r}) \\ &= \frac{1}{4}\int \mathrm{d}^3r\, \langle ab|\frac{\delta v_{12}[\rho]}{\delta\rho(\vec{r})}|cd\rangle(\rho_{ca}\rho_{db}-\rho_{cb}\rho_{da}+\sigma_{ac,bd})\rho(\vec{r}), \end{aligned} \tag{IV.11}$$

and is usually called the "rearrangement term" since due to the density dependence of the nuclear interaction. It basically represents the response of the system to a small density variation. It is worth mentioning that this quantity depends on the one-body and two-body correlation matrix densities of the correlated state $|\Phi\rangle$, whose elements read

$$\rho_{ab} \equiv \langle\Phi|c_b^\dagger c_a|\Phi\rangle, \tag{IV.12a}$$

$$\sigma_{ab,cd} \equiv \langle\Phi|c_a^\dagger c_c^\dagger c_d c_b|\Phi\rangle - \rho_{ba}\rho_{dc}+\rho_{bc}\rho_{da}. \tag{IV.12b}$$

These dependences make the configuration mixing equation non-linear, and it should be kept in mind that the computation of those two quantities is required to specify the rearrangement term. We notice that this first equation really looks like the so-called shell-model secular equation. This is not so surprising because the expansion (IV.4a) is comparable to that performed in shell-model theory, except that it is more general, since *a priori* not restricted to a given major shell.

The second equation involves a one-body mean-field Hamiltonian which also depends on the two types of matrix densities through the rearrangement term, according to

$$h[\rho,\sigma] = K + \Gamma[\rho] + R[\rho,\sigma], \tag{IV.13}$$

where K and $\Gamma[\rho]$ respectively stand for kinetic and mean-field-type contributions. This Hamiltonian can be seen as a generalization of the HF field since it is constructed from the density matrix of the many-configuration system (IV.12a), rather than from a simple Slater determinant. As for the quantity $G[\sigma]$, it is referred to as the source term and includes the effect of correlations beyond this mean field. Again, this second equation looks like the so-called HF equation (A.14). Actually, we can even prove that if only the reference state is included in expansion (IV.4a), i.e. if $|\Phi\rangle = |\phi_0\rangle$, the two-body correlation density matrix vanishes, the one-body density matrix reduces to the HF density matrix and we fall back on the HF equations [209]. The MPMH method can be seen as a generalization of the HF approximation where the residual correlations are taken into account in the source term. In short, the MPMH configuration mixing method is an approach that aims to combine and generalize mean-field and shell-model approximations to capitalize on their respective advantages while incorporating additional beyond mean-field effects.

Let us finally point out that the resolution of both MPMH equations (IV.9) is based on an iterative process. We start with an HF solution (characterized by the density matrices $\rho = \rho_{\mathrm{HF}}$ and $\sigma = 0$) that furnishes an initial set of individual wave functions from which we build the many-body configuration basis and solve the first equation (IV.9a). This provides mixing coefficients from which we can calculate ρ and σ and solve the second equation (IV.9b). With the new set of individual wave functions, the process starts over, and is repeated again and again until convergence of the matrices ρ and σ. The mixing coefficients and individual wave functions are then obtained fully self-consistently. Practically, the complete procedure becomes time-consuming when the matrix H to diagonalize is large. Furthermore, the fully self-consistent MPMH method has been developed only

for even–even nuclei so far. Waiting for a soon extension of the self-consistency to odd and odd–odd nuclei, we resort to a simpler scheme in which the diagonalization of equation (IV.9a) is only performed once from the initial data ($\rho = \rho_{\text{HF}}, \sigma = 0$). By doing so, the outputs produced by even–even, odd and odd–odd nuclei can be compared as they are all treated on a same footing, and we also avoid numerical issues when dealing with medium-mass isotopes. In return, the rearrangement term cannot be included (we have said that we needed in particular to know σ in order to specify the rearrangement term, which is not, here) and the self-consistency is lost. We will see that this is not problematic for our purposes by showing in due time how the restoration of the self-consistency impacts the results. We also specify that the results given in the following are all obtained by truncating the one-body basis to the finite order $n = 10$.

2. Even–even nuclei in *sd* shell

2.1. First excitation energies

In this section, we study and compare excitation energies of the first (as indicated by the subscript) excited states $J^\pi = 2_1^+$ of even–even nuclei for DG, D1S and D2 Gogny interactions, in the *sd* shell. This means that the possible multiparticle–multihole excitations are restrained to the SPEs belonging to this major shell, namely $1d_{5/2}, 2s_{1/2}$ and $1d_{3/2}$ levels. Preliminary works in this direction were carried out for D1S in [19, 213–215].

We analyze in Figure IV.2 the difference between the excitation energies 2_1^+ predicted by the MPMH and the experimental values for the *sd*-shell isotopes, namely Ne, Mg, Si, S and Ar. This difference is defined as

$$\Delta\mathcal{E}_{\text{MPMH}}[2_1^+] \equiv \mathcal{E}_{\text{MPMH}}[2_1^+] - \mathcal{E}_{\text{exp}}[2_1^+], \tag{IV.14}$$

where $\mathcal{E}_{\text{MPMH}}[2_1^+]$ and $\mathcal{E}_{\text{exp}}[2_1^+]$ respectively denote the excitation energies of the first excited state evaluated by the MPMH method and experimentally [202]. Note that we have excluded ^{26}S, ^{28}Ar and ^{30}Ar from our study since these nuclei are known to be unbound experimentally.

Generally speaking, we see that MPMH results are very close to experimental values for all three interactions, with *on average* differences of the order of a few hundred keV. To be more quantitative, we have computed the usual mean values and standard deviations, respectively defined by

$$\langle x \rangle \equiv \frac{1}{N}\sum_{i=1}^{N} |x_i|, \tag{IV.15a}$$

$$\sigma(x) \equiv \sqrt{\langle x^2 \rangle - \langle x \rangle^2}, \tag{IV.15b}$$

for the whole bunch of nuclei in Table IV.1, and then for each isotopic chain in Table IV.2. Of the three interactions, Table IV.1 shows that the MPMH predictions obtained with DG are the most qualitative. Notably, the mean difference is almost half that of D2 and the standard deviation more than three times smaller than that of D1S. On the contrary, the D2 interaction deteriorates the relatively good mean value of D1S. This may be explained by the fact that, unlike DG and D1S interactions, D2 was not controlled on quantities evaluated beyond the mean field in its fitting process or subsequently. It appears how important it may be to target the quantities we wish a faithful reproduction of right from the fitting stage.

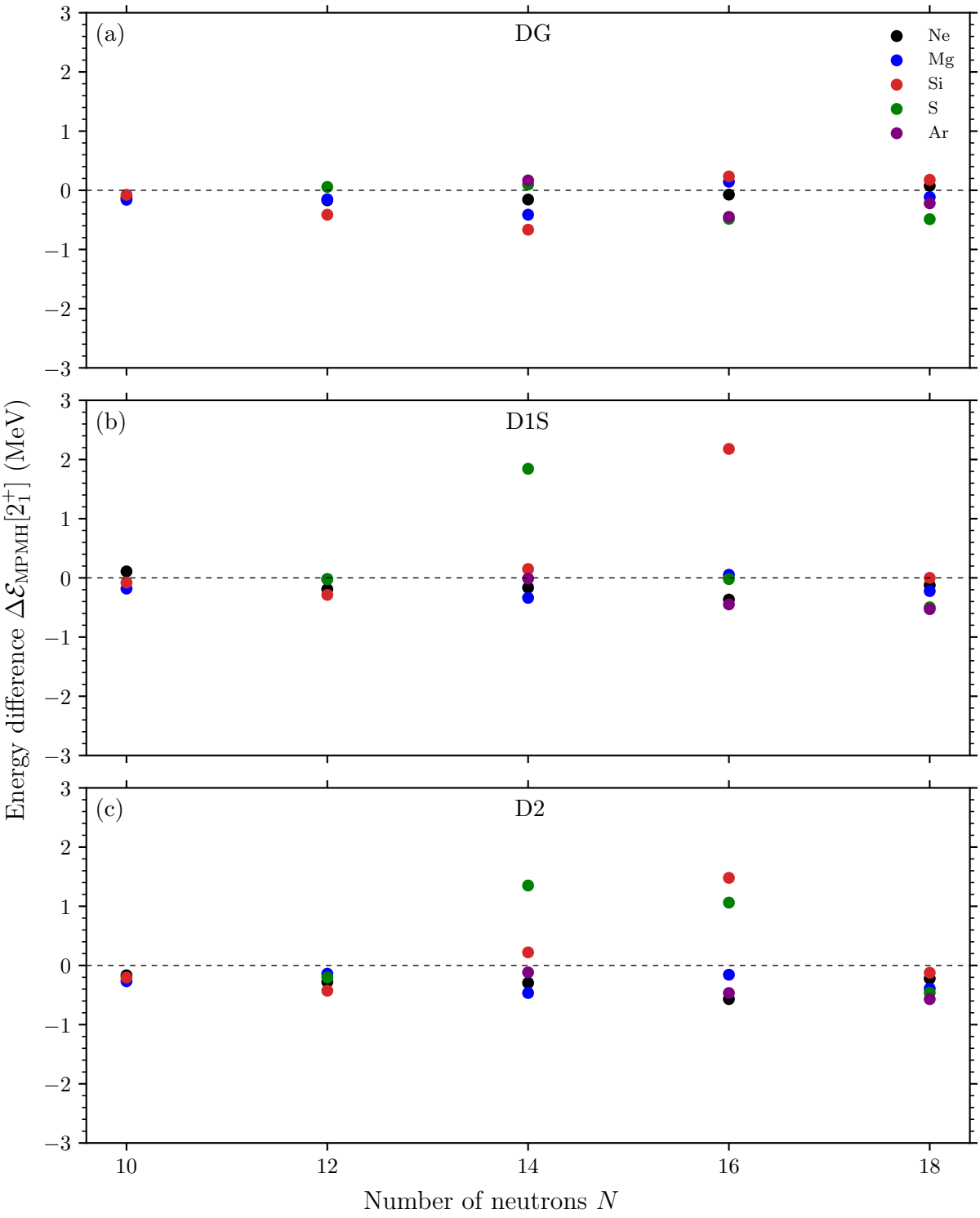

Figure IV.2 – Energy difference between first excitation energies predicted by the MPMH and experimental data, expressed by (IV.14), as a function of the number of neutrons N. The results are shown for DG, D1S and D2 interaction, in panels (a), (b) and (c), respectively. Horizontal dashed lines display perfect agreement with experiment [202]. The *sd*-shell isotopes studied are labelled by different colors, as indicated in the legend.

If we now look at the mean differences and standard deviations in each isotopic chain (even if there is not much elements), as displayed in Table IV.2, we deduce that our

	All isotopes	
Interaction	$\langle x \rangle$ (keV)	$\sigma(x)$ (keV)
DG	232	171
D1S	356	561
D2	438	382

Table IV.1 – Mean value and standard deviation of the difference $x \equiv \Delta\mathcal{E}_{\mathrm{MPMH}}[2_1^+]$, as defined in (IV.15), evaluated for the complete set of studied isotopes, with DG, D1S and D2 interactions.

comparison between the interactions is broadly maintained in separate isotopic chains. Specifically, the mean values and standard deviations are the lowest with the DG interaction for all isotopic chains, except in Mg isotopes for which the mean value is slightly lower with D1S. Again, D2 is not as good as its counterparts, except in Si isotopes, the mean value and standard deviation being lower than those of D1S. This is also true in S and Ar isotopes where D2 values deviate less from the mean values than D1S ones. We will thereby preferentially compare the DG outputs with those of D1S since we want to put forward the amendments with respect to the most convincing interaction to date.

Let us now try to justify the improvements brought by interaction DG. As we will see later on, there is a strong link between the description of first excitation energies and the SPE spectra. Indeed, the smaller the energy gap between the ground state and the first excited state, the greater the probability of particle–hole excitations from the lower towards the higher state. On the other hand, the DG interaction promotes a finite range to the spin–orbit force and includes a finite-range tensor force, which are fully refitted along with the other terms. These latter are known to significantly impact the position of SPEs. Knowing moreover that the central and density-dependent part of DG is close to that of D2, it is reasonable to think that one or both of the spin–orbit and tensor forces are (mainly) responsible for the observed effects. Since the trend described here is *global*, and that the tensor term plays a dominant role only in some specific configurations of SPEs, we can legitimately attribute the overall effect to the spin–orbit term, whose intensity has been lowered from 130 MeVfm^5 to 115.849 MeVfm^5 in the $T = 1$ channel when going from D1S and D2 interactions to DG. Actually this deduction has already been tested when dealing with the fitting procedure since the first excitation energies have been evaluated for several DG-type parametrizations (see subsection II.1.2.4). We have found out, by gently tuning its intensity, that the spin–orbit term is responsible for the fine overall reproduction of this observable, which was a little too strong in this purpose, with D1S and D2 interactions.

Even though the MPMH predictions are satisfactory as a whole for all three interactions, Figure IV.2 reveals that some first excitation energies of Si (red dots) and S (green dots) isotopes are overestimated by more than 1 MeV with D1S and D2. More precisely, ^{30}Si and ^{30}S stand out with an overestimation of 2.179 MeV and 1.480 MeV respectively, with D1S. With D2, the disagreement is lowered for these nuclei, to 1.843 MeV and 1.351 MeV, respectively, but ^{32}S which was particularly well predicted by D1S with an underestimation of 20 keV, is degraded with D2 and reach an overestimation of 1.062 MeV. These nuclei are at the origin of the highest mean values and standard deviations of Si and S isotopic chains among all the others, as shown in Table IV.2, for D1S and D2

	Ne		Mg		Si		S		Ar	
Interaction	$\langle x \rangle$ (keV)	$\sigma(x)$ (keV)	$\langle x \rangle$ (keV)	$\sigma(x)$ (keV)	$\langle x \rangle$ (keV)	$\sigma(x)$ (keV)	$\langle x \rangle$ (keV)	$\sigma(x)$ (keV)	$\langle x \rangle$ (keV)	$\sigma(x)$ (keV)
DG	120	44	197	121	313	232	281	236	279	150
D1S	191	104	163	129	539	923	596	861	329	279
D2	306	155	284	143	491	564	769	529	384	237

Table IV.2 – Same as in Table IV.1, but for each isotopic chain.

interactions. On the opposite, DG does not exhibit such pathologies since the absolute differences are always lower than 1 MeV, as indicated in panel (a) of Figure IV.2. For ^{30}Si, ^{30}S and ^{32}S, they are respectively 234 keV, 97 keV and −482 keV. Note however that ^{28}Si which was well reproduced by D1S and D2 interactions, with differences of 150 keV and 221 keV, is less by DG as the difference becomes −666 keV. [1] Therefore, DG seems to cure (or at least considerably reduce) the overestimated first excitation energies of ^{30}Si, ^{30}S and ^{32}S isotopes by lowering them to values of the order of those found in nuclei of approximately the same mass. [2] This is confirmed in Table IV.2 as the mean values of Si and S are more reasonable with DG, and of the order of that of Ar isotopes, even if their standard deviations remain the highest. This phenomenon cannot be assigned to some kind of long-range correlations as one could have assumed for an analysis based on HFB results, for instance, because they are all taken into account in the MPMH procedure. In the next subsection, we discuss a more fundamental interpretation, based on an interplay between spin–orbit and tensor effects.

Finally, we remind that the excitation energies evaluated in this section were obtained without solving the second MPMH equation (IV.9b) ensuring the full self-consistency. In a recent article [19], a comparison of the outputs with and without considering the full self-consistency for the D1S interaction evinced that the general trend was maintained when switching on the resolution of the second equation, but that the overall agreement with experiment was substantially improved. In particular, the excitations energies were corrected up to 600 keV for the nuclei ^{30}Si and ^{30}S in which the reproduction was the less satisfying. There are then good chance that the restoration of self-consistency in a subsequent study generates even better MPMH predictions.

2.2. Interplay between spin–orbit and tensor interactions

As presented in the previous chapter (see subsection III.2), the tensor effects are most pronounced for nuclei in which the low spin-partner states are completely filled while their higher spin-partner states are empty, according to Ostuka's picture. In the *sd* shell, this situation corresponds to the proton and neutron states $1d_{5/2}$ filled with six particles and their proton and neutron spin partner states $1d_{3/2}$ empty, as illustrated in Figure III.3. Isotopes ^{30}Si, ^{30}S and ^{32}S whose first excitation energies are overestimated by D1S and D2 interactions are remarkably enough all of this sort. Then there are reasons to believe that these discrepancies are in particular due to the lack of a tensor force in the D1S and

1. This is not an actual devil nucleus, as shown in subsection IV.2.4.
2. Actually, in ^{30}Si and ^{30}S, not only the 2_1^+ state is overestimated, but also the higher 4_1^+ and 6_1^+ states with D1S and D2 interactions. This led the authors of [19] to characterize this effect as a "monopole shift", in analogy with a similar phenomenon observed in shell-model calculations.

D2 analytical expressions.

To get some insight, we have first plotted the proton and neutron SPEs of Si and S isotopes at the HF approximation in Figure IV.3. Note that for open-shell isotopes, we have considered the equal filling approximation. In panel (a), we see that the $(1d_{5/2})_\pi$ and $(2s_{1/2})_\pi$ states are not very different from one interaction to another, while the DG $(1d_{3/2})_\pi$ state starts to slightly move downwards from $N = 12$ to $N = 16$, with respect to those of D1S and D2, thus reducing the $(2s_{1/2} - 1d_{3/2})_\pi$ gap. On the neutron side, the $(1d_{5/2})_\nu$ and $(1d_{3/2})_\nu$ states get closer with DG than with D1S and D2 interactions in panel (b). This convergence of neutron levels appears stronger than the decline of the proton $(1d_{3/2})_\pi$ state and is not restricted to some specific isotopes. The exact same tendency is observed with S isotopes in panels (c) and (d). In that sense, it appears that the diminishing of the $(1d_{5/2})_\pi$ state is believably largely due to the tensor force since it is dominant in $N = 14$ and $N = 16$ isotopes. On the other hand, as the lowering of the difference $(1d_{5/2} - 1d_{3/2})_\nu$ is observed all along the isotopic chains, without isolated behaviors, it is rather a signature of the spin–orbit interaction. Indeed, as the $T = 1$ intensity of the spin–orbit term was decreased when going from $W_0 = 130\,\mathrm{MeVfm}^5$ with D1S and D2 interactions to $W_5 - H_5 = 115.849\,\mathrm{MeVfm}^5$ with DG, we expect the spin–orbit splitting to be lessened. Thus, it seems that for isotopes in which *both* proton and neutron gaps are shrunk, particle–hole excitations happen more likely and the energy needed to reach the first excited state is noticeably lowered. We highlight that the good reproduction of Si and S isotopes with DG is to us a *combination* of spin–orbit and tensor effects. If this was only due to the spin–orbit force, then we would expect a diminution of the excitations energies of all Si and S isotopes, which is not the case. If this was only a consequence of the tensor force, the small descent of $(1d_{3/2})_\pi$ would probably not be enough to lower the excitations energies by a few hundred keV, as we will see in the next paragraph. Besides, we have interpreted the overall better agreement of the excitation energies to be mainly due to the spin–orbit term; this also applies to Si and S isotopes.

In order to compare the energy gaps between orbitals predicted by the three interactions in the nuclei of interest, we have displayed the energy differences between proton and neutron SPEs in Table IV.3 for ^{28}Si, ^{30}Si, ^{30}S and ^{32}S isotopes. As explained qualitatively, we see that proton $(1d_{5/2} - 2s_{1/2})_\pi$ and neutron $(2s_{1/2} - 1d_{3/2})_\nu$ gaps for ^{30}Si are reduced in the case of DG, compared to D1S and D2. Whereas it is decreased by nearly 1 MeV in the proton sector when going from D1S to DG, it reduces further to 2 MeV in the neutron sector. In ^{30}S the effects are essentially the same on proton $(2s_{1/2} - 1d_{3/2})_\pi$ and neutron $(1d_{5/2} - 2s_{1/2})_\nu$ gaps, with a reduction of about 1 MeV for DG, with respect to D1S. Finally, in ^{32}S the proton $(2s_{1/2} - 1d_{3/2})_\pi$ and neutron $(2s_{1/2} - 1d_{3/2})_\nu$ gaps remain quite unchanged, with a neutron gap smaller by about 300 keV when going from D1S to DG. It is interesting that of these three isotopes, this latter is the one whose first excitation energy is the least well reproduced, and is also the only one to be underestimated. When looking at panel (c) in Figure IV.3, we observe that for ^{32}S the descent of $(1d_{3/2})_\pi$ with DG (considered as a consequence of the tensor force) is somewhat compensated by the ascent of $(2s_{1/2})_\pi$ with D1S, such that both interactions predict similar proton gaps. As the spin–orbit and tensor forces are not expected to act on s states at first approximation, the higher $(2s_{1/2})_\pi$ states of D1S and D2 compared to DG should be of another nature. Perhaps this is attributable to the central and density-dependent terms of DG, which are a bit different from those of its counterparts. In general, we notice that the shrinking of the neutron energy gaps is often quantitatively significant when going from D1S to DG. For this reason, the spin–orbit term which we assume to be mainly responsible for it must

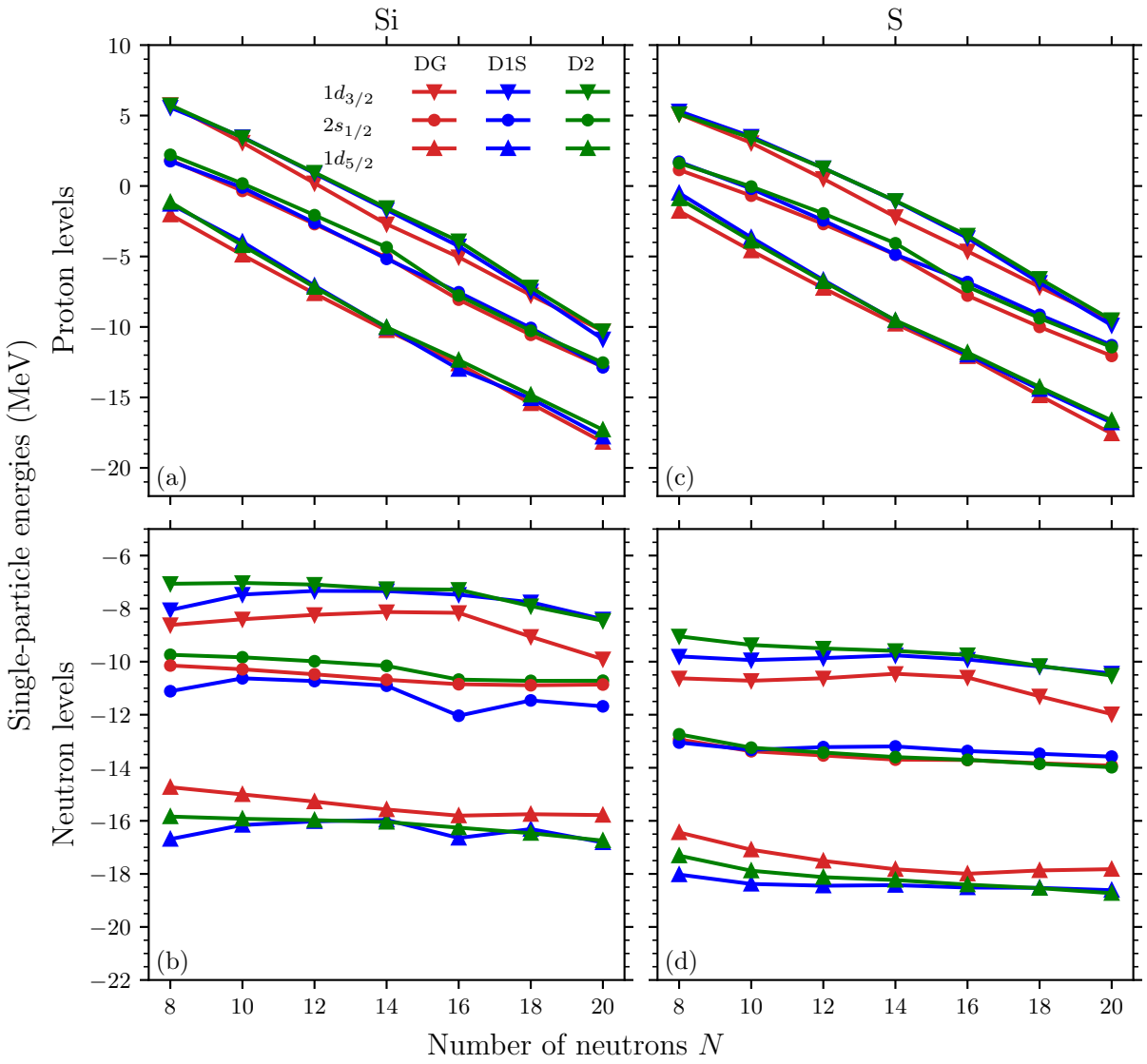

Figure IV.3 – Single-particle energies of the *sd* shell along Si (left panels) and S (right panels) isotopic chains, for proton (upper panels) and neutron (lower panels) levels. Results are given for DG, D1S and D2 interactions.

be considered when dealing with SPEs of Si and S isotopes.

We close this subsection by discussing the relative contributions of the particle-like and proton–neutron components of the tensor force to the effects we have underlined. According to Ostuka's picture, this proton–neutron component is maximal when both proton–proton and neutron–neutron contributions are. With the example of ^{32}S, we indeed see that neutron and proton $1d_{5/2}$ states are full such that particle-like contributions of the tensor force between $(1d_{5/2})_\pi$ and $(1d_{3/2})_\pi$ states as well as between $(1d_{5/2})_\nu$ and $(1d_{3/2})_\nu$ are maximum. At the same time, attraction between $(1d_{5/2})_\pi$ and $(1d_{3/2})_\nu$ as well as between $(1d_{5/2})_\nu$ and $(1d_{3/2})_\pi$ is also maximum. It is therefore not possible to isolate particle-like and proton–neutron contributions of the tensor interaction with this type of nuclei. However, we can do so if we focus on mirror nuclei ^{22}Si and ^{22}O whose SPEs are shown in Figures IV.3 and IV.4. In ^{22}Si, no neutron–neutron tensor interaction is expected since the neutron *sd* shell is empty, and the lower spin-partner states completely filled. On the other side, the proton–proton and proton–neutron tensor interactions between

Interaction	$(1d_{5/2}-2s_{1/2})_\pi$ (MeV)	$(2s_{1/2}-1d_{3/2})_\pi$ (MeV)	$(1d_{5/2}-2s_{1/2})_\nu$ (MeV)	$(2s_{1/2}-1d_{3/2})_\nu$ (MeV)
		^{28}Si		
DG	5.173	2.370	4.891	2.554
D1S	4.877	3.484	5.058	3.568
D2	5.671	2.799	5.887	2.898
		^{30}Si		
DG	4.547	3.021	4.955	2.691
D1S	5.457	3.267	4.608	4.563
D2	4.579	3.865	5.581	3.389
		^{30}S		
DG	4.918	2.679	4.132	3.238
D1S	4.694	3.793	5.229	3.433
D2	5.470	3.016	4.636	4.003
		^{32}S		
DG	4.320	3.144	4.288	3.111
D1S	5.161	3.131	5.147	3.450
D2	4.671	3.638	4.704	3.951

Table IV.3 – Proton and neutron energy gaps of ^{28}Si, ^{30}Si, ^{30}S and ^{32}S isotopes predicted by DG, D1S and D2 interactions at the HF approximation.

$(1d_{5/2})_\pi$, which is full, and the empty $(1d_{3/2})_\nu$ and $(1d_{3/2})_\pi$ states should be important. Actually the state $(1d_{3/2})_\pi$ is almost not impacted, going from 5.568 MeV with D1S, to 5.760 MeV with DG. On the contrary, the state $(1d_{3/2})_\nu$ is significantly lowered, from -7.339 MeV to -8.128 MeV, when going from D1S to DG. The roles of neutrons and protons are reversed for ^{22}O. We see that $(1d_{3/2})_\pi$ is notably lowered, from -4.226 MeV to -5.171 MeV, while $(1d_{3/2})_\nu$ remains quite unchanged, going from 1.016 MeV to 1.040 MeV, with D1S and DG interactions, respectively.

It appears, based on Otsuka's picture, that the proton–neutron contribution of our tensor interaction has more prominent effects on SPEs (and then on excitation energies) than the particle-like ones. This may be related to the additional $T = 0$ pairing TBMEs we have constrained in the fitting code of DG (see subsection II.1.2.2). In fact, previous studies [19, 216] suggested that the uncontrolled $T = 0$ matrix elements could be associated with shifts in the excitation energy spectra, as we have observed in the first excitation energies of some Si and S isotopes with D1S and D2. It seems that the control of the $T = 0$ channel with the addition of the proton–neutron component of the tensor force (together with the spin–orbit interaction) regulates this channel and predicts more reasonable excitation energies for ^{30}Si, ^{30}S and ^{32}S nuclei. This argument is in qualitative agreement with Otsuka's analysis where the monopole tensor force in the $T = 0$ channel is three times stronger than in the $T = 1$ channel (see equation (III.56)). Finally since we are dealing with even–even nuclei so far, we can separate particle-like from proton–neutron contributions of the tensor interaction as we have done in (I.62). We find that the particle-like and proton–neutron intensities are respectively given by $W_7 - H_7 = -196.063$ MeV and $H_7 = 196.481$ MeV, with the interaction DG. This proximity in the magnitude of the

intensities hints that the effects described here are not specific to the values attributed to W_7 and H_7 in the fitting process. The proton–neutron contribution of the tensor force is stronger than the particle-like one, as expected.

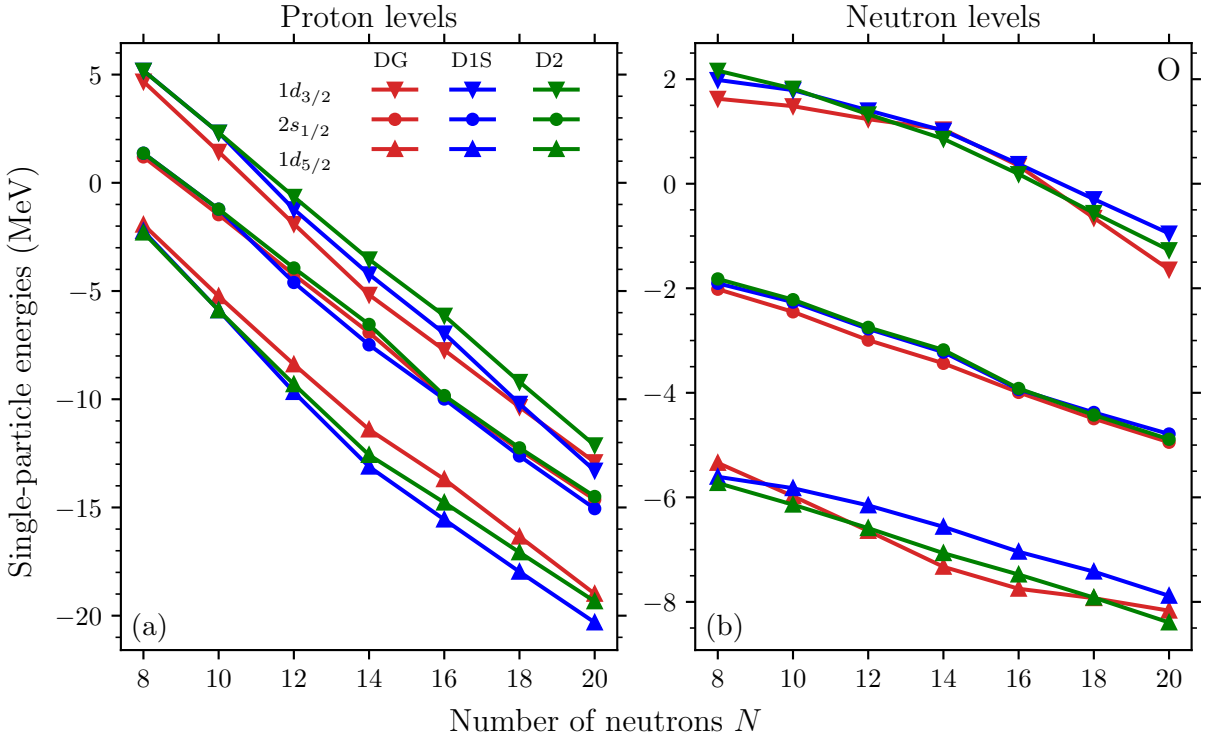

Figure IV.4 – Same as in Figure IV.3, but for the O isotopic chain with proton (left panel) and neutron (right panel) levels.

2.3. Multiparticle–multihole excitations

We now would like to provide more information on how the nucleons are distributed in the *sd* subshells from one interaction to another, and how their migration from the ground to the first excited state translates.

2.3.1. Occupation of the ground and first excited states

Ground state

We start by looking at the occupation of the ground states 0^+ in the Si and S isotopic chains. In Figure IV.5 is represented the average number of protons (left panels) and neutrons (right panels) in the single-particle states composing the ground state, as a function of the neutron number N, of Si isotopes, for DG, D1S and D2 interactions. The same quantities are displayed for the S isotopic chain in Figure IV.6.

In the proton sector of Figure IV.5 (left panels), we observe that the six protons of the *sd* shell are mainly occupying the lowest state $1d_{5/2}$ for all three interactions in ^{24}Si, as expected. As the number of neutrons increases, though, this state is gradually depopulated in favor of the higher $2s_{1/2}$ state, and to a lesser extent, in the favor of the highest $1d_{3/2}$ state. More precisely, this phenomenon is specifically marked from isotopes $N = 12$ to $N = 16$ and then fades away. On the other hand, it predominates with the

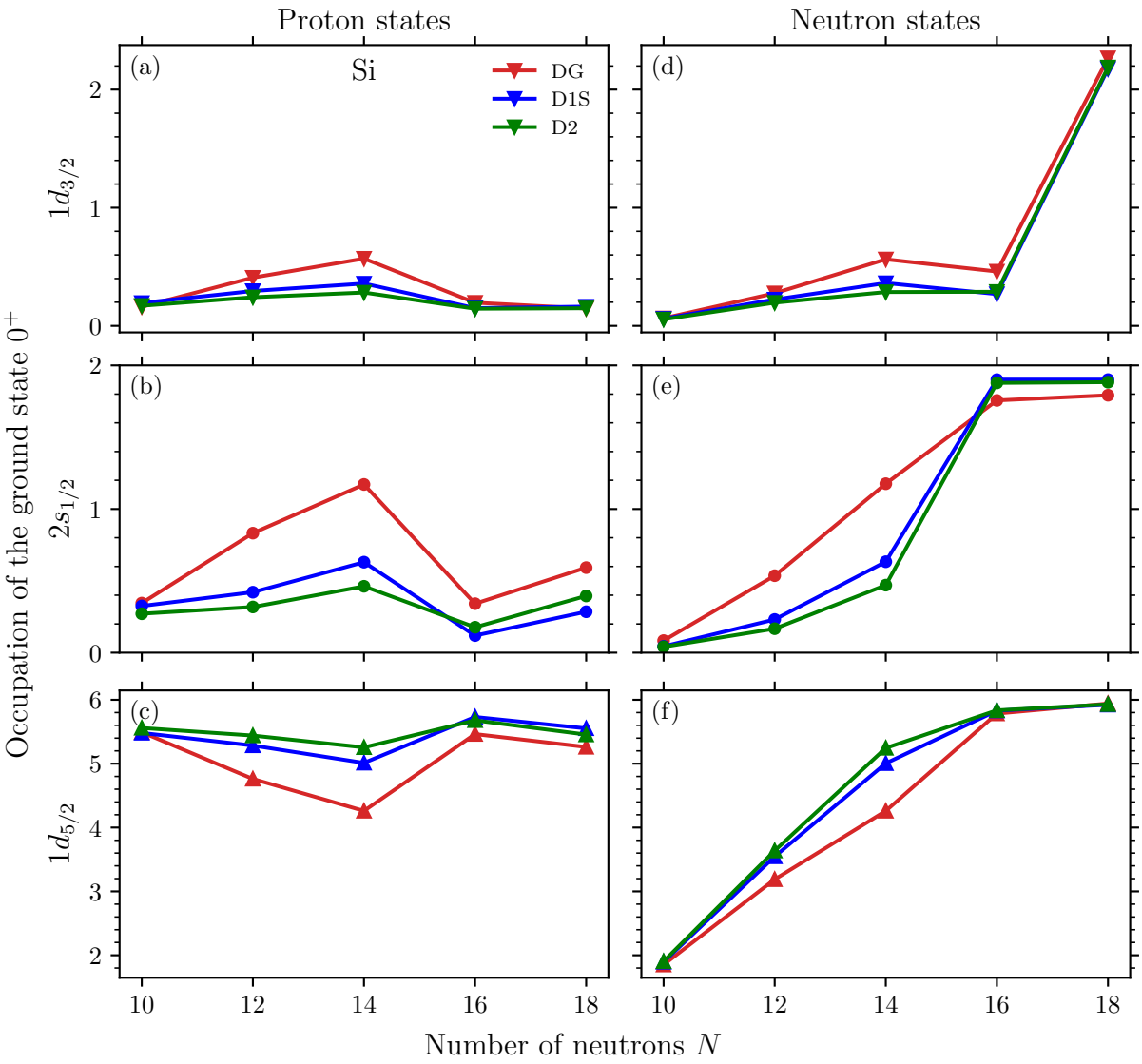

Figure IV.5 – Occupation of the ground states 0^+ of Si isotopes defined as the number of protons (left panels) and neutrons (right panels) filling the *sd* subshells, namely the $1d_{5/2}$ (lower panels), $2s_{1/2}$ (middle panels) and $1d_{3/2}$ (upper panels) levels.

DG interaction, compared to D1S and D2. In ^{30}Si for instance, 0.341 and 0.196 protons are filling the respective $2s_{1/2}$ and $1d_{3/2}$ states with DG, against 0.150 and 0.119 protons in those same states with D1S. These differences are readily understandable when we compare the proton gaps $(1d_{5/2} - 2s_{1/2})$ and $(2s_{1/2} - 1d_{3/2})$ provided in Table IV.3 of the DG and D1S interactions for this isotope. They are indeed about 900 keV and 250 keV larger with D1S, respectively, so that proton excitations from $1d_{5/2}$ towards higher states are less likely with D1S than are with DG. This effect being particularly pronounced for ^{28}Si and ^{30}Si isotopes, i.e. when the tensor force acts strongly, we have reasons to believe that this latter is to a great extent responsible for it. Let us note that the number of protons is fixed here so that, according to Ostuka's picture, the filling of $(1d_{5/2})_\nu$ causes the lowering of $(1d_{3/2})_\pi$ and allows protons to reach the top state more easily, as observed. This confirms the importance of the proton–neutron contribution of the tensor force in the arrangement of single-particle levels.

In the neutron sector (right panels), we see in panel (f) that the state $1d_{5/2}$ is progres-

sively populated as the number of neutrons increases. Again, DG stands out because the occupation of $1d_{5/2}$ and $2s_{1/2}$ states are reduced to the benefit of the higher $1d_{3/2}$ state from $N = 12$ to $N = 16$ isotopes. In ^{30}Si for example, 1.756 and 0.460 neutrons are filling the respective $2s_{1/2}$ and $1d_{3/2}$ states with DG, against 1.901 and 0.269 neutrons in those same states with D1S. We notice here that neutrons from both $1d_{5/2}$ and $2s_{1/2}$ states are jumping towards $1d_{3/2}$. Like before, this is explained by the shrinking of the neutron gap $(2s_{1/2} - 1d_{3/2})$ of about 1.9 MeV when going from D1S to DG interactions. Note by the way that the reduction of the proton gaps for this nucleus was not as strong as this one, as shown in the previous paragraph. Finally, for heavier isotopes, the tensor effects become less visible as the highest state starts to fill up.

We notice that the analysis we have just carried out for Si isotopes can be extended to the S isotopic chain of Figure IV.6. Keeping in mind that the proton $2s_{1/2}$ state is now filled, the exact same remarks can be made. The migration of nucleons towards higher states is in particular pronounced from $N = 12$ to $N = 16$ isotopes, for the reasons we have discriminated. We do not repeat the study and let the reader see that the trends on both proton and neutron sides are similar.

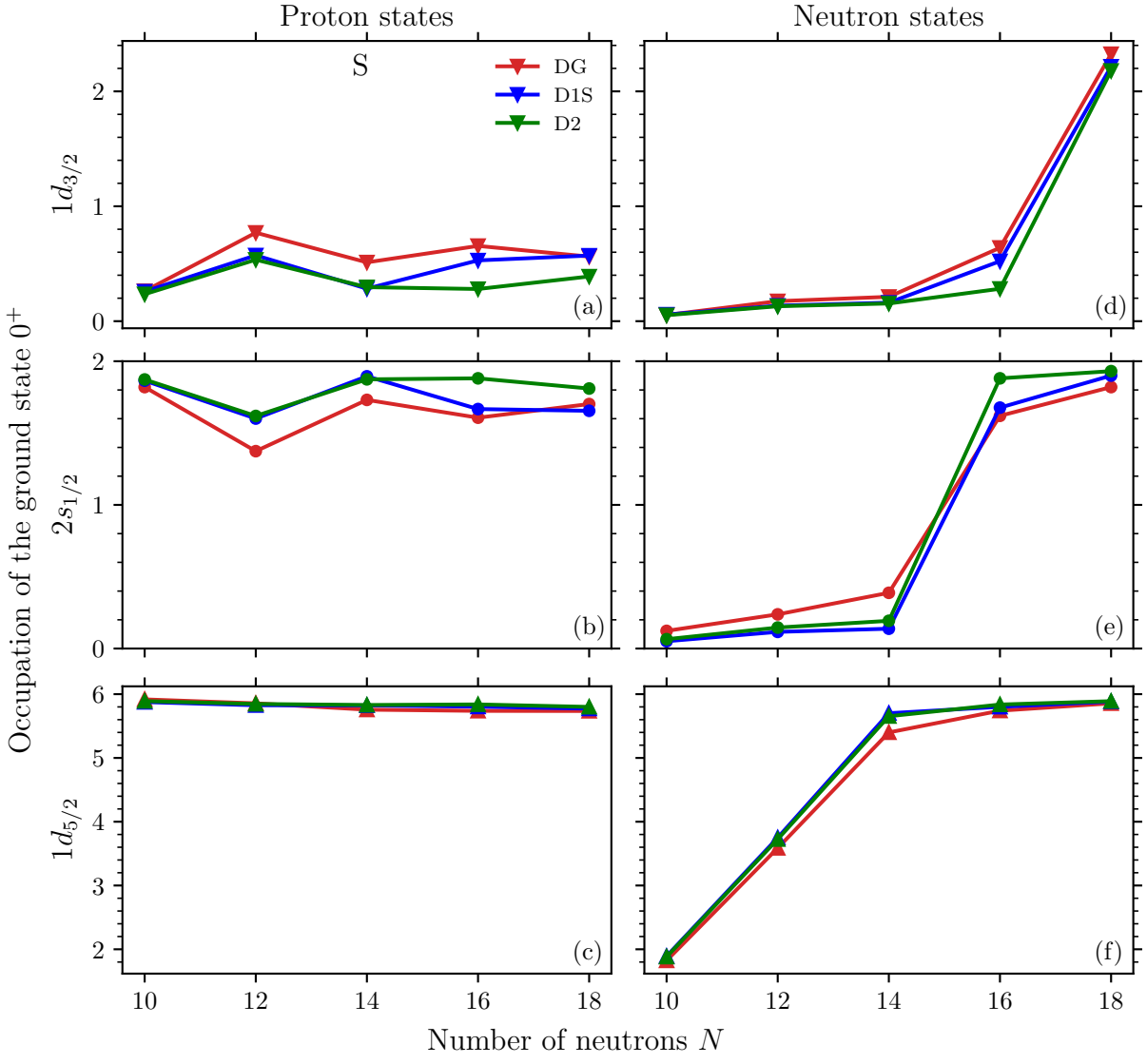

Figure IV.6 – Same as in Figure IV.5, but for the S isotopic chain.

First excited state

We now focus on the second purpose of this subsection, namely learning how the nucleons rearrange in the *sd* subshells in the first excited state, in comparison with the ground state. As in Figures IV.5 and IV.6, the occupations in terms of single-particle states for Si and S isotopes are shown in Figures IV.7 and IV.8, respectively, but now for the first excited state 2_1^+.

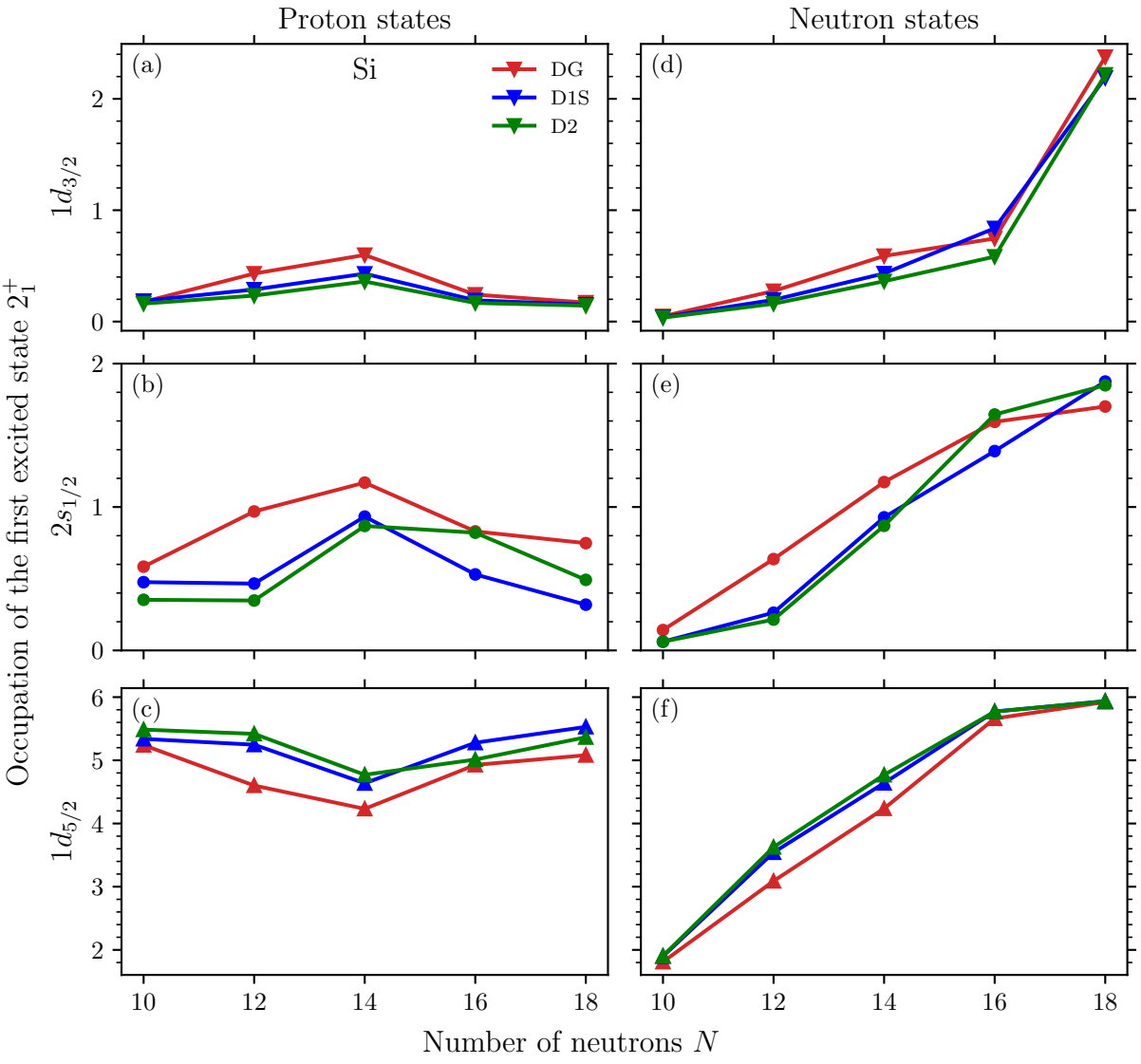

Figure IV.7 – Occupation of the first excited states 2_1^+ of Si isotopes defined as the number of protons (left panels) and neutrons (right panels) filling the *sd* subshells, namely the $1d_{5/2}$ (lower panels), $2s_{1/2}$ (middle panels) and $1d_{3/2}$ (upper panels) levels.

In Figure IV.7, we first notice that the peculiar behavior of the interaction DG, spotted in the ground state for isotopes from $N = 12$ to $N = 16$, remains present in the first excited state, in proton and neutron sectors. This is rather reassuring since our interpretation of the tensor effects based on energy gaps must also hold for first excited states we try to describe the physics of. In the proton sector (left panels), it turns out that the $2s_{1/2}$ and $1d_{3/2}$ states are globally more populated than the same levels in the ground state of Figure IV.5. Indeed, 0.830 and 0.242 protons (to be compared with the values 0.341 and 0.196 in the ground state) respectively occupy these states in ^{30}Si, with the DG interaction. On

the neutron side (right panels), particles also switch to higher energy states. In ^{30}Si, 0.746 neutrons (to be compared with the value 0.460 in the ground state) reach the $1d_{3/2}$ level with the DG interaction. The same pattern is observed with most of the other isotopes, be it with the DG, D1S or D2 interactions. We claim that this general phenomenon simply stems from the increment of energy brought to the system in the first excited state such that nucleons are more likely to spread to upper levels. This engenders strong variations in the structure of the MPMH wave function of the system, with breaking of pairs, as we are going to see.

Once again, the results obtained for Si isotopes can be transposed to S isotopes, displayed in Figure IV.8. The behavior of the interaction DG and the larger number of particles filling the highest *sd* subshells, with respect to the ground-state case, are maintained.

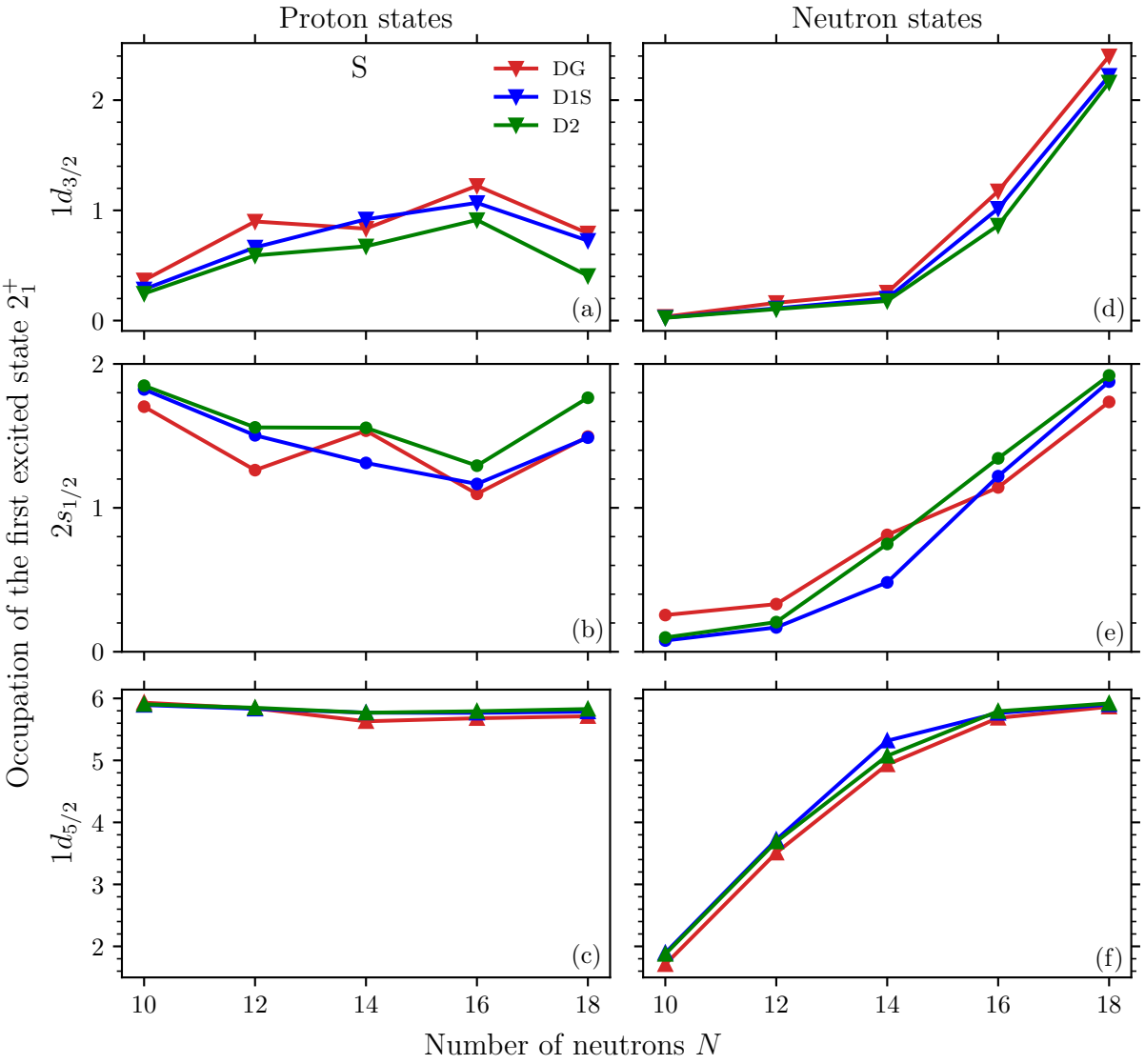

Figure IV.8 – Same as in Figure IV.7, but for the S isotopic chain.

2.3.2. Excitations of the wave function of the system

We recall that the MPMH wave function of the system $|\Phi\rangle$ is a superposition of weighted multiparticle–multihole excitations, characterized by an excitation order M, of an HF-type reference state (see first subsection). In order to determine which types of excitation are responsible for the distribution of nucleons in the *sd* subshells we have just described, and in what proportions, we represent the components of the MPMH wave function by means of bar charts. The decomposition is provided for closed-subshell nuclei ^{28}Si, ^{30}Si, ^{30}S and ^{32}S, with each DG, D1S and D2 interactions, and in both the ground state and the first excited state, as shown in Figures IV.9 and IV.10, respectively. Note that a limit of 12p–12h excitations is in force in the *sd* shell.

In Figure IV.9, generally speaking, the component $M = 0$ appears as the dominant contribution to the total ground-state wave function for all interactions and isotopes (except for the specific case of ^{28}Si for D1S and DG, we put aside and discuss in the next subsection). This component does not necessitate the displacement of nucleons towards the upper single-particle states, unlike $M \geq 1$ excitations, and is therefore energetically favorable. Then, as the excitation order grows, more and more nucleons are moved, which increases the energy cost and reduces the probability of such excitations. Let us point out that the proportion of the $M = 4$ component is always greater than that of $M = 3$. The $M = 3$ component needfully involves breaking a pair of nucleons, which turns out to be less likely than exciting two pairs of nucleons, corresponding to the main contribution of $M = 4$ excitations. We now concentrate on the changes occurring when going from D1S to DG interaction. We see that the portion of $M = 0$ components is systematically diminished to the benefit of excitations of higher orders, $M > 1$. For instance, in ^{30}Si, the components $M = 0, M = 2, M = 3$ and $M = 4$ respectively represent 58.9% (76.2%), 31.0% (20.3%), 3.8% (1.3%) and 5.2% (2.0%) of the ground-state wave function with DG (D1S) interaction, the $M = 1$ and $M > 4$ components being negligible. Actually this is explained by the smaller proton and neutron gaps of DG with respect to D1S (see Table IV.3). Since the gaps are shrunk, the collectivity of the wave function diversifies as more components of higher excitation orders, now energetically more favorable, come into play.

We now look at how the components of the wave function of the system rearrange in the first excited state 2_1^+ of Figure IV.10. We first mention that the $M = 0$ contribution vanishes identically as the low single-particle states are fully occupied, at the HF approximation, in the isotopes displayed. As a consequence, nucleons must shift towards higher states for the first excited state to gain energy. Overall, the same tendency is observed as in the ground state, the lowest component $M = 1$, corresponding to the pair-breaking mechanism, is preponderant and the higher excitation orders less represented. This time, it appears that the $M = 3$ component is always greater than the $M = 2$ component. As more energy is brought to the system in the first excited state than in the ground state, it seems that breaking a pair of nucleons is now more likely than exciting it. For the same reasons as in the ground state, the portion of the lowest $M = 1$ components is systematically reduced in favor of excitations of higher orders $M > 1$, when going from D1S to DG. For example, in ^{30}Si, the components $M = 1, M = 2, M = 3, M = 4$ and $M = 5$ respectively represent 58.5% (70.5%), 12.2% (8.6%), 21.4% (17.0%), 5.2% (2.4%) and 2.3% (1.3%) of the ground-state wave function with DG (D1S) interaction, the $M > 5$ components being negligible. Compared with the ground state, this example illustrates that there are more high-order excitations in the first excited state. In particular, $M > 2$ excitations are much more represented; the wave function of the system exhibits more

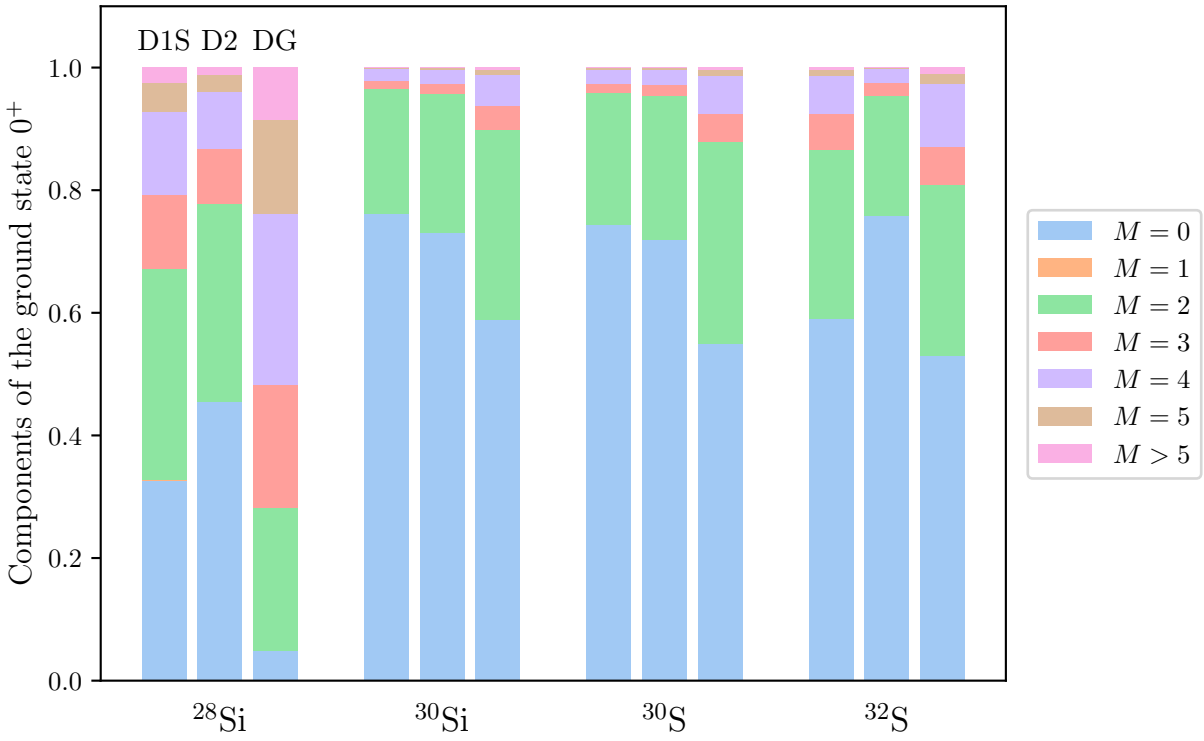

Figure IV.9 – Decomposition of the wave function of the system in the ground state 0^+ in terms of multiparticle–multihole excitations of order M. Results are shown for DG, D1S and D2 interactions in ^{28}Si, ^{30}Si, ^{30}S and ^{32}S isotopes.

collectivity in the first excited state than in the ground state. Again, this was expected as the increment of energy brought in the first excited state allows more sophisticated excitations to show up.

2.4. The case of ^{28}Si

Finally, we come to the case of ^{28}Si, whose first excitation energy predicted by DG is the furthest from the experimental value in *sd* shell, with an underestimation of 666 keV. We try to give some clues as to why, of the four isotopes is the *sd* shell in which the tensor force plays an important role, only this nucleus presents such a mismatch.

First, we recall that taking full self-consistency into account in the MPMH procedure improves the overall agreement with experimental data. For D1S, we have said that it reduced of about 600 keV the overestimated first excitation energies of ^{30}Si and ^{30}S. We can then reasonably anticipate a better reproduction of ^{28}Si excitation energy with fully self-consistent calculations. Second, it is a bit surprising that this nucleus is so well reproduced with D1S and D2 interactions (with small overestimations of 150 keV and 221 keV, respectively) in the light of our physical interpretation based on a combination of spin–orbit and tensor effects, whereas the other isotopes ^{30}Si, ^{30}S and ^{32}S are not. We may assume that the physics of this nucleus is, exceptionally and involuntary, already caught in the central and density-dependent part of the D1S and D2 interactions. Consequently, the adjusted spin–orbit and tensor forces of the DG interaction, whose central and density-dependent part is not very different from that of the former interactions, may imply a double counting of alike effects. One might also be tempted to say that the intensity of

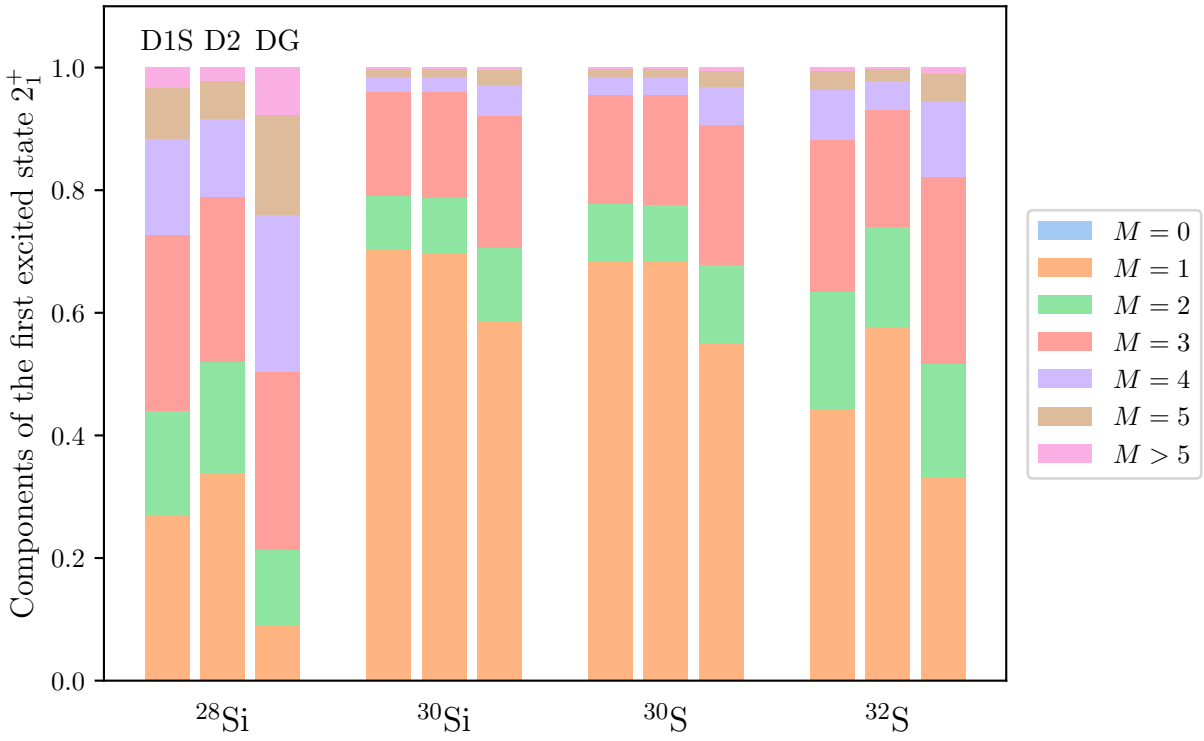

Figure IV.10 – Same as in Figure IV.9, but for the first excited state 2_1^+.

the spin–orbit or tensor terms is somewhat too strong, leading to an excessive drop in the excitation energy of ^{28}Si. However we have noticed that lowering these intensities would also raise the excitation energies of the other Si and S isotopes, ending up in worsening their good overall reproduction. Third, it seems that ^{28}Si presents complex spectroscopic properties. Indeed, Figures IV.5 and IV.7 show in particular that of all Si isotopes, ^{28}Si is the one showing the most distinctly a depletion of the $1d_{5/2}$ state for the higher proton and neutron states. The phenomenon is particularly striking for the DG interaction and $2s_{1/2}$ states. Yet, its associated proton $(1d_{5/2}-2s_{1/2})_\pi$ and neutron $(1d_{5/2}-2s_{1/2})_\nu$ gaps are not even smaller than those of its neighbors, as indicated in Table IV.3. To conclude we can also point out that according to Figures IV.9 and IV.10, this nucleus displays a pretty rich collectivity in its wave function, even more pronounced with the DG interaction. This might be the sign that uncommon processes occur in this $N = Z$ nucleus.

3. Odd nuclei in *sd* shell

3.1. Spin–parities

We continue by focusing on the same kind of results, but now for odd nuclei in the *sd* shell. In total, sixty odd nuclei belong to the *sd* shell, among which nine are unbound experimentally. These, namely ^{25}P, ^{25}S, ^{27}Cl, ^{29}Cl, ^{27}Ar, ^{29}Ar, ^{29}K, ^{31}K and ^{33}K, will then be discarded in our analysis. On top of them, ^{27}F and ^{29}Ne will not be considered either since, as negative-parity isotopes, their spectroscopy involve pf subshells we do not take into account here. We are finally left with forty-nine positive-parity odd nuclei in the *sd* shell. In odd nuclei, the density of states is known to be higher than in even–even nuclei at low energy. The consequence is that inversions between low-lying states predicted

theoretically may occur more frequently. To account for this effect with DG, D1S and D2 interactions, we compare in Figures IV.11 and IV.12 their predicted spin–parities in the ground state and first excited state, respectively, with experimental data, whenever they exist.

In Figure IV.11, we see that overall, all three interactions present a good reproduction of measured spin–parities in the ground state. We can be more quantitative thanks to Table IV.4, in which are shown the agreement rates with experiment for each spin–parity and globally, for DG, D1S and D2 interactions. On the left side, a global reproduction of more than 80% is reached for all three interactions in the ground state. Even though D2 appears to be better than DG, they are actually pretty similar as only four more nuclei out of forty-seven are correctly reproduced with D2. Predictions of the three interactions are identical with respect to $1/2^+$, DG is slightly better for $3/2^+$ and the real difference lies in the $5/2^+$ states which are degraded when going from D1S and D2 to DG. Lastly, we mention that the two nuclei whose experimental spin–parities are yet unknown (circles without surrounding squares) will not change this trend as the three interactions predict same results.

	Agreement rate (%)							
	Ground state				First excited state			
Interaction	$1/2^+$	$3/2^+$	$5/2^+$	Total	$1/2^+$	$3/2^+$	$5/2^+$	Total
DG	75.0	94.4	70.6	80.9	75.0	30.0	71.4	62.1
D1S	75.0	83.3	100.0	87.2	70.0	70.0	71.4	70.3
D2	75.0	88.9	100.0	89.4	70.0	50.0	71.4	64.9

Table IV.4 – Agreement rates with experiment in the prediction of spin–parities in the ground state (left side) and in the first excited state (right side), for DG, D1S and D2 interactions.

The overall reproduction of measured spin–parities in the first excited state is quite deteriorated compared to those of the ground state for all three interactions, as illustrated in Figure IV.12. This was expected since the level inversions already present in certain ground states are generally reflected in the associated first excited states, to which are added new inversions, related to the first excited state, in other nuclei. Even so, we observe on the right side of Table IV.4 a global reproduction of more than 60% for all three interactions in the first excited state. This time D1S appears as the best candidate, but only three nuclei out of thirty-seven make the difference with DG. With a 24.5% drop in the overall agreement rate compared to the ground state, D2 is the most impacted interaction. This drop is about 18.7% and 17.0% for DG and D1S interactions, respectively. When looking at separate spin–parities, it turns out that the reproduction is slenderly better with DG for $1/2^+$, equal with all interactions for $5/2^+$, but that the difference really manifests in $3/2^+$ states. Indeed, Figure IV.12 reveals that many experimentally measured $3/2^+$ states are actually predicted as $5/2^+$ states. This is particularly remarkable with interaction DG. Let us also note that no $7/2^+$ states are predicted by DG, contrary to D1S and D2 interactions, in accordance with available experimental data. Finally, it must be pointed out that experimental spin–parities related to first excited states of twelve nuclei are missing, and that some of them present different theoretical outputs with DG, D1S and D2. It is then not excluded that future data could change a

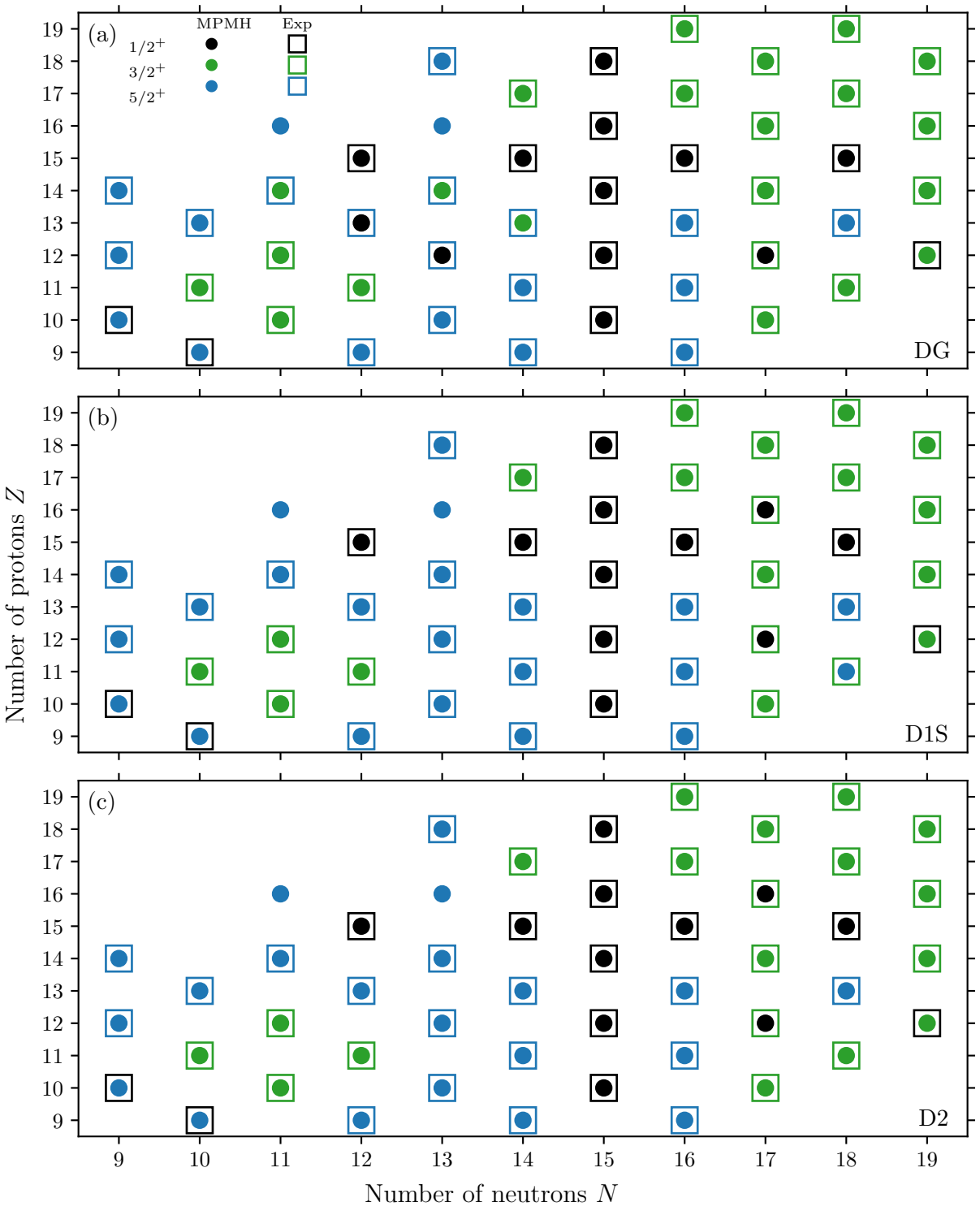

Figure IV.11 – Comparison between spin–parities $J^\pi \in \{1/2^+, 3/2^+, 5/2^+\}$ predicted by the MPMH method for DG (upper panel), D1S (middle panel) and D2 (lower panel) interactions and experimental data [202], in the ground state. MPMH and experimental results are represented by circles and squares, respectively.

bit the trend we have just described.

Now, we would like to have a better understanding on why some spin–parities are not properly reproduced by the three interactions. We suppose that the high density of

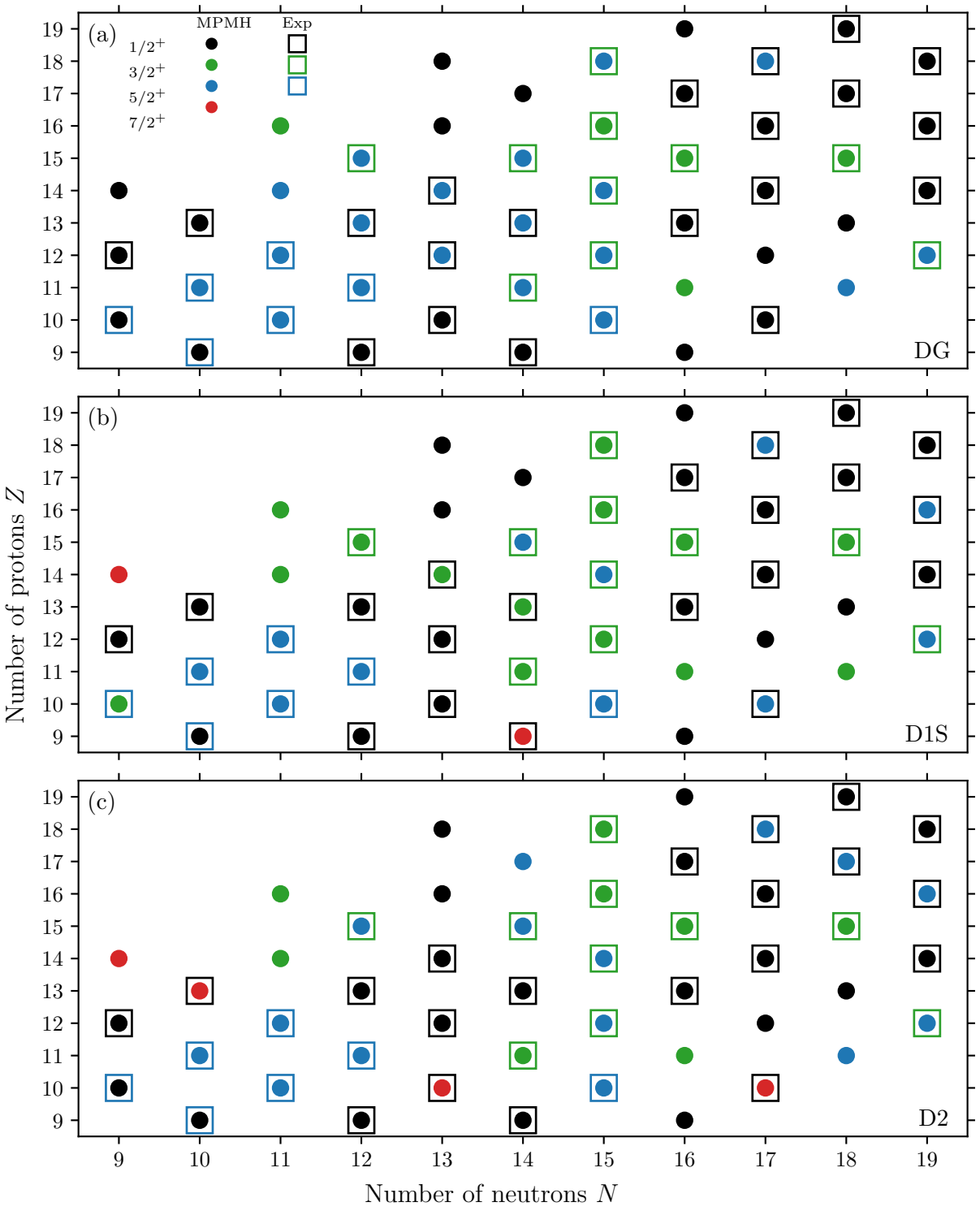

Figure IV.12 – Same as in Figure IV.11, but now for the first excited state. Spin–parities are here such that $J^\pi \in \{1/2^+, 3/2^+, 5/2^+, 7/2^+\}$.

states in odd nuclei at low density is responsible for it. Accordingly, some spin–parities would be wrongly assigned to ground and first excited states whereas the right associated state may be close by in energy. To get to the bottom of it, we have evaluated the energy difference between the ground state (as well as the first excited state) and the lowest state having the spin–parity measured experimentally, for all nuclei whose spin–parities do not

fit experimental data, with DG, D1S and D2 interactions. The resulting mean values, together with standard deviations, evaluated by means of relations (IV.15), are displayed in Table IV.5.

	Ground state		First excited state	
Interaction	$\langle\Delta\mathcal{E}\rangle$ (MeV)	$\sigma(\Delta\mathcal{E})$ (MeV)	$\langle\Delta\mathcal{E}\rangle$ (MeV)	$\sigma(\Delta\mathcal{E})$ (MeV)
DG	0.597	0.737	0.520	0.426
D1S	1.214	1.088	0.515	0.440
D2	1.684	0.780	0.553	0.446

Table IV.5 – Mean values and standard deviations of the theoretical energy difference $\Delta\mathcal{E}$ between ground states (left side) or first excited states (right side) and the lowest states whose spin–parities are those of experimental measurements, for DG, D1S and D2 interactions.

In the ground state (left side of the table), the mean difference is about 600 keV for DG, which means that, on average, the state showing the spin–parity determined from experiment is not that far from the one this spin–parity has been attributed to by the MPMH method (for nuclei whose spin–parities does not match experimental values). It is more litigious with D1S and D2 since the gap with experiment widens. We should nonetheless bear in mind that fewer spin–parities are incorrectly reproduced by these interactions, so these mean values would drop if we took into account the spin–parities they faithfully reproduce while DG does not. We also underline that the standard deviations are relatively important; some differences are very low and then not expected to be handled by these interactions, while others are rather strong and then more embarrassing. In the first excited state (right side of the table), the mean differences are about 500 keV for all three interactions, with lower standard deviations. Consequently, although agreement rates are lower in the first excited states than in the ground states, this is not problematic at this stage. Indeed, the related level inversions are hardly avoidable since they involve fine spectroscopic effects these interactions are not meant to perfectly account for. Gogny interactions have been fitted and mainly tested on even–even nuclei so far. It is accordingly not so surprising that results for odd nuclei exhibit some limitations. Moreover, the full self-consistency should be considered before making definite conclusions, as it is supposed to refine the results.

3.2. First excitation energies

We now turn into the calculation of the difference between the excitation energies of the first excited state evaluated by the MPMH method and experimentally, which is defined as

$$\Delta\mathcal{E}_{\text{MPMH}}[J^\pi] \equiv \mathcal{E}_{\text{MPMH}}[J^\pi] - \mathcal{E}_{\text{exp}}[J^\pi], \tag{IV.16}$$

where $\mathcal{E}_{\text{MPMH}}[J^\pi]$ and $\mathcal{E}_{\text{exp}}[J^\pi]$ respectively denote the excitation energies, of spin–parity J^π, of the first excited state evaluated by the MPMH method and from experiment [202]. Note that among the forty-nine odd nuclei we have retained, the first excitation energies of thirty-seven of them are known experimentally. In the light of our discussion from previous subsection, the theoretical excitation energies $\mathcal{E}_{\text{MPMH}}[J^\pi]$ of those nuclei are

associated with the first state showing the spin–parity measured experimentally. The results are presented in Figure IV.13 for DG, D1S and D2 interactions.

In contrast to even–even nuclei, the results appear more nuanced between interactions for odd nuclei. With D1S and D2, the excitation energies of certain nuclei are particularly overestimated, which is not the case with DG interaction. Quantitatively, Table IV.6 displays the mean values and standard deviations as defined in (IV.15), for each appearing spin–parity and in total. Our observations are confirmed since MPMH results are the greatest with DG. In particular, the mean difference is almost half that of D1S and the standard deviation less than half of it. As for D2, its mean value is relatively important but its standard deviation approximately that of D1S. The same hierarchy can be set up in each type of spin–parity states. Mean values and standard deviations are always the lowest with DG, especially for $1/2^+$ and $3/2^+$ states in which the outputs are remarkably improved with respect to D1S and D2. On the contrary, D2 shows important discrepancies with experiment in these states. For this reason, we will preferably compare the results brought by DG with those of D1S to highlight its advantages with respect to the reliable interaction we have at hand (between D1S and D2). Because this effect is *global*, we tend to identify the spin–orbit force as being mainly responsible for it. The complete justification follows that exposed in subsection IV.2.1 for even–even nuclei. Here also, already at the level of the fitting process, we have noticed that the intensity of the spin–orbit term proper to D1S and D2 interactions was a bit too high to produce a good overall reproduction of excitations energies. By generating parametrizations of lower spin–orbit intensities, like DG, the outputs proved to be more pertinent.

	$1/2^+$		$3/2^+$		$5/2^+$		Total	
Interaction	$\langle x \rangle$ (keV)	$\sigma(x)$ (keV)	$\langle x \rangle$ (keV)	$\sigma(x)$ (keV)	$\langle x \rangle$ (keV)	$\sigma(x)$ (keV)	$\langle x \rangle$ (keV)	$\sigma(x)$ (keV)
DG	423	253	288	188	105	82	337	263
D1S	874	794	631	657	131	74	659	698
D2	1098	539	898	799	132	139	821	673

Table IV.6 – Mean values and standard deviations of the difference $x \equiv \Delta\mathcal{E}_{\text{MPMH}}[J^\pi]$, as defined in (IV.16), evaluated for each spin–parity $J^\pi \in \{1/2^+, 3/2^+, 5/2^+\}$ and globally, with DG, D1S and D2 interactions.

A closer look at Figure IV.13 unveils that the energy difference appreciably increases from $N = 14$ with D1S and D2 interactions. Interestingly, we have mentioned in the previous section that isotopes with neutrons in the region between $N = 14$ and $N = 16$ were specifically sensitive to the tensor force. It makes all the more sense that Si (red symbols) and S (green symbols) isotopes have excitation energies among the least well reproduced of all the nuclei belonging to this region, with both D1S and D2 interactions. In concrete terms, ^{29}Si and ^{31}Si are respectively overestimated by 1.640 MeV and 2.518 MeV with D1S. With D2, the disagreements reach by 1.862 MeV and 2.320 MeV for these two nuclei. On top of them, ^{31}S and ^{33}S, which were decently described by D1S with energy differences of 698 keV and 258 keV, are worsened with D2, with overestimations of 1.636 MeV and 1.357 MeV, respectively. Besides, we notice that beyond $N = 17$, two other Si and S isotopes, namely ^{33}Si and ^{35}S, exhibit also high energy differences, 1.806 MeV (1.624 MeV) and 1.112 MeV (1.801 MeV) with D1S (D2), respectively. Even if the tensor force in the neutron sector is not expected to be as strong as the one acting in $N = 13$ to $N = 17$ iso-

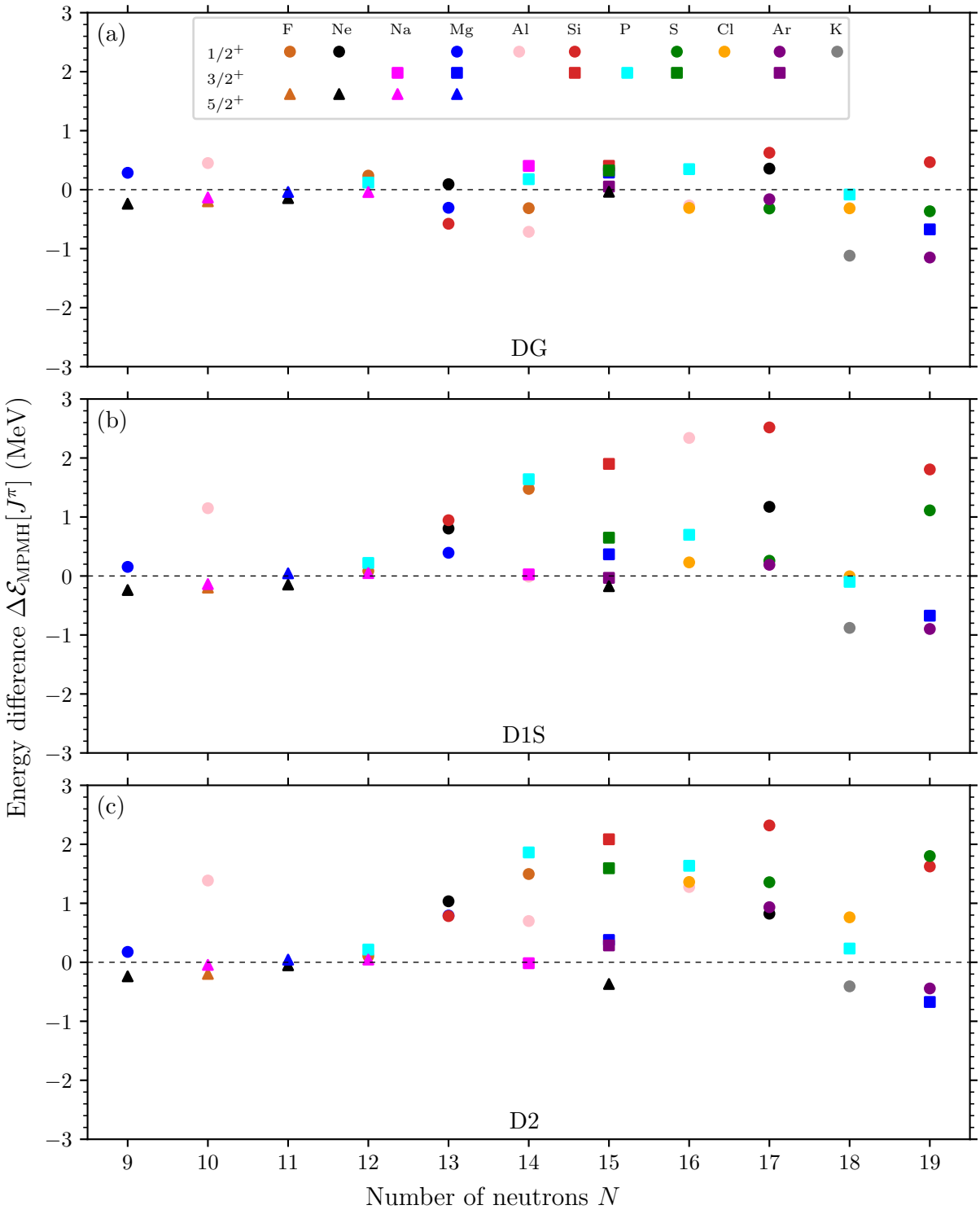

Figure IV.13 – Energy difference between the first excitation energies predicted by the MPMH and experimental data, expressed by (IV.16), as a function of the number of neutrons N. The results are shown for DG, D1S and D2 interactions, in panels (a), (b) and (c), respectively. Horizontal dashed lines display perfect agreement with experiment. The *sd*-shell isotopes studied are labelled by different colors and their spin–parities $J^\pi \in \{1/2^+, 3/2^+, 5/2^+\}$ by different shapes, as indicated in the legend.

topes, we shall discuss in the next subsection that the overall action of the tensor term may not be negligible. On the other hand, DG does not present such pathologies since the differences are always lower than 1 MeV, as indicated in panel (a). For ^{29}Si, ^{31}Si, ^{33}Si, ^{31}S, ^{33}S and ^{35}S, they are respectively 178 keV, 626 keV, 466 keV, 348 keV, −319 keV and −366 keV. Therefore, as for even–even Si and S isotopes, DG seems to cure (or at least notably reduce) the overestimated first excitation energies of odd Si and S isotopes. Note that we have commented on nuclei with an odd number of neutrons to make the link with the previous section; however the study also applies to nuclei with an odd number of protons.

Finally, we mention again that the restoration of the full self-consistency is supposed to make the agreement with experiment better. Unlike even–even nuclei, though, there have been no previous studies in odd nuclei to give us information on the order of magnitude of the correction to be expected.

3.3. Single-particle energies

We have detailed in previous subsection that ^{29}Si, ^{31}Si, ^{33}Si, ^{31}S, ^{33}S and ^{35}S isotopes are predicted with too high first excitation energies with either D1S or D2. In the same way as isotopes ^{28}Si, ^{30}Si, ^{30}S and ^{32}S discussed in subsection IV.2.2, this effect may be seen as an interplay between spin–orbit and tensor forces.

In order to ascertain that the analysis made for even–even nuclei still hold for their odd counterparts, we have represented in Figure IV.14 the proton and neutron SPEs of Si and S isotopes at the HF level, invoking the equal filling approximation. As expected, no particular behavior on SPEs stand out with odd Si and S isotopes. The results are qualitatively very similar to those of Figure IV.3 regarding the reduction of proton and neutron gaps when going from D1S to DG interactions. The general interpretation based on a combination of spin–orbit and tensor effects remains the same.

Table IV.7 allows us to be more precise by quantifying proton and neutron gaps for the Si and S isotopes we are interested in, with all three interactions. In ^{29}Si, proton $(2s_{1/2} - 1d_{3/2})_\pi$ and neutron $(2s_{1/2} - 1d_{3/2})_\nu$ gaps are both reduced by about 800 keV when going from D1S to DG, while only this neutron gap is significantly shrunk, by about 1.7 MeV and 2 MeV, in ^{31}Si and ^{33}Si, respectively. In ^{29}S, proton $(2s_{1/2} - 1d_{3/2})_\pi$ and neutron $(1d_{5/2} - 2s_{1/2})_\nu$ are respectively diminished by about 500 keV and 900 keV when going from D1S to DG. A reduction of the same order takes place in this neutron gap for ^{29}S whereas the proton gap $(1d_{5/2} - 2s_{1/2})_\pi$ is decreased by about 600 keV. Finally, only neutron gaps $(1d_{5/2} - 2s_{1/2})_\nu$ and $(2s_{1/2} - 1d_{3/2})_\nu$ are substantially modified with DG, showing a decline of about 1.1 MeV and 900 keV, respectively, with respect to D1S. These figures are interesting since they testimony the way the gaps are changed when the upper $(1d_{3/2})_\nu$ level starts to fill up. On the one hand, we notice, by comparing Tables IV.3 and IV.7, that the same kinds of gap reductions appear for ^{28}Si and ^{29}Si isotopes when going from D1S to DG. This pattern also shows up for ^{30}S and ^{31}Si isotopes. This was expected as we have designated the tensor force to justify, to some extent, the shrinking of the gaps. Here, as only (about) one additional neutron is filling the $(2s_{1/2})_\nu$ state in ^{29}Si and ^{31}Si, compared to ^{28}Si and ^{30}S, the tensor effects should roughly remain the same according to Otsuka's picture. On the other hand, between ^{30}Si and ^{31}Si, as well as between ^{32}S and ^{33}S, (about) one additional neutron lies in the $(1d_{3/2})_\nu$ state. As this spin-partner state is no longer empty, the intensity of the tensor force is supposed to fall in the associated nuclei. We observe that while both proton and neutron gaps of ^{30}Si and ^{32}S were *greatly* enlarged when going from D1S to DG, only neutron gaps are so for

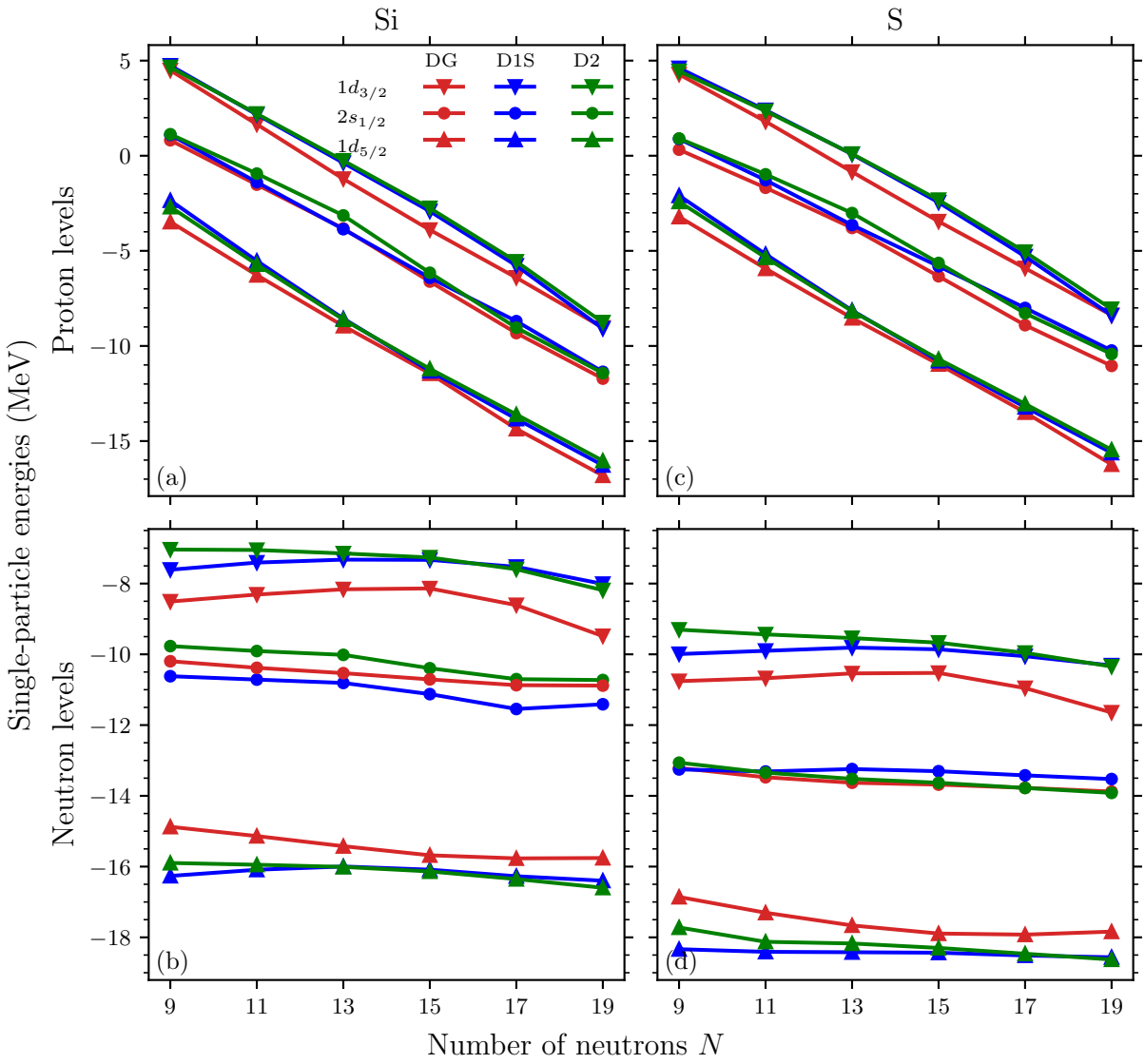

Figure IV.14 – Single-particle energies of the *sd* shell along Si (left panels) and S (right panels) isotopic chains, for proton (upper panels) and neutron (lower panels) levels. Results are given for DG, D1S and D2 interactions

^{31}Si and ^{33}S. Referring to Ostuka's interpretation, this phenomenon cannot be ascribed to the proton–proton contribution of the tensor force as it is unchanged within Si and S isotopes. However, the intensity of the proton–neutron contribution is diminished in ^{31}Si and ^{33}S with respect to ^{30}Si and ^{32}S because of the filling of the $(1d_{3/2})_\nu$ state. It then seems that the widening of the proton gaps for these isotopes are related to the proton–neutron component of the tensor force. This reasoning is supported by isotopes ^{33}Si and ^{35}S, in which the proton–neutron tensor force is expected to be even lower, as we see small proton gaps.

Obviously, our interpretation must be taken with a grain of salt. Indeed, if the effects were fully understandable within Otsuka's picture, we would observe a diminution of the neutron gaps between D1S and DG interactions when going from ^{30}Si to ^{31}Si and ^{33}Si, as well as from ^{31}S to ^{33}S and ^{35}S, since the intensity of the neutron–neutron tensor force is supposed to decrease. This is manifestly not the case. Second because all the terms making up the Gogny interactions participate in the description of SPEs. In particular, the

Interaction	$(1d_{5/2}-2s_{1/2})_\pi$ (MeV)	$(2s_{1/2}-1d_{3/2})_\pi$ (MeV)	$(1d_{5/2}-2s_{1/2})_\nu$ (MeV)	$(2s_{1/2}-1d_{3/2})_\nu$ (MeV)
		^{29}Si		
DG	4.832	2.718	4.971	2.572
D1S	4.902	3.498	4.962	3.795
D2	5.047	3.399	5.744	3.130
		^{31}Si		
DG	5.036	2.912	4.896	2.263
D1S	5.135	2.922	4.727	3.998
D2	4.560	3.476	5.651	3.107
		^{33}Si		
DG	5.096	2.679	4.873	1.399
D1S	4.908	2.273	4.987	3.402
D2	4.607	2.667	5.871	2.539
		^{31}S		
DG	4.625	2.883	4.209	3.157
D1S	4.976	3.358	5.130	3.446
D2	5.056	3.313	4.668	3.960
		^{33}S		
DG	4.584	2.994	4.150	2.818
D1S	5.209	2.709	5.091	3.368
D2	4.764	3.223	4.685	3.819
		^{35}S		
DG	5.182	2.664	3.960	2.233
D1S	5.377	1.850	5.037	3.212
D2	5.032	2.365	4.709	3.572

Table IV.7 – Proton and neutron energy gaps of ^{29}Si, ^{31}Si, ^{33}Si, ^{31}S, ^{33}S and ^{35}S isotopes predicted by DG, D1S and D2 interactions at the HF level employed with the equal filling approximation.

spin–orbit term, considered predominantly responsible for the overall better agreement of first excitation energies, cannot be discarded. Likewise, it is difficult to entirely attribute the displacement of the $1s_{1/2}$ states for DG, with respect to D1S and D2 interactions in Figure IV.14, to spin–orbit and tensor forces, since they are not supposed to act on it to first approximation.

3.4. Multiparticle–multihole excitations

We now reiterate the study carried out in subsection IV.2.3 on the locations of the nucleons within the *sd* subshells in the ground and first excited states, but now for odd nuclei. We begin by focusing on the occupation of the ground states for Si and S isotopic chains. In Figure IV.15 is displayed the average number of protons (left panels) and

neutrons (right panels) in the single-particle states constituting the ground state, as a function of the neutron number N, of Si isotopes, for DG, D1S and D2 interactions. The same quantities are represented for the S isotopic chain in Figure IV.16.

In Figure IV.15, generally speaking, we observe the same tendency in both proton and neutron sectors as that illustrated in Figure IV.5 for even–even isotopes. The increasing concentration of nucleons in the upper states $2s_{1/2}$ and $1d_{3/2}$, prominent with the interaction DG, prevails for isotopes with $N = 13$ and $N = 15$. This corroborates the same observation made for even–even isotopes with a number of neutrons ranging from $N = 12$ to $N = 16$.

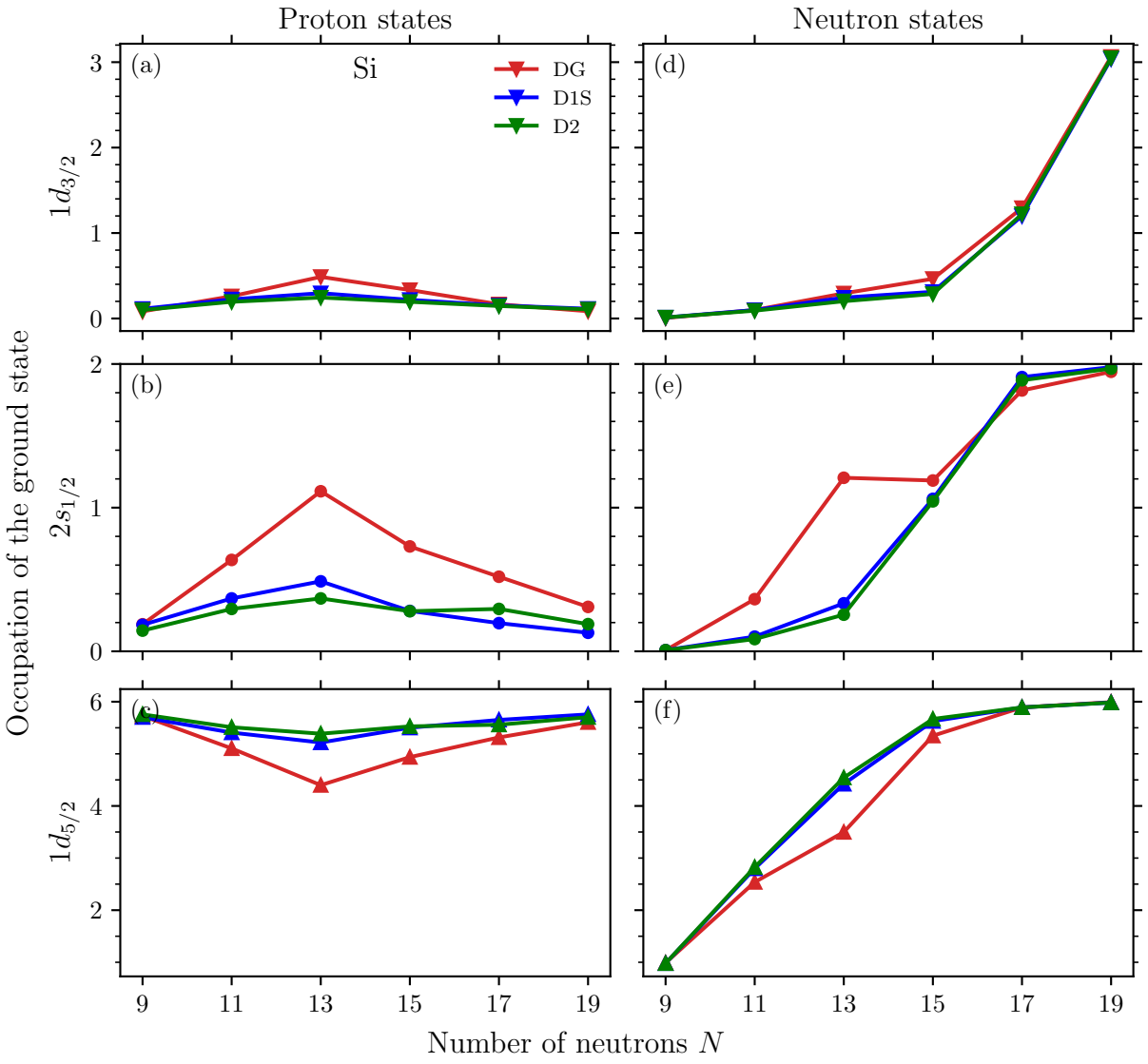

Figure IV.15 – Occupation of the ground states of Si isotopes defined as the number of proton (left panels) and neutrons (right panels) filling the *sd* subshells, namely the $1d_{5/2}$ (lower panels), $2s_{1/2}$ (middle panels) and $1d_{3/2}$ (upper panels) levels.

Now, let us point out some differences brought by odd isotopes. In the proton sector (left panels), for example, 0.730 and 0.333 protons are filling the respective $2s_{1/2}$ and $1d_{3/2}$ states of ^{29}Si with DG. In comparison, we have said that those same states were less occupied (0.341 and 0.196 protons, respectively) in ^{30}Si. It is difficult to draw conclusions based on the proton gaps of those isotopes as $(1d_{5/2} - 2s_{1/2})_\pi$ is slightly broader while

$(2s_{1/2}-1d_{3/2})_\pi$ slightly narrower for ^{29}Si, with respect to those of ^{30}Si. Nevertheless we are tempted to say that the single neutron *a priori* lying in the $(2s_{1/2})_\nu$ state of ^{29}Si has more chances to form a pair with a proton than when already paired to another neutron in ^{30}Si. Such proton–neutron pair can then scatter towards the upper states, explaining the higher occupations of $(2s_{1/2})_\pi$ and $(1d_{3/2})_\pi$ states in ^{29}Si. In the neutron sector (right panels) of ^{29}Si, 1.189 and 0.464 neutrons are located in the states $2s_{1/2}$ and $1d_{3/2}$, respectively. In ^{30}Si, we have found 1.756 and 0.460 neutrons in those same states. The fact that on average more neutrons fill the $2s_{1/2}$ state with ^{30}Si was predictable as this nucleus is by definition made up of one extra neutron. However, the reason why nearly the same number of neutrons occupy the highest level may be less on, given that their neutron gaps $(2s_{1/2}-1d_{3/2})_\nu$ are not so different (with the DG interaction). In fact, even though only one neutron is in $(2s_{1/2})_\nu$ with ^{29}Si, which then offers less possibilities to reach the $(1d_{5/2})_\nu$ than with two neutrons, the energy to supply is lower and this configuration more favorable.

Finally, we notice that for ^{33}Si, in which the tensor force is not supposed to be strong in the neutron sector, 0.309 (0.129) and 0.085 (0.114) protons as well as 1.946 (1.978) and 3.063 (3.038) neutrons sit in the respective $2s_{1/2}$ and $1d_{3/2}$ states, with DG (D1S) interactions. This fits the data of Table IV.7 as the proton gap $(2s_{1/2}-1d_{3/2})_\pi$ is much less reduced than the neutron gap $(2s_{1/2}-1d_{3/2})_\nu$ when going from D1S to DG, namely 400 keV versus 2 MeV. It means that the reduction of the neutron gap is principally responsible for the better reproduction of the first excitation energy of ^{33}Si with DG. This was quite unexpected.

For S isotopes as well, the migration of nucleons towards $2s_{1/2}$ and $1d_{3/2}$ states is important for $N = 13$ and $N = 15$, and is in particular marked for the interaction DG, as shown in Figure IV.16. By considering now two protons in the $2s_{1/2}$ state, the same type of remarks we have just made can be adjusted for odd S isotopes.

Let us eventually examine the occupation of the single-particle states for DG, D1S and D2, but now in the first excited state. The average number of nucleons filling $1d_{5/2}, 2s_{1/2}$ and $1d_{3/2}$ proton and neutron states along Si and S isotopic chains are given in Figures IV.17 and IV.18, respectively.

First of all, we notice in Figure IV.17 that the depletion of the lowest state to the benefit of the upper states in $N = 13$ and $N = 15$ isotopes is still in force in both proton and neutron sectors for Si nuclei. It should be noted, though, that it is less apparent in the transition from D1S to DG than it was for the ground state or even the first excited state in even–even isotopes (see Figure IV.7). In the same manner as in those latter, we also observe that the $2s_{1/2}$ and $1d_{3/2}$ levels are more populated in the first excited state than in the ground state, for the Si isotopes we have selected. Indeed, in ^{29}Si for instance, 0.958 and 0.369 protons (to be compared with the values 0.730 and 0.333 in the ground state) respectively stand in $2s_{1/2}$ and $1d_{3/2}$ states. On the other side, 1.511 and 0.505 neutrons (to be compared with the values 1.189 and 0.464 in the ground state) reach those same states in the neutron sector. In ^{30}Si, we recall that 0.830 and 0.242 protons as well as 1.594 and 0.746 neutrons occupy the corresponding $2s_{1/2}$ and $1d_{3/2}$ states. As more protons are in the upper subshells, our interpretation based on proton–neutron excitations in the ground state seems to hold here, in the first excited state. Complementarily, as more neutrons are filling the highest state for ^{30}Si, it appears that more excitations are related with the neutron pair than with the single neutron.

Once again, the results obtained for Si isotopes can be transposed to S isotopes.

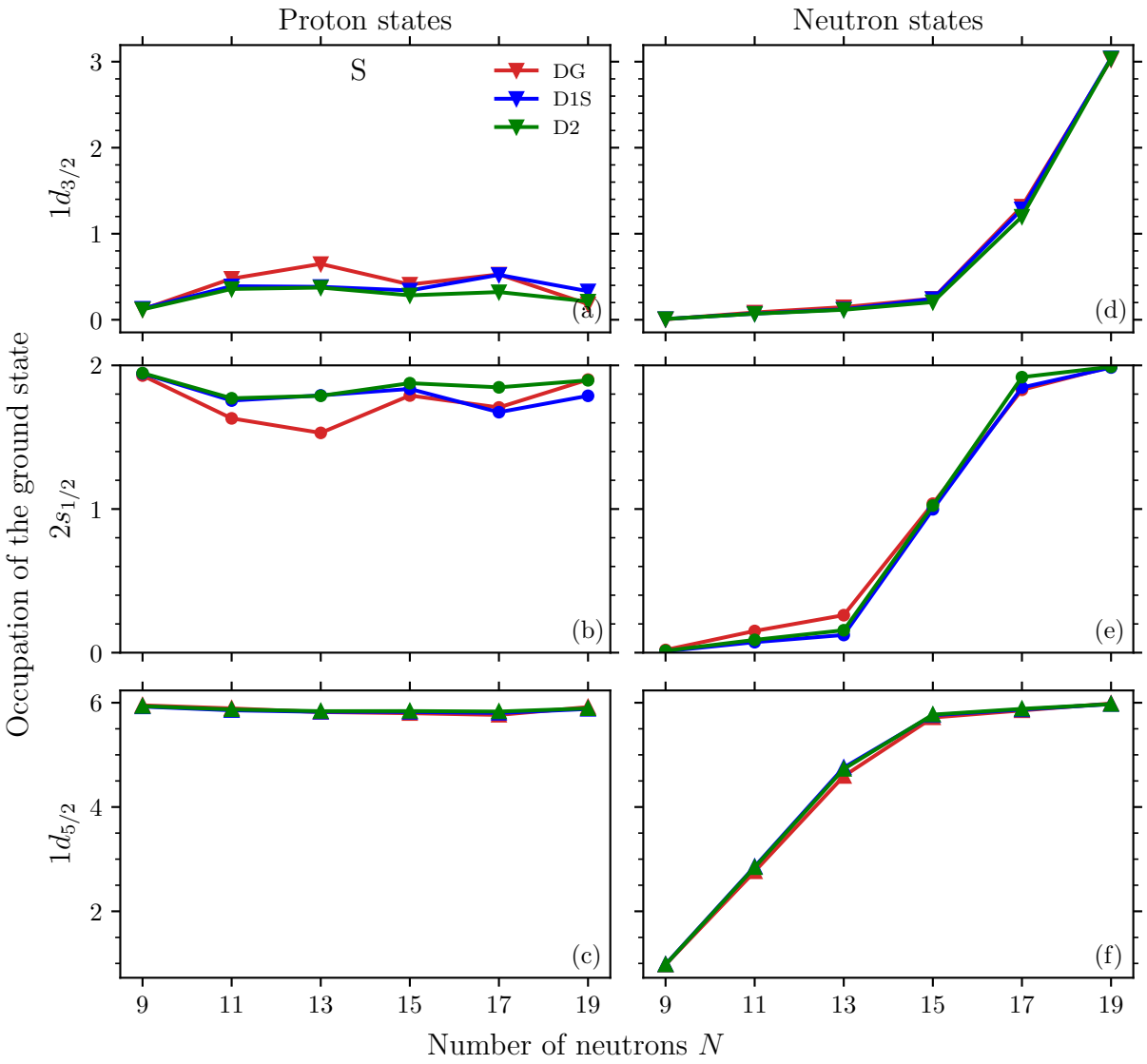

Figure IV.16 – Same as in Figure IV.15, but for the S isotopic chain.

Indeed, the general pattern we have just exposed is recovered for S isotopes, as displayed in Figure IV.18.

4. Odd–odd nuclei in *sd* shell

4.1. Spin–parities

We finally end our study of the MPMH spectroscopy in the *sd* shell with odd–odd nuclei. In total, thirty-six odd–odd nuclei belong to the *sd* shell, among which nine are unbound experimentally. These, namely ^{28}F, ^{24}P, ^{26}Cl, ^{28}Cl, ^{30}Cl, ^{28}K, ^{30}K, ^{32}K and ^{34}K, will then not be considered in the following. In odd–odd nuclei, the density of states at low energy is known to be even higher than in odd nuclei. Just like we have observed for odd nuclei, the spin–parity J^π of a given odd–odd nucleus measured from experiment consequently does not necessarily matches that predicted with the MPMH. The situation is illustrated in Figures IV.19 and IV.20 where the predicted spin–parities in the ground

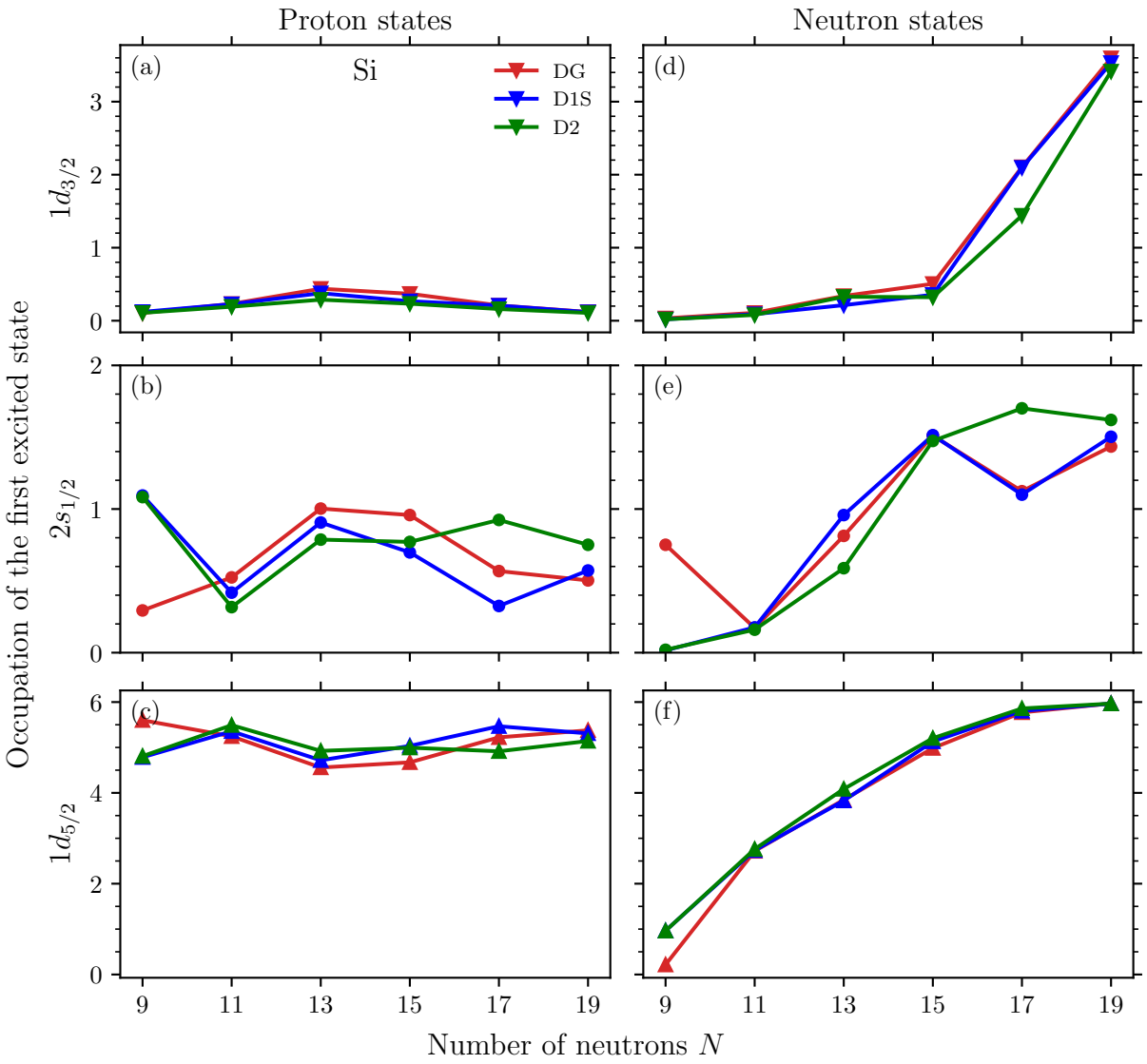

Figure IV.17 – Occupation of the Si isotopes first excited states defined as the number of proton (left panels) and neutrons (right panels) filling the *sd* subshells, namely the $1d_{5/2}$ (lower panels), $2s_{1/2}$ (middle panels) and $1d_{3/2}$ (upper panels) levels.

and first excited state, respectively, are compared with experimental data, when available.

In Figure IV.19, it appears that overall, the reproduction of measured spin–parities in the ground state is more mixed than in odd nuclei (see Figure IV.11). For D1S and D2 interactions, it seems slightly less good but for DG the damaging is pronounced. The precise agreement rates with experiment for DG, D1S and D2 interactions are listed in Table IV.8. Note that we have not distinguished the results by spin–parities as there are not enough cases for this to be relevant. We effectively see that the agreement in the ground state is mainly tarnished for DG, with less than one spin–parity in two correctly predicted. On the opposite, the agreement remains satisfactory for D1S and D2 interactions, with a reproduction of more than 75%.

In the first excited state, the general prediction of spin–parities is worsened compared to those of the ground state for all three interactions, as shown in Figure IV.20. As for odd nuclei, this phenomenon was expected since the mixing of low-energy levels observed in the ground states propagates in the associated first excited states, to which are added new

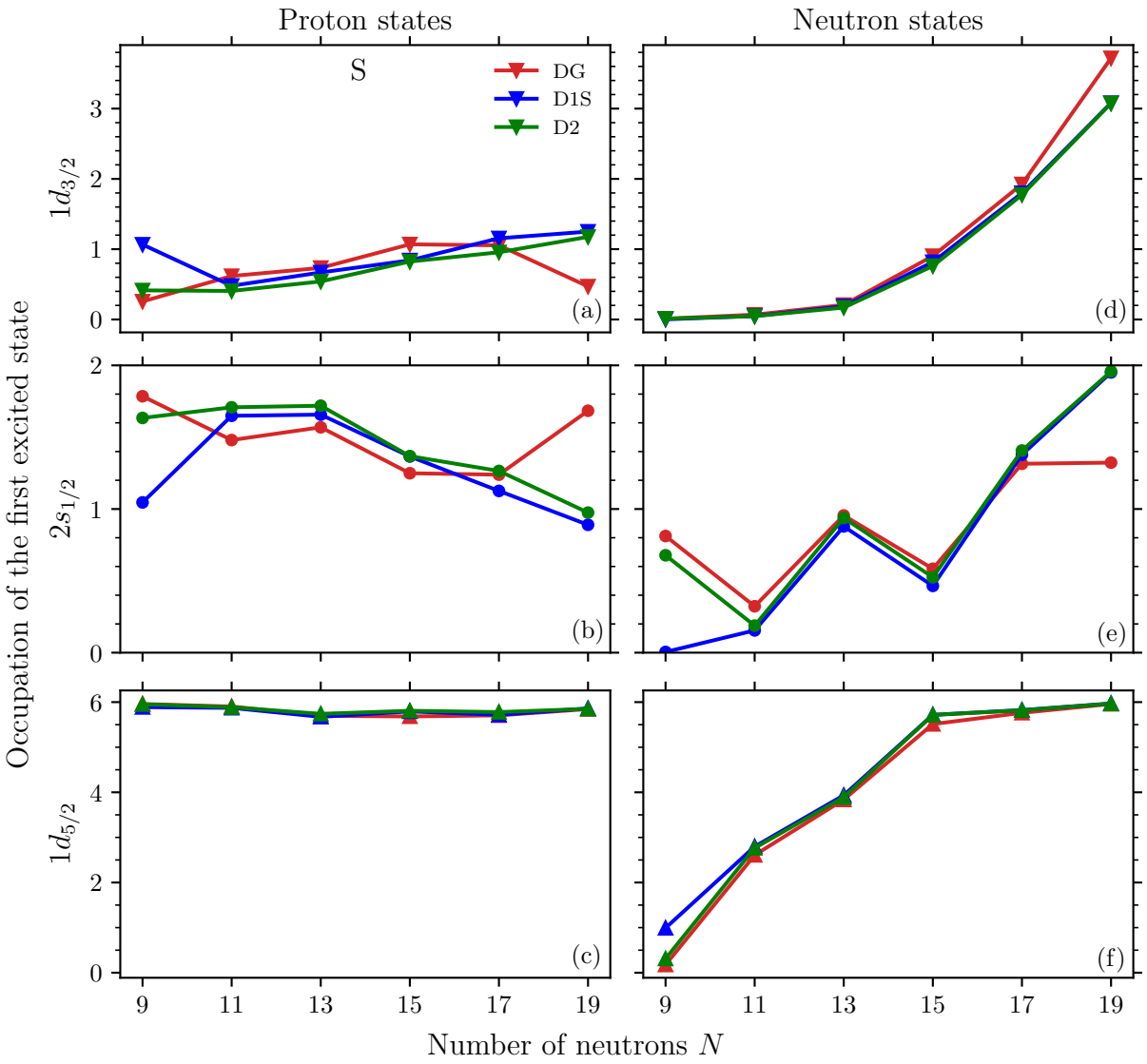

Figure IV.18 – Same as in Figure IV.17, but for the S isotopic chain.

	Agreement rate (%)	
	Ground state	First excited state
Interaction		
DG	44.0	27.3
D1S	76.0	45.5
D2	84.0	40.9

Table IV.8 – Agreement rates with experiment in the prediction of spin–parities in the ground state (left side) and in the first excited state (right side), for DG, D1S and D2 interactions.

inversions specific to the first excited states. The interactions D1S and D2 are importantly affected in the first excited state, with an agreement falling below 50%. The accuracy is even lower with DG, just over a quarter, but only three nuclei out of twenty-two make the difference with D1S. With a 43.1% drop in the overall reproduction of spin–parities when

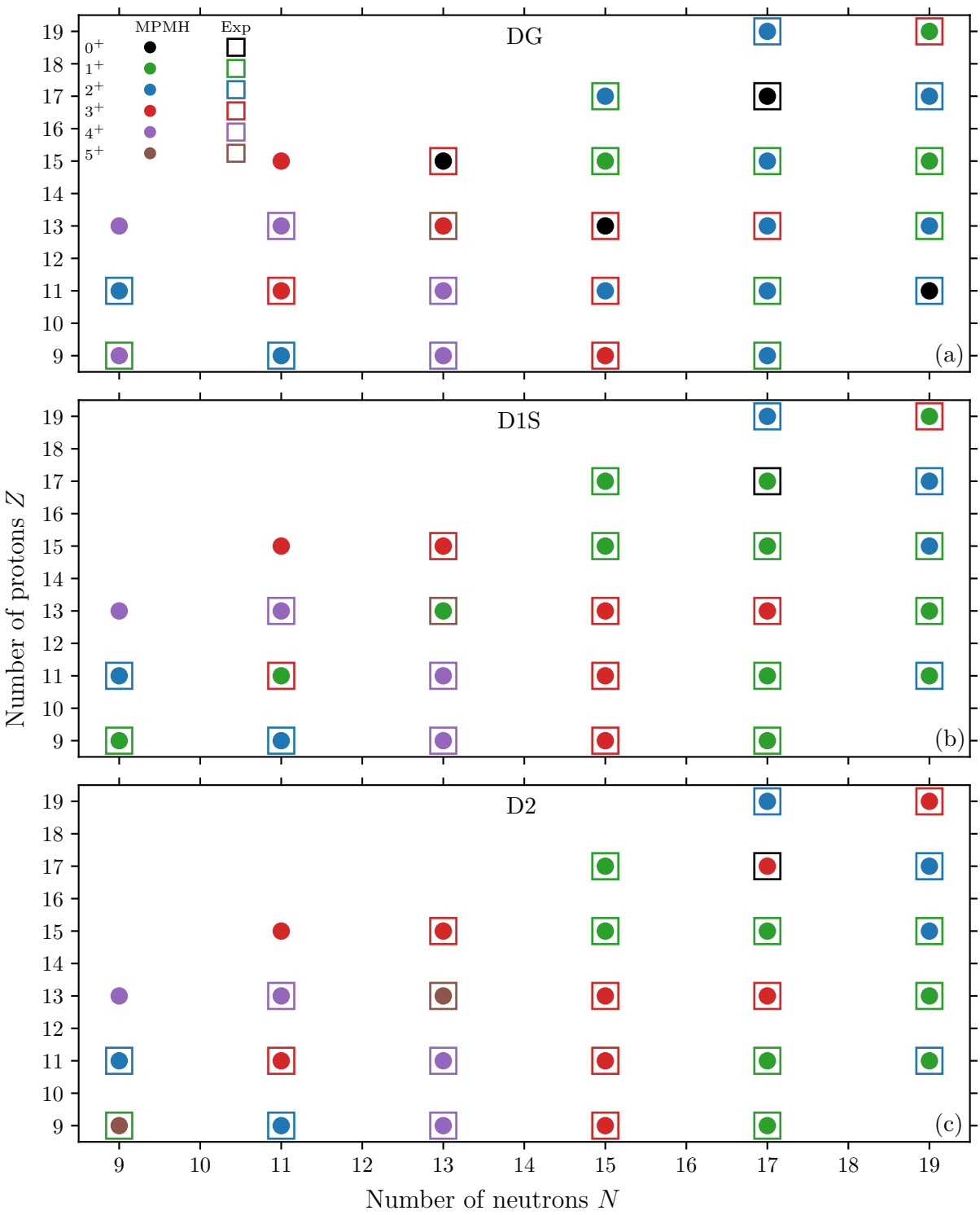

Figure IV.19 – Comparison between spin–parities $J^\pi \in \{0^+, 1^+, 2^+, 3^+, 4^+, 5^+\}$ predicted by the MPMH method for DG (upper panel), D1S (middle panel) and D2 (lower panel) interactions and experimental data [202] for the ground state. MPMH and experimental results are represented by circles and squares, respectively.

going from the ground to the first excited state, D2 is the most affected, followed by D1S (30.5%) and DG (16.7%). The same decline has been observed in odd nuclei, although less prominent. We lastly mention that experimental measurements of six nuclei are still

missing. Most theoretical outputs of the MPMH method for these nuclei are different with DG, and with D1S and D2. This could modulate our statistics, when experimental data come out.

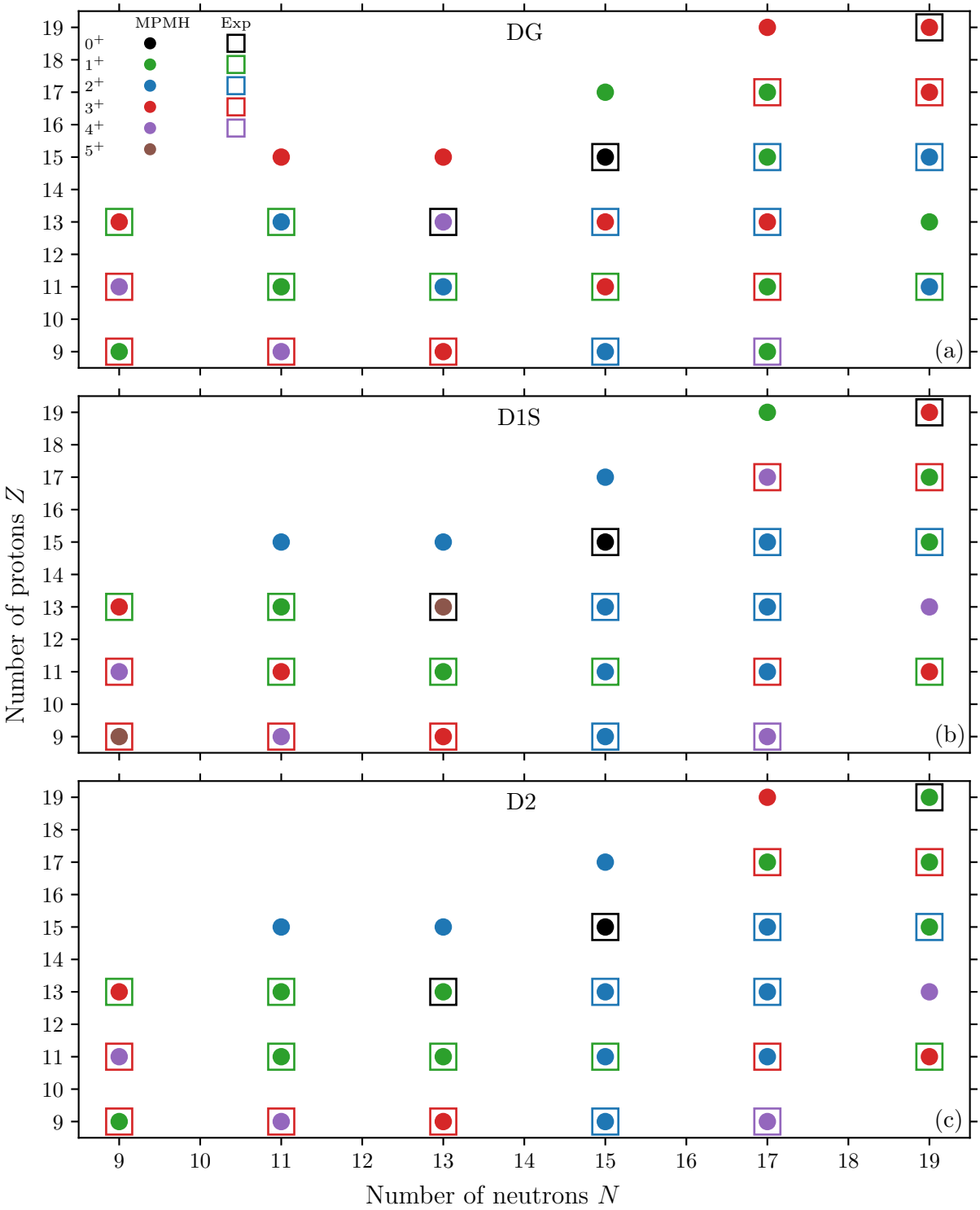

Figure IV.20 – Same as in Figure IV.19, but now for the first excited state.

For odd nuclei, we have shown that the existence of several states within a relatively small range in energy was responsible for the discrepancies in the description of spin–parities in both ground and first excited states. As this description is even poorer for

odd–odd nuclei, we assume that our explanation still holds. We then carry out the same analysis. In Table IV.9, the mean values and standard deviations of the energy difference between the ground state (as well as the first excited state) and the lowest state having the spin–parity measured experimentally, for all nuclei whose spin–parities do not fit experimental data are provided, for DG, D1S and D2 interactions. In the ground state (left side of the table), the mean difference is about 400 keV for DG, and reduced to less than 300 keV for D1S and D2. This shows that the distribution of low-energy states is on average more compact for odd–odd than for odd nuclei (see Table IV.5), as expected. Standard deviations are also smaller, meaning that there are less disparities within energy differences $\Delta\mathcal{E}$. In the first excited state (right side of the table), the mean differences are slightly higher, about 400 to 500 keV for all three interactions, with reasonable standard deviations. These are of the order of what we have observed for odd nuclei. It turns out that most of spin–parity mismatches between theoretical and experimental predictions are caused by level inversions of no more than a few hundred keV. At present, Gogny interactions cannot be expected to utterly reproduce such fine structure effects in odd–odd nuclei, even more subtle than in odd nuclei, for which they have not been tuned. Besides, full self-consistent MPMH calculations should be performed to have a more meticulous picture.

	Ground state		First excited state	
Interaction	$\langle\Delta\mathcal{E}\rangle$ (keV)	$\sigma(\Delta\mathcal{E})$ (keV)	$\langle\Delta\mathcal{E}\rangle$ (keV)	$\sigma(\Delta\mathcal{E})$ (keV)
DG	390	208	442	291
D1S	232	210	485	489
D2	296	448	469	441

Table IV.9 – Mean values and standard deviations of the theoretical energy difference $\Delta\mathcal{E}$ between ground states (left side) or first excited states (right side) and the lowest states whose spin–parities are those of experimental measurements, for DG, D1S and D2 interactions.

4.2. First excitation energies

We now evaluate the difference between the excitation energies of the first excited state evaluated by the MPMH approach and experimentally, which has been defined in (IV.16). Note that among the twenty-seven odd–odd nuclei we have retained, the first excitation energies of twenty-one of them are known experimentally. According to our discussion of the previous subsection, the theoretical excitation energies of those nuclei are associated with the first state showing the spin–parity measured experimentally. The results are plotted in Figure IV.21 for DG, D1S and D2 interactions.

In general, the excitation energies are satisfactorily reproduced by all three interactions in odd–odd nuclei. With differences rarely above a few hundred keV, they look better than in odd nuclei and thinly worse than in even–even nuclei. To be more precise, the mean values and standard deviations, as defined in (IV.15), are displayed in Table IV.10, for DG, D1S and D2 interactions. Note that we have not calculated these quantities for each spin–parity or isotopic chain as there are not enough representatives. The outputs are better with DG, putting finishing touches to the quality of this interaction in the description of

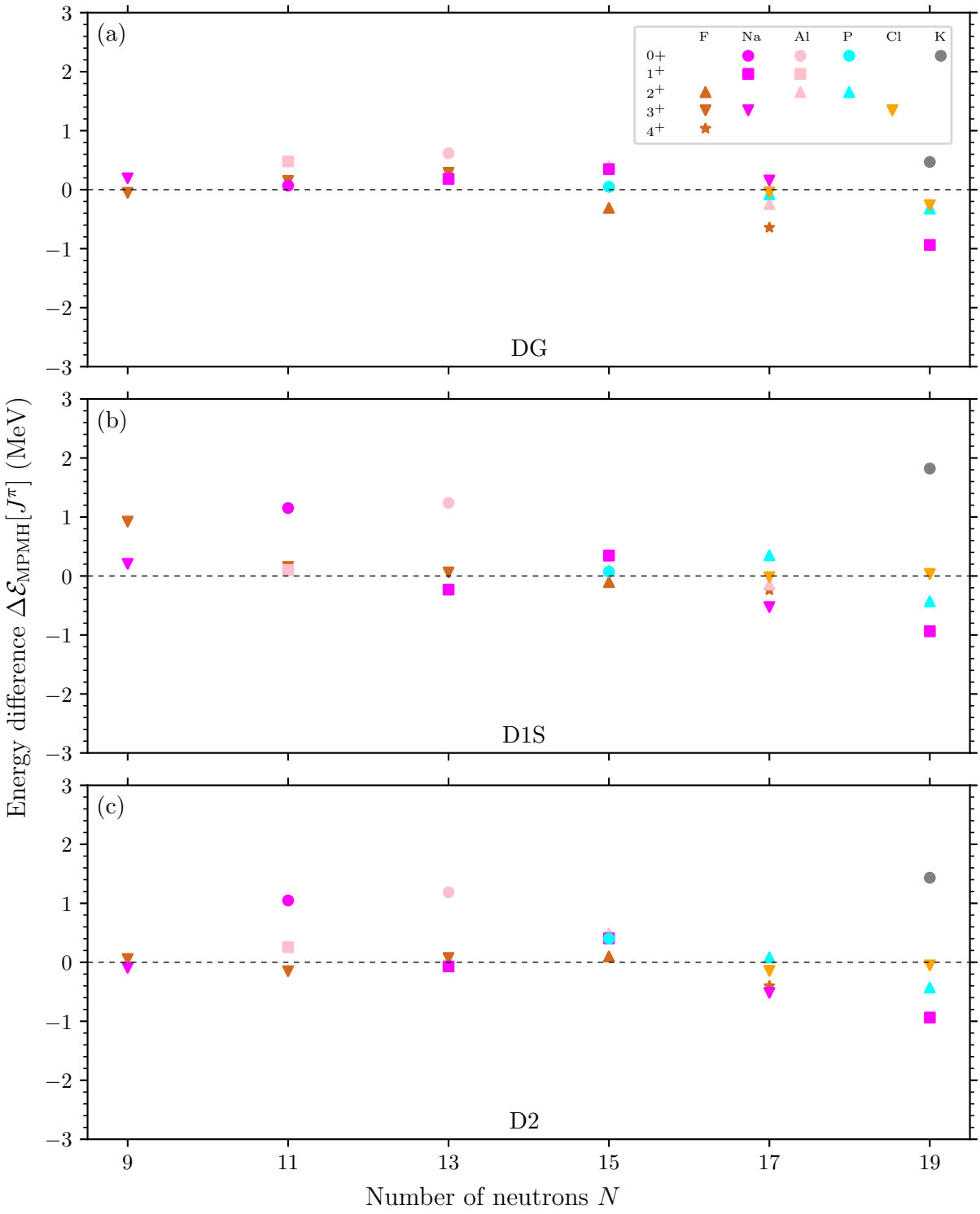

Figure IV.21 – Energy difference between the first excitation energies predicted by the MPMH and experimental data, expressed by (IV.16), as a function of the number of neutrons N. The results are shown for DG, D1S and D2 interactions, in panels (a), (b) and (c), respectively. Horizontal dashed lines display perfect agreement with experiment. The *sd*-shell isotopes studied are labelled by different colors and their spin–parities $J^\pi \in \{0^+, 1^+, 2^+, 3^+, 4^+\}$ by different shapes, as indicated in the legend.

first excitation energies, beyond the mean field, of all *sd*-shell nuclei. The mean difference is about 100 keV smaller than that of D1S or D2, and the standard deviation less than half that of D1S. We notice that D1S and D2 results are pretty similar, but since we have mostly compared DG to D1S so far, we shall continue this way for the sake of clarity. Since we are describing a global effect here, it is principally attributed to the spin–orbit interaction, as for the other types of nuclei. This is something we have realized during the fitting process, as lessening the intensity of the spin–orbit term improved the description of odd–odd nuclei in terms of their first excitation energies.

Interaction	$\langle x \rangle$ (keV)	$\sigma(x)$ (keV)
DG	299	230
D1S	437	491
D2	400	413

Table IV.10 – Mean values and standard deviations of the difference $x \equiv \Delta\mathcal{E}_{\text{MPMH}}[J^\pi]$, as defined in (IV.16), evaluated with DG, D1S and D2 interactions.

We can discriminate three nuclei whose energy differences are over 1 MeV with D1S and D2 interactions. Because they are manifestly decreased by DG, they play a crucial role in the overall higher mean values discussed above. In ^{22}Na (magenta circle), the excitation energy of the first excited state is overestimated by 1.151 MeV with D1S, 1.048 MeV with D2, and only 68 keV with DG. As for ^{26}Al (pink circle), it is 1.238 MeV, 1.186 MeV and 617 keV with D1S, D2 and DG, respectively. Finally, for ^{38}K (gray circle), we find out 1.821 MeV, 1.433 MeV and 470 keV, with the same interactions. The results are slightly better with D2 than D1S, but not sufficiently lowered to achieve the accuracy of DG, invariably below 1 MeV. It is interesting to notice that these nuclei have all 0^+ experimental spin–parities (as indicated by the circles) and a same number of protons and neutron, i.e. $N = Z$. Another nucleus, namely ^{30}Na (magenta square), also stands out with an overestimated energy difference of 937 keV for all three interactions. Actually this is the experimental first excitation energy of this nucleus as the associated spin–parity is assigned to the ground state by the MPMH method (conventionally chosen as the origin of the energy spectrum). In fact, we are approaching the $N = 20$ island of inversion with this nucleus [217]. The sole mixing of *sd*-shell states considered here is no longer sufficient to describe the spectroscopy of this nucleus. The *pf*-shell states, and in particular $(1f_{7/2})_\nu$, should be taken into account as they may intrude the lower orbitals.

Finally, we recall that the full self-consistency, we still do not know the order of magnitude of in odd–odd nuclei, is supposed to enhance the MPMH predictions.

4.3. Single-particle energies

In previous subsection, we have observed that ^{22}Na, ^{26}Al and ^{38}K isotopes are described with overestimated first excitation energies, with both D1S and D2. The tensor force is expected to be diminished in those nuclei as no one presents a completely filled spin-partner state while the other is empty. Only in ^{26}Al we may expect some effect as the $1d_{5/2}$ states start to fill up.

In order to understand what is going on in the above-mentioned nuclei, we plot in Figure IV.22 the proton and neutron SPEs of Na and Al isotopes at the HF level, obtained

with the equal filling approximation. We specify that the full isotopic chains have been displayed to emphasize the potential gap reductions of the nuclei we are interested in with respect to their neighbors, and to see the modifications relatively to the Si and S cases we have investigated in detail. For K nuclei, unfortunately, such study is not viable as most odd–odd isotopes are unbound. We will then content to give the values of the gaps associated with ^{38}K in what follows. On the whole, the descent of the proton state $1d_{3/2}$, more pronounced at $N = 13$ and $N = 15$, and the global reductions of neutron gaps observed with DG are still in place in Na and Al isotopes. In the neutron sector, the phenomenon is less marked than in Si and S isotopes (see Figure IV.14), but still clear.

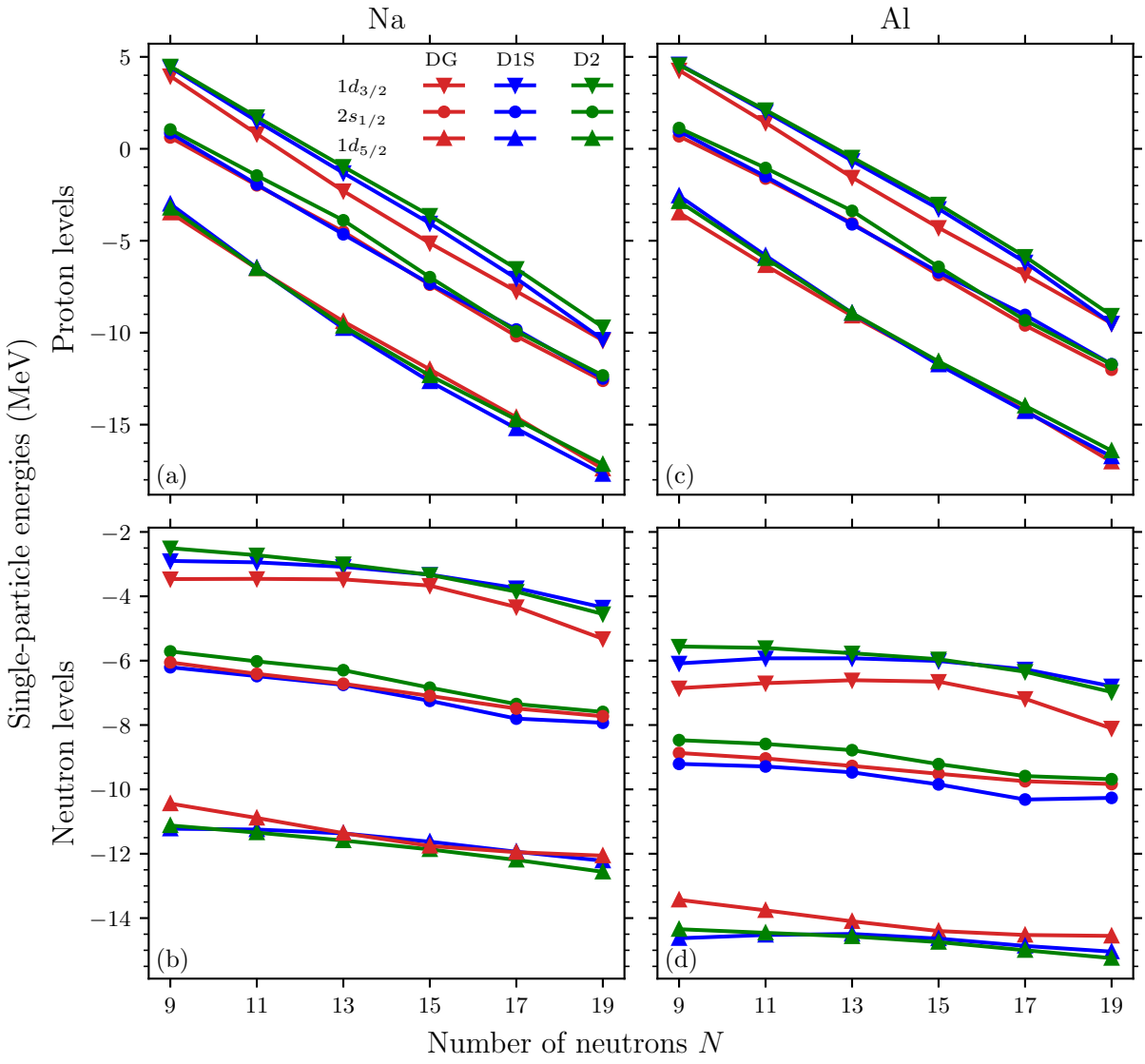

Figure IV.22 – Single-particle energies of the *sd* shell along Na (left panels) and Al (right panels) isotopic chains, for proton (upper panels) and neutron (lower panels) levels. Results are given for DG, D1S and D2 interactions.

Going further, we furnish the proton and neutron gaps of ^{22}Na, ^{26}Al and ^{38}K predicted by all three interactions in Table IV.11. We indeed observe the shrinking of several gaps for all isotopes when going from D1S to DG, at the origin of more reasonable first excitation energies. In ^{22}Na and ^{26}Al, the reductions are salient in proton and neutron $(2s_{1/2} - 1d_{3/2})$ gaps. Of about 600 keV in both $(2s_{1/2} - 1d_{3/2})$ gaps in ^{22}Na, they reach about 1 MeV and

900 keV in $(2s_{1/2} - 1d_{3/2})_\pi$ and $(2s_{1/2} - 1d_{3/2})_\nu$ in ^{26}Al, respectively. On the other hand, the main reductions take place in proton and neutron gaps $(1d_{5/2} - 2s_{1/2})$ in ^{38}K. They are diminished by about 400 keV and 500 keV, respectively. Let us note by the way that these gaps are also systematically narrowed when going from D1S to D2. This coincides with the lower excitation energies obtained for the three nuclei with D2, but the effect is *a priori* too weak to sufficiently lower them. We point out that the gap reductions are stronger in ^{26}Al, in which the tensor force is supposed to show some action, than in ^{22}Na and ^{38}K, in which its action is very limited. Its more dominant action in ^{26}Al compared to ^{22}Na is graphically observable, in particular in the proton sector, when focusing on their respective gaps, in panels (a) and (c) of Figure IV.22. We then claim that the drop in the energy differences of ^{22}Na and ^{38}K when going from D1S to DG is mainly due to the lower spin–orbit intensity while a non-negligible tensor component must additionally be taken into account to explain those of ^{26}Al.

	^{22}Na			
Interaction	$(1d_{5/2} - 2s_{1/2})_\pi$ (MeV)	$(2s_{1/2} - 1d_{3/2})_\pi$ (MeV)	$(1d_{5/2} - 2s_{1/2})_\nu$ (MeV)	$(2s_{1/2} - 1d_{3/2})_\nu$ (MeV)
DG	4.523	2.792	4.479	2.951
D1S	4.534	3.441	4.764	3.535
D2	5.048	3.187	5.321	3.299
	^{26}Al			
DG	5.037	2.488	4.828	2.665
D1S	4.826	3.456	5.022	3.545
D2	5.560	2.910	5.789	3.013
	^{38}K			
DG	4.887	1.586	4.794	1.766
D1S	5.324	1.692	5.292	1.936
D2	5.186	2.018	5.148	2.287

Table IV.11 – Proton and neutron energy gaps of ^{22}Na, ^{26}Al and ^{38}K isotopes predicted by DG, D1S and D2 interactions at the HF level, with the equal filling approximation.

Finally, we would like to say that the diminutions of the energy gaps are in general less important here than in even–even and odd Si and S isotopes whose excitation energies are overestimated (with D1S or D2). This is in accordance with the fact that the excitation energies of these nuclei are usually more overestimated than those we focus on in this section. When going from D1S to DG, the reduction of the proton and neutron gaps $(2s_{1/2} - 1d_{3/2})$ of ^{26}Al must indeed be multiplied by a factor 1.7 to get those of ^{28}Si, displayed in Table IV.3. This shows how strong the tensor effects become when the lower spin-partner states of the *sd* shell are filled. Another interesting example is that of ^{27}Si, since it has only one more proton than ^{26}Al. In this nucleus, the proton and neutron gaps $(2s_{1/2} - 1d_{3/2})$ are reduced by about 900 keV and 1.1 MeV when going from D1S to DG. Thus, the addition of one proton increases the diminution of the gap $(2s_{1/2} - 1d_{3/2})_\pi$ by about 300 keV, and by about 100 keV for the gap $(2s_{1/2} - 1d_{3/2})_\nu$. Once again, it seems that the proton–neutron component of the tensor force is noteworthy.

4.4. Multiparticle–multihole excitations

We eventually look at how the nucleons are distributed within the single-particle levels in the ground and first excited states of ^{22}Na, ^{26}Al and ^{38}K isotopes. We begin with the occupation of the ground state in Na and Al isotopic chains. In Figures IV.23 and IV.24 are represented the average number of protons (left panels) and neutrons (right panels) in the single-particle states making up the ground state, as a function of the neutron number N, of Na and Al isotopes, respectively, for DG, D1S and D2 interactions.

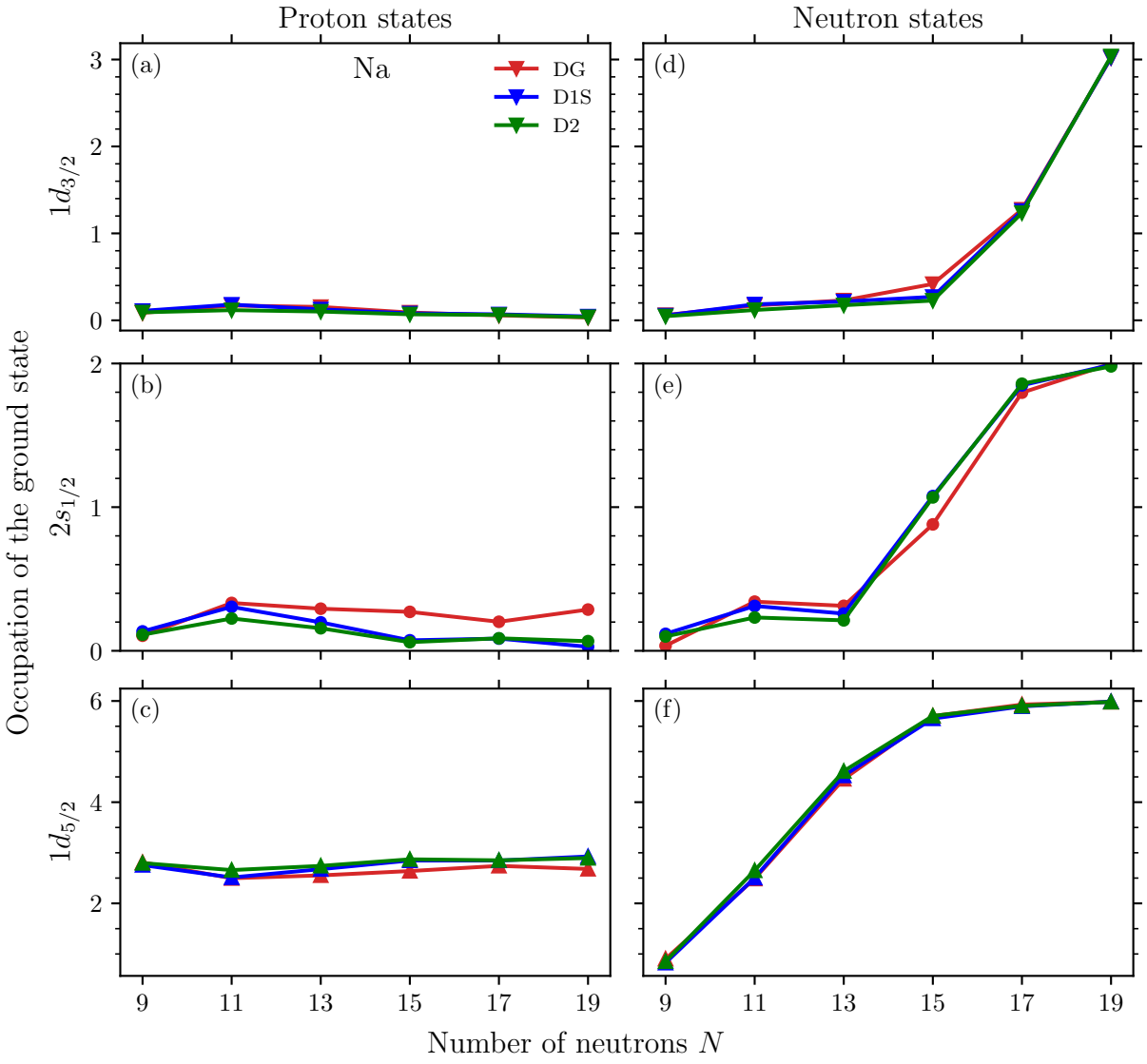

Figure IV.23 – Occupation of the ground states of Na isotopes, defined as the number of proton (left panels) and neutrons (right panels) filling the *sd* subshells, namely the $1d_{5/2}$ (lower panels), $2s_{1/2}$ (middle panels) and $1d_{3/2}$ (upper panels) levels.

In Figure IV.23, we observe, from $N = 13$ in the proton sector (left panels), a depletion of the lowest state in favor of the $2s_{1/2}$ state, and to a lesser extent, in favor of the $1d_{3/2}$ state, with the interaction DG. This is basically the phenomenon showing up in Si and S isotopes, but with greater amplitude (see Figures IV.15 and IV.16). In the neutron sector (right panels), the same trend can be spotted, but only from $N = 15$. In ^{22}Na, only a small ascent of the $2s_{1/2}$ states is perceptible in panels (b) and (e). This fits the

small variations of the gaps $(2s_{1/2} - 1d_{3/2})$ of Table IV.11 when going from D1S to DG. Concretely, 0.333 and 0.170 protons are filling the respective $2s_{1/2}$ and $1d_{3/2}$ states with DG, against 0.306 and 0.181 with D1S. On the neutron side, 0.342 and 0.171 neutrons lie in these same states with DG, versus 0.312 and 0.184 with D1S.

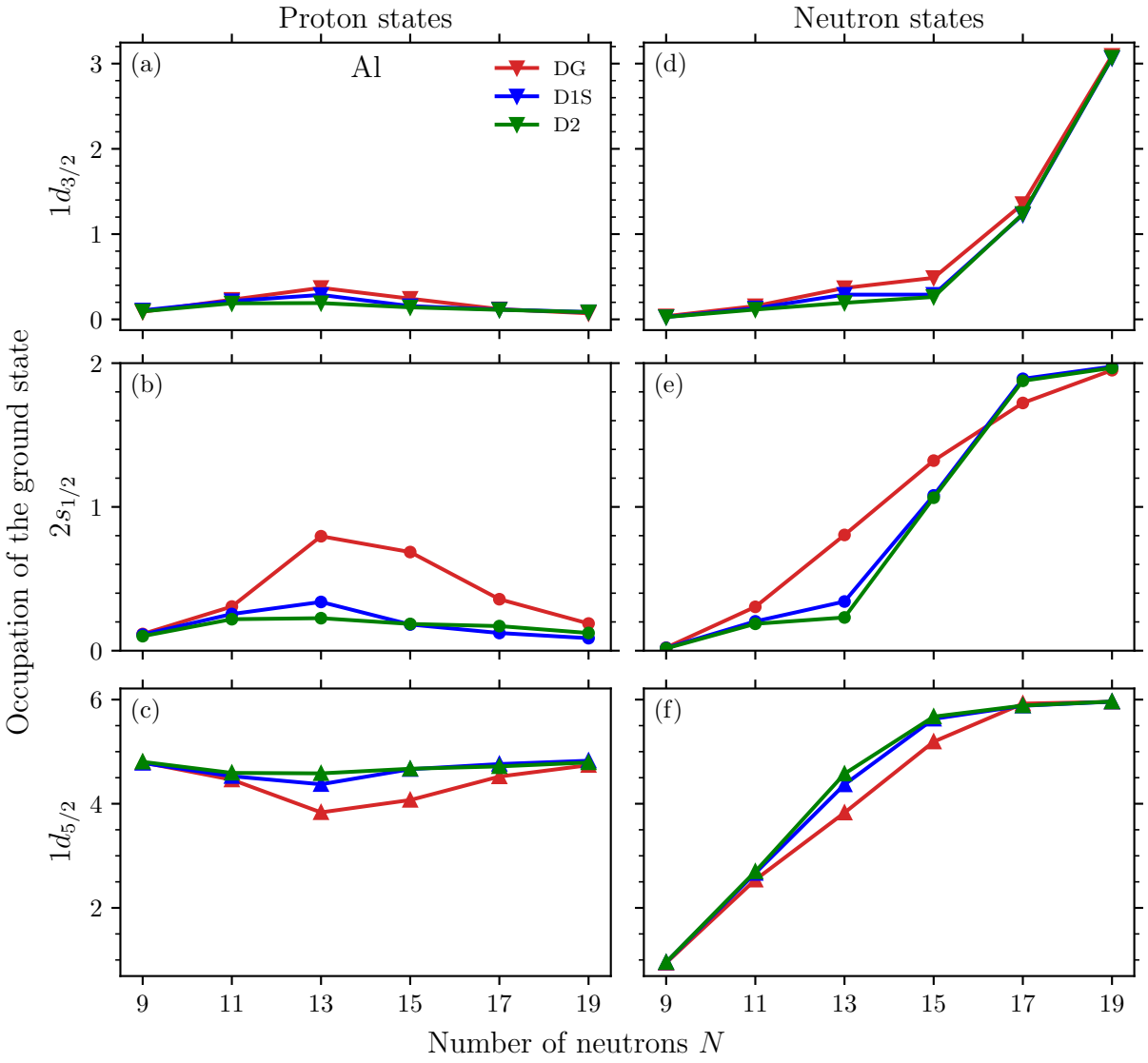

Figure IV.24 – Same as in Figure IV.24, but for the Al isotopic chain.

The same depletion occurs from $N = 13$ in the Al isotopic chain of Figure IV.24. This time, the effect is more visible, in both proton and neutron sectors, although a bit less than in Si and S isotopes. Such behavior was expected since more protons fill the $1d_{5/2}$ state (which renders transitions towards upper states more likely), and the gap reductions seem more prominent with Al isotopes, based on the examples of ^{22}Na and ^{26}Al. Indeed, 0.796 and 0.370 protons (0.805 and 0.368 neutrons) occupy the respective $1d_{5/2}$ and $2s_{1/2}$ states with DG, against 0.339 and 0.287 protons (0.342 and 0.290 neutrons) with D1S. Note that the increasing intensity of the phenomenon with the average number of protons filling the lowest state (three in Na, five in Al and six in Si as well as in S isotopes), sustains the idea that the tensor term naturally plays a role in the occupation of the single-particle states.

We have not represented the occupation of K isotopes as most of their odd–odd members are unbound experimentally. We still give the results for ^{38}K. The states $1d_{5/2}, 2s_{1/2}$ and $1d_{3/2}$ are filled by $5.867, 1.593$ and 3.539 protons, as well as $5.877, 1.610$ and 3.513 protons, with DG, against $5.980, 1.818$ and 3.202 protons, as well as $5.980, 1.829$ and 3.191 protons, with D1S. The migration towards the upper states is manifest with DG. The relatively significant reductions of the proton and neutron gaps $(1d_{5/2} - 2s_{1/2})$ explain the transitions between the states they link, but also the smaller reductions of the proton and neutron gaps $(2s_{1/2} - 1d_{3/2})$ exhibit a discernible influence.

Finally, we turn into the occupation of the *sd* subshells for DG, D1S and D2, but now for the first excited state. The average number of nucleons standing in the $1d_{5/2}, 2s_{1/2}$ and $1d_{3/2}$ proton and neutron states along Na and Al isotopic chains are provided in Figures IV.25 and IV.26, respectively.

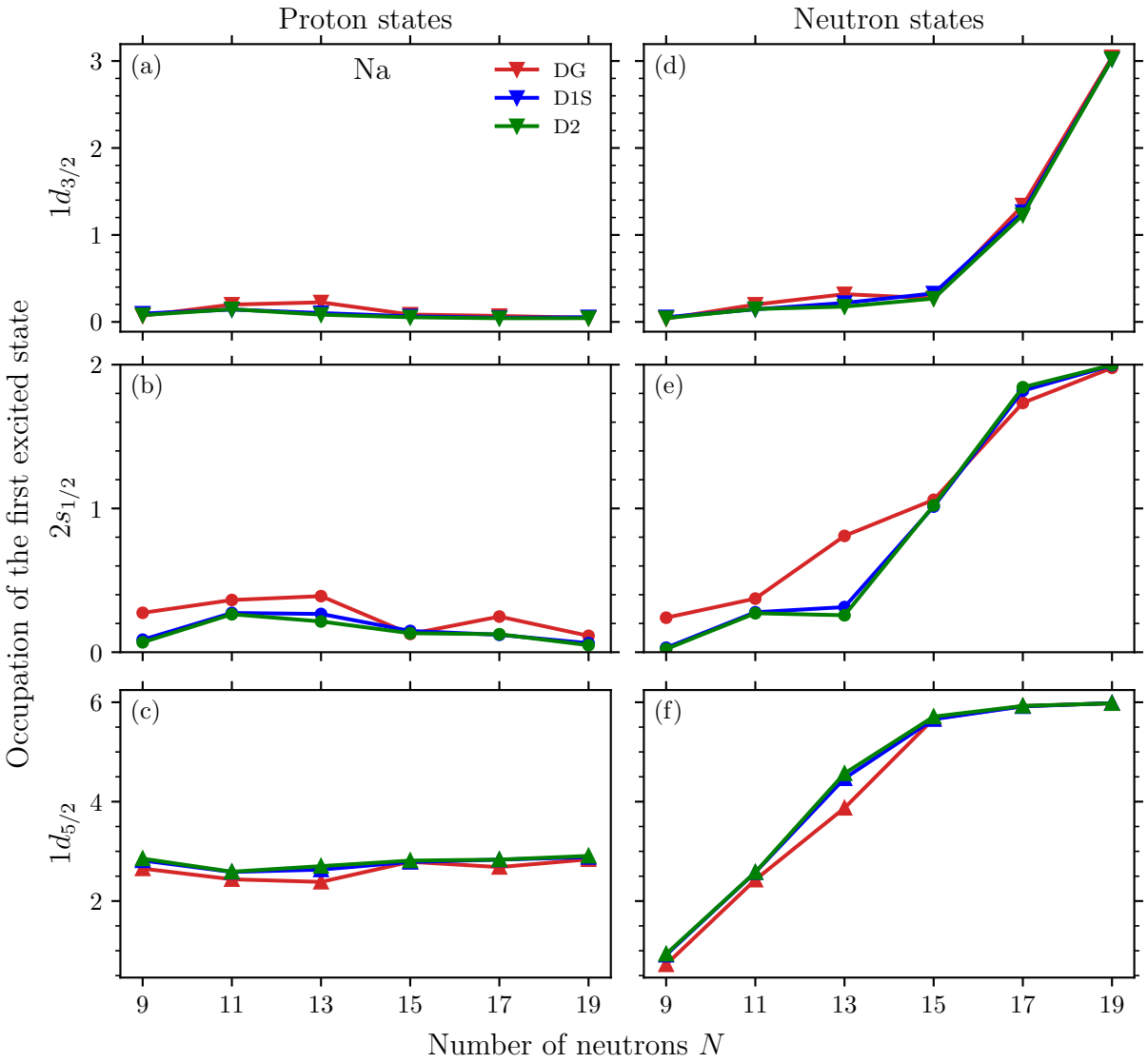

Figure IV.25 – Occupation of the first excited states of Na isotopes, defined as the number of proton (left panels) and neutrons (right panels) filling the *sd* subshells, namely the $1d_{5/2}$ (lower panels), $2s_{1/2}$ (middle panels) and $1d_{3/2}$ (upper panels) levels.

In Figure IV.25, we see that the phenomenon we have described in the ground state

is still present, and even more pronounced, especially in the neutron sector, in the first excited state. The augmentation of the number of particles occupying the $1d_{3/2}$ states with interaction DG is now distinct. On the other hand, the migration of nucleons from $1d_{5/2}$ towards $2s_{1/2}$ states with DG appears sooner, from $N = 9$. This globally results in upper states being more occupied in the first excited state than in the ground state. For ^{22}Na, 0.363 and 0.199 protons (to be compared with 0.306 and 0.181 in the ground state) as well as 0.373 and 0.199 neutrons (to be compared with 0.342 and 0.171 in the ground state) are populating the $2s_{1/2}$ and $1d_{3/2}$ levels in the first excited state, respectively.

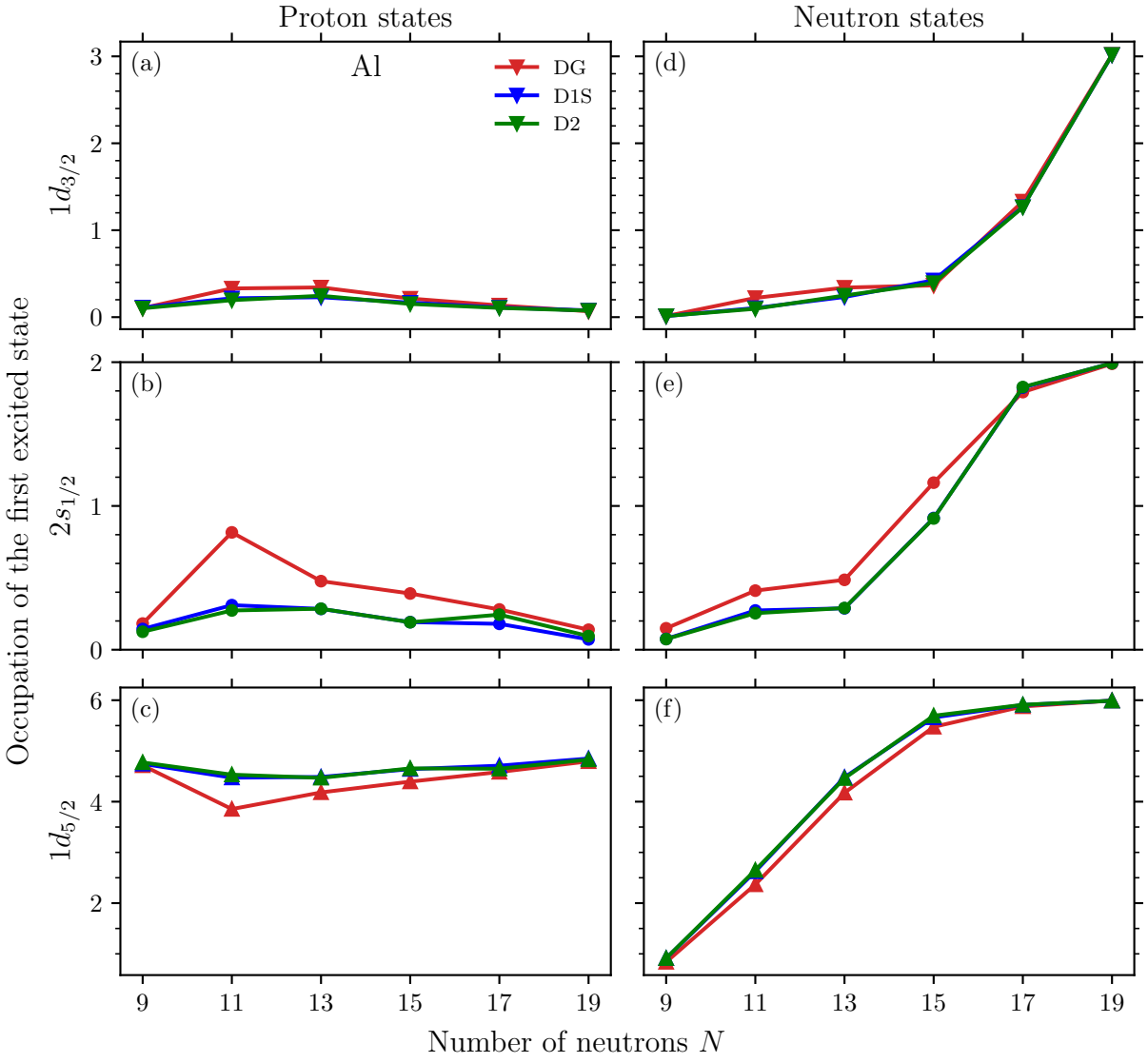

Figure IV.26 – Same as in Figure IV.25, but for the Al isotopic chain.

For Al isotopes, the situation is quite the opposite to the one detailed for Na isotopes, when going from the ground to the first excited state, as illustrated in Figure IV.26. In fact, even if the peculiar behavior is also taking place sooner, from $N = 11$, it is less marked than in the ground state. As a consequence, the upper states are now in general less occupied in the first excited state than in the ground state. For ^{26}Al, 0.477 and 0.342 protons (to be compared with 0.796 and 0.370 in the ground state) as well as 0.486 and 0.340 neutrons (to be compared with 0.805 and 0.368 in the ground state) are lying in the $2s_{1/2}$ and $1d_{3/2}$ levels of the first excited state, respectively.

It is also interesting to compare the occupation of the single-particle states of ^{26}Al and ^{27}Si in the first excited state, here with interaction DG. In ^{27}Si, 1.003 and 0.438 protons, as well as 0.813 and 0.339 neutrons occupy the $2s_{1/2}$ and $1d_{3/2}$ states, respectively. Unsurprisingly, more protons reach these states in ^{27}Si than in ^{26}Al as an additional proton is involved. With the same number of neutrons, though, more neutrons reach the $2s_{1/2}$ state in ^{27}Si. Yet, their gaps $(1d_{5/2} - 2s_{1/2})_\nu$ are pretty similar, 4.828 MeV for ^{26}Al and 4.891 MeV for ^{27}Si, with DG. This suggests that the single proton and neutron in ^{26}Al tend to pair up, and that their scattering to higher-energy states will be less energetically favorable than that of the single neutron in ^{27}Si.

Finally, in ^{38}K as well, less nucleons are filling the first excited state with respect to the ground state. To be quantitative, 2.000 protons and neutrons (to be compared with 1.593 protons and 1.610 neutrons in the ground state) are saturating the $2s_{1/2}$ states, while 3.018 protons and 3.017 neutrons (to be compared with 3.539 protons and 3.513 neutrons) stay in the $1d_{3/2}$ states.

Conclusion

We constructed a generalized fully finite-range Gogny interaction provided with spin–orbit and tensor terms. The associated analytical expression encompasses almost all previous ones and is intrinsically free from ultraviolet divergences at the Hartree–Fock–Bogoliubov level and when going beyond the mean field. In this venture, we had to extend the existing fitting procedure to integrate new constraints and filters in order to efficiently discriminate trustworthy sets of parameters. The constraints took the form of requirements, drawn from the shell model, on two-body matrix elements allowing to control for the first time the proton–neutron pairing properties of a Gogny interaction. To make this possible, the spherical two-body matrix elements of the newly introduced finite-range spin–orbit and tensor forces were derived analytically. As for the filters, they were founded on the three following points:

(i) a spin–orbit intensity in the $T = 1$ channel approximately equal to that of the original Gogny interaction at the zero-range limit;

(ii) an isospin-dependent spin–orbit parameter of the order of that established by Sharma *et al.* [142] to better reproduce the kink in Pb isotopes;

(iii) tensor parameters close to those of Anguiano and Grasso [61], obtained by fitting the $1f$ splittings of three nuclei while considering the combined actions of spin–orbit and tensor forces.

The choice of the spin–orbit and tensor ranges used as inputs in the fitting code were guided by the exchanges of π and ω mesons in the one-boson-exchange models. The outcoming parametrizations were successively tested in infinite nuclear matter and from the perspectives of mean-field and beyond mean-field approaches, before the best compromise was found for the parametrization referred to as DG. We additionally asked our globally refitted parametrization not to deviate too much from the former parametrization D2, to preserve its qualitative features.

In nuclear matter, we found that interaction DG presents satisfactory results, in particular regarding:

(i) physical quantities correctly reproduced by D2 (standard quantities evaluated at the saturation density, potential energy in (S, T) channels, equations of state in symmetric and neutron matters, effective masses and Landau parameters);

(ii) partial waves, with spin–orbit and tensor forces showing good behavior in P waves;

(iii) instabilities, as all stability criteria resulted from both central and non-central terms in the context of the Landau theory of Fermi liquids were fulfilled.

The first point was expected since both the spin–orbit and tensor forces are zero in the nuclear matter framework we considered, the others are unprecedented. In particular, the contributions of the tensor force to the second and third points had to be computed.

The consistency of an effective interaction is truly evaluated in finite nuclei. We accordingly deduced the mean and pairing Hartree–Fock–Bogoliubov fields associated

with the finite-range spin–orbit and tensor terms, in a two-center basis. For the generalized Gogny interaction, mean-field calculations within the Hartree–Fock–Bogoliubov approach revealed interesting outputs, that are:

(i) a slight decrease in the binding energies of many nuclei;

(ii) charge radii and nuclear density distributions of the order of those of the former D1S and D2 interactions;

(iii) a better reproduction of the kink in Pb isotopes;

(iv) a reduction of the pairing energies in some isotopes and isotones of the $Z = 50$ and $N = 50$ chains;

(v) significant modifications in the splittings and Fermi gaps of many nuclei;

(vi) changes in the nature of the quadrupole deformations of certain light nuclei, in agreement with experimental data;

(vii) a lowering of fission barrier heights, in line with experiment, as well as deformation shifts in the potential energy surfaces of Th isotopes and standard actinides.

Most of these points were interpreted as coming from a subtle interplay between the spin–orbit and tensor forces. However, point two was mainly attributed to the central and density-dependent part, while points six and seven seemed principally due to the tensor component.

When we developed our interaction, we decided to adopt the philosophy of the original Gogny interaction, that is to aim for a fine description not at the level of the mean field, but beyond it. As a consequence, some space for the correlations beyond the mean field were deliberately introduced. Within the multiparticle–multihole configuration mixing method, we showed that the first excitation energies of even–even and odd nuclei were strongly improved by the generalized Gogny interaction. Here also, the competition between spin–orbit and tensor forces was held responsible, sometimes one contribution more predominantly than the other, for the outcomes, in connection with their respective effects on shell evolution.

From the set of results we have listed, the generalized Gogny interaction stood out as a quality interaction in the landscape of phenomenological effective interactions fashioned to date. Nevertheless, several improvements and extensions could be envisaged in the future, including:

(i) larger analyses and enhancements applied to the current DG parametrization;

(ii) the search for a new parametrization of the generalized Gogny interaction;

(iii) extensions of the analytical expression of the generalized Gogny interaction.

We begin with the first point. It may be interesting to test parametrization DG within the random phase approximation, and more specifically regarding the sum rules in the Landau theory of Fermi liquids, which are violated in a significant way by the tensor force. Similarly, the nuclear density distributions, known to be better described at this approximation [17], would certainly better fit the experimental data also with interaction DG. We did not discuss the astrophysical applications of interaction DG. Yet, interaction D2 [218], and more generally Gogny interactions, can show reliable properties in neutron stars [128, 219, 220], in particular through the filters on the potential energy in (S, T) channels and on the neutron matter equation of state. It may be enlightening to undertake work in this direction. To confirm our observations on the effect of the

tensor force on the axial quadrupole deformations, a detailed study of the moments of inertia of the related nuclei would be welcomed. As for fission barriers of pre-actinides and actinides, we already pointed out that extensions to asymmetric potential energy surfaces and triaxiality, as well as a dynamical treatment of the process, would unavoidably enable to further dissect the role of the tensor force. Eventually, as the full self-consistency of the multiparticle–multihole configuration mixing method is supposed to refine the excitation energies, such procedure should be done for all even–even, odd and odd–odd nuclei. There is incidentally no reason for this study to be limited to the first excitation energies, and could be employed for higher ones as well.

Another possibility is to trade the DG parametrization for a new one, still built up from the analytical expression of the generalized Gogny interaction. In the fitting code of DG, we imposed *constraints* on four two-body matrix elements, two in the *sd* shell, two in the *pf* shell. Such procedure could be adapted to *filters* by asking for the reproduction of a large number of matrix elements, like all the sixty-three of the *sd* shell for instance, since their evaluation is pretty fast in the fitting code. A standard deviation would be calculated and all the parametrizations whose latter exceeds a chosen accuracy would be automatically rejected. This would for sure improve the predictions on the excitation energies evaluated within the multiparticle–multihole configuration mixing method. To reduce the second fission barriers that were predicted too high in actinides with the original Gogny interaction, a filter on the surface energy coefficient calculated in a semi-infinite nuclear matter, was added in the fitting procedure of D1S [16]. These calculations could be generalized to the finite-range tensor force and implemented in the fitting code with the same objective.

Instead of looking for new parametrizations, the degrees of freedom could be increased by directly extending the analytical expression of the generalized Gogny interaction. There are several options, more or less difficult to set up, which are:

(i) adding another finite-range density-dependent term;

(ii) replacing the phenomenological density-dependent term by a genuine finite-range three-body density-dependent term;

(iii) adding another finite-range spin–orbit or tensor term, or both at the same time;

(iv) attaching a density dependence to the finite-range spin–orbit or tensor term, or both at the same time.

Adding another finite-range density-dependent term would require the least amount of work. As we have said, the fitting code is already made up for such purpose, and no additional analytical calculations are necessary. A preliminary work we have carried out in this direction, from the analytical form of D2, turned out encouraging as it was quite easy to control the energy drift in Sn isotopes while amending the predictions in some (S, T) channels.

A *genuine* three-body interaction, analogous to that of the original Skyrme interaction [106], with a finite range, could replace the current *phenomenologically* determined two-body density-dependent term [221]. In the absence of a density-dependent term raised to some fractional power, it is likely that reproduction of the saturation point will also require the incorporation of a tensor term, this time of short range. Such extension is less straightforward than the former one, though, since it is accompanied with analytical calculations and a subsequent implementation in the different codes. These changes on the density dependence should make the interaction better in many respects, including notably the relative positions of the single-particle states, which we have seen, especially in the *s* states, can be improved.

Otherwise, we could incorporate a new finite-range spin–orbit term, a new finite-range tensor term, or both at the same time. Once again, the fitting code is ready for this and no more work is required as four extra constraints related to two-body matrix elements have already been implemented. Finding a way to filter the new parameters appropriately appears a priori as the only requisite. This would bring us progressively to the number of parameters of M3Y and GPT interactions, so that it may be rewarding to draw inspiration from their fitting protocols [52, 118].

Finally, some of the analytical extensions enumerated could be combined by providing density dependences to one or several spin–orbit and tensor terms, or even both at the same time. Actually, considering a zero-range density-dependent spin–orbit term in the Gogny interaction was conceived a few years ago, but not pursued [222]. Chances are that the description of nuclear density distributions, Landau parameters (and then sum rules and stability criteria) as well as the kink in Pb isotopes will be enhanced by such generalizations according to what we have suggested throughout the document. To achieve this, relevant constraints on these or other quantities will have to be formulated, in order to properly take advantage of the latitude brought by the extensions. Anyone interested in such developments must be warned that they are far from being trivial. On the analytical aspect, the spin–orbit and tensor forces were the most challenging to derive while the density dependence brings rearrangement terms, eventually leading to even more quantities to be calculated. On the numerical aspect, the density-dependent and tensor terms already involved numerical integrals in the Hartree–Fock–Bogoliubov fields, noticeably increasing the need for computational resources to find out a solution. The situation will evidently become more intricate when finite-range density-dependent spin–orbit and tensor terms will be taken into account. Computation times will have to be kept to a reasonable level, particularly in the case of large-scale calculations such as those required to generate potential energy surfaces. However, with modern computing power, such considerations remain viable.

Sur le coteau, là-bas où sont les tombes,
Un beau palmier, comme un panache vert,
Dresse sa tête, où le soir les colombes
Viennent nicher et se mettre à couvert.

Mais le matin elles quittent les branches ;
Comme un collier qui s'égrène, on les voit
S'éparpiller dans l'air bleu, toutes blanches,
Et se poser plus loin sur quelque toit.

Mon âme est l'arbre où tous les soirs, comme elles,
De blancs essaims de folles visions
Tombent des cieux en palpitant des ailes,
Pour s'envoler dès les premiers rayons.

— Théophile Gautier, « Les colombes », *La Comédie de la mort*

Appendices

Appendix A

Infinite nuclear matter

> "Whoever undertakes to set himself up as a judge of Truth and Knowledge is shipwrecked by the laughter of the gods."
>
> — Albert Einstein

Homogeneous infinite nuclear matter refers to a boundless neutral medium composed of a large number of nucleons exclusively interacting through the nuclear force. As such, this is a model portraying an ideal system of infinite volume exhibiting translational invariance with no surface effects. It is in particular very useful to describe the core of heavy nuclei whose structure, fairly uniform, is broadly comparable to nuclear matter. In this appendix, we will evaluate various physical quantities as well as stability criteria and sum rules derived from Landau parameters calculated in infinite nuclear matter. They will indeed serve as filters in the selection of parameterizations of the generalized Gogny interaction.

Chapter contents

The first section tries to recall in a concise and pedagogical way the formalisms of infinite nuclear matter (INM) [223] and Hartee–Fock (HF) approximation [4, 224, 225]. The two following sections are mainly based on the thesis of Chappert [17], where we have added the calculations in the general case of asymmetric infinite nuclear matter, which had not been completed, for future applications. Besides, we have extended those calculations to the newly introduced finite-range tensor and spin–orbit interactions. The derivations of the Landau parameters associated with central and density-dependent interactions are established from [226], and continued for the tensor and spin–orbit forces. Finally, the stability criteria and sum rules of tensor-dependent interactions found in the literature [163, 164] are applied to the generalized Gogny interaction.

1. Hartree–Fock approximation in nuclear matter

Let us mention right away the conditions under which we will be working all along this appendix. By *homogeneous* INM, we mean that it manifests the same properties everywhere in the medium. Moreover, we will postulate both an *(isospin)-asymmetric* and a *spin-saturated* INM. Asymmetric INM refers to a medium where there is not as many protons as neutrons. As for spin-saturated (or spin-symmetric, or even spin-unpolarized) INM, we mean that there is no spin excess, i.e. there is as many protons and neutrons of spin up than protons and neutrons of spin down. Formally, if we designate by $N_\uparrow$ and $N_\downarrow$ (respectively by $Z_\uparrow$ and $Z_\downarrow$) the number of neutrons (respectively protons) with spin up and with spin down, an asymmetric medium corresponds to $N_\uparrow + N_\downarrow \neq Z_\uparrow + Z_\downarrow$, while a spin-saturated medium satisfies $N_\uparrow + Z_\uparrow = N_\downarrow + Z_\downarrow$. These are the three characteristics of what we simply call infinite nuclear matter in the following. Sometimes we will specify the asymmetry of the medium (see the asymmetry parameter defined in (A.29)) or, in footnotes, the changes to be made when other assumptions are released.

In this chapter, various physical quantities will be evaluated in INM at the HF approximation. It is therefore appropriate to recall the INM and HF formalisms, thanks to [4, 17].

1.1. Plane wave representation

In INM, nucleons are described by plane wave functions. The associated quantum states of this basis are characterized by the set of quantum numbers

$$|\vec{k}st\rangle, \tag{A.1}$$

where $\vec{k}$ is the wave vector describing the spatial degrees of freedom, and $s = \pm 1/2$ and $t = \pm 1/2$ the projections of the spin and isospin along the quantization axis, chosen to be Oz, respectively.

The plane wave functions then take the form

$$\Phi_{\vec{k}st}(\vec{r},\sigma,\tau) = \langle \vec{r}\sigma\tau|\vec{k}st\rangle = \phi_{\vec{k}}(\vec{r})\xi_s(\sigma)\zeta_t(\tau), \tag{A.2}$$

where $\xi_s(\sigma)$ and $\zeta_t(\tau)$ are the (normalized) spin and isospin wave functions, associated with σ and τ, the Pauli matrices describing the spin and isospin degrees of freedom, respectively, and where the spatial plane wave functions are expressed as

$$\phi_{\vec{k}}(\vec{r}) = \frac{1}{\sqrt{\mathcal{V}}}\,\mathrm{e}^{\mathrm{i}\vec{k}\cdot\vec{r}}, \tag{A.3}$$

with the normalization coefficient $1/\sqrt{\mathcal{V}}$ involving the volume $\mathcal{V}$ of the nuclear medium. If the nucleons are moving in a finite volume, the situation is equivalent to particles trapped in a three-dimensional box in such a way that the boundary conditions impose quantified momenta $\vec{k}$. If, instead, the volume is infinite, we have no such conditions and the momenta are considered continuous. To go from a finite to an infinite volume, one must therefore perform the following transformation

$$\sum_{\vec{k}} \to \frac{\mathcal{V}}{(2\pi)^3}\int \mathrm{d}^3k. \tag{A.4}$$

We demand the plane wave functions to be orthogonal, i.e. to satisfy the orthogonality relation, for continuous momenta,

$$\sum_{\sigma\tau}\int \mathrm{d}^3r\,\Phi^*_{\vec{k}st}(\vec{r},\sigma,\tau)\Phi_{\vec{k}'s't'}(\vec{r},\sigma,\tau) = \delta(\vec{k}-\vec{k}')\delta_{ss'}\delta_{tt'}. \tag{A.5}$$

1.2. Hartree–Fock approximation

In general, the Schrödinger equation governing the dynamics of the A nucleons within a nucleus is

$$H|\psi\rangle \equiv \left[\sum_{i=1}^{A}\frac{p_i^2}{2m} + \sum_{i<j} v_{ij}\right]|\psi\rangle = \mathcal{E}|\psi\rangle. \tag{A.6}$$

This equation is not exactly solvable because of the interaction term v_{ij} which implies that the A-body wave function $|\psi\rangle$ depends on the degrees of freedom of all the nucleons, leading to a tremendous problem for which there unfortunately exists no general solution. One way to get around this issue is to assume that the nucleons move independently of each other in an average potential, called the *mean field*, created by their neighbors. This is the independent particle picture. In this approximation, the A-body wave function Φ_{HF} becomes separable and can therefore be expressed as a product of one-particle wave

functions φ^{HF}. To account for the antisymmetry of fermionic systems, this wave function is expressed as a Slater determinant of the type

$$\Phi_{\mathrm{HF}}(\xi_1,\ldots,\xi_A) = \frac{1}{\sqrt{A!}}\begin{vmatrix} \varphi_1^{\mathrm{HF}}(\xi_1) & \cdots & \varphi_A^{\mathrm{HF}}(\xi_1) \\ \vdots & \ddots & \vdots \\ \varphi_1^{\mathrm{HF}}(\xi_A) & \cdots & \varphi_A^{\mathrm{HF}}(\xi_A) \end{vmatrix}, \tag{A.7}$$

where ξ_i stands for the degrees of freedom of the i-th individual wave function φ_i^{HF}, with $i \in \{1,\ldots,A\}$.

Based on the independent particle picture, the Hartree–Fock (HF) method is a variational approach in which the Slater determinant Φ_{HF} is taken as trial wave function. Then, the Hartree–Fock energy, corresponding to the average energy of the nucleus in the (normalized) determinantal state $|\Phi_{\mathrm{HF}}\rangle$, is simply $\mathcal{E}_{\mathrm{HF}} \equiv \langle\Phi_{\mathrm{HF}}|H|\Phi_{\mathrm{HF}}\rangle$. In order to evaluate the HF energy, we shall rewrite the nuclear Hamiltonian (A.6) in the second quantization formalism, i.e.

$$H = \sum_{ab}\langle a|t_{\mathrm{K}}|b\rangle c_a^\dagger c_b + \frac{1}{4}\sum_{abcd}\langle ac|v_{12}^{(\mathrm{a})}|bd\rangle c_a^\dagger c_c^\dagger c_d c_b, \tag{A.8}$$

with the above states characterizing the individual wave functions of the Slater determinant. We have defined the usual one-body kinetic operator in terms of the momentum operator $p \equiv \hbar k$ as

$$t_{\mathrm{K}} \equiv \frac{p^2}{2m}, \tag{A.9}$$

as well as the antisymmetrized interaction

$$v_{12}^{(\mathrm{a})} \equiv v_{12}(1 - P_r P_\sigma P_\tau). \tag{A.10}$$

As for the A-body HF wave function (A.7), it becomes, in second quantization,

$$|\Phi_{\mathrm{HF}}\rangle = \prod_{a\in F} c_a^\dagger\,|0\rangle, \tag{A.11}$$

where F is the Fermi sea and $|0\rangle$ the vacuum particle state. Using Wick's theorem, we show that the total energy of the nucleus reads, at the HF approximation,

$$\mathcal{E}_{\mathrm{HF}} = \sum_{ab}\langle a|t_{\mathrm{K}}|b\rangle\rho_{ba} + \frac{1}{2}\sum_{abcd}\langle ac|v_{12}^{(\mathrm{a})}|bd\rangle\rho_{ba}\rho_{db}, \tag{A.12}$$

where we have defined the one-body density matrix as $\rho_{ba} \equiv \langle\Phi_{\mathrm{HF}}|c_a^\dagger c_b|\Phi_{\mathrm{HF}}\rangle$. One can show that choosing a Slater determinant as trial wave function amounts to requiring that the density matrix satisfies the relation $\rho^2 = \rho$. Thus, the HF approach consists in minimizing the HF energy while preserving this condition by means of Lagrange multipliers. This amounts to minimizing the functional

$$\mathcal{F}[\rho] \equiv \mathcal{E}_{\mathrm{HF}}[\rho] - \Lambda(\rho^2 - \rho), \tag{A.13}$$

where Λ is a matrix composed of Lagrange multipliers ensuring the requirement $\rho^2 = \rho$. The stationary condition $\mathrm{d}\mathcal{F} = 0$ finally leads to the so-called HF equation,

$$\boxed{\left[h^{\mathrm{HF}}, \rho\right] = 0,} \tag{A.14}$$

where we have defined the individual (or one-body) Hamiltonian to which each nucleon of the nucleus is subjected, as $h^{\mathrm{HF}} \equiv \partial \mathcal{E}_{\mathrm{HF}}/\partial\rho$. This relation tells us there exists a basis in which both the individual Hamiltonian and the density matrix are diagonal. In this basis, hereafter called the *HF basis*, the density matrix is simply

$$\rho_{ab} = \delta_{ab}\rho_{aa} = \begin{cases} 1 & \text{if } |a\rangle \text{ is occupied,} \\ 0 & \text{otherwise.} \end{cases} \tag{A.15}$$

Let us then rewrite the HF energy in this basis, in terms of HF fields, as

$$\mathcal{E}_{\mathrm{HF}} = \mathcal{E}_{\mathrm{K}} + \mathcal{E}_{\mathrm{P}} = \mathcal{E}_{\mathrm{K}} + \mathcal{E}_{\mathrm{MF}}, \tag{A.16}$$

where the kinetic energy

$$\mathcal{E}_{\mathrm{K}} \equiv \sum_a K_{aa}\rho_{aa}, \tag{A.17}$$

is expressed in terms of the kinetic field

$$\boxed{K_{aa} \equiv \langle a|t_{\mathrm{K}}|a\rangle,} \tag{A.18}$$

and the potential energy drawing, at the HF approximation, its only contribution from the mean-field energy,

$$\mathcal{E}_{\mathrm{P}} = \mathcal{E}_{\mathrm{MF}} \equiv \frac{1}{2}\sum_a \Gamma_{aa}\rho_{aa}, \tag{A.19}$$

is expressed in terms of the mean field in the HF basis,

$$\boxed{\Gamma_{aa} \equiv \sum_b \langle ab|v_{12}^{(\mathrm{a})}|ab\rangle\rho_{bb}.} \tag{A.20}$$

As for the individual Hamiltonian in the HF basis, $h_{aa}^{\mathrm{HF}} \equiv \partial\mathcal{E}_{\mathrm{HF}}/\partial\rho_{aa}$, it reads

$$h_{aa}^{\mathrm{HF}} = K_{aa} + \Gamma_{aa} + \partial\Gamma_{aa}, \tag{A.21}$$

where we have introduced the rearrangement field in the HF basis,

$$\boxed{\partial\Gamma_{aa} \equiv \frac{1}{2}\sum_{a'b'} \langle a'b'|\frac{\partial v_{12}^{(\mathrm{a})}}{\partial\rho_{aa}}|a'b'\rangle\rho_{a'a'}\rho_{b'b'}.} \tag{A.22}$$

Since each of the fields describing the individual Hamiltonian at the HF approximation in the HF basis (A.21) is diagonal (as the density matrices are), the individual Hamiltonian is diagonal itself. Therefore, each non-zero matrix element of this Hamiltonian corresponds to an eigenvalue $\varepsilon_a^{\mathrm{HF}}$, identified as an individual (or one-body) energy, i.e.

$$\varepsilon_a^{\mathrm{HF}} = h_{aa}^{\mathrm{HF}} = K_{aa} + \Gamma_{aa} + \partial\Gamma_{aa}. \tag{A.23}$$

In INM, the plane wave functions are exact solutions of the one-particle Schrödinger equation. Thus, the individual wave functions φ_i^{HF} ($i \in \{1, \ldots, A\}$) of the Slater determinant (A.7) are simply those of the plane waves (A.2). In other words, the states appearing in the above HF quantities will be (A.1) in INM. Note also that in practical calculations, we will not bother with the density matrix (A.15) since it is always equal to unity, in the HF basis, for the occupied states on which the summations are performed.

2. Energy in infinite nuclear matter

In this section, we will derive the energy in INM at the HF approximation, in the HF basis, as outlined in the previous section.

To be able to do so, we will first need the evaluate the local nuclear density in this formalism. In general, the local nuclear density is given by

$$\rho(\vec{r}) \equiv \sum_{\sigma\tau} \langle \vec{r}\sigma\tau|\rho|\vec{r}\sigma\tau\rangle \tag{A.24}$$

$$= \sum_{\sigma\tau}\sum_{ab} \Phi_a^*(\vec{r},\sigma,\tau)\Phi_b(\vec{r},\sigma,\tau)\rho_{ba}. \tag{A.25}$$

From the first to the second line, we have used two completeness relations associated with the sets of quantum numbers a and b characterizing some states. The chosen wave functions are denoted by Φ, and $\rho_{ba} \equiv \langle a|\rho|b\rangle$ are the (matrix elements of the) density matrix expressed in this basis.

Then, the density of isospin-t particles in INM reads

$$\begin{aligned}
\rho_t(\vec{r}) &\equiv \sum_{\sigma\tau}\sum_{\vec{k}_1 s_1}\sum_{\vec{k}_2 s_2} \Phi^*_{\vec{k}_1 s_1 t_1}(\vec{r},\sigma,\tau)\Phi_{\vec{k}_1 s_2 t_2}(\vec{r},\sigma,\tau)\rho_{\vec{k}_1 s_1 t,\vec{k}_2 s_2 t} \\
&= \frac{\mathcal{V}}{(2\pi)^3}\sum_s \int \mathrm{d}^3k\, \phi^*_{\vec{k}st}(\vec{r},\sigma,\tau)\phi_{\vec{k}st}(\vec{r},\sigma,\tau) \\
&= \frac{2\mathcal{V}}{(2\pi)^2}\sum_s \int_0^{k_\mathrm{F}^t} \mathrm{d}k\, k^2 \phi^*_{\vec{k}st}(\vec{r},\sigma,\tau)\phi_{\vec{k}st}(\vec{r},\sigma,\tau) \\
&= \frac{(k_\mathrm{F}^t)^3}{3\pi^2},
\end{aligned} \tag{A.26}$$

where we have used the particular form of the density matrix in the HF basis (A.15), the plane wave functions (A.2) and the orthogonality relation (A.5). Above, the Fermi momentum of the isospin-t particle is denoted by k_F^t. We notice that the local density is, as expected, *constant* in infinite nuclear matter, i.e. $\rho(\vec{r}) = \rho$, as a signature of its invariance by translation. Now, the total nuclear density is nothing but the sum of the neutron ρ_ν and proton ρ_π density contributions, i.e.

$$\boxed{\rho = \rho_\nu + \rho_\pi = \frac{2k_\mathrm{F}^3}{3\pi^2},} \tag{A.27}$$

where the total Fermi momentum can be expressed as

$$k_\mathrm{F}^3 = \frac{(k_\mathrm{F}^\nu)^3 + (k_\mathrm{F}^\pi)^3}{2}. \tag{A.28}$$

In order to evaluate the proportion of neutrons and protons in INM, we introduce the asymmetry parameter

$$\beta \equiv \frac{\rho_\nu - \rho_\pi}{\rho}. \tag{A.29}$$

When there are (not) as many neutrons as protons, $\beta = 0$ ($\beta \neq 0$), infinite nuclear matter is said to be symmetric (asymmetric). When entirely composed of neutrons (protons), $\beta = 1$ ($\beta = -1$), we talk about neutron (proton) infinite nuclear matter.

At the HF approximation, the energy is given by (A.16) in the HF basis, so that

$$\begin{aligned}\mathcal{E} &= \mathcal{E}_{\rm K} + \mathcal{E}_{\rm pot} \\ &= \sum_{\vec{k}st} \langle \vec{k}st|t_{\rm K}|\vec{k}st\rangle \rho_{\vec{k}st,\vec{k}st} \\ &\qquad + \frac{1}{2}\sum_{\vec{k}_1 s_1 t_1}\sum_{\vec{k}_2 s_2 t_2} \langle \vec{k}_1 s_1 t_1\, \vec{k}_2 s_2 t_2|v_{12}^{\rm (a)}|\vec{k}_1 s_1 t_1\ \vec{k}_2 s_2 t_2\rangle \rho_{\vec{k}_1 s_1 t_1,\vec{k}_2 s_2 t_2}.\end{aligned} \tag{A.30}$$

In the following, we will therefore derive this energy by separately evaluating its kinetic and potential contributions in asymmetric, as well as in the particular cases of symmetric ($\beta = 0$) and neutron ($\beta = 1$) infinite nuclear matter. It is indeed the building blocks of the physical quantities we will compute in the next section.

2.1. Kinetic energy

The total kinetic energy reads

$$\begin{aligned}\mathcal{E}_{\rm K} &\equiv \sum_{\vec{k}st} \langle \vec{k}st|t_{\rm K}|\vec{k}st\rangle \rho_{\vec{k}st,\vec{k}st} \\ &= \sum_{\vec{k}st} \frac{\hbar^2 k^2}{2m} \\ &= \frac{\mathcal{V}}{\pi^2}\sum_t \int_0^{k_{\rm F}^t} {\rm d}k\, \frac{\hbar^2 k^4}{2m} \\ &= \sum_t \frac{3}{5}\frac{\hbar^2 (k_{\rm F}^t)^2}{2m}\rho_t \mathcal{V},\end{aligned} \tag{A.31}$$

where we made it possible to separate the proton and neutron contributions to the kinetic energy. Note that the number of nucleons filling INM is $A = \rho\mathcal{V}$, such that the kinetic energy per nucleon can be expressed as

$$\boxed{\frac{\mathcal{E}_{\rm K}}{A} = \sum_t \frac{3}{5}\frac{\hbar^2 (k_{\rm F}^t)^2}{2m}\frac{\rho_t}{\rho}.} \tag{A.32}$$

We shall keep the kinetic energy written this way since it is the most suitable one for computing the different particular cases we will consider in the following.

2.2. Potential energy

The total potential energy is

$$\mathcal{E}_{\rm P} \equiv \frac{1}{2}\sum_{\vec{k}_1 s_1 t_1}\sum_{\vec{k}_2 s_2 q_2} \langle \vec{k}_1 s_1 t_1\, \vec{k}_2 s_2 t_2|v_{12}^{\rm (a)}|\vec{k}_1 s_1 t_1\ \vec{k}_2 s_2 q_2\rangle \rho_{\vec{k}_1 s_1 t_1,\vec{k}_2 s_2 t_2}, \tag{A.33}$$

where the antisymmetrized two-body interaction is given by $v_{12}^{\rm (a)} \equiv v_{12}(1 - P_r P_\sigma P_\tau)$. In the following, we will evaluate this potential for each term of the generalized Gogny interaction (II.1).

2.2.1. Central and density-dependent contributions

Let us start with the contributions of the central and density-dependent (CDD) interactions to the potential energy (A.33). The antisymmetrized CDD interactions can be encompassed in the following expression,

$$\begin{aligned} v_{12}^{\mathrm{CDD,(a)}} &\equiv v_{12}^{\mathrm{CDD}}(1 - P_r P_\sigma P_\tau) \\ &= (W + BP_\sigma - HP_\tau - MP_\sigma P_\tau) V(r_{12}) D[\rho](1 - P_r P_\sigma P_\tau) \\ &= \mathcal{P}_{\mathrm{D}} V(r_{12}) D[\rho] + \mathcal{P}_{\mathrm{E}} V(r_{12}) D[\rho] P_r, \end{aligned} \tag{A.34}$$

with the Gaussian potential

$$V(r_{12}) \equiv \mathrm{e}^{-(\vec{r}_1 - \vec{r}_2)^2/\mu^2}, \tag{A.35}$$

and the functional of the density, specific to the density-dependent interaction,

$$D[\rho] \equiv \frac{\rho^\alpha(\vec{r}_1) + \rho^\alpha(\vec{r}_2)}{2}. \tag{A.36}$$

The central contributions to the potential energy are obtained by setting $\alpha = 0$ and summing over the central ranges μ_1 and μ_2. To get the density-dependent term, it suffices to consider $\alpha \neq 0$ and choose a third range μ_3 (up to some factor $1/(\mu\sqrt{\pi})^3$ we do not keep in the following for simplicity). On the other hand, the spin-isospin components of the direct and exchange components of the CDD interaction are respectively

$$\mathcal{P}_{\mathrm{D}} \equiv W + BP_\sigma - HP_\tau - MP_\sigma P_\tau, \tag{A.37a}$$

$$\mathcal{P}_{\mathrm{E}} \equiv M + HP_\sigma - BP_\tau - WP_\sigma P_\tau. \tag{A.37b}$$

Separating the spatial and spin-isospin two-body matrix elements (TBMEs) as well as the direct and exchange components of the CDD interaction, the potential energy becomes

$$\begin{aligned} \mathcal{E}_{\mathrm{P}} = \frac{1}{2} \sum_{\vec{k}_1 s_1 t_1} \sum_{\vec{k}_2 s_2 t_2} \Big[&\langle \vec{k}_1 \vec{k}_2 | V(r_{12}) D[\rho] | \vec{k}_1 \vec{k}_2 \rangle \langle s_1 t_1 s_2 t_2 | \mathcal{P}_{\mathrm{D}} | s_1 t_1 s_2 t_2 \rangle \\ &+ \langle \vec{k}_1 \vec{k}_2 | V(r_{12}) D[\rho] | \vec{k}_2 \vec{k}_1 \rangle \langle s_1 t_1 s_2 t_2 | \mathcal{P}_{\mathrm{E}} | s_1 t_1 s_2 t_2 \rangle \Big]. \end{aligned} \tag{A.38}$$

Let us now start by calculating the spatial TBMEs of the potential energy. The direct component reads, by definition,

$$\begin{aligned} \langle \vec{k}_1 \vec{k}_2 | V(r_{12}) D[\rho] | \vec{k}_1 \vec{k}_2 \rangle &\equiv \int \mathrm{d}^3 r_1 \int \mathrm{d}^3 r_2 \, \phi^*_{\vec{k}_1}(\vec{r}_1) \phi^*_{\vec{k}_2}(\vec{r}_2) V(r_{12}) D[\rho] \phi_{\vec{k}_1}(\vec{r}_1) \phi_{\vec{k}_2}(\vec{r}_2) \\ &= \frac{1}{\mathcal{V}^2} \int \mathrm{d}^3 r_1 \int \mathrm{d}^3 r_2 \, \mathrm{e}^{-(\vec{r}_1 - \vec{r}_2)^2/\mu^2} \frac{\rho^\alpha(\vec{r}_1) + \rho^\alpha(\vec{r}_2)}{2} \\ &= \frac{\rho^\alpha}{\mathcal{V}^2} \int \mathrm{d}^3 r \int \mathrm{d}^3 R \, \mathrm{e}^{-r^2/\mu^2} \\ &= \frac{\rho^\alpha}{\mathcal{V}} \int \mathrm{d}^3 r \, \mathrm{e}^{-r^2/\mu^2}. \end{aligned} \tag{A.39}$$

where, from the second to the third line, we have used the translational invariance of INM, i.e. $\rho(\vec{r}_1) = \rho(\vec{r}_2) = \rho$, and moved from nucleon coordinates $(\vec{r}_1, \vec{r}_2)$ to the relative and center-of-mass coordinates $(\vec{r}, \vec{R})$, defined as [1]

$$\vec{r} \equiv \vec{r}_1 - \vec{r}_2, \quad \text{and} \quad \vec{R} \equiv \frac{\vec{r}_1 + \vec{r}_2}{2}, \tag{A.40}$$

1. Note that these conventions for the relative and center-of-mass coordinates are different from the ones we will consider in the calculations related to the spherical (see (B.224)) and axial (see (C.513)) harmonic oscillators.

whose Jacobian is equal to unity. Finally, considering the relative distance between two nucleons as being potentially infinite in INM, that is, assuming an infinite volume of the medium, $\mathcal{V} \to \infty$, the Gauss integral (D.118) eventually furnishes

$$\boxed{\langle \vec{k}_1 \vec{k}_2 | V(r_{12}) D[\rho] | \vec{k}_1 \vec{k}_2 \rangle = \frac{\rho^\alpha}{\mathcal{V}} (\mu\sqrt{\pi})^3.} \tag{A.41}$$

Since the above matrix element does not explicitly depend on the momenta $\vec{k}_1$ and $\vec{k}_2$, the contribution of the direct spatial term to the potential energy is straightforward, and at the continuous limit (A.4), reads

$$\boxed{\sum_{\vec{k}_1 \vec{k}_2} \langle \vec{k}_1 \vec{k}_2 | V(r_{12}) D[\rho] | \vec{k}_1 \vec{k}_2 \rangle = \frac{\mathcal{V}\rho^\alpha}{(2\pi)^6} (\mu\sqrt{\pi})^3 \frac{4\pi (k_{\mathrm{F}}^{t_1})^3}{3} \frac{4\pi (k_{\mathrm{F}}^{t_2})^3}{3},} \tag{A.42}$$

where $k_{\mathrm{F}}^{t_1}$ and $k_{\mathrm{F}}^{t_2}$ are the Fermi momenta associated with $\vec{k}_1$ and $\vec{k}_2$, respectively.

Let us continue with the exchange component. We find, by definition,

$$\begin{aligned} \langle \vec{k}_1 \vec{k}_2 | V(r_{12}) D[\rho] | \vec{k}_2 \vec{k}_1 \rangle &\equiv \int \mathrm{d}^3 r_1 \int \mathrm{d}^3 r_2 \, \phi^*_{\vec{k}_1}(\vec{r}_1) \phi^*_{\vec{k}_2}(\vec{r}_2) V(r_{12}) D[\rho] \phi_{\vec{k}_2}(\vec{r}_1) \phi_{\vec{k}_1}(\vec{r}_2) \\ &= \frac{1}{\mathcal{V}^2} \int \mathrm{d}^3 r_1 \int \mathrm{d}^3 r_2 \, \mathrm{e}^{-\mathrm{i}(\vec{k}_1 - \vec{k}_2)\cdot(\vec{r}_1 - \vec{r}_2)} \mathrm{e}^{-(\vec{r}_1 - \vec{r}_2)^2/\mu^2} \frac{\rho^\alpha(\vec{r}_1) + \rho^\alpha(\vec{r}_2)}{2} \\ &= \frac{\rho^\alpha}{\mathcal{V}} \int \mathrm{d}^3 r \, \mathrm{e}^{-\mathrm{i}(\vec{k}_1 - \vec{k}_2)\cdot\vec{r}} \mathrm{e}^{-r^2/\mu^2}, \end{aligned} \tag{A.43}$$

where we have performed the same steps as for the direct term (A.39). The last integral can be evaluated by completing the square of the argument of the above exponential according to

$$-\left[\frac{r^2}{\mu^2} + \mathrm{i}(\vec{k}_1 - \vec{k}_2)\cdot\vec{r} - \frac{(\vec{k}_1 - \vec{k}_2)^2 \mu^2}{4}\right]^2 - \frac{(\vec{k}_1 - \vec{k}_2)^2 \mu^2}{4}, \tag{A.44}$$

so that, we obtain, after the change of variable $\vec{x} \equiv \vec{r}/\mu + \mathrm{i}(\vec{k}_1 - \vec{k}_2)\mu/2$ and a Gaussian integration (D.118),

$$\boxed{\langle \vec{k}_1 \vec{k}_2 | V(r_{12}) D[\rho] | \vec{k}_2 \vec{k}_1 \rangle = \frac{\rho^\alpha}{\mathcal{V}} (\mu\sqrt{\pi})^3 \mathrm{e}^{-(\vec{k}_1 - \vec{k}_2)^2 \mu^2/4}.} \tag{A.45}$$

This time, the contribution of the exchange spatial term to the potential energy is not straightforward because the associated matrix element depends explicitly on the momenta $\vec{k}_1$ and $\vec{k}_2$. Indeed, we have

$$\sum_{\vec{k}_1 \vec{k}_2} \langle \vec{k}_1 \vec{k}_2 | V(r_{12}) D[\rho] | \vec{k}_2 \vec{k}_1 \rangle = \frac{\mathcal{V}\rho^\alpha}{(2\pi)^6} (\mu\sqrt{\pi})^3 \int \mathrm{d}^3 k_1 \int \mathrm{d}^3 k_2 \, \mathrm{e}^{-(\vec{k}_1 - \vec{k}_2)^2 \mu^2/4}. \tag{A.46}$$

Since the calculation of this integral is a bit long and wearisome, we have reported it in section D.7.2, for clarity. We find out, at the continuous limit (A.4),

$$\boxed{\sum_{\vec{k}_1 \vec{k}_2} \langle \vec{k}_1 \vec{k}_2 | V(r_{12}) D[\rho] | \vec{k}_2 \vec{k}_1 \rangle = \frac{\mathcal{V}\rho^\alpha}{(2\pi)^6} (\mu\sqrt{\pi})^3 I(X_{t_1}, X_{t_2}),} \tag{A.47}$$

where we have defined the dimensionless quantity $X_t \equiv \mu k_{\mathrm{F}}^t$, and where $I(X_{t_1}, X_{t_2})$, derived in (D.141), is given by

$$I(X_{t_1}, X_{t_2}) = \left(\frac{2}{\mu}\right)^6 \frac{\pi^2}{6} Q(X_{t_1}, X_{t_2}), \tag{A.48}$$

with

$$\begin{aligned} Q(X_{t_1}, X_{t_2}) \equiv\ & \mathrm{e}^{-\left(\frac{X_{t_1}+X_{t_2}}{2}\right)^2}\left(X_{t_1}^2 + X_{t_2}^2 - X_{t_1}X_{t_2} - 2\right) \\ & - \mathrm{e}^{-\left(\frac{X_{t_1}-X_{t_2}}{2}\right)^2}\left(X_{t_1}^2 + X_{t_2}^2 + X_{t_1}X_{t_2} - 2\right) \\ & + \frac{\sqrt{\pi}}{2}\operatorname{erf}\left(\frac{X_{t_1}+X_{t_2}}{2}\right)\left(X_{t_1}^3 + X_{t_2}^3\right) \\ & - \frac{\sqrt{\pi}}{2}\operatorname{erf}\left(\frac{X_{t_1}-X_{t_2}}{2}\right)\left(X_{t_1}^3 - X_{t_2}^3\right). \end{aligned} \tag{A.49}$$

Now that we have obtained some expressions for the spatial parts of the potential energy (A.38), let us do the same for its spin-isospin parts. By going from the two-particle representation to the coupled one, we get, for the direct part,

$$\begin{aligned} \langle s_1 q_1 s_2 t_2 | W + BP_\sigma - HP_\tau - MP_\sigma P_\tau | s_1 q_1 s_2 t_2 \rangle = & \sum_{SM_S}\sum_{TM_T} \langle 1/2 s_1 1/2 s_2 | S M_S \rangle^2 \\ & \times \langle 1/2 t_1 1/2 t_2 | T M_T \rangle^2 (W - (-)^S B + (-)^T H - (-)^{S+T} M), \end{aligned} \tag{A.50}$$

where the brackets denote the Clebsch–Gordan coefficients. Since we have $s_1, s_2 = \pm 1/2$, the summations over s_1 and s_2 in the potential energy make the spin Clebsch–Gordan coefficients disappear. Note that we cannot apply the same procedure for the isospin Clebsch–Gordan coefficients as we have shown that the space parts of the potential energy explicitly depend on the isospins (see equations (A.42) and (A.47)). The process is the same for the exchange spin-isospin part, and the potential energy (A.38) becomes

$$\begin{aligned} \mathcal{E}_{\mathrm{P}} = & \frac{1}{2}\sum_{t_1 t_2}\sum_{TM_T} \langle 1/2 t_1 1/2 t_2 | T M_T \rangle^2 \sum_S (2S+1) \\ & \times \sum_{\vec{k}_1 \vec{k}_2} \Big[\langle \vec{k}_1 \vec{k}_2 | V(r_{12}) D[\rho] | \vec{k}_1 \vec{k}_2 \rangle \Big(W - (-)^S B + (-)^T H - (-)^{S+T} M \Big) \\ & + \langle \vec{k}_1 \vec{k}_2 | V(r_{12}) D[\rho] | \vec{k}_2 \vec{k}_1 \rangle \Big(M - (-)^S H + (-)^T B - (-)^{S+T} W \Big) \Big], \end{aligned} \tag{A.51}$$

where we have additionally performed the summation over M_S. The potential energy can be written in the condensed notation

$$\begin{aligned} \mathcal{E}_{\mathrm{P}} = 8\sqrt{\pi} \sum_{t_1 t_2}\sum_{ST} \mathcal{L}^T_{t_1 t_2} \sum_{\vec{k}_1 \vec{k}_2} \Big[& \mathcal{A}^{ST} \langle \vec{k}_1 \vec{k}_2 | V(r_{12}) D[\rho] | \vec{k}_1 \vec{k}_2 \rangle \\ & - \mathcal{B}^{ST} \langle \vec{k}_1 \vec{k}_2 | V(r_{12}) D[\rho] | \vec{k}_2 \vec{k}_1 \rangle \Big], \end{aligned} \tag{A.52}$$

where we have defined

$$\mathcal{L}^T_{t_1 t_2} \equiv \frac{1}{2T+1} \sum_{M_T} \langle 1/2 t_1 1/2 t_2 | T M_T \rangle^2, \tag{A.53a}$$

$$\mathcal{A}^{ST} \equiv \frac{(2S+1)(2T+1)}{16\sqrt{\pi}} \Big(W - (-)^S B + (-)^T H - (-)^{S+T} M \Big), \tag{A.53b}$$

$$\mathcal{B}^{ST} \equiv -\frac{(2S+1)(2T+1)}{16\sqrt{\pi}} \Big(M - (-)^S H + (-)^T B - (-)^{S+T} W \Big). \tag{A.53c}$$

Noticing that the volume can be written $\mathcal{V} = A/\rho = A \times 3\pi^2\mu^3/2X^3$, with $X \equiv \mu k_{\mathrm{F}}$, and plugging the expressions of the space parts (A.42) and (A.47), we write down the potential energy per nucleon as

$$\frac{\mathcal{E}_{\mathrm{P}}}{A} = 2\frac{\rho^\alpha}{X^3}\sum_{ST}\sum_{t_1t_2}\mathcal{L}^T_{t_1t_2}\left[\mathcal{A}^{ST}\frac{(X_{t_1}X_{t_2})^3}{6} - \mathcal{B}^{ST}Q(X_{t_1},X_{t_2})\right], \tag{A.54}$$

where $Q(X_{t_1},X_{t_2})$ is defined above. Using the particular values of the Clebsch–Gordan coefficients and the fact that $T^2 = T$, we obtain, from (A.53a),

$$\mathcal{L}^T_{t_1t_2} = \frac{1}{2T+1}\left[T\delta_{t_1t_2} + \frac{1}{2}\delta_{t_1,-t_2}\right], \tag{A.55}$$

so that, by doing the summations over the projections of the isospins t_1 and t_2, we separate the proton π and neutron ν contributions according to

$$\begin{aligned}\frac{\mathcal{E}_{\mathrm{P}}}{A} = 2\frac{\rho^\alpha}{X^3}\sum_{ST}\frac{1}{2T+1}\Bigg[&\frac{\mathcal{A}^{ST}}{6}\Big(TX_\pi^6 + TX_\nu^6 + X_\pi^3X_\nu^3\Big)\\ &- \mathcal{B}^{ST}\Big(TQ(X_\pi,X_\pi) + TQ(X_\nu,X_\nu) + Q(X_\pi,X_\nu)\Big)\Bigg].\end{aligned} \tag{A.56}$$

It remains to perform the last two summations over S and T. Thus, the contribution from the central and density-dependent terms to the potential energy per nucleon in asymmetric INM reads

$$\boxed{\begin{aligned}\frac{\mathcal{E}_{\mathrm{P}}}{A} = \frac{\rho^\alpha}{X^3}\Bigg[&\frac{\mathcal{A}}{6}\Big(X_\pi^6 + X_\nu^6\Big) - \frac{\mathcal{A}'}{6}\Big(X_\pi^3 - X_\nu^3\Big)^2\\ &+ (\mathcal{B}' - \mathcal{B})\Big(Q(X_\pi,X_\pi) + Q(X_\nu,X_\nu)\Big) - 2\mathcal{B}'Q(X_\pi,X_\nu)\Bigg],\end{aligned}} \tag{A.57}$$

with the quantities

$$\mathcal{A} \equiv \sum_{ST}\mathcal{A}^{ST} = \frac{1}{2\sqrt{\pi}}\Big(2W + B - H - \frac{M}{2}\Big), \tag{A.58a}$$

$$\mathcal{B} \equiv \sum_{ST}\mathcal{A}^{ST} = \frac{1}{2\sqrt{\pi}}\Big(\frac{W}{2} + B - H - 2M\Big), \tag{A.58b}$$

$$\mathcal{A}' \equiv \sum_{ST}\frac{\mathcal{A}^{ST}}{2T+1} = \frac{1}{2\sqrt{\pi}}\Big(W + \frac{B}{2}\Big), \tag{A.58c}$$

$$\mathcal{B}' \equiv \sum_{ST}\frac{\mathcal{B}^{ST}}{2T+1} = -\frac{1}{2\sqrt{\pi}}\Big(M + \frac{H}{2}\Big). \tag{A.58d}$$

2.2.2. Tensor contribution

Let us continue with the contribution of the tensor interaction to the total potential energy (A.33). The antisymmetrized tensor interaction can be expressed as

$$\begin{aligned}v_{12}^{\mathrm{T},(\mathrm{a})} &\equiv v_{12}^{\mathrm{T}}(1 - P_rP_\sigma P_\tau)\\ &= (W - HP_\tau)V(r_{12})S_{12}(1 - P_rP_\tau)\\ &= \mathcal{P}_{\mathrm{D}}V(r_{12})S_{12} + \mathcal{P}_{\mathrm{E}}V(r_{12})S_{12}P_r,\end{aligned} \tag{A.59}$$

where the Gaussian potential is expressed in (A.35), and where the tensor operator S_{12}, given by (D.49), removes the operator P_σ since it acts symmetrically on the spin variables (see discussion in section II). As for the isospin components of the direct and exchange tensor interaction, they are respectively

$$\mathcal{P}_{\mathrm{D}} \equiv W - HP_\tau, \tag{A.60a}$$
$$\mathcal{P}_{\mathrm{E}} \equiv H - WP_\tau. \tag{A.60b}$$

Using the equivalent form of the tensor operator (D.58) and separating the spatial and spin-isospin TBMEs as well as the direct and exchange components of the tensor interaction, the potential energy becomes

$$\begin{aligned}\mathcal{E}_{\mathrm{P}} = \frac{1}{2}\sum_l (-)^l \sum_{\vec{k}_1 s_1 t_1} \sum_{\vec{k}_2 s_2 q_2} \\ \times \Big[\langle \vec{k}_1\vec{k}_2|V(r_{12})[\hat{r}_{12}\otimes\hat{r}_{12}]^{(2)}_{-l}|\vec{k}_1\vec{k}_2\rangle\langle s_1t_1s_2t_2|\mathcal{P}_{\mathrm{D}}[\vec{\sigma}_1\otimes\vec{\sigma}_2]^{(2)}_l|s_1t_1s_2t_2\rangle \\ + \langle \vec{k}_1\vec{k}_2|V(r_{12})[\hat{r}_{12}\otimes\hat{r}_{12}]^{(2)}_{-l}|\vec{k}_2\vec{k}_1\rangle\langle s_1t_1s_2t_2|\mathcal{P}_{\mathrm{E}}[\vec{\sigma}_1\otimes\vec{\sigma}_2]^{(2)}_l|s_1t_1s_2t_2\rangle\Big].\end{aligned} \tag{A.61}$$

Let us first consider the direct spin-isospin TBMEs. The spin and isospin degrees of freedom split up in such a way that

$$\langle s_1t_1s_2t_2|\mathcal{P}_{\mathrm{D}}[\vec{\sigma}_1\otimes\vec{\sigma}_2]^{(2)}_l|s_1t_1s_2t_2\rangle = \langle t_1t_2|\mathcal{P}_{\mathrm{D}}|t_1t_2\rangle\langle s_1s_2|[\vec{\sigma}_1\otimes\vec{\sigma}_2]^{(2)}_l|s_1s_2\rangle. \tag{A.62}$$

Then, the spin TBMEs can be evaluated by means of the general formula (D.20). We obtain

$$\langle s_1s_2|[\vec{\sigma}_1\otimes\vec{\sigma}_2]^{(2)}_l|s_1s_2\rangle = 4\sqrt{\frac{2}{3}}s_1s_2\delta_{l,0}, \tag{A.63}$$

so that the spin part of the potential energy associated with the direct component of the tensor interaction vanishes, i.e.

$$\sum_{s_1s_2}\langle s_1s_2|[\vec{\sigma}_1\otimes\vec{\sigma}_2]^{(2)}_l|s_1s_2\rangle = 0. \tag{A.64}$$

At the HF approximation (in the HF basis), the direct component of the tensor interaction does not contribute to the potential energy.

As for the exchange spin-isospin TBMEs, they also split up according to

$$\langle s_1t_1s_2t_2|\mathcal{P}_{\mathrm{E}}[\vec{\sigma}_1\otimes\vec{\sigma}_2]^{(2)}_l|s_2t_2s_1t_1\rangle = \langle t_1t_2|\mathcal{P}_{\mathrm{E}}|t_2t_1\rangle\langle s_1s_2|[\vec{\sigma}_1\otimes\vec{\sigma}_2]^{(2)}_l|s_2s_1\rangle\,. \tag{A.65}$$

The spin TBMEs evaluated with (D.20) gives

$$\langle s_1s_2|[\vec{\sigma}_1\otimes\vec{\sigma}_2]^{(2)}_l|s_2s_1\rangle = 4\sqrt{\frac{2}{3}}s_1s_2\delta_{l,0}(\delta_{s_1s_2}+\delta_{s_1,-s_2}), \tag{A.66}$$

so that the spin part of the potential energy associated with the exchange component of the tensor interaction vanishes, i.e.

$$\sum_{s_1s_2}\langle s_1s_2|[\vec{\sigma}_1\otimes\vec{\sigma}_2]^{(2)}_l|s_2s_1\rangle = 0. \tag{A.67}$$

At the HF approximation (in the HF basis), the exchange component of the tensor interaction does not contribute to the potential energy either. It follows that *the tensor*

contribution to the potential energy is zero at the HF approximation (in the HF basis).[2] It is therefore not necessary to calculate the spatial TBMEs of the tensor interaction as their contribution to the potential energy is already zero. However, it is easy to see that they (only the exchange TBMEs, to be precise) do not vanish in general (see subsection B.4.2.3).

2.2.3. Spin–orbit contribution

Finally, let us look at the contribution of the spin–orbit interaction to the potential energy (A.33). The spin–orbit interaction we consider here is the equivalent writing (D.80). The antisymmetrized spin–orbit interaction can then be written

$$\begin{aligned} v_{12}^{\mathrm{SO,(a)}} &\equiv v_{12}^{\mathrm{SO}}(1 - P_r P_\sigma P_\tau) \\ &= (W - HP_\tau)\Big[\overleftarrow{\nabla}_{12} G(r_{12}) \times \vec{\nabla}_{12}\Big] \cdot (\vec{\sigma}_1 + \vec{\sigma}_2)(1 - P_r P_\tau) \\ &= \mathcal{P}_{\mathrm{D}}\Big[\overleftarrow{\nabla}_{12} G(r_{12}) \times \vec{\nabla}_{12}\Big] \cdot (\vec{\sigma}_1 + \vec{\sigma}_2) \\ &\qquad + \mathcal{P}_{\mathrm{E}}\Big[\overleftarrow{\nabla}_{12} G(r_{12}) \times \vec{\nabla}_{12}\Big] \cdot (\vec{\sigma}_1 + \vec{\sigma}_2) P_r, \end{aligned} \tag{A.68}$$

where we will not need to specify the function $G(r_{12})$, and where we have intentionally omitted the factor $\mathrm{i}B(\mu)/4$ for conciseness (see subsection D.5.1 to get their definitions). Note also that the operator $\vec{\sigma}_1 + \vec{\sigma}_2 = 2\vec{S}$, with $\vec{S}$ given by (II.3), removes the operator P_σ since it acts symmetrically on the spin variables (see discussion in section II). The isospin components of the direct and exchange spin–orbit interaction are respectively

$$\mathcal{P}_{\mathrm{D}} \equiv W - HP_\tau, \tag{A.69a}$$

$$\mathcal{P}_{\mathrm{E}} \equiv H - WP_\tau. \tag{A.69b}$$

Separating the spatial and spin-isospin TBMEs as well as the direct and exchange components of the spin–orbit interaction above, the potential energy becomes

$$\begin{aligned} \mathcal{E}_{\mathrm{P}} = \frac{1}{2} \sum_{\vec{k}_1 s_1 t_1} \sum_{\vec{k}_2 s_2 t_2} \Big[&\langle \vec{k}_1 \vec{k}_2 | \Big[\overleftarrow{\nabla}_{12} G(r_{12}) \times \vec{\nabla}_{12}\Big] | \vec{k}_1 \vec{k}_2 \rangle \cdot \langle s_1 t_1 s_2 t_2 | \mathcal{P}_{\mathrm{D}} (\vec{\sigma}_1 + \vec{\sigma}_2) | s_1 t_1 s_2 t_2 \rangle \\ + &\langle \vec{k}_1 \vec{k}_2 | \Big[\overleftarrow{\nabla}_{12} G(r_{12}) \times \vec{\nabla}_{12}\Big] | \vec{k}_2 \vec{k}_1 \rangle \cdot \langle s_1 t_1 s_2 t_2 | \mathcal{P}_{\mathrm{E}} (\vec{\sigma}_1 + \vec{\sigma}_2) | s_1 t_1 s_2 t_2 \rangle \Big]. \end{aligned} \tag{A.70}$$

Let us first consider the direct spatial TBMEs. By definition, we have,

$$\begin{aligned} &\langle \vec{k}_1 \vec{k}_2 | \Big[\overleftarrow{\nabla}_{12} G(r_{12}) \times \vec{\nabla}_{12}\Big] | \vec{k}_1 \vec{k}_2 \rangle \\ &\equiv \int \mathrm{d}^3 r_1 \int \mathrm{d}^3 r_2 \, \phi^*_{\vec{k}_1}(\vec{r}_1) \phi^*_{\vec{k}_2}(\vec{r}_2) \Big[\overleftarrow{\nabla}_{12} G(r_{12}) \times \vec{\nabla}_{12}\Big] \phi_{\vec{k}_1}(\vec{r}_1) \phi_{\vec{k}_2}(\vec{r}_2) \\ &= \frac{1}{\mathcal{V}^2} \int \mathrm{d}^3 r_1 \int \mathrm{d}^3 r_2 \left(\mathrm{e}^{-\mathrm{i}\vec{k}_1 \cdot \vec{r}_1} \mathrm{e}^{-\mathrm{i}\vec{k}_2 \cdot \vec{r}_2} \overleftarrow{\nabla}_{12} \right) G(r_{12}) \times \left(\vec{\nabla}_{12} \mathrm{e}^{\mathrm{i}\vec{k}_1 \cdot \vec{r}_1} \mathrm{e}^{\mathrm{i}\vec{k}_2 \cdot \vec{r}_2} \right) \\ &= \frac{1}{\mathcal{V}^2} \int \mathrm{d}^3 r_1 \int \mathrm{d}^3 r_2 \, G(r_{12}) \Big[(\vec{k}_1 - \vec{k}_2) \times (\vec{k}_1 - \vec{k}_2) \Big] = 0. \end{aligned} \tag{A.71}$$

At the HF approximation *in INM* (in the HF basis), the direct component of the spin–orbit interaction does not contribute to the potential energy. Let us see also what is going

2. Let us emphasize that this result does not depend on the infinite nuclear matter framework, since the associated spatial matrix elements are generally non-zero for the tensor interaction. Nevertheless, it is specific to the HF basis at the HF approximation which conditions the form of the spin matrix elements, then zero for the tensor interaction.

on with the direct spin-isospin TBME. The spin and isospin degrees of freedom split up in such a way that

$$\langle s_1 t_1 s_2 t_2 | \mathcal{P}_{\mathrm{D}} [\vec{\sigma}_1 + \vec{\sigma}_2]_l^{(1)} | s_1 t_1 s_2 t_2 \rangle = \langle t_1 t_2 | \mathcal{P}_{\mathrm{D}} | t_1 t_2 \rangle \langle s_1 s_2 | [\vec{\sigma}_1 + \vec{\sigma}_2]_l^{(1)} | s_1 s_2 \rangle. \tag{A.72}$$

Then, the spin TBMEs can be evaluated by means of the general formula (D.22). We obtain

$$\langle s_1 s_2 | [\vec{\sigma}_1 + \vec{\sigma}_2]_l^{(1)} | s_1 s_2 \rangle = 2(s_1 + s_2)\delta_{l,0}, \tag{A.73}$$

so that the spin part of the potential energy associated with the direct spin–orbit interaction vanishes, i.e.

$$\sum_{s_1 s_2} \langle s_1 s_2 | [\vec{\sigma}_1 + \vec{\sigma}_2]_l^{(1)} | s_1 s_2 \rangle = 0. \tag{A.74}$$

Just like for the tensor interaction, the direct component of the spin–orbit interaction does not contribute to the potential energy at the HF approximation (in the HF basis).

As for the exchange spatial TBMEs, they read, by definition,

$$\begin{aligned}
&\langle \vec{k}_1 \vec{k}_2 | \Big[\overleftarrow{\nabla}_{12} G(r_{12}) \times \vec{\nabla}_{12} \Big] | \vec{k}_2 \vec{k}_1 \rangle \\
&\equiv \int \mathrm{d}^3 r_1 \int \mathrm{d}^3 r_2 \, \phi^*_{\vec{k}_1}(\vec{r}_1) \phi^*_{\vec{k}_2}(\vec{r}_2) \Big[\overleftarrow{\nabla}_{12} G(r_{12}) \times \vec{\nabla}_{12} \Big] \phi_{\vec{k}_2}(\vec{r}_1) \phi_{\vec{k}_1}(\vec{r}_2) \\
&= \frac{1}{\mathcal{V}^2} \int \mathrm{d}^3 r_1 \int \mathrm{d}^3 r_2 \left(\mathrm{e}^{-\mathrm{i}\vec{k}_1 \cdot \vec{r}_1} \mathrm{e}^{-\mathrm{i}\vec{k}_2 \cdot \vec{r}_2} \overleftarrow{\nabla}_{12} \right) G(r_{12}) \times \left(\vec{\nabla}_{12} \mathrm{e}^{\mathrm{i}\vec{k}_2 \cdot \vec{r}_1} \mathrm{e}^{\mathrm{i}\vec{k}_1 \cdot \vec{r}_2} \right) \\
&= -\frac{1}{\mathcal{V}^2} \int \mathrm{d}^3 r_1 \int \mathrm{d}^3 r_2 \, G(r_{12}) \Big[(\vec{k}_1 - \vec{k}_2) \times (\vec{k}_1 - \vec{k}_2) \Big] = 0.
\end{aligned} \tag{A.75}$$

At the HF approximation *in INM* (in the HF basis), the exchange component of the spin–orbit interaction does not contribute to the potential energy either. Thus, *in INM, the spin–orbit interaction does not contribute to the potential energy since its spatial matrix elements vanish.* As for the exchange spin-isospin TBMEs, they also split up according to

$$\langle s_1 t_1 s_2 t_2 | \mathcal{P}_{\mathrm{E}} [\vec{\sigma}_1 + \vec{\sigma}_2]_l^{(1)} | s_1 t_1 s_2 t_2 \rangle = \langle t_1 t_2 | \mathcal{P}_{\mathrm{E}} | t_2 t_1 \rangle \langle s_1 s_2 | [\vec{\sigma}_1 + \vec{\sigma}_2]_l^{(1)} | s_2 s_1 \rangle. \tag{A.76}$$

Then, the spin TBMEs can be evaluated by means of (D.22). We obtain

$$\langle s_1 s_2 | [\vec{\sigma}_1 + \vec{\sigma}_2]_l^{(1)} | s_2 s_1 \rangle = 2(s_1 + s_2)\delta_{s_1 s_2}\delta_{l,0}, \tag{A.77}$$

so that the spin part of the potential energy associated with the direct spin–orbit interaction vanishes, i.e.

$$\sum_{s_1 s_2} \langle s_1 s_2 | [\vec{\sigma}_1 + \vec{\sigma}_2]_l^{(1)} | s_1 s_2 \rangle = 0. \tag{A.78}$$

Just like for the tensor interaction, the exchange component of the spin–orbit interaction does not contribute to the potential energy at the HF approximation (in the HF basis).

It follows that *the spin–orbit contribution to the potential energy is zero at the HF approximation (in the HF basis).* [3]

3. This result, common to the tensor interaction (see previous subsection), adds to the fact that the spin–orbit interaction does not contribute to the potential energy in INM also because of its spatial matrix elements being zero; which is not the case of the tensor term.

2.3. Energy in symmetric nuclear matter

In the case of symmetric INM ($\beta = 0$), there are as many neutrons as protons, so that $k_{\mathrm{F}}^{\nu} = k_{\mathrm{F}}^{\pi} = k_{\mathrm{F}}$, and then $X_\nu = X_\pi = X$. The kinetic energy per nucleon (A.32) then becomes

$$\boxed{\frac{\mathcal{E}_{\mathrm{K}}^{\mathrm{S}}}{A} = \frac{3}{5}\frac{\hbar^2 k_{\mathrm{F}}^2}{2m}.} \tag{A.79}$$

As for the potential energy per nucleon (A.33), it simplifies as

$$\boxed{\frac{\mathcal{E}_{\mathrm{P}}^{\mathrm{S}}}{A} = 2\rho^\alpha \sum_{ST}\left[\mathcal{A}^{ST}\frac{X^3}{6} - \mathcal{B}^{ST}\left(\mathrm{e}^{-X^2}\left(\frac{1}{X} - \frac{2}{X^3}\right) - \frac{3}{X} + \frac{2}{X^3} + \sqrt{\pi}\,\mathrm{erf}(X)\right)\right].} \tag{A.80}$$

Note that we have restored the dependence in S and T to be able to evaluate the contribution of the energy in the symmetric matter in each channel (S, T) of the interaction.

2.4. Energy in neutron nuclear matter

In the case of infinite neutron (or simply neutron) INM ($\beta = 1$), the medium is only composed of neutrons, so that $k_{\mathrm{F}}^{\pi} = 0$ and $k_{\mathrm{F}}^{\nu} = 2^{1/3}k_{\mathrm{F}}$, and then $X_\pi = 0$ and $X_\nu = 2^{1/3}X$. The kinetic energy per nucleon (A.32) then becomes

$$\boxed{\frac{\mathcal{E}_{\mathrm{K}}^{\mathrm{N}}}{A} = \frac{3}{5}\frac{\hbar^2 (k_{\mathrm{F}}^{\nu})^2}{2m}.} \tag{A.81}$$

As for the potential energy per nucleon (A.33), it simplifies as

$$\boxed{\frac{V_{\mathrm{pot}}^{\nu}}{A} = 4\rho^\alpha \sum_{ST}\frac{T}{2T+1}\left[\mathcal{A}^{ST}\frac{X^3}{6} - \mathcal{B}^{ST}\frac{Q(X_\nu, X_\nu)}{X_\nu^3}\right],} \tag{A.82}$$

where we have restored the dependence in S and T just like for symmetric INM.

3. Physical quantities in infinite nuclear matter

In this section, we will take advantage of the energy considerations from the previous section to evaluate various physical quantities in asymmetric, as well as for symmetric ($\beta = 0$) and neutron ($\beta = 1$) INM.

3.1. Incompressibility

The incompressibility corresponds to the amount of energy needed to modify the density of the medium – here of INM – around the equilibrium position (the energy minimum). The incompressibility is defined by

$$K_\infty \equiv 9\rho^2 \left.\frac{\partial^2 \mathcal{E}/A}{\partial \rho^2}\right|_{\rho_0}, \tag{A.83}$$

which is only valid at the energy minimum corresponding to some nuclear density ρ_0 called the *saturation density*. Mathematically speaking, the first derivative of the energy at that

point is zero (extremum condition), that is to say $\partial\mathcal{E}/\partial\rho|_{\rho_0} = 0$. Given the expression of our kinetic (A.32) and potential (A.33) energies, it will be easier to perform the derivation on the Fermi momentum k_F rather than on the density. The relation between the density and the Fermi momentum (A.27) allows us to write

$$K_\infty \equiv k_\mathrm{F}^2 \frac{\partial^2 \mathcal{E}/A}{\partial k_\mathrm{F}^2}\bigg|_{k_\mathrm{F}^0}, \tag{A.84}$$

where the Fermi momentum corresponding to the saturation density is, using (A.27), $k_\mathrm{F}^0 = (3\pi^2\rho_0/2)^{1/3}$. The extremum condition then becomes $\partial\mathcal{E}/\partial k_\mathrm{F}|_{k_\mathrm{F}^0} = 0$.

Let us start by considering the contribution of the kinetic energy to the incompressibility. Combining equation (A.32) and the Fermi momenta as functions of the asymmetry parameter β, $k_\mathrm{F}^\nu = k_\mathrm{F}(1+\beta)^{1/3}$ and $k_\mathrm{F}^\pi = k_\mathrm{F}(1-\beta)^{1/3}$, we eventually get

$$\boxed{k_\mathrm{F}^2 \frac{\partial^2 \mathcal{E}_\mathrm{K}/A}{\partial k_\mathrm{F}^2}\bigg|_{k_\mathrm{F}^0} = 2\frac{\mathcal{E}_\mathrm{K}}{A}\bigg|_{k_\mathrm{F}^0}.} \tag{A.85}$$

As for the contribution from the potential energy (A.33), the calculation is quite long and error-prone but we made it to the end. In asymmetric INM with some asymmetry parameter β, we obtain

$$\begin{aligned}
k_\mathrm{F}^2 \frac{\partial^2 \mathcal{E}_\mathrm{P}/A}{\partial k_\mathrm{F}^2} = {} & \frac{3(\alpha-1)(3\alpha-4)\rho^\alpha}{X^3}\bigg[\frac{\mathcal{A}}{6}\Big(X_\pi^6 + X_\nu^6\Big) - \frac{\mathcal{A}'}{6}\Big(X_\pi^3 - X_\nu^3\Big)^2 \\
& + (\mathcal{B}-\mathcal{B}')\Big(Q(X_\pi,X_\pi) + Q(X_\nu,X_\nu)\Big) - 2\mathcal{B}'Q(X_\pi,X_\nu)\bigg] \\
& - \frac{6(\alpha-1)\rho^\alpha}{X^2}\bigg[\mathcal{A}\Big((1-\beta)^{1/3}X_\pi^5 + (1+\beta)^{1/3}X_\nu^5\Big) \\
& - \mathcal{A}'\Big((1-\beta)^{1/3}X_\pi^5 - (1+\beta)^{1/3}X_\nu^5\Big)\Big(X_\pi^3 - X_\nu^3\Big) \\
& + (\mathcal{B}-\mathcal{B}')\bigg(\frac{\partial}{\partial X}Q(X_\pi,X_\pi) + \frac{\partial}{\partial X}Q(X_\nu,X_\nu)\bigg) \\
& - 2\mathcal{B}'\frac{\partial}{\partial X}Q(X_\pi,X_\nu)\bigg] \\
& + \frac{\rho^\alpha}{X}\bigg[5\mathcal{A}\Big((1-\beta)^{2/3}X_\pi^4 + (1+\beta)^{2/3}X_\nu^4\Big) \\
& - \mathcal{A}'\Big(2\Big((1-\beta)^{2/3}X_\pi^4 - (1+\beta)^{2/3}X_\nu^4\Big)\Big(X_\pi^3 - X_\nu^3\Big) \\
& + 3\Big((1-\beta)^{1/3}X_\pi^2 - (1+\beta)^{1/3}X_\nu^2\Big)^2\Big) \\
& + (\mathcal{B}-\mathcal{B}')\bigg(\frac{\partial^2}{\partial X^2}Q(X_\pi,X_\pi) + \frac{\partial^2}{\partial X^2}Q(X_\nu,X_\nu)\bigg) \\
& - 2\mathcal{B}'\frac{\partial^2}{\partial X^2}Q(X_\pi,X_\nu)\bigg],
\end{aligned} \tag{A.86}$$

that has to be evaluated at $k_\mathrm{F} = k_\mathrm{F}^0$. Note that the derivatives of the function Q are performed with respect to $X = \mu k_\mathrm{F}$ instead of k_F to get rid of overall μ factors. The first

derivative reads

$$\begin{aligned}\frac{\partial}{\partial X}Q(X_\pi,X_\nu) = \mathrm{e}^{-\left(\frac{X_\pi+X_\nu}{2}\right)^2}\Bigg[&(1-\beta)^{1/3}(2X_\pi-X_\nu)+(1+\beta)^{1/3}(2X_\nu-X_\pi)\\ &-\Big((1-\beta)^{1/3}+(1+\beta)^{1/3}\Big)\\ &\times\left(\left(\frac{X_\pi+X_\nu}{2}\right)\Big(X_\pi^2+X_\nu^2-X_\pi X_\nu-2\Big)-\left(\frac{X_\pi^3+X_\nu^3}{2}\right)\right)\Bigg]\\ &-\mathrm{e}^{-\left(\frac{X_\pi-X_\nu}{2}\right)^2}\Bigg[(1-\beta)^{1/3}(2X_\pi+X_\nu)+(1+\beta)^{1/3}(2X_\nu+X_\pi)\\ &-\Big((1-\beta)^{1/3}-(1+\beta)^{1/3}\Big)\\ &\times\left(\left(\frac{X_\pi-X_\nu}{2}\right)\Big(X_\pi^2+X_\nu^2+X_\pi X_\nu-2\Big)-\left(\frac{X_\pi^3-X_\nu^3}{2}\right)\right)\Bigg]\\ &+\frac{3\sqrt{\pi}}{2}\Bigg[\Big((1-\beta)^{1/3}X_\pi^2+(1+\beta)^{1/3}X_\nu^2\Big)\,\mathrm{erf}\left(\frac{X_\pi+X_\nu}{2}\right)\\ &-\Big((1-\beta)^{1/3}X_\pi^2-(1+\beta)^{1/3}X_\nu^2\Big)\,\mathrm{erf}\left(\frac{X_\pi-X_\nu}{2}\right)\Bigg],\end{aligned} \tag{A.87}$$

and the second derivative is

$$\begin{aligned}\frac{\partial^2}{\partial X^2}Q(X_\pi,X_\nu) = \mathrm{e}^{-\left(\frac{X_\pi+X_\nu}{2}\right)^2}\Bigg\{&2\Big((1-\beta)^{2/3}+(1+\beta)^{2/3}-(1-\beta)^{1/3}(1+\beta)^{1/3}\Big)\\ &-\Big((1-\beta)^{1/3}+(1+\beta)^{1/3}\Big)\\ &\times\Bigg[\left(\frac{(1-\beta)^{1/3}+(1+\beta)^{1/3}}{2}\right)\Bigg(\Big(X_\pi^2+X_\nu^2-X_\pi X_\nu-2\Big)\\ &+(X_\pi+X_\nu)\Big(\frac{X_\pi^3+X_\nu^3}{2}\Big)\Bigg)-3\Big((1-\beta)^{1/3}X_\pi^2+(1+\beta)^{1/3}X_\nu^2\Big)\\ &+\left(\frac{X_\pi+X_\nu}{2}\right)\Big(2\Big((1-\beta)^{1/3}(2X_\pi-X_\nu)\\ &+(1+\beta)^{1/3}(2X_\nu-X_\pi)\Big)-\Big((1-\beta)^{1/3}+(1+\beta)^{1/3}\Big)\\ &\times\left(\frac{X_\pi+X_\nu}{2}\right)\Big(X_\pi^2+X_\nu^2-X_\pi X_\nu-2\Big)\Big)\Bigg]\Bigg\}\\ &-\mathrm{e}^{-\left(\frac{X_\pi-X_\nu}{2}\right)^2}\Bigg\{2\Big((1-\beta)^{2/3}+(1+\beta)^{2/3}\\ &+(1-\beta)^{1/3}(1+\beta)^{1/3}\Big)-\Big((1-\beta)^{1/3}-(1+\beta)^{1/3}\Big)\\ &\times\Bigg[\left(\frac{(1-\beta)^{1/3}-(1+\beta)^{1/3}}{2}\right)\Bigg(\Big(X_\pi^2+X_\nu^2+X_\pi X_\nu-2\Big)\\ &+(X_\pi-X_\nu)\Big(\frac{X_\pi^3-X_\nu^3}{2}\Big)\Bigg)-3\Big((1-\beta)^{1/3}X_\pi^2-(1+\beta)^{1/3}X_\nu^2\Big)\\ &+\left(\frac{X_\pi-X_\nu}{2}\right)\Big(2\Big((1-\beta)^{1/3}(2X_\pi+X_\nu)\\ &+(1+\beta)^{1/3}(2X_\nu+X_\pi)\Big)-\Big((1-\beta)^{1/3}-(1+\beta)^{1/3}\Big)\\ &\times\left(\frac{X_\pi-X_\nu}{2}\right)\Big(X_\pi^2+X_\nu^2+X_\pi X_\nu-2\Big)\Big)\Bigg]\Bigg\}\end{aligned} \tag{A.88}$$

$$+ 3\sqrt{\pi}\Bigg[\Big((1-\beta)^{2/3}X_\pi + (1+\beta)^{2/3}X_\nu\Big)\,\mathrm{erf}\left(\frac{X_\pi + X_\nu}{2}\right) - \Big((1-\beta)^{2/3}X_\pi - (1+\beta)^{2/3}X_\nu\Big)\,\mathrm{erf}\left(\frac{X_\pi - X_\nu}{2}\right)\Bigg].$$

Note that the derivatives of $Q(X_\pi, X_\pi)$ and $Q(X_\nu, X_\nu)$ can easily be deduced from the above ones by making the substitutions $X_\nu \to X_\pi$ and $1+\beta \to 1-\beta$, and $X_\pi \to X_\nu$ and $1-\beta \to 1+\beta$, respectively.

3.1.1. Incompressibility in symmetric nuclear matter

In the case of symmetric INM ($\beta = 0$), there are as many neutrons as protons, so that $k_\mathrm{F}^\nu = k_\mathrm{F}^\pi = k_\mathrm{F}$, and then $X_\nu = X_\pi = X$. Thus, the contribution of the potential energy to the incompressibility (A.86) is greatly simplified, and becomes

$$\boxed{\begin{aligned} k_\mathrm{F}^2\frac{\partial^2\mathcal{E}_\mathrm{P}^\mathrm{S}/A}{\partial k_\mathrm{F}^2} = {}& \frac{3(\alpha-1)(3\alpha-4)\rho^\alpha}{X^3}\left[\frac{\mathcal{A}}{3}X^6 - 2\mathcal{B}Q(X,X)\right] \\ & + \frac{12(\alpha-1)\rho^\alpha}{X^2}\left[\mathcal{A}X^5 - 2\mathcal{B}\frac{\partial}{\partial X}Q(X,X)\right] \\ & + \frac{2\rho^\alpha}{X}\left[5\mathcal{A}X^4 - \mathcal{B}\frac{\partial^2}{\partial X^2}Q(X,X)\right], \end{aligned}} \tag{A.89}$$

that has to be evaluated at $k_\mathrm{F} = k_\mathrm{F}^0$, and where the function Q is simply

$$Q(X,X) = \mathrm{e}^{-X^2}(X^2-2) - 3X^2 + 2 + \sqrt{\pi}X^3\,\mathrm{erf}(X), \tag{A.90}$$

while the derivatives are given by

$$\frac{1}{3}\frac{\partial}{\partial X}Q(X,X) = 2X\left(\mathrm{e}^{-X^2} - 1\right) + \sqrt{\pi}X^2\,\mathrm{erf}(X), \tag{A.91}$$

and

$$\frac{1}{6}\frac{\partial^2}{\partial X^2}Q(X,X) = \mathrm{e}^{-X^2}(1-X^2) - 1 + \sqrt{\pi}X\,\mathrm{erf}(X). \tag{A.92}$$

Plugging these expressions in equation (A.89), we consistently recover the results from Chappert's thesis [17].

3.1.2. Incompressibility in neutron nuclear matter

In the case of neutron INM ($\beta = 1$), the medium is only composed of neutrons, so that $k_\mathrm{F}^\pi = 0$ and $k_\mathrm{F}^\nu = 2^{1/3}k_\mathrm{F}$, and then $X_\pi = 0$ and $X_\nu = 2^{1/3}X$. Thus, the contribution of the potential energy to the incompressibility (A.86) is greatly simplified, and becomes

$$\boxed{\begin{aligned} k_\mathrm{F}^2\frac{\partial^2\mathcal{E}_\mathrm{P}^\nu/A}{\partial k_\mathrm{F}^2} = {}& \frac{3(\alpha-1)(3\alpha-4)\rho^\alpha}{X^3}\left[(\mathcal{A}-\mathcal{A}')\frac{X_\nu^6}{6} + (\mathcal{B}'-\mathcal{B})Q(X_\nu,X_\nu)\right] \\ & - \frac{6(\alpha-1)\rho^\alpha}{X^2}\left[2^{1/3}(\mathcal{A}-\mathcal{A}')X_\nu^5 + (\mathcal{B}'-\mathcal{B})\frac{\partial}{\partial X}Q(X_\nu,X_\nu)\right] \\ & + \frac{\rho^\alpha}{X}\left[2^{2/3}5(\mathcal{A}-\mathcal{A}')X_\nu^4 + (\mathcal{B}'-\mathcal{B})\frac{\partial^2}{\partial X^2}Q(X_\nu,X_\nu)\right], \end{aligned}} \tag{A.93}$$

that has to be evaluated at $k_{\rm F} = k_{\rm F}^0$, and where the function Q is simply

$$Q(X_\nu, X_\nu) = \mathrm{e}^{-X_\nu^2}\Big(X_\nu^2 - 2\Big) - 3X_\nu^2 + 2 + \sqrt{\pi} X_\nu^3 \,\mathrm{erf}(X_\nu), \tag{A.94}$$

while the derivatives are given by

$$\frac{1}{2^{1/3}3}\frac{\partial}{\partial X} Q(X_\nu, X_\nu) = 2X_\nu\Big(\mathrm{e}^{-X_\nu^2} - 1\Big) + \sqrt{\pi} X_\nu^2 \,\mathrm{erf}(X_\nu), \tag{A.95}$$

and

$$\frac{1}{2^{2/3}6}\frac{\partial^2}{\partial X^2} Q(X_\nu, X_\nu) = \mathrm{e}^{-X_\nu^2}\Big(1 - X_\nu^2\Big) - 1 + \sqrt{\pi} X_\nu \,\mathrm{erf}(X_\nu). \tag{A.96}$$

3.2. Symmetry energy

The symmetry energy quantifies the variation of the total energy as a function of the asymmetry β of the medium, here in INM. The symmetry energy is defined by

$$\mathcal{E}_{\rm sym} \equiv \frac{1}{2}\frac{\partial^2 \mathcal{E}/A}{\partial \beta^2}\bigg|_{\beta=0}. \tag{A.97}$$

We notice that the derivative is evaluated at zero asymmetry ($\beta = 0$), i.e. in symmetric INM. Indeed, the symmetric matter is the reference point around which the energy fluctuations due to the asymmetry are evaluated.

Let us start by considering the contribution of the kinetic energy to the symmetry energy. From equation (A.32), we obtain

$$\boxed{\frac{1}{2}\frac{\partial^2 \mathcal{E}_{\rm K}/A}{\partial \beta^2}\bigg|_{\beta=0} = \frac{1}{3}\frac{\hbar^2 (k_{\rm F}^t)^2}{2M} = \frac{5}{9}\frac{\mathcal{E}_{\rm K}^{\rm S}}{A},} \tag{A.98}$$

that we have defined with respect to the kinetic energy per nucleon of symmetric matter (A.79). As for the contribution from the potential energy (A.33), the calculation is once again quite long and tedious. However, the evaluation in $\beta = 0$ simplifies the result so that we eventually find out

$$\boxed{\begin{aligned}\frac{1}{2}\frac{\partial^2 \mathcal{E}_{\rm P}/A}{\partial \beta^2}\bigg|_{\beta=0} = \frac{\rho^\alpha}{3}\Bigg[&(\mathcal{A} - 2\mathcal{A}')X^3 + 2\mathcal{B}\bigg(\Big(\frac{1}{X} + X\Big)\mathrm{e}^{-X^2} - \frac{1}{X}\bigg) \\ &+ 2\mathcal{B}' X\Big(1 - \mathrm{e}^{-X^2}\Big)\Bigg].\end{aligned}} \tag{A.99}$$

3.3. Effective mass

The effective mass m^* corresponds to the renormalized mass the nucleons would have if they were considered as moving freely, rather than submitted to the nuclear potential with their actual mass m. By definition, the (inverse of the) effective mass of an isospin-t particle reads

$$\frac{1}{m_t^*} \equiv \frac{1}{\hbar^2 k}\frac{\mathrm{d}\varepsilon_t(\vec{k})}{\mathrm{d}k}\bigg|_{k=k_{\rm F}^t}, \tag{A.100}$$

where the one-body energy of an isospin-t particle, is given, according to (B.126), in INM, by

$$\varepsilon_t(\vec{k}) = \frac{\hbar^2 k^2}{2m} + \Gamma_t(\vec{k}) + \partial\Gamma. \tag{A.101}$$

Two remarks are in order regarding the rearrangement field $\partial\Gamma$ (at the HF approximation, in the HF basis). It is the same for both protons and neutrons (see subsection C.2.1.4, where the conclusion still holds at the HF approximation), but more importantly, it does not depend on the momentum $\vec{k}$ as it can be inferred from its expression (A.22). As a consequence, it does not contribute to the effective mass defined above. Thus, we have

$$\frac{1}{m_t^*} = \frac{1}{m} + \frac{1}{\hbar^2 k}\frac{\mathrm{d}\Gamma_t(\vec{k})}{\mathrm{d}k}\bigg|_{k=k_{\mathrm{F}}^t}. \tag{A.102}$$

We will then have to derive the mean field $\Gamma_t(\vec{k})$ for each term of the generalized Gogny interaction. Actually, we do not need to make the full calculation as we already computed the potential energy in the previous section, which is linked to the mean field by (A.19).

3.3.1. Central and density-dependent contributions

The central and density-dependent interactions are encompassed in the expression (A.34). Following the exact same steps that led to the contributions of those interactions to the potential energy (A.54), we eventually find out

$$\boxed{\begin{aligned}\Gamma_t(\vec{k}) = 4\rho^\alpha \sum_{ST}\sum_{t'}\frac{1}{2T+1}\Big(1+(2T-1)\delta_{tt'}\Big) \\ \times\left[\frac{\mathcal{A}^{ST}}{6}X_{q'}^3 + \mathcal{B}^{ST}\left(g_{\mu k}\left(\mu\frac{k-k_{\mathrm{F}}^{t'}}{2}\right) - g_{\mu k}\left(\mu\frac{k+k_{\mathrm{F}}^{t'}}{2}\right)\right)\right],\end{aligned}} \tag{A.103}$$

which is the mean field associated with the central and density-dependent interactions. In this expression, we have defined the function

$$g_y(x) \equiv \frac{\sqrt{\pi}}{2}\,\mathrm{erf}(x) + \frac{1}{y}\,\mathrm{e}^{-x^2}. \tag{A.104}$$

Taking the derivative of the mean field and evaluating it at $k = k_{\mathrm{F}}^t$, we get

$$\begin{aligned}\frac{\mathrm{d}\Gamma_t(\vec{k})}{\mathrm{d}k}\bigg|_{k=k_{\mathrm{F}}^t} &= -4\rho^\alpha \sum_{ST}\sum_{t'}\frac{1}{2T+1}\Big(1+(2T-1)\delta_{tt'}\Big) \\ &\times \mathcal{B}^{ST}\left[\mathrm{e}^{-\left(\frac{X_t-X_{t'}}{2}\right)^2}\left(\frac{1}{X_t k_{\mathrm{F}}^t} + \frac{X_t - X_{t'}}{2k_{\mathrm{F}}^t} - \frac{\mu}{2}\right)\right. \\ &\left. - \mathrm{e}^{-\left(\frac{X_t+X_{t'}}{2}\right)^2}\left(\frac{1}{X_t k_{\mathrm{F}}^t} + \frac{X_t + X_{t'}}{2k_{\mathrm{F}}^t} - \frac{\mu}{2}\right)\right],\end{aligned} \tag{A.105}$$

where we have used the following derivatives,

$$\frac{\mathrm{d}}{\mathrm{d}k}g_{\mu k}\left(\mu\frac{k\pm k_{\mathrm{F}}^{t'}}{2}\right) = -\,\mathrm{e}^{\left(\mu\frac{k\pm k_{\mathrm{F}}^{t'}}{2}\right)^2}\left(\frac{1}{\mu k^2} + \mu\frac{k\pm k_{\mathrm{F}}^{t'}}{2k} - \frac{\mu}{2}\right). \tag{A.106}$$

Finally, the contribution of the central and density-dependent terms to the effective mass can be written as

$$\boxed{\frac{m}{m_t^*} = 1 - \frac{4m\mu^2\rho^\alpha}{\hbar^2}\sum_{ST}\frac{1}{2T+1}\frac{\mathcal{B}^{ST}}{X_t^3}\Big(2Tf(t,t) + f(t,-t)\Big),} \tag{A.107}$$

where we have defined the isospin-dependent function

$$f(t,t') \equiv \left(1 - \frac{X_t X_{t'}}{2}\right) \mathrm{e}^{-\left(\frac{X_t - X_{t'}}{2}\right)^2} - \left(1 + \frac{X_t X_{t'}}{2}\right) \mathrm{e}^{-\left(\frac{X_t + X_{t'}}{2}\right)^2}. \tag{A.108}$$

Note that we have directly taken into account the contribution coming from the kinetic energy (which is the unity term of the right-hand side part) since, as we show in the following subsections, the tensor and spin–orbit mean fields cancel out and therefore do not contribute to the effective mass.

3.3.2. Tensor contribution

Let us now focus on the mean field associated with the tensor interaction (A.59). In a similar manner that the potential energy associated with the tensor interaction is zero (see subsection A.2.2.2), we show, following the same steps, that the corresponding mean field vanishes, because of its spin part. In fact, we show it explicitly in subsection B.4.2.3 as the expression of the mean field at the HFR approximation is the same as the one in the HF basis of the HF approximation we consider here. Then, the tensor interaction does not contribute to the effective mass (A.102).

3.3.3. Spin–orbit contribution

The mean field associated with the spin–orbit interaction (A.68) does not contribute to the effective mass (A.102) either, but for a different reason than the tensor interaction. Indeed, we show that the direct spin part of the spin–orbit mean field does not vanish. In fact, we show it explicitly in subsection B.4.2.4 as the expression of the mean field at the HFR approximation is same as the one in the HF basis of the HF approximation we consider here. What is then responsible for the spin–orbit mean field to be zero is, as we have shown in subsection A.2.2.3, that its spatial matrix elements are zero in the plane wave function representation.

4. Landau parameters

In this section, we will derive what are called the stability criteria and sum rules associated with the generalized Gogny interaction within the theory of normal Fermi liquids, in symmetric INM. Those are valuable indicators of the consistency of the parametrizations coming out of the fitting code. To do so, we will first need to introduce the effective quasiparticle interaction and make the link with the Landau parameters.

4.1. Effective quasiparticle interaction

In this subsection, we quickly recall how the effective quasiparticle interaction is defined in the context of the time-dependent Hartree–Fock (TDHF) theory in the limit of small amplitudes, before deriving its expression for a density-dependent interaction.

We start from the TDHF equations and assume a weak external field, that is to say we only allow oscillations with small amplitudes of the stationary density, which is itself solution of the stationary HF equations. Working in the particle–hole representation within

the HF basis, we show [4, 165] that we fall back on the Random Phase Approximation (RPA) equations if we assume a residual interaction given by

$$\langle ph'|V_{\rm ph}|hp'\rangle = \frac{\partial^2 \mathcal{E}_{\rm HF}}{\partial\rho_{hp}\partial\rho_{p'h'}}, \tag{A.109}$$

where $\mathcal{E}_{\rm HF}$ is the HF energy (A.12). Note that the residual interaction at the RPA level traduces the oscillations of small amplitudes of the system and is referred to as the *quasiparticle (or particle–hole) interaction*, then denoted as $V_{\rm ph}$. For a density-dependent interaction like the generalized Gogny interaction (II.1), the second derivative of the HF energy with respect to the density matrices provides

$$\boxed{\begin{aligned}\langle ph'|V_{\rm ph}|hp'\rangle = \langle ph'|v_{12}^{\rm (a)}|hp'\rangle + \sum_i \langle h'i|\frac{\partial v_{12}^{\rm (a)}}{\partial\rho_{hp}}|p'i\rangle + \sum_i \langle pi|\frac{\partial v_{12}^{\rm (a)}}{\partial\rho_{p'h'}}|hi\rangle \\ + \frac{1}{2}\sum_{ij}\langle ij|\frac{\partial^2 v_{12}^{\rm (a)}}{\partial\rho_{hp}\partial\rho_{p'h'}}|ij\rangle,\end{aligned}} \tag{A.110}$$

where the summations are performed on the occupied states, i.e. on the hole states in the particle–hole representation. The last three quantities of the right-hand side term are specific to density-dependent interactions as they involve derivatives of the density; they are called the rearrangement terms. Since the particle–hole interaction is here expressed in terms of the effective interaction v_{12}, we adequately call it the *effective quasiparticle (or particle–hole) interaction*.

4.2. Theory of normal Fermi liquids

Let us start by briefly recalling what a normal Fermi liquid is and what it implies to assume INM as being one [171, 227–231].

We consider an ideal system made up of a non-interacting homogeneous gas of fermions at zero temperature. The system presents translational invariance and the one-body wave functions are the plane waves (A.2). Accordingly, the wave function of the whole system corresponds to an antisymmetric linear combination of those plane waves. An eigenstate of the system is defined by listing which are the occupied plane waves. This information is provided by the distribution function $\rho(\vec{k})$, where $\vec{k}$ is the momentum of the plane wave. Under the above hypotheses, the distribution function of the system *in the ground state* corresponds to an isotropic distribution of the type

$$\rho(\vec{k}) = \begin{cases} 1 & \text{for } |\vec{k}| \leq k_{\rm F}, \\ 0 & \text{for } |\vec{k}| > k_{\rm F}. \end{cases} \tag{A.111}$$

This implies that the Fermi surface of a normal Fermi liquid in momentum space is spherical. [4] Now, the fundamental assumption of Landau's theory of Fermi liquids is that

4. We here use the notations introduced at the beginning of section A.1. In the case of a spin-polarized medium, corresponding to $N_\uparrow + Z_\uparrow \neq N_\downarrow + Z_\downarrow$, two distinct Fermi surfaces, one for spin up and another for spin down nucleons show up. Besides, the problem becomes more difficult since the spin excess introduces an anisotropy in the system so that the Fermi surfaces are not spherical in general. In particular, the Fermi surfaces deviate from spherical shapes because of the coupling between momentum and spin implied by the *tensor term* of the interaction. These observations remain true in a spin-isospin polarized medium, corresponding to $N_\uparrow + Z_\downarrow \neq N_\downarrow + Z_\uparrow$, but with four Fermi surfaces (one for each spin and isospin projection) [232].

when one gradually turns on the interaction, the ideal system adiabatically develops into the real system in such a way that the classification of states remains the same. It means that in the interacting system the one-body wave functions remain the plane waves and the distribution function in the ground state is still given by the definition above. Note, however, that the distribution function now describes the occupation of quasiparticle states. Indeed, if one adds a particle with momentum $|\vec{k}| > k_{\mathrm{F}}$ (or, equivalently, a hole with momentum $|\vec{k}| \leq k_{\mathrm{F}}$) to the ideal ground state and turns on the interaction, the system becomes a real ground state plus a quasiparticle of momentum $\vec{k}$. If a system obeys Landau's assumption, it is said to be a *normal Fermi liquid*. Note that, for quasiparticles to be a meaningful concept, they must have reasonably long lifetimes. One can show that in a normal Fermi liquid, the characteristic length of a quasiparticle with momentum $\vec{k}$ at zero temperature is proportional to $(k - k_{\mathrm{F}})^2$, because of the Pauli principle. Since the typical lifetime of a quasiparticle is inversely proportional to its characteristic length, assuming the quasiparticles to be close enough to the Fermi surface guarantees them sufficiently long lifetimes.

The energy $\mathcal{E}$ of the real system depends on the distribution function of the quasiparticles. Landau [227–229] investigated how this energy is modified when one changes the distribution function $\rho(\vec{k})$ by an amount $\delta\rho(\vec{k})$. Geometrically, this equates to translate the Fermi sphere by a small momentum (giving a uniform velocity to the system) without modifying its size or its shape. The resulting change in energy at the first order in $\delta\rho(\vec{k})$ is

$$\delta\mathcal{E} = \sum_{\vec{k}} \varepsilon(\vec{k})\delta\rho(\vec{k}), \tag{A.112}$$

where the summation should in principle also run over spin and isospin projections, but we decided to forget those degrees of freedom for a moment, to simplify the treatment. The quantity $\varepsilon(\vec{k})$ is interpreted as the energy of a quasiparticle with momentum $\vec{k}$. In other words, the quasiparticle energy is obtained by varying the energy with respect to the quasiparticle distribution, i.e.

$$\varepsilon(\vec{k}) \equiv \frac{\delta\mathcal{E}[\rho]}{\delta\rho(\vec{k})}. \tag{A.113}$$

Actually, Landau found out that result demanding the conservation of the quasiparticle momentum [171]. Moreover, the energy of a quasiparticle is modified if the distribution of the other quasiparticles changes. Thus, Landau also took into account the second order variations of the distribution function by writing the total change in energy as

$$\delta\mathcal{E} = \sum_{\vec{k}} \varepsilon_0(\vec{k})\delta\rho(\vec{k}) + \frac{1}{2}\sum_{\vec{k}\vec{k}'} \mathcal{F}(\vec{k},\vec{k}')\delta\rho(\vec{k})\delta\rho(\vec{k}'). \tag{A.114}$$

It appears that $\varepsilon_0(\vec{k})$ corresponds to the energy of a non-interacting quasiparticle. By means of relation (A.113), a variation of the distribution function of the other quasiparticles changes $\varepsilon_0(\vec{k})$ into

$$\varepsilon(\vec{k}) = \varepsilon_0(\vec{k}) + \sum_{\vec{k}'} \mathcal{F}(\vec{k},\vec{k}')\delta\rho(\vec{k}'), \tag{A.115}$$

so that the function $\mathcal{F}(\vec{k},\vec{k}')$ describes the interaction between the quasiparticles. Formally, it can be written as the second functional derivative of the energy with respect to

the distribution function,

$$\boxed{\mathcal{F}(\vec{k},\vec{k}') \equiv \frac{\delta\varepsilon[\rho(\vec{k})]}{\delta\rho(\vec{k}')} \equiv \frac{\delta^2\mathcal{E}[\rho]}{\delta\rho(\vec{k})\delta\rho(\vec{k}')},} \tag{A.116}$$

where we have denoted by $\vec{k}$ and $\vec{k}'$ the momenta of the two particles, instead of $\vec{k}_1$ and $\vec{k}_2$ as we did in the appendix, since this notation is more transparent at the Landau limit discussed below. From now on, this quantity is called the *quasiparticle (or particle–hole) interaction* in the light of its physical interpretation. Note that it is only defined at the Landau limit, i.e. near the Fermi surface where $|\vec{k}| \simeq |\vec{k}'| \simeq k_\mathrm{F}$, because of the reasonably long lifetime requirement we discussed earlier. Let us report that the Landau limit is sometimes called the limit of equal momenta or, accordingly, the long-wavelength limit. Thus, at this limit, the particle–hole interaction only depends on the angle between the momenta $\vec{k}$ and $\vec{k}'$, sometimes referred to as the Landau angle θ. We also observe that this quasiparticle interaction is defined in the same way as the effective quasiparticle interaction calculated at the TDHF approximation in the limit of small amplitude oscillations (A.109). Then, those quantities coincide at the Landau limit, that is to say $\mathcal{F}(\vec{k}_\mathrm{F},\vec{\sigma}_1,\vec{\tau}_1;\vec{k}'_\mathrm{F},\vec{\sigma}_2,\vec{\tau}_2) = \langle \vec{k}_\mathrm{F}\vec{\sigma}_1\vec{\tau}_1;\vec{k}'_\mathrm{F}\vec{\sigma}_2\vec{\tau}_2|V_\mathrm{ph}|\vec{k}_\mathrm{F}\vec{\sigma}_1\vec{\tau}_1;\vec{k}'_\mathrm{F}\vec{\sigma}_2\vec{\tau}_2\rangle \equiv V_\mathrm{ph}^\mathrm{L}$, where we have restored the spin and isospin dependences of the quasiparticle interaction. Midgal [169] was the first to establish this link between the theory of normal Fermi liquids and heavy atomic nuclei, in the framework of INM. This equivalence was in particular showed by Gogny and Padjen for the D1 interaction in [172].

Therefore, in homogeneous and symmetric INM, the particle–hole interaction can be parametrized as [5]

$$\begin{aligned} V_\mathrm{ph}^\mathrm{L} = N_0^{-1}\Big[& f(\theta) + g(\theta)(\vec{\sigma}_1\cdot\vec{\sigma}_2) + f'(\theta)(\vec{\tau}_1\cdot\vec{\tau}_2) + g'(\theta)(\vec{\sigma}_1\cdot\vec{\sigma}_2)(\vec{\tau}_1\cdot\vec{\tau}_2) \\ & + h(\theta)\frac{q_\mathrm{F}^2}{k_\mathrm{F}^2}S_{12}(\hat{q}_{12}) + h'(\theta)\frac{q_\mathrm{F}^2}{k_\mathrm{F}^2}S_{12}(\hat{q}_{12})(\vec{\tau}_1\cdot\vec{\tau}_2)\Big], \end{aligned} \tag{A.118}$$

where the density of quasiparticle states at the Fermi surface is defined by

$$N_0 \equiv \frac{2m^*\mathcal{V}k_\mathrm{F}}{\pi^2\hbar^2}. \tag{A.119}$$

This factor ensures that the parameters f, f', g, g', h and h' are dimensionless quantities. Note that these parameters to be determined only depend on the angle between the momenta $\vec{k}_\mathrm{F}$ and $\vec{k}'_\mathrm{F}$ of the quasiparticle pair. As for $S_{12}(\hat{q}_{12})$, it is the tensor operator in momentum space defined, by analogy with (D.49) in coordinate space, as

$$S_{12}(\hat{q}_{12}) = (\vec{\sigma}_1\cdot\hat{q}_{12})(\vec{\sigma}_2\cdot\hat{q}_{12}) - \frac{1}{3}\vec{\sigma}_1\cdot\vec{\sigma}_2, \tag{A.120}$$

5. In isospin-asymmetric nuclear matter, the above equation would become

$$\mathcal{F}_{tt'}(\vec{k},\vec{k}') \equiv \frac{\delta^2\mathcal{E}[\rho]}{\delta\rho_t(\vec{k})\delta\rho_{t'}(\vec{k}')}, \tag{A.117}$$

since there would then be three different contributions to the quasiparticle interaction, of neutron–neutron $F_{\nu\nu}$, proton–proton $F_{\pi\pi}$ and proton–neutron $F_{\pi\nu}$ types, that would complicate the problem a bit [232–234]. Fortunately, the charge independence (see equation (I.11) and the discussion below) assumed here implies that these three contributions are equal.

where the direction pointed by the relative momentum is $\hat{q}_{12} \equiv \vec{q}_{12}/|\vec{q}_{12}|$, in momentum space. This expression is the most general form of the quasiparticle interaction considering the symmetry constraints to be satisfied (see section I.1.2). Actually, because of the presence of a medium, the Galilean translational invariance is broken and two new non-central terms, dubbed as the center-of-mass tensor and the cross-vector interactions, arise [235, 236]. Nevertheless, we have not taken them into account in our treatment. [6] The first four terms are called the central terms as they are related to the central part of the interaction while the two last ones are the tensor terms which are related to the non-central part of the interaction. Accordingly, the central parameters f, g, f' and g' respectively contribute to the $(S = 0, T = 0)$, $(S = 1, T = 0)$, $(S = 0, T = 1)$ and $(S = 1, T = 1)$ channels of the interaction while the tensor parameters h and h' respectively contribute to the $(S = 1, T = 0)$ and $(S = 1, T = 1)$ channels of the interaction, but not in the $S = 0$ channel, as expected for a tensor interaction (see section II). In the following, we will then cast these parameters into the quantities $f^{ST}(\theta)$, where $f^{00}(\theta) \equiv f(\theta)$, $f^{10}(\theta) \equiv g(\theta)$, $f^{01}(\theta) \equiv f'(\theta)$ and $f^{11}(\theta) \equiv g'(\theta)$, and $h^{1T}(\theta)$, where $h^{10}(\theta) = h(\theta)$ and $h^{11}(\theta) = h'(\theta)$. Now, since the particle–hole interaction only depends on the Landau angle θ between the quasiparticles, these quantities can be expanded in series of Legendre polynomials with argument $\hat{k} \cdot \hat{k}' = \cos\theta$, according to

$$f^{ST}(\theta) = \sum_l f_l^{ST} P_l(\cos\theta), \tag{A.121a}$$

$$h^{1T}(\theta) = \sum_l h_l^{1T} P_l(\cos\theta), \tag{A.121b}$$

where the coefficients f_l^{ST} and h_l^{1T} of these expansions are the so-called *Landau parameters* that one needs to evaluate, in principle for all values of l, to fully characterize the particle–hole interaction. In fact, those coefficients converge quite rapidly (in the sense that their absolute value decreases sharply as l increases; see section II.2.5 for more details), so that we only need to calculate the coefficients for the first values of l in practice. Finally, note that, contrary to the central terms, the tensor terms exhibit a factor $q_\mathrm{F}^2/k_\mathrm{F}^2$, where the relative momentum at the Fermi surface is $\vec{q}_\mathrm{F} \equiv \vec{k}_\mathrm{F} - \vec{k}'_\mathrm{F}$, whose magnitude reads

$$q_\mathrm{F} = k_\mathrm{F}\sqrt{2(1 - \cos\theta)}. \tag{A.122}$$

This factor is conventional but often chosen as it is well-suited to calculate the response function. We will not calculate the response function here, but we will stick to this convention to simplify the contribution of the tensor force to the sum rules (see subsection A.4.4). Note that some authors have defined the tensor terms without this factor, claiming that it leads to a faster convergence of the corresponding Landau parameters [236]. In any case, there exists a recurrence relation linking the two conventions [236]. Defining $h^{1T}(\theta) \equiv q_\mathrm{F}^2/k_\mathrm{F}^2 \widetilde{h}^{1T}(\theta)$, expanding this relation as in (A.121), using the orthogonality relation (D.107) of the Legendre polynomials and then their recurrence relation (D.108), we eventually obtain

$$h_l^{1T}(\theta) = 2\left[\widetilde{h}_l^{1T}(\theta) - \frac{l}{2l-1}\widetilde{h}_{l-1}^{1T}(\theta) - \frac{l+1}{2l+3}\widetilde{h}_{l+1}^{1T}(\theta)\right], \quad \text{for } l \in \mathbb{N}. \tag{A.123}$$

In the following subsections, we will then give analytical expressions for the Landau parameters $f_l^{ST}(\theta)$ and $h_l^{1T}(\theta)$ of the generalized Gogny interaction.

6. Logically, these terms should have been introduced, in coordinate space, already at the level of the generalized Gogny interaction (II.1), so that they would have appeared naturally in the quasiparticle interaction above. We have chosen to stick to the usual tensor force present in the nucleon–nucleon interaction (see equation (I.14)), which is why we do not consider these terms here.

4.2.1. Central and density-dependent contributions

In this subsection, we shall derive the various Landau parameters associated with the finite-range central and density-dependent terms of the generalized Gogny interaction (II.1). The antisymmetrized central and density-dependent (CDD) interactions are characterized by the set of equations (A.34)–(A.36), with their direct and exchange spin-isospin components (A.37) respectively written under the equivalent forms

$$\begin{aligned}\mathcal{P}_{\rm D} \equiv &\left(W + \frac{B}{2} - \frac{H}{2} - \frac{M}{4}\right) + \left(\frac{B}{2} - \frac{M}{4}\right)(\vec{\sigma}_1 \cdot \vec{\sigma}_2) \\ &- \left(\frac{H}{2} + \frac{M}{4}\right)(\vec{\tau}_1 \cdot \vec{\tau}_2) - \frac{M}{4}(\vec{\sigma}_1 \cdot \vec{\sigma}_2)(\vec{\tau}_1 \cdot \vec{\tau}_2),\end{aligned} \tag{A.124a}$$

$$\begin{aligned}\mathcal{P}_{\rm E} \equiv &\left(M + \frac{H}{2} - \frac{B}{2} - \frac{W}{4}\right) + \left(\frac{H}{2} - \frac{W}{4}\right)(\vec{\sigma}_1 \cdot \vec{\sigma}_2) \\ &- \left(\frac{B}{2} + \frac{W}{4}\right)(\vec{\tau}_1 \cdot \vec{\tau}_2) - \frac{W}{4}(\vec{\sigma}_1 \cdot \vec{\sigma}_2)(\vec{\tau}_1 \cdot \vec{\tau}_2).\end{aligned} \tag{A.124b}$$

We notice that the direct spin-isospin components of the CDD interactions can be deduced from the exchange ones upon replacing W, B, H, M by M, H, B, W.

In order to get the contributions from the central and density-dependent interactions to the matrix elements of the particle–hole interaction (A.110), we shall evaluate the following antisymmetrized matrix elements in the particle–hole representation,

$$\begin{aligned}\langle \vec{k}_p \vec{k}_{h'} | v_{12}^{\rm CDD,(a)} | \vec{k}_h \vec{k}_{p'} \rangle = &\langle \vec{k}_p \vec{k}_{h'} | V(r_{12}) D[\rho] | \vec{k}_h \vec{k}_{p'} \rangle \mathcal{P}_{\rm D} \\ &+ \langle \vec{k}_p \vec{k}_{h'} | V(r_{12}) D[\rho] | \vec{k}_{p'} \vec{k}_h \rangle \mathcal{P}_{\rm E},\end{aligned} \tag{A.125}$$

where we have explicitly separated the direct and exchange as well as the spatial and spin-isospin parts. Since the spin-isospin part is fully specified by (A.124), we focus on the spatial parts. In fact, the calculation is pretty similar to what we have done in (A.43). The only difference is that the conservation of the quasiparticle pair momentum is invoked here, i.e. $\vec{k}_p + \vec{k}_{h'} = \vec{k}_h + \vec{k}_{p'}$. We eventually find out

$$\langle \vec{k}_p \vec{k}_{h'} | V(r_{12}) D[\rho] | \vec{k}_h \vec{k}_{p'} \rangle = \frac{\rho^\alpha}{\mathcal{V}} (\mu\sqrt{\pi})^3 \, {\rm e}^{-\mu^2 (\vec{k}_p - \vec{k}_h)^2/4}, \tag{A.126a}$$

$$\langle \vec{k}_p \vec{k}_{h'} | V(r_{12}) D[\rho] | \vec{k}_{p'} \vec{k}_h \rangle = \frac{\rho^\alpha}{\mathcal{V}} (\mu\sqrt{\pi})^3 \, {\rm e}^{-\mu^2 (\vec{k}_p - \vec{k}_{p'})^2/4}, \tag{A.126b}$$

where, from $\alpha = 0$, we obtain the central contributions and from $\alpha \neq 0$ the density-dependent one. Now, at the Landau limit, $|\vec{k}_p| = |\vec{k}_h| = |\vec{k}_{\rm F}|$ and $|\vec{k}_{p'}| = |\vec{k}_{h'}| = |\vec{k}'_{\rm F}|$, so that the above relations become

$$\langle \vec{k}_{\rm F} \vec{k}'_{\rm F} | V(r_{12}) D[\rho] | \vec{k}_{\rm F} \vec{k}'_{\rm F} \rangle = \frac{\rho^\alpha}{\mathcal{V}} (\mu\sqrt{\pi})^3 \equiv G_\mu^\alpha(0), \tag{A.127a}$$

$$\langle \vec{k}_{\rm F} \vec{k}'_{\rm F} | V(r_{12}) D[\rho] | \vec{k}'_{\rm F} \vec{k}_{\rm F} \rangle = \frac{\rho^\alpha}{\mathcal{V}} (\mu\sqrt{\pi})^3 \, {\rm e}^{-\mu^2 \vec{q}_{\rm F}^{\,2}/4} \equiv G_\mu^\alpha(\vec{q}_{\rm F}), \tag{A.127b}$$

where we have defined the function $G_\mu^\alpha(\vec{k}) \equiv \rho^\alpha (\mu\sqrt{\pi})^3/\mathcal{V} \times {\rm e}^{-\mu^2 \vec{k}^{\,2}/4}$ and considered the relative momentum at the Fermi surface, $\vec{q}_{\rm F} = \vec{k}_{\rm F} - \vec{k}'_{\rm F}$. In order to connect these expressions to the parameters appearing in (A.118), we also define

$$\widetilde{G}_\mu^\alpha(\vec{k}) \equiv N_0 G_\mu^\alpha(\vec{k}) = \frac{2m^* k_{\rm F} \rho^\alpha}{\pi^2 \hbar^2} (\mu\sqrt{\pi})^3 \, {\rm e}^{-\mu^2 \vec{k}^{\,2}/4}. \tag{A.128}$$

Then, with (A.124) and (A.125), we have,

$$f^{00}(\theta) = \Big(W + \frac{B}{2} - \frac{H}{2} - \frac{M}{4}\Big)\widetilde{G}^{\alpha}_{\mu}(0) + \Big(M + \frac{H}{2} - \frac{B}{2} - \frac{W}{4}\Big)\widetilde{G}^{\alpha}_{\mu}(\vec{q}_{\mathrm{F}}), \tag{A.129a}$$

$$f^{10}(\theta) = \Big(\frac{B}{2} - \frac{M}{4}\Big)\widetilde{G}^{\alpha}_{\mu}(0) + \Big(\frac{H}{2} - \frac{W}{4}\Big)\widetilde{G}^{\alpha}_{\mu}(\vec{q}_{\mathrm{F}}), \tag{A.129b}$$

$$f^{01}(\theta) = -\Big(\frac{H}{2} + \frac{M}{4}\Big)\widetilde{G}^{\alpha}_{\mu}(0) - \Big(\frac{B}{2} + \frac{W}{4}\Big)\widetilde{G}^{\alpha}_{\mu}(\vec{q}_{\mathrm{F}}), \tag{A.129c}$$

$$f^{11}(\theta) = -\frac{M}{4}\widetilde{G}^{\alpha}_{\mu}(0) - \frac{W}{4}\widetilde{G}^{\alpha}_{\mu}(\vec{q}_{\mathrm{F}}). \tag{A.129d}$$

To get the Landau parameters out of the f^{ST}, we expanded them in Legendre polynomials according to (A.121a). Let us see how to do the same with the function

$$\widetilde{G}^{\alpha}_{\mu}(\vec{q}_{\mathrm{F}}) = N_0 \frac{\rho^{\alpha}}{\mathcal{V}} (\mu\sqrt{\pi})^3 \, \mathrm{e}^{-\mu^2 k_{\mathrm{F}}^2 (1-\cos\theta)/2}, \tag{A.130}$$

where we have used the magnitude of the relative momentum at the Fermi surface (A.122). The plane wave expansion of the exponential (D.116) furnishes

$$\mathrm{e}^{\mu^2 k_{\mathrm{F}}^2 \cos\theta/2} = \mathrm{e}^{\mathrm{i}(-\mathrm{i}\mu^2 k_{\mathrm{F}}^2)\cos\theta/2} = \sum_l (2l+1)\mathrm{i}^l j_l\Big(-\mathrm{i}\mu^2 k_{\mathrm{F}}^2/2\Big) P_l(\cos\theta). \tag{A.131}$$

If the argument of the Bessel function of the first kind j_l had been real, we would have directly considered its analytical expression for a given l, the first three examples of which are given by (D.115). Here, however, the argument is purely imaginary, so we have no choice but to expand the function in infinite series according to (D.114). In practice this series will be truncated to a finite order, which is not a problem since this series converges rather quickly. We therefore find out

$$\mathrm{e}^{\mu^2 k_{\mathrm{F}}^2 \cos\theta/2} = \frac{\sqrt{\pi}}{2} \sum_l (2l+1) \sum_m \frac{\big(\mu^2 k_{\mathrm{F}}^2/4\big)^{2m+l}}{m!\,\Gamma(m+l+3/2)} P_l(\cos\theta), \tag{A.132}$$

and finally obtain

$$\boxed{\widetilde{G}^{\alpha}_{\mu}(\vec{q}_{\mathrm{F}}) = \widetilde{G}^{\alpha}_{\mu}(0) \sum_l G_l P_l(\cos\theta),} \tag{A.133}$$

where the coefficients of this expansion in Legendre polynomials are defined by

$$G_l \equiv \frac{\sqrt{\pi}}{2}(2l+1)\,\mathrm{e}^{-\mu^2 k_{\mathrm{F}}^2/2} \sum_m \frac{\big(\mu^2 k_{\mathrm{F}}^2/4\big)^{2m+l}}{m!\,\Gamma(m+l+3/2)}. \tag{A.134}$$

Thus, the contributions of the central and density-dependent interactions to the Landau parameters defined in (A.121), can be evaluated, for $l \in \mathbb{N}$, by means of the relations

$$\boxed{f_l^{00} = \widetilde{G}^{\alpha}_{\mu}(0)\bigg[\Big(W + \frac{B}{2} - \frac{H}{2} - \frac{M}{4}\Big)\delta_{l,0} + \Big(M + \frac{H}{2} - \frac{B}{2} - \frac{W}{4}\Big)G_l\bigg],} \tag{A.135a}$$

$$\boxed{f_l^{10} = \widetilde{G}^{\alpha}_{\mu}(0)\bigg[\Big(\frac{B}{2} - \frac{M}{4}\Big)\delta_{l,0} + \Big(\frac{H}{2} - \frac{W}{4}\Big)G_l\bigg],} \tag{A.135b}$$

$$\boxed{f_l^{01} = -\widetilde{G}^{\alpha}_{\mu}(0)\bigg[\Big(\frac{H}{2} + \frac{M}{4}\Big)\delta_{l,0} + \Big(\frac{B}{2} + \frac{W}{4}\Big)G_l\bigg],} \tag{A.135c}$$

$$\boxed{f_l^{11} = -\widetilde{G}^{\alpha}_{\mu}(0)\bigg[\frac{M}{4}\delta_{l,0} + \frac{W}{4}G_l\bigg].} \tag{A.135d}$$

We keep in mind that we must set $\alpha = 0$ in the quantity $\widetilde{G}^{\alpha}_{\mu}(0)$ to get the contributions of the central terms, and divide it by the coefficient $(\mu\sqrt{\pi})^3$ to get the one of the density-dependent term.

4.2.2. Rearrangement contributions

In this subsection, we continue by deriving the Landau parameters associated with the rearrangement terms of the generalized Gogny interaction (II.1). We recall in passing that only the density-dependent term gives rise to such terms. According to (A.110), there are three rearrangement terms. To compute the first one, it will be useful to write the derivative of the antisymmetrized interaction as

$$\begin{aligned}\frac{\partial v_{12}^{(\mathrm{a})}}{\partial \rho_{hp}} &= \frac{\partial v_{12}^{(\mathrm{a})}}{\partial \rho(\vec{r}_1)}\frac{\partial \rho(\vec{r}_1)}{\partial \rho_{hp}} + \frac{\partial v_{12}^{(\mathrm{a})}}{\partial \rho(\vec{r}_2)}\frac{\partial \rho(\vec{r}_2)}{\partial \rho_{hp}} \\ &= \frac{\alpha}{2}\frac{V(r_{12})}{(\mu\sqrt{\pi})^3}\left[\rho^{\alpha-1}(\vec{r}_1)\frac{\partial \rho(\vec{r}_1)}{\partial \rho_{hp}} + \rho^{\alpha-1}(\vec{r}_2)\frac{\partial \rho(\vec{r}_2)}{\partial \rho_{hp}}\right](\mathcal{P}_{\mathrm{D}} + \mathcal{P}_{\mathrm{E}}P_r),\end{aligned} \tag{A.136}$$

where the spin-isospin components of the direct $\mathcal{P}_{\mathrm{D}}$ and exchange $\mathcal{P}_{\mathrm{E}}$ density-dependent interaction are given by (A.124). Using the definition (A.24) of the local nuclear density, we can rewrite the above derivatives thanks to the formula

$$\begin{aligned}\frac{\partial \rho(\vec{r})}{\partial \rho_{hp}} &= \sum_{\sigma\tau}\Phi_p^*(\vec{r},\sigma,\tau)\Phi_h(\vec{r},\sigma,\tau) \\ &= \sum_{\sigma\tau}\int \mathrm{d}^3r'\,\Phi_p^*(\vec{r},\sigma,\tau)\delta(\vec{r}-\vec{r}')\Phi_h(\vec{r},\sigma,\tau) \\ &= \langle p|\delta(\vec{r}-\vec{r}')|h\rangle.\end{aligned} \tag{A.137}$$

Then, the derivative (A.136) becomes

$$\begin{aligned}\frac{\partial v_{12}^{(\mathrm{a})}}{\partial \rho_{hp}} = \frac{\alpha}{2}\frac{V(r_{12})}{(\mu\sqrt{\pi})^3}&\langle p|\rho^{\alpha-1}(\vec{r}_1)\delta(\vec{r}_1-\vec{r}_3) + \rho^{\alpha-1}(\vec{r}_2)\delta(\vec{r}_2-\vec{r}_3)|h\rangle \\ &\times(\mathcal{P}_{\mathrm{D}} + \mathcal{P}_{\mathrm{E}}P_r),\end{aligned} \tag{A.138}$$

and the first rearrangement term appearing in (A.110) can be written

$$\begin{aligned}\sum_i \langle h'i|\frac{\partial v_{12}^{(\mathrm{a})}}{\partial \rho_{hp}}|p'i\rangle = \frac{\alpha}{2}\sum_i \langle h'ip|\frac{V(r_{12})}{(\mu\sqrt{\pi})^3}\Big[&\rho^{\alpha-1}(\vec{r}_1)\delta(\vec{r}_1-\vec{r}_3) \\ &+ \rho^{\alpha-1}(\vec{r}_2)\delta(\vec{r}_2-\vec{r}_3)\Big](\mathcal{P}_{\mathrm{D}}^{12} + \mathcal{P}_{\mathrm{E}}^{12}P_r^{12})|p'ih\rangle,\end{aligned} \tag{A.139}$$

since the quantities only acting on the particles 1 and 2, spotted by their indices 12, can be incorporated in the three-body matrix element, having no action on the third particle p and third hole h. Defining

$$\begin{aligned}v_{12}^{\mathrm{d}_1} \equiv \frac{\alpha}{2}\sum_i \langle i|\frac{V(r_{23})}{(\mu\sqrt{\pi})^3}\Big[&\rho^{\alpha-1}(\vec{r}_2)\delta(\vec{r}_1-\vec{r}_2) + \rho^{\alpha-1}(\vec{r}_3)\delta(\vec{r}_1-\vec{r}_3)\Big] \\ &\times(\mathcal{P}_{\mathrm{D}}^{23} + \mathcal{P}_{\mathrm{E}}^{23}P_r^{23})|i\rangle,\end{aligned} \tag{A.140}$$

we find out, after a circular permutation of the variables in (A.139),

$$\sum_i \langle h'i|\frac{\partial v_{12}^{(\mathrm{a})}}{\partial \rho_{hp}}|p'i\rangle = \langle ph'|v_{12}^{\mathrm{d}_1}|hp'\rangle. \tag{A.141}$$

We then start by evaluating the direct component of (A.140), which reads

$$v_{12}^{\mathrm{d}_1}|_{\mathrm{D}} \equiv \frac{\alpha}{2}\sum_i \langle i|\frac{V(r_{23})}{(\mu\sqrt{\pi})^3}\Big[\rho^{\alpha-1}(\vec{r}_2)\delta(\vec{r}_1-\vec{r}_2)+\rho^{\alpha-1}(\vec{r}_3)\delta(\vec{r}_1-\vec{r}_3)\Big]\mathcal{P}_{\mathrm{D}}^{23}|i\rangle. \tag{A.142}$$

Considering the continuous limit (A.4), we obtain (with i renamed 3 for convenience),

$$\begin{aligned} v_{12}^{\mathrm{d}_1}|_{\mathrm{D}} = \frac{\alpha}{2}\frac{\mathcal{V}}{(2\pi)^3}\sum_{u_3}\langle u_3|\mathcal{P}_{\mathrm{D}}^{23}|u_3\rangle \times \int \mathrm{d}^3r_3 \int \mathrm{d}^3k_3\, \phi^*_{\vec{k}_3}(\vec{r}_3)\frac{V(r_{23})}{(\mu\sqrt{\pi})^3} \\ \times \Big[\rho^{\alpha-1}(\vec{r}_2)\delta(\vec{r}_1-\vec{r}_2)+\rho^{\alpha-1}(\vec{r}_3)\delta(\vec{r}_1-\vec{r}_3)\Big]\phi_{\vec{k}_3}(\vec{r}_3). \end{aligned} \tag{A.143}$$

On the one hand, the calculation of the nuclear density (A.27) at the continuous limit (A.4) immediately brings

$$\frac{\mathcal{V}}{(2\pi)^3}\int \mathrm{d}^3k_3\,|\phi_{\vec{k}_3}(\vec{r}_3)|^2 = \frac{\rho(\vec{r}_3)}{4}, \tag{A.144}$$

where the factor 4 comes from the spin and isospin degeneracies. On the other hand, expressing the scalar product of Pauli matrices, we have

$$\langle s_3|\vec{\sigma}_2\cdot\vec{\sigma}_3|s_3\rangle = \sum_k (-)^k \sigma_2^{-k}\langle s_3|\sigma_3^k|s_3\rangle = 2s_3\sigma_2^0, \tag{A.145}$$

where we have used the unified relation of the matrix elements of the Pauli matrices (D.18). We obviously get an equivalent relation for the Pauli matrices associated with the isospin, so that

$$\sum_{s_3}\langle s_3|\vec{\sigma}_2\cdot\vec{\sigma}_3|s_3\rangle = \sum_{t_3}\langle t_3|\vec{\tau}_2\cdot\vec{\tau}_3|t_3\rangle = 0, \tag{A.146}$$

in such a way that, eventually only the unity operator of $\mathcal{P}_{\mathrm{D}}^{23}$ contributes to the matrix elements, i.e.

$$\sum_{s_3t_3}\langle s_3t_3|\mathcal{P}_{\mathrm{D}}^{23}|s_3t_3\rangle = 4\Big(W+\frac{B}{2}-\frac{H}{2}-\frac{M}{4}\Big). \tag{A.147}$$

Gathering those two results and taking into account the translational invariance of INM, i.e. $\rho(\vec{r}_3)=\rho$, it follows that

$$\begin{aligned} v_{12}^{\mathrm{d}_1}|_{\mathrm{D}} &= \frac{\alpha\rho}{2}\Big(W+\frac{B}{2}-\frac{H}{2}-\frac{M}{4}\Big)\int \mathrm{d}^3r_3\,\frac{V(r_{23})}{(\mu\sqrt{\pi})^3}\Big[\rho^{\alpha-1}(\vec{r}_2)\delta(\vec{r}_1-\vec{r}_2)+\rho^{\alpha-1}(\vec{r}_3)\delta(\vec{r}_1-\vec{r}_3)\Big] \\ &= \frac{\alpha\rho}{2}\Big(W+\frac{B}{2}-\frac{H}{2}-\frac{M}{4}\Big)\Big[\rho^{\alpha-1}(\vec{r}_1)\frac{V(r_{12})}{(\mu\sqrt{\pi})^3}+\rho^{\alpha-1}(\vec{r}_2)\delta(\vec{r}_1-\vec{r}_2)\Big], \end{aligned} \tag{A.148}$$

where the first integral has been evaluated by means of the Gauss integral (D.118). Now, to get the direct contribution of the first rearrangement term (A.141), we need to evaluate the TBMEs

$$\begin{aligned} \langle ph'|v_{12}^{\mathrm{d}_1}|_{\mathrm{D}}|hp'\rangle &= \langle \vec{k}_p\vec{k}_{h'}|v_{12}^{\mathrm{d}_1}|_{\mathrm{D}}|\vec{k}_h\vec{k}_{p'}\rangle \\ &= \frac{\alpha\rho}{2}\Big(W+\frac{B}{2}-\frac{H}{2}-\frac{M}{4}\Big) \\ &\quad\times \langle \vec{k}_p\vec{k}_{h'}|\Big[\rho^{\alpha-1}(\vec{r}_1)\frac{V(r_{12})}{(\mu\sqrt{\pi})^3}+\rho^{\alpha-1}(\vec{r}_2)\delta(\vec{r}_1-\vec{r}_2)\Big]|\vec{k}_h\vec{k}_{p'}\rangle. \end{aligned} \tag{A.149}$$

By definition,

$$\begin{aligned}\langle\vec{k}_p\vec{k}_{h'}|v_{12}^{\mathrm{d}_1}|_{\mathrm{D}}|\vec{k}_h\vec{k}_{p'}\rangle &= \frac{\alpha\rho}{2}\Big(W+\frac{B}{2}-\frac{H}{2}-\frac{M}{4}\Big)\\ \times\int \mathrm{d}^3r_1\int \mathrm{d}^3r_2\,\phi^*_{\vec{k}_p}(\vec{r}_1)\phi^*_{\vec{k}_{h'}}(\vec{r}_2)\Big[\rho^{\alpha-1}(\vec{r}_1)\frac{V(r_{12})}{(\mu\sqrt{\pi})^3}+\rho^{\alpha-1}(\vec{r}_2)\delta(\vec{r}_1-\vec{r}_2)\Big]\phi_{\vec{k}_h}(\vec{r}_1)\phi_{\vec{k}_{p'}}(\vec{r}_2)&\\ = \frac{\alpha\rho}{2\mathcal{V}^2}\Big(W+\frac{B}{2}-\frac{H}{2}-\frac{M}{4}\Big)&\\ \times\int \mathrm{d}^3r_1\int \mathrm{d}^3r_2\,\mathrm{e}^{-\mathrm{i}(\vec{k}_p-\vec{k}_h)\cdot\vec{r}_1}\mathrm{e}^{\mathrm{i}(\vec{k}_{p'}-\vec{k}_{h'})\cdot\vec{r}_2}\Big[\rho^{\alpha-1}(\vec{r}_1)\frac{V(r_{12})}{(\mu\sqrt{\pi})^3}+\rho^{\alpha-1}(\vec{r}_2)\delta(\vec{r}_1-\vec{r}_2)\Big].&\end{aligned} \tag{A.150}$$

Using the conservation of the quasiparticle pair momentum $\vec{k}_p+\vec{k}_h=\vec{k}_{p'}+\vec{k}_{h'}$, the translational invariance of INM, i.e. $\rho(\vec{r}_1)=\rho(\vec{r}_2)=\rho$, and going from the nucleon to the center-of-mass and relative coordinates defined in (A.40), whose Jacobian is equal to unity, while splitting the integral into two parts, we successively obtain

$$\begin{aligned}\langle\vec{k}_p\vec{k}_{h'}|v_{12}^{\mathrm{d}_1}|_{\mathrm{D}}|\vec{k}_h\vec{k}_{p'}\rangle &= \frac{\alpha\rho}{2\mathcal{V}^2}\Big(W+\frac{B}{2}-\frac{H}{2}-\frac{M}{4}\Big)\\ \times\int \mathrm{d}^3r_1\int \mathrm{d}^3r_2\,\mathrm{e}^{-\mathrm{i}(\vec{k}_p-\vec{k}_h)\cdot(\vec{r}_1-\vec{r}_2)}\Big[\rho^{\alpha-1}(\vec{r}_1)\frac{V(r_{12})}{(\mu\sqrt{\pi})^3}+\rho^{\alpha-1}(\vec{r}_2)\delta(\vec{r}_1-\vec{r}_2)\Big].&\\ = \frac{\alpha\rho^\alpha}{2\mathcal{V}^2}\Big(W+\frac{B}{2}-\frac{H}{2}-\frac{M}{4}\Big)&\\ \times\Big[\int \mathrm{d}^3R\int \mathrm{d}^3r\,\mathrm{e}^{-\mathrm{i}(\vec{k}_p-\vec{k}_h)\cdot\vec{r}}\frac{\mathrm{e}^{-r^2/\mu^2}}{(\mu\sqrt{\pi})^3}+\int \mathrm{d}^3R\int \mathrm{d}^3r\,\mathrm{e}^{-\mathrm{i}(\vec{k}_p-\vec{k}_h)\cdot\vec{r}}\delta(\vec{r})\Big].&\end{aligned} \tag{A.151}$$

Considering an infinite volume, $\mathcal{V}\to\infty$, and repeating the steps that led to (A.45), we can perform the two integrals with Gaussian integrals (D.118). Indeed,

$$\begin{aligned}\langle\vec{k}_p\vec{k}_{h'}|v_{12}^{\mathrm{d}_1}|_{\mathrm{D}}|\vec{k}_h\vec{k}_{p'}\rangle &= \frac{\alpha\rho^\alpha}{2\mathcal{V}}\Big(W+\frac{B}{2}-\frac{H}{2}-\frac{M}{4}\Big)\\ &\quad\times\Big[\int \mathrm{d}^3r\,\mathrm{e}^{-\mathrm{i}(\vec{k}_p-\vec{k}_h)\cdot\vec{r}}\frac{\mathrm{e}^{-r^2/\mu^2}}{(\mu\sqrt{\pi})^3}+\int \mathrm{d}^3r\,\mathrm{e}^{-\mathrm{i}(\vec{k}_p-\vec{k}_h)\cdot\vec{r}}\delta(\vec{r})\Big]\\ &= \frac{\alpha\rho^\alpha}{2\mathcal{V}}\Big(W+\frac{B}{2}-\frac{H}{2}-\frac{M}{4}\Big)\Big[\mathrm{e}^{-(\vec{k}_p-\vec{k}_h)^2\mu^2/4}+1\Big].\end{aligned} \tag{A.152}$$

At the Landau limit, we have $|\vec{k}_p|=|\vec{k}_h|=|\vec{k}_{\mathrm{F}}|$ and $|\vec{k}_{p'}|=|\vec{k}_{h'}|=|\vec{k}'_{\mathrm{F}}|$, so that the direct component of the first rearrangement term reads

$$\boxed{\langle\vec{k}_{\mathrm{F}}\vec{k}'_{\mathrm{F}}|v_{12}^{\mathrm{d}_1}|_{\mathrm{D}}|\vec{k}_{\mathrm{F}}\vec{k}'_{\mathrm{F}}\rangle = \frac{\alpha\rho^\alpha}{\mathcal{V}}\Big(W+\frac{B}{2}-\frac{H}{2}-\frac{M}{4}\Big).} \tag{A.153}$$

We continue by evaluating the exchange component of (A.140), which is

$$v_{12}^{\mathrm{d}_1}|_{\mathrm{E}} \equiv \frac{\alpha}{2}\sum_i\langle i|\frac{V(r_{23})}{(\mu\sqrt{\pi})^3}\Big[\rho^{\alpha-1}(\vec{r}_2)\delta(\vec{r}_1-\vec{r}_2)+\rho^{\alpha-1}(\vec{r}_3)\delta(\vec{r}_1-\vec{r}_3)\Big]\mathcal{P}_{\mathrm{E}}^{23}P_r^{23}|i\rangle. \tag{A.154}$$

The calculation is trickier than the direct term because of the space exchange operator P_r^{23} that forces us to consider directly the two-body matrix element

$$\begin{aligned}\langle ph'|v_{12}^{\mathrm{d}_1}|_{\mathrm{E}}|hp'\rangle = \frac{\alpha}{2}\sum_i\langle ph'i|\frac{V(r_{23})}{(\mu\sqrt{\pi})^3}\Big[\rho^{\alpha-1}(\vec{r}_2)\delta(\vec{r}_1-\vec{r}_2)+\rho^{\alpha-1}(\vec{r}_3)\delta(\vec{r}_1-\vec{r}_3)\Big]&\\ \times\mathcal{P}_{\mathrm{E}}^{23}|hip'\rangle,&\end{aligned} \tag{A.155}$$

since $P_r^{23}|hp'i\rangle = |hip'\rangle$. Considering again the continuous limit (A.4), we obtain (with i renamed 3 for convenience),

$$\begin{aligned}\langle ph'|v_{12}^{\mathrm{d}_1}|_{\mathrm{E}}|hp'\rangle = \frac{\alpha}{2}\frac{\mathcal{V}}{(2\pi)^3}\sum_{u_3}\langle u_3|\mathcal{P}_{\mathrm{E}}^{23}|u_3\rangle \times \int \mathrm{d}^3k_3 \int \mathrm{d}^3r_3 \int \mathrm{d}^3r_2 \int \mathrm{d}^3r_1 \\ \times \phi^*_{\vec{k}_p}(\vec{r}_1)\phi^*_{\vec{k}_{h'}}(\vec{r}_2)\phi^*_{\vec{k}_3}(\vec{r}_3)\frac{V(r_{23})}{(\mu\sqrt{\pi})^3}\Big[\rho^{\alpha-1}(\vec{r}_2)\delta(\vec{r}_1-\vec{r}_2) \\ + \rho^{\alpha-1}(\vec{r}_3)\delta(\vec{r}_1-\vec{r}_3)\Big]\phi_{\vec{k}_h}(\vec{r}_1)\phi_{\vec{k}_3}(\vec{r}_2)\phi_{\vec{k}_{p'}}(\vec{r}_3).\end{aligned} \tag{A.156}$$

To get the spin-isospin contribution, we just need to change W, B, H, M for M, H, B, W in (A.147), so that

$$\sum_{s_3t_3}\langle s_3t_3|\mathcal{P}_{\mathrm{E}}^{23}|s_3t_3\rangle = 4\Big(M + \frac{H}{2} - \frac{B}{2} - \frac{W}{4}\Big). \tag{A.157}$$

Then, we have

$$\begin{aligned}\langle ph'|v_{12}^{\mathrm{d}_1}|_{\mathrm{E}}|hp'\rangle &= \langle \vec{k}_p\vec{k}_{h'}|v_{12}^{\mathrm{d}_1}|_{\mathrm{E}}|\vec{k}_h\vec{k}_{p'}\rangle \\ &= \frac{2}{(2\pi)^3}\frac{\alpha}{\mathcal{V}^2}\Big(M + \frac{H}{2} - \frac{B}{2} - \frac{W}{4}\Big)\int \mathrm{d}^3k_3 \\ &\quad \times \int \mathrm{d}^3r_3 \int \mathrm{d}^3r_2 \int \mathrm{d}^3r_1\, \mathrm{e}^{-\mathrm{i}(\vec{k}_p-\vec{k}_h)\cdot\vec{r}_1}\mathrm{e}^{-\mathrm{i}(\vec{k}_3-\vec{k}_{p'})\cdot\vec{r}_2}\mathrm{e}^{-\mathrm{i}(\vec{k}_{h'}-\vec{k}_3)\cdot\vec{r}_3} \\ &\quad \times \frac{V(r_{23})}{(\mu\sqrt{\pi})^3}\Big[\rho^{\alpha-1}(\vec{r}_2)\delta(\vec{r}_1-\vec{r}_2) + \rho^{\alpha-1}(\vec{r}_3)\delta(\vec{r}_1-\vec{r}_3)\Big].\end{aligned} \tag{A.158}$$

Splitting the integral into two parts and evaluating the integrals over $\vec{r}_1$, we get

$$\begin{aligned}\langle \vec{k}_p\vec{k}_{h'}|v_{12}^{\mathrm{d}_1}|_{\mathrm{E}}|\vec{k}_h\vec{k}_{p'}\rangle &= \frac{2}{(2\pi)^3}\frac{\alpha}{\mathcal{V}^2}\Big(M + \frac{H}{2} - \frac{B}{2} - \frac{W}{4}\Big) \\ &\quad \times \Bigg[\int \mathrm{d}^3k_3 \int \mathrm{d}^3r_3 \int \mathrm{d}^3r_2 \int \mathrm{d}^3r_1\, \rho^{\alpha-1}(\vec{r}_2)\delta(\vec{r}_1-\vec{r}_2)\frac{V(r_{23})}{(\mu\sqrt{\pi})^3} \\ &\quad \times \mathrm{e}^{-\mathrm{i}(\vec{k}_p-\vec{k}_h)\cdot\vec{r}_1}\mathrm{e}^{-\mathrm{i}(\vec{k}_3-\vec{k}_{p'})\cdot\vec{r}_2}\mathrm{e}^{-\mathrm{i}(\vec{k}_{h'}-\vec{k}_3)\cdot\vec{r}_3} \\ &\quad + \int \mathrm{d}^3k_3 \int \mathrm{d}^3r_3 \int \mathrm{d}^3r_2 \int \mathrm{d}^3r_1\, \rho^{\alpha-1}(\vec{r}_3)\delta(\vec{r}_1-\vec{r}_3)\frac{V(r_{23})}{(\mu\sqrt{\pi})^3} \\ &\quad \times \mathrm{e}^{-\mathrm{i}(\vec{k}_p-\vec{k}_h)\cdot\vec{r}_1}\mathrm{e}^{-\mathrm{i}(\vec{k}_3-\vec{k}_{p'})\cdot\vec{r}_2}\mathrm{e}^{-\mathrm{i}(\vec{k}_{h'}-\vec{k}_3)\cdot\vec{r}_3}\Bigg] \\ &= \frac{2}{(2\pi)^3}\frac{\alpha}{\mathcal{V}^2}\Big(M + \frac{H}{2} - \frac{B}{2} - \frac{W}{4}\Big) \\ &\quad \times \Bigg[\int \mathrm{d}^3k_3 \int \mathrm{d}^3r_3 \int \mathrm{d}^3r_2\, \rho^{\alpha-1}(\vec{r}_2)\frac{V(r_{23})}{(\mu\sqrt{\pi})^3} \\ &\quad \times \mathrm{e}^{-\mathrm{i}(\vec{k}_p+\vec{k}_3-\vec{k}_h-\vec{k}_{p'})\cdot\vec{r}_2}\mathrm{e}^{-\mathrm{i}(\vec{k}_{h'}-\vec{k}_3)\cdot\vec{r}_3} \\ &\quad + \int \mathrm{d}^3k_3 \int \mathrm{d}^3r_3 \int \mathrm{d}^3r_2\, \rho^{\alpha-1}(\vec{r}_3)\frac{V(r_{23})}{(\mu\sqrt{\pi})^3} \\ &\quad \times \mathrm{e}^{-\mathrm{i}(\vec{k}_3-\vec{k}_{p'})\cdot\vec{r}_2}\mathrm{e}^{-\mathrm{i}(\vec{k}_p+\vec{k}_{h'}-\vec{k}_h-\vec{k}_3)\cdot\vec{r}_3}\Bigg].\end{aligned} \tag{A.159}$$

The conservation of the quasiparticle pair momentum $\vec{k}_p + \vec{k}_{h'} = \vec{k}_h + \vec{k}_{p'}$ provides

$$\begin{aligned}
\langle \vec{k}_p \vec{k}_{h'} | v_{12}^{\mathrm{d_1}} |_{\mathrm{E}} | \vec{k}_h \vec{k}_{p'} \rangle &= \frac{2}{(2\pi)^3} \frac{\alpha}{\mathcal{V}^2} \left(M + \frac{H}{2} - \frac{B}{2} - \frac{W}{4} \right) \\
&\quad \times \left[\int \mathrm{d}^3 k_3 \int \mathrm{d}^3 r_3 \int \mathrm{d}^3 r_2 \, \rho^{\alpha-1}(\vec{r}_2) \frac{V(r_{23})}{(\mu\sqrt{\pi})^3} \mathrm{e}^{-\mathrm{i}(\vec{k}_{h'} - \vec{k}_3)\cdot(\vec{r}_3 - \vec{r}_2)} \right. \\
&\quad \left. + \int \mathrm{d}^3 k_3 \int \mathrm{d}^3 r_3 \int \mathrm{d}^3 r_2 \, \rho^{\alpha-1}(\vec{r}_3) \frac{V(r_{23})}{(\mu\sqrt{\pi})^3} \mathrm{e}^{-\mathrm{i}(\vec{k}_{p'} - \vec{k}_3)\cdot(\vec{r}_3 - \vec{r}_2)} \right] \\
&= \frac{2}{(2\pi)^3} \frac{\alpha \rho^{\alpha-1}}{\mathcal{V}^2} \left(M + \frac{H}{2} - \frac{B}{2} - \frac{W}{4} \right) \\
&\quad \times \left[\int \mathrm{d}^3 r_1 \int \mathrm{d}^3 r_2 \, \frac{V(r_{12})}{(\mu\sqrt{\pi})^3} \mathrm{e}^{-\mathrm{i}\vec{k}_{h'}\cdot(\vec{r}_1 - \vec{r}_2)} \int \mathrm{d}^3 k_3 \, \mathrm{e}^{-\mathrm{i}\vec{k}_3\cdot(\vec{r}_1 - \vec{r}_2)} \right. \\
&\quad \left. + \int \mathrm{d}^3 r_1 \int \mathrm{d}^3 r_2 \, \frac{V(r_{12})}{(\mu\sqrt{\pi})^3} \mathrm{e}^{-\mathrm{i}\vec{k}_{p'}\cdot(\vec{r}_1 - \vec{r}_2)} \int \mathrm{d}^3 k_3 \, \mathrm{e}^{-\mathrm{i}\vec{k}_3\cdot(\vec{r}_1 - \vec{r}_2)} \right],
\end{aligned} \tag{A.160}$$

where we have renamed the integration variable $\vec{r}_3$ into $\vec{r}_1$ and used the translational invariance of INM, i.e. $\rho(\vec{r}_1) = \rho(\vec{r}_2) = \rho$. The integral over $\vec{k}_3$ reads

$$\begin{aligned}
\int \mathrm{d}^3 k_3 \, \mathrm{e}^{-\mathrm{i}\vec{k}_3\cdot(\vec{r}_1 - \vec{r}_2)} &= 2\pi \int_0^{k_\mathrm{F}} \mathrm{d}k_3 \, k_3^2 \int_0^\pi \mathrm{d}\theta \sin\theta \, \mathrm{e}^{-\mathrm{i}k_3 r \cos\theta} \\
&= 2\pi \int_0^{k_\mathrm{F}} \mathrm{d}k_3 \, k_3 \frac{1}{\mathrm{i}r} \left[\mathrm{e}^{-\mathrm{i}k_3 r \cos\theta} \right]_0^\pi \\
&= \frac{4\pi}{r} \int_0^{k_\mathrm{F}} \mathrm{d}k_3 \, k_3 \sin(k_3 r) \\
&= \frac{4\pi}{r} \frac{1}{r^2} \int_0^{k_\mathrm{F} r} \mathrm{d}(k_3 r) \, k_3 r \sin(k_3 r) \\
&= \frac{4\pi}{r} \frac{\sin k_\mathrm{F} r - k_\mathrm{F} r \cos k_\mathrm{F} r}{r^2} = \frac{4\pi k_\mathrm{F}^2}{r} j_1(k_\mathrm{F} r),
\end{aligned} \tag{A.161}$$

with $\vec{r} \equiv \vec{r}_1 - \vec{r}_2$ and the spherical Bessel function of the first kind given by (D.115c). Finally, the expression of the constant nuclear density in INM (A.27) gives

$$\frac{1}{(2\pi)^3} \int \mathrm{d}^3 k_3 \, \mathrm{e}^{-\mathrm{i}\vec{k}_3\cdot(\vec{r}_1 - \vec{r}_2)} = \frac{3\rho}{4} \frac{j_1(k_\mathrm{F} r)}{k_\mathrm{F} r}. \tag{A.162}$$

Moving from the nucleon to the center-of-mass and relative coordinates defined in (A.40) and considering an infinite volume, $\mathcal{V} \to \infty$, we find out

$$\begin{aligned}
\langle \vec{k}_p \vec{k}_{h'} | v_{12}^{\mathrm{d_1}} |_{\mathrm{E}} | \vec{k}_h \vec{k}_{p'} \rangle &= \frac{3\alpha\rho^\alpha}{2\mathcal{V}^2} \left(M + \frac{H}{2} - \frac{B}{2} - \frac{W}{4} \right) \\
&\quad \times \left[\int \mathrm{d}^3 R \int \mathrm{d}^3 r \, \mathrm{e}^{-\mathrm{i}\vec{k}_{h'}\cdot\vec{r}} \frac{\mathrm{e}^{-r^2/\mu^2}}{(\mu\sqrt{\pi})^3} \frac{j_1(k_\mathrm{F} r)}{k_\mathrm{F} r} \right. \\
&\quad \left. + \int \mathrm{d}^3 R \int \mathrm{d}^3 r \, \mathrm{e}^{-\mathrm{i}\vec{k}_{p'}\cdot\vec{r}} \frac{\mathrm{e}^{-r^2/\mu^2}}{(\mu\sqrt{\pi})^3} \frac{j_1(k_\mathrm{F} r)}{k_\mathrm{F} r} \right], \\
&= \frac{3\alpha\rho^\alpha}{2\mathcal{V}} \left(M + \frac{H}{2} - \frac{B}{2} - \frac{W}{4} \right) \\
&\quad \times \left[\int \mathrm{d}^3 r \, \mathrm{e}^{-\mathrm{i}\vec{k}_{h'}\cdot\vec{r}} \frac{\mathrm{e}^{-r^2/\mu^2}}{(\mu\sqrt{\pi})^3} \frac{j_1(k_\mathrm{F} r)}{k_\mathrm{F} r} \right. \\
&\quad \left. + \int \mathrm{d}^3 r \, \mathrm{e}^{-\mathrm{i}\vec{k}_{p'}\cdot\vec{r}} \frac{\mathrm{e}^{-r^2/\mu^2}}{(\mu\sqrt{\pi})^3} \frac{j_1(k_\mathrm{F} r)}{k_\mathrm{F} r} \right],
\end{aligned} \tag{A.163}$$

At the Landau limit, we have $|\vec{k}_p| = |\vec{k}_h| = |\vec{k}_\mathrm{F}|$ and $|\vec{k}_{p'}| = |\vec{k}_{h'}| = |\vec{k}'_\mathrm{F}|$, so that the two integrals coincide and we obtain

$$\begin{aligned}\langle \vec{k}_\mathrm{F}\vec{k}'_\mathrm{F}|v_{12}^{\mathrm{d}_1}|_\mathrm{E}|\vec{k}_\mathrm{F}\vec{k}'_\mathrm{F}\rangle &= \frac{3\alpha\rho^\alpha}{\mathcal{V}}\left(M+\frac{H}{2}-\frac{B}{2}-\frac{W}{4}\right)\\ &\quad\times\int \mathrm{d}^3r\,\mathrm{e}^{-\mathrm{i}k_\mathrm{F}r\cos\theta}\frac{\mathrm{e}^{-r^2/\mu^2}}{(\mu\sqrt{\pi})^3}\frac{j_1(k_\mathrm{F}r)}{k_\mathrm{F}r}\\ &= \frac{6\pi\alpha\rho^\alpha}{\mathcal{V}}\left(M+\frac{H}{2}-\frac{B}{2}-\frac{W}{4}\right)\\ &\quad\times\int \mathrm{d}r\,r^2\frac{\mathrm{e}^{-r^2/\mu^2}}{(\mu\sqrt{\pi})^3}\frac{j_1(k_\mathrm{F}r)}{k_\mathrm{F}r}\int_0^\pi \mathrm{d}\theta\sin\theta\,\mathrm{e}^{-\mathrm{i}k_\mathrm{F}r\cos\theta}.\end{aligned} \tag{A.164}$$

The angular integral is simply

$$\begin{aligned}\int_0^\pi \mathrm{d}\theta\sin\theta\,\mathrm{e}^{-\mathrm{i}k_\mathrm{F}r\cos\theta} &= \frac{1}{\mathrm{i}k_\mathrm{F}r}\int_0^\pi \mathrm{d}\theta\,\mathrm{i}k_\mathrm{F}r\sin\theta\,\mathrm{e}^{-\mathrm{i}k_\mathrm{F}r\cos\theta}\\ &= \frac{2\sin k_\mathrm{F}r}{k_\mathrm{F}r} = 2j_0(k_\mathrm{F}r),\end{aligned} \tag{A.165}$$

with the spherical Bessel function of the first kind given by (D.115a). Finally, the exchange component of the first rearrangement term reads

$$\begin{aligned}\langle \vec{k}_\mathrm{F}\vec{k}'_\mathrm{F}|v_{12}^{\mathrm{d}_1}|_\mathrm{E}|\vec{k}_\mathrm{F}\vec{k}'_\mathrm{F}\rangle &= \frac{12\pi\alpha\rho^\alpha}{\mathcal{V}}\left(M+\frac{H}{2}-\frac{B}{2}-\frac{W}{4}\right)\\ &\quad\times\int_0^\infty \mathrm{d}r\,r^2\frac{\mathrm{e}^{-r^2/\mu^2}}{(\mu\sqrt{\pi})^3}\frac{j_1(k_\mathrm{F}r)}{k_\mathrm{F}r}j_0(k_\mathrm{F}r),\end{aligned} \tag{A.166}$$

This is consistently the expression found in [18]. Let us now evaluate the above radial integral, hereafter called I^{d_1}, analytically. Using the expressions of the spherical Bessel functions of the first kind (D.115a) and (D.115b), and linearizing the sine and cosine functions, we have to evaluate

$$I^{\mathrm{d}_1} \equiv \frac{1}{2k_\mathrm{F}^2}\frac{1}{(\mu\sqrt{\pi})^3}\int_0^\infty \mathrm{d}r\,\mathrm{e}^{-r^2/\mu^2}\left[\frac{1-\cos 2k_\mathrm{F}r}{(k_\mathrm{F}r)^2}-\frac{\sin 2k_\mathrm{F}r}{k_\mathrm{F}r}\right]. \tag{A.167}$$

The series expansions of the sine and cosine functions, and the parity of the integrands provide

$$\begin{aligned}I^{\mathrm{d}_1} &= \frac{1}{k_\mathrm{F}^2}\frac{1}{(\mu\sqrt{\pi})^3}\int_{-\infty}^{+\infty}\mathrm{d}r\,\mathrm{e}^{-r^2/\mu^2}\left[\sum_n\frac{(-)^n}{(2n+2)!}(2k_\mathrm{F}r)^{2n}-\frac{1}{2}\sum_n\frac{(-)^n}{(2n+1)!}(2k_\mathrm{F}r)^{2n}\right]\\ &= \frac{\sqrt{\pi}}{k_\mathrm{F}^3}\frac{1}{(\mu\sqrt{\pi})^3}\left[\sum_n\frac{(-)^n(\mu k_\mathrm{F})^{2n+1}}{(2n+1)(2n+2)n!}-\frac{1}{2}\sum_n\frac{(-)^n(\mu k_\mathrm{F})^{2n+1}}{(2n+1)n!}\right],\end{aligned} \tag{A.168}$$

where we have inverted the integrals and sums, and used the expression (D.120). We recognize the series expansion of the error function (D.97) in the second right-hand side, so that

$$\begin{aligned}I^{\mathrm{d}_1} &= \frac{\sqrt{\pi}}{2k_\mathrm{F}^3}\frac{1}{(\mu\sqrt{\pi})^3}\left[2\sum_n\frac{(-)^n(\mu k_\mathrm{F})^{2n+1}}{(2n+1)n!}\left(1-\frac{2n+1}{2n+2}\right)-\frac{\sqrt{\pi}}{2}\operatorname{erf}(\mu k_\mathrm{F})\right]\\ &= \frac{\sqrt{\pi}}{2k_\mathrm{F}^3}\frac{1}{(\mu\sqrt{\pi})^3}\left[\sqrt{\pi}\operatorname{erf}(\mu k_\mathrm{F})-\sum_n\frac{(-)^n(\mu k_\mathrm{F})^{2n+1}}{(n+1)!}-\frac{\sqrt{\pi}}{2}\operatorname{erf}(\mu k_\mathrm{F})\right].\end{aligned} \tag{A.169}$$

Setting $X \equiv \mu k_{\mathrm{F}}$ and recognizing the series expansion of the function $(\mathrm{e}^{-X^2}-1)/X$ in the second right-hand side term, we finally get

$$I^{\mathrm{d}_1} = \frac{1}{2\pi X^3}\left[\frac{1}{X}\left(\mathrm{e}^{-X^2}-1\right)+\frac{\sqrt{\pi}}{2}\,\mathrm{erf}(X)\right]. \tag{A.170}$$

Thus, the exchange first rearrangement term becomes

$$\boxed{\begin{aligned}\langle \vec{k}_{\mathrm{F}}\vec{k}'_{\mathrm{F}}|v_{12}^{\mathrm{d}_1}|_{\mathrm{E}}|\vec{k}_{\mathrm{F}}\vec{k}'_{\mathrm{F}}\rangle = \frac{6\alpha\rho^{\alpha}}{\mathcal{V}X^3}\left(M+\frac{H}{2}-\frac{B}{2}-\frac{W}{4}\right)\\ \times\left[\frac{1}{X}\left(\mathrm{e}^{-X^2}-1\right)+\frac{\sqrt{\pi}}{2}\,\mathrm{erf}(X)\right],\end{aligned}} \tag{A.171}$$

where the values of the error function (D.96) are tabulated in the fitting code.

In order to compute the second rearrangement term of the quasiparticle interaction (A.110), it will be useful to give an expression for the derivative appearing therein. According to (A.138), it directly reads

$$\begin{aligned}\frac{\partial v_{12}^{(\mathrm{a})}}{\partial\rho_{p'h'}} = \frac{\alpha}{2}\frac{V(r_{12})}{(\mu\sqrt{\pi})^3}\langle h'|\rho^{\alpha-1}(\vec{r}_1)\delta(\vec{r}_1-\vec{r}_3)+\rho^{\alpha-1}(\vec{r}_2)\delta(\vec{r}_2-\vec{r}_3)|p'\rangle\\ \times(\mathcal{P}_{\mathrm{D}}+\mathcal{P}_{\mathrm{E}}P_r),\end{aligned} \tag{A.172}$$

In the same way as for the first rearrangement term, we see that the second rearrangement term can be written

$$\sum_i \langle pi|\frac{\partial v_{12}^{(\mathrm{a})}}{\partial\rho_{p'h'}}|hi\rangle = \langle ph'|v_{12}^{\mathrm{d}_2}|hp'\rangle, \tag{A.173}$$

where we have defined

$$\begin{aligned}v_{12}^{\mathrm{d}_2} \equiv \frac{\alpha}{2}\sum_i\langle i|\frac{V(r_{13})}{(\mu\sqrt{\pi})^3}\left[\rho^{\alpha-1}(\vec{r}_1)\delta(\vec{r}_1-\vec{r}_2)+\rho^{\alpha-1}(\vec{r}_3)\delta(\vec{r}_2-\vec{r}_3)\right]\\ \times(\mathcal{P}_{\mathrm{D}}^{13}+\mathcal{P}_{\mathrm{E}}^{13}P_r^{13})|i\rangle.\end{aligned} \tag{A.174}$$

We then start by evaluating the direct component of the above one-body matrix element, which reads

$$v_{12}^{\mathrm{d}_2}|_{\mathrm{D}} \equiv \frac{\alpha}{2}\sum_i\langle i|\frac{V(r_{13})}{(\mu\sqrt{\pi})^3}\left[\rho^{\alpha-1}(\vec{r}_1)\delta(\vec{r}_1-\vec{r}_2)+\rho^{\alpha-1}(\vec{r}_3)\delta(\vec{r}_2-\vec{r}_3)\right]\mathcal{P}_{\mathrm{D}}^{13}|i\rangle. \tag{A.175}$$

The procedure is similar to the one undertaken for the direct component of the first rearrangement term, leading to the result (A.148). Here, it comes

$$v_{12}^{\mathrm{d}_2}|_{\mathrm{D}} = \frac{\alpha\rho}{2}\left(W+\frac{B}{2}-\frac{H}{2}-\frac{M}{4}\right)\left[\rho^{\alpha-1}(\vec{r}_1)\frac{V(r_{12})}{(\mu\sqrt{\pi})^3}+\rho^{\alpha-1}(\vec{r}_1)\delta(\vec{r}_1-\vec{r}_2)\right]. \tag{A.176}$$

We now need to evaluate the two-body matrix elements

$$\begin{aligned}\langle ph'|v_{12}^{\mathrm{d}_2}|_{\mathrm{D}}|hp'\rangle &= \langle \vec{k}_p\vec{k}_{h'}|v_{12}^{\mathrm{d}_2}|_{\mathrm{D}}|\vec{k}_h\vec{k}_{p'}\rangle\\ &= \frac{\alpha\rho}{2}\left(W+\frac{B}{2}-\frac{H}{2}-\frac{M}{4}\right)\\ &\quad\times\langle\vec{k}_p\vec{k}_{h'}|\left[\rho^{\alpha-1}(\vec{r}_1)\frac{V(r_{12})}{(\mu\sqrt{\pi})^3}+\rho^{\alpha-1}(\vec{r}_1)\delta(\vec{r}_1-\vec{r}_2)\right]|\vec{k}_h\vec{k}_{p'}\rangle.\end{aligned} \tag{A.177}$$

By following the steps leading to (A.152), we finally get

$$\langle \vec{k}_p \vec{k}_{h'} | v_{12}^{\mathrm{d}_2} |_{\mathrm{D}} | \vec{k}_h \vec{k}_{p'} \rangle = \frac{\alpha \rho^\alpha}{2\mathcal{V}} \left(W + \frac{B}{2} - \frac{H}{2} - \frac{M}{4} \right) \left[\mathrm{e}^{-(\vec{k}_p - \vec{k}_h)^2 \mu^2 / 4} + 1 \right], \tag{A.178}$$

which is in fact exactly the expression we have found out for the first rearrangement term (A.152). At the Landau limit, we have $|\vec{k}_p| = |\vec{k}_h| = |\vec{k}_{\mathrm{F}}|$ and $|\vec{k}_{p'}| = |\vec{k}_{h'}| = |\vec{k}'_{\mathrm{F}}|$, so that the direct component of the second rearrangement term reads

$$\boxed{\langle \vec{k}_{\mathrm{F}} \vec{k}'_{\mathrm{F}} | v_{12}^{\mathrm{d}_2} |_{\mathrm{D}} | \vec{k}_{\mathrm{F}} \vec{k}'_{\mathrm{F}} \rangle = \frac{\alpha \rho^\alpha}{\mathcal{V}} \left(W + \frac{B}{2} - \frac{H}{2} - \frac{M}{4} \right),} \tag{A.179}$$

just like the direct component of the first rearrangement term (A.153).

We continue by evaluating the exchange component of (A.174), which is

$$v_{12}^{\mathrm{d}_2} |_{\mathrm{E}} \equiv \frac{\alpha}{2} \sum_i \langle i | \frac{V(r_{13})}{(\mu\sqrt{\pi})^3} \left[\rho^{\alpha-1}(\vec{r}_1) \delta(\vec{r}_1 - \vec{r}_2) + \rho^{\alpha-1}(\vec{r}_3) \delta(\vec{r}_2 - \vec{r}_3) \right] W_{\mathrm{E}}^{13} \mathcal{P}_r^{13} | i \rangle. \tag{A.180}$$

Once again, we have to deal with the space exchange operator P_r^{13} that forces us to consider directly the two-body matrix element

$$\begin{aligned} \langle ph' | v_{12}^{\mathrm{d}_2} |_{\mathrm{E}} | hp' \rangle = \frac{\alpha}{2} \sum_i \langle ph' i | \frac{V(r_{13})}{(\mu\sqrt{\pi})^3} \left[\rho^{\alpha-1}(\vec{r}_1) \delta(\vec{r}_1 - \vec{r}_2) + \rho^{\alpha-1}(\vec{r}_3) \delta(\vec{r}_2 - \vec{r}_3) \right] \\ \times \mathcal{P}_{\mathrm{E}}^{13} | ip'h \rangle, \end{aligned} \tag{A.181}$$

since $P_r^{13} | hp'i \rangle = | ip'h \rangle$. The derivation is analogous to the first rearrangement term leading to (A.163). We obtain

$$\begin{aligned} \langle ph' | v_{12}^{\mathrm{d}_2} |_{\mathrm{E}} | hp' \rangle &= \langle \vec{k}_p \vec{k}_{h'} | v_{12}^{\mathrm{d}_2} |_{\mathrm{E}} | \vec{k}_h \vec{k}_{p'} \rangle \\ &= \frac{3\alpha\rho^\alpha}{2\mathcal{V}} \left(M + \frac{H}{2} - \frac{B}{2} - \frac{W}{4} \right) \left[\int \mathrm{d}^3 r \, \mathrm{e}^{-\mathrm{i}\vec{k}_h \cdot \vec{r}} \frac{\mathrm{e}^{-r^2/\mu^2}}{(\mu\sqrt{\pi})^3} \frac{j_1(k_{\mathrm{F}} r)}{k_{\mathrm{F}} r} \right. \\ &\qquad \left. + \int \mathrm{d}^3 r \, \mathrm{e}^{-\mathrm{i}\vec{k}_p \cdot \vec{r}} \frac{\mathrm{e}^{-r^2/\mu^2}}{(\mu\sqrt{\pi})^3} \frac{j_1(k_{\mathrm{F}} r)}{k_{\mathrm{F}} r} \right]. \end{aligned} \tag{A.182}$$

At the Landau limit, we have $|\vec{k}_p| = |\vec{k}_h| = |\vec{k}_{\mathrm{F}}|$, and we end up with the same expression we have obtained with the first rearrangement term, namely

$$\begin{aligned} \langle \vec{k}_{\mathrm{F}} \vec{k}'_{\mathrm{F}} | v_{12}^{\mathrm{d}_2} |_{\mathrm{E}} | \vec{k}_{\mathrm{F}} \vec{k}'_{\mathrm{F}} \rangle = \frac{3\alpha\rho^\alpha}{\mathcal{V}} \left(M + \frac{H}{2} - \frac{B}{2} - \frac{W}{4} \right) \\ \times \int \mathrm{d}^3 r \, \mathrm{e}^{-\mathrm{i} k_{\mathrm{F}} r \cos\theta} \frac{\mathrm{e}^{-r^2/\mu^2}}{(\mu\sqrt{\pi})^3} \frac{j_1(k_{\mathrm{F}} r)}{k_{\mathrm{F}} r}, \end{aligned} \tag{A.183}$$

so that the exchange component of the second rearrangement term eventually reads

$$\begin{aligned} \langle \vec{k}_{\mathrm{F}} \vec{k}'_{\mathrm{F}} | v_{12}^{\mathrm{d}_2} |_{\mathrm{E}} | \vec{k}_{\mathrm{F}} \vec{k}'_{\mathrm{F}} \rangle = \frac{12\pi\alpha\rho^\alpha}{\mathcal{V}} \left(M + \frac{H}{2} - \frac{B}{2} - \frac{W}{4} \right) \\ \times \int_0^\infty \mathrm{d} r \, r^2 \frac{\mathrm{e}^{-r^2/\mu^2}}{(\mu\sqrt{\pi})^3} \frac{j_1(k_{\mathrm{F}} r)}{k_{\mathrm{F}} r} j_0(k_{\mathrm{F}} r). \end{aligned} \tag{A.184}$$

This is the same exchange term as the first rearrangement term (A.171), where the radial integral has been calculated in (A.170). We then get

$$\boxed{\langle \vec{k}_{\rm F}\vec{k}'_{\rm F}|v_{12}^{\rm d_2}|_{\rm E}|\vec{k}_{\rm F}\vec{k}'_{\rm F}\rangle = \frac{6\alpha\rho^{\alpha}}{\mathcal{V}X^3}\Big(M+\frac{H}{2}-\frac{B}{2}-\frac{W}{4}\Big) \times\left[\frac{1}{X}\Big(\mathrm{e}^{-X^2}-1\Big)+\frac{\sqrt{\pi}}{2}\,\mathrm{erf}(X)\right],} \tag{A.185}$$

just like for the first rearrangement term .

Finally, to derive the third rearrangement term of the quasiparticle interaction (A.110), we proceed in the way as before, with a second derivative. Taking advantage of the first derivative (A.138), this latter reads

$$\begin{aligned}\frac{\partial^2 v_{12}^{(\rm a)}}{\partial\rho_{hp}\partial\rho_{p'h'}} &\equiv \frac{\partial}{\partial\rho_{p'h'}}\left(\frac{\partial v_{12}^{(\rm a)}}{\partial\rho_{hp}}\right)\\ &= \frac{\alpha(\alpha-1)}{2}\frac{V(r_{12})}{(\mu\sqrt{\pi})^3}\langle ph'|\rho^{\alpha-2}(\vec{r}_1)\delta(\vec{r}_1-\vec{r}_3)\delta(\vec{r}_1-\vec{r}_4)\\ &\qquad +\rho^{\alpha-2}(\vec{r}_2)\delta(\vec{r}_2-\vec{r}_3)\delta(\vec{r}_2-\vec{r}_4)|hp'\rangle(\mathcal{P}_{\rm D}+\mathcal{P}_{\rm E}P_r),\end{aligned} \tag{A.186}$$

Thus, the third rearrangement term appearing in (A.110) can be written

$$\begin{aligned}\frac{1}{2}\sum_{ij}\langle ij|\frac{\partial^2 v_{12}^{(\rm a)}}{\partial\rho_{hp}\partial\rho_{p'h'}}|ij\rangle &= \frac{\alpha(\alpha-1)}{4}\sum_{ij}\langle ijph'|\frac{V(r_{12})}{(\mu\sqrt{\pi})^3}\\ \times\Big[\rho^{\alpha-2}(\vec{r}_1)\delta(\vec{r}_1-\vec{r}_3)\delta(\vec{r}_1-\vec{r}_4)&+\rho^{\alpha-2}(\vec{r}_2)\delta(\vec{r}_2-\vec{r}_3)\delta(\vec{r}_2-\vec{r}_4)\Big]\\ &\times(\mathcal{P}_{\rm D}^{12}+\mathcal{P}_{\rm E}^{12}P_r^{12})|ijhp'\rangle,\end{aligned} \tag{A.187}$$

since the quantities only acting on the particles 1 and 2, spotted by their indices 12, can be incorporated in the four-body matrix element, having no action on the third particle p and third hole h, nor on the fourth particle p' and fourth hole h'. Defining

$$\begin{aligned}v_{12}^{\rm d_3} \equiv \frac{\alpha(\alpha-1)}{4}\sum_{ij}\langle ij|\frac{V(r_{34})}{(\mu\sqrt{\pi})^3}\Big[&\rho^{\alpha-2}(\vec{r}_3)\delta(\vec{r}_1-\vec{r}_3)\delta(\vec{r}_2-\vec{r}_3)\\ &+\rho^{\alpha-1}(\vec{r}_4)\delta(\vec{r}_1-\vec{r}_4)\delta(\vec{r}_2-\vec{r}_4)\Big](\mathcal{P}_{\rm D}^{34}+\mathcal{P}_{\rm E}^{34}P_r^{34})|ij\rangle,\end{aligned} \tag{A.188}$$

we find out, after two circular permutations of the variables in (A.187),

$$\frac{1}{2}\sum_{ij}\langle ij|\frac{\partial^2 v_{12}^{(\rm a)}}{\partial\rho_{hp}\partial\rho_{p'h'}}|ij\rangle = \langle ph'|v_{12}^{\rm d_3}|hp'\rangle. \tag{A.189}$$

We then start by evaluating the direct component of (A.188), which reads

$$\begin{aligned}v_{12}^{\rm d_3}|_{\rm D} \equiv \frac{\alpha(\alpha-1)}{4}\sum_{ij}\langle ij|\frac{V(r_{34})}{(\mu\sqrt{\pi})^3}\Big[&\rho^{\alpha-2}(\vec{r}_3)\delta(\vec{r}_1-\vec{r}_3)\delta(\vec{r}_2-\vec{r}_3)\\ &+\rho^{\alpha-1}(\vec{r}_4)\delta(\vec{r}_1-\vec{r}_4)\delta(\vec{r}_2-\vec{r}_4)\Big]\mathcal{P}_{\rm D}^{34}|ij\rangle,\end{aligned} \tag{A.190}$$

Considering the continuous limit (A.4), we obtain (with i and j respectively renamed 3 and 4 for convenience),

$$\begin{aligned} v_{12}^{\mathrm{d}_3}|_{\mathrm{D}} = \frac{\alpha(\alpha-1)}{4}\frac{\mathcal{V}^2}{(2\pi)^6}\sum_{u_3u_4}\langle u_3u_4|\mathcal{P}_{\mathrm{D}}^{34}|u_3u_4\rangle \times \int \mathrm{d}^3r_3\int \mathrm{d}^3r_4\int \mathrm{d}^3k_3\int \mathrm{d}^3k_4 \\ \times \phi^*_{\vec{k}_3}(\vec{r}_3)\phi^*_{\vec{k}_4}(\vec{r}_4)\frac{V(r_{34})}{(\mu\sqrt{\pi})^3}\Big[\rho^{\alpha-2}(\vec{r}_3)\delta(\vec{r}_1-\vec{r}_3)\delta(\vec{r}_2-\vec{r}_3) \\ + \rho^{\alpha-2}(\vec{r}_4)\delta(\vec{r}_1-\vec{r}_4)\delta(\vec{r}_2-\vec{r}_4)\Big]\phi_{\vec{k}_3}(\vec{r}_3)\phi_{\vec{k}_4}(\vec{r}_4). \end{aligned} \tag{A.191}$$

On the one hand, expressing the scalar product of Pauli matrices as we have done in (A.145), we find

$$\langle s_3s_4|\vec{\sigma}_3\cdot\vec{\sigma}_4|s_3s_4\rangle = \sum_k(-)^k\langle s_3|\sigma_3^k|s_3\rangle\langle s_4|\sigma_4^{-k}|s_4\rangle = 4s_3s_4, \tag{A.192}$$

where we have used the unified relation of the matrix elements of the Pauli matrices (D.18). We obviously get an equivalent relation for the Pauli matrices associated with the isospin, so that

$$\sum_{s_3s_4}\langle s_3s_4|\vec{\sigma}_3\cdot\vec{\sigma}_4|s_3s_4\rangle = \sum_{t_3t_4}\langle t_3t_4|\vec{\tau}_3\cdot\vec{\tau}_4|t_3t_4\rangle = 0, \tag{A.193}$$

in such a way that, eventually only the unity operator of $\mathcal{P}_{\mathrm{D}}^{34}$ contributes to the matrix elements, i.e.

$$\sum_{s_3t_3}\sum_{s_4t_4}\langle s_3t_3\, s_4t_4|\mathcal{P}_{\mathrm{D}}^{34}|s_3t_3\, s_4t_4\rangle = 16\Big(W+\frac{B}{2}-\frac{H}{2}-\frac{M}{4}\Big). \tag{A.194}$$

Combining this result with the nuclear density (A.144), and invoking the translational invariance of INM, i.e. $\rho(\vec{r}_1)=\rho(\vec{r}_2)=\rho$, it follows that

$$\begin{aligned} v_{12}^{\mathrm{d}_3}|_{\mathrm{D}} = \frac{\alpha(\alpha-1)\rho^2}{4}\Big(W+\frac{B}{2}-\frac{H}{2}-\frac{M}{4}\Big)\int \mathrm{d}^3r_3\int \mathrm{d}^3r_4\,\frac{V(r_{34})}{(\mu\sqrt{\pi})^3} \\ \times\Big[\rho^{\alpha-2}(\vec{r}_3)\delta(\vec{r}_1-\vec{r}_3)\delta(\vec{r}_2-\vec{r}_3)+\rho^{\alpha-2}(\vec{r}_4)\delta(\vec{r}_1-\vec{r}_4)\delta(\vec{r}_2-\vec{r}_4)\Big]. \end{aligned} \tag{A.195}$$

Now, to get the direct contribution of the third rearrangement term (A.189), we need to evaluate the two-body matrix elements

$$\begin{aligned} \langle ph'|v_{12}^{\mathrm{d}_3}|_{\mathrm{D}}|hp'\rangle &= \langle \vec{k}_p\vec{k}_{h'}|v_{12}^{\mathrm{d}_3}|_{\mathrm{D}}|\vec{k}_h\vec{k}_{p'}\rangle \\ &= \frac{\alpha(\alpha-1)\rho^2}{4}\Big(W+\frac{B}{2}-\frac{H}{2}-\frac{M}{4}\Big)\int \mathrm{d}^3r_3\int \mathrm{d}^3r_4 \\ &\quad\times\langle \vec{k}_p\vec{k}_{h'}|\frac{V(r_{34})}{(\mu\sqrt{\pi})^3}\Big[\rho^{\alpha-2}(\vec{r}_3)\delta(\vec{r}_1-\vec{r}_3)\delta(\vec{r}_2-\vec{r}_3) \\ &\quad+\rho^{\alpha-2}(\vec{r}_4)\delta(\vec{r}_1-\vec{r}_4)\delta(\vec{r}_2-\vec{r}_4)\Big]|\vec{k}_h\vec{k}_{p'}\rangle. \end{aligned} \tag{A.196}$$

By definition,

$$\begin{aligned} \langle \vec{k}_p\vec{k}_{h'}|v_{12}^{\mathrm{d}_3}|_{\mathrm{D}}|\vec{k}_h\vec{k}_{p'}\rangle = \frac{\alpha(\alpha-1)\rho^2}{4}\Big(W+\frac{B}{2}-\frac{H}{2}-\frac{M}{4}\Big)\int \mathrm{d}^3r_1\int \mathrm{d}^3r_2\int \mathrm{d}^3r_3\int \mathrm{d}^3r_4 \\ \times\phi^*_{\vec{k}_p}(\vec{r}_1)\phi^*_{\vec{k}_{h'}}(\vec{r}_2)\frac{V(r_{34})}{(\mu\sqrt{\pi})^3}\Big[\rho^{\alpha-2}(\vec{r}_3)\delta(\vec{r}_1-\vec{r}_3)\delta(\vec{r}_2-\vec{r}_3) \\ +\rho^{\alpha-2}(\vec{r}_4)\delta(\vec{r}_1-\vec{r}_4)\delta(\vec{r}_2-\vec{r}_4)\Big]\phi_{\vec{k}_h}(\vec{r}_1)\phi_{\vec{k}_{p'}}(\vec{r}_2) \end{aligned}$$

$$
\begin{aligned}
&= \frac{\alpha(\alpha-1)\rho^2}{4\mathcal{V}^2}\Big(W + \frac{B}{2} - \frac{H}{2} - \frac{M}{4}\Big) \\
&\times \Bigg[\int \mathrm{d}^3 r_3 \int \mathrm{d}^3 r_4\, \mathrm{e}^{-\mathrm{i}(\vec{k}_p+\vec{k}_{h'}-\vec{k}_h-\vec{k}_{p'})\cdot\vec{r}_3} \frac{V(r_{34})}{(\mu\sqrt{\pi})^3}\rho^{\alpha-2}(\vec{r}_3) \\
&+ \int \mathrm{d}^3 r_3 \int \mathrm{d}^3 r_4\, \mathrm{e}^{-\mathrm{i}(\vec{k}_p+\vec{k}_{h'}-\vec{k}_h-\vec{k}_{p'})\cdot\vec{r}_4} \frac{V(r_{34})}{(\mu\sqrt{\pi})^3}\rho^{\alpha-2}(\vec{r}_4)\Bigg],
\end{aligned}
\tag{A.197}
$$

where we have performed the straight integrals over $\vec{r}_1$ and $\vec{r}_2$, and separated the expression into two parts. Then, using the conservation of the quasiparticle pair momentum $\vec{k}_p + \vec{k}_h = \vec{k}_{p'} + \vec{k}_{h'}$, we obtain

$$
\begin{aligned}
\langle \vec{k}_p\vec{k}_{h'}|v_{12}^{\mathrm{d}_3}|_{\mathrm{D}}|\vec{k}_h\vec{k}_{p'}\rangle &= \frac{\alpha(\alpha-1)\rho^2}{2\mathcal{V}^2}\Big(W + \frac{B}{2} - \frac{H}{2} - \frac{M}{4}\Big) \\
&\times \int \mathrm{d}^3 r_1 \int \mathrm{d}^3 r_2\, \frac{V(r_{12})}{(\mu\sqrt{\pi})^3}\rho^{\alpha-2}(\vec{r}_1),
\end{aligned}
\tag{A.198}
$$

since the two integrals are equal, as we see when exchanging the integration variables $\vec{r}_3$ and $\vec{r}_4$ in the second integral. Note that we have also relabelled $\vec{r}_3$ as $\vec{r}_1$ and $\vec{r}_4$ as $\vec{r}_2$. Using the translational invariance of INM, i.e. $\rho(\vec{r}_1) = \rho$, and going from the nucleon to the center-of-mass and relative coordinates defined in (A.40), it comes

$$
\begin{aligned}
\langle \vec{k}_p\vec{k}_{h'}|v_{12}^{\mathrm{d}_3}|_{\mathrm{D}}|\vec{k}_h\vec{k}_{p'}\rangle &= \frac{\alpha(\alpha-1)\rho^\alpha}{2\mathcal{V}^2}\Big(W + \frac{B}{2} - \frac{H}{2} - \frac{M}{4}\Big)\int \mathrm{d}^3 r \int \mathrm{d}^3 R\, \frac{\mathrm{e}^{-r^2/\mu^2}}{(\mu\sqrt{\pi})^3} \\
&= \frac{\alpha(\alpha-1)\rho^\alpha}{2\mathcal{V}}\Big(W + \frac{B}{2} - \frac{H}{2} - \frac{M}{4}\Big)\int \mathrm{d}^3 r\, \frac{\mathrm{e}^{-r^2/\mu^2}}{(\mu\sqrt{\pi})^3} \\
&= \frac{\alpha(\alpha-1)\rho^\alpha}{2\mathcal{V}}\Big(W + \frac{B}{2} - \frac{H}{2} - \frac{M}{4}\Big),
\end{aligned}
\tag{A.199}
$$

where we have considered an infinite volume $\mathcal{V} \to \infty$ and performed the integral by means of the Gauss integral (D.118). At the Landau limit, we have $|\vec{k}_p| = |\vec{k}_h| = |\vec{k}_{\mathrm{F}}|$ and $|\vec{k}_{p'}| = |\vec{k}_{h'}| = |\vec{k}'_{\mathrm{F}}|$, so that the direct contribution of the third rearrangement term reads

$$
\boxed{\langle \vec{k}_{\mathrm{F}}\vec{k}'_{\mathrm{F}}|v_{12}^{\mathrm{d}_3}|_{\mathrm{D}}|\vec{k}_{\mathrm{F}}\vec{k}'_{\mathrm{F}}\rangle = \frac{\alpha(\alpha-1)\rho^\alpha}{2\mathcal{V}}\Big(W + \frac{B}{2} - \frac{H}{2} - \frac{M}{4}\Big).}
\tag{A.200}
$$

We continue by evaluating the exchange component of (A.188), which is

$$
\begin{aligned}
v_{12}^{\mathrm{d}_3}|_{\mathrm{E}} \equiv \frac{\alpha(\alpha-1)}{4}\sum_{ij}\langle ij|\frac{V(r_{34})}{(\mu\sqrt{\pi})^3}\Big[&\rho^{\alpha-2}(\vec{r}_3)\delta(\vec{r}_1-\vec{r}_3)\delta(\vec{r}_2-\vec{r}_3) \\
&+ \rho^{\alpha-1}(\vec{r}_4)\delta(\vec{r}_1-\vec{r}_4)\delta(\vec{r}_2-\vec{r}_4)\Big]\mathcal{P}_{\mathrm{D}}^{34}P_r^{34}|ij\rangle,
\end{aligned}
\tag{A.201}
$$

Here, contrary to the first two rearrangement terms (A.155) and (A.181), we can evaluate the above quantity without having to consider the full two-body matrix element $\langle ph'|v_{12}^{\mathrm{d}_2}|_{\mathrm{E}}|hp'\rangle$ since $P_r^{34}|ij\rangle = |ji\rangle$. However, it turns out that it is not possible to simplify the result as we have done for the direct terms in (A.148) and (A.176). Therefore, it will be more efficient to simply follow the procedure adopted for the first two exchange terms. We then have

$$
\begin{aligned}
\langle ph'|v_{12}^{\mathrm{d}_3}|_{\mathrm{E}}|hp'\rangle = \frac{V(r_{34})}{(\mu\sqrt{\pi})^3}\Big[&\rho^{\alpha-2}(\vec{r}_3)\delta(\vec{r}_1-\vec{r}_3)\delta(\vec{r}_2-\vec{r}_3) \\
&+ \rho^{\alpha-1}(\vec{r}_4)\delta(\vec{r}_1-\vec{r}_4)\delta(\vec{r}_2-\vec{r}_4)\Big]\mathcal{P}_{\mathrm{E}}^{34}|hp'ji\rangle.
\end{aligned}
\tag{A.202}
$$

Considering again the continuous limit (A.4), we obtain (with i and j respectively renamed 3 and 4 for convenience),

$$\begin{aligned}\langle ph'|v_{12}^{\mathrm{d}_3}|_{\mathrm{E}}|hp'\rangle &= \frac{\alpha(\alpha-1)}{4}\frac{\mathcal{V}^2}{(2\pi)^6}\sum_{u_3u_4}\langle u_3u_4|\mathcal{P}_{\mathrm{E}}^{34}|u_3u_4\rangle \\ &\times\int \mathrm{d}^3k_3\int \mathrm{d}^3k_4\int \mathrm{d}^3r_4\int \mathrm{d}^3r_3\int \mathrm{d}^3r_2\int \mathrm{d}^3r_1\,\phi^*_{\vec{k}_p}(\vec{r}_1)\phi^*_{\vec{k}_{h'}}(\vec{r}_2)\phi^*_{\vec{k}_3}(\vec{r}_3)\phi^*_{\vec{k}_4}(\vec{r}_4) \\ &\times\frac{V(r_{34})}{(\mu\sqrt{\pi})^3}\Big[\rho^{\alpha-2}(\vec{r}_3)\delta(\vec{r}_1-\vec{r}_3)\delta(\vec{r}_2-\vec{r}_3)+\rho^{\alpha-2}(\vec{r}_4)\delta(\vec{r}_1-\vec{r}_4)\delta(\vec{r}_2-\vec{r}_4)\Big] \\ &\qquad\times\phi_{\vec{k}_h}(\vec{r}_1)\phi_{\vec{k}_{p'}}(\vec{r}_2)\phi_{\vec{k}_4}(\vec{r}_3)\phi_{\vec{k}_3}(\vec{r}_4).\end{aligned} \tag{A.203}$$

To get the spin-isospin contribution, we just need to change W, B, H, M for M, H, B, W in (A.194), so that

$$\sum_{s_3t_3}\sum_{s_4t_4}\langle s_3t_3\,s_4t_4|\mathcal{P}_{\mathrm{E}}^{34}|s_3t_3\,s_4t_4\rangle = 16\Big(M+\frac{H}{2}-\frac{B}{2}-\frac{W}{4}\Big). \tag{A.204}$$

Thus,

$$\begin{aligned}\langle ph'|v_{12}^{\mathrm{d}_3}|_{\mathrm{E}}|hp'\rangle &= \langle\vec{k}_p\vec{k}_{h'}|v_{12}^{\mathrm{d}_3}|_{\mathrm{E}}|\vec{k}_h\vec{k}_{p'}\rangle \\ &= \frac{4\alpha(\alpha-1)}{(2\pi)^6\mathcal{V}^2}\Big(M+\frac{H}{2}-\frac{B}{2}-\frac{W}{4}\Big) \\ &\times\int \mathrm{d}^3k_3\int \mathrm{d}^3k_4\int \mathrm{d}^3r_4\int \mathrm{d}^3r_3\int \mathrm{d}^3r_2\int \mathrm{d}^3r_1\,\mathrm{e}^{-\mathrm{i}(\vec{k}_p-\vec{k}_h)\cdot\vec{r}_1}\mathrm{e}^{-\mathrm{i}(\vec{k}_{h'}-\vec{k}_{p'})\cdot\vec{r}_2} \\ &\times\frac{V(r_{34})}{(\mu\sqrt{\pi})^3}\Big[\rho^{\alpha-2}(\vec{r}_3)\delta(\vec{r}_1-\vec{r}_3)\delta(\vec{r}_2-\vec{r}_3)+\rho^{\alpha-2}(\vec{r}_4)\delta(\vec{r}_1-\vec{r}_4)\delta(\vec{r}_2-\vec{r}_4)\Big] \\ &\qquad\times\mathrm{e}^{-\mathrm{i}(\vec{k}_3-\vec{k}_4)\cdot\vec{r}_3}\mathrm{e}^{-\mathrm{i}(\vec{k}_4-\vec{k}_3)\cdot\vec{r}_4}.\end{aligned} \tag{A.205}$$

Splitting the integral into two parts and evaluating the integrals over $\vec{r}_1$ and $\vec{r}_2$ taking into account the conservation of the quasiparticle pair momentum $\vec{k}_p+\vec{k}_h=\vec{k}_{p'}+\vec{k}_{h'}$, we obtain

$$\begin{aligned}\langle\vec{k}_p\vec{k}_{h'}|v_{12}^{\mathrm{d}_3}|_{\mathrm{E}}|\vec{k}_h\vec{k}_{p'}\rangle &= \frac{4\alpha(\alpha-1)}{(2\pi)^6\mathcal{V}^2}\Big(M+\frac{H}{2}-\frac{B}{2}-\frac{W}{4}\Big) \\ &\times\Bigg[\int \mathrm{d}^3k_3\int \mathrm{d}^3k_4\int \mathrm{d}^3r_4\int \mathrm{d}^3r_3\int \mathrm{d}^3r_2\int \mathrm{d}^3r_1\,\frac{V(r_{34})}{(\mu\sqrt{\pi})^3} \\ &\times\rho^{\alpha-2}(\vec{r}_3)\delta(\vec{r}_1-\vec{r}_3)\delta(\vec{r}_2-\vec{r}_3)\mathrm{e}^{-\mathrm{i}(\vec{k}_p-\vec{k}_h)\cdot(\vec{r}_1-\vec{r}_2)}\mathrm{e}^{-\mathrm{i}(\vec{k}_3-\vec{k}_4)\cdot(\vec{r}_3-\vec{r}_4)} \\ &+\int \mathrm{d}^3k_3\int \mathrm{d}^3k_4\int \mathrm{d}^3r_4\int \mathrm{d}^3r_3\int \mathrm{d}^3r_2\int \mathrm{d}^3r_1\,\frac{V(r_{34})}{(\mu\sqrt{\pi})^3} \\ &\times\rho^{\alpha-2}(\vec{r}_4)\delta(\vec{r}_1-\vec{r}_4)\delta(\vec{r}_2-\vec{r}_4)\mathrm{e}^{-\mathrm{i}(\vec{k}_p-\vec{k}_h)\cdot(\vec{r}_1-\vec{r}_2)}\mathrm{e}^{-\mathrm{i}(\vec{k}_3-\vec{k}_4)\cdot(\vec{r}_3-\vec{r}_4)}\Bigg] \\ &= \frac{4\alpha(\alpha-1)}{(2\pi)^6\mathcal{V}^2}\Big(M+\frac{H}{2}-\frac{B}{2}-\frac{W}{4}\Big) \\ &\times\Bigg[\int \mathrm{d}^3k_3\int \mathrm{d}^3k_4\int \mathrm{d}^3r_4\int \mathrm{d}^3r_3\,\rho^{\alpha-2}(\vec{r}_3)\frac{V(r_{34})}{(\mu\sqrt{\pi})^3} \\ &\qquad\times\mathrm{e}^{-\mathrm{i}(\vec{k}_3-\vec{k}_4)\cdot(\vec{r}_3-\vec{r}_4)} \\ &\times\int \mathrm{d}^3k_3\int \mathrm{d}^3k_4\int \mathrm{d}^3r_4\int \mathrm{d}^3r_3\,\rho^{\alpha-2}(\vec{r}_4)\frac{V(r_{34})}{(\mu\sqrt{\pi})^3} \\ &\qquad\times\mathrm{e}^{-\mathrm{i}(\vec{k}_3-\vec{k}_4)\cdot(\vec{r}_3-\vec{r}_4)}.\end{aligned} \tag{A.206}$$

We now relabel the integration variables $\vec{r}_3$ as $\vec{r}_1$ and $\vec{r}_4$ as $\vec{r}_2$, and use the translational invariance of INM, i.e. $\rho(\vec{r}_1) = \rho(\vec{r}_2) = \rho$ to find out that the above integrals are the same and read

$$\begin{aligned}\langle \vec{k}_p \vec{k}_{h'} | v_{12}^{\mathrm{d}_3} |_{\mathrm{E}} | \vec{k}_h \vec{k}_{p'} \rangle &= \frac{8\alpha(\alpha-1)\rho^{\alpha-2}}{(2\pi)^6 \mathcal{V}^2} \Big(M + \frac{H}{2} - \frac{B}{2} - \frac{W}{4} \Big) \\ &\times \int \mathrm{d}^3 r_1 \int \mathrm{d}^3 r_2 \, \frac{V(r_{12})}{(\mu\sqrt{\pi})^3} \int \mathrm{d}^3 k_3 \, \mathrm{e}^{-\mathrm{i}\vec{k}_3 \cdot (\vec{r}_1 - \vec{r}_2)} \int \mathrm{d}^3 k_4 \, \mathrm{e}^{\mathrm{i}\vec{k}_4 \cdot (\vec{r}_1 - \vec{r}_2)}.\end{aligned} \tag{A.207}$$

It is not difficult to see that

$$\int \mathrm{d}^3 k_3 \, \mathrm{e}^{-\mathrm{i}\vec{k}_3 \cdot (\vec{r}_1 - \vec{r}_2)} = \int \mathrm{d}^3 k_4 \, \mathrm{e}^{\mathrm{i}\vec{k}_4 \cdot (\vec{r}_1 - \vec{r}_2)}, \tag{A.208}$$

that we have already evaluated in (A.162). Now, moving from the nucleon to the center-of-mass and relative coordinates defined in (A.40) and considering an infinite volume, $\mathcal{V} \to \infty$, we obtain

$$\begin{aligned}\langle \vec{k}_p \vec{k}_{h'} | v_{12}^{\mathrm{d}_3} |_{\mathrm{E}} | \vec{k}_h \vec{k}_{p'} \rangle &= \frac{9\alpha(\alpha-1)\rho^{\alpha}}{2\mathcal{V}^2} \Big(M + \frac{H}{2} - \frac{B}{2} - \frac{W}{4} \Big) \\ &\times \int \mathrm{d}^3 r \int \mathrm{d}^3 R \, \frac{\mathrm{e}^{-r^2/\mu^2}}{(\mu\sqrt{\pi})^3} \left[\frac{j_1(k_{\mathrm{F}} r)}{k_{\mathrm{F}} r} \right]^2 \\ &= \frac{18\pi\alpha(\alpha-1)\rho^{\alpha}}{\mathcal{V}} \Big(M + \frac{H}{2} - \frac{B}{2} - \frac{W}{4} \Big) \\ &\times \int_0^{\infty} \mathrm{d}r \, r^2 \frac{\mathrm{e}^{-r^2/\mu^2}}{(\mu\sqrt{\pi})^3} \left[\frac{j_1(k_{\mathrm{F}} r)}{k_{\mathrm{F}} r} \right]^2.\end{aligned} \tag{A.209}$$

At the Landau limit, we have $|\vec{k}_p| = |\vec{k}_h| = |\vec{k}_{\mathrm{F}}|$ and $|\vec{k}_{p'}| = |\vec{k}_{h'}| = |\vec{k}'_{\mathrm{F}}|$, so that the exchange component of the third rearrangement term reads

$$\begin{aligned}\langle \vec{k}_{\mathrm{F}} \vec{k}'_{\mathrm{F}} | v_{12}^{\mathrm{d}_3} |_{\mathrm{E}} | \vec{k}_{\mathrm{F}} \vec{k}'_{\mathrm{F}} \rangle &= \frac{18\pi\alpha(\alpha-1)\rho^{\alpha}}{\mathcal{V}} \Big(M + \frac{H}{2} - \frac{B}{2} - \frac{W}{4} \Big) \\ &\times \int_0^{\infty} \mathrm{d}r \, r^2 \frac{\mathrm{e}^{-r^2/\mu^2}}{(\mu\sqrt{\pi})^3} \left[\frac{j_1(k_{\mathrm{F}} r)}{k_{\mathrm{F}} r} \right]^2,\end{aligned} \tag{A.210}$$

This is consistently the expression found in [18]. Let us now evaluate the above radial integral, hereafter called I^{d_3}, analytically. The procedure is the same as the one that led to (A.170), although more complex. We eventually obtain

$$I^{\mathrm{d}_3} = \frac{1}{6\pi X^6} \Big[\mathrm{e}^{-X^2} (X^2 - 2) - (3X^2 - 2) + \sqrt{\pi} X^3 \, \mathrm{erf}(X) \Big]. \tag{A.211}$$

The exchange contribution of the third rearrangement terms then becomes

$$\boxed{\begin{aligned}\langle \vec{k}_{\mathrm{F}} \vec{k}'_{\mathrm{F}} | v_{12}^{\mathrm{d}_3} |_{\mathrm{E}} | \vec{k}_{\mathrm{F}} \vec{k}'_{\mathrm{F}} \rangle &= \frac{3\alpha(\alpha-1)\rho^{\alpha}}{\mathcal{V} X^6} \Big(M + \frac{H}{2} - \frac{B}{2} - \frac{W}{4} \Big) \\ &\times \Big[\mathrm{e}^{-X^2} (X^2 - 2) - (3X^2 - 2) + \sqrt{\pi} X^3 \, \mathrm{erf}(X) \Big],\end{aligned}} \tag{A.212}$$

where we recall that $X \equiv \mu k_{\mathrm{F}}$, and that the values of the error function are tabulated in the fitting code.

Now that we have calculated all the rearrangement terms of the quasiparticle interaction, let us see how to express them in terms of the Landau parameters. It has been shown that these terms contribute only to the channel $(S = 0, T = 0)$ of the quasiparticle interaction (see equations (A.147) and (A.157) for the first two terms, as well as (A.194) and (A.204) for the third term). Putting together the direct contributions on one side and the exchange contributions on the other side of the three rearrangement terms, we have

$$f^{00}(\theta) = \widetilde{G}^{\alpha}_{\mu}(0)\Bigg[\frac{(3+\alpha)\alpha}{2}\Big(W + \frac{B}{2} - \frac{H}{2} - \frac{M}{4}\Big) + \frac{3\alpha}{X^3}\Big(4K_1(X) + \frac{\alpha-1}{X^3}K_2(X)\Big)\Big(M + \frac{H}{2} - \frac{B}{2} - \frac{W}{4}\Big)\Bigg], \tag{A.213}$$

where we have defined the functions

$$K_1(X) \equiv \frac{1}{X}\Big(\mathrm{e}^{-X^2} - 1\Big) + \frac{\sqrt{\pi}}{2}\,\mathrm{erf}(X), \tag{A.214a}$$

$$K_2(X) \equiv \mathrm{e}^{-X^2}(X^2 - 2) - (3X^2 - 2) + \sqrt{\pi}X^3\,\mathrm{erf}(X), \tag{A.214b}$$

as well as

$$\widetilde{G}^{\alpha}_{\mu}(0) \equiv N_0 G^{\alpha}_{\mu}(0) = N_0\frac{\rho^{\alpha}}{\mathcal{V}}, \tag{A.215}$$

where N_0 is the density of quasiparticle states at the Fermi surface (A.119), ensuring the connection of our matrix elements with the parameters appearing in (A.118). Note that we have defined $G^{\alpha}_{\mu}(0)$ without the factor $(\mu\sqrt{\pi})^3$, contrary to what we did in (A.128). The reason is that the rearrangement terms are exclusively derived from the density-dependent term, for which the potential (A.35) must then be divided by this factor. Now, since the right-hand side of (A.213) does not depend on the angle θ between the quasiparticles, the rearrangement terms only contribute to the component $l = 0$ of the Landau parameter f^{00}_l. Indeed, the expansion (A.121a) is independent of θ only for $l = 0$ as $P_0(\cos\theta) = 1$. Thus, the contribution of the rearrangement terms to the Landau parameters reads

$$\boxed{f^{00}_l = \widetilde{G}^{\alpha}_{\mu}(0)\delta_{l,0}\Bigg[\frac{(3+\alpha)\alpha}{2}\Big(W + \frac{B}{2} - \frac{H}{2} - \frac{M}{4}\Big) + \frac{3\alpha}{X^3}\Big(4K_1(X) + \frac{\alpha-1}{X^3}K_2(X)\Big)\Big(M + \frac{H}{2} - \frac{B}{2} - \frac{W}{4}\Big)\Bigg].} \tag{A.216}$$

4.2.3. Tensor contribution

In this subsection, we shall derive the Landau parameters associated with the finite-range tensor term of the generalized Gogny interaction (II.1). The antisymmetrized tensor interaction is characterized by the equation (A.59), with its direct and exchange spin-isospin components (A.60) respectively written under the equivalent forms

$$\mathcal{P}_{\mathrm{D}} \equiv \Big(W - \frac{H}{2}\Big) - \frac{H}{2}\vec{\tau}_1 \cdot \vec{\tau}_2, \tag{A.217a}$$

$$\mathcal{P}_{\mathrm{E}} \equiv \Big(H - \frac{W}{2}\Big) - \frac{W}{2}\vec{\tau}_1 \cdot \vec{\tau}_2. \tag{A.217b}$$

We notice that the direct isospin components of the tensor interaction can be deduced from the exchange ones by switching W and H, in the same idea as what we did for the central and density-dependent terms.

In order to get the contribution from the tensor interaction to the matrix elements of the particle–hole interaction (A.110), we shall evaluate the following antisymmetrized matrix elements in the particle–hole representation,

$$\begin{aligned}\langle \vec{k}_p \vec{k}_{h'} | v_{12}^{\mathrm{T},(\mathrm{a})} | \vec{k}_h \vec{k}_{p'} \rangle = {} & \langle \vec{k}_p \vec{k}_{h'} | V(r_{12}) S_{12}(\hat{r}_{12}) | \vec{k}_h \vec{k}_{p'} \rangle \mathcal{P}_{\mathrm{D}} \\ & + \langle \vec{k}_p \vec{k}_{h'} | V(r_{12}) S_{12}(\hat{r}_{12}) | \vec{k}_{p'} \vec{k}_h \rangle \mathcal{P}_{\mathrm{E}},\end{aligned} \tag{A.218}$$

where we have explicitly separated the direct and exchange as well as the spatial-spin and isospin parts. We have also specified that the above tensor operator acts in the coordinate space by adding $\hat{r}_{12}$ as argument. Since the isospin part is fully specified by (A.217), we focus on the spatial-spin parts. For the direct spatial-spin part, we have, by definition,

$$\begin{aligned}\langle \vec{k}_p \vec{k}_{h'} | V(r_{12}) S_{12}(\hat{r}_{12}) | \vec{k}_h \vec{k}_{p'} \rangle &= \int \mathrm{d}^3 r_1 \int \mathrm{d}^3 r_2 \, \phi^*_{\vec{k}_p}(\vec{r}_1) \phi^*_{\vec{k}_{h'}}(\vec{r}_2) V(r_{12}) S_{12}(\hat{r}_{12}) \phi_{\vec{k}_h}(\vec{r}_1) \phi_{\vec{k}_{p'}}(\vec{r}_2) \\ &= \sum_k (-)^k [\vec{\sigma}_1 \otimes \vec{\sigma}_2]^{(2)}_{-k} \frac{1}{\mathcal{V}^2} \\ &\quad \times \int \mathrm{d}^3 r_1 \int \mathrm{d}^3 r_2 \, \mathrm{e}^{\mathrm{i}(\vec{k}_h - \vec{k}_p)\cdot(\vec{r}_1 - \vec{r}_2)} V(r_{12}) [\hat{r}_{12} \otimes \hat{r}_{12}]^{(2)}_k \\ &= \sum_k (-)^k [\vec{\sigma}_1 \otimes \vec{\sigma}_2]^{(2)}_{-k} \frac{1}{\mathcal{V}} \int \mathrm{d}^3 r \, \mathrm{e}^{\mathrm{i}\vec{q}_{12}\cdot\vec{r}} V(r) [\hat{r} \otimes \hat{r}]^{(2)}_k .\end{aligned} \tag{A.219}$$

From the first to the second line, we have used the equivalent form (D.58) of the tensor operator and invoked the conservation the quasiparticle pair momentum, that is to say $\vec{k}_p + \vec{k}_{h'} = \vec{k}_h + \vec{k}_{p'}$. From the second to the third line, we have defined the relative momentum of the quasiparticle pair $\vec{q}_{12} \equiv \vec{k}_h - \vec{k}_p = \vec{k}_{h'} - \vec{k}_{p'}$ and moved from the nucleon to the relative and center-of-mass coordinates defined in (A.40). Now, using the writing (B.211) and the plane wave expansion of the exponential in terms of the spherical harmonics (D.117), the above integral becomes

$$\begin{aligned}\frac{1}{\mathcal{V}} \int \mathrm{d}^3 r \, \mathrm{e}^{\mathrm{i}\vec{q}_{12}\cdot\vec{r}} V(r) [\hat{r} \otimes \hat{r}]^{(2)}_k &= \frac{4\pi}{\mathcal{V}} \sqrt{\frac{8\pi}{15}} \int \mathrm{d}r \, r^2 V(r) \sum_{lm} \mathrm{i}^l j_l(q_{12} r) Y_l^{m*}(\hat{q}_{12}) \int \mathrm{d}\hat{r} \, Y_l^m(\hat{r}) Y_2^k(\hat{r}) \\ &= \frac{4\pi}{\mathcal{V}} (-)^{k+1} Y_2^{-k*}(\hat{q}_{12}) \int \mathrm{d}r \, r^2 V(r) j_2(q_{12} r) \\ &= -\frac{4\pi}{\mathcal{V}} [\hat{q}_{12} \otimes \hat{q}_{12}]^{(2)}_k \int \mathrm{d}r \, r^2 V(r) j_2(q_{12} r).\end{aligned} \tag{A.220}$$

From the first to the second line, we have used the orthogonality relation of the spherical harmonics (B.205) and from the second to the third line the writing (B.211) in momentum space. Considering the tensor operator in momentum space (A.120), we finally obtain

$$\langle \vec{k}_p \vec{k}_{h'} | V(r_{12}) S_{12}(\hat{r}_{12}) | \vec{k}_h \vec{k}_{p'} \rangle = -\frac{4\pi}{\mathcal{V}} S_{12}(\hat{q}_{12}) \int \mathrm{d}r \, r^2 V(r) j_2(q_{12} r). \tag{A.221}$$

The calculation of the exchange spatial-spin part is done in the same manner. We eventually find out

$$\langle \vec{k}_p \vec{k}_{h'} | V(r_{12}) S_{12}(\hat{r}_{12}) | \vec{k}_{p'} \vec{k}_h \rangle = -\frac{4\pi}{\mathcal{V}} S_{12}(\hat{q}'_{12}) \int \mathrm{d}r \, r^2 V(r) j_2(q'_{12} r), \tag{A.222}$$

with a relative momentum between the quasiparticle pair given by $\vec{q}'_{12} \equiv \vec{k}_{p'} - \vec{k}_p = \vec{k}_{h'} - \vec{k}_h$. Now, at the Landau limit, we have $|\vec{k}_p| = |\vec{k}_h| = |\vec{k}_{\mathrm{F}}|$ and $|\vec{k}_{p'}| = |\vec{k}_{h'}| = |\vec{k}'_{\mathrm{F}}|$, so that

$|\vec{q}_{12}| = 0$ and $|\vec{q}'_{12}| = q_\mathrm{F}$, the relative momentum at the Fermi surface, which is given by (A.122). This implies

$$\langle \vec{k}_\mathrm{F}\vec{k}'_\mathrm{F}|V(r_{12})S_{12}(\hat{r}_{12})|\vec{k}_\mathrm{F}\vec{k}'_\mathrm{F}\rangle = 0, \tag{A.223a}$$

$$\langle \vec{k}_\mathrm{F}\vec{k}'_\mathrm{F}|V(r_{12})S_{12}(\hat{r}_{12})|\vec{k}'_\mathrm{F}\vec{k}_\mathrm{F}\rangle = -\frac{4\pi}{\mathcal{V}}S_{12}(\hat{q}'_{12})\int \mathrm{d}r\, r^2 V(r) j_2(q_\mathrm{F} r). \tag{A.223b}$$

Therefore, the direct spatial-spin part of the tensor interaction vanishes at the Landau limit. *The direct component of the (finite-range) tensor force does not contribute to the Landau parameters.* Moreover, from (A.110), (A.217b) and (A.223a), we get

$$h^{10}(\theta)\frac{q_\mathrm{F}^2}{k_\mathrm{F}^2}S_{12}(\hat{q}_\mathrm{F}) = \left(H - \frac{W}{2}\right)\langle \vec{k}_\mathrm{F}\vec{k}'_\mathrm{F}|V(r_{12})S_{12}(\hat{r}_{12})|\vec{k}'_\mathrm{F}\vec{k}_\mathrm{F}\rangle, \tag{A.224a}$$

$$h^{11}(\theta)\frac{q_\mathrm{F}^2}{k_\mathrm{F}^2}S_{12}(\hat{q}_\mathrm{F}) = -\frac{W}{2}\langle \vec{k}_\mathrm{F}\vec{k}'_\mathrm{F}|V(r_{12})S_{12}(\hat{r}_{12})|\vec{k}'_\mathrm{F}\vec{k}_\mathrm{F}\rangle, \tag{A.224b}$$

since $\hat{q}_{12} = \hat{q}_\mathrm{F}$ as this quantity only indicates the direction of the relative momentum between the quasiparticles. Expanding the parameters h^{1T} in series of Legendre polynomials according to (A.121b), the resulting coefficients, the Landau parameters associated with the tensor interaction, are given by (D.110), that is to say, in our case

$$h_l^{10} = \left(H - \frac{W}{2}\right)H_l(q_\mathrm{F}), \tag{A.225a}$$

$$h_l^{11} = -\frac{W}{2}H_l(q_\mathrm{F}), \tag{A.225b}$$

where, after the change of variable $u \equiv \cos\theta$, we have defined the function

$$H_l(k) \equiv -\frac{2\pi}{\mathcal{V}}(2l+1)\int_{-1}^{1}\mathrm{d}u\,\frac{P_l(u)}{2(1-u)}\int_0^\infty \mathrm{d}r\, r^2 V(r) j_2(kr). \tag{A.226}$$

This is the final expression Pastore *et al.* also get in their review of linear response function in homogeneous INM [234].

Let us now try to simplify this expression. To do so, we first set

$$A_l(r) \equiv \int_{-1}^{1}\mathrm{d}u\,\frac{P_l(u)}{2(1-u)}j_2(q_\mathrm{F} r), \tag{A.227}$$

to evaluate the first integral. The simple change of variable $x \equiv q_\mathrm{F} r = x_\mathrm{F}\sqrt{2(1-u)}$ with $x_\mathrm{F} \equiv k_\mathrm{F} r$ provides

$$\begin{aligned} A_l(r) &= \int_0^{2x_\mathrm{F}}\mathrm{d}x\,\frac{x}{x_\mathrm{F}^2}\frac{x_\mathrm{F}^2}{x^2}P_l\left(1-\frac{x^2}{2x_\mathrm{F}^2}\right)j_2(x) \\ &= \int_0^{2x_\mathrm{F}}\frac{\mathrm{d}x}{x}\left[\left(\frac{3}{x^2}-\frac{1}{x}\right)\sin x - \frac{3}{x^2}\cos x\right]P_l\left(1-\frac{x^2}{2x_\mathrm{F}^2}\right), \end{aligned} \tag{A.228}$$

where we have plugged the expression of the second spherical Bessel function of the first kind (D.115c). By virtue of the series expansion (D.105) of the Legendre polynomial, we obtain

$$A_l(r) = \sum_{i=0}^{l}\frac{(-)^i(l+i)!}{(i!)^2(l-i)!}\frac{1}{(2x_\mathrm{F})^{2i}}I_{2(i-2)}(r), \tag{A.229}$$

with the integral

$$I_{2(i-2)}(r) \equiv \int_0^{2x_\mathrm{F}} \mathrm{d}x \left[(3-x^2)\sin x - 3x\cos x\right] x^{2(i-2)}. \tag{A.230}$$

Setting $n \equiv i-2$, we shall evaluate the integral

$$I_{2n}(r) = \int_0^{2x_\mathrm{F}} \mathrm{d}x \left(3x^{2n}\sin x - x^{2n+2}\sin x - 3x^{2n+1}\cos x\right) \tag{A.231}$$

for $n \geq -2$. For $n \geq 0$, we derive the following results using integration by parts,

$$\int_0^{2x_\mathrm{F}} \mathrm{d}x\, x^{2n+1}\cos x = (2x_\mathrm{F})^{2n+1}\sin 2x_\mathrm{F} - (2n+1)J_{2n}(r), \tag{A.232a}$$

$$\begin{aligned}\int_0^{2x_\mathrm{F}} \mathrm{d}x\, x^{2n+2}\sin x = &-(2x_\mathrm{F})^{2n+2}\cos 2x_\mathrm{F} \\ &+ (2n+2)\Big[(2x_\mathrm{F})^{2n+1}\sin 2x_\mathrm{F} - (2n+1)J_{2n}(r)\Big],\end{aligned} \tag{A.232b}$$

where we have defined the integral

$$J_{2n}(r) \equiv \int_0^{2x_\mathrm{F}} \mathrm{d}x\, x^{2n}\sin x. \tag{A.233}$$

Gathering all the contributions, we obtain

$$I_{2n}(r) = (2n+2)(2n+4)J_{2n}(r) - (2n+5)(2x_\mathrm{F})^{2n+1}\sin 2x_\mathrm{F} + (2x_\mathrm{F})^{2n+2}\cos 2x_\mathrm{F}. \tag{A.234}$$

It only remains to evaluate the integral $J_{2n}(r)$. From the formula (D.121), we find

$$\begin{aligned}J_{2n} &= (2n)!\left[\sum_{t=0}^{n}(-)^{t+1}\frac{x^{2n-2t}}{(2n-2t)!}\cos x + \sum_{t=0}^{n-1}(-)^t\frac{x^{2n-2t-1}}{(2n-2t-1)!}\sin x\right]_0^{2x_\mathrm{F}} \\ &= (2n)!\left[(-)^{n+1}\cos x + \sum_{t=0}^{n-1}(-)^t\frac{x^{2n-2t}}{(2n-2t)!}\left((2n-2t)\frac{\sin x}{x} - \cos x\right)\right]_0^{2x_\mathrm{F}} \\ &= (2n)!\Bigg[(-)^n(1-\cos 2x_\mathrm{F}) \\ &\qquad + \sum_{t=0}^{n-1}(-)^t\frac{(2x_\mathrm{F})^{2n-2t}}{(2n-2t)!}\left((2n-2t)\frac{\sin 2x_\mathrm{F}}{2x_\mathrm{F}} - \cos 2x_\mathrm{F}\right)\Bigg].\end{aligned} \tag{A.235}$$

For $n = -1$, we have to evaluate

$$I_{-2}(r) = \int_0^{2x_\mathrm{F}} \mathrm{d}x \left(\frac{3\sin x}{x^2} - \sin x - \frac{3\cos x}{x}\right). \tag{A.236}$$

Integration by parts provides

$$\int_0^{2x_\mathrm{F}} \mathrm{d}x\, \frac{\cos x}{x} = \frac{\sin 2x_\mathrm{F}}{2x_\mathrm{F}} - 1 + \int_0^{2x_\mathrm{F}} \mathrm{d}x\, \frac{\sin x}{x^2}, \tag{A.237}$$

so that we end up with

$$I_{-2}(r) = \cos 2x_\mathrm{F} - \frac{3\sin 2x_\mathrm{F}}{2x_\mathrm{F}} + 2. \tag{A.238}$$

For $n=-2$, we have to evaluate

$$I_{-4}(r)=\int_0^{2x_\mathrm{F}}\mathrm{d}x\left(\frac{3\sin x}{x^4}-\frac{\sin x}{x^2}-\frac{3\cos x}{x^3}\right). \tag{A.239}$$

Integration by parts provides

$$\int_0^{2x_\mathrm{F}}\mathrm{d}x\,\frac{\sin x}{x^2}=-\left[\frac{\cos x}{x^2}\right]_0^{2x_\mathrm{F}}-2\int_0^{2x_\mathrm{F}}\mathrm{d}x\,\frac{\cos x}{x^3}, \tag{A.240a}$$

$$\int_0^{2x_\mathrm{F}}\mathrm{d}x\,\frac{\cos x}{x^3}=\left[\frac{\sin x}{x^3}\right]_0^{2x_\mathrm{F}}+3\int_0^{2x_\mathrm{F}}\mathrm{d}x\,\frac{\sin x}{x^4}, \tag{A.240b}$$

so that we end up with

$$I_{-4}(r)=\left[\frac{x\cos x-\sin x}{x^3}\right]_0^{2x_\mathrm{F}}=\frac{2x_\mathrm{F}\cos 2x_\mathrm{F}-\sin 2x_\mathrm{F}}{(2x_\mathrm{F})^3}+\frac{1}{3}. \tag{A.241}$$

Thus, the function $A_l(r)$ defined in (A.229) is fully specified. Injecting it in (A.226), we finally find out

$$H_l(q_\mathrm{F})=-\frac{2\pi}{\mathcal{V}}(2l+1)\sum_{i=0}^{l}\frac{(-)^i(l+i)!}{(i!)^2(l-i)!}\int_0^\infty\mathrm{d}r\,r^{2(1-i)}\,\mathrm{e}^{-r^2/\mu^2}I_{2(i-2)}(r). \tag{A.242}$$

We then give the expressions of the above quantity for the first values of l, which have been implemented in the fitting code (and verified with Mathematica). The corresponding integrals are evaluated in a similar manner as we have done for the previous terms. We have:

$$H_0=-\frac{\pi^{3/2}}{4\mathcal{V}k_\mathrm{F}^3}\left[\frac{2}{3}X^3+X\mathrm{e}^{-X^2}-\frac{\sqrt{\pi}}{2}\,\mathrm{erf}(X)\right], \tag{A.243a}$$

$$H_1=-\frac{3\pi^{3/2}}{4\mathcal{V}k_\mathrm{F}^3}\left[\frac{2}{3}X^3-X\left(\mathrm{e}^{-X^2}+4\right)+\frac{5}{2}\sqrt{\pi}\,\mathrm{erf}(X)\right], \tag{A.243b}$$

$$H_2=-\frac{5\pi^{3/2}}{4\mathcal{V}k_\mathrm{F}^3}\left[\frac{2}{3}X^3+X\left(\mathrm{e}^{-X^2}-12\right)+\frac{24}{X}\left(\mathrm{e}^{-X^2}-1\right)+\frac{35}{2}\sqrt{\pi}\,\mathrm{erf}(X)\right], \tag{A.243c}$$

$$\begin{aligned}H_3=-\frac{7\pi^{3/2}}{4\mathcal{V}k_\mathrm{F}^3}\Bigg[&\frac{2}{3}X^3-X\left(\mathrm{e}^{-X^2}+24\right)+\frac{40}{X}\left(\mathrm{e}^{-X^2}-3\right)-\frac{80}{X^3}\left(\mathrm{e}^{-X^2}-1\right)\\&+\frac{105}{2}\sqrt{\pi}\,\mathrm{erf}(X)\Bigg],\end{aligned} \tag{A.243d}$$

$$\begin{aligned}H_4=-\frac{9\pi^{3/2}}{4\mathcal{V}k_\mathrm{F}^3}\Bigg[&\frac{2}{3}X^3+X\left(\mathrm{e}^{-X^2}-40\right)+\frac{8}{X}\left(17\mathrm{e}^{-X^2}-45\right)+\frac{112}{X^3}\left(\mathrm{e}^{-X^2}+5\right)\\&+\frac{672}{X^5}\left(\mathrm{e}^{-X^2}-1\right)+\frac{231}{2}\sqrt{\pi}\,\mathrm{erf}(X)\Bigg],\end{aligned} \tag{A.243e}$$

$$\begin{aligned}H_5=-\frac{11\pi^{3/2}}{4\mathcal{V}k_\mathrm{F}^3}\Bigg[&\frac{2}{3}X^3-X\left(\mathrm{e}^{-X^2}+60\right)+\frac{8}{X}\left(23\mathrm{e}^{-X^2}-105\right)\\&-\frac{64}{X^3}\left(8\mathrm{e}^{-X^2}-35\right)-\frac{864}{X^5}\left(3\mathrm{e}^{-X^2}+7\right)-\frac{8\,640}{X^7}\left(\mathrm{e}^{-X^2}+1\right)\\&+\frac{429}{2}\sqrt{\pi}\,\mathrm{erf}(X)\Bigg],\end{aligned} \tag{A.243f}$$

$$H_6 = -\frac{13\pi^{3/2}}{4\mathcal{V}k_{\mathrm{F}}^3}\bigg[\frac{2}{3}X^3 + X\Big(\mathrm{e}^{-X^2} - 84\Big) + \frac{80}{X}\Big(5\mathrm{e}^{-X^2} - 21\Big) - \frac{320}{X^3}\Big(2\mathrm{e}^{-X^2} + 21\Big) + \frac{480}{X^5}\Big(19\mathrm{e}^{-X^2} - 63\Big) + \frac{10\,560}{X^7}\Big(5\mathrm{e}^{-X^2} + 9\Big) + \frac{147\,840}{X^9}\Big(\mathrm{e}^{-X^2} - 1\Big) + \frac{715}{2}\sqrt{\pi}\,\mathrm{erf}(X)\bigg], \tag{A.243g}$$

$$H_7 = -\frac{15\pi^{3/2}}{4\mathcal{V}k_{\mathrm{F}}^3}\bigg[\frac{2}{3}X^3 - X\Big(\mathrm{e}^{-X^2} + 112\Big) + \frac{16}{X}\Big(31\mathrm{e}^{-X^2} - 189\Big) - \frac{160}{X^3}\Big(11\mathrm{e}^{-X^2} - 105\Big) - \frac{480}{X^5}\Big(47\mathrm{e}^{-X^2} + 231\Big) - \frac{1\,920}{X^7}\Big(11\mathrm{e}^{-X^2} - 297\Big) - \frac{174\,720}{X^9}\Big(7\mathrm{e}^{-X^2} + 11\Big) - \frac{3\,144\,960}{X^{11}}\Big(\mathrm{e}^{-X^2} - 1\Big) + \frac{1\,105}{2}\sqrt{\pi}\,\mathrm{erf}(X)\bigg], \tag{A.243h}$$

where we have defined $X \equiv \mu k_{\mathrm{F}}$ and used the error function defined in (D.96). Thanks to the relations (A.225) these expressions allow us to fully determine the Landau parameters associated with the tensor force.

4.2.4. Spin–orbit contribution

In this subsection, we prove that the spin–orbit interaction characterized by (A.68) does not contribute to the Landau parameters in INM.

Following the steps that led to (A.71) and (A.75) along with the conservation of the quasiparticle pair momentum, $\vec{k}_p + \vec{k}_{h'} = \vec{k}_h + \vec{k}_{p'}$, the direct and exchange spatial matrix elements of the spin–orbit interaction in the particle–hole representation respectively read

$$\begin{aligned}&\langle \vec{k}_p \vec{k}_{h'} | \Big[\overleftarrow{\nabla}_{12} G(r_{12}) \times \vec{\nabla}_{12}\Big] | \vec{k}_h \vec{k}_{p'} \rangle \\ &= \frac{1}{\mathcal{V}^2} \int \mathrm{d}^3 r_1 \int \mathrm{d}^3 r_2\, \mathrm{e}^{-\mathrm{i}(\vec{k}_p - \vec{k}_h)\cdot(\vec{r}_1 - \vec{r}_2)} G(r_{12}) \Big[(\vec{k}_p - \vec{k}_{h'}) \times (\vec{k}_h - \vec{k}_{p'})\Big],\end{aligned} \tag{A.244a}$$

$$\begin{aligned}&\langle \vec{k}_p \vec{k}_{h'} | \Big[\overleftarrow{\nabla}_{12} G(r_{12}) \times \vec{\nabla}_{12}\Big] | \vec{k}_{p'} \vec{k}_h \rangle \\ &= -\frac{1}{\mathcal{V}^2} \int \mathrm{d}^3 r_1 \int \mathrm{d}^3 r_2\, \mathrm{e}^{-\mathrm{i}(\vec{k}_p - \vec{k}_h)\cdot(\vec{r}_1 - \vec{r}_2)} G(r_{12}) \Big[(\vec{k}_p - \vec{k}_{h'}) \times (\vec{k}_h - \vec{k}_{p'})\Big].\end{aligned} \tag{A.244b}$$

Now, at the Landau limit, we have $|\vec{k}_p| = |\vec{k}_h| = |\vec{k}_{\mathrm{F}}|$ and $|\vec{k}_{p'}| = |\vec{k}_{h'}| = |\vec{k}'_{\mathrm{F}}|$, so that

$$\begin{aligned}&\langle \vec{k}_{\mathrm{F}} \vec{k}'_{\mathrm{F}} | \Big[\overleftarrow{\nabla}_{12} G(r_{12}) \times \vec{\nabla}_{12}\Big] | \vec{k}_{\mathrm{F}} \vec{k}'_{\mathrm{F}} \rangle \\ &= \frac{1}{\mathcal{V}^2} \int \mathrm{d}^3 r_1 \int \mathrm{d}^3 r_2\, G(r_{12}) \Big[(\vec{k}_{\mathrm{F}} - \vec{k}'_{\mathrm{F}}) \times (\vec{k}_{\mathrm{F}} - \vec{k}'_{\mathrm{F}})\Big] = 0,\end{aligned} \tag{A.245a}$$

$$\begin{aligned}&\langle \vec{k}_{\mathrm{F}} \vec{k}'_{\mathrm{F}} | \Big[\overleftarrow{\nabla}_{12} G(r_{12}) \times \vec{\nabla}_{12}\Big] | \vec{k}'_{\mathrm{F}} \vec{k}_{\mathrm{F}} \rangle \\ &= -\frac{1}{\mathcal{V}^2} \int \mathrm{d}^3 r_1 \int \mathrm{d}^3 r_2\, G(r_{12}) \Big[(\vec{k}_{\mathrm{F}} - \vec{k}'_{\mathrm{F}}) \times (\vec{k}_{\mathrm{F}} - \vec{k}'_{\mathrm{F}})\Big] = 0.\end{aligned} \tag{A.245b}$$

Therefore, at the Landau limit, the spatial matrix elements associated with the spin–orbit interaction vanish. Thus, *the spin–orbit interaction does not contribute to the Landau parameters in INM.* This is the reason why there are no such parameters in the expression of the quasiparticle interaction (A.118).

4.3. Stability criteria

In this subsection, we introduce and derive stability criteria associated with the Landau parameters (in homogeneous and symmetric INM), with and without tensor terms.

4.3.1. Stability criteria without tensor forces

We start by establishing stability criteria [17, 170, 171, 230] considering the quasiparticle interaction (A.118) without tensor terms, i.e. with $h(\theta) = h'(\theta) = 0$.

We have said in the previous subsection that the quasiparticle ground state defines a spherical Fermi surface in momentum space. Then, this state effectively corresponds to a ground state if it is stable against small deformations, i.e. if it is associated with a minimum of the free energy

$$F \equiv \mathcal{E} - \mu_{\rm c} A, \tag{A.246}$$

where $\mu_{\rm c}$ is the chemical potential and A the number of nucleons. In order to slightly distort the Fermi surface, let us define an infinitesimal displacement $u(\theta, \varphi)$ in momentum space in terms of spherical harmonics (B.204) according to

$$u(\theta, \varphi) = \sum_{lm} u_{lm} Y_l^m(\theta, \varphi), \tag{A.247}$$

for which we assume the reality condition $u_{lm}^* = (-)^m u_{l-m}$. Then, the change in the distribution function (A.111) becomes

$$\delta\rho(\vec{k}) = \begin{cases} 1 & \text{if } \ k_{\rm F} \leq |\vec{k}| \leq k_{\rm F} + u(\theta, \varphi), \\ 0 & \text{otherwise.} \end{cases} \tag{A.248}$$

Considering the continuous limit (A.4) to transform the summations of equation (A.114) while considering the above distribution function, the variation in free energy is given by

$$\begin{aligned} \delta F = {} & \frac{\mathcal{V}}{(2\pi)^3} \sum_{sq} \int \mathrm{d}\hat{r} \int_{k_{\rm F}}^{k_{\rm F}+u(\theta,\varphi)} \mathrm{d}k\, k^2 (\varepsilon_0(k) - \mu_{\rm c}) \\ & + \frac{1}{2} \frac{\mathcal{V}^2}{(2\pi)^6} \sum_{sq} \sum_{s'q'} \int \mathrm{d}\hat{r} \int \mathrm{d}\hat{r}' \int_{k_{\rm F}}^{k_{\rm F}+u(\theta,\varphi)} \mathrm{d}k\, k^2 \int_{k_{\rm F}}^{k_{\rm F}+u(\theta',\varphi')} \mathrm{d}k'\, k'^2 \mathcal{F}(\vec{k}, \vec{k}'), \end{aligned} \tag{A.249}$$

Since we are interested in small displacements of the Fermi surface, we will only keep the lowest orders in $u(\theta, \varphi)$. For the first right-hand side term, the lowest order is 2 as we notice that $\varepsilon_0(k_{\rm F}) = \mu_{\rm c}$, so that the terms of order 1 vanish. For the second right-hand side term, it is 1, for each integral. Performing the integrations over momenta, we get

$$\delta F = \frac{\mathcal{V}}{(2\pi)^3} \frac{\hbar^2 k_{\rm F}^3}{2m^*} \sum_{sq} \int \mathrm{d}\hat{r}\, u^2(\theta, \varphi) + \frac{\mathcal{V}^2 k_{\rm F}^4}{(2\pi)^6} \sum_{sq} \sum_{s'q'} \int \mathrm{d}\hat{r}\, u(\theta, \varphi) \int \mathrm{d}\hat{r}'\, u(\theta', \varphi') \mathcal{F}(\xi), \tag{A.250}$$

where ξ is the angle between the directions (θ, φ) and (θ', φ'). As the quasiparticle interaction only depends on this angle, we can expand it in Legendre polynomials,

$$\mathcal{F}(\xi) = \sum_l \mathcal{F}_l P_l(\cos\xi). \tag{A.251}$$

Let us remark here that we have assumed the displacement (A.247) and the quasiparticle interaction (A.251) to be independent on the spin and isospin variables for simplicity. We

will see later how the result generalizes when these dependences are restored. Inserting (A.247) and (A.251) in (A.250), and using the properties of the spherical harmonics (B.205) and (B.207) as well as the Legendre expansion (D.106), we eventually obtain

$$\delta F = \frac{\mathcal{V}}{(2\pi)^3}\frac{\hbar^2 k_{\mathrm{F}}^3}{2m^*}\sum_{lm}|u_{lm}|^2\Big(1+N_0\frac{\mathcal{F}_l}{2l+1}\Big), \tag{A.252}$$

where N_0 is the density of quasiparticle states at the Fermi surface (A.119). Thus, if the free energy is minimal for a spherical Fermi surface corresponding to the ground state, any variation of the free energy must be positive, i.e. $\delta F > 0$. It implies the stability criterion

$$f_l^{00} > -(2l+1), \quad \text{for } l \in \mathbb{N}, \tag{A.253}$$

where we have used the notations leading to (A.121). Since we have assumed (A.247) and (A.251) to be independent on the spin and isospin variables, this result only holds in the $(S=0,T=0)$ channel. However, we can extend it to the other channels by repeating the calculation while displacing the Fermi surface in the directions $\vec{u}(\theta,\varphi)\cdot\vec{\sigma}$, $u(\theta,\varphi)\tau_z$ and $\vec{u}(\theta,\varphi)\cdot\vec{\sigma}\tau_z$, where Oz is chosen as quantization axis. It brings the same stability criteria for the channels $(S=1,T=0)$, $(S=0,T=1)$ and $(S=1,T=0)$, respectively, i.e.

$$\boxed{f_l^{ST} > -(2l+1), \quad \text{for } l \in \mathbb{N}.} \tag{A.254}$$

For the ground state to be stable when the quasiparticle interaction is purely composed of central terms, the above stability criteria have to be fulfilled at any time.

4.3.2. Stability criteria with tensor forces

We now focus on the stability criteria considering the full quasiparticle interaction (A.118) with tensor terms, i.e. with $h(\theta), h'(\theta) \neq 0$. We will give the new stability criteria and only sketch their derivation [163], this latter being pretty similar (although more intricate) to the one without non-central terms of the previous subsection.

As the tensor terms only act in the $S=1$ channel of the quasiparticle interaction, we can immediately state that the stability criteria in the $S=0$ channel remain the same as in (A.254), i.e.

$$\boxed{f_l^{0T} > -(2l+1), \quad \text{for } l \in \mathbb{N}.} \tag{A.255}$$

Nevertheless, they are modified in the $S=1$ channel, as expected. As before, we consider a variation of the free energy engendered by some displacement of the Fermi surface. The displacements in the $(S=1,T=0)$ and $(S=1,T=1)$ channels are respectively $\vec{u}(\theta,\varphi)\cdot\vec{\sigma}$ and $\vec{u}(\theta,\varphi)\cdot\vec{\sigma}\tau_z$, in agreement with the fact that the tensor interaction explicitly involves the spin variables. In the $(S=1,T=0)$ channel, we show that the change in free energy is eventually given by its matrix elements coupled to the particle–hole quantum numbers

J and J' as [163]

$$\begin{aligned}\langle l'J'|F|lJ\rangle = \delta_{ll'}\delta_{JJ'}\Bigg(1 + \frac{1}{2l+1}f_l^{10} + \frac{2l}{(2l-1)(2l+1)}h_{l-1}^{10} \\ + \frac{2(l+1)}{(2l+1)(2l+3)}h_{l+1}^{10}\Bigg) \\ + \delta_{JJ'}\Bigg(15(-)^J \begin{pmatrix}1 & 1 & 2\\ 0 & 0 & 0\end{pmatrix}\begin{pmatrix}l & l' & 2\\ 0 & 0 & 0\end{pmatrix}\begin{Bmatrix}1 & l' & J\\ l & 1 & 2\end{Bmatrix} \\ \times \left[\sqrt{\frac{2l+1}{2l'+1}}h_{l'}^{10} + \sqrt{\frac{2l'+1}{2l+1}}h_l^{10}\right] \\ - \frac{3\sqrt{(2l+1)(2l'+1)}}{2J+1}\begin{pmatrix}l & 1 & J\\ 0 & 0 & 0\end{pmatrix}\begin{pmatrix}l' & 1 & J\\ 0 & 0 & 0\end{pmatrix}h_J^{10} \\ - 3\sqrt{(2l+1)(2l'+1)}\sum_{l''}\begin{pmatrix}l & 1 & l''\\ 0 & 0 & 0\end{pmatrix}\begin{pmatrix}l' & 1 & l''\\ 0 & 0 & 0\end{pmatrix}\begin{Bmatrix}1 & l' & J\\ 1 & l & l''\end{Bmatrix}h_{l''}^{10}\Bigg),\end{aligned} \tag{A.256}$$

where the parentheses and the brackets respectively denote the Wigner-3j and 6j symbols. For the $(S = 1, T = 1)$ channel, we find out the exact same relation after substituting f_l^{10} by f_l^{11} and h_l^{10} by h_l^{11}, for all l. Thus, the condition for stability of the ground state becomes that the matrix F (whose elements are given above for the $(S = 1, T = 0)$ channel) has only positive eigenvalues. Note in passing that switching off the tensor interaction, i.e. demanding $h_l^{10} = 0$ in the equation above and $h_l^{11} = 0$ in the $(S = 1, T = 1)$ channel, for all l, consistently brings back the stability criteria without tensor terms (A.254) in the associated channels.

Let us now analyze how to extract the eigenvalues of the matrix F from the above expression. First, we note that J and J' are the total momenta that couple the angular and intrinsic momenta of two quasiparticle pairs, in such a way that $|l-1| \leq J \leq l+1$ and $|l'-1| \leq J' \leq l'+1$ (as can in particular be inferred from the Wigner-6j symbols). By the way, those momenta have to be equal, $J = J'$, otherwise the matrix elements are zero. Besides, the properties of the Wigner-3j symbols impose l and l' to be of the same parity. Therefore, for a given J, there is only one 2×2 matrix to diagonalize, the case $J = l = l'$ being a diagonal sub-block. The case $J = 0$, $l = l' = 1$ is also diagonal since the sub-block $J = l = l' = 1$ is, as stated above. We then give the stability criteria for the first values of J, l and l'.

From the diagonal matrix elements, we obtain:

$$\text{for } J = 0, l = l' = 1, \qquad 1 + \frac{1}{3}f_1^{10} - \frac{10}{3}h_0^{10} + \frac{4}{3}h_1^{10} - \frac{2}{15}h_2^{10} > 0, \tag{A.257a}$$

$$\text{for } J = 1, l = l' = 1, \qquad 1 + \frac{1}{3}f_1^{10} + \frac{5}{3}h_0^{10} - \frac{2}{3}h_1^{10} + \frac{1}{15}h_2^{10} > 0, \tag{A.257b}$$

$$\text{for } J = 2, l = l' = 2, \qquad 1 + \frac{1}{5}f_2^{10} + \frac{7}{15}h_1^{10} - \frac{2}{5}h_2^{10} + \frac{3}{35}h_3^{10} > 0, \tag{A.257c}$$

$$\text{for } J = 3, l = l' = 3, \qquad 1 + \frac{1}{7}f_3^{10} + \frac{9}{35}h_2^{10} - \frac{2}{7}h_3^{10} + \frac{5}{63}h_4^{10} > 0, \tag{A.257d}$$

$$\text{for } J = 4, l = l' = 4, \qquad 1 + \frac{1}{9}f_4^{10} + \frac{11}{63}h_3^{10} - \frac{2}{9}h_4^{10} + \frac{7}{99}h_5^{10} > 0, \tag{A.257e}$$

$$\text{for } J = 5, l = l' = 5, \qquad 1 + \frac{1}{11}f_5^{10} + \frac{13}{99}h_4^{10} - \frac{2}{11}h_5^{10} + \frac{9}{143}h_6^{10} > 0. \tag{A.257f}$$

The first four conditions are extracted from [163]. We have checked them all, and evaluate the two last ones for our purposes.

For a given J, the sub-matrix 2×2 of F to diagonalize is defined by

$$F^J \equiv \begin{pmatrix} \langle J-1\,J|F|J-1\,J\rangle & \langle J-1\,J|F|J+1\,J\rangle \\ \langle J+1\,J|F|J-1\,J\rangle & \langle J+1\,J|F|J+1\,J\rangle \end{pmatrix}. \tag{A.258}$$

The standard diagonalization procedure consists in finding the solutions $\lambda_\pm^J$, then called the eigenvalues, of the equation $\det(F^J - \lambda_\pm^J \mathbb{1}) = 0$, where the left-hand side is a second order polynomial in $\lambda_\pm^J$. Therefore, the stability criteria for the sub-matrix simply read

$$\lambda_\pm^J \equiv \frac{-b_J \pm \sqrt{\Delta_J}}{2} > 0, \tag{A.259}$$

where

$$b_J \equiv -\Big(\langle J-1\,J|A|J-1\,J\rangle + \langle J+1\,J|A|J+1\,J\rangle\Big), \tag{A.260a}$$
$$c_J \equiv -\langle J-1\,J|A|J+1\,J\rangle\langle J+1\,J|A|J-1\,J\rangle, \tag{A.260b}$$
$$\Delta_J \equiv b_J^2 - 4c_J. \tag{A.260c}$$

We will therefore give the matrix elements involved in the sub-matrices of the form (A.258) from which the stability criteria are obtained by means of (A.259). Those coupled matrix elements are:

$$\text{for } J=1, \quad \begin{cases} \langle 01|F|01\rangle = 1 + f_0^{10}, \\ \langle 01|F|21\rangle = \langle 21|F|01\rangle = -\sqrt{2}\Big(h_0^{10} - \frac{2}{3}h_1^{10} + \frac{1}{5}h_2^{10}\Big), \\ \langle 21|F|21\rangle = 1 + \frac{1}{5}f_2^{10} - \frac{7}{15}h_1^{10} + \frac{2}{5}h_2^{10} - \frac{3}{35}h_3^{10}, \end{cases} \tag{A.261a}$$

$$\text{for } J=2, \quad \begin{cases} \langle 12|F|12\rangle = 1 + \frac{1}{3}f_1^{10} - \frac{1}{3}h_0^{10} + \frac{2}{15}h_1^{10} - \frac{1}{75}h_2^{10}, \\ \langle 12|F|32\rangle = \langle 32|F|12\rangle = -\sqrt{6}\Big(\frac{1}{5}h_1^{10} - \frac{6}{25}h_2^{10} + \frac{3}{35}h_3^{10}\Big), \\ \langle 32|F|32\rangle = 1 + \frac{1}{7}f_3^{10} - \frac{36}{175}h_2^{10} + \frac{8}{35}h_2^{10} - \frac{4}{63}h_4^{10}, \end{cases} \tag{A.261b}$$

$$\text{for } J=3, \quad \begin{cases} \langle 23|F|23\rangle = 1 + \frac{1}{5}f_2^{10} - \frac{2}{15}h_1^{10} + \frac{12}{105}h_2^{10} - \frac{6}{245}h_3^{10}, \\ \langle 23|F|43\rangle = \langle 43|F|23\rangle = -\sqrt{3}\Big(\frac{6}{35}h_2^{10} - \frac{12}{49}h_3^{10} + \frac{10}{105}h_4^{10}\Big), \\ \langle 43|F|43\rangle = 1 + \frac{1}{9}f_4^{10} - \frac{55}{441}h_3^{10} + \frac{10}{63}h_4^{10} - \frac{5}{99}h_5^{10}, \end{cases} \tag{A.261c}$$

$$\text{for } J=4, \quad \begin{cases} \langle 34|F|34\rangle = 1 + \frac{1}{7}f_3^{10} - \frac{3}{35}h_2^{10} + \frac{2}{9}h_3^{10} - \frac{29}{189}h_4^{10}, \\ \langle 34|F|54\rangle = \langle 54|F|34\rangle = -\sqrt{5}\Big(\frac{2}{21}h_3^{10} - \frac{4}{27}h_4^{10} + \frac{2}{33}h_5^{10}\Big), \\ \langle 54|F|54\rangle = 1 + \frac{1}{11}f_5^{10} - \frac{26}{297}h_4^{10} + \frac{4}{33}h_5^{10} - \frac{18}{143}h_6^{10}. \end{cases} \tag{A.261d}$$

The two first sets of matrix elements are extracted from [163]. We have checked them all, and evaluate the two last ones for our purposes. We take this opportunity to give two additional off-diagonal matrix elements we need in section II.2.5, namely

$$\text{for } J=5, \quad \langle 45|F|45\rangle = 1 + \frac{1}{9}f_4^{10} - \frac{4}{63}h_3^{10} + \frac{8}{99}h_4^{10} - \frac{46}{363}h_5^{10}, \tag{A.262a}$$

$$\text{for } J=6, \quad \langle 56|F|56\rangle = 1 + \frac{1}{11}f_5^{10} - \frac{5}{99}h_4^{10} + \frac{10}{143}h_5^{10} - \frac{45}{1\,859}h_6^{10}. \tag{A.262b}$$

We remind that all those matrix elements given for the $(S=1, T=0)$ channel can immediately be deduced for the $(S=1, T=1)$ channel, applying the changes $f_l^{10} \to f_l^{11}$ and $h_l^{10} \to h_l^{11}$, for all l.

4.4. Sum rules

In this subsection, we introduce and derive the sum rules associated with the Landau parameters (in homogeneous and symmetric INM), with and without tensor terms. We start with the framework that applies to both cases.

Within the theory of normal Fermi liquids, we can express the forward scattering amplitude of a quasiparticle pair on the Fermi surface [164, 170] in terms of parameters in pretty much the same way as we did for the quasiparticle interaction (A.118), i.e.

$$\begin{aligned}\mathcal{S} = N_0^{-1}\Big[&b(\theta) + c(\theta)(\vec{\sigma}_1\cdot\vec{\sigma}_2) + b'(\theta)(\vec{\tau}_1\cdot\vec{\tau}_2) + c'(\theta)(\vec{\sigma}_1\cdot\vec{\sigma}_2)(\vec{\tau}_1\cdot\vec{\tau}_2)\\ &+ d(\theta)\frac{q_\mathrm{F}^2}{k_\mathrm{F}^2}S_{12}(\hat{q}_{12}) + d'(\theta)\frac{q_\mathrm{F}^2}{k_\mathrm{F}^2}S_{12}(\hat{q}_{12})(\vec{\tau}_1\cdot\vec{\tau}_2)\Big],\end{aligned} \tag{A.263}$$

with $\mathcal{S} \equiv \mathcal{S}(\vec{k}_\mathrm{F}, \vec{\sigma}_1, \vec{\tau}_1; \vec{k}'_\mathrm{F}, \vec{\sigma}_2, \vec{\tau}_2)$ and N_0 the density of quasiparticle states at the Fermi surface defined in (A.119) ensuring that b, b', c, c', d, d' are dimensionless quantities. Note that these parameters to be determined only depend on the momenta $\vec{k}_\mathrm{F}$ and $\vec{k}'_\mathrm{F}$ of the quasiparticle pair. Now, just like the Landau parameters, we will cast these parameters into common notations $b^{ST}(\theta)$ and $d^{1T}(\theta)$ reflecting the (S,T) channel in which they contribute, namely $b^{00}(\theta) \equiv b(\theta)$, $b^{10}(\theta) \equiv c(\theta)$, $b^{01}(\theta) \equiv b'(\theta)$, $b^{11}(\theta) \equiv c'(\theta)$, and $d^{10}(\theta) \equiv d(\theta)$, $d^{11}(\theta) \equiv d'(\theta)$. As we have done for the parameters of the quasiparticle interaction (A.121), we will expand these parameters in Legendre polynomials, as they only depend on the Landau angle θ between the two quasiparticles,

$$b^{ST}(\theta) = \sum_l b_l^{ST} P_l(\cos\theta), \tag{A.264a}$$

$$d^{1T}(\theta) = \sum_l d_l^{1T} P_l(\cos\theta). \tag{A.264b}$$

Now, the Pauli exclusion principle imposes the forward scattering amplitude to be antisymmetric under the exchange of the two (ingoing or outgoing) quasiparticles, what we write as

$$P\mathcal{S} \equiv P_r P_\sigma P_\tau \mathcal{S} = -\mathcal{S}, \tag{A.265}$$

where the operators P_r, P_σ and P_τ respectively exchange momenta, spins and isospins of the two quasiparticles. Let us evaluate this action when *the momenta of the quasiparticles are equal*, i.e. when $\vec{k}_\mathrm{F} = \vec{k}'_\mathrm{F}$, and then $P_r = \mathbb{1}$. Since then $\vec{q}_{12} = 0$, the tensors terms do not contribute.[7] By means of the definitions (D.8) of the exchange operators as well as the properties (D.13), we obtain

$$\begin{aligned}4P\mathcal{S}(\vec{q}_{12}=0) = &(b + 3b' + 3c + 9c') + (b + 3b' - c - 3c')(\vec{\sigma}_1\cdot\vec{\sigma}_2)\\ &+ (b - b' + 3c - 3c')(\vec{\tau}_1\cdot\vec{\tau}_2) + (b - b' - c + c')(\vec{\sigma}_1\cdot\vec{\sigma}_2)(\vec{\tau}_1\cdot\vec{\tau}_2).\end{aligned} \tag{A.267}$$

7. This is the main reason we chose the first convention for the tensor terms (see discussion after (A.121)). Indeed, the tensor terms are expected to vanish for $\vec{q}_{12} = 0$, in accordance with the expression of the one-pion-exchange contribution to the tensor interaction (II.11). If we had chosen the other convention, the tensor terms would not have been zero in this case. To ensure the vanishing anyway, the coefficients of the expansion in Legendre polynomials (A.121b) should additionally satisfy the condition [236]

$$\sum_{l=0}^{\infty} h_l^{1T} = 0, \tag{A.266}$$

which is necessarily violated if the series is truncated at some finite order, as we practically do (see section II.2.5). Nevertheless, this is not too pathological as we know the coefficients to converge quite rapidly.

Considering the antisymmetrization condition of the forward scattering amplitude together with the above relation in each of the four (S,T) channels, we get, from the properties (D.11), four equations that are

$$\begin{cases} 5b + 3b' + 3c + 9c' = 0, \\ b + 3b' + 3c - 3c' = 0, \\ b + 3b' + 3c - 3c' = 0, \\ b - b' - c + 5c' = 0. \end{cases} \tag{A.268}$$

We notice that the second and third equations are the same. Moreover, multiplying the second line by two, the fourth line by three and adding the result, we fall back on the first equation. Thus, only two of the three remaining equations are linearly independent. We decide to keep the first and second ones. Using the notations we have introduced to bring some physics insight, we write down the two linearly independent equations as

$$\begin{cases} 5b^{00} + 3b^{10} + 3b^{01} + 9b^{11} = 0, \\ b^{00} + 3b^{10} + 3b^{01} - 3b^{11} = 0. \end{cases} \tag{A.269}$$

Summing the equations and plugging the expansions (A.264a) in the result (keeping in mind that $\theta = 0$ as $\vec{k}_{\mathrm{F}} = \vec{k}'_{\mathrm{F}}$), we get the first sum rule,

$$\boxed{\sum_l \left(b_l^{00} + b_l^{10} + b_l^{01} + b_l^{11} \right) = 0.} \tag{A.270}$$

Now, dividing the first equation by two and subtracting it three half of the second one, we obtain the second sum rule,

$$\boxed{\sum_l \left(b_l^{00} - 3b_l^{10} - 3b_l^{01} + 9b_l^{11} \right) = 0.} \tag{A.271}$$

Note we could have chosen other combinations of the two linearly independent equations (A.269) that would have led to different sum rules. Nevertheless, those are convenient since their physical interpretation is obvious. The first and second sum rules are the relations we obtain when considering the antisymmetrization condition (A.265) in the triplet–odd $(S = 1, T = 1)$ and singlet–odd $(S = 0, T = 0)$ channels, respectively. As such, they project onto the triplet–odd and singlet–odd states respectively, ensuring that the forward scattering amplitude of two quasiparticles with *same momenta* vanishes in odd partial waves. Note by the way that there are no such sum rules in even-parity states since the forward scattering amplitude is not expected to vanish for quasiparticles with same momenta in even partial waves. This is indeed what we find out when we consider the antisymmetrization condition (A.265) in the triplet–even $(S = 1, T = 0)$ and singlet–even $(S = 0, T = 1)$ channels. In conclusion, the Pauli exclusion principle is satisfied when the forward scattering amplitude is only composed of central terms if and only if the above sum rules hold.

4.4.1. Sum rules without tensor forces

Let us now write down the sum rules in terms of Landau parameters when there are no tensor forces [17, 164, 170].

When there are no tensor forces, the link between the forward scattering amplitude and the quasiparticle interaction is quite simple so that their respective parameters can be expressed in relation to each other according to

$$b_l^{ST} = \frac{f_l^{ST}}{1 + f_l^{ST}/(2l+1)}, \quad \text{for } l \in \mathbb{N}. \tag{A.272}$$

Then, the sum rules (A.270) and (A.271) merely become

$$\boxed{\sum_l \left[\frac{f_l^{00}}{1 + f_l^{00}/(2l+1)} + \frac{f_l^{10}}{1 + f_l^{10}/(2l+1)} + \frac{f_l^{01}}{1 + f_l^{01}/(2l+1)} + \frac{f_l^{11}}{1 + f_l^{11}/(2l+1)} \right] = 0,} \tag{A.273}$$

as well as

$$\boxed{\sum_l \left[\frac{f_l^{00}}{1 + f_l^{00}/(2l+1)} - \frac{3f_l^{10}}{1 + f_l^{10}/(2l+1)} - \frac{3f_l^{01}}{1 + f_l^{01}/(2l+1)} + \frac{9f_l^{11}}{1 + f_l^{11}/(2l+1)} \right] = 0.} \tag{A.274}$$

In the absence of tensor forces, the two equations above must be satisfied for the Pauli exclusion principle to hold.

4.4.2. Sum rules with tensor forces

Let us finally write down the sum rules in terms of Landau parameters in the presence of tensor forces [164].

As we have seen in the framework outlined earlier, the tensor parameters $d(\theta)$ and $d'(\theta)$ do not take part in the sum rules since they are derived in the limit of equal momenta for which $\vec{q}_{12} = 0$. However, the spin-dependent nature of the tensor forces complicates the equation connecting the forward scattering amplitude to the quasiparticle interaction. To solve it, we need to couple the angular and intrinsic momenta of the quasiparticle pair to the total momentum J. Then, we show that the parameters in the $S = 1$ channel can be written in terms of the forward scattering amplitude coupled to J as

$$b_l^{1T} = \frac{1}{3} \sum_J \frac{2J+1}{2l+1} \mathcal{S}_{ll}^{JT}, \tag{A.275}$$

where $\mathcal{S}_{ll}^{JT}$ is the forward scattering amplitude composed of a diagonal part (for $J = l = l'$ and $J = 0, l = l' = 1$) and a non diagonal part (for $l = J \pm 1$ and $l' = J \mp 1$), such that

$$\mathcal{S}_{ll}^{JT} = \begin{cases} \dfrac{\mathcal{F}_{ll}^{JT}}{1 + \mathcal{F}_{ll}^{JT}/(2l+1)} & \text{for the diagonal part,} \\ \mathcal{D}^{-1} \left[\mathcal{F}_{ll}^{JT} \left(1 + \dfrac{\mathcal{F}_{l'l'}^{JT}}{2l'+1} \right) - \dfrac{(\mathcal{F}_{ll'}^{JT})^2}{2l'+1} \right] & \text{for the non diagonal part,} \end{cases} \tag{A.276}$$

with the quantity

$$\mathcal{D} \equiv \left(1 + \frac{\mathcal{F}_{ll}^{JT}}{2l+1} \right) \left(1 + \frac{\mathcal{F}_{l'l'}^{JT}}{2l'+1} \right) - \frac{(\mathcal{F}_{ll'}^{JT})^2}{(2l+1)(2l'+1)}. \tag{A.277}$$

The quasiparticle interaction coupled to J is related to the matrix elements of the free energy F expressed in the formalism we have defined before, according to

$$\mathcal{F}_{ll'}^{JT} = \sqrt{(2l+1)(2l'+1)}\Big(\langle l'J|F|lJ\rangle - \delta_{ll'}\Big), \tag{A.278}$$

where the matrix elements are given by (A.256) for $T=0$, and by the same relation with the transformations $f_l^{10} \to f_l^{11}$ and $h_l^{10} \to h_l^{11}$, for all l, when $T=1$.

As for the parameters in the $S=0$ channel, they are still given by (A.272) since the tensor forces do not act in this channel, i.e.

$$b_l^{0T} = \frac{f_l^{0T}}{1 + f_l^{0T}/(2l+1)}, \quad \text{for } l \in \mathbb{N}. \tag{A.279}$$

Then, the sum rules (A.270) and (A.271) become

$$\boxed{\sum_l \left[\frac{f_l^{00}}{1+f_l^{00}/(2l+1)} + \frac{f_l^{01}}{1+f_l^{01}/(2l+1)} + \frac{1}{3}\sum_J \frac{2J+1}{2l+1}\Big(\mathcal{S}_{ll}^{J0} + \mathcal{S}_{ll}^{J1}\Big)\right] = 0,} \tag{A.280}$$

as well as

$$\boxed{\sum_l \left[\frac{f_l^{00}}{1+f_l^{00}/(2l+1)} - \frac{3f_l^{01}}{1+f_l^{01}/(2l+1)} + \sum_J \frac{2J+1}{2l+1}\Big(3\mathcal{S}_{ll}^{J1} - \mathcal{S}_{ll}^{J0}\Big)\right] = 0,} \tag{A.281}$$

where the first values of $\mathcal{S}_{ll}^{JT}$ can easily be deduced from the first values of the diagonal (A.257) and coupled (A.261) matrix elements, together with the relations (A.276) and (A.278) [8].

By switching off the tensor interaction in (A.256), i.e. by demanding $h_l^{10} = 0$ (and $h_l^{11} = 0$ in the $(S=1, T=1)$ channel) for all l, we find out

$$\langle l'J|F|lJ\rangle = \delta_{ll'}\left(1 + \frac{f_l^{1T}}{2l+1}\right), \tag{A.284}$$

so that (A.276) reduces, for both the diagonal and non diagonal parts, to

$$\mathcal{S}_{ll}^{JT} = \frac{f_l^{1T}}{1 + f_l^{1T}/(2l+1)}, \tag{A.285}$$

in such a way that we recover (A.272) for all S and T, and consistently fall back on the sum rules without tensor forces, given by (A.273) and (A.274).

8. In the article [164], the first and second sum rules when tensor forces are taken into account respectively read

$$\sum_l \left[\frac{f_l^{00}}{1+f_l^{00}/(2l+1)} + \sum_J \frac{2J+1}{2l+1}\mathcal{S}_{ll}^{J1}\right] = 0, \tag{A.282}$$

and

$$\sum_l \left[\frac{2}{3}\frac{f_l^{00}}{1+f_l^{00}/(2l+1)} + \frac{f_l^{01}}{1+f_l^{01}/(2l+1)} + \frac{1}{3}\sum_J \frac{2J+1}{2l+1}\mathcal{S}_{ll}^{J0}\right] = 0. \tag{A.283}$$

These are equivalent to ours since the first relation can be obtained by multiplying our first sum rule by three and adding it the second one, and the second relation by multiplying our first sum rule by nine and subtracting it the second one. In practice, these sum rules are violated (see section II.2.5.3), so that the two writings are no longer equivalent. As we are proposing a generalization of the sum rules (A.273) and (A.274) in the presence of tensor forces, we have implemented the forms (A.281) and (A.281) that restore these when the tensor forces are set to zero.

Appendix B

Spherical symmetry

"I am now convinced that theoretical physics is actual philosophy." [1]

— Max Born

In this appendix, we deal with the quantities involved in the fitting procedure, evaluated in the spherical harmonic oscillator representation. After recalling this formalism, we derive the associated two-body matrix elements of the generalized Gogny interaction, coupled to the quantum numbers (J, T), as those are involved in the inversion process leading to the parameters of the tensor and spin–orbit terms. Then, we calculate different energies at the restricted Hartree–Fock approximation serving as constraints in the fitting code, while the last section is devoted to listing the useful formulas of the spherical symmetry.

Chapter contents

1. This quote is of course dedicated to Guillaume Blanchon and his HF code, with the "stockage merdier $9j$".

The first section briefly recalls the formalism of the spherical harmonic oscillator (HO) representation, based on [17, 175, 181]. The second section is devoted to the derivation of the two-body matrix elements (TBMEs) in this basis, for both the common central and density-dependent terms [17, 175, 181], and the newly introduced finite-range tensor and spin–orbit terms. Actually those two last terms have already been computed in [181], yet in an old-fashioned way. We also detail how the radial integral of the density-dependent term is implemented in the fitting code. On the other hand, we have coupled all the TBMEs to the quantum numbers (J, T) as in [137], since they are put into relation with the (J, T)-coupled TBMEs of [137, 139] in the inversion procedure (see section II.1.2.2). The Hartree–Fock restricted (HFR) approximation is presented and the following calculatory sections are mainly based on Chappert thesis [17], where we have taken into account the contributions of the tensor and spin–orbit forces.

1. Spherical harmonic oscillator representation

In the fitting code, the TBMEs are expressed in a one-center spherical HO representation that we then need to specify. The states $|a\rangle$ of this basis are characterized by the set of quantum numbers

$$|a\rangle = |r_a u_a\rangle = |n_a l_a m_{la} s_a t_a\rangle, \tag{B.1}$$

where the triplet $r_a = (n_a, l_a, m_{la})$ specifies the orbitals of the spherical HO, while the doublet $u_a = (s_a = \pm 1/2, t_a = \pm 1/2)$ corresponds to the projections of the spin and isospin along the quantization axis, chosen to be Oz, respectively.

The spherically symmetric HO wave functions then take the form

$$\Phi_a(\vec{r}, \sigma, \tau) \equiv \langle \vec{r}\tau\sigma|a\rangle = \phi_{r_a}(\vec{r})\xi_{s_a}(\sigma)\zeta_{t_a}(\tau), \tag{B.2}$$

where $\xi_{s_a}(\sigma)$ and $\zeta_{t_a}(\tau)$ are the (normalized) spin and isospin wave functions, associated with σ and τ, the Pauli matrices describing the spin and isospin degrees of freedom, respectively, and where the spatial spherical wave functions are expressed, in spherical coordinates $\vec{r} = (r, \hat{r}) = (r, \theta, \varphi)$, as

$$\phi_{r_a}(\vec{r}) = \left[\frac{2}{b^3}\frac{n_a!}{\Gamma(n_a + l_a + 3/2)}\right]^{1/2} \mathrm{e}^{-r^2/2b^2}\left(\frac{r}{b}\right)^{l_a} L_{n_a}^{l_a+1/2}\left(\frac{r^2}{b^2}\right) Y_{l_a}^{m_{la}}(\hat{r}), \tag{B.3}$$

where $b = \sqrt{\hbar/M\omega}$ is the oscillator length, with $\hbar\omega$ the oscillator frequency and M the mass of the nucleus considered. Note that $L_{n_a}^{l_a+1/2}(r^2/b^2)$ refers to the generalized Laguerre polynomial and $Y_{l_a}^{m_{l_a}}(\hat{r})$ the spherical harmonics, whose expression can be found in (B.204). We impose the spherical HO wave functions to satisfy the orthogonality relation

$$\sum_{\sigma\tau}\int \mathrm{d}^3r\, \Phi_a^*(\vec{r},\sigma,\tau)\Phi_b(\vec{r},\sigma,\tau) = \delta_{r_a r_b}\delta_{s_a s_b}\delta_{t_a t_b}. \tag{B.4}$$

In the following, we will often meet the spherical HO wave functions (B.3) with their quantum numbers equal to zero. For convenience, we write them down once and for all,

$$\phi_0(\vec{r}) = \frac{1}{\sqrt{4\pi}}\left[\frac{4}{\sqrt{\pi}b^3}\right]^{1/2} \mathrm{e}^{-r^2/2b^2}, \tag{B.5}$$

with the associated spherical harmonics given by $Y_0^0(\hat{r}) = 1/\sqrt{4\pi}$, according to (B.208). The angular dependence of the spherical wave functions (B.3) being entirely contained in the spherical harmonics, we can simply define their radial part as

$$\phi_{(r_a)}(r) \equiv \phi_{r_a}(\vec{r})/Y_{l_a}^{m_{l_a}}(\hat{r}), \tag{B.6}$$

where we have introduced the notation $(r_a) = (n_a, l_a)$. Note that we also have the particular case $\phi_{(0)}(r) = \sqrt{4\pi}\phi_0(\vec{r})$. Finally, we can define the spherical HO wave functions deprived of their exponential as

$$\hat{\phi}_{(r_a)}(r) \equiv \mathrm{e}^{r^2/2b^2}\phi_{(r_a)}(r), \tag{B.7}$$

where we have additionally removed the angular dependence according to (B.6).

2. Derivation of the two-body matrix elements

In this section, we will derive the TBMEs associated with each of the terms of the generalized Gogny interaction in the formalism outlined above. In the first subsection, we will describe the conventions adopted in the coupling process of the TBMEs to the quantum numbers (J,T), and then derive them explicitly. As far as possible, we will try to make the calculations of the TBMEs of each term independent of one another, so that the reader can follow these notes in the desired order. Nevertheless, comparisons between the results obtained with the various terms will allow us to highlight their similarities and differences.

2.1. Coupling to (J,T) process

The TBME of the generalized Gogny interaction v_{12}, given in (II.1), considered in the fitting code are coupled to the quantum numbers (J,T), normalized and antisymmetrized (na), in the same way as in [137]. They write

$$\begin{aligned}\langle\widetilde{a}\widetilde{b}JT|v_{12}|\widetilde{c}\widetilde{d}JT\rangle_{\mathrm{na}} = {} & \frac{1}{\sqrt{(1+\delta_{\widetilde{a}\widetilde{b}})(1+\delta_{\widetilde{c}\widetilde{d}})}} \\ & \times\Big[\langle\widetilde{a}\widetilde{b}JT|v_{12}|\widetilde{c}\widetilde{d}JT\rangle + (-)^{j_c+j_d+J+T}\langle\widetilde{a}\widetilde{b}JT|v_{12}|\widetilde{d}\widetilde{c}JT\rangle\Big],\end{aligned} \tag{B.8}$$

where the states are defined by the set of quantum numbers

$$|\widetilde{a}\rangle = |j_a n_a l_a\rangle, \tag{B.9}$$

with j_i the projection of the (one-body) total angular momentum $\vec{j}_i = \vec{l}_i + \vec{s}_i$, where $\vec{l}_i$ and $\vec{s}_i$ are respectively the (one-body) orbital and intrinsic angular momenta. As for J and T, they correspond to the quantum numbers associated with the two-body total angular momentum $\vec{J} = \vec{j}_a + \vec{j}_b = \vec{j}_c + \vec{j}_d$ and the two-body isospin operator, which is not an angular momentum (see equation (D.7) and the discussion below), $\vec{T} = \vec{t}_a + \vec{t}_b = \vec{t}_c + \vec{t}_d$ (where the $\vec{t}_i$ are the (one-body) isospin operators), respectively. It is important to differentiate these states from the "pure" spherical HO states (B.1). Note that we have subsequently introduced the Kronecker delta $\delta_{\widetilde{a}\widetilde{b}} = \delta_{j_a j_b}\delta_{n_a n_b}\delta_{l_a l_b}$.

We notice that those TBMEs are diagonal in J and T and do not depend on their projections M_J and M_T, while in general they are written $\langle \alpha J M_J T M_T | v_{12} | \alpha' J' M'_J T' M'_T \rangle$, where α and α' are the set of quantum numbers, here $\tilde{a}\tilde{b}$ and $\tilde{c}\tilde{d}$, characterizing the state. This is in fact a consequence of the invariance of the two-body nuclear interaction v_{12} under rotations in coordinate plus spin and isospin spaces (see section I.1.2). If the interaction is rotationally invariant, it commutes with $\vec{J}$, and in particular with $\vec{J}^2$, the component J_z and the usual ladder operators J_+ and J_-. Dropping for a moment the isospin dependence, we can then write down [7]

$$\langle \alpha J M_J | v_{12} \vec{J}^2 | \alpha' J' M'_J \rangle - \langle \alpha J M_J | \vec{J}^2 v_{12} | \alpha' J' M'_J \rangle = 0, \tag{B.10}$$

so that

$$\langle \alpha J M_J | v_{12} | \alpha' J' M'_J \rangle [J(J+1) - J'(J'+1)] = 0. \tag{B.11}$$

Therefore, the TBMEs of the interaction are zero unless we have $J = J'$, that is to say

$$\langle \alpha J M_J | v_{12} | \alpha' J' M'_J \rangle = \delta_{JJ'} \langle \alpha J M_J | v_{12} | \alpha' J M'_J \rangle. \tag{B.12}$$

Then, the relation (B.10) with $\vec{J}^2$ replaced by J_z similarly provides

$$\langle \alpha J M_J | v_{12} | \alpha' J M'_J \rangle [M_J - M'_J] = 0. \tag{B.13}$$

Therefore, the TBMEs of the interaction are zero unless we also have $M_J = M'_J$, that is to say

$$\langle \alpha J M_J | v_{12} | \alpha' J M'_J \rangle = \delta_{M_J M'_J} \langle \alpha J M_J | v_{12} | \alpha' J M_J \rangle. \tag{B.14}$$

Finally, since the action of the ladder operator J_+ is

$$J_+ | J M_J - 1 \rangle \equiv \sqrt{J(J+1) - M_J(M_J - 1)} | J M_J \rangle, \tag{B.15}$$

we deduce, for $-J + 1 \leq M_J \leq J + 1$,

$$\langle \alpha J M_J | v_{12} | \alpha' J M_J \rangle = \frac{\langle \alpha J M_J | v_{12} J_+ | \alpha' J M_J - 1 \rangle}{\sqrt{J(J+1) - M_J(M_J - 1)}}. \tag{B.16}$$

On the other hand, the TBME of the right-hand side can be written

$$\begin{aligned} \langle \alpha J M_J | v_{12} J_+ | \alpha' J M_J - 1 \rangle = \sqrt{J(J+1) - M_J(M_J - 1)} \\ \times \langle \alpha J M_J - 1 | v_{12} | \alpha' J M_J - 1 \rangle, \end{aligned} \tag{B.17}$$

where we have used the fact that v_{12} and J_+ commute as well as the identity $J_+ = J_-^\dagger$. Combining the last two equations, we obtain, for all allowed values of M_J,

$$\langle \alpha J M_J | v_{12} | \alpha' J M_J \rangle = \langle \alpha J M_J - 1 | v_{12} | \alpha' J M_J - 1 \rangle, \quad \text{where } -J < M_J < J. \tag{B.18}$$

This proves that the TBMEs of the interaction are independent of M_J.

All in all, the TBMEs of the interaction are diagonal in J and M_J, and do not depend on M_J, what we can formally express as

$$\boxed{\langle \alpha J M_J | v_{12} | \alpha' J' M_J' \rangle = \delta_{JJ'} \delta_{M_J M_J'} \langle \alpha J | v_{12} | \alpha' J \rangle.} \tag{B.19}$$

Actually, the above calculations are a simple application of the Wigner–Eckart theorem to the interaction v_{12}, viewed as a scalar (i.e. a spherical tensor of rank 0) [224], where the reduced TBMEs are conventionally related to the standard TBMEs by

$$\langle \alpha J \| v_{12} \| \alpha' J \rangle \equiv \sqrt{2J+1} \langle \alpha J | v_{12} | \alpha' J \rangle. \tag{B.20}$$

The same procedure can be undertaken in the isospin space to show that the TBME of the interaction are diagonal in T and M_T, and do not depend on M_T, what we can formally express as

$$\boxed{\langle \alpha T M_T | v_{12} | \alpha' T' M_T' \rangle = \delta_{TT'} \delta_{M_T M_T'} \langle \alpha T | v_{12} | \alpha' T \rangle.} \tag{B.21}$$

Indeed, the interaction being rotationally invariant in the isospin space due to the charge invariance (see equation (I.11) and the related discussion), it commutes with $\vec{T}$, and in particular with $\vec{T}^2$, the component T_z and the ladder operators T_+ and T_-. This result can also be found by viewing the interaction v_{12} as an isoscalar (i.e. a spherical tensor of rank 0 in the isospin space) [224], with the convention (B.20) for the isospin (J should be replaced by T). We then understand why the TBMEs are directly considered under the form appearing on the left-hand side of (B.8).

Thus, it remains to evaluate the contributions of each term of the generalized Gogny interaction to the non-normalized and non-antisymmetrized TBME $\langle \widetilde{a}\widetilde{b} JT | v_{12} | \widetilde{c}\widetilde{d} JT \rangle$ and $\langle \widetilde{a}\widetilde{b} JT | v_{12} | \widetilde{d}\widetilde{c} JT \rangle$; we do so in the next subsections.

2.2. Central two-body matrix elements

We start by deriving the TBMEs of the central terms whose expression we recall below,

$$v_{12}^{\mathrm{C}} = (W + BP_\sigma - HP_\tau - MP_\sigma P_\tau) V(r_{12}), \tag{B.22}$$

where $V(r_{12})$ is the Gaussian potential given by

$$V(r_{12}) \equiv \mathrm{e}^{-(\vec{r}_1 - \vec{r}_2)^2/\mu^2}. \tag{B.23}$$

As explained in the previous section, we need to express the TBMEs with the conventions chosen in [137]. The central TBMEs are therefore recoupled to (J,T), normalized and antisymmetrized (na) according to (B.8), i.e.

$$\begin{aligned} \langle \widetilde{a}\widetilde{b} JT | v_{12}^{\mathrm{C}} | \widetilde{c}\widetilde{d} JT \rangle_{\mathrm{na}} = {} & \frac{1}{\sqrt{(1+\delta_{\widetilde{a}\widetilde{b}})(1+\delta_{\widetilde{c}\widetilde{d}})}} \\ & \times \Big[\langle \widetilde{a}\widetilde{b} JT | v_{12}^{\mathrm{C}} | \widetilde{c}\widetilde{d} JT \rangle + (-)^{j_c + j_d + J + T} \langle \widetilde{a}\widetilde{b} JT | v_{12}^{\mathrm{C}} | \widetilde{d}\widetilde{c} JT \rangle \Big], \end{aligned} \tag{B.24}$$

We can effortlessly evaluate the isospin dependence of the non-normalized and non-antisymmetrized central TBMEs, and write them as

$$\langle \widetilde{ab} JT|v_{12}^{\mathrm{C}}|\widetilde{cd} JT\rangle = \langle \widetilde{ab} J|\underbrace{(W + BP_\sigma + (-)^T H + (-)^T M P_\sigma)V(r_{12})}_{\widetilde{v}_{12}^{\mathrm{C}}}|\widetilde{cd} J\rangle. \tag{B.25}$$

The transformation from jj coupling to LS coupling provides [237]

$$\begin{aligned}\langle \widetilde{ab} J|\tilde{v}_{12}^{\mathrm{C}}|\widetilde{cd} J\rangle = \sum_{LS}\sum_{L'S'} \hat{j}_a\hat{j}_b\hat{j}_c\hat{j}_d\hat{L}\hat{L}'\hat{S}\hat{S}' \begin{Bmatrix} l_a & l_b & L \\ 1/2 & 1/2 & S \\ j_a & j_b & J \end{Bmatrix}\begin{Bmatrix} l_c & l_d & L' \\ 1/2 & 1/2 & S' \\ j_c & j_d & J \end{Bmatrix} \\ \times \underbrace{\langle n_a l_a \frac{1}{2}\, n_b l_b \frac{1}{2}\, LSJ|\tilde{v}_{12}^{\mathrm{C}}|n_c l_c \frac{1}{2}\, n_d l_d \frac{1}{2}\, L'S'J\rangle}_{B^{\mathrm{C}}},\end{aligned} \tag{B.26}$$

where the braces denote the Wigner-9j symbols and where we have defined $\hat{L} \equiv \sqrt{2L+1}$. The space and spin parts split up in such a way that

$$\begin{aligned}B^{\mathrm{C}} = \sum_{M_L M_S}\sum_{M'_L M'_S} \langle LM_L SM_S|JM_L + M_S\rangle\langle L'M'_L S'M'_S|JM'_L + M'_S\rangle \\ \times \underbrace{\langle n_a l_a\, n_b l_b\, LM_L|V(r_{12})|n_c l_c\, n_d l_d\, L'M'_L\rangle}_{C^{\mathrm{C}}} \\ \times \underbrace{\langle \frac{1}{2}\,\frac{1}{2}\, SM_S|(W + BP_\sigma + (-)^T H + (-)^T M P_\sigma)|\frac{1}{2}\,\frac{1}{2}\, S'M'_S\rangle}_{D^{\mathrm{C}}},\end{aligned} \tag{B.27}$$

where the brackets denote the Clebsch–Gordan coefficients.

On the one hand, the formulas (D.11) allow us to simplify the above spin TBME as

$$D^{\mathrm{C}} = \Big[(W - B + (-)^T H - (-)^T M) + S(S+1)(B + (-)^T M)\Big]\delta_{SS'}\delta_{M_S M'_S}. \tag{B.28}$$

We see that the central TBMEs are divided into two pieces, one proportional to the combination of parameters $(W - B + (-)^T H - (-)^T M)$, the other to $S(S+1)(B + (-)^T M)$. The corresponding TBMEs are denoted by V_a^{C} and V_b^{C} in the second part II.1.2.2, respectively. In this way, we have decorrelated the isospin from the spin degrees of freedom so that the combination of parameters involved in the central TBMEs (B.24) can be determined for a given total isospin T.

On the other hand, the above space TBMEs read

$$\begin{aligned}C^{\mathrm{C}} = \sum_{m_{la} m_{lb}}\sum_{m_{lc} m_{ld}} \langle l_a m_{la} l_b m_{lb}|LM_L\rangle\langle l_c m_{lc} l_c m_{lc}|L'M'_L\rangle \\ \times \underbrace{\langle n_a l_a m_{la}\, n_b l_b m_{lb}|V(r_{12})|n_c l_c m_{lc}\, n_d l_d m_{ld}\rangle}_{v^{\mathrm{C}}_{r_a r_b r_c r_d}}.\end{aligned} \tag{B.29}$$

Thus, we need to evaluate the central TBMEs in the spherical HO basis, whose wave functions are defined in (B.3). By definition,

$$v^{\mathrm{C}}_{r_a r_b r_c r_d} \equiv \int \mathrm{d}^3 r_1 \int \mathrm{d}^3 r_2\, \phi^*_{r_a}(\vec{r}_1)\phi^*_{r_b}(\vec{r}_2)V(r_{12})\phi_{r_c}(\vec{r}_1)\phi_{r_d}(\vec{r}_2). \tag{B.30}$$

Since the wave functions and the central potential commute, we can rearrange the terms according to

$$v^{\mathrm{C}}_{r_a r_b r_c r_d} = \int \mathrm{d}^3 r_1 \int \mathrm{d}^3 r_2 \, \phi^*_{r_a}(\vec{r}_1)\phi_{r_c}(\vec{r}_1) V(r_{12}) \phi^*_{r_b}(\vec{r}_2)\phi_{r_d}(\vec{r}_2). \tag{B.31}$$

Using twice the Gogny separable development in spherical symmetry (B.219), we obtain

$$\begin{aligned} v^{\mathrm{C}}_{r_a r_b r_c r_d} = & \sum_{r_\mu r_\nu} T^{(r_\mu)}_{(r_a)(r_c)} T^{(r_\nu)}_{(r_b)(r_d)} \langle l_a m_{la} | Y^{m_{l\mu}*}_{l_\mu} | l_c m_{lc} \rangle \langle l_b m_b | Y^{m_{l\nu}*}_{l_\nu} | l_d m_{ld} \rangle \\ & \times \int \mathrm{d}^3 r_1 \int \mathrm{d}^3 r_2 \, \phi_0(\vec{r}_1)\phi_0(\vec{r}_2) V(r_{12}) \phi_{r_\mu}(\vec{r}_1)\phi_{r_\nu}(\vec{r}_2). \end{aligned} \tag{B.32}$$

Then, applying twice the Moshinsky transformation in spherical symmetry (B.225), we get

$$\begin{aligned} v^{\mathrm{C}}_{r_a r_b r_c r_d} = & \sum_{r_\mu r_\nu} T^{(r_\mu)}_{(r_a)(r_c)} T^{(r_\nu)}_{(r_b)(r_d)} \langle l_a m_{la} | Y^{m_{l\mu}*}_{l_\mu} | l_c m_{lc} \rangle \langle l_b m_{lb} | Y^{m_{l\nu}*}_{l_\nu} | l_d m_{ld} \rangle \\ & \times \sum_{r_\lambda r_\sigma} M^{r_\lambda r_\sigma}_{r_\mu r_\nu} \int \mathrm{d}^3 r \, \phi_0(\vec{r}) V(\sqrt{2} r) \phi_{r_\lambda}(\vec{r}) \int \mathrm{d}^3 R \, \phi^*_0(\vec{R}) \phi_{r_\sigma}(\vec{R}), \end{aligned} \tag{B.33}$$

since the Jacobian of the change of variables $(\vec{r}_1, \vec{r}_2) \to (\vec{r}, \vec{R})$, given by (B.224), is equal to unity and the spherical Moshinsky coefficient, specified by (B.227), fixes the range of values of r_σ according to (B.229) and (B.230). Note that in the particular case $r'_\mu = r'_\nu = 0$, the spherical Moshinsky coefficient reduces to (B.234). Note also that $\phi_0(\vec{R}) = \phi^*_0(\vec{R})$ because of (B.5).

The integral over $\vec{R}$ is readily carried out considering the orthogonality relation of the spherical HO wave functions (B.4). On the other hand, we can simplify the integral over $\vec{r}$ by pulling out its angular part by means of (B.6), namely

$$\begin{aligned} \int \mathrm{d}^3 r \, \phi_0(\vec{r}) V(\sqrt{2} r) \phi_{r_\sigma}(\vec{r}) &= \int \mathrm{d}r \, r^2 \phi_{(0)}(r) V(\sqrt{2} r) \phi_{(r_\sigma)}(r) \int \mathrm{d}^2 \hat{r} \, Y^{m_{l\sigma}}_{l_\lambda}(\hat{r}) Y^{0*}_0(\hat{r}) \\ &= \delta_{l_\sigma,0} \delta_{m_{l\sigma},0} \int \mathrm{d}r \, r^2 \phi_{(0)}(r) V(\sqrt{2} r) \phi_{(r_\sigma)}(r), \end{aligned} \tag{B.34}$$

where we have used the orthogonality relation of the spherical harmonics (B.205) and the fact that $Y^0_0(\hat{r}) = Y^{0*}_0(\hat{r})$ because of (B.208). Thus, the only thing that remains to be done is to evaluate the above radial integral. Considering the particular wave functions (B.5) and

$$\phi_{(n_\sigma,0)}(r) = \left[\frac{2}{b^3} \frac{n_\sigma!}{\Gamma(n_\sigma + 3/2)} \right]^{1/2} \mathrm{e}^{-r^2/2b^2} L^{1/2}_{n_\sigma}\left(\frac{r^2}{b^2} \right), \tag{B.35}$$

we can write down

$$\begin{aligned} \int_0^\infty \mathrm{d}r \, r^2 \phi_{(0,0)}(r) V(\sqrt{2} r) \phi_{(n_\sigma,0)}(r) = & \left[\frac{8}{b^6 \sqrt{\pi}} \frac{n_\sigma!}{\Gamma(n_\sigma + 3/2)} \right]^{1/2} \\ & \times \int_0^\infty \mathrm{d}r \, r^2 \mathrm{e}^{-(\mu^2 + 2b^2) r^2 / \mu^2 b^2} L^{1/2}_{n_\sigma}\left(\frac{r^2}{b^2} \right). \end{aligned} \tag{B.36}$$

Taking advantage of the series expansion of the generalized Laguerre polynomial (D.100), we find

$$\begin{aligned} \int_0^\infty \mathrm{d}r \, r^2 \phi_{(0,0)}(r) V(\sqrt{2} r) \phi_{(n_\sigma,0)}(r) = & \left[\frac{8}{b^6 \sqrt{\pi}} n_\sigma! \, \Gamma(n_\sigma + 3/2) \right]^{1/2} \\ & \times \sum_{i=0}^{n_\sigma} \frac{(-)^i}{i! (n_\sigma - i)! \, \Gamma(i + 3/2)} \int_0^\infty \mathrm{d}r \, r^{2i+2} \mathrm{e}^{-r^2/p^2}, \end{aligned} \tag{B.37}$$

where we have set the change of variable $p \equiv \mu b/\sqrt{\mu^2+2b^2}$. Using the formula (D.119), we can determine the above integral, and we end up with

$$\int_0^\infty \mathrm{d}r\, r^2 \phi_{(0,0)}(r) V(\sqrt{2}r) \phi_{(n_\sigma,0)}(r) = \left[\frac{2}{\sqrt{\pi}} n_\sigma! \,\Gamma(n_\sigma+3/2)\right]^{1/2} \sum_{i=0}^{n_\lambda} \frac{(-)^i G^{-i-3/2}}{i!(n_\sigma-i)!}, \tag{B.38}$$

with

$$\boxed{G \equiv 1 + \frac{2b^2}{\mu^2}.} \tag{B.39}$$

Finally, by gathering all the terms, we get an expression for the TBMEs of the central terms in the spherical HO basis, that reads

$$\boxed{\begin{aligned} v^{\mathrm{C}}_{r_a r_b r_c r_d} = \sum_{r_\mu r_\nu} T^{(r_\mu)}_{(r_a)(r_c)} T^{(r_\nu)}_{(r_b)(r_d)} \langle l_a m_{la} | Y^{m_{l\mu}*}_{l_\mu} | l_c m_{lc} \rangle \langle l_b m_{lb} | Y^{m_{l\nu}*}_{l_\nu} | l_d m_{ld} \rangle \\ \times M^{0\, r_\sigma}_{r_\mu r_\nu} \left[\frac{2}{\sqrt{\pi}} n_\sigma! \,\Gamma(n_\sigma+3/2)\right]^{1/2} \sum_{i=0}^{n_\sigma} \frac{(-)^i G^{-i-3/2}}{i!(n_\sigma-i)!}, \end{aligned}} \tag{B.40}$$

where G is given in (B.39). In this expression, $r_\sigma = (n_\sigma, 0, 0)$, with n_σ given by (B.232), while the conditions (B.213) and (B.223) have to be fulfilled at any time.

In the specific cases of $1s$ and $2s$ states, the quantum numbers are $r_a = r_b = r_c = r_d = (0,0,0)$ and $r_a = r_b = r_c = r_d = (1,0,0)$, respectively. Then, the contributions to the central terms to the $1s$ and $2s$ TBMEs can respectively be written

$$\begin{aligned} f_{1s} &\equiv \langle 000\,000 | V(r_{12}) | 000\,000 \rangle \\ &= G^{-3/2}, \end{aligned} \tag{B.41a}$$

$$\begin{aligned} f_{2s} &\equiv \langle 100\,100 | V(r_{12}) | 100\,100 \rangle \\ &= G^{-3/2}\left(\frac{41}{64} - \frac{79}{48}G^{-1} + \frac{385}{96}G^{-2} - \frac{175}{48}G^{-3} + \frac{105}{64}G^{-4}\right). \end{aligned} \tag{B.41b}$$

2.3. Density-dependent two-body matrix elements

We continue by deriving the TBME of the (finite-range) density-dependent interaction whose expression we recall below,

$$V^{\mathrm{DD}} = (W + BP_\sigma - HP_\tau - MP_\sigma P_\tau) V(r_{12}) D[\rho], \tag{B.42}$$

where $V(r_{12})$ is the Gaussian potential (B.23), and

$$D[\rho] \equiv \frac{\rho^\alpha(\vec{r}_1) + \rho^\alpha(\vec{r}_2)}{2} \tag{B.43}$$

the density functional which represents the density of the nucleus under study at its center-of-mass position. For conciseness, we have omitted the factor $1/(\mu\sqrt{\pi})^3$, but it is obviously taken into account in the fitting code.

The coupling procedure to the quantum numbers (J,T) and the spin dependence of the density-dependent term being formally identical to those of the central terms, we refer the reader to the previous subsection for their construction for the density-dependent term. Let us simply note that the density-dependent TBMEs proportional to the combinations of parameters $(W - B + (-)^T H - (-)^T M)$ and $S(S+1)(B + (-)^T M)$, as discussed

right after equation (B.28), are respectively denoted by $V_a^{\rm DD}$ and $V_b^{\rm DD}$ in the second part II.1.2.2.

Thus, we only need to evaluate the TBMEs of the density-dependent interaction, expressed as

$$v^{\rm DD}_{r_a r_b r_c r_d} \equiv \langle n_a l_a m_{la}\, n_b l_b m_{lb}|V(r_{12})D[\rho]|n_c l_c m_{lc}\, n_d l_d m_{ld}\rangle, \tag{B.44}$$

in the spherical HO basis, whose wave functions are defined in (B.3). By definition,

$$v^{\rm DD}_{r_a r_b r_c r_d} \equiv \int \mathrm{d}^3 r_1 \int \mathrm{d}^3 r_2\, \phi^*_{r_a}(\vec{r}_1)\phi^*_{r_b}(\vec{r}_2)V(r_{12})D[\rho]\phi_{r_c}(\vec{r}_1)\phi_{r_d}(\vec{r}_2). \tag{B.45}$$

Since the density functional commutes with the wave functions, we can rearrange the terms and, as for the central terms, consider the Gogny separable development in spherical symmetry (B.219) twice, to express

$$\begin{aligned} v^{\rm DD}_{r_a r_b r_c r_d} = \sum_{r_\mu r_\nu} & T^{(r_\mu)}_{(r_a)(r_c)} T^{(r_\nu)}_{(r_b)(r_d)} \langle l_a m_{la}|Y^{m_{l\mu}*}_{l_\mu}|l_c m_{lc}\rangle\langle l_b m_{lb}|Y^{m_{l\nu}*}_{l_\nu}|l_d m_{ld}\rangle \\ & \times \frac{1}{2}\Bigg[\int \mathrm{d}^3 r_1 \int \mathrm{d}^3 r_2\, \phi_0(\vec{r}_1)\phi_0(\vec{r}_2)\rho^\alpha(\vec{r}_1)V(r_{12})\phi_{r_\mu}(\vec{r}_1)\phi_{r_\nu}(\vec{r}_2) \\ & \quad + \int \mathrm{d}^3 r_1 \int \mathrm{d}^3 r_2\, \phi_0(\vec{r}_1)\phi_0(\vec{r}_2)\rho^\alpha(\vec{r}_2)V(r_{12})\phi_{r_\mu}(\vec{r}_1)\phi_{r_\nu}(\vec{r}_2)\Bigg]. \end{aligned} \tag{B.46}$$

We notice that the second integral is deduced from the first one by exchanging the quantum numbers r_μ and r_ν. Then, we only need to focus on the first integral to find an expression for the above TBMEs. This time, we have no interest in employing the Moshinsky transformation since the density would couple the relative and center-of-mass coordinates. Instead, we can perform the integral over $\vec{r}_2$ by means of the following formula [181], [2]

$$\int \mathrm{d}^3 r_2\, \mathrm{e}^{-(\vec{r}_1-\vec{r}_2)^2/\mu^2}\phi_0(\vec{r}_2)\phi_{r_\nu}(\vec{r}_2) = K\lambda_{(r_\nu)}\phi_0(\vec{r}_1, b\sqrt{g})\phi_{r_\nu}(\vec{r}_1, b\sqrt{g}), \tag{B.47}$$

where, in the above wave functions, the oscillator length b is replaced by $b\sqrt{g}$, with $g \equiv 1+\mu^2/b^2$. The new quantities are expressed in terms of g as $K \equiv \pi[b\sqrt{g-1}]^3/2$ and $\lambda_{(r_\nu)} \equiv g^{-n_\nu - l_\nu/2}$. Thus, we will have to evaluate integrals of the form

$$I_{r_\mu r_\nu} \equiv \int \mathrm{d}^3 r\, \phi_0(\vec{r})\phi_{r_\mu}(\vec{r})\rho^\alpha(\vec{r})\phi_0(\vec{r}, b\sqrt{g})\phi_{r_\nu}(\vec{r}, b\sqrt{g}). \tag{B.48}$$

Taking into account that the density is spherically symmetric, i.e. $\rho(\vec{r}) = \rho(r)$, as well as the definitions (B.5) and (B.6), we get

$$\begin{aligned} I_{r_\mu r_\nu} = \frac{1}{4\pi}\frac{4}{\sqrt{\pi}b^3}\int \mathrm{d}r\, r^2 \rho^\alpha(r)\mathrm{e}^{-r^2/2b^2}\mathrm{e}^{-r^2/2gb^2}\phi_{(r_\mu)}(r)\phi_{(r_\nu)}(r, b\sqrt{g}) \\ \times \int \mathrm{d}^2\hat{r}\, Y^{m_{l\mu}}_{l_\mu}(\hat{r})Y^{m_{l\nu}}_{l_\nu}(\hat{r}). \end{aligned} \tag{B.49}$$

Invoking the orthogonality of the spherical harmonics (B.205) and pulling out the exponentials of the wave functions according to (B.7), the integral becomes

$$I_{r_\mu r_\nu} = \frac{(-)^{m_{l\mu}}}{(\sqrt{\pi}b)^3}\delta_{l_\mu l_\nu}\delta_{m_{l\mu},-m_{l\nu}} \underbrace{\int_0^\infty \mathrm{d}r\, r^2 \rho^\alpha(r)\mathrm{e}^{-(1+g)r^2/gb^2}\hat{\phi}_{(r_\mu)}(r)\hat{\phi}_{(r_\nu)}(r, b\sqrt{g})}_{J_{(r_\mu)(r_\nu)}}. \tag{B.50}$$

2. In fact, this formula is demonstrated from the generating functions of the spherical HO, in the same idea the relation (C.109), with the generating functions of the axial HO, is obtained. As the introduction of the generating functions in spherical symmetry would have been long and useful only here, we have chosen to leave it at admitting this relation.

At this point, there is at least two ways to evaluate the integral $J_{(r_\mu)(r_\nu)}$ numerically. The most straightforward one consists in setting the change of variable $x \equiv (1+g)r^2/gb^2$, to find out

$$J_{(r_\mu)(r_\nu)} = \frac{1}{2}\left[\frac{gb^2}{1+g}\right]^{3/2} \int_0^\infty \mathrm{d}x\, \sqrt{x}\mathrm{e}^{-x} f_{(r_\mu)(r_\nu)}(x), \tag{B.51}$$

where we have defined the function

$$f_{(r_\mu)(r_\nu)}(x) \equiv \rho^\alpha\left(\sqrt{\frac{gb^2}{1+g}}\sqrt{x}\right)\hat{\phi}_{(r_\mu)}\left(\sqrt{\frac{gb^2}{1+g}}\sqrt{x}\right)\hat{\phi}_{(r_\nu)}\left(\sqrt{\frac{gb^2}{1+g}}\sqrt{x}, b\sqrt{g}\right). \tag{B.52}$$

We can then apply the generalized Gauss–Laguerre quadrature which states that

$$\int_0^\infty \mathrm{d}x\, \sqrt{x}\mathrm{e}^{-x} f_{(r_\mu)(r_\nu)}(x) \simeq \sum_{i=1}^{n} w_i f_{(r_\mu)(r_\nu)}(x_i), \tag{B.53}$$

where n is the quadrature order, x_i the i-th root of the generalized Laguerre polynomial $L_n^{1/2}(x)$ and w_i a weight factor that reads

$$w_i \equiv \frac{\Gamma(n+3/2)x_i}{n!(n+1)^2\left[L_{n+1}^{1/2}(x_i)\right]^2}. \tag{B.54}$$

Gathering the results, the integral (B.48) we wanted to calculate can be approximated by

$$\boxed{I_{r_\mu r_\nu} \simeq \frac{(-)^{m_{l_\mu}}}{2}\left[\frac{1}{\pi}\frac{g}{1+g}\right]^{3/2}\delta_{l_\mu l_\nu}\delta_{m_{l_\mu},-m_{l_\nu}}\sum_{i=1}^{n} w_i f_{(r_\mu)(r_\nu)}(x_i),} \tag{B.55}$$

with w_i and $f_{(r_\mu)(r_\nu)}(x_i)$ given above. The last summation can then be evaluated numerically, up to a certain order n.

The second method requires more work but is numerically advantageous. This is the one adopted in the fitting procedure. Starting from the general definition of the local nuclear density (A.25), we can write down

$$\rho(\vec{r}) = 2\sum_{r_a} \phi^*_{r_a}(\vec{r})\phi_{r_a}(\vec{r})\left(\rho^\pi_{r_a,r_a} + \rho^\nu_{r_a,r_a}\right), \tag{B.56}$$

where the factor 2 comes from the spin degeneracy and where we have separated the proton π and neutron ν density matrices. Pulling out the angular dependencies of the wave functions and using the addition theorem (B.206), we obtain

$$\begin{aligned}\rho(\vec{r}) &= 2\sum_{nl}\phi_{(n,l)}(r)\phi_{(n,l)}(r)\sum_{m_l} Y_l^{m_l *}(\hat{r})Y_l^{m_l}(\hat{r})\left(\rho^\pi_{nl,nl} + \rho^\nu_{nl,nl}\right)\\ &= \frac{1}{2\pi}\sum_{nl}(2l+1)\frac{2}{b^3}\frac{n!}{\Gamma(n+l+3/2)}\mathrm{e}^{-r^2/b^2}\left(\frac{r}{b}\right)^{2l}\left[L_n^{l+1/2}\left(\frac{r^2}{b^2}\right)\right]^2\left(\rho^\pi_{nl,nl} + \rho^\nu_{nl,nl}\right),\end{aligned} \tag{B.57}$$

where we have proved that the nuclear density does not depend on the orientation in space, as expected in spherical symmetry. Note that the density matrix does not depend on m_l as the occupation of the major shells is only specified by n and l (see equation (B.117)

and the related discussion). The relation between the generalized Laguerre polynomials and the confluent hypergeometric function (D.103) permits to get

$$\rho(r) = \frac{1}{b^3}\mathrm{e}^{-r^2/b^2}\left[\frac{1}{2\pi}\sum_{nl}(2l+1)\frac{2\Gamma(n+l+3/2)}{n!\Gamma(l+3/2)^2}\left(\frac{r}{b}\right)^{2l} \times {}_1F_1(-n, l+3/2, r^2/b^2)^2\left(\rho^{\pi}_{nl,nl}+\rho^{\nu}_{nl,nl}\right)\right]. \tag{B.58}$$

Inserting this expression for the density in the radial integral appearing in (B.50), we obtain

$$J_{(r_\mu)(r_\nu)} = \frac{1}{b^{3(\alpha+1)}}\frac{1}{g^{3/4}}\int_0^\infty \mathrm{d}r\, r^2\mathrm{e}^{-(\alpha+1+1/g)r^2/gb^2}F_{(r_\mu)}\left(\frac{r^2}{b^2}\right)F_{(r_\nu)}\left(\frac{r^2}{gb^2}\right)\widetilde{\rho}^{\alpha}\left(\frac{r^2}{b^2}\right), \tag{B.59}$$

where we have used the relation (D.103) again with the generalized Laguerre polynomials of the wave functions, and defined the quantities

$$F_{(r_\mu)}\left(\frac{r^2}{b^2}\right) \equiv \left[\frac{2\Gamma(n_\mu+l_\mu+3/2)}{n_\mu!}\right]^{1/2}\frac{1}{\Gamma(l_\mu+3/2)}\left(\frac{r}{b}\right)^{l_\mu} \times {}_1F_1(-n_\mu, l_\mu+3/2, r^2/b^2), \tag{B.60a}$$

$$F_{(r_\nu)}\left(\frac{r^2}{gb^2}\right) \equiv \left[\frac{2\Gamma(n_\nu+l_\mu+3/2)}{n_\nu!}\right]^{1/2}\frac{1}{\Gamma(l_\mu+3/2)}\left(\frac{r}{\sqrt{g}b}\right)^{l_\nu} \times {}_1F_1(-n_\nu, l_\mu+3/2, r^2/gb^2), \tag{B.60b}$$

$$\widetilde{\rho}\left(\frac{r^2}{b^2}\right) \equiv \frac{1}{2\pi}\sum_{nl}(2l+1)\frac{2\Gamma(n+l+3/2)}{n!\Gamma(l+3/2)^2}\left(\frac{r}{b}\right)^{2l} \times {}_1F_1(-n, l+3/2, r^2/b^2)^2\left(\rho^{\pi}_{nl,nl}+\rho^{\nu}_{nl,nl}\right). \tag{B.60c}$$

The change of variable $x \equiv r/b\sqrt{\alpha+1+1/g}$ eventually furnishes

$$J_{(r_\mu)(r_\nu)} = \frac{1}{b^{3\alpha}}\frac{1}{g^{3/4}}\frac{1}{\sqrt{\alpha+1+1/g}}\int_0^\infty \mathrm{d}x\,\mathrm{e}^{-x^2}f_{(r_\mu)(r_\nu)}(x^2), \tag{B.61}$$

with the function

$$f_{(r_\mu)(r_\nu)}(x^2) \equiv \frac{x^2}{\alpha+1+1/g}F_{(r_\mu)}\left(\frac{x^2}{\alpha+1+1/g}\right)F_{(r_\nu)}\left(\frac{x^2}{g(\alpha+1+1/g)}\right) \times \widetilde{\rho}^{\alpha}\left(\frac{x^2}{\alpha+1+1/g}\right). \tag{B.62}$$

The Gauss–Hermite quadrature allows to approximate integrals defined on the entire space according to

$$\int_{-\infty}^{+\infty}\mathrm{d}x\,\mathrm{e}^{-x^2}f(x) \simeq \sum_{i=0}^{n} w_i f(x_i), \tag{B.63}$$

where n is the quadrature order, x_i the i-th root of the Hermite polynomial $H_n(x)$ at which the function f is evaluated, and w_i a weight factor that reads

$$w_i \equiv \frac{2^{n-1}n!\sqrt{\pi}}{n^2[H_{n-1}(x_i)]^2}. \tag{B.64}$$

Here, the integral (B.61) runs from zero to infinity, but since the roots of the Hermite polynomials are symmetric (to each root x_i corresponds another root $-x_i$) and the integrand is even, we can approximate it with the Gauss–Hermite quadrature according to

$$\int_0^\infty \mathrm{d}x\, \mathrm{e}^{-x^2} f_{(r_\mu)(r_\nu)}(x^2) \simeq \sum_{i=0}^{n} w_i f_{(r_\mu)(r_\nu)}(x^2), \tag{B.65}$$

where $f_{(r_\mu)(r_\nu)}(x^2)$ is given by (B.62). When we will truncate the series at a certain order n, it will then be necessary to consider $2n$ roots and weight factors associated with the complete quadrature (B.63). In the fitting code, the quadrature order is $n = 10$ as the series converges quite rapidly, so that the first twenty Gauss–Hermite roots and weights are needed. Gathering the results, the integral (B.48) we wanted to evaluate can be approximated by

$$\boxed{I_{r_\mu r_\nu} \simeq \frac{(-)^{m_{l\mu}}}{(\sqrt{\pi} g^{1/4} b^{\alpha+1})^3} \frac{1}{\sqrt{\alpha+1+1/g}} \delta_{l_\mu l_\nu} \delta_{m_{l\mu},-m_{l\nu}} \sum_{i=1}^{n} w_i f_{(r_\mu)(r_\nu)}(x_i^2),} \tag{B.66}$$

with w_i and $f_{(r_\mu)(r_\nu)}(x_i^2)$ given above.

Finally, in both cases, the TBMEs of the density-dependent interaction, in the spherical HO basis, read

$$\boxed{\begin{aligned} v^{\mathrm{DD}}_{r_a r_b r_c r_d} = \frac{1}{2} K \sum_{r_\mu r_\nu} T^{(r_\mu)}_{(r_a)(r_c)} T^{(r_\nu)}_{(r_b)(r_d)} \langle l_a m_{la} | Y^{m_{l\mu}*}_{l_\mu} | l_c m_{lc} \rangle \langle l_b m_{lb} | Y^{m_{l\nu}*}_{l_\nu} | l_d m_{ld} \rangle \\ \times \Big[\lambda_{(r_\nu)} I_{r_\mu r_\nu} + \lambda_{(r_\mu)} I_{r_\nu r_\mu} \Big], \end{aligned}} \tag{B.67}$$

where the integrals $I_{r_\mu r_\nu}$ and $I_{r_\nu r_\mu}$ are either given by (B.55) or (B.66). In this expression, we have $l_\mu = l_\nu$ and $m_{l\mu} = -m_{l\nu}$ while the conditions (B.213) and (B.223) have to be fulfilled at any time.

2.4. Tensor two-body matrix elements

In order to easily compute the TBMEs of the tensor interaction, we shall separate the space and spin-isospin degrees of freedom according to the equivalent form of the tensor operator (D.58). The tensor interaction then reads

$$v^{\mathrm{T}}_{12} = (W - HP_\tau) V(r_{12}) [\hat{r}_{12} \otimes \hat{r}_{12}]^{(2)} \cdot [\vec{\sigma}_1 \otimes \vec{\sigma}_2]^{(2)}, \tag{B.68}$$

where $V(r_{12})$ is the Gaussian potential (B.23). As for the previous terms, the normalized and antisymmetrized (na) TBMEs, recoupled to (J, T), of the tensor interaction can be written by means of (B.8), i.e.

$$\begin{aligned} \langle \widetilde{a}\widetilde{b} JT | v^{\mathrm{T}}_{12} | cdJT \rangle_{\mathrm{na}} = \frac{1}{\sqrt{(1+\delta_{\widetilde{ab}})(1+\delta_{\widetilde{cd}})}} \\ \times \Big[\langle \widetilde{a}\widetilde{b} JT | v^{\mathrm{T}}_{12} | \widetilde{c}\widetilde{d} JT \rangle + (-)^{j_c + j_d + J + T} \langle \widetilde{a}\widetilde{b} JT | v^{\mathrm{T}}_{12} | \widetilde{d}\widetilde{c} JT \rangle \Big], \end{aligned} \tag{B.69}$$

We can extract the isospin dependence of the non-normalized and non-antisymmetrized tensor TBMEs according to

$$\langle \widetilde{a}\widetilde{b} JT | v^{\mathrm{T}}_{12} | \widetilde{c}\widetilde{d} JT \rangle = (W + (-)^T H) \langle \widetilde{a}\widetilde{b} J | \widetilde{v}^{\mathrm{T}}_{12} | \widetilde{c}\widetilde{d} J \rangle, \tag{B.70}$$

where $\widetilde{V}^{\mathrm{T}}$ corresponds to (B.68) deprived of its combination of parameters. Gathering the results, we find

$$\begin{aligned}\langle\widetilde{a}\widetilde{b}JT|v_{12}^{\mathrm{T}}|\widetilde{c}\widetilde{d}JT\rangle_{\mathrm{na}} = &\frac{W+(-)^{T}H}{\sqrt{(1+\delta_{\widetilde{a}\widetilde{b}})(1+\delta_{\widetilde{c}\widetilde{d}})}}\\ &\times\Big[\langle\widetilde{a}\widetilde{b}J|\widetilde{v}_{12}^{\mathrm{T}}|\widetilde{c}\widetilde{d}J\rangle+(-)^{j_c+j_d+J+T}\langle\widetilde{a}\widetilde{b}J|\widetilde{v}_{12}^{\mathrm{T}}|\widetilde{d}\widetilde{c}J\rangle\Big].\end{aligned} \tag{B.71}$$

In the following, we will then evaluate

$$\langle\widetilde{a}\widetilde{b}J|\widetilde{v}_{12}^{\mathrm{T}}|\widetilde{c}\widetilde{d}J\rangle=\sum_{k}(-)^{k}\langle\widetilde{a}\widetilde{b}J|\widetilde{v}_{12}^{\mathrm{T},k}|\widetilde{c}\widetilde{d}J\rangle, \tag{B.72}$$

where the k-th component of the tensor interaction is defined as

$$\widetilde{v}_{12}^{\mathrm{T},k}\equiv V(r_{12})[\hat{r}_{12}\otimes\hat{r}_{12}]_{-k}^{(2)}[\vec{\sigma}_1\otimes\vec{\sigma}_2]_{k}^{(2)}. \tag{B.73}$$

The transformation from jj coupling to LS coupling provides

$$\begin{aligned}\langle\widetilde{a}\widetilde{b}J|\widetilde{v}_{12}^{\mathrm{T},k}|\widetilde{c}\widetilde{d}J\rangle=&\sum_{LS}\sum_{L'S'}\hat{j}_a\hat{j}_b\hat{j}_c\hat{j}_d\hat{L}\hat{L}'\hat{S}\hat{S}'\begin{Bmatrix}l_a & l_b & L\\ 1/2 & 1/2 & S\\ j_a & j_b & J\end{Bmatrix}\begin{Bmatrix}l_c & l_d & L'\\ 1/2 & 1/2 & S'\\ j_c & j_d & J\end{Bmatrix}\\ &\times\underbrace{\langle n_a l_a\frac{1}{2}\,n_b l_b\frac{1}{2}\,LSJ|\widetilde{v}_{12}^{\mathrm{T},k}|n_c l_c\frac{1}{2}\,n_d l_d\frac{1}{2}\,L'S'J\rangle}_{B_k^{\mathrm{T}}},\end{aligned} \tag{B.74}$$

where the space and spin parts split up in such a way that

$$\begin{aligned}B_k^{\mathrm{T}}=&\sum_{M_L M_S}\sum_{M_L' M_S'}\langle LM_L SM_S|JM_L+M_S\rangle\langle L'M_L'S'M_S'|JM_L'+M_S'\rangle\\ &\underbrace{\langle n_a l_a\,n_b l_b\,LM_L|V(r_{12})[\hat{r}_{12}\otimes\hat{r}_{12}]_{-k}^{(2)}|n_c l_c\,n_d l_d\,L'M_L'\rangle}_{C_{-k}^{\mathrm{T}}}\\ &\times\underbrace{\langle\frac{1}{2}\,\frac{1}{2}\,SM_S|[\vec{\sigma}_1\otimes\vec{\sigma}_2]_k^{(2)}|\frac{1}{2}\,\frac{1}{2}\,S'M_S'\rangle}_{D_k^{\mathrm{T}}}.\end{aligned} \tag{B.75}$$

On the one hand, the Wigner–Eckart theorem relates the above spin TBME to its reduced counterpart according to [237]

$$D_k^{\mathrm{T}}=(-)^{S-M_S}\begin{pmatrix}S & 2 & S'\\ -M_S & k & M_S'\end{pmatrix}\langle\frac{1}{2}\,\frac{1}{2}\,S\|[\vec{\sigma}_1\otimes\vec{\sigma}_2]^{(2)}\|\frac{1}{2}\,\frac{1}{2}\,S'\rangle, \tag{B.76}$$

where the double bar denotes the reduced TBME, that can itself be expressed as

$$\langle\frac{1}{2}\,\frac{1}{2}\,S\|[\vec{\sigma}_1\otimes\vec{\sigma}_2]^{(2)}\|\frac{1}{2}\,\frac{1}{2}\,S'\rangle=\sqrt{5}\hat{S}\hat{S}'\begin{Bmatrix}1/2 & 1/2 & S\\ 1/2 & 1/2 & S'\\ 1 & 1 & 2\end{Bmatrix}\langle\frac{1}{2}\|\vec{\sigma}_1\|\frac{1}{2}\rangle\langle\frac{1}{2}\|\vec{\sigma}_2\|\frac{1}{2}\rangle, \tag{B.77}$$

with the reduced (one-body) matrix elements

$$\langle\frac{1}{2}\|\vec{\sigma}_i\|\frac{1}{2}\rangle=\sqrt{6},\quad\text{for } i\in\{1,2\}, \tag{B.78}$$

since we are dealing with Pauli matrices, verifying (D.6). Note that the Wigner-3j symbol appearing above with parentheses implies $2 \leq S + S'$, so that, necessarily, $S = S' = 1$. This result was expected as we know that the tensor term only acts in the $S = 1$ channel of the interaction (see section II.1.1). Gathering the equations, we obtain, for the spin part of the tensor TBMEs,

$$D_k^{\mathrm{T}} = 6\sqrt{5}(-)^{S-M_S}\hat{S}\hat{S}' \begin{pmatrix} S & 2 & S' \\ -M_S & k & M'_S \end{pmatrix} \begin{Bmatrix} 1/2 & 1/2 & S \\ 1/2 & 1/2 & S' \\ 1 & 1 & 2 \end{Bmatrix}. \tag{B.79}$$

As for the tensor space part, we find

$$\begin{aligned} C_{-k}^{\mathrm{T}} = \sum_{m_{la}m_{lb}} \sum_{m_{lc}m_{ld}} & \langle l_a m_{la} l_b m_{lb} | L M_L \rangle \langle l_c m_{lc} l_c m_{lc} | L' M'_L \rangle \\ & \times \underbrace{\langle n_a l_a m_{la}\, n_b l_b m_{lb} | V(r_{12}) [\hat{r}_{12} \otimes \hat{r}_{12}]^{(2)}_{-k} | n_c l_c m_{lc}\, n_d l_d m_{ld} \rangle}_{v^{\mathrm{T}\,-k}_{r_a r_b r_c r_d}}. \end{aligned} \tag{B.80}$$

Thus, we need to evaluate the tensor TBMEs in the spherical HO basis, whose wave functions are defined in (B.3). By definition,

$$v^{\mathrm{T}\,-k}_{r_a r_b r_c r_d} \equiv \int \mathrm{d}^3 r_1 \int \mathrm{d}^3 r_2\, \phi^*_{r_a}(\vec{r}_1) \phi^*_{r_b}(\vec{r}_2) V(r_{12}) [\hat{r}_{12} \otimes \hat{r}_{12}]^{(2)}_{-k} \phi_{r_c}(\vec{r}_1) \phi_{r_d}(\vec{r}_2), \tag{B.81}$$

Since the sandwiched quantity commutes with the wave functions, we have

$$v^{\mathrm{T}\,-k}_{r_a r_b r_c r_d} = \int \mathrm{d}^3 r_1 \int \mathrm{d}^3 r_2\, \phi^*_{r_a}(\vec{r}_1) \phi_{r_c}(\vec{r}_1) V(r_{12}) [\hat{r}_{12} \otimes \hat{r}_{12}]^{(2)}_{-k} \phi^*_{r_b}(\vec{r}_2) \phi_{r_d}(\vec{r}_2). \tag{B.82}$$

Applying twice the Gogny separable development in spherical symmetry (B.219), we obtain

$$\begin{aligned} v^{\mathrm{T}\,-k}_{r_a r_b r_c r_d} = & \sum_{r_\mu r_\nu} T^{(r_\mu)}_{(r_a)(r_c)} T^{(r_\nu)}_{(r_b)(r_d)} \langle l_a m_{la} | Y^{m_{l\mu}*}_{l_\mu} | l_c m_{lc} \rangle \langle l_b m_{lb} | Y^{m_{l\nu}*}_{l_\nu} | l_d m_{ld} \rangle \\ & \times \int \mathrm{d}^3 r_1 \int \mathrm{d}^3 r_2\, \phi_0(\vec{r}_1) \phi_0(\vec{r}_1) V(r_{12}) [\hat{r}_{12} \otimes \hat{r}_{12}]^{(2)}_{-k} \phi_{r_\mu}(\vec{r}_2) \phi_{r_\nu}(\vec{r}_2). \end{aligned} \tag{B.83}$$

Now, applying twice the Moshinsky transformation in spherical symmetry (B.225), we get

$$\begin{aligned} v^{\mathrm{T}\,-k}_{r_a r_b r_c r_d} = & \sum_{r_\mu r_\nu} T^{(r_\mu)}_{(r_a)(r_c)} T^{(r_\nu)}_{(r_b)(r_d)} \langle l_a m_{la} | Y^{m_{l\mu}*}_{l_\mu} | l_c m_{lc} \rangle \langle l_b m_{lb} | Y^{m_{l\nu}*}_{l_\nu} | l_d m_{ld} \rangle \\ & \times \sum_{r_\lambda r_\sigma} M^{r_\lambda\, r_\sigma}_{r_\mu\, r_\nu} \int \mathrm{d}^3 r\, \phi_0(\vec{r}) V(\sqrt{2} r) [\hat{r} \otimes \hat{r}]^{(2)}_{-k} \phi_{r_\lambda}(\vec{r}) \int \mathrm{d}^3 R\, \phi^*_0(\vec{R}) \phi_{r_\sigma}(\vec{R}), \end{aligned} \tag{B.84}$$

since the Jacobian of the change of variables $(\vec{r}_1, \vec{r}_2) \to (\vec{r}, \vec{R})$, given by (B.224), is equal to unity and the spherical Moshinsky coefficient, specified by (B.227), fixes the range of values of r_σ according to (B.229) and (B.230). Note that in the particular case $r'_\mu = r'_\nu = 0$, the spherical Moshinsky coefficient reduces to (B.234). Note also that $\phi_0(\vec{R}) = \phi^*_0(\vec{R})$ because of (B.5).

The integral over $\vec{R}$ is readily carried out considering the orthogonality relation of the spherical HO wave functions (B.4). On the other hand, using the writing (B.211) in

spherical symmetry, we can simplify the integral over $\vec{r}$ by pulling out its angular part by means of (B.6), namely

$$\begin{aligned}\int \mathrm{d}^3r\, \phi_0(\vec{r})V(\sqrt{2}r)[\hat{r}\otimes\hat{r}]^{(2)}_{-k}\phi_{r_\sigma}(\vec{r}) &= \sqrt{\frac{8\pi}{15}}\int \mathrm{d}^3r\, \phi_0(\vec{r})V(\sqrt{2}r)\phi_{r_\sigma}(\vec{r})Y_2^{-k}(\hat{r}) \\ &= \sqrt{\frac{8\pi}{15}}\frac{1}{\sqrt{4\pi}}\int \mathrm{d}r\, r^2\phi_{(0)}(r)V(\sqrt{2}r)\phi_{(r_\sigma)}(r) \\ &\qquad \times \int \mathrm{d}^2\hat{r}\, Y_2^{-k}(\hat{r})Y_{l_\sigma}^{m_{l\sigma}}(\hat{r}) \\ &= (-)^k\sqrt{\frac{2}{15}}\delta_{l_\sigma,2}\delta_{m_{l\sigma},k} \\ &\qquad \times \int \mathrm{d}r\, r^2\phi_{(0)}(r)V(\sqrt{2}r)\phi_{(r_\sigma)}(r),\end{aligned} \tag{B.85}$$

where we have used the orthogonality of the spherical harmonics (B.205). Thus, the only thing that remains to be done is to evaluate the above integral. Considering the particular wave functions (B.5) and

$$\phi_{(n_\sigma,2)} = \left[\frac{2}{b^3}\frac{n_\sigma!}{\Gamma(n_\sigma+7/2)}\right]^{1/2}\mathrm{e}^{-r^2/2b^2}\left(\frac{r}{b}\right)^2 L_{n_\sigma}^{5/2}\left(\frac{r^2}{b^2}\right), \tag{B.86}$$

as well as the series expansion of the generalized Laguerre polynomial (D.100), we obtain, after a development similar to the one made for the central TBMEs,

$$\begin{aligned}\int \mathrm{d}r\, r^2\phi_{(0,0)}(r)V(\sqrt{2}r)\phi_{(n_\sigma,2)}(r) &= \left[\frac{2}{\sqrt{\pi}}n_\sigma!\,\Gamma(n_\sigma+7/2)\right]^{1/2} \\ &\qquad \times \sum_{i=0}^{n_\sigma}\frac{(-)^i G^{-i-5/2}}{i!(n_\sigma-i)!(i+5/2)},\end{aligned} \tag{B.87}$$

where G is defined in (B.39). Finally, by gathering all the results, we get an expression for the TBMEs of the tensor interaction in the spherical HO basis, that reads

$$\boxed{\begin{aligned}v^{\mathrm{T}\,-k}_{r_ar_br_cr_d} &= (-)^k\sqrt{\frac{2}{15}}\sum_{r_\mu r_\nu}T^{(r_\mu)}_{(r_a)(r_c)}T^{(r_\nu)}_{(r_b)(r_d)}\langle l_a m_{la}|Y_{l_\mu}^{m_{l\mu}*}|l_c m_{lc}\rangle\langle l_b m_{lb}|Y_{l_\nu}^{m_{l\nu}*}|l_d m_{ld}\rangle \\ &\qquad \times M^{0\,r_\sigma}_{r_\mu r_\nu}\left[\frac{2}{\sqrt{\pi}}n_\sigma!\,\Gamma(n_\sigma+7/2)\right]^{1/2}\sum_{i=0}^{n_\sigma}\frac{(-)^i G^{-i-5/2}}{i!(n_\sigma-i)!(i+5/2)},\end{aligned}} \tag{B.88}$$

where G is expressed in (B.39). In this expression, $r_\sigma = (n_\sigma, 2, k)$, with n_σ given by (B.232), while the conditions (B.213) and (B.223) have to be fulfilled at any time.

2.5. Spin–orbit two-body matrix elements

In order to easily compute the TBMEs of the spin–orbit interaction, we shall separate the space and spin-isospin degrees of freedom according to the equivalent form of the spin–orbit operator (D.85). The interaction we are considering in this section then reads

$$v_{12}^{\mathrm{SO}} = \widetilde{B}(\mu)(W - HP_\tau)V(r_{12})[\vec{r}_{12}\otimes\vec{\nabla}_{12}]^{(1)}\cdot[\vec{\sigma}_1+\vec{\sigma}_2]^{(1)}, \tag{B.89}$$

where $V(r_{12})$ is the Gaussian potential (B.23) and $\widetilde{B}(\mu)$ the coefficient given by

$$\widetilde{B}(\mu) \equiv -\frac{1}{2\sqrt{2}} B(\mu) = \frac{\sqrt{2}}{\mu^2} \frac{1}{(\mu\sqrt{\pi})^3}, \tag{B.90}$$

with $B(\mu)$ defined in (II.7). As for the previous terms, the normalized and antisymmetrized (na) TBMEs, coupled to (J,T), of the spin–orbit interaction can be written by means of (B.8), i.e.

$$\begin{aligned}\langle \widetilde{ab} JT | v_{12}^{\mathrm{SO}} | \widetilde{cd} JT \rangle_{\mathrm{na}} = & \frac{1}{\sqrt{(1+\delta_{\widetilde{ab}})(1+\delta_{\widetilde{cd}})}} \\ & \times \Big[\langle \widetilde{ab} JT | v_{12}^{\mathrm{SO}} | \widetilde{cd} JT \rangle + (-)^{j_c+j_d+J+T} \langle \widetilde{ab} JT | v_{12}^{\mathrm{SO}} | \widetilde{dc} JT \rangle \Big],\end{aligned} \tag{B.91}$$

We can extract the isospin dependence of the non-normalized and non-antisymmetrized spin–orbit TBMEs, as we have done for the tensor interaction, according to

$$\langle \widetilde{ab} JT | v_{12}^{\mathrm{SO}} | \widetilde{cd} JT \rangle = \widetilde{B}(\mu)(W + (-)^T H) \langle \widetilde{ab} J | \widetilde{v}_{12}^{\mathrm{SO}} | \widetilde{cd} J \rangle, \tag{B.92}$$

where $\widetilde{V}^{\mathrm{SO}}$ corresponds to (B.89) deprived of its combination of parameters. Gathering the results, we find

$$\begin{aligned}\langle \widetilde{ab} JT | v_{12}^{\mathrm{SO}} | \widetilde{cd} JT \rangle_{\mathrm{na}} = & \widetilde{B}(\mu) \frac{W + (-)^T H}{\sqrt{(1+\delta_{\widetilde{ab}})(1+\delta_{\widetilde{cd}})}} \\ & \times \Big[\langle \widetilde{ab} J | \widetilde{v}_{12}^{\mathrm{SO}} | \widetilde{cd} J \rangle + (-)^{j_c+j_d+J+T} \langle \widetilde{ab} J | \widetilde{v}_{12}^{\mathrm{SO}} | \widetilde{dc} J \rangle \Big].\end{aligned} \tag{B.93}$$

In the following, we will then evaluate

$$\langle \widetilde{ab} J | \widetilde{v}_{12}^{\mathrm{SO}} | \widetilde{cd} J \rangle = \sum_k (-)^k \langle \widetilde{ab} J | \widetilde{v}_{12}^{\mathrm{SO},k} | \widetilde{cd} J \rangle, \tag{B.94}$$

where the k-th component of the spin–orbit interaction is defined as

$$\widetilde{v}_{12}^{\mathrm{SO},k} \equiv V(r_{12}) [\vec{r}_{12} \otimes \vec{\nabla}_{12}]^{(1)}_{-k} [\vec{\sigma}_1 + \vec{\sigma}_2]^{(1)}_k. \tag{B.95}$$

The transformation from jj coupling to LS coupling provides

$$\begin{aligned}\langle \widetilde{ab} J | \widetilde{v}_{12}^{\mathrm{SO},k} | \widetilde{cd} J \rangle = & \sum_{LS} \sum_{L'S'} \hat{j}_a \hat{j}_b \hat{j}_c \hat{j}_d \hat{L} \hat{L}' \hat{S} \hat{S}' \begin{Bmatrix} l_a & l_b & L \\ 1/2 & 1/2 & S \\ j_a & j_b & J \end{Bmatrix} \begin{Bmatrix} l_c & l_d & L' \\ 1/2 & 1/2 & S' \\ j_c & j_d & J \end{Bmatrix} \\ & \times \underbrace{\langle n_a l_a \tfrac{1}{2}\, n_b l_b \tfrac{1}{2}\, LSJ | \widetilde{v}_{12}^{\mathrm{SO},k} | n_c l_c \tfrac{1}{2}\, n_d l_d \tfrac{1}{2}\, L'S'J \rangle}_{B_k^{\mathrm{SO}}},\end{aligned} \tag{B.96}$$

where the space and spin parts split up in such a way that

$$\begin{aligned}B_k^{\mathrm{SO}} = & \sum_{M_L M_S} \sum_{M'_L M'_S} \langle LM_L SM_S | JM_L + M_S \rangle \langle L'M'_L S'M'_S | JM'_L + M'_S \rangle \\ & \underbrace{\langle n_a l_a\, n_b l_b\, LM_L | V(r_{12}) [\vec{r}_{12} \otimes \hat{\nabla}_{12}]^{(1)}_{-k} | n_c l_c\, n_d l_d\, L'M'_L \rangle}_{C_{-k}^{\mathrm{SO}}} \\ & \times \underbrace{\langle \tfrac{1}{2}\tfrac{1}{2} SM_S | [\vec{\sigma}_1 + \vec{\sigma}_2]^{(1)}_k | \tfrac{1}{2}\tfrac{1}{2} S'M'_S \rangle}_{D_k^{\mathrm{SO}}}.\end{aligned} \tag{B.97}$$

On the one hand, the Wigner–Eckart theorem relates the above spin TBME to its reduced counterpart according to [237]

$$D_k^{\mathrm{SO}} = (-)^{S-M_S} \begin{pmatrix} S & 1 & S' \\ -M_S & k & M'_S \end{pmatrix} \langle \frac{1}{2}\,\frac{1}{2}\, S \| \vec{\sigma}_1 + \vec{\sigma}_2 \| \frac{1}{2}\,\frac{1}{2}\, S' \rangle. \tag{B.98}$$

Separating the contributions from the first and second particles in the spin reduced TBME, we obtain

$$\langle \frac{1}{2}\,\frac{1}{2}\, S \| \vec{\sigma}_1 + \vec{\sigma}_2 \| \frac{1}{2}\,\frac{1}{2}\, S' \rangle = \underbrace{\langle \frac{1}{2}\,\frac{1}{2}\, S \| \vec{\sigma}_1 \| \frac{1}{2}\,\frac{1}{2}\, S' \rangle}_{E_1} + \underbrace{\langle \frac{1}{2}\,\frac{1}{2}\, S \| \vec{\sigma}_2 \| \frac{1}{2}\,\frac{1}{2}\, S' \rangle}_{E_2}, \tag{B.99}$$

where we have [237]

$$E_1 = (-)^{S'} \hat{S}\hat{S}' \begin{Bmatrix} 1/2 & S & 1/2 \\ S' & 1/2 & 1 \end{Bmatrix} \langle \frac{1}{2} \| \vec{\sigma}_1 \| \frac{1}{2} \rangle, \tag{B.100a}$$

$$E_2 = (-)^{S} \hat{S}\hat{S}' \begin{Bmatrix} 1/2 & S & 1/2 \\ S' & 1/2 & 1 \end{Bmatrix} \langle \frac{1}{2} \| \vec{\sigma}_2 \| \frac{1}{2} \rangle, \tag{B.100b}$$

with the above reduced matrix elements given by (B.78). On the one hand, the Wigner-3j symbol appearing in (B.98) implies that S and S' cannot be simultaneously equal to 0. On the other hand, if $S = 0$ and $S' = 1$ or $S = 1$ and $S' = 0$, the quantities E_1 and E_2 expressed above cancel one another so that the spin–orbit TBMEs vanish. Thus, the only possibility is $S = S' = 1$, just like for the tensor interaction (see discussion right after equation (B.78)). Once again, this result was expected since we know that the spin–orbit term only acts in the $S = 1$ channel of the interaction (see section II.1.1). Gathering the equations, we obtain, for the spin part of the spin–orbit TBMEs,

$$D_k^{\mathrm{SO}} = 2\sqrt{6}(-)^{S-M_S} \hat{S}\hat{S}' \begin{pmatrix} S & 1 & S' \\ -M_S & k & M'_S \end{pmatrix} \begin{Bmatrix} 1/2 & S & 1/2 \\ S' & 1/2 & 1 \end{Bmatrix}. \tag{B.101}$$

As for the spin–orbit space part, we find

$$\begin{aligned} C_{-k}^{\mathrm{SO}} = \sum_{m_{la} m_{lb}} \sum_{m_{lc} m_{ld}} & \langle l_a m_{la} l_b m_{lb} | L M_L \rangle \langle l_c m_{lc} l_c m_{lc} | L' M'_L \rangle \\ & \times \underbrace{\langle n_a l_a m_{la}\, n_b l_b m_{lb} | V(r_{12}) [\vec{r}_{12} \otimes \hat{\nabla}_{12}]^{(1)}_{-k} | n_c l_c m_{lc}\, n_d l_d m_{ld} \rangle}_{v^{\mathrm{SO}\,-k}_{r_a r_b r_c r_d}}. \end{aligned} \tag{B.102}$$

Thus, we need to evaluate the spin–orbit TBME in the spherical HO basis, whose wave functions are defined in (B.3). Decoupling the tensor product, we have,

$$v^{\mathrm{SO}\,-k}_{r_a r_b r_c r_d} = \sum_{\alpha\beta} \langle 1\alpha 1\beta | 1 - k \rangle \underbrace{\langle n_a l_a m_{la}\, n_b l_b m_{lb} | r_{12}^{\alpha} V(r_{12}) \nabla_{12}^{\beta} | n_c l_c m_{lc}\, n_d l_d m_{ld} \rangle}_{v^{\mathrm{SO}\,\alpha\beta}_{r_a r_b r_c r_d}}, \tag{B.103}$$

with, by definition,

$$v^{\mathrm{SO}\,\alpha\beta}_{r_a r_b r_c r_d} \equiv \int \mathrm{d}^3 r_1 \int \mathrm{d}^3 r_2\, \phi^*_{r_a}(\vec{r}_1) \phi^*_{r_b}(\vec{r}_2) V(r_{12}) r_{12}^{\alpha} \Big[\nabla_{12}^{\beta} \phi_{r_c}(\vec{r}_1) \phi_{r_d}(\vec{r}_2) \Big]. \tag{B.104}$$

This time, the sandwiched quantity does not commute with the wave functions because of the gradient operator. Then, by separating the gradients acting on the first and second particles, we obtain

$$\begin{aligned} v^{\mathrm{SO}\,\alpha\beta}_{r_a r_b r_c r_d} = & \int \mathrm{d}^3 r_1 \int \mathrm{d}^3 r_2\, \phi^*_{r_a}(\vec{r}_1) \phi^*_{r_b}(\vec{r}_2) V(r_{12}) r_{12}^{\alpha} \Big[\nabla_1^{\beta} \phi_{r_c}(\vec{r}_1) \Big] \phi_{r_d}(\vec{r}_2) \\ & - \int \mathrm{d}^3 r_1 \int \mathrm{d}^3 r_2\, \phi^*_{r_a}(\vec{r}_1) \phi^*_{r_b}(\vec{r}_2) V(r_{12}) r_{12}^{\alpha} \phi_{r_c}(\vec{r}_1) \Big[\nabla_2^{\beta} \phi_{r_d}(\vec{r}_2) \Big]. \end{aligned} \tag{B.105}$$

In the following, we will call $I_1^{\alpha\beta}$ and $I_2^{\alpha\beta}$ the first and second integrals of the above right-hand side term (we purposely omit the other indices for conciseness). We fill focus on the integral $I_1^{\alpha\beta}$, the integral $I_2^{\alpha\beta}$ being easily deductible from it. We have to evaluate the action of the gradient operator on the wave functions with the help of the gradient formula in spherical symmetry (B.218). We find

$$\begin{aligned} I_1^{\alpha\beta} = \frac{1}{b}\sum_{j=\pm 1}(-)^{l_c+m_{lc}+\beta+1}\begin{pmatrix} l_c & 1 & l_c+j \\ m_{lc} & \beta & -m_{lc}-\beta \end{pmatrix} \\ \times\Bigg[a_j^{(r_c)}\int \mathrm{d}^3r_1\int \mathrm{d}^3r_2\,\phi_{r_a}^*(\vec{r}_1)\phi_{n_c-j,l_c+j,m_{lc}+\beta}(\vec{r}_1)V(r_{12})r_{12}^\alpha\phi_{r_b}^*(\vec{r}_2)\phi_{r_d}(\vec{r}_2) \\ + c_j^{(r_c)}\int \mathrm{d}^3r_1\int \mathrm{d}^3r_2\,\phi_{r_a}^*(\vec{r}_1)\phi_{n_c,l_c+j,m_{lc}+\beta}(\vec{r}_1)V(r_{12})r_{12}^\alpha\phi_{r_b}^*(\vec{r}_2)\phi_{r_d}(\vec{r}_2)\Bigg], \end{aligned} \tag{B.106}$$

where the coefficients $a_j^{(r_c)}$ and $c_j^{(r_c)}$ are defined in (B.217). Now, using the Gogny separable development in spherical symmetry (B.219) four times, we end up with

$$\begin{aligned} I_1^{\alpha\beta} = \frac{1}{b}\sum_{j=\pm 1}(-)^{l_c+m_{lc}+\beta+1}\begin{pmatrix} l_c & 1 & l_c+j \\ m_{lc} & \beta & -m_{lc}-\beta \end{pmatrix} \\ \times\sum_{l_\mu m_{l\mu}}\sum_{r_\nu} T_{(r_b)(r_d)}^{(r_\nu)}\langle l_a m_{la}|Y_{l_\mu}^{m_{l\mu}*}|l_c+j\,m_{lc}+\beta\rangle\langle l_b m_{lb}|Y_{l_\nu}^{m_{l\nu}*}|l_d m_{ld}\rangle \\ \times\Bigg[a_j^{(r_c)}\sum_{n_\mu} T_{(r_a)(n_c-j,l_c+j)}^{(r_\mu)} \\ \times\int \mathrm{d}^3r_1\int \mathrm{d}^3r_2\,\phi_0(\vec{r}_1)\phi_0(\vec{r}_2)V(r_{12})r_{12}^\alpha\phi_{r_\mu}(\vec{r}_1)\phi_{r_\nu}(\vec{r}_2) \\ + c_j^{(r_c)}\sum_{n'_\mu} T_{(r_a)(n_c,l_c+j)}^{(r'_\mu)}\int \mathrm{d}^3r_1\int \mathrm{d}^3r_2\,\phi_0(\vec{r}_1)\phi_0(\vec{r}_2)V(r_{12})r_{12}^\alpha\phi_{r'_\mu}(\vec{r}_1)\phi_{r_\nu}(\vec{r}_2)\Bigg]. \end{aligned} \tag{B.107}$$

Let us note that we have introduced the notations $r_\mu = (n_\mu, l_\mu, m_{l\mu})$ and $r'_\mu = (n'_\mu, l_\mu, m_{l\mu})$ since the quantum numbers n_μ and n'_μ run over distinct ranges of values, as they appear in different Talman coefficients (see condition (B.223)). In the following, we will focus on the first integral, the second one is deduced by the transformation $r_\mu \to r'_\mu$. Then, applying twice the Moshinsky transformation in spherical symmetry (B.225) on the first integral, we get

$$\begin{aligned} \int \mathrm{d}^3r_1\int \mathrm{d}^3r_2\,\phi_0(\vec{r}_1)\phi_0(\vec{r}_2)V(r_{12})r_{12}^\alpha\phi_{r_\mu}(\vec{r}_1)\phi_{r_\nu}(\vec{r}_2) = \sqrt{2}\sum_{r_\lambda r_\sigma} M_{r_\mu r_\nu}^{r_\lambda r_\sigma} \\ \times\int \mathrm{d}^3r\,\phi_0(\vec{r})V(\sqrt{2}r)r^\alpha\phi_{r_\sigma}(\vec{r})\int \mathrm{d}^3R\,\phi_0^*(\vec{R})\phi_{r_\lambda}(\vec{R}), \end{aligned} \tag{B.108}$$

since the Jacobian of the change of variables $(\vec{r}_1, \vec{r}_2) \to (\vec{r}, \vec{R})$, given by (B.224), is equal to unity and the spherical Moshinsky coefficient, specified by (B.227), fixes the range of values of r_σ according to (B.229) and (B.230). Note that in the particular case $r'_\mu = r'_\nu = 0$, the spherical Moshinsky coefficient reduces to (B.234). Note also that $\phi_0(\vec{R}) = \phi_0^*(\vec{R})$ because of (B.5).

The integral over $\vec{R}$ is readily carried out considering the orthogonality relation of the spherical HO wave functions (B.4). On the other hand, using the writing (B.210) in spherical symmetry, we can simplify the integral over $\vec{r}$ by pulling out its angular part by

means of (B.6), namely

$$\begin{aligned}\int \mathrm{d}^3r\,\phi_0(\vec{r})V(\sqrt{2}r)r^\alpha\phi_{r_\sigma}(\vec{r}) &= \sqrt{\frac{4\pi}{3}}\int \mathrm{d}^3r\,r\phi_0(\vec{r})V(\sqrt{2}r)\phi_{r_\sigma}(\vec{r})Y_1^\alpha(\hat{r})\\ &= \sqrt{\frac{4\pi}{3}}\frac{1}{\sqrt{4\pi}}\int \mathrm{d}r\,r^3\phi_{(0)}(r)V(\sqrt{2}r)\phi_{(r_\sigma)}(r)\\ &\qquad\times\int \mathrm{d}^2\hat{r}\,Y_1^\alpha(\hat{r})Y_{l_\sigma}^{m_{l\sigma}}(\hat{r})\\ &= \frac{(-)^\alpha}{\sqrt{3}}\delta_{l_\sigma,1}\delta_{m_{l\sigma},-\alpha}\\ &\qquad\times\int \mathrm{d}r\,r^3\phi_{(0)}(r)V(\sqrt{2}r)\phi_{(r_\sigma)}(r),\end{aligned} \tag{B.109}$$

where we have used the orthogonality of the spherical harmonics (B.205). Finally, using the identity $r\phi_{(0,0)}(r) = \sqrt{3/2}b\phi_{(0,1)}(r)$ of the spherical HO wave functions (B.3), we obtain

$$\begin{aligned}\int \mathrm{d}^3r\,\phi_0(\vec{r})V(\sqrt{2}r)r_{12}^\alpha\phi_{r_\sigma}(\vec{r}) &= \frac{(-)^\alpha b}{\sqrt{2}}\delta_{l_\sigma,1}\delta_{m_{l\sigma},-\alpha}\\ &\qquad\times\int \mathrm{d}r\,r^2\phi_{(0,1)}(r)V(\sqrt{2}r)\phi_{(n_\sigma,1)}(r).\end{aligned} \tag{B.110}$$

Thus, the only thing that remains to be done is to evaluate the above integral. Considering the particular wave functions

$$\phi_{(0,1)}(r) = \left[\frac{8}{3\sqrt{\pi}b^3}\right]^{1/2}\frac{r}{b}\,\mathrm{e}^{-r^2/2b^2}, \tag{B.111}$$

and

$$\phi_{(n_\sigma,1)}(r) = \left[\frac{2}{b^3}\frac{n_\sigma!}{\Gamma(n_\sigma+5/2)}\right]^{1/2}\frac{r}{b}\,\mathrm{e}^{-r^2/2b^2}L_{n_\sigma}^{3/2}\left(\frac{r^2}{b^2}\right), \tag{B.112}$$

as well as the series expansion of the generalized Laguerre polynomial (D.100), we obtain, after a development similar to the ones made for the central and tensor TBMEs,

$$\begin{aligned}\int \mathrm{d}r\,r^2\phi_{(0,1)}(r)V(\sqrt{2}r)\phi_{(n_\sigma,1)}(r) &= \left[\frac{4}{3\sqrt{\pi}}n_\sigma!\,\Gamma(n_\sigma+5/2)\right]^{1/2}\\ &\qquad\times\sum_{i=0}^{n_\sigma}\frac{(-)^iG^{-i-5/2}}{i!(n_\sigma-i)!},\end{aligned} \tag{B.113}$$

where G is defined in (B.39). Gathering all the results, we can write down the expression

for the first integral $I_1^{\alpha\beta}$, given by (B.106), namely

$$
\begin{aligned}
I_1^{\alpha\beta} = & \sum_{j=\pm 1} (-)^{l_c+m_{lc}+\alpha+\beta+1} \begin{pmatrix} l_c & 1 & l_c+j \\ m_{lc} & \beta & -m_{lc}-\beta \end{pmatrix} \\
& \times \sum_{l'_\mu m'_{l\mu}} \sum_{r_\nu} T^{(r_\nu)}_{(r_b)(r_d)} \langle l_a m_{la} | Y^{m'_{l\mu}*}_{l'_\mu} | l_c + j\, m_{lc}+\beta \rangle \langle l_b m_{lb} | Y^{m_{l\nu}*}_{l_\nu} | l_d m_{ld} \rangle \\
& \times \Bigg[a_j^{(r_c)} T^{(r_\mu^{(1)})}_{(r_a)(n_c-j,l_c+j)} M^{0\, r_\sigma^{(1)}}_{r_\mu^{(1)} r_\nu} \left[\frac{4}{3\sqrt{\pi}} n_\sigma^{(1)}!\, \Gamma(n_\sigma^{(1)}+5/2) \right]^{1/2} \\
& \qquad \times \sum_{i=0}^{n_\sigma^{(1)}} \frac{(-)^i G^{-i-5/2}}{i!(n_\sigma^{(1)}-i)!} \\
& \quad + c_j^{(r_c)} T^{(r_\mu^{(2)})}_{(r_a)(n_c,l_c+j)} M^{0\, r_\sigma^{(2)}}_{r_\mu^{(2)} r_\nu} \left[\frac{4}{3\sqrt{\pi}} n_\sigma^{(2)}!\, \Gamma(n_\sigma^{(2)}+5/2) \right]^{1/2} \\
& \qquad \times \sum_{i=0}^{n_\sigma^{(2)}} \frac{(-)^i G^{-i-5/2}}{i!(n_\sigma^{(2)}-i)!} \Bigg].
\end{aligned}
\tag{B.114}
$$

where G is expressed in (B.39). For clarity, we have changed the notations a bit in the above expression. They are $r_\mu^{(i)} = (n_\mu^{(i)}, l'_\mu, m'_{l\mu})$ for $i \in \{1,2\}$ and $r_\nu = (n_\nu, l_\nu, m_\nu)$. Moreover, we have $r_\sigma^{(1)} = (n_\sigma^{(1)}, 2, k)$ and $r_\sigma^{(2)} = (n_\sigma^{(2)}, 2, k)$ with $n_\sigma^{(1)} = (X_\mu^{(1)} + X_\nu - 2)/2$ and $n_\sigma^{(2)} = (X_\mu^{(2)} + X_\nu - 2)/2$, according to (B.232). We see that $n_\sigma^{(1)}$ and $n_\sigma^{(2)}$ respectively depend on the values of $n_\mu^{(1)}$ and $n_\mu^{(2)}$, hence the notations chosen. Moreover, the conditions (B.213) and (B.223) have to be fulfilled at any time. For the sake of completeness, we also write down the full expression of the integral $I_2^{\alpha\beta}$ whose derivation is analogous to the one of $I_1^{\alpha\beta}$. We have

$$
\begin{aligned}
I_2^{\alpha\beta} = & \sum_{j=\pm 1} (-)^{l_d+m_{ld}+\alpha+\beta+1} \begin{pmatrix} l_d & 1 & l_d+j \\ m_{ld} & \beta & -m_{ld}-\beta \end{pmatrix} \\
& \times \sum_{l'_\nu m'_{l\nu}} \sum_{r_\mu} T^{(r_\mu)}_{(r_a)(r_c)} \langle l_a m_{la} | Y^{m_{l\mu}*}_{l_\mu} | l_c m_{lc} \rangle \langle l_b m_{lb} | Y^{m'_{l\nu}*}_{l'_\nu} | l_d + j\, m_{ld}+\beta \rangle \\
& \times \Bigg[a_j^{(r_d)} T^{(r_\nu^{(1)})}_{(r_b)(n_d-j,l_d+j)} M^{0\, r_\sigma^{(3)}}_{r_\mu r_\nu^{(1)}} \left[\frac{4}{3\sqrt{\pi}} n_\sigma^{(3)}!\, \Gamma(n_\sigma^{(3)}+5/2) \right]^{1/2} \\
& \qquad \times \sum_{i=0}^{n_\sigma^{(3)}} \frac{(-)^i G^{-i-5/2}}{i!(n_\sigma^{(3)}-i)!} \\
& \quad + c_j^{(r_d)} T^{(r_\nu^{(2)})}_{(r_b)(n_d,l_d+j)} M^{0\, r_\sigma^{(4)}}_{r_\mu r_\nu^{(2)}} \left[\frac{4}{3\sqrt{\pi}} n_\sigma^{(4)}!\, \Gamma(n_\sigma^{(4)}+5/2) \right]^{1/2} \\
& \qquad \times \sum_{i=0}^{n_\sigma^{(4)}} \frac{(-)^i G^{-i-5/2}}{i!(n_\sigma^{(4)}-i)!} \Bigg],
\end{aligned}
\tag{B.115}
$$

where G is expressed in (B.39). Once again, we have changed the notations a bit in the above expression. They are $r_\nu^{(i)} = (n_\nu^{(i)}, l'_\nu, m'_{l\nu})$ for $i \in \{1,2\}$ and $r_\mu = (n_\mu, l_\mu, m_\mu)$. Besides, we have $r_\sigma^{(3)} = (n_\sigma^{(3)}, 2, k)$ and $r_\sigma^{(4)} = (n_\sigma^{(4)}, 2, k)$ with $n_\sigma^{(3)} = (X_\mu + X_\nu^{(1)} - 2)/2$ and $n_\sigma^{(4)} = (X_\mu + X_\nu^{(2)} - 2)/2$, according to (B.232). We see that $n_\sigma^{(3)}$ and $n_\sigma^{(4)}$ respectively

depend on the values of $n_\nu^{(1)}$ and $n_\nu^{(2)}$, hence the notations chosen (see the previous paragraph). From equation (B.103) and these expressions, we directly deduce the TBME of the spin–orbit interaction in the spherical HO basis.

3. From HF to HFR approximation

As presented in section I.2.2.1, in the fitting procedure, the different quantities are evaluated at the Hartree–Fock restricted (HFR) approximation. The HFR approximation consists in a more restrained HF approach (presented in subsection A.1.2), where the density matrix is imposed to be diagonal, i.e.

$$\rho_{ab} = \delta_{ab}\rho_{aa} = \begin{cases} 1 & \text{if } |a\rangle \text{ is occupied,} \\ 0 & \text{otherwise.} \end{cases} \tag{B.116}$$

In addition, we have mentioned that the splitting of the states according to the projections of their total angular momentum does not show up in the fitting procedure since the spin–orbit interaction, inducing that effect, is neglected. The spherical HO states are then fully specified by their quantum numbers n and l, through their major shells $N \equiv 2n + l$, and the density matrix at the HFR approximation simply is

$$\rho_{nl,nl} = \begin{cases} 1 & \text{if } |nl\rangle \text{ is occupied,} \\ 0 & \text{otherwise.} \end{cases} \tag{B.117}$$

Thus, at the HFR approximation, the total HF energy (A.12) reduces to

$$\mathcal{E}_{\text{HFR}} = \sum_a \langle a|t|a\rangle\rho_{aa} + \frac{1}{2}\sum_{ac}\langle ab|v_{12}^{(\text{a})}|ab\rangle\rho_{bb}\rho_{aa}, \tag{B.118}$$

or, in terms of HFR fields, as

$$\mathcal{E}_{\text{HFR}} = \mathcal{E}_{\text{K}}^{\text{HFR}} + \mathcal{E}_{\text{P}}^{\text{HFR}} = \mathcal{E}_{\text{K}}^{\text{HFR}} + \mathcal{E}_{\text{MF}}^{\text{HFR}}, \tag{B.119}$$

where the kinetic energy

$$\mathcal{E}_{\text{K}}^{\text{HFR}} \equiv \sum_a K_{aa}\rho_{aa}, \tag{B.120}$$

is expressed in terms of the kinetic field

$$\boxed{K_{aa} \equiv \langle a|t|a\rangle,} \tag{B.121}$$

and the potential energy

$$\mathcal{E}_{\text{P}}^{\text{HFR}} = \mathcal{E}_{\text{MF}}^{\text{HFR}} \equiv \frac{1}{2}\sum_a \Gamma_{aa}\rho_{aa}, \tag{B.122}$$

is expressed in terms of the mean field

$$\boxed{\Gamma_{aa} \equiv \sum_b \langle ab|v_{12}^{(\text{a})}|ab\rangle\rho_{bb}.} \tag{B.123}$$

The individual (or one-body) Hamiltonian to which each nucleon of the nucleus is subjected satisfies the relation $h_{aa}^{\text{HFR}} \equiv \partial\mathcal{E}_{\text{HFR}}/\partial\rho_{aa}$, so that

$$h_{aa}^{\text{HFR}} = K_{aa} + \Gamma_{aa} + \partial\Gamma_{aa}, \tag{B.124}$$

where the rearrangement field is

$$\boxed{\partial\Gamma_{ab} \equiv \frac{1}{2}\sum_{a'b'}\langle a'b'|\frac{\partial v_{12}^{(\mathrm{a})}}{\partial\rho_{aa}}|a'b'\rangle\rho_{a'a'}\rho_{b'b'}.} \tag{B.125}$$

Since each of the fields describing the individual Hamiltonian at the HFR approximation (B.124) is diagonal (as the density matrices are), the individual Hamiltonian is diagonal itself. Therefore, each non-zero matrix element of this Hamiltonian corresponds to an eigenvalue $\varepsilon_a^{\mathrm{HFR}}$, identified as an individual (or one-body) energy, i.e.

$$\varepsilon_a^{\mathrm{HFR}} = h_{aa}^{\mathrm{HFR}} = K_{aa} + \Gamma_{aa} + \partial\Gamma_{aa}. \tag{B.126}$$

Note that in practical calculations, we will not bother with the density matrix (B.117) since it is always equal to unity, at the HFR approximation, for the occupied states on which the summations are performed. Moreover, although the spin–orbit interaction is not taken into account in the fitting procedure, we will still evaluate how the quantities calculated at the HFR approximation are modified when a spin–orbit term is considered.

4. Derivation of the Hartree–Fock restricted fields

In order to evaluate later the total (B.119) and individual (B.126) energies at the HFR approximation, let us calculate the various HFR fields introduced in the previous section.

4.1. Kinetic field

At the HFR approximation, the kinetic field is given by (B.121). By virtue of the virial theorem, we can evaluate its contribution in the spherical HO representation, and obtain

$$\boxed{K_{aa} = \frac{\hbar\omega}{2}\left(2n_a + l_a + \frac{3}{2}\right).} \tag{B.127}$$

4.2. Mean field

At the HFR approximation, the mean field is given by (B.123). For the sake of clarity, we will decompose this field into a direct and an exchange component in the following, as $\Gamma_{aa} \equiv \Gamma_{aa}|_{\mathrm{D}} + \Gamma_{aa}|_{\mathrm{E}}$, where

$$\Gamma_{aa}|_{\mathrm{D}} \equiv \sum_b \langle ab|v_{12}|ab\rangle\rho_{bb}, \tag{B.128a}$$

$$\Gamma_{aa}|_{\mathrm{E}} \equiv \sum_b \langle ab|v_{12}|ba\rangle\rho_{bb}. \tag{B.128b}$$

It is now necessary to evaluate these contributions for the fields of the generalized Gogny interaction (II.1).

4.2.1. Central contribution

Let us start by deriving the direct mean field associated with the central terms. The central terms are given by (B.22), where we now use the shorthand notation for the spin-isospin part,

$$\mathcal{P} \equiv W + BP_\sigma - HP_\tau - MP_\sigma P_\tau. \tag{B.129}$$

The spatial and spin-isospin degrees of freedom split up in such a way that

$$\Gamma^{\mathrm{C}}_{aa}|_{\mathrm{D}} = \sum_{r_b u_b} \langle r_a r_b|V(r_{12})|r_a r_b\rangle\langle u_a u_b|W_{\mathrm{D}}|u_a u_b\rangle. \tag{B.130}$$

On the one hand, the spin-isospin TBMEs of the central terms are easy to compute since their spin-isospin part is only a combination of spin- and isospin-exchange operators. We find out, in general,

$$\begin{aligned}\langle u_a u_b|\mathcal{P}|u_c u_d\rangle = &\Big(W\delta_{s_a s_c}\delta_{s_b s_d} + B\delta_{s_a s_d}\delta_{s_b s_c}\Big)\delta_{t_a t_c}\delta_{t_b t_d} \\ &- \Big(H\delta_{s_a s_c}\delta_{s_b s_d} + M\delta_{s_a s_d}\delta_{s_b s_c}\Big)\delta_{t_a t_d}\delta_{t_b t_c}.\end{aligned} \tag{B.131}$$

In the particular case of the HFR approximation, this equation reduces to

$$\langle u_a u_b|\mathcal{P}|u_a u_b\rangle = W + B\delta_{s_a s_d} - (H + M\delta_{s_a s_b})\delta_{t_a t_b}, \tag{B.132}$$

so that we immediately get

$$\sum_{s_b}\langle s_a t_a\, s_b t_b|\mathcal{P}|s_a t_a\, s_b t_b\rangle = 2W + B - (2H + M)\delta_{t_a t_b}. \tag{B.133}$$

On the other hand, the spatial TBMEs associated with the central terms have been calculated in (B.40). The respective definitions of the integral over three spherical harmonics (B.212) and of the particular value of the Moshinsky coefficient (B.231), coupled with the properties of the Wigner-3j symbols, allow to simplify the spatial part according to

$$\sum_{m_{lb}}\langle n_a l_a m_{la}\, n_b l_b m_{lb}|V(r_{12})|n_a l_a m_{la}\, n_b l_b m_{lb}\rangle = S^{\mathrm{C}}_{n_a l_a n_b l_b}|_{\mathrm{D}}, \tag{B.134}$$

where he have defined

$$S^{\mathrm{C}}_{n_a l_a n_b l_b}|_{\mathrm{D}} \equiv \frac{1}{4\pi}(2l_b + 1)\sum_{n_\mu n_\nu} T^{(n_\mu 0)}_{(n_a l_a)(n_a l_a)} T^{(n_\nu 0)}_{(n_b l_b)(n_b l_b)} I_{n_\mu n_\nu 0}, \tag{B.135}$$

with the quantity

$$I_{nn'l} \equiv \frac{1}{2^{n+n'+l}}\frac{(n+n'+l)!\Gamma(n+n'+l+3/2)}{[n!n'!\Gamma(n+l+3/2)\Gamma(n'+l+3/2)]^{1/2}}\sum_{i=0}^{n+n'+l}\frac{(-)^i G^{-i-3/2}}{i!(n+n'+l-i)!}. \tag{B.136}$$

Finally, the direct mean field associated with the central terms writes

$$\boxed{\Gamma^{\mathrm{C}}_{aa}|_{\mathrm{D}} = \sum_{n_b l_b t_b}(2W + B - (2H + M)\delta_{t_a t_b})S^{\mathrm{C}}_{n_a l_a n_b l_b}|_{\mathrm{D}}.} \tag{B.137}$$

The calculation of the exchange mean field associated with the central terms is similar. We have

$$\Gamma^{\mathrm{C}}_{aa}|_{\mathrm{E}} = \sum_{r_b u_b}\langle r_a r_b|V(r_{12})|r_b r_a\rangle\langle u_a u_b|W_{\mathrm{E}}|u_b u_a\rangle. \tag{B.138}$$

Using (B.131) in the particular case of the HFR approximation, we directly get for the spin-isospin part,

$$\sum_{s_b}\langle s_a t_a\, s_b t_b|\mathcal{P}|s_b t_b\, s_a t_a\rangle = 2M + H - (2B + W)\delta_{t_a t_b}. \tag{B.139}$$

The exchange spatial part is obtained in the same way as the direct part, with the last three indices of the spatial TBME reversed. Following the same steps, we eventually get

$$\sum_{m_{lb}} \langle n_a l_a m_{la}\, n_b l_b m_{lb}|V(r_{12})|n_b l_b m_{lb}\, n_a l_a m_{la}\rangle = S^{\mathrm{C}}_{n_a l_a n_b l_b}|_{\mathrm{E}}, \tag{B.140}$$

where he have defined

$$\begin{aligned} S^{\mathrm{C}}_{n_a l_a n_b l_b}|_{\mathrm{E}} \equiv{}& \frac{1}{4\pi}(2l_b+1) \\ &\times \sum_{n_\mu n_\nu l_\mu} (2l_\mu+1) \begin{pmatrix} l_a & l_b & l_\mu \\ 0 & 0 & 0 \end{pmatrix}^2 T^{(n_\mu l_\mu)}_{(n_a l_a)(n_b l_b)} T^{(n_\nu l_\mu)}_{(n_b l_b)(n_a l_a)} I_{n_\mu n_\nu l_\mu}, \end{aligned} \tag{B.141}$$

where the quantity I is defined in (B.136). Finally, the exchange mean field associated with the central terms writes

$$\boxed{\Gamma^{\mathrm{C}}_{aa}|_{\mathrm{E}} = \sum_{n_b l_b t_b} (2M + H - (2B+W)\delta_{q_a q_b}) S^{\mathrm{C}}_{n_a l_a n_b l_b}|_{\mathrm{E}}.} \tag{B.142}$$

Note that the ranges of values taken by the quantum numbers n_μ, n_ν and l_μ appearing in the equations above can easily be deduced from (B.213) and (B.223). In the expressions (B.137) and (B.142), we have not performed the summation on the isospin with the future purpose of separating the proton and neutron contributions.

4.2.2. Density-dependent contribution

Let us continue with the derivation of the direct mean field associated with the density-dependent term. The density-dependent term is given by (B.42), where we now use the shorthand notation for the spin-isospin part (B.129), which is precisely the one of the central terms. The spatial and spin-isospin degrees of freedom split up in such a way that

$$\Gamma^{\mathrm{DD}}_{aa}|_{\mathrm{D}} = \sum_{r_b u_b} \langle r_a r_b|V(r_{12})D[\rho]|r_a r_b\rangle\langle u_a u_b|\mathcal{P}|u_a u_b\rangle. \tag{B.143}$$

Since the spin-isospin part of the density-dependent term is exactly the same as the one of the central terms (B.133), we immediately find

$$\sum_{s_b} \langle s_a t_a\, s_b t_b|\mathcal{P}_{\mathrm{D}}|s_a t_a\, s_b t_b\rangle = 2W + B - (2H+M)\delta_{t_a t_b}. \tag{B.144}$$

On the other hand, the spatial TBMEs associated with the density-dependent term have been calculated in (B.46). Integrating the angular parts of the integrals appearing in (B.46) and using the definition of the integral over three spherical harmonics (B.212), along with with the properties of the Wigner-3j symbols, permits to simplify the spatial part according to

$$\sum_{m_{lb}} \langle n_a l_a m_{la}\, n_b l_b m_{lb}|V(r_{12})D[\rho]|n_a l_a m_{la}\, n_b l_b m_{lb}\rangle = S^{\mathrm{DD}}_{n_a l_a n_b l_b}|_{\mathrm{D}}, \tag{B.145}$$

where he have defined

$$S^{\mathrm{DD}}_{n_a l_a n_b l_b}|_{\mathrm{D}} \equiv \frac{1}{4\pi}(2l_b+1) \sum_{n_\mu n_\nu} T^{(n_\mu 0)}_{(n_a l_a)(n_a l_a)} T^{(n_\nu 0)}_{(n_b l_b)(n_b l_b)} \frac{1}{2}\Big[J_{n_\mu n_\nu 0} + J_{n_\nu n_\mu 0}\Big], \tag{B.146}$$

with the integral

$$J_{nn'l} = K\lambda_{(n'l)} \int_0^\infty \mathrm{d}r\, r^2 \phi_{(00)}(r)\phi_{(nl)}(r)\rho^\alpha(r)\phi_{(00)}(r, b\sqrt{g})\phi_{(n'l)}(r, b\sqrt{g}), \tag{B.147}$$

which is nothing but the integral appearing in (B.50), with $l_\mu = l_\nu$, that we have already evaluated numerically.

Finally, the direct mean field associated with the density-dependent term writes

$$\boxed{\Gamma^{\mathrm{DD}}_{aa}|_{\mathrm{D}} = \sum_{n_b l_b t_b} (2W + B - (2H + M)\delta_{t_a t_b}) S^{\mathrm{DD}}_{n_a l_a n_b l_b}|_{\mathrm{D}}.} \tag{B.148}$$

The calculation of the exchange mean field associated with the density-dependent term is similar. We obtain

$$\Gamma^{\mathrm{C}}_{aa}|_{\mathrm{E}} = \sum_{r_b u_b} \langle r_a r_b | V(r_{12}) D[\rho] | r_b r_a \rangle \langle u_a u_b | \mathcal{P} | u_b u_a \rangle. \tag{B.149}$$

Since the spin-isospin part of the density-dependent term is exactly the same as the one of the central terms (B.139), we immediately find

$$\sum_{s_b} \langle s_a t_a\, s_b t_b | \mathcal{P} | s_b t_b\, s_a t_a \rangle = 2M + H - (2B + W)\delta_{t_a t_b}. \tag{B.150}$$

The exchange spatial part is obtained in the same way as the direct part, with the last three indices of the spatial TBME reversed. Following the same steps, we eventually get

$$\sum_{m_{lb}} \langle n_a l_a m_{la}\, n_b l_b m_{lb} | V(r_{12}) D[\rho] | n_b l_b m_{lb}\, n_a l_a m_{la} \rangle = S^{\mathrm{DD}}_{n_a l_a n_b l_b}|_{\mathrm{E}}, \tag{B.151}$$

where he have defined

$$\begin{aligned} S^{\mathrm{DD}}_{n_a l_a n_b l_b}|_{\mathrm{E}} \equiv{}& \frac{1}{4\pi}(2l_b + 1) \sum_{n_\mu n_\nu l_\mu} (2l_\mu + 1) \\ &\times \begin{pmatrix} l_a & l_b & l_\mu \\ 0 & 0 & 0 \end{pmatrix}^2 T^{(n_\mu l_\mu)}_{(n_a l_a)(n_b l_b)} T^{(n_\nu l_\mu)}_{(n_b l_b)(n_a l_a)} \frac{1}{2}\Big[J_{n_\mu n_\nu l_\mu} + J_{n_\nu n_\nu l_\mu}\Big], \end{aligned} \tag{B.152}$$

where the integral J is defined in (B.147). Finally, the exchange mean field associated with the density-dependent term writes

$$\boxed{\Gamma^{\mathrm{DD}}_{aa}|_{\mathrm{E}} = \sum_{n_b l_b q_b} (2M + H - (2B + W)\delta_{q_a q_b}) S^{\mathrm{DD}}_{n_a l_a n_b l_b}|_{\mathrm{E}}.} \tag{B.153}$$

Note that the ranges of values taken by the quantum numbers n_μ, n_ν and l_μ appearing in the equations above can easily be deduced from (B.213) and (B.223). As for the central terms, in the expressions (B.148) and (B.153), we have not performed the summation on the isospin with the future purpose of separating the proton and neutron contributions.

4.2.3. Tensor contribution

We now look at the derivation of the direct mean field associated with the tensor term. The tensor interaction is given by (B.68), where we use the shorthand notation for the spin-isospin part,

$$\mathcal{P} \equiv W - HP_\tau. \tag{B.154}$$

Separating the spatial and spin-isospin degrees of freedom, we obtain

$$\Gamma^{\mathrm{T}}_{aa}|_{\mathrm{D}} = \sum_{r_b u_b} \langle r_a r_b|V(r_{12})[\hat{r}_{12}\otimes\hat{r}_{12}]^{(2)}_{-k}|r_a r_b\rangle\langle u_a u_b|\mathcal{P}[\vec{\sigma}_1\otimes\vec{\sigma}_2]^{(2)}_{k}|u_a u_b\rangle. \tag{B.155}$$

Let us evaluate the spin-isospin TBMEs of the tensor term. The isospin TBMEs are trivial and read, in general,

$$\langle t_a t_b|\mathcal{P}|t_c t_d\rangle = W\delta_{t_a t_c}\delta_{t_b t_d} - H\delta_{t_a t_d}\delta_{t_b t_c}. \tag{B.156}$$

As for the spin TBMEs, we have calculated their general expression in (D.20). In the particular case of the HFR approximation, this expression reduces to

$$\langle s_a s_b|[\vec{\sigma}_1\otimes\vec{\sigma}_2]^{(2)}_{k}|s_a s_b\rangle = 4\sqrt{\frac{2}{3}}s_a s_c\delta_{k,0}, \tag{B.157}$$

so that the spin part of the tensor direct mean field vanishes, i.e.

$$\sum_{s_b}\langle s_a s_b|[\vec{\sigma}_1\otimes\vec{\sigma}_2]^{(2)}_{k}|s_a s_b\rangle = 0. \tag{B.158}$$

Thus, at the HFR approximation, the direct tensor mean field is zero.

The calculation of the exchange mean field associated with the tensor term is similar. We obtain

$$\Gamma^{\mathrm{T}}_{aa}|_{\mathrm{E}} = \sum_{r_b u_b} \langle r_a r_b|V(r_{12})[\hat{r}_{12}\otimes\hat{r}_{12}]^{(2)}_{-k}|r_b r_a\rangle\langle u_a u_b|\mathcal{P}[\vec{\sigma}_1\otimes\vec{\sigma}_2]^{(2)}_{k}|u_b u_a\rangle. \tag{B.159}$$

Again, from equation (D.20), we deduce the following spin TBMEs at the HFB approximation,

$$\langle s_a s_b|[\vec{\sigma}_1\otimes\vec{\sigma}_2]^{(2)}_{k}|s_b s_a\rangle = 4\sqrt{\frac{2}{3}}s_a s_c\delta_{k,0}(\delta_{s_a s_b} + \delta_{s_a,-s_b}), \tag{B.160}$$

so that the spin part of the tensor exchange mean field vanishes as well, i.e.

$$\sum_{s_b}\langle s_a s_b|[\vec{\sigma}_1\otimes\vec{\sigma}_2]^{(2)}_{k}|s_b s_a\rangle = 0. \tag{B.161}$$

Thus, at the HFR approximation, the exchange tensor mean field is also zero. It follows that, *the tensor mean field vanishes at the HFR approximation.*[3] It is therefore not necessary to calculate the spatial contribution to the tensor mean field.

4.2.4. Spin–orbit contribution

Finally, we discuss the derivation of the direct mean field associated with the spin–orbit term. The spin–orbit interaction is given by (B.89), where we now use the shorthand notation for the spin-isospin part (B.154), which is precisely the one of the tensor term. Separating the spatial and spin-isospin degrees of freedom, we obtain

$$\Gamma^{\mathrm{SO}}_{aa}|_{\mathrm{D}} = \sum_{r_b u_b} \langle r_a r_b|V(r_{12})[\vec{r}_{12}\otimes\vec{\nabla}_{12}]^{(1)}_{-k}|r_a r_b\rangle\langle u_a u_b|\mathcal{P}[\vec{\sigma}_1+\vec{\sigma}_2]^{(1)}_{k}|u_a u_b\rangle. \tag{B.162}$$

3. Here, the HFR approximation is essential to infer that the tensor term gives no contribution. Indeed, at the less restrictive HF approximation, the (exchange) tensor mean field does not vanish.

Let us evaluate the spin-isospin TBMEs of the spin–orbit term. The isospin TBMEs are precisely the ones of the tensor term (B.156). As for the spin TBME, we have calculated their general expression in (D.22). In the particular case of the HFR approximation, this expression reduces to

$$\langle s_a s_b|[\vec{\sigma}_1+\vec{\sigma}_2]^{(1)}_k|s_a s_b\rangle = 2(s_a+s_b)\delta_{k,0}, \tag{B.163}$$

so that the spin part of the spin-orbit direct mean field simply reads

$$\sum_{s_b}\langle s_a s_b|[\vec{\sigma}_1\otimes\vec{\sigma}_2]^{(2)}_k|s_a s_b\rangle = 4s_a\delta_{k,0}. \tag{B.164}$$

The calculation of the exchange mean field associated with the spin–orbit term is similar. We obtain

$$\Gamma^{\mathrm{SO}}_{aa}|_{\mathrm{E}} = \sum_{r_b u_b}\langle r_a r_b|V(r_{12})[\vec{r}_{12}\otimes\vec{\nabla}_{12}]^{(1)}_{-k}|r_b r_a\rangle\langle u_a u_b|\mathcal{P}[\vec{\sigma}_1+\vec{\sigma}_2]^{(1)}_k|u_b u_a\rangle. \tag{B.165}$$

Again, from equation (D.22), we deduce the following spin TBMEs at the HFB approximation,

$$\langle s_a s_b|[\vec{\sigma}_1+\vec{\sigma}_2]^{(1)}_k|s_b s_a\rangle = 2(s_a+s_b)\delta_{s_a s_b}\delta_{k,0}, \tag{B.166}$$

so that the spin part of the spin–orbit exchange mean field vanishes, i.e.

$$\sum_{s_b}\langle s_a s_b|[\vec{\sigma}_1+\vec{\sigma}_2]^{(1)}_k|s_b s_a\rangle = 0. \tag{B.167}$$

Thus, *at the HFR approximation, the spin–orbit exchange mean field is zero*, since its spin part is. This is not the case of the direct mean field; its spin part does not vanish and there is no reason for the spatial part to vanish either. The only thing we can infer regarding the direct space part is that $k=0$ since we can deduce from the ranges of values taken by the quantum numbers appearing in (B.114) and (B.115), that $k = m_{lc}+m_{ld}-m_{la}-m_{lb}$. If we were considering the spin–orbit interaction at the HFR approximation in the fitting code, we should then evaluate its direct mean-field contribution, but we neglect it, as stated earlier.

4.3. Rearrangement field

At the HFR approximation, the rearrangement field is given by (B.125). Only the density-dependent term has such a non-zero rearrangement field since it is the only term that explicitly depends on the local nuclear density. By definition (A.25), in the spherical HO representation, this density can be written

$$\rho(\vec{r}) = \sum_{\sigma\tau}\sum_{ab}\Phi^*_a(\vec{r},\sigma,\tau)\Phi_b(\vec{r},\sigma,\tau)\rho_{ba}, \tag{B.168}$$

where the wave functions are the ones of the spherical HO, defined by (B.2). Thus, the rearrangement field involves the derivative

$$\begin{aligned}\frac{\partial\rho(\vec{r})}{\partial\rho_{aa}} &= \sum_{\sigma\tau}\Phi^*_a(\vec{r},\sigma,\tau)\Phi_a(\vec{r},\sigma,\tau)\\ &= \phi^*_{r_a}(\vec{r})\phi_{r_a}(\vec{r}),\end{aligned} \tag{B.169}$$

where we have used the orthogonality of the spin and isospin wave functions (contained in (B.4)) when going from the first to the second line. Then, it appears that the rearrangement field is independent of the isospin t_a. Because of this property, we will in fact not need to calculate the rearrangement field for the quantities we are interested in, as we will see.

5. Hartree–Fock restricted energy

At the HFR approximation, the total energy of the nucleus is given by (B.119). In this section, we shall then evaluate both its kinetic and potential contributions.

5.1. Kinetic energy

At the HFR approximation, the kinetic energy is given by (B.120). Explicitly,

$$\mathcal{E}_{\rm K}^{\rm HFR} \equiv \sum_a K_{aa}\rho_{aa} = \sum_{\substack{n_a l_a m_{la} \\ s_a t_a}} \frac{\hbar\omega}{2}\Big(2n_a + l_a + \frac{3}{2}\Big)\rho_{aa}, \tag{B.170}$$

where we have used the expression of the kinetic field derived in (B.127). We end up with

$$\boxed{\begin{aligned}\mathcal{E}_{\rm K}^{\rm HFR} = 2\sum_{(n_a l_a)_\pi}(2l_a+1)\Big(2n_a + l_a + \frac{3}{2}\Big)\frac{\hbar\omega}{2} \\ + 2\sum_{(n_a l_a)_\nu}(2l_a+1)\Big(2n_a + l_a + \frac{3}{2}\Big)\frac{\hbar\omega}{2}.\end{aligned}} \tag{B.171}$$

The degeneracy factor $2(2l_a+1)$ appears because a given state has the same kinetic energy no matter the values of its quantum numbers s_a and m_{la}, at the origin of factors 2 and $(2l_a+1)$, respectively. Note that the summations concern the proton π and neutron ν occupied states (n_a, l_a), in the spherical HO basis. We will need this kinetic energy for the oxygen ^{16}O and zirconium ^{90}Zr. By adding the successive contributions of each shell up to the proton and neutron Fermi levels according to the above relation, we eventually obtain

$$\mathcal{E}_{\rm K}^{\rm HFR}\Big[^{16}{\rm O}\Big]/(A=16) = \frac{9}{8}\hbar\omega, \tag{B.172a}$$

$$\mathcal{E}_{\rm K}^{\rm HFR}\Big[^{90}{\rm Zr}\Big]/(A=90) = \frac{71}{36}\hbar\omega, \tag{B.172b}$$

where we have normalized the kinetic energies by the number of nucleons A in the corresponding nuclei.

5.2. Potential energy

At the HFR approximation, the potential energy is given by (B.122). For the sake of clarity, we will decompose the potential energy into a direct and an exchange component in the following, as $\mathcal{E}_{\rm P} \equiv \mathcal{E}_{\rm P}|_{\rm D} + \mathcal{E}_{\rm P}|_{\rm E}$, where

$$\mathcal{E}_{\rm P}|_{\rm D} \equiv \frac{1}{2}\sum_a \Gamma_{aa}|_{\rm D}\rho_{aa}, \tag{B.173a}$$

$$\mathcal{E}_{\rm P}|_{\rm E} \equiv \frac{1}{2}\sum_a \Gamma_{aa}|_{\rm E}\rho_{aa}. \tag{B.173b}$$

It is now necessary to evaluate these contributions for the fields of the generalized Gogny interaction (II.1). Note that in the following, we will use the notation

$$\widetilde{S}_{n_a l_a n_b l_b} \equiv (2l_a+1)S_{n_a l_a n_b l_b}, \tag{B.174}$$

for the direct and exchange contributions of both the central and density-dependent terms, since they do not explicitly depend on the quantum number m_{la}.

5.2.1. Central contribution

Let us start by deriving the direct component of the potential energy associated with the central terms. We have, using (B.137),

$$\begin{aligned}\mathcal{E}_{\mathrm{P}}^{\mathrm{D}}|_{\mathrm{D}} &\equiv \frac{1}{2}\sum_{a}\Gamma_{aa}^{\mathrm{D}}|_{\mathrm{D}}\rho_{aa},\\ &= \frac{1}{2}\sum_{s_a t_a t_b}\sum_{n_a l_a}\sum_{n_b l_b}(2M+B-(2H+M)\delta_{t_a t_b})\widetilde{S}^{\mathrm{C}}_{n_a l_a n_b l_b}|_{\mathrm{D}}.\end{aligned} \tag{B.175}$$

Separating the proton and neutron shells, we obtain, in the general case of an asymmetric nucleus,

$$\begin{aligned}\mathcal{E}_{\mathrm{P}}^{\mathrm{D}}|_{\mathrm{D}} = {}& (2W+B-2H-M)\sum_{(n_a l_a)_\pi}\sum_{(n_b l_b)_\pi}\widetilde{S}^{\mathrm{C}}_{n_a l_a n_b l_b}|_{\mathrm{D}}\\ &+(2W+B-2H-M)\sum_{(n_a l_a)_\nu}\sum_{(n_b l_b)_\nu}\widetilde{S}^{\mathrm{C}}_{n_a l_a n_b l_b}|_{\mathrm{D}}\\ &+2(2W+B)\sum_{(n_a l_a)_\pi}\sum_{(n_b l_b)_\nu}\widetilde{S}^{\mathrm{C}}_{n_a l_a n_b l_b}|_{\mathrm{D}},\end{aligned} \tag{B.176}$$

where we have taken advantage of the symmetry of the quantity $S^{\mathrm{C}}_{n_a l_a n_b l_b}|_{\mathrm{D}}$ under the exchange of indices $(n_a, l_a) \leftrightarrow (n_b, l_b)$, and where the summations over $(n_a l_a)_\pi$ and $(n_b l_b)_\nu$ run over the full set of quantum numbers characterizing the states occupied by protons π and neutrons ν. When the nucleus is symmetric, this set is the same for both proton and neutron quantum numbers. Then, the potential energy becomes

$$\boxed{\mathcal{E}_{\mathrm{P}}^{\mathrm{D}}|_{\mathrm{D}} = (4W+2B-2H-M)F^{\mathrm{D}}[X],} \tag{B.177}$$

where we have defined (X denoting the nucleus under study),

$$F^{\mathrm{D}}[X] \equiv 2\sum_{(n_a l_a)_\pi}\sum_{(n_b l_b)_\nu}\widetilde{S}^{\mathrm{C}}_{n_a l_a n_b l_b}|_{\mathrm{D}}. \tag{B.178}$$

This identity holds for the symmetric ^{16}O, but, in principle, not for the asymmetric ^{90}Zr. Let us now consider an asymmetric nucleus that has more neutrons than protons, i.e. $\nu_{\max} = \pi_{\max} + \nu_+$, where $\nu_{\max}$ and $\pi_{\max}$ are the numbers of neutrons and protons respectively, and where ν_+ is the neutron excess. This choice is conventional, the proton excess is treated in a similar way. From equation (B.176), we get

$$\begin{aligned}\mathcal{E}_{\mathrm{P}}^{\mathrm{D}}|_{\mathrm{D}} = {}& 2(4W+2B-2H-M)\sum_{(n_a l_a)_\pi}\sum_{(n_b l_b)_\nu}\widetilde{S}^{\mathrm{C}}_{n_a l_a n_b l_b}|_{\mathrm{D}}\\ &+(2W+B-2H-M)\sum_{(n_a l_a)_{\nu=\pi_{\max}+1}}^{\nu_{\max}}\sum_{(n_b l_b)_{\nu=\pi_{\max}+1}}^{\nu_{\max}}\widetilde{S}^{\mathrm{C}}_{n_a l_a n_b l_b}|_{\mathrm{D}}.\end{aligned} \tag{B.179}$$

We observe that a new contribution, proportional to $(2W+B-2H-M)$, is added in the case of an asymmetric nucleus. However, this contribution is negligible compared to that of $(4W+2B-2H-M)$ for weakly asymmetric nuclei like the ^{90}Zr, since then $\nu_+ - 1 \ll \nu_{\max}, \pi_{\max}$. As a consequence, we will legitimately assume that the identity (B.177) also holds for the ^{90}Zr.

The calculation of the exchange component of the potential energy associated with the central terms is similar. We obtain, using (B.142),

$$\begin{aligned}\mathcal{E}_{\mathrm{P}}^{\mathrm{C}}|_{\mathrm{E}} &\equiv \frac{1}{2}\sum_{a}\Gamma_{aa}^{\mathrm{D}}|_{\mathrm{E}}\rho_{aa},\\ &= \frac{1}{2}\sum_{s_a t_a t_b}\sum_{n_a l_a}\sum_{n_b l_b}(2M+B-(2H+M)\delta_{t_a t_b})\widetilde{S}^{\mathrm{C}}_{n_a l_a n_b l_b}|_{\mathrm{E}}.\end{aligned} \tag{B.180}$$

For a symmetric nucleus like the ^{16}O, we end up with

$$\boxed{\mathcal{E}_{\mathrm{P}}^{\mathrm{C}}|_{\mathrm{E}} = (4M+2H-2B-W)F^{\mathrm{E}}[X],} \tag{B.181}$$

where we have defined (X denoting the nucleus under study),

$$F^{\mathrm{E}}[X] \equiv 2\sum_{(n_a l_a)_\pi}\sum_{(n_b l_b)_\nu}\widetilde{S}^{\mathrm{C}}_{n_a l_a n_b l_b}|_{\mathrm{E}}, \tag{B.182}$$

while, for an asymmetric nucleus with a neutron excess, we find

$$\begin{aligned}\mathcal{E}_{\mathrm{P}}^{\mathrm{C}}|_{\mathrm{E}} &= 2(4M+2H-2B-W)\sum_{(n_a l_a)_\pi}\sum_{(n_b l_b)_\nu}\widetilde{S}^{\mathrm{C}}_{n_a l_a n_b l_b}|_{\mathrm{E}}\\ &+ (2M+H-2B-W)\sum_{(n_a l_a)_{\nu=\pi_{\max}+1}}^{\nu_{\max}}\sum_{(n_b l_b)_{\nu=\pi_{\max}+1}}^{\nu_{\max}}\widetilde{S}^{\mathrm{C}}_{n_a l_a n_b l_b}|_{\mathrm{E}}.\end{aligned} \tag{B.183}$$

Here again, the contribution proportional to $(2M+H-2B-W)$ is negligible compared to that of $(4M+2H-2B-W)$ for weakly asymmetric nuclei like the ^{90}Zr. We will then assume that the identity (B.181) also holds for the ^{90}Zr.

5.2.2. Density-dependent contribution

The procedure introduced above is similar for the density-dependent interaction. Using (B.148), we find that the direct component of the potential energy associated with the density-dependent term reads

$$\begin{aligned}\mathcal{E}_{\mathrm{P}}^{\mathrm{DD}}|_{\mathrm{D}} &\equiv \frac{1}{2}\sum_{a}\Gamma_{aa}^{\mathrm{DD}}|_{\mathrm{D}}\rho_{aa},\\ &= \frac{1}{2}\sum_{s_a t_a t_b}\sum_{n_a l_a}\sum_{n_b l_b}(2M+B-(2H+M)\delta_{t_a t_b})\widetilde{S}^{\mathrm{DD}}_{n_a l_a n_b l_b}|_{\mathrm{D}}.\end{aligned} \tag{B.184}$$

Separating the proton and neutron shells, we obtain, in the general case of an asymmetric nucleus,

$$\begin{aligned}\mathcal{E}_{\mathrm{P}}^{\mathrm{DD}}|_{\mathrm{D}} &= (2W+B-2H-M)\sum_{(n_a l_a)_\pi}\sum_{(n_b l_b)_\pi}\widetilde{S}^{\mathrm{DD}}_{n_a l_a n_b l_b}|_{\mathrm{D}}\\ &+ (2W+B-2H-M)\sum_{(n_a l_a)_\nu}\sum_{(n_b l_b)_\nu}\widetilde{S}^{\mathrm{DD}}_{n_a l_a n_b l_b}|_{\mathrm{D}}\\ &+ 2(2W+B)\sum_{(n_a l_a)_\pi}\sum_{(n_b l_b)_\nu}\widetilde{S}^{\mathrm{DD}}_{n_a l_a n_b l_b}|_{\mathrm{D}},\end{aligned} \tag{B.185}$$

where we have taken advantage of the symmetry of the quantity $S^{\mathrm{DD}}_{n_a l_a n_b l_b}|_{\mathrm{D}}$ under the exchange of indices $(n_a, l_a) \leftrightarrow (n_b, l_b)$. When the nucleus is symmetric, this set is the same for both proton and neutron quantum numbers. Then, the potential energy becomes

$$\boxed{\mathcal{E}_{\mathrm{P}}^{\mathrm{DD}}|_{\mathrm{D}} = 2(4W+2B-2H-M)\sum_{(n_a l_a)_\pi}\sum_{(n_b l_b)_\nu}\widetilde{S}^{\mathrm{DD}}_{n_a l_a n_b l_b}|_{\mathrm{D}}.} \tag{B.186}$$

Following the procedure developed for the central terms, we find, for an asymmetric nucleus with a neutron excess,

$$\begin{aligned}\mathcal{E}_{\mathrm{P}}^{\mathrm{DD}}|_{\mathrm{D}} &= 2(4W+2B-2H-M)\sum_{(n_al_a)_\pi}\sum_{(n_bl_b)_\nu}\widetilde{S}^{\mathrm{DD}}_{n_al_an_bl_b}|_{\mathrm{D}} \\ &\quad+(2W+B-2H-M)\sum_{(n_al_a)_{\nu=\pi_{\max}+1}}^{\nu_{\max}}\sum_{(n_bl_b)_{\nu=\pi_{\max}+1}}^{\nu_{\max}}\widetilde{S}^{\mathrm{DD}}_{n_al_an_bl_b}|_{\mathrm{D}}.\end{aligned} \tag{B.187}$$

As it was the case for the central terms, we observe that a new contribution, proportional to $(2W+B-2H-M)$, is added in the case of an asymmetric nucleus. Here again, we will neglect this contribution for weakly asymmetric nuclei like the ^{90}Zr, so that the relation (B.186) holds for this nucleus as well.

The calculation of the exchange component of the potential energy associated with the density-dependent is similar. We obtain, using (B.153),

$$\begin{aligned}\mathcal{E}_{\mathrm{P}}^{\mathrm{DD}}|_{\mathrm{E}} &\equiv \frac{1}{2}\sum_a \Gamma^{\mathrm{DD}}_{aa}|_{\mathrm{E}}\rho_{aa}, \\ &= \frac{1}{2}\sum_{s_aq_aq_b}\sum_{n_al_a}\sum_{n_bl_b}(2M+B-(2H+M)\delta_{q_aq_b})\widetilde{S}^{\mathrm{DD}}_{n_al_an_bl_b}|_{\mathrm{E}}.\end{aligned} \tag{B.188}$$

For a symmetric nucleus like the ^{16}O, we end up with

$$\boxed{\mathcal{E}_{\mathrm{P}}^{\mathrm{DD}}|_{\mathrm{E}} = 2(4M+2H-2B-W)\sum_{(n_al_a)_\pi}\sum_{(n_bl_b)_\nu}\widetilde{S}^{\mathrm{DD}}_{n_al_an_bl_b}|_{\mathrm{E}},} \tag{B.189}$$

while, for an asymmetric nucleus with a neutron excess, we find

$$\begin{aligned}\mathcal{E}_{\mathrm{P}}^{\mathrm{DD}}|_{\mathrm{E}} &= 2(4M+2H-2B-W)\sum_{(n_al_a)_\pi}\sum_{(n_bl_b)_\nu}\widetilde{S}^{\mathrm{DD}}_{n_al_an_bl_b}|_{\mathrm{E}} \\ &\quad+(2M+H-2B-W)\sum_{(n_al_a)_{\nu=\pi_{\max}+1}}^{\nu_{\max}}\sum_{(n_bl_b)_{\nu=\pi_{\max}+1}}^{\nu_{\max}}\widetilde{S}^{\mathrm{DD}}_{n_al_an_bl_b}|_{\mathrm{E}}.\end{aligned} \tag{B.190}$$

Here again, the contribution proportional to $(2M+H-2B-W)$ is negligible compared to that of $(4M+2H-2B-W)$ for weakly asymmetric nuclei like the ^{90}Zr. We will then assume that the identity (B.188) also holds for the ^{90}Zr.

5.2.3. Tensor contribution

We have shown in subsection B.4.2.3 that the mean field associated with the tensor interaction vanishes at the HFR approximation. Thus, the tensor interaction does not contribute to the HFR potential energy $\mathcal{E}_{\mathrm{P}}^{\mathrm{HFR}}$.

5.2.4. Spin–orbit contribution

We have shown in subsection B.4.2.4 that the exchange mean field associated with the spin–orbit interaction vanishes at the HFR approximation. Thus, it brings no contribution to the potential energy. However, the direct mean field is not zero and may then contribute to the potential energy. By definition, this direct component of the potential energy associated with the spin–orbit term reads

$$\mathcal{E}_{\mathrm{P}}^{\mathrm{SO}}|_{\mathrm{D}} \equiv \frac{1}{2}\sum_a \Gamma^{\mathrm{SO}}_{aa}|_{\mathrm{D}}\rho_{aa}. \tag{B.191}$$

According to (B.164), the spin part of the above potential energy reads

$$\sum_{s_a} 4 s_a \delta_{k,0} = 0. \tag{B.192}$$

Thus, *the potential energy associated with the spin–orbit interaction vanishes at the HFR approximation*, since the spin parts of both its direct and exchange components are zero. Even if the spin–orbit interaction had been considered at the HFR approximation, it would have provided no contribution to the potential energy $\mathcal{E}_{\rm P}^{\rm HFR}$.

6. Calculation of the energy difference $\Delta\varepsilon$

One of the quantities constrained in the fitting code is the energy difference between the neutron and proton $2s_{1/2}$ states in the calcium ^{48}Ca, at the HFR approximation, that we write as

$$\Delta\varepsilon \equiv \varepsilon^{\nu}_{2s_{1/2}} - \varepsilon^{\pi}_{2s_{1/2}}, \tag{B.193}$$

where ε denotes the individual energy of the corresponding state at the HFR approximation, given by (B.126). At this approximation, neither the kinetic field given by (B.127), nor the rearrangement field (see equation (B.169) and the discussion below), depend on the isospin. Thus, only the neutron and proton mean fields contribute to $\Delta\varepsilon$, in such a way that

$$\Delta\varepsilon = \Gamma^{\nu}_{2s_{1/2}} - \Gamma^{\pi}_{2s_{1/2}}. \tag{B.194}$$

It is now necessary to evaluate these contributions for the fields of the generalized Gogny interaction (II.1).

6.1. Central interaction

Let us start by evaluating the contribution to this energy difference $\Delta\varepsilon$ coming from the central terms. It is

$$\Delta\varepsilon^{\rm C} = \Gamma^{{\rm C}\,\nu}_{2s_{1/2}} - \Gamma^{{\rm C}\,\pi}_{2s_{1/2}}, \tag{B.195}$$

where the expressions of the central mean fields will be deduced from (B.137) and (B.142). These contributions eventually furnish, after filling the shells, for the neutron mean field,

$$\begin{aligned}\Gamma^{{\rm C}\,\nu}_{2s_{1/2}} = \sum_{(n_b l_b)_\nu} \Big[&\Big(2W + B - (2H + M)\Big)\widetilde{S}^{\rm C}_{10\,n_b l_b}|_{\rm D} \\ &- \Big(2M + H - (2B + W)\Big)\widetilde{S}^{\rm C}_{10\,n_b l_b}|_{\rm E}\Big] \\ + \sum_{(n_b l_b)_\pi} \Big[&(2W + B)\widetilde{S}^{\rm C}_{10\,n_b l_b}|_{\rm D} - (2M + H)\widetilde{S}^{\rm C}_{10\,n_b l_b}|_{\rm E}\Big],\end{aligned} \tag{B.196}$$

and, for the proton mean field,

$$\begin{aligned}\Gamma^{{\rm C}\,\pi}_{2s_{1/2}} = &\sum_{(n_b l_b)_\nu} \Big[(2W + B)\widetilde{S}^{\rm C}_{10\,n_b l_b}|_{\rm D} - (2M + H)\widetilde{S}^{\rm C}_{10\,n_b l_b}|_{\rm E}\Big] \\ &+ \sum_{(n_b l_b)_\pi} \Big[\Big(2W + B - (2H + M)\Big)\widetilde{S}^{\rm C}_{10\,n_b l_b}|_{\rm D} \\ &\qquad - \Big((2M + H) - (2B + W)\Big)\widetilde{S}^{\rm C}_{10\,n_b l_b}|_{\rm E}\Big].\end{aligned} \tag{B.197}$$

Gathering the results, we obtain

$$\begin{aligned}\Delta\varepsilon^{\mathrm{C}} = &-(2H+M)\left[\sum_{(n_b l_b)_\nu}\widetilde{S}^{\mathrm{C}}_{10\,n_b l_b}|_{\mathrm{D}} - \sum_{(n_b l_b)_\pi}\widetilde{S}^{\mathrm{C}}_{10\,n_b l_b}|_{\mathrm{D}}\right]\\ &+(2B+W)\left[\sum_{(n_b l_b)_\nu}\widetilde{S}^{\mathrm{C}}_{10\,n_b l_b}|_{\mathrm{E}} - \sum_{(n_b l_b)_\pi}\widetilde{S}^{\mathrm{C}}_{10\,n_b l_b}|_{\mathrm{E}}\right].\end{aligned} \tag{B.198}$$

The ^{48}Ca has twenty protons and twenty-eight neutrons. The proton Fermi level is therefore $2s$ ($n=1, l=0$), which is saturated, and the neutron Fermi level $1f$ ($n=0, l=3$), which contains eight neutrons among the fourteen available slots. Then, the central contribution to the energy difference (B.193) reads

$$\boxed{\Delta\varepsilon^{\mathrm{C}} = (2H+M)f_{\mathrm{D}} + (2B+W)f_{\mathrm{E}},} \tag{B.199}$$

where we have defined

$$f_{\mathrm{D}} \equiv -\frac{4}{7}\widetilde{S}^{\mathrm{C}}_{10\,03}|_{\mathrm{D}}, \tag{B.200a}$$

$$f_{\mathrm{E}} \equiv +\frac{4}{7}\widetilde{S}^{\mathrm{C}}_{10\,03}|_{\mathrm{E}}, \tag{B.200b}$$

with the prefactors traducing the occupation of the neutron Fermi level.

6.2. Density-dependent interaction

The calculation of the contribution from the density-dependent term to $\Delta\varepsilon$ is similar to the central terms. We have

$$\Delta\varepsilon^{\mathrm{DD}} = \Gamma^{\mathrm{DD}\,\nu}_{2s_{1/2}} - \Gamma^{\mathrm{DD}\,\pi}_{2s_{1/2}}, \tag{B.201}$$

where the expressions of the density-dependent mean fields will be deduced from (B.148) and (B.153). We eventually find out, in a similar way we have done for the central terms,

$$\boxed{\Delta\varepsilon^{\mathrm{DD}} = (2H+M)g_{\mathrm{D}} + (2B+W)g_{\mathrm{E}},} \tag{B.202}$$

where we have defined

$$g_{\mathrm{D}} \equiv -\frac{4}{7}\widetilde{S}^{\mathrm{DD}}_{10\,03}|_{\mathrm{D}}, \tag{B.203a}$$

$$g_{\mathrm{E}} \equiv +\frac{4}{7}\widetilde{S}^{\mathrm{DD}}_{10\,03}|_{\mathrm{E}}. \tag{B.203b}$$

6.3. Tensor interaction

We have shown in subsection B.4.2.3 that the mean field associated with the tensor interaction vanishes at the HFR approximation. Thus, the tensor interaction does not contribute to the energy difference $\Delta\varepsilon$ at this approximation, $\Delta\varepsilon^{\mathrm{T}} = 0$.

6.4. Spin–orbit interaction

We have shown in subsection B.4.2.4 that the exchange mean field associated with the spin–orbit interaction vanishes at the HFR approximation, but the direct one does not. Then, the spin–orbit interaction contributes to the energy difference $\Delta\varepsilon$ at the HFR approximation, $\Delta\varepsilon^{\mathrm{SO}} \neq 0$. As already mentioned, we neglect this contribution in the fitting procedure. Otherwise, it should have been taken into account while distinguishing the HO states by their quantum numbers j, projections of the total angular momentum.

7. Formulas for the spherical symmetry

In this section, we give the main formulas used to carry out the above calculations in the framework of the spherical harmonic oscillator representation. We will not attempt to justify the developments leading to those and refer the reader in particular to [175, 181] for more detailed presentations.

7.1. Spherical harmonics

The spherical harmonics considered in the spherical HO wave functions (B.3) are conventionally defined as

$$Y_l^{m_l}(\theta,\varphi) \equiv (-)^{m_l}\sqrt{\frac{(2l+1)}{4\pi}\frac{(l-m_l)!}{(l+m_l)!}}P_l^{m_l}(\cos\theta)\,\mathrm{e}^{\mathrm{i}m_l\varphi}, \tag{B.204}$$

where $P_l^{m_l}(\cos\theta)$ are the associated Legendre polynomials. By definition, the spherical harmonics satisfy the orthogonality relation

$$\int \mathrm{d}^2\hat{r}\, Y_l^{m_l}(\hat{r})Y_{l'}^{m_l'*}(\hat{r}) = \delta_{ll'}\delta_{m_l m_l'}, \tag{B.205}$$

as well as the so-called addition theorem

$$\sum_{m_l} Y_l^{m_l*}(\hat{r})Y_l^{m_l}(\hat{r}) = \frac{2l+1}{4\pi}, \tag{B.206}$$

where we recall the notation for the angular variables, $\hat{r} = (\theta,\varphi)$, and where we have used the reality condition

$$Y_l^{m_l*}(\hat{r}) = (-)^{m_l}Y_l^{-m_l}(\hat{r}). \tag{B.207}$$

In the calculations, we often met the spherical harmonics (B.204) with their quantum numbers equal to zero. They simply read

$$Y_0^0(\hat{r}) = \frac{1}{\sqrt{4\pi}}. \tag{B.208}$$

One shows that the spherical harmonics can be written as a product of irreducible tensors of the form [238]

$$Y_l^{m_l}(\hat{r}) = \frac{1}{r^l}\sqrt{\frac{1}{4\pi}\frac{(2l+1)!}{2^l(l!)^2}}\Big[\ldots[[\vec{r}\otimes\vec{r}]^{(2)}\otimes\vec{r}]^{(3)}\ldots\otimes\vec{r}\Big]^l_{m_l}. \tag{B.209}$$

In the particular case $l = 1$, useful for tensor calculations, this relation brings

$$Y_1^{m_l}(\hat{r}) = \frac{1}{r}\sqrt{\frac{3}{4\pi}}r^{m_l}, \tag{B.210}$$

and in the particular case $l = 2$, useful for spin–orbit calculations,

$$Y_2^{m_l}(\hat{r}) = \frac{1}{r^2}\sqrt{\frac{15}{8\pi}}[\vec{r}\otimes\vec{r}]^{(2)}_{m_l}. \tag{B.211}$$

Finally, the integral of the product of three spherical harmonics reads

$$\int \mathrm{d}^2\hat{r}\, Y_{l_a}^{m_{la}*}(\hat{r}) Y_{l_\mu}^{m_{l\mu}*}(\hat{r}) Y_{l_c}^{m_{lc}}(\hat{r}) = (-)^{m_{lc}} \sqrt{\frac{(2l_a+1)(2l_\mu+1)(2l_c+1)}{4\pi}} \times \begin{pmatrix} l_a & l_\mu & l_c \\ 0 & 0 & 0 \end{pmatrix} \begin{pmatrix} l_a & l_\mu & l_c \\ m_{la} & m_{l\mu} & -m_{lc} \end{pmatrix}, \tag{B.212}$$

which is non-zero if and only if the conditions

$$m_{li} \leq |l_i| \text{ for } i \in \{a, \mu, c\}, \tag{B.213a}$$
$$|l_a - l_c| \leq l_\mu \leq l_a + l_c, \tag{B.213b}$$
$$m_{l\mu} = -(m_{la} + m_{lc}), \tag{B.213c}$$

imposed by the above Wigner-3j symbols, denoted by the parentheses, are satisfied.

7.2. Action of the gradient operator in spherical symmetry

We can decompose the action of the gradient operator on the spherical harmonic oscillator wave functions according to its components in the spherical basis (see definition (D.14)). Then, each spherical component $\beta = 0, \pm 1$ of the gradient operator acts in the following way on a wave function $\phi_r(\vec{r}) = \phi_{(n,l)}(r) Y_l^{m_l}(\hat{r})$ [181],

$$\nabla_\beta \phi_r(\vec{r}) \equiv \sum_{j=\pm 1} (-)^{l+m_l+\beta+1} \begin{pmatrix} l & 1 & l+j \\ m_l & \beta & -m_l-\beta \end{pmatrix} g_j^l(r) \phi_{(n,l)}(r) Y_{l+j}^{m_l+\beta}(\hat{r}), \tag{B.214}$$

where the operator $g_j^l(r)$ is defined by

$$g_j^l(r) \equiv j\sqrt{l + \frac{1}{2}(j+1)} \left[\frac{\mathrm{d}}{\mathrm{d}r} - j\frac{l(j-1)}{r} \right]. \tag{B.215}$$

Using the definition of the spherical HO wave functions (B.3), it is not difficult to prove the recurrence relation

$$g_j^l(r)\phi_{(n,l)}(r) = \frac{1}{b}\Big[a_j^{(n,l)} \phi_{(n-j,l+j)}(r) + c_j^{(n,l)} \phi_{(n,l+j)}(r) \Big], \tag{B.216}$$

with the coefficients

$$\begin{aligned} a_j^{(n,l)} &\equiv -\sqrt{\Big(n - \frac{1}{2}(j-1)\Big)\Big(l + \frac{1}{2}(j+1)\Big)}, \\ c_j^{(n,l)} &\equiv -\sqrt{\Big(n + l + \frac{1}{2}(j+1)\Big)\Big(l + \frac{1}{2}(j+1)\Big)}. \end{aligned} \tag{B.217}$$

Combining equations (B.214) and (B.216) leads to the final form of the gradient formula, i.e. for $\beta = 0, \pm 1$,

$$\nabla_\beta \phi_r(\vec{r}) = \frac{1}{b} \sum_{j=\pm 1} (-)^{l+m_l+\beta+1} \begin{pmatrix} l & 1 & l+j \\ m_l & \beta & -m_l-\beta \end{pmatrix} \times \Big[a_j^{(n,l)} \phi_{n-j,l+j,m_l+\beta}(\vec{r}) + c_j^{(n,l)} \phi_{n,l+j,m_l+\beta}(\vec{r}) \Big]. \tag{B.218}$$

7.3. Talman coefficients in spherical symmetry

The Gogny separable development [181] (see section D.3 for a quick presentation) applied on spherical HO wave functions provides the relation

$$\boxed{\phi^*_{r_a}(\vec{r})\phi_{r_b}(\vec{r}) = \sum_{r_\mu} T^{(r_\mu)}_{(r_a)(r_b)} \langle l_a m_{la}|Y^{m_{l\mu}*}_{l_\mu}|l_b m_{lb}\rangle \phi_0(\vec{r})\phi_{r_\mu}(\vec{r}),} \tag{B.219}$$

where, by definition,

$$\langle l_a m_{la}|Y^{m_{l\mu}*}_{l_\mu}|l_b m_{lb}\rangle \equiv \int \mathrm{d}^2\hat{r}\, Y^{m_{la}*}_{l_a}(\hat{r}) Y^{m_{l\mu}*}_{l_\mu}(\hat{r}) Y^{m_{lb}}_{l_b}(\hat{r}), \tag{B.220}$$

with the integral over three spherical harmonics given in (B.212), and where it appears a coefficient called the spherical Talman coefficient, that reads

$$\boxed{\begin{aligned} T^{(r_\mu)}_{(r_a)(r_b)} &= (-)^{n_\mu} N^{(r_\mu)}_{(r_a)(r_b)} \sum_{ij} \frac{(-)^{i+j}}{i!(n_a-i)!j!(n_b-j)!} \\ &\times \frac{\Gamma\left[\frac{1}{2}(l_a+l_b+l_\mu)+i+j+3/2\right]\Gamma\left[\frac{1}{2}(l_a+l_b-l_\mu)+i+j+1\right]}{\Gamma[l_a+i+3/2]\,\Gamma[l_b+j+3/2]\,\Gamma\left[\frac{1}{2}(l_a+l_b-l_\mu)-n_\mu+i+j+1\right]}, \end{aligned}} \tag{B.221}$$

with

$$\boxed{N^{(r_\mu)}_{(r_a)(r_b)} \equiv \left[2\pi^{3/2}\frac{n_a!\,\Gamma[n_a+l_a+3/2]\,n_b!\,\Gamma[n_b+l_b+3/2]}{n_\mu!\,\Gamma[n_\mu+l_\mu+3/2]}\right]^{1/2}.} \tag{B.222}$$

The spherical Talman coefficient is non-zero if and only if the following inequalities are satisfied,

$$\max\left(0, \frac{|N_a-N_b|-l_\mu}{2}\right) \leq n_\mu \leq \frac{N_a+N_b-l_\mu}{2}, \tag{B.223}$$

with $X_a \equiv 2n_a + l_a$.

7.4. Moshinsky coefficients in spherical symmetry

The Moshinsky transformation allows us to move from the nucleon coordinates $(\vec{r}_1, \vec{r}_2)$ to the relative and center-of-mass coordinates $(\vec{r}, \vec{R})$, defined as [4]

$$\vec{r} \equiv \frac{\vec{r}_1 - \vec{r}_2}{\sqrt{2}}, \quad \text{and} \quad \vec{R} \equiv \frac{\vec{r}_1 + \vec{r}_2}{\sqrt{2}}. \tag{B.224}$$

The Moshinky transformation applied on spherical HO wave functions furnishes the relation

$$\boxed{\phi_{r_\mu}(\vec{r}_1)\phi_{r_\nu}(\vec{r}_2) = \sum_{r_\lambda r_\sigma} M^{r_\lambda r_\sigma}_{r_\mu r_\nu} \phi_{r_\lambda}(\vec{R})\phi_{r_\sigma}(\vec{r}),} \tag{B.225}$$

4. This convention is important; another definition of the relative and center-of-mass coordinates $(\vec{r}, \vec{R})$ would bring a different expression of the Moshinsky coefficient.

where it appears a coefficient called the spherical Moshinsky coefficient, that reads [175] [5]

$$\boxed{M^{r_\lambda r_\sigma}_{r_\mu r_\nu} = \sum_{r_a r_b}\sum_{r_c r_d}(-)^{X_d}\left(\frac{1}{\sqrt{2}}\right)^{X_a+X_b+X_c+X_d} C^{r_\mu *}_{r_a r_c} C^{r_\nu *}_{r_b r_d} C^{r_\lambda}_{r_a r_b} C^{r_\sigma}_{r_c r_d},} \tag{B.227}$$

with

$$\boxed{C^{r_\mu}_{r_a r_b} \equiv (-)^{n_a+n_b-n_\mu} N^{(r_\mu)}_{(r_a)(r_b)} \langle l_\mu m_{l\mu} | Y^{m_{la}}_{l_a} | l_b m_{lb}\rangle \delta_{X_\mu, X_a+X_b},} \tag{B.228}$$

where $N^{(r_\mu)}_{(r_a)(r_b)}$ is given by (B.222).

One can show that the spherical Moshinsky coefficient implies

$$n_\sigma = \frac{X_\mu + X_\nu - X_\lambda - l_\sigma}{2}, \tag{B.229}$$

as well as

$$m_{l\sigma} = m_{l\mu} + m_{l\nu} - m_{l\lambda}, \tag{B.230}$$

while the range of values taken by r_λ is only constrained by $m_{l\lambda} \leq |l_\lambda|$. Thus, the summation over r_σ in (B.225) actually corresponds to a simple summation over l_σ.

In the case $r_\lambda = 0$, the spherical Moshinsky coefficient simplifies according to

$$\boxed{\begin{aligned} M^{0\, r_\sigma}_{r_\mu r_\nu} &= (-)^{l_\mu - l_\nu + l_\sigma/2}\sqrt{4\pi}\left(\frac{1}{\sqrt{2}}\right)^{X_\mu+X_\nu} \\ &\times \left[\frac{2}{\sqrt{\pi}}\frac{n_\sigma!\,\Gamma(n_\sigma + l_\sigma + 3/2)}{n_\mu!\,\Gamma(n_\mu + l_\mu + 3/2) n_\nu!\,\Gamma(n_\nu + l_\nu + 3/2)}\right]^{1/2} \langle l_\sigma m_{l\sigma} | Y^{m_{l\mu}}_{l_\mu} | l_\nu m_{l\nu}\rangle, \end{aligned}} \tag{B.231}$$

which implies

$$n_\sigma = \frac{X_\mu + X_\nu - l_\sigma}{2}, \tag{B.232}$$

and

$$m_{l\sigma} = m_{l\mu} + m_{l\nu}. \tag{B.233}$$

In the case $r_\mu = r_\nu = 0$, the spherical Moshinsky coefficient reduces to

$$\boxed{M^{r_\lambda r_\sigma}_{0\,0} = \delta_{r_\lambda, 0}\delta_{r_\sigma, 0}.} \tag{B.234}$$

5. In his article about the separable development [181], Gogny uses the convention of Baranger and Davies [239] for the Moshinsky coefficient. Its Moshinsky coefficient that we call $M^{r_\lambda r_\sigma}_{r_\mu r_\nu}|_{\mathrm{G}}$, is linked to ours by the relation

$$M^{r_\lambda r_\sigma}_{r_\mu r_\nu}|_{\mathrm{G}} = (-)^{l_\lambda + l_\sigma - m_{l\lambda}} M^{r_\lambda r_\sigma}_{r_\mu r_\nu}. \tag{B.226}$$

Appendix C

Axial symmetry

> « Chaque fois que la science avance d'un pas, c'est qu'un imbécile la pousse, sans le faire exprès. »
>
> — Émile Zola, *La joie de vivre*

In this appendix, we deal with the Hartree–Fock–Bogoliubov fields of the generalized Gogny interaction in a two-center axially symmetric harmonic oscillator representation. These fields are the building blocks necessary to set up the above-mentioned formalism and to deduce various quantities of interest. After a brief presentation on the properties of the axial wave functions and the symmetries of the related fields in the first section, we derive these latter one by one, including the newly introduced finite-range tensor and spin–orbit fields, in a second section. The last section essentially recalls some useful formulas for these calculations.

Chapter contents

The first section introduces the axial harmonic oscillator (HO) states considered in the calculations as well as the symmetries of the Hartree–Fock–Bogoliubov (HFB) fields that will be taken up to simplify the search for their expressions. The second section is devoted to the derivation of these fields, for both the common central and density-dependent terms [175, 176], and the newly introduced finite-range tensor and spin–orbit interactions. The derivation of the central and density-dependent fields is not the focus of this work, but has the merit of smoothly introducing the methods used to derive the tensor and spin-orbit fields, while proposing generalized expressions that do not impose time reversal invariance. We also detail how the integrals involved in the mean- and pairing fields can be evaluated, analytically or numerically depending on the case. We eventually specify the new expressions of these fields when time-reversal invariance is imposed (as in the `HFB3` code we use in this thesis). For the central and density-dependent fields, we consistently recover the expressions found by Chappert [17]. Finally, some useful formulas for the axial symmetry are given in the last section [175, 176].

1. Preliminary considerations

1.1. Axial harmonic oscillator wave functions

As explained, the HFB quasiparticle states will be expanded on a harmonic oscillator (HO) wave function basis whose states are characterized by the set of quantum numbers

$$|a\rangle = |j_a r_a u_a\rangle = |j_a m_a \nu_a t_a s_a\rangle = |j_a m_a n_{\perp a} n_{za} t_a \Omega_a\rangle, \tag{C.1}$$

where the triplet $r_a = (m_a, \nu_a) = (m_a, n_{\perp a}, n_{za})$ specifies the orbitals of the axial HO, while the doublet $u_a = (t_a = \pm 1/2, s_a = \pm 1/2)$ corresponds to the projections of the spin and the isospin along the quantization axis, chosen to be Oz, respectively. Equivalently, since these states display an axial symmetry about Oz, they are eigenstates of the corresponding total angular momentum J_z. Thus, we can specify our HO state by the projection of J_z, namely $\Omega_a \equiv m_a + s_a$, rather than by the quantum number s_a. As for the quantum number j_a, it defines the shift from the origin, along Oz, of the wave function.

The axially symmetric HO wave function then takes the form

$$\Phi_a(\vec{r}, \sigma, \tau) \equiv \langle \vec{r}\tau\sigma|a\rangle = \phi_{j_a r_a}(\vec{r})\xi_{s_a}(\sigma)\zeta_{t_a}(\tau), \tag{C.2}$$

where $\xi_{s_a}(\sigma)$ and $\zeta_{t_a}(\tau)$ are the (normalized) spin and isospin wave functions, associated with σ and τ, the Pauli matrices describing the spin and isospin degrees of freedom,

respectively, and where the spatial axial wave functions are decomposed, in cylindrical coordinates $\vec{r} = (\vec{r}_\perp, z) = (r_\perp, \varphi, z)$, into

$$\phi_{j_a r_a}(\vec{r}) \equiv \phi_{m_a n_{\perp a}}(\vec{r}_\perp)\phi_{j_a n_{za}}(z), \tag{C.3}$$

The first function is a two-dimensional radial HO wave function, which depends on the direction $\vec{r}_\perp$ perpendicular to the symmetry axis Oz, and reads

$$\phi_{m_a n_{\perp a}}(\vec{r}_\perp) \equiv \frac{1}{b_\perp\sqrt{\pi}}\left[\frac{n_{\perp a}!}{(n_{\perp a}+|m_a|)!}\right]^{1/2} \mathrm{e}^{-r_\perp^2/2b_\perp^2}\left(\frac{r_\perp}{b_\perp}\right)^{|m_a|} L_{n_{\perp a}}^{|m_a|}\left(\frac{r_\perp^2}{b_\perp^2}\right)\mathrm{e}^{\mathrm{i}m_a\varphi}, \tag{C.4}$$

where $L_{n_{\perp a}}^{|m_a|}(r_\perp^2/b_\perp^2)$ denotes the generalized Laguerre polynomial. The second function is an off-center one-dimensional wave function along z that reads

$$\phi_{j_a n_{za}}(z) = \phi_{n_{za}}(z - d_{j_a}) \equiv \frac{1}{(b_z\sqrt{\pi})^{1/2}}\frac{1}{(2^{n_{za}}n_{za}!)^{1/2}}\mathrm{e}^{-(z-d_{j_a})^2/2b_z^2} H_{n_{za}}\left(\frac{z-d_{j_a}}{b_z}\right), \tag{C.5}$$

where $H_{n_{za}}((z-d_{j_a})/b_z)$ denotes the (off-center) Hermite polynomial. Note that we either specify the position of the center with the index j_a or directly with the distance d_{j_a} in the argument of the wave function (but not both at the same time).

We impose the axial HO wave functions to satisfy the orthogonality relation

$$\sum_{\sigma\tau}\int \mathrm{d}^3r\, \Phi_a^*(\vec{r},\sigma,\tau)\Phi_b(\vec{r},\sigma,\tau) = \delta_{r_a r_b}\delta_{s_a s_b}\delta_{t_a t_b}. \tag{C.6}$$

The oscillator lengths appearing in the HO wave functions are linked to the HO parameters $\beta_\perp$ and β_z, and the oscillator frequencies $\hbar\omega_\perp$ and $\hbar\omega_z$, by the relations

$$b_\perp = \frac{1}{\sqrt{\beta_\perp}} = \sqrt{\frac{\hbar}{m\omega_\perp}}, \tag{C.7a}$$

$$b_z = \frac{1}{\sqrt{\beta_z}} = \sqrt{\frac{\hbar}{m\omega_z}}, \tag{C.7b}$$

where m is the mass of the nucleus under study. In the following, we will often meet the above HO wave functions with their quantum numbers equal to zero. For convenience, we write them down once and for all,

$$\phi_{00}(\vec{r}_\perp) = \frac{1}{b_\perp\sqrt{\pi}}\mathrm{e}^{-r_\perp^2/2b_\perp^2}, \tag{C.8a}$$

$$\phi_{j_a 0}(z) = \frac{1}{(b_z\sqrt{\pi})^{1/2}}\mathrm{e}^{-(z-d_{j_a})^2/2b_z^2}. \tag{C.8b}$$

Most of the time, we will simply write $\phi_{j_a 0}(\vec{r}) = \phi_{00}(\vec{r}_\perp)\phi_{j_a 0}(z)$ the corresponding axial HO wave function, with $0 = (0,0,0)$ as index. At some point, we will also need the radial HO wave functions without their angular dependence, that is to say the quantities

$$\widetilde{\phi}_{|m_a| n_{\perp a}}(r_\perp) \equiv \mathrm{e}^{-\mathrm{i}m_a\varphi}\phi_{m_a n_{\perp a}}(\vec{r}_\perp). \tag{C.9}$$

Finally, we can define the HO wave functions deprived of their exponential, i.e.

$$\hat{\phi}_{m_a n_{\perp a}}(r_\perp) \equiv \mathrm{e}^{r_\perp^2/2b_\perp^2}\widetilde{\phi}_{m_a n_{\perp a}}(r_\perp), \tag{C.10a}$$

$$\hat{\phi}_{j_a n_{za}}(z) \equiv \mathrm{e}^{(z-d_a)^2/2b_z^2}\phi_{j_a n_{za}}(z), \tag{C.10b}$$

where we have additionally removed the angular dependence in the radial wave function according to (C.9).

1.2. Properties and symmetries of the harmonic oscillator states

One important property of the harmonic oscillator states (C.1) we are considering is the way they transform under the time-reversal operator T. By definition, [1]

$$T|a\rangle \equiv |\overline{a}\rangle \equiv \sigma_a|-a\rangle, \tag{C.14}$$

where the factor σ_a corresponds to the double of the projection of the spin along the Oz axis according to (D.6), namely $\sigma_a \equiv 2s_a$, with the current notations. Note that we have removed the constant $\hbar$ since we do not need to deal with it at this stage. We have also set

$$|-a\rangle \equiv |j_a - m_a n_{\perp a} n_{za} t_a - \Omega_a\rangle. \tag{C.15}$$

Let us now define what we call the simplex operator S,

$$S \equiv \Pi\, \mathrm{e}^{-\mathrm{i}\pi J_y}, \tag{C.16}$$

where Π is the parity operator and $J_y \equiv L_y + S_y$ the total angular momentum operator along Oy, decomposed into orbital L_y and intrinsic S_y momentum operators. The quantity $\mathrm{e}^{-\mathrm{i}\pi J_y}$ corresponds to a rotation of an angle π about the Oy axis in full space (coordinate plus spin spaces). The axial coordinates are then transformed according to $(r_\perp, \varphi, z) \to (r_\perp, -\varphi + \pi, z)$, which has, according to (C.3), the following effect

$$\mathrm{e}^{-\mathrm{i}\pi L_y}|j_a m_a n_{\perp a} n_{za} t_a \Omega_a\rangle = (-)^{m_a + n_{za}}|j_a - m_a n_{\perp a} n_{za} t_a \Omega_a\rangle. \tag{C.17}$$

As for the parity operator, it corresponds to a reflection along all coordinates, i.e. in axial coordinates, to the coordinates transformation $(r_\perp, \varphi, z) \to (r_\perp, \varphi + \pi, -z)$. With (C.3), we then get

$$\Pi|a\rangle = (-)^{m_a + n_{za}}|a\rangle. \tag{C.18}$$

Combining results (C.12), (C.17) and (C.18), we finally have

$$S|a\rangle = \sigma_a|-a\rangle. \tag{C.19}$$

Thus, we see that the simplex operator and the time-reversal operator have the same action of the axial HO states, such that

$$\boxed{S_T|a\rangle \equiv TS^{-1}|a\rangle = |a\rangle,} \tag{C.20}$$

where we have defined the T-simplex operator S_T. In other words, the axial HO states remain invariant under the T-simplex operator, this is a symmetry of the system characterized by its state $|a\rangle$.

1. Actually, this result arises naturally if we consider the usual definition of the time-reversal operator,

$$T \equiv K\mathrm{e}^{-\mathrm{i}\pi S_y}, \tag{C.11}$$

where K is the complex conjugation operator and S_y the spin operator along Oy. On the one hand, using Euler's formula in terms of Pauli matrices, we get $\mathrm{e}^{-\mathrm{i}\pi S_y} = -\mathrm{i}\sigma_y$, where σ_y is the Pauli matrix defined in (D.2). The matrix representation of σ_y and $|s_a\rangle$ directly provides

$$\mathrm{e}^{-\mathrm{i}\pi S_y}|s_a\rangle = \sigma_a|-s_a\rangle. \tag{C.12}$$

On the other hand, the definition of the axial HO wave functions (C.3) brings

$$K|j_a m_a \nu_a t_a s_a\rangle = |j_a - m_a \nu_a t_a s_a\rangle. \tag{C.13}$$

Combining these results, we obtain (C.14).

1.3. Symmetries of the Hartree–Fock–Bogoliubov fields

Finally we give the symmetries of the HFB fields we have introduced in the previous subsection. We will indeed exploit these symmetries in the next section to considerably simplify the calculation of the fields.

First, since we have considered a Bogoliubov transformation (III.1) which preserves the quantum numbers Ω and t, the density matrices and the pairing tensor defined in terms of the matrices of this transformation (III.4) themselves preserve these quantum numbers. In other words, they are diagonal in Ω and t in the chosen basis, what we write as

$$\rho_{ab} = \delta_{\Omega_a\Omega_b}\delta_{t_at_b}\rho^{t_a\Omega_a}_{m_a\nu_a,\,m_b\nu_b}, \tag{C.21a}$$
$$\overline{\rho}_{ab} = \delta_{\Omega_a\Omega_b}\delta_{t_at_b}\overline{\rho}^{t_a\Omega_a}_{m_a\nu_a,\,m_b\nu_b}, \tag{C.21b}$$
$$\kappa_{ab} = \delta_{\Omega_a\Omega_b}\delta_{t_at_b}\kappa^{t_a\Omega_a}_{m_a\nu_a,\,m_b\nu_b}, \tag{C.21c}$$

where we recall that the superscripts identify, in our convention, the conserved quantum numbers. Plugging these expressions in the various HFB fields, and taking into account that the nuclear interaction v_{12} is invariant under a full rotation (in both coordinate and spin spaces) and under a rotation in the isospin space (see equations (I.7) and (I.11)), we find out that the fields preserve the quantum numbers Ω and t as well. Explicitly,

$$\Gamma_{ab} = \delta_{\Omega_a\Omega_b}\delta_{t_at_b}\Gamma^{t_a\Omega_a}_{m_a\nu_a,\,m_b\nu_b}, \tag{C.22a}$$
$$\overline{\Gamma}_{ab} = \delta_{\Omega_a\Omega_b}\delta_{t_at_b}\overline{\Gamma}^{t_a\Omega_a}_{m_a\nu_a,\,m_b\nu_b}, \tag{C.22b}$$
$$\Delta_{ab} = \delta_{\Omega_a\Omega_b}\delta_{t_at_b}\Delta^{t_a\Omega_a}_{m_a\nu_a,\,m_b\nu_b}, \tag{C.22c}$$
$$\partial\Gamma_{ab} = \delta_{\Omega_a\Omega_b}\delta_{t_at_b}\partial\Gamma^{t_a\Omega_a}_{m_a\nu_a,\,m_b\nu_b}, \tag{C.22d}$$
$$\partial\overline{\Gamma}_{ab} = \delta_{\Omega_a\Omega_b}\delta_{t_at_b}\partial\overline{\Gamma}^{t_a\Omega_a}_{m_a\nu_a,\,m_b\nu_b}, \tag{C.22e}$$
$$\partial\Delta_{ab} = \delta_{\Omega_a\Omega_b}\delta_{t_at_b}\partial\Delta^{t_a\Omega_a}_{m_a\nu_a,\,m_b\nu_b}, \tag{C.22f}$$
$$\partial\overline{\Delta}_{ab} = \delta_{\Omega_a\Omega_b}\delta_{t_at_b}\partial\overline{\Delta}^{t_a\Omega_a}_{m_a\nu_a,\,m_b\nu_b}. \tag{C.22g}$$

Let us continue by analyzing how the fields transform when their indices are interchanged. We start with the mean field (III.37), by noticing that

$$\begin{aligned}\Gamma_{ba} &= \sum_{cd>0}\left[\langle bc|v_{12}^{(\mathrm{a})}|ad\rangle\rho_{dc} + \langle b\overline{c}|v_{12}^{(\mathrm{a})}|a\overline{d}\rangle\overline{\rho}_{cd}\right]\\ &= \sum_{cd>0}\left[\langle bd|v_{12}^{(\mathrm{a})}|ac\rangle\rho_{cd} + \langle b\overline{d}|v_{12}^{(\mathrm{a})}|a\overline{c}\rangle\overline{\rho}_{dc}\right]\\ &= \sum_{cd>0}\left[\langle ac|v_{12}^{(\mathrm{a})}|bd\rangle\rho_{dc} + \langle a\overline{c}|v_{12}^{(\mathrm{a})}|b\overline{d}\rangle\overline{\rho}_{cd}\right] \equiv \Gamma_{ab}.\end{aligned} \tag{C.23}$$

From the first to the second line, we have exchanged the dummy indices c and d, and from the second to the third line, we have used the fact that the two-body matrix elements are real in the axial HO representation (see (III.16)) and that the density matrices are symmetric. The result is obviously the same with the other mean field (III.38). Then, the HFB mean fields are symmetric (under the exchange of their indices).

As for the pairing field (III.32), we have

$$\begin{aligned}\Delta_{ba} &= \sum_{cd>0} \langle b\bar{a}|v_{12}^{(\mathrm{a})}|c\bar{d}\rangle\kappa_{cd} \\ &= \sum_{cd>0} \langle b\bar{a}|v_{12}^{(\mathrm{a})}|d\bar{c}\rangle\kappa_{dc} \\ &= \sum_{cd>0} \langle a\bar{b}|v_{12}^{(\mathrm{a})}|c\bar{d}\rangle\kappa_{dc}. \end{aligned} \tag{C.24}$$

From the first to the second line, we have exchanged the dummy indices c and d, and from the second to the third line, we have used the facts that the interaction is invariant under the exchange of the two particles and time-reversal symmetry, and that the two-body matrix elements are real in the axial HO representation (see (III.14), (III.15) and (III.16)). We emphasize that the HFB pairing field is *not* symmetric as the mean fields are since, in general, the pairing tensor is not symmetric itself, $\kappa_{dc} \neq \kappa_{cd}$ (contrary to the density matrices). It is only when time-reversal invariance is imposed that the pairing tensor becomes symmetric and then the pairing field as well.

The rearrangement fields, whether they are associated with mean fields ((III.42) and (III.43)) or the pairing field ((III.44) and (III.45)), are invariant under the exchange of their indices, i.e.

$$\partial\Gamma_{ab} = \partial\Gamma_{ba}, \tag{C.25a}$$
$$\partial\overline{\Gamma}_{ab} = \partial\overline{\Gamma}_{ba}, \tag{C.25b}$$
$$\partial\Delta_{ab} = \partial\Delta_{ba}, \tag{C.25c}$$
$$\partial\overline{\Delta}_{ab} = \partial\overline{\Delta}_{ba}. \tag{C.25d}$$

Indeed, based on their expressions, they are symmetric if the derivatives $\partial v_{12}^{(\mathrm{a})}/\partial\rho_{ba}$ and $\partial v_{12}^{(\mathrm{a})}/\partial\overline{\rho}_{ba}$ are. They are, since the density matrices are.

2. Derivation of the fields

In this section, we will derive the fields associated with each of the terms of the generalized Gogny interaction (II.1), in the framework outlined in the above section. As far as possible, we will try to make the calculations of these fields independent of one another, so that the reader can follow these notes in the desired order. Nevertheless, comparisons between the results obtained with the various terms will allow us to highlight their similarities and differences.

2.1. Central and density-dependent contributions

In this subsection, we shall derive the various fields associated with the finite-range central and density-dependent terms of the generalized Gogny interaction (II.1). The antisymmetrized finite-range central and density-dependent (CDD) interactions can be encompassed in the following expression,

$$\begin{aligned} v_{12}^{\mathrm{CDD},(\mathrm{a})} &\equiv v_{12}^{\mathrm{CDD}}(1 - P_r P_\sigma P_\tau) \\ &= (W + BP_\sigma - HP_\tau - MP_\sigma P_\tau)V(r_{12})D[\rho](1 - P_r P_\sigma P_\tau) \\ &= \mathcal{P}_{\mathrm{D}}V(r_{12})D[\rho] + \mathcal{P}_{\mathrm{E}}V(r_{12})D[\rho]P_r, \end{aligned} \tag{C.26}$$

with the Gaussian potential

$$V(r_{12}) \equiv \mathrm{e}^{-(\vec{r}_1-\vec{r}_2)^2/\mu^2}, \tag{C.27}$$

and the functional of the density, specific to the density-dependent interaction,

$$D[\rho] \equiv \frac{\rho^\alpha(\vec{r}_1)+\rho^\alpha(\vec{r}_2)}{2}, \tag{C.28}$$

where the local nuclear density is defined in (III.50). The central contributions to the generalized Gogny interaction are obtained by setting $\alpha = 0$ above and summing (C.26) over the central ranges μ_1 and μ_2. To get the density-dependent term, it suffices to choose a third range μ_3 in (C.26), with $\alpha = 1/3$. On the other hand, the spin-isospin components of the direct and exchange CDD fields are respectively

$$\mathcal{P}_\mathrm{D} \equiv W + BP_\sigma - HP_\tau - MP_\sigma P_\tau, \tag{C.29a}$$
$$\mathcal{P}_\mathrm{E} \equiv M + HP_\sigma - BP_\tau - WP_\sigma P_\tau. \tag{C.29b}$$

We notice that the direct components of the CDD fields can be deduced from the exchange ones by replacing W, B, H, M by M, H, B, W and removing the operator P_τ. Thus, in the following, we will start by deriving the exchange CDD fields from which, then, we will deduce the direct ones.

2.1.1. Central and density-dependent mean fields

We start by deriving the mean field Γ, expressed in (III.37), of the central and density-dependent interactions (C.26), which is not time-reversal invariant for the moment. Given that the density matrices (C.21) and the fields (C.22) are diagonal in t and Ω, this CDD mean field can be written

$$\begin{aligned}\Gamma^{t\Omega}_{r_a r_b} = \sum_{\substack{t'\Omega'>0\\ r_c r_d}} \Big[&\langle t s_a r_a \; t' s_c r_c | v_{12}^{\mathrm{CDD,(a)}} | t s_b r_b \; t' s_d r_d \rangle \rho^{t'\Omega'}_{r_d r_c} \\ &+ \langle t s_a r_a \; \overline{t' s_c r_c} | v_{12}^{\mathrm{CDD,(a)}} | t s_b r_b \; \overline{t' s_d r_d} \rangle \overline{\rho}^{t'\Omega'}_{r_c r_d} \Big].\end{aligned} \tag{C.30}$$

Let us first concentrate on the exchange CDD mean field, which reads

$$\begin{aligned}\Gamma^{t\Omega}_{r_a r_b}|_\mathrm{E} = \sum_{\substack{t'\Omega'>0\\ r_c r_d}} \Big[&\langle r_a r_c | V(r_{12}) D[\rho] P_r | r_b r_d \rangle \langle t s_a \; t' s_c | \mathcal{P}_\mathrm{E} | t s_b \; t' s_d \rangle \rho^{t'\Omega'}_{r_d r_c} \\ &+ \sigma_c \sigma_d \langle r_a - r_c | V(r_{12}) D[\rho] P_r | r_b - r_d \rangle \langle t s_a \; t' - s_c | \mathcal{P}_\mathrm{E} | t s_b \; t' - s_d \rangle \overline{\rho}^{t'\Omega'}_{r_c r_d} \Big].\end{aligned} \tag{C.31}$$

Let us try to reduce the range of values taken by the quantum numbers involved in the above matrix elements. We first assume that $\Omega > 0$ (the case $\Omega < 0$ can easily be deduced considering the transformation $\Omega \to -\Omega$). In this case, the projections m_a and m_b are positive or zero (because $\Omega = m_a + s_a = m_b + s_b > 0$, where $s_a = \pm 1/2$ and $s_b = \pm 1/2$) and differ at most from 1 (if $s_a = -s_b$). Then we can set in the following $m_a \equiv m$ and $m_b \equiv m + \lambda$, with $m \geq 0$ and $|\lambda| \leq 1$. Consequently, if we set $s_a \equiv s$, we will have $s_b = s - \lambda$, where $s = \pm 1/2$. In fact, since Γ is symmetric under the exchange of its indices (see equation (C.23)), it is enough to restrict ourselves to $\lambda \in \{0, 1\}$, the case $\lambda = -1$ being deduced from the case $\lambda = 1$ by symmetry.

In the same way, as $\Omega' > 0$, the projections m_c and m_d are positive or zero (because $\Omega' = m_c + s_c = m_d + s_d > 0$, where $s_c = \pm 1/2$ and $s_d = \pm 1/2$) and differ at most from

1 (if $s_c = -s_d$). On the other hand, we know that the central and density-dependent interactions commute with $\vec{L}$ (and $\vec{S}$, as they also commute with $\vec{J}$; see discussion in subsection D.6.1). In other words, these interactions must remain invariant under any rotation in the coordinate space where they behave like scalars. As a consequence, the projections m of L_z (since Oz is the quantization axis) of the ingoing pair and outgoing pair must be equal, that is to say

$$m_a + m_c = m_b + m_d, \qquad \text{in the first matrix element,} \tag{C.32a}$$
$$m_a - m_c = m_b - m_d, \qquad \text{in the second matrix element.} \tag{C.32b}$$

Therefore, we can set $m_d \equiv m'$ and $s_d \equiv s'$, with $m' \geq 0$ and $s' = \pm 1/2$, in the first matrix element of the above equation, which implies, according to the conservation law, $m_c = m' + \lambda$ and $s_c = s' - \lambda$. In the second matrix element, we will rather set $m_c \equiv m'$ and $s_c \equiv s'$, which implies $m_d = m' + \lambda$ and $s_d = s' - \lambda$. The reason for this particular choice will appear later; it allows to simplify the final expression of the direct CDD mean field (see equation (C.41)).

With these notations, the exchange CDD mean field becomes

$$\begin{aligned}\Gamma^{t\Omega=m+s}_{m\nu_a,\, m+\lambda\,\nu_b}|_{\mathrm{E}} = &\sum_{\substack{t'\Omega'>0\\ m'\nu_c\nu_d}} \\ &\times \Big[\langle m\nu_a\ m'+\lambda\,\nu_c|V(r_{12})D[\rho]P_r|m+\lambda\,\nu_b\ m'\nu_d\rangle \\ &\quad\times\langle ts\ t's'-\lambda|\mathcal{P}_{\mathrm{E}}|ts-\lambda\ t's'\rangle\rho^{t'm'+s'}_{m'\nu_d,\,m'+\lambda\,\nu_c} \\ &+4s'(s'-\lambda)\langle m\nu_a\ -m'\nu_c|V(r_{12})D[\rho]P_r|m+\lambda\,\nu_b\ -(m'+\lambda)\,\nu_d\rangle \\ &\quad\times\langle ts\ t'-s'|\mathcal{P}_{\mathrm{E}}|ts-\lambda\ t'-(s'-\lambda)\rangle\overline{\rho}^{t'm'+s'}_{m'\nu_c,\,m'+\lambda\,\nu_d}\Big].\end{aligned} \tag{C.33}$$

Let us first focus on the spin-isospin part. We set

$$X^{(+)ts\lambda}_{\Omega'm'\nu_d\nu_c}|_{\mathrm{E}} \equiv \sum_{t'}\langle ts\ t's'-\lambda|\mathcal{P}_{\mathrm{E}}|ts-\lambda\ t's'\rangle\rho^{t'm'+s'}_{m'\nu_d,\,m'+\lambda\,\nu_c}, \tag{C.34a}$$
$$X^{(-)ts\lambda}_{\Omega'm'\nu_c\nu_d}|_{\mathrm{E}} \equiv \sum_{t'}4s'(s'-\lambda)\langle ts\ t'-s'|\mathcal{P}_{\mathrm{E}}|ts-\lambda\ t'-(s'-\lambda)\rangle\overline{\rho}^{t'm'+s'}_{m'\nu_c,\,m'+\lambda\,\nu_d}, \tag{C.34b}$$

in the first and second matrix elements respectively. Using the expression of $\mathcal{P}_{\mathrm{E}}$, given by (C.29), we can evaluate the above spin-isospin matrix elements. We find

$$X^{(+)ts\lambda}_{\Omega'm'\nu_d\nu_c}|_{\mathrm{E}} = \sum_{t'}\Big[(M-B\delta_{tt'})\delta_{\lambda,0}+(H-W\delta_{tt'})\delta_{ss'}\Big]\rho^{t'm'+s'}_{m'\nu_d,\,m'+\lambda\,\nu_c}, \tag{C.35a}$$
$$X^{(-)ts\lambda}_{\Omega'm'\nu_c\nu_d}|_{\mathrm{E}} = \sum_{t'}\Big[(M-B\delta_{tt'})\delta_{\lambda,0}+(H-W\delta_{tt'})(1-4s\lambda)\delta_{s+s',\lambda}\Big]\overline{\rho}^{t'm'+s'}_{m'\nu_c,\,m'+\lambda\,\nu_d}. \tag{C.35b}$$

Now, setting

$$R^{(+)ts\lambda}_{m'\nu_d\nu_c}|_{\mathrm{E}} \equiv \sum_{\Omega'}\Theta(\Omega')X^{(+)ts\lambda}_{\Omega'm'\nu_d\nu_c}|_{\mathrm{E}} = \sum_{s'=\pm s}\Theta(m'+s')X^{(+)ts\lambda}_{m'+s'm'\nu_d\nu_c}|_{\mathrm{E}}, \tag{C.36a}$$
$$R^{(-)ts\lambda}_{m'\nu_c\nu_d}|_{\mathrm{E}} \equiv \sum_{\Omega'}\Theta(\Omega')X^{(-)ts\lambda}_{\Omega'm'\nu_c\nu_d}|_{\mathrm{E}} = \sum_{s'=\pm s}\Theta(m'+s')X^{(-)ts\lambda}_{m'+s'm'\nu_c\nu_d}|_{\mathrm{E}}, \tag{C.36b}$$

we end up with

$$\boxed{\begin{aligned} R^{(+)ts\lambda}_{m'\nu_d\nu_c}|_{\mathrm{E}} &= \sum_{t'}\Big\{\Theta(m'+s)\Big[(M-B\delta_{tt'})\delta_{\lambda,0}+(H-W\delta_{tt'})\Big]\rho^{t'm'+s}_{m'\nu_d,\,m'+\lambda\,\nu_c} \\ &\quad+\Theta(m'-s)(M-B\delta_{tt'})\delta_{\lambda,0}\rho^{t'm'-s}_{m'\nu_d,\,m'+\lambda\,\nu_c}\Big\}, \end{aligned} \tag{C.37a}$$

$$\boxed{\begin{aligned} R^{(-)ts\lambda}_{m'\nu_c\nu_d}|_{\mathrm{E}} &= \sum_{t'}\Big\{\Theta(m'+s)\Big[(M-B\delta_{tt'})\delta_{\lambda,0}-(H-W\delta_{tt'})\delta_{\lambda,2s}\Big]\overline{\rho}^{t'm'+s}_{m'\nu_c,\,m'+\lambda\,\nu_d} \\ &\quad+\Theta(m'-s)\Big[H+M-(W+B)\delta_{tt'}\Big]\delta_{\lambda,0}\overline{\rho}^{t'm'-s}_{m'\nu_c,\,m'+\lambda\,\nu_d}\Big\}, \end{aligned} \tag{C.37b}$$

and the exchange CDD mean field can be written

$$\boxed{\begin{aligned} \Gamma^{t\Omega=m+s}_{m\nu_a,\,m+\lambda\,\nu_b}|_{\mathrm{E}} &= \sum_{\substack{m'\geq 0\\ \nu_c\nu_d}}\Big[\langle m\nu_a\ m'+\lambda\,\nu_c|V(r_{12})F[\rho]|m'\nu_d\ m+\lambda\,\nu_b\rangle R^{(+)ts\lambda}_{m'\nu_d\nu_c}|_{\mathrm{E}} \\ &\quad+\langle m\nu_a\ -m'\nu_c|V(r_{12})D[\rho]|-(m'+\lambda)\,\nu_d\ m+\lambda\,\nu_b\rangle R^{(-)ts\lambda}_{m'\nu_c\nu_d}|_{\mathrm{E}}\Big], \end{aligned} \tag{C.38}$$

where we have replaced the summations $\sum_{m'}\sum_{\Omega'>0}$ by $\sum_{m'\geq 0}\sum_{\Omega'}\Theta(\Omega')$ and applied the operator P_r.

To get the direct CDD mean field out of the exchange one, it suffices to exchange W, B, H, M by M, H, B, W and omit the operator P_r. The latter is therefore

$$\begin{aligned} \Gamma^{t\Omega=m+s}_{m\nu_a,\,m+\lambda\,\nu_b}|_{\mathrm{D}} &= \sum_{\substack{m'\geq 0\\ \nu_c\nu_d}}\Big[\langle m\nu_a\ m'+\lambda\,\nu_c|V(r_{12})D[\rho]|m+\lambda\,\nu_b\ m'\nu_d\rangle R^{(+)ts\lambda}_{m'\nu_d\nu_c}|_{\mathrm{D}} \\ &\quad+\langle m\nu_a\ -m'\nu_d|V(r_{12})D[\rho]|m+\lambda\,\nu_b\ -(m'+\lambda)\,\nu_c\rangle R^{(-)ts\lambda}_{m'\nu_d\nu_c}|_{\mathrm{D}}\Big], \end{aligned} \tag{C.39}$$

where we have switched the dummy indices ν_c and ν_d in the second matrix element of the right-hand side term. The quantities appearing in the direct CDD mean field are

$$\begin{aligned} R^{(+)ts\lambda}_{m'\nu_d\nu_c}|_{\mathrm{D}} &= \sum_{t'}\Big\{\Theta(m'+s)\Big[(W-H\delta_{tt'})\delta_{\lambda,0}+(B-M\delta_{tt'})\Big]\rho^{t'm'+s}_{m'\nu_d,\,m'+\lambda\,\nu_c} \\ &\quad+\Theta(m'-s)(W-H\delta_{tt'})\delta_{\lambda,0}\rho^{t'm'-s}_{m'\nu_d,\,m'+\lambda\,\nu_c}\Big\}, \end{aligned} \tag{C.40a}$$

$$\begin{aligned} R^{(-)ts\lambda}_{m'\nu_d\nu_c}|_{\mathrm{D}} &= \sum_{t'}\Big\{\Theta(m'+s)\Big[(W-H\delta_{tt'})\delta_{\lambda,0}-(B-M\delta_{tt'})\delta_{\lambda,2s}\Big]\overline{\rho}^{t'm'+s}_{m'\nu_d,\,m'+\lambda\,\nu_c} \\ &\quad+\Theta(m'-s)\Big(W+B-(H+M)\delta_{tt'}\Big)\delta_{\lambda,0}\overline{\rho}^{t'm'-s}_{m'\nu_d,\,m'+\lambda\,\nu_c}\Big\}. \end{aligned} \tag{C.40b}$$

Now, by writing down the two spatial matrix elements involved in the direct CDD mean field, we notice that they are equal, because of the expression of the axial wave functions (C.3) and the fact that they commute with the quantity $V(r_{12})D[\rho]$. This is the reason for our particular choice discussed above (see discussion after (C.31)). The direct CDD mean field is then simplified according to

$$\boxed{\Gamma^{t\Omega=m+s}_{m\nu_a,\,m+\lambda\,\nu_b}|_{\mathrm{D}} = \sum_{\substack{m'\geq 0\\ \nu_c\nu_d}}\langle m\nu_a\ m'+\lambda\,\nu_c|V(r_{12})D[\rho]|m+\lambda\,\nu_b\ m'\nu_d\rangle R^{ts\lambda}_{m'\nu_d\nu_c}|_{\mathrm{D}},} \tag{C.41}$$

where we have

$$R^{ts\lambda}_{m'\nu_d\nu_c}|_{\rm D} \equiv R^{(+)ts\lambda}_{m'\nu_d\nu_c}|_{\rm D} + R^{(-)ts\lambda}_{m'\nu_d\nu_c}|_{\rm D}, \tag{C.42}$$

that is to say,

$$\begin{aligned}
R^{ts\lambda}_{m'\nu_d\nu_c}|_{\rm D} = \sum_{t'} \Big\{ & \Theta(m'+s)\Big[\Big((W - H\delta_{tt'})\delta_{\lambda,0} + (B - M\delta_{tt'})\Big)\rho^{t'm'+s}_{m'\nu_d,\, m'+\lambda\,\nu_c} \\
& + \Big((W - H\delta_{tt'})\delta_{\lambda,0} - (B - M\delta_{tt'})\delta_{\lambda,2s}\Big)\overline{\rho}^{t'm'+s}_{m'\nu_d,\, m'+\lambda\,\nu_c}\Big] \\
& + \Theta(m'-s)\delta_{\lambda,0}\Big[(W - H\delta_{tt'})\rho^{t'm'-s}_{m'\nu_d,\, m'+\lambda\,\nu_c} \\
& + \Big(W + B - (H+M)\delta_{tt'}\Big)\overline{\rho}^{t'm'-s}_{m'\nu_d,\, m'+\lambda\,\nu_c}\Big]\Big\}.
\end{aligned} \tag{C.43}$$

From the boxed equations, we can now explicitly write down the expressions of the direct and exchange CDD mean fields Γ for each value of λ. We recall that these fields are *not* time-reversal invariant. Note also that if $\lambda = 1$, then $s = 1/2$ since the identity $s_b \equiv s - 1 = \pm 1/2$ holds only if $s = 1/2$.

- Exchange CDD mean field Γ for $\lambda = 0$:

$$\begin{aligned}
\Gamma^{t\Omega=m+s}_{m\nu_a,\, m\nu_b}|_{\rm E} = \sum_{\substack{m'\geq 0 \\ \nu_c\overline{\nu}_d}} & \Big[\langle m\nu_a\ m'\nu_c|V(r_{12})D[\rho]|m'\nu_d\ m\nu_b\rangle R^{(+)ts0}_{m'\nu_d\nu_c}|_{\rm E} \\
& + \langle m\nu_a\ -m'\nu_c|V(r_{12})D[\rho]|-m'\nu_d\ m\nu_b\rangle R^{(-)ts0}_{m'\nu_c\nu_d}|_{\rm E}\Big],
\end{aligned} \tag{C.44}$$

where

$$R^{(+)ts0}_{m'\nu_d\nu_c}|_{\rm E} = \sum_{t'} \Big[\Theta(m'+s)\Big(H + M - (W+B)\delta_{tt'}\Big)\rho^{t'm'+s}_{m'\nu_d,\, m'\nu_c} + \Theta(m'-s)(M - B\delta_{tt'})\rho^{t'm'-s}_{m'\nu_d,\, m'\nu_c}\Big], \tag{C.45a}$$

$$R^{(-)ts0}_{m'\nu_c\nu_d}|_{\rm E} = \sum_{t'} \Big[\Theta(m'+s)(M - B\delta_{tt'})\overline{\rho}^{t'm'+s}_{m'\nu_c,\, m'\nu_d} + \Theta(m'-s)\Big(H + M - (W+B)\delta_{tt'}\Big)\overline{\rho}^{t'm'-s}_{m'\nu_c,\, m'\nu_d}\Big]. \tag{C.45b}$$

- Direct CDD mean field Γ for $\lambda = 0$:

$$\Gamma^{t\Omega=m+s}_{m\nu_a,\, m\nu_b}|_{\rm D} = \sum_{\substack{m'\geq 0 \\ \nu_c\overline{\nu}_d}} \langle m\nu_a\ m'\nu_c|V(r_{12})D[\rho]|m\nu_b\ m'\nu_d\rangle R^{ts0}_{m'\nu_d\nu_c}|_{\rm D}, \tag{C.46}$$

where

$$\begin{aligned}
R^{ts0}_{m'\nu_d\nu_c}|_{\rm D} = & \sum_{t'} \Big[\Theta(m'+s)\rho^{t'm'+s}_{m'\nu_d,\, m'\nu_c} + \Theta(m'-s)\overline{\rho}^{t'm'-s}_{m'\nu_d,\, m'\nu_c}\Big] \\
& \times \Big(W + B - (H+M)\delta_{tt'}\Big) \\
& + \Big[\Theta(m'+s)\overline{\rho}^{t'm'+s}_{m'\nu_d,\, m'\nu_c} + \Theta(m'-s)\rho^{t'm'-s}_{m'\nu_d,\, m'\nu_c}\Big](W - H\delta_{tt'}),
\end{aligned} \tag{C.47}$$

Let us note that the quantities $R^{(\pm)ts0}|_{\rm E}$ and $R^{ts0}|_{\rm D}$ are symmetric under the exchange of ν_c and ν_d since the density matrices ρ and $\overline{\rho}$ are symmetric (under the exchange of their indices) and diagonal in m'.

- Exchange CDD mean field Γ for $\lambda = 1$:

$$\boxed{\begin{aligned}\Gamma^{t\Omega=m+1/2}_{m\nu_a,\,m+1\,\nu_b}|_{\mathrm{E}} = \sum_{\substack{m'\geq 0\\ \nu_c\nu_d}} \Big[&\langle m\nu_a\ m'+1\,\nu_c|V(r_{12})D[\rho]|m'\nu_d\ m+1\,\nu_b\rangle R^{(+)t1/2\,1}_{m'\nu_d\nu_c}|_{\mathrm{E}}\\ &+\langle m\nu_a\ -m'\nu_c|V(r_{12})D[\rho]|-(m'+1)\,\nu_d\ m+1\,\nu_b\rangle R^{(-)t1/2\,1}_{m'\nu_c\nu_d}|_{\mathrm{E}}\Big],\end{aligned}} \tag{C.48}$$

where

$$\boxed{\begin{aligned}R^{(+)t1/2\,1}_{m'\nu_d\nu_c}|_{\mathrm{E}} &= \sum_{t'}(H-W\delta_{tt'})\rho^{t'm'+1/2}_{m'\nu_d,\,m'+1\,\nu_c}, &\text{(C.49a)}\\ R^{(-)t1/2\,1}_{m'\nu_c\nu_d}|_{\mathrm{E}} &= -\sum_{t'}(H-W\delta_{tt'})\overline{\rho}^{t'm'+1/2}_{m'\nu_c,\,m'+1\,\nu_d}. &\text{(C.49b)}\end{aligned}}$$

- Direct CDD mean field Γ for $\lambda = 1$:

$$\boxed{\Gamma^{t\Omega=m+1/2}_{m\nu_a,\,m+1\,\nu_b}|_{\mathrm{D}} = \sum_{\substack{m'\geq 0\\ \nu_c\nu_d}} \langle m\nu_a\ m'+1\,\nu_c|V(r_{12})D[\rho]|m+1\,\nu_b\ m'\nu_d\rangle R^{t1/2\,1}_{m'\nu_d\nu_c}|_{\mathrm{D}},} \tag{C.50}$$

where

$$\boxed{R^{t1/2\,1}_{m'\nu_d\nu_c}|_{\mathrm{D}} = \sum_{t'}(B-M\delta_{tt'})\Big[\rho^{t'm'+1/2}_{m'\nu_d,\,m'+1\,\nu_c} - \overline{\rho}^{t'm'+1/2}_{m'\nu_d,\,m'+1\,\nu_c}\Big].} \tag{C.51}$$

This time, the quantities $R^{(\pm)t1/2\,1}|_{\mathrm{E}}$ and $R^{t1/2\,1}|_{\mathrm{D}}$ are not symmetric under the exchange of ν_c and ν_d since the density matrices ρ and $\overline{\rho}$ are not diagonal in m', though symmetric.

The CDD mean field $\overline{\Gamma}$ can easily be deduced by exchanging ρ and $\overline{\rho}$ in the expressions of the CDD mean field Γ, as we notice by comparing the expressions of the mean fields (III.37) and (III.38). We can see that only the quantities $R^{(\pm)}$ are impacted by this transformation. We will call them $\overline{R}^{(\pm)}$ in the following. It turns out that there exists some straight relations between the quantities $R^{(\pm)}$ and $\overline{R}^{(\pm)}$ for the CDD interactions. They read

$$\boxed{\begin{aligned}\overline{R}^{(\pm)ts0}_{m'\nu_d\nu_c}|_{\mathrm{E}} &= R^{(\mp)t-s0}_{m'\nu_d\nu_c}|_{\mathrm{E}}, &\text{(C.52a)}\\ \overline{R}^{ts0}_{m'\nu_d\nu_c}|_{\mathrm{D}} &= R^{t-s0}_{m'\nu_d\nu_c}|_{\mathrm{D}}, &\text{(C.52b)}\\ \overline{R}^{(\pm)t1/2\,1}_{m'\nu_d\nu_c}|_{\mathrm{E}} &= -R^{(\mp)t1/2\,1}_{m'\nu_d\nu_c}|_{\mathrm{E}}, &\text{(C.52c)}\\ \overline{R}^{t1/2\,1}_{m'\nu_d\nu_c}|_{\mathrm{D}} &= -R^{t1/2\,1}_{m'\nu_d\nu_c}|_{\mathrm{D}}, &\text{(C.52d)}\end{aligned}}$$

as we can deduce from (C.45), (C.47), (C.49) and (C.51). Accordingly, we can explicitly write down the expressions of the direct and exchange CDD mean fields $\overline{\Gamma}$ for each value of λ. We recall that these fields are *not* time-reversal invariant. Note also that if $\lambda = 1$, then $s = 1/2$ since the identity $s_b \equiv s - 1 = \pm 1/2$ holds only if $s = 1/2$.

- Exchange CDD mean field $\overline{\Gamma}$ for $\lambda = 0$:

$$\boxed{\begin{aligned}\overline{\Gamma}^{t\Omega=m+s}_{m\nu_a,\,m\nu_b}|_{\mathrm{E}} = \sum_{\substack{m'\geq 0\\ \nu_c\nu_d}} \Big[&\langle m\nu_a\ m'\nu_c|V(r_{12})D[\rho]|m'\nu_d\ m\nu_b\rangle R^{(-)t-s0}_{m'\nu_d\nu_c}|_{\mathrm{E}}\\ &+\langle m\nu_a\ -m'\nu_c|V(r_{12})D[\rho]|-m'\nu_d\ m\nu_b\rangle R^{(+)t-s0}_{m'\nu_c\nu_d}|_{\mathrm{E}}\Big],\end{aligned}} \tag{C.53}$$

where the quantities $R^{(\pm)ts0}|_{\mathrm{E}}$ are given by (C.45).

- Direct CDD mean field $\overline{\Gamma}$ for $\lambda = 0$:

$$\boxed{\overline{\Gamma}^{t\Omega=m+s}_{m\nu_a,\,m\nu_b}|_{\rm D} = \sum_{\substack{m'\geq 0\\ \nu_c\nu_d}} \langle m\nu_a\ m'\nu_c|V(r_{12})D[\rho]|m\nu_b\ m'\nu_d\rangle R^{t-s0}_{m'\nu_d\nu_c}|_{\rm D},} \tag{C.54}$$

where the quantity $R^{ts0}|_{\rm D}$ is given by (C.47).

- Exchange CDD mean field $\overline{\Gamma}$ for $\lambda = 1$:

$$\boxed{\begin{aligned}\overline{\Gamma}^{t\Omega=m+1/2}_{m\nu_a,\,m+1\,\nu_b}|_{\rm E} = -\sum_{\substack{m'\geq 0\\ \nu_c\nu_d}} \Big[&\langle m\nu_a\ m'+1\,\nu_c|V(r_{12})D[\rho]|m'\nu_d\ m+1\,\nu_b\rangle R^{(-)t1/2\,1}_{m'\nu_d\nu_c}|_{\rm E}\\ &+\langle m\nu_a\ -m'\nu_c|V(r_{12})D[\rho]|-(m'+1)\,\nu_d\ m+1\,\nu_b\rangle R^{(+)t1/2\,1}_{m'\nu_c\nu_d}|_{\rm E}\Big],\end{aligned}} \tag{C.55}$$

where the quantities $R^{(\pm)t1/2\,1}|_{\rm E}$ are given by (C.49).

- Direct CDD mean field $\overline{\Gamma}$ for $\lambda = 1$:

$$\boxed{\overline{\Gamma}^{t\Omega=m+1/2}_{m\nu_a,\,m+1\,\nu_b}|_{\rm D} = -\sum_{\substack{m'\geq 0\\ \nu_c\nu_d}} \langle m\nu_a\ m'+1\,\nu_c|V(r_{12})D[\rho]|m+1\,\nu_b\ m'\nu_d\rangle R^{t1/2\,1}_{m'\nu_d\nu_c}|_{\rm D},} \tag{C.56}$$

where the quantity $R^{t1/2\,1}|_{\rm D}$ is given by (C.51).

We observe that the same quantities R appear in both Γ and $\overline{\Gamma}$ mean fields. Thus, the remarks concerning their symmetries made before remain valid, and the fields can be calculated simultaneously in an HFB code.

Time-reversal invariant mean fields

Now, we assume the time-reversal invariance of the CDD mean fields Γ and $\overline{\Gamma}$, i.e. we set $\rho = \overline{\rho}$. In this case, we have $R^{(\pm)} = \overline{R}^{(\pm)}$, so that the mean fields coincide, $\Gamma = \overline{\Gamma}$. They simplify according to the following expressions, where the notation $|^{\rm T}$ identifies the time-reversal invariant quantities.

The exchange CDD mean fields, (C.38) and the corresponding field $\overline{\Gamma}$, become

$$\boxed{\begin{aligned}\Gamma^{t\Omega=m+s}_{m\nu_a,\,m+\lambda\,\nu_b}|^{\rm T}_{\rm E} = \sum_{\substack{m'\geq 0\\ \nu_c\nu_d}} \Big[&\langle m\nu_a\ m'+\lambda\,\nu_c|V(r_{12})D[\rho]|m'\nu_d\ m+\lambda\,\nu_b\rangle R^{(+)ts\lambda}_{m'\nu_d\nu_c}|^{\rm T}_{\rm E}\\ &+\langle m\nu_a\ -m'\nu_c|V(r_{12})D[\rho]|-(m'+\lambda)\,\nu_d\ m+\lambda\,\nu_b\rangle R^{(-)ts\lambda}_{m'\nu_c\nu_d}|^{\rm T}_{\rm E}\Big],\end{aligned}} \tag{C.57}$$

where the quantities (C.37) simplify according to

$$\boxed{\begin{aligned}R^{(+)ts\lambda}_{m'\nu_d\nu_c}|_{\rm E} = \sum_{t'}\Big\{&\Theta(m'+s)\Big[(M-B\delta_{tt'})\delta_{\lambda,0}+(H-W\delta_{tt'})\Big]\rho^{t'm'+s}_{m'\nu_d,\,m'+\lambda\,\nu_c}\\ &+\Theta(m'-s)(M-B\delta_{tt'})\delta_{\lambda,0}\rho^{t'm'-s}_{m'\nu_d,\,m'+\lambda\,\nu_c}\Big\},\end{aligned}} \tag{C.58a}$$

$$\boxed{\begin{aligned}R^{(-)ts\lambda}_{m'\nu_c\nu_d}|_{\rm E} = \sum_{t'}\Big\{&\Theta(m'+s)\Big[(M-B\delta_{tt'})\delta_{\lambda,0}-(H-W\delta_{tt'})\delta_{\lambda,2s}\Big]\rho^{t'm'+s}_{m'\nu_c,\,m'+\lambda\,\nu_d}\\ &+\Theta(m'-s)\Big(H+M-(W+B)\delta_{tt'}\Big)\rho^{t'm'-s}_{m'\nu_c,\,m'+\lambda\,\nu_d}\Big\}.\end{aligned}} \tag{C.58b}$$

In a similar way, the direct CDD mean fields, (C.41) and the corresponding field $\overline{\Gamma}$, become

$$\boxed{\Gamma^{t\Omega=m+s}_{m\nu_a,\,m+\lambda\,\nu_b}|^{\rm T}_{\rm D} = \sum_{\substack{m'\geq 0\\ \nu_c\nu_d}} \langle m\nu_a\ m'+\lambda\,\nu_c|V(r_{12})D[\rho]|m+\lambda\,\nu_b\ m'\nu_d\rangle R^{ts\lambda}_{m'\nu_d\nu_c}|^{\rm T}_{\rm D},} \tag{C.59}$$

where the quantity (C.43) simplifies according to

$$\boxed{\begin{aligned} R^{ts\lambda}_{m'\nu_d\nu_c}|^{\mathrm{T}}_{\mathrm{D}} &= \sum_{t'} \\ &\times \Big\{\Theta(m'+s)\Big[2(W-H\delta_{tt'})\delta_{\lambda,0}+(B-M\delta_{tt'})(1-\delta_{\lambda,2s})\Big]\rho^{t'm'+s}_{m'\nu_d,\,m'+\lambda\,\nu_c} \\ &\qquad + \Theta(m'-s)\delta_{\lambda,0}\Big[2W+B-(2H+M)\delta_{tt'}\Big]\rho^{t'm'-s}_{m'\nu_d,\,m'+\lambda\,\nu_c}\Big\}. \end{aligned}} \tag{C.60}$$

From the boxed equations, we can now explicitly write down the expressions of the *time-reversal invariant* direct and exchange CDD mean field for each value of λ. Note also that if $\lambda = 1$, then $s = 1/2$ since the identity $s_b \equiv s-1 = \pm 1/2$ holds only if $s = 1/2$.

- Time-reversal invariant exchange CDD mean field for $\lambda = 0$:

$$\boxed{\begin{aligned} \Gamma^{t\Omega=m+s}_{m\nu_a,\,m\nu_b}|^{\mathrm{T}}_{\mathrm{E}} = \sum_{\substack{m'\geq 0\\ \nu_c\nu_d}} &\Big[\langle m\nu_a\ m'\nu_c|V(r_{12})D[\rho]|m'\nu_d\ m\nu_b\rangle R^{ts0}_{m'\nu_d\nu_c}|^{\mathrm{T}}_{\mathrm{E}} \\ &+ \langle m\nu_a\ -m'\nu_c|V(r_{12})D[\rho]|-m'\nu_d\ m\nu_b\rangle R^{t-s0}_{m'\nu_d\nu_c}|^{\mathrm{T}}_{\mathrm{E}}\Big], \end{aligned}} \tag{C.61}$$

where we have set

$$R^{ts0}_{m'\nu_d\nu_c}|^{\mathrm{T}}_{\mathrm{E}} \equiv R^{(+)ts0}_{m'\nu_d\nu_c}|^{\mathrm{T}}_{\mathrm{E}} = R^{(-)t-s0}_{m'\nu_d\nu_c}|^{\mathrm{T}}_{\mathrm{E}}, \tag{C.62}$$

that is to say,

$$\boxed{\begin{aligned} R^{ts0}_{m'\nu_d\nu_c}|^{\mathrm{T}}_{\mathrm{E}} = \sum_{t'} &\Big[\Theta(m'+s)\Big(H+M-(W+B)\delta_{tt'}\Big)\rho^{t'm'+s}_{m'\nu_d,\,m'\nu_c} \\ &+ \Theta(m'-s)(M-B\delta_{tt'})\rho^{t'm'-s}_{m'\nu_d,\,m'\nu_c}\Big]. \end{aligned}} \tag{C.63}$$

- Time-reversal invariant direct CDD mean field Γ for $\lambda = 0$:

$$\boxed{\Gamma^{t\Omega=m+1/2}_{m\nu_a,\,m\nu_b}|^{\mathrm{T}}_{\mathrm{D}} = \sum_{\substack{m'\geq 0\\ \nu_c\nu_d}} \langle m\nu_a\ m'\nu_c|V(r_{12})D[\rho]|m\nu_b\ m'\nu_d\rangle R^{t0}_{m'\nu_d\nu_c}|^{\mathrm{T}}_{\mathrm{D}},} \tag{C.64}$$

with

$$\boxed{\begin{aligned} R^{t0}_{m'\nu_d\nu_c}|^{\mathrm{T}}_{\mathrm{D}} = \sum_{t'} &\Big(2W+B-(2H+M)\delta_{tt'}\Big) \\ &\times \Big[\rho^{t'm'+1/2}_{m'\nu_d,\,m'\nu_c} + \Theta(m'-1/2)\rho^{t'm'-1/2}_{m'\nu_d,\,m'\nu_c}\Big], \end{aligned}} \tag{C.65}$$

where we have removed the superscript s in the above quantity since it does not depend on its particular value, and then set $s = 1/2$ in the CDD mean field. We notice that the quantities $R^{ts0}|^{\mathrm{T}}_{\mathrm{E}}$ and $R^{t0}|^{\mathrm{T}}_{\mathrm{D}}$ are symmetric under the exchange of ν_c and ν_d as they already are when time-reversal invariance is not yet imposed. In particular, this symmetry was used to exchange the indices of the quantity $R^{t-s0}|^{\mathrm{T}}_{\mathrm{E}}$ appearing in (C.61).

- Time-reversal invariant exchange CDD mean field Γ for $\lambda = 1$:

$$\boxed{\begin{aligned} \Gamma^{t\Omega=m+1/2}_{m\nu_a,\,m+1\,\nu_b}|^{\mathrm{T}}_{\mathrm{E}} = \sum_{\substack{m'\geq 0\\ \nu_c\nu_d}} &\Big[\langle m\nu_a\ m'+1\,\nu_c|V(r_{12})D[\rho]|m'\nu_d\ m+1\,\nu_b\rangle R^{t1/2\,1}_{m'\nu_d\nu_c}|^{\mathrm{T}}_{\mathrm{E}} \\ &- \langle m\nu_a\ -m'\nu_c|V(r_{12})D[\rho]|-(m'+1)\,\nu_d\ m+1\,\nu_b\rangle R^{t1/2\,1}_{m'\nu_c\nu_d}|^{\mathrm{T}}_{\mathrm{E}}\Big], \end{aligned}} \tag{C.66}$$

where we have set

$$R^{t1/2\,1}_{m'\nu_d\nu_c}|^{\mathrm{T}}_{\mathrm{E}} \equiv R^{(+)t1/2\,1}_{m'\nu_d\nu_c}|^{\mathrm{T}}_{\mathrm{E}} = -R^{(-)t1/2\,1}_{m'\nu_d\nu_c}|^{\mathrm{T}}_{\mathrm{E}}, \tag{C.67}$$

that is to say,

$$\boxed{R^{t1/2\,1}_{m'\nu_d\nu_c}|^{\mathrm{T}}_{\mathrm{E}} = \sum_{t'}(H - W\delta_{tt'})\rho^{t'm'+1/2}_{m'\nu_d,\,m'+1\,\nu_c}.} \tag{C.68}$$

We notice that the quantity $R^{t1/2\,1}_{m'\nu_d\nu_c}|^{\mathrm{T}}_{\mathrm{E}}$ is not symmetric under the exchange of ν_c and ν_d since the density matrix ρ is not diagonal in m', though symmetric.

- Time-reversal invariant direct CDD mean field Γ for $\lambda = 1$:

$$\boxed{\Gamma^{t\Omega=m+1/2}_{m\nu_a,\,m+1\,\nu_b}|^{\mathrm{T}}_{\mathrm{D}} = 0} \tag{C.69}$$

since we have

$$\boxed{R^{t1/2\,1}_{m'\nu_d\nu_c}|^{\mathrm{T}}_{\mathrm{D}} = 0.} \tag{C.70}$$

These expressions show that the direct mean field is always easier to calculate than the exchange one, especially when time-reversal invariance is demanded. This is one of the main reasons why zero-range effective interactions, in which the exchange field has the same form as the direct field, are widely used in the literature. We note that we recover the expressions of the time-reversal invariant mean fields obtained by Chappert [17].

2.1.2. Central and density-dependent pairing field

We continue by deriving the pairing field (III.32) of the central and density-dependent interaction (C.26), which is not time-reversal invariant for the moment. Given that the pairing tensor (C.21) and the fields (C.22) are diagonal in t and Ω, this CDD pairing field can be written

$$\Delta^{t\Omega}_{r_a r_b} = \sum_{\substack{t'\Omega'>0\\ r_c r_d}} \langle ts_a r_a\ \overline{ts_b r_b}|v^{\mathrm{CDD,(a)}}_{12}|t's_c r_c\ \overline{t's_d r_d}\rangle \kappa^{t'\Omega'}_{r_c r_d}. \tag{C.71}$$

As for the CDD mean fields, let us first concentrate on the exchange component of the CDD pairing field. It reads

$$\begin{aligned}\Delta^{t\Omega}_{r_a r_b}|_{\mathrm{E}} = \sum_{\substack{t'\Omega'>0\\ r_c r_d}} &\langle r_a - r_b|V(r_{12})D[\rho]P_r|r_c - r_d\rangle \\ &\times \sigma_b\sigma_d\langle ts_a\ t - s_b|\mathcal{P}_{\mathrm{E}}|t's_c\ t' - s_d\rangle\kappa^{t'\Omega'}_{r_c r_d}.\end{aligned} \tag{C.72}$$

We name the quantum numbers of the above matrix element in the same way as we have done for the second matrix element of the CDD mean field (C.33), while keeping in mind that here $\lambda \in \{-1, 0, 1\}$ since the pairing field is not symmetric under the exchange of its indices, contrary to the mean field (see equation (C.24) and the discussion below). With these notations, the exchange CDD pairing field becomes

$$\begin{aligned}\Delta^{t\Omega=m+s}_{m\nu_a,\,m+\lambda\,\nu_b}|_{\mathrm{E}} = \sum_{\substack{t'\Omega'>0\\ m'\nu_c\nu_d}} &\langle m\nu_a\ -(m+\lambda)\,\nu_b|V(r_{12})D[\rho]P_r|m'\nu_c\ -(m'+\lambda)\,\nu_d\rangle \\ &\times 4(s-\lambda)(s'-\lambda)\langle ts\ t-(s-\lambda)|\mathcal{P}_{\mathrm{E}}|t's'\ t'-(s'-\lambda)\rangle\kappa^{t'm'+s'}_{m'\nu_c,\,m'+\lambda\,\nu_d}.\end{aligned} \tag{C.73}$$

Once again, let us first focus on the spin-isospin part. We set

$$\begin{aligned}A^{ts\lambda}_{\Omega'm'\nu_c\nu_d}|_{\mathrm{E}} \equiv \sum_{t'} &4(s-\lambda)(s'-\lambda)\langle ts\ t-(s-\lambda)|\mathcal{P}_{\mathrm{E}}|t's'\ t'-(s'-\lambda)\rangle \\ &\times \kappa^{t'm'+s'}_{m'\nu_c,\,m'+\lambda\,\nu_d},\end{aligned} \tag{C.74}$$

Using the expression of $\mathcal{P}_{\rm E}$, given by (C.29), we can evaluate the above spin-isospin matrix elements. Taking into account the sum over t, we find

$$A^{ts\lambda}_{\Omega' m'\nu_c\nu_d}|_{\rm E} = \Big[(M-B)\delta_{ss'} + (W-H)(1-4s\lambda)\delta_{\lambda,s+s'}\Big]\kappa^{t\,m'+s'}_{m'\nu_c,\,m'+\lambda\,\nu_d}, \tag{C.75}$$

Now, setting

$$S^{ts\lambda}_{m'\nu_c\nu_d}|_{\rm E} \equiv \sum_{\Omega'}\Theta(\Omega')A^{ts\lambda}_{\Omega' m'\nu_c\nu_d}|_{\rm E} = \sum_{s'=\pm s}\Theta(m'+s')A^{ts\lambda}_{m'+s'm'\nu_c\nu_d}|_{\rm E}, \tag{C.76}$$

we end up with

$$\boxed{\begin{aligned} S^{ts\lambda}_{m'\nu_c\nu_d}|_{\rm E} = {}& \Theta(m'+s)\Big[(M-B)+(H-W)\delta_{\lambda,2s}\Big]\kappa^{t\,m'+s}_{m'\nu_c,\,m'+\lambda\,\nu_d} \\ & - \Theta(m'-s)\delta_{\lambda,0}(H-W)\kappa^{t\,m'-s}_{m'\nu_c,\,m'+\lambda\,\nu_d}, \end{aligned}} \tag{C.77}$$

and the exchange CDD pairing field can be written

$$\begin{aligned} \Delta^{t\Omega=m+s}_{m\nu_a,\,m+\lambda\,\nu_b}|_{\rm E} = {} & \sum_{\substack{m'\geq 0\\ \nu_c\nu_d}} \\ & \times \langle m\nu_a\ -(m+\lambda)\,\nu_b|V(r_{12})D[\rho]|-(m'+\lambda)\,\nu_d\ m'\nu_c\rangle S^{ts\lambda}_{m'\nu_c\nu_d}|_{\rm E}, \end{aligned} \tag{C.78}$$

where, as for the CDD mean fields, we have simply replaced the summations $\sum_{m'}\sum_{\Omega'>0}$ by $\sum_{m'\geq 0}\sum_{\Omega'}\Theta(\Omega')$ and applied the operator P_r. Now, writing the above matrix element under its integral form, we see that it is equivalent, because of the expression of the axial wave functions (C.3) and the fact that they commute with the quantity $V(r_{12})D[\rho]$, to $\langle m\nu_a\ -m'\nu_c|V(r_{12})D[\rho]|-(m'+\lambda)\,\nu_d\ (m+\lambda)\,\nu_b\rangle$. Thus, the exchange CDD pairing field reads

$$\boxed{\begin{aligned} \Delta^{t\Omega=m+s}_{m\nu_a,\,m+\lambda\,\nu_b}|_{\rm E} = {} & \sum_{\substack{m'\geq 0\\ \nu_c\nu_d}} \\ & \times \langle m\nu_a\ -m'\nu_c|V(r_{12})D[\rho]|-(m'+\lambda)\,\nu_d\ (m+\lambda)\,\nu_b\rangle S^{ts\lambda}_{m'\nu_c\nu_d}|_{\rm E}. \end{aligned}} \tag{C.79}$$

To get the direct CDD pairing field out of the exchange one, we first exchange W, B, H, M by M, H, B, W and omit the operator P_r to obtain

$$\begin{aligned} \Delta^{t\Omega=m+s}_{m\nu_a,\,m+\lambda\,\nu_b}|_{\rm D} = {} & \sum_{\substack{m'\geq 0\\ \nu_c\nu_d}} \\ & \times \langle m\nu_a\ -(m+\lambda)\,\nu_b|V(r_{12})D[\rho]|m'\nu_c\ -(m'+\lambda)\,\nu_d\rangle S^{ts\lambda}_{m'\nu_c\nu_d}|_{\rm D}. \end{aligned} \tag{C.80}$$

Just like we have done with the exchange term, we notice that the matrix element can be written $\langle m\nu_a\ (m+\lambda)\,\nu_d|V(r_{12})D[\rho]|m'\nu_c\ (m+\lambda)\,\nu_b\rangle$. Finally exchanging the dummy indices ν_c and ν_d, the direct CDD pairing field becomes

$$\boxed{\begin{aligned} \Delta^{t\Omega=m+s}_{m\nu_a,\,m+\lambda\,\nu_b}|_{\rm D} = {} & \sum_{\substack{m'\geq 0\\ \nu_c\nu_d}} \\ & \times \langle m\nu_a\ (m'+\lambda)\,\nu_c|V(r_{12})D[\rho]|m'\nu_d\ (m+\lambda)\,\nu_b\rangle S^{ts\lambda}_{m'\nu_d\nu_c}|_{\rm D}, \end{aligned}} \tag{C.81}$$

where

$$\boxed{\begin{aligned} S^{ts\lambda}_{m'\nu_d\nu_c}|_{\rm D} = \Theta(m'+s)\Big[(W-H)+(B-M)\delta_{\lambda,2s}\Big]\kappa^{t\,m'+s}_{m'\nu_d,\,m'+\lambda\,\nu_c} \\ -\Theta(m'-s)\delta_{\lambda,0}(B-M)\kappa^{t\,m'-s}_{m'\nu_d,\,m'+\lambda\,\nu_c}. \end{aligned}} \tag{C.82}$$

Finally, the full CDD pairing field (direct plus exchange components) can be written as

$$\boxed{\begin{aligned} \Delta^{t\Omega=m+s}_{m\nu_a,\,m+\lambda\,\nu_b} = \sum_{\substack{m'\geq 0\\ \nu_c\nu_d}} \\ \times\Big[\langle m\nu_a\ m'+\lambda\,\nu_c|V(r_{12})D[\rho]|m'\nu_d\ m+\lambda\,\nu_b\rangle S^{ts\lambda}_{m'\nu_d\nu_c}|_{\rm D} \\ +\langle m\nu_a\ -m'\nu_c|V(r_{12})D[\rho]|-(m'+\lambda)\,\nu_d\ m+\lambda\,\nu_b\rangle S^{ts\lambda}_{m'\nu_c\nu_d}|_{\rm E}\Big]. \end{aligned}} \tag{C.83}$$

We see that the pairing field has the same structure as the exchange mean field (C.38). This is the reason for our specific transformations leading to (C.79) and (C.81). Indeed, the pairing fields can therefore be calculated simultaneously with the exchange mean fields in an HFB code.

From the boxed equations, we can now explicitly write down the expressions of the above CDD pairing field for each value of λ. We recall that this field is *not* time-reversal invariant. We also note that if $|\lambda|=1$, then $\lambda=2s$ as we deduce from $s_b\equiv s-\lambda=\pm 1/2$ when $\lambda\neq 0$.

- CDD pairing field for $\lambda=0$:

$$\boxed{\begin{aligned} \Delta^{t\Omega=m+s}_{m\nu_a,\,m\nu_b} = \sum_{\substack{m'\geq 0\\ \nu_c\nu_d}}\Big[\langle m\nu_a\ m'\nu_c|V(r_{12})D[\rho]|m'\nu_d\ m\nu_b\rangle S^{ts0}_{m'\nu_d\nu_c} \\ +\langle m\nu_a\ -m'\nu_c|V(r_{12})D[\rho]|-m'\nu_d\ m\nu_b\rangle S^{t-s0}_{m'\nu_c\nu_d}\Big], \end{aligned}} \tag{C.84}$$

where we have set

$$S^{ts0}_{m'\nu_d\nu_c}\equiv S^{ts0}_{m'\nu_d\nu_c}|_{\rm D} = S^{t-s0}_{m'\nu_d\nu_c}|_{\rm E}, \tag{C.85}$$

with

$$\boxed{S^{ts0}_{m'\nu_c\nu_d} = \Theta(m'+s)(W-H)\kappa^{t\,m'+s}_{m'\nu_c,\,m'\nu_d} - \Theta(m'-s)(B-M)\kappa^{t\,m'-s}_{m'\nu_c,\,m'\nu_d}.} \tag{C.86}$$

- CDD pairing field for $|\lambda|=1$:

$$\boxed{\begin{aligned} \Delta^{t\Omega=m+s}_{m\nu_a,\,m+2s\,\nu_b} = \sum_{\substack{m'\geq 0\\ \nu_c\nu_d}}\Big[\langle m\nu_a\ m'+2s\,\nu_c|V(r_{12})D[\rho]|m'\nu_d\ m+2s\,\nu_b\rangle S^{ts\,2s}_{m'\nu_d\nu_c} \\ -\langle m\nu_a\ -m'\nu_c|V(r_{12})D[\rho]|-(m'+2s)\,\nu_d\ m+2s\,\nu_b\rangle S^{ts\,2s}_{m'\nu_c\nu_d}\Big], \end{aligned}} \tag{C.87}$$

where we have set

$$S^{ts\,2s}_{m'\nu_d\nu_c}\equiv S^{ts\,2s}_{m'\nu_d\nu_c}|_{\rm D} = -S^{ts\,2s}_{m'\nu_d\nu_c}|_{\rm E}, \tag{C.88}$$

with

$$\boxed{S^{ts\,2s}_{m'\nu_c\nu_d} = \Theta(m'+s)(W+B-H-M)\kappa^{t\,m'+s}_{m'\nu_c,\,m'+2s\,\nu_d}.} \tag{C.89}$$

Note that the quantities S^{ts0} and $S^{ts\,2s}$ are not symmetric under the exchange of ν_d and ν_c since the pairing tensor κ is not.

Time-reversal invariant fields

Now, we assume the time-reversal invariance of the CDD pairing field, i.e. the pairing tensor κ becomes symmetric under the exchange of its indices. Then, the pairing field becomes symmetric (see discussion below equation (C.24)) and it suffices to consider its expression for $\lambda \in \{0, 1\}$. If $\lambda = 1$, then $s = 1/2$ since the identity $s_b \equiv s - 1 = \pm 1/2$ holds only if $s = 1/2$.

- Time-reversal invariant CDD pairing field for $\lambda = 0$:

$$\boxed{\begin{aligned}\Delta^{t\Omega=m+s}_{m\nu_a,\,m\nu_b}|^{\mathrm{T}} = \sum_{\substack{m'\geq 0\\ \nu_c\nu_d}} \Big[&\langle m\nu_a\ m'\nu_c|V(r_{12})D[\rho]|m'\nu_d\ m\nu_b\rangle S^{ts0}_{m'\nu_d\nu_c} \\ &+ \langle m\nu_a\ -m'\nu_c|V(r_{12})D[\rho]|-m'\nu_d\ m\nu_b\rangle S^{t-s0}_{m'\nu_d\nu_c}\Big],\end{aligned}} \tag{C.90}$$

where the quantity S^{ts0} is given in (C.86). This time, this quantity is symmetric under the exchange of ν_c and ν_d since the pairing tensor is symmetric and diagonal in m'.

- Time-reversal invariant CDD pairing field for $\lambda = 1$:

$$\boxed{\begin{aligned}\Delta^{t\Omega=m+1/2}_{m\nu_a,\,m+1\,\nu_b}|^{\mathrm{T}} = \sum_{\substack{m'\geq 0\\ \nu_c\nu_d}} \Big[&\langle m\nu_a\ m'+1\,\nu_c|V(r_{12})D[\rho]|m'\nu_d\ m+1\,\nu_b\rangle S^{t1/2\,1}_{m'\nu_d\nu_c} \\ &- \langle m\nu_a\ -m'\nu_c|V(r_{12})D[\rho]|-(m'+1)\,\nu_d\ m+1\,\nu_b\rangle S^{t1/2\,1}_{m'\nu_c\nu_d}\Big],\end{aligned}} \tag{C.91}$$

where

$$\boxed{S^{t1/2\,1}_{m'\nu_c\nu_d} = (W + B - H - M)\kappa^{t\,m'+1/2}_{m'\nu_c,\,m'+1\,\nu_d}.} \tag{C.92}$$

The quantity $S^{t1/2\,1}$ is not symmetric under the exchange of ν_c and ν_d since the pairing tensor κ is not diagonal in m', though symmetric. We note that we recover the expressions of the time-reversal invariant pairing fields obtained by Chappert [17].

2.1.3. Central and density-dependent spatial matrix elements

In the previous subsection, we have treated the spin-isospin parts of the central and density-dependent mean- and pairing fields. In order to fully specify these fields, it remains to determine their spatial parts, which we now undertake.

Identifying the position of the centers by the quantum numbers j, the spatial dependence of the CDD fields lies in the two-body matrix elements of the form

$$v^{j_aj_cj_bj_d}_{r_ar_cr_br_d} \equiv \langle j_ar_a\ j_cr_c|V(r_{12})D[\rho]|j_br_b\ j_dr_d\rangle. \tag{C.93}$$

By expliciting the functional of the density (C.28), we get

$$\begin{aligned}v^{j_aj_cj_bj_d}_{r_ar_cr_br_d} = \frac{1}{2}\int \mathrm{d}^3r_1 \int \mathrm{d}^3r_2 \\ \times \phi^*_{j_ar_a}(\vec{r}_1)\phi^*_{j_cr_c}(\vec{r}_2)V(r_{12})\Big[\rho^\alpha(\vec{r}_1) + \rho^\alpha(\vec{r}_2)\Big]\phi_{j_br_b}(\vec{r}_1)\phi_{j_dr_d}(\vec{r}_2).\end{aligned} \tag{C.94}$$

Since the wave functions and the sandwiched quantity commute, we can rearrange the terms and break the integral into two parts, according to

$$\begin{aligned}v^{j_aj_cj_bj_d}_{r_ar_cr_br_d} = \frac{1}{2}\int \mathrm{d}^3r_1 \int \mathrm{d}^3r_2\, V(r_{12})\Big[&\rho^\alpha(\vec{r}_1)\phi^*_{j_ar_a}(\vec{r}_1)\phi_{j_br_b}(\vec{r}_1)\phi^*_{j_cr_c}(\vec{r}_2)\phi_{j_dr_d}(\vec{r}_2) \\ &+ \rho^\alpha(\vec{r}_2)\phi^*_{j_ar_a}(\vec{r}_1)\phi_{j_br_b}(\vec{r}_1)\phi^*_{j_cr_c}(\vec{r}_2)\phi_{j_dr_d}(\vec{r}_2)\Big].\end{aligned} \tag{C.95}$$

Now, using twice the Gogny separable development in axial symmetry (C.495), on $\vec{r}_1$ coordinates in the first integral and on $\vec{r}_2$ coordinates in the second one, we find

$$\begin{aligned} v^{j_a j_c j_b j_d}_{r_a r_c r_b r_d} = \frac{1}{2}\int \mathrm{d}^3 r_1 \int \mathrm{d}^3 r_2\, V(r_{12}) \\ \times \Big[\rho^\alpha(\vec{r}_1)\phi^*_{j_a r_a}(\vec{r}_1)\phi_{j_b r_b}(\vec{r}_1)\sum_{r_\mu} T^{r_\mu}_{j_c r_c\, j_d r_d}\phi_{j_{cd}0}(\vec{r}_2)\phi_{j_{cd} r_\mu}(\vec{r}_2) \\ + \rho^\alpha(\vec{r}_2)\phi^*_{j_c r_c}(\vec{r}_2)\phi_{j_d r_d}(\vec{r}_2)\sum_{r'_\mu} T^{r'_\mu}_{j_a r_a\, j_b r_b}\phi_{j_{ab}0}(\vec{r}_1)\phi_{j_{ab} r'_\mu}(\vec{r}_1)\Big]. \end{aligned} \tag{C.96}$$

Now, we switch the coordinates $\vec{r}_1$ and $\vec{r}_2$ in the second integral, taking into account the fact that the potential $V(r_{12})$ is central. Setting $\vec{r} \equiv \vec{r}_1$ as well as $\vec{r}\,' \equiv \vec{r}_2$, we finally obtain

$$\begin{aligned} v^{j_a j_c j_b j_d}_{r_a r_c r_b r_d} = \frac{1}{2}\int \mathrm{d}^3 r\, \rho^\alpha(\vec{r})\Big[\phi^*_{j_a r_a}(\vec{r})\phi_{j_b r_b}(\vec{r})\sum_{r_\mu} T^{r_\mu}_{j_c r_c\, j_d r_d} G_{j_{cd} r_\mu}(\vec{r}) \\ + \phi^*_{j_c r_c}(\vec{r})\phi_{j_d r_d}(\vec{r})\sum_{r'_\mu} T^{r'_\mu}_{j_a r_a\, j_b r_b} G_{j_{ab} r'_\mu}(\vec{r})\Big], \end{aligned} \tag{C.97}$$

where we have set

$$G_{j r_\mu}(\vec{r}) \equiv \int \mathrm{d}^3 r'\, V(|\vec{r} - \vec{r}\,'|)\phi_{j0}(\vec{r}\,')\phi_{j r_\mu}(\vec{r}\,'), \tag{C.98}$$

that we will now try to evaluate. Since the wave functions and the potential can be separated along their $r_\perp$ and z parts, we can separate the above quantity in the same way, according to

$$G_{j r_\mu}(\vec{r}) = G^{(2)}_{m_\mu n_{\perp\mu}}(\vec{r}_\perp)\, G^{(1)}_{j n_{z\mu}}(z), \tag{C.99}$$

where

$$G^{(N)}_\mu(\vec{u}) \equiv \int \mathrm{d}^N u'\, \mathrm{e}^{-(\vec{u}-\vec{u}')^2/\mu^2_{\mathrm{CDD}}}\phi_0(\vec{u}' - \vec{d})\phi_\mu(\vec{u}' - \vec{d}), \tag{C.100}$$

with the condensed notation

$$\phi_\mu(\vec{u}' - \vec{d}) \equiv \begin{cases} \phi_{m_\mu n_{\perp\mu}}(\vec{r}_\perp) & \text{for } N = 2, \\ \phi_{n_{z\mu}}(z - d_j) & \text{for } N = 1. \end{cases} \tag{C.101}$$

Note that the range of the central and density-dependent terms has been dubbed μ_{CDD} to avoid confusions with the set of quantum numbers $\mu = (m_\mu, n_{\perp\mu}, n_{z\mu})$. By means of the fundamental relation linking the wave functions to their generating functions in N dimensions (C.485), we can evaluate (C.100) for both $N = 1$ and $N = 2$ cases. Indeed, by expliciting the wave functions, we get

$$\sum_\mu \chi^*_\mu(\vec{t})G^{(N)}_\mu(\vec{u}) = \left(\frac{\beta}{\pi}\right)^{N/2}\int \mathrm{d}^N u'\, \mathrm{e}^{-(\vec{u}-\vec{u}')^2/\mu^2_{\mathrm{CDD}}}\mathrm{e}^{-\beta(\vec{u}'-\vec{d})^2 + 2\sqrt{\beta}\,\vec{t}\cdot(\vec{u}'-\vec{d}) - t^2}. \tag{C.102}$$

Let us now complete the square of the argument of the exponential appearing in the integral above. It reads, after simplifications,

$$-\left[\frac{1}{g\mu_{\mathrm{CDD}}}\vec{u}' - g\mu_{\mathrm{CDD}}\left(\frac{\vec{u}}{\mu^2_{\mathrm{CDD}}} + \beta\vec{d} + \sqrt{\beta}\vec{t}\right)\right]^2 - \beta g^2(\vec{u}-\vec{d})^2 + 2\sqrt{\beta}g^2\vec{t}\cdot(\vec{u}-\vec{d}) - g^2t^2, \tag{C.103}$$

where we have defined

$$g \equiv \frac{1}{\sqrt{1 + \beta\mu^2_{\mathrm{CDD}}}}. \tag{C.104}$$

Setting $\vec{v} \equiv (1/g\mu_{\text{CDD}})\vec{u}' - g\mu(\vec{u}/\mu_{\text{CDD}}^2 + \beta\vec{d} + \sqrt{\beta}\vec{t})$, the Gauss integral (D.118) over this new variable furnishes

$$\sum_{\mu} \chi_{\mu}^{*}(\vec{t}) G_{\mu}^{(N)}(\vec{u}) = \left(\frac{\beta}{\pi}\right)^{N/2} \pi^{N/2} (g\mu_{\text{CDD}})^{N} \mathrm{e}^{-\beta g^2(\vec{u}-\vec{d})^2 + 2\sqrt{\beta} g^2 \vec{t}\cdot(\vec{u}-\vec{d}) - g^2 t^2}. \tag{C.105}$$

Now, applying the fundamental relation (C.485) again, but in reverse order, considering an off-centered wave function, namely using,

$$\sum_{\mu} \chi_{\mu}^{*}(\vec{t}) \phi_{\mu}\Big(g(\vec{u}-\vec{d})\Big) = \left(\frac{\beta}{\pi}\right)^{N/4} \mathrm{e}^{-\beta g^2(\vec{u}-\vec{d})^2/2 + 2\sqrt{\beta} g^2(\vec{u}-\vec{d}) - g^2 t^2}, \tag{C.106}$$

we find

$$\sum_{\mu} \chi_{\mu}^{*}(\vec{t}) G_{\mu}^{(N)}(\vec{u}) = \left(\frac{\beta}{\pi}\right)^{N/4} \pi^{N/2} (g\mu_{\text{CDD}})^{N} \mathrm{e}^{-\beta g^2(\vec{u}-\vec{d})^2/2} \sum_{\mu} \chi_{\mu}^{*}(\vec{t}) \phi_{\mu}\Big(g(\vec{u}-\vec{d})\Big), \tag{C.107}$$

such that, with the definition (C.8) and the first property of (C.491),

$$\sum_{\mu} \chi_{\mu}^{*}(\vec{t}) G_{\mu}^{(N)}(\vec{u}) = (g\mu_{\text{CDD}}\sqrt{\pi})^{N} \phi_0\Big(g(\vec{u}-\vec{d})\Big) \sum_{\mu} g^{X_\mu} \chi_{\mu}^{*}(\vec{t}) \phi_{\mu}\Big(g(\vec{u}-\vec{d})\Big), \tag{C.108}$$

where X_μ is given in (C.492). This equality is only true if the coefficients of the expansion of the generating function $\chi_{\mu}^{*}(\vec{t})$ on both sides are equal, that is to say if

$$\boxed{G_{\mu}^{(N)}(\vec{u}) = (g\mu_{\text{CDD}}\sqrt{\pi})^{N} g^{X_\mu} \phi_0\Big(g(\vec{u}-\vec{d})\Big) \phi_{\mu}\Big(g(\vec{u}-\vec{d})\Big).} \tag{C.109}$$

We can deduce the expressions of the above quantity for $N = 1$ and $N = 2$, i.e.

$$G_{n_{\perp\mu} m_\mu}^{(2)}(\vec{r}_\perp) = N_\perp \phi_{00}(g_\perp \vec{r}_\perp) \phi_{m_\mu n_{\perp\mu}}(g_\perp \vec{r}_\perp), \tag{C.110a}$$

$$G_{j n_{z\mu}}^{(1)}(z) = N_z \phi_0\Big(g_z(z-d_j)\Big) \phi_{n_{z\mu}}\Big(g_z(z-d_j)\Big), \tag{C.110b}$$

where

$$N_\perp \equiv \pi\mu_{\text{CDD}}^2 g_\perp^{2n_{\perp\mu}+|m_\mu|+2}, \qquad \text{and} \qquad N_z \equiv \sqrt{\pi}\mu_{\text{CDD}} g_z^{2n_{z\mu}+1}, \tag{C.111}$$

as well as

$$g_\perp \equiv \frac{b_\perp}{\sqrt{\mu_{\text{CDD}}^2 + b_\perp^2}}, \qquad \text{and} \qquad g_z \equiv \frac{b_z}{\sqrt{\mu_{\text{CDD}}^2 + b_z^2}}. \tag{C.112}$$

Finally,

$$G_{j r_\mu}(\vec{r}_g) = N_r \phi_{j0}(\vec{r}_g) \phi_{j r_\mu}(\vec{r}_g), \tag{C.113}$$

where $\vec{r}_g \equiv (g_\perp \vec{r}_\perp, g_z(z-d_j))$, and

$$N_r \equiv N_\perp N_z = (\mu_{\text{CDD}}\sqrt{\pi})^3 g_\perp^{2n_{\perp\mu}+|m_\mu|+2} g_z^{n_{z\mu}+1}. \tag{C.114}$$

Central interactions

Let us start by seeking an expression for the spatial matrix elements associated with the central terms. For this, we start from equation (C.97) where we set $\alpha = 0$ and, for convenience, we exchange r_μ with r'_μ, such that

$$\begin{aligned} v^{j_a j_c j_b j_d}_{r_a r_c r_b r_d} = \frac{1}{2}\int \mathrm{d}^3 r \Big[\phi^*_{j_a r_a}(\vec{r})\phi_{j_b r_b}(\vec{r}) \sum_{r'_\mu} T^{r'_\mu}_{j_c r_c\, j_d r_d} G_{j_c d r'_\mu}(\vec{r}) \\ + \phi^*_{j_c r_c}(\vec{r})\phi_{j_d r_d}(\vec{r}) \sum_{r_\mu} T^{r_\mu}_{j_a r_a\, j_b r_b} G_{j_a b r_\mu}(\vec{r}) \Big]. \end{aligned} \tag{C.115}$$

Using the Gogny separable development (C.495) again, we obtain

$$\begin{aligned} v^{j_a j_c j_b j_d}_{r_a r_c r_b r_d} = \frac{1}{2}\sum_{r_\mu r'_\mu} T^{r_\mu}_{j_a r_a\, j_b r_b} T^{r'_\mu}_{j_c r_c\, j_d r_d} \\ \times \int \mathrm{d}^3 r \left[G_{j_a b r_\mu}(\vec{r})\phi_{j_c d 0}(\vec{r})\phi_{j_c d r'_\mu}(\vec{r}) + G_{j_c d r'_\mu}(\vec{r})\phi_{j_a b 0}(\vec{r})\phi_{j_a b r_\mu}(\vec{r}) \right]. \end{aligned} \tag{C.116}$$

Using the expression of $G_{j r_\mu}(\vec{r})$ given by (C.98) to exchange the integration variables $\vec{r}$ and $\vec{r}\,'$ in the second quantity appearing in the bracket, we find out that the latter is identical to the first one, hence

$$v^{j_a j_c j_b j_d}_{r_a r_c r_b r_d} = \sum_{r_\mu r'_\mu} T^{r_\mu}_{j_a r_a\, j_b r_b} T^{r'_\mu}_{j_c r_c\, j_d r_d} \int \mathrm{d}^3 r\, G_{j_a b r_\mu}(\vec{r})\phi_{j_c d 0}(\vec{r})\phi_{j_c d r'_\mu}(\vec{r}). \tag{C.117}$$

We notice that the above integral takes the form

$$I_{j r_\mu j' r'_\mu} \equiv \int \mathrm{d}^3 r\, G_{j r_\mu}(\vec{r})\phi_{j' 0}(\vec{r})\phi_{j' r'_\mu}(\vec{r}), \tag{C.118}$$

that we can separate along the $r_\perp$ and z directions, as we can do it for both the wave functions and the function $G_{j r_\mu}(\vec{r})$, given by (C.99), i.e. we can write

$$I_{j r_\mu j' r'_\mu} = I^{(2)}_{m_\mu n_{\perp\mu} m'_\mu n'_{\perp\mu}} I^{(1)}_{j n_{z\mu} j' n'_{z\mu}}, \tag{C.119}$$

where

$$I^{(N)}_{j\mu j'\mu'} \equiv \int \mathrm{d}^N u\, G^{(N)}_{j\mu}(\vec{u})\phi_0(\vec{u} - \vec{d}_{j'})\phi_{\mu'}(\vec{u} - \vec{d}_{j'}), \tag{C.120}$$

with $N = 1$ or $N = 2$. The expression of $G^{(N)}_{j\mu}(\vec{u})$ has just been evaluated in (C.109), with (C.104), while we have used the condensed notation (C.101) again. In the following, the range of the central terms will be denoted by μ_{C}. Our integral then becomes

$$I^{(N)}_{j\mu j'\mu'} = (g\mu_{\mathrm{C}}\sqrt{\pi})^N g^{X_\mu} \int \mathrm{d}^N u\, \phi_0(\vec{u} - \vec{d}_{j'})\phi_0\Big(g(\vec{u} - \vec{d}_j)\Big)\phi_{\mu'}(\vec{u} - \vec{d}_{j'})\phi_\mu\Big(g(\vec{u} - \vec{d}_j)\Big). \tag{C.121}$$

Expliciting the wave functions and using twice the fundamental relation linking the wave functions to their generating functions (C.485), we get

$$\begin{aligned} \sum_{\mu\mu'} \chi^*_\mu(\vec{t})\chi^*_{\mu'}(\vec{t}\,')I^{(N)}_{j\mu j'\mu'} = \left(\frac{g\mu_{\mathrm{C}}\beta}{\sqrt{\pi}}\right)^N \int \mathrm{d}^N u\, \mathrm{e}^{-g^2\beta(\vec{u}-\vec{d}_j)^2 + 2g^2\sqrt{\beta}\vec{t}\cdot(\vec{u}-\vec{d}_j) - g^2 t^2} \\ \times \mathrm{e}^{-\beta(\vec{u}-\vec{d}_{j'})^2 + 2\sqrt{\beta}\vec{t}\,'\cdot(\vec{u}-\vec{d}_{j'}) - t'^2}, \end{aligned} \tag{C.122}$$

where we have used the properties (C.491) of the generating functions. Completing the square of the argument of the exponential, we find, after simplifications,

$$-\left[\sqrt{\beta(1+g^2)}\vec{u}-\frac{g^2\vec{t}+\vec{t}'+\sqrt{\beta}(g^2\vec{d}_j+\vec{d}_{j'})}{\sqrt{1+g^2}}\right]^2-\frac{g^2}{1+g^2}\left[\sqrt{\beta}(\vec{d}_j-\vec{d}_{j'})+(\vec{t}-\vec{t}')\right]^2. \quad \text{(C.123)}$$

Setting $\vec{v}\equiv\sqrt{\beta(1+g^2)}\vec{u}-(g^2\vec{t}+\vec{t}'+\sqrt{\beta}(g^2\vec{d}_j+\vec{d}_{j'}))/\sqrt{1+g^2}$, the Gauss integral (D.118) over this new variable furnishes

$$\sum_{\mu\mu'}\chi^*_\mu(\vec{t})\chi^*_{\mu'}(\vec{t}')I^{(N)}_{j\mu j'\mu'}=\left(\frac{g\mu_{\mathrm{C}}\sqrt{\beta}}{\sqrt{1+g^2}}\right)^N \mathrm{e}^{-\delta^2+2\vec{\delta}\cdot\vec{T}-T^2}, \quad \text{(C.124)}$$

where we have defined

$$\vec{\delta}\equiv\frac{g\sqrt{\beta}}{\sqrt{1+g^2}}(\vec{d}_{j'}-\vec{d}_j), \quad \text{(C.125a)}$$

$$\vec{T}\equiv\frac{g}{\sqrt{1+g^2}}(\vec{t}-\vec{t}'). \quad \text{(C.125b)}$$

Applying the fundamental relation (C.485) again, but in reverse order, considering a wave function with a parameter $\beta=1$ defined by $\psi_\lambda(\sqrt{\beta}\vec{r})=\beta^{-N/4}\phi_\lambda(\vec{r})$, we obtain

$$\sum_{\mu\mu'}\chi^*_\mu(\vec{t})\chi^*_{\mu'}(\vec{t}')I^{(N)}_{j\mu j'\mu'}=\left(\frac{g\mu_{\mathrm{C}}\sqrt{\beta}}{\sqrt{1+g^2}}\right)^N \pi^{N/4}\mathrm{e}^{-\delta^2/2}\sum_\lambda\chi^*_\lambda(\vec{T})\psi_\lambda(\vec{\delta}). \quad \text{(C.126)}$$

Using the properties (C.491) and (C.493) of the generating functions, we can prove the equality

$$\chi^*_\lambda(\vec{T})=\left(\frac{g}{\sqrt{1+g^2}}\right)^{X_\lambda}\sum_{\mu\mu'}(-)^{X_\mu}\frac{\mathcal{N}_\mu\mathcal{N}_{\mu'}}{\mathcal{N}_{\mu+\mu'}}\chi_\mu(\vec{t})\chi_{\mu'}(\vec{t}')\delta_{\mu+\mu',-\lambda}, \quad \text{(C.127)}$$

where the coefficients $\mathcal{N}_\mu$ are given by (C.488) and X_μ by (C.492), such that eventually

$$\begin{aligned}\sum_{\mu\mu'}\chi^*_\mu(\vec{t})\chi^*_{\mu'}(\vec{t}')I^{(N)}_{j\mu j'\mu'}=&\left(\frac{g\mu_{\mathrm{C}}\sqrt{\beta}}{\sqrt{1+g^2}}\right)^N \pi^{N/4}\mathrm{e}^{-\delta^2/2}\sum_{\mu\mu'}(-)^{X_\mu}\frac{\mathcal{N}_\mu\mathcal{N}_{\mu'}}{\mathcal{N}_{\mu+\mu'}}\\&\times\left(\frac{g}{\sqrt{1+g^2}}\right)^{X_\mu+X_{\mu'}}\chi^*_\mu(\vec{t})\chi^*_{\mu'}(\vec{t}')\psi_{\mu+\mu'}(\vec{\delta}),\end{aligned} \quad \text{(C.128)}$$

where we have taken advantage of the properties (C.491) and (C.493) again. This equality is only true if the coefficients of the expansions of the generating functions $\chi^*_\mu(\vec{t})$ and $\chi^*_{\mu'}(\vec{t}')$ on both sides are equal, that is to say if

$$\boxed{I^{(N)}_{j\mu j'\mu'}=\frac{(-)^{X_\mu}\pi^{N/4}(\mu_{\mathrm{C}}\sqrt{\beta})^N}{(2+\beta\mu^2)^{(X_\mu+X_{\mu'}+N)/2}}\frac{\mathcal{N}_\mu\mathcal{N}_{\mu'}}{\mathcal{N}_{\mu+\mu'}}\mathrm{e}^{-\delta^2/2}\psi_{\mu+\mu'}(\vec{\delta}),} \quad \text{(C.129)}$$

where we have plugged the expression of g, given by (C.104). We can deduce the expression of the above quantity for $N=2$,

$$\begin{aligned}I^{(2)}_{m_\mu n_{\perp\mu}m'_\mu n'_{\perp\mu}}=&\,\delta_{m_\mu,-m'_\mu}\frac{\beta_\perp\mu_{\mathrm{C}}^2}{(2+\beta_\perp\mu_{\mathrm{C}}^2)^{n_{\perp\mu}+n'_{\perp\mu}+|m_\mu|+1}}\\&\times\frac{(n_{\perp\mu}+n'_{\perp\mu}+|m_\mu|)!}{\left[n_{\perp\mu}!(n_{\perp\mu}+|m_\mu|)!\,n'_{\perp\mu}!(n'_{\perp\mu}+|m_\mu|)!\right]^{1/2}},\end{aligned} \quad \text{(C.130)}$$

since (C.488) and (C.492). For $N = 1$, we have

$$I^{(1)}_{jn_{z\mu}j'n'_{z\mu}} = \frac{(-)^{n_{z\mu}}\pi^{1/4}\mu_{\mathrm{C}}\sqrt{\beta_z}}{(2+\beta_z\mu_{\mathrm{C}}^2)^{(n_{z\mu}+n'_{z\mu}+1)/2}}\left[\frac{(n_{z\mu}+n'_{z\mu})!}{n_{z\mu}!n'_{z\mu}!}\right]^2 \mathrm{e}^{-\delta_z^2/2}\psi_{n_{z\mu}+n'_{z\mu}}(\delta_z), \tag{C.131}$$

since (C.490) and (C.492), and where

$$\delta_z \equiv \sqrt{\frac{\beta_z}{2+\beta_z\mu_{\mathrm{C}}^2}}(d_{j'} - d_j). \tag{C.132}$$

Note that we could have applied the Moshinsky transformation in axial symmetry (C.516), directly on the wave functions appearing in equation (C.116) in order to move to center-of-mass and relative coordinates and solve the integral. This consistently brings the same result. We will not detail the related calculations here since this method will already be applied to derive the tensor and spin–orbit matrix elements in the following.

Density-dependent interaction

Now, let us continue by finding an expression for the spatial matrix elements associated with the density-dependent term. For this, we start from equation (C.97) again, but with $\alpha = 1/3 \neq 0$. The only angular dependence of the function $G_{jr_\mu}(\vec{u})$, given by (C.99), is contained in the wave function $\phi_{jr_\mu}(\vec{r}_g)$. Thus, by extracting the angular dependence of the wave function as we have done in (C.9), i.e. by writing

$$\phi_{jr_\mu}(\vec{r}_g) = \widetilde{\phi}_{j|r_\mu|}(r_g)\mathrm{e}^{\mathrm{i}m_\mu\varphi}, \tag{C.133}$$

we can similarly extract the angular dependence of the function $G_{jr_\mu}(\vec{r}_g)$,

$$G_{jr_\mu}(\vec{r}_g) = \widetilde{G}_{j|r_\mu|}(r_g)\mathrm{e}^{\mathrm{i}m_\mu\varphi}, \tag{C.134}$$

where

$$\widetilde{G}_{j|r_\mu|}(r_g) \equiv N_r\phi_{j0}(r_g)\widetilde{\phi}_{jr_\mu}(r_g). \tag{C.135}$$

Extracting the phases of the wave functions appearing in the two-body matrix element and taking into account that the local density is axially symmetric, i.e. $\rho(\vec{r}) = \rho(r)$, we obtain

$$\begin{aligned} v^{j_aj_cj_bj_d}_{r_ar_cr_br_d} = \pi\delta_{m_a+m_c,m_b+m_d}\int \mathrm{d}^2r\rho^\alpha(r)\Big[&\widetilde{\phi}_{j_a|r_a|}(r)\widetilde{\phi}_{j_b|r_b|}(r)\sum_{r_\mu} T^{r_\mu}_{j_cr_c\,j_dr_d}\widetilde{G}_{j_cd|r_\mu|}(r_g) \\ &+ \widetilde{\phi}_{j_c|r_c|}(r)\widetilde{\phi}_{j_d|r_d|}(r)\sum_{r'_\mu} T^{r'_\mu}_{j_ar_a\,j_br_b}\widetilde{G}_{j_ab|r'_\mu|}(r_g)\Big], \end{aligned} \tag{C.136}$$

where the Kronecker delta enforces the condition $m_a + m_c = m_b + m_d$ already deduced in (C.32), as a consequence of the fact that the central and density-dependent interactions commute with L_z (see section D.6).

Finally, setting

$$F_{j_ar_aj_br_b}(r_g) \equiv \sum_{r_\mu} T^{r_\mu}_{j_ar_a\,j_br_b}\widetilde{G}_{j_cd|r_\mu|}(r_g), \tag{C.137}$$

the two-body matrix elements can analytically be written

$$\boxed{\begin{aligned} v^{j_aj_cj_bj_d}_{r_ar_cr_br_d} = \pi\delta_{m_a+m_c,m_b+m_d}\int \mathrm{d}^2r\,\rho^\alpha(r) \\ \times\Big[\widetilde{\phi}_{j_a|r_a|}(r)\widetilde{\phi}_{j_b|r_b|}(r)F_{j_cdr_cr_d}(r_g) + \widetilde{\phi}_{j_c|r_c|}(r)\widetilde{\phi}_{j_d|r_d|}(r)F_{j_abr_ar_b}(r_g)\Big], \end{aligned}} \tag{C.138}$$

In the following, we will see how to approximate this integral which can be hardly evaluated analytically because of the expression of the local density, given by (III.50). More precisely, we will approximate an integral of the form

$$I \equiv \int \mathrm{d}^2 r\, \rho^\alpha(r) \widetilde{\phi}_{j_a|r_a|}(r) \widetilde{\phi}_{j_b|r_b|}(r) F_{j_c d r_c r_d}(r_g), \tag{C.139}$$

where we purposely omit the r and j indices for conciseness. First, we split up the wave functions and the function $F_{j_{cd} r_c r_d}(r_g)$ according to their radial and z parts, that is to say,

$$F_{j_{cd} r_c r_d}(r_g) = \sum_{n_{\perp\mu}} T^{m_\mu n_{\perp\mu}}_{m_c n_{\perp c} m_d n_{\perp d}} G_{|m_\mu| n_{\perp\mu}}(g_\perp r_\perp) \times \sum_{n_{z\mu}} T^{n_{z\mu}}_{j_c n_{zc}\, j_d n_{zd}} G_{n_{z\mu}}(g_z(z - d_{cd})), \tag{C.140}$$

where

$$G_{|m_\mu| n_{\perp\mu}}(g_\perp r_\perp) = N_\perp \phi_{00}(g_\perp r_\perp) \phi_{m_\mu n_{\perp\mu}}(g_\perp r_\perp), \tag{C.141a}$$

$$G_{n_{z\mu}}(g_z(z - d_{cd})) = N_z \phi_0(g_z(z - d_{cd})) \phi_{n_{z\mu}}(g_z(z - d_{cd})), \tag{C.141b}$$

with

$$N_\perp \equiv \pi \mu_{\mathrm{DD}}^2 g_\perp^{2n_{\perp\mu} + |m_\mu| + 2}, \tag{C.142a}$$

$$N_z \equiv \sqrt{\pi} \mu_{\mathrm{DD}} g_z^{n_{z\mu}+1}. \tag{C.142b}$$

Note that the range of the density-dependent term has been dubbed μ_{DD}. The integral (C.139) then becomes

$$I = \int_{-\infty}^{+\infty} \mathrm{d}z\, I_z(z) \underbrace{\int_0^\infty \mathrm{d}r_\perp\, I_\perp(r_\perp) \rho^\alpha(r_\perp, z)}_{I_1(z)}, \tag{C.143}$$

where

$$\begin{aligned} I_1(z) = {} & N_\perp \sum_{n_{\perp\mu}} T^{m_\mu n_{\perp\mu}}_{m_c n_{\perp c} m_d n_{\perp d}} \\ & \times \int_0^\infty \mathrm{d}r_\perp\, r_\perp \phi_{|m_a| n_{\perp a}}(r_\perp) \phi_{|m_b| n_{\perp b}}(r_\perp) \phi_{00}(g_\perp r_\perp) \phi_{|m_\mu| n_{\perp\mu}}(g_\perp r_\perp) \rho^\alpha(r_\perp, z). \end{aligned} \tag{C.144}$$

In order to apply the Gauss–Laguerre quadrature, we pull the exponentials out of the wave functions using (C.10), so that

$$\begin{aligned} I_1(z) = {} & N_\perp \sum_{n_{\perp\mu}} T^{m_\mu n_{\perp\mu}}_{m_c n_{\perp c} m_d n_{\perp d}} \int_0^\infty \mathrm{d}r_\perp\, r_\perp \mathrm{e}^{-(1+g_\perp^2) r_\perp^2 / b_\perp^2} \\ & \times \hat{\phi}_{|m_a| n_{\perp a}}(r_\perp) \hat{\phi}_{|m_b| n_{\perp b}}(r_\perp) \hat{\phi}_{00}(g_\perp r_\perp) \hat{\phi}_{|m_\mu| n_{\perp\mu}}(g_\perp r_\perp) \rho^\alpha(r_\perp, z). \end{aligned} \tag{C.145}$$

Setting $x \equiv (1 + g_\perp^2) r_\perp^2 / b_\perp^2$, we end up with

$$I_1(z) = \frac{N_\perp b_\perp^2}{2(1 + g_\perp^2)} \sum_{n_{\perp\mu}} T^{m_\mu n_{\perp\mu}}_{m_c n_{\perp c} m_d n_{\perp d}} \int_0^\infty \mathrm{d}x\, \mathrm{e}^{-x} f_{|m_\mu| n_{\perp\mu}}(x, z), \tag{C.146}$$

where we have defined

$$\begin{aligned} f_{|m_\mu| n_{\perp\mu}}(x, z) \equiv {} & \hat{\phi}_{|m_a| n_{\perp a}}\left(\frac{b_\perp}{\sqrt{1 + g_\perp^2}} \sqrt{x} \right) \hat{\phi}_{|m_b| n_{\perp b}}\left(\frac{b_\perp}{\sqrt{1 + g_\perp^2}} \sqrt{x} \right) \\ & \times \hat{\phi}_{00}\left(\frac{g_\perp b_\perp}{\sqrt{1 + g_\perp^2}} \sqrt{x} \right) \hat{\phi}_{|m_\mu| n_{\perp\mu}}\left(\frac{g_\perp b_\perp}{\sqrt{1 + g_\perp^2}} \sqrt{x} \right) \\ & \times \rho^\alpha\left(\frac{b_\perp}{\sqrt{1 + g_\perp^2}} \sqrt{x}, z \right). \end{aligned} \tag{C.147}$$

By means of the Gauss–Laguerre quadrature, we can approximate the above integral according to

$$\int_0^\infty \mathrm{d}x\, \mathrm{e}^{-x} f_{|m_\mu|n_{\perp\mu}}(x,z) \simeq \sum_{i=0}^{n} v_i f_{|m_\mu|n_{\perp\mu}}(x_i,z), \tag{C.148}$$

where n is the quadrature order, x_i the i-th root of the Laguerre polynomial $L_n(x)$ at which the function (C.147) is evaluated, and v_i a weight factor that reads

$$v_i \equiv \frac{x_i}{(n+1)^2[L_{n+1}(x_i)]^2}. \tag{C.149}$$

We obtain

$$\begin{aligned} I_1(z) \simeq \frac{N_\perp b_\perp^2}{2(1+g_\perp^2)} \sum_{n_{\perp\mu}} T^{m_\mu n_{\perp\mu}}_{m_c n_{\perp c} m_d n_{\perp d}} \sum_{i=0}^{n} v_i \\ \times \hat{\phi}_{|m_a|n_{\perp a}}(\widetilde{x}_i)\hat{\phi}_{|m_b|n_{\perp b}}(\widetilde{x}_i)\hat{\phi}_{00}(g_\perp \widetilde{x}_i)\hat{\phi}_{|m_\mu|n_{\perp\mu}}(g_\perp\widetilde{x}_i)\rho^\alpha(\widetilde{x}_i,z), \end{aligned} \tag{C.150}$$

with

$$\widetilde{x}_i \equiv \frac{b_\perp}{\sqrt{1+g_\perp^2}}\sqrt{x_i}. \tag{C.151}$$

To get an expression for (C.143), it remains to evaluate

$$I_2(\widetilde{x}_i) \equiv \int_{-\infty}^{+\infty} \mathrm{d}z\, I_z(z)\rho^\alpha(\widetilde{x}_i,z). \tag{C.152}$$

We have

$$\begin{aligned} I_2(\widetilde{x}_i) = N_z \sum_{n_{z\mu}} T^{n_{z\mu}}_{j_c n_{zc}\, j_d n_{zd}} \int_{-\infty}^{+\infty} \mathrm{d}z\, \phi_{n_{za}}(z-d_a)\phi_{n_{zb}}(z-d_b)\phi_0\Big(g_z(z-d_{cd})\Big) \\ \times \phi_{n_{z\mu}}\Big(g_z(z-d_{cd})\Big)\rho^\alpha(\widetilde{x}_i,z). \end{aligned} \tag{C.153}$$

In order to apply the Gauss–Hermite quadrature, we pull the exponentials out of the wave functions using (C.10), so that

$$\begin{aligned} I_2(\widetilde{x}_i) = N_z \sum_{n_{z\mu}} T^{n_{z\mu}}_{j_c n_{zc}\, j_d n_{zd}} \int_{-\infty}^{+\infty} \mathrm{d}z\, \mathrm{e}^{-[(z-d_a)^2+(z-d_b)^2+2g_z^2(z-d_{cd})^2]/2b_z^2}\hat{\phi}_{n_{za}}(z-d_a) \\ \times \hat{\phi}_{n_{zb}}(z-d_b)\hat{\phi}_0\Big(g_z(z-d_{cd})\Big)\hat{\phi}_{n_{z\mu}}\Big(g_z(z-d_{cd})\Big)\rho^\alpha(\widetilde{x}_i,z). \end{aligned} \tag{C.154}$$

Let us now complete the square of the argument of the exponential appearing in the integral above. It reads

$$\begin{aligned} -\left[\frac{\sqrt{1+g_z^2}}{b_z}z - \frac{d_a+d_b+2g_z^2 d_{cd}}{2b_z\sqrt{1+g_z^2}}\right]^2 + \frac{1}{2b_z^2}\left[\frac{(d_a+d_b+2g_z^2d_{cd})^2}{2(1+g_z^2)}\right. \\ \left. - \Big(d_a^2+d_b^2+2g_z^2d_{cd}^2\Big)\right], \end{aligned} \tag{C.155}$$

in such a way that we get

$$\begin{aligned} I_2(\widetilde{x}_i) = N_z \mathrm{e}^{[(d_a+d_b+2g_z^2d_{cd})^2/(2(1+g_z^2))-(d_a^2+d_b^2+2g_z^2d_{cd}^2)]/2b_z^2} \sum_{n_{z\mu}} T^{n_{z\mu}}_{j_c n_{zc}\, j_d n_{zd}} \\ \times \int_{-\infty}^{+\infty} \mathrm{d}z\, \mathrm{e}^{-\left[\sqrt{1+g_z^2}z/b_z-(d_a+d_b+2g_z^2d_{cd})/2b_z\sqrt{1+g_z^2}\right]^2}\hat{\phi}_{n_{za}}(z-d_a) \\ \times \hat{\phi}_{n_{zb}}(z-d_b)\hat{\phi}_0\Big(g_z(z-d_{cd})\Big)\hat{\phi}_{n_{z\mu}}\Big(g_z(z-d_{cd})\Big)\rho^\alpha(\widetilde{x}_i,z). \end{aligned} \tag{C.156}$$

The change of variable $y \equiv \sqrt{1+g_z^2}z/b_z - (d_a+d_b+2g_z^2 d_{cd})/2b_z\sqrt{1+g_z^2}$ provides

$$\begin{aligned} I_2(\widetilde{x}_i) = {} & \frac{N_z b_z}{\sqrt{1+g_z^2}} \mathrm{e}^{[(d_a+d_b+2g_z^2 d_{cd})^2/(2(1+g_z^2))-(d_a^2+d_b^2+2g_z^2 d_{cd}^2)]/2b_z^2} \\ & \times \sum_{n_{z\mu}} T^{n_{z\mu}}_{j_c n_{zc}\, j_d n_{zd}} \int_{-\infty}^{+\infty} \mathrm{d}y\, \mathrm{e}^{-y^2} g_{n_{z\mu}}(\widetilde{x}_i, y), \end{aligned} \tag{C.157}$$

where

$$\begin{aligned} g_{n_{z\mu}}(\widetilde{x}_i, y) \equiv {} & \hat{\phi}_{n_{za}}\left(\frac{b_z}{\sqrt{1+g_z^2}}y + \frac{d_a+d_b+2g_z^2 d_{cd}}{2(1+g_z^2)} - d_a\right) \\ & \times \hat{\phi}_{n_{zb}}\left(\frac{b_z}{\sqrt{1+g_z^2}}y + \frac{d_a+d_b+2g_z^2 d_{cd}}{2(1+g_z^2)} - d_b\right) \\ & \times \hat{\phi}_0\left(g_z\left(\frac{b_z}{\sqrt{1+g_z^2}}y + \frac{d_a+d_b+2g_z^2 d_{cd}}{2(1+g_z^2)} - d_{cd}\right)\right) \\ & \times \hat{\phi}_{n_{z\mu}}\left(g_z\left(\frac{b_z}{\sqrt{1+g_z^2}}y + \frac{d_a+d_b+2g_z^2 d_{cd}}{2(1+g_z^2)} - d_{cd}\right)\right) \\ & \times \rho^{\alpha}\left(\widetilde{x}_i, \frac{b_z}{\sqrt{1+g_z^2}}y + \frac{d_a+d_b+2g_z^2 d_{cd}}{2(1+g_z^2)}\right). \end{aligned} \tag{C.158}$$

By means of the Gauss–Hermite quadrature, we can approximate the above integral according to

$$\int_{-\infty}^{+\infty} \mathrm{d}y\, \mathrm{e}^{-y^2} g_{n_{z\mu}}(\widetilde{x}_i, y) \simeq \sum_{j=0}^{m} w_j g_{n_{z\mu}}(\widetilde{x}_i, y_j), \tag{C.159}$$

where m is the quadrature order, y_j the j-th root of the Hermite polynomial $H_m(y)$ at which the function (C.158) is evaluated, and w_j a weight factor that reads

$$w_j \equiv \frac{2^{m-1} m! \sqrt{\pi}}{m^2 [H_{m-1}(y_j)]^2}. \tag{C.160}$$

We obtain

$$\begin{aligned} I_2(\widetilde{x}_i) \simeq {} & \frac{N_z b_z}{\sqrt{1+g_z^2}} \mathrm{e}^{[(d_a+d_b+2g_z^2 d_{cd})^2/(2(1+g_z^2))-(d_a^2+d_b^2+2g_z^2 d_{cd}^2)]/2b_z^2} \\ & \times \sum_{n_{z\mu}} T^{n_{z\mu}}_{j_c n_{zc}\, j_d n_{zd}} \sum_{j=0}^{m} w_j \hat{\phi}_{n_{za}}(\widetilde{y}_j - d_a) \hat{\phi}_{n_{zb}}(\widetilde{y}_j - d_b) \\ & \times \hat{\phi}_0\Big(g_z(\widetilde{y}_j - d_{cd})\Big) \hat{\phi}_{n_{z\mu}}\Big(g_z(\widetilde{y}_j - d_{cd})\Big) \rho^{\alpha}(\widetilde{x}_i, \widetilde{y}_j), \end{aligned} \tag{C.161}$$

with

$$\widetilde{y}_j \equiv \frac{b_z}{\sqrt{1+g_z^2}} y_j + \frac{d_a+d_b+2g_z^2 d_{cd}}{2(1+g_z^2)}. \tag{C.162}$$

Combining the results (C.150) and (C.161), we can furnish an approximate expression for the integral (C.139) at the quadrature order (n, m). We find

$$\begin{aligned} I \simeq & \frac{N_\perp b_\perp^2}{2(1+g_\perp^2)} \frac{N_z b_z}{\sqrt{1+g_z^2}} \mathrm{e}^{[(d_a+d_b+2g_z^2 d_{cd})^2/(2(1+g_z^2))-(d_a^2+d_b^2+2g_z^2 d_{cd}^2)]/2b_z^2} \\ & \times \sum_{r_\mu} T^{r_\mu}_{j_a r_a\, j_b r_b} \sum_{i=0}^{n} \sum_{j=0}^{m} v_i w_j \hat{\phi}_{|r_a|}(\widetilde{x}_i, \widetilde{y}_j - d_a) \hat{\phi}_{|r_b|}(\widetilde{x}_i, \widetilde{y}_j - d_b) \\ & \times \hat{\phi}_0\Big(g_\perp \widetilde{x}_i, g_z(\widetilde{y}_j - d_{cd})\Big) \hat{\phi}_{|r_\mu|}\Big(g_\perp \widetilde{x}_i, g_z(\widetilde{y}_j - d_{cd})\Big) \rho^\alpha(\widetilde{x}_i, \widetilde{y}_j), \end{aligned} \tag{C.163}$$

where we have gathered the axial and z-relative Talman coefficients as well as the $\widetilde{x}_i$- and $\widetilde{y}_j$-dependent wave functions, where the latter coordinates are respectively given by (C.151) and (C.162).

2.1.4. Rearrangement fields associated with the mean fields

As already mentioned in the first section, since the generalized Gogny interaction (II.1) contains a density-dependent term, rearrangement fields arise. In this subsection, we will derive the rearrangement fields associated with the mean fields (III.37) and (III.38). According to their expressions (III.42) and (III.43), we first need to evaluate the derivative of the interaction (C.26) (that we will simply call the density-dependent interaction (DD) in the following, the central terms not giving rise to rearrangement fields), with respect to ρ_{ba} and $\overline{\rho}_{ba}$. This interaction only depends on the density through the local nuclear density $\rho(\vec{r})$, so that we can write

$$\frac{\partial v_{12}^{\mathrm{DD}}}{\partial \rho_{ba}} = \int \mathrm{d}^3 r \, \frac{\partial v_{12}^{\mathrm{DD}}}{\partial \rho(\vec{r})} \frac{\partial \rho(\vec{r})}{\partial \rho_{ba}}, \tag{C.164a}$$

$$\frac{\partial v_{12}^{\mathrm{DD}}}{\partial \overline{\rho}_{ba}} = \int \mathrm{d}^3 r \, \frac{\partial v_{12}^{\mathrm{DD}}}{\partial \rho(\vec{r})} \frac{\partial \rho(\vec{r})}{\partial \overline{\rho}_{ba}}. \tag{C.164b}$$

We have to derive the nuclear density we have defined in (III.50). We find out [2]

$$\frac{1+\delta_{ab}}{2} \frac{\partial \rho(\vec{r})}{\partial \rho_{ba}} = \frac{1+\delta_{ab}}{2} \frac{\partial \rho(\vec{r})}{\partial \overline{\rho}_{ba}} = \delta_{m_a m_b} \phi^*_{j_b m_a \nu_b}(\vec{r}) \phi_{j_a m_a \nu_a}(\vec{r}), \tag{C.165}$$

where $a = (t, \Omega, \nu_a, m_a)$ and $b = (t, \Omega, \nu_b, m_b)$. We deduce from (C.164) that the partial derivatives of v_{12}^{DD} with respect to ρ_{ba} and $\overline{\rho}_{ba}$ are equal. The rearrangement fields $\partial\Gamma$ and $\partial\overline{\Gamma}$ are then constructed from the same "derived interaction" ∂v_{12}^{ab}, that we define as

$$\partial v_{12}^{ab} \equiv \frac{1+\delta_{ab}}{2} \frac{\partial v_{12}^{\mathrm{DD}}}{\partial \rho_{ba}} = \frac{1+\delta_{ab}}{2} \frac{\partial v_{12}^{\mathrm{DD}}}{\partial \overline{\rho}_{ba}} = \delta_{m_a m_b} \int \mathrm{d}^3 r \, \frac{\partial v_{12}^{\mathrm{DD}}}{\partial \rho(\vec{r})} \phi^*_{j_b m_a \nu_b}(\vec{r}) \phi_{j_a m_a \nu_a}(\vec{r}), \tag{C.166}$$

where we have omitted the superscript DD in the name of the derived interaction since, by definition, only the density-dependent term generates such a quantity. It follows that

2. To perform this derivative, it may be worthwhile to expand the summations over ν and ν' to see that $\rho_{m\nu_a, m\nu_b}$ and $\rho_{m\nu_b, m\nu_a}$ (respectively, $\overline{\rho}_{m\nu_a, m\nu_b}$ and $\overline{\rho}_{m\nu_b, m\nu_a}$) bring the same contribution when derived with respect to ρ_{ba} (with respect to $\overline{\rho}_{ba}$, respectively) because of their symmetry under the exchange of their indices. That explains the factor 2 in the denominator in the case $\nu_a \neq \nu_b$. Moreover, when $m = 0$, we necessarily have $s_a = s_b = 1/2$ because $\Omega > 0$, so that we do not need to take into account the case $\Omega = m - 1/2$.

the matrix elements composing the rearrangement fields $\partial\Gamma$ and $\partial\overline{\Gamma}$ are the same, so that the rearrangement fields themselves are equal, i.e.

$$\boxed{\partial\Gamma_{ab} = \partial\overline{\Gamma}_{ab}.} \tag{C.167}$$

To fully specify the derived interaction, it remains to evaluate the derivative of the DD interaction with respect to the total nuclear density. Given the form of this interaction, (C.26), we find

$$\frac{\partial v_{12}^{\mathrm{DD}}}{\partial\rho(\vec{r})} = \frac{\alpha}{2}(W + BP_\sigma - HP_\tau - MP_\sigma P_\tau)V(r_{12})\Big(\delta(\vec{r}-\vec{r}_1) + \delta(\vec{r}-\vec{r}_2)\Big)\rho^{\alpha-1}(\vec{r}). \tag{C.168}$$

Consequently, the derived interaction can be written

$$\boxed{\partial v_{12}^{ab} = (W + BP_\sigma - HP_\tau - MP_\sigma P_\tau)V(r_{12})D'_{ab}[\rho],} \tag{C.169}$$

where

$$\boxed{\begin{aligned} D'_{ab}[\rho] \equiv \frac{\alpha}{2}\delta_{m_a m_b}\Big[&\rho^{\alpha-1}(\vec{r}_1)\phi^*_{j_b m_a \nu_b}(\vec{r}_1)\phi_{j_a m_a \nu_a}(\vec{r}_1) \\ &+ \rho^{\alpha-1}(\vec{r}_2)\phi^*_{j_b m_a \nu_b}(\vec{r}_2)\phi_{j_a m_a \nu_a}(\vec{r}_2)\Big]. \end{aligned}} \tag{C.170}$$

We notice that the derived interaction is similar to the density-dependent interaction v_{12}^{DD}; only the functional $D[\rho]$ is replaced by $D'_{ab}[\rho]$ in its expression. The antisymmetrized derived interaction also looks like the antisymmetrized DD interaction (C.26), since

$$\partial v_{12}^{ab,(\mathrm{a})} \equiv \partial v_{12}^{ab}(1 - P_r P_\sigma P_\tau) = \mathcal{P}_{\mathrm{D}} V(r_{12})D'_{ab}[\rho] + \mathcal{P}_{\mathrm{E}} V(r_{12})D'_{ab}[\rho], \tag{C.171}$$

where the combinations of exchange operators $\mathcal{P}_{\mathrm{D}}$ and $\mathcal{P}_{\mathrm{E}}$ are given by (C.29). With these notations, the rearrangement fields (III.42) and (III.43) are

$$\begin{aligned} \partial\Gamma_{ab} = \sum_{a'b'c'd'>0} \Big[&\langle a'c'|\partial v_{12}^{ab,(\mathrm{a})}|b'd'\rangle \frac{1}{2}\Big(\rho_{b'a'}\rho_{d'c'} + \overline{\rho}_{b'a'}\overline{\rho}_{d'c'}\Big) \\ &+ \langle a'\overline{c'}|\partial v_{12}^{ab,(\mathrm{a})}|b'\overline{d'}\rangle \rho_{b'a'}\overline{\rho}_{d'c'}\Big]. \end{aligned} \tag{C.172}$$

Let us remark that the antisymmetrized derived interaction is diagonal in m (as we have $m \equiv m_a = m_b$), since $D'_{ab}[\rho]$ is. On the other hand, we recall that the rearrangement fields are also diagonal in $t \equiv t_a = t_b$ and in $\Omega \equiv \Omega_a = \Omega_b$ (see (C.22)). Moreover, we notice that $\partial v_{12}^{ab,(a)}$ does not explicitly depend on t, nor on Ω (because it does not depend on the spins s_a and s_b). Accordingly, the matrix elements of the rearrangement field above, and the rearrangement field itself, are independent of t and Ω. We can then remove these indices and write

$$\partial\Gamma^{t\Omega}_{m_a\nu_a, m_b\nu_b} = \delta_{m_a m_b}\partial\Gamma_{m_a\nu_a, m_a\nu_b}. \tag{C.173}$$

We shall then evaluate

$$\begin{aligned} \partial\Gamma_{m\nu_a, m\nu_b} = \sum_{a'b'c'd'>0} \Big[&\langle a'c'|\partial v_{12}^{ab,(\mathrm{a})}|b'd'\rangle \frac{1}{2}\Big(\rho_{b'a'}\rho_{d'c'} + \overline{\rho}_{b'a'}\overline{\rho}_{d'c'}\Big) \\ &+ \langle a'\overline{c'}|\partial v_{12}^{ab,(\mathrm{a})}|b'\overline{d'}\rangle \rho_{b'a'}\overline{\rho}_{d'c'}\Big], \end{aligned} \tag{C.174}$$

where, as explained before, $a = (m, \nu_a)$, $b = (m, \nu_b)$ and $a' = (t', \Omega', m'_a, \nu'_a)$. In order to simplify the rearrangement field, it is convenient to introduce new fields, analogous to the

mean fields (III.37) and (III.38), but where the matrix elements of the antisymmetrized derived interaction, rather than the matrix elements of the standard antisymmetrized interaction, are considered. These fields, called the "auxiliary mean fields" in the following, are defined as

$$\boxed{\begin{aligned}(\widetilde{\Gamma}^{ab})_{a'b'} &\equiv \sum_{c'd'>0}\Big[\langle a'c'|\partial v_{12}^{ab,(\mathrm{a})}|b'd'\rangle\rho_{d'c'} + \langle a'\overline{c'}|\partial v_{12}^{ab,(\mathrm{a})}|b'\overline{d'}\rangle\overline{\rho}_{c'd'}\Big], \qquad \text{(C.175a)}\\ (\widetilde{\overline{\Gamma}}^{ab})_{a'b'} &\equiv \sum_{c'd'>0}\Big[\langle a'c'|\partial v_{12}^{ab,(\mathrm{a})}|b'd'\rangle\overline{\rho}_{d'c'} + \langle a'\overline{c'}|\partial v_{12}^{ab,(\mathrm{a})}|b'\overline{d'}\rangle\rho_{c'd'}\Big]. \qquad \text{(C.175b)}\end{aligned}}$$

The rearrangement field can then be written as

$$\boxed{\partial\Gamma_{ab} = \frac{1}{2}\sum_{a'b'>0}\Big[(\widetilde{\Gamma}^{ab})_{a'b'}\rho_{b'a'} + (\widetilde{\overline{\Gamma}}^{ab})_{a'b'}\overline{\rho}_{b'a'}\Big].} \qquad \text{(C.176)}$$

Indeed, plugging (C.175) in (C.176), we get

$$\begin{aligned}\partial\Gamma_{ab} &= \frac{1}{2}\sum_{a'b'c'd'>0}\Big[\Big(\langle a'c'|\partial v_{12}^{ab,(\mathrm{a})}|b'd'\rangle\rho_{d'c'} + \langle a'\overline{c'}|\partial v_{12}^{ab,(\mathrm{a})}|b'\overline{d'}\rangle\overline{\rho}_{c'd'}\Big)\rho_{b'a'}\\ &\qquad + \Big(\langle a'c'|\partial v_{12}^{ab,(\mathrm{a})}|b'd'\rangle\overline{\rho}_{d'c'} + \langle a'\overline{c'}|\partial v_{12}^{ab,(\mathrm{a})}|b'\overline{d'}\rangle\rho_{c'd'}\Big)\overline{\rho}_{b'a'}\Big]\\ &= \sum_{a'b'c'd'>0}\Big[\langle a'c'|\partial v_{12}^{ab,(\mathrm{a})}|b'd'\rangle\frac{1}{2}\Big(\rho_{b'a'}\rho_{d'c'} + \overline{\rho}_{b'a'}\overline{\rho}_{d'c'}\Big)\\ &\qquad + \langle a'\overline{c'}|\partial v_{12}^{ab,(\mathrm{a})}|b'\overline{d'}\rangle\frac{1}{2}\Big(\rho_{b'a'}\overline{\rho}_{d'c'} + \overline{\rho}_{b'a'}\rho_{c'd'}\Big)\Big].\end{aligned} \qquad \text{(C.177)}$$

Now, relabelling the quantum numbers and considering the symmetry of the density matrices ρ and $\overline{\rho}$ under the exchange of their indices, we obtain

$$\begin{aligned}\sum_{a'b'c'd'>0}\langle a'\overline{c'}|\partial v_{12}^{ab,(\mathrm{a})}|b'\overline{d'}\rangle\overline{\rho}_{b'a'}\rho_{c'd'} &= \sum_{a'b'c'd'>0}\langle c'\overline{a'}|\partial v_{12}^{ab,(\mathrm{a})}|d'\overline{b'}\rangle\overline{\rho}_{d'c'}\rho_{a'b'} \qquad \text{(C.178)}\\ &= \sum_{a'b'c'd'>0}\langle c'\overline{a'}|\partial v_{12}^{ab,(\mathrm{a})}|d'\overline{b'}\rangle\overline{\rho}_{c'd'}\rho_{b'a'}. \qquad \text{(C.179)}\end{aligned}$$

It only remains to prove that $\langle c'\overline{a'}|\partial v_{12}^{ab,(\mathrm{a})}|d'\overline{b'}\rangle = \langle a'\overline{c'}|\partial v_{12}^{ab,(\mathrm{a})}|b'\overline{d'}\rangle$, and then we will have equality between (C.174) and (C.176). We can write

$$\begin{aligned}\langle a'\overline{c'}|\partial v_{12}^{ab,(\mathrm{a})}|b'\overline{d'}\rangle &= \Big(\langle\overline{a'}c'|T_1^\dagger T_2^\dagger\Big)\,\partial v_{12}^{ab,(\mathrm{a})}\Big(T_2T_1|\overline{b'}d'\rangle\Big)\\ &= \Big[\langle\overline{a'}c'|\Big(T_1^\dagger T_2^\dagger\partial v_{12}^{ab,(\mathrm{a})}T_2T_1|\overline{b'}d'\rangle\Big)\Big]^*\\ &= \langle\overline{a'}c'|\partial v_{12}^{ab,(\mathrm{a})}|\overline{b'}d'\rangle^*\\ &= \langle\overline{a'}c'|\partial v_{12}^{ab,(\mathrm{a})}|\overline{b'}d'\rangle\\ &= \langle c'\overline{a'}|\partial v_{12}^{ab,(\mathrm{a})}|d'\overline{b'}\rangle. \qquad \text{(C.180)}\end{aligned}$$

From the first to the second line, we have noticed that the derived interaction is Hermitian, i.e. $\partial v_{12}^{ab\dagger} = \partial v_{12}^{ab}$, according to its expression (C.169). From the second to the third line, we have considered the fact that ∂v_{12}^{ab} is time-reversal invariant, since v_{12} is (see equation (I.9)). [3] From the third to the fourth line, we have observed that the matrix elements

3. Indeed, applying the time-reversal operator on ∂v_{12}^{ab}, we find

$$\overline{\partial v_{12}^{ab}} = \frac{1+\delta_{ab}}{2}\frac{\overline{\partial v_{12}^{\mathrm{DD}}}}{\partial\rho_{ba}} = \frac{1+\delta_{ab}}{2}\frac{\partial v_{12}^{\mathrm{DD}}}{\partial\overline{\rho}_{ba}} = \frac{1+\delta_{ab}}{2}\frac{\partial v_{12}^{\mathrm{DD}}}{\partial\rho_{ba}} = \partial v_{12}^{ab}, \qquad \text{(C.181)}$$

since v_{12}^{DD} is time-reversal invariant.

of ∂v_{12}^{ab} are real, as we can carry out the exact same analysis we have done to show that the matrix elements of v_{12} are real (see equation (III.16)). Finally, from the fourth to the last line, we have taken into account the invariance of ∂v_{12}^{ab} under the exchange of the two particles, as it appears clearly from its expression (C.169). [4] Thus, the rearrangement field associated with the mean fields can be written (C.176).

With this writing of the rearrangement field, we can benefit from the results already derived for the mean fields in subsection C.2.1.1. We just have to replace the standard antisymmetrized interaction $v_{12}^{\mathrm{DD},(\mathrm{a})}$ by the antisymmetrized derived one, $\partial v_{12}^{ab,(\mathrm{a})}$ (they are detailed further, in (C.186)).

It remains to treat the summation in (C.176). Let us consider the first term only (the second one is identical, we just need to put a bar on top of the quantities). It reads

$$T^{ab} \equiv \frac{1}{2} \sum_{a'b'>0} \widetilde{\Gamma}^{ab}_{a'b'} \rho_{b'a'} = \sum_{\substack{\Omega'>0 \\ m'_a m'_b}} (g^{ab})^{\Omega'}_{m'_a m'_b}, \tag{C.182}$$

with

$$(g^{ab})^{\Omega'}_{m'_a m'_b} \equiv \frac{1}{2} \sum_{t'\nu'_a\nu'_b} (\widetilde{\Gamma}^{ab})^{t'\Omega'}_{m'_a\nu'_a,m'_b\nu'_b} \rho^{t'\Omega'}_{m'_a\nu'_a,m'_b\nu'_b}, \tag{C.183}$$

where we have used the symmetry of the density matrix ρ under the exchange of its indices. First carrying out the summation over $m'_a = \Omega' \pm 1/2$ and $m'_b = \Omega' \pm 1/2$, then considering $m' \equiv \Omega' \pm 1/2$ and finally gathering the terms using the symmetry of g^{ab} under the exchange of its indices m'_a and m'_b (since both $\widetilde{\Gamma}^{ab}$ and ρ exhibit this symmetry), we successively find

$$\begin{aligned}
T^{ab} &= \sum_{\Omega'>0} \Big[(g^{ab})^{\Omega'}_{\Omega'-1/2,\Omega'-1/2} + (g^{ab})^{\Omega'}_{\Omega'-1/2,\Omega'+1/2} \\
&\qquad\qquad + (g^{ab})^{\Omega'}_{\Omega'+1/2,\Omega'-1/2} + (g^{ab})^{\Omega'}_{\Omega'+1/2,\Omega'+1/2} \Big] \\
&= \sum_{m'\geq 0} \Big[(g^{ab})^{m'+1/2}_{m',m'} + (g^{ab})^{m'+1/2}_{m'+1,m'} + (g^{ab})^{m'+1/2}_{m',m'+1} + (g^{ab})^{m'+1/2}_{m'+1,m'+1} \Big] \\
&= \sum_{m'\geq 0} \Big[(g^{ab})^{m'+1/2}_{m',m'} + 2(g^{ab})^{m'+1/2}_{m',m'+1} + \Theta(m'-1/2)(g^{ab})^{m'-1/2}_{m',m'} \Big] \\
&= \sum_{m'\geq 0} \Big[\Big(\sum_{s'=\pm 1/2} \Theta(m'+s')(g^{ab})^{m'+s'}_{m',m'} \Big) + 2(g^{ab})^{m'+1/2}_{m',m'+1} \Big].
\end{aligned} \tag{C.184}$$

Thus, the rearrangement field (C.174) eventually becomes

$$\boxed{\begin{aligned}
\partial\Gamma_{ab} = \frac{1}{2} \sum_{\substack{t'm'\geq 0 \\ \nu'_a\nu'_b}} \Big[&\Big(\sum_{s'=\pm 1/2} \Theta(m'+s') (\widetilde{\Gamma}^{ab})^{t'm'+s'}_{m'\nu'_a,m'\nu'_b} \rho^{t'm'+s'}_{m'\nu'_a,m'\nu'_b} \Big) \\
&+ 2(\widetilde{\Gamma}^{ab})^{t'm'+1/2}_{m'\nu'_a,m'+1\,\nu'_b} \rho^{t'm'+1/2}_{m'\nu'_a,m'+1\,\nu'_b} \\
&+ \Big(\sum_{s'=\pm 1/2} \Theta(m'+s') (\widetilde{\overline{\Gamma}}^{ab})^{t'm'+s'}_{m'\nu'_a,m'\nu'_b} \overline{\rho}^{t'm'+s'}_{m'\nu'_a,m'\nu'_b} \Big) \\
&+ 2(\widetilde{\overline{\Gamma}}^{ab})^{t'm'+1/2}_{m'\nu'_a,m'+1\,\nu'_b} \overline{\rho}^{t'm'+1/2}_{m'\nu'_a,m'+1\,\nu'_b} \Big],
\end{aligned}} \tag{C.185}$$

4. Note that all the properties of the derived interaction we have listed are also satisfied by the nuclear interaction v_{12}. In fact, this was to be expected since the rearrangement fields must retain the properties of the mean- and pairing fields, which are imposed by the symmetries of v_{12} (see subsection I.1.2).

where we recall that $a = (m, \nu_a)$ and $b = (m, \nu_b)$. Note that we will also take care to consider the direct *and* exchange contributions of the auxiliary mean fields, that is to say $\widetilde{\Gamma}^{ab} \equiv \widetilde{\Gamma}^{ab}|_{\mathrm{D}} + \widetilde{\Gamma}^{ab}|_{\mathrm{E}}$ and $\widetilde{\overline{\Gamma}}^{ab} \equiv \widetilde{\overline{\Gamma}}^{ab}|_{\mathrm{D}} + \widetilde{\overline{\Gamma}}^{ab}|_{\mathrm{E}}$. Explicitly, they read:

$$(\widetilde{\Gamma}^{ab})^{t'\Omega'=m'+s'}_{m'\nu'_a,\,m'\nu'_b}|_{\mathrm{E}} = \sum_{\substack{m''\geq 0\\ \nu'_c\nu'_d}} \Big[\langle m'\nu'_a\ m''\nu'_c|V(r_{12})F'_{ab}[\rho]|m''\nu'_d\ m'\nu'_b\rangle R^{(+)t's'0}_{m''\nu'_d\nu'_c}|_{\mathrm{E}} + \langle m'\nu'_a\ -m''\nu'_c|V(r_{12})F'_{ab}[\rho]|-m''\nu'_d\ m'\nu'_b\rangle R^{(-)t's'0}_{m''\nu'_c\nu'_d}|_{\mathrm{E}}\Big], \tag{C.186a}$$

$$(\widetilde{\Gamma}^{ab})^{t'\Omega'=m'+s'}_{m'\nu'_a,\,m'\nu'_b}|_{\mathrm{D}} = \sum_{\substack{m''\geq 0\\ \nu'_c\nu'_d}} \langle m'\nu'_a\ m''\nu'_c|V(r_{12})F'_{ab}[\rho]|m'\nu'_b\ m''\nu'_d\rangle R^{t's'0}_{m''\nu'_d\nu'_c}|_{\mathrm{D}}, \tag{C.186b}$$

$$(\widetilde{\Gamma}^{ab})^{t'\Omega'=m'+1/2}_{m'\nu'_a,\,m'+1\,\nu'_b}|_{\mathrm{E}} = \sum_{\substack{m''\geq 0\\ \nu'_c\nu'_d}} \times \Big[\langle m'\nu'_a\ m''+1\,\nu'_c|V(r_{12})F'_{ab}[\rho]|m''\nu'_d\ m'+1\,\nu'_b\rangle\, R^{(+)t'1/2\,1}_{m''\nu'_d\nu'_c}|_{\mathrm{E}} + \langle m'\nu'_a\ -m''\nu'_c|V(r_{12})F'_{ab}[\rho]|-(m''+1)\,\nu'_d\ m'+1\,\nu'_b\rangle R^{(-)t'1/2\,1}_{m''\nu'_c\nu'_d}|_{\mathrm{E}}\Big], \tag{C.186c}$$

$$(\widetilde{\Gamma}^{ab})^{t'\Omega'=m'+1/2}_{m'\nu'_a,\,m'+1\,\nu'_b}|_{\mathrm{D}} = \sum_{\substack{m''\geq 0\\ \nu'_c\nu'_d}} \times \langle m'\nu'_a\ m''+1\,\nu'_c|V(r_{12})F'_{ab}[\rho]|m'+1\,\nu'_b\ m''\nu'_d\rangle R^{t'1/2\,1}_{m''\nu'_d\nu'_c}|_{\mathrm{D}}, \tag{C.186d}$$

$$(\widetilde{\overline{\Gamma}}^{ab})^{t'\Omega'=m'+s'}_{m'\nu'_a,\,m'\nu'_b}|_{\mathrm{E}} = \sum_{\substack{m''\geq 0\\ \nu'_c\nu'_d}} \Big[\langle m'\nu'_a\ m''\nu'_c|V(r_{12})F'_{ab}[\rho]|m''\nu'_d\ m'\nu'_b\rangle R^{(-)t'-s'0}_{m''\nu'_d\nu'_c}|_{\mathrm{E}} + \langle m'\nu'_a\ -m''\nu'_c|V(r_{12})F'_{ab}[\rho]|-m''\nu'_d\ m'\nu'_b\rangle R^{(+)t'-s'0}_{m''\nu'_c\nu'_d}|_{\mathrm{E}}\Big], \tag{C.186e}$$

$$(\widetilde{\overline{\Gamma}}^{ab})^{t'\Omega'=m'+s'}_{m'\nu'_a,\,m'\nu'_b}|_{\mathrm{D}} = \sum_{\substack{m''\geq 0\\ \nu'_c\nu'_d}} \langle m'\nu'_a\ m''\nu'_c|V(r_{12})F'_{ab}[\rho]|m'\nu'_b\ m''\nu'_d\rangle R^{t'-s'0}_{m''\nu'_d\nu'_c}|_{\mathrm{D}}, \tag{C.186f}$$

$$(\widetilde{\overline{\Gamma}}^{ab})^{t'\Omega'=m'+1/2}_{m'\nu'_a,\,m'+1\,\nu'_b}|_{\mathrm{E}} = -\sum_{\substack{m''\geq 0\\ \nu'_c\nu'_d}} \times \Big[\langle m'\nu'_a\ m''+1\,\nu'_c|V(r_{12})F'_{ab}[\rho]|m''\nu'_d\ m'+1\,\nu'_b\rangle R^{(-)t'1/2\,1}_{m''\nu'_d\nu'_c}|_{\mathrm{E}} + \langle m'\nu'_a\ -m''\nu'_c|V(r_{12})F'_{ab}[\rho]|-(m''+1)\,\nu'_d\ m'+1\,\nu'_b\rangle R^{(+)t'1/2\,1}_{m''\nu'_c\nu'_d}|_{\mathrm{E}}\Big], \tag{C.186g}$$

$$(\widetilde{\overline{\Gamma}}^{ab})^{t'\Omega'=m'+1/2}_{m'\nu'_a,\,m'+1\,\nu'_b}|_{\mathrm{D}} = -\sum_{\substack{m''\geq 0\\ \nu'_c\nu'_d}} \times \langle m'\nu'_a\ m''+1\,\nu'_c|V(r_{12})F'_{ab}[\rho]|m'+1\,\nu'_b\ m''\nu'_d\rangle R^{t'1/2\,1}_{m''\nu'_d\nu'_c}|_{\mathrm{D}}, \tag{C.186h}$$

where the quantities R appearing are given by (C.45), (C.47), (C.49) or (C.51).

Now, we assume the time-reversal invariance of the rearrangement field associated with the mean fields, i.e. we set $\rho = \overline{\rho}$. In this case, the fields we have introduced coincide, that is to say $\widetilde{\Gamma}^{ab} = \widetilde{\overline{\Gamma}}^{ab}$. The rearrangement field then simplifies according to the following expressions, where the notation $|^{\mathrm{T}}$ identifies the time-reversal invariant quantities. The

exchange contribution reads

$$\boxed{\begin{aligned}\partial\Gamma_{ab}|^{\mathrm{T}}_{\mathrm{E}} = \sum_{\substack{t'm'\geq 0\\ \nu'_a\nu'_b}} \Big[&(\widetilde{\Gamma}^{ab})^{t'm'+1/2}_{m'\nu'_a,m'\nu'_b}|^{\mathrm{T}}_{\mathrm{E}}\,\rho^{t'm'+1/2}_{m'\nu'_a,m'\nu'_b}\\ &+\Theta(m'-1/2)(\widetilde{\Gamma}^{ab})^{t'm'-1/2}_{m'\nu'_a,m'\nu'_b}|^{\mathrm{T}}_{\mathrm{E}}\,\rho^{t'm'-1/2}_{m'\nu'_a,m'\nu'_b} + 2(\widetilde{\Gamma}^{ab})^{t'm'+1/2}_{m'\nu'_a,m'+1\,\nu'_b}|^{\mathrm{T}}_{\mathrm{E}}\,\rho^{t'm'+1/2}_{m'\nu'_a,m'+1\,\nu'_b}\Big],\end{aligned}} \tag{C.187}$$

while the direct one is

$$\boxed{\partial\Gamma_{ab}|^{\mathrm{T}}_{\mathrm{D}} = \sum_{\substack{t'm'\geq 0\\ \nu'_a\nu'_b}} \Big[(\widetilde{\Gamma}^{ab})^{t'm'+1/2}_{m'\nu'_a,m'\nu'_b}|^{\mathrm{T}}_{\mathrm{D}}\Big(\rho^{t'm'+1/2}_{m'\nu'_a,m'\nu'_b} + \Theta(m'-1/2)\rho^{t'm'-1/2}_{m'\nu'_a,m'\nu'_b}\Big)\Big],} \tag{C.188}$$

because, the direct parts of the auxiliary mean fields (C.175), similarly to the direct mean fields, are diagonal in m and independent of Ω. Indeed, explicitly:

$$\begin{aligned}(\widetilde{\Gamma}^{ab})^{t'\Omega'=m'+s'}_{m'\nu'_a,\,m'\nu'_b}|^{\mathrm{T}}_{\mathrm{E}} = \sum_{\substack{m''\geq 0\\ \nu'_c\nu'_d}} \Big[&\langle m'\nu'_a\ m''\nu'_c|V(r_{12})F'_{ab}[\rho]|m''\nu'_d\ m'\nu'_b\rangle R^{t's'0}_{m''\nu'_d\nu'_c}|^{\mathrm{T}}_{\mathrm{E}}\\ &+\langle m'\nu'_a\ -m''\nu'_c|V(r_{12})F'_{ab}[\rho]|-m''\nu'_d\ m'\nu'_b\rangle R^{t'-s'0}_{m''\nu'_c\nu'_d}|^{\mathrm{T}}_{\mathrm{E}}\Big],\end{aligned} \tag{C.189a}$$

$$(\widetilde{\Gamma}^{ab})^{t'\Omega'=m'+s'}_{m'\nu'_a,\,m'\nu'_b}|^{\mathrm{T}}_{\mathrm{D}} = \sum_{\substack{m''\geq 0\\ \nu'_c\nu'_d}} \langle m'\nu'_a\ m''\nu'_c|V(r_{12})F'_{ab}[\rho]|m'\nu'_b\ m''\nu'_d\rangle R^{t'0}_{m''\nu'_d\nu'_c}|^{\mathrm{T}}_{\mathrm{D}}, \tag{C.189b}$$

$$\begin{aligned}(\widetilde{\Gamma}^{ab})^{t'\Omega'=m'+1/2}_{m'\nu'_a,\,m'+1\,\nu'_b}|^{\mathrm{T}}_{\mathrm{E}} = \sum_{\substack{m''\geq 0\\ \nu'_c\nu'_d}} \Big[&\langle m'\nu'_a\ m''+1\,\nu'_c|V(r_{12})F'_{ab}[\rho]|m''\nu'_d\ m'+1\,\nu'_b\rangle\\ &-\langle m'\nu'_a\ -m''\nu'_d|V(r_{12})F'_{ab}[\rho]|-(m''+1)\,\nu'_c\ m'+1\,\nu'_b\rangle\Big] R^{t'1/2\,1}_{m''\nu'_d\nu'_c}|^{\mathrm{T}}_{\mathrm{E}},\end{aligned} \tag{C.189c}$$

$$(\widetilde{\Gamma}^{ab})^{t'\Omega'=m'+1/2}_{m'\nu'_a,\,m'+1\,\nu'_b}|^{\mathrm{T}}_{\mathrm{D}} = 0, \tag{C.189d}$$

where the quantities R appearing are given by (C.63), (C.65) or (C.68). We note that we recover the expressions of the time-reversal invariant rearrangement fields associated with mean fields obtained by Chappert [17].

2.1.5. Rearrangement fields associated with the pairing field

In this subsection, we will derive the rearrangement fields associated with the pairing field (III.32). According to their expressions (III.44) and (III.45), we first need to evaluate the derivative of the interaction (C.26) (that we will simply call the density-dependent interaction (DD) in the following, the central terms not giving rise to rearrangement fields), with respect to ρ_{ba} and $\overline{\rho}_{ba}$. In the previous subsection, we have shown that the derivatives of this interaction with respect to ρ_{ba} and $\overline{\rho}_{ba}$ were the same, so that, as for the rearrangement fields associated with the mean fields, $\partial\Gamma$ and $\partial\overline{\Gamma}$, the rearrangement fields associated with the pairing field, $\partial\Delta$ and $\partial\overline{\Delta}$, are constructed from the same "derived interaction" ∂v^{ab}_{12}, that we have defined in (C.169). As a consequence, the matrix elements composing the rearrangement fields $\partial\Delta$ and $\partial\overline{\Delta}$ are the same, so that the rearrangement fields themselves are equal, i.e.

$$\boxed{\partial\Delta = \partial\overline{\Delta},} \tag{C.190}$$

where

$$\partial\Delta_{ab} = \sum_{a'b'c'd'>0} \langle \overline{a}'c'|\partial v_{12}^{ab,(\mathrm{a})}|\overline{b}'d'\rangle \kappa_{c'a'}\kappa_{d'b'}. \tag{C.191}$$

Introducing the antisymmetrized derived interaction as in (C.171), we remark that it is diagonal in m (as $m \equiv m_a = m_b$), since $D'_{ab}[\rho]$ is. On the other hand, we recall that the rearrangement fields are also diagonal in $t \equiv t_a = t_b$ and in $\Omega \equiv \Omega_a = \Omega_b$ (see (C.22)). Moreover, we notice that $\partial v_{12}^{ab,(\mathrm{a})}$ does not explicitly depend on t, nor on Ω (because it does not depend on the spins s_a and s_b). Accordingly, the matrix elements of the rearrangement field above, and the rearrangement field itself, are independent of t and Ω. We can then remove these indices and write, as for the rearrangement field associated with the mean fields,

$$\partial\Delta^{t\Omega}_{m_a\nu_a,m_b\nu_b} = \delta_{m_am_b}\partial\Delta_{m_a\nu_a,m_a\nu_b}. \tag{C.192}$$

We shall then evaluate

$$\partial\Delta_{m\nu_a,m\nu_b} = \sum_{a'b'c'd'>0} \langle \overline{a}'c'|\partial v_{12}^{ab,(\mathrm{a})}|\overline{b}'d'\rangle \kappa_{c'a'}\kappa_{d'b'}, \tag{C.193}$$

where, as explained before, $a = (m, \nu_a)$, $b = (m, \nu_b)$ and $a' = (t', \Omega', m'_a, \nu'_a)$. In order to simplify the rearrangement field, it is convenient to introduce a new field, analogous to the pairing field (III.32), but where the matrix elements of the antisymmetrized derived interaction, rather than the matrix elements of the standard antisymmetrized interaction, are considered. This field, called the "auxiliary pairing field" in the following, is defined as

$$\boxed{(\widetilde{\Delta}^{ab})_{c'a'} \equiv \sum_{b'd'>0} \langle c'\overline{a}'|\partial v_{12}^{ab,(\mathrm{a})}|b'\overline{d}'\rangle \kappa_{b'd'}.} \tag{C.194}$$

Using the property (C.180) of the matrix elements of the antisymmetrized derived interaction we have shown and exchanging the indices b' and d' in the summation, we obtain

$$(\widetilde{\Delta}^{ab})_{c'a'} = \sum_{b'd'>0} \langle \overline{a}'c'|\partial v_{12}^{ab,(a)}|\overline{b}'d'\rangle \kappa_{d'b'}, \tag{C.195}$$

The rearrangement field can then be rewritten as

$$\partial\Delta_{ab} = \sum_{a'b'>0} (\widetilde{\Delta}^{ab})_{a'b'}\kappa_{a'b'}, \tag{C.196}$$

where we have exchanged the dummy indices a' and c' and renamed c' by b'.

With this writing of the rearrangement field, we can benefit from the results already derived for the density-dependent pairing field in subsection C.2.1.2. We just have to replace the standard antisymmetrized interaction $v_{12}^{\mathrm{DD},(a)}$ by the antisymmetrized derived one, $\partial v_{12}^{ab,(a)}$ (they are detailed further, in (C.201)).

It remains to treat the summation in (C.196). We have

$$\partial\Delta_{ab} = \sum_{\substack{\Omega'>0 \\ m'_am'_b}} (g^{ab})^{\Omega'}_{m'_am'_b}, \tag{C.197}$$

with

$$(g^{ab})^{\Omega'}_{m'_am'_b} \equiv \sum_{t'\nu'_a\nu'_b} (\widetilde{\Delta}^{ab})^{t'\Omega'}_{m'_a\nu'_a,m'_b\nu'_b}\kappa^{t'\Omega'}_{m'_a\nu'_a,m'_b\nu'_b}, \tag{C.198}$$

where we recall that the pairing tensor κ is not symmetric under the exchange of its indices (contrary to ρ). First carrying out the summation over $m'_a = \Omega' \pm 1/2$ and $m'_b = \Omega' \pm 1/2$,

then considering $m' \equiv \Omega' \pm 1/2$ and finally gathering the terms keeping in mind that this time g^{ab} is not symmetric under the exchange of its indices m'_a and m'_b (since neither $\widetilde{\Delta}^{ab}$ nor κ exhibit this symmetry in general), we successively find

$$\begin{aligned}
\partial\Delta_{ab} &= \sum_{\Omega'>0} \Big[(g^{ab})^{\Omega'}_{\Omega'-1/2,\Omega'-1/2} + (g^{ab})^{\Omega'}_{\Omega'-1/2,\Omega'+1/2} \\
&\qquad + (g^{ab})^{\Omega'}_{\Omega'+1/2,\Omega'-1/2} + (g^{ab})^{\Omega'}_{\Omega'+1/2,\Omega'+1/2} \Big] \\
&= \sum_{m'\geq 0} \Big[(g^{ab})^{m'+1/2}_{m',m'} + (g^{ab})^{m'+1/2}_{m'+1,m'} + (g^{ab})^{m'+1/2}_{m',m'+1} + (g^{ab})^{m'+1/2}_{m'+1,m'+1} \Big] \\
&= \sum_{m'\geq 0} \Big[(g^{ab})^{m'+1/2}_{m',m'} + (g^{ab})^{m'+1/2}_{m'+1,m'} + (g^{ab})^{m'+1/2}_{m',m'+1} \\
&\qquad + \Theta(m'-1/2)(g^{ab})^{m'-1/2}_{m',m'} \Big] \\
&= \sum_{m'\geq 0} \Big[\Big(\sum_{s=\pm 1/2} \Theta(m'+s)(g^{ab})^{m'+s}_{m',m'} \Big) + (g^{ab})^{m'+1/2}_{m'+1,m'} + (g^{ab})^{m'+1/2}_{m',m'+1} \Big].
\end{aligned} \tag{C.199}$$

Thus, the rearrangement field (C.193) eventually becomes

$$\boxed{\begin{aligned}
\partial\Delta_{ab} = \sum_{\substack{t'm'\geq 0 \\ \nu'_a\nu'_b}} \Big[&\Big(\sum_{s'=\pm 1/2} \Theta(m'+s')(\widetilde{\Delta}^{ab})^{t'm'+s'}_{m'\nu'_a,m'\nu'_b} \kappa^{t'm'+s'}_{m'\nu'_a,m'\nu'_b} \Big) \\
&+ (\widetilde{\Delta}^{ab})^{t'm'+1/2}_{m'+1\,\nu'_a,m'\nu'_b} \kappa^{t'm'+1/2}_{m'+1\,\nu'_a,m'\nu'_b} + (\widetilde{\Delta}^{ab})^{t'm'+1/2}_{m'\nu'_a,m'+1\,\nu'_b} \kappa^{t'm'+1/2}_{m'\nu'_a,m'+1\,\nu'_b} \Big],
\end{aligned}} \tag{C.200}$$

where we recall that $a = (m, \nu_a)$ and $b = (m, \nu_b)$. Explicitly, equations (C.84) and (C.91) allow us to write the auxiliary pairing fields as:

$$\begin{aligned}
(\widetilde{\Delta}^{ab})^{t'\Omega'=m'+s'}_{m'\nu'_a,\,m'\nu'_b} = \sum_{\substack{m''\geq 0 \\ \nu'_c\nu'_d}} \Big[&\langle m'\nu'_a \; - m'\nu'_b | V(r_{12}) D'_{ab}[\rho] | m''\nu'_c \; - m''\nu'_d \rangle S^{t's'0}_{m''\nu'_c\nu'_d} \\
&+ \langle m'\nu'_a \; - m'\nu'_b | V(r_{12}) D'_{ab}[\rho] | -m''\nu'_d \; m''\nu'_c \rangle S^{t'-s'0}_{m''\nu'_c\nu'_d} \Big],
\end{aligned} \tag{C.201a}$$

$$\begin{aligned}
(\widetilde{\Delta}^{ab})^{t'\Omega'=m'+1/2}_{m'\nu'_a,\,m'+1\,\nu'_b} = &\sum_{\substack{m''\geq 0 \\ \nu'_c\nu'_d}} \\
&\times \Big[\langle m'\nu'_a \; - (m'+1)\,\nu'_b | V(r_{12}) D'_{ab}[\rho] | m''\nu'_c \; - (m''+1)\,\nu'_d \rangle \\
&- \langle m'\nu'_a \; - (m'+1)\,\nu'_b | V(r_{12}) D'_{ab}[\rho] | -(m''+1)\,\nu'_d \; m''\nu'_c \rangle \Big] S^{t'1/2\,1}_{m''\nu'_c\nu'_d},
\end{aligned} \tag{C.201b}$$

$$\begin{aligned}
(\widetilde{\Delta}^{ab})^{t'\Omega'=m'+1/2}_{m'+1\,\nu'_a,\,m'\nu'_b} = &\sum_{\substack{m''\geq 0 \\ \nu'_c\nu'_d}} \\
&\times \Big[\langle m'+1\,\nu'_a \; - m'\nu'_b | V(r_{12}) D'_{ab}[\rho] | m''+1\,\nu'_c \; - m''\nu'_d \rangle \\
&- \langle m'+1\,\nu'_a \; - m'\nu'_b | V(r_{12}) D'_{ab}[\rho] | -m''\nu'_d \; m''+1\,\nu'_c \rangle \Big] S^{t'-1/2\,-1}_{m''+1\,\nu'_c\nu'_d}.
\end{aligned} \tag{C.201c}$$

where the quantities S appearing are given by (C.86) and (C.92).

Now, we assume the time-reversal invariance of the rearrangement field associated with the pairing field, $\partial\Delta^{ab}$. It implies that the pairing tensor κ becomes symmetric under the exchange of its indices. Then, the auxiliary pairing field $\widetilde{\Delta}^{ab}$ becomes symmetric as well, such that the last two terms of (C.200) become equal and the rearrangement field

simplifies as

$$\boxed{\partial\Delta_{ab}|^{\mathrm{T}} = \sum_{\substack{t'm'\geq 0\\ \nu'_a\nu'_b}} \Big[\Big(\sum_{s'=\pm 1/2} \Theta(m'+s')(\widetilde{\Delta}^{ab})^{t'm'+s'}_{m'\nu'_a,m'\nu'_b}\kappa^{t'm'+s'}_{m'\nu'_a,m'\nu'_b}\Big) + 2(\widetilde{\Delta}^{ab})^{t'm'+1/2}_{m'\nu'_a,m'+1\,\nu'_b}\kappa^{t'm'+1/2}_{m'\nu'_a,m'+1\,\nu'_b}\Big],} \tag{C.202}$$

where the notation $|^{\mathrm{T}}$ identifies the time-reversal invariant quantities and where the expressions of $\widetilde{\Delta}^{ab}|^{\mathrm{T}} = \widetilde{\Delta}^{ab}$ are given by (C.201). We note that we recover the expressions of the time-reversal invariant rearrangement fields associated with pairing fields obtained by Chappert [17].

2.1.6. Rearrangement spatial matrix elements

When we derived the rearrangement fields arising from the density-dependent term (see subsection C.2.1.4), we ended up with a spatial dependence contained in two-body matrix elements of the form

$$v^{j_aj_cj_bj_d}_{r_ar_cr_br_d,\,a'b'} \equiv \langle j_ar_a\ j_cr_c|V(r_{12})D'_{a'b'}[\rho]|j_br_b\ j_dr_d\rangle, \tag{C.203}$$

where the functional $D'_{a'b'}[\rho]$ was given by (C.170), that is

$$\begin{aligned} D'_{a'b'}[\rho] \equiv \frac{\alpha}{2}\delta_{m'_am'_b}\Big[&\rho^{\alpha-1}(\vec{r}_1)\phi^*_{j'_bm'_a\nu'_b}(\vec{r}_1)\phi_{j'_am'_a\nu'_a}(\vec{r}_1) \\ &+ \rho^{\alpha-1}(\vec{r}_2)\phi^*_{j'_bm'_a\nu'_b}(\vec{r}_2)\phi_{j'_am'_a\nu'_a}(\vec{r}_2)\Big], \end{aligned} \tag{C.204}$$

where we recall that $a' = (j'_a, m'_a, \nu'_a)$ and $b' = (j'_b, m'_b, \nu'_b)$. Note that because of the similarity between $D[\rho]$, given by (C.28), and $D'_{a'b'}[\rho]$, it is not necessary to do the entire calculation of the above matrix element. It is sufficient to replace $\rho^\alpha(r)$ by

$$\alpha\delta_{m'_am'_b}\rho^{\alpha-1}(r)\phi^*_{j'_bm'_a\nu'_b}(\vec{r})\phi_{j'_am'_a\nu'_a}(\vec{r}) = \alpha\delta_{m'_am'_b}\rho^{\alpha-1}(r)\widetilde{\phi}_{j'_a|m'_a|\nu'_a}(r)\widetilde{\phi}_{j'_b|m'_a|\nu'_b}(r) \tag{C.205}$$

in equation (C.138). The equality comes from the fact that the two wave functions have opposite phases that compensate one another. The substitution directly provides

$$\begin{aligned} v^{j_aj_cj_bj_d}_{r_ar_cr_br_d,\,a'b'} = \pi\alpha\delta_{m'_am'_b}\delta_{m_a+m_c,m_b+m_d}&\int \mathrm{d}^2r\,\rho^{\alpha-1}(r)\widetilde{\phi}_{j'_a|m'_a|\nu'_a}(r)\widetilde{\phi}_{j'_b|m'_a|\nu'_b}(r) \\ \times\Big[\widetilde{\phi}_{j_a|m_a|\nu_a}(r)\widetilde{\phi}_{j_b|m_b|\nu_b}(r)&F_{j_cdr_cr_d}(r_g) + \widetilde{\phi}_{j_c|m_c|\nu_c}(r)\widetilde{\phi}_{j_d|m_d|\nu_d}(r)F_{j_abr_ar_b}(r_g)\Big]. \end{aligned} \tag{C.206}$$

As for the spatial matrix elements of the mean- and pairing fields, we end up having to approximate an integral which can be hardly evaluated analytically because of the expression of the density, given by (III.50). The procedure is quite similar; our aim we will be to approximate an integral of the form

$$I \equiv \int \mathrm{d}^2r\,\rho^{\alpha-1}(r)\widetilde{\phi}_{j'_a|m'_a|\nu'_a}(r)\widetilde{\phi}_{j'_b|m'_a|\nu'_b}(r)\widetilde{\phi}_{j_a|m_a|\nu_a}(r)\widetilde{\phi}_{j_b|m_b|\nu_b}(r)F_{j_cdr_cr_d}(r_g), \tag{C.207}$$

where we purposely omitted the r and j indices in I for conciseness. As before, we split up the wave functions and the function $F_{j_cdr_cr_d}(r_g)$ according to their radial and z parts, so that the integral becomes

$$I = \int_{-\infty}^{+\infty}\mathrm{d}z\,I_z(z)\underbrace{\int_0^\infty \mathrm{d}r_\perp\,I_\perp(r_\perp)\rho^{\alpha-1}(r_\perp,z)}_{I_1(z)}, \tag{C.208}$$

where

$$I_1(z) = N_\perp \sum_{n_{\perp\mu}} T^{m_\mu n_{\perp\mu}}_{m_c n_{\perp c} m_d n_{\perp d}} \int_0^\infty \mathrm{d}r_\perp \, r_\perp \phi_{|m_a|n_{\perp a}}(r_\perp)\phi_{|m_b|n_{\perp b}}(r_\perp) \\ \times \phi_{|m'_a|n'_{\perp a}}(r_\perp)\phi_{|m'_a|n'_{\perp b}}(r_\perp)\phi_{00}(g_\perp r_\perp)\phi_{|m_\mu|n_{\perp\mu}}(g_\perp r_\perp)\rho^{\alpha-1}(r_\perp, z). \tag{C.209}$$

In order to apply the Gauss–Laguerre quadrature, we pull the exponentials out of the wave functions using (C.10), so that

$$I_1(z) = N_\perp \sum_{n_{\perp\mu}} T^{m_\mu n_{\perp\mu}}_{m_c n_{\perp c} m_d n_{\perp d}} \int_0^\infty \mathrm{d}r_\perp \, r_\perp \mathrm{e}^{-(2+g_\perp^2)r_\perp^2/b_\perp^2} \hat{\phi}_{|m_a|n_{\perp a}}(r_\perp)\hat{\phi}_{|m_b|n_{\perp b}}(r_\perp) \\ \times \hat{\phi}_{|m'_a|n'_{\perp a}}(r_\perp)\hat{\phi}_{|m'_a|n'_{\perp b}}(r_\perp)\hat{\phi}_{00}(g_\perp r_\perp)\hat{\phi}_{|m_\mu|n_{\perp\mu}}(g_\perp r_\perp)\rho^{\alpha-1}(r_\perp, z). \tag{C.210}$$

Setting $x \equiv (2+g_\perp^2)r_\perp^2/b_\perp^2$, we end up with

$$I_1(z) = \frac{N_\perp b_\perp^2}{2(2+g_\perp^2)} \sum_{n_{\perp\mu}} T^{m_\mu n_{\perp\mu}}_{m_c n_{\perp c} m_d n_{\perp d}} \int_0^\infty \mathrm{d}x \, \mathrm{e}^{-x} f_{|m_\mu|n_{\perp\mu}}(x, z), \tag{C.211}$$

where we have defined

$$f_{|m_\mu|n_{\perp\mu}}(x,z) \equiv \hat{\phi}_{|m_a|n_{\perp a}}\left(\frac{b_\perp}{\sqrt{2+g_\perp^2}}\sqrt{x}\right)\hat{\phi}_{|m_b|n_{\perp b}}\left(\frac{b_\perp}{\sqrt{2+g_\perp^2}}\sqrt{x}\right) \\ \times \hat{\phi}_{|m'_a|n'_{\perp a}}\left(\frac{b_\perp}{\sqrt{2+g_\perp^2}}\sqrt{x}\right)\hat{\phi}_{|m'_a|n'_{\perp b}}\left(\frac{b_\perp}{\sqrt{2+g_\perp^2}}\sqrt{x}\right) \\ \times \hat{\phi}_{00}\left(\frac{g_\perp b_\perp}{\sqrt{2+g_\perp^2}}\sqrt{x}\right)\hat{\phi}_{|m_\mu|n_{\perp\mu}}\left(\frac{g_\perp b_\perp}{\sqrt{2+g_\perp^2}}\sqrt{x}\right) \\ \times \rho^{\alpha-1}\left(\frac{b_\perp}{\sqrt{2+g_\perp^2}}\sqrt{x}, z\right). \tag{C.212}$$

By means of the Gauss–Laguerre quadrature, we can approximate the above integral according to

$$\int_0^\infty \mathrm{d}x \, \mathrm{e}^{-x} f_{|m_\mu|n_{\perp\mu}}(x,z) \simeq \sum_{i=0}^{n} v_i f_{|m_\mu|n_{\perp\mu}}(x_i, z), \tag{C.213}$$

where n is the quadrature order, x_i the i-th root of the Laguerre polynomial $L_n(x)$ at which the function (C.212) is evaluated, and v_i a weight factor that reads

$$v_i \equiv \frac{x_i}{(n+1)^2[L_{n+1}(x_i)]^2}. \tag{C.214}$$

We obtain

$$I_1(\widetilde{x}_i, z) = \frac{N_\perp b_\perp^2}{2(2+g_\perp^2)} \sum_{n_{\perp\mu}} T^{m_\mu n_{\perp\mu}}_{m_c n_{\perp c} m_d n_{\perp d}} \sum_{i=0}^{n} v_i(x_i)\hat{\phi}_{|m_a|n_{\perp a}}(\widetilde{x}_i)\hat{\phi}_{|m_b|n_{\perp b}}(\widetilde{x}_i) \\ \times \hat{\phi}_{|m'_a|n'_{\perp a}}(\widetilde{x}_i)\hat{\phi}_{|m'_a|n'_{\perp b}}(\widetilde{x}_i)\hat{\phi}_{00}(g_\perp \widetilde{x}_i)\hat{\phi}_{|m_\mu|n_{\perp\mu}}(g_\perp \widetilde{x}_i)\rho^{\alpha-1}(\widetilde{x}_i, z), \tag{C.215}$$

where

$$\widetilde{x}_i \equiv \frac{b_\perp}{\sqrt{2+g_\perp^2}}\sqrt{x_i}. \tag{C.216}$$

To get an expression for (C.208), it remains to evaluate

$$I_2(\widetilde{x}_i) \equiv \int_{-\infty}^{+\infty} \mathrm{d}z\, I_z(z)\rho^{\alpha-1}(\widetilde{x}_i, z). \tag{C.217}$$

We have

$$\begin{aligned} I_2(\widetilde{x}_i) = N_z \sum_{n_{z\mu}} T^{n_{z\mu}}_{j_c n_{zc}\, j_d n_{zd}} \int_{-\infty}^{+\infty} \mathrm{d}z\, \phi_{n_{za}}(z-d_a)\phi_{n_{zb}}(z-d_b)\phi_{n'_{za}}(z-d'_a) \\ \times \phi_{n'_{zb}}(z-d'_b)\phi_0\Big(g_z(z-d_{cd})\Big)\phi_{n_{z\mu}}\Big(g_z(z-d_{cd})\Big)\rho^{\alpha-1}(\widetilde{x}_i, z). \end{aligned} \tag{C.218}$$

In order to apply the Gauss–Hermite quadrature, we pull the exponentials out of the wave functions using (C.10), so that

$$\begin{aligned} I_2(\widetilde{x}_i) = N_z \sum_{n_{z\mu}} T^{n_{z\mu}}_{j_c n_{zc}\, j_d n_{zd}} \int_{-\infty}^{+\infty} \mathrm{d}z\, \mathrm{e}^{-[(z-d_a)^2+(z-d_b)^2+(z-d'_a)^2+(z-d'_b)^2+2g_z^2(z-d_{cd})^2]/2b_z^2} \\ \times \hat{\phi}_{n_{za}}(z-d_a)\hat{\phi}_{n_{zb}}(z-d_b)\hat{\phi}_{n'_{za}}(z-d'_a)\hat{\phi}_{n'_{zb}}(z-d'_b) \\ \times \hat{\phi}_0\Big(g_z(z-d_{cd})\Big)\hat{\phi}_{n_{z\mu}}\Big(g_z(z-d_{cd})\Big)\rho^{\alpha-1}(\widetilde{x}_i, z). \end{aligned} \tag{C.219}$$

Let us now complete the square of the argument of the exponential appearing in the integral above. It reads

$$\begin{aligned} -\left[\frac{\sqrt{2+g_z^2}}{b_z}z - \frac{d_a+d_b+d'_a+d'_b+2g_z^2 d_{cd}}{2b_z\sqrt{2+g_z^2}}\right]^2 \\ + \frac{1}{2b_z^2}\left[\frac{(d_a+d_b+d'_a+d'_b+2g_z^2 d_{cd})^2}{2(2+g_z^2)} - \Big(d_a^2+d_b^2+d_a'^2+d_b'^2+2g_z^2 d_{cd}^2\Big)\right], \end{aligned} \tag{C.220}$$

in such a way that we get

$$\begin{aligned} I_2(\widetilde{x}_i) = N_z \mathrm{e}^{[(d_a+d_b+d'_a+d'_b+2g_z^2 d_{cd})^2/(2(2+g_z^2))-(d_a^2+d_b^2+d_a'^2+d_b'^2+2g_z^2 d_{cd}^2)]/2b_z^2} \\ \times \sum_{n_{z\mu}} T^{n_{z\mu}}_{j_c n_{zc}\, j_d n_{zd}} \int_{-\infty}^{+\infty} \mathrm{d}z\, \mathrm{e}^{-\left[\sqrt{2+g_z^2}z/b_z-(d_a+d_b+d'_a+d'_b+2g_z^2 d_{cd})/2b_z\sqrt{2+g_z^2}\right]^2} \\ \times \hat{\phi}_{n_{za}}(z-d_a)\hat{\phi}_{n_{zb}}(z-d_b)\hat{\phi}_{n'_{za}}(z-d'_a)\hat{\phi}_{n'_{zb}}(z-d'_b) \\ \times \hat{\phi}_0\Big(g_z(z-d_{cd})\Big)\hat{\phi}_{n_{z\mu}}\Big(g_z(z-d_{cd})\Big)\rho^{\alpha-1}(\widetilde{x}_i, z). \end{aligned} \tag{C.221}$$

The change of variable $y \equiv \sqrt{2+g_z^2}z/b_z - (d_a+d_b+d'_a+d'_b+2g_z^2 d_{cd})/2b_z\sqrt{2+g_z^2}$ provides

$$\begin{aligned} I_2(\widetilde{x}_i) = \frac{N_z b_z}{\sqrt{2+g_z^2}} \mathrm{e}^{[(d_a+d_b+d'_a+d'_b+2g_z^2 d_{cd})^2/(2(2+g_z^2))-(d_a^2+d_b^2+d_a'^2+d_b'^2+2g_z^2 d_{cd}^2)]/2b_z^2} \\ \times \sum_{n_{z\mu}} T^{n_{z\mu}}_{j_c n_{zc}\, j_d n_{zd}} \int_{-\infty}^{+\infty} \mathrm{d}y\, \mathrm{e}^{-y^2} g_{n_{z\mu}}(\widetilde{x}_i, y), \end{aligned} \tag{C.222}$$

where we have defined

$$
\begin{aligned}
g_{n_{z\mu}}(\widetilde{x}_i, y) \equiv\ & \hat{\phi}_{n_{za}}\left[\frac{b_z}{\sqrt{2+g_z^2}}y + \frac{d_a + d_b + d'_a + d'_b + 2g_z^2 d_{cd}}{2(2+g_z^2)} - d_a\right] \\
& \times \hat{\phi}_{n_{zb}}\left[\frac{b_z}{\sqrt{2+g_z^2}}y + \frac{d_a + d_b + d'_a + d'_b + 2g_z^2 d_{cd}}{2(2+g_z^2)} - d_b\right] \\
& \times \hat{\phi}_{n'_{za}}\left[\frac{b_z}{\sqrt{2+g_z^2}}y + \frac{d_a + d_b + d'_a + d'_b + 2g_z^2 d_{cd}}{2(2+g_z^2)} - d'_a\right] \\
& \times \hat{\phi}_{n'_{zb}}\left[\frac{b_z}{\sqrt{2+g_z^2}}y + \frac{d_a + d_b + d'_a + d'_b + 2g_z^2 d_{cd}}{2(2+g_z^2)} - d'_b\right] \\
& \times \hat{\phi}_0\left[g_z\left(\frac{b_z}{\sqrt{2+g_z^2}}y + \frac{d_a + d_b + d'_a + d'_b + 2g_z^2 d_{cd}}{2(2+g_z^2)} - d_{cd}\right)\right] \\
& \times \hat{\phi}_{n_{z\mu}}\left[g_z\left(\frac{b_z}{\sqrt{2+g_z^2}}y + \frac{d_a + d_b + d'_a + d'_b + 2g_z^2 d_{cd}}{2(2+g_z^2)} - d_{cd}\right)\right] \\
& \times \rho^{\alpha-1}\left[\frac{b_\perp}{\sqrt{2+g_\perp^2}}\sqrt{x_i}, \frac{b_z}{\sqrt{2+g_z^2}}y + \frac{d_a + d_b + d'_a + d'_b + 2g_z^2 d_{cd}}{2(2+g_z^2)}\right].
\end{aligned}
\tag{C.223}
$$

By means of the Gauss–Hermite quadrature, we can approximate the above integral according to

$$
\int_{-\infty}^{+\infty} \mathrm{d}y\, \mathrm{e}^{-y^2} g_{n_{z\mu}}(\widetilde{x}_i, y) \simeq \sum_{j=0}^{m} w_j g_{n_{z\mu}}(\widetilde{x}_i, y_j),
\tag{C.224}
$$

where m is the quadrature order, y_j the j-th root of the Hermite polynomial $H_m(y)$ at which the function (C.223) is evaluated, and w_j a weight factor that reads

$$
w_j \equiv \frac{2^{m-1} m! \sqrt{\pi}}{m^2 [H_{m-1}(y_j)]^2}.
\tag{C.225}
$$

We obtain

$$
\begin{aligned}
I_2(\widetilde{x}_i, \widetilde{y}_j) = & \frac{N_z b_z}{\sqrt{2+g_z^2}} \mathrm{e}^{[(d_a+d_b+d'_a+d'_b+2g_z^2 d_{cd})^2/(2(2+g_z^2)) - (d_a^2+d_b^2+d_a'^2+d_b'^2+2g_z^2 d_{cd}^2)]/2b_z^2} \\
& \times \sum_{n_{z\mu}} T^{n_{z\mu}}_{j_c n_{zc} j_d n_{zd}} \sum_{j=0}^{m} w_j(y_j) \hat{\phi}_{n_{za}}(\widetilde{y}_j - d_a) \hat{\phi}_{n_{zb}}(\widetilde{y}_j - d_b) \hat{\phi}_{n'_{za}}(\widetilde{y}_j - d'_a) \\
& \times \hat{\phi}_{n'_{zb}}(\widetilde{y}_j - d'_b) \hat{\phi}_0\Big(g_z(\widetilde{y}_j - d_{cd})\Big) \hat{\phi}_{n_{z\mu}}\Big(g_z(\widetilde{y}_j - d_{cd})\Big) \rho^{\alpha-1}(\widetilde{x}_i, \widetilde{y}_j),
\end{aligned}
\tag{C.226}
$$

with

$$
\widetilde{y}_j \equiv \frac{b_z}{\sqrt{2+g_z^2}}y + \frac{d_a + d_b + d'_a + d'_b + 2g_z^2 d_{cd}}{2(2+g_z^2)}.
\tag{C.227}
$$

Combining the results (C.215) and (C.226), we can furnish an approximate expression for the integral (C.208) at the quadrature order (n, m). We find

$$\begin{aligned} I = \frac{N_\perp b_\perp^2}{2(2+g_\perp^2)} \frac{N_z b_z}{\sqrt{2+g_z^2}} \mathrm{e}^{[(d_a+d_b+d'_a+d'_b+2g_z^2 d_{cd})^2/(2(2+g_z^2))-(d_a^2+d_b^2+d_a'^2+d_b'^2+2g_z^2 d_{cd}^2)]/2b_z^2} \\ \times \sum_{r_\mu} T^{r_\mu}_{j_a r_a\, j_b r_b} \sum_{i=0}^{n}\sum_{j=0}^{m} v_i w_j \hat{\phi}_{|m_a|\nu_a}(\widetilde{x}_i, \widetilde{y}_j - d_a)\hat{\phi}_{|m_b|\nu_b}(\widetilde{x}_i, \widetilde{y}_j - d_b) \\ \times \hat{\phi}_{|m'_a|\nu'_a}(\widetilde{x}_i, \widetilde{y}_j - d'_a)\hat{\phi}_{|m'_a|\nu'_b}(\widetilde{x}_i, \widetilde{y}_j - d'_b)\hat{\phi}_0\Big(g_\perp \widetilde{x}_i, g_z(\widetilde{y}_j - d_{cd})\Big) \\ \times \hat{\phi}_{|m_\mu|\nu_\mu}\Big(g_\perp \widetilde{x}_i, g_z(\widetilde{y}_j - d_{cd})\Big)\rho^{\alpha-1}(\widetilde{x}_i, \widetilde{y}_j), \end{aligned} \tag{C.228}$$

where we have gathered the axial and z-relative Talman coefficients as well as the $\widetilde{x}_i$- and $\widetilde{y}_j$-dependent wave functions, where the latter coordinates are respectively given by (C.216) and (C.227).

2.2. Tensor contribution

In this subsection, we shall derive the mean- and pairing fields associated with the finite-range tensor term of the generalized Gogny interaction (II.1). Note that there are no rearrangement fields associated with the tensor term since it is density-independent. The antisymmetrized finite-range tensor interaction considered in the following reads

$$\begin{aligned} v_{12}^{\mathrm{T,(a)}} &\equiv v_{12}^{\mathrm{T}}(1 - P_r P_\sigma P_\tau) \\ &= (W - HP_\tau)V(r_{12})S_{12}(1 - P_r P_\tau) \\ &= \mathcal{P}_{\mathrm{D}} V(r_{12})S_{12} + \mathcal{P}_{\mathrm{E}} V(r_{12})S_{12}P_r, \end{aligned} \tag{C.229}$$

where the tensor operator S_{12}, given by (D.49), removes the operator P_σ since it acts symmetrically on the spin variables (see discussion in section II). To perform the calculations, we will use the equivalent form (D.58) of the tensor operator. Note also that the isospin components of the direct and exchange tensor fields are respectively

$$\mathcal{P}_{\mathrm{D}} \equiv W - HP_\tau, \tag{C.230a}$$

$$\mathcal{P}_{\mathrm{E}} \equiv H - WP_\tau. \tag{C.230b}$$

We notice that the direct components of the tensor fields can be deduced from the exchange ones by switching W and H and removing the operator P_r, in the same idea as what we have done for the central and density-dependent terms. Thus, in the following, we will start by deriving the exchange tensor fields from which, then, we will deduce the direct ones.

2.2.1. Tensor mean fields

We start by deriving the mean field Γ, given by (III.37), of the tensor interaction (C.229), which is not time-reversal invariant for the moment. Given that the density matrices (C.21) and the fields (C.22) are diagonal in t and Ω, this tensor mean field can be written

$$\begin{aligned} \Gamma^{t\Omega}_{r_a r_b} = \sum_{\substack{t'\Omega'>0 \\ r_c r_d}} \Big[&\langle t s_a r_a\ t' s_c r_c | v_{12}^{\mathrm{T,(a)}} | t s_b r_b\ t' s_d r_d \rangle \rho^{t'\Omega'}_{r_d r_c} \\ &+ \langle t s_a r_a\ \overline{t' s_c r_c} | v_{12}^{\mathrm{T,(a)}} | t s_b r_b\ \overline{t' s_d r_d} \rangle \overline{\rho}^{t'\Omega'}_{r_c r_d} \Big]. \end{aligned} \tag{C.231}$$

Let us first concentrate on the exchange tensor mean field. It reads

$$\begin{aligned}\Gamma^{t\Omega}_{r_a r_b}|_{\mathrm{E}} = \sum_{\substack{t'\Omega'>0\\ r_c r_d}} \sum_{k} (-)^k \Big[&\langle r_a r_c | V(r_{12}) [\hat{r}_{12} \otimes \hat{r}_{12}]^{(2)}_{-k} P_r | r_b r_d \rangle \\ &\times \langle t s_a \; t' s_c | \mathcal{P}_{\mathrm{E}} [\vec{\sigma}_1 \otimes \vec{\sigma}_2]^{(2)}_k | t s_b \; t' s_d \rangle \rho^{t'\Omega'}_{r_d r_c} \\ + \sigma_c \sigma_d \langle r_a - r_c | V(r_{12}) &[\hat{r}_{12} \otimes \hat{r}_{12}]^{(2)}_{-k} P_r | r_b - r_d \rangle \\ &\times \langle t s_a \; t' - s_c | \mathcal{P}_{\mathrm{E}} [\vec{\sigma}_1 \otimes \vec{\sigma}_2]^{(2)}_k | t s_b \; t' - s_d \rangle \overline{\rho}^{t'\Omega'}_{r_c r_d} \Big].\end{aligned} \tag{C.232}$$

From the arguments already mentioned for the central and density-dependent terms (see discussion right after (C.31)), we will set in the following $m_a \equiv m$ and $m_b \equiv m + \lambda$ as well as $s_a \equiv s$ and $s_b \equiv s - \lambda$, with $m \geq 0$ and $\lambda \in \{0, 1\}$ in both matrix elements.

Now, contrary to the CDD interactions, the tensor interaction does not commute with $\vec{L}$ (nor $\vec{S}$), as it is shown in subsection D.6.2. Consequently, the conservation laws (C.32) no longer hold. Nevertheless, since the matrix elements must remain scalars in the coordinate space, the Wigner–Eckart theorem imposes the more general conservation laws

$$m_a + m_c = m_b + m_d - k, \qquad \text{in the first matrix element,} \tag{C.233a}$$

$$m_a - m_c = m_b - m_d - k, \qquad \text{in the second matrix element.} \tag{C.233b}$$

Then, as $\Omega' > 0$, we know that m_c and m_d are positive or zero and differ at most from 1. Therefore, we can set $m_d \equiv m'$ and $s_d \equiv s'$, with $m' \geq 0$ and $s' = \pm 1/2$, in the first matrix element of the above equation, which implies, according to the associated conservation law, $m_c = m' + \lambda - k$ and $s_c = s' - \lambda + k$. In the second matrix element, we will rather set $m_c = m'$ and $s_c = s'$, which implies $m_d = m' + \lambda - k$ and $s_d = s' - \lambda + k$. The reason for this particular choice is the same as for the central and density-dependent terms; it allows to simplify the final expression of the direct tensor mean field (see equation (C.250)). Let us remark in passing that since $\lambda \in \{0, 1\}$, the value $k = -2$ is forbidden. It appears in fact only for the case $\lambda = -1$ which is simply deduced from the case $\lambda = 1$ by symmetry. Thus, for the tensor mean field, we will not need to evaluate the spatial integral involving the component $[\hat{r}_{12} \otimes \hat{r}_{12}]^{(2)}_2$. Finally, to ease the notations, we will write $\lambda' \equiv \lambda - k$, with $|\lambda'| \leq 1$. The summation over k will thus be replaced by that over λ'.

With these notations, the exchange tensor mean field becomes

$$\begin{aligned}\Gamma^{t\Omega=m+s}_{m\nu_a,\, m+\lambda\,\nu_b}|_{\mathrm{E}} = \sum_{\substack{t'\Omega'>0\\ m'\nu_c\nu_d}} \sum_{\lambda'} (-)^{\lambda-\lambda'} \\ \times \Big[\langle m\nu_a \; m' + \lambda' \, \nu_c | V(r_{12}) [\hat{r}_{12} \otimes \hat{r}_{12}]^{(2)}_{\lambda'-\lambda} P_r | m + \lambda \, \nu_b \; m' \nu_d \rangle \\ \times \langle t s \; t' s' - \lambda' | \mathcal{P}_{\mathrm{E}} [\vec{\sigma}_1 \otimes \vec{\sigma}_2]^{(2)}_{\lambda-\lambda'} | t \, s - \lambda \; t' s' \rangle \rho^{t'm'+s'}_{m'\nu_d,\, m'+\lambda'\nu_c} \\ + 4 s'(s' - \lambda') \langle m\nu_a \; - m'\nu_c | V(r_{12}) [\hat{r}_{12} \otimes \hat{r}_{12}]^{(2)}_{\lambda'-\lambda} P_r | m + \lambda \, \nu_b \; - (m' + \lambda') \, \nu_d \rangle \\ \times \langle t s \; t' - s' | \mathcal{P}_{\mathrm{E}} [\vec{\sigma}_1 \otimes \vec{\sigma}_2]^{(2)}_{\lambda-\lambda'} | t \, s - \lambda \; t' - (s' - \lambda') \rangle \overline{\rho}^{t'm'+s'}_{m'\nu_c,\, m'+\lambda'\nu_d} \Big].\end{aligned} \tag{C.234}$$

Let us first focus on the spin-isospin part, which is no longer trivial for the tensor interaction. We set

$$X^{(+)ts\lambda}_{\Omega' m' \nu_d \nu_c \lambda'}|_{\mathrm{E}} \equiv Y^{(+)s\lambda}_{s'\lambda'} \times Z^{(+)t}_{\Omega' m' \nu_d \nu_c \lambda'}|_{\mathrm{E}}, \tag{C.235a}$$

$$X^{(-)ts\lambda}_{\Omega' m' \nu_c \nu_d \lambda'}|_{\mathrm{E}} \equiv Y^{(-)s\lambda}_{s'\lambda'} \times Z^{(-)t}_{\Omega' m' \nu_c \nu_d \lambda'}|_{\mathrm{E}}, \tag{C.235b}$$

in the first and second matrix elements respectively, where their spin parts read

$$Y^{(+)s\lambda}_{s'\lambda'} \equiv \langle s\ s'-\lambda'|[\vec{\sigma}_1\otimes\vec{\sigma}_2]^{(2)}_{\lambda-\lambda'}|s-\lambda\ s'\rangle, \tag{C.236a}$$
$$Y^{(-)s\lambda}_{s'\lambda'} \equiv 4s'(s'-\lambda')\langle s\ -s'|[\vec{\sigma}_1\otimes\vec{\sigma}_2]^{(2)}_{\lambda-\lambda'}|s-\lambda\ -(s'-\lambda')\rangle, \tag{C.236b}$$

and their isospin parts are

$$Z^{(+)t}_{\Omega' m'\nu_d\nu_c\lambda'}|_{\rm E} \equiv \sum_{t'}(H-W\delta_{tt'})\,\rho^{t'\Omega'}_{m'\nu_d,\,m'+\lambda'\nu_c}, \tag{C.237a}$$
$$Z^{(-)t}_{\Omega' m'\nu_c\nu_d\lambda'}|_{\rm E} \equiv \sum_{t'}(H-W\delta_{tt'})\,\overline{\rho}^{t'\Omega'}_{m'\nu_c,\,m'+\lambda'\nu_d}, \tag{C.237b}$$

or, by explicitly separating their particle-like and proton-neutron contributions,

$$\boxed{Z^{(+)t}_{\Omega' m'\nu_d\nu_c\lambda'}|_{\rm E} = (H-W)\,\rho^{t\Omega'}_{m'\nu_d,\,m'+\lambda'\nu_c} + H\,\rho^{-t\Omega'}_{m'\nu_d,\,m'+\lambda'\nu_c},} \tag{C.238a}$$
$$\boxed{Z^{(-)t}_{\Omega' m'\nu_c\nu_d\lambda'}|_{\rm E} = (H-W)\,\overline{\rho}^{t\Omega'}_{m'\nu_c,\,m'+\lambda'\nu_d} + H\,\overline{\rho}^{-t\Omega'}_{m'\nu_c,\,m'+\lambda'\nu_d}.} \tag{C.238b}$$

On the other hand, since the direct and exchange tensor mean fields have the same spin part, we also have implicitly set

$$Y^{(\pm)s\lambda}_{s'\lambda'} \equiv Y^{(\pm)s\lambda}_{s'\lambda'}|_{\rm D} = Y^{(\pm)s\lambda}_{s'\lambda'}|_{\rm E}. \tag{C.239}$$

To evaluate the quantities $Y^{(\pm)}$, we need to find out the general expression of the spin matrix element $\langle s_a\ s_c|[\vec{\sigma}_1\otimes\vec{\sigma}_2]^{(2)}_{\lambda-\lambda'}|s_b\ s_d\rangle$. It is given by (D.20). Applying this formula to (C.236) keeping in mind that $\lambda\in\{0,1\}$, we obtain

$$\begin{aligned} Y^{(+)s\lambda}_{s'\lambda'} &= 4ss'\delta_{\lambda,0}\left[\sqrt{\frac{2}{3}}\delta_{\lambda',0}+\delta_{\lambda',2s'}\right] \\ &\quad -\delta_{\lambda,1}\delta_{s,1/2}\left[2s'\delta_{\lambda',0}+\sqrt{\frac{2}{3}}\delta_{\lambda',1}\delta_{s',1/2}-2\delta_{\lambda',-1}\delta_{s',-1/2}\right], \end{aligned} \tag{C.240a}$$

$$\begin{aligned} Y^{(-)s\lambda}_{s'\lambda'} &= -4ss'\delta_{\lambda,0}\left[\sqrt{\frac{2}{3}}\delta_{\lambda',0}+\delta_{\lambda',2s'}\right] \\ &\quad +\delta_{\lambda,1}\delta_{s,1/2}\left[2s'\delta_{\lambda',0}+\sqrt{\frac{2}{3}}\delta_{\lambda',1}\delta_{s',1/2}-2\delta_{\lambda',-1}\delta_{s',-1/2}\right], \end{aligned} \tag{C.240b}$$

where we notice that

$$Y^{s\lambda}_{s'\lambda'} \equiv Y^{(+)s\lambda}_{s'\lambda'} = -Y^{(-)s\lambda}_{s'\lambda'}, \tag{C.241}$$

with

$$\boxed{\begin{aligned} Y^{s\lambda}_{s'\lambda'} &\equiv 4ss'\delta_{\lambda,0}\left[\sqrt{\frac{2}{3}}\delta_{\lambda',0}+\delta_{\lambda',2s'}\right] \\ &\quad -\delta_{\lambda,1}\delta_{s,1/2}\left[2s'\delta_{\lambda',0}+\sqrt{\frac{2}{3}}\delta_{\lambda',1}\delta_{s',1/2}-2\delta_{\lambda',-1}\delta_{s',-1/2}\right]. \end{aligned}} \tag{C.242}$$

We check that the spin diagonal part of the tensor mean field corresponds to $\lambda=0$ and its non-diagonal part to $\lambda=1$. Note that if the tensor mean field is spin diagonal, then it is also diagonal in m, in agreement with the fact that the tensor mean field is diagonal in Ω ($\Omega_a=\Omega_b$ and $s_a=s_b$ imply $m_a=m_b$).

Then, from (C.235), we get

$$X^{(+)ts\lambda}_{\Omega' m' \nu_d \nu_c \lambda'}|_{\rm E} \equiv Y^{s\lambda}_{s'\lambda'} \times Z^{(+)t}_{\Omega' m' \nu_d \nu_c \lambda'}|_{\rm E}, \tag{C.243a}$$

$$X^{(-)ts\lambda}_{\Omega' m' \nu_c \nu_d \lambda'}|_{\rm E} \equiv -Y^{s\lambda}_{s'\lambda'} \times Z^{(-)t}_{\Omega' m' \nu_c \nu_d \lambda'}|_{\rm E}. \tag{C.243b}$$

Now, setting

$$R^{(+)ts\lambda}_{m' \nu_d \nu_c \lambda'}|_{\rm E} \equiv \sum_{\Omega'} \Theta(\Omega') X^{(+)ts\lambda}_{\Omega' m' \nu_d \nu_c \lambda'}|_{\rm E} = \sum_{s'=\pm s} \Theta(m'+s') X^{(+)ts\lambda}_{m'+s' m' \nu_d \nu_c \lambda'}|_{\rm E}, \tag{C.244a}$$

$$R^{(-)ts\lambda}_{m' \nu_c \nu_d \lambda'}|_{\rm E} \equiv \sum_{\Omega'} \Theta(\Omega') X^{(-)ts\lambda}_{\Omega' m' \nu_c \nu_d \lambda'}|_{\rm E} = \sum_{s'=\pm s} \Theta(m'+s') X^{(-)ts\lambda}_{m'+s' m' \nu_c \nu_d \lambda'}|_{\rm E}, \tag{C.244b}$$

we end up with

$$\boxed{\begin{aligned} R^{(+)ts\lambda}_{m' \nu_d \nu_c \lambda'}|_{\rm E} &= \Theta(m'+s) Y^{s\lambda}_{s\lambda'} Z^{(+)t}_{m'+s\, m' \nu_d \nu_c \lambda'}|_{\rm E} \\ &\quad + \Theta(m'-s) Y^{s\lambda}_{-s\lambda'} Z^{(+)t}_{m'-s\, m' \nu_d \nu_c \lambda'}|_{\rm E}, \end{aligned}} \tag{C.245a}$$

$$\boxed{\begin{aligned} R^{(-)ts\lambda}_{m' \nu_c \nu_d \lambda'}|_{\rm E} &= -\Theta(m'+s) Y^{s\lambda}_{s\lambda'} Z^{(-)t}_{m'+s\, m' \nu_c \nu_d \lambda'}|_{\rm E} \\ &\quad - \Theta(m'-s) Y^{s\lambda}_{-s\lambda'} Z^{(-)t}_{m'-s\, m' \nu_c \nu_d \lambda'}|_{\rm E}, \end{aligned}} \tag{C.245b}$$

and the exchange tensor mean field can be written

$$\boxed{\begin{aligned} \Gamma^{t\Omega=m+s}_{m\nu_a,\, m+\lambda\, \nu_b}|_{\rm E} = \sum_{\substack{m'\geq 0 \\ \nu_c \nu_d}} \sum_{\lambda'=-1}^{1} (-)^{\lambda-\lambda'} \\ \times \Big[\langle m\nu_a\ m'+\lambda'\, \nu_c | V(r_{12}) [\hat{r}_{12} \otimes \hat{r}_{12}]^{(2)}_{\lambda'-\lambda} | m' \nu_d\ m+\lambda\, \nu_b \rangle R^{(+)ts\lambda}_{m' \nu_d \nu_c \lambda'}|_{\rm E} \\ + \langle m\nu_a\ -m' \nu_c | V(r_{12}) [\hat{r}_{12} \otimes \hat{r}_{12}]^{(2)}_{\lambda'-\lambda} | -(m'+\lambda')\, \nu_d\ m+\lambda\, \nu_b \rangle R^{(-)ts\lambda}_{m' \nu_c \nu_d \lambda'}|_{\rm E} \Big], \end{aligned}} \tag{C.246}$$

where, as previously done for the central and density-dependent terms, we have replaced the summations $\sum_{m'} \sum_{\Omega'>0}$ by $\sum_{m'\geq 0} \sum_{\Omega'} \Theta(\Omega')$ and applied the operator P_r.

To get the direct tensor mean field out of the exchange one, it suffices to exchange H and W and omit the operator P_r. The latter is therefore

$$\begin{aligned} \Gamma^{t\Omega=m+s}_{m\nu_a,\, m+\lambda\, \nu_b}|_{\rm D} = \sum_{\substack{m'\geq 0 \\ \nu_c \nu_d}} \sum_{\lambda'=-1}^{1} (-)^{\lambda-\lambda'} \\ \times \Big[\langle m\nu_a\ m'+\lambda'\, \nu_c | V(r_{12}) [\hat{r}_{12} \otimes \hat{r}_{12}]^{(2)}_{\lambda'-\lambda} | m+\lambda\, \nu_b\ m' \nu_d \rangle R^{(+)ts\lambda}_{m' \nu_d \nu_c \lambda'}|_{\rm D} \\ + \langle m\nu_a\ -m' \nu_d | V(r_{12}) [\hat{r}_{12} \otimes \hat{r}_{12}]^{(2)}_{\lambda'-\lambda} | m+\lambda\, \nu_b\ -(m'+\lambda')\, \nu_c \rangle R^{(-)ts\lambda}_{m' \nu_d \nu_c \lambda'}|_{\rm D} \Big], \end{aligned} \tag{C.247}$$

where we have switched the dummy indices ν_c and ν_d in the second matrix element of the right-hand side term. The quantities appearing in the direct tensor mean field are

$$R^{(+)ts\lambda}_{m' \nu_d \nu_c \lambda'}|_{\rm D} = \Theta(m'+s) Y^{s\lambda}_{s\lambda'} Z^{(+)t}_{m'+s\, m' \nu_d \nu_c \lambda'}|_{\rm D} + \Theta(m'-s) Y^{s\lambda}_{-s\lambda'} Z^{(+)t}_{m'-s\, m' \nu_d \nu_c \lambda'}|_{\rm D}, \tag{C.248a}$$

$$R^{(-)ts\lambda}_{m' \nu_c \nu_d \lambda'}|_{\rm D} = -\Theta(m'+s) Y^{s\lambda}_{s\lambda'} Z^{(-)t}_{m'+s\, m' \nu_c \nu_d \lambda'}|_{\rm D} - \Theta(m'-s) Y^{s\lambda}_{-s\lambda'} Z^{(-)t}_{m'-s\, m' \nu_c \nu_d \lambda'}|_{\rm D}, \tag{C.248b}$$

where the quantities Y are given by (C.242), and

$$\boxed{Z^{(+)t}_{\Omega' m' \nu_d \nu_c \lambda'}|_{\rm D} = (W-H)\, \rho^{t\Omega'}_{m' \nu_d,\, m'+\lambda' \nu_c} + W\, \rho^{-t\Omega'}_{m' \nu_d,\, m'+\lambda' \nu_c},} \tag{C.249a}$$

$$\boxed{Z^{(-)t}_{\Omega' m' \nu_c \nu_d \lambda'}|_{\rm D} = (W-H)\, \overline{\rho}^{t\Omega'}_{m' \nu_c,\, m'+\lambda' \nu_d} + W\, \overline{\rho}^{-t\Omega'}_{m' \nu_c,\, m'+\lambda' \nu_d}.} \tag{C.249b}$$

Now, by writing down the two spatial matrix elements involved in the direct tensor mean field, we notice that they are equal, because of the expression of the axial wave functions (C.3) and the fact that they commute with the tensor $[\hat{r}_{12} \otimes \hat{r}_{12}]^{(2)}_{\lambda'-\lambda}$. This is the reason for our particular choice discussed earlier (see discusion after (C.232)). The direct tensor mean field is then simplified according to

$$\boxed{\begin{aligned}\Gamma^{t\Omega=m+s}_{m\nu_a,\,m+\lambda\,\nu_b}|_{\mathrm{D}} = &\sum_{\substack{m'\geq 0\\ \nu_c\overline{\nu}_d}}\sum_{\lambda'=-1}^{1}(-)^{\lambda-\lambda'}\\ &\times\langle m\nu_a\ m'+\lambda'\,\nu_c|V(r_{12})[\hat{r}_{12}\otimes\hat{r}_{12}]^{(2)}_{\lambda'-\lambda}|m+\lambda\,\nu_b\ m'\nu_d\rangle R^{ts\lambda}_{m'\nu_d\nu_c\lambda'}|_{\mathrm{D}},\end{aligned}} \tag{C.250}$$

where we have

$$R^{ts\lambda}_{m'\nu_d\nu_c\lambda'}|_{\mathrm{D}} \equiv R^{(+)ts\lambda}_{m'\nu_d\nu_c\lambda'}|_{\mathrm{D}} + R^{(-)ts\lambda}_{m'\nu_d\nu_c\lambda'}|_{\mathrm{D}}, \tag{C.251}$$

that is to say,

$$\boxed{\begin{aligned}R^{ts\lambda}_{m'\nu_d\nu_c\lambda'}|_{\mathrm{D}} = \Theta(m'+s)Y^{s\lambda}_{s\lambda'}\Big[Z^{(+)t}_{m'+s\,m'\nu_d\nu_c\lambda'}|_{\mathrm{D}} - Z^{(-)t}_{m'+s\,m'\nu_d\nu_c\lambda'}|_{\mathrm{D}}\Big]\\ +\Theta(m'-s)Y^{s\lambda}_{-s\lambda'}\Big[Z^{(+)t}_{m'-s\,m'\nu_d\nu_c\lambda'}|_{\mathrm{D}} - Z^{(-)t}_{m'-s\,m'\nu_d\nu_c\lambda'}|_{\mathrm{D}}\Big],\end{aligned}} \tag{C.252}$$

where the quantities Y and $Z^{(\pm)}|_{\mathrm{D}}$ are respectively given by (C.242) and (C.249).

From the boxed equations, we can now explicitly write down the expressions of the direct and exchange tensor mean fields Γ for each value of λ. We recall that these fields are *not* time-reversal invariant, and that the quantities $Z^{(\pm)}|_{\mathrm{E}}$ and $Z^{(\pm)}|_{\mathrm{D}}$, respectively given by (C.238) and (C.249), are the same no matter the value of λ. Finally, note that if $\lambda = 1$, then $s = 1/2$ (as we could have already seen in (C.240)) since the identity $s_b \equiv s - 1 = \pm 1/2$ holds only if $s = 1/2$.

- Exchange tensor mean field Γ for $\lambda = 0$:

$$\boxed{\begin{aligned}\Gamma^{t\Omega=m+s}_{m\nu_a,\,m\nu_b}|_{\mathrm{E}} = &\sum_{\substack{m'\geq 0\\ \nu_c\overline{\nu}_d}}\sum_{\lambda'=-1}^{1}(-)^{\lambda'}\\ &\times\Big[\langle m\nu_a\ m'+\lambda'\,\nu_c|V(r_{12})[\hat{r}_{12}\otimes\hat{r}_{12}]^{(2)}_{\lambda'}|m'\nu_d\ m\nu_b\rangle R^{(+)ts0}_{m'\nu_d\nu_c\lambda'}|_{\mathrm{E}}\\ &+\langle m\nu_a\ -m'\nu_c|V(r_{12})[\hat{r}_{12}\otimes\hat{r}_{12}]^{(2)}_{\lambda'}|-(m'+\lambda')\,\nu_d\ m\nu_b\rangle R^{(-)ts0}_{m'\nu_c\nu_d\lambda'}|_{\mathrm{E}}\Big],\end{aligned}} \tag{C.253}$$

where

$$\boxed{\begin{aligned}R^{(+)ts0}_{m'\nu_d\nu_c\lambda'}|_{\mathrm{E}} = &\Theta(m'+s)Y^{s0}_{s\lambda'}Z^{(+)t}_{m'+s\,m'\nu_d\nu_c\lambda'}|_{\mathrm{E}}\\ &+\Theta(m'-s)Y^{s0}_{-s\lambda'}Z^{(+)t}_{m'-s\,m'\nu_d\nu_c\lambda'}|_{\mathrm{E}},\end{aligned}} \tag{C.254a}$$

$$\boxed{\begin{aligned}R^{(-)ts0}_{m'\nu_c\nu_d\lambda'}|_{\mathrm{E}} = &-\Theta(m'+s)Y^{s0}_{s\lambda'}Z^{(-)t}_{m'+s\,m'\nu_c\nu_d\lambda'}|_{\mathrm{E}}\\ &-\Theta(m'-s)Y^{s0}_{-s\lambda'}Z^{(-)t}_{m'-s\,m'\nu_c\nu_d\lambda'}|_{\mathrm{E}},\end{aligned}} \tag{C.254b}$$

with

$$\boxed{Y^{s0}_{\pm s\lambda'} = \pm\left[\sqrt{\frac{2}{3}}\delta_{\lambda',0} + \delta_{\lambda',\pm 2s}\right].} \tag{C.255}$$

- Direct tensor mean field Γ for $\lambda = 0$:

$$\boxed{\begin{aligned}\Gamma^{t\Omega=m+s}_{m\nu_a,\,m\nu_b}|_{\mathrm{D}} = &\sum_{\substack{m'\geq 0\\ \nu_c\nu_d}}\sum_{\lambda'=-1}^{1}(-)^{\lambda'}\\ &\times\langle m\nu_a\; m'+\lambda'\,\nu_c|V(r_{12})[\hat{r}_{12}\otimes\hat{r}_{12}]^{(2)}_{\lambda'}|m\nu_b\; m'\nu_d\rangle R^{ts0}_{m'\nu_d\nu_c\lambda'}|_{\mathrm{D}},\end{aligned}} \tag{C.256}$$

where

$$\boxed{\begin{aligned}R^{ts0}_{m'\nu_d\nu_c\lambda'}|_{\mathrm{D}} = &\,\Theta(m'+s)Y^{s0}_{s\lambda'}\Big[Z^{(+)t}_{m'+s\,m'\nu_d\nu_c\lambda'}|_{\mathrm{D}} - Z^{(-)t}_{m'-s\,m'\nu_d\nu_c\lambda'}|_{\mathrm{D}}\Big]\\ &+\Theta(m'-s)Y^{s0}_{-s\lambda'}\Big[Z^{(+)t}_{m'+s\,m'\nu_d\nu_c\lambda'}|_{\mathrm{D}} - Z^{(-)t}_{m'-s\,m'\nu_d\nu_c\lambda'}|_{\mathrm{D}}\Big],\end{aligned}} \tag{C.257}$$

with the quantities Y given by (C.255). Note that the quantities $R^{(\pm)ts0}|_{\mathrm{E}}$ and $R^{ts0}|_{\mathrm{D}}$ are symmetric under the exchange of ν_c and ν_d only if $\lambda'=0$ such that the corresponding quantities $Z^{(\pm)}|_{\mathrm{E}}$ and $Z^{(\pm)}|_{\mathrm{D}}$ display this symmetry as their density matrices ρ and $\overline{\rho}$, besides being symmetric, are diagonal in m'.

- Exchange tensor mean field Γ for $\lambda=1$:

$$\boxed{\begin{aligned}\Gamma^{t\Omega=m+1/2}_{m\nu_a,\,m+1\,\nu_b}|_{\mathrm{E}} = &\sum_{\substack{m'\geq 0\\ \nu_c\nu_d}}\sum_{\lambda'=-1}^{1}(-)^{\lambda'-1}\\ &\times\Big[\langle m\nu_a\; m'+\lambda'\,\nu_c|V(r_{12})[\hat{r}_{12}\otimes\hat{r}_{12}]^{(2)}_{\lambda'-1}|m'\nu_d\; m+1\,\nu_b\rangle R^{(+)t1/2\,1}_{m'\nu_d\nu_c\lambda'}|_{\mathrm{E}}\\ &+\langle m\nu_a\;\; -m'\nu_c|V(r_{12})[\hat{r}_{12}\otimes\hat{r}_{12}]^{(2)}_{\lambda'-1}|-(m'+\lambda')\,\nu_d\; m+1\,\nu_b\rangle R^{(-)t1/2\,1}_{m'\nu_c\nu_d\lambda'}|_{\mathrm{E}}\Big],\end{aligned}} \tag{C.258}$$

where

$$\boxed{\begin{aligned}R^{(+)t1/2\,1}_{m'\nu_d\nu_c\lambda'}|_{\mathrm{E}} = &\,Y^{1/2\,1}_{1/2\,\lambda'}Z^{(+)t}_{m'+1/2\,m'\nu_d\nu_c\lambda'}|_{\mathrm{E}}\\ &+\Theta(m'-1/2)Y^{1/2\,1}_{-1/2\,\lambda'}Z^{(+)t}_{m'-1/2\,m'\nu_d\nu_c\lambda'}|_{\mathrm{E}},\end{aligned}} \tag{C.259a}$$

$$\boxed{\begin{aligned}R^{(-)t1/2\,1}_{m'\nu_c\nu_d\lambda'}|_{\mathrm{E}} = &-Y^{1/2\,1}_{1/2\,\lambda'}Z^{(-)t}_{m'+1/2\,m'\nu_c\nu_d\lambda'}|_{\mathrm{E}}\\ &-\Theta(m'-1/2)Y^{1/2\,1}_{-1/2\,\lambda'}Z^{(-)t}_{m'-1/2\,m'\nu_c\nu_d\lambda'}|_{\mathrm{E}},\end{aligned}} \tag{C.259b}$$

with

$$\boxed{Y^{1/2\,1}_{1/2\,\lambda'} = -\left[\delta_{\lambda',0}+\sqrt{\frac{2}{3}}\delta_{\lambda',1}\right],} \tag{C.260a}$$

$$\boxed{Y^{1/2\,1}_{-1/2\,\lambda'} = \delta_{\lambda',0}+2\delta_{\lambda',-1}.} \tag{C.260b}$$

- Direct tensor mean field Γ for $\lambda=1$:

$$\boxed{\begin{aligned}\Gamma^{t\Omega=m+1/2}_{m\nu_a,\,m+1\,\nu_b}|_{\mathrm{D}} = &\sum_{\substack{m'\geq 0\\ \nu_c\nu_d}}\sum_{\lambda'=-1}^{1}(-)^{\lambda'-1}\\ &\times\langle m\nu_a\; m'+\lambda'\,\nu_c|V(r_{12})[\hat{r}_{12}\otimes\hat{r}_{12}]^{(2)}_{\lambda'-1}|m+1\,\nu_b\; m'\nu_d\rangle R^{t1/2\,1}_{m'\nu_d\nu_c\lambda'}|_{\mathrm{D}},\end{aligned}} \tag{C.261}$$

where

$$\boxed{\begin{aligned}R^{t1/2\,1}_{m'\nu_d\nu_c\lambda'}|_{\mathrm{D}} = &\,Y^{1/2\,1}_{1/2\,\lambda'}\Big[Z^{(+)t}_{m'+1/2\,m'\nu_d\nu_c\lambda'}|_{\mathrm{D}} - Z^{(-)t}_{m'+1/2\,m'\nu_d\nu_c\lambda'}|_{\mathrm{D}}\\ &+\Theta(m'-1/2)Y^{1/2\,1}_{-1/2\,\lambda'}\Big[Z^{(+)t}_{m'-1/2\,m'\nu_d\nu_c\lambda'}|_{\mathrm{D}} - Z^{(-)t}_{m'-1/2\,m'\nu_d\nu_c\lambda'}|_{\mathrm{D}}\Big],\end{aligned}} \tag{C.262}$$

with the quantities Y given by (C.260). Here again, the quantities $R^{(\pm)t1/2\,1}|_{\mathrm{E}}$ and $R^{t1/2\,1}|_{\mathrm{D}}$ are symmetric under the exchange of ν_c and ν_d only if $\lambda'=0$ such that the corresponding

quantities $Z^{(\pm)}|_{\rm E}$ and $Z^{(\pm)}|_{\rm D}$ display this symmetry as their density matrices ρ and $\overline{\rho}$, besides being symmetric, are diagonal in m'.

The tensor mean field $\overline{\Gamma}$ can easily be deduced by exchanging ρ and $\overline{\rho}$ in the expressions of the tensor mean field Γ, as we notice by comparing the expressions of the mean fields (III.37) and (III.38). We can see that only the quantities $R^{(\pm)}$ are impacted by this transformation. We will call them $\overline{R}^{(\pm)}$ in the following. Unfortunately, there are no straight relations between the quantities $R^{(\pm)}$ and $\overline{R}^{(\pm)}$ for the tensor interaction, as there were for the central and density-dependent terms (see equations (C.52)). As a consequence, the tensor mean fields Γ and $\overline{\Gamma}$ will be computed simultaneously in the code, but with different quantities $R^{(\pm)}$ and $\overline{R}^{(\pm)}$. In addition, note that the quantities Y making up the $R^{(\pm)}$ remain the same under this transformation, hence

$$\overline{Y}^{s\lambda}_{s'\lambda'} = Y^{s\lambda}_{s'\lambda'}. \tag{C.263}$$

Accordingly, the exchange tensor mean field $\overline{\Gamma}$ can be expressed as

$$\begin{aligned}\overline{\Gamma}^{t\Omega=m+s}_{m\nu_a,\,m+\lambda\,\nu_b}|_{\rm E} = \sum_{\substack{m'\geq 0\\ \nu_c\overline{\nu}_d}}\sum_{\lambda'=-1}^{1}(-)^{\lambda+\lambda'} \\ \times\Big[\langle m\nu_a\ m'+\lambda'\,\nu_c|V(r_{12})[\hat{r}_{12}\otimes\hat{r}_{12}]^{(2)}_{\lambda'-\lambda}|m'\nu_d\ m+\lambda\,\nu_b\rangle\overline{R}^{(+)ts\lambda}_{m'\nu_d\nu_c\lambda'}|_{\rm E} \\ +\langle m\nu_a\ -m'\nu_c|V(r_{12})[\hat{r}_{12}\otimes\hat{r}_{12}]^{(2)}_{\lambda'-\lambda}|-(m'+\lambda')\,\nu_d\ m+\lambda\,\nu_b\rangle\overline{R}^{(-)ts\lambda}_{m'\nu_c\nu_d\lambda'}|_{\rm E}\Big],\end{aligned} \tag{C.264}$$

where

$$\begin{aligned}\overline{R}^{(+)ts\lambda}_{m'\nu_d\nu_c\lambda'}|_{\rm E} &= \Theta(m'+s)Y^{s\lambda}_{s\lambda'}\overline{Z}^{(+)t}_{m'+s\,m'\nu_d\nu_c\lambda'}|_{\rm E} \\ &\quad+\Theta(m'-s)Y^{s\lambda}_{-s\lambda'}\overline{Z}^{(+)t}_{m'-s\,m'\nu_d\nu_c\lambda'}|_{\rm E},\end{aligned} \tag{C.265a}$$

$$\begin{aligned}\overline{R}^{(-)ts\lambda}_{m'\nu_c\nu_d\lambda'}|_{\rm E} &= -\Theta(m'+s)Y^{s\lambda}_{s\lambda'}\overline{Z}^{(-)t}_{m'+s\,m'\nu_c\nu_d\lambda'}|_{\rm E} \\ &\quad-\Theta(m'-s)Y^{s\lambda}_{-s\lambda'}\overline{Z}^{(-)t}_{m'-s\,m'\nu_c\nu_d\lambda'}|_{\rm E},\end{aligned} \tag{C.265b}$$

with the quantities Y expressed in (C.242), and with

$$\overline{Z}^{(+)t}_{\Omega'm'\nu_d\nu_c\lambda'}|_{\rm E} \equiv \sum_{t'}(H-W\delta_{tt'})\,\overline{\rho}^{t'\Omega'}_{m'\nu_d,\,m'+\lambda'\nu_c}, \tag{C.266a}$$

$$\overline{Z}^{(-)t}_{\Omega'm'\nu_c\nu_d\lambda'}|_{\rm E} \equiv \sum_{t'}(H-W\delta_{tt'})\,\rho^{t'\Omega'}_{m'\nu_c,\,m'+\lambda'\nu_d}, \tag{C.266b}$$

or, by explicitly separating their particle-like and proton-neutron contributions,

$$\overline{Z}^{(+)t}_{\Omega'm'\nu_d\nu_c\lambda'}|_{\rm E} = (H-W)\,\overline{\rho}^{t\Omega'}_{m'\nu_d,\,m'+\lambda'\nu_c} + H\,\overline{\rho}^{-t\Omega'}_{m'\nu_d,\,m'+\lambda'\nu_c}, \tag{C.267a}$$

$$\overline{Z}^{(-)t}_{\Omega'm'\nu_c\nu_d\lambda'}|_{\rm E} = (H-W)\,\rho^{t\Omega'}_{m'\nu_c,\,m'+\lambda'\nu_d} + H\,\rho^{-t\Omega'}_{m'\nu_c,\,m'+\lambda'\nu_d}. \tag{C.267b}$$

As for the direct tensor mean field $\overline{\Gamma}$, it reads

$$\begin{aligned}\overline{\Gamma}^{t\Omega=m+s}_{m\nu_a,\,m+\lambda\,\nu_b}|_{\rm D} = \sum_{\substack{m'\geq 0\\ \nu_c\overline{\nu}_d}}\sum_{\lambda'=-1}^{1}(-)^{\lambda-\lambda'} \\ \times\langle m\nu_a\ m'+\lambda'\,\nu_c|V(r_{12})[\hat{r}_{12}\otimes\hat{r}_{12}]^{(2)}_{\lambda'-\lambda}|m+\lambda\,\nu_b\ m'\nu_d\rangle\overline{R}^{ts\lambda}_{m'\nu_d\nu_c\lambda'}|_{\rm D},\end{aligned} \tag{C.268}$$

where

$$\boxed{\begin{aligned}\overline{R}^{ts\lambda}_{m'\nu_d\nu_c\lambda'}|_{\mathrm{D}} &= \Theta(m'+s)Y^{s\lambda}_{s\lambda'}\Big[\overline{Z}^{(+)t}_{m'+s\,m'\nu_d\nu_c\lambda'}|_{\mathrm{D}} - \overline{Z}^{(-)t}_{m'+s\,m'\nu_d\nu_c\lambda'}|_{\mathrm{D}}\Big] \\ &\quad + \Theta(m'-s)Y^{s\lambda}_{-s\lambda'}\Big[\overline{Z}^{(+)t}_{m'-s\,m'\nu_d\nu_c\lambda'}|_{\mathrm{D}} - \overline{Z}^{(-)t}_{m'-s\,m'\nu_d\nu_c\lambda'}|_{\mathrm{D}}\Big],\end{aligned}} \tag{C.269}$$

with the quantities Y expressed in (C.242), and with

$$\boxed{\begin{aligned}\overline{Z}^{(+)t}_{\Omega'm'\nu_d\nu_c\lambda'}|_{\mathrm{D}} &= (W-H)\,\overline{\rho}^{t\Omega'}_{m'\nu_d,\,m'+\lambda'\nu_c} + W\,\overline{\rho}^{-t\Omega'}_{m'\nu_d,\,m'+\lambda'\nu_c}, \qquad \text{(C.270a)}\\ \overline{Z}^{(-)t}_{\Omega'm'\nu_c\nu_d\lambda'}|_{\mathrm{D}} &= (W-H)\,\rho^{t\Omega'}_{m'\nu_c,\,m'+\lambda'\nu_d} + W\,\rho^{-t\Omega'}_{m'\nu_c,\,m'+\lambda'\nu_d}. \qquad \text{(C.270b)}\end{aligned}}$$

From the boxed equations, we can now explicitly write down the expressions of the direct and exchange tensor mean fields $\overline{\Gamma}$ for each value of λ. We recall that these fields are *not* time-reversal invariant, and that the quantities $\overline{Z}^{(\pm)}|_{\mathrm{E}}$ and $\overline{Z}^{(\pm)}|_{\mathrm{D}}$, respectively given by (C.267) and (C.270), are the same no matter the value of λ. Finally, note that if $\lambda = 1$, then $s = 1/2$ (as we could have already seen in (C.240)) since the identity $s_b \equiv s - 1 = \pm 1/2$ holds only if $s = 1/2$.

- Exchange tensor mean field $\overline{\Gamma}$ for $\lambda = 0$:

$$\boxed{\begin{aligned}\overline{\Gamma}^{t\Omega=m+s}_{m\nu_a,\,m\nu_b}|_{\mathrm{E}} &= \sum_{\substack{m'\geq 0\\ \nu_c\nu_d}}\sum_{\lambda'=-1}^{1}(-)^{\lambda'} \\ &\quad\times\Big[\langle m\nu_a\ m'+\lambda'\,\nu_c|V(r_{12})[\hat{r}_{12}\otimes\hat{r}_{12}]^{(2)}_{\lambda'}|m'\nu_d\ m\nu_b\rangle\overline{R}^{(+)ts0}_{m'\nu_d\nu_c\lambda'}|_{\mathrm{E}} \\ &\quad+\langle m\nu_a\ -m'\nu_c|V(r_{12})[\hat{r}_{12}\otimes\hat{r}_{12}]^{(2)}_{\lambda'}|-(m'+\lambda')\,\nu_d\ m\nu_b\rangle\overline{R}^{(-)ts0}_{m'\nu_c\nu_d\lambda'}|_{\mathrm{E}}\Big],\end{aligned}} \tag{C.271}$$

where

$$\boxed{\begin{aligned}\overline{R}^{(+)ts0}_{m'\nu_d\nu_c\lambda'}|_{\mathrm{E}} &= \Theta(m'+s)Y^{s0}_{s\lambda'}\overline{Z}^{(+)t}_{m'+s\,m'\nu_d\nu_c\lambda'}|_{\mathrm{E}} \\ &\quad+\Theta(m'-s)Y^{s0}_{-s\lambda'}\overline{Z}^{(+)t}_{m'-s\,m'\nu_d\nu_c\lambda'}|_{\mathrm{E}}, \qquad \text{(C.272a)}\\ \overline{R}^{(-)ts0}_{m'\nu_c\nu_d\lambda'}|_{\mathrm{E}} &= -\Theta(m'+s)Y^{s0}_{s\lambda'}\overline{Z}^{(-)t}_{m'+s\,m'\nu_c\nu_d\lambda'}|_{\mathrm{E}} \\ &\quad-\Theta(m'-s)Y^{s0}_{-s\lambda'}\overline{Z}^{(-)t}_{m'-s\,m'\nu_c\nu_d\lambda'}|_{\mathrm{E}}, \qquad \text{(C.272b)}\end{aligned}}$$

with the quantities Y given by (C.255).

- Direct tensor mean field $\overline{\Gamma}$ for $\lambda = 0$:

$$\boxed{\begin{aligned}\overline{\Gamma}^{t\Omega=m+s}_{m\nu_a,\,m\nu_b}|_{\mathrm{D}} &= \sum_{\substack{m'\geq 0\\ \nu_c\nu_d}}\sum_{\lambda'=-1}^{1}(-)^{\lambda'} \\ &\quad\times\langle m\nu_a\ m'+\lambda'\,\nu_c|V(r_{12})[\hat{r}_{12}\otimes\hat{r}_{12}]^{(2)}_{\lambda'}|m\nu_b\ m'\nu_d\rangle\overline{R}^{ts0}_{m'\nu_d\nu_c\lambda'}|_{\mathrm{D}},\end{aligned}} \tag{C.273}$$

where

$$\boxed{\begin{aligned}\overline{R}^{ts0}_{m'\nu_d\nu_c\lambda'}|_{\mathrm{D}} &= \Theta(m'+s)Y^{s0}_{s\lambda'}\Big[\overline{Z}^{(+)t}_{m'+s\,m'\nu_d\nu_c\lambda'}|_{\mathrm{D}} - \overline{Z}^{(-)t}_{m'+s\,m'\nu_d\nu_c\lambda'}|_{\mathrm{D}}\Big] \\ &\quad+\Theta(m'-s)Y^{s0}_{-s\lambda'}\Big[\overline{Z}^{(+)t}_{m'-s\,m'\nu_d\nu_c\lambda'}|_{\mathrm{D}} - \overline{Z}^{(-)t}_{m'-s\,m'\nu_d\nu_c\lambda'}|_{\mathrm{D}}\Big],\end{aligned}} \tag{C.274}$$

with the quantities Y given by (C.255). Note that the quantities $\overline{R}^{(\pm)ts0}|_{\mathrm{E}}$ and $\overline{R}^{ts0}|_{\mathrm{D}}$ are symmetric under the exchange of ν_c and ν_d only if $\lambda' = 0$ such that the corresponding quantities $\overline{Z}^{(\pm)}|_{\mathrm{E}}$ and $\overline{Z}^{(\pm)}|_{\mathrm{D}}$ display this symmetry as their density matrices ρ and $\overline{\rho}$ are, besides being symmetric, diagonal in m'.

- Exchange tensor mean field $\overline{\Gamma}$ for $\lambda = 1$:

$$\begin{aligned}\overline{\Gamma}^{t\Omega=m+1/2}_{m\nu_a,\,m+1\,\nu_b}|_{\mathrm{E}} = &\sum_{\substack{m'\geq 0\\ \nu_c\nu_d}}\sum_{\lambda'=-1}^{1}(-)^{\lambda'-1}\\ &\times\Big[\langle m\nu_a\ m'+\lambda'\,\nu_c|V(r_{12})[\hat{r}_{12}\otimes\hat{r}_{12}]^{(2)}_{\lambda'-1}|m'\nu_d\ m+1\,\nu_b\rangle\overline{R}^{(+)t1/2\,1}_{m'\nu_d\nu_c\lambda'}|_{\mathrm{E}}\\ &+\langle m\nu_a\ -m'\nu_c|V(r_{12})[\hat{r}_{12}\otimes\hat{r}_{12}]^{(2)}_{\lambda'-1}|-(m'+\lambda')\,\nu_d\ \ m+1\,\nu_b\rangle\overline{R}^{(-)t1/2\,1}_{m'\nu_c\nu_d\lambda'}|_{\mathrm{E}}\Big],\end{aligned} \tag{C.275}$$

where

$$\overline{R}^{(+)t1/2\,1}_{m'\nu_d\nu_c\lambda'}|_{\mathrm{E}} = Y^{1/2\,1}_{1/2\,\lambda'}\overline{Z}^{(+)t}_{m'+1/2\,m'\nu_d\nu_c\lambda'}|_{\mathrm{E}} + \Theta(m'-1/2)Y^{1/2\,1}_{-1/2\,\lambda'}\overline{Z}^{(+)t}_{m'-1/2\,m'\nu_d\nu_c\lambda'}|_{\mathrm{E}}, \tag{C.276a}$$

$$\overline{R}^{(-)t1/2\,1}_{m'\nu_c\nu_d\lambda'}|_{\mathrm{E}} = -Y^{1/2\,1}_{1/2\,\lambda'}\overline{Z}^{(-)t}_{m'+1/2\,m'\nu_c\nu_d\lambda'}|_{\mathrm{E}} - \Theta(m'-1/2)Y^{1/2\,1}_{-1/2\,\lambda'}\overline{Z}^{(-)t}_{m'-1/2\,m'\nu_c\nu_d\lambda'}|_{\mathrm{E}}, \tag{C.276b}$$

with the quantities Y given by (C.260).

- Direct tensor mean field $\overline{\Gamma}$ for $\lambda = 1$:

$$\begin{aligned}\overline{\Gamma}^{t\Omega=m+1/2}_{m\nu_a,\,m+1\,\nu_b}|_{\mathrm{D}} = &\sum_{\substack{m'\geq 0\\ \nu_c\nu_d}}\sum_{\lambda'=-1}^{1}(-)^{\lambda'-1}\\ &\times\langle m\nu_a\ m'+\lambda'\,\nu_c|V(r_{12})[\hat{r}_{12}\otimes\hat{r}_{12}]^{(2)}_{\lambda'-1}|m+1\,\nu_b\ m'\nu_d\rangle\overline{R}^{t1/2\,1}_{m'\nu_d\nu_c\lambda'}|_{\mathrm{D}},\end{aligned} \tag{C.277}$$

where

$$\begin{aligned}\overline{R}^{t1/2\,1}_{m'\nu_d\nu_c\lambda'}|_{\mathrm{D}} = &\,Y^{1/2\,1}_{1/2\,\lambda'}\Big[\overline{Z}^{(+)t}_{m'+1/2\,m'\nu_d\nu_c\lambda'}|_{\mathrm{D}} - \overline{Z}^{(-)t}_{m'+1/2\,m'\nu_d\nu_c\lambda'}|_{\mathrm{D}}\Big]\\ &+\Theta(m'-1/2)Y^{1/2\,1}_{-1/2\,\lambda'}\Big[\overline{Z}^{(+)t}_{m'-1/2\,m'\nu_d\nu_c\lambda'}|_{\mathrm{D}} - \overline{Z}^{(-)t}_{m'-1/2\,m'\nu_d\nu_c\lambda'}|_{\mathrm{D}}\Big],\end{aligned} \tag{C.278}$$

with the quantities Y given by (C.260). Here again, the quantities $\overline{R}^{(\pm)t1/2\,1}|_{\mathrm{E}}$ and $\overline{R}^{t1/2\,1}|_{\mathrm{D}}$ are symmetric under the exchange of ν_c and ν_d only if $\lambda' = 0$ such that the corresponding quantities $\overline{Z}^{(\pm)}|_{\mathrm{E}}$ and $\overline{Z}^{(\pm)}|_{\mathrm{D}}$ display this symmetry as their density matrices ρ and $\overline{\rho}$, besides being symmetric, are diagonal in m'.

Time-reversal invariant fields

Now, we assume the time-reversal invariance of the tensor mean fields Γ and $\overline{\Gamma}$, i.e. we set $\rho = \overline{\rho}$. In this case, as the quantity $Y^{s\lambda}_{s'\lambda'}$ remains unchanged under time-reversal symmetry and $Z^{(\pm)} = \overline{Z}^{(\pm)}$, we have $R^{(\pm)} = \overline{R}^{(\pm)}$, so that eventually the mean fields coincide, $\Gamma = \overline{\Gamma}$. They simplify according to the following expressions.

The exchange tensor mean fields (C.246) and (C.264) become

$$\begin{aligned}\Gamma^{t\Omega=m+s}_{m\nu_a,\,m+\lambda\,\nu_b}|^{\mathrm{T}}_{\mathrm{E}} = &\sum_{\substack{m'\geq 0\\ \nu_c\nu_d}}\sum_{\lambda'=-1}^{1}(-)^{\lambda-\lambda'}\\ &\times\Big[\langle m\nu_a\ m'+\lambda'\,\nu_c|V(r_{12})[\hat{r}_{12}\otimes\hat{r}_{12}]^{(2)}_{\lambda'-\lambda}|m'\nu_d\ m+\lambda\,\nu_b\rangle R^{ts\lambda}_{m'\nu_d\nu_c\lambda'}|^{\mathrm{T}}_{\mathrm{E}}\\ &-\langle m\nu_a\ -m'\nu_c|V(r_{12})[\hat{r}_{12}\otimes\hat{r}_{12}]^{(2)}_{\lambda'-\lambda}|-(m'+\lambda')\,\nu_d\ m+\lambda\,\nu_b\rangle R^{ts\lambda}_{m'\nu_c\nu_d\lambda'}|^{\mathrm{T}}_{\mathrm{E}}\Big],\end{aligned} \tag{C.279}$$

where the quantities (C.245) and (C.265) simplify according to

$$\boxed{R^{ts\lambda}_{m'\nu_d\nu_c\lambda'}|^{\mathrm{T}}_{\mathrm{E}} \equiv R^{(+)ts\lambda}_{m'\nu_d\nu_c\lambda'}|^{\mathrm{T}}_{\mathrm{E}} = -R^{(-)ts\lambda}_{m'\nu_d\nu_c\lambda'}|^{\mathrm{T}}_{\mathrm{E}},} \tag{C.280}$$

with

$$\boxed{R^{ts\lambda}_{m'\nu_d\nu_c\lambda'}|^{\mathrm{T}}_{\mathrm{E}} = \Theta(m'+s)Y^{s\lambda}_{s\lambda'}Z^{t}_{m'+s\,m'\nu_d\nu_c\lambda'}|^{\mathrm{T}}_{\mathrm{E}} + \Theta(m'-s)Y^{s\lambda}_{-s\lambda'}Z^{t}_{m'-s\,m'\nu_d\nu_c\lambda'}|^{\mathrm{T}}_{\mathrm{E}},} \tag{C.281}$$

since we notice that

$$\boxed{Z^{t}_{\Omega'm'\nu_d\nu_c\lambda'}|^{\mathrm{T}}_{\mathrm{E}} \equiv Z^{(+)t}_{\Omega'm'\nu_d\nu_c\lambda'}|^{\mathrm{T}}_{\mathrm{E}} = Z^{(-)t}_{\Omega'm'\nu_d\nu_c\lambda'}|^{\mathrm{T}}_{\mathrm{E}},} \tag{C.282}$$

where

$$\boxed{Z^{t}_{\Omega'm'\nu_d\nu_c\lambda'}|^{\mathrm{T}}_{\mathrm{E}} = (H-W)\rho^{t\Omega'}_{m'\nu_d,\,m'+\lambda'\nu_c} + H\rho^{-t\Omega'}_{m'\nu_d,\,m'+\lambda'\nu_c},} \tag{C.283}$$

while the quantities Y, given by (C.242), remain unchanged under time-reversal symmetry.

On the other hand, the direct tensor mean fields (C.250) and (C.268) become

$$\boxed{\overline{\Gamma}^{t\Omega=m+s}_{m\nu_a,\,m+\lambda\,\nu_b}|^{\mathrm{T}}_{\mathrm{D}} = 0,} \tag{C.284}$$

since the quantities (C.252) and (C.269) simplify according to

$$\boxed{R^{ts\lambda}_{m'\nu_d\nu_c\lambda'}|^{\mathrm{T}}_{\mathrm{D}} = 0,} \tag{C.285}$$

as we notice that

$$\boxed{Z^{(+)t}_{\Omega'm'\nu_d\nu_c\lambda'}|^{\mathrm{T}}_{\mathrm{D}} = Z^{(-)t}_{\Omega'm'\nu_d\nu_c\lambda'}|^{\mathrm{T}}_{\mathrm{D}}.} \tag{C.286}$$

In other words, *the direct tensor mean field is zero when the time-reversal symmetry is imposed.* Thus, the full time-reversal tensor mean field (direct plus exchange components) can be written

$$\boxed{\begin{aligned}\Gamma^{t\Omega=m+s}_{m\nu_a,\,m+\lambda\,\nu_b}|^{\mathrm{T}} = \sum_{\substack{m'\geq 0\\ \nu_c\overline{\nu}_d}}\sum_{\lambda'=-1}^{1}(-)^{\lambda-\lambda'} \\ \times\Big[\langle m\nu_a\ m'+\lambda'\,\nu_c|V(r_{12})[\hat{r}_{12}\otimes\hat{r}_{12}]^{(2)}_{\lambda'-\lambda}|m'\nu_d\ m+\lambda\,\nu_b\rangle R^{ts\lambda}_{m'\nu_d\nu_c\lambda'}|^{\mathrm{T}} \\ -\langle m\nu_a\ -m'\nu_c|V(r_{12})[\hat{r}_{12}\otimes\hat{r}_{12}]^{(2)}_{\lambda'-\lambda}|-(m'+\lambda')\,\nu_d\ m+\lambda\,\nu_b\rangle R^{ts\lambda}_{m'\nu_c\nu_d\lambda'}|^{\mathrm{T}}\Big],\end{aligned}} \tag{C.287}$$

where

$$R^{ts\lambda}_{m'\nu_d\nu_c\lambda'}|^{\mathrm{T}} \equiv R^{ts\lambda}_{m'\nu_d\nu_c\lambda'}|^{\mathrm{T}}_{\mathrm{E}}, \tag{C.288}$$

with $R^{ts\lambda}_{m'\nu_d\nu_c\lambda'}|^{\mathrm{T}}_{\mathrm{E}}$ given by (C.281), and

$$Z^{t}_{\Omega'm'\nu_d\nu_c\lambda'}|^{\mathrm{T}} = Z^{t}_{\Omega'm'\nu_d\nu_c\lambda'}|^{\mathrm{T}}_{\mathrm{E}}, \tag{C.289}$$

with $Z^{t}_{\Omega'm'\nu_d\nu_c\lambda'}|^{\mathrm{T}}_{\mathrm{E}}$ given by (C.283).

From the boxed equations, we can now explicitly write down the expressions of the *time-reversal invariant* tensor mean field for each value of λ. Note that the quantity $Z|_{\mathrm{E}}$, given by (C.282), is the same no matter the value of λ. Finally, note that if $\lambda = 1$, then $s = 1/2$ (as we could have already seen in (C.240)) since the identity $s_b \equiv s - 1 = \pm 1/2$ holds only if $s = 1/2$.

- Time-reversal invariant tensor mean field for $\lambda = 0$:

$$\boxed{\begin{aligned}\Gamma^{t\Omega=m+s}_{m\nu_a,\,m\nu_b}|^{\mathrm{T}} = &\sum_{\substack{m'\geq 0\\ \nu_c\overline{\nu}_d}}\sum_{\lambda'=-1}^{1}(-)^{\lambda'}\\ &\times\Big[\langle m\nu_a\ m'+\lambda'\,\nu_c|V(r_{12})[\hat{r}_{12}\otimes\hat{r}_{12}]^{(2)}_{\lambda'}|m'\nu_d\ m\nu_b\rangle R^{ts0}_{m'\nu_d\nu_c\lambda'}|^{\mathrm{T}}\\ &-\langle m\nu_a\ -m'\nu_c|V(r_{12})[\hat{r}_{12}\otimes\hat{r}_{12}]^{(2)}_{\lambda'}|-(m'+\lambda')\,\nu_d\ m\nu_b\rangle R^{ts0}_{m'\nu_c\nu_d\lambda'}|^{\mathrm{T}}\Big],\end{aligned}} \tag{C.290}$$

where

$$\boxed{R^{ts0}_{m'\nu_d\nu_c\lambda'}|^{\mathrm{T}} = \Theta(m'+s)Y^{s0}_{s\lambda'}Z^{t}_{m'+s\,m'\nu_d\nu_c\lambda'}|^{\mathrm{T}} + \Theta(m'-s)Y^{s0}_{-s\lambda'}Z^{t}_{m'-s\,m'\nu_d\nu_c\lambda'}|^{\mathrm{T}},} \tag{C.291}$$

with the quantities Y given by (C.255).

- Time-reversal invariant tensor mean field for $\lambda = 1$:

$$\boxed{\begin{aligned}\Gamma^{t\Omega=m+1/2}_{m\nu_a,\,m+1\,\nu_b}|^{\mathrm{T}} = &\sum_{\substack{m'\geq 0\\ \nu_c\overline{\nu}_d}}\sum_{\lambda'=-1}^{1}(-)^{\lambda'-1}\\ &\times\Big[\langle m\nu_a\ m'+\lambda'\,\nu_c|V(r_{12})[\hat{r}_{12}\otimes\hat{r}_{12}]^{(2)}_{\lambda'-1}|m'\nu_d\ m+1\,\nu_b\rangle R^{t1/2\,1}_{m'\nu_d\nu_c\lambda'}|^{\mathrm{T}}\\ &-\langle m\nu_a\ -m'\nu_c|V(r_{12})[\hat{r}_{12}\otimes\hat{r}_{12}]^{(2)}_{\lambda'-1}|-(m'+\lambda')\,\nu_d\ m+1\,\nu_b\rangle R^{t1/2\,1}_{m'\nu_c\nu_d\lambda'}|^{\mathrm{T}}\Big],\end{aligned}} \tag{C.292}$$

where

$$\boxed{R^{t1/2\,1}_{m'\nu_d\nu_c\lambda'}|^{\mathrm{T}} = Y^{1/2\,1}_{1/2\,\lambda'}Z^{t}_{m'+1/2\,m'\nu_d\nu_c\lambda'}|^{\mathrm{T}} + \Theta(m'-1/2)Y^{1/2\,1}_{-1/2\,\lambda'}Z^{t}_{m'-1/2\,m'\nu_d\nu_c\lambda'}|^{\mathrm{T}},} \tag{C.293}$$

with the quantities Y given by (C.260). Note that the quantities $R^{ts0}|^{\mathrm{T}}$ and $R^{t1/2\,1}|^{\mathrm{T}}$ are symmetric under the exchange of ν_c and ν_d only if $\lambda' = 0$ such that the corresponding quantities $Z|^{\mathrm{T}}$ display this symmetry as their density matrix ρ, besides being symmetric, is diagonal in m'.

2.2.2. Tensor pairing field

We continue by deriving the pairing field (III.32) of the tensor interaction (C.229), which is not time-reversal invariant for the moment. Given that the pairing tensor (C.21) and the fields (C.22) are diagonal in t and Ω, this tensor pairing field can be written

$$\Delta^{t\Omega}_{r_ar_b} = \sum_{\substack{t'\Omega'>0\\ r_cr_d}}\langle ts_ar_a\ \overline{ts_br_b}|v^{\mathrm{T},(\mathrm{a})}_{12}|t's_cr_c\ \overline{t's_dr_d}\rangle\kappa^{t'\Omega'}_{r_cr_d}. \tag{C.294}$$

As for the tensor mean fields, let us first concentrate on the exchange component of the tensor pairing field. It reads

$$\begin{aligned}\Delta^{t\Omega}_{r_ar_b}|_{\mathrm{E}} = &\sum_{\substack{t'\Omega'>0\\ r_cr_d}}\sum_{k}(-)^k\langle r_a-r_b|V(r_{12})[\hat{r}_{12}\otimes\hat{r}_{12}]^{(2)}_{-k}P_r|r_c-r_d\rangle\\ &\times\sigma_b\sigma_d\langle ts_a\ t-s_b|\mathcal{P}_{\mathrm{E}}[\vec{\sigma}_1\otimes\vec{\sigma}_2]^{(2)}_{k}|t's_c\ t'-s_d\rangle\kappa^{t'\Omega'}_{r_cr_d}.\end{aligned} \tag{C.295}$$

We name the quantum numbers of the above matrix element in the same way as we have done for the second matrix element of the tensor mean field (C.234), while keeping in mind that here $\lambda \in \{-1, 0, 1\}$ since the pairing field is not symmetric under the exchange of its

indices, contrary to the mean field (see discussion (C.24) and the discussion below). Note in passing that all the spatial integrals of the tensor pairing field have to be evaluated so that all the components of $[\hat{r}_{12}\otimes\hat{r}_{12}]^{(2)}_{-k}$ exist. With these notations, the exchange tensor pairing field becomes

$$\begin{aligned}\Delta^{t\Omega=m+s}_{m\nu_a,\,m+\lambda\,\nu_b}|_{\rm E} = &\sum_{\substack{t'\Omega'>0\\ m'\nu_c\nu_d}}\sum_{\lambda'}(-)^{\lambda-\lambda'}\times 4(s-\lambda)(s'-\lambda')\\ \times\langle m\nu_a\ -(m+\lambda)\,\nu_b|V(r_{12})[\hat{r}_{12}\otimes\hat{r}_{12}]^{(2)}_{\lambda'-\lambda}P_r|m'\nu_c\ -(m'+\lambda')\,\nu_d\rangle\\ \times\langle ts\ t-(s-\lambda)|\mathcal{P}_{\rm E}[\vec{\sigma}_1\otimes\vec{\sigma}_2]^{(2)}_{\lambda-\lambda'}|t's'\ t'-(s'-\lambda')\rangle\kappa^{t'm'+s'}_{m'\nu_c,\,m'+\lambda'\nu_d}.\end{aligned}\tag{C.296}$$

Once again, let us first focus on the spin-isospin part. We set

$$A^{ts\lambda}_{\Omega'm'\nu_c\nu_d\lambda'}|_{\rm E}\equiv B^{s\lambda}_{s'\lambda'}\times C^{t}_{\Omega'm'\nu_c\nu_d\lambda'}|_{\rm E},\tag{C.297}$$

where the spin part reads

$$B^{s\lambda}_{s'\lambda'}\equiv 4(s-\lambda)(s'-\lambda')\langle s\ -(s-\lambda)|[\vec{\sigma}_1\otimes\vec{\sigma}_2]^{(2)}_{\lambda-\lambda'}|s'\ -(s'-\lambda')\rangle,\tag{C.298}$$

and the isospin part is

$$C^{t}_{\Omega'm'\nu_c\nu_d\lambda'}|_{\rm E}=(H-W)\kappa^{t\,m'+s'}_{m'\nu_c,\,m'+\lambda'\nu_d},\tag{C.299}$$

where we notice that there is only a particle-like contribution coming from the tensor pairing field. On the other hand, since the direct and exchange tensor pairing fields have the same spin part, we also have implicitly set

$$B^{s\lambda}_{s'\lambda'}\equiv B^{s\lambda}_{s'\lambda'}|_{\rm D}=B^{s\lambda}_{s'\lambda'}|_{\rm E}.\tag{C.300}$$

Using carefully the expression of the spin matrix element (D.20), we obtain

$$\boxed{\begin{aligned}B^{s\lambda}_{s'\lambda'}=-16s(s-\lambda)^2(s'-\lambda')\Bigg\{&\delta_{ss'}\left[\sqrt{\frac{2}{3}}\delta_{\lambda\lambda'}-\delta_{\lambda+\lambda',2s}\right]\\ &+\delta_{s,-s'}\left[\sqrt{\frac{2}{3}}\delta_{\lambda,0}\delta_{\lambda',0}+2\delta_{\lambda,2s}\delta_{\lambda,-\lambda'}-\delta_{\lambda-\lambda',2s}\right]\Bigg\},\end{aligned}}\tag{C.301}$$

where we have separated the $s=s'$ and $s\neq s'$ contributions to the tensor pairing field, its spin diagonal part being given by $\lambda=0$ and the non-diagonal one by $\lambda\neq 0$, as expected. Note that if the tensor pairing field is spin diagonal, then it is also diagonal in m, just like the tensor mean fields are.

Then, from (C.297), we get

$$A^{ts\lambda}_{\Omega'm'\nu_c\nu_d\lambda'}|_{\rm E}=(H-W)B^{s\lambda}_{s'\lambda'}\kappa^{t\,m'+s'}_{m'\nu_c,\,m'+\lambda'\nu_d}.\tag{C.302}$$

Now, setting

$$S^{ts\lambda}_{m'\nu_c\nu_d\lambda'}|_{\rm E}\equiv\sum_{\Omega'}\Theta(\Omega')A^{ts\lambda}_{\Omega'm'\nu_c\nu_d\lambda'}|_{\rm E}=\sum_{s'=\pm s}\Theta(m'+s')A^{ts\lambda}_{m'+s'm'\nu_c\nu_d\lambda'}|_{\rm E},\tag{C.303}$$

we end up with

$$\boxed{\begin{aligned}S^{ts\lambda}_{m'\nu_c\nu_d\lambda'}|_{\rm E}=(H-W)\Big[&\Theta(m'+s)B^{s\lambda}_{s\lambda'}\kappa^{t\,m'+s}_{m'\nu_c,\,m'+\lambda'\nu_d}\\ &+\Theta(m'-s)B^{s\lambda}_{-s\lambda'}\kappa^{t\,m'-s}_{m'\nu_c,\,m'+\lambda'\nu_d}\Big],\end{aligned}}\tag{C.304}$$

and the exchange tensor pairing field can be written

$$\Delta^{t\Omega=m+s}_{m\nu_a,\,m+\lambda\,\nu_b}|_{\rm E} = \sum_{\substack{m'\geq 0\\ \nu_c\bar{\nu}_d}}\sum_{\lambda'=-1}^{1}(-)^{\lambda-\lambda'} \times \langle m\nu_a\ -(m+\lambda)\,\nu_b|V(r_{12})[\hat{r}_{12}\otimes\hat{r}_{12}]^{(2)}_{\lambda'-\lambda}|-(m'+\lambda')\,\nu_d\ m'\nu_c\rangle S^{ts\lambda}_{m'\nu_c\nu_d\lambda'}|_{\rm E}, \tag{C.305}$$

where, as we have done for the tensor mean fields, we have replaced the summations $\sum_{m'}\sum_{\Omega'>0}$ by $\sum_{m'\geq 0}\sum_{\Omega'}\Theta(\Omega')$ and applied the operator P_r. Now, writing the above matrix element under its integral form, we see that, because of the expression of the axial wave functions (C.3) and the fact that they commute with the tensor $[\hat{r}_{12}\otimes\hat{r}_{12}]^{(2)}_{\lambda'-\lambda}$, it is equivalent to $\langle m\nu_a\ -m'\nu_c|V(r_{12})[\hat{r}_{12}\otimes\hat{r}_{12}]^{(2)}_{\lambda'-\lambda}|-(m'+\lambda')\,\nu_d\ m+\lambda\,\nu_b\rangle$. Thus, the exchange tensor pairing field reads

$$\boxed{\Delta^{t\Omega=m+s}_{m\nu_a,\,m+\lambda\,\nu_b}|_{\rm E} = \sum_{\substack{m'\geq 0\\ \nu_c\bar{\nu}_d}}\sum_{\lambda'=-1}^{1}(-)^{\lambda-\lambda'} \times \langle m\nu_a\ -m'\nu_c|V(r_{12})[\hat{r}_{12}\otimes\hat{r}_{12}]^{(2)}_{\lambda'-\lambda}|-(m'+\lambda')\,\nu_d\ m+\lambda\,\nu_b\rangle S^{ts\lambda}_{m'\nu_c\nu_d\lambda'}|_{\rm E}.} \tag{C.306}$$

To get the direct tensor pairing field out of the exchange one, we first switch H and W and omit the operator P_r to obtain

$$\Delta^{t\Omega=m+s}_{m\nu_a,\,m+\lambda\,\nu_b}|_{\rm D} = \sum_{\substack{m'\geq 0\\ \nu_c\bar{\nu}_d}}\sum_{\lambda'=-1}^{1}(-)^{\lambda-\lambda'} \times \langle m\nu_a\ -(m+\lambda)\,\nu_b|V(r_{12})[\hat{r}_{12}\otimes\hat{r}_{12}]^{(2)}_{\lambda'-\lambda}|m'\nu_c\ -(m'+\lambda')\,\nu_d\rangle S^{ts\lambda}_{m'\nu_c\nu_d\lambda'}|_{\rm D}. \tag{C.307}$$

Just like we have done with the exchange term, we notice that the matrix element can be written $\langle m\nu_a\ m'+\lambda'\,\nu_d|V(r_{12})[\hat{r}_{12}\otimes\hat{r}_{12}]^{(2)}_{\lambda'-\lambda}|m'\nu_c\ m+\lambda\,\nu_b\rangle$. Finally exchanging the dummy indices ν_c and ν_d, the direct tensor pairing field becomes

$$\boxed{\Delta^{t\Omega=m+s}_{m\nu_a,\,m+\lambda\,\nu_b}|_{\rm D} = \sum_{\substack{m'\geq 0\\ \nu_c\bar{\nu}_d}}\sum_{\lambda'=-1}^{1}(-)^{\lambda-\lambda'} \times \langle m\nu_a\ m'+\lambda'\,\nu_c|V(r_{12})[\hat{r}_{12}\otimes\hat{r}_{12}]^{(2)}_{\lambda'-\lambda}|m'\nu_d\ m+\lambda\,\nu_b\rangle S^{ts\lambda}_{m'\nu_d\nu_c\lambda'}|_{\rm D},} \tag{C.308}$$

where

$$\boxed{S^{ts\lambda}_{m'\nu_d\nu_c\lambda'}|_{\rm D} = (W-H)\Big[\Theta(m'+s)B^{s\lambda}_{s\lambda'}\kappa^{t\,m'+s}_{m'\nu_d,\,m'+\lambda'\nu_c} + \Theta(m'-s)B^{s\lambda}_{-s\lambda'}\kappa^{t\,m'-s}_{m'\nu_d,\,m'+\lambda'\nu_c}\Big],} \tag{C.309}$$

with the quantities B given by (C.301).

Finally, the identity

$$\boxed{S^{ts\lambda}_{m'\nu_c\nu_d\lambda'} \equiv -S^{ts\lambda}_{m'\nu_c\nu_d\lambda'}|_{\rm E} = S^{ts\lambda}_{m'\nu_c\nu_d\lambda'}|_{\rm D}} \tag{C.310}$$

allows us to write down the full tensor pairing field (direct plus exchange components) as

$$\boxed{\begin{aligned}\Delta^{t\Omega=m+s}_{m\nu_a,\,m+\lambda\,\nu_b} &= \sum_{\substack{m'\geq 0\\ \nu_c\nu_d}}\sum_{\lambda'=-1}^{1}(-)^{\lambda-\lambda'}\\ &\times\Big[\langle m\nu_a\ m'+\lambda'\,\nu_c|V(r_{12})[\hat{r}_{12}\otimes\hat{r}_{12}]^{(2)}_{\lambda'-\lambda}|m'\nu_d\ m+\lambda\,\nu_b\rangle S^{ts\lambda}_{m'\nu_d\nu_c\lambda'}\\ &-\langle m\nu_a\ -m'\nu_c|V(r_{12})[\hat{r}_{12}\otimes\hat{r}_{12}]^{(2)}_{\lambda'-\lambda}|-(m'+\lambda')\,\nu_d\ m+\lambda\,\nu_b\rangle S^{ts\lambda}_{m'\nu_c\nu_d\lambda'}\Big],\end{aligned}} \tag{C.311}$$

As it was the case with the CDD pairing field, we see that the tensor pairing field has the same structure as the tensor mean field (C.246). This is the reason of our specific transformations leading to (C.306) and (C.308). Indeed, the pairing fields can therefore be calculated simultaneously with the mean fields in an HFB code.

From the boxed equations, we can now explicitly write down the expressions of the above tensor pairing field for each value of λ. We recall that this field is *not* time-reversal invariant. We also note that if $|\lambda|=1$, then $\lambda=2s$ as we deduce from $s_b\equiv s-\lambda=\pm 1/2$ when $\lambda\neq 0$.

- Tensor pairing field for $\lambda=0$:

$$\boxed{\begin{aligned}\Delta^{t\Omega=m+s}_{m\nu_a,\,m\nu_b} &= \sum_{\substack{m'\geq 0\\ \nu_c\nu_d}}\sum_{\lambda'=-1}^{1}(-)^{\lambda'}\\ &\times\Big[\langle m\nu_a\ m'+\lambda'\,\nu_c|V(r_{12})[\hat{r}_{12}\otimes\hat{r}_{12}]^{(2)}_{\lambda'}|m'\nu_d\ m\nu_b\rangle S^{ts0}_{m'\nu_d\nu_c\lambda'}\\ &-\langle m\nu_a\ -m'\nu_c|V(r_{12})[\hat{r}_{12}\otimes\hat{r}_{12}]^{(2)}_{\lambda'}|-(m'+\lambda')\,\nu_d\ m\nu_b\rangle S^{ts0}_{m'\nu_c\nu_d\lambda'}\Big],\end{aligned}} \tag{C.312}$$

where

$$\boxed{\begin{aligned}S^{ts0}_{m'\nu_c\nu_d\lambda'} &= (W-H)\Big[\Theta(m'+s)B^{s0}_{s\lambda'}\kappa^{t\,m'+s}_{m'\nu_c,\,m'+\lambda'\nu_d}\\ &\qquad+\Theta(m'-s)B^{s0}_{-s\lambda'}\kappa^{t\,m'-s}_{m'\nu_c,\,m'+\lambda'\nu_d}\Big],\end{aligned}} \tag{C.313}$$

with

$$\boxed{B^{s0}_{\pm s\lambda'}=\mp\left[\sqrt{\frac{2}{3}}\delta_{\lambda',0}+\delta_{\lambda',\pm 2s}\right].} \tag{C.314}$$

- Tensor pairing field for $|\lambda|=1$:

$$\boxed{\begin{aligned}\Delta^{t\Omega=m+s}_{m\nu_a,\,m+2s\,\nu_b} &= \sum_{\substack{m'\geq 0\\ \nu_c\nu_d}}\sum_{\lambda'=-1}^{1}(-)^{\lambda'-2s}\\ &\times\Big[\langle m\nu_a\ m'+\lambda'\,\nu_c|V(r_{12})[\hat{r}_{12}\otimes\hat{r}_{12}]^{(2)}_{\lambda'-2s}|m'\nu_d\ m+2s\,\nu_b\rangle S^{ts\,2s}_{m'\nu_d\nu_c\lambda'}\\ &-\langle m\nu_a\ -m'\nu_c|V(r_{12})[\hat{r}_{12}\otimes\hat{r}_{12}]^{(2)}_{\lambda'-2s}|-(m'+\lambda')\,\nu_d\ m+2s\,\nu_b\rangle S^{ts\,2s}_{m'\nu_c\nu_d\lambda'}\Big],\end{aligned}} \tag{C.315}$$

where

$$\boxed{\begin{aligned}S^{ts\,2s}_{m'\nu_c\nu_d\lambda'} &= (W-H)\Big[\Theta(m'+s)B^{s\,2s}_{s\lambda'}\kappa^{t\,m'+s}_{m'\nu_c,\,m'+\lambda'\nu_d}\\ &\qquad+\Theta(m'-s)B^{s\,2s}_{-s\lambda'}\kappa^{t\,m'-s}_{m'\nu_c,\,m'+\lambda'\nu_d}\Big],\end{aligned}} \tag{C.316}$$

with

$$\boxed{B^{s\,2s}_{s\lambda'} = \delta_{\lambda',0} + \sqrt{\frac{2}{3}}\delta_{\lambda',2s},} \tag{C.317a}$$

$$\boxed{B^{s\,2s}_{-s\lambda'} = -\Big[\delta_{\lambda',0} + 2\delta_{\lambda',-2s}\Big].} \tag{C.317b}$$

Note that the quantities S^{ts0} and $S^{ts\,2s}$ are not symmetric under the exchange of ν_c and ν_d since the pairing tensor κ is not.

Time-reversal invariant fields

Now, we assume the time-reversal invariance of the tensor pairing field, i.e. the pairing tensor κ becomes symmetric under the exchange of its indices. Then, the pairing field becomes symmetric (see discussion below equation (C.24)) and it suffices to consider its expression for $\lambda \in \{0, 1\}$. For $\lambda = 0$, its expression is still given by (C.312), with $S^{ts0}|^{\mathrm{T}} = S^{ts0}$. If $\lambda = 1$, then $s = 1/2$ (as we could have already seen in (C.301)) since the identity $s_b \equiv s - 1 = \pm 1/2$ holds only if $s = 1/2$.

- Time-reversal invariant tensor pairing field for $\lambda = 1$:

$$\begin{aligned}\boxed{\Delta^{t\Omega=m+1/2}_{m\nu_a,\,m+1\,\nu_b}|^{\mathrm{T}} = \sum_{\substack{m'\geq 0\\ \nu_c\nu_d}}\sum_{\lambda'=-1}^{1}(-)^{\lambda'-1}} \\ \times\Big[\langle m\nu_a\ m'+\lambda'\,\nu_c|V(r_{12})[\hat{r}_{12}\otimes\hat{r}_{12}]^{(2)}_{\lambda'-1}|m'\nu_d\ m+1\,\nu_b\rangle S^{t1/2\,1}_{m'\nu_d\nu_c\lambda'}|^{\mathrm{T}} \\ -\langle m\nu_a\ -m'\nu_c|V(r_{12})[\hat{r}_{12}\otimes\hat{r}_{12}]^{(2)}_{\lambda'-1}|-(m'+\lambda')\,\nu_d\ m+1\,\nu_b\rangle S^{t1/2\,1}_{m'\nu_c\nu_d\lambda'}|^{\mathrm{T}}\Big],\end{aligned} \tag{C.318}$$

where

$$\begin{aligned}\boxed{S^{t1/2\,1}_{m'\nu_c\nu_d\lambda'}|^{\mathrm{T}} = (W-H)\Big[B^{1/2\,1}_{1/2\,\lambda'}\kappa^{t\,m'+1/2}_{m'\nu_c,\,m'+\lambda'\nu_d}} \\ \boxed{+\Theta(m'-1/2)B^{1/2\,1}_{-1/2\,\lambda'}\kappa^{t\,m'-1/2}_{m'\nu_c,\,m'+\lambda'\nu_d}\Big],}\end{aligned} \tag{C.319}$$

with

$$\boxed{S^{t1/2\,1}_{m'\nu_c\nu_d\lambda'}|^{\mathrm{T}} = S^{t1/2\,1}_{m'\nu_c\nu_d\lambda'},} \tag{C.320}$$

and

$$\boxed{B^{1/2\,1}_{1/2\,\lambda'} = \delta_{\lambda',0} + \sqrt{\frac{2}{3}}\delta_{\lambda',1},} \tag{C.321a}$$

$$\boxed{B^{1/2\,1}_{-1/2\,\lambda'} = -\Big[\delta_{\lambda',0} + 2\delta_{\lambda',-1}\Big].} \tag{C.321b}$$

Note that the quantities S^{ts0} and $S^{t1/2\,1}$ are symmetric under the exchange of ν_c and ν_d only if $\lambda' = 0$ such that the pairing tensor κ, besides being symmetric, is diagonal in m'.

2.2.3. Tensor spatial matrix elements

In the previous subsection, we have treated the spin-isospin parts of the tensor mean- and pairing fields. In order to fully specify these fields, it remains to determine their spatial parts, which we now undertake.

Identifying the position of the centers by the quantum numbers j, the spatial dependence of the tensor fields lies in the two-body matrix elements of the form

$$v^{j_a j_c j_b j_d,\,k}_{r_a r_c r_b r_d} \equiv \langle j_a r_a\ j_c r_c|V(r_{12})[\hat{r}_{12}\otimes\hat{r}_{12}]^{(2)}_{-k}|j_b r_b\ j_d r_d\rangle, \tag{C.322}$$

where we recall that $k = \lambda - \lambda'$ (see equation (C.233) and the related discussion). By definition,

$$v^{j_a j_c j_b j_d,\, k}_{r_a r_c r_b r_d} = \int \mathrm{d}^3 r_1 \int \mathrm{d}^3 r_2 \, \phi^*_{j_a r_a}(\vec{r}_1)\phi^*_{j_c r_c}(\vec{r}_2) V(r_{12})[\hat{r}_{12} \otimes \hat{r}_{12}]^{(2)}_{-k} \phi_{j_b r_b}(\vec{r}_1)\phi_{j_d r_d}(\vec{r}_2). \quad \text{(C.323)}$$

Since the wave functions and the sandwiched quantity commute, we can rearrange the terms according to

$$v^{j_a j_c j_b j_d,\, k}_{r_a r_c r_b r_d} = \int \mathrm{d}^3 r_1 \int \mathrm{d}^3 r_2 \, V(r_{12})[\hat{r}_{12} \otimes \hat{r}_{12}]^{(2)}_{-k} \phi^*_{j_a r_a}(\vec{r}_1)\phi_{j_b r_b}(\vec{r}_1)\phi^*_{j_c r_c}(\vec{r}_2)\phi_{j_d r_d}(\vec{r}_2). \quad \text{(C.324)}$$

Now, using twice the Gogny separable development in axial symmetry (C.495), on both $\vec{r}_1$ and $\vec{r}_2$ coordinates, we find

$$\begin{aligned} v^{j_a j_c j_b j_d,\, k}_{r_a r_c r_b r_d} = \sum_{r_\mu r_\nu} T^{r_\mu}_{j_a r_a\, j_b r_b} T^{r_\nu}_{j_c r_c\, j_d r_d} \int \mathrm{d}^3 r_1 \int \mathrm{d}^3 r_2 \\ \times V(r_{12})[\hat{r}_{12} \otimes \hat{r}_{12}]^{(2)}_{-k} \phi_{j_{ab}0}(\vec{r}_1)\phi_{j_{cd}0}(\vec{r}_2)\phi_{j_{ab} r_\mu}(\vec{r}_2)\phi_{j_{cd} r_\nu}(\vec{r}_2), \end{aligned} \quad \text{(C.325)}$$

where the axial Talman coefficients are specified in (C.497) and the ranges of values taken by r_μ and r_ν can be deduced from (C.503), (C.504) and (C.510). Applying twice the Moshinsky transformation in axial symmetry (C.514), we get

$$\begin{aligned} v^{j_a j_c j_b j_d,\, k}_{r_a r_c r_b r_d} = \sum_{r_\mu r_\nu} T^{r_\mu}_{j_a r_a\, j_b r_b} T^{r_\nu}_{j_c r_c\, j_d r_d} \sum_{r_\lambda} M^{r_\lambda\, r_\sigma}_{r_\mu\, r_\nu} \\ \times \int \mathrm{d}^3 r \, V(\sqrt{2} r)[\hat{r} \otimes \hat{r}]^{(2)}_{-k} \phi_0(\vec{r} - \vec{d}_{abcd})\phi_{r_\sigma}(\vec{r} - \vec{d}_{abcd}) \\ \times \int \mathrm{d}^3 R \, \phi^*_0(\vec{R} - \vec{D}_{abcd})\phi_{r_\lambda}(\vec{R} - \vec{D}_{abcd}), \end{aligned} \quad \text{(C.326)}$$

since the Jacobian of the change of variables $(\vec{r}_1, \vec{r}_2) \to (\vec{r}, \vec{R})$ is equal to unity, the quantity $\hat{r}$ is scale-invariant and the axial Moshinsky coefficient, specified by (C.516), fixes the range of values of r_σ according to (C.521), (C.522) and (C.530). Note that in the particular case $r'_\mu = r'_\nu = 0$, the axial Moshinsky coefficient reduces to $M^{r'_\lambda r'_\sigma}_{0\,0} = \delta_{r'_\lambda,0}\delta_{r'_\sigma,0}$ because of (C.526) and (C.533). Note also that $\phi_0(\vec{R}) = \phi^*_0(\vec{R})$, by virtue of (C.8). Finally, from (C.496) and (C.515), we can express the above distances as

$$\vec{d}_{abcd} \equiv \frac{\vec{d}_{ab} - \vec{d}_{cd}}{\sqrt{2}}, \quad \text{and} \quad \vec{D}_{abcd} \equiv \frac{\vec{d}_{ab} + \vec{d}_{cd}}{\sqrt{2}}, \quad \text{(C.327)}$$

with

$$\vec{d}_{ab} \equiv \frac{\vec{d}_a + \vec{d}_b}{2}. \quad \text{(C.328)}$$

The integral over $\vec{R}$ is readily carried out considering the orthogonality relation of the axial wave function (C.6), so that, eventually,

$$\boxed{\begin{aligned} v^{j_a j_c j_b j_d,\, k}_{r_a r_c r_b r_d} = \sum_{r_\mu r_\nu} T^{r_\mu}_{j_a r_a\, j_b r_b} T^{r_\nu}_{j_c r_c\, j_d r_d} M^{0\, r_\sigma}_{r_\mu\, r_\nu} \\ \times \int \mathrm{d}^3 r \, V(\sqrt{2} r)[\hat{r} \otimes \hat{r}]^{(2)}_{-k} \phi_0(\vec{r} - \vec{d}_{abcd})\phi_{r_\sigma}(\vec{r} - \vec{d}_{abcd}), \end{aligned}} \quad \text{(C.329)}$$

with the Moshinsky coefficient $M^{0\, r_\sigma}_{r_\mu\, r_\nu}$ given by merging the results (C.523) and (C.531) and the new values taken by r_σ specified by (C.524), (C.525) and (C.532).

Thus, in the following, we shall evaluate the integral defined by

$$I^k_{r_\sigma}(\vec{d}_{abcd}) \equiv \int \mathrm{d}^3 r\, V(\sqrt{2}r)[\hat{r}\otimes\hat{r}]^{(2)}_{-k}\phi_0(\vec{r}-\vec{d}_{abcd})\phi_{r_\sigma}(\vec{r}-\vec{d}_{abcd}). \tag{C.330}$$

First, we recall that, in axial symmetry where $\vec{r}=(r_\perp,\varphi,z)$, the components of the tensor $[\hat{r}\otimes\hat{r}]^{(2)}$ are

$$[\hat{r}\otimes\hat{r}]^{(2)}_0 = \frac{1}{\sqrt{6}}\frac{2z^2-r_\perp^2}{r_\perp^2+z^2}, \tag{C.331a}$$

$$[\hat{r}\otimes\hat{r}]^{(2)}_{\pm1} = \mp\frac{zr_\perp \mathrm{e}^{\pm\mathrm{i}\varphi}}{r_\perp^2+z^2}, \tag{C.331b}$$

$$[\hat{r}\otimes\hat{r}]^{(2)}_{\pm2} = \frac{1}{2}\frac{r_\perp^2 \mathrm{e}^{\pm2\mathrm{i}\varphi}}{r_\perp^2+z^2}. \tag{C.331c}$$

Accordingly, it appears that the integral (C.330) can be separated along the directions Oz and perpendicular to Oz if and only if the quantity $V(\sqrt{2}r)/r^2$ is the product of a function of $r_\perp$ by a function of z. In particular, if the tensor potential is Gaussian, as it is the case for the analytical form of the Gogny interaction we are studying, the quantity $V(\sqrt{2}r)/r^2$ cannot be written as a product of a function of $r_\perp$ by a function of z, such that the integral cannot be separated along the directions Oz and perpendicular to Oz. One way to address this issue is to consider the relation

$$\frac{1}{r^2} = \int_0^\infty \mathrm{d}\xi\, \mathrm{e}^{-\xi r^2}, \tag{C.332}$$

so that the integral (C.330) becomes separable. Indeed, for a Gaussian tensor potential, we have

$$\begin{aligned} V(\sqrt{2}r)[\hat{r}\otimes\hat{r}]^{(2)}_{-k} &= \mathrm{e}^{-2r^2/\mu^2}\frac{P_{-k}(r_\perp,z)}{r^2}\mathrm{e}^{-\mathrm{i}k\varphi} \\ &= \int_0^\infty \mathrm{d}\xi\, \mathrm{e}^{-r^2(2/\mu^2+\xi)}P_{-k}(r_\perp,z)\mathrm{e}^{-\mathrm{i}k\varphi}, \end{aligned} \tag{C.333}$$

where the polynomial P_{-k} is defined by

$$P_0 = \frac{2z^2-r_\perp^2}{\sqrt{6}}, \tag{C.334a}$$

$$P_{\pm1} = \mp zr_\perp, \tag{C.334b}$$

$$P_{\pm2} = \frac{r_\perp^2}{2}, \tag{C.334c}$$

in such a way that the integral (C.330) separates according to

$$\begin{aligned} I^k_{r_\sigma}(\vec{d}_{abcd}) = &\int_0^\infty \mathrm{d}\xi \int_{-\infty}^{+\infty} \mathrm{d}z\, \mathrm{e}^{-z^2(2/\mu^2+\xi)}\phi_0(z-d_{abcd})\phi_{n_{z\sigma}}(z-d_{abcd}) \\ &\times \int \mathrm{d}^2 r_\perp\, \mathrm{e}^{-r_\perp^2(2/\mu^2+\xi)}\mathrm{e}^{-\mathrm{i}k\varphi}\phi_{00}(\vec{r}_\perp)\phi_{m_\sigma n_{\perp\sigma}}(\vec{r}_\perp)P_{-k}(r_\perp,z). \end{aligned} \tag{C.335}$$

According to the definition (C.8), $\phi_{00}(\vec{r}_\perp) = \phi_{00}(r_\perp)$ since this wave function has no angular dependence. Furthermore, we can write $\phi_{m_\sigma n_{\perp\sigma}}(\vec{r}_\perp) = \mathrm{e}^{\mathrm{i}m_\sigma\varphi}\widetilde{\phi}_{|m_\sigma|n_{\perp\sigma}}(r_\perp)$, thanks

to the relation (C.9). From these equations, we can easily evaluate the angular part of the integral over $r_\perp$, so that

$$I^k_{r_\sigma}(\vec{d}_{abcd}) = 2\pi\delta_{k,m_\sigma}\int_0^\infty \mathrm{d}\xi \int_{-\infty}^{+\infty} \mathrm{d}z\, \mathrm{e}^{-z^2(2/\mu^2+\xi)}\phi_0(z-d_{abcd})\phi_{n_{z\sigma}}(z-d_{abcd}) \times \int_0^\infty \mathrm{d}r_\perp\, r_\perp \mathrm{e}^{-r_\perp^2(2/\mu^2+\xi)}\phi_{00}(r_\perp)\widetilde{\phi}_{|m_\sigma|n_{\perp\sigma}}(r_\perp)P_{-k}(r_\perp,z). \tag{C.336}$$

Note that the Kronecker delta enforces the symmetry condition $k = m_b - m_a + m_d - m_c$, in accordance with the fact that the tensor interaction does not commute with L_z (see discussion right after (C.232)). Otherwise, we would recover the conservation law of the central and density-dependent interactions that do commute with L_z (see equation (C.136) and the discussion below). Mathematically speaking, the tensor interaction involves a tensor of rank 2, so that its projection satisfies $-2 \leq k \leq 2$ while the central and density-dependent interactions only involve scalars, i.e. tensors of rank 0, for which the projection is necessarily $k = 0$, so that $m_a + m_c = m_c + m_d$, as expected.

Finally, we can include the different cases encountered in the unified expression

$$\boxed{I^k_{r_\sigma}(\vec{d}_{abcd}) = 2\pi\delta_{k,m_\sigma}\sum_{m=0}^{2}\sum_{n=0}^{2} P^{mn}_{-k}\int_0^\infty \mathrm{d}\xi\, K^{z\,m}_{n_{z\sigma}}(\xi,d_{abcd})K^{\perp\,n}_{|m_\sigma|n_{\perp\sigma}}(\xi),} \tag{C.337}$$

where

$$P^{mn}_0 = \frac{1}{\sqrt{6}}(2\delta_{m,2}\delta_{n,0} - \delta_{m,0}\delta_{n,2}), \tag{C.338a}$$

$$P^{mn}_{\pm1} = \mp\delta_{m,1}\delta_{n,1}, \tag{C.338b}$$

$$P^{mn}_{\pm2} = \frac{1}{2}\delta_{m,0}\delta_{n,2}, \tag{C.338c}$$

and

$$K^{z\,m}_{n_{z\sigma}}(\xi,d_{abcd}) = \int_{-\infty}^{+\infty}\mathrm{d}z\, z^m\, \mathrm{e}^{-z^2(2/\mu^2+\xi)}\phi_0(z-d_{abcd})\phi_{n_{z\sigma}}(z-d_{abcd}), \tag{C.339}$$

$$K^{\perp\,n}_{|m_\sigma|n_{\perp\sigma}}(\xi) = \int_0^\infty \mathrm{d}r_\perp\, r_\perp^{n+1}\, \mathrm{e}^{-r_\perp^2(2/\mu^2+\xi)}\phi_{00}(r_\perp)\widetilde{\phi}_{|m_\sigma|n_{\perp\sigma}}(r_\perp). \tag{C.340}$$

To complete the calculation of the spatial part of the tensor term, we need to evaluate the above integrals. Since the wave functions are not off-center along $r_\perp$, the calculation of the associated integral is quite easy and we will then start with this one.

The series expansion of the generalized Laguerre polynomial (D.100) making up the radial wave function $\widetilde{\phi}_{|m_\sigma|n_{\perp\sigma}}(r_\perp)$ of (C.340) combined to the result (D.119) leads to

$$\boxed{K^{\perp\,n}_{|m_\sigma|n_{\perp\sigma}}(\xi) = \frac{b_\perp^n}{2\pi}[n_{\perp\sigma}!(n_{\perp\sigma}+|m_\sigma|)!]^{1/2} \times \sum_{i=0}^{n_{\perp\sigma}}\frac{(-)^i}{i!(n_{\perp\sigma}-i)!(i+|m_\sigma|)!}\Gamma(i+n/2+|m_\sigma|/2+1)G_\perp^{-i-n/2-|m_\sigma|/2-1}(\xi),} \tag{C.341}$$

with

$$\boxed{G_\perp(\xi) \equiv \frac{2b_\perp^2+\mu^2+\mu^2 b_\perp^2\xi}{\mu^2},} \tag{C.342}$$

the analogous version of the spherical quantity (B.39) for the radial part of the axial symmetry, when $\xi = 0$.

The wave functions being off-center along z, the calculation of the associated integral is a bit more tedious. From the expressions of the wave functions relative to z, (C.5), and the series expansion of the Hermite polynomial (D.98), we obtain

$$K^{z\,m}_{n_{z\sigma}}(\xi, d_{abcd}) = \frac{1}{b_z^{n_{z\sigma}+1}}\left[\frac{2^{n_{z\sigma}} n_{z\sigma}!}{\pi}\right]^{1/2} \sum_{j=0}^{\lfloor n_{z\sigma}/2\rfloor} \frac{(-)^j}{2^{2j} j!(n_{z\sigma}-2j)!} b_z^{2j} \times \underbrace{\int_{-\infty}^{+\infty} \mathrm{d}z\, z^m (z-d_{abcd})^{n_{z\sigma}-2j}\, \mathrm{e}^{-z^2(2/\mu^2+\xi)} \mathrm{e}^{-(z-d_{abcd})^2/b_z^2}}_{A}. \tag{C.343}$$

Shifting $z' = z - d_{abcd}$ and using the binomial formula, the above integral becomes

$$A = \sum_{l=0}^{m} \frac{m!}{l!(m-l)!} d_{abcd}^{m-l} \underbrace{\int_{-\infty}^{+\infty} \mathrm{d}z'\, z'^{\,n_{z\sigma}+l-2j}\, \mathrm{e}^{-(z'+d_{abcd})^2(2/\mu^2+\xi)} \mathrm{e}^{-z'^2/b_z^2}}_{B}. \tag{C.344}$$

Let us now complete the square of the argument of the exponential appearing in the integral above. It reads

$$-\left[\frac{\sqrt{G_z(\xi)}}{b_z} z' + \left(\frac{2}{\mu^2}+\xi\right)\frac{b_z d_{abcd}}{\sqrt{G_z(\xi)}}\right]^2 - \left(\frac{2}{\mu^2}+\xi\right)\frac{d_{abcd}^2}{G_z(\xi)}, \tag{C.345}$$

where we have set

$$\boxed{G_z(\xi) \equiv \frac{2b_z^2 + \mu^2 + \mu^2 b_z^2 \xi}{\mu^2},} \tag{C.346}$$

the analogous version of the spherical quantity (B.39) for the z part in axial symmetry, when $\xi = 0$. Then, the integral B can be rewritten as

$$B = \mathrm{e}^{-(2/\mu^2+\xi)d_{abcd}^2/G_z(\xi)} \times \int_{-\infty}^{+\infty} \mathrm{d}z'\, z'^{\,n_{z\sigma}+l-2j}\, \mathrm{e}^{-\left[\sqrt{G_z(\xi)}z'/b_z + (2/\mu^2+\xi)b_z d_{abcd}/\sqrt{G_z(\xi)}\right]^2}. \tag{C.347}$$

Another change of variable, namely $u \equiv \sqrt{G_z(\xi)}z'/b_z + (2/\mu^2+\xi)b_z d_{abcd}/\sqrt{G_z(\xi)}$, where ξ is considered fixed here, gives

$$B = \frac{b_z}{\sqrt{G_z(\xi)}} \mathrm{e}^{-(2/\mu^2+\xi)d_{abcd}^2/G_z(\xi)} \times \underbrace{\int_{-\infty}^{+\infty} \mathrm{d}u \left[\frac{b_z}{\sqrt{G_z(\xi)}} u - \left(\frac{2}{\mu^2}+\xi\right)\frac{b_z^2 d_{abcd}}{G_z(\xi)}\right]^{n_{z\sigma}+l-2j} \mathrm{e}^{-u^2}}_{C}. \tag{C.348}$$

Applying the binomial formula again, we end up with

$$C = \sum_{p=0}^{n_{z\sigma}+l-2j} (-)^{n_{z\sigma}+l-p} \frac{(n_{z\sigma}+l-2j)!}{p!(n_{z\sigma}+l-2j-p)!} \times \left[\frac{b_z}{\sqrt{G_z(\xi)}}\right]^p \left[\left(\frac{2}{\mu^2}+\xi\right)\frac{b_z^2 d_{abcd}}{G_z(\xi)}\right]^{n_{z\sigma}+l-2j-p} J_p, \tag{C.349}$$

where the integral

$$J_p \equiv \int_{-\infty}^{+\infty} \mathrm{d}u\, u^p\, \mathrm{e}^{-u^2} \tag{C.350}$$

is given by (D.120). Finally, by gathering all the terms, we find

$$\begin{aligned} K^{z\,m}_{n_{z\sigma}}(\xi, d_{abcd}) = (-)^{n_{z\sigma}} \left[\frac{2^{n_{z\sigma}} n_{z\sigma}!}{\pi}\right]^{1/2} \mathrm{e}^{-F_z(\xi) d_{abcd}^2} \sum_{j=0}^{\lfloor n_{z\sigma}/2 \rfloor} \frac{(-)^j}{2^{2j} j! (n_{z\sigma}-2j)!} \\ \times \sum_{l=0}^{m} (-)^l \frac{m!}{l!(m-l)!} d_{abcd}^{m-l} \sum_{\substack{p=0 \\ p\in 2\mathbb{N}}}^{n_{z\sigma}+l-2j} \frac{(n_{z\sigma}+l-2j)!}{p!(n_{z\sigma}+l-2j-p)!} \\ \times b_z^{n_{z\sigma}+2l-2j-p} G_z^{-p/2-1/2}(\xi) \Big[F_z(\xi) d_{abcd}\Big]^{n_{z\sigma}+l-2j-p} \Gamma\left(\frac{p+1}{2}\right), \end{aligned} \tag{C.351}$$

where the notation $p \in 2\mathbb{N}$ indicates that p has to be even. The quantities appearing are

$$F_z(\xi) \equiv \left(\frac{2}{\mu^2} + \xi\right) \frac{1}{G_z(\xi)} = \frac{2 + \mu^2 \xi}{2b_z^2 + \mu^2 + \mu^2 b_z^2 \xi}, \tag{C.352}$$

and $G_z(\xi)$, that is expressed in (C.346). Then, to get an expression for (C.337), it remains to evaluate the integral over ξ. Initially, we wrote this integral as

$$\int_0^\infty \mathrm{d}\xi\, K^{z\,m}_{n_{z\sigma}}(\xi, d_{abcd}) K^{\perp\,n}_{|m_\sigma|n_{\perp\sigma}}(\xi) = \int_0^\infty \mathrm{d}\xi\, \mathrm{e}^{-\xi} f^{mn}_{|m_\sigma|n_{\perp\sigma}n_{z\sigma}}(\xi, d_{abcd}), \tag{C.353}$$

where we defined

$$f^{mn}_{|m_\sigma|n_{\perp\sigma}n_{z\sigma}}(\xi, d_{abcd}) \equiv \mathrm{e}^{\xi} K^{z\,m}_{n_{z\sigma}}(\xi, d_{abcd}) K^{\perp\,n}_{|m_\sigma|n_{\perp\sigma}}(\xi). \tag{C.354}$$

This writing allowed us to perform a Gauss–Laguerre quadrature to approximate the above integral according to

$$\int_0^\infty \mathrm{d}\xi\, \mathrm{e}^{-\xi} f^{mn}_{|m_\sigma|n_{\perp\sigma}n_{z\sigma}}(\xi, d_{abcd}) \simeq \sum_{q=0}^{N} w_q f^{mn}_{|m_\sigma|n_{\perp\sigma}n_{z\sigma}}(\xi_q, d_{abcd}), \tag{C.355}$$

with N the quadrature order, ξ_q the q-th root of the Laguerre polynomial $L_N(\xi_q)$ at which the function (C.354) is evaluated, and w_q a weight factor that reads

$$w_q \equiv \frac{\xi_q}{(N+1)^2 [L_{N+1}(\xi_q)]^2}. \tag{C.356}$$

Sadly, the integrand increases quite fast so that it is not smooth enough to ensure a decent convergence. Indeed, we needed to push the quadrature order to $N = 200$ for the fields to converge with a precision of 10^{-6} in their matrix elements. In order to reduce this number, we made the change of variable $\xi \equiv x/1-x$ to get

$$\int_0^\infty \mathrm{d}\xi\, K^{z\,m}_{n_{z\sigma}}(\xi, d_{abcd}) K^{\perp\,n}_{|m_\sigma|n_{\perp\sigma}}(\xi) = \int_0^1 \mathrm{d}x\, g^{mn}_{|m_\sigma|n_{\perp\sigma}n_{z\sigma}}(x, d_{abcd}), \tag{C.357}$$

with the function

$$g^{mn}_{|m_\sigma|n_{\perp\sigma}n_{z\sigma}}(x, d_{abcd}) \equiv \frac{1}{(1-x)^2} K^{z\,m}_{n_{z\sigma}}\left(\frac{x}{1-x}, d_{abcd}\right) K^{\perp\,n}_{|m_\sigma|n_{\perp\sigma}}\left(\frac{x}{1-x}\right). \tag{C.358}$$

Now using a Gauss–Legendre quadrature on the interval $[0,1]$, the integral is approximated according to

$$\int_0^1 \mathrm{d}x\, g^{mn}_{|m_\sigma|n_{\perp\sigma}n_{z\sigma}}(x, d_{abcd}) \simeq \sum_{q=0}^{N'} \widetilde{w}_q g^{mn}_{|m_\sigma|n_{\perp\sigma}n_{z\sigma}}(\widetilde{x}_q, d_{abcd}). \tag{C.359}$$

It is important to mention that the weight factors read

$$\widetilde{w}_q \equiv \frac{1}{(1-\widetilde{x}_q^2)[P'_N(\widetilde{x}_q)]^2}, \tag{C.360}$$

and that the Gauss–Legendre nodes on the interval $[0,1]$, $\widetilde{x}_q$, are related to the ones on the interval $[-1,1]$, x_q, for traditional Gauss–Legendre quadratures as

$$\widetilde{x}_q \equiv \frac{x_q+1}{2}, \tag{C.361}$$

as we performed a translation. With this new method, the order $N = 20$ is enough to reach a precision of 10^{-6} in the fields.

At the one-center limit, all centers coincide ($j_a = j_b = j_c = j_d$), so that $d_{abcd} = 0$. Obviously, the spin-isospin matrix elements (of the tensor interaction) evaluated in the previous subsections remain the same. As for the tensor spatial matrix elements (C.329), they remain valid provided that the integral (C.330) is evaluated for $d_{abcd} = 0$ and that the Talman coefficients relative to z are those given by (C.511) rather than by (C.506), in the same way that the conditions (C.512) rather than (C.510) will have to be taken into account at this limit. When the integral (C.330) is evaluated for $d_{abcd} = 0$, only its part relative to z, whose final expression is given by (C.351), is affected. It simplifies as

$$\boxed{\begin{aligned} K^{z\,m}_{n_{z\sigma}}(\xi,0) = \left[\frac{2^{n_{z\sigma}} n_{z\sigma}!}{\pi}\right]^{1/2} b_z^m \sum_{j=0}^{\lfloor n_{z\sigma}/2\rfloor} \frac{(-)^j}{2^{2j} j!(n_{z\sigma}-2j)!} \delta_{n_{z\sigma}+m-2j,2\mathbb{N}} \\ \times G_z^{-n_{z\sigma}/2-m/2+j-1/2}(\xi)\, \Gamma\left(\frac{n_{z\sigma}+m-2j+1}{2}\right), \end{aligned}} \tag{C.362}$$

where $G_z(\xi)$ is expressed in (C.346) and where the notation $\delta_{n_{z\sigma}+m-2j,2\mathbb{N}}$ indicates that the sum $n_{z\sigma}+m-2j$ must be even. To get an expression for (C.337) at the one-center limit, it is enough to repeat the procedure presented in the two-center case in (C.355), while imposing $d_{abcd} = 0$.

2.3. Spin–orbit contribution

In this subsection, we shall derive the mean- and pairing fields associated with the finite-range spin–orbit term of the generalized Gogny interaction (II.1). Note that there are no rearrangement fields associated with the spin–orbit term since it does not depend on the density. The antisymmetrized finite-range spin–orbit interaction considered in the following reads

$$\begin{aligned} v_{12}^{\mathrm{SO},(\mathrm{a})} &\equiv v_{12}^{\mathrm{SO}}(1 - P_r P_\sigma P_\tau) \\ &= (W - HP_\tau) B(\mu) V(r_{12}) \vec{L}\cdot\vec{S}(1 - P_r P_\tau) \\ &= \mathcal{P}_{\mathrm{D}} \widetilde{B}(\mu) V(r_{12}) [\vec{r}_{12} \otimes \vec{\nabla}_{12}]^{(1)} \cdot [\vec{\sigma}_1 + \vec{\sigma}_2]^{(1)} \\ &\quad + \mathcal{P}_{\mathrm{E}} \widetilde{B}(\mu) V(r_{12}) [\vec{r}_{12} \otimes \vec{\nabla}_{12}]^{(1)} \cdot [\vec{\sigma}_1 + \vec{\sigma}_2]^{(1)} P_r, \end{aligned} \tag{C.363}$$

where the angular momenta involved in the second equation have been defined in (II.3) and (II.4). Note that $\vec{S}$ removes the operator P_σ since it acts symmetrically on the spin variables (see discussion in section II). Note that we have used the equivalent form (D.85) of the spin–orbit operator in the third equation, with the factor

$$\widetilde{B}(\mu) \equiv -\frac{1}{2\sqrt{2}} B(\mu) = \frac{\sqrt{2}}{\mu^2} \frac{1}{(\mu\sqrt{\pi})^3}, \tag{C.364}$$

ensuring that we recover the exact expression of the zero-range spin–orbit interaction at the zero-range limit (see subsection D.5.1 for more details), where $B(\mu)$ is given by (II.7). The isospin components of the direct and exchange fields are respectively

$$\mathcal{P}_{\mathrm{D}} \equiv W - HP_\tau, \tag{C.365a}$$
$$\mathcal{P}_{\mathrm{E}} \equiv H - WP_\tau. \tag{C.365b}$$

We notice that the direct components of the spin–orbit fields can be deduced from the exchange ones by switching W and H and removing the operator P_r, as we have done for the other terms of the Gogny interaction. Thus, in the following, we will start by deriving the exchange spin–orbit fields from which, then, we will deduce the direct ones.

2.3.1. Spin–orbit mean fields

We start by deriving the mean field Γ, given by (III.37), of the spin–orbit interaction (C.363), which is not time-reversal invariant for the moment. Given that density matrices (C.21) and the fields (C.22) are diagonal in t and Ω, this spin–orbit mean field can be written

$$\begin{aligned}\Gamma^{t\Omega}_{r_a r_b} = \sum_{\substack{t'\Omega'>0 \\ r_c r_d}} \Big[&\langle t s_a r_a \; t' s_c r_c | v_{12}^{\mathrm{SO,(a)}} | t s_b r_b \; t' s_d r_d \rangle \rho^{t'\Omega'}_{r_d r_c} \\ &+ \langle t s_a r_a \; \overline{t' s_c r_c} | v_{12}^{\mathrm{SO,(a)}} | t s_b r_b \; \overline{t' s_d r_d} \rangle \overline{\rho}^{t'\Omega'}_{r_c r_d} \Big].\end{aligned} \tag{C.366}$$

Let us first concentrate on the exchange spin–orbit mean field. It reads

$$\begin{aligned}\Gamma^{t\Omega}_{r_a r_b}|_{\mathrm{E}} = \widetilde{B}(\mu) \sum_{\substack{t'\Omega'>0 \\ r_c r_d}} \sum_k (-)^k \Big[&\langle r_a r_c | V(r_{12}) [\vec{r}_{12} \otimes \vec{\nabla}_{12}]^{(1)}_{-k} P_r | r_b r_d \rangle \\ &\times \langle t s_a \; t' s_c | \mathcal{P}_{\mathrm{E}} [\vec{\sigma}_1 + \vec{\sigma}_2]^{(1)}_k | t s_b \; t' s_d \rangle \rho^{t'\Omega'}_{r_d r_c} \\ + \sigma_c \sigma_d \langle r_a - r_c | V(r_{12}) [\vec{r}_{12} \otimes \vec{\nabla}_{12}]^{(1)}_{-k} P_r | r_b - r_d \rangle &\\ &\times \langle t s_a \; t' - s_c | \mathcal{P}_{\mathrm{E}} [\vec{\sigma}_1 + \vec{\sigma}_2]^{(1)}_k | t s_b \; t' - s_d \rangle \overline{\rho}^{t'\Omega'}_{r_c r_d} \Big].\end{aligned} \tag{C.367}$$

The analysis on symmetries exposed for the tensor interaction remains valid for the spin–orbit term since the spin–orbit operator $\vec{L} \cdot \vec{S}$ does not commute with $\vec{L}$ or $\vec{S}$ either, as it is shown in subsection D.6.3. The structure of the fields of the spin-orbit interaction will therefore be similar to that of the tensor interaction. In particular, the conservation laws (C.233) still hold for the spin–orbit interaction, with $-1 \leq k \leq 1$. We use the same conventions and notations as for the tensor term, and thus refer the reader to the previous section for more details.

The exchange spin–orbit mean field becomes

$$\begin{aligned}\Gamma^{t\Omega=m+s}_{m\nu_a,\,m+\lambda\,\nu_b}|_{\rm E} = \widetilde{B}(\mu) \sum_{\substack{t'\Omega'>0\\ m'\nu_c\nu_d}} \sum_{\lambda'} (-)^{\lambda-\lambda'} \\ \times \Big[\langle m\nu_a\ m'+\lambda'\,\nu_c|V(r_{12})[\vec{r}_{12}\otimes\vec{\nabla}_{12}]^{(1)}_{\lambda'-\lambda}P_r|m+\lambda\,\nu_b\ m'\nu_d\rangle \\ \times \langle ts\ t's'-\lambda'|\mathcal{P}_{\rm E}[\vec{\sigma}_1+\vec{\sigma}_2]^{(1)}_{\lambda-\lambda'}|t\,s-\lambda\ t's'\rangle\rho^{t'm'+s'}_{m'\nu_d,\,m'+\lambda'\nu_c} \\ + 4s'(s'-\lambda')\langle m\nu_a\ -m'\nu_c|V(r_{12})[\vec{r}_{12}\otimes\vec{\nabla}_{12}]^{(1)}_{\lambda'-\lambda}P_r|m+\lambda\,\nu_b\ -(m'+\lambda')\,\nu_d\rangle \\ \times \langle ts\ t'-s'|\mathcal{P}_{\rm E}[\vec{\sigma}_1+\vec{\sigma}_2]^{(1)}_{\lambda-\lambda'}|t\,s-\lambda\ t'-(s'-\lambda')\rangle\overline{\rho}^{t'm'+s'}_{m'\nu_c,\,m'+\lambda'\nu_d}\Big].\end{aligned} \tag{C.368}$$

Let us first focus on the spin-isospin part, which is not trivial for the spin–orbit interaction either. As for the tensor term, we set

$$X^{(+)ts\lambda}_{\Omega'm'\nu_d\nu_c\lambda'}|_{\rm E} \equiv Y^{(+)s\lambda}_{s'\lambda'} \times Z^{(+)t}_{\Omega'm'\nu_d\nu_c\lambda'}|_{\rm E}, \tag{C.369a}$$

$$X^{(-)ts\lambda}_{\Omega'm'\nu_c\nu_d\lambda'}|_{\rm E} \equiv Y^{(-)s\lambda}_{s'\lambda'} \times Z^{(-)t}_{\Omega'm'\nu_c\nu_d\lambda'}|_{\rm E}, \tag{C.369b}$$

in the first and second matrix elements respectively, where their spin parts read

$$Y^{(+)s\lambda}_{s'\lambda'} \equiv \langle s\ s'-\lambda'|[\vec{\sigma}_1+\vec{\sigma}_2]^{(1)}_{\lambda-\lambda'}|s-\lambda\ s'\rangle, \tag{C.370a}$$

$$Y^{(-)s\lambda}_{s'\lambda'} \equiv 4s'(s'-\lambda')\langle s\ -s'|[\vec{\sigma}_1+\vec{\sigma}_2]^{(1)}_{\lambda-\lambda'}|s-\lambda\ -(s'-\lambda')\rangle, \tag{C.370b}$$

and their isospin parts are

$$Z^{(+)t}_{\Omega'm'\nu_d\nu_c\lambda'}|_{\rm E} \equiv \sum_{t'}(H-W\delta_{tt'})\,\rho^{t'\Omega'}_{m'\nu_d,\,m'+\lambda'\nu_c}, \tag{C.371a}$$

$$Z^{(-)t}_{\Omega'm'\nu_c\nu_d\lambda'}|_{\rm E} \equiv \sum_{t'}(H-W\delta_{tt'})\,\overline{\rho}^{t'\Omega'}_{m'\nu_c,\,m'+\lambda'\nu_d}, \tag{C.371b}$$

or, by explicitly separating their particle-like and proton-neutron contributions,

$$\boxed{Z^{(+)t}_{\Omega'm'\nu_d\nu_c\lambda'}|_{\rm E} = (H-W)\,\rho^{t\Omega'}_{m'\nu_d,\,m'+\lambda'\nu_c} + H\,\rho^{-t\Omega'}_{m'\nu_d,\,m'+\lambda'\nu_c},} \tag{C.372a}$$

$$\boxed{Z^{(-)t}_{\Omega'm'\nu_c\nu_d\lambda'}|_{\rm E} = (H-W)\,\overline{\rho}^{t\Omega'}_{m'\nu_c,\,m'+\lambda'\nu_d} + H\,\overline{\rho}^{-t\Omega'}_{m'\nu_c,\,m'+\lambda'\nu_d}.} \tag{C.372b}$$

Note that these quantities are identical to those of the tensor term (C.238), provided that we consider the tensor coefficients W and H instead of the spin–orbit ones. On the other hand, since the direct and exchange spin–orbit mean fields have the same spin part, we also have implicitly set

$$Y^{(\pm)s\lambda}_{s'\lambda'} \equiv Y^{(\pm)s\lambda}_{s'\lambda'}|_{\rm D} = Y^{(\pm)s\lambda}_{s'\lambda'}|_{\rm E}. \tag{C.373}$$

To evaluate the quantities $Y^{(\pm)}$, we need to find out the general expression of the spin matrix element $\langle s_a\ s_c|[\vec{\sigma}_1+\vec{\sigma}_2]^{(1)}_{\lambda-\lambda'}|s_b\ s_d\rangle$. It is given by (D.22). Applying this formula to (C.370) keeping in mind that $\lambda\in\{0,1\}$, we obtain

$$Y^{(+)s\lambda}_{s'\lambda'} = \delta_{\lambda,0}\Big[2(s+s')\delta_{\lambda',0}+\sqrt{2}\lambda'\delta_{\lambda',2s'}\Big] - \sqrt{2}\delta_{\lambda,1}\delta_{s,1/2}\delta_{\lambda',0}, \tag{C.374a}$$

$$Y^{(-)s\lambda}_{s'\lambda'} = \delta_{\lambda,0}\Big[2(s-s')\delta_{\lambda',0}-\sqrt{2}\lambda'\delta_{\lambda',2s'}\Big] - \sqrt{2}\delta_{\lambda,1}\delta_{s,1/2}\delta_{\lambda',0}, \tag{C.374b}$$

where we notice that

$$Y^{s\lambda}_{s'\lambda'} \equiv Y^{(+)s\lambda}_{s'\lambda'} = Y^{(-)s\lambda}_{-s'-\lambda'}, \tag{C.375}$$

with

$$\boxed{Y^{s\lambda}_{s'\lambda'} = \delta_{\lambda,0}\Big[2(s+s')\delta_{\lambda',0} + \sqrt{2}\lambda'\delta_{\lambda',2s'}\Big] - \sqrt{2}\delta_{\lambda,1}\delta_{s,1/2}\delta_{\lambda',0}.} \tag{C.376}$$

We check that the spin diagonal part of the spin–orbit mean field corresponds to $\lambda = 0$ and its non-diagonal part to $\lambda = 1$. Note that if the spin–orbit mean field is spin diagonal, then it is also diagonal in m, in agreement with the fact that the spin–orbit mean field is diagonal in Ω ($\Omega_a = \Omega_b$ and $s_a = s_b$ imply $m_a = m_b$).

Then, from (C.369), we get

$$X^{(+)ts\lambda}_{\Omega' m'\nu_d\nu_c\lambda'}|_{\rm E} \equiv Y^{s\lambda}_{s'\lambda'} \times Z^{(+)t}_{\Omega' m'\nu_d\nu_c\lambda'}|_{\rm E}, \tag{C.377a}$$

$$X^{(-)ts\lambda}_{\Omega' m'\nu_c\nu_d\lambda'}|_{\rm E} \equiv Y^{s\lambda}_{-s'-\lambda'} \times Z^{(-)t}_{\Omega' m'\nu_c\nu_d\lambda'}|_{\rm E}. \tag{C.377b}$$

Now, setting

$$R^{(+)ts\lambda}_{m'\nu_d\nu_c\lambda'}|_{\rm E} \equiv \sum_{\Omega'} \Theta(\Omega') X^{(+)ts\lambda}_{\Omega' m'\nu_d\nu_c\lambda'}|_{\rm E} = \sum_{s'=\pm s} \Theta(m'+s') X^{(+)ts\lambda}_{m'+s' m'\nu_d\nu_c\lambda'}|_{\rm E}, \tag{C.378a}$$

$$R^{(-)ts\lambda}_{m'\nu_c\nu_d\lambda'}|_{\rm E} \equiv \sum_{\Omega'} \Theta(\Omega') X^{(-)ts\lambda}_{\Omega' m'\nu_c\nu_d\lambda'}|_{\rm E} = \sum_{s'=\pm s} \Theta(m'+s') X^{(-)ts\lambda}_{m'+s' m'\nu_c\nu_d\lambda'}|_{\rm E}, \tag{C.378b}$$

we end up with

$$\boxed{\begin{aligned} R^{(+)ts\lambda}_{m'\nu_d\nu_c\lambda'}|_{\rm E} &= \Theta(m'+s) Y^{s\lambda}_{s\lambda'} Z^{(+)t}_{m'+s\, m'\nu_d\nu_c\lambda'}|_{\rm E} \\ &\quad + \Theta(m'-s) Y^{s\lambda}_{-s\lambda'} Z^{(+)t}_{m'-s\, m'\nu_d\nu_c\lambda'}|_{\rm E}, \end{aligned}} \tag{C.379a}$$

$$\boxed{\begin{aligned} R^{(-)ts\lambda}_{m'\nu_c\nu_d\lambda'}|_{\rm E} &= \Theta(m'+s) Y^{s\lambda}_{-s-\lambda'} Z^{(-)t}_{m'+s\, m'\nu_c\nu_d\lambda'}|_{\rm E} \\ &\quad + \Theta(m'-s) Y^{s\lambda}_{s-\lambda'} Z^{(-)t}_{m'-s\, m'\nu_c\nu_d\lambda'}|_{\rm E}, \end{aligned}} \tag{C.379b}$$

and the exchange spin–orbit mean field can be written

$$\boxed{\begin{aligned} \Gamma^{t\Omega=m+s}_{m\nu_a,\, m+\lambda\,\nu_b}|_{\rm E} &= \widetilde{B}(\mu) \sum_{\substack{m'\geq 0 \\ \nu_c\nu_d}} \sum_{\lambda'=-1}^{1} (-)^{\lambda-\lambda'} \\ &\quad \times \Big[\langle m\nu_a\ m'+\lambda'\,\nu_c | V(r_{12}) [\vec{r}_{12} \otimes \vec{\nabla}_{12}]^{(1)}_{\lambda'-\lambda} | m'\nu_d\ m+\lambda\,\nu_b\rangle R^{(+)ts\lambda}_{m'\nu_d\nu_c\lambda'}|_{\rm E} \\ &\quad + \langle m\nu_a\ -m'\nu_c | V(r_{12}) [\vec{r}_{12} \otimes \vec{\nabla}_{12}]^{(1)}_{\lambda'-\lambda} | -(m'+\lambda')\,\nu_d\ m+\lambda\,\nu_b\rangle R^{(-)ts\lambda}_{m'\nu_c\nu_d\lambda'}|_{\rm E}\Big], \end{aligned}} \tag{C.380}$$

where, as previously done for the other terms, we have replaced the summations $\sum_{m'} \sum_{\Omega'>0}$ by $\sum_{m'\geq 0} \sum_{\Omega'} \Theta(\Omega')$ and applied the operator P_r.

To get the direct spin–orbit mean field out of the exchange one, it suffices to exchange H and W and omit the operator P_r. The latter is therefore

$$\boxed{\begin{aligned} \Gamma^{t\Omega=m+s}_{m\nu_a,\, m+\lambda\,\nu_b}|_{\rm D} &= \widetilde{B}(\mu) \sum_{\substack{m'\geq 0 \\ \nu_c\nu_d}} \sum_{\lambda'=-1}^{1} (-)^{\lambda-\lambda'} \\ &\quad \times \Big[\langle m\nu_a\ m'+\lambda'\,\nu_c | V(r_{12}) [\vec{r}_{12} \otimes \vec{\nabla}_{12}]^{(1)}_{\lambda'-\lambda} | m+\lambda\,\nu_b\ m'\nu_d\rangle R^{(+)ts\lambda}_{m'\nu_d\nu_c\lambda'}|_{\rm D} \\ &\quad + \langle m\nu_a\ -m'\nu_c | V(r_{12}) [\vec{r}_{12} \otimes \vec{\nabla}_{12}]^{(1)}_{\lambda'-\lambda} | m+\lambda\,\nu_b\ -(m'+\lambda')\,\nu_d\rangle R^{(-)ts\lambda}_{m'\nu_c\nu_d\lambda'}|_{\rm D}\Big], \end{aligned}} \tag{C.381}$$

composed of the quantities

$$\boxed{\begin{aligned} R^{(+)ts\lambda}_{m'\nu_d\nu_c\lambda'}|_{\rm D} &= \Theta(m'+s)Y^{s\lambda}_{s\lambda'}Z^{(+)t}_{m'+s\,m'\nu_d\nu_c\lambda'}|_{\rm D} \\ &\quad + \Theta(m'-s)Y^{s\lambda}_{-s\lambda'}Z^{(+)t}_{m'-s\,m'\nu_d\nu_c\lambda'}|_{\rm D}, \end{aligned}} \tag{C.382a}$$

$$\boxed{\begin{aligned} R^{(-)ts\lambda}_{m'\nu_c\nu_d\lambda'}|_{\rm D} &= \Theta(m'+s)Y^{s\lambda}_{-s-\lambda'}Z^{(-)t}_{m'+s\,m'\nu_c\nu_d\lambda'}|_{\rm D} \\ &\quad + \Theta(m'-s)Y^{s\lambda}_{s-\lambda'}Z^{(-)t}_{m'-s\,m'\nu_c\nu_d\lambda'}|_{\rm D}, \end{aligned}} \tag{C.382b}$$

the quantities Y given by (C.376), and where

$$\boxed{Z^{(+)t}_{\Omega'm'\nu_d\nu_c\lambda'}|_{\rm D} = (W-H)\,\rho^{t\Omega'}_{m'\nu_d,\,m'+\lambda'\nu_c} + W\,\rho^{-t\Omega'}_{m'\nu_d,\,m'+\lambda'\nu_c},} \tag{C.383a}$$

$$\boxed{Z^{(-)t}_{\Omega'm'\nu_c\nu_d\lambda'}|_{\rm D} = (W-H)\,\overline{\rho}^{t\Omega'}_{m'\nu_c,\,m'+\lambda'\nu_d} + W\,\overline{\rho}^{-t\Omega'}_{m'\nu_c,\,m'+\lambda'\nu_d}.} \tag{C.383b}$$

Note that these quantities are identical to those of the tensor term (C.249), provided that we consider the tensor coefficients W and H instead of the spin–orbit ones. It is crucial to notice that, contrary to the central, density-dependent and tensor cases, the first and the second matrix elements appearing in the above direct spin–orbit mean field are not equal. Indeed, the action of the gradient operator on the wave functions prevents such a simplification. [5]

From the boxed equations, we can now explicitly write down the expressions of the direct and exchange spin–orbit mean fields Γ for each value of λ. We recall that these fields are *not* time-reversal invariant, and note that the quantities $Z^{(\pm)}|_{\rm E}$ and $Z^{(\pm)}|_{\rm D}$, respectively given by (C.372) and (C.383), are the same no matter the value of λ. Finally, note that if $\lambda = 1$, then $s = 1/2$ (as we could have already seen in (C.376)) since the identity $s_b \equiv s - 1 = \pm 1/2$ holds only if $s = 1/2$.

- Exchange spin–orbit mean field Γ for $\lambda = 0$:

$$\boxed{\begin{aligned} \Gamma^{t\Omega=m+s}_{m\nu_a,\,m\nu_b}|_{\rm E} &= \widetilde{B}(\mu)\sum_{\substack{m'\geq 0\\ \nu_c\nu_d}}\sum_{\lambda'=-1}^{1}(-)^{\lambda'} \\ &\quad\times\Big[\langle m\nu_a\ m'+\lambda'\,\nu_c|V(r_{12})[\vec{r}_{12}\otimes\vec{\nabla}_{12}]^{(1)}_{\lambda'}|m'\nu_d\ m\nu_b\rangle R^{(+)ts0}_{m'\nu_d\nu_c\lambda'}|_{\rm E} \\ &\quad+\langle m\nu_a\ -m'\nu_c|V(r_{12})[\vec{r}_{12}\otimes\vec{\nabla}_{12}]^{(1)}_{\lambda'}|-(m'+\lambda')\,\nu_d\ m\nu_b\rangle R^{(-)ts0}_{m'\nu_c\nu_d\lambda'}|_{\rm E}\Big], \end{aligned}} \tag{C.384}$$

where

$$\boxed{\begin{aligned} R^{(+)ts0}_{m'\nu_d\nu_c\lambda'}|_{\rm E} &= \Theta(m'+s)Y^{s0}_{s\lambda'}Z^{(+)t}_{m'+s\,m'\nu_d\nu_c\lambda'}|_{\rm E} \\ &\quad + \Theta(m'-s)Y^{s0}_{-s\lambda'}Z^{(+)t}_{m'-s\,m'\nu_d\nu_c\lambda'}|_{\rm E}, \end{aligned}} \tag{C.385a}$$

$$\boxed{\begin{aligned} R^{(-)ts0}_{m'\nu_c\nu_d\lambda'}|_{\rm E} &= \Theta(m'+s)Y^{s0}_{-s-\lambda'}Z^{(-)t}_{m'+s\,m'\nu_c\nu_d\lambda'}|_{\rm E} \\ &\quad + \Theta(m'-s)Y^{s0}_{s-\lambda'}Z^{(-)t}_{m'-s\,m'\nu_c\nu_d\lambda'}|_{\rm E}, \end{aligned}} \tag{C.385b}$$

with

$$\boxed{Y^{s0}_{s\lambda'} = 4s\delta_{\lambda',0} + \sqrt{2}\lambda'\delta_{\lambda',2s},} \tag{C.386a}$$

$$\boxed{Y^{s0}_{-s\lambda'} = \sqrt{2}\lambda'\delta_{\lambda',-2s}.} \tag{C.386b}$$

5. We insist on this distinctive feature of the spin–orbit term which, at first, had escaped us and led to wrong expressions of the spin–orbit fields.

- Direct spin–orbit mean field Γ for $\lambda = 0$:

$$\begin{aligned}\Gamma^{t\Omega=m+s}_{m\nu_a,\,m+\lambda\,\nu_b}|_{\mathrm{D}} = \widetilde{B}(\mu) \sum_{\substack{m'\geq 0\\ \nu_c\nu_d}} \sum_{\lambda'=-1}^{1} (-)^{\lambda'} \\ \times \Big[\langle m\nu_a\ m'+\lambda'\,\nu_c|V(r_{12})[\vec{r}_{12}\otimes\vec{\nabla}_{12}]^{(1)}_{\lambda'}|m+\lambda\,\nu_b\ m'\nu_d\rangle R^{(+)ts0}_{m'\nu_d\nu_c\lambda'}|_{\mathrm{D}} \\ + \langle m\nu_a\ -m'\nu_c|V(r_{12})[\vec{r}_{12}\otimes\vec{\nabla}_{12}]^{(1)}_{\lambda'}|m+\lambda\,\nu_b\ -(m'+\lambda')\,\nu_d\rangle R^{(-)ts0}_{m'\nu_c\nu_d\lambda'}|_{\mathrm{D}}\Big],\end{aligned} \tag{C.387}$$

where

$$\begin{aligned}R^{(+)ts0}_{m'\nu_d\nu_c\lambda'}|_{\mathrm{D}} &= \Theta(m'+s)Y^{s0}_{s\lambda'}Z^{(+)t}_{m'+s\,m'\nu_d\nu_c\lambda'}|_{\mathrm{D}} \\ &\quad + \Theta(m'-s)Y^{s0}_{-s\lambda'}Z^{(+)t}_{m'-s\,m'\nu_d\nu_c\lambda'}|_{\mathrm{D}},\end{aligned} \tag{C.388a}$$

$$\begin{aligned}R^{(-)ts0}_{m'\nu_c\nu_d\lambda'}|_{\mathrm{D}} &= \Theta(m'+s)Y^{s0}_{-s-\lambda'}Z^{(-)t}_{m'+s\,m'\nu_c\nu_d\lambda'}|_{\mathrm{D}} \\ &\quad + \Theta(m'-s)Y^{s0}_{s-\lambda'}Z^{(-)t}_{m'-s\,m'\nu_c\nu_d\lambda'}|_{\mathrm{D}},\end{aligned} \tag{C.388b}$$

with the quantities Y given by (C.386). Just like the equivalent quantities for the tensor mean field, $R^{(\pm)ts0}|_{\mathrm{E}}$ and $R^{(\pm)ts0}|_{\mathrm{D}}$ are symmetric under the exchange of ν_c and ν_d only if $\lambda' = 0$ such that the corresponding quantities $Z^{(\pm)}|_{\mathrm{E}}$ and $Z^{(\pm)}|_{\mathrm{D}}$ display this symmetry as their density matrices ρ and $\overline{\rho}$, besides being symmetric, are diagonal in m'.

- Exchange spin–orbit mean field Γ for $\lambda = 1$:

$$\begin{aligned}\Gamma^{t\Omega=m+1/2}_{m\nu_a,\,m+1\,\nu_b}|_{\mathrm{E}} = -\widetilde{B}(\mu) \sum_{\substack{m'\geq 0\\ \nu_c\nu_d}} \\ \times \Big[\langle m\nu_a\ m'\nu_c|V(r_{12})[\vec{r}_{12}\otimes\vec{\nabla}_{12}]^{(1)}_{-1}|m'\nu_d\ m+1\,\nu_b\rangle R^{(+)t1/2\,1}_{m'\nu_d\nu_c0}|_{\mathrm{E}} \\ + \langle m\nu_a\ -m'\nu_c|V(r_{12})[\vec{r}_{12}\otimes\vec{\nabla}_{12}]^{(1)}_{-1}|-m'\nu_d\ m+1\,\nu_b\rangle R^{(-)t1/2\,1}_{m'\nu_d\nu_c0}|_{\mathrm{E}}\Big],\end{aligned} \tag{C.389}$$

where

$$R^{(+)t1/2\,1}_{m'\nu_d\nu_c0}|_{\mathrm{E}} = Y^{1/2\,1}_{1/2\,0}\Big[Z^{(+)t}_{m'+1/2\,m'\nu_d\nu_c0}|_{\mathrm{E}} + \Theta(m'-1/2)Z^{(+)t}_{m'-1/2\,m'\nu_d\nu_c0}|_{\mathrm{E}}\Big], \tag{C.390a}$$

$$R^{(-)t1/2\,1}_{m'\nu_d\nu_c0}|_{\mathrm{E}} = Y^{1/2\,1}_{1/2\,0}\Big[Z^{(-)t}_{m'+1/2\,m'\nu_d\nu_c0}|_{\mathrm{E}} + \Theta(m'-1/2)Z^{(-)t}_{m'-1/2\,m'\nu_d\nu_c0}|_{\mathrm{E}}\Big], \tag{C.390b}$$

with

$$Y^{1/2\,1}_{\pm 1/2\,\lambda'} = -\sqrt{2}\delta_{\lambda',0}, \tag{C.391}$$

that imposes $\lambda' = 0$ in the above mean field.

- Direct spin–orbit mean field Γ for $\lambda = 1$:

$$\begin{aligned}\Gamma^{t\Omega=m+s}_{m\nu_a,\,m+\lambda\,\nu_b}|_{\mathrm{D}} = -\widetilde{B}(\mu) \sum_{\substack{m'\geq 0\\ \nu_c\nu_d}} \\ \times \Big[\langle m\nu_a\ m'\nu_c|V(r_{12})[\vec{r}_{12}\otimes\vec{\nabla}_{12}]^{(1)}_{-1}|m+1\,\nu_b\ m'\nu_d\rangle R^{(+)t1/2\,1}_{m'\nu_d\nu_c0}|_{\mathrm{D}} \\ + \langle m\nu_a\ -m'\nu_c|V(r_{12})[\vec{r}_{12}\otimes\vec{\nabla}_{12}]^{(1)}_{-1}|m+1\,\nu_b\ -m'\nu_d\rangle R^{(-)t1/2\,1}_{m'\nu_c\nu_d0}|_{\mathrm{D}}\Big],\end{aligned} \tag{C.392}$$

where

$$R^{(+)t1/2\,1}_{m'\nu_d\nu_c0}|_{\mathrm{D}} = Y^{1/2\,1}_{1/2\,0}\Big[Z^{(+)t}_{m'+1/2\,m'\nu_d\nu_c0}|_{\mathrm{D}} + \Theta(m'-1/2)Z^{(+)t}_{m'-1/2\,m'\nu_d\nu_c0}|_{\mathrm{D}}\Big], \tag{C.393a}$$

$$R^{(-)t1/2\,1}_{m'\nu_d\nu_c0}|_{\mathrm{D}} = Y^{1/2\,1}_{1/2\,0}\Big[Z^{(-)t}_{m'+1/2\,m'\nu_d\nu_c0}|_{\mathrm{D}} + \Theta(m'-1/2)Z^{(-)t}_{m'-1/2\,m'\nu_d\nu_c0}|_{\mathrm{D}}\Big], \tag{C.393b}$$

with the quantity Y given by (C.391), that imposes $\lambda' = 0$ in the above mean field. The quantities $R^{(\pm)t1/2\,1}|_{\rm E}$ and $R^{(\pm)t1/2\,1}|_{\rm D}$ are symmetric under the exchange of ν_c and ν_d since the corresponding quantities $Z^{(\pm)}|_{\rm E}$ and $Z^{(\pm)}|_{\rm D}$ display this symmetry as their density matrices ρ and $\overline{\rho}$ are symmetric and diagonal in m'. In particular, this symmetry was used to exchange the indices of the quantities $R^{(-)t1/2\,1}|_{\rm E}$ and $R^{(-)t1/2\,1}|_{\rm D}$ appearing above.

The spin–orbit mean field $\overline{\Gamma}$ can easily be deduced by exchanging ρ and $\overline{\rho}$ in the expressions of the spin–orbit mean field Γ, as we notice by comparing the expressions of the mean fields (III.37) and (III.38). We can see that only the quantities $R^{(\pm)}$ are impacted by this transformation. We will call them $\overline{R}^{(\pm)}$ in the following. Unfortunately, there are no straight relations between the quantities $R^{(\pm)}$ and $\overline{R}^{(\pm)}$ for the spin–orbit interaction, as it was already the case for the tensor term. As a consequence, the spin–orbit mean fields Γ and $\overline{\Gamma}$ will be computed simultaneously in the code, but with different quantities $R^{(\pm)}$ and $\overline{R}^{(\pm)}$. Furthermore, note that the quantities $Y^{(\pm)}$ making up $R^{(\pm)}$ remain the same under this transformation, hence

$$\overline{Y}^{s\lambda}_{s'\lambda'} = Y^{s\lambda}_{s'\lambda'}. \tag{C.394}$$

Accordingly, the exchange spin–orbit mean field $\overline{\Gamma}$ can be expressed as

$$\begin{aligned}\overline{\Gamma}^{t\Omega=m+s}_{m\nu_a,\,m+\lambda\,\nu_b}|_{\rm E} = \widetilde{B}(\mu) \sum_{\substack{m'\geq 0\\ \nu_c\nu_d}} \sum_{\lambda'=-1}^{1} (-)^{\lambda-\lambda'} \\ \times \Big[\langle m\nu_a\ m'+\lambda'\,\nu_c|V(r_{12})[\vec{r}_{12}\otimes\vec{\nabla}_{12}]^{(1)}_{\lambda'-\lambda}|m'\nu_d\ m+\lambda\,\nu_b\rangle \overline{R}^{(+)ts\lambda}_{m'\nu_d\nu_c\lambda'}|_{\rm E} \\ + \langle m\nu_a\ -m'\nu_c|V(r_{12})[\vec{r}_{12}\otimes\vec{\nabla}_{12}]^{(1)}_{\lambda'-\lambda}|-(m'+\lambda')\,\nu_d\ m+\lambda\,\nu_b\rangle \overline{R}^{(-)ts\lambda}_{m'\nu_c\nu_d\lambda'}|_{\rm E}\Big],\end{aligned} \tag{C.395}$$

where

$$\begin{aligned}\overline{R}^{(+)ts\lambda}_{m'\nu_d\nu_c\lambda'}|_{\rm E} &= \Theta(m'+s) Y^{s\lambda}_{s\lambda'} \overline{Z}^{(+)t}_{m'+s\,m'\nu_d\nu_c\lambda'}|_{\rm E} \\ &\quad + \Theta(m'-s) Y^{s\lambda}_{-s\lambda'} \overline{Z}^{(+)t}_{m'-s\,m'\nu_d\nu_c\lambda'}|_{\rm E}, \qquad \text{(C.396a)} \\ \overline{R}^{(-)ts\lambda}_{m'\nu_c\nu_d\lambda'}|_{\rm E} &= \Theta(m'+s) Y^{s\lambda}_{-s-\lambda'} \overline{Z}^{(-)t}_{m'+s\,m'\nu_c\nu_d\lambda'}|_{\rm E} \\ &\quad + \Theta(m'-s) Y^{s\lambda}_{s-\lambda'} \overline{Z}^{(-)t}_{m'-s\,m'\nu_c\nu_d\lambda'}|_{\rm E}, \qquad \text{(C.396b)}\end{aligned}$$

with the quantities Y expressed in (C.376), and with

$$\overline{Z}^{(+)t}_{\Omega' m'\nu_d\nu_c\lambda'}|_{\rm E} \equiv \sum_{t'} (H - W\delta_{tt'})\, \overline{\rho}^{t'\Omega'}_{m'\nu_d,\,m'+\lambda'\nu_c}, \tag{C.397a}$$

$$\overline{Z}^{(-)t}_{\Omega' m'\nu_c\nu_d\lambda'}|_{\rm E} \equiv \sum_{t'} (H - W\delta_{tt'})\, \rho^{t'\Omega'}_{m'\nu_c,\,m'+\lambda'\nu_d}, \tag{C.397b}$$

or, by explicitly separating their particle-like and proton-neutron contributions,

$$\overline{Z}^{(+)t}_{\Omega' m'\nu_d\nu_c\lambda'}|_{\rm E} = (H - W)\, \overline{\rho}^{t\Omega'}_{m'\nu_d,\,m'+\lambda'\nu_c} + H\, \overline{\rho}^{-t\Omega'}_{m'\nu_d,\,m'+\lambda'\nu_c}, \tag{C.398a}$$

$$\overline{Z}^{(-)t}_{\Omega' m'\nu_c\nu_d\lambda'}|_{\rm E} = (H - W)\, \rho^{t\Omega'}_{m'\nu_c,\,m'+\lambda'\nu_d} + H\, \rho^{-t\Omega'}_{m'\nu_c,\,m'+\lambda'\nu_d}. \tag{C.398b}$$

Note that these quantities are identical to those of the tensor term (C.267), provided that we consider the tensor coefficients W and H instead of the spin–orbit ones.

As for the direct spin–orbit mean field, it reads

$$\begin{aligned}\overline{\Gamma}^{t\Omega=m+s}_{m\nu_a,\,m+\lambda\,\nu_b}|_{\rm D} = \widetilde{B}(\mu)\sum_{\substack{m'\geq 0\\ \nu_c\overline{\nu}_d}}\sum_{\lambda'=-1}^{1}(-)^{\lambda-\lambda'}\\ \times\Big[\langle m\nu_a\ m'+\lambda'\,\nu_c|V(r_{12})[\vec{r}_{12}\otimes\vec{\nabla}_{12}]^{(1)}_{\lambda'-\lambda}|m+\lambda\,\nu_b\ m'\nu_d\rangle\overline{R}^{(+)ts\lambda}_{m'\nu_d\nu_c\lambda'}|_{\rm D}\\ +\langle m\nu_a\ -m'\nu_c|V(r_{12})[\vec{r}_{12}\otimes\vec{\nabla}_{12}]^{(1)}_{\lambda'-\lambda}|m+\lambda\,\nu_b\ -(m'+\lambda')\,\nu_d\rangle\overline{R}^{(-)ts\lambda}_{m'\nu_c\nu_d\lambda'}|_{\rm D}\Big],\end{aligned} \tag{C.399}$$

where

$$\begin{aligned}\overline{R}^{(+)ts\lambda}_{m'\nu_d\nu_c\lambda'}|_{\rm D} &= \Theta(m'+s)Y^{s\lambda}_{s\lambda'}\overline{Z}^{(+)t}_{m'+s\,m'\nu_d\nu_c\lambda'}|_{\rm D}\\ &\quad+\Theta(m'-s)Y^{s\lambda}_{-s\lambda'}\overline{Z}^{(+)t}_{m'-s\,m'\nu_d\nu_c\lambda'}|_{\rm D},\end{aligned} \tag{C.400a}$$

$$\begin{aligned}\overline{R}^{(-)ts\lambda}_{m'\nu_c\nu_d\lambda'}|_{\rm D} &= \Theta(m'+s)Y^{s\lambda}_{-s-\lambda'}\overline{Z}^{(-)t}_{m'+s\,m'\nu_c\nu_d\lambda'}|_{\rm D}\\ &\quad+\Theta(m'-s)Y^{s\lambda}_{s-\lambda'}\overline{Z}^{(-)t}_{m'-s\,m'\nu_c\nu_d\lambda'}|_{\rm D},\end{aligned} \tag{C.400b}$$

with the quantities Y expressed in (C.376), and with

$$\overline{Z}^{(+)t}_{\Omega'm'\nu_d\nu_c\lambda'}|_{\rm D} = (W-H)\,\overline{\rho}^{t\Omega'}_{m'\nu_d,\,m'+\lambda'\nu_c} + W\,\overline{\rho}^{-t\Omega'}_{m'\nu_d,\,m'+\lambda'\nu_c}, \tag{C.401a}$$

$$\overline{Z}^{(-)t}_{\Omega'm'\nu_c\nu_d\lambda'}|_{\rm D} = (W-H)\,\rho^{t\Omega'}_{m'\nu_c,\,m'+\lambda'\nu_d} + W\,\rho^{-t\Omega'}_{m'\nu_c,\,m'+\lambda'\nu_d}. \tag{C.401b}$$

Note that these quantities are identical to those of the tensor term (C.270), provided that we consider the tensor coefficients W and H instead of the spin–orbit ones.

From the boxed equations, we can now explicitly write down the expressions of the direct and exchange spin–orbit mean fields $\overline{\Gamma}$ for each value of λ. We recall that these fields are *not* time-reversal invariant and note that the quantities $\overline{Z}^{(\pm)}|_{\rm E}$ and $\overline{Z}^{(\pm)}|_{\rm D}$, respectively given by (C.398) and (C.401), are the same no matter the value of λ. Finally, note that if $\lambda=1$, then $s=1/2$ (as we could have already seen in (C.376)) since the identity $s_b\equiv s-1=\pm1/2$ holds only if $s=1/2$.

- Exchange spin–orbit mean field $\overline{\Gamma}$ for $\lambda=0$:

$$\begin{aligned}\overline{\Gamma}^{t\Omega=m+s}_{m\nu_a,\,m\nu_b}|_{\rm E} = \widetilde{B}(\mu)\sum_{\substack{m'\geq 0\\ \nu_c\overline{\nu}_d}}\sum_{\lambda'=-1}^{1}(-)^{\lambda'}\\ \times\Big[\langle m\nu_a\ m'+\lambda'\,\nu_c|V(r_{12})[\vec{r}_{12}\otimes\vec{\nabla}_{12}]^{(1)}_{\lambda'}|m'\nu_d\ m\nu_b\rangle\overline{R}^{(+)ts0}_{m'\nu_d\nu_c\lambda'}|_{\rm E}\\ +\langle m\nu_a\ -m'\nu_c|V(r_{12})[\vec{r}_{12}\otimes\vec{\nabla}_{12}]^{(1)}_{\lambda'}|-(m'+\lambda')\,\nu_d\ m\nu_b\rangle\overline{R}^{(-)ts0}_{m'\nu_c\nu_d\lambda'}|_{\rm E}\Big],\end{aligned} \tag{C.402}$$

where

$$\begin{aligned}\overline{R}^{(+)ts0}_{m'\nu_d\nu_c\lambda'}|_{\rm E} &= \Theta(m'+s)Y^{s0}_{s\lambda'}\overline{Z}^{(+)t}_{m'+s\,m'\nu_d\nu_c\lambda'}|_{\rm E}\\ &\quad+\Theta(m'-s)Y^{s0}_{-s\lambda'}\overline{Z}^{(+)t}_{m'-s\,m'\nu_d\nu_c\lambda'}|_{\rm E},\end{aligned} \tag{C.403a}$$

$$\begin{aligned}\overline{R}^{(-)ts0}_{m'\nu_c\nu_d\lambda'}|_{\rm E} &= \Theta(m'+s)Y^{s0}_{-s-\lambda'}\overline{Z}^{(-)t}_{m'+s\,m'\nu_c\nu_d\lambda'}|_{\rm E}\\ &\quad+\Theta(m'-s)Y^{s0}_{s-\lambda'}\overline{Z}^{(-)t}_{m'-s\,m'\nu_c\nu_d\lambda'}|_{\rm E},\end{aligned} \tag{C.403b}$$

with the quantities Y given by (C.386).

- Direct spin–orbit mean field $\overline{\Gamma}$ for $\lambda=0$:

$$\begin{aligned}\overline{\Gamma}^{t\Omega=m+s}_{m\nu_a,\,m+\lambda\,\nu_b}|_{\mathrm{D}} = \widetilde{B}(\mu)\sum_{\substack{m'\geq 0\\ \nu_c\nu_d}}\sum_{\lambda'=-1}^{1}(-)^{\lambda'}\\ \times\Big[\langle m\nu_a\ m'+\lambda'\,\nu_c|V(r_{12})[\vec{r}_{12}\otimes\vec{\nabla}_{12}]^{(1)}_{\lambda'}|m\nu_b\ m'\nu_d\rangle\overline{R}^{(+)ts0}_{m'\nu_d\nu_c\lambda'}|_{\mathrm{D}}\\ +\langle m\nu_a\ -m'\nu_c|V(r_{12})[\vec{r}_{12}\otimes\vec{\nabla}_{12}]^{(1)}_{\lambda'}|m\nu_b\ -(m'+\lambda')\,\nu_d\rangle\overline{R}^{(-)ts0}_{m'\nu_c\nu_d\lambda'}|_{\mathrm{D}}\Big],\end{aligned} \tag{C.404}$$

where

$$\begin{aligned}\overline{R}^{(+)ts0}_{m'\nu_d\nu_c\lambda'}|_{\mathrm{D}} &= \Theta(m'+s)Y^{s0}_{s\lambda'}\overline{Z}^{(+)t}_{m'+s\,m'\nu_d\nu_c\lambda'}|_{\mathrm{D}}\\ &\quad+\Theta(m'-s)Y^{s0}_{-s\lambda'}\overline{Z}^{(+)t}_{m'-s\,m'\nu_d\nu_c\lambda'}|_{\mathrm{D}},\end{aligned} \tag{C.405a}$$

$$\begin{aligned}\overline{R}^{(-)ts0}_{m'\nu_c\nu_d\lambda'}|_{\mathrm{D}} &= \Theta(m'+s)Y^{s0}_{-s-\lambda'}\overline{Z}^{(-)t}_{m'+s\,m'\nu_c\nu_d\lambda'}|_{\mathrm{D}}\\ &\quad+\Theta(m'-s)Y^{s0}_{s-\lambda'}\overline{Z}^{(-)t}_{m'-s\,m'\nu_c\nu_d\lambda'}|_{\mathrm{D}},\end{aligned} \tag{C.405b}$$

with the quantities Y given by (C.386). Note that the quantities $\overline{R}^{(\pm)ts0}|_{\mathrm{E}}$ and $\overline{R}^{(\pm)ts0}|_{\mathrm{D}}$ are symmetric under the exchange of ν_c and ν_d only if $\lambda'=0$ such that the corresponding quantities $Z^{(\pm)}|_{\mathrm{E}}$ and $Z^{(\pm)}|_{\mathrm{D}}$ display this symmetry as their density matrices ρ and $\overline{\rho}$, besides being symmetric, are diagonal in m'.

- Exchange spin–orbit mean field $\overline{\Gamma}$ for $\lambda=1$:

$$\begin{aligned}\overline{\Gamma}^{t\Omega=m+1/2}_{m\nu_a,\,m+1\,\nu_b}|_{\mathrm{E}} = -\widetilde{B}(\mu)\sum_{\substack{m'\geq 0\\ \nu_c\nu_d}}\\ \times\Big[\langle m\nu_a\ m'\nu_c|V(r_{12})[\vec{r}_{12}\otimes\vec{\nabla}_{12}]^{(1)}_{-1}|m'\nu_d\ m+1\,\nu_b\rangle\overline{R}^{(+)t1/2\,1}_{m'\nu_d\nu_c0}|_{\mathrm{E}}\\ +\langle m\nu_a\ -m'\nu_c|V(r_{12})[\vec{r}_{12}\otimes\vec{\nabla}_{12}]^{(1)}_{-1}|-m'\nu_d\ \ m+1\,\nu_b\rangle\overline{R}^{(-)t1/2\,1}_{m'\nu_d\nu_c0}|_{\mathrm{E}}\Big],\end{aligned} \tag{C.406}$$

where

$$\overline{R}^{(+)t1/2\,1}_{m'\nu_d\nu_c0}|_{\mathrm{E}} = Y^{1/2\,1}_{1/2\,0}\Big[\overline{Z}^{(+)t}_{m'+1/2\,m'\nu_d\nu_c0}|_{\mathrm{E}}+\Theta(m'-1/2)\overline{Z}^{(+)t}_{m'-1/2\,m'\nu_d\nu_c0}|_{\mathrm{E}}\Big], \tag{C.407a}$$

$$\overline{R}^{(-)t1/2\,1}_{m'\nu_d\nu_c0}|_{\mathrm{E}} = Y^{1/2\,1}_{1/2\,0}\Big[\overline{Z}^{(-)t}_{m'+1/2\,m'\nu_d\nu_c0}|_{\mathrm{E}}+\Theta(m'-1/2)\overline{Z}^{(-)t}_{m'-1/2\,m'\nu_d\nu_c0}|_{\mathrm{E}}\Big], \tag{C.407b}$$

with the quantities Y given by (C.391), that imposes $\lambda'=0$ in the above mean field.

- Direct spin–orbit mean field $\overline{\Gamma}$ for $\lambda=1$:

$$\begin{aligned}\overline{\Gamma}^{t\Omega=m+1/2}_{m\nu_a,\,m+1\,\nu_b}|_{\mathrm{D}} = -\widetilde{B}(\mu)\sum_{\substack{m'\geq 0\\ \nu_c\nu_d}}\\ \times\Big[\langle m\nu_a\ m'\nu_c|V(r_{12})[\vec{r}_{12}\otimes\vec{\nabla}_{12}]^{(1)}_{-1}|m+1\,\nu_b\ m'\nu_d\rangle\overline{R}^{(+)t1/2\,1}_{m'\nu_d\nu_c0}|_{\mathrm{D}}\\ +\langle m\nu_a\ -m'\nu_c|V(r_{12})[\vec{r}_{12}\otimes\vec{\nabla}_{12}]^{(1)}_{-1}|m+1\,\nu_b\ -m'\nu_d\rangle\overline{R}^{(-)t1/2\,1}_{m'\nu_d\nu_c0}|_{\mathrm{D}}\Big],\end{aligned} \tag{C.408}$$

where

$$\overline{R}^{(+)t1/2\,1}_{m'\nu_d\nu_c0}|_{\mathrm{D}} = Y^{1/2\,1}_{1/2\,0}\Big[\overline{Z}^{(+)t}_{m'+1/2\,m'\nu_d\nu_c0}|_{\mathrm{D}}+\Theta(m'-1/2)\overline{Z}^{(+)t}_{m'-1/2\,m'\nu_d\nu_c0}|_{\mathrm{D}}\Big], \tag{C.409a}$$

$$\overline{R}^{(-)t1/2\,1}_{m'\nu_d\nu_c0}|_{\mathrm{D}} = Y^{1/2\,1}_{1/2\,0}\Big[\overline{Z}^{(-)t}_{m'+1/2\,m'\nu_d\nu_c0}|_{\mathrm{D}}+\Theta(m'-1/2)\overline{Z}^{(-)t}_{m'-1/2\,m'\nu_d\nu_c0}|_{\mathrm{D}}\Big], \tag{C.409b}$$

with the quantity Y given by (C.391), that imposes $\lambda' = 0$ in the above mean field. The quantities $\overline{R}^{(\pm)t1/2\,1}|_{\mathrm{E}}$ and $\overline{R}^{(\pm)t1/2\,1}|_{\mathrm{D}}$ are symmetric under the exchange of ν_c and ν_d since the corresponding quantities $\overline{Z}^{(\pm)}|_{\mathrm{E}}$ and $\overline{Z}^{(\pm)}|_{\mathrm{D}}$ display this symmetry as their density matrices ρ and $\overline{\rho}$ are symmetric and diagonal in m'. In particular, this symmetry has been used to exchange the indices of the quantities $\overline{R}^{(-)t1/2\,1}|_{\mathrm{E}}$ and $\overline{R}^{(-)t1/2\,1}|_{\mathrm{D}}$ appearing above.

Time-reversal invariant fields

Now, we assume the time-reversal invariance of the spin–orbit mean fields Γ and $\overline{\Gamma}$, i.e. we set $\rho = \overline{\rho}$. In this case, as the quantity $Y^{s\lambda}_{s'\lambda'}$ remains unchanged under time-reversal symmetry and $Z^{(\pm)} = \overline{Z}^{(\pm)}$, we have $R^{(\pm)} = \overline{R}^{(\pm)}$, so that eventually the mean fields coincide, $\Gamma = \overline{\Gamma}$. They simplify according to the following expressions.

The exchange spin–orbit mean fields (C.380) and (C.395) become

$$\begin{aligned}\Gamma^{t\Omega=m+s}_{m\nu_a,\,m+\lambda\,\nu_b}|^{\mathrm{T}}_{\mathrm{E}} &= \widetilde{B}(\mu)\sum_{\substack{m'\geq 0\\ \nu_c\overline{\nu}_d}}\sum_{\lambda'=-1}^{1}(-)^{\lambda-\lambda'}\\ &\times\Big[\langle m\nu_a\; m'+\lambda'\,\nu_c|V(r_{12})[\vec{r}_{12}\otimes\vec{\nabla}_{12}]^{(1)}_{\lambda'-\lambda}|m'\nu_d\; m+\lambda\,\nu_b\rangle R^{(+)ts\lambda}_{m'\nu_d\nu_c\lambda'}|^{\mathrm{T}}_{\mathrm{E}}\\ &+\langle m\nu_a\; -m'\nu_c|V(r_{12})[\vec{r}_{12}\otimes\vec{\nabla}_{12}]^{(1)}_{\lambda'-\lambda}|-(m'+\lambda')\,\nu_d\; m+\lambda\,\nu_b\rangle R^{(-)ts\lambda}_{m'\nu_c\nu_d\lambda'}|^{\mathrm{T}}_{\mathrm{E}}\Big],\end{aligned}\tag{C.410}$$

where the quantities (C.379) and (C.396) simplify according to

$$\begin{aligned}R^{(+)ts\lambda}_{m'\nu_d\nu_c\lambda'}|^{\mathrm{T}}_{\mathrm{E}} &= \Theta(m'+s)Y^{s\lambda}_{s\lambda'}Z^{t}_{m'+s\,m'\nu_d\nu_c\lambda'}|^{\mathrm{T}}_{\mathrm{E}}\\ &\quad+\Theta(m'-s)Y^{s\lambda}_{-s\lambda'}Z^{t}_{m'-s\,m'\nu_d\nu_c\lambda'}|^{\mathrm{T}}_{\mathrm{E}},\end{aligned}\tag{C.411a}$$

$$\begin{aligned}R^{(-)ts\lambda}_{m'\nu_c\nu_d\lambda'}|^{\mathrm{T}}_{\mathrm{E}} &= \Theta(m'+s)Y^{s\lambda}_{-s-\lambda'}Z^{t}_{m'+s\,m'\nu_c\nu_d\lambda'}|^{\mathrm{T}}_{\mathrm{E}}\\ &\quad+\Theta(m'-s)Y^{s\lambda}_{s-\lambda'}Z^{t}_{m'-s\,m'\nu_c\nu_d\lambda'}|^{\mathrm{T}}_{\mathrm{E}},\end{aligned}\tag{C.411b}$$

since we notice that

$$Z^{t}_{\Omega' m'\nu_d\nu_c\lambda'}|^{\mathrm{T}}_{\mathrm{E}} \equiv Z^{(+)t}_{\Omega' m'\nu_d\nu_c\lambda'}|^{\mathrm{T}}_{\mathrm{E}} = Z^{(-)t}_{\Omega' m'\nu_d\nu_c\lambda'}|^{\mathrm{T}}_{\mathrm{E}},\tag{C.412}$$

while the quantities Y, given by (C.376), remain unchanged under time-reversal symmetry.

In a similar way, the direct spin–orbit mean fields (C.381) and (C.399) become

$$\begin{aligned}\Gamma^{t\Omega=m+s}_{m\nu_a,\,m+\lambda\,\nu_b}|^{\mathrm{T}}_{\mathrm{D}} &= \widetilde{B}(\mu)\sum_{\substack{m'\geq 0\\ \nu_c\overline{\nu}_d}}\sum_{\lambda'=-1}^{1}(-)^{\lambda-\lambda'}\\ &\times\Big[\langle m\nu_a\; m'+\lambda'\,\nu_c|V(r_{12})[\vec{r}_{12}\otimes\vec{\nabla}_{12}]^{(1)}_{\lambda'-\lambda}|m+\lambda\,\nu_b\; m'\nu_d\rangle R^{(+)ts\lambda}_{m'\nu_d\nu_c\lambda'}|^{\mathrm{T}}_{\mathrm{D}}\\ &+\langle m\nu_a\; -m'\nu_c|V(r_{12})[\vec{r}_{12}\otimes\vec{\nabla}_{12}]^{(1)}_{\lambda'-\lambda}|m+\lambda\,\nu_b\; -(m'+\lambda')\,\nu_d\rangle R^{(-)ts\lambda}_{m'\nu_c\nu_d\lambda'}|^{\mathrm{T}}_{\mathrm{D}}\Big],\end{aligned}\tag{C.413}$$

where the quantities (C.382) and (C.400) simplify according to

$$\begin{aligned}R^{(+)ts\lambda}_{m'\nu_d\nu_c\lambda'}|^{\mathrm{T}}_{\mathrm{D}} &= \Theta(m'+s)Y^{s\lambda}_{s\lambda'}Z^{t}_{m'+s\,m'\nu_d\nu_c\lambda'}|^{\mathrm{T}}_{\mathrm{D}}\\ &\quad+\Theta(m'-s)Y^{s\lambda}_{-s\lambda'}Z^{t}_{m'-s\,m'\nu_d\nu_c\lambda'}|^{\mathrm{T}}_{\mathrm{D}},\end{aligned}\tag{C.414a}$$

$$\begin{aligned}R^{(-)ts\lambda}_{m'\nu_c\nu_d\lambda'}|^{\mathrm{T}}_{\mathrm{D}} &= \Theta(m'+s)Y^{s\lambda}_{-s-\lambda'}Z^{t}_{m'+s\,m'\nu_c\nu_d\lambda'}|^{\mathrm{T}}_{\mathrm{D}}\\ &\quad+\Theta(m'-s)Y^{s\lambda}_{s-\lambda'}Z^{t}_{m'-s\,m'\nu_c\nu_d\lambda'}|^{\mathrm{T}}_{\mathrm{D}},\end{aligned}\tag{C.414b}$$

since we notice that

$$\boxed{Z^{t}_{\Omega' m' \nu_d \nu_c \lambda'}|^{\mathrm{T}}_{\mathrm{D}} \equiv Z^{(+)t}_{\Omega' m' \nu_d \nu_c \lambda'}|^{\mathrm{T}}_{\mathrm{D}} = Z^{(-)t}_{\Omega' m' \nu_d \nu_c \lambda'}|^{\mathrm{T}}_{\mathrm{D}},} \tag{C.415}$$

while the quantities Y, given by (C.376), remain unchanged under time-reversal symmetry.

From the boxed equations, we can now explicitly write down the expressions of the *time-reversal invariant* direct and exchange spin–orbit mean fields for each value of λ. Note that the quantities $Z|_{\mathrm{E}}$ and $Z|_{\mathrm{D}}$, respectively given by (C.412) and (C.415), are the same no matter the value of λ. Finally, note that if $\lambda = 1$, then $s = 1/2$ (as we could have already seen in (C.376)) since the identity $s_b \equiv s - 1 = \pm 1/2$ holds only if $s = 1/2$.

- Time-reversal invariant exchange spin–orbit mean field for $\lambda = 0$:

$$\begin{aligned}\boxed{\Gamma^{t\Omega=m+s}_{m\nu_a,\, m\nu_b}|^{\mathrm{T}}_{\mathrm{E}} = \widetilde{B}(\mu) \sum_{\substack{m'\geq 0\\ \nu_c\nu_d}} \sum_{\lambda'=-1}^{1} (-)^{\lambda'} \\ \times \Big[\langle m\nu_a\ m' + \lambda'\,\nu_c | V(r_{12}) [\vec{r}_{12} \otimes \vec{\nabla}_{12}]^{(1)}_{\lambda'} | m'\nu_d\ m\nu_b\rangle R^{(+)ts0}_{m'\nu_d\nu_c\lambda'}|^{\mathrm{T}}_{\mathrm{E}} \\ + \langle m\nu_a\ -m'\nu_c | V(r_{12}) [\vec{r}_{12} \otimes \vec{\nabla}_{12}]^{(1)}_{\lambda'} | -(m' + \lambda')\,\nu_d\ m\nu_b\rangle R^{(-)ts0}_{m'\nu_c\nu_d\lambda'}|^{\mathrm{T}}_{\mathrm{E}}\Big],}\end{aligned} \tag{C.416}$$

where

$$\boxed{\begin{aligned} R^{(+)ts0}_{m'\nu_d\nu_c\lambda'}|^{\mathrm{T}}_{\mathrm{E}} &= \Theta(m' + s) Y^{s0}_{s\lambda'} Z^{t}_{m'+s\, m'\nu_d\nu_c\lambda'}|^{\mathrm{T}}_{\mathrm{E}} \\ &\quad + \Theta(m' - s) Y^{s0}_{-s\lambda'} Z^{t}_{m'-s\, m'\nu_d\nu_c\lambda'}|^{\mathrm{T}}_{\mathrm{E}}, \end{aligned}} \tag{C.417a}$$

$$\boxed{\begin{aligned} R^{(-)ts0}_{m'\nu_c\nu_d\lambda'}|^{\mathrm{T}}_{\mathrm{E}} &= \Theta(m' + s) Y^{s0}_{-s-\lambda'} Z^{t}_{m'+s\, m'\nu_c\nu_d\lambda'}|^{\mathrm{T}}_{\mathrm{E}} \\ &\quad + \Theta(m' - s) Y^{s0}_{s-\lambda'} Z^{t}_{m'-s\, m'\nu_c\nu_d\lambda'}|^{\mathrm{T}}_{\mathrm{E}}, \end{aligned}} \tag{C.417b}$$

with the quantities Y given by (C.386).

- Time-reversal invariant direct spin–orbit mean field for $\lambda = 0$:

$$\begin{aligned}\boxed{\Gamma^{t\Omega=m+s}_{m\nu_a,\, m\nu_b}|^{\mathrm{T}}_{\mathrm{D}} = \widetilde{B}(\mu) \sum_{\substack{m'\geq 0\\ \nu_c\nu_d}} \sum_{\lambda'=-1}^{1} (-)^{\lambda'} \\ \times \Big[\langle m\nu_a\ m' + \lambda'\,\nu_c | V(r_{12}) [\vec{r}_{12} \otimes \vec{\nabla}_{12}]^{(1)}_{\lambda'} | m\nu_b\ m'\nu_d\rangle R^{(+)ts0}_{m'\nu_d\nu_c\lambda'}|^{\mathrm{T}}_{\mathrm{D}} \\ + \langle m\nu_a\ -m'\nu_c | V(r_{12}) [\vec{r}_{12} \otimes \vec{\nabla}_{12}]^{(1)}_{\lambda'} | m\nu_b\ -(m' + \lambda')\,\nu_d\rangle R^{(-)ts0}_{m'\nu_c\nu_d\lambda'}|^{\mathrm{T}}_{\mathrm{D}}\Big],}\end{aligned} \tag{C.418}$$

where

$$\boxed{\begin{aligned} R^{(+)ts0}_{m'\nu_d\nu_c\lambda'}|^{\mathrm{T}}_{\mathrm{D}} &= \Theta(m' + s) Y^{s0}_{s\lambda'} Z^{t}_{m'+s\, m'\nu_d\nu_c\lambda'}|^{\mathrm{T}}_{\mathrm{D}} \\ &\quad + \Theta(m' - s) Y^{s0}_{-s\lambda'} Z^{t}_{m'-s\, m'\nu_d\nu_c\lambda'}|^{\mathrm{T}}_{\mathrm{D}}, \end{aligned}} \tag{C.419a}$$

$$\boxed{\begin{aligned} R^{(-)ts0}_{m'\nu_c\nu_d\lambda'}|^{\mathrm{T}}_{\mathrm{D}} &= \Theta(m' + s) Y^{s0}_{-s-\lambda'} Z^{t}_{m'+s\, m'\nu_c\nu_d\lambda'}|^{\mathrm{T}}_{\mathrm{D}} \\ &\quad + \Theta(m' - s) Y^{s0}_{s-\lambda'} Z^{t}_{m'-s\, m'\nu_c\nu_d\lambda'}|^{\mathrm{T}}_{\mathrm{D}}, \end{aligned}} \tag{C.419b}$$

with the quantities Y given by (C.386). Note that the quantities $R^{ts0}|^{\mathrm{T}}_{\mathrm{E}}$ and $R^{ts0}|^{\mathrm{T}}_{\mathrm{D}}$ are symmetric under the exchange of ν_c and ν_d only if $\lambda' = 0$ such that the corresponding quantities $Z|_{\mathrm{E}}$ and $Z|_{\mathrm{D}}$ display this symmetry as their density matrix ρ, besides being symmetric, is diagonal in m'.

- Time-reversal invariant exchange spin–orbit mean field for $\lambda = 1$:

$$\boxed{\begin{aligned}\Gamma^{t\Omega=m+1/2}_{m\nu_a,\,m+1\,\nu_b}|^{\mathrm{T}}_{\mathrm{E}} &= -\widetilde{B}(\mu)\sum_{\substack{m'\geq 0\\ \nu_c\nu_d}}\\ &\times\Big[\langle m\nu_a\ m'\nu_c|V(r_{12})[\vec{r}_{12}\otimes\vec{\nabla}_{12}]^{(1)}_{-1}|m'\nu_d\ m+1\,\nu_b\rangle\\ &+\langle m\nu_a\ -m'\nu_c|V(r_{12})[\vec{r}_{12}\otimes\vec{\nabla}_{12}]^{(1)}_{-1}|-m'\nu_d\ m+1\,\nu_b\rangle\Big]R^{t1/2\,1}_{m'\nu_d\nu_c0}|^{\mathrm{T}}_{\mathrm{E}},\end{aligned}} \tag{C.420}$$

where

$$\boxed{R^{t1/2\,1}_{m'\nu_d\nu_c0}|^{\mathrm{T}}_{\mathrm{E}} \equiv R^{(+)t1/2\,1}_{m'\nu_d\nu_c0}|^{\mathrm{T}}_{\mathrm{E}} = R^{(-)t1/2\,1}_{m'\nu_d\nu_c0}|^{\mathrm{T}}_{\mathrm{E}},} \tag{C.421}$$

with

$$\boxed{R^{t1/2\,1}_{m'\nu_d\nu_c0}|^{\mathrm{T}}_{\mathrm{E}} = Y^{1/2\,1}_{1/2\,0}\Big[Z^{t}_{m'+1/2\,m'\nu_d\nu_c0}|^{\mathrm{T}}_{\mathrm{E}} + \Theta(m'-1/2)Z^{t}_{m'-1/2\,m'\nu_d\nu_c0}|^{\mathrm{T}}_{\mathrm{E}}\Big],} \tag{C.422}$$

and the quantity Y given by (C.391), that imposes $\lambda'=0$ in the above mean field.

- Time-reversal invariant direct spin–orbit mean field for $\lambda=1$:

$$\boxed{\begin{aligned}\Gamma^{t\Omega=m+1/2}_{m\nu_a,\,m+1\,\nu_b}|^{\mathrm{T}}_{\mathrm{D}} &= -\widetilde{B}(\mu)\sum_{\substack{m'\geq 0\\ \nu_c\nu_d}}\\ &\times\Big[\langle m\nu_a\ m'\nu_c|V(r_{12})[\vec{r}_{12}\otimes\vec{\nabla}_{12}]^{(1)}_{-1}|m+1\,\nu_b\ m'\nu_d\rangle\\ &+\langle m\nu_a\ -m'\nu_c|V(r_{12})[\vec{r}_{12}\otimes\vec{\nabla}_{12}]^{(1)}_{-1}|m+1\,\nu_b\ -m'\nu_d\rangle\Big]R^{t1/2\,1}_{m'\nu_d\nu_c0}|^{\mathrm{T}}_{\mathrm{D}},\end{aligned}} \tag{C.423}$$

where

$$\boxed{R^{t1/2\,1}_{m'\nu_d\nu_c0}|^{\mathrm{T}}_{\mathrm{D}} = Y^{1/2\,1}_{1/2\,0}\Big[Z^{t}_{m'+1/2\,m'\nu_d\nu_c0}|^{\mathrm{T}}_{\mathrm{D}} + \Theta(m'-1/2)Z^{t}_{m'-1/2\,m'\nu_d\nu_c0}|^{\mathrm{T}}_{\mathrm{D}}\Big],} \tag{C.424}$$

and the quantity Y given by (C.391), that imposes $\lambda'=0$ in the above mean field. Therefore, the quantities $R^{t1/2\,1}|^{\mathrm{T}}_{\mathrm{E}}$ and $R^{t1/2\,1}|^{\mathrm{T}}_{\mathrm{D}}$ are symmetric under the exchange of ν_c and ν_d since the corresponding quantities $Z|^{\mathrm{T}}_{\mathrm{E}}$ and $Z|^{\mathrm{T}}_{\mathrm{D}}$ display this symmetry as their density matrix ρ is symmetric and diagonal in m'.

2.3.2. Spin–orbit pairing field

We continue by deriving the pairing field (III.32) of the spin–orbit interaction (C.363), which is not time-reversal invariant for the moment. Given that the pairing tensor (C.21) and the fields (C.22) are diagonal in t and Ω, this spin–orbit pairing field can be written

$$\Delta^{t\Omega}_{r_ar_b} = \sum_{\substack{t'\Omega'>0\\ r_cr_d}}\langle ts_ar_a\ \overline{ts_br_b}|v^{(\mathrm{SO}),(\mathrm{a})}_{12}|t's_cr_c\ \overline{t's_dr_d}\rangle\kappa^{t'\Omega'}_{r_cr_d}. \tag{C.425}$$

As for the spin–orbit mean fields, let us first concentrate on the exchange component of the spin–orbit pairing field. It reads

$$\begin{aligned}\Delta^{t\Omega}_{r_ar_b}|_{\mathrm{E}} = \widetilde{B}(\mu)\sum_{\substack{t'\Omega'>0\\ r_cr_d}}\sum_k(-)^k\langle r_a-r_b|V(r_{12})[\vec{r}_{12}\otimes\vec{\nabla}_{12}]^{(1)}_{-k}P_r|r_c-r_d\rangle\\ \times\sigma_b\sigma_d\langle ts_a\ t-s_b|\mathcal{P}_{\mathrm{E}}[\vec{\sigma}_1+\vec{\sigma}_2]^{(1)}_k|t's_c\ t'-s_d\rangle\kappa^{t'\Omega'}_{r_cr_d}.\end{aligned} \tag{C.426}$$

We name the quantum numbers of the above matrix element in the same way as we have done for the second matrix element of the spin–orbit mean field (C.368), while keeping in

mind that here $\lambda \in \{-1, 0, 1\}$ since the pairing field is not symmetric under the exchange of its indices, contrary to the mean field (see equation (C.24) and the discussion below). With these notations, the exchange spin–orbit pairing field becomes

$$\begin{aligned}\Delta^{t\Omega=m+s}_{m\nu_a,\,m+\lambda\,\nu_b}|_{\mathrm{E}} &= \widetilde{B}(\mu) \sum_{\substack{t'\Omega'>0\\ m'\nu_c\nu_d}} \sum_{\lambda'} (-)^{\lambda-\lambda'} \times 4(s-\lambda)(s'-\lambda') \\ &\times \langle m\nu_a \ -(m+\lambda)\,\nu_b|V(r_{12})[\vec{r}_{12}\otimes\vec{\nabla}_{12}]^{(1)}_{\lambda'-\lambda}P_r|m'\nu_c \ -(m'+\lambda')\,\nu_d\rangle \\ &\quad\times\langle ts\ t-(s-\lambda)|\mathcal{P}_{\mathrm{E}}[\vec{\sigma}_1+\vec{\sigma}_2]^{(1)}_{\lambda-\lambda'}|t's'\ t'-(s'-\lambda')\rangle\kappa^{t'm'+s'}_{m'\nu_c,\,m'+\lambda'\nu_d}.\end{aligned} \tag{C.427}$$

Once again, let us first concentrate on the spin-isospin part. We set

$$A^{ts\lambda}_{\Omega'm'\nu_c\nu_d\lambda'}|_{\mathrm{E}} \equiv B^{s\lambda}_{s'\lambda'} \times C^{t}_{\Omega'm'\nu_c\nu_d\lambda'}|_{\mathrm{E}}, \tag{C.428}$$

where the spin part reads

$$B^{s\lambda}_{s'\lambda'} \equiv 4(s-\lambda)(s'-\lambda')\langle s \ -(s-\lambda)|[\vec{\sigma}_1+\vec{\sigma}_2]^{(1)}_{\lambda-\lambda'}|s' \ -(s'-\lambda')\rangle, \tag{C.429}$$

and the isospin part is

$$C^{t}_{\Omega'm'\nu_c\nu_d\lambda'}|_{\mathrm{E}} = (H-W)\kappa^{t\,m'+s'}_{m'\nu_c,\,m'+\lambda'\nu_d}, \tag{C.430}$$

where we notice that there is only a particle-like contribution to the density coming from the spin–orbit pairing field. Note that this quantity is identical to the one of the tensor term (C.299), provided that we consider the tensor coefficients W and H instead of the spin–orbit ones. On the other hand, since the direct and exchange spin–orbit pairing fields have the same spin part, we also have implicitly set

$$B^{s\lambda}_{s'\lambda'} \equiv B^{s\lambda}_{s'\lambda'}|_{\mathrm{D}} = B^{s\lambda}_{s'\lambda'}|_{\mathrm{E}}. \tag{C.431}$$

Using carefully the expression of the spin matrix element (D.22), we obtain

$$\boxed{\begin{aligned}B^{s\lambda}_{s'\lambda'} = 4(s-\lambda)(s'-\lambda')\Big\{\delta_{ss'}\Big[2\lambda\delta_{\lambda\lambda'} - \sqrt{2}(\lambda-\lambda')\delta_{\lambda+\lambda',2s}\Big] \\ - 2s\sqrt{2}\delta_{s,-s'}\delta_{\lambda-\lambda',2s}\Big\},\end{aligned}} \tag{C.432}$$

where we have separated the $s = s'$ and $s \neq s'$ contributions to the spin–orbit pairing field, its spin diagonal part being given by $\lambda = 0$ and the non-diagonal one by $\lambda \neq 0$, as expected. Note that if the spin–orbit pairing field is diagonal, then it is also diagonal in m, just like the spin–orbit mean fields are.

Then, from (C.428), we get

$$A^{ts\lambda}_{\Omega'm'\nu_c\nu_d\lambda'}|_{\mathrm{E}} = (H-W)B^{s\lambda}_{s'\lambda'}\kappa^{t\,m'+s'}_{m'\nu_c,\,m'+\lambda'\nu_d}. \tag{C.433}$$

Now, setting

$$S^{ts\lambda}_{m'\nu_c\nu_d\lambda'}|_{\mathrm{E}} \equiv \sum_{\Omega'}\Theta(\Omega')A^{ts\lambda}_{\Omega'm'\nu_c\nu_d\lambda'}|_{\mathrm{E}} = \sum_{s'=\pm s}\Theta(m'+s')A^{ts\lambda}_{m'+s'm'\nu_c\nu_d\lambda'}|_{\mathrm{E}}, \tag{C.434}$$

we end up with

$$\boxed{\begin{aligned}S^{ts\lambda}_{m'\nu_c\nu_d\lambda'}|_{\mathrm{E}} = (H-W)\Big[\Theta(m'+s)B^{s\lambda}_{s\lambda'}\kappa^{t\,m'+s}_{m'\nu_c,\,m'+\lambda'\nu_d} \\ + \Theta(m'-s)B^{s\lambda}_{-s\lambda'}\kappa^{t\,m'-s}_{m'\nu_c,\,m'+\lambda'\nu_d}\Big],\end{aligned}} \tag{C.435}$$

and the exchange spin–orbit mean field can be written

$$\boxed{\begin{aligned}\Delta^{t\Omega=m+s}_{m\nu_a,\,m+\lambda\,\nu_b}|_{\rm E} &= \widetilde{B}(\mu)\sum_{\substack{m'\geq 0\\ \nu_c\nu_d}}\sum_{\lambda'=-1}^{1}(-)^{\lambda-\lambda'}\\ &\times\langle m\nu_a\ -(m+\lambda)\,\nu_b|V(r_{12})[\vec{r}_{12}\otimes\vec{\nabla}_{12}]^{(1)}_{\lambda'-\lambda}|-(m'+\lambda')\,\nu_d\ m'\nu_c\rangle S^{ts\lambda}_{m'\nu_c\nu_d\lambda'}|_{\rm E},\end{aligned}} \tag{C.436}$$

where, as for the spin–orbit mean fields, we have replaced the summations $\sum_{m'}\sum_{\Omega'>0}$ by $\sum_{m'\geq 0}\sum_{\Omega'}\Theta(\Omega')$ and applied the operator P_r. One might be tempted to say, like the central, density-dependent and tensor cases, that the above matrix element is equivalent to $\langle m\nu_a\ -m'\nu_c|V(r_{12})[\vec{r}_{12}\otimes\vec{\nabla}_{12}]^{(1)}_{\lambda'-\lambda}|-(m'+\lambda')\,\nu_d\ m+\lambda\,\nu_b\rangle$. Unfortunately, this statement is wrong as the gradient operator of the spin–orbit term prevents the commutation of the wave functions (the situation is similar to what we have discussed for the spin–orbit mean field below equation (C.381)).

To get the direct spin–orbit mean field out of the exchange one, we first switch H and W and omit the operator P_r to obtain

$$\boxed{\begin{aligned}\Delta^{t\Omega=m+s}_{m\nu_a,\,m+\lambda\,\nu_b}|_{\rm D} &= \widetilde{B}(\mu)\sum_{\substack{m'\geq 0\\ \nu_c\nu_d}}\sum_{\lambda'=-1}^{1}(-)^{\lambda-\lambda'}\\ &\times\langle m\nu_a\ -(m+\lambda)\,\nu_b|V(r_{12})[\vec{r}_{12}\otimes\vec{\nabla}_{12}]^{(1)}_{\lambda'-\lambda}|m'\nu_c\ -(m'+\lambda')\,\nu_d\rangle S^{ts\lambda}_{m'\nu_c\nu_d\lambda'}|_{\rm D},\end{aligned}} \tag{C.437}$$

where

$$\boxed{\begin{aligned}S^{ts\lambda}_{m'\nu_c\nu_d\lambda'}|_{\rm D} = (W-H)\Big[&\Theta(m'+s)B^{s\lambda}_{s\lambda'}\kappa^{t\,m'+s}_{m'\nu_c,\,m'+\lambda'\nu_d}\\ &+\Theta(m'-s)B^{s\lambda}_{-s\lambda'}\kappa^{t\,m'-s}_{m'\nu_c,\,m'+\lambda'\nu_d}\Big],\end{aligned}} \tag{C.438}$$

with the quantities B given by (C.432).

Finally, the identity

$$\boxed{S^{ts\lambda}_{m'\nu_c\nu_d\lambda'} \equiv -S^{ts\lambda}_{m'\nu_c\nu_d\lambda'}|_{\rm E} = S^{ts\lambda}_{m'\nu_c\nu_d\lambda'}|_{\rm D},} \tag{C.439}$$

allows us to write down the full spin–orbit pairing field (direct plus exchange components) as

$$\boxed{\begin{aligned}\Delta^{t\Omega=m+s}_{m\nu_a,\,m+\lambda\,\nu_b} &= \widetilde{B}(\mu)\sum_{\substack{m'\geq 0\\ \nu_c\nu_d}}\sum_{\lambda'=-1}^{1}(-)^{\lambda-\lambda'}\\ &\times\Big[\langle m\nu_a\ -(m+\lambda)\,\nu_b|V(r_{12})[\vec{r}_{12}\otimes\vec{\nabla}_{12}]^{(1)}_{\lambda'-\lambda}|m'\nu_c\ -(m'+\lambda')\,\nu_d\rangle\\ &-\langle m\nu_a\ -(m+\lambda)\,\nu_b|V(r_{12})[\vec{r}_{12}\otimes\vec{\nabla}_{12}]^{(1)}_{\lambda'-\lambda}|-(m'+\lambda')\,\nu_d\ m'\nu_c\rangle\Big]S^{ts\lambda}_{m'\nu_c\nu_d\lambda'}.\end{aligned}} \tag{C.440}$$

Contrary to the CDD and tensor pairing fields, we see that the spin–orbit pairing field does not share the structure of an exchange spin–orbit mean field (due to the gradient operator that prevents the required transformations). Regrettably, the spin–orbit pairing fields can therefore not be calculated simultaneously with the spin–orbit mean fields in an HFB code.

From the boxed equations, we can now explicitly write down the expressions of the above spin–orbit pairing field for each value of λ. We recall that this field is *not* time-reversal invariant. We also note that if $|\lambda| = 1$, then $\lambda = 2s$ as we can deduce from $s_b \equiv s - \lambda = \pm 1/2$ when $\lambda \neq 0$.

- Spin–orbit pairing field for $\lambda = 0$:

$$\boxed{\begin{aligned}\Delta^{t\Omega=m+s}_{m\nu_a,\,m+\lambda\,\nu_b} = -\widetilde{B}(\mu) \sum_{\substack{m'\geq 0\\ \nu_c\nu_d}} \sum_{\lambda'=\pm 1} \\ \times \Big[\langle m\nu_a \;-m\nu_b|V(r_{12})[\vec{r}_{12}\otimes\vec{\nabla}_{12}]^{(1)}_{\lambda'}|m'\nu_c \;-(m'+\lambda')\,\nu_d\rangle \\ -\langle m\nu_a \;-m\nu_b|V(r_{12})[\vec{r}_{12}\otimes\vec{\nabla}_{12}]^{(1)}_{\lambda'}|-(m'+\lambda')\,\nu_d\; m'\nu_c\rangle\Big] S^{ts0}_{m'\nu_c\nu_d\lambda'}.\end{aligned}} \tag{C.441}$$

where

$$\boxed{\begin{aligned}S^{ts0}_{m'\nu_c\nu_d\lambda'} = (W-H)\Big[\Theta(m'+s)B^{s0}_{s\lambda'}\kappa^{t\,m'+s}_{m'\nu_c,\,m'+\lambda'\nu_d} \\ +\Theta(m'-s)B^{s0}_{-s\lambda'}\kappa^{t\,m'-s}_{m'\nu_c,\,m'+\lambda'\nu_d}\Big],\end{aligned}} \tag{C.442}$$

with

$$\boxed{B^{s0}_{\pm s\lambda'} = -2s\sqrt{2}\delta_{\lambda',\pm 2s},} \tag{C.443}$$

that imposes $\lambda' = \pm 1$ in the above pairing field.

- Spin–orbit pairing field for $|\lambda| = 1$:

$$\boxed{\begin{aligned}\Delta^{t\Omega=m+s}_{m\nu_a,\,m+2s\,\nu_b} = \widetilde{B}(\mu) \sum_{\substack{m'\geq 0\\ \nu_c\nu_d}} \sum_{\lambda'=-1}^{1} (-)^{\lambda'-2s} \\ \times \Big[\langle m\nu_a \;-(m+2s)\,\nu_b|V(r_{12})[\vec{r}_{12}\otimes\vec{\nabla}_{12}]^{(1)}_{\lambda'-2s}|m'\nu_c \;-(m'+\lambda')\,\nu_d\rangle \\ -\langle m\nu_a \;-(m+2s)\,\nu_b|V(r_{12})[\vec{r}_{12}\otimes\vec{\nabla}_{12}]^{(1)}_{\lambda'-2s}|-(m'+\lambda')\,\nu_d\; m'\nu_c\rangle\Big] S^{ts\,2s}_{m'\nu_c\nu_d\lambda'},\end{aligned}} \tag{C.444}$$

where

$$\boxed{\begin{aligned}S^{ts\,2s}_{m'\nu_c\nu_d\lambda'} = (W-H)\Big[\Theta(m'+s)B^{s\,2s}_{s\lambda'}\kappa^{t\,m'+s}_{m'\nu_c,\,m'+\lambda'\nu_d} \\ +\Theta(m'-s)B^{s\,2s}_{-s\lambda'}\kappa^{t\,m'-s}_{m'\nu_c,\,m'+\lambda'\nu_d}\Big],\end{aligned}} \tag{C.445}$$

with

$$\boxed{\begin{aligned}B^{s\,2s}_{s\lambda'} &= 2s\sqrt{2}\delta_{\lambda',0} + 4s\delta_{\lambda',2s}, &\text{(C.446a)}\\ B^{s\,2s}_{-s\lambda'} &= -2s\sqrt{2}\delta_{\lambda',0}. &\text{(C.446b)}\end{aligned}}$$

Note that the quantities S^{ts0} and $S^{ts\,2s}$ are not symmetric under the exchange of ν_c and ν_d since the pairing tensor κ is not.

Time-reversal invariant fields

Now, we assume the time-reversal invariance of the spin–orbit pairing field, i.e. the pairing tensor κ becomes symmetric under the exchange of its indices. Then, the pairing field becomes symmetric (see discussion discussion below equation (C.24)) and it suffices to consider its expression for $\lambda \in \{0, 1\}$. For $\lambda = 0$, its expression is still given by (C.441). In this case, the quantity S^{ts0} is not symmetric under the exchange of ν_c and ν_d since the pairing tensor κ is not diagonal in m' (as $\lambda' \neq 0$), though symmetric. If $\lambda = 1$, then $s = 1/2$ (as we could have already seen in (C.432)) since the identity $s_b \equiv s - 1 = \pm 1/2$ holds only if $s = 1/2$.

- Time-reversal invariant spin–orbit pairing field for $\lambda = 1$:

$$\boxed{\begin{aligned}\Delta^{t\Omega=m+1/2}_{m\nu_a,\,m+1\,\nu_b} &= \widetilde{B}(\mu)\sum_{\substack{m'\geq 0\\ \nu_c\nu_d}}\sum_{\lambda'=0}^{1}(-)^{\lambda'-1}\\ &\times\Big[\langle m\nu_a\ m+1\,\nu_b|V(r_{12})[\vec{r}_{12}\otimes\vec{\nabla}_{12}]^{(1)}_{\lambda'-1}|m'\nu_c\ -(m'+\lambda')\,\nu_d\rangle\Big]\\ &-\langle m\nu_a\ m+1\,\nu_b|V(r_{12})[\vec{r}_{12}\otimes\vec{\nabla}_{12}]^{(1)}_{\lambda'-1}|-(m'+\lambda')\,\nu_d\ m'\nu_c\rangle S^{t1/2\,1}_{m'\nu_c\nu_d\lambda'}\Big],\end{aligned}} \tag{C.447}$$

where

$$\boxed{S^{t1/2\,1}_{m'\nu_c\nu_d\lambda'} = (W-H)\Big[B^{1/2\,1}_{1/2\,\lambda'}\kappa^{t\,m'+1/2}_{m'\nu_c,\,m'+\lambda'\nu_d}+\Theta(m'-1/2)B^{1/2\,1}_{-1/2\,\lambda'}\kappa^{t\,m'-1/2}_{m'\nu_c,\,m'+\lambda'\nu_d}\Big],} \tag{C.448}$$

with

$$\boxed{\begin{aligned}B^{1/2\,1}_{1/2\,\lambda'} &= \sqrt{2}\delta_{\lambda',0}+2\delta_{\lambda',1}, &\text{(C.449a)}\\ B^{1/2\,1}_{-1/2\,\lambda'} &= -\sqrt{2}\delta_{\lambda',0}, &\text{(C.449b)}\end{aligned}}$$

that impose $\lambda' \in \{0,1\}$ in the above pairing field. Note that the quantity $S^{t1/2\,1}$ is symmetric under the exchange of ν_c and ν_d only if $\lambda' = 0$ such that the pairing tensor κ, besides being symmetric, is diagonal in m'.

2.3.3. Spin–orbit spatial matrix elements

In the previous subsection, we have treated the spin-isospin parts of the spin–orbit mean- and pairing fields. In order to fully specify these fields, it remains to determine their spatial parts, which we now undertake.

Identifying the position of the centers by the quantum numbers j, the spatial dependence of the spin–orbit fields lies in the two-body matrix elements of the form

$$v^{j_aj_cj_bj_d,\,k}_{r_ar_cr_br_d} \equiv \langle j_a r_a\ j_c r_c|V(r_{12})[\vec{r}_{12}\otimes\vec{\nabla}_{12}]^{(1)}_{-k}|j_b r_b\ j_d r_d\rangle, \tag{C.450}$$

where we recall that $k = \lambda - \lambda'$ (see equation (C.233) and the related discussion). By definition,

$$v^{j_aj_cj_bj_d,\,k}_{r_ar_cr_br_d} = \int \mathrm{d}^3r_1\int \mathrm{d}^3r_2\,\phi^*_{j_ar_a}(\vec{r}_1)\phi^*_{j_cr_c}(\vec{r}_2)V(r_{12})[\vec{r}_{12}\otimes\vec{\nabla}_{12}]^{(1)}_{-k}\phi_{j_br_b}(\vec{r}_1)\phi_{j_dr_d}(\vec{r}_2). \tag{C.451}$$

Contrary to the previous terms, this time the wave functions do not commute with the sandwhiched quantity because of the gradient operator. Accordingly, we have no choice but to apply the gradient operator on the wave functions on its right. Decoupling the tensor product and separating the action of the gradient on the coordinates $\vec{r}_1$ and $\vec{r}_2$, we get

$$\begin{aligned}v^{j_aj_cj_bj_d,\,k}_{r_ar_cr_br_d} &= \sum_{\alpha\beta}\langle 1\alpha 1\beta|1-k\rangle\\ &\times\Big\{\int \mathrm{d}^3r_1\int \mathrm{d}^3r_2\,\phi^*_{j_ar_a}(\vec{r}_1)\phi^*_{j_cr_c}(\vec{r}_2)V(r_{12})r^\alpha_{12}\Big[\nabla^\beta_1\phi_{j_br_b}(\vec{r}_1)\Big]\phi_{j_dr_d}(\vec{r}_2)\\ &-\int \mathrm{d}^3r_1\int \mathrm{d}^3r_2\,\phi^*_{j_ar_a}(\vec{r}_1)\phi^*_{j_cr_c}(\vec{r}_2)V(r_{12})r^\alpha_{12}\phi_{j_br_b}(\vec{r}_1)\Big[\nabla^\beta_2\phi_{j_dr_d}(\vec{r}_2)\Big]\Big\},\end{aligned} \tag{C.452}$$

where the Clebsch–Gordan coefficient is not zero only if $\alpha+\beta = -k$. In the following, we will call $I^{\alpha\beta}_1$ and $I^{\alpha\beta}_2$ the first and second integrals of the above right-hand side term (we

purposely omit the r and j indices for conciseness). We fill focus on the integral $I_1^{\alpha\beta}$, the integral $I_2^{\alpha\beta}$ being easily deductible from it.

By separating the radial and z parts of the axial wave function on which the gradient acts, namely by writing $\phi_{j_b r_b}(\vec{r}_1) = \phi_{m_b n_{\perp b}}(\vec{r}_{\perp 1})\phi_{j_b n_{zb}}(z_1)$, we can first express the action of the gradient on the wave function along z using (C.483), to obtain, for $\beta = 0$,

$$\nabla_1^0 \phi_{j_b n_{zb}}(z_1) = \sqrt{\frac{\beta_z}{2}}\left[\sqrt{n_{zb}}\,\phi_{j_b, n_{zb}-1}(z_1) - \sqrt{n_{zb}+1}\,\phi_{j_b, n_{zb}+1}(z_1)\right], \tag{C.453}$$

since the chain rule applied on the off-center wave function $\phi_{j_b n_{zb}}(z_1)$ furnishes

$$\frac{\mathrm{d}}{\mathrm{d}z_1}\Big[\phi_{n_{zb}}(z_1 - d_b)\Big] = \left[\frac{\mathrm{d}\phi_{n_{zb}}}{\mathrm{d}z_1}\right](z_1 - d_b). \tag{C.454}$$

As for the action of the gradient on the radial wave function, we find, from (C.484), for $\beta = \pm 1$,

$$\begin{aligned}
\nabla_1^\beta \phi_{m_b n_{\perp b}}(\vec{r}_{\perp 1}) = {} & \Theta(2m_b + \beta)\sqrt{\frac{\beta_\perp}{2}}\left[\sqrt{n_{\perp b} + m_b + \frac{1+\beta}{2}}\,\phi_{m_b+\beta, n_{\perp b}}(\vec{r}_{\perp 1})\right. \\
& \left. + \sqrt{n_{\perp b} + \frac{1-\beta}{2}}\,\phi_{m_b+\beta, n_{\perp b}-\beta}(\vec{r}_{\perp 1})\right] \\
& - \Theta(-2m_b - \beta)\sqrt{\frac{\beta_\perp}{2}}\left[\sqrt{n_{\perp b} - m_b + \frac{1-\beta}{2}}\,\phi_{m_b+\beta, n_{\perp b}}(\vec{r}_{\perp 1})\right. \\
& \left. + \sqrt{n_{\perp b} + \frac{1+\beta}{2}}\,\phi_{m_b+\beta n_{\perp b}+\beta}(\vec{r}_{\perp 1})\right],
\end{aligned} \tag{C.455}$$

Thus, the action of the gradient operator on the axial wave function is

$$\nabla_1^\beta \phi_{j_b r_b}(\vec{r_1}) = \delta_{\beta,0}\phi_{m_b n_{\perp b}}(\vec{r}_{\perp 1})\nabla_1^0 \phi_{j_b n_{zb}}(z_1) + \delta_{|\beta|,1}\phi_{j_b n_{zb}}(z_1)\nabla_1^\beta \phi_{m_b n_{\perp b}}(\vec{r}_{\perp 1}), \tag{C.456}$$

where the action of the gradient for $\beta = 0$ and $\beta = \pm 1$ is respectively given by (C.453) and (C.455).

As for the previous terms, we apply the Gogny separable development in axial symmetry (C.495) on both the $\vec{r}_1$ and $\vec{r}_2$ coordinates. The one on the $\vec{r}_1$ coordinates is the same as for the previous terms, and is straightforward, i.e.

$$\phi^*_{j_c r_c}(\vec{r}_2)\phi_{j_d r_d}(\vec{r}_2) = \sum_{r_\nu} T^{r_\nu}_{j_c r_c\, j_d r_d}\phi_{j_{cd}0}(\vec{r}_2)\phi_{j_{cd} r_\nu}(\vec{r}_2). \tag{C.457}$$

Nevertheless, the Gogny separable development on the $\vec{r}_2$ coordinates is less on. Indeed, because of the gradient, we have to apply the Gogny separable development several times, sometimes on radial wave functions by means of (C.495), sometimes on wave functions

along z by means of (C.498). After doing so, we end up with

$$\begin{aligned}
\phi^*_{j_a r_a}(\vec{r}_1)\Big[\nabla_1^\beta \phi_{j_b r_b}(\vec{r}_1)\Big] &= \delta_{\beta,0}\sqrt{\frac{\beta_z}{2}}\phi_{j_{ab}0}(\vec{r}_1)\sum_{n_{\perp\mu}} T^{m_\mu n_{\perp\mu}}_{m_a n_{\perp a}\, m_b n_{\perp b}}\phi_{m_\mu n_{\perp\mu}}(\vec{r}_{\perp 1}) \\
\times\Bigg\{\sqrt{n_{zb}}\sum_{n^{(1)}_{z\mu}} T^{n^{(1)}_{z\mu}}_{j_a n_{za}\, j_b, n_{zb}-1}\phi_{j_{ab}n^{(1)}_{z\mu}}(z_1) &- \sqrt{n_{zb}+1}\sum_{n^{(2)}_{z\mu}} T^{n^{(2)}_{z\mu}}_{j_a n_{za}\, j_b, n_{zb}+1}\phi_{j_{ab}n^{(2)}_{z\mu}}(z_1)\Bigg\} \\
&+\delta_{|\beta|,1}\sqrt{\frac{\beta_\perp}{2}}\phi_{j_{ab}0}(\vec{r}_1)\sum_{n_{z\mu}} T^{n_{z\mu}}_{j_a n_{za}\, j_b n_{zb}}\phi_{j_{ab}n_{z\mu}}(z_1) \\
\times\Bigg\{\Theta(2m_b+\beta)\Bigg[\sqrt{n_{\perp b}+m_b+\frac{1+\beta}{2}}\sum_{n^{(1)}_{\perp\mu}} T^{m'_\mu n^{(1)}_{\perp\mu}}_{m_a n_{\perp a}\, m_b+\beta, n_{\perp b}}\phi_{m'_\mu n^{(1)}_{\perp\mu}}(\vec{r}_{\perp 1}) \\
&+\sqrt{n_{\perp b}+\frac{1-\beta}{2}}\sum_{n^{(2)}_{\perp\mu}} T^{m'_\mu n^{(2)}_{\perp\mu}}_{m_a n_{\perp a}\, m_b+\beta, n_{\perp b}-\beta}\phi_{m'_\mu n^{(2)}_{\perp\mu}}(\vec{r}_{\perp 1})\Bigg] \\
-\Theta(-2m_b-\beta)\Bigg[\sqrt{n_{\perp b}-m_b+\frac{1-\beta}{2}}\sum_{n^{(1)}_{\perp\mu}} T^{m'_\mu n^{(1)}_{\perp\mu}}_{m_a n_{\perp a}\, m_b+\beta, n_{\perp b}}\phi_{m'_\mu n^{(1)}_{\perp\mu}}(\vec{r}_{\perp 1}) \\
&+\sqrt{n_{\perp b}+\frac{1+\beta}{2}}\sum_{n^{(3)}_{\perp\mu}} T^{m'_\mu n^{(3)}_{\perp\mu}}_{m_a n_{\perp a}\, m_b+\beta, n_{\perp b}+\beta}\phi_{m'_\mu n^{(3)}_{\perp\mu}}(\vec{r}_{\perp 1})\Bigg]\Bigg\},
\end{aligned} \tag{C.458}$$

where the values taken by $n^{(i)}_{\perp\mu}$ for $i \in \{0,1,2,3\}$ (where $n^{(0)}_{\perp\mu} \equiv n_{\perp\mu}$) can be obtained from (C.504), $m^{(\prime)}_\mu$ can be expressed through (C.503), and the values taken by $n^{(j)}_{z\mu}$ for $j \in \{0,1,2\}$ (where $n^{(0)}_{z\mu} \equiv n_{z\mu}$) can be found in (C.510). The integral we want to evaluate then becomes

$$\begin{aligned}
I_1^{\alpha\beta} = \sum_{r_\nu} T^{r_\nu}_{j_c r_c\, j_d r_d}\int \mathrm{d}^3 r_1 \int \mathrm{d}^3 r_2 \\
\times V(r_{12}) r_{12}^\alpha \phi^*_{j_a r_a}(\vec{r}_1)\Big[\nabla_1^\beta \phi_{j_b r_b}(\vec{r}_1)\Big]\phi_{j_{cd}0}(\vec{r}_2)\phi_{j_{cd}r_\nu}(\vec{r}_2),
\end{aligned} \tag{C.459}$$

where the quantity $\phi^*_{j_a r_a}(\vec{r}_1)\Big[\nabla_1^\beta \phi_{j_b r_b}(\vec{r}_1)\Big]$ is provided above, and where the expressions or values taken by $r_\nu = (m_\nu, n_{\perp\nu}, n_{z\nu})$ can be deduced from (C.503), (C.504) and (C.510).

We now apply the Moshinsky transformation in axial symmetry (C.516). We see that we can extract the wave function $\phi_{j_{ab}0}(\vec{r}_1)$ from (C.458), so that the Moshinsky transformation for $r_\nu = 0$ is identical to the one of the previous terms, and is straightforward, i.e.

$$\phi_{j_{ab}0}(\vec{r}_1)\phi_{j_{cd}0}(\vec{r}_2) = \phi_0(\vec{R} - \vec{D}_{abcd})\phi_0(\vec{r} - \vec{d}_{abcd}), \tag{C.460}$$

since the Jacobian of the change of variables $(\vec{r}_1, \vec{r}_2) \to (\vec{r}, \vec{R})$ is equal to unity and the axial Moshinsky coefficient, specified by (C.516), satisfies the identity $M_{0\,0}^{r_{\lambda'}\, r_{\sigma'}} = \delta_{r_{\lambda'},0}\delta_{r_{\sigma'},0}$ because of (C.526) and (C.533). By writing $\phi_{j_{cd}r_\nu}(\vec{r}_2) = \phi_{m_\nu n_{\perp\nu}}(\vec{r}_{\perp 2})\phi_{j_{cd}n_{z\nu}}(z_2)$, we see that the same situation occurs for the Moshinsky transformation in the case $r_\nu \neq 0$ as for the Gogny separable development on the $\vec{r}_2$ coordinates. Indeed, we have to apply the Moshinsky transformation several times, sometimes on radial wave functions by means of (C.514), sometimes on wave functions along z by means of (C.527). Depending on the Moshinsky transformation considered, different integrals come out. The orthogonality relation of the off-center axial wave functions allows us to evaluate both the radial integrals,

given by

$$\int \mathrm{d}^2 R_\perp \, \phi_0^*(\vec{R}_\perp)\phi_{m_\lambda^{(\prime)} n_{\perp\lambda}^{(i)}}(\vec{R}_\perp) = \delta_{n_{\perp\lambda}^{(i)},0}\delta_{m_\lambda^{(\prime)},0} \quad \text{for } i \in \{0,1,2,3\}, \tag{C.461}$$

and the integrals along z, given by

$$\int \mathrm{d}Z \, \phi_0^*(Z - D_{abcd})\phi_{n_{z\lambda}^{(j)}}(Z - D_{abcd}) = \delta_{n_{z\lambda}^{(j)},0} \quad \text{for } j \in \{0,1,2\}, \tag{C.462}$$

where we have used the relations $\phi_{00}(\vec{R}_\perp) = \phi_{00}^*(\vec{R}_\perp)$ and $\phi_0(Z) = \phi_0^*(Z)$, by virtue of (C.8). The distances found in the last three equations are expressed by (C.327), with (C.328). Noticing that, when changing variables, $r_{12}^\alpha = \sqrt{2} r^\alpha$, we are finally led to

$$\boxed{I_1^{\alpha\beta} = \sum_{r_\nu} T^{r_\nu}_{j_c r_c \, j_d r_d} \int \mathrm{d}^3 r \, V(\sqrt{2}r) r^\alpha \phi_0(\vec{r} - \vec{d}_{abcd}) F^\beta_{1,r_\nu r_\sigma}(\vec{r} - \vec{d}_{abcd}),} \tag{C.463}$$

where

$$\begin{aligned}
F^\beta_{1,r_\nu r_\sigma}(\vec{r} - \vec{d}_{abcd}) \equiv{}& \frac{\delta_{\beta,0}}{b_z} \sum_{n_{\perp\mu}} T^{m_\mu n_{\perp\mu}}_{n_{\perp a} m_a \, n_{\perp b} m_b} M^{00 \, m_\sigma n_{\perp\sigma}}_{m_\mu n_{\perp\mu} \, m_\nu n_{\perp\nu}} \phi_{m_\sigma n_{\perp\sigma}}(\vec{r}_\perp) \\
&\times \Bigg\{ \sqrt{n_{zb}} \sum_{n_{z\mu}^{(1)}} T^{n_{z\mu}^{(1)}}_{j_a n_{za} \, j_b, n_{zb}-1} M^{0 \, n_{z\sigma}^{(1)}}_{n_{z\mu}^{(1)} n_{z\nu}} \phi_{n_{z\sigma}^{(1)}}(z - d_{abcd}) \\
&- \sqrt{n_{zb}+1} \sum_{n_{z\mu}^{(2)}} T^{n_{z\mu}^{(2)}}_{j_a n_{za} \, j_b, n_{zb}+1} M^{0 \, n_{z\sigma}^{(2)}}_{n_{z\mu}^{(2)} n_{z\nu}} \phi_{n_{z\sigma}^{(2)}}(z - d_{abcd}) \Bigg\} \\
&+ \frac{\delta_{|\beta|,1}}{b_\perp} \sum_{n_{z\mu}} T^{n_{z\mu}}_{j_a n_{za} \, j_b n_{zb}} M^{0 \, n_{z\sigma}}_{n_{z\mu} n_{z\nu}} \phi_{n_{z\sigma}}(z - d_{abcd}) \\
&\times \Bigg\{ \Theta(2m_b + \beta) \\
&\Bigg[\sqrt{n_{\perp b} + m_b + \frac{1+\beta}{2}} \sum_{n_{\perp\mu}^{(1)}} T^{m'_\mu n_{\perp\mu}^{(1)}}_{m_a n_{\perp a} \, m_b+\beta, n_{\perp b}} M^{00 \, m'_\sigma n_{\perp\sigma}^{(1)}}_{m'_\mu n_{\perp\mu}^{(1)} \, m_\nu n_{\perp\nu}} \phi_{m'_\sigma n_{\perp\sigma}^{(1)}}(\vec{r}_\perp) \\
&+ \sqrt{n_{\perp b} + \frac{1-\beta}{2}} \sum_{n_{\perp\mu}^{(2)}} T^{m'_\mu n_{\perp\mu}^{(2)}}_{m_a n_{\perp a} \, m_b+\beta, n_{\perp b}-\beta} M^{00 \, m'_\sigma n_{\perp\sigma}^{(2)}}_{m'_\mu n_{\perp\mu}^{(2)} \, m_\nu n_{\perp\nu}} \phi_{m'_\sigma n_{\perp\sigma}^{(2)}}(\vec{r}_\perp) \Bigg] \\
&- \Theta(-2m_b - \beta) \\
&\Bigg[\sqrt{n_{\perp b} - m_b + \frac{1-\beta}{2}} \sum_{n_{\perp\mu}^{(1)}} T^{m'_\mu n_{\perp\mu}^{(1)}}_{m_a n_{\perp a} \, m_b+\beta, n_{\perp b}} M^{00 \, m'_\sigma n_{\perp\sigma}^{(1)}}_{m'_\mu n_{\perp\mu}^{(1)} \, m_\nu n_{\perp\nu}} \phi_{m'_\sigma n_{\perp\sigma}^{(1)}}(\vec{r}_\perp) \\
&+ \sqrt{n_{\perp b} + \frac{1+\beta}{2}} \sum_{n_{\perp\mu}^{(3)}} T^{m'_\mu n_{\perp\mu}^{(3)}}_{m_a n_{\perp a} \, m_b+\beta, n_{\perp b}+\beta} M^{00 \, m'_\sigma n_{\perp\sigma}^{(3)}}_{m'_\mu n_{\perp\mu}^{(3)} \, m_\nu n_{\perp\nu}} \phi_{m'_\sigma n_{\perp\sigma}^{(3)}}(\vec{r}_\perp) \Bigg] \Bigg\},
\end{aligned} \tag{C.464}$$

where we recall that the quantities β_z and b_z as well as $\beta_\perp$ and $b_\perp$ are respectively linked by the relations (C.7). The radial Moshinsky coefficients $M^{00 \, m_\sigma^{(\prime)} n_{\perp\sigma}^{(i)}}_{m_\mu^{(\prime)} n_{\perp\mu}^{(i)} \, m_\nu n_{\perp\nu}}$ are given by (C.516) while the expressions of $n_{\perp\sigma}^{(i)}$ for $i \in \{0,1,2,3\}$ (where $n_{\perp\sigma}^{(0)} \equiv n_{\perp\sigma}$) and $m_\sigma^{(\prime)}$ can respectively be obtained from (C.524) and (C.525). As for the Moshinsky coefficients relative to z,

$M^{0\,n_{z\sigma}^{(j)}}_{n_{z\mu}^{(j)}\,n_{z\nu}}$, they are given by (C.528) while the expressions of $n_{z\sigma}^{(j)}$ for $j \in \{0,1,2\}$ (where $n_{z\mu}^{(0)} \equiv n_{z\sigma}$) can be obtained from (C.532).

For the sake of completeness, we write the full expression of the integral $I_2^{\alpha\beta}$ whose derivation is analogous to the one of $I_1^{\alpha\beta}$ we have just presented. We have

$$\boxed{I_2^{\alpha\beta} = \sum_{r_\mu} T^{r_\mu}_{j_a r_a\, j_b r_b} \int \mathrm{d}^3 r\, V(\sqrt{2}r) r^\alpha \phi_0(\vec{r} - \vec{d}_{abcd}) F^\beta_{2,r_\mu r_\rho}(\vec{r} - \vec{d}_{abcd}),} \tag{C.465}$$

where

$$\begin{aligned}
\boxed{
F^\beta_{2,r_\mu r_\rho}(\vec{r} - \vec{d}_{abcd}) \equiv{}& \frac{\delta_{\beta,0}}{b_z} \sum_{n_{\perp\nu}} T^{m_\nu n_{\perp\nu}}_{m_c n_{\perp c}\, m_d n_{\perp d}} M^{00\, m_\rho n_{\perp\rho}}_{m_\mu n_{\perp\mu}\, m_\nu n_{\perp\nu}} \phi_{m_\rho n_{\perp\rho}}(\vec{r}_\perp) \\
&\times \Bigg\{ \sqrt{n_{zd}} \sum_{n_{z\nu}^{(1)}} T^{n_{z\nu}^{(1)}}_{j_c n_{zc}\, j_d, n_{zd}-1} M^{0\, n_{z\rho}^{(1)}}_{n_{z\mu} n_{z\nu}^{(1)}} \phi_{n_{z\rho}^{(1)}}(z - d_{abcd}) \\
&- \sqrt{n_{zd}+1} \sum_{n_{z\nu}^{(2)}} T^{n_{z\nu}^{(2)}}_{j_c n_{zc}\, j_d, n_{zd}+1} M^{0\, n_{z\rho}^{(2)}}_{n_{z\mu} n_{z\nu}^{(1)}} \phi_{n_{z\rho}^{(2)}}(z - d_{abcd}) \Bigg\} \\
&+ \frac{\delta_{|\beta|,1}}{b_\perp} \sum_{n_{z\nu}} T^{n_{z\nu}}_{j_c n_{zc}\, j_d n_{zd}} M^{0\, n_{z\rho}}_{n_{z\mu} n_{z\nu}} \phi_{n_{z\rho}}(z - d_{abcd}) \\
&\times \Bigg\{ \Theta(2m_d + \beta) \\
&\Bigg[\sqrt{n_{\perp d} + m_d + \frac{1+\beta}{2}} \sum_{n_{\perp\nu}^{(1)}} T^{m'_\nu n_{\perp\nu}^{(1)}}_{m_c n_{\perp c}\, m_d+\beta, n_{\perp d}} M^{00\, m'_\rho n_{\perp\rho}^{(1)}}_{m_\mu n_{\perp\mu}\, m'_\nu n_{\perp\nu}^{(1)}} \phi_{m'_\rho n_{\perp\rho}^{(1)}}(\vec{r}_\perp) \\
&+ \sqrt{n_{\perp d} + \frac{1-\beta}{2}} \sum_{n_{\perp\nu}^{(2)}} T^{m'_\nu n_{\perp\nu}^{(2)}}_{m_c n_{\perp c}\, m_d+\beta, n_{\perp d}-\beta} M^{00\, m'_\rho n_{\perp\rho}^{(2)}}_{m_\mu n_{\perp\mu}\, m'_\nu n_{\perp\nu}^{(2)}} \phi_{m'_\rho n_{\perp\rho}^{(2)}}(\vec{r}_\perp) \Bigg] \\
&- \Theta(-2m_d - \beta) \\
&\Bigg[\sqrt{n_{\perp d} - m_d + \frac{1-\beta}{2}} \sum_{n_{\perp\nu}^{(1)}} T^{m'_\nu n_{\perp\nu}^{(1)}}_{m_c n_{\perp c}\, m_d+\beta, n_{\perp d}} M^{00\, m'_\rho n_{\perp\rho}^{(1)}}_{m_\mu n_{\perp\mu}\, m'_\nu n_{\perp\nu}^{(1)}} \phi_{m'_\rho n_{\perp\rho}^{(1)}}(\vec{r}_\perp) \\
&+ \sqrt{n_{\perp d} + \frac{1+\beta}{2}} \sum_{n_{\perp\nu}^{(3)}} T^{m'_\nu n_{\perp\nu}^{(3)}}_{m_c n_{\perp c}\, m_d+\beta, n_{\perp d}+\beta} M^{00\, m'_\rho n_{\perp\rho}^{(3)}}_{m_\mu n_{\perp\mu}\, m'_\nu n_{\perp\nu}^{(3)}} \phi_{m'_\rho n_{\perp\rho}^{(3)}}(\vec{r}_\perp) \Bigg] \Bigg\}.
}
\end{aligned} \tag{C.466}$$

As for the expressions of the Talman and Moshinsky coefficients as well as the expressions or the values taken by the various indices, they can be deduced from the same equations as for the integral $I_1^{\alpha\beta}$.

Thus, in order to evaluate both $I_1^{\alpha\beta}$ and $I_2^{\alpha\beta}$ integrals, we will need to find an expression for

$$I^\alpha_{r_\eta} = \int \mathrm{d}^3 r\, V(\sqrt{2}r) r^\alpha \phi_0(\vec{r} - \vec{d}_{abcd}) \phi_{r_\eta}(\vec{r} - \vec{d}_{abcd}), \tag{C.467}$$

with $\eta = \sigma$ to get $I_1^{\alpha\beta}$ and $\eta = \rho$ to get $I_2^{\alpha\beta}$. In fact, $I^\alpha_{r_\sigma}$ and $I^\alpha_{r_\rho}$ are the same integrals, only the expressions or values taken by r_σ and r_ρ may differ.

First, we recall that, in axial symmetry where $\vec{r} = (r_\perp, \varphi, z)$, the components r^α of

the vector $\vec{r}$ are

$$r^0 = z, \tag{C.468a}$$

$$r^{\pm 1} = \mp \frac{1}{\sqrt{2}} r_\perp \mathrm{e}^{\pm \mathrm{i}\varphi}. \tag{C.468b}$$

Here, the integral (C.467) is much simpler to evaluate than the one the tensor term (C.330) because, in the absence of a $1/r^2$ dependence, it is directly separable into a product of integrals along the directions Oz and perpendicular to Oz when considering a Gaussian potential. Indeed,

$$V(\sqrt{2}r) r^\alpha = \mathrm{e}^{-2r^2/\mu^2} Q_\alpha(r_\perp, z) \mathrm{e}^{\mathrm{i}\alpha\varphi}, \tag{C.469}$$

where the polynomial Q_α is defined by

$$Q_0 = z, \tag{C.470a}$$

$$Q_{\pm 1} = \mp \frac{1}{\sqrt{2}} r_\perp, \tag{C.470b}$$

in such a way that the integral (C.467) separates according to

$$\begin{aligned} I^\alpha_{r_\eta}(\vec{d}_{abcd}) = &\int_{-\infty}^{+\infty} \mathrm{d}z\, \mathrm{e}^{-2z^2/\mu^2} \phi_0(z - d_{abcd}) \phi_{n_{z\eta}}(z - d_{abcd}) \\ &\times \int \mathrm{d}^2 r_\perp\, \mathrm{e}^{-2r_\perp^2/\mu^2} \mathrm{e}^{\mathrm{i}\alpha\varphi} \phi_{00}(\vec{r}_\perp) \phi_{m_\eta n_{\perp\eta}}(\vec{r}_\perp) Q_\alpha(r_\perp, z). \end{aligned} \tag{C.471}$$

According to the definition (C.8), $\phi_{00}(\vec{r}_\perp) = \phi_{00}(r_\perp)$ since this wave function has no angular dependence. Furthermore, we can write $\phi_{m_\eta n_{\perp\eta}}(\vec{r}_\perp) = \mathrm{e}^{\mathrm{i}m_\eta\varphi} \widetilde{\phi}_{|m_\eta| n_{\perp\eta}}(r_\perp)$, thanks to the relation (C.9). Then, just like the tensor term, we can easily evaluate the angular part of the integral over $r_\perp$, so that

$$\begin{aligned} I^\alpha_{r_\eta}(\vec{d}_{abcd}) = &2\pi \delta_{\alpha,-m_\eta} \int_{-\infty}^{+\infty} \mathrm{d}z\, \mathrm{e}^{-2z^2/\mu^2} \phi_0(z - d_{abcd}) \phi_{n_{z\eta}}(z - d_{abcd}) \\ &\times \int_0^\infty \mathrm{d}r_\perp\, r_\perp \mathrm{e}^{-2r_\perp^2/\mu^2} \phi_{00}(r_\perp) \widetilde{\phi}_{|m_\eta| n_{\perp\eta}}(r_\perp) Q_\alpha(r_\perp, z). \end{aligned} \tag{C.472}$$

Note that the Kronecker delta enforces the symmetry condition $\alpha = m_a - m_b + m_c - m_d$, in accordance with the fact that the spin–orbit interaction does not commute with L_z (see discussion right after (C.367)). Otherwise, we would recover the conservation law of the central and density-dependent interactions that do commute with L_z (see equation (C.136) and the discussion below). Mathematically speaking, the spin–orbit interaction involves a tensor of rank 1, so that its projection satisfies $-1 \leq k = -(\alpha + \beta) \leq 1$. The situation is then similar to the one of the tensor interaction, except that this latter involves a tensor of rank 2 (see equation (C.336) and discussion below).

Finally, we can include the different cases encountered in the unified expression

$$\boxed{I^\alpha_{r_\eta}(\vec{d}_{abcd}) = 2\pi \delta_{\alpha,-m_\eta} \sum_{m=0}^{1} \sum_{n=0}^{1} Q^{mn}_\alpha K^{z\,m}_{n_{z\eta}}(0, d_{abcd}) K^{\perp\,n}_{|m_\eta| n_{\perp\eta}}(0),} \tag{C.473}$$

where

$$Q^{mn}_0 = \delta_{m,1} \delta_{n,0}, \tag{C.474a}$$

$$Q^{mn}_{\pm 1} = \mp \frac{1}{\sqrt{2}} \delta_{m,0} \delta_{n,1}, \tag{C.474b}$$

and

$$K^{z\,m}_{n_{z\eta}}(0,d_{abcd}) = \int_{-\infty}^{+\infty} \mathrm{d}z\, z^m\, \mathrm{e}^{-2z^2/\mu^2}\phi_0(z-d_{abcd})\phi_{n_{z\eta}}(z-d_{abcd}), \tag{C.475}$$

$$K^{\perp\,n}_{|m_\eta|n_{\perp\eta}}(0) = \int_0^{\infty} \mathrm{d}r_\perp\, r_\perp^{n+1}\, \mathrm{e}^{-2r_\perp^2/\mu^2}\phi_{00}(r_\perp)\widetilde{\phi}_{|m_\eta|n_{\perp\eta}}(r_\perp). \tag{C.476}$$

Note that these expressions correspond to the more general expressions obtained in the calculation of the tensor spatial matrix elements, namely (C.339) and (C.340), in the case $\xi = 0$, hence the chosen notation. Consequently (and luckily), we do not need to evaluate them again.

Indeed, from (C.341) in the case $\xi = 0$, we find

$$\boxed{\begin{aligned} K^{\perp\,n}_{|m_\eta|n_{\perp\eta}}(0) &= \frac{b_\perp^n}{2\pi}[n_{\perp\eta}!(n_{\perp\eta}+|m_\eta|)!]^{1/2} \\ &\times \sum_{i=0}^{n_{\perp\eta}} \frac{(-)^i}{i!(n_{\perp\eta}-i)!(i+|m_\eta|)!}\Gamma(i+n/2+|m_\eta|/2+1)G_\perp^{-i-n/2-|m_\eta|/2-1}(0), \end{aligned}} \tag{C.477}$$

with

$$\boxed{G_\perp(0) \equiv \frac{2b_\perp^2+\mu^2}{\mu^2},} \tag{C.478}$$

the analogous version of the spherical quantity (B.39) for the radial part in axial symmetry.

In the same way, from (C.351) in the case $\xi = 0$, we obtain

$$\boxed{\begin{aligned} K^{z\,m}_{n_{z\eta}}(0,d_{abcd}) &= (-)^{n_{z\eta}}\left[\frac{2^{n_{z\eta}}n_{z\eta}!}{\pi}\right]^{1/2} \mathrm{e}^{-F_z(0)d_{abcd}^2} \sum_{j=0}^{\lfloor n_{z\eta}/2\rfloor} \frac{(-)^j}{2^{2j}j!(n_{z\eta}-2j)!} \\ &\times \sum_{l=0}^{m}(-)^l\frac{m!}{l!(m-l)!}d_{abcd}^{m-l} \sum_{\substack{p=0\\ p\in 2\mathbb{N}}}^{n_{z\eta}+l-2j}(-)^p\frac{(n_{z\eta}+l-2j)!}{p!(n_{z\eta}+l-2j-p)!} \\ &\times b_z^{n_{z\sigma}+2l-2j-p}G_z^{-p/2-1/2}(0)\Big[F_z(0)d_{abcd}\Big]^{n_{z\eta}+l-2j-p}\Gamma\left(\frac{p+1}{2}\right), \end{aligned}} \tag{C.479}$$

where the notation $p \in 2\mathbb{N}$ indicates that p has to be even. The quantities appearing are

$$\boxed{G_z(0) \equiv \frac{2b_z^2+\mu^2}{\mu^2},} \tag{C.480}$$

the analogous version of the spherical quantity (B.39) for the z part in axial symmetry, as well as

$$\boxed{F_z(0) = \frac{2}{\mu^2 G_z(0)} = \frac{2}{2b_z^2+\mu^2}.} \tag{C.481}$$

We notice that *the finite-range spin–orbit two-body matrix elements of the generalized Gogny interaction* (II.1)*, in a two-center axially symmetric representation, are purely analytical.*

At the one-center limit, all centers coincide ($j_a = j_b = j_c = j_d$), so that $d_{abcd} = 0$. Obviously, the spin-isospin matrix elements (of the spin–orbit interaction) evaluated in the previous subsections remain the same. As for the spin–orbit spatial matrix elements,

deduced from the integrals (C.463) and (C.465), they remain valid provided that the integral (C.467) is evaluated for $d_{abcd} = 0$ and that the Talman coefficients relative to z are those given by (C.511) rather than by (C.506), in the same way that the conditions (C.512) rather than (C.510) will have to be taken into account at this limit. When the integral (C.467) is evaluated for $d_{abcd} = 0$, only its part relative to z, whose final expression is given by (C.479), is affected. It simplifies as

$$\boxed{\begin{aligned} K^{z\,m}_{n_{z\eta}}(0,0) = \left[\frac{2^{n_{z\eta}} n_{z\eta}!}{\pi}\right]^{1/2} b_z^m \sum_{i=0}^{\lfloor n_{z\eta}/2 \rfloor} \frac{(-)^j}{2^{2j} j!(n_{z\eta}-2j)!} \delta_{n_{z\eta}+m-2j,2\mathbb{N}} \\ \times G_z^{-n_{z\eta}/2-m/2+j-1/2}(0)\,\Gamma\left(\frac{n_{z\eta}+m-2j+1}{2}\right), \end{aligned}} \tag{C.482}$$

where $G_z(0)$ is expressed in (C.478) and where the notation $\delta_{n_{z\eta}+m-2j,2\mathbb{N}}$ indicates that the sum $n_{z\eta} + m - 2j$ must be even. To evaluate (C.473) at the one-center limit, it is then enough to replace the expression of $K^{z\,m}_{n_{z\eta}}(0, d_{abcd})$ by the expression of $K^{z\,m}_{n_{z\eta}}(0,0)$.

3. Formulas for the axial symmetry

In this section, we give the main formulas used to carry out the above calculations in the chosen framework, namely the two-center axial harmonic oscillator representation. We will not attempt to justify the developments leading to those and refer the reader to [175, 176] for more detailed presentations.

3.1. Action of the gradient operator in axial symmetry

We give the action of the gradient operator on the harmonic oscillators wave functions in one and two dimensions.

In one dimension, we find out, from the recurrence relations (D.99) between the Hermite polynomials,

$$\frac{\mathrm{d}\phi_{n_z}}{\mathrm{d}z}(z) = \sqrt{\frac{\beta_z}{2}}\left[\sqrt{n_z}\,\phi_{n_z-1}(z) - \sqrt{n_z+1}\,\phi_{n_z+1}(z)\right]. \tag{C.483}$$

In two dimensions, we find out, from the recurrence relations (D.102) between the generalized Laguerre polynomials,

$$\begin{aligned} \nabla^\lambda \phi_{m n_\perp}(\vec{r}_\perp) = \sqrt{\frac{\beta_\perp}{2}}\Bigg[\sqrt{n_\perp + m + \frac{1+\lambda}{2}}\,\phi_{m+\lambda,n_\perp}(\vec{r}_\perp) \\ + \sqrt{n_\perp + \frac{1-\lambda}{2}}\,\phi_{m+\lambda,n_\perp-\lambda}(\vec{r}_\perp)\Bigg] \quad \text{if } m > -\frac{\lambda}{2}, \end{aligned} \tag{C.484a}$$

$$\begin{aligned} \nabla^\lambda \phi_{m n_\perp}(\vec{r}_\perp) = -\sqrt{\frac{\beta_\perp}{2}}\Bigg[\sqrt{n_\perp - m + \frac{1-\lambda}{2}}\,\phi_{m+\lambda,n_\perp}(\vec{r}_\perp) \\ + \sqrt{n_\perp + \frac{1+\lambda}{2}}\,\phi_{m+\lambda,n_\perp+\lambda}(\vec{r}_\perp)\Bigg] \quad \text{if } m < -\frac{\lambda}{2}, \end{aligned} \tag{C.484b}$$

where ∇^λ with $\lambda = \pm 1$ is the gradient operator expressed in the spherical basis (see definition (D.14)).

3.2. Generating functions in axial symmetry

The generating functions χ take all their interest in the fundamental relation which links them to the functions of the harmonic oscillator ϕ, here in dimension $N = 1$ or $N = 2$, according to

$$\sum_n \chi_n^*(\vec{t})\phi_n(\vec{r}) = \left(\frac{\beta}{\pi}\right)^{N/4} \mathrm{e}^{-\beta r^2/2+2\sqrt{\beta}\,\vec{t}\cdot\vec{r}-t^2}, \tag{C.485}$$

where n denotes the set of quantum numbers in dimension N and β the corresponding oscillator parameter, i.e. $n = (m, n_\perp)$ and $\beta = \beta_\perp$ if $N = 2$, and, $n = n_z$ and $\beta = \beta_z$ if $N = 1$. The axial generating functions associated with the axial harmonic oscillators, that satisfy the above relation, are given by

$$\chi_r(\vec{t}) \equiv \chi_{mn_\perp}(\vec{t}_\perp)\chi_{n_z}(t_z), \tag{C.486}$$

where the radial generating function is

$$\chi_{mn_\perp}(\vec{t}_\perp) \equiv \mathcal{N}_{mn_\perp} t_\perp^{2n_\perp+|m|} \mathrm{e}^{\mathrm{i}m\varphi_t}, \tag{C.487}$$

with the coefficient

$$\mathcal{N}_{mn_\perp} \equiv \frac{(-)^{n_\perp}}{(n_\perp!(n_\perp+|m|)!)^{1/2}}, \tag{C.488}$$

while the generating function along z is

$$\chi_{n_z}(t_z) \equiv \mathcal{N}_{n_z} t_z^{n_z}, \tag{C.489}$$

with the coefficient

$$\mathcal{N}_{n_z} \equiv \left(\frac{2^{n_z}}{n_z!}\right)^{1/2}. \tag{C.490}$$

In our calculations, we will need the following properties satisfied by the above generating functions, for $a \in \mathbb{R}$,

$$\chi_n(a\vec{t}) = a^{X_n}\chi_n(\vec{t}), \tag{C.491a}$$

$$\chi_n^*(\vec{t}) = \chi_{-n}(\vec{t}), \tag{C.491b}$$

where

$$X_n \equiv \begin{cases} 2n_\perp + |m| & \text{if } N = 2, \\ n_z & \text{if } N = 1, \end{cases} \quad \text{and} \quad -n \equiv \begin{cases} (n_\perp, -m) & \text{if } N = 2, \\ n_z & \text{if } N = 1. \end{cases} \tag{C.492}$$

We will also need the sum and product rules

$$\chi_{n_\mu}(\vec{t})\chi_{n_{\mu'}}(\vec{t}) = \sum_\nu \frac{\mathcal{N}_{n_\mu}\mathcal{N}_{n_{\mu'}}}{\mathcal{N}_{n_\nu}} \delta_{\mu+\mu',\nu}\chi_{n_\nu}(\vec{t}), \tag{C.493a}$$

$$\chi_{n_\nu}(\vec{t}_1+\vec{t}_2) = \sum_{\mu\mu'} \frac{\mathcal{N}_{n_\mu}\mathcal{N}_{n_{\mu'}}}{\mathcal{N}_{n_\nu}} \delta_{\mu+\mu',\nu}\chi_{n_\mu}(\vec{t}_1)\chi_{n_{\mu'}}(\vec{t}_2), \tag{C.493b}$$

where

$$\mu+\mu' = \nu \iff \begin{cases} X_\mu + X_{\mu'} = X_\nu \text{ and } m_\mu + m_{\mu'} = m_\nu & \text{if } N = 2, \\ n_{z\mu} + n_{z\mu'} = n_{z\nu} & \text{if } N = 1, \end{cases} \tag{C.494}$$

with $X \equiv 2n_\perp + |m|$.

3.3. Talman coefficients in axial symmetry

The Gogny separable development [181] (see section D.3 for a quick presentation) applied on two-center axial HO wave functions provides the relation

$$\boxed{\phi^*_{j_a r_a}(\vec{r})\phi_{j_b r_b}(\vec{r}) = \sum_{r_\mu} T^{r_\mu}_{j_a r_a\, j_b r_b}\phi_{j_{ab}0}(\vec{r})\phi_{j_{ab} r_\mu}(\vec{r}),} \tag{C.495}$$

where the quantum number j_{ab} locates the associated wave functions at a distance

$$\vec{d}_{ab} = \frac{\vec{d}_a + \vec{d}_b}{2}, \tag{C.496}$$

and where the axial Talman coefficient can be decomposed into the product

$$T^{r_\mu}_{j_a r_a\, j_b r_b} = T^{m_\mu n_{\perp\mu}}_{m_a n_{\perp a}\, m_b n_{\perp b}} \times T^{n_{z\mu}}_{j_a n_{za}\, j_b n_{zb}}. \tag{C.497}$$

The quantity $T^{m_\mu n_{\perp\mu}}_{m_a n_{\perp a}\, m_b n_{\perp b}}$ denotes the radial Talman coefficient and $T^{n_{z\mu}}_{j_a n_{za}\, j_b n_{zb}}$ the Talman coefficient relative to the z coordinate. Note that only the Talman coefficient relative to z is impacted by the decentering of the wave functions, in relation with the fact that these ones are only decentered along z. We now need to specify the expressions of the Talman coefficients and the ranges of values taken by the quantum numbers $r_\mu = (m_\mu, n_{\perp\mu}, n_{z\mu})$.

3.3.1. Radial Talman coefficient

It is also possible to apply the separable Gogny expansion directly to the radial HO wave functions to get

$$\phi^*_{m_a n_{\perp a}}(\vec{r}_\perp)\phi_{m_b n_{\perp b}}(\vec{r}_\perp) = \sum_{n_{\perp\mu}} T^{m_\mu n_{\perp\mu}}_{m_a n_{\perp a}\, m_b n_{\perp b}}\phi_{00}(\vec{r}_\perp)\phi_{m_\mu n_{\perp\mu}}(\vec{r}_\perp). \tag{C.498}$$

We can show [175, 176] that the radial Talman coefficient reads

$$\boxed{\begin{aligned} T^{m_\mu n_{\perp\mu}}_{m_a n_{\perp a}\, m_b n_{\perp b}} &= (-)^{n_{\perp a}+n_{\perp b}-n_{\perp\mu}} \\ &\times \Big[n_{\perp a}!(n_{\perp a}+|m_a|)!n_{\perp b}!(n_{\perp b}+|m_b|)!n_{\perp\mu}!(n_{\perp\mu}+|m_\mu|)!\Big]^{1/2} \\ &\times \sum_m \left[\left(\frac{X'_a \pm (m+|m_a|)}{2}\right)!\left(\frac{X'_b \pm (m+|m_b|)}{2}\right)!\left(\frac{X'_\mu \pm (m+|m_\mu|)}{2}\right)!\right]^{-1}, \end{aligned}} \tag{C.499}$$

where we have set

$$X'_a \equiv \frac{X_\mu + X_b - X_a}{2}, \tag{C.500a}$$

$$X'_b \equiv \frac{X_\mu + X_a - X_b}{2}, \tag{C.500b}$$

$$X'_\mu \equiv \frac{X_a + X_b - X_\mu}{2}, \tag{C.500c}$$

have used the notation

$$\left(\frac{X \pm |m|}{2}\right)! \equiv \left(\frac{X+|m|}{2}\right)!\left(\frac{X-|m|}{2}\right)! = n_\perp!(n_\perp+|m|)!, \tag{C.501}$$

and where, besides having to be of the same parity as $X'_a + m_a$, the index m must verify

$$\begin{aligned} -\max(X'_a + m_a, X'_b + m_b, X_\mu + m_a + m_b) \\ \leq m \leq \min(X'_a - m_a, X'_b - m_b, X_\mu + m_a + m_b). \end{aligned} \tag{C.502}$$

Note in addition that the radial Talman coefficient implies

$$\boxed{m_\mu = m_b - m_a,} \tag{C.503}$$

and is different from zero if and only the inequalities

$$\boxed{\frac{|X_a - X_b| - |m_\mu|}{2} \leq n_{\perp\mu} \leq \frac{X_a + X_b - |m_\mu|}{2}} \tag{C.504}$$

are fulfilled.

3.3.2. Talman coefficient relative to the z coordinate

It is also possible to apply the separable Gogny expansion directly to the HO wave functions relative to z, to get

$$\boxed{\phi^*_{j_a n_{za}}(z)\phi_{j_b n_{zb}}(z) = \sum_{n_{z\mu}} T^{n_{z\mu}}_{j_a n_{za}\, j_b n_{zb}} \phi_{j_{ab}0}(z)\phi_{j_{ab} n_{z\mu}}(z).} \tag{C.505}$$

In the general case where the wave functions do not belong to the same center ($j_a \neq j_b$), we can show [175, 176] that the Talman coefficient relative to z reads

$$\boxed{T^{n_{z\mu}}_{j_a n_{za}\, j_b n_{zb}} = \sqrt{n_{za}! n_{zb}! n_{z\mu}!} \sum_n \frac{1}{n!(n_{z\mu} - n)!} \frac{R^{j_a j_b}_{n_{za}-n, n_{zb}-n_{z\mu}+n}}{\sqrt{(n_{za} - n)!(n_{zb} - n_{z\mu} + n)!}},} \tag{C.506}$$

where

$$\boxed{R^{j_a j_b}_{n_{za} n_{zb}} \equiv (-)^{n_{zb}} \mathrm{e}^{-\sigma^2_{ab}} \sqrt{\frac{n_{za}! n_{zb}!}{2^{n_{za}+n_{zb}}}} \sum_{p=0}^{n_{za}} \sum_{q=0}^{n_{zb}} \frac{H_{p+q}(\sigma_{ab})}{p! q! \left(\frac{n_{za}-p}{2}\right)! \left(\frac{n_{zb}-q}{2}\right)!},} \tag{C.507}$$

with

$$\boxed{\sigma_{ab} \equiv \frac{d_b - d_a}{2} \sqrt{\beta_z},} \tag{C.508}$$

the HO parameter β_z being defined in (C.7), and the condition

$$\max(0, n_{z\mu} - n_{zb}) \leq n \leq \min(n_{za}, n_{z\mu}). \tag{C.509}$$

Note in addition that the Talman coefficient relative to z is different from zero, for $j_a \neq j_b$, if and only the inequalities

$$0 \leq n_{z\mu} \leq n_{za} + n_{zb} \tag{C.510}$$

are fulfilled.

In the particular case where the wave functions belong to the same center ($j_a = j_b$), the above Talman coefficient relative to z simplifies according to

$$\boxed{T^{n_{z\mu}}_{n_{za} n_{zb}} = \frac{\sqrt{n_{za}! n_{zb}! n_{z\mu}!}}{\left(\frac{n_{za}-n_{zb}+n_{z\mu}}{2}\right)! \left(\frac{n_{zb}-n_{za}+n_{z\mu}}{2}\right)! \left(\frac{n_{za}+n_{zb}-n_{z\mu}}{2}\right)!},} \tag{C.511}$$

where we have not specified the position of the centers since they now coincide. The Talman coefficient relative to z is different from zero, for $j_a = j_b$, if the statements

$$n_{z\mu} \text{ has the same parity as } n_{za} + n_{zb}, \tag{C.512a}$$
$$|n_{za} - n_{zb}| \leq n_{z\mu} \leq n_{za} + n_{zb}, \tag{C.512b}$$

are fulfilled.

3.4. Moshinsky coefficients in axial symmetry

The Moshinsky transformation allows us to move from the nucleon coordinates $(\vec{r}_1, \vec{r}_2)$ to the relative and center-of-mass coordinates $(\vec{r} = (\vec{r}_\perp, z), \vec{R} = (\vec{R}_\perp, Z))$, defined as[6]

$$\vec{r} \equiv \frac{\vec{r}_1 - \vec{r}_2}{\sqrt{2}}, \quad \text{and} \quad \vec{R} \equiv \frac{\vec{r}_1 + \vec{r}_2}{\sqrt{2}}. \tag{C.513}$$

The Moshinky transformation of two-center axial HO wave functions is encoded in the relation

$$\phi_{j_a r_a}(\vec{r}_1)\phi_{j_b r_b}(\vec{r}_2) = \sum_{r_\lambda} M^{r_\lambda r_\sigma}_{r_a r_b} \phi_{r_\lambda}(\vec{R} - \vec{D}_{ab})\phi_{r_\sigma}(\vec{r} - \vec{d}_{ab}), \tag{C.514}$$

where the distances appearing are defined by

$$\vec{d}_{ab} \equiv \frac{\vec{d}_a - \vec{d}_b}{\sqrt{2}}, \quad \text{and} \quad \vec{D}_{ab} \equiv \frac{\vec{d}_a + \vec{d}_b}{\sqrt{2}}, \tag{C.515}$$

and where the axial Moshinsky coefficient can be decomposed into the product

$$M^{r_\lambda r_\sigma}_{r_a r_b} = M^{m_\lambda n_{\perp\lambda}\, m_\sigma n_{\perp\sigma}}_{m_a n_{\perp a}\, m_b n_{\perp b}} \times M^{n_{z\lambda} n_{z\sigma}}_{n_{za} n_{zb}}. \tag{C.516}$$

The quantity $M^{m_\lambda n_{\perp\lambda}\, m_\sigma n_{\perp\sigma}}_{m_a n_{\perp a}\, m_b n_{\perp b}}$ denotes the radial Moshinsky coefficient and $M^{n_{z\lambda} n_{z\sigma}}_{n_{za} n_{zb}}$ the Moshinsky coefficient relative to the z coordinate. Note that neither the radial Moshinsky coefficient nor the Moshinsky coefficient relative to the z coordinate are impacted by the decentering of the wave functions. We now need to specify the expressions of the Moshinsky coefficients as well as the ranges of values taken by the quantum numbers $r_\sigma = (m_\sigma, n_{\perp\sigma}, n_{z\sigma})$.

3.4.1. Radial Moshinsky coefficient

It is also possible to apply the Moshinksy transformation directly to the radial HO wave functions to get

$$\phi_{m_a n_{\perp a}}(\vec{r}_{\perp 1})\phi_{m_b n_{\perp b}}(\vec{r}_{\perp 2}) = \sum_{m_\lambda n_{\perp\lambda}} M^{m_\lambda n_{\perp\lambda}\, m_\sigma n_{\perp\sigma}}_{m_a n_{\perp a}\, m_b n_{\perp b}} \phi_{m_\lambda n_{\perp\lambda}}(\vec{R}_\perp)\phi_{m_\sigma n_{\perp\sigma}}(\vec{r}_\perp), \tag{C.517}$$

We can show [175, 176] that the radial Moshinsky coefficient reads

$$\boxed{\begin{aligned} M^{m_\lambda n_{\perp\lambda}\, m_\sigma n_{\perp\sigma}}_{m_a n_{\perp a}\, m_b n_{\perp b}} &= \frac{(-)^{n_{\perp a}+n_{\perp b}+n_{\perp\lambda}+n_{\perp\sigma}}}{2^{(X_a+X_b)/2}} \\ &\times \left[\left(\frac{X_a \pm m_a}{2}\right)!\left(\frac{X_b \pm m_b}{2}\right)!\left(\frac{X_\lambda \pm m_\lambda}{2}\right)!\left(\frac{X_\sigma \pm m_\sigma}{2}\right)!\right]^{1/2} \\ &\times \sum_{n_\perp m} \frac{(-)^m}{\left(\frac{X \pm |m|}{2}\right)!\left(\frac{X_b - X \pm |m_b - m|}{2}\right)!\left(\frac{X_\sigma - X \pm |m_\sigma - m|}{2}\right)!\left(\frac{X_\sigma - X_b + X \pm |m_\sigma - m_b + m|}{2}\right)!}, \end{aligned}} \tag{C.518}$$

6. This convention is important; another definition of the relative and center-of-mass coordinates $(\vec{r}, \vec{R})$ would bring a different expression of the Moshinsky coefficient.

where we have set $X \equiv 2n_\perp + |m|$, used the notation (C.501) and where the index $n_\perp$ must verify the inequalities

$$\begin{aligned}\max(0, X_b - X_\lambda - |m| + |m + m_\lambda - m_b|) \\ \leq 2n_\perp \leq \min(X_b - |m| + |m - m_b|, X_\sigma - |m| + |m - m_\sigma|),\end{aligned} \tag{C.519}$$

and the index m, the inequalities,

$$\begin{aligned}-\min(X_b - m_b, X_\sigma - m_\sigma, X_\lambda + m_\lambda - 2m_b, X_a + m_a - 2m_\sigma) \\ \leq 2m \leq \min(X_b + m_b, X_\sigma + m_\sigma, X_\lambda + m_\lambda + 2m_b, X_a + m_a + 2m_\sigma).\end{aligned} \tag{C.520}$$

Note in addition that the radial Moshinsky coefficient implies

$$n_{\perp\sigma} = \frac{X_a + X_b - X_\lambda - |m_\sigma|}{2}, \tag{C.521}$$

and

$$m_\sigma = m_a + m_b - m_\lambda, \tag{C.522}$$

while the range of values taken by $n_{\perp\lambda}$ and m_λ are not constrained.

In the case $r_\lambda = 0$, the radial Moshinsky coefficient simplifies according to

$$\boxed{M^{00\, m_\sigma n_{\perp\sigma}}_{m_a n_{\perp a}\, m_b n_{\perp b}} = \frac{(-)^{(|m_a|-|m_b|-|m_\sigma|)/2}}{2^{(X_a+X_b)/2}} \left[\frac{\left(\frac{X_a+X_b\pm|m_a+m_b|}{2}\right)!}{\left(\frac{X_a\pm|m_a|}{2}\right)!\left(\frac{X_b\pm|m_b|}{2}\right)!}\right]^{1/2},} \tag{C.523}$$

which implies

$$n_{\perp\sigma} = \frac{X_a + X_b - |m_\sigma|}{2}, \tag{C.524}$$

and

$$m_\sigma = m_a + m_b. \tag{C.525}$$

In the case $r_a = r_b = 0$, the radial Moshinsky coefficient simplifies according to

$$\boxed{M^{m_\lambda n_{\perp\lambda}\, m_\sigma n_{\perp\sigma}}_{00\,00} = \delta_{n_{\perp\lambda},0}\delta_{n_{\perp\sigma},0}\delta_{m_\lambda,0}\delta_{m_\sigma,0}.} \tag{C.526}$$

3.4.2. Moshinsky coefficient relative to the z coordinate

It is also possible to apply the Moshinsky transformation directly to the HO wave functions relative to z, to get

$$\phi_{n_{za}}(z_1 - d_a)\phi_{n_{zb}}(z_2 - d_b) = \sum_{n_{z\lambda}} M^{n_{z\lambda}n_{z\sigma}}_{n_{za}n_{zb}} \phi_{n_{z\lambda}}(Z - D_{ab})\phi_{n_{z\sigma}}(z - d_{ab}), \tag{C.527}$$

where the distances appearing in the wave functions are defined in (C.515). We can show [175, 176] that the Moshinsky coefficient relative to z reads

$$\boxed{\begin{aligned}M^{n_{z\lambda}n_{z\sigma}}_{n_{za}n_{zb}} = &\left[\frac{n_{za}!n_{zb}!n_{z\lambda}!n_{z\sigma}!}{2^{n_{za}+n_{zb}}}\right]^{1/2} \\ &\times \sum_{n_z} \frac{(-)^{n_z}}{n_z!(n_{zb}-n_z)!(n_{z\sigma}-n_z)!(n_{z\lambda}-n_{zb}+n_z)!},\end{aligned}} \tag{C.528}$$

with the condition

$$\max(0, n_{zb} - n_{z\lambda}) \leq n_z \leq \min(n_{zb}, n_{z\sigma}). \tag{C.529}$$

Note in addition that the Moshinky coefficient relative to z implies

$$n_{z\sigma} = n_{za} + n_{zb} - n_{z\lambda}. \tag{C.530}$$

In the case $r_\lambda = 0$, the Moshinsky coefficient relative to z simplifies according to

$$\boxed{M^{0\, n_{z\sigma}}_{n_{za} n_{zb}} = \frac{(-)^{n_{zb}}}{2^{(n_{za}+n_{zb})/2}} \left[\frac{(n_{za}+n_{zb})!}{n_{za}! n_{zb}!}\right]^{1/2},} \tag{C.531}$$

which implies

$$n_{z\sigma} = n_{za} + n_{zb}. \tag{C.532}$$

In the case $r_a = r_b = 0$, the Moshinsky coefficient relative to z simplifies according to

$$\boxed{M^{n_{z\lambda} n_{z\sigma}}_{0\,0} = \delta_{n_{z\lambda},0}\, \delta_{n_{z\sigma},0}.} \tag{C.533}$$

Chapter D

Miscellaneous

> "For particulars, as every one knows, make for virtue and happiness; generalities are intellectually necessary evils."
>
> — Aldous Huxley, *Brave New World*

In this appendix, we provide most of the formulas used to carry out the derivations as well as generalities and various properties useful for understanding the whole document, and that were not mentioned elsewhere. We begin by recalling some definitions and properties related to the spin and isospin formalisms. Then, the general form of the nuclear two-body nuclear interaction and the so-called Gogny separable development are demonstrated. We continue by bringing up notable features of the tensor and spin–orbit interactions and discussing the behavior of the generalized Gogny interaction under rotations. Finally, the main functions, polynomials, series expansions and integrals we take advantage of all along the calculations are enumerated.

Chapter contents

1. Pauli matrices and exchange operators

In this section, we give some useful properties of the Pauli matrices we benefit from in the developments. We do the same for the spin- and isospin-exchange operators as they are expressed in terms of the Pauli matrices.

By definition, the Pauli vector reads

$$\vec{\sigma} = \sigma_x \hat{x} + \sigma_y \hat{y} + \sigma_z \hat{z}, \tag{D.1}$$

where $\hat{x}$, $\hat{y}$ and $\hat{y}$ are the components of the unit vector $\hat{r} \equiv \vec{r}/|\vec{r}|$, giving the directions of the Pauli vector components, which are the common Pauli matrices defined by

$$\sigma_x \equiv \begin{pmatrix} 0 & 1 \\ 1 & 0 \end{pmatrix}, \qquad \sigma_y \equiv \begin{pmatrix} 0 & -\mathrm{i} \\ \mathrm{i} & 0 \end{pmatrix}, \qquad \sigma_z \equiv \begin{pmatrix} 1 & 0 \\ 0 & -1 \end{pmatrix}. \tag{D.2}$$

Using these definitions, one quickly obtains

$$\vec{\sigma}^2 = 3\mathbb{1}. \tag{D.3}$$

Similarly, it is not difficult to show that the product of any two Pauli matrices can be written as

$$\sigma_i \sigma_j = \delta_{ij}\mathbb{1} + \mathrm{i}\epsilon_{ijk}\sigma_k, \tag{D.4}$$

where δ_{ij} denotes the Kronecker delta and ϵ_{ijk} the Levi-Civita symbol. This relation helps us derive the following identity where we first expand the scalar product,

$$\begin{aligned} (\vec{\sigma}\cdot\hat{r})^2 = (\vec{\sigma}\cdot\hat{r})(\vec{\sigma}\cdot\hat{r}) &= \sum_i \sigma_i \hat{r}_i \sum_j \sigma_j \hat{r}_j \\ &= \sum_{ij} \hat{r}_i \hat{r}_j (\delta_{ij}\mathbb{1} + \mathrm{i}\epsilon_{ijk}\sigma_k) \\ &= \hat{r}\cdot\hat{r} + \mathrm{i}\sigma(\hat{r}\times\hat{r}) = \hat{r}\cdot\hat{r} = \mathbb{1}, \end{aligned} \tag{D.5}$$

and finally use the component expression of the cross product (marked by $\times$). We now point out that the Pauli vector is related to the spin operator $\vec{s}$ by the simple relation

$$\vec{\sigma} = \frac{2}{\hbar}\vec{s}. \tag{D.6}$$

This identity is then also true for each component of the Pauli vector and the spin operator. We note that those relations hold for the isospin as well. To distinguish them from the above ones, we replace σ by τ. In particular, the Pauli vector (associated with the isospin) is related to the isospin operator $\vec{t}$ by the simple relation

$$\vec{\tau} = 2\vec{t}. \tag{D.7}$$

We emphasize that the isospin, although describable by a formalism very close to that of the spin, is not an angular momentum; it is an dimensionless quantity, hence the absence of the constant $\hbar$ in this definition. The spin-exchange and isospin-exchange operators between the particles 1 and 2 can respectively be defined in terms of Pauli vectors as

$$P_\sigma \equiv \frac{\mathbb{1} + \vec{\sigma}_1\cdot\vec{\sigma}_2}{2}, \tag{D.8a}$$

$$P_\tau \equiv \frac{\mathbb{1} + \vec{\tau}_1\cdot\vec{\tau}_2}{2}, \tag{D.8b}$$

where the Pauli vectors associated with the first particle are $\vec{\sigma}_1$ and $\vec{\tau}_1$, and the ones associated with the second particle are $\vec{\sigma}_2$ and $\vec{\tau}_2$. As their names suggest, those operators respectively exchange the spin and isospin projections of the two particles. Formally,

$$P_\sigma|s_1 s_2\rangle = |s_2 s_1\rangle, \tag{D.9a}$$
$$P_\tau|t_1 t_2\rangle = |t_2 t_1\rangle, \tag{D.9b}$$

where s_1 and s_2 as well as t_1 and t_2 are the projections of the spin and isospin, respectively, along the quantization axis, chosen to be Oz. As a consequence of these equalities, we have $P_\sigma^2 = P_\tau^2 = \mathbb{1}$. Now, since the particles we are dealing with are nucleons, that is to say in particular spin-1/2 and isospin-1/2 particles, we have the relations

$$\begin{aligned} P_\sigma &= \frac{1}{2}\mathbb{1} + 2\vec{s}_1\cdot\vec{s}_2 = \frac{1}{2}\mathbb{1} + \vec{S}^2 - \vec{s}_1^{\,2} - \vec{s}_2^{\,2} \\ &= \vec{S}^2 - \mathbb{1}, \end{aligned} \tag{D.10a}$$

$$\begin{aligned} P_\tau &= \frac{1}{2}\mathbb{1} + 2\vec{t}_1\cdot\vec{t}_2 = \frac{1}{2}\mathbb{1} + \vec{T}^2 - \vec{t}_1^{\,2} - \vec{t}_2^{\,2} \\ &= \vec{T}^2 - \mathbb{1}. \end{aligned} \tag{D.10b}$$

Using those results, we can infer the action of the spin-exchange and isospin-exchange operators on the states coupled to the total spin and total isospin as

$$P_\sigma\,|SM_S\rangle = [S(S+1) - 1]\,|SM_S\rangle = (-)^{S+1}\,|SM_S\rangle, \tag{D.11a}$$
$$P_\tau\,|TM_T\rangle = [T(T+1) - 1]\,|TM_T\rangle = (-)^{T+1}\,|TM_T\rangle, \tag{D.11b}$$

where the rightmost equalities come from the fact that $S, T \in \{0, 1\}$. Alternatively, the definitions (D.8) provide

$$(\vec{\sigma}_1\cdot\vec{\sigma}_2)\,|SM_S\rangle = [2(-)^{S+1} - 1]\,|SM_S\rangle, \tag{D.12a}$$
$$(\vec{\tau}_1\cdot\vec{\tau}_2)\,|TM_T\rangle = [2(-)^{T+1} - 1]\,|TM_T\rangle. \tag{D.12b}$$

Finally, the definitions (D.8) combined with the identities $P_\sigma^2 = P_\tau^2 = \mathbb{1}$ imply

$$(\vec{\sigma}_1\cdot\vec{\sigma}_2)^2 = 3\mathbb{1} - 2\vec{\sigma}_1\cdot\vec{\sigma}_2, \tag{D.13a}$$
$$(\vec{\tau}_1\cdot\vec{\tau}_2)^2 = 3\mathbb{1} - 2\vec{\tau}_1\cdot\vec{\tau}_2. \tag{D.13b}$$

In the spherical basis, the Pauli vector writes

$$\vec{\sigma} = \sigma_{+1}\hat{e}_+ + \sigma_{-1}\hat{e}_- + \sigma_z\hat{z}, \tag{D.14}$$

where the unit vectors $\hat{e}_+$ and $\hat{e}_-$ can be expressed as linear combinations of $\hat{x}$ and $\hat{y}$, just like these components of the Pauli vector are expressed as linear combinations of the Pauli matrices (D.2) as [1]

$$\sigma_{+1} \equiv -\frac{\sigma_x}{\sqrt{2}} + \mathrm{i}\frac{\sigma_y}{\sqrt{2}}, \tag{D.16a}$$
$$\sigma_{-1} \equiv \frac{\sigma_x}{\sqrt{2}} + \mathrm{i}\frac{\sigma_y}{\sqrt{2}}. \tag{D.16b}$$

1. Those components should not be confused with the ladder operators σ^+ and σ^-, often encountered in quantum mechanics, which are related to them by the relations

$$\sigma^+ \equiv -\sqrt{2}\sigma_{+1}, \tag{D.15a}$$
$$\sigma^- \equiv \sqrt{2}\sigma_{-1}. \tag{D.15b}$$

By definition, the spherical components of the Pauli vector act in the following way on the projections of the spin,

$$\sigma_{+1}|-1/2\rangle = -\sqrt{2}\,|1/2\rangle, \tag{D.17a}$$

$$\sigma_{-1}|1/2\rangle = \sqrt{2}\,|-1/2\rangle, \tag{D.17b}$$

$$\sigma_z|s\rangle = 2s|s\rangle. \tag{D.17c}$$

We then propose a unified notation to describe the matrix element of any spherical component of the Pauli vector as

$$\langle s_a|\sigma_m|s_b\rangle = 2s_a\delta_{s_a s_b}\delta_{m,0} - m\sqrt{2}\delta_{s_a,s_b+m}, \qquad \text{for } m = 0, \pm 1. \tag{D.18}$$

When dealing with the tensor interaction, we have to find out an expression for the matrix elements of the operator $[\vec{\sigma}_1 \otimes \vec{\sigma}_2]^{(2)}_k$. By first decoupling this tensor product, we get

$$\langle s_a\ s_c|[\vec{\sigma}_1 \otimes \vec{\sigma}_2]^{(2)}_k|s_b\ s_d\rangle = \sum_m \langle 1m1k-m|2k\rangle\langle s_a|\sigma_m|s_b\rangle\langle s_c|\sigma_{k-m}|s_d\rangle, \tag{D.19}$$

where we have used the properties of the Clebsch–Gordan coefficients, denoted by the brackets. Simplifying this expression by means of the unified expression (D.18) and plugging the particular values of the Clebsch–Gordan coefficients that appear, we get, after a lengthy but straight calculation,

$$\boxed{\begin{aligned}\langle s_a\ s_c|[\vec{\sigma}_1 \otimes \vec{\sigma}_2]^{(2)}_k|s_b\ s_d\rangle = 4s_a s_c\Bigg\{&\delta_{s_a s_b}\left[\sqrt{\frac{2}{3}}\delta_{s_c s_d}\delta_{k,0} - \delta_{s_c,-s_d}\delta_{k,2s_c}\right]\\ &- \delta_{s_a,-s_b}\left[\delta_{s_c s_d}\delta_{k,2s_a} - \delta_{s_c,-s_d}\left(\sqrt{\frac{2}{3}}\delta_{s_a,-s_c}\delta_{k,0} + 2\delta_{s_a s_c}\delta_{k,4s_a}\right)\right]\Bigg\}.\end{aligned}} \tag{D.20}$$

When dealing with the spin–orbit interaction, it is an expression for the matrix elements of the operator $[\vec{\sigma}_1 + \vec{\sigma}_2]^{(1)}_k$ that we need to find out. Separating the two contributions, we first obtain

$$\langle s_a\ s_c|[\vec{\sigma}_1 + \vec{\sigma}_2]^{(1)}_k|s_b\ s_d\rangle = \langle s_a|\sigma_{1,k}|s_b\rangle\delta_{s_c s_d} + \langle s_c|\sigma_{2,k}|s_d\rangle\delta_{s_a s_b}. \tag{D.21}$$

Now taking advantage of the unified relation (D.18), we get, without difficulty,

$$\boxed{\begin{aligned}\langle s_a\ s_c|[\vec{\sigma}_1 + \vec{\sigma}_2]^{(1)}_k|s_b\ s_d\rangle = {}&2(s_a + s_c)\delta_{s_a s_b}\delta_{s_c s_d}\delta_{k,0}\\ &- \sqrt{2}k\Big[\delta_{s_a s_b}\delta_{s_c,-s_d}\delta_{k,2s_c} + \delta_{s_a,-s_b}\delta_{s_c s_d}\delta_{k,2s_a}\Big].\end{aligned}} \tag{D.22}$$

2. Construction of the realistic two-body nuclear interaction

In the following, we seek to determine the most general form of the two-body nuclear interaction preserving the eight symmetries exposed in section I.1.2.

Because of charge independence, the isospin dependence of the two-body nuclear interaction must be scalar. According to the property (D.3) of Pauli matrices, the only possible scalars are the unity operator $\mathbb{1}$, the scalar product $\vec{\tau}_1 \cdot \vec{\tau}_2$ and powers of $\vec{\tau}_1 \cdot \vec{\tau}_2$. However, the additional property (D.13) reduces the powers of $\vec{\tau}_1 \cdot \vec{\tau}_2$ to linear combinations of $\mathbb{1}$ and $\vec{\tau}_1 \cdot \vec{\tau}_2$. Thus, the most general isospin dependence of the interaction is contained in the expression

$$v(\vec{r}, \vec{p}; \vec{\sigma}_1, \vec{\tau}_1; \vec{\sigma}_2, \vec{\tau}_2) = v^{(0)}(\vec{r}, \vec{p}; \vec{\sigma}_1; \vec{\sigma}_2) + v^{(1)}(\vec{r}, \vec{p}; \vec{\sigma}_1; \vec{\sigma}_2)\vec{\tau}_1 \cdot \vec{\tau}_2, \tag{D.23}$$

where we have omitted the unity operator for clarity.

Spin dependences

Now, let us have a look at the possible spin dependences of the two-body nuclear interaction. We can already state that this dependence will be independent, linear or quadratic in Pauli matrices. Indeed, the properties of Pauli matrices allow to express the higher dependences as linear combinations of independent, linear or quadratic terms in Pauli matrices (see for instance section D.1).

We begin with the linear dependence. According to the rotational symmetry, the spin dependence of the interaction must be scalar. The only possibilities at linear order are, for $i \in \{0,1\}$,

$$v^{(i)}(\vec{r},\vec{p};\vec{\sigma}_1;\vec{\sigma}_2) = \vec{a}_1 \cdot \vec{\sigma}_1 + \vec{a}_2 \cdot \vec{\sigma}_2. \tag{D.24}$$

The symmetry under the exchange of the two nucleons implies $\vec{a}_1 = \vec{a}_2 \equiv \vec{a}/2$, so that $v^{(i)}(\vec{r},\vec{p};\vec{\sigma}_1;\vec{\sigma}_2) = \vec{a} \cdot \vec{S}$, where we have defined $\vec{S} \equiv (\vec{\sigma}_1 + \vec{\sigma}_2)/2$. The vector $\vec{a}$ has to be chosen among the available vectors the interaction may depend on, namely $\vec{r}$, $\vec{p}$ and a combination of them, $\vec{L} \equiv \vec{r} \times \vec{p}$. Note that since $\vec{S}$ and all those vectors are Hermitian, the Hermiticity condition is guaranteed. Besides, $\vec{S}$ is invariant under a parity transformation and odd under time-reversal symmetry, so that the vector $\vec{a}$ must have the same behaviour for the nuclear interaction to be both parity and time-reversal invariant. The vectors $\vec{r}$ and $\vec{p}$, being odd under parity, are not suitable. Only the vector $\vec{L}$ behaves the appropriate way. Moreover, the vectors $\vec{S}$ and $\vec{L}$ are both Hermitian. Thus, at linear order in Pauli matrices, the spin dependence of the interaction is given by $\vec{L} \cdot \vec{S}$, because of its symmetries.

We continue with the quadratic dependence. Once again, the rotational symmetry imposes the spin dependence of the interaction to be scalar. At second order, the possibilities are *a priori*, for $i \in \{0,1\}$,

$$\begin{aligned} v^{(i)}(\vec{r},\vec{p};\vec{\sigma}_1;\vec{\sigma}_2) = \vec{a}_1 \cdot \vec{\sigma}_1^2 + \vec{a}_2 \cdot \vec{\sigma}_2^2 + \vec{\sigma}_1 \cdot \vec{\sigma}_2 + \vec{b} \cdot (\vec{\sigma}_1 \times \vec{\sigma}_2) \\ + (\vec{\sigma}_1 \cdot \vec{c}_1)(\vec{\sigma}_2 \cdot \vec{c}_2) + (\vec{\sigma}_1 \times \vec{d}_1) \cdot (\vec{\sigma}_2 \times \vec{d}_2). \end{aligned} \tag{D.25}$$

The first two terms are actually proportional to the unity operator because of (D.3). The third term is invariant under the exchange of the two nucleons, under parity and time-reversal symmetries, and obviously Hermitian, we can keep it. The vector $(\vec{\sigma}_1 \times \vec{\sigma}_2)$ appearing in the fourth term is odd under the exchange of the two nucleons (by definition of the vector product) and invariant under parity and time-reversal symmetries. The vector $\vec{b}$ that has to be either $\vec{r}$, $\vec{p}$ or $\vec{L}$ must then behave the same way. Nevertheless, none of these vectors does. For the fifth term the conclusion is the same unless we choose $\vec{c}_1 = \vec{c}_2 \equiv \vec{c}$. In this case, the term is invariant under the exchange of the two nucleons, under parity and time-reversal symmetries, and obviously Hermitian, whatever the vector $\vec{c}$, be it $\vec{r}$, $\vec{p}$ or $\vec{L}$. In the case $\vec{c} \equiv \vec{L}$, note however that the invariance under the exchange of the two nucleons is not satisfied as $(\vec{\sigma}_1 \cdot \vec{L})$ and $(\vec{\sigma}_2 \cdot \vec{L})$ do not commute (since the components of $\vec{L}$ fulfil the canonical commutation relations). In order to avoid this issue, we rather build the symmetric quantity $[(\vec{\sigma}_1 \cdot \vec{L})(\vec{\sigma}_2 \cdot \vec{L}) + (\vec{\sigma}_2 \cdot \vec{L})(\vec{\sigma}_1 \cdot \vec{L})]/2$, which then respect all the symmetries. Finally, the last term can be expressed as a linear combination of the third and fifth terms. Indeed, the quadruple product furnishes $(\vec{\sigma}_1 \times \vec{d}_1) \cdot (\vec{\sigma}_2 \times \vec{d}_2) = (\vec{\sigma}_1 \cdot \vec{\sigma}_2)(\vec{d}_1 \cdot \vec{d}_2) - (\vec{\sigma}_1 \cdot \vec{d}_2)(\vec{\sigma}_2 \cdot \vec{d}_1)$. In the first right-hand side term, the scalar product $(\vec{d}_1 \cdot \vec{d}_2)$ must be conveniently constructed from the available vectors $\vec{r}$, $\vec{p}$ and $\vec{L}$ (see below). As for the second right-hand side term, it has to be discarded when $\vec{d}_1 \neq \vec{d}_2$ according to what we have previously said. Thus, at second order in Pauli

matrices, the spin dependence of the interaction may be given by $\vec{\sigma}_1 \cdot \vec{\sigma}_2$, $(\vec{\sigma}_1 \cdot \vec{r})(\vec{\sigma}_2 \cdot \vec{r})$, $(\vec{\sigma}_1 \cdot \vec{p})(\vec{\sigma}_2 \cdot \vec{p})$ or $[(\vec{\sigma}_1 \cdot \vec{L})(\vec{\sigma}_2 \cdot \vec{L}) + (\vec{\sigma}_2 \cdot \vec{L})(\vec{\sigma}_1 \cdot \vec{L})]/2$, because of its symmetries.

Spatial dependences

Lastly, we focus on the possible spatial dependences of the two-body nuclear interaction. First, we notice that the Hermiticity condition applied to the time-reversal symmetry permits to rewrite the requirement (I.9) as

$$v(\vec{r}, -\vec{p}; -\vec{\sigma}_1, \vec{\tau}_1; -\vec{\sigma}_2, \vec{\tau}_2) = v^{\mathrm{T}}(\vec{r}, \vec{p}; \vec{\sigma}_1, \vec{\tau}_1; \vec{\sigma}_2, \vec{\tau}_2), \tag{D.26}$$

where the transpose operation merely reverses the order of the operators constituting the interaction [3].

According to the rotational symmetry, the spatial dependence of the two-body nuclear interaction must be scalar. Moreover, the possible scalars must be invariant under time-reversal symmetry (D.26). The time-reversal invariant scalars made up of the available vectors $\vec{r}$, $\vec{p}$ and $\vec{L}$ are $\vec{r}^2 \equiv \vec{r} \cdot \vec{r}$, $\vec{p}^2 \equiv \vec{p} \cdot \vec{p}$, $\vec{L}^2 \equiv \vec{L} \cdot \vec{L}$ and $(\vec{r} \cdot \vec{p} + \vec{p} \cdot \vec{r})^2$.[2] On the other hand, the last scalar can be expressed as a function of the first three,

$$\begin{aligned}(\vec{r} \cdot \vec{p} + \vec{p} \cdot \vec{r})^2 &= (\vec{r} \cdot \vec{p})^2 + (\vec{p} \cdot \vec{r})^2 + (\vec{r} \cdot \vec{p})(\vec{p} \cdot \vec{r}) + (\vec{p} \cdot \vec{r})(\vec{r} \cdot \vec{p}) \\ &= 2(\vec{r} \cdot \vec{p})(\vec{p} \cdot \vec{r}) + 2(\vec{p} \cdot \vec{r})(\vec{r} \cdot \vec{p}) + 3\mathrm{i}\hbar[(\vec{r} \cdot \vec{p}) - (\vec{p} \cdot \vec{r})] \\ &= 2(\vec{r}^2\vec{p}^2 + \vec{p}^2\vec{r}^2) - 4\vec{L}^2 - 9\hbar^2. \end{aligned} \tag{D.27}$$

From the first to the second line, we have used the canonical commutation relations leading to $(\vec{r} \cdot \vec{p})^2 = (\vec{r} \cdot \vec{p})(\vec{p} \cdot \vec{r}) + 3\mathrm{i}\hbar(\vec{r} \cdot \vec{p})$ and $(\vec{p} \cdot \vec{r})^2 = (\vec{p} \cdot \vec{r})(\vec{r} \cdot \vec{p}) - 3\mathrm{i}\hbar(\vec{p} \cdot \vec{r})$. From the second to the third line, we have taken advantage of the quadruple products giving $(\vec{r} \cdot \vec{p})(\vec{p} \cdot \vec{r}) = \vec{r}^2\vec{p}^2 - \vec{L}^2$ and $(\vec{p} \cdot \vec{r})(\vec{r} \cdot \vec{p}) = \vec{p}^2\vec{r}^2 - \vec{L}^2$. Therefore, the time-reversal invariant scalars are necessarily functions of $\vec{r}^2$, $\vec{p}^2$ and $\vec{L}^2$. In addition, they are invariant under the exchange of two nucleons and parity transformations, as well as obviously Hermitian. Thus, the spatial dependence of the interaction is expressed in terms of $\vec{r}^2$, $\vec{p}^2$ and $\vec{L}^2$, because of its symmetries, what we write down as, for $i \in \{0, 1\}$,

$$v^{(i)}(\vec{r}, \vec{p}) = v^{(i)}(\vec{r}^2, \vec{p}^2, \vec{L}^2), \tag{D.28}$$

the spin dependence having been treated above.

By bringing together the studies of the isospin, spin and space dependences, we can infer the general form the two-body nuclear interaction takes when all eight symmetries are reproduced, namely it can be formulated as

$$v_{12} = v^{00} + v^{10}(\vec{\sigma}_1 \cdot \vec{\sigma}_2) + v^{01}(\vec{\tau}_1 \cdot \vec{\tau}_2) + v^{11}(\vec{\sigma}_1 \cdot \vec{\sigma}_2)(\vec{\tau}_1 \cdot \vec{\tau}_2), \tag{D.29}$$

where

$$v^{ST} = \sum_{k=1}^{5} f_k^{ST}(\vec{r}^2, \vec{p}^2, \vec{L}^2) O_k, \quad \text{for } S, T \in \{0, 1\}, \tag{D.30}$$

with $f_k^{ST}(\vec{r}^2, \vec{p}^2, \vec{L}^2)$, functions of the scalars $\vec{r}^2$, $\vec{p}^2$ and $\vec{L}^2$ called form factors, and O_k

2. It is worth mentioning that the combinations $(\vec{r} \cdot \vec{p})^2$ and $(\vec{p} \cdot \vec{r})^2$ are not suitable as they are not time-reversal invariant, because $\vec{r}$ and $\vec{p}$ do not commute, and then the condition (D.26) is not fulfilled.

operators of one of the following forms,

$$O_k = \begin{cases} \mathbb{1} & \text{if } k=1, \\ \vec{L}\cdot\vec{S} & \text{if } k=2, \\ S_{12}(\hat{r}) \equiv (\vec{\sigma}_1\cdot\hat{r})(\vec{\sigma}_2\cdot\hat{r}) - \frac{1}{3}\vec{\sigma}_1\cdot\vec{\sigma}_2 & \text{if } k=3, \\ S_{12}(\hat{p}) \equiv (\vec{\sigma}_1\cdot\hat{p})(\vec{\sigma}_2\cdot\hat{p}) - \frac{1}{3}\vec{\sigma}_1\cdot\vec{\sigma}_2 & \text{if } k=4, \\ Q_{12} \equiv \frac{1}{2}\Big[(\vec{\sigma}_1\cdot\vec{L})(\vec{\sigma}_2\cdot\vec{L}) + (\vec{\sigma}_2\cdot\vec{L})(\vec{\sigma}_1\cdot\vec{L})\Big] & \text{if } k=5. \end{cases} \tag{D.31}$$

This is the most general expression of the realistic two-body nuclear interaction, obtained from the symmetries to be fulfilled, we have discussed at the beginning of the document.

3. The Gogny separable development

The Gogny separable development [175, 181] is a powerful tool that allows to separate the spatial degrees of freedom of a two-body potential, be it central or non-central, in any basis of the harmonic oscillator (HO). Schematically, the separable development reads

$$v(\vec{r}_1 - \vec{r}_2) \sim \sum_{r_\mu} \hat{\phi}_{r_\mu}(\vec{r}_1) f_{r_\mu}(\vec{r}_2), \tag{D.32}$$

where $v(\vec{r}_1 - \vec{r}_2)$ is the two-body potential (in this thesis, the generalized Gogny interaction (II.1)), r_μ the set of quantum numbers characterizing the spatial degrees of freedom in some HO basis (namely (B.1) in spherical symmetry, and (C.1) in axial symmetry), $\hat{\phi}_{r_\mu}(\vec{r}_1)$ the HO wave function deprived of its exponential factor (their radial part is given by (B.7) in spherical symmetry, and by (C.10) in axial symmetry), and $f_{r_\mu}(\vec{r}_2)$ some function of $\vec{r}_2$. Formally, the separable development stipulates that the potential and the development of the right-hand side part are equivalent in the sense that *their two-body matrix elements (TBMEs) evaluated in any basis of the harmonic oscillator are equal*, i.e.

$$\langle r_a r_b | v(\vec{r}_1 - \vec{r}_2) | r_c r_d \rangle = \sum_{r_\mu} \langle r_a r_b | \hat{\phi}_{r_\mu}(\vec{r}_1) f_{r_\mu}(\vec{r}_2) | r_c r_d \rangle. \tag{D.33}$$

Thus, the TBMEs of the potential in some HO basis can be written as a product of one-body matrix elements according to

$$\langle r_a r_b | v(\vec{r}_1 - \vec{r}_2) | r_c r_d \rangle = \sum_{r_\mu=1}^{m} \langle r_a | \hat{\phi}_{r_\mu}(\vec{r}_1) | r_c \rangle \langle r_b | f_{r_\mu}(\vec{r}_2) | r_d \rangle, \tag{D.34}$$

or, equivalently, by means of the symmetry under the exchange of the two particles (I.2),

$$\langle r_a r_b | v(\vec{r}_1 - \vec{r}_2) | r_c r_d \rangle = \sum_{r_\mu=1}^{m'} \langle r_a | f_{r_\mu}(\vec{r}_1) | r_c \rangle \langle r_b | \hat{\phi}_{r_\mu}(\vec{r}_2) | r_d \rangle, \tag{D.35}$$

where, in general, $m \neq m'$. These separations are very useful, both analytically and numerically. Analytically, they simplify the calculations by decorrelating the spatial coordinates of the two particles. Numerically, they allow to optimize the loops, especially when implementing fields (see appendix C), by reducing the number of time-demanding operations. Actually, the existence of such a development relies on the following property of the HO wave functions [181],

$$\boxed{\phi^*_{r_a}(\vec{r})\phi_{r_c}(\vec{r}) = \sum_{r_\mu} T^{r_\mu}_{r_a r_c} \phi_0(\vec{r})\phi_{r_\mu}(\vec{r}).} \tag{D.36}$$

As it is essential to demonstrate the separable development, this property itself is sometimes called, as we do in the thesis, the separable Gogny development. For the spherical and axial symmetries, the corresponding properties are given by (B.219) and (C.495), from which we can extract the value of the factor $T^{r_\mu}_{r_a r_c} \equiv \langle r_a|\hat{\phi}_{r_\mu}(\vec{r}_1)|r_c\rangle$, involving the so-called Talman coefficients. In the next subsections, we prove the Gogny separable development for central and non-central potentials.

3.1. Central potentials

Let us start with a central potential which, by definition, only depends on the relative distance between the two nucleons, $v(|\vec{r}_1 - \vec{r}_2|)$. Its TBMEs in some HO representation are

$$\langle r_a r_b|v(|\vec{r}_1 - \vec{r}_2|)|r_c r_d\rangle = \int \mathrm{d}^3 r_1 \int \mathrm{d}^3 r_2\, \phi^*_{r_a}(\vec{r}_1)\phi^*_{r_b}(\vec{r}_2) v(|\vec{r}_1 - \vec{r}_2|)\phi_{r_c}(\vec{r}_1)\phi_{r_d}(\vec{r}_2), \quad \text{(D.37)}$$

where ϕ denotes the HO wave function. Since the potential is central, it commutes with the wave functions; we can then apply the relation (D.36) to obtain

$$\begin{aligned}\langle r_a r_b|v(|\vec{r}_1 - \vec{r}_2|)|r_c r_d\rangle = &\sum_{r_\mu} T^{r_\mu}_{r_a r_c} \\ &\times \int \mathrm{d}^3 r_2\, \phi^*_{r_b}(\vec{r}_2) \int \mathrm{d}^3 r_1\, \phi_0(\vec{r}_1)\phi_{r_\mu}(\vec{r}_1) v(|\vec{r}_1 - \vec{r}_2|)\phi_{r_d}(\vec{r}_2).\end{aligned} \quad \text{(D.38)}$$

Defining the quantity

$$f_{r_\mu}(\vec{r}_2) \equiv \int \mathrm{d}^3 r_1\, \phi_0(\vec{r}_1)\phi_{r_\mu}(\vec{r}_1) v(|\vec{r}_1 - \vec{r}_2|), \quad \text{(D.39)}$$

we finally get the first form of the Gogny separable development (D.34). If instead of applying the relation (D.36) on the wave functions evaluated in $\vec{r}_1$, we apply it on the ones evaluated in $\vec{r}_2$, we equivalently end up with the second form of the Gogny separable development (D.35).

3.2. Non-central potentials

We continue with the non-central potentials, which, in the case of the generalized Gogny interaction (II.1) we are interested in, are summarized in the tensor and spin–orbit potentials.

The tensor potential can in fact be written in terms of a central potential as

$$v^{\mathrm{T}} \equiv v(|\vec{r}_1 - \vec{r}_2|)S_{12}, \quad \text{(D.40)}$$

where S_{12} is the tensor operator (II.9). But since the tensor operator commutes with the HO wave functions appearing in (D.37), it barely behaves like a central potential, and its separable development is immediately demonstrated, with

$$f_{r_\mu}(\vec{r}_2, \vec{\sigma}_1, \vec{\sigma}_2) \equiv \int \mathrm{d}^3 r_1\, \phi_0(\vec{r}_1)\phi_{r_\mu}(\vec{r}_1) v(|\vec{r}_1 - \vec{r}_2|)S_{12}. \quad \text{(D.41)}$$

Once again, applying the relation (D.36) on the wave functions evaluated in $\vec{r}_2$ would lead to the second form of the Gogny separable development (D.35).

The spin–orbit potential can also be written in terms of a central potential as

$$v^{\mathrm{SO}} \equiv v(|\vec{r}_1 - \vec{r}_2|)(\vec{r}_{12} \times \vec{\nabla}_{12}) \cdot \vec{S}, \quad \text{(D.42)}$$

where $\vec{S}$ is given by (II.3) and where we have freed ourselves from fractors to define the relative position $\vec{r}_{12} \equiv \vec{r}_1 - \vec{r}_2$ and the relative gradient $\vec{\nabla}_{12} \equiv \vec{\nabla}_1 - \vec{\nabla}_2$. Here the demonstration is a bit trickier as the non-central part of the spin–orbit potential does not commute with the HO wave functions because of the gradient operator. Separating the spatial from the spin degrees of freedom according to

$$\langle r_a r_b | v^{\mathrm{SO}} | r_c r_d \rangle = \langle r_a r_b | v(|\vec{r}_1 - \vec{r}_2|)(\vec{r}_{12} \times \vec{\nabla}_{12}) | r_c r_d \rangle \cdot \vec{S}, \tag{D.43}$$

we have,

$$\begin{aligned} &\langle r_a r_b | v(|\vec{r}_1 - \vec{r}_2|)(\vec{r}_{12} \times \vec{\nabla}_{12}) | r_c r_d \rangle = \\ &\quad \int \mathrm{d}^3 r_1 \int \mathrm{d}^3 r_2 \, \phi^*_{r_a}(\vec{r}_1) \phi^*_{r_b}(\vec{r}_2) v(|\vec{r}_1 - \vec{r}_2|)(\vec{r}_{12} \times \vec{\nabla}_{12}) \phi_{r_c}(\vec{r}_1) \phi_{r_d}(\vec{r}_2). \end{aligned} \tag{D.44}$$

Splitting the integral into two parts, we obtain

$$\begin{aligned} &\langle r_a r_b | v(|\vec{r}_1 - \vec{r}_2|)(\vec{r}_{12} \times \vec{\nabla}_{12}) | r_c r_d \rangle = \\ &\quad \int \mathrm{d}^3 r_1 \int \mathrm{d}^3 r_2 \, \phi^*_{r_a}(\vec{r}_1) \phi^*_{r_b}(\vec{r}_2) \phi_{r_d}(\vec{r}_2) v(|\vec{r}_1 - \vec{r}_2|)(\vec{r}_{12} \times \vec{\nabla}_1) \phi_{r_c}(\vec{r}_1) \\ &\quad - \int \mathrm{d}^3 r_1 \int \mathrm{d}^3 r_2 \, \phi^*_{r_a}(\vec{r}_1) \phi_{r_c}(\vec{r}_1) \phi^*_{r_b}(\vec{r}_2) v(|\vec{r}_1 - \vec{r}_2|)(\vec{r}_{12} \times \vec{\nabla}_2) \phi_{r_d}(\vec{r}_2). \end{aligned} \tag{D.45}$$

By virtue of the formula (D.36) applied on both parts, we find out

$$\begin{aligned} \langle r_a r_b | v(|\vec{r}_1 - \vec{r}_2|)(\vec{r}_{12} \times \vec{\nabla}_{12}) | r_c r_d \rangle = &\sum_{r_\mu} T^{r_\mu}_{r_b r_d} \langle r_a | \vec{f}_{r_\mu}(\vec{r}_1) | r_c \rangle \\ &- \sum_{r_\nu} T^{r_\nu}_{r_a r_c} \langle r_b | \vec{f}_{r_\nu}(\vec{r}_2) | r_d \rangle. \end{aligned} \tag{D.46}$$

where we have defined the vector quantities

$$\vec{f}_{r_\mu}(\vec{r}_1) \equiv \int \mathrm{d}^3 r_2 \, \phi_0(\vec{r}_2) \phi_{r_\mu}(\vec{r}_2) v(|\vec{r}_1 - \vec{r}_2|) \vec{r}_{12} \times \vec{\nabla}_1, \tag{D.47a}$$

$$\vec{f}_{r_\nu}(\vec{r}_2) \equiv \int \mathrm{d}^3 r_1 \, \phi_0(\vec{r}_1) \phi_{r_\nu}(\vec{r}_1) v(|\vec{r}_1 - \vec{r}_2|) \vec{r}_{12} \times \vec{\nabla}_2. \tag{D.47b}$$

Finally adding the spin part, it comes

$$\begin{aligned} \langle r_a r_b | v^{\mathrm{SO}} | r_c r_d \rangle = &\sum_{r_\mu} \langle r_b | \hat{\phi}_{r_\mu}(\vec{r}_2) | r_d \rangle \langle r_a | \vec{f}_{r_\mu}(\vec{r}_1) | r_c \rangle \cdot \vec{S} \\ &- \sum_{r_\nu} \langle r_a | \hat{\phi}_{r_\nu}(\vec{r}_1) | r_c \rangle \langle r_b | \vec{f}_{r_\nu}(\vec{r}_2) | r_d \rangle \cdot \vec{S}. \end{aligned} \tag{D.48}$$

Thus, each of the above parts of the spin–orbit potential can be decomposed into a product of a one-body matrix element in $\vec{r}_1$ and another one in $\vec{r}_2$. This is precisely the definition of the Gogny separable development (D.32), which separately holds for both parts. Note that we had no choice but to apply the formula (D.36) on the wave functions evaluated in $\vec{r}_2$ in the first integral, and on the ones evaluated in $\vec{r}_1$ in the second integral of (D.45). Therefore, contrary to the central and tensor potentials, we cannot decide to apply this formula on the wave functions depending on the other variables to get the second form of the separable development (D.35). To do so, we rather notice that the spin–orbit potential is symmetric under the exchange of variables $(\vec{r}_1, \vec{\sigma}_1) \leftrightarrow (\vec{r}_2, \vec{\sigma}_2)$.

4. Tensor interaction

4.1. Expression of the tensor operator

As expressed in the first part (II.9), the convention chosen for the tensor operator of the generalized Gogny interaction (II.1) is

$$S_{12} \equiv (\vec{\sigma}_1 \cdot \hat{r}_{12})(\vec{\sigma}_2 \cdot \hat{r}_{12}) - \frac{1}{3}\vec{\sigma}_1 \cdot \vec{\sigma}_2. \tag{D.49}$$

Another convention often adopted in the literature is the following,

$$\widetilde{S}_{12} = 3(\vec{\sigma}_1 \cdot \hat{r}_{12})(\vec{\sigma}_2 \cdot \hat{r}_{12}) - \vec{\sigma}_1 \cdot \vec{\sigma}_2, \tag{D.50}$$

which simply corresponds to the first one multiplied by a factor 3. Actually, these two conventions are equivalent, the only requirement being that the tensor operator is isotropic, i.e. that its integral over all directions vanishes, that is to say

$$\boxed{\int \mathrm{d}^2\hat{r}\, S_{12} \equiv \int \mathrm{d}^2\hat{r}\, \widetilde{S}_{12} = 0,} \tag{D.51}$$

where $\hat{r} = (\theta, \varphi)$.

Indeed, Oz being the quantization axis, we show that whatever the orientation of the spins of the nucleons (which are spin-1/2 particles, with either spin up or spin down), we find out the relation

$$(\vec{\sigma}_1 \cdot \hat{r}_{12})(\vec{\sigma}_2 \cdot \hat{r}_{12}) = \vec{\sigma}_1 \cdot \vec{\sigma}_2 \cos^2\theta, \tag{D.52}$$

where we make it clear that θ refers to the angle of the relative position between the two particles $\vec{r}_{12}$ and the axis Oz. Then,

$$\int \mathrm{d}^2\hat{r}\, S_{12} = \vec{\sigma}_1 \cdot \vec{\sigma}_2 \int_0^{2\pi} \mathrm{d}\varphi \int_0^{\pi} \mathrm{d}\theta \sin\theta \cos^2\theta - \frac{1}{3}\vec{\sigma}_1 \cdot \vec{\sigma}_2 \int \mathrm{d}^2\hat{r} = 0, \tag{D.53}$$

as expected. The outcome is obviously the same with the other convention (D.50).

4.2. The tensor operator is a tensor

In this subsection, we will answer the question: "Why is the tensor interaction called the tensor interaction?" (and it is not even a joke).

We shall write the tensor operator (D.49) in some specific way. Considering the components of the three-dimensional vectors $\hat{r}_{12}$, $\vec{\sigma}_1$ and $\vec{\sigma}_2$, we deduce

$$\begin{aligned}(\vec{\sigma}_1 \cdot \hat{r}_{12})(\vec{\sigma}_2 \cdot \hat{r}_{12}) &= \sum_{ij}^{3} \sigma_{1i}\sigma_{2j}\hat{r}_{12i}\hat{r}_{12j} \\ &= \frac{1}{2}\sum_{ij}^{3}(\sigma_{1i}\sigma_{2j} + \sigma_{1j}\sigma_{2i})\hat{r}_{12i}\hat{r}_{12j},\end{aligned} \tag{D.54}$$

where in the last equation we have symmetrized the right-hand side quantity with respect to the exchange of the indices 1 and 2. This step is crucial as it ensures that the tensor operator is invariant under the exchange of the two particles, which is one of the fundamental symmetries the nuclear interaction has to fulfil (see subsection I.1.2).

On the other hand, we notice that $\sum_i (\hat{r}_{12i})^2 = 1$ since $|\hat{r}_{12}| = 1$. Therefore,

$$\vec{\sigma}_1 \cdot \vec{\sigma}_2 = \sum_{ij}^{3} \vec{\sigma}_1 \cdot \vec{\sigma}_2 \delta_{ij} \hat{r}_{12i} \hat{r}_{12j}. \tag{D.55}$$

By merging the two previous results, we can write down the tensor operator (D.49) as

$$S_{12} = \sum_{ij} T_{ij} \hat{r}_{12i} \hat{r}_{12j}, \tag{D.56}$$

where T_{ij} is an irreducible tensor of rank 2, whose expression reads

$$T_{ij} = \frac{1}{2}\big(\sigma_{1i}\sigma_{2j} + \sigma_{1j}\sigma_{2i}\big) - \frac{\delta_{ij}}{3} \vec{\sigma}_1 \cdot \vec{\sigma}_2. \tag{D.57}$$

It is precisely because the tensor operator can be expressed in terms of a tensor, unlike the other terms of the nuclear interaction, that it is called the "tensor interaction".

4.3. Equivalent forms of the tensor operator

In this subsection, we want to show that the tensor operator (D.49) is strictly equivalent to the following forms involving tensors of rank 2,

$$\boxed{S_{12} = [\hat{r}_{12} \otimes \hat{r}_{12}]^{(2)} \cdot [\vec{\sigma}_1 \otimes \vec{\sigma}_2]^{(2)},} \tag{D.58}$$

and [3]

$$\boxed{S_{12} = \sqrt{5}\Big[[\hat{r}_{12} \otimes \hat{r}_{12}]^{(2)} \otimes [\vec{\sigma}_1 \otimes \vec{\sigma}_2]^{(2)}\Big]^{(0)},} \tag{D.59}$$

as well as tensors of rank 1,

$$\boxed{S_{12} = 2(\vec{S} \cdot \hat{r}_{12})^2 - \frac{2}{3}\vec{S}^2.} \tag{D.60}$$

Indeed, expanding the scalar product, using the coupling procedure between irreducible tensors and some symmetry properties of the Clebsch–Gordan coefficients, we successively obtain

$$\begin{aligned}
(\vec{\sigma}_1 \cdot \hat{r}_{12})(\vec{\sigma}_2 \cdot \hat{r}_{12}) &= \sum_{\mu_1\mu_2} (-)^{\mu_1+\mu_2} \hat{r}_{12}^{\mu_1} \hat{r}_{12}^{\mu_2} \sigma_1^{-\mu_1} \sigma_2^{-\mu_2} \\
&= \sum_{\mu_1\mu_2} (-)^{\mu_1+\mu_2} \sum_{\lambda\mu} \sum_{\lambda'\mu'} \langle 1\mu_1 1\mu_2 | \lambda\mu \rangle \langle 1\mu_1 1\mu_2 | \lambda' - \mu' \rangle [\hat{r}_{12} \otimes \hat{r}_{12}]^{(\lambda)}_{\mu} [\vec{\sigma}_1 \otimes \vec{\sigma}_2]^{(\lambda')}_{\mu'} \\
&= \sum_{\lambda\mu} \sum_{\lambda'\mu'} (-)^{\mu-\lambda'} \sum_{\mu_1\mu_2} \langle 1\mu_1 1\mu_2 | \lambda\mu \rangle \langle 1\mu_1 1\mu_2 | \lambda' - \mu' \rangle [\hat{r}_{12} \otimes \hat{r}_{12}]^{(\lambda)}_{\mu} [\vec{\sigma}_1 \otimes \vec{\sigma}_2]^{(\lambda')}_{\mu'} \\
&= \sum_{\lambda\mu} \sum_{\lambda'\mu'} (-)^{\mu-\lambda} \delta_{\lambda\lambda'} \delta_{\mu,-\mu'} [\hat{r}_{12} \otimes \hat{r}_{12}]^{(\lambda)}_{\mu} [\vec{\sigma}_1 \otimes \vec{\sigma}_2]^{(\lambda')}_{\mu'} \\
&= \sum_{\lambda\mu} (-)^{\mu-\lambda} [\hat{r}_{12} \otimes \hat{r}_{12}]^{(\lambda)}_{\mu} [\vec{\sigma}_1 \otimes \vec{\sigma}_2]^{(\lambda)}_{-\mu}.
\end{aligned} \tag{D.61}$$

3. This is the form adopted by Gogny in his article about the separable development [181].

Because of the invariance of the quantity $[\hat{r}_{12} \otimes \hat{r}_{12}]^{(\lambda)}_{\mu}$ under the exchange of the $\hat{r}_{12}$, we can write, using the coupling procedure,

$$[\hat{r}_{12} \otimes \hat{r}_{12}]^{(\lambda)}_{\mu} = \sum_{\mu_1\mu_2} \langle 1\mu_1 1\mu_2|\lambda\mu\rangle \hat{r}^{\mu_1}_{12}\hat{r}^{\mu_2}_{12}, \tag{D.62a}$$

$$= \sum_{\mu_1\mu_2} \langle 1\mu_2 1\mu_1|\lambda\mu\rangle \hat{r}^{\mu_1}_{12}\hat{r}^{\mu_2}_{12}. \tag{D.62b}$$

On the other hand, the symmetry properties of the Clebsch–Gordan coefficients provide

$$\langle 1\mu_1 1\mu_2|\lambda\mu\rangle = (-)^{\lambda}\langle 1\mu_2 1\mu_1|\lambda\mu\rangle. \tag{D.63}$$

Thus, the only way the equations (D.62) can be true without $[\hat{r}_{12} \otimes \hat{r}_{12}]^{(\lambda)}_{\mu}$ being zero is if $\lambda = 0$ or $\lambda = 2$. When $\lambda = 0$, we get the following contribution from equation (D.61),

$$\begin{aligned}[\hat{r}_{12} \otimes \hat{r}_{12}]^{(0)}_{0}[\vec{\sigma}_1 \otimes \vec{\sigma}_2]^{(0)}_{0} &= \sum_{\mu_1\mu_2} \langle 1\mu_1 1\mu_2|00\rangle \hat{r}^{\mu_1}_{12}\hat{r}^{\mu_2}_{12} \sum_{\nu_1\nu_2} \langle 1\nu_1 1\nu_2|00\rangle \sigma_1^{\nu_1}\sigma_2^{\nu_2} \\ &= \frac{1}{3}\Big(\sum_{\mu}(-)^{\mu}\hat{r}^{\mu}_{12}\hat{r}^{-\mu}_{12}\Big)\Big(\sum_{\nu}(-)^{\nu}\sigma_1^{\nu}\sigma_2^{-\nu}\Big) \\ &= \frac{1}{3}(\hat{r}_{12}\cdot\hat{r}_{12})(\vec{\sigma}_1\cdot\vec{\sigma}_2) = \frac{1}{3}\vec{\sigma}_1\cdot\vec{\sigma}_2. \end{aligned} \tag{D.64}$$

This last term compensates the second right-hand side term of the form (D.49). When $\lambda = 2$, we get, by definition of the scalar product in the spherical basis,

$$\sum_{\mu}(-)^{\mu}[\hat{r}_{12} \otimes \hat{r}_{12}]^{(2)}_{\mu}[\vec{\sigma}_1 \otimes \vec{\sigma}_2]^{(2)}_{-\mu} \equiv [\hat{r}_{12} \otimes \hat{r}_{12}]^{(2)} \cdot [\vec{\sigma}_1 \otimes \vec{\sigma}_2]^{(2)}. \tag{D.65}$$

Therefore, combining this result with (D.61) and (D.64), we end up with the first equivalent form of the tensor operator (D.58). If, instead, we use the coupling procedure when $\lambda = 2$, we get the following contribution from equation (D.61),

$$\begin{aligned}\sum_{\mu}(-)^{\mu}[\hat{r}_{12} \otimes \hat{r}_{12}]^{(2)}_{\mu}[\vec{\sigma}_1 \otimes \vec{\sigma}_2]^{(2)}_{-\mu} &= \sum_{\mu}(-)^{\mu}\sum_{\lambda'\mu'}\langle 2\mu 2 - \mu|\lambda'\mu'\rangle \Big[[\hat{r}_{12} \otimes \hat{r}_{12}]^{(2)} \otimes [\vec{\sigma}_1 \otimes \vec{\sigma}_2]^{(2)}\Big]^{(\lambda')}_{\mu'} \\ &= \sum_{\lambda'} \underbrace{\sum_{\mu}(-)^{\mu}\langle 2\mu 2 - \mu|\lambda' 0\rangle}_{\sqrt{5}\delta_{\lambda',0}} \Big[[\hat{r}_{12} \otimes \hat{r}_{12}]^{(2)} \otimes [\vec{\sigma}_1 \otimes \vec{\sigma}_2]^{(2)}\Big]^{(\lambda')}_{0} \\ &= \sqrt{5}\Big[[\hat{r}_{12} \otimes \hat{r}_{12}]^{(2)} \otimes [\vec{\sigma}_1 \otimes \vec{\sigma}_2]^{(2)}\Big]^{(0)}. \end{aligned} \tag{D.66}$$

Thus, combining this result with (D.61) and (D.64), we end up with the second equivalent form of the tensor operator (D.59).

The third equivalent form of the tensor operator is deduced from (D.49), noticing that we find out, on one side,

$$\vec{\sigma}_1\cdot\vec{\sigma}_2 = 2\vec{S}^2 - 3\mathbb{1}, \tag{D.67}$$

by combining relations (D.8) and (D.10a), and, on the other side,

$$\begin{aligned} 2(\vec{S}\cdot\hat{r}_{12})^2 &= \frac{1}{2}\Big[(\vec{\sigma}_1+\vec{\sigma}_2)\cdot\hat{r}_{12}\Big]^2 \\ &= \frac{1}{2}\Big[(\vec{\sigma}_1\cdot\hat{r}_{12})^2 + (\vec{\sigma}_2\cdot\hat{r}_{12})^2 + 2(\vec{\sigma}_1\cdot\hat{r}_{12})(\vec{\sigma}_2\cdot\hat{r}_{12})\Big] \\ &= \mathbb{1} + (\vec{\sigma}_1\cdot\hat{r}_{12})(\vec{\sigma}_2\cdot\hat{r}_{12}), \end{aligned} \tag{D.68}$$

by considering the identities (II.3) and (D.5).

5. Spin–orbit interaction

5.1. The spin–orbit interaction at the zero-range limit

In this subsection, we determine the expression the coefficient $B(\mu)$ below must take so that, we recover, from the finite-range spin–orbit term we consider in the generalized Gogny interaction (II.1), i.e.

$$v_{12}^{\mathrm{SO}} = B(\mu)(W - HP_\tau)V(r_{12},\mu)\vec{L}\cdot\vec{S}, \tag{D.69}$$

the exact zero-range spin–orbit term of the original Gogny interaction at the zero-range limit, that is

$$\frac{\mathrm{i}}{4}W_0\Big[\big(\overleftarrow{\nabla}_1 - \overleftarrow{\nabla}_2\big)\delta(\vec{r}_1-\vec{r}_2)\times\big(\vec{\nabla}_1-\vec{\nabla}_2\big)\Big]\cdot(\vec{\sigma}_1+\vec{\sigma}_2), \tag{D.70}$$

where $V(r_{12},\mu)$ is the Gaussian potential given by (II.2), with the dependence on the range μ specified for clarity. We also recall that here the symbol $\times$ denotes the cross product. Actually, in the following calculations, we will restrict ourselves to the particular case of a Gaussian potential only at the end. Indeed, we will treat a more general potential, whose only requirement will be to verify the equation (D.72).

First, the definitions (II.3)–(II.6) of the quantities appearing in the spin–orbit interaction (D.69) allows us to rewrite it as

$$v_{12}^{\mathrm{SO}} = -\frac{\mathrm{i}}{4}B(\mu)(W-HP_\tau)V(r_{12},\mu)\Big[\vec{r}_{12}\times\vec{\nabla}_{12}\Big]\cdot(\vec{\sigma}_1+\vec{\sigma}_2), \tag{D.71}$$

where we have defined the relative gradient $\vec{\nabla}_{12}\equiv\vec{\nabla}_1-\vec{\nabla}_2$. Now, let us consider a potential $V(r_{12},\mu)$ from which we can find a function $G(r_{12},\mu)$ satisfying

$$\vec{\nabla}_{12}G(r_{12},\mu) = V(r_{12},\mu)\vec{r}_{12}. \tag{D.72}$$

In the particular case of a Gaussian potential, we have (up to some constant), [4]

$$G(r_{12},\mu) = -\frac{\mu^2}{4}\mathrm{e}^{-(\vec{r}_1-\vec{r}_2)^2/\mu^2}. \tag{D.73}$$

The expression (D.71) then becomes

$$v_{12}^{\mathrm{SO}} = -\frac{\mathrm{i}}{4}B(\mu)(W-HP_\tau)\Big[\vec{\nabla}_{12}G(r_{12},\mu)\times\vec{\nabla}_{12}\Big]\cdot(\vec{\sigma}_1+\vec{\sigma}_2). \tag{D.74}$$

Let us now consider the spatial two-body matrix element of the above expression in some basis, such as encountered in the document. By definition,

$$\begin{aligned}\langle r_a r_b|\vec{\nabla}_{12}G(r_{12},\mu)\times\vec{\nabla}_{12}|r_c r_d\rangle \equiv \int \mathrm{d}^3r_1\int\mathrm{d}^3r_2\,\phi^*_{r_a}(\vec{r}_1)\phi^*_{r_b}(\vec{r}_2)\\ \times\big(\vec{\nabla}_1-\vec{\nabla}_2\big)G(r_{12},\mu)\times\big(\vec{\nabla}_1-\vec{\nabla}_2\big)\phi_{r_c}(\vec{r}_1)\phi_{r_d}(\vec{r}_2).\end{aligned} \tag{D.75}$$

The product rule provides

$$\begin{aligned}&\langle r_a r_b|\vec{\nabla}_{12}G(r_{12},\mu)\times\vec{\nabla}_{12}|r_c r_d\rangle = \\ &\int\mathrm{d}^3r_1\int\mathrm{d}^3r_2\,\Big[\phi^*_{r_b}(\vec{r}_2)\vec{\nabla}_1\big(\phi^*_{r_a}(\vec{r}_1)G(r_{12},\mu)\big)-\phi^*_{r_a}(\vec{r}_1)\vec{\nabla}_2\big(\phi^*_{r_b}(\vec{r}_2)G(r_{12},\mu)\big)\Big]\\ &\qquad\times\big(\vec{\nabla}_1-\vec{\nabla}_2\big)\phi_{r_c}(\vec{r}_1)\phi_{r_d}(\vec{r}_2)\\ &-\int\mathrm{d}^3r_1\int\mathrm{d}^3r_2\,\Big[\phi^*_{r_b}(\vec{r}_2)G(r_{12},\mu)\vec{\nabla}_1\phi^*_{r_a}(\vec{r}_1)-\phi^*_{r_a}(\vec{r}_1)G(r_{12},\mu)\vec{\nabla}_2\phi^*_{r_b}(\vec{r}_2)\Big]\\ &\qquad\times\big(\vec{\nabla}_1-\vec{\nabla}_2\big)\phi_{r_c}(\vec{r}_1)\phi_{r_d}(\vec{r}_2).\end{aligned} \tag{D.76}$$

4. Watch out, $\vec{\nabla}_{12}\neq\vec{\nabla}_{r_{12}}$, where $\vec{\nabla}_{r_{12}}$ denotes the derivative with respect to r_{12}.

From the first right-hand side term, we can extract the following quantity, that we transform using the identity $\vec{\nabla} \times (\varphi \vec{A}) = \varphi \vec{\nabla} \times \vec{A} + (\vec{\nabla}\varphi) \times \vec{A}$, where φ and $\vec{A}$ are scalar and vector fields respectively, and the fact that the curl of a gradient acting on a scalar field is zero, i.e. $\vec{\nabla} \times \vec{\nabla}\varphi = 0$,

$$\begin{aligned} &\int \mathrm{d}^3 r_1 \int \mathrm{d}^3 r_2 \, \phi^*_{r_b}(\vec{r}_2) \vec{\nabla}_1 \Big(\phi^*_{r_a}(\vec{r}_1) G(r_{12}, \mu) \Big) \times \vec{\nabla}_1 \phi_{r_c}(\vec{r}_1) \phi_{r_d}(\vec{r}_2) \\ &\quad = \int \mathrm{d}^3 r_2 \, \phi^*_{r_b}(\vec{r}_2) \phi_{r_d}(\vec{r}_2) \int \mathrm{d}^3 r_1 \, \vec{\nabla}_1 \times \Big(\phi^*_{r_a}(\vec{r}_1) G(r_{12}, \mu) \vec{\nabla}_1 \phi_{r_c}(\vec{r}_1) \Big). \end{aligned} \tag{D.77}$$

Stokes' theorem allows to express the last volume integral as a surface integral, as

$$\begin{aligned} &\int_{\mathbb{R}^3} \mathrm{d}^3 r_1 \, \vec{\nabla}_1 \times \Big(\phi^*_{r_a}(\vec{r}_1) G(r_{12}, \mu) \vec{\nabla}_1 \phi_{r_c}(\vec{r}_1) \Big) \\ &\qquad = \int_{\partial \mathbb{R}^3} \mathrm{d}^2 r_1 \cdot \Big(\phi^*_{r_a}(\vec{r}_1) G(r_{12}, \mu) \vec{\nabla}_1 \phi_{r_c}(\vec{r}_1) \Big). \end{aligned} \tag{D.78}$$

The surface integral is zero provided that its integrand goes sufficiently rapidly to zero when $|\vec{r}_1| \to \infty$ (with $\vec{r}_2$ fixed). This is the case considering the behavior of harmonic oscillator wave functions and of the quantity $G(r_{12}, \mu)$ at infinity. Note that the conclusion is the same with the other three contributions coming from the first right-hand side term of (D.76), so that this term is zero. As for the second right-hand side term, it can be rewritten in such a way that

$$\begin{aligned} &\langle r_a r_b | \vec{\nabla}_{12} G(r_{12}, \mu) \times \vec{\nabla}_{12} | r_c r_d \rangle = \\ &\quad - \int \mathrm{d}^3 r_1 \int \mathrm{d}^3 r_2 \, \phi^*_{r_a}(\vec{r}_1) \phi^*_{r_b}(\vec{r}_2) \Big(\overleftarrow{\nabla}_1 - \overleftarrow{\nabla}_2 \Big) G(r_{12}, \mu) \times \Big(\vec{\nabla}_1 - \vec{\nabla}_2 \Big) \phi_{r_c}(\vec{r}_1) \phi_{r_d}(\vec{r}_2) \\ &\equiv - \langle r_a r_b | \overleftarrow{\nabla}_{12} G(r_{12}, \mu) \times \vec{\nabla}_{12} | r_c r_d \rangle. \end{aligned} \tag{D.79}$$

Since this equality holds in any basis, the finite-range spin–orbit interaction (D.74) has the equivalent writing

$$v_{12}^{\mathrm{SO}} = \frac{\mathrm{i}}{4} B(\mu)(W - HP_\tau) \Big[\overleftarrow{\nabla}_{12} G(r_{12}, \mu) \times \vec{\nabla}_{12} \Big] \cdot (\vec{\sigma}_1 + \vec{\sigma}_2). \tag{D.80}$$

Now that we have a finite-range spin–orbit term that looks like its zero-range counterpart (D.70), we can identify them at the zero-range limit. We are then looking for the expression of $B(\mu)$ so that the equality

$$\lim_{\mu \to 0} \frac{\mathrm{i}}{4} B(\mu) W \Big[\overleftarrow{\nabla}_{12} G(r_{12}, \mu) \times \vec{\nabla}_{12} \Big] \cdot (\vec{\sigma}_1 + \vec{\sigma}_2) = \frac{\mathrm{i}}{4} W_0 \Big[\overleftarrow{\nabla}_{12} \delta(\vec{r}_1 - \vec{r}_2) \times \vec{\nabla}_{12} \Big] \cdot (\vec{\sigma}_1 + \vec{\sigma}_2) \tag{D.81}$$

is true. Note that we have set the parameter $H = 0$ at the zero-range limit since we know the zero-range spin–orbit term of the original Gogny interaction to contribution only to the $(S = 1, T = 1)$ channel of the interaction. As we are only interested, at this point, in the analytical form the finite-range spin–orbit term has to take and not in the particular values of its parameters, we can also set $W = W_0$. The equation above therefore reduces to

$$\lim_{\mu \to 0} B(\mu) G(r_{12}, \mu) = \delta(\vec{r}_1 - \vec{r}_2). \tag{D.82}$$

Integrating this equality and simplifying the left-hand side by means of an integration by parts, we find that we must eventually have

$$\boxed{\lim_{\mu \to 0} -\frac{2\pi}{3} B(\mu) \int_0^\infty \mathrm{d}r_{12} \, r_{12}^4 V(r_{12}, \mu) = 1.} \tag{D.83}$$

This is an equivalent writing of what Brink and Vautherin found out to recover the expression of the zero-range spin–orbit force of the Skyrme interaction [106]. This is reassuring, since the spin–orbit force is the same for both original Skyrme and Gogny interactions. For a Gaussian potential $V(r_{12})$ such as (II.2), the integration provides

$$\boxed{B(\mu) = -\frac{4}{\mu^2}\frac{1}{(\mu\sqrt{\pi})^3}.} \tag{D.84}$$

It is therefore this expression of the coefficient $B(\mu)$ that we consider in the finite-range spin–orbit term of the generalized Gogny interaction (II.1). We know this coefficient to be correct as we have recovered, using it, both the exact zero-range spherical spin–orbit matrix elements and axial spin–orbit fields of Appendices B and C, at the zero-range limit.

5.2. Equivalent forms of the spin–orbit operator

In this subsection, we want to show that the spin–orbit operator $\vec{L}\cdot\vec{S}$ is strictly equivalent to the following forms involving tensors of rank 1,

$$\boxed{\vec{L}\cdot\vec{S} = -\frac{1}{2\sqrt{2}}[\vec{r}_{12}\otimes\vec{\nabla}_{12}]^{(1)}\cdot[\vec{\sigma}_1+\vec{\sigma}_2]^{(1)},} \tag{D.85}$$

and

$$\boxed{\vec{L}\cdot\vec{S} = \sqrt{\frac{3}{2}}\Big[[\vec{r}_{12}\otimes\vec{\nabla}_{12}]^{(1)}\otimes[\vec{\sigma}_1+\vec{\sigma}_2]^{(1)}\Big]^{(0)}.} \tag{D.86}$$

Indeed, using the definitions (II.3)–(II.5) of the $\vec{L}$, $\vec{S}$ and $\vec{p}_{12}$ operators, we obtain

$$\vec{L}\cdot\vec{S} = -\frac{\mathrm{i}}{4}(\vec{r}_{12}\times\vec{\nabla}_{12})\cdot(\vec{\sigma}_1+\vec{\sigma}_2), \tag{D.87}$$

where we recall that the symbol $\times$ refers to the cross product between two vectors. Those two vectors can equivalently be seen as tensors of rank 1. Accordingly, we can define their tensor product, symbolized by $\otimes$, from their cross product according to

$$[\vec{r}_{12}\otimes\vec{\nabla}_{12}]^{(1)} = \frac{\mathrm{i}}{\sqrt{2}}\vec{r}_{12}\times\vec{\nabla}_{12}, \tag{D.88}$$

where the notation $[]^{(1)}$ states that we are dealing with a tensor of rank 1. This formula can easily be demonstrated by expliciting, for example, the components of each of the quantities in the spherical basis, and showing that they are all equal. As for the quantity $(\vec{\sigma}_1+\vec{\sigma}_2)$, it is a vector, and then also a tensor of rank 1 that we denote as $[\vec{\sigma}_1+\vec{\sigma}_2]^{(1)}$ from now on. Then, combining the two last identities, we end up with the first equivalent form of the spin–orbit operator (D.85).

Now, starting from the first equivalent form and following the procedure that led to (D.66) for the tensor operator, i.e. using the coupling procedure between irreducible

tensors and some properties of the Clebsch–Gordan coefficients, we end up with

$$\begin{aligned}
\vec{L}\cdot\vec{S} &= -\frac{1}{\sqrt{2}}\sum_{\mu}(-)^{\mu}[\vec{r}_{12}\otimes\vec{\nabla}_{12}]^{(1)}_{\mu}[\vec{\sigma}_1+\vec{\sigma}_2]^{(1)}_{-\mu} \\
&= -\frac{1}{\sqrt{2}}\sum_{\mu}(-)^{\mu}\sum_{\lambda'\mu'}\langle 1\mu 1-\mu|\lambda'\mu'\rangle\Big[[\vec{r}_{12}\otimes\vec{\nabla}_{12}]^{(1)}\otimes[\vec{\sigma}_1+\vec{\sigma}_2]^{(1)}\Big]^{(\lambda')}_{\mu'} \\
&= -\frac{1}{\sqrt{2}}\sum_{\lambda'}\underbrace{\sum_{\mu}(-)^{\mu}\langle 1\mu 1-\mu|\lambda' 0\rangle}_{-\sqrt{3}\delta_{\lambda',0}}\Big[[\vec{r}_{12}\otimes\vec{\nabla}_{12}]^{(1)}\otimes[\vec{\sigma}_1+\vec{\sigma}_2]^{(1)}\Big]^{(\lambda')}_{0} \\
&= \sqrt{\frac{3}{2}}\Big[[\vec{r}_{12}\otimes\vec{\nabla}_{12}]^{(1)}\otimes[\vec{\sigma}_1+\vec{\sigma}_2]^{(1)}\Big]^{(0)},
\end{aligned} \tag{D.89}$$

which is the second equivalent form of the spin–orbit operator (D.86) we wanted to reach.

6. Commutation relations

When constructing the two-body nuclear interaction (see subsection I.1.2), we learnt that the different terms involved in the generalized Gogny interaction (II.1) commute with the total angular momentum $\vec{J}\equiv\vec{L}+\vec{S}$. This means that the interaction is a scalar in the (coordinate plus spin) space, i.e. it is invariant under a full rotation, in both coordinate and spin spaces. In this section, we examine whether those terms are also invariant under separate rotations in coordinate and spin spaces, i.e. if they commute with the angular $\vec{L}$ and intrinsic $\vec{S}$ momenta.

6.1. Central and density-dependent interactions

By definition, a central term is invariant under any rotation in the coordinate space. This is confirmed by the obvious commutation relations $[P_\sigma,\vec{L}]=[P_\tau,\vec{L}]=0$. Since the central terms also commute with the total momentum $\vec{J}=\vec{L}+\vec{S}$, they then commute with the intrinsic momentum $\vec{S}$, i.e. they are invariant under any rotation in the spin space. Alternatively, we show that $[P_\sigma,\vec{S}]=[P_\tau,\vec{S}]=0$ since $P_\sigma=\vec{S}^2-\mathbb{1}$.

The functional of the density (A.36) does not change these relations so that they remain true for the density-dependent interaction.

6.2. Tensor interaction

By definition, the tensor force is a non-central interaction. It is therefore expected not to commute with the angular momentum $\vec{L}$. Let us show it explicitly with the equivalent form (D.58) of the tensor operator. We are particularly interested in proving it for the component L_z since the quantization axis is chosen to be Oz (and then the conservation laws of the quantum numbers associated with the spin projections are written on this

axis). For the component L_z, we find out

$$\begin{aligned}
[S_{12}, L_z] &= 2[(\vec{S}\cdot\hat{r}_{12})(\vec{S}\cdot\hat{r}_{12}), L_z] \\
&= 2\Big((\vec{S}\cdot\hat{r}_{12})[\vec{S}\cdot\hat{r}_{12}, L_z] + [\vec{S}\cdot\hat{r}_{12}, L_z]\,(\vec{S}\cdot\hat{r}_{12})\Big) \\
&= 4(\vec{S}\cdot\hat{r}_{12})[\vec{S}\cdot\hat{r}_{12}, L_z] \\
&= 4(\vec{S}\cdot\hat{r}_{12})\sum_i S_i[\hat{r}_{12i}, L_z] \\
&= 4\mathrm{i}\hbar(\vec{S}\cdot\hat{r}_{12})\sum_{ij}\epsilon_{izj}S_i\hat{r}_{12j} \\
&= -4\mathrm{i}\hbar(\vec{S}\cdot\hat{r}_{12})(\vec{S}\times\hat{r}_{12})_z \neq 0,
\end{aligned} \tag{D.90}$$

where we have benefited from the usual canonical commutation relations, leading to the z component $(\vec{S}\times\hat{r}_{12})_z$, which has been expressed in terms of the Levi-Civita symbol ϵ_{izj}. Note that from the second to the third line, we have pretended that the operator $\vec{S}\cdot\hat{r}_{12}$ commutes with $[\vec{S}\cdot\hat{r}_{12}, L_z]$ (or with $(\vec{S}\times\hat{r}_{12})_z$, according to what we have just shown). As this is not trivial, let us show it explicitly,

$$\begin{aligned}
[(\vec{S}\cdot\hat{r}_{12}), (\vec{S}\times\hat{r}_{12})_z] &= \sum_{ijk}\epsilon_{zij}[S_k\hat{r}_{12k}, S_i\hat{r}_{12j}] \\
&= \sum_{ijk}\epsilon_{zij}[S_k, S_i]\,\hat{r}_{12j}\hat{r}_{12k} \\
&= \mathrm{i}\hbar\sum_{ijkl}\epsilon_{zji}\epsilon_{kli}S_l\hat{r}_{12j}\hat{r}_{12k} \\
&= \mathrm{i}\hbar\sum_{jkl}\Big(S_l\hat{r}_{12j}\hat{r}_{12k}\delta_{zk}\delta_{jl} - S_l\hat{r}_{12j}\hat{r}_{12k}\delta_{zl}\delta_{jk}\Big) \\
&= \mathrm{i}\hbar\sum_j[S_j, \hat{r}_{12z}]\,\hat{r}_{12j} = 0.
\end{aligned} \tag{D.91}$$

We obtain analogous results for the other components L_x and L_y. It appears that the tensor interaction does not commute with $\vec{L}$, i.e. it is not invariant under a rotation in the coordinate space. As it commutes, however, with the total angular momentum $\vec{J} = \vec{L} + \vec{S}$, we must have $[S_{12}, \vec{S}] = -[S_{12}, \vec{L}]$, in such a way that the tensor interaction does not commute with the intrinsic momentum $\vec{S}$ either, i.e. it is not invariant under a rotation in the spin space. Let us check this out; in particular for the component S_z, for the same reason given above. Following the same steps, we get

$$\begin{aligned}
[S_{12}, S_z] &= 4(\vec{S}\cdot\hat{r}_{12})\sum_i[S_i, S_z]\,\hat{r}_{12i} \\
&= 4\mathrm{i}\hbar(\vec{S}\cdot\hat{r}_{12})\sum_{ij}\epsilon_{izj}S_j\hat{r}_{12i} \\
&= 4\mathrm{i}\hbar(\vec{S}\cdot\hat{r}_{12})(\vec{S}\times\hat{r}_{12})_z \neq 0,
\end{aligned} \tag{D.92}$$

where we have used (D.91) again, as $(\vec{S}\times\hat{r}_{12})_z = \mathrm{i}\hbar[\vec{S}\cdot\hat{r}_{12}, L_z]$, and the usual canonical commutation relations. We then consistently get $[S_{12}, S_z] = -[S_{12}, L_z]$, and analogous relations for the other components S_x and S_y.

6.3. Spin–orbit interaction

The spin–orbit interaction being a non-central force as well, the conclusions are the same as for the tensor interaction. It does not commute with either $\vec{L}$ or $\vec{S}$, i.e. it is

not invariant under separate rotations in coordinate and spin spaces. Formally, for the component L_z, we find out

$$\begin{aligned}[\vec{L}\cdot\vec{S}, L_z] &= \sum_i [L_i S_i, L_z] \\ &= \mathrm{i}\hbar \sum_{ij} \epsilon_{izj} L_j S_i \\ &= \mathrm{i}\hbar (\vec{L}\times\vec{S})_z \neq 0, \end{aligned} \tag{D.93}$$

where we have used the same relations as in the previous subsection. We obtain analogous results for the other components L_x and L_y. For the component S_z, we get

$$\begin{aligned}[\vec{L}\cdot\vec{S}, S_z] &= \sum_i [L_i S_i, S_z] \\ &= \mathrm{i}\hbar \sum_{ij} \epsilon_{izj} L_i S_j \\ &= -\mathrm{i}\hbar (\vec{L}\times\vec{S})_z \neq 0, \end{aligned} \tag{D.94}$$

where we have used the same relations as in the previous subsection again. We then consistently get $[\vec{L}\cdot\vec{S}, S_z] = -[\vec{L}\cdot\vec{S}, L_z]$, and analogous relations for the other components S_x and S_y.

7. Mathematical stuff

In this section, we give some definitions and properties of the functions, polynomials, series expansions and integrals used in the calculations. Our aim is to facilitate the reader's task of verifying the analytical developments by providing only the material used in this thesis, with the chosen conventions. The equations are mainly extracted from [240, 241].

7.1. Functions, polynomials and series expansions

The Heaviside step function is defined as

$$\Theta(x) \equiv \begin{cases} 1 & \text{if } x \geq 0, \\ 0 & \text{if } x < 0. \end{cases} \tag{D.95}$$

The error function is defined, for $x \in \mathbb{R}$, as

$$\mathrm{erf}(x) \equiv \frac{2}{\sqrt{\pi}} \int_0^x \mathrm{d}t\ \mathrm{e}^{-t^2}. \tag{D.96}$$

The series expansion of the error function, for $x \in \mathbb{C}$, is

$$\mathrm{erf}(x) = \frac{2}{\sqrt{\pi}} \sum_{n=0}^{\infty} \frac{(-)^n x^{2n+1}}{(2n+1)n!}. \tag{D.97}$$

The series expansion of the Hermite polynomial, for $x \in \mathbb{R}$, reads

$$H_n(x) = n! \sum_{i=0}^{\lfloor n/2 \rfloor} \frac{(-)^i (2x)^{n-2i}}{i!(n-2i)!}, \quad \text{with } n \in \mathbb{N}, \tag{D.98}$$

where $\lfloor\rfloor$ denotes the floor function.
The Hermite polynomials verify the recurrence relations

$$H_{n+1}(x) = 2xH_n(x) - 2nH_{n-1}(x), \tag{D.99a}$$
$$H'_n(x) = 2nH_{n-1}(x), \tag{D.99b}$$
$$H''_n(x) = 2xH'_n(x) - 2nH_n(x), \tag{D.99c}$$

where the prime stands for the derivative operation.
The series expansion of the generalized Laguerre polynomial, for $x \in \mathbb{R}$, is given by

$$L_n^\alpha(x) = \Gamma(n+\alpha+1)\sum_{i=0}^{n}\frac{(-)^i x^i}{i!(n-i)!\Gamma(i+\alpha+1)}, \quad \text{with } n \in \mathbb{N} \text{ and } \alpha \in \mathbb{R}, \tag{D.100}$$

where Γ is the so-called gamma function, defined, for $x \in \mathbb{R}$, as

$$\Gamma(x) \equiv \int_0^\infty \mathrm{d}t\, t^{x-1}\mathrm{e}^{-x}. \tag{D.101}$$

The generalized Laguerre polynomials verify the recurrence relations

$$L_n^\alpha(x) = L_n^{\alpha+1}(x) - L_{n-1}^{\alpha+1}(x), \tag{D.102a}$$
$$xL_n^{\alpha+1}(x) = (n+\alpha+1)L_n^\alpha(x) - (n+1)L_{n+1}^\alpha(x), \tag{D.102b}$$
$$nL_n^\alpha(x) = (2n+\alpha-x-1)L_{n-1}^\alpha(x) - (n+\alpha-1)L_{n-2}^\alpha(x), \tag{D.102c}$$
$$L_n^{\alpha\,\prime}(x) = -L_{n-1}^{\alpha+1}(x), \tag{D.102d}$$
$$xL_n^{\alpha\,\prime}(x) = nL_n^\alpha(x) - (n+\alpha)L_{n-1}^\alpha(x), \tag{D.102e}$$
$$xL_n^{\alpha\,\prime\prime}(x) = (x-\alpha-1)L_n^{\alpha\,\prime}(x) - nL_n^\alpha(x). \tag{D.102f}$$

The generalized Laguerre polynomials are related to the confluent hypergeometric function by the formula

$$L_n^\alpha(x) = \frac{\Gamma(n+\alpha+1)}{\Gamma(\alpha+1)n!}\,{}_1F_1(-n;\alpha+1;x), \tag{D.103}$$

where the confluent hypergeometric function is a generalized hypergeometric series given by

$${}_1F_1(a;b;x) = \sum_{n=0}^{\infty}\frac{a^{(n)}x^n}{b^{(n)}n!}, \tag{D.104}$$

where $a^{(n)} \equiv a(a+1)\dots(a+n-1)$ denotes the rising factorial.
One series expansion of the Legendre polynomial, for $-1 \le x \le 1$, is given by

$$P_l(x) = \sum_{i=0}^{l}\frac{(l+i)!}{(i!)^2(l-i)!}\left(\frac{x-1}{2}\right)^i, \quad \text{with } l \in \mathbb{N}. \tag{D.105}$$

Another one, given in terms of the spherical harmonics (B.204), reads

$$P_l(\cos\xi) = \frac{4\pi}{2l+1}\sum_{m=-l}^{l}Y_l^{m*}(\theta,\varphi)Y_l^m(\theta',\varphi'), \tag{D.106}$$

where ξ is the angle between the directions (θ,φ) and (θ',φ').
The Legendre polynomials verify the orthogonality relation

$$\int_{-1}^{1}\mathrm{d}x\, P_l(x)P'_l(x) = \frac{2}{2l+1}\delta_{ll'}, \tag{D.107}$$

as well as the recurrence relation

$$(l+1)P_{l+1}(x) = (2l+1)xP_l(x) - lP_{l-1}(x). \tag{D.108}$$

The completeness of the Legendre polynomials implies that any continuous function f on the interval $[-1,1]$ can be expanded in Legendre polynomials according to

$$f(x) = \sum_{l=0}^{\infty} a_l P_l(x), \tag{D.109}$$

provided that the coefficients of the expansion are given by

$$a_l \equiv \frac{2l+1}{2}\int_{-1}^{1} \mathrm{d}x\, f(x)P_l(x). \tag{D.110}$$

The series expansion of the Bessel function of the first kind, for $x \in \mathbb{C}$, is given by

$$J_\alpha(x) = \sum_{m=0}^{\infty} \frac{(-)^m}{m!\Gamma(m+\alpha+1)}\left(\frac{x}{2}\right)^{2m+\alpha}, \quad \text{with } \alpha \in \mathbb{Z}/2. \tag{D.111}$$

When the argument is purely imaginary, we have in particular

$$J_\alpha(\mathrm{i}x) = \mathrm{i}^\alpha \sum_{m=0}^{\infty} \frac{1}{m!\Gamma(m+\alpha+1)}\left(\frac{x}{2}\right)^{2m+\alpha}, \quad \text{with } \alpha \in \mathbb{Z}/2. \tag{D.112}$$

The spherical Bessel function of the first kind is defined in terms of the Bessel function of the first kind, for $x \in \mathbb{C}$, as

$$j_n(x) \equiv \sqrt{\frac{\pi}{2x}} J_{n+1/2}(x), \quad \text{with } n \in \mathbb{Z}. \tag{D.113}$$

When the argument is purely imaginary, we have in particular

$$j_n(\mathrm{i}x) = \mathrm{i}^n \frac{\sqrt{\pi}}{2} \sum_{m=0}^{\infty} \frac{1}{m!\Gamma(m+n+3/2)}\left(\frac{x}{2}\right)^{2m+n}, \quad \text{with } n \in \mathbb{Z}. \tag{D.114}$$

We provide the expressions of the first spherical Bessel functions of the first kind, for $x \in \mathbb{R}$, which appear in the developments,

$$j_0(x) = \frac{\sin x}{x}, \tag{D.115a}$$

$$j_1(x) = \frac{\sin x}{x^2} - \frac{\cos x}{x}, \tag{D.115b}$$

$$j_2(x) = \left(\frac{3}{x^2} - 1\right)\frac{\sin x}{x} - \frac{3\cos x}{x^2}. \tag{D.115c}$$

The plane wave expansion of the exponential function in terms of Legendre polynomials reads

$$\mathrm{e}^{\mathrm{i}\vec{k}\cdot\vec{r}} = \sum_{l=0}^{\infty}(2l+1)\mathrm{i}^l j_l(kr)P_l(\cos\theta), \tag{D.116}$$

where $j_l(kr)$ is the l-th spherical Bessel function of the first kind defined above, and $\cos\theta \equiv \hat{k}\cdot\hat{r}$ the direction between the vectors $\vec{k}$ and $\vec{r}$.
By means of (D.106), we can similarly expand the exponential functions in spherical harmonics (B.204) according to

$$\mathrm{e}^{\mathrm{i}\vec{k}\cdot\vec{r}} = 4\pi \sum_{l=0}^{\infty}\sum_{m=-l}^{l} \mathrm{i}^l j_l(kr)Y_l^{m*}(\hat{r})Y_l^m(\hat{k}). \tag{D.117}$$

7.2. Integrals

The Gauss integral in N dimensions reads

$$\int_{-\infty}^{+\infty} \mathrm{d}^N x \, \mathrm{e}^{-\alpha x^2} = \left(\frac{\pi}{\alpha}\right)^{N/2}, \quad \text{with } \alpha \in \mathbb{R}^*. \tag{D.118}$$

From the definition of the gamma function (D.101), we can show the following relation

$$\int_0^{\infty} \mathrm{d}x \, x^n \mathrm{e}^{-\alpha x^\beta} = \frac{\Gamma[(n+1)/\beta]}{\beta \alpha^{(n+1)/\beta}}, \quad \text{with } n \in \mathbb{N} \text{ and } \alpha, \beta \in \mathbb{R}^*. \tag{D.119}$$

We can take advantage of this result to evaluate the following integral, for $\alpha \in \mathbb{R}^*$ and $\beta = 2$, according to the parity of the exponent $n \in \mathbb{N}$,

$$\int_{-\infty}^{+\infty} \mathrm{d}x \, x^n \mathrm{e}^{-\alpha x^2} = \begin{cases} \frac{\Gamma[(n+1)/2]}{\alpha^{(n+1)/2}} = \frac{\sqrt{\pi}}{\alpha^{(n+1)/2}} \frac{(2n)!}{4^n n!} & \text{if } n \text{ is even,} \\ 0 & \text{if } n \text{ is odd.} \end{cases} \tag{D.120}$$

By induction, using successive integrations by parts, we can show that

$$\begin{aligned} \int \mathrm{d}x \, x^n \sin x = \cos x \sum_{k=0}^{\lfloor n/2 \rfloor} (-)^{k+1} \frac{n!}{(n-2k)!} x^{n-2k} \\ + \sin x \sum_{k=0}^{\lfloor (n-1)/2 \rfloor} (-)^k \frac{n!}{(n-2k-1)!} x^{n-2k-1}, \quad \text{with } n \in \mathbb{N}, \end{aligned} \tag{D.121}$$

where we have omitted the constant of integration, for conciseness.
When dealing with infinite nuclear matter, a double integral of the following form has to be calculated (see equation (A.46)),

$$I \equiv \int \mathrm{d}^3 k_1 \int \mathrm{d}^3 k_2 \, \mathrm{e}^{-(\vec{k}_1 - \vec{k}_2)^2 \mu^2/4}, \tag{D.122}$$

where the magnitude of the momentum $\vec{k}_1$ goes from 0 to $k_{\mathrm{F}}^{t_1}$, and from 0 to $k_{\mathrm{F}}^{t_2}$ for the momentum $\vec{k}_2$. We choose the spherical coordinates in such a way that $\vec{k}_1$ and $\vec{k}_2$ are related by a rotation of polar angle θ, and have the same azimuthal angle φ. This allows us to write $(\vec{k}_1 - \vec{k}_2)^2 = k_1^2 + k_2^2 - 2k_1 k_2 \cos\theta$. Setting the change of variables $\vec{x} = \mu \vec{k}_1/2$ and $\vec{y} = \mu \vec{k}_2/2$, the integral becomes

$$I = \left(\frac{2}{\mu}\right)^6 \int \mathrm{d}^3 x \int \mathrm{d}^3 y \, \mathrm{e}^{-(\vec{x} - \vec{y})^2}, \tag{D.123}$$

where the magnitude of the vector $\vec{x}$ goes from 0 to $L_1 \equiv \mu k_{\mathrm{F}}^{t_1}/2$, and from 0 to $L_2 \equiv \mu k_{\mathrm{F}}^{t_2}/2$ for $\vec{y}$. We can now evaluate the integral according to

$$\begin{aligned} I &= 2\pi \left(\frac{2}{\mu}\right)^6 \int \mathrm{d}^3 x \int_0^{L_2} \mathrm{d}y \, y^2 \mathrm{e}^{-x^2 - y^2} \int_0^{\pi} \mathrm{d}\theta \sin\theta \, \mathrm{e}^{2xy\cos\theta} \\ &= 4\pi^2 \left(\frac{2}{\mu}\right)^6 \int_0^{L_1} \mathrm{d}x \, x \int_0^{L_2} \mathrm{d}y \, y \left[\mathrm{e}^{-(x-y)^2} - \mathrm{e}^{-(x+y)^2}\right] \end{aligned} \tag{D.124}$$

Noticing that

$$-\int_0^{L_1} \mathrm{d}x \, x \, \mathrm{e}^{-(x+y)^2} = \int_{-L_1}^{0} \mathrm{d}x \, x \, \mathrm{e}^{-(x+y)^2}, \tag{D.125}$$

we can rewrite our integral as

$$I = 4\pi^2\left(\frac{2}{\mu}\right)^6 \int_{-L_1}^{L_1} \mathrm{d}x\, xJ(x), \tag{D.126}$$

where we have defined the integral

$$J(x) \equiv \int_0^{L_2} \mathrm{d}y\, y\, \mathrm{e}^{-(x-y)^2}, \tag{D.127}$$

that we are now going to evaluate. We get

$$\begin{aligned} J(x) &= \int_0^{L_2} \mathrm{d}y\, (y - x + x)\, \mathrm{e}^{-(y-x)^2} \\ &= \frac{1}{2}\Big(\mathrm{e}^{-x^2} - \mathrm{e}^{-(L_2-x)^2}\Big) + x\Big(\mathrm{E}(x) + \mathrm{E}(L_2 - x)\Big), \end{aligned} \tag{D.128}$$

where we have defined the function

$$\mathrm{E}(x) \equiv \frac{\sqrt{\pi}}{2}\,\mathrm{erf}(x) = \int_0^x \mathrm{d}t\, \mathrm{e}^{-t^2}, \tag{D.129}$$

in order to avoid carrying the factor $2/\sqrt{\pi}$ of the error function (D.96). Thus, our integral can be rewritten

$$I = 4\pi^2\left(\frac{2}{\mu}\right)^6 \left(\frac{1}{2}J_1 + J_2\right), \tag{D.130}$$

with the integrals

$$J_1 \equiv -\int_{-L_1}^{L_1} \mathrm{d}x\, x\, \mathrm{e}^{-(L_2-x)^2}, \tag{D.131a}$$

$$J_2 \equiv \int_{-L_1}^{L_1} \mathrm{d}x\, x^2\, \mathrm{E}(L_2 - x), \tag{D.131b}$$

where the odd functions cancel out when integrated over this symmetric interval. On the one hand, we obtain

$$\begin{aligned} J_1 &= -\int_{-L_1-L_2}^{L_1-L_2} \mathrm{d}x\, (x + L_2)\, \mathrm{e}^{-x^2} \\ &= \frac{1}{2}\Big(\mathrm{e}^{-(L_1-L_2)^2} - \mathrm{e}^{(L_1+L_2)^2}\Big) - L_2\Big(\mathrm{E}(L_1 - L_2) + \mathrm{E}(L_1 + L_2)\Big). \end{aligned} \tag{D.132}$$

On the other hand, we find out

$$\begin{aligned} J_2 &= -\int_{-L_1-L_2}^{L_1-L_2} \mathrm{d}x\, (x + L_2)^2\, \mathrm{E}(x) \\ &= \frac{L_1^3}{3}\mathrm{E}(L_1 + L_2) - \frac{L_1^3}{3}\mathrm{E}(L_1 - L_2) + \frac{1}{3}J_3, \end{aligned} \tag{D.133}$$

using an integration by parts and defining

$$J_3 \equiv \int_{-L_1-L_2}^{L_1-L_2} \mathrm{d}x\, (x^3 + 3x^2L_2 + 3xL_2^2 + L_2^3)\mathrm{e}^{-x^2}. \tag{D.134}$$

Let us evaluate this last integral by defining another integral, namely

$$K_n \equiv \int_{-L_1-L_2}^{L_1-L_2} \mathrm{d}x\, x^n \mathrm{e}^{-x^2}, \quad \text{with } n \in \mathbb{N}. \tag{D.135}$$

An integration by parts provides

$$K_n = \frac{n-1}{2} K_{n-2} + \frac{1}{2}\Big[(-L_1 - L_2)^{n-1}\,\mathrm{e}^{-(L_1+L_2)^2} - (L_1 - L_2)^{n-1}\,\mathrm{e}^{-(L_1-L_2)^2}\Big]. \tag{D.136}$$

Since the maximum value we encounter is $n = 3$, we only need to evaluate the integral K_n in the particular cases $n = 0$ and $n = 1$. We straightforwardly get

$$K_0 = \mathrm{E}(L_1 - L_2) + \mathrm{E}(L_1 + L_2), \tag{D.137a}$$

$$K_1 = \frac{1}{2}\Big[\mathrm{e}^{-(L_1+L_2)^2} - \mathrm{e}^{-(L_1-L_2)^2}\Big]. \tag{D.137b}$$

The integral (D.134) then reads

$$\begin{aligned} J_3 &= K_3 + 3L_2K_2 + 3L_2^2K_1 + L_2^3K_0 \\ &= \mathrm{e}^{-(L_1+L_2)^2}\left(\frac{1}{2} + \frac{3}{2}L_2^2 - \frac{3}{2}L_2(L_1+L_2) + \frac{1}{2}(L_1+L_2)^2\right) \\ &\quad - \mathrm{e}^{-(L_1-L_2)^2}\left(\frac{1}{2} + \frac{3}{2}L_2^2 + \frac{3}{2}L_2(L_1-L_2) + \frac{1}{2}(L_1-L_2)^2\right) \\ &\quad + \left(\frac{3}{2}L_2 + L_2^3\right)\Big(\mathrm{E}(L_1+L_2) + \mathrm{E}(L_1-L_2)\Big), \end{aligned} \tag{D.138}$$

so that the integral (D.133) reduces to

$$\begin{aligned} J_2 &= \frac{1}{3}\mathrm{e}^{-(L_1+L_2)^2}\left(\frac{1}{2} + \frac{L_1^2}{2} + \frac{L_2^2}{2} - \frac{L_1L_2}{2}\right) \\ &\quad - \frac{1}{3}\mathrm{e}^{-(L_1-L_2)^2}\left(\frac{1}{2} + \frac{L_1^2}{2} + \frac{L_2^2}{2} + \frac{L_1L_2}{2}\right) \\ &\quad + \mathrm{E}(L_1+L_2)\left(\frac{L_1^3}{3} + \frac{L_2^3}{2} + \frac{L_2}{2}\right) + \mathrm{E}(L_1-L_2)\left(-\frac{L_1^3}{3} + \frac{L_2^3}{2} + \frac{L_2}{2}\right). \end{aligned} \tag{D.139}$$

Gathering all those results in (D.130), we find

$$\begin{aligned} I = \left(\frac{2}{\mu}\right)^6 \frac{\pi^2}{3}\Big\{ &\mathrm{e}^{-(L_1+L_2)^2}\Big[2(L_1^2 + L_2^2 - L_1L_2) - 1\Big] \\ &- \mathrm{e}^{-(L_1-L_2)^2}\Big[2(L_1^2 + L_2^2 + L_1L_2) - 1\Big] + 4\mathrm{E}(L_1+L_2)(L_1^3 + L_2^3) \\ &- 4\mathrm{E}(L_1-L_2)(L_1^3 - L_2^3)\Big\}, \end{aligned} \tag{D.140}$$

and finally, by setting, $X_{t_i} \equiv \mu k_{\mathrm{F}}^{t_i} = 2L_i$ for $i \in \{1, 2\}$ and using (D.129), we get the following expression for the integral (D.122),

$$I(X_{t_1}, X_{t_2}) = \left(\frac{2}{\mu}\right)^6 \frac{\pi^2}{6} Q(X_{t_1}, X_{t_2}), \tag{D.141}$$

where

$$\begin{aligned} Q(X_{t_1}, X_{t_2}) \equiv\ & \mathrm{e}^{-\left(\frac{X_{t_1}+X_{t_2}}{2}\right)^2}\Big(X_{t_1}^2 + X_{t_2}^2 - X_{t_1}X_{t_2} - 2\Big) \\ &- \mathrm{e}^{-\left(\frac{X_{t_1}-X_{t_2}}{2}\right)^2}\Big(X_{t_1}^2 + X_{t_2}^2 + X_{t_1}X_{t_2} - 2\Big) \\ &+ \frac{\sqrt{\pi}}{2}\,\mathrm{erf}\left(\frac{X_{t_1}+X_{t_2}}{2}\right)(X_{t_1}^3 + X_{t_2}^3) \\ &- \frac{\sqrt{\pi}}{2}\,\mathrm{erf}\left(\frac{X_{t_1}-X_{t_2}}{2}\right)(X_{t_1}^3 - X_{t_2}^3). \end{aligned} \tag{D.142}$$

References

[1] M. Gell-Mann, "A schematic model of baryons and mesons," Physics Letters **8**, 214–215 (1964).

[2] G. Zweig, "An SU_3 model for strong interaction symmetry and its breaking; Version 2," (1964).

[3] S. Okubo and R. E. Marshak, "Velocity dependence of the two-nucleon interaction," Annals of Physics **4**, 166–179 (1958).

[4] P. Ring and P. Schuck, *The Nuclear Many-Body Problem*, Physics and astronomy online library (Springer, 2004).

[5] M. Bender, P.-H. Heenen, and P.-G. Reinhard, "Self-consistent mean-field models for nuclear structure," Reviews of Modern Physics **75**, 121–180 (2003).

[6] D. Lacroix, "Review of mean-field theory," in *Ecole Joliot-Curie (30 years) "Physics at the femtometer scale"* (La Colle sur Loup, France, 2011).

[7] J.-F. Berger, "Structure Nucléaire Théorique," Formation NPAC (2008).

[8] P. Ring, "Relativistic mean field theory in finite nuclei," Progress in Particle and Nuclear Physics **37**, 193–263 (1996).

[9] P.-G. Reinhard, "The relativistic mean-field description of nuclei and nuclear dynamics," Reports on Progress in Physics **52**, 439 (1989).

[10] T. H. R. Skyrme, "The effective nuclear potential," Nuclear Physics **9**, 615–634 (1958).

[11] T. H. R. Skyrme, "The spin-orbit interaction in nuclei," Nuclear Physics **9**, 635–640 (1958).

[12] D. Gogny, "Proceedings of the International Conference on Nuclear Physics, Munich, August 27-September 1, 1973," (1973) p. 48.

[13] D. Gogny, "Self-consistent pairing calculations," (North-Holland Publishing Company, 1975).

[14] J. Dechargé and D. Gogny, "Hartree-Fock-Bogolyubov calculations with the $D1$ effective interaction on spherical nuclei," Physical Review C **21**, 1568–1593 (1980).

[15] J.-F. Berger, M. Girod, and D. Gogny, "Time-dependent quantum collective dynamics applied to nuclear fission," Computer Physics Communications **63**, 365–374 (1991).

[16] J.-F. Berger, M. Girod, and D. Gogny, "Constrained hartree-fock and beyond," Nuclear Physics A **502**, 85–104 (1989).

[17] F. Chappert, *Nouvelles paramétrisations de l'interaction nucléaire effective de Gogny*, Theses, Université Paris Sud - Paris XI (2007).

[18] F. Chappert, N. Pillet, M. Girod, and J.-F. Berger, "Gogny force with a finite-range density dependence," Physical Review C **91**, 034312 (2015).

[19] C. Robin, N. Pillet, M. Dupuis, J. Le Bloas, D. Peña Arteaga, and J.-F. Berger, "Description of nuclear systems with a self-consistent configuration-mixing approach. II. Application to structure and reactions in even-even sd-shell nuclei," Physical Review C **95** (2017).

[20] N. Pillet, private discussions.

[21] W. Rarita and J. Schwinger, "On the Neutron-Proton Interaction," Physical Review **59**, 436–452 (1941).

[22] W. Rarita and J. Schwinger, "On the Exchange Properties of the Neutron-Proton Interaction," Physical Review **59**, 556–564 (1941).

[23] R. V. Reid, "Local phenomenological nucleon-nucleon potentials," Annals of Physics **50**, 411–448 (1968).

[24] M. Lacombe, B. Loiseau, J. M. Richard, R. Vinh Mau, J. Côté, P. Pirès, and R. de Tourreil, "Parametrization of the Paris $N-N$ potential," Physical Review C **21**, 861–873 (1980).

[25] R. Machleidt, K. Holinde, and Ch. Elster, "The Bonn meson-exchange model for the nucleon—nucleon interaction," Physics Reports **149**, 1–89 (1987).

[26] R. B. Wiringa, R. A. Smith, and T. L. Ainsworth, "Nucleon-nucleon potentials with and without $\Delta(1232)$ degrees of freedom," Physical Review C **29**, 1207–1221 (1984).

[27] R. B. Wiringa, V. G. J. Stoks, and R. Schiavilla, "Accurate nucleon-nucleon potential with charge-independence breaking," Physical Review C **51**, 38–51 (1995).

[28] H. Sagawa and G. Colò, "Tensor interaction in mean-field and density functional theory approaches to nuclear structure," Progress in Particle and Nuclear Physics **76**, 76–115 (2014).

[29] M. Anguiano, G. Co', V. De Donno, and A. M. Lallena, "Tensor effective interaction in self-consistent random-phase approximation calculations," Physical Review C **83** (2011).

[30] T. Otsuka, T. Suzuki, R. Fujimoto, H. Grawe, and Y. Akaishi, "Evolution of Nuclear Shells due to the Tensor Force," Physical Review Letters **95**, 232502 (2005).

[31] T. Otsuka, "Exotic nuclei and nuclear forces," Physica Scripta **2013**, 014007 (2013).

[32] T. Otsuka, A. Gade, O. Sorlin, T. Suzuki, and Y. Utsuno, "Evolution of shell structure in exotic nuclei," Reviews of Modern Physics **92**, 015002 (2020).

[33] L.-G. Cao, G. Colò, H. Sagawa, P. F. Bortignon, and L. Sciacchitano, "Effects of the tensor force on the multipole response in finite nuclei," Physical Review C **80**, 064304 (2009).

[34] B. S. Hu, Q. Wu, Q. Yuan, Y. Z. Ma, X. Q. Yan, and F. R. Xu, "Nuclear multipole responses from chiral effective field theory interactions," Physical Review C **101**, 044309 (2020).

[35] C. L. Bai, H. Sagawa, H. Q. Zhang, X. Z. Zhang, G. Colò, and F. R. Xu, "Effect of tensor correlations on Gamow–Teller states in 90Zr and 208Pb," Physics Letters B **675**, 28–31 (2009).

[36] C. L. Bai, H. Q. Zhang, X. Z. Zhang, F. R. Xu, H. Sagawa, and G. Colò, "Quenching of Gamow-Teller strength due to tensor correlations in ^{90}Zr and ^{208}Pb," Physical Review C **79**, 041301 (2009).

[37] A. P. Severyukhin and H. Sagawa, "Tensor correlation effects on Gamow–Teller resonances in 120Sn and N = 80, 82 isotones," Progress of Theoretical and Experimental Physics **2013**, 103D03 (2013).

[38] R. N. Bernard and M. Anguiano, "Interplay between tensor force and deformation in even–even nuclei," Nuclear Physics A **953**, 32–64 (2016).

[39] R. N. Bernard, N. Pillet, L. M. Robledo, and M. Anguiano, "Description of the asymmetric to symmetric fission transition in the neutron-deficient thorium isotopes: Role of the tensor force," Physical Review C **101** (2020).

[40] G. Co', M. Anguiano, and A. M. Lallena, "Tensor force and deformation in even-even nuclei," Physical Review C **104**, 014313 (2021).

[41] T. Otsuka, T. Suzuki, and Y. Utsuno, "Exotic Nuclei and Yukawa's Forces," Nuclear Physics A **805**, 127c–136c (2008), iNPC 2007.

[42] X.-R. Zhou and H. Sagawa, "Effect of tensor force on the shell structure of superheavy nuclei," Journal of Physics: Conference Series **420**, 012009 (2013).

[43] M. El Adri and M. Oulne, "Tensor force effect on the neutron shell closure in superheavy elements," The European Physical Journal Plus **136** (2021).

[44] Fl. Stancu, D. M. Brink, and H. Flocard, "The tensor part of Skyrme's interaction," Physics Letters B **68**, 108–112 (1977).

[45] M. Beiner, H. Flocard, N. Van Giai, and P. Quentin, "Nuclear ground-state properties and self-consistent calculations with the skyrme interaction: (I). Spherical description," Nuclear Physics A **238**, 29–69 (1975).

[46] B. A. Brown, T. Duguet, T. Otsuka, D. Abe, and T. Suzuki, "Tensor interaction contributions to single-particle energies," Physical Review C **74**, 061303 (2006).

[47] D. M. Brink and Fl. Stancu, "Evolution of nuclear shells with the Skyrme density dependent interaction," Physical Review C **75**, 064311 (2007).

[48] G. Colò, H. Sagawa, S. Fracasso, and P. F. Bortignon, "Spin–orbit splitting and the tensor component of the Skyrme interaction," Physics Letters B **646**, 227–231 (2007).

[49] M. Zalewski, J. Dobaczewski, W. Satuła, and T. R. Werner, "Spin-orbit and tensor mean-field effects on spin-orbit splitting including self-consistent core polarizations," Physical Review C **77**, 024316 (2008).

[50] M. Zalewski, P. Olbratowski, M. Rafalski, W. Satuła, T. R. Werner, and R. A. Wyss, "Global nuclear structure effects of the tensor interaction," Physical Review C **80**, 064307 (2009).

[51] T. Lesinski, M. Bender, K. Bennaceur, T. Duguet, and J. Meyer, "Tensor part of the Skyrme energy density functional: Spherical nuclei," Physical Review C **76**, 014312 (2007).

[52] G. Bertsch, J. Borysowicz, H. McManus, and W. G. Love, "Interactions for inelastic scattering derived from realistic potentials," Nuclear Physics A **284**, 399–419 (1977).

[53] H. Nakada, "Hartree-Fock calculations on unstable nuclei with several types of effective interactions," Nuclear Physics A **722**, C117–C122 (2003).

[54] H. Nakada, "Hartree-Fock approach to nuclear matter and finite nuclei with M3Y-type nucleon-nucleon interactions," Physical Review C **68**, 014316 (2003).

[55] H. Nakada, "Mean-field approach to nuclear structure with semi-realistic nucleon-nucleon interactions," Physical Review C **78**, 054301 (2008).

[56] H. Nakada, "Modified parameter sets of M3Y-type semi-realistic nucleon-nucleon interactions for nuclear structure studies," Physical Review C **81**, 027301 (2010).

[57] N. Onishi and J. W. Negele, "Two-body and three-body effective interactions in nuclei," Nuclear Physics A **301**, 336–348 (1978).

[58] T. Otsuka, T. Matsuo, and D. Abe, "Mean Field with Tensor Force and Shell Structure of Exotic Nuclei," Physical Review Letters **97**, 162501 (2006).

[59] G. Co', V. De Donno, M. Anguiano, and A. M. Lallena, "Effective tensor forces and neutron rich nuclei," **267**, 012022 (2011).

[60] M. Anguiano, M. Grasso, G. Co', V. De Donno, and A. M. Lallena, "Tensor and tensor-isospin terms in the effective Gogny interaction," Physical Review C **86** (2012).

[61] M. Grasso and M. Anguiano, "Tensor parameters in Skyrme and Gogny effective interactions: Trends from a ground-state-focused study," Physical Review C **88**, 054328 (2013).

[62] H. A. Bethe, "Thomas-Fermi Theory of Nuclei," Physical Review **167**, 879–907 (1968).

[63] R. K. Bhaduri and C. S. Warke, "Effective, Central, Density-Dependent Potential from Tensor Force in Nuclear Matter," Physical Review Letters **20**, 1379–1382 (1968).

[64] H. Yukawa, "On the Interaction of Elementary Particles. I," Proceedings of the Physico-Mathematical Society of Japan. 3rd Series **17**, 48–57 (1935).

[65] M. Riordan, "The Discovery of Quarks," Science **256**, 1287–1293 (1992).

[66] H. Fritzsch, M. Gell-Mann, and H. Leutwyler, "Advantages of the color octet gluon picture," Physics Letters B **47**, 365–368 (1973).

[67] H. Fritzsch, "The history of QCD," CERN Courier **27** (2012).

[68] S. Bethke, "Experimental tests of asymptotic freedom," Progress in Particle and Nuclear Physics **58**, 351–386 (2007).

[69] J. Greensite, *An introduction to the confinement problem*, Vol. 821 (2011).

[70] D. J. Gross, "The discovery of asymptotic freedom and the emergence of QCD," Proceedings of the National Academy of Sciences **102**, 9099–9108 (2005).

[71] D. J. Gross and F. Wilczek, "Ultraviolet Behavior of Non-Abelian Gauge Theories," Physical Review Letters **30**, 1343–1346 (1973).

[72] H. D. Politzer, "Reliable Perturbative Results for Strong Interactions?" Physical Review Letters **30**, 1346–1349 (1973).

[73] R. Machleidt, "Nuclear Forces," Scholarpedia **9**, 30710 (2014), revision #143358.

[74] K. G. Wilson, "Confinement of quarks," Physical Review D **10**, 2445–2459 (1974).

[75] N. Ishii, S. Aoki, and T. Hatsuda, "Nuclear Force from Lattice QCD," Physical Review Letters **99**, 022001 (2007).

[76] H.-W. Hammer, S. König, and U. van Kolck, "Nuclear effective field theory: Status and perspectives," Reviews of Modern Physics **92**, 025004 (2020).

[77] S. Weinberg, "Phenomenological Lagrangians," Physica A: Statistical Mechanics and its Applications **96**, 327–340 (1979).

[78] S. Weinberg, "Effective chiral lagrangians for nucleon-pion interactions and nuclear forces," Nuclear Physics B **363**, 3–18 (1991).

[79] R. Machleidt and D. R. Entem, "Chiral effective field theory and nuclear forces," Physics Reports **503**, 1–75 (2011).

[80] H. Leutwyler, "Chiral perturbation theory," Scholarpedia **7**, 8708 (2012), revision #138476.

[81] E. Tiesinga, P. J. Mohr, D. B. Newell, and B. N. Taylor, "CODATA recommended values of the fundamental physical constants: 2018," Reviews of Modern Physics **93**, 025010 (2021).

[82] P. Möller and A. J. Sierk, "80 Years of the liquid drop—50 years of the macroscopic–microscopic model," International Journal of Mass Spectrometry **349-350**, 19–25 (2013), 100 years of Mass Spectrometry.

[83] C. F. V. Weizsäcker, "Zur Theorie der Kernmassen," Zeitschrift fur Physik **96**, 431–458 (1935).

[84] H. A. Bethe and R. F. Bacher, "Nuclear Physics A. Stationary States of Nuclei," Reviews of Modern Physics **8**, 82–229 (1936).

[85] V. M. Strutinsky, "Shell effects in nuclear masses and deformation energies," Nuclear Physics A **95**, 420–442 (1967).

[86] V. M. Strutinsky, ""Shells" in deformed nuclei," Nuclear Physics A **122**, 1–33 (1968).

[87] W. D. Myers and W. J. Swiatecki, "Nuclear masses and deformations," Nuclear Physics **81**, 1–60 (1966).

[88] P. Möller, W. D. Myers, W. J. Swiatecki, and J. Treiner, "Nuclear mass formula with a finite-range droplet model and a folded-Yukawa single-particle potential," Atomic Data and Nuclear Data Tables **39**, 225–233 (1988).

[89] P. Möller, A. J. Sierk, T. Ichikawa, and H. Sagawa, "Nuclear ground-state masses and deformations: FRDM(2012)," Atomic Data and Nuclear Data Tables **109-110**, 1–204 (2016).

[90] D. Lacroix, "Introduction - Strong interaction in the nuclear medium: new trends," (2010), arXiv:1001.5001 [nucl-th].

[91] H. Hergert, "A Guided Tour of ab initio Nuclear Many-Body Theory," Frontiers in Physics **8**, 379 (2020).

[92] M. Goeppert Mayer, "Nuclear Configurations in the Spin-Orbit Coupling Model. I. Empirical Evidence," Physical Review **78**, 16–21 (1950).

[93] M. Goeppert Mayer, "Nuclear Configurations in the Spin-Orbit Coupling Model. II. Theoretical Considerations," Physical Review **78**, 22–23 (1950).

[94] O. Haxel, J. H. D. Jensen, and H. E. Suess, "On the "Magic Numbers" in Nuclear Structure," Physical Review **75**, 1766–1766 (1949).

[95] B. A. Brown and B. H. Wildenthal, "Status of the Nuclear Shell Model," Annual Review of Nuclear and Particle Science **38**, 29–66 (1988).

[96] E. Caurier, G. Martínez-Pinedo, F. Nowacki, A. Poves, and A. P. Zuker, "The shell model as a unified view of nuclear structure," Reviews of Modern Physics **77**, 427–488 (2005).

[97] M. Goeppert Mayer, "On Closed Shells in Nuclei," Physical Review **74**, 235–239 (1948).

[98] M. Goeppert Mayer, "On Closed Shells in Nuclei. II," Physical Review **75**, 1969–1970 (1949).

[99] R. D. Woods and D. S. Saxon, "Diffuse Surface Optical Model for Nucleon-Nuclei Scattering," Physical Review **95**, 577–578 (1954).

[100] J. Carlson, S. Gandolfi, F. Pederiva, S. C. Pieper, R. Schiavilla, K. E. Schmidt, and R. B. Wiringa, "Quantum Monte Carlo methods for nuclear physics," Reviews of Modern Physics **87**, 1067–1118 (2015).

[101] C. Lanczos, "An iteration method for the solution of the eigenvalue problem of linear differential and integral operators," (1950).

[102] S. Goriely, S. Hilaire, M. Girod, and S. Péru, "First Gogny-Hartree-Fock-Bogoliubov Nuclear Mass Model," Physical Review Letters **102**, 242501 (2009).

[103] N. Pillet, "From Nuclei to Stars," Formation NPAC (2015).

[104] K. A. Brueckner, "Two-Body Forces and Nuclear Saturation. III. Details of the Structure of the Nucleus," Physical Review **97**, 1353–1366 (1955).

[105] B. Bally, private communication.

[106] D. Vautherin and D. M. Brink, "Hartree-Fock Calculations with Skyrme's Interaction. I. Spherical Nuclei," Physical Review C **5**, 626–647 (1972).

[107] D. Vautherin, "Hartree-Fock Calculations with Skyrme's Interaction. II. Axially Deformed Nuclei," Physical Review C **7**, 296–316 (1973).

[108] N. Anantaraman, H. Toki, and G. F. Bertsch, "An effective interaction for inelastic scattering derived from the Paris potential," Nuclear Physics A **398**, 269–278 (1983).

[109] P. Ring, S. Wang, Q. Zhao, and J. Meng, "Relativistic Brueckner-Hartree-Fock Theory in Infinite Nuclear Matter," EPJ Web of Conferences **252**, 02001 (2021).

[110] P. Ring, S. Wang, H. Tong, Q. Zhao, C. Wang, and J. Meng, "Relativistic Brueckner-Hartree-Fock Theory: an ab initio Approach for Nuclear Matter and for Finite Nuclei," Journal of Physics: Conference Series **2453**, 012031 (2023).

[111] L. I. Schiff, "Nonlinear Meson Theory of Nuclear Forces. I. Neutral Scalar Mesons with Point-Contact Repulsion," Physical Review **84**, 1–9 (1951).

[112] M. H. Johnson and E. Teller, "Classical Field Theory of Nuclear Forces," Physical Review **98**, 783–787 (1955).

[113] H.-P. Duerr and E. Teller, "Interaction of Antiprotons with Nuclear Fields," Physical Review **101**, 494–495 (1956).

[114] J. D. Walecka, "A theory of highly condensed matter." Annals of Physics **83**, 491–529 (1974).

[115] B. D. Serot and J. D. Walecka, "Advances in Nuclear Physics," (1986).

[116] N. Pillet, "Dérivation analytique des équations nécessaires à la mise au point d'une interaction de Gogny généralisée," internal CEA document (2012).

[117] J.-F. Berger, J.-P. Blaizot, D. Bouche, P. Chaix, J.-P. Delaroche, M. Dupuis, M. Girod, J. Gogny, B. Grammaticos, D. Iracane, J. Lachkar, F. Mariotte, N. Pillet, and N. Van Giai, "Daniel Gogny," The European Physical Journal A **53** (2017).

[118] D. Gogny, P. Pires, and R. De Tourreil, "A smooth realistic local nucleon-nucleon force suitable for nuclear Hartree-Fock calculations," Physics Letters B **32**, 591–595 (1970).

[119] V. Gillet, "The phenomenology of the effective two-body forces for C12 and O16 in the particle-hole models," Nuclear Physics **51**, 410–426 (1964).

[120] V. Gillet and N. Vinh Mau, "Particle-hole description of carbon 12 and oxygen 16," Nuclear Physics **54**, 321–351 (1964).

[121] D. M. Brink and E. Boeker, "Effective interactions for Hartree-Fock calculations," Nuclear Physics A **91**, 1–26 (1967).

[122] A. B. Volkov, "Equilibrium deformation calculations of the ground state energies of 1p shell nuclei," Nuclear Physics **74**, 33–58 (1965).

[123] M. Farine, D. Von-Eiff, P. Schuck, J.-F. Berger, J. Dechargé, and M. Girod, "Towards a new effective interaction of the Gogny type," Journal of Physics G: Nuclear and Particle Physics **25**, 863 (1999).

[124] F. Chappert, M. Girod, and S. Hilaire, "Towards a new Gogny force parameterization: Impact of the neutron matter equation of state," Physics Letters B **668**, 420–424 (2008).

[125] R. F. Casten and B. M. Sherrill, "The study of exotic nuclei," Progress in Particle and Nuclear Physics **45**, S171–S233 (2000).

[126] B. Friedman and V. R. Pandharipande, "Hot and cold, nuclear and neutron matter," Nuclear Physics A **361**, 502–520 (1981).

[127] S. Goriely, S. Hilaire, M. Girod, and S. Péru, "The Gogny-Hartree-Fock-Bogoliubov nuclear-mass model," The European Physical Journal A **52**, 202 (2016).

[128] C. Gonzalez-Boquera, M. Centelles, X. Viñas, and L. M. Robledo, "New Gogny interaction suitable for astrophysical applications," Physics Letters B **779**, 195–200 (2018).

[129] B. S. Pudliner, V. R. Pandharipande, J. Carlson, S. C. Pieper, and R. B. Wiringa, "Quantum Monte Carlo calculations of nuclei with $A < 7$," Physical Review C **56**, 1720–1750 (1997).

[130] F. Arias de Saavedra, C. Bisconti, G. Co', and A. Fabrocini, "Renormalized Fermi hypernetted chain approach in medium–heavy nuclei," Physics Reports **450**, 1–95 (2007).

[131] O. Sorlin and M.-G. Porquet, "Nuclear magic numbers: New features far from stability," Progress in Particle and Nuclear Physics **61**, 602–673 (2008).

[132] P. D. Cottle and K. W. Kemper, "Single-neutron energies near $N = 28$ and the absence of the $N = 34$ subshell closure in the Ti isotopes," Physical Review C **78**, 037304 (2008).

[133] L. Batail, D. Davesne, S. Péru, P. Becker, A. Pastore, and J. Navarro, "A three-ranged Gogny interaction in touch with pion exchange: promising results to improve infinite matter properties," The European Physical Journal A **59** (2023).

[134] D. Davesne, P. Becker, A. Pastore, and J. Navarro, "Does the Gogny Interaction Need a Third Gaussian?" Acta Physica Polonica B **48**, 265 (2017).

[135] L. Batail, *Etude des modes de respiration nucléaire dans le formalisme QRPA : un défi pour les interactions effectives modernes*, Theses, Université de Lyon (2021).

[136] J. Beringer *et al.* (Particle Data Group), "Review of Particle Physics," Physical Review D **86**, 010001 (2012).

[137] B. A. Brown, W. A. Richter, R. E. Julies, and B. H. Wildenthal, "Semi-empirical effective interactions for the 1s-0d shell," Annals of Physics **182**, 191–236 (1988).

[138] B. A. Brown and W. A. Richter, "New "USD" Hamiltonians for the *sd* shell," Physical Review C **74**, 034315 (2006).

[139] M. Honma, T. Otsuka, B. A. Brown, and T. Mizusaki, "New effective interaction for pf-shell nuclei and its implications for the stability of the $N = Z = 28$ closed core," Physical Review C **69**, 034335 (2004).

[140] M. W. Kirson, "Oscillator parameters in nuclei," Nuclear Physics A **781**, 350–362 (2007).

[141] J. Blomqvist and A. Molinari, "Collective 0- vibrations in even spherical nuclei with tensor forces," Nuclear Physics A **106**, 545–569 (1968).

[142] M. M. Sharma, G. Lalazissis, J. König, and P. Ring, "Isospin Dependence of the Spin-Orbit Force and Effective Nuclear Potentials," Physical Review Letters **74**, 3744–3747 (1995).

[143] N. Schwierz, I. Wiedenhover, and A. Volya, "Parameterization of the Woods-Saxon Potential for Shell-Model Calculations," (2007), arXiv:0709.3525 [nucl-th].

[144] B. Frois and C. N. Papanicolas, "Electron Scattering and Nuclear Structure," Annual Review of Nuclear and Particle Science **37**, 133–176 (1987).

[145] W. D. Myers and W. J. Swiatecki, "Nuclear masses and deformations," Nuclear Physics **81**, 1–60 (1966).

[146] W. D. Myers and W. J. Swiatecki, "Average nuclear properties," Annals of Physics **55**, 395–505 (1969).

[147] W. D. Myers, "Droplet model nuclear density distributions and single-particle potential wells," Nuclear Physics A **145**, 387–400 (1970).

[148] P. Möller and J. Rayford Nix, "Global nuclear-structure calculations," Nuclear Physics A **520**, c369–c376 (1990), nuclear Structure in the Nineties.

[149] P. Möller, J. Rayford Nix, W. D. Myers, and W. J. Swiatecki, "Nuclear Ground-State Masses and Deformations," Atomic Data and Nuclear Data Tables **59**, 185–381 (1995).

[150] J.-P. Blaizot, J.-F. Berger, J. Dechargé, and M. Girod, "Microscopic and macroscopic determinations of nuclear compressibility," Nuclear Physics A **591**, 435–457 (1995).

[151] C. Mahaux and R. Sartor, "Single-Particle Motion in Nuclei," in *Advances in Nuclear Physics*, edited by J. W. Negele and E. Vogt (Springer US, Boston, MA, 1991) pp. 1–223.

[152] I. E. Lagaris and V. R. Pandharipande, "Variational calculations of realistic models of nuclear matter," Nuclear Physics A **359**, 349–364 (1981).

[153] M. Baldo, P. Schuck, and X. Viñas, "Kohn–Sham density functional inspired approach to nuclear binding," Physics Letters B **663**, 390–394 (2008).

[154] A. Lejeune, P. Grange, M. Martzolff, and J. Cugnon, "Hot nuclear matter in an extended Brueckner approach," Nuclear Physics A **453**, 189–219 (1986).

[155] I. Bombaci and U. Lombardo, "Asymmetric nuclear matter equation of state," Physical Review C **44**, 1892–1900 (1991).

[156] E. N. E. van Dalen, C. Fuchs, and A. Faessler, "Momentum, density, and isospin dependence of symmetric and asymmetric nuclear matter properties," Physical Review C **72**, 065803 (2005).

[157] H. F. Arellano and J.-P. Delaroche, "Low-density homogeneous symmetric nuclear matter: Disclosing dinucleons in coexisting phases," The European Physical Journal A **51**, 7 (2015).

[158] H. F. Arellano, F. Isaule, and A. Rios, "Di-nucleon structures in homogeneous nuclear matter based on two- and three-nucleon interactions," The European Physical Journal A **52**, 299 (2016).

[159] V. Rotival, *Fonctionnelles d'énergie non-empiriques pour la structure nucléaire*, Theses, Université Paris-Diderot - Paris VII (2008).

[160] D. Davesne, J. Meyer, A. Pastore, and J. Navarro, "Partial wave decomposition of the N3LO equation of state," Physica Scripta **90**, 114002 (2015).

[161] D. Davesne, P. Becker, A. Pastore, and J. Navarro, "Infinite matter properties and zero-range limit of non-relativistic finite-range interactions," Annals of Physics **375**, 288–312 (2016).

[162] G. Blanchon, private communication.

[163] S.-O. Bäckman, O. Sjöberg, and A. D. Jackson, "The role of tensor forces in Fermi liquid theory," Nuclear Physics A **321**, 10–24 (1979).

[164] B. L. Friman and A. K. Dhar, "Sum rules for Landau parameters in nuclear matter," Physics Letters B **85**, 1–4 (1979).

[165] D. Gogny, "Lecture on the RPA formalism for density-dependent interactions," internal CEA document (2004).

[166] P. Ring and J. Speth, "RPA-calculations in ^{208}Pb with a density dependent interaction," Physics Letters B **44**, 477–480 (1973).

[167] P. Ring and J. Speth, "Nuclear structure calculations with a density-dependent force in ^{208}Pb," Nuclear Physics A **235**, 315–351 (1974).

[168] J. Speth, L. Zamick, and P. Ring, "E0 properties in the lead region," Nuclear Physics A **232**, 1–12 (1974).

[169] A. B. Migdal, *Theory of finite Fermi systems and application to atomic nuclei*, Interscience monographs and texts in physics and astronomy (Wiley-Interscience Publ., 1967).

[170] S.-O. Bäckman, G. E. Brown, and J. A. Niskanen, "The nucleon-nucleon interaction and the nuclear many-body problem," Physics Reports **124**, 1–68 (1985).

[171] G. E. Brown, "Landau, Brueckner-Bethe, and Migdal Theories of Fermi Systems," Reviews of Modern Physics **43**, 1–14 (1971).

[172] D. Gogny and R. Padjen, "The propagation and damping of the collective modes in nuclear matter," Nuclear Physics A **293**, 365–378 (1977).

[173] A. Pastore, D. Davesne, Y. Lallouet, M. Martini, K. Bennaceur, and J. Meyer, "Nuclear response for the Skyrme effective interaction with zero-range tensor terms. II. Sum rules and instabilities," Physical Review C **85**, 054317 (2012).

[174] M. Anguiano, A. M. Lallena, G. Co', V. De Donno, M. Grasso, and R. N. Bernard, "Gogny interactions with tensor terms," The European Physical Journal A **52** (2016).

[175] J.-F. Berger, *Approche microscopique auto-consistante des processus nucléaires collectifs de grande amplitude à basse énergie : application à la diffusion d'ions lourds et à la fission*, Thèse d'état, Université Paris Sud - Paris XI (1985).

[176] A. Zdeb, N. Pillet, N. Dubray, J.-P. Ebran, and J.-F. Berger, "Implementation in the HFB3 code of the finite range density-dependent term of the D2 Gogny interaction in a 2-center harmonic oscillator basis," internal CEA document (2021).

[177] M. Bender, K. Rutz, P.-G. Reinhard, and J. A. Maruhn, "Consequences of the center–of–mass correction in nuclear mean–field models," The European Physical Journal A **7**, 467–478 (2000).

[178] F. Laloë, "Cours sur les symétries," DEA de physique quantique.

[179] N. Dubray *et al.*, to be published.

[180] J. Newsome, to be published.

[181] D. Gogny, "Simple separable expansions for calculating matrix elements of two-body local interactions with harmonic oscillator functions," Nuclear Physics A **237**, 399–418 (1975).

[182] N. Dubray, private communication.

[183] P. Carpentier, to be published.

[184] R. R. Scheerbaum, "The role of spin-unsaturated closed shells in nuclear spin-orbit splitting," Physics Letters B **63**, 381–384 (1976).

[185] A. L. Goodman and J. Borysowicz, "The mass dependence of the spin-orbit splitting in the A = 176–208 mass region," Nuclear Physics A **295**, 333–344 (1978).

[186] D. C. Zheng and L. Zamick, "The effects of the spin-orbit and tensor interactions in nuclei," Annals of Physics **206**, 106–121 (1991).

[187] M. Wang, W. J. Huang, F. G. Kondev, G. Audi, and S. Naimi, "The AME 2020 atomic mass evaluation (II). Tables, graphs and references*," Chinese Physics C **45**, 030003 (2021).

[188] H. Atac, M. Constantinou, Z.-E. Meziani, M. Paolone, and N. Sparveris, "Measurement of the neutron charge radius and the role of its constituents," Nature Communications **12** (2021).

[189] I. Angeli and K. P. Marinova, "Table of experimental nuclear ground state charge radii: An update," Atomic Data and Nuclear Data Tables **99**, 69–95 (2013).

[190] N. Pillet and S. Hilaire, "Towards an extended Gogny force," The European Physical Journal A **53** (2017).

[191] J. P. Delaroche, M. Girod, J. Libert, H. Goutte, S. Hilaire, S. Péru, N. Pillet, and G. F. Bertsch, "Structure of even-even nuclei using a mapped collective Hamiltonian and the D1S Gogny interaction," Physical Review C **81**, 014303 (2010).

[192] Y. Kanada-En'yo, "Effects of density-dependent spin-orbit interactions in Skyrme-Hartree-Fock-Bogoliubov calculations of the charge radii and densities of Pb isotopes," (2022), arXiv:2209.11411 [nucl-th].

[193] R. F. Garcia Ruiz *et al.*, "Unexpectedly large charge radii of neutron-rich calcium isotopes," Nature Physics **12**, 594–598 (2016).

[194] A. J. Miller *et al.*, "Proton superfluidity and charge radii in proton-rich calcium isotopes," Nature Physics **15**, 432–436 (2019).

[195] G. Co', M. Anguiano, and A. M. Lallena, "Charge radii of Ca isotopes and correlations," Physical Review C **105**, 034320 (2022).

[196] J. W. Negele, "Structure of Finite Nuclei in the Local-Density Approximation," Physical Review C **1**, 1260–1321 (1970).

[197] S. Haddad and S. H. Suleiman, "Neutron Charge Distribution and Charge Density Distributions in Lead Isotopes," Acta Physica Polonica B (1999).

[198] J. Zenihiro, H. Sakaguchi, T. Murakami, M. Yosoi, Y. Yasuda, S. Terashima, Y. Iwao, H. Takeda, M. Itoh, H. P. Yoshida, and M. Uchida, "Neutron density distributions of ^{204,206,208}Pb deduced via proton elastic scattering at E_p = 295 MeV," Physical Review C **82**, 044611 (2010).

[199] H. De Vries, C. W. De Jager, and C. De Vries, "Nuclear charge-density-distribution parameters from elastic electron scattering," Atomic Data and Nuclear Data Tables **36**, 495–536 (1987).

[200] S. Yoshida, H. Sagawa, J. Zenihiro, and T. Uesaka, "Trajectory in 2D plot of isoscalar and isovector densities of ^{48}Ca and ^{208}Pb, and symmetry energy," Physical Review C **102**, 064307 (2020).

[201] S. Miyahara and H. Nakada, "Shape evolution of Zr nuclei and roles of the tensor force," Physical Review C **98**, 064318 (2018).

[202] "National Nuclear Data Center," `https://www.nndc.bnl.gov`.

[203] G. Audi, A. H. Wapstra, and C. Thibault, "The Ame2003 atomic mass evaluation: (II). Tables, graphs and references," Nuclear Physics A **729**, 337–676 (2003), the 2003 NUBASE and Atomic Mass Evaluations.

[204] Y. Suzuki, H. Nakada, and S. Miyahara, "Effects of a realistic tensor force on nuclear quadrupole deformation near the "shore" of the island of inversion," Physical Review C **94**, 024343 (2016).

[205] Reference Input Parameter Library – 2, IAEA, Vienna (2002), tecDoc (2003), unpublished; available at `https://www-nds.iaea.org`.

[206] M. Samyn, S. Goriely, and J. M. Pearson, "Further explorations of Skyrme-Hartree-Fock-Bogoliubov mass formulas. V. Extension to fission barriers," Physical Review C **72**, 044316 (2005).

[207] J.-P. Delaroche, M. Girod, H. Goutte, and J. Libert, "Structure properties of even–even actinides at normal and super deformed shapes analysed using the Gogny force," Nuclear Physics A **771**, 103–168 (2006).

[208] N. Pillet, J.-F. Berger, and E. Caurier, "Variational multiparticle-multihole configuration mixing method applied to pairing correlations in nuclei," Physical Review C **78**, 024305 (2008).

[209] C. Robin, *Fully self-consistent multiparticle-multihole configuration mixing method: applications to a few light nuclei*, Theses, Université Paris Sud - Paris XI (2014).

[210] J. C. Morrison and C. Fischer Froese, "Multiconfiguration Hartree-Fock method and many-body perturbation theory: A unified approach," Physical Review A **35**, 2429–2439 (1987).

[211] C. Froese Fischer, M. Godefroid, T. Brage, P. Jönsson, and G. Gaigalas, "Advanced multiconfiguration methods for complex atoms: I. Energies and wave functions," Journal of Physics B: Atomic, Molecular and Optical Physics **49**, 182004 (2016).

[212] P. G. Szalay, T. Müller, G. Gidofalvi, H. Lischka, and R. Shepard, "Multiconfiguration Self-Consistent Field and Multireference Configuration Interaction Methods and Applications," Chemical Reviews **112**, 108–181 (2012).

[213] N. Pillet, V. G. Zelevinsky, M. Dupuis, J.-F. Berger, and J. M. Daugas, "Low-lying spectroscopy of a few even-even silicon isotopes investigated with the multiparticle-multihole Gogny energy density functional," Physical Review C **85**, 044315 (2012).

[214] J. Le Bloas, N. Pillet, M. Dupuis, J. M. Daugas, L. M. Robledo, C. Robin, and V. G. Zelevinsky, "First characterization of *sd*-shell nuclei with a multiconfiguration approach," Physical Review C **89**, 011306 (2014).

[215] C. Robin, N. Pillet, D. Peña Arteaga, and J.-F. Berger, "Description of nuclear systems with a self-consistent configuration-mixing approach: Theory, algorithm, and application to the ^{12}C test nucleus," Physical Review C **93**, 024302 (2016).

[216] S. Krewald, K. W. Schmid, and A. Faessler, "The influence of correlations on the odd-mass Nuclei ^{21}Ne and ^{25}Mg," Zeitschrift für Physik **269** (1974).

[217] P. Doornenbal *et al.*, "Exploring the "island of inversion" by in-beam γ-ray spectroscopy of the neutron-rich sodium isotopes ^{31,32,33}Na," Physical Review C **81**, 041305 (2010).

[218] X. Viñas, C. Gonzalez-Boquera, M. Centelles, L. M. Robledo, and C. Mondal, "Gogny forces in the astrophysical context," (2018), arXiv:1810.07469 [nucl-th].

[219] C. Mondal, X. Viñas, M. Centelles, and J. N. De, "Structure and composition of the inner crust of neutron stars from Gogny interactions," Physical Review C **102**, 015802 (2020).

[220] C. Gonzalez-Boquera, M. Centelles, X. Viñas, and A. Rios, "Higher-order symmetry energy and neutron star core-crust transition with Gogny forces," Physical Review C **96**, 065806 (2017).

[221] P. Da Costa, *Interactions effectives de portée nulle et régularisées pour les calculs à l'approximation du champ moyen et au-delà*, Theses, Université de Lyon (2022).

[222] M. Oertel, F. Chappert, J.-F. Berger, and M. Girod, "Density dependent spin-orbit interaction from relativistic approaches," (2006), unpublished.

[223] J. D. Walecka, *Theoretical Nuclear and Subnuclear Physics*, Theoretical Nuclear and Subnuclear Physics (Imperial College Press, 2004).

[224] J. Suhonen, *From Nucleons to Nucleus: Concepts of Microscopic Nuclear Theory*, Theoretical and Mathematical Physics (Springer Berlin Heidelberg, 2007).

[225] J.-P. Blaizot and G. Ripka, *Quantum Theory of Finite Systems* (MIT Press, 1986).

[226] N. Pillet, "Derivation of the D2 Landau parameters," internal CEA document (2011).

[227] L. D. Landau, "The Theory of a Fermi Liquid," Soviet Physics JETP **3**, 920 (1957).

[228] L. D. Landau, "Oscillations in a Fermi Liquid," Soviet Physics JETP **5**, 101 (1957).

[229] L. D. Landau, "On the Theory of a Fermi Liquid," Soviet Physics JETP **8**, 70 (1959).

[230] P. Nozières, *Theory of Interacting Fermi Systems*, Frontiers in physics (W. A. Benjamin, 1964).

[231] S.-O. Bäckman, "A calculation of some parameters in Migdal's theory of nuclei," Nuclear Physics A **120**, 593–621 (1968).

[232] J. Dabrowski and P. Haensel, "The deformation of the Fermi surface in polarized nuclear matter," Annals of Physics **97**, 452–469 (1976).

[233] N. Rudra and J. N. De, "Landau parameters for asymmetric nuclear matter with a finite-range density-dependent interaction," Nuclear Physics A **545**, 608–622 (1992).

[234] A. Pastore, D. Davesne, and J. Navarro, "Linear response of homogeneous nuclear matter with energy density functionals," Physics Reports **563**, 1–67 (2015).

[235] A. Schwenk and B. L. Friman, "Polarization Contributions to the Spin Dependence of the Effective Interaction in Neutron Matter," Physical Review Letters **92** (2004).

[236] E. Olsson, P. Haensel, and C. J. Pethick, "Static response of Fermi liquids with tensor interactions," Physical Review C **70** (2004), 10.1103/physrevc.70.025804.

[237] I. Talmi, *Simple Models of Complex Nuclei: The Shell Model and Interacting Boson Model*, Beitrage Zur Wirtschaftsinformatik (Harwood Academic Publishers, 1993).

[238] V. K. Khersonskii, A. N. Moskalev, and D. A. Varshalovich, *Quantum Theory Of Angular Momemtum* (World Scientific Publishing Company, 1988).

[239] M. Baranger and K. T. R. Davies, "Oscillator brackets for Hartree-Fock calculations," Nuclear Physics **79**, 403–416 (1966).

[240] M. Abramowitz, I. A. Stegun, and R. H. Romer, "Handbook of mathematical functions with formulas, graphs, and mathematical tables," (1988).

[241] I. S. Gradshteyn and I. M. Ryzhik, *Table of integrals, series, and products* (Academic press, 2014).